# **AERONAUTICAL ENGINEERING**

A CONTINUING BIBLIOGRAPHY WITH INDEXES

(NASA-SP-7037(319)) AERONAUTICAL ENGINEERING: A CONTINUING BIBLIOGRAPHY WITH INDEXES (SUPPLEMENT 319) (NASA) 133 p

N96-10985

Unclas

00/01 0065431



National Aeronautics and Space Administration

Scientific and Technical Information Office

### The NASA STI Office ... in Profile

Since its founding, NASA has been dedicated to the advancement of aeronautics and space science. The NASA Scientific and Technical Information (STI) Office plays a key part in helping NASA maintain this important role.

The NASA STI Office provides access to the NASA STI Database, the largest collection of aeronautical and space science STI in the world. The Office is also NASA's institutional mechanism for disseminating the results of its research and development activities.

Specialized services that help round out the Office's diverse offerings include creating custom thesauri, translating material to or from 34 foreign languages, building customized databases, organizing and publishing research results ... even providing videos.

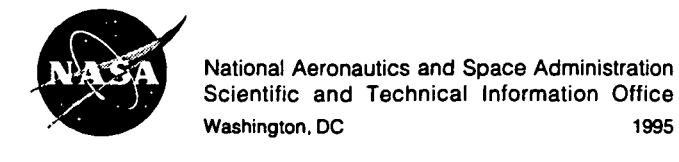
For more information about the NASA STI Office, you can:

- Phone the NASA Access Help Desk at (301) 621-0390
- Fax your question to the NASA Access Help Desk at (301) 621-0134
- E-mail your question via the Internet to help@sti.nasa.gov
- Write to:

NASA Access Help Desk NASA Center for AeroSpace Information 800 Elkridge Landing Road Linthicum Heights, MD 21090-2934

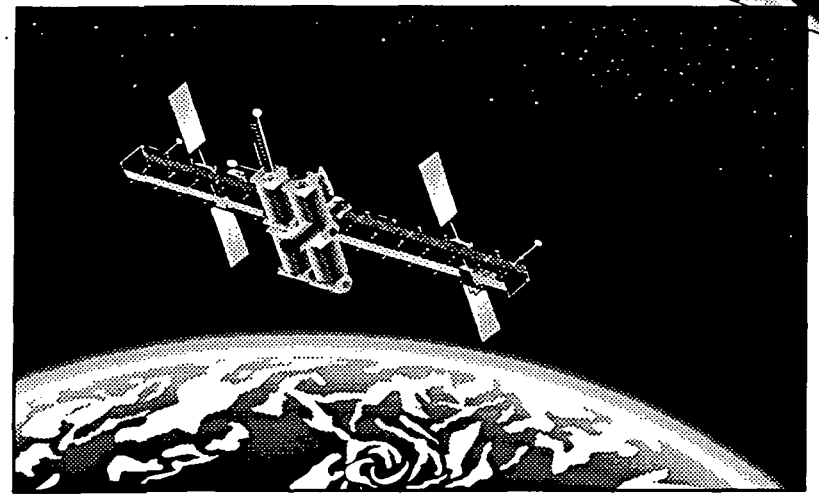
# AERONAUTICAL ENGINEERING

A CONTINUING BIBLIOGRAPHY WITH INDEXES



# The New NASA Video Catalog is Here





To order your free copy call the NASA Access Help Desk at (301) 621-0390 or fax to (301) 621-0134 or e-mail to helpdesk@sti.nasa.gov

# **EXPLORE THE UNIVERSE**

This publication was prepared by the NASA Center for AeroSpace Information, 800 Elkridge Landing Road, Linthicum Heights, MD 21090-2934, (301) 621-0390.

### INTRODUCTION

This issue of *Aeronautical Engineering — A Continuing Bibliography with Indexes* (NASA SP-7037) lists 349 reports, journal articles, and other documents recently announced in the NASA STI Database.

Accession numbers cited in this issue include:

Scientific and Technical Aerospace Reports (STAR) (N-10000 Series) N95-2 Open Literature (A-60000 Series) A95-1

N95-22478 — N95-24194 A95-73327 — A95-77372

The coverage includes documents on the engineering and theoretical aspects of design, construction, evaluation, testing, operation, and performance of aircraft (including aircraft engines) and associated components, equipment, and systems. It also includes research and development in aerodynamics, aeronautics, and ground support equipment for aeronautical vehicles.

Each entry in the publication consists of a standard bibliographic citation accompanied, in most cases, by an abstract. The listing of the entries is arranged by the first nine *STAR* specific categories and the remaining *STAR* major categories. This arrangement offers the user the most advantageous breakdown for individual objectives. The citations include the original accession numbers from the respective announcement journals.

Seven indexes—subject, personal author, corporate source, foreign technology, contract number, report number, and accession number—are included.

A cumulative index for 1995 will be published in early 1996.

The NASA CASI price code table, addresses of organizations, and document availability information are located at the back of this issue.



# SCAN Goes Electronic!

If you have NASA Mail or if you can access the Internet, you can get biweekly issues of *SCAN* delivered to your desk—top absolutely free!

Electronic SCAN takes advantage of computer technology to alert you to the latest aerospace-related, worldwide scientific and technical information that has been published.

No more waiting while the paper copy is printed and mailed to you. You can review Electronic SCAN the same day it is released! And you get all 191—or any combination of—subject areas of announcements with abstracts to browse at your leisure. When you locate a publication of interest, you can print the announcement or electronically add it to your publication order list.

Start your free access to *Electronic SCAN* today. Over 1,000 announcements of new reports, books, conference proceedings, journal articles . . . and more—delivered to your computer every two weeks.

For instant access via Internet:

ftp.sti.nasa.gov gopher.sti.nasa.gov listserv@sti.nasa.gov

For additional information:

e-mail: help@sti.nasa.gov scan@sti.nasa.gov

(Enter this address on the "To" line. Leave the subject line blank and send. You will receive an automatic reply with instructions in minutes.)

Phone: (301) 621-0390 Fax: (301) 621-0134

Write: NASA Access Help Desk

**NASA STI Office** 

NASA Center for AeroSpace Information

800 Elkridge Landing Road

Linthicum Heights, MD 21090-2934

Electronic SCAN
Timely
Flexible
Complete
Free!



### TABLE OF CONTENTS

Category 01	Aeronautics	261
	<b>Áerodynamics</b> aerodynamics of bodies, combinations, wings, rotors, and control surfaces; nal flow in ducts and turbomachinery.	262
Category 03 Includes	Air Transportation and Safety passenger and cargo air transport operations; and aircraft accidents.	276
	Aircraft Communications and Navigation digital and voice communication with aircraft; air navigation systems and ground based); and air traffic control.	278
Category 05 Includes	Aircraft Design, Testing and Performance aircraft simulation technology.	280
Category 06 Includes	Aircraft Instrumentation cockpit and cabin display devices; and flight instruments.	286
	Aircraft Propulsion and Power prime propulsion systems and systems components, e.g., gas turbine and compressors; and onboard auxiliary power plants for aircraft.	288
Category 08 Includes	Aircraft Stability and Control aircraft handling qualities; piloting; flight controls; and autopilots.	290
	Research and Support Facilities (Air) airports, hangars and runways; aircraft repair and overhaul facilities; wind shock tubes; and aircraft engine test stands.	295
facilities ( communi design, 1	Astronautics astronautics (general); astrodynamics; ground support systems and (space); launch vehicles and space vehicles; space transportation; space cations, spacecraft communications, command and tracking; spacecraft esting and performance; spacecraft instrumentation; and spacecraft n and power.	297
physical	Chemistry and Materials chemistry and materials (general); composite materials; inorganic and chemistry; metallic materials; nonmetallic materials; propellants and fuels; rials processing.	300
cal engin phy; lase	Engineering engineering (general); communications and radar; electronics and electri- eering; fluid mechanics and heat transfer; instrumentation and photogra- rs and masers; mechanical engineering; quality assurance and reliability; tural mechanics.	304

Catego	Includes production	Geosciences geosciences (general); earth resources and remote sensing; energy on and conversion; environment pollution; geophysics; meteorology and egy; and oceanography.	316	
Cateogory 14 Life Sciences Includes life sciences (general); aerospace medicine; behavioral sciences; man/system technology and life support; and space biology.				
Category 15 Mathematical and Computer Sciences Includes mathematical and computer sciences (general); computer operations and hardware; computer programming and software; computer systems; cybernetics; numerical analysis; statistics and probability; systems analysis; and theoretical mathematics.			321	
Catego	Includes high-ene	<b>Physics</b> physics (general); acoustics; atomic and molecular physics; nuclear and rgy; optics; plasma physics; solid-state physics; and thermodynamics and I physics.	323	
	Includes tion and i	Social Sciences social sciences (general); administration and management; documenta- information science; economics and cost anaylsis; law, political science, se policy; and urban technology and transportation.	N.A.	
	Includes	Space Sciences space sciences (general); astronomy; astrophysics; lunar and planetary on; solar physics; and space radiation.	N.A.	
Catego	ry 19	General	325	
Subject	Index		A-1	
		Index	B-1	
•		e Index		
Foreign Technology Index				
Contract Number IndexE-1				
-		Index		
Accessi		ber Index	G-1	

.

### TYPICAL REPORT CITATION AND ABSTRACT

#### NASA SPONSORED

ON MICROFICHE

ACCESSION NUMBER → N95-10318\*# Dow Chemical Co., Midland, MI.

← CORPORATE SOURCE

TITLE ightarrow NOVEL MATRIX RESINS FOR COMPOSITES FOR AIRCRAFT PRIMARY STRUCTURES, PHASE 1 Final Report, Apr. 1989 -

Mar. 1992

AUTHORS → EDMUND P. WOO, P. M. PUCKETT, S. MAYNARD, M. T. BISHOP, K. J. BRUZA, J. P. GODSCHALX, AND M. J. MULLINS Aug. 1992 ← PUBLICATION DATE

CONTRACT NUMBERS → (Contracts NAS1-18841; RTOP 510-02-11-02)

REPORT NUMBERS → (NASA-CR-189657; NAS1.26:189657) Avail: CASI HC A08/MFA02 ← AVAILABILITY AND

PRICE CODE

The objective of the contract is the development of matrix resins with improved processability and properties for composites for primarily aircraft structures. To this end, several resins/systems were identified for subsonic and supersonic applications. For subsonic aircraft, a series of epoxy resins suitable for RTM and powder prepreg was shown to give composites with about 40 ksi compressive strength after impact (CAI) and 200 F/wet mechanical performance. For supersonic applications, a thermoplastic toughened cyanate prepreg system has demonstrated excellent resistance to heat aging at 360 F for 4000 hours, 40 ksi CAI and useful mechanical properties at greater than or equal to 310 F. An AB-BCB-maleimide resin was identified as a leading candidate for the HSCT. Composite panels fabricated by RTM show CAI of approximately 50 ksi, 350 F/wet performance and excellent retention of mechanical properties after aging at 400 F for 4000 hours. Author

### TYPICAL JOURNAL ARTICLE CITATION AND ABSTRACT

#### NASA SPONSORED

ACCESSION NUMBER → A95-60192\* National Aeronautics and Space Administration. Ames. ← CORPORATE SOURCE Research Center, Moffett Field, CA.

> TITLE → AERODYNAMIC INTERACTIONS BETWEEN A ROTOR AND WING IN HOVER

**AUTHORS** → FORT F. FELKER NASA. Ames Research Center, Moffett Field, 

AUTHOR'S AFFILIATION CA, US and JEFFREY S. LIGHT NASA. Ames Research Center,

Journal of the American Helicopter Society - JOURNAL TITLE Moffett Field, CA, US

PUBLICATION DATE → 2 Jun. 1986 p. 53-61

REPORT NUMBER → (HTN-94-00714) Copyright

An experimental investigation of rotor/wing aerodynamic interactions in hover is described. The investigation consisted of both a largescale and a small-scale test. A 0.658-scale V-22 rotor and wing was used in the large-scale test. Wing download, wing surface pressure. rotor performance, and rotor downwash data from the large-scale test are presented. A small-scale experiment was conducted to determine how changes in the rotor/wing geometry affected the aerodynamic interactions. These geometry variations included the distance between the rotor and wing, wing incidence angle, wing flap angle, rotor rotation direction, and configurations both with the rotor axis at the tip of the wind (tilt rotor configuration) and with the rotor axis at the center of the wing (compound helicopter configuration). Author (Hemer)

# AERONAUTICAL ENGINEERING

A Continuing Bibliography (Suppl. 319)

July 1995

# 01 AERONAUTICS (GENERAL)

A95-74042\* National Aeronautics and Space Administration. Langley Research Center, Hampton, VA.

OPTIMIZATION OF CONTOURED HYPERSONIC SCRAMJET INLETS WITH A LEAST-SQUARES PARABOLIZED NAVIER-STOKES PROCEDURE

J. J. KORTE NASA. Langley Research Center, Hampton, VA, US and A. H. AUSLENDER Lockheed Enigneering and Sciences Company, Hampton, VA, US Computing Systems in Engineering (ISSN 0956-0521) vol. 4, no. 1 February 1993 p. 13-26 (HTN-95-20976) Copyright

A new optimization procedure, in which a parabolized Navier-Stokes solver is coupled with a non-linear least-squares optimization algorithm, is applied to the design of a Mach 14, laminar two-dimensional hypersonic subscale flight inlet with an internal contraction ratio of 15:1 and a length-to-throat half-height ratio of 150:1. An automated numerical search of multiple geometric wall contours, which are defined by polynomical splines, results in an optimal geometry that yields the maximum total-pressure recovery for the compression process. Optimal inlet geometry is obtained for both inviscid and viscous flows, with the assumption that the gas is either calorically or thermally perfect. The analysis with a calorically perfect gas results in an optimized inviscid inlet design that is defined by two cubic splines and yields a mass-weighted totalpressure recovery of 0.787, which is a 23% improvement compared with the optimized shock-canceled two-ramp inlet design. Similarly, the design procedure obtains the optimized contour for a viscous calorically perfect gas to yield a mass-weighted total-pressure recovery value of 0.749. Additionally, an optimized contour for a viscous thermally perfect gas is obtained to yield a mass-weighted total-pressure recovery value of 0.768. The design methodology incorporates both complex fluid dynamic physics and optimal search techniques without an excessive compromise of computational speed; hence, this methodology is a practical technique that is applicable to optimal inlet design procedures. Author (Herner)

#### A95-75752

### AUTOMATIC RIVETING CELL FOR COMMERCIAL AIRCRAFT FLOOR GRID ASSEMBLY

NIGEL R. ROCHE Deutsche Aerospace Airbur GmbH Aerospace Engineering (Warrendale, Pennsylvania) (ISSN 0736-2536) vol. 15, no. 1 January-February 1995 p. 7-10 (BTN-95-EIX95182617807) Copyright

A new floor grid structure assembly cell was created to allow manufacture of the A330/A340 widebody program into the Airbus manufacturing process. The cell is composed of three stations. Manufacturing in stations 1 and 3 is done manually, while operations are automated in station 2. The main part of the automatic station is a five-axis traveling-column robot with automatically changeable tools. These tools are Cherry Buck riveting machines and drilling machines. The riveting machines have a mass up to 350 kg, and perform drilling, sealing, installing, and closing operations in programmed sequences.

#### A95-75753

#### **MAINTENANCE CHALLENGES AND TRENDS**

LINDA E. TREGO Aerospace Engineering (Warrendale, Pennsylvania) (ISSN 0736-2536) vol. 15, no. 1 January-February 1995 p. 11-14

(BTN-95-EIX95182617808) Copyright

Airlines are faced with an increasing number of maintenance challenges. In the case of Delta Airlines, their approach to these challenges is a process of reengineering which consists of a review of all activities, and elimination of work that does add value to the process. This includes the examination of airlines's maintenance activities such as HMVs (heavy maintenance visits, or 'D' checks) and engine overhauls, and revising processes to eliminate all unnecessary work. By changing the way HMVs are performed, Delta eliminated the time needed to accomplish B-757 HMVs by 20%, and reduced work hours to 20%.

#### A95-75754

#### MAINTENANCE PROGRAMS

LINDA E. TREGO Aerospace Engineering (Warrendale, Pennsylvania) (ISSN 0736-2536) vol. 15, no. 1 January-February 1995 p. 15-20

(BTN-95-EIX95182617809) Copyright

Although maintenance programs differ among airlines and for different aircraft, the same fundamental maintenance requirements apply to all. The method for determining the maintenance program for a system/powerplant including the APU is by using MSG-3, a progressive logic diagram that is applied to the aircraft's MSI (maintenance significant items). The basic planning requirements are derived from the Maintenance Steering Group (MSG-3), which is task oriented. MSIs are those significant items whose failure could 1) affect safety (on ground or flight) and 2) be undetectable or are not likely to be detected during operations, and/or 3) have significant operational impact, and/or 4) have significant economic impact. El

### A95-75756

### **CONDITION MONITORING AND DIAGNOSTICS**

Aerospace Engineering (Warrendale, Pennsylvania) (ISSN 0736-2536) vol. 15, no. 1 January-February 1995 p. 25-26 (BTN-95-EIX95182617811) Copyright

Condition monitoring and diagnostics is being utilized by engineers to detect faults, maintain conditions within certain limits, predict possible future behavior, and improve the future design of aircraft and their subsystems. It has been defined as a field in which physical parameters of an operating machine are periodically or continuously sensed, measured, and recorded for the purpose of reducing, analyzing, comparing, and displaying data, and ultimately to support decisions related to the operation and maintenance of the machine.

#### A95-76765

### CALCULATION OF WING-ALONE AERODYNAMICS TO HIGH ANGLES OF ATTACK

F. G. MOORE Naval Surface Warfare Cent, Dahlgren, VA, United States and R. M. MCINVILLE Journal of Spacecraft and Rockets (ISSN 0022-4650) vol. 32, no. 1 January-February 1995

p. 187-190 refs (BTN-95-EIX95212645713) Copyright

A fourth-order semiempirical method has been developed to estimate wing-alone aerodynamics at all Mach numbers and angles of attack. The method utilizes the linearized theory approaches of the National Space Science Data Center (NSWCDD) Aeroprediction Code along with wing-alone data bases to evaluate constants needed in the fourth-order equation. In deriving the new method, many extrapolations were needed at low Mach numbers and high aspect ratios (ARs). As a result, additional accurate wing-alone wind-tunnel data are needed for AR = 4.0, lambda = 1.0, at all Mach numbers and M less than 1.5, alpha greater than 30 deg, at all ARs.

N95-23506# AVRO International Aerospace, Woodford (England). Engineering Test Facilities.

### HEALTH AND USAGE MONITORING SYSTEMS: CORROSION SURVEILLANCE

J. D. SMART and D. C. WEETMAN (Real Time Corrosion Management Ltd., Grandby Row, England.) In AGARD, Corrosion Detection and Management of Advanced Airframe Materials 11 p Jan. 1995

Copyright Avail: CASI HC A03/MF A03

A predictive method of determining the inspection requirements for specific areas of individual aircraft could offer major advantages in terms of safety and maintenance and repair costs. An approach such as Health and Usage Monitoring in Service, in which the condition of components is monitored whilst in operation, would allow inspection requirements to be minimized and maintenance to be carried out as it becomes necessary. To use such an approach on aircraft would require very sensitive monitoring techniques. Modern electrochemical corrosion instrumentation could offer the required levels of sensitivity for detecting and characterizing the corrosion processes which precede the development of observable damage. This paper details a program carried out to assess the suitability of such electrochemical monitoring instrumentation for aerospace applications and to assess the feasibility of producing an aircraft system on which a predictive corrosion monitoring system could be based. Author

# N95-23519# Department of the Air Force, Tinker AFB, OK. OKLAHOMA CITY AIR LOGISTICS CENTER (USAF) AGING AIRCRAFT CORROSION PROGRAM

DONALD E. NIESER In AGARD, Corrosion Detection and Management of Advanced Airframe Materials 12 p Jan. 1995
Copyright Avail: CASI HC A03/MF A03

Because of projected reductions in future defense budgets, less money will be available for new aircraft acquisitions. Consequently, many of the current aircraft will have to be maintained well into the twenty-first century. As they continue to age, the timedependent effects of material degradation, due to corrosion, will become more significant. Having to maintain aircraft three to four times their original design life presents a unique new set of complex technical problems and challenges. The primary concern is the reduction of airframe fatigue life and static strength due to widespread corrosion damage, fatigue, embrittlement, material loss due to corrosion, intergranular corrosion attack, fretting and stress concentrations. In an effort to ensure continued airworthiness and flight safety, an aggressive program plan has been developed and implemented at Tinker AFB to try to solve the corrosion problems and fatigue related problems to present the occurrence of catastrophic structural failures. The program consists of (1) invasive disassembly of a complete C/KC-135 and sections of B-52 and Boeing 707 aircraft, (2) corrosion documentation/information system development, (3) analysis and testing the effects of corrosion on structural integrity, as well as corrosion growth rates, (4) corrosion modeling and development of C/KC-135 service life extension strategies, (5) and comprehensive evaluation of nondestructive inspection/testing (NDI/NDT) equipment for hidden corrosion detection and quantification. This program has been extensively coordinated with USAF Wright Labs, AFOSR, Naval Air Warfare Center, FAA Aging Aircraft Center, NASA Langley, industry and academia.

Author

N95-24025\*# National Aeronautics and Space Administration. Lewis Research Center, Cleveland, OH.

**RESEARCH AND TECHNOLOGY, 1994** 

Jan. 1995 171 p

(NASA-TM-106764; E-9207; NAS 1.15:106764) Avail: CASI HC A08/MF A02

This report selectively summarizes the NASA Lewis Research Center's research and technology accomplishments for the fiscal year 1994. It comprises approximately 200 short articles submitted by the staff members of the technical directorates. The report is organized into six major sections: Aeronautics, Aerospace Technology, Space Flight Systems, Engineering and Computational Support, Lewis Research Academy, and Technology Transfer. A table of contents and author index have been developed to assist the reader in finding articles of special interest. This report is not intended to be a comprehensive summary of all research and technology work done over the past fiscal year. Most of the work is reported in Lewis-published technical reports, journal articles, and presentations prepared by Lewis staff members and contractors. In addition, university grants have enabled faculty members and graduate students to engage in sponsored research that is reported at technical meetings or in journal articles. For each article in this report a Lewis contact person has been identified, and where possible, reference documents are listed so that additional information can be easily obtained. The diversity of topics attests to the breadth of research and technology being pursued and to the skill mix of the staff that makes it possible.

# 02 AERODYNAMICS

Includes aerodynamics of bodies, combinations, wings, rotors, and control surfaces; and internal flow in ducts and turbomachinery.

### A95-73441

### TIME-OF-FLIGHT MASS SPECTROMETER FOR IMPULSE FACILITIES

K. A. SKINNER Univ of Queensland, St. Lucia, Australia and R. J. STALKER AIAA Journal (ISSN 0001-1452) vol. 32, no. 11 November 1994 p. 2325-2328 refs (BTN-95-EIX95142553057) Copyright

A time-of-flight mass spectrometer has been coupled with a compact sampling system to measure species concentrations in hypersonic flows produced by an impulse facility. The ability to detect molecular species present at levels of only 2% by number has been shown.

#### A95-73444

### TWO-EQUATION TURBULENCE MODEL FOR UNSTEADY SEPARATED FLOWS AROUND AIRFOILS

G. JIN Inst de Mecanique des Fluides de Toulouse, Toulouse, France and M. BRAZA AIAA Journal (ISSN 0001-1452) vol. 32, no. 11 November 1994 p. 2316-2320 refs (BTN-95-EIX95142553054) Copyright

The turbulent incompressible flow around an airfoil NACA 0012 at a Reynolds number range of 10(exp 6) is simulated by an unsteady approach, using the phase-averaging decomposition. This decomposition provides the phase-averaged Navier-Stokes equations. The unsteady vorticity is introduced into the production term of turbulent energy to improve the behavior of the two-equation model with respect to the physics of the flow.

#### A95-73461

# LAPLACE INTERACTION LAW FOR THE COMPUTATION OF VISCOUS AIRFOIL FLOW IN LOW- AND HIGH-SPEED AERODYNAMICS

F. ARNOLD Deutsche Aerospace Airbus GmbH, Bremen, Germany and F. THIELE AIAA Journal (ISSN 0001-1452) vol. 32, no. 11 November 1994 p. 2178-2185 refs (BTN-95-EIX95142553037) Copyright

A new interaction law that accelerates convergence of interactive boundary-layer methods is presented. The law is derived from the Laplace equation and allows the automatic implementation of the Kutta condition for lifting airfoil flows. The accurate influence coefficients of the Laplace interaction law (LIL) facilitate efficient prediction of high-lift flows about multi-element airfoils by direct numerical simulation. Taking into account suitable turbulent closure relations for boundary-layer equations, a fast and reliable computer code has been developed for industrial applications at Deutsche Aerospace Airbus. Very fast convergence and good agreement of calculated results with experiments are observed over a reasonable range of multi-element airfoil flows up to maximum lift. The LIL coupling technique can also be extended to transonic flows. A quasisimultaneous iteration procedure, similar to well-known thinairfoil coupling techniques follows, and accelerated convergence is obtained using the more appropriate influence coefficients of LIL.

Author (EI)

#### A95-73462

### EFFECTS OF EXPANSIONS ON A SUPERSONIC BOUNDARY LAYER: SURFACE PRESSURE MEASUREMENTS

JONATHAN A. DAWSON Ohio State Univ, Columbus, OH, United States, MO SAMIMY, and STEPHEN A. ARNETTE AIAA Journal (ISSN 0001-1452) vol. 32, no. 11 November 1994 p. 2169-2177 refs.

(BTN-95-EIX95142553036) Copyright

Multipoint wall pressure measurements are used to investigate the response of a Mach 3, fully developed, compressible, turbulent boundary layer (Re theta approximately = 25,000) to centered and gradual (R/delta approximately = 50) expansions, both of 7- and 14deg deflection. Although rms fluctuation levels decrease across the expansions, the rms normalized by the local static pressure remains nominally constant. Just downstream of the expansions, normalized power spectra are more concentrated at low frequencies (fless than 10-15 kHz) than upstream, suggesting small-scale turbulence is quenched. This spectra alteration is more prominent for centered expansions and larger deflections. The spectra evolve very quickly after the centered expansions and very slowly after the gradual expansions. Downstream of the expansions, space-time correlations do not lend themselves to the derivation of convection velocities, signifying a severe distortion of the boundary layers. Measurements immediately after the gradual expansions compare well with those further downstream of the centered expansions of the same deflection, suggesting the distance from the beginning of the expansions is the appropriate length scale for characterizing the boundary-layer evolution. After the expansions, a band of elevated spanwise coherence (around 15-30 kHz) and elevated spanwise correlation levels emerge. Increases in streamwise coherence and correlation are less pronounced. At the last measurement stations, the boundary layers remain far from equilibrium. Author (EI)

#### A95-73465

### AERODYNAMIC SHAPE OPTIMIZATION USING PRECONDITIONED CONJUGATE GRADIENT METHODS

GREG W. BURGREEN Old Dominion Univ, Norfolk, VA, United States and OKTAY BAYSAL AIAA Journal (ISSN 0001-1452) vol. 32, no. 11 November 1994 p. 2145-2152 refs (BTN-95-EIX95142553033) Copyright

In an effort to further improve upon the latest advancements made in aerodynamic shape optimization procedures, a systematic study is performed to examine several current solution methodologies as applied to various aspects of the optimization procedure. It is demonstrated that preconditioned conjugate gradient-like meth-

odologies dramatically decrease the computational efforts required for such procedures. The design problem investigated is the shape optimization of the upper and lower surfaces of an initially symmetric (NACA 0012) airfoil in inviscid transonic flow and at zero degrees angle of attack. The complete surface shape is represented using a Bezier-Bernstein polynomial. The present optimization method is demonstrated to automatically obtain super-critical airfoil shapes over a variety of freestream Mach numbers. Furthermore, the best optimization strategy examined resulted in a factor of 8 decrease in computational time as well as a factor of 4 decrease in memory over the most efficient strategies in current use.

Author (EI)

#### A95-73493

### ANALYTICAL STUDY OF THE NEUTRAL STABILITY OF A MODEL HYPERSONIC BOUNDARY LAYER

DANIEL R. BOWER State Univ of New York at Buffalo, Buffalo, NY, United States and CHING SHI LIU AIAA Journal (ISSN 0001-1452) vol. 32, no. 12 December 1994 p. 2366-2371 refs (BTN-95-EIX95152577589) Copyright

The neutral modes of a hypersonic boundary layer flow over an adiabatic flat plate are considered. A formulation of the governing second-order linear equation for the pressure disturbance is developed that lends itself to the application of the WKB method over the entire boundary layer. This formulation provides analytic eigenvalues and eigenfunction relations for the pressure disturbances and is applicable to flows at moderate Mach numbers as well. Solutions are determined for the cases of the wave speed c = 0 and c = 1, and show good qualitative agreement with numerical computations as well as results in the limit M(sub INF) to infinity.

Author (EI)

#### A95-73494

### COMPUTATION OF OSCILLATING AIRFOIL FLOWS WITH ONE- AND TWO-EQUATION TURBULENCE MODELS

J. A. EKATERINARIS Navy-NASA Joint Inst of Aeronautics, Moffett Field, CA, United States and F. R. MENTER AIAA Journal (ISSN 0001-1452) vol. 32, no. 12 December 1994 p. 2359-2365 refs (BTN-95-EIX95152577588) Copyright

The ability of one- and two-equation turbulence models to predict unsteady separated flows over airfoils is evaluated. An implicit, factorized, upwind-biased numerical scheme is used for the integration of the compressible, Reynolds-averaged Navier-Stokes equations. The turbulent eddy viscosity is obtained from the computed mean flowfield by integration of the turbulent field equations. One- and two-equation turbulence models are first tested for a separated airfoil flow at fixed angle of incidence. The same models are then applied to compute the unsteady flowfields about airfoils undergoing oscillatory motion at low subsonic Mach numbers. Experimental cases where the flow has been tripped at the leadingedge and where natural transition was allowed to occur naturally are considered. The more recently developed turbulence models capture the physics of unsteady separated flow significantly better than the standard k- epsilon and k- omega models. However, certain differences in the hysteresis effects are observed. For an untripped high-Reynolds-number flow, it was found necessary to take into account the leading-edge transitional flow region to capture the correct physical mechanism that leads to dynamic stall.

Author (EI)

### A95-73495

# COUPLED FEM-BEM APPROACH FOR MEAN FLOW EFFECTS ON VIBRO-ACOUSTIC BEHAVIOR OF PLANAR STRUCTURES

FRANCK SGARD Univ of Sherbrooke, Sherbrooke, Que, Canada, NOUREDDINE ATALLA, and JEAN NICOLAS AIAA Journal (ISSN 0001-1452) vol. 32, no. 12 December 1994 p. 2351-2358 refs (BTN-95-EIX95152577587) Copyright

The importance of the mean flow effects on the forced vibrational behavior of a baffled plate, as well as on its acoustic radiation patterns, is investigated for a plate with different kinds of boundary conditions. The analysis is based on a finite element method for the calculation of the plate transverse vibrations and the use of the

extended Kirchoff's integral equation to account for fluid loading with mean flow. A variational boundary element method is used to compute the acoustic radiation impedance. The formulation shows explicitly the effects of mean flow in terms of added mass, stiffness and radiation damping.

A95-73496\* National Aeronautics and Space Administration. Langley Research Center, Hampton, VA.

### MACH WAVE EMISSION FROM A HIGH-TEMPERATURE SUPERSONIC JET

JOHN M. SEINER National Aeronautics and Space Administration. Langley Research Center, Hampton, VA, THONSE R. S. BHAT, and MICHAEL K. PONTON AIAA Journal (ISSN 0001-1452) vol. 32, no. 12 December 1994 p. 2345-2356 refs (BTN-95-EIX95152577586) Copyright

The paper considers the compressible Rayleigh equation as a model for the Mach wave emission mechanism associated with high-temperature supersonic jets. Solutions to the compressible Rayleigh equation reveal the existence of several families of supersonically convecting instability waves. These waves directly radiate noise to the jet far field. The predicted noise characteristics are compared to previously acquired experimental data for an axisymmetric Mach 2 fully pressure balanced jet (i.e., P(sub e)/ P(sub a) = 1.0) operating over a range of jet total temperatures from ambient to 1370 K. The results of this comparison show that the firstorder supersonic instability wave and the Kelvin-Helmholtz first-, second-, and third-order modes have directional radiation characteristics that are in agreement with observed data. The assumption of equal initial amplitudes for all of the waves leads to the conclusion that the flapping mode of instability dominates the noise radiation process of supersonic jets. At a jet temperature of 1370 K, supersonic instability waves are predicted to dominate the noise radiated at high frequency at narrow angles to the jet axis. Author (EI)

#### A95-73497

### EFFICIENT SENSITIVITY ANALYSIS FOR ROTARY-WING AEROMECHANICAL PROBLEMS

ANNE MARIE SPENCE Univ of Maryland, College Park, MD, United States and ROBERTO CELI AIAA Journal (ISSN 0001-1452) vol. 32, no. 12 December 1994 p. 2337-2344 refs (BTN-95-EIX95152577585) Copyright

This paper describes a method for the calculation of the sensitivities of rotating blade root loads and hub loads to changes of blade design parameters using a chain rule differentiation approach. The algorithm exploits features of the formulation of the blade and fuselage equations of motion, and of the solution technique, to calculate the sensitivities at a fraction of the cost of an aeroelastic analysis. The mathematical model of the blade includes nonlinearities because of moderately large elastic deflections and the fuselage is described by nonlinear Euler equations, so that the resulting model is valid for both straight and turning flight. The results indicate that the semianalytical technique is very accurate and computationally efficient.

Author (EI)

### A95-73516

### FLOW VISUALIZATION STUDIES ON SIDEWALL EFFECTS IN TWO-DIMENSIONAL TRANSONIC AIRFOIL TESTING

NORIKAZU SUDANI Nati Aerospace Lab, Tokyo, Japan, MAMORU SATO, HIROSHI KANDA, and KENICHI MATSUNO Journal of Aircraft (ISSN 0021-8669) vol. 31, no. 6 November-December 1994 p. 1233-1239 refs

(BTN-95-EIX95152582313) Copyright

The effects of sidewall boundary layers in two-dimensional transonic airfoil testing were investigated using oil-flow or liquid crystal visualization techniques. Three different chord models were tested in order to clarify the sidewall effects and to seek a suitable aspect ratio of the airfoil. The oil-flow visualization data systematically reveal the surface flow patterns affected by the sidewalls and suggest a minimum aspect ratio for conducting reliable two-dimensional tests. The results of the liquid crystal visualization also show

the three dimensionality of the transition behavior and the necessity of the high aspect ratio. In addition, investigations on effects of the sidewall boundary-layer suction and application of a sidewall interference correction produce significant results for improvement of airfoil testing by removal of the sidewall effects.

Author (EI)

A95-73518\* National Aeronautics and Space Administration. Ames Research Center, Moffett Field, CA.

### PROGRESS IN HIGH-LIFT AERODYNAMIC CALCULATIONS

STUART E. ROGERS National Aeronautics and Space Administration. Ames Research Center, Moffett Field, CA Journal of Aircraft (ISSN 0021-8669) vol. 31, no. 6 November-December 1994 p. 1244-1251 refs

(BTN-95-EIX95152582315) Copyright

The current work presents progress in the effort to numerically simulate the flow over high-lift aerodynamic components, namely multielement airfoils in either a takeoff or landing configuration. The computational approach utilizes an incompressible flow solver and an overlaid chimera grid approach. A detailed grid resolution study is presented for flow over a three-element airfoil. Two turbulence models - a one-equation Baldwin-Barth model and a two-equation k-omega model - are compared. Excellent agreement with experiment is obtained for the lift coefficient at all angles of attack, including the prediction of maximum lift when using the two-equation model. Results for two other flap riggings are shown.

# A95-73519 SIDEWASH ON THE VERTICAL TAIL IN SUBSONIC AND SUPERSONIC FLOWS

CHYN-SHAN CHIU China Junior Coll of Technology, Taipei, Taiwan, Province of China and I. J. LIN, Journal of Aircraft (ISSN 0021-8669) vol. 31, no. 6 November-December 1994 p. 1252-1256 refs (BTN-95-EIX95152582316) Copyright

A generalized vortex-lattice method is used for the investigation of sidewash on the single and twin vertical tails due to rolling wing in subsonic and supersonic flows. The current results of sidewash on the single vertical tail in incompressible inviscid flow are almost the same as Michael's calculations. The sidewash on the single vertical tail through high angle of attack is presented. The difference of sidewash on the single and twin vertical tail that is induced by the rolling wing in subsonic and supersonic flows is also studied.

Author (EI)

#### A95-73520

### LIMIT CYCLE PHENOMENA IN COMPUTATIONAL TRANSONIC AEROELASTICITY

KENNETH A. KOUSEN Univ of California, Los Angeles, CA, United States and ODDVAR O. BENDIKSEN Journal of Aircraft (ISSN 0021-8669) vol. 31, no. 6 November-December 1994 p. 1257-1263 refs

(BTN-95-EIX95152582317) Copyright

Limit cycle behavior has been observed in past transonic flutter calculations by the authors, using a two degree-of-freedom typical section model coupled to an unsteady Euler equations solver. In this article, the structural nonlinearity of freeplay has been added to the typical section model, and its effects on the dynamic stability problem are assessed. In addition, limit cycle behavior in the sweptwing model of Isogai is demonstrated and related to the observed presence of multiple flutter points in the transonic dip region.

Author (EI)

### A95-73523

### COMPUTATION OF THE POSTSTALL BEHAVIOR OF A CIRCULATION CONTROLLED AIRFOIL

SAMUEL W. LINTON Sterling Software at NASA Ames Research Cent, Moffett Field, CA, United States Journal of Aircraft (ISSN 0021-8669) vol. 31, no. 6 November-December 1994 p. 1273-1280 refs

(BTN-95-EIX95152582320) Copyright

This article describes the numerical simulation of stalled and

unstalled flows over a circulation controlled airfoil (CCA) using a fully implicit Navier-Stokes code, and the comparison with experimental results. Mach numbers of 0.3 and 0.5 and jet total to freestream pressure ratios of 1.4 and 1.8 are investigated. The Baldwin-Lomax and k-epsilon turbulence models are used, each modified to include the effect of strong streamline curvature. The numerical solutions of the poststall CCA show a highly regular unsteady periodic flowfield. This is the result of an alternation between adverse pressure gradient and shock-induced separation of the boundary layer on the airfoil trailing edge.

Author (EI)

### A95-73524

### EXPERIMENTAL INVESTIGATION OF THE FLOWFIELD ABOUT AN UPSWEPT AFTERBODY

RONALD J. EPSTEIN von Karman Inst for Fluid Dynamics, Rhode-Saint-Genese, Belgium, MARIO C. CARBONARO, and F. CAUDRON Journal of Aircraft (ISSN 0021-8669) vol. 31, no. 6 November-December 1994 p. 1281-1290 refs (BTN-95-EIX95152582321) Copyright

In general, the flowfield about the aft portion of an aircraft fuselage employing an upswept afterbody is complex and can have a detailed vortex structure. Directional pressure probe measurements show that the afterbody wake evolution is weakly dependent on the Reynolds number. Pressure taps are used to investigate the effect of base slant on the base pressure distribution. The base pressure distribution is found to increase along the upswept ramp in the freestream direction. Using oil flow visualizations general conclusions are drawn about the surface flow topology. Two distinct regions of flow separation are identified. An analytical model of the crossflow wake structure is developed from the experimental data. This model allows for conclusions to be drawn about the crossflow vortex structure and provides simple analytical expressions for the vorticity and swirl velocity distributions in the crossflow plane.

Author (EI)

### A95-73525

### UNSTRUCTURED GRID SOLUTIONS TO A WING/PYLON/ STORE CONFIGURATION

PARESH PARIKH VIGYAN, Inc. Hampton, VA, United States, SHAHYAR PIRZADEH, and NEAL T. FRINK Journal of Aircraft (ISSN 0021-8669) vol. 31, no. 6 November-December 1994 p. 1291-1296 refs

(BTN-95-EIX95152582322) Copyright

The purpose of this article is to validate an inviscid flow solution package based on a new unstructured grid methodology using experimental data on a wing/pylon/tinned store configuration. The solution package consists of an advancing front grid generator, VGRID, and an efficient Euler equation solver, USM3D. Comparisons of computed data vs experimental data are made for two freestream Mach numbers at five store locations relative to the wing. Both rigid body aerodynamics and mutual interference effects are explored. A very good agreement is observed between computed and wind-tunnel data.

Author (EI)

### A95-73527

### MOVING WALL EFFECT IN RELATION TO OTHER DYNAMIC STALL FLOW MECHANISMS

LARS E. ERICSSON Journal of Aircraft (ISSN 0021-8669) vol. 31, no. 6 November-December 1994 p. 1303-1309 refs (BTN-95-EIX95152582324) Copyright

An analysis is performed to determine the importance of the socalled moving wall effect relative to other unsteady flow mechanisms present in the dynamic stall process. Analysis of existing theoretical and experimental results indicates that the tangential moving wall effect on the initial boundary-layer development, close to the flow stagnation point, is not satisfactorily represented in current numerical methods. The analysis shows that this moving wall effect plays a dominant role in inducing self-excited oscillations, such as the wing rock of advanced aircraft, and also plays a significant role in so called supermaneuvers of these aircraft.

Author (EI) A95-73529\* National Aeronautics and Space Administration. Langley Research Center, Hampton, VA.

### SEPARATION CONTROL ON HIGH-LIFT AIRFOILS VIA MICRO-VORTEX GENERATORS

JOHN C. LIN National Aeronautical and Space Administration. Langley Research Center, Hampton, VA, STEPHEN K. ROBINSON, ROBERT J. MCGHEE, and WALTER O. VALAREZO Journal of Aircraft (ISSN 0021-8669) vol. 31, no. 6 November-December 1994 p. 1317-1323 refs

(BTN-95-EIX95152582326) Copyright

An experimental investigation has been conducted to evaluate boundary-layer separation control on a two-dimensional single-flap, three-element, high-lift system at near-flight Reynolds numbers with small surface-mounted vortex generators. The wind-tunnel testing was carried out in the NASA Langley Low-Turbulence Pressure Tunnel as part of a cooperative program between McDonnell Douglas Aerospace and NASA Langley Research Center to develop code validation data bases and to improve physical understanding of multielement airfoil flows. This article describes results obtained for small (subboundary-layer) vane-type vortex generators mounted on a multielement airfoil in a landing configuration. Measurements include lift, drag, surface pressure, wake profile, and fluctuating surface heat fluxes. The results reveal that vortex generators as small as 0.18% of reference (slat and flap stowed) wing chord ('micro-vortex generators') can effectively reduce boundary-layer separation on the flap for landing configurations. Reduction of flap separation can significantly improve performance of the high-lift system by reducing drag and increasing lift for a given approach angle of attack. At their optimum chordwise placement on the flap, the micro-vortex generators are hidden inside the wing when the flap is retracted, thus extracting no cruise drag penalty. Author (EI)

#### A95-73530

### STUDY OF AN AIRFOIL WITH A FLAP AND SPOILER

ABDULLAH AL SHABIBI Sultan Qaboos Univ, Muscat, Oman, MUNIR AL HAMMADI, and JOSEPH MATHEW Journal of Aircraft (ISSN 0021-8669) vol. 31, no. 6 November-December 1994 p. 1324-1327 refs

(BTN-95-EIX95152582327) Copyright

An experimental investigation of an airfoil with a spoiler and flap was carried out. Results of these studies are presented. The coefficient of lift was seen to decline sharply in the range of spoiler angles ranging from 0 to 15 deg, due to the early separation that the spoiler introduces on the airfoil. Experiments with wing-flap combinations for flap angles ranging from 0 to 45 deg showed that there is an optimum wing-flap gap for a wing-flap configuration. A considerable increase in the intensities of turbulences were seen at higher flap angles that should contribute to the sharp increase in the drag at the higher flap angles. A wake frequency spectrum for varying angles of attack has been made and is presented.

Author (EI)

A95-73532\* National Aeronautics and Space Administration. Langlev Research Center, Hampton, VA.

### ANALYSIS OF A HIGHER HARMONIC CONTROL TEST TO REDUCE BLADE VORTEX INTERACTION NOISE

THOMAS F. BROOKS National Aeronautics and Space Administration. Langley Research Center, Hampton, VA, EARL R. BOOTH, JR., D. DOUGLAS BOYD, JR., WOLF R. SPLETTSTOESSER, KLAUS-J. SCHULTZ, ROLAND KUBE, GEORG H. NIESL, and OLIVIER STREBY Journal of Aircraft (ISSN 0021-8669) vol. 31, no. 6 November-December 1994 p. 1341-1349 refs (BTN-95-FIX95152582330). Convright

(BTN-95-EIX95152582330) Copyright
A noise study using an aeroelastically scaled BO-105 rotor was conducted in the German-Dutch Wind Tunnel to examine the use of higher harmonic control (HHC) of blade pitch to reduce impulsive blade-vortex interaction (BVI) noise. The noise directivity was measured over a large plane underneath the rotor using a traversing inflow microphone array. Noise and vibration measurements were made for a range of matched rotor operating conditions where prescribed (or open loop) HHC pitch, at various amplitudes and phases, was superimposed on normal (baseline) collective and

cyclic trim pitch. Acoustic data are presented for 3, 4, and 5P HHC applied to a typical landing approach rotor operating condition where BVI noise is normally intense. Noise reductions of up to 6 dB were found for the advancing side BVI noise radiating upstream of the rotor, and also for the retreating side BVI noise radiating below and downstream of the rotor. The relative levels between the sides were modified by HHC control phase. To help give insight to the physics of the HHC/BVI noise problem, high-resolution loading and noise prediction results are presented for comparison to the data. The predictions are based on a new high-resolution version of the CAMRAD rotor performance program under development at Langley, called HIRES.

### A95-73539

### POSTINSTABILITY BEHAVIOR OF A TWO-DIMENSIONAL AIRFOIL WITH A STRUCTURAL NONLINEARITY

S. J. PRICE McGill Univ, Montreal, Que, Canada, B. H. K. LEE, and H. ALIGHANBARI Journal of Aircraft (ISSN 0021-8669) vol. 31, no. 6 November-December 1994 p. 1395-1401 refs (BTN-95-EIX95152582337) Copyright

A two-dimensional airfoil with a free-play nonlinearity in pitch subject to incompressible flow has been analyzed. The aerodynamic forces on the airfoil were evaluated using Wagner's function and the resulting equations integrated numerically to give time histories of the airfoil motion. Regions of limit cycle oscillation are detected for velocities well below the linear flutter boundary, and the existence of these regions is strongly dependent on the initial conditions and properties of the airfoil. Furthermore, for small structural preloads, narrow regions of chaotic motion are obtained, as suggested by power spectral densities, phase-plane plots, and Poincare sections of the airfoil time histories. The existence of this chaotic motion is strongly dependent on a number of airfoil parameters, including, mass, frequency ratio, structural damping, and preload.

Author (EI)

#### A95-73541

### STATIC PRESSURE DISTRIBUTION IN THE INLET OF A HELICOPTER TURBINE COMPRESSOR

JOHANNES P. VANDERWALT Univ of the Witwatersrand, Johannesburg, South Africa and ALAN NURICK Journal of Aircraft (ISSN 0021-8669) vol. 31, no. 6 November-December 1994 p. 1411-1413 refs

(BTN-95-EIX95152582339) Copyright

The parallel compressor model was used to demonstrate that when the airflow into a compressor is distorted, the velocity at the inlet to the compressor will be virtually constant with consequent variations in the static pressure. Refined parallel compressor models have been proposed in which it is assumed that the compressor tends to induce a constant air inlet velocity with static pressure gradients that are in sympathy with the total pressure gradients. Four basic elements have been identified to be important for distortion measurement: (1) circumferential intensity; (2) extent; (3) multiple-per-rev elements defined at constant radius; and (4) a radial intensity element.

### A95-73546

### FLOW STUDY OF SUPERSONIC WING-NACELLE CONFIGURATION

KASIM BIBER Wichita State Univ, Wichita, KS, United States and JOEL MENDOZA Journal of Aircraft (ISSN 0021-8669) vol. 31, no. 6 November-December 1994 p. 1424-1426 refs (BTN-95-EIX95152582344) Copyright

Nacelle/airframe integration is of major importance for aerodynamically efficient supersonic transport aircraft design and development. When the nacelle is integrated with an aircraft wing, its flowfield is affected by the wing boundary layer, depending on the nacelle proximity to the wing surface. The shock-boundary layer flow interaction between the nacelle and wing is studied, as well as the wing interference effects on the nacelle flowfield. The nacelle leading-edge shock wave appears to be steady and attached to the inlet lip for all test cases. The boundary layer on the wing lower

surface is turbulent and the shock expansion waves from the nacelle do not have a significant impingement effect on its character.

#### A95-73547

### ANALYTIC PREDICTION OF LIFT FOR DELTA WINGS WITH PARTIAL LEADING-EDGE THRUST

LANCE W. TRAUB Univ of the Witwatersrand, Johannesburg, South Africa Journal of Aircraft (ISSN 0021-8669) vol. 31, no. 6 November-December 1994 p. 1426-1429 refs (BTN-95-EIX95152582345) Copyright

Expressions were derived to analytically determine the lift an drag coefficients of delta wings with partial leading-edge thrust in subsonic flow. The method uses the suction analogy, with an assumed theoretical leading-edge thrust distribution. Separate expressions to estimate the effective thrust based on the empirical method of Carlson and Mack and the method of Kulfan were derived. Some airfoil and wing geometric parameters, as well as the potential constant, are required in the equations. The two methods were compared with experimental results, and good agreement was shown at moderate angles of attack which improves as the wing aspect ratio was reduced.

A95-73548\* National Aeronautics and Space Administration. Langley Research Center, Hampton, VA.

### COMPUTATIONAL STUDY OF PLUME-INDUCED SEPARATION ON A HYPERSONIC POWERED MODEL

L. D. HUEBNER National Aeronautics and Space Administration. Langley Research Center, Hampton, VA Journal of Aircraft (ISSN 0021-8669) vol. 31, no. 6 November-December 1994 p. 1429-1431 refs

(BTN-95-EIX95152582346) Copyright

The computation of hypersonic air-breathing vehicle flowfields were studied under simulated powered conditions. Two-dimensional parabolized Navier-Stokes (PNS) and full Reynolds-averaged Navier-Stokes (RANS) calculations were performed to predict the possible existence and effects of flow separation on the cowl of a hypersonic airbreathing model employing scramjet exhaust flow simulation at representative Mach 10 wind tunnel conditions. Flow separation resulted in a negligible difference in lift and thrust, while there was a small increase in pitching moment. If the cowl trailing edge was at a position such that part of the cowl was an expansion surface, the separation would likely be greater, as would the impact on lift and thrust.

A95-73552\* National Aeronautics and Space Administration. Langley Research Center, Hampton, VA.

### AERODYNAMIC CHARACTERISTICS OF A HYPERSONIC VISCOUS OPTIMIZED WAVERIDER AT HIGH ALTITUDES

DIDIER F. G. RAULT National Aeronautics and Space Administration, Langley Research Center, Hampton, VA Journal of Spacecraft and Rockets (ISSN 0022-4650) vol. 31, no. 5 September-October 1994 p. 719-727 refs

(BTN-95-EIX95152583251) Copyright

The aerodynamic characteristics of a University of Maryland viscous optimized waverider are studied at altitudes ranging from 97 to 145 km and incidence angles of 0 to 30 deg. The direct simulation Monte Carlo method is used to simulate and analyze the flowfield around the waverider and evaluate surface loads. It is shown that the vehicle lift-to-drag ratio decreases rapidly as flight altitude is increased, and is confined to values less than 0.3. At high altitudes, the waverider is surrounded by a thick viscous shock layer, and the friction forces, which are typically large at high Knudsen numbers, are shown to significantly reduce lift and increase drag. Author (EI)

#### A95-73557

### BASE DRAG PREDICTION ON MISSILE CONFIGURATIONS

F. G. MOORE Naval Surface Warfare Cent, Dahlgren, VA, United States, F. WILCOX, and T. HYMER Journal of Spacecraft and Rockets (ISSN 0022-4650) vol. 31, no. 5 September-October 1994 p. 759-765 refs

(BTN-95-EIX95152583256) Copyright

New wind-tunnel data have been taken, and a new empirical model has been developed for predicting base drag on missile configurations. The new wind-tunnel data were taken at NASA Langley Research Center in the unitary wind tunnel at Mach numbers from 2.0 to 4.5, angles of attack to 16 deg, fin control deflections up to 20 deg, fin thickness-to-chord ratio of 0.05 to 0.15, and fin locations flush with the base to two chord lengths upstream of the base. The newly developed empirical model uses these data along with previous wind-tunnel data. It estimates base drag as a function of all the preceding variables along with boattail and power-on or power-off effects. In comparing the new empirical model to that used in the former aeroprediction code, the new model gives improved accuracy compared to wind-tunnel data. The new model also is more robust due to inclusion of additional variables. On the other hand, additional wind-tunnel data are needed to validate or modify the current empirical model in areas where data are not available.

Author (EI)

#### A95-73558

### AERODYNAMIC CHARACTERISTICS OF A CANARD-CONTROLLED MISSILE AT HIGH ANGLES OF ATTACK

EDMUND H. SMITH Naval Air Warfare Cent, China Lake, CA, United States, SHESHAGIRI HEBBAR, and MAX F. PLATZER Journal of Spacecraft and Rockets (ISSN 0022-4650) vol. 31, no. 5 September-October 1994 p. 766-772 refs (BTN-95-EIX95152583257) Copyright

A low-speed wind-tunnel investigation was conducted to examine the aerodynamic characteristics of a one-third-scale model of a canard-controlled missile at high angles of attack using force and moment measurements. The data were taken at a nominal Mach number of 0.2 for angles of attack up to 50 deg at three different canard deflection settings. The test runs were limited to 0- and 45deg missile roll angles (symmetric configurations) and two sets of tails (aft fins), one with the full area including the roll damping tabs (rollerons) and the other without the rollerons. The data indicate that the rollerons act as an effective fin area at low speeds and high angles of attack, and make the missile more stable. The test data were also used to validate the aerodynamic characteristics of the missile as predicted by the Missile Datcom program. The agreement between the Datcom predictions and the test data is fairly good, with the latter indicating a slightly higher static stability. Author (EI)

#### A95-73560

### THREE-DIMENSIONAL STRUCTURE OF A SUPERSONIC JET IMPINGING ON AN INCLINED PLATE

KYOUNG-HO KIM Hyundai Motor Co and KEUN-SHIK CHANG Journal of Spacecraft and Rockets (ISSN 0022-4650) vol. 31, no. 5 September-October 1994 p. 778-782 refs (BTN-95-EIX95152583259) Copyright

The flow structure of an underexpanded supersonic let impinging on an inclined flat plate has been numerically investigated using a total-variation-diminishing scheme for the Euler equations. The impinging jet is characterized by many discontinuities, such as barrel shock, exhaust gas jet boundary, Mach disk, reflected shock, plate shock, subtail shock, contact surface, and sometimes a stagnation bubble. Furthermore, if the plate is inclined, the jet structure becomes three-dimensional and severely distorted. The effect of plate inclination has been investigated in the present paper by studying the formation of the asymmetric stagnation bubble and the magnitude and location of the maximum wall pressure. Comparison with the existing experimental results over a broad range of data sets on pressure and shock structure has led to the conclusion that the present inviscid numerical model can offer fairly good prediction of the impinging jet for moderate plate inclinations. The maximum wall pressure was found to be larger on the inclined plate than on the normal plate. Author (EI)

#### A95-73561

### IMPROVED VERSION OF THE NAVAL SURFACE WARFARE CENTER AEROPREDICTION CODE (AP93)

F. G. MOORE Naval Surface Warfare Cent, Dahlgren, VA, United

States, T. HYMER, and R. MCINVILLE Journal of Spacecraft and Rockets (ISSN 0022-4650) vol. 31, no. 5 September-October 1994 p. 783-791 refs

(BTN-95-EIX95152583260) Copyright

A new and improved version of the naval Surface Warfare Center, Dahlgren Division aeroprediction code has been developed. The new code, AP93, contains new technology that allows planar aerodynamics of axisymmetric solid-rocket-type weapons to be computed over the entire Mach-number range that weapons fly and for angles of attack up to 30 deg. Comparisons of the new AP93 code with the AP81 show that the AP93 on the average reduces the normal force and center-of-pressure errors of the AP81 code almost by half, and gives a slight improvement in axial force errors.

A95-75097\* National Aeronautics and Space Administration. Langley Research Center, Hampton, VA.

### SENSITIVITY OF ACOUSTIC PREDICTIONS TO VARIATION OF INPUT PARAMETERS

KENNETH S. BRENTNER NASA. Langley Research Center, Hampton, VA, US, CASEY L. BURLEY NASA. Langley Research Center, Hampton, VA, US, and MICHAEL A. MARCOLINI NASA. Langley Research Center, Hampton, VA, US American Helicopter Society, Journal (ISSN 0002-8711) vol. 39, no. 3 July 1994 p. 43-52 (HTN-95-80855) Copyright

Rotor noise prediction codes predict the thickness and loading noise produced by a helicopter rotor, given the blade motion, rotor operating conditions, and fluctuating force distribution over the blade surface. However, the criticality of these various inputs, and their respective effects on the predicted acoustic field, have never been fully addressed. This paper examines the importance of these inputs, and the sensitivity of the acoustic predicitions to a variation of each parameter. The effects of collective and cyclic pitch, as well as coning and cyclic flapping, are presented. Blade loading inputs are examined to determine the necessary spatial and temporal resolution, as well as the importance of the chordwise distribution. The acoustic predictions show regions in the acoustic field where significant errors occur when simplified blade motions or blade loadings are used. An assessment of the variation in the predicted acoustic field is balanced by a consideration of Central Processing Unit (CPU) time necessary for the various approximations.

Author (Herner)

### A95-75101

### THE INFLUENCE OF ALTERNATE INTER-BLADE CONNECTIONS ON GROUND RESONANCE

N. M. SELA Technion-Israel Institute of Technology, Haifa, Israel and A. ROSEN Technion-Israel Institute of Technology, Haifa, Israel American Helicopter Society, Journal (ISSN 0002-8711) vol. 39, no. 3 July 1994 p. 73-78 (HTN-95-80859) Copyright

The present analysis is an extension to a previous work by the authors where the ground resonance problem of a helicopter with a rotor incorporating inter-connected blades was analyzed. As before the blades are inter-connected with springs and dampers, but in the present analysis the direction of inter-blade connections is opposite to that analyzed previously. Using the Modified Multiblade Coordinate Transformation (MMCT), a set of constant coefficient equations is obtained. Examination of the equations reveals that the present arrangement of the inter-connecting springs and dampers is less effective than the previous one for three-bladed rotors, equally, effective for four-bladed rotors, and more effective for rotors incorporating five blades or more.

#### A95-75728

# DETERMINATION OF WALL BOUNDARY CONDITIONS FOR HIGH-SPEED-RATIO DIRECT SIMULATION MONTE CARLO CALCULATIONS

FRANK G. COLLINS Univ of Tennessee Space Inst, Tullahoma, TN, United States and E. C. KNOX Journal of Spacecraft and Rockets (ISSN 0022-4650) vol. 31, no. 6 November-December 1994 p. 965-970 refs

#### (BTN-95-EIX95182617457) Copyright

A procedure for determining the velocity distribution function for the molecules that are reflected from an element of surface when a vehicle is moving in the transition or free-molecule flow regimes at high speed ratios is described. This distribution function could be used as the boundary condition for DSMC calculations. The method uses measurements of the momentum accommodation coefficients to determine the parameters for the Nocilla model of the reflected velocity distribution function. The use of this function as a boundary condition with the DSMC method would yield more accurate predictions of flow fields than are presently obtained using the assumption of diffuse scattering from the body surface. Several sets of Nocilla model parameters are determined as examples of the application of the procedure.

A95-75729\* National Aeronautics and Space Administration. Langley Research Center, Hampton, VA.

# ZONALLY DECOUPLED DIRECT SIMULATION MONTE CARLO SOLUTIONS OF HYPERSONIC BLUNT-BODY WAKE FLOWS

RICHARD G. WILMOTH National Aeronautics and Space Administration, Langley Research Center, Hampton, VA, ROBERT A. MITCHELTREE, JAMES N. MOSS, and VIRENDRA K. DOGRA Journal of Spacecraft and Rockets (ISSN 0022-4650) vol. 31, no. 6 November-December 1994 p. 971-979 refs (BTN-95-EIX95182617458) Copyright

Direct simulation Monte Carlo (DSMC) solutions are presented for the hypersonic flow behind a blunt body in which the wake region is solved in a zonally decoupled manner. The forebody flow is solved separately using either a DSMC or a Navier-Stokes method, and the forebody exit-plane solution is specified as the inflow condition to the decoupled DSMC solution of the wake region. Results are presented for a 70-deg, blunted cone at flow conditions that can be accommodated in existing low-density wind tunnels with the Knudsen number (based on the base diameter) ranging from 0.03 to 0.001. The zonally decoupled solutions show good agreement with fully coupled DSMC solutions of the wake flow densities and velocities. The wake closure predicted by the zonally decoupled solutions is in better agreement with fully coupled results than that predicted by a fully coupled Navier-Stokes method, indicating the need to account for rarefaction in the wake for the cases considered. The combined use of Navier-Stokes for the forebody with a decoupled DSMC solution for the wake provides an efficient method for solving transitional blunt-body flows where the forebody flow is continuum and the wake is rarefied. Author (EI)

### A95-75731

### CONVECTIVE AND RADIATIVE HEAT TRANSFER ANALYSIS FOR THE FIRE 2 FOREBODY

ROBERT B. GREENDYKE VIGYAN, Inc., Hampton, VA, United States and LIN C. HARTUNG Journal of Spacecraft and Rockets (ISSN 0022-4650) vol. 31, no. 6 November-December 1994 p. 986-992 refs

(BTN-95-EIX95182617460) Copyright

A Navier-Stokes flowfield solution method using finite-rate chemistry and two-temperature thermal nonequilibrium was used in combination with two nonequilibrium radiative heat transfer codes to calculate heating for the FIRE II vehicle. An axisymmetric model of the actual body shape was used. One radiative heating code was used in uncoupled fashion with the flowfield solver's energy equations, while the other code was used in both coupled and uncoupled variations. Several trajectory points ranging from highly nonequilibrium flow to near-equilibrium flow were used for a study of both convective and radiative heating over the vehicle. Considerable variation in radiative heating was seen at the extremes, while agreement was good in the intermediate trajectory points. Total heat transfer calculations gave good comparison until the peak heating trajectory points were encountered and returned to good agreement for the last two equilibrium points. Author (EI)

#### A95-75733

### WING VERTICAL POSITION EFFECTS ON WING-BODY CARRYOVER FOR NONCIRCULAR MISSILES

BRIAN E. EST Univ of Missouri-Rolla, Rolla, MO, United States and H. F. NELSON Journal of Spacecraft and Rockets (ISSN 0022-4650) vol. 31, no. 6 November-December 1994 p. 999-1006 refs (BTN-95-EIX95182617462) Copyright

The preliminary design component buildup factor K(sub W(B)), a measure of the wing-body interference caused by upwash, is investigated for unbanked, supersonic missiles with noncircular body cross section. The aerodynamic effects of wing vertical location relative to the missile fuselage centerline, Mach number, and fuselage cross-sectional shape are parametrically varied to develop a preliminary design data base of K(sub W(B)) values for circular, square, and triangular missile bodies. A spatial marching Euler code ZEUS is used to determine the delta-wing normal force in the presence of the body. Euler K(sub W(B)) predictions are compared to the slender body theory presently used for computing low angleof-attack K(sub W(B)) in missile preliminary design engineering methods. Euler values of K(sub W(B)) exhibit sensitivity to wing vertical position, Mach number, and body cross-sectional shape, whereas slender body theory is a function of wing semispan to body radius ratios, S/R, only. Euler values of K(sub W(B)) are generally found to differ from slender body theory values by less than 15% for smaller S/R, and they approach slender body theory values at larger Author (EI)

# A95-75736 SUPERSONIC NEAR-WAKE AFTERBODY BOATTAILING EFFECTS ON AXISYMMETRIC BODIES

J. L. HERRIN Univ of Illinois at Urbana-Champaign, Urbana, IL, United States and J. C. DUTTON Journal of Spacecraft and Rockets (ISSN 0022-4650) vol. 31, no. 6 November-December 1994 p. 1021-1028 refs (BTN-95-EIX95182617465) Copyright

An experimental investigation of the near-wake flowfield downstream of a conical boattailed afterbody in supersonic flow is presented. The afterbody investigated is typical of those for conventional boattailed missiles and projectiles in unpowered flight. Flow visualization, mean static pressure measurements, and three-component laser Doppler velocimeter data have been obtained throughout the near wake of the body. The effects of afterbody boattailing on the physics of the near-wake flow are determined by comparing the present data with similar data obtained on a cylindrical afterbody. Results indicate that a net afterbody drag reduction of 21% is achieved with the current boattailed afterbody for a freestream Mach number of 2.46. The shear-layer growth rate, and therefore mass entrainment from the recirculation region behind the base, is shown to be significantly reduced by afterbody boattailing due to the reduction in turbulence levels throughout the near wake as compared to the cylindrical afterbody. Author (EI)

#### A95-75758

### TRANSIENT STRUCTURE OF VORTEX BREAKDOWN ON A DELTA WING

J. -C. LIN Lehigh Univ, Bethlehem, PA, United States and D. ROCKWELL AIAA Journal (ISSN 0001-1452) vol. 33, no. 1 January 1995 p. 6-12 refs

(BTN-95-EIX95182619073) Copyright

The transient relaxation process of the leading-edge vortex on a delta wing pitched to high angle of attack is quantitatively characterized using high-image density particle image velocimetry. Instantaneous distributions of azimuthal vorticity and patterns of sectional streamlines over an entire plane allow definition of a new, rapidly evolving mechanism at the onset of vortex breakdown; it marks the transition from a relatively high to low upstream propagation speed of the breakdown.

Author (EI)

A95-75761\* National Aeronautics and Space Administration. Ames Research Center, Moffett Field, CA.

### AEROACOUSTIC MODEL FOR WEAK SHOCK WAVES BASED ON BURGERS EQUATION

SANFORD S. DAVIS National Aeronautics and Space Administration, Ames Research Center, Moffett Field, CA AIAA Journal (ISSN 0001-1452) vol. 33, no. 1 January 1995 p. 27-32 refs (BTN-95-EIX95182619076) Copyright

The adiabatic form of the Euler equations are cast in a form emphasizing its signal propagation properties and solved using an approximate eigenfunction analysis. Second-order rarefaction waves appear as direct eigenfunction solutions. The underlying scalar equation describing nonlinear shock wave evolution is rederived as a first-order Burgers equation. The characteristic sonic boom N waves are predicted using an implicit aeroacoustic-based finite-difference algorithm with numerical damping designed to suppress spurious oscillations at shock-wave discontinuities. The evolution of these sonic-boom-type signals to the mid- and far field are computed directly with the numerical method.

Author (EI)

#### A95-75763

### TURBULENT TRANSONIC AIRFOIL FLOW SIMULATION USING A PRESSURE-BASED ALGORITHM

GANG ZHOU Chalmers Univ of Technology, Gothenburg, Sweden, LARS DAVIDSON, and ERIK OLSSON AIAA Journal (ISSN 0001-1452) vol. 33, no. 1 January 1995 p. 42-47 refs (BTN-95-EIX95182619078) Copyright

There are few successful computational reports for transonic airfoil flow worked out with the pressure-based method. In this study, an advanced approach based on a pressure correction scheme is developed to solve the Reynolds-averaged Navier-Stokes equations for turbulent transonic flow around the airfoil RAE 2822. An implicit numerical dissipation model is adopted to create a dissipation mechanism based on pressure gradients to damp the destabilizing numerical effects, without smearing the physical discontinuity at shocks. The standard k-epsilon turbulence closure with a nearwall one-equation model is used. The computational results are compared with experimental data. Several discretization schemes such as the second-order upwind, hybrid, and MUSCL schemes for convection terms are investigated. The computational results show that the proposed pressure-based method has a resolution comparable to, or better than, the traditional time-marching methods.

Author (EI)

### A95-75765

### SIMULATION OF TRANSVERSE GAS INJECTION IN TURBULENT SUPERSONIC AIR FLOWS

F. GRASSO Univ of Rome 'La Sapienza', Rome, Italy and V. MAGI AIAA Journal (ISSN 0001-1452) vol. 33, no. 1 January 1995 p. 56-62 refs

(BTN-95-EIX95182619080) Copyright

The present paper deals with the simulation of the fluid dynamic behavior of transverse gas injection in turbulent supersonic air streams. The Favre-averaged Navier-Stokes equations are solved for a multicomponent mixture of gases. A two-equation k-epsilon turbulence model is employed that properly accounts for low Reynolds effects. The governing equations are solved by a finite volume approach with the k-epsilon model equations fully coupled with those of the mean flow, and an implicit treatment of the source terms. Several test cases are considered and the results are compared with available experimental measurements.

Author (EI)

#### A95-75778

### VISCOUS-INVISCID INTERACTION METHOD FOR UNSTEADY LOW-SPEED AIRFOIL FLOWS

ISMAIL H. TUNCER Naval Postgraduate Sch, Monterey, CA, United States, JOHN A. EKATERINARIS, and MAX F. PLATZER AIAA Journal (ISSN 0001-1452) vol. 33, no. 1 January 1995 p. 151-154 refs

(BTN-95-EIX95182619093) Copyright

A Reynolds-averaged Navier-Stokes solver was coupled with

a potential flow panel code in an attempt to split the flowfield into viscous and inviscid flow zones. The objective was to reduce the computational domain in which Navier-Stokes equations are solved. This method confines the Navier-Stokes computations to the close proximity of the vortical boundary-layer and the wake regions. It is capable of predicting low Mach number, attached or mildly separated flowfields as accurately as the full-domain Navier-Stokes solutions. For a typical flowfield, the Navier-Stokes/potential flow interactive solution method is about 40% more efficient than the full Navier-Stokes method in terms of CPU times.

#### A95-76589

### SCALING OF INCIPIENT SEPARATION IN SUPERSONIC/ TRANSONIC SPEED LAMINAR FLOWS

GEORGE R. INGER Iowa State Univ, Ames, IA, United States AIAA Journal (ISSN 0001-1452) vol. 33, no. 1 January 1995 p. 178-181 refs

(BTN-95-EIX95182619104) Copyright

Interactions between oblique shock waves and boundary layers must be understood to predict the performance of aero-dynamic devices such as flaps, spoilers, and inlets. These involve strong viscous/inviscid interaction flow with a large local adverse pressure gradient that often provokes boundary-layer separation. The prediction of the onset of such separation and the delineation of the underlying scaling laws that govern it continue to be important in aerodynamic studies of high speed aircraft and missiles, these vehicles operate and are tested over a wide range of Mach and Reynolds numbers. This paper re-examines the fundamental similitude rules pertaining to the laminar (high-altitude) flight regime of supersonic vehicles, with the goal of establishing a single unified scaling law for both supersonic and moderately hypersonic Mach numbers.

### A95-76590

### SIMPLE METHOD OF SUPERSONIC FLOW VISUALIZATION USING WATERTABLE

A. K. PAL Jadavpur Univ, Calcutta, India and B. BOSE AIAA Journal (ISSN 0001-1452) vol. 33, no. 1 January 1995 p. 181-182 refs

(BTN-95-EIX95182619105) Copyright

A simple and novel optical method for the quantitative evaluation of physical flow variables in a high-speed flow has been obtained from photographs of the flow pattern, obtained in a watertable using the established theory of hydraulic analogy. Here, the photographic method for flow visualization is demonstrated at supersonic speeds. It is also shown that it may be extended to study different model configurations.

### A95-76605

### **MULTIAXIS PILOT RATINGS FOR DAMAGED AIRCRAFT**

YAUG-FEA JENG Oklahoma State Univ, Stillwater, OK, United States and ROBERT L. SWAIM Journal of Guidance, Control, and Dynamics (ISSN 0731-5090) vol. 17, no. 6 November-December 1994 p. 1241-1244 refs

(BTN-95-EIX95182619128) Copyright

A systematic methodology for the prediction of loss of control for various maneuvers performed by a specific aircraft with various types and degrees of damage is presented. The study monitors the development of loss of control while the scale of the specific damage is increasing. This study also investigates the sensitivity of the specific aircraft to different types of damage while a specific maneuver is being performed. The result shows the existence of the critical degrees of specific damage that cause the pilot to lose control as represented by a pilot opinion rating (POR) of greater than 9 on the Cooper-Harper rating scale.

### A95-76615

### ANALYTICAL AEROPROPULSIVE/AEROELASTIC HYPERSONIC-VEHICLE MODEL WITH DYNAMIC ANALYSIS

FRANK R. CHAVEZ Univ of Maryland at Coll Park, College Park, MD, United States and DAVID K. SCHMIDT Journal of Guidance,

Control, and Dynamics (ISSN 0731-5090) vol. 17, no. 6 November-December 1994 p. 1308-1319 refs (BTN-95-EIX95182619138) Copyright

Dynamic characteristics determination of hypersonic vehicles needs an integrated approach since the propulsion system and airframe are so highly coupled. A first step toward the development of an integrated approach that is intentionally generic and basic is presented. Further, analytical expressions are developed to allow for characterization of the vehicle's dynamics early in the design cycle, so that configuration trade-off may be performed with some cognizance of the attitude dynamics. It is shown that the vehicle's aerodynamics and propulsive forces are both very significant in the evaluation of key derivatives that dictate the vehicle's dynamic characteristics. It is also shown that the vehicle selected is highly unstable in pitch and exhibits strong airframe/engine/elastic coupling in the aeroelastic and attitude dynamics.

A95-76636\* National Aeronautics and Space Administration. Langley Research Center, Hampton, VA.

### APPLICATION OF TRANSONIC SMALL DISTURBANCE THEORY TO THE ACTIVE FLEXIBLE WING MODEL

WALTER A. SILVA National Aeronautics and Space Administration, Langley Research Center, Hampton, VA and ROBERT M. BENNETT Journal of Aircraft (ISSN 0021-8669) vol. 32, no. 1 January-February 1995 p. 16-22 refs (BTN-95-EIX95182619210) Copyright

The CAP-TSD code, developed at the NASA Langley Research Center, is applied to the active flexible wing wind-tunnel model for prediction of transonic aeroelastic behavior. A semispan computational model is used for evaluation of symmetric motions, and a full-span model is used for evaluation of antisymmetric motions. Static aeroelastic solutions using the computational aeroelasticity programtransonic small disturbance, are computed. Dynamic (flutter) analyses are then performed as perturbations about the static aeroelastic deformations and presented as flutter boundaries in terms of Mach number and dynamic pressure. Flutter boundaries that take into account modal refinements, vorticity and entropy corrections, antisymmetric motions, and sensitivity to the modeling of the wingtip ballast stores are also presented and compared with experimental flutter results.

A95-76643\* National Aeronautics and Space Administration.
Langley Research Center, Hampton, VA.
ROLLING MANFILVER LOAD ALL EVIATION USING ACTIVE

### ROLLING MANEUVER LOAD ALLEVIATION USING ACTIVE CONTROLS

JESSICA A. WOODS-VEDELER National Aeronautics and Space Administration, Langley Research Center, Hampton, VA, ANTHONY S. POTOTZKY, and SHERWOOD T. HOADLEY Journal of Aircraft (ISSN 0021-8669) vol. 32, no. 1 January-February 1995 p. 68-76 refs

(BTN-95-EIX95182619217) Copyright

Rolling maneuver load alleviation (RMLA) has been demonstrated on the Active Flexible Wing wind-tunnel model in the NASA Langley Transonic Dynamics Tunnel (TDT). The objective was to develop a systematic approach for designing active control laws to alleviate wing loads generated during rolling maneuvers. Two RMLA control laws were developed that utilized outboard control surface pairs (leading and trailing edge) to counteract the loads and used inboard trailing-edge control surface pairs to maintain roll performance. Rolling maneuver load tests were performed in the TDT at several dynamic pressures including two below and one 11% above the open-loop flutter dynamic pressure. Above open-loop flutter, the RMLA system was operated simultaneously with an active flutter suppression system. At all dynamic pressures for which baseline results were obtained, torsion moment loads were reduced for both RMLA control laws. Results for bending moment load reductions were mixed; however, design equations developed in this study provided conservative estimates of load reduction in all cases. Author (EI)

A95-76646
DYNAMIC INVESTIGATION OF THE ANGULAR MOTION OF A

#### **ROTATING BODY-PARACHUTE SYSTEM**

D. LEVIN Technion - Israel Inst of Technology, Haifa, Israel and Z. SHPUND Journal of Aircraft (ISSN 0021-8669) vol. 32, no. 1 January-February 1995 p. 93-99 refs (BTN-95-EIX95182619220) Copyright

The modern design of parachute-payload systems that undergo specific trajectories has to cope with dynamic behavior characteristics, which were of secondary importance in the past. Static and dynamic measurements, as well as computational simulations, are being employed to help the designers in converging to an optimal solution. However, some aerodynamic dynamic data are often impossible to obtain either computationally or experimentally through direct measurement. Novel experimental techniques have to be implemented in order to expand the analysis capability or to validate the design of specific configurations. A test technique that allows three degrees of freedom for investigating experimentally the dynamic behavior of parachute-payload systems is presented. The system is utilized to investigate the effect of the parachute geometrical variables on the dynamic stability of the parachute-payload system. The crosstype parachute-payload systems that were tested exhibit three zones of different dynamic stability modes and the occurrence of dynamic instability for statically stable configurations. These results show the need for obtaining more dynamic data for the complete understanding of the dynamic behavior of closely coupled parachute-payload Author (EI) configurations.

#### A95-76651

### STABILITY DERIVATIVES OF A FLAPPED PLATE IN UNSTEADY GROUND EFFECT

A. O. NUHAIT King Saud Univ, Riyadh, Saudi Arabia and M. F. ZEDAN Journal of Aircraft (ISSN 0021-8669) vol. 32, no. 1 January-February 1995 p. 124-129 refs (BTN-95-EIX95182619225) Copyright

The stability derivatives of a flapped plate moving in ground proximity are evaluated using an unsteady ground effect model. The model, which has been developed previously, was extended to account for the flap. The results show that ground proximity has a substantial effect on the derivatives of the aerodynamic coefficients. The derivatives obtained by the present unsteady model disagree with those obtained by the customary steady ground effect model, especially very close to the ground. The effect of the flight-path angle (in addition to the pitch angle or angle of attack) on aerodynamic coefficients is found to be substantial and, therefore, their derivatives with respect to it are very important. Because of its own nature, the steady approach fails to account for the flight-path angle and, therefore, it cannot provide the derivatives with respect to this angle near ground.

Author (EI)

### A95-76653

# AERODYNAMICS OF A FINITE WING WITH SIMULATED ICE A. KHODADOUST Univ of Illinois at Urbana-Champaign, Urbana, IL, United States and M. B. BRAGG Journal of Aircraft (ISSN 0021-

8669) vol. 32, no. 1 January-February 1995 p. 137-144 refs (BTN-95-EIX95182619227) Copyright

The flowfield about a semispan finite wing with a simulated leading-edge ice accretion is studied experimentally. The finite wing was tested in both a straight and swept wing configuration. Surface pressures, fluorescent oil flow visualization, and helium bubble flow visualization studies of the flowfield are reported. The presence of the simulated ice accretion produces a large leading-edge separation bubble which results in a global change of the pressure field, reduction of lift, and increase in drag. Fluorescent oil flow visualization and pressure distributions from the centerline of the straight wing at low angles of attack show a predominantly two-dimensional flowfield on the wing's upper surface. Three-dimensional effects due to the tipinduced vortex and root-wall interaction become important at high angles of attack. Oil flow visualization shows that wall suction near the wing root drastically changes the flowfield near the root. The measured span loads on the straight wing compare well with the computational results when the endwall is properly modeled. The swept wing has a highly three-dimensional flowfield. Pressure distributions indicate higher lift near the root and lower lift near the

tip. Helium bubble traces show a strong spanwise flow component on the swept wing. These results are in good qualitative agreement with Navier-Stokes calculations. Author (EI)

#### A95-76656

### AERODYNAMIC CHARACTERISTICS OF EXTERNAL STORE CONFIGURATIONS AT LOW SPEEDS

O. OZCAN Istanbul Technical Univ, Istanbul, Turkey, M. F. UNAL, A. R. ASLAN, Y. BOZKURT, and N. H. AYDIN Journal of Aircraft (ISSN 0021-8669) vol. 32, no. 1 January-February 1995 p. 161-170 refs

(BTN-95-EIX95182619230) Copyright

Aerodynamic characteristics of external store configurations used on interceptor aircraft were investigated experimentally and computationally. Balance measurements, flow visualization, and static pressure measurements were made in a low-speed wind tunnel. The experimental and computational data revealed the global structure of the flow around a basic configuration. Six groups of models were used in the present study. This article discusses the results for the first and second group of models. The incompressible flow over a limited number of models was computed by solving the Navier-Stokes equations. The solution method is based on the Galerkin finite element discretization of space and the fractional step discretization of time. Reasonably good agreement was observed between the experimental and computational static pressure distributions on a basic geometry. The computational data, which revealed details of reverse flow regions, supported and supplemented the experimental data. Author (EI)

# A95-76659 UNSTEADY GROUND EFFECTS ON AERODYNAMIC COEFFICIENTS OF FINITE WINGS WITH CAMBER

A. O. NUHAIT King Saud Univ, Riyadh, Saudi Arabia Journal of Aircraft (ISSN 0021-8669) vol. 32, no. 1 January-February 1995 p. 186-192 refs

(BTN-95-EIX95182619233) Copyright

A numerical investigation on finite thin cambered wings moving near ground in unsteady flow was conducted. The numerical model is based on the general three-dimensional vortex-lattice method in which the wake is computed as part of the solution. The image technique is used to simulate the ground effects. The computed results indicate that the percentage changes in the aerodynamic coefficients (C(sub L) and C(sub M)) increase with proximity to the ground. The greater the sink rate, the weaker the increase, which is consistent with the trend shown by other experimental investigators for flat wings. Increasing the aspect ratio increases the ground effect, causing wings to start feeling the ground at higher positions. The ground effects are weaker as the camber ratio increases, consistent with the results of two-dimensional plates. Moving the position of maximum camber backward has a similar effect. Meanlines of NACA five-digit series showed bigger increase in C(sub L) and C(sub M) compared to NACA four-digit and six-digit series meanlines. Increasing the angle of attack increases the ground effects in conflict with the results of two-dimensional plates. Author (EI)

#### A95-76661

### STUDY OF THE DROPLET SPRAY CHARACTERISTICS OF A SUBSONIC WIND TUNNEL

MICHAEL B. BRAGG Univ of Illinois at Urbana-Champaign, Urbana, IL, United States and ABDOLLAH KHODADOUST Journal of Aircraft (ISSN 0021-8669) vol. 32, no. 1 January-February 1995 p. 199-204 refs

(BTN-95-EIX95182619235) Copyright

A finite difference, two-dimensional potential flow solver, and a three-dimensional particle trajectory code have been written to compute water droplet trajectories in a subsonic incompressible flow wind tunnel. This method was used to study the spray cloud in the test section of a two-dimensional wind tunnel resulting from the injection of a distribution of water droplets in the settling chamber ahead of the inlet. The results of this computational study showed that the trajectories of the larger water droplets were affected by the droplet inertia and gravity

more dramatically than that for the smaller particles. The calculated liquid water content across the test section indicated a high concentration near the tunnel centerline. The largest droplets were present at the test section only in the center one-third of the wind tunnel, whereas the smaller droplets spanned almost the entire test section width. This resulted in a computed droplet size distribution skewed toward the larger droplets in comparison with the initial Langmuir-D distribution. The distribution of particle sizes and concentrations required at the droplet injection point in the settling chamber for a Langmuir-D distribution of uniform liquid water content in the center third of the test section was computed.

#### A95-76740

### REVIEW AND DEVELOPMENT OF BASE PRESSURE AND BASE HEATING CORRELATIONS IN SUPERSONIC FLOW

J. PARKER LAMB Univ of Texas at Austin, Austin, TX, United States and WILLIAM L. OBERKAMPF Journal of Spacecraft and Rockets (ISSN 0022-4650) vol. 32, no. 1 January-February 1995 p. 8-23 refs

(BTN-95-EIX95212645688) Copyright

A comprehensive review of experimental base pressure and base heating data related to supersonic and hypersonic flight vehicles is presented. Particular attention is paid to free-flight data as well as to wind-tunnel data for models without rear sting support. Using theoretically based correlation parameters, a series of internally consistent, empirical predictions are developed for planar and axisymmetric geometries (wedges, cones, and cylinders). These equations encompass the speed range from low supersonic to hypersonic flow and laminar and turbulent forebody boundary layers. A wide range of cone and wedge angles and cone bluntness ratios is included in the data base used to develop the correlations. The present investigation also includes an analysis of the effect of the angle of attack and the specific-heat ratio of the gas. Angle-ofattack effects are considered on sharp and blunted cones and cylindrical afterbodies. Author (EI)

### A95-76742

### NUMERICAL INVESTIGATION OF SUPERSONIC FLOWS AROUND A SPIKED BLUNT BODY

MASAFUMI YAMAUCHI Tokyo Noko Univ, Tokyo, Japan, KOZO FUJII, and FUMIO HIGASHINO Journal of Spacecraft and Rockets (ISSN 0022-4650) vol. 32, no. 1 January-February 1995 p. 32-42 refs

(BTN-95-EIX95212645690) Copyright

In supersonic flow, a spike attached to the nose reduces the drag of a blunt body. Supersonic flows around a spiked blunt body are numerically simulated to examine the effects of the spike length, Mach number, and angle of attack. Three-dimensional thin-layer compressible Navier-Stokes equations are solved using a high-resolution upwind scheme with LU-ADI time-integration algorithm. The computed results show that the drag of the spiked blunt body is significantly influenced by the spike length, Mach number, and angle of attack. Scales of the separated region are not significantly influenced by the freestream Mach number. For the spiked blunt body at angle of attack, the flowfield becomes complex with spiral flows. The computed results are in reasonable agreement with experimental data.

#### A95-76744

### INTEGRATED DESIGN OF HYPERSONIC WAVERIDERS INCLUDING INLETS AND TAILFINS

SHEAM-CHYUN LIN Natl Taiwan Inst of Technology, Taipei, Taiwan, Province of China and YU-SHAN LUO Journal of Spacecraft and Rockets (ISSN 0022-4650) vol. 32, no. 1 January-February 1995 p. 48-54 refs

(BTN-95-EIX95212645692) Copyright

A generic aerospace vehicle including an airframe, inlet, and tail-wings is developed by means of the waverider concept. The stream surfaces of the hypersonic flow past a cone with both transverse and longitudinal curvatures are used to design the forebody configuration. By suitably choosing the even polynomial

stream surfaces, the airframe, horizontal stabilizers, and inlet can be constructed together. In addition, several small caret-waveriders are patched on this configuration as the vertical fins for the furnishment of a hypersonic vehicle. Also calculated are the mass flow rate, lift, drag, and lift-to-drag ratio. Moreover, effects of the various parameters on the shape and aerodynamic performance of this high-speed vehicle are found and discussed in detail. Hence, an overall aerodynamic design of a hypersonic vehicle is established in a simple and systematic way.

Author (EI)

A95-76746\* National Aeronautics and Space Administration. Lewis Research Center, Cleveland, OH.

### NUMERICAL ANALYSIS OF HYPERSONIC LOW-DENSITY SCRAMJET INLET FLOW

CHAN H. CHUNG National Aeronautics and Space Administration. Lewis Research Center, Cleveland, OH, SUK C. KIM, KENNETH J. DEWITT, and HENRY T. NAGAMATSU Journal of Spacecraft and Rockets (ISSN 0022-4650) vol. 32, no. 1 January-February 1995 p. 60-66 refs

(BTN-95-EIX95212645694) Copyright

Hypersonic low-density flow around a two-dimensional scramjet inlet model has been analyzed using the direct simulation Monte Carlo (DSMC) method. The predominant features of hypersonic flows, such as a thick viscous layer due to the low-density fluid together with shock-boundary-layer interaction and shock impingement as well as shock-induced separation, are encountered in this type of flowfield. Three hypersonic flowfields with different degrees of rarefaction are investigated. The freestream Knudsen numbers of the flowfields based on the height of the duct passage are in the range of 0.02-0.12. Conventional continuum gas dynamics based on the concept of a local equilibrium may not be adequate to describe this type of flowfield accurately. The pressures obtained by the DSMC simulation are compared with available experimental data. Good agreement is obtained with previous experimental data and with theoretical solutions for similar wedge flow cases near the leading edge of the ramp centerbody. Good agreement is observed with the experimental data of Minucci and Nagamatsu except for some discrepancies, especially in the lower-density cases, which may be partially attributed to three-dimensional effects and/or to experimental uncertainty. Author (EI)

### A95-76747

### ANALYTICAL SOLUTION AND PARAMETER ESTIMATION OF PROJECTILE DYNAMICS

SUSANNE WEISS DLR, German Aerospace Research Establishment, Braunschweig, Germany, KARL-FRIEDRICH DOHERR, and HARTMUT SCHILLING Journal of Spacecraft and Rockets (ISSN 0022-4650) vol. 32, no. 1 January-February 1995 p. 67-74 refs (BTN-95-EIX95212645695) Copyright

For the determination of the pitch, yaw, and roll characteristics of conventional projectiles an approach is presented that allows fast estimation of the projectile parameters from test data. To avoid numerical integration and the corresponding integration errors and convergence problems, an analytical solution of the six-degree-offreedom differential equations of motion is introduced. Here, instead of time, the arc length of the flight path is taken as the independent variable. Also, linear aerodynamics without Magnus effects is assumed. The projectile parameters are determined by minimizing the squared sum of the differences between the measured and the simulated trajectory using a nongradient direct search method. As an example, yaw-card measurements from tests with KE rods (highkinetic-energy projectiles) are analyzed. It is shown that the main aerodynamic coefficients can be extracted from these data. In addition, it is possible to identify the size and the location of the muzzle jump as well as the jump due to sabot separation.

Author (EI)

# A95-76764 LASER VELOCIMETRY SEED-PARTICLE BEHAVIOR IN SHEAR LAYERS AT MACH 12

J. D. SCHMISSEUR Wright Lab, Wright-Patterson Air Force Base,

OH, United States and M. S. MAURICE Journal of Spacecraft and Rockets (ISSN 0022-4650) vol. 32, no. 1 January-February 1995 p. 185-187 refs

(BTN-95-EIX95212645712) Copyright

The seed particle behavior in a Mach 12 flowfield was examined through laser velocimetry measurements in the Aeromechanics Division Twenty-Inch Hypersonic Wind Tunnel. Data were collected in the shear layer generated by the nozzle wall at the nozzle exit plane. Two diameters of alumina, nominally 0.3 and 1.0 micron, were used as seed material to investigate the particle response characteristics.

N95-22666\*# National Aeronautics and Space Administration. Ames Research Center, Moffett Field, CA.

### FLOW VISUALIZATION STUDIES OF VTOL AIRCRAFT MODELS DURING HOVER IN GROUND EFFECT

NIKOS J. MOURTOS (San Jose State Univ., CA.), STEPHANE COUILLAUD (San Jose State Univ., CA.), DALE CARTER (San Jose State Univ., CA.), CRAIG HANGE, DOUG WARDWELL, and RICHARD J. MARGASON Jan. 1995 48 p Original contains color illustrations

(Contract(s)/Grant(s): RTOP 505-68-32)

(NASA-TM-108860; A-95025; NAS 1.15:108860) Avail: CASI HC A03/MF A01; 28 functional color pages

A flow visualization study of several configurations of a jet-powered vertical takeoff and landing (VTOL) aircraft model during hover in ground effect was conducted. A surface oil flow technique was used to observe the flow patterns on the lower surfaces of the model. There were significant configuration effects. Wing height with respect to fuselage, the presence of an engine inlet duct beside the fuselage, and nozzle pressure ratio are seen to have strong effects on the surface flow angles on the lower surface of the wing. This test was part of a program to improve the methods for predicting the hot gas ingestion (HGI) for jet-powered vertical/short takeoff and landing (V/STOL) aircraft. The tests were performed at the Jet Calibration and Hover Test (JCAHT) Facility at Ames Research Center.

Author

N95-22802\*# National Aeronautics and Space Administration. Langley Research Center, Hampton, VA.

WING PRESSURE DISTRIBUTIONS FROM SUBSONIC TESTS OF A HIGH-WING TRANSPORT MODEL

ZACHARY T. APPLIN, GARL L. GENTRY, JR., and M. A. TAKALLU (Lockheed Engineering and Sciences Co., Hampton, VA.) Jan. 1995 442 p

(Contract(s)/Grant(s): RTOP 505-59-10-13)

(NASA-TM-4583; L-17380; NAS 1.15:4583) Avail: CASI HC A19/ MF A04

A wind tunnel investigation was conducted on a generic, highwing transport model in the Langley 14- by 22-Foot Subsonic Tunnel. This report contains pressure data that document effects of various model configurations and free-stream conditions on wing pressure distributions. The untwisted wing incorporated a full-span, leading-edge Krueger flap and a part-span, double-slotted trailingedge flap system. The trailing-edge flap was tested at four different deflection angles (20 deg, 30 deg, 40 deg, and 60 deg). Four wing configurations were tested: cruise, flaps only, Krueger flap only, and high lift (Krueger flap and flaps deployed). Tests were conducted at free-stream dynamic pressures of 20 psf to 60 psf with corresponding chord Reynolds numbers of 1.22 x 10(exp 6) to 2.11 x 10(exp 6) and Mach numbers of 0.12 to 0.20. The angles of attack presented range from 0 deg to 20 deg and were determined by wing configuration. The angle of sideslip ranged from minus 20 deg to 20 deg. In general, pressure distributions were relatively insensitive to freestream speed with exceptions primarily at high angles of attack or high flap deflections. Increasing trailing-edge Krueger flap significantly reduced peak suction pressures and steep gradients on the wing at high angles of attack. Installation of the empennage had no effect on wing pressure distributions. Unpowered engine nacelles reduced suction pressures on the wing and the flaps. Author

N95-22917\*# Lockheed-Fort Worth Co., Fort Worth, TX. **EULER TECHNOLOGY ASSESSMENT PROGRAM FOR** PRELIMINARY AIRCRAFT DESIGN EMPLOYING SPLITFLOW **CODE WITH CARTESIAN UNSTRUCTURED GRID METHOD** Report, 1 Feb. - 1 Aug. 1994

DENNIS B. FINLEY Mar. 1995 100 p

(Contract(s)/Grant(s): NAS1-19000; RTOP 505-68-30-03) (NASA-CR-4649; NAS 1.26:4649) Avail: CASI HC A05/MF A02

This report documents results from the Euler Technology Assessment program. The objective was to evaluate the efficacy of Euler computational fluid dynamics (CFD) codes for use in preliminary aircraft design. Both the accuracy of the predictions and the rapidity of calculations were to be assessed. This portion of the study was conducted by Lockheed Fort Worth Company, using a recently developed in-house Cartesian-grid code called SPLITFLOW. The Cartesian grid technique offers several advantages for this study, including ease of volume grid generation and reduced number of cells compared to other grid schemes. SPLITFLOW also includes grid adaptation of the volume grid during the solution convergence to resolve high-gradient flow regions. This proved beneficial in resolving the large vortical structures in the flow for several configurations examined in the present study. The SPLITFLOW code predictions of the configuration forces and moments are shown to be adequate for preliminary design analysis, including predictions of sideslip effects and the effects of geometry variations at low and high angles of attack. The time required to generate the results from initial surface definition is on the order of several hours, including grid generation, which is compatible with the needs of the design environment.

N95-23095\*# Boeing Defense and Space Group, Seattle, WA. **EULER TECHNOLOGY ASSESSMENT FOR PRELIMINARY** AIRCRAFT DESIGN EMPLOYING OVERFLOW CODE WITH **MULTIBLOCK STRUCTURED-GRID METHOD Technical** Report, 1 Feb. - 1 Aug. 1994

DAVID A. TREIBER and DENNIS A. MUILENBURG Hampton, VA NASA Mar. 1995 66 p

(Contract(s)/Grant(s): NAS1-18762; RTOP 505-68-30-03)

(NASA-CR-4651; NAS 1.26:4651) Avail: CASI HC A04/MF A01

The viability of applying a state-of-the-art Euler code to calculate the aerodynamic forces and moments through maximum lift coefficient for a generic sharp-edge configuration is assessed. The OVER-FLOW code, a method employing overset (Chimera) grids, was used to conduct mesh refinement studies, a wind-tunnel wall sensitivity study, and a 22-run computational matrix of flow conditions, including sideslip runs and geometry variations. The subject configuration was a generic wing-body-tail geometry with chined forebody, swept wing leading-edge, and deflected part-span leading-edge flap. The analysis showed that the Euler method is adequate for capturing some of the non-linear aerodynamic effects resulting from leading-edge and forebody vortices produced at high angle-of-attack through C(sub Lmax). Computed forces and moments, as well as surface pressures, match well enough useful preliminary design information to be extracted. Vortex burst effects and vortex interactions with the configuration are also investigated.

N95-23182\*# Wayne State Univ., Detroit, Ml. Dept. of Mathematics.

**ACTIVE CONTROL OF PANEL VIBRATIONS INDUCED BY A BOUNDARY LAYER FLOW Technical Report, 31 Aug. 1990 -**31 Oct. 1994

PAO-LIU CHOW 24 Jan. 1995 30 p (Contract(s)/Grant(s): NAG1-1175)

(NASA-CR-197867; NAS 1.26:197867) Avail: CASI HC A03/MF

The problems of active and passive control of sound and vibration has been investigated by many researchers for a number of years. However, few of the articles are concerned with the sound and vibration with flow-structure interaction. Experimental and numerical studies on the coupling between panel vibration and acoustic radiation due to flow excitation have been done by Maestrello and his associates at NASA/Langley Research Center. Since the coupled

system of nonlinear partial differential equations is formidable, an analytical solution to the full problem seems impossible. For this reason, we have to simplify the problem to that of the nonlinear panel vibration induced by a uniform flow or a boundary-layer flow with a given wall pressure distribution. Based on this simplified model, we have been able to consider the control and stabilization of the nonlinear panel vibration, which have not been treated satisfactorily by other authors. Although the sound radiation has not been included, the vibration suppression will clearly reduce the sound radiation power from the panel. The major research findings are presented in three sections. In section two we describe results on the boundary control of nonlinear panel vibration, with or without flow excitation. Sections three and four are concerned with some analytical and numerical results in the optimal control of the linear and nonlinear panel vibrations, respectively, excited by the flow pressure fluctuations. Finally, in section five, we draw some conclusions from research findings. Derived from text

N95-23185\*# Lockheed Aeronautical Systems Co., Marietta, GA. AN ASSESSMENT OF VISCOUS EFFECTS IN COMPUTATIONAL SIMULATION OF BENIGN AND BURST VORTEX FLOWS ON GENERIC FIGHTER WIND-TUNNEL **MODELS USING TEAM CODE Contractor Report, 1 Feb. - 1** Aug. 1994

TIM A. KINARD, BRENDA W. HARRIS, and PRADEEP RAJ Hampton, VA NASA Mar. 1995 82 p

(Contract(s)/Grant(s): NAS1-19000; RTOP 505-68-30-03)

(NASA-CR-4650; NAS 1.26:4650) Avail: CASI HC A05/MF A01

Vortex flows on a twin-tail and a single-tail modular transonic vortex interaction (MTVI) model, representative of a generic fighter configuration, are computationally simulated in this study using the Three-dimensional Euler/Navier-Stokes Aerodynamic Method (TEAM). The primary objective is to provide an assessment of viscous effects on benign (10 deg angle of attack) and burst (35 deg angle of attack) vortex flow solutions. This study was conducted in support of a NASA project aimed at assessing the viability of using Euler technology to predict aerodynamic characteristics of aircraft configurations at moderate-to-high angles of attack in a preliminary design environment. The TEAM code solves the Euler and Reynoldsaverage Navier-Stokes equations on patched multiblock structured grids. Its algorithm is based on a cell-centered finite-volume formulation with multistage time-stepping scheme. Viscous effects are assessed by comparing the computed inviscid and viscous solutions with each other and experimental data. Also, results of Euler solution sensitivity to grid density and numerical dissipation are presented for the twin-tail model. The results show that proper accounting of viscous effects is necessary for detailed design and optimization but Euler solutions can provide meaningful guidelines for preliminary design of flight vehicles which exhibit vortex flows in parts of their flight envelope.

N95-23193\*# Joint Inst. for Advancement of Flight Sciences. Hampton, VA.

AN APPROXIMATE THEORETICAL METHOD FOR MODELING THE STATIC THRUST PERFORMANCE OF NON-**AXISYMMETRIC TWO-DIMENSIONAL CONVERGENT-DIVERGENT NOZZLES M.S. Thesis - George Washington** 

CRAIG A. HUNTER Mar. 1995 51 p

(Contract(s)/Grant(s): NCC1-14; NCC1-24; RTOP 537-07-20) (NASA-CR-195050; NAS 1.26:195050) Avail: CASI HC A04/MF A01

An analytical/numerical method has been developed to predict the static thrust performance of non-axisymmetric, two-dimensional convergent-divergent exhaust nozzles. Thermodynamic nozzle performance effects due to over- and underexpansion are modeled using one-dimensional compressible flow theory. Boundary layer development and skin friction losses are calculated using an approximate integral momentum method based on the classic karman-Polhausen solution. Angularity effects are included with these two models in a computational Nozzle Performance Analysis Code, NPAC. In four different case studies, results from NPAC are compared to experimental data obtained from subscale nozzle testing to demonstrate the capabilities and limitations of the NPAC method. In several cases, the NPAC prediction matched experimental gross thrust efficiency data to within 0.1 percent at a design NPR, and to within 0.5 percent at off-design conditions.

Author

N95-23218\*# Old Dominion Univ., Norfolk, VA. Dept. of Aerospace Engineering.

AERODYNAMIC DESIGN OPTIMIZATION WITH SENSITIVITY ANALYSIS AND COMPUTATIONAL FLUID DYNAMICS Final Report, period ending 31 May 1995

OKTAY BAYSAL Mar. 1995 8 p (Contract(s)/Grant(s): NAG1-1188)

(NASA-CR-197419; NAS 1.26:197419) Avail: CASI HC A02/MF A01

An investigation was conducted from October 1, 1990 to May 31, 1994 on the development of methodologies to improve the designs (more specifically, the shape) of aerodynamic surfaces of coupling optimization algorithms (OA) with Computational Fluid Dynamics (CFD) algorithms via sensitivity analyses (SA). The study produced several promising methodologies and their proof-of-concept cases, which have been reported in the open literature. Author

N95-23250°# National Aeronautics and Space Administration. Ames Research Center, Moffett Field, CA.

EXPERIMENTAL RESULTS FOR A HYPERSONIC NOZZLE/ AFTERBODY FLOW FIELD

FRANK W. SPAID (McDonnell-Douglas Aerospace, Saint Louis, MO.), EARL R. KEENER (Eloret Corp., Palo Alto, CA.), and FRANK C. L. HUI Mar. 1995 106 p

(Contract(s)/Grant(s): RTOP 505-70-62)

(NASA-TM-4638; A-94119; NAS 1.15:4638) Avail: CASI HC A06/ MF A02

This study was conducted to experimentally characterize the flow field created by the interaction of a single-expansion rampnozzle (SERN) flow with a hypersonic external stream. Data were obtained from a generic nozzle/afterbody model in the 3.5 Foot Hypersonic Wind Tunnel at the NASA Ames Research Center, in a cooperative experimental program involving Ames and McDonnell Douglas Aerospace. The model design and test planning were performed in close cooperation with members of the Ames computational fluid dynamics (CFD) team for the National Aerospace Plane (NASP) program. This paper presents experimental results consisting of oil-flow and shadow graph flow-visualization photographs, afterbody surface-pressure distributions, rake boundary-layer measurements, Preston-tube skin-friction measurements, and flow field surveys with five-hole and thermocouple probes. The probe data consist of impact pressure, flow direction, and total temperature profiles in the interaction flow field. **Author** 

N95-23283\*# Mississippi State Univ., Mississippi State, MS. Dept. of Aerospace Engineering.

CROSSFLOW INSTABILITY CONTROL ON A SWEPT-WING: PRELIMINARY STUDIES Abstract Only

DAVID H. BRIDGES In Hampton Univ., 1994 NASA-HU American Society for Engineering Education (ASEE) Summer Faculty Fellowship Program p 63 Dec. 1994

Avail: CASI HC A01/MF A02

The pressure distribution on a swept wing causes the streamlines at the edge of the boundary layer to be curved. This pressure gradient normal to the external streamline creates a velocity component normal to the external streamline within the boundary layer which is referred to as the crossflow velocity. Because the crossflow velocity profile perpendicular to the wing surface has an inflection point, the profile is unstable. The stationary instability mode takes the form of crossflow vortices. Under these conditions, the boundary layer on the

wing is extremely unstable and transition to turbulent flow takes place much closer to the leading edge of the wing than it would on an unswept wing. Higher skin friction drag is associated with turbulent flow, and so better aircraft performance could be obtained if the crossflow could be eliminated One method of controlling crossflow that is being investigated is boundary-layer suction. An extensive airfoil suction experiment in the 8 feet Transonic Pressure Tunnel (TPT) at NASA Langley Research Center will begin late in 1994. Because of the size, complexity, and expense associated with this test, a number of 'risk-reduction' tests are currently being conducted. The 20 x 28 in. Shear Flow Control Tunnel at NASA Langley is being used for some of these tests. Prior to the summer of 1994, a flat plate with a swept leading edge was installed in the 20 x 28 in. tunnel, with a displacement body mounted on the tunnel ceiling that created a pressure distribution on the plate similar to the pressure distribution on a swept wing. The flow over the plate was investigated during the summer of 1994 using a laser Doppler velocimeter (LDV) system. The LDV measurements indicated the possible presence of multiple disturbance modes, a rarely-seen phenomena since, in most tests, one disturbance mode dominates. The possible existence of multiple disturbance modes in the flat plate boundary layer, however, means that the flow in the 20 x 28 in, tunnel is of interest itself, and will be investigated more thoroughly in the future. With a view to these investigations, the boundary layer traverse mechanism in the 20 x 28 in, tunnel was modified to improve its performance, and strain gauges were mounted on the traverse in order to monitor its deflection during a test. Other preliminary work conducted in the 20 x 28 in. tunnel included the use of an infrared camera system. Previous work with this system showed that transition indeed could be detected, but the signal produced by the crossflow vortices was too weak to be detected. It was hoped that spraying the flat plate with naphthalene would augment the heat transfer associated with the crossflow vortices so that they would show up in a IR image; however, experiments showed that this would not work. Another set of tests was conducted in the 20 x 28 in. tunnel to determine the tripping requirements for a set of airfoil-shaped struts that will be used in the 8 feet TPT experiment. Since the Reynolds number associated with these struts is small, a laminar boundary layer would separate early, causing large fluctuations in the flow field. A turbulent boundary layer would remain attached further back, but tripping from laminar to turbulent flow at low Reynolds number is very difficult. However, trip strip configurations were found that should effectively trip the boundary layer at the required conditions. Currently underway is an investigation of the data acquisition requirements for the 8 feet TPT experiment, with the purpose of the finding the minimum amount of data needed to characterize sufficiently the swept-wing boundary layer. This study is being conducted using a numerically generated data set. Author

N95-23294\*# Texas A&M Univ., College Station, TX. Dept. of Aerospace Engineering.

CONTROL OF FLOW SEPARATION IN AIRFOIL/WING DESIGN APPLICATIONS Abstract Only

THOMAS A. GALLY In Hampton Univ., 1994 NASA-HU American Society for Engineering Education (ASEE) Summer Faculty Fellowship Program p 75 Dec. 1994

Avail: CASI HC A01/MF A02

Existing aerodynamic design methods have generally concentrated on the optimization of airfoil or wing shapes to produce a minimum drag while satisfying some basic constraints such as lift, pitching moment, or thickness. Since the minimization of drag almost always precludes the existence of separated flow, the evaluation and validation of these design methods for their robustness and accuracy when separated flow is present has not been aggressively pursued. However, two new applications for these design tools may be expected to include separated flow and the issues of aerodynamic design with this feature must be addressed. The first application of the aerodynamic design tools is the design of airfoils or wings to provide an optimal performance over a wide range of flight conditions (multipoint

design). While the definition of 'optimal performance' in the multipoint setting is currently being hashed out, it is recognized that given a wide enough range of flight conditions, it will not be possible to ensure a minimum drag constraint at all conditions, and in fact some amount of separated flow (presumably small) may have to be allowed at the more demanding flight conditions. Thus a multipoint design method must be tolerant of the existence of separated flow and may include some controls upon its extent. The second application is in the design of wings with extended high speed buffet boundaries of their flight envelopes. Buffet occurs on a wing when regions of flow separation have grown to the extent that their time varying pressures induce possible destructive effects upon the wing structure or adversely effect either the aircraft controllability or the passenger comfort. A conservative approach to the expansion of the buffet flight boundary is to simply expand the flight envelope of nonseparated flow under the assumption that buffet will also thus be alleviated. However, having the ability to design a wing with separated flow and thus to control the location, extent, and severity of the separated flow regions may allow aircraft manufacturers to gain an advantage in the early design stages of an aircraft, when configuration changes are relatively inexpensive to make. Continuing the work begun last year, an airfoil design package has been modified to provide some control over the existence and extent of flow separation. This package consists of a 2-D Navier-Stokes flow solver which is coupled to the CDISC (constrained direct/iterative surface curvature) design method. The first modification is a prediction method for determining whether separation is likely based solely upon a given pressure distribution. If separation is predicted but is undesirable, the new routines will modify the pressure distribution to alleviate the problem. This new pressure distribution is then used in the design method to generate a new aerodynamic shape. Since separation may be acceptable in some cases, particularly if the separation does not extend to the trailing edge, another added logic estimates the extent of separation based upon a correlation with calculated separated flow cases. If the flow behind a shock induced separation is not predicted to reattach before the trailing edge, the logic weakens the shock strength and otherwise alters the pressure distribution in order to promote reattachment. This later addition is as yet unreliable due to secondary separation effects, but additional work is being pursued to improve the method. Author

N95-23333\*# California Univ., Davis, CA. Dept. of Mechanical and Aeronautical Engineering.

HIGH-LIFT FLOW-PHYSICS FLIGHT EXPERIMENTS ON A SUBSONIC CIVIL TRANSPORT AIRCRAFT (B737-100)
Abstract Only

CORNELIS P. VANDAM In Hampton Univ., 1994 NASA-HU American Society for Engineering Education (ASEE) Summer Faculty Fellowship Program p 115 Dec. 1994 Avail: CASI HC A01/MF A02

As part of the subsonic transport high-lift program, flight experiments are being conducted using NASA Langley's B737-100 to measure the flow characteristics of the multi-element high-lift systern at full-scale high-Reynolds-number conditions. The instrumentation consists of hot-film anemometers to measure boundary-layer states, an infra-red camera to detect transition from laminar to turbulent flow, Preston tubes to measure wall shear stress, boundary-layer rakes to measure off-surface velocity profiles, and pressure orifices to measure surface pressure distributions. The initial phase of this research project was recently concluded with two flights on July 14. This phase consisted of a total of twenty flights over a period of about ten weeks. In the coming months the data obtained in this initial set of flight experiments will be analyzed and the results will be used to finalize the instrumentation layout for the next set of flight experiments scheduled for Winter and Spring of 1995. The main goal of these upcoming flights will be: (1) to measure more detailed surface pressure distributions across the wing for a range of flight conditions and flap settings; (2) to visualize the

surface flows across the multi-element wing at high-lift conditions using fluorescent mini tufts; and (3) to measure in more detail the changes in boundary-layer state on the various flap elements as a result of changes in flight condition and flap deflection. These flight measured results are being correlated with experimental data measured in ground-based facilities as well as with computational data calculated with methods based on the Navier-Stokes equations or a reduced set of these equations. Also these results provide insight into the extent of laminar flow that exists on actual multi-element lifting surfaces at full-scale high-life conditions. Preliminary results indicate that depending on the deflection angle, the slat and flap elements have significant regions of laminar flow over a wide range of angles of attack. Boundary-layer transition mechanisms that were observed include attachment-line contamination on the slat and inflectional instability on the slat and fore flap. Also, the results agree fairly well with the predictions reported in a paper presented at last year's AIAA Fluid Dynamics Conference. The fact that extended regions of laminar flow are shown to exist on the various elements of the high-lift system raises the question what the effect is of loss of laminar flow as a result of insect contamiantion, rain or ice accumulation on high-life performance. **Author** 

N95-23462\*# Toledo Univ., OH.

ENHANCED ANALYSIS AND USERS MANUAL FOR RADIAL-INFLOW TURBINE CONCEPTUAL DESIGN CODE RTD Final Contractor Report

ARTHUR J. GLASSMAN Cleveland NASA Mar. 1995 24 p (Contract(s)/Grant(s): NAG3-1165; RTOP 505-69-50) (NASA-CR-195454; E-9538; NAS 1.26:195454) Avail: CASI HC A03/MF A01

Modeling enhancements made to a radial-inflow turbine conceptual design code are documented in this report. A stator-endwall clearance-flow model was added for use with pivoting vanes. The rotor calculations were modified to account for swept blades and splitter blades. Stator and rotor trailing-edge losses and a vaneless-space loss were added to the loss model. Changes were made to the disk-friction and rotor-clearance loss calculations. The loss model was then calibrated based on experimental turbine performance. A complete description of code input and output along with sample cases are included in the report.

N95-23669\*# Tennessee Univ., Tullahoma, TN. Space Inst. SUPERSONIC LAMINAR FLOW CONTROL RESEARCH Semiannual Report No. 2, Jul. - Dec. 1994

C. F. LO Dec. 1994 64 p (Contract(s)/Grant(s): NAG2-881)

(NASA-CR-197938; NAS 1.26:197938) Avail: CASI HC A04/MF A01

The objective of the research is to understand supersonic laminar flow stability, transition and active control. Some prediction techniques will be developed or modified to analyze laminar flow stability. The effects of super laminar flow with distributed heating and cooling on active control will be studied. The primary tasks of the research applying to the NASA/Ames Proof of Concept (POC) and Laminar Flow Supersonic Wind Tunnel (LFSWT) nozzle design with laminar flow control are as follows: (1) predictions of supersonic laminar boundary layer stability and transition; (2) effects of wall heating and cooling for supersonic laminar flow control; and (3) performance evaluation of POC and LFSWT nozzles design with wall heating and cooling effects applying at different locations and various length. A paper addressing the effect of heating and cooling strips on boundary layer stability of nozzles and test sections of supersonic wind tunnels is included as an appendix.

Derived from text

### 03

### AIR TRANSPORTATION AND SAFETY

Includes passenger and cargo air transport operations; and aircraft accidents.

### A95-73522

### DESIGN CONSTRAINTS IN THE PAYLOAD-RANGE DIAGRAM OF ULTRAHIGH CAPACITY TRANSPORT AIRPLANES

RODRIGO MARTINEZ-VAL Universidad Politecnica de Madrid, Madrid, Spain, EMILIO PEREZ, TOMAS MUNOZ, and CRISTINA CUERNO Journal of Aircraft (ISSN 0021-8669) vol. 31, no. 6 November-December 1994 p. 1268-1272 refs (BTN-95-EIX95152582319) Copyright

The economic and productivity potential of ultrahigh capacity airplanes, assessed through the payload-range diagram and the direct operating cost, is considered in the present work from a designer's viewpoint. Two different scenarios are envisaged: first, with current requirements and constraints; and second, after including some achievable improvements. The design constraints analyzed are maximum takeoff weight-based wing loading, maximum wingspan, minimum aspect ratio, maximum zero fuel weight-based wing loading, and maximum fuel capacity. Furthermore, to account for possible advantages of unconventional concepts, the common wing-tailplane and a three-surface arrangement are dealt with in parallel yielding a total of four cases: two configurations in two scenarios. The payload-range diagrams obtained are compatible with very dense, transatlantic, and transpacific routes; however, the three-surface solution in the second scenario exhibits very poor payload vs range flexibility. The benefits of the four cases are considered by computing the direct operating cost relative to that of a B747-400, providing clear economic arguments in favor of these ultrahigh capacity aircraft. Author (EI)

#### Δ95-73536

### EFFECT OF UNDERWING FROST ON A TRANSPORT AIRCRAFT AIRFOIL AT FLIGHT REYNOLDS NUMBER

M. B. BRAGG Univ of Illinois at Urbana-Champaign, Urbana, IL, United States, D. C. HEINRICH, W. O. VALAREZO, and R. J. MCGHEE Journal of Aircraft (ISSN 0021-8669) vol. 31, no. 6 November-December 1994 p. 1372-1379 refs (BTN-95-EIX95152582334) Copyright

The effect of underwing frost on a transport aircraft airfoil in a takeoff configuration was studied. Underwing frost can occur when the lower surface of the wing is cooled by fuel cold-soaked in the wing tanks during cruise. Frost may accrete on the wing lower surface while the aircraft is awaiting takeoff. A two-dimensional test was performed in the NASA Langley Low-Turbulence Pressure Tunnel on a representative high-lift airfoil with a leading-edge slat and trailing-edge flap. Frost was simulated on the lower surface using distributed roughness particles. The test was conducted at M = 0.2 and Re =  $5 \times 10(\exp 6)$  to  $1.6 \times 10(\exp 7)$ . The effects of the frost on performance were generally small, with the largest effects occurring for the open-slat case with the frost starting at 12% chord. In this situation, it was found that the frost contaminated the upper surface boundary layer at high angles of attack, increasing drag and Author (EI) reducing maximum lift.

### A95-73588

# MULTIPLE SITE FATIGUE DAMAGE IN FUSELAGE SKIN SPLICES: EXPERIMENTAL SIMULATION AND THEORETICAL PREDICTION

GRAEME F. EASTAUGH Carleton Univ, PAUL V. STRAZNICKY, and DAVID L. SIMPSON Canadian Aeronautics and Space Journal (ISSN 0008-2821) vol. 40, no. 4 December 1994 p. 151-159 refs (BTN-95-EIX95152584676) Copyright

The results of experimental and theoretical research into multiple site fatigue damage (MSD) in the skin splices of pressurized fuselages are described. First, a special coupon-type splice test specimen has been designed that approximates on-aircraft condi-

tions and enables realistic MSD to be created and studied in a laboratory environment. The coupon specimens usually used in industry and research are not suitable for studying MSD crack growth because the net section stress increases atypically as the cracks progress and because the specimens tend to fail before MSD has developed adequately. The specimen concept described in this paper is intended to overcome these problems. Second, an efficient computer program for predicting MSD crack growth within a framebay has been developed. Rooke's technique of compounding stress intensity factors is applied in a new way, and graphical output of multiple crack growth curves can be produced in a few minutes on a SUN computer workstation. In an initial evaluation, the program agreed well with experimental results.

#### A95-76604

### OPTIMAL LATERAL-ESCAPE MANEUVERS FOR MICROBURST ENCOUNTERS DURING FINAL APPROACH

H. G. VISSER Delft Univ of Technology, Delft, Netherlands Journal of Guidance, Control, and Dynamics (ISSN 0731-5090) vol. 17, no. 6 November-December 1994 p. 1234-1240 refs (BTN-95-EIX95182619127) Copyright

The optimization of lateral-escape trajectories in a microburst wind field for an aircraft on final approach is studied to minimize the peak value of altitude drop. To investigate the characteristics of open-loop extremal solutions for various locations of the microburst, an extensive numerical effort is performed. The results show that a lateral-escape maneuver may significantly improve an aircraft's survivability, in comparison to an escape maneuver restricted to the vertical plane. One of the most significant observations is that, in contrast to nonturning escape maneuvers, lateral-escape maneuvers often exhibit a climb, rather than a descent, in the initial phase. It is hoped that the insight obtained may help the development of near-optimal lateral-escape guidance strategies for onboard application.

### A95-76645

### EFFECT OF CURVATURE IN THE NUMERICAL SIMULATION OF AN ELECTROTHERMAL DE-ICER PAD

J. R. HUANG Univ of Toledo, Toledo, OH, United States, THEO G. KEITH, JR., and KENNETH J. DEWITT Journal of Aircraft (ISSN 0021-8669) vol. 32, no. 1 January-February 1995 p. 84-92 refs (BTN-95-EIX95182619219) Copyright

A finite element method, which incorporates an assumed phase state technique, is presented for the solution of one- and two-dimensional heat conduction problems with phase change. A simulation of an electrothermal de-iced aircraft surface is made using this method. The major interest of this study is the effect of the surface curvature on the numerical results. Comparison of predicted temperatures within a rectangular simulation and those within an airfoil reveals the extent and importance of modeling curvature effects. When surface curvature is less than 0.25, curvature effects may be neglected and a rectangular shape may be used instead of the actual geometry.

Author (EI)

N95-23201# Manchester Univ. (England). Dept. of Pure and Applied Physics.

# COLLABORATIVE RESEARCH ON AIRCRAFT ICING AND CHARGING PROCESSES IN ICE Final Annual Technical Report, 1 Sep. 1992 - 31 Aug. 1994

C. P. SAUNDERS 1 Sep. 1994 44 p (Contract(s)/Grant(s): AF-AFOSR-0376-91)

(AD-A285102; EOARD-TR-94-07) Avail: CASI HC A03/MF A01

This study is into the electrification processes that occur when ice crystals collide with other bodies. The work is of relevance to the charging of ice pellets falling in thunderstorms when they collide with ice crystals, and to the charging of aircraft when they fly through ice phase precipitation. The study relates the thunderstorm field measurements made over recent years to the laboratory simulations of thunderstorm conditions. Charging is shown to be dependent on the water content in the cloud, on the ice crystal sizes, on the speed of impact, and on the temperature. Several theories to account for this

charge transfer behavior are discussed, including measurements of a charge layer at an ice interface that may be indicative of charge being available for transfer during ice particle collisions. The major conclusion is that all the proposed mechanisms have problems in accounting for the observed charging behavior. Further field studies, are needed in which the growth or sublimation state of ice pellets in thunderstorms may be identified so that laboratory simulations can be made more relevant.

N95-23598# National Transportation Safety Board, Washington,

REPORT OF PROCEEDINGS: AVIATION ACCIDENT **INVESTIGATION SYMPOSIUM. VOLUME 2: PARTICIPANT PRESENTATIONS** 

1994 331 p Symposium held in Tysons Corner, VA, 29-31 Mar. 1994

(PB94-917007; NTSB/RP-94/02-VOL-2) Avail: CASI HC A15/MF A03

Volume 2 contains presentations made by participants in the Safety Board's Aviation Accident Investigation Symposium held at Tysons Corner, Virginia, from March 29 through 31, 1994. Volume 1 contains the Safety Board's responses to a number of recommendations made by the aviation industry during the symposium. The symposium provided a forum for the aviation industry to discuss and critique Safety Board programs and practices, as well as procedures used during aviation accident investigations. Participants included representatives from U.S. air carriers, airframe and engine manufacturers, aviation associations and unions, government officials and interested parties, as well as foreign investigative authorities and manufacturers. **Author** 

N95-23609# National Transportation Safety Board, Washington, DC.

AIRCRAFT ACCIDENT REPORT. RUNWAY OVERRUN FOLLOWING REJECTED TAKEOFF. CONTINENTAL AIRLINES FLIGHT 795, MCDONNELL DOUGLAS MD-82, N18835. LAGUARDIA AIRPORT, FLUSHING, NY, 2 MARCH 1994

(PB95-910401; NTSB/AAR-95/01) Avail: CASI HC A05/MF A01

This report explains the accident involving Continental Airlines flight 795, an MD-82 airplane, which experienced a runway overrun following a rejected takeoff from runway 13 at LaGuardia Airport, Flushing, New York, on March 2, 1994. Safety issues discussed in the report include the availability of takeoff performance data for flightcrews, the proper functioning of pitot/static heat systems, the duration of cockpit voice recordings, and problems associated with passenger evacuations from airplanes. Safety recommendations concerning these issues were addressed to the Federal Aviation Administration and to Continental Airlines, Inc.

N95-24012# Wichita State Univ., Wichita, KS. THE AIRLINE QUALITY REPORT, 1994

BRENT D. BOWEN (Nebraska Univ., Omaha, NE.) and DEAN E. HEADLEY Apr. 1994 48 p

(NIAR-94-11) Avail: CASI HC A03/MF A01

The Airline Quality Rating was developed and first announced in early 1991 as an objective method of comparing airline performance on combined multiple factors important to consumers. Development history and calculation details for the AQR rating system are detailed in The Airline Quality Rating (NIAR Report 91-11) issued in April, 1991, by the National Institute for Aviation Research at Wichita State University. A full reporting of the monthly Airline Quality Rating scores for 1991 and 1992 is available in Airline Quality Report 1992 (NIAR Report 92-11) and Airline Quality Rating Report 1993 (NIAR Report 93-11) by contacting Wichita State University. The Airline Quality Rating 1994 (NIAR Report 94-11) is a summary of month-bymonth quality ratings for the nine major domestic U.S. airlines operating during 1993. Using the Airline Quality Rating (AQR) system and monthly performance data for each airline for the calendar year of 1993, individual and comparative ratings are reported. This research monograph, NIAR Report 94-11, contains a brief summary of the AQR methodology, detailed data and charts that track comparative quality for major domestic airlines across the 12 month period of 1993, and industry average results. Also, comparative Airline quality Rating data for 1992 is included to provide a longer term view of quality in the industry.

N95-24024# Civil Aeromedical Inst., Oklahoma City, OK. AIRCRAFT FIRES, SMOKE TOXICITY, AND SURVIVAL: AN **OVERVIEW Final Report** 

ARVIND K. CHATURVEDI and DONALD C. SANDERS Feb. 1995

(DOT/FAA/AM-95/8) Avail: CASI HC A02/MF A01

In-flight fires in modern aircraft are rare, but post-crash fires do occur. Cabin occupants frequently survive initial forces of such crashes but are incapacitated from smoke inhalation. According to an international study, there were 95 fire-related civil passenger aircraft accidents world-wide over a 26-year period, claiming approximately 2400 lives. Between 1985-1991, about 16% (32) of all US transport aircraft accidents involved fire and 22% (140) of the deaths in these accidents resulted from fire/smoke toxicity. Our laboratory database (1967-1993) indicates that 360 individuals in 134 fatal fire-related civil aircraft (air carrier and general aviation) accidents had carboxyhemoglobin saturation levels, with or without cyanide in blood, high enough to impair performance. Combustion toxicology is now moving from a descriptive to a mechanistic phase. Methods for gas analyses have been developed and combustion/ animal-exposure assemblies have been constructed. Material/fireretardant toxicity and interactions between smoke gases are being studied. Relationships between gas exposure concentrations, blood levels, and incapacitation onset are being established in animal models. Continuing basic research in smoke toxicity will be necessary to understand its complexities, and thus enhance aviation safety and fire survival chances.

N95-24050# Wichita State Univ., Wichita, KS. National Inst. for Aviation Research.

A MULTIBODY/FINITE ELEMENT ANALYSIS APPROACH FOR **MODELING OF CRASH DYNAMIC RESPONSES** 

DEREN MA Apr. 1994 210 p

(NIAR-94-3) Avail: CASI HC A10/MF A03

Occupant models are robust tools for gaining insight into the gross motion of ground vehicle or aircraft occupants and evaluating loads and deformations of their critical parts in the studies of crashworthiness. One of the most important issues in occupant modeling is how the large motion of rigid segments of occupants such as the limbs and the small deformations of flexible bodies such as the spine column are handled. In this dissertation, mathematical models of the occupants with a finite element model of the spine are developed based on the principles of the rigid/flexible multibody dynamics and finite element methods along with numerical techniques. An exhaustive study of the occupant modeling and postcrash dynamic behavior of the vehicle occupants under various crash environments is performed by both experimental and analytical means. With the validated occupant model containing the lumbar spine, the gross motion of occupant segments, including displacements, velocities and accelerations are evaluated. The spinal axial loads, bending moments, shear forces, internal forces, nodal forces, and deformation time histories are also determined. In addition, variables such as Head Injury Criteria (HIC), Severity Index (SI) and Dynamic Response Index (DRI) are evaluated to determine possibilities of the injuries in particular crash scenario. This detailed information helps assess the level of spinal injury, determine mechanisms of spinal injury, and design and develop better occupant safety devices. Derived from text

N95-24065# Federal Aviation Administration, Washington, DC. Flight Standards Service.

**OCEANIC OPERATIONS: AN AUTHORITATIVE GUIDE TO OCEANIC OPERATIONS** 

Sep. 1994 243 p

(FAA-AFS-550; FAA-AC-91-70) Avail: CASI HC A11/MF A03

This advisory circular (AC) contains information and guidance to be used by operators and pilots planning oceanic flights. Information is presented on the following topics: United States aviation and the International Civil Aviation Organization; oceanic operations for all aircraft in all geographic areas; North Atlantic operations; Northern Pacific operations; Southern Pacific operations; Caribbean operations; Gulf of Mexico operations; Iong-range navigation; helicopter oceanic operations; crew training for oceanic operations; general aviation short-range aircraft oceanic operations; polar flights; and oceanic operations to the former Soviet Union and other Soviet Block nations.

# N95-24071# Civil Aeromedical Inst., Oklahoma City, OK. A REVIEW OF CIVIL AVIATION FATAL ACCIDENTS IN WHICH LOST/DISORIENTED WAS A CAUSE/FACTOR: 1981-1990 Final Report

WILLIAM E. COLLINS Jan. 1995 11 p (DOT/FAA/AM-95/1) Avail: CASI HC A03/MF A01

The National Transportation Safety Board (NTSB) analyzes circumstances and data from civil aviation accidents and describes one or more causes and/or related factors to help explain each accident. Among the formally accepted NTSB categories of accident causation is one termed 'lost/disoriented:' that term generally differs from 'spatial disorientation' and refers more to a loss of geographic awareness and, perhaps, resulting confusion on the part of the pilot. The present study was undertaken to provide information regarding the circumstances surrounding these fatal general aviation accidents in recent years, and to define demographic and behavioral characteristics of the 'lost' disoriented' pilots. Those reports were examined and analyzed in terms of type of accident, age and experience of pilots, actions of pilots, night or day, and other conditions. The computer search yielded a total of 120 accidents in which 'lost/disoriented' was among the findings noted by investigators of general aviation accidents for the 10-year period. Those accidents resulted in 169 fatalities. Related causes and circumstances associated with the accidents were analyzed and categorized. 'Lost/disoriented' accident frequency for the 1981-90 period peaked at 22 fatal accidents in 1985 and declined steadily thereafter, 75% of the pilots had no instrument rating, 64% of the accidents were associated with adverse weather, and just over half occurred at night. Other analyses suggest that educational efforts should continue to emphasize proper flight planning and the flight hazards of adverse weather conditions so that the recently lowered rates of 'lost/disoriented' accidents can be maintained or improved.

N95-24105# National Transportation Safety Board, Washington, DC.

# AVIATION ACCIDENT INVESTIGATION SYMPOSIUM. VOLUME 1: INDUSTRY RECOMMENDATIONS AND SAFETY BOARD RESPONSES

17 Mar. 1994 73 p Symposium held in Tysons Corner, VA, 29-31 Mar. 1994

(PB94-917005; NTSB/RP-94/01-VOL-1) Avail: CASI HC A04/MF A01

Volume 1 contains the Safety Board's responses to a number of recommendations made by the aviation industry during the Safety Board's Aviation Accident Investigation Symposium. The symposium provided a forum for the aviation industry to discuss and critique Safety Board programs and practices, as well as procedures used during aviation accident investigations. Participants included representatives from U.S. air carriers, airframe and engine manufacturers, aviation associations and unions, government officials and interested parties, as well as foreign investigative authorities andmanufacturers.

Author (revised)

#### 04

### AIRCRAFT COMMUNICATIONS AND NAVIGATION

Includes digital and voice communication with aircraft; air navigation systems (satellite and ground based); and air traffic control.

#### A95-73433

### ON THE EXACT SOLUTIONS OF PSEUDORANGE EQUATIONS

JAMES CHAFFEE JChaffee & Associates, Austin, TX, United States and JONATHAN ABEL IEEE Transactions on Aerospace and Electronic Systems (ISSN 0018-9251) vol. 30, no. 4 October 1994 p. 1021-1030 refs

(BTN-95-EIX95142555477) Copyright

Three formulations of exact solution algorithms to the system of determined pseudorange equations are derived. It is demonstrated that pseudorange equations are hyperbolic in nature and may have two solutions, even when the emitter configuration is nonsingular. Conditions for uniqueness and for the existence of multiple solutions are derived in terms of the Lorentz inner product. The bifurcation parameter for systems of pseudorange equations is also expressed in terms of the Lorentz functional. The solution is expressed as a product of the geometric dilution of precision (GDOP) matrix, representing the linear part of the solution, and a vector of nonlinear terms. Using this formulation, stability of solutions is discussed.

Author (EI)

#### A95-73435

### ENHANCING FILTER ROBUSTNESS IN CASCADED GPS-INS INTEGRATIONS

SPIRO P. KARATSINIDES Smiths Industries, Grand Rapids, MI, United States IEEE Transactions on Aerospace and Electronic Systems (ISSN 0018-9251) vol. 30, no. 4 October 1994 p. 1001-1008 refs

(BTN-95-EIX95142555475) Copyright

Filter robustness is defined as the ability of the global positioning system/inertial navigation system (GPS/INS) Kalman filter to cope with adverse environments and input conditions, to successfully identify such conditions, and to take evasive action. A formulation of two techniques for a cascaded GPS-INS Kalman filter integration is discussed. This is an integration in which the navigation solution from a GPS receiver is used as a measurement in the filter to estimate inertial errors and instrument biases. A method of suppressing transients is also presented together with a method of formulating the filter noise statistics dynamically based on the inputs from the GPS and the INS.

### A95-73571

# THERMAL FORCE MODELING FOR GLOBAL POSITIONING SYSTEM SATELLITES USING THE FINITE ELEMENT METHOD

YVONNE VIGUE California Inst of Technology, Pasadena, CA, United States, BOB E. SCHUTZ, and P. A. M. ABUSALI Journal of Spacecraft and Rockets (ISSN 0022-4650) vol. 31, no. 5 September-October 1994 p. 855-859 refs (BTN-95-EIX95152583270) Copyright

Geophysical applications of the Global Positioning System (GPS) require the capability to estimate and propagate satellite orbits with high precision. An accurate model of all the forces acting on a satellite is an essential part of achieving high orbit accuracy. Methods of analyzing the perturbation due to thermal radiation and determining its effects on the long-term orbital behaviour of GPS satellites are presented. The thermal imbalance force, a nongravitational orbit perturbation previously considered negligible, is the focus of this paper. The Earth's shadowing of a satellite in orbit causes periodic changes in the satellite's thermal environment. Simulations show that neglecting thermal imbalance in the satellite force model gives orbit errors larger than 10 m over several days for eclipsing satellites. This orbit mismodeling can limit accuracy in orbit determination and in estimation of baselines used for geophysical applications.

Author (EI)

#### A95-75714

### REAL-TIME NAVIGATION USING THE GLOBAL POSITIONING

DAN SIMON TRW Test Lab, Mesa, AZ, United States and HOSSNY EL-SHERIEF IEEE Aerospace and Electronic Systems Magazine (ISSN 0885-8985) vol. 10, no. 1 January 1995 p. 31-37 refs (BTN-95-EIX95172595298) Copyright

This paper presents the results of an investigation of the application of the Global Positioning System (GPS) to real-time integrated missile navigation. We present quantifiable measures of navigation accuracy as a function of GPS user segment parameters. These user segment parameters include antenna phase response accuracy, single versus dual frequency, and Kalman filter structure and size. We also formulate some new phase-locked loop (PLL) filter designs for application in GPS receivers, and demonstrate their superiority over more conventional filters.

Author (EI)

#### A95-76622

# SWITCHED BIAS PROPORTIONAL NAVIGATION FOR HOMING GUIDANCE AGAINST HIGHLY MANEUVERING TARGETS

K. RAVINDRABABU Indian Inst of Science, Bangalore, India, I. G. SARMA, and K. N. SWAMY Journal of Guidance, Control, and Dynamics (ISSN 0731-5090) vol. 17, no. 6 November-December 1994 p. 1357-1363 refs

(BTN-95-EIX95182619145) Copyright

A new form of the proportional navigation (PN) guidance law for short-range homing missiles is proposed. Named the Switched Bias Proportional Navigation (SBPN) law, it is derived by invoking slidingmode control theory and is structured around the basic PN, with an additive switched bias term. This additional term depends only on the polarity of the line-of-sight rate, which is readily available with a seeker. It is shown that the bias term acts as an estimate of the target acceleration and other unmodeled dynamics. An adaptive procedure is suggested to select the gain of this term, which results in improved performance. The SBPN is almost as simple to implement as the PN law itself, as it does not require any additional information related to the engagement, in the form of either measurements or estimates. Simulation results show that the acceleration profiles of SBPN closely follow those of augmented PN guidance law, after a short initial transient. They further demonstrate the robustness of the proposed SBPN in the presence of missile velocity variation. Author (EI)

### A95-76631

### DRAG FUNCTION MODELING FOR AIR TRAFFIC SIMULATION

MARK R. ANDERSON Virginia Polytechnic Inst and State Univ, Blacksburg, VA, United States and DANIEL E. SCHAB Journal of Guidance, Control, and Dynamics (ISSN 0731-5090) vol. 17, no. 6 November-December 1994 p. 1383-1385 refs (BTN-95-EIX95182619154) Copyright

A new approach to developing a drag function expression for commercial air traffic or combat aircraft threat models is presented. The idea is to determine parameters of a simplified drag coefficient function so that the performance of the modeled aircraft closely matches that of the actual aircraft. The drag function parameters are varied using a form of parameter identification or multidimensional curve fitting. In other words, the parameters of the air traffic model drag function are actually extracted from performance data rather than estimated from wind tunnel data. Thus, the performance of the air traffic model will match the actual aircraft.

### A95-76674

### SIMULATION ON THE 3-D TURBULENT FLOW IN THE PASSAGES OF FINOCYL GRAIN

YU LIU Northwestern Polytechnical Univ, Xi'an, China, HONGQING HE, XINPING WU, and TIMIN CAI Tuijin Jishu/Journal of Propulsion Technology (ISSN 1001-4055) no. 6 December 1994 p. 10-17 In CHINESE refs

(BTN-95-EIX95202638962) Copyright

The SIMPLE algorithm was used to simulate the 3-D flow in the

chamber of solid propellant rocket engine with the following physical factors taken into account: finocyl grain, 3-D mass addition and incompressible turbulent flow, moving boundaries of propellant burning surfaces, and heat radiation of gas, etc. The equations used are: 3-D continuity, momentum, and energy equations; k-epsilon equations of turbulent model; and 3-D flux equations of heat radiation, etc. In addition, the tracking technique with marked grid was used to treat the moving boundaries of burning surfaces. Our results show that the geometry matches between the fin-canals and main passage, and the degree of propellant mass addition, will significantly influence the parameter distribution of flow field and sometimes even returning flow and eddy flow may occur.

#### A95-76676

# NEW FAILURE DETECTION APPROACH AND ITS APPLICATION TO GPS AUTONOMOUS INTEGRITY MONITORING

REN DA American GNC Corp, Canoga Park, CA, United States and CHING-FANG LIN IEEE Transactions on Aerospace and Electronic Systems (ISSN 0018-9251) vol. 31, no. 1 January 1995 p. 499-506 refs

(BTN-95-EIX95202637613) Copyright

This investigation presents a new approach for detecting failures which affect only subsets of system measurements. In addition to a main Kalman filter, which processes all the measurements to give the optimal state estimate, a bank of auxiliary Kalman filters is also used, which process subsets of the measurements to provide the state estimates which serve as failure detection references. After the statistical property of the differences between the state estimate of the main Kalman filter and those of the auxiliaries is derived with an application of the orthogonal projection theory. failure detection is undertaken by checking the consistency between the state estimate of the main Kalman filter and those of the auxiliaries by means of the chi-square statistical hypothesis test. The effectiveness of the proposed procedure is illustrated in a problem of GPS (Global Positioning System) autonomous integrity monitoring for a GPS/SDINS (Strapdown Inertial Navigation System) integrated navigation system. Author (EI)

### A95-76683

# SOLUTIONS OF GENERALIZED PROPORTIONAL NAVIGATION WITH MANEUVERING AND NONMANEUVERING TARGETS

PIN-JAR YUAN Chung Shan Inst of Science and Technology, Lungtan, Taiwan, Province of China and SHIH-CHE HSU IEEE Transactions on Aerospace and Electronic Systems (ISSN 0018-9251) vol. 31, no. 1 January 1995 p. 469-474 refs (BTN-95-EIX95202637606) Copyright

In this generalized proportional navigation (GPN), the commanded acceleration is applied in a direction with a bias angle to the normal direction of line-of-sight (LOS) and its magnitude is proportional to the product of closing speed and LOS rate between interceptor and its target. Some solutions of GPN were obtained before under the assumption that the magnitude of commanded acceleration is proportional to the LOS rate only. Now in this article, the exact and complete closed-form solutions are derived under this modified guidance scheme for both maneuvering and nonmaneuvering targets. Some related important characteristics, such as capture capability and energy cost, are investigated and discussed. The variation of bias angle will induce the change of capture area and energy cost required. Also, a typical example of target maneuver is introduced to describe the effect of target maneuver easily. It shows that the target maneuver will decrease the capture area and increase the energy cost for effective intercept of target. Author (EI)

### A95-76697

#### COVARIANCE ANALYSIS OF STRAPDOWN INS CONSIDERING GYROCOMPASS CHARACTERISTICS

HEUNG WON PARK Seoul Natl Univ, Seoul, Korea, Republic of, JANG GYU LEE, and CHAN GOOK PARK IEEE Transactions on

Aerospace and Electronic Systems (ISSN 0018-9251) vol. 31, no. 1 January 1995 p. 320-328 refs (BTN-95-EIX95202637592) Copyright

A complete error covariance analysis for strapdown inertial navigation system (SDINS) is presented. The authors have found that in SDINS the cross-coupling terms in gyrocompass alignment errors can significantly influence the SDINS error propagation. Initial heading error has a close correlation with the east component of gyro bias error, while initial level tilt errors are closely related to accelerometer bias errors. In addition, pseudostate variables are introduced in covariance analysis for SDINS utilizing the characteristics of gyrocompass alignment errors. This approach simplifies the covariance analysis because it makes the initial error covariance matrix to a diagonal form. Thus a real implementation becomes easier. The approach is conformed by comparing the results for a simplified case with the covariance analysis obtained from the conventional SDINS error model.

N95-23318\*# Saint Cloud State Coll., MN. Dept. of Electrical Engineering.

# DIFFERENTIAL GPS AND SYSTEM INTEGRATION OF THE LOW VISIBILITY LANDING AND SURFACE OPERATIONS (LVLASO) DEMONSTRATION Abstract Only

JAMES M. RANKIN In Hampton Univ., 1994 NASA-HU American Society for Engineering Education (ASEE) Summer Faculty Fellowship Program p 100 Dec. 1994

Avail: CASI HC A01/MF A02

The LVLASO Flight Demonstration of ASTA concepts (FDAC) integrates NASA-Langley's electronic moving map display and Transport Systems Research Vehicle (TSRV) (a modified Boeing 737 aircraft); ARINC's VHF data link, GPS ground station, and automated controller workstation; and Norden's surface radar/airport movement safety system. Aircraft location is shown on the electronic map display in the cockpit. An approved taxi route as well as other aircraft and surface traffic are also displayed. An Ashtech Z12 Global Positioning System (GPS) receiver on the TSRV estimates the aircraft's position. In Differential mode (DSPS), the Ashtech receiver accepts differential C/A code pseudorange corrections from a GPS ground station. The GPS ground station provides corrections up to ten satellites. The corrections are transmitted on a VHF data link at a 1 Hz. rate using the RTCM-104 format. DGPS position estimates will be within 5 meters of actual aircraft position. DGPS position estimates are blended with position, velocity, acceleration, and heading data from the TSRV Air Data/Inertial Reference System (ADIRS). The ADIRS data is accurate in the short-term, but drifts over time. The DGPS data is used to keep the ADIRS position accurate. Ownship position, velocity, heading, and turn rate are sent at a 20 Hz. rate to the electronic map display. Airport traffic is detected by the airport surface radar system. Aircraft and vehicles such as fuel trucks and baggage carts are detected. The traffic's location, velocity, and heading are sent to the TSRV. To prevent traffic symbology from jumping each second when a location update arrives, velocity and heading are used to predict a new traffic location for each display update. Possible runway incursions and collisions can be shown on the electronic map. Integrating the different systems used in the FDAC requires attention to the underlying coordinate systems. The airport diagram displayed on the electronic map is obtained from published navigational charts. The charts reference the North American Datum of 1927 (NAD27) or a local state-plane coordinate system. GPS uses the World Geodetic Standard of 1984 (WGS84). Both NAD27 and WGS84 model the Earth as an ellipsoid, however, they use a different origin and different size ellipsoids. Latitudes and longitudes given in these systems can be converted to a Cartesian system with the origin at the Earth's center. The surface radar detects traffic in a locally-level, rho-theta coordiante system. The electronic airport diagram is stored using a flat XY coordinate system. The map origin is at the tower and is referenced as True North up. All ownship and other traffic positions must be converted to the electronic map's frame of reference for display. **Author** 

N95-23393\* National Aeronautics and Space Administration. Ames Research Center, Moffett Field, CA.

### **CUEING LIGHT CONFIGURATION FOR AIRCRAFT**

#### **NAVIGATION Patent**

MARY K. KAISER, inventor (to NASA) and WALTER J. JOHNSON, inventor (to NASA) 24 May 1994 9 p Filed 27 Aug. 1992 (NASA-CASE-ARC-11982-1; US-PATENT-5,315,296; US-PATENT-APPL-SN-935939; US-PATENT-CLASS-340-946; US-PATENT-CLASS-73-178H; US-PATENT-CLASS-340-953; US-PATENT-CLASS-340-961; US-PATENT-CLASS-340-981; US-PATENT-CLASS-362-62; INT-PATENT-CLASS-G08B-21/00) Avail: US Patent and Trademark Office

A pattern of light is projected from multiple sources located on an aircraft to form two clusters. The pattern of each cluster changes as the aircraft flies above and below a predetermined nominal altitude. The initial patterns are two horizontal, spaced apart lines. Each is capable of changing to a delta formation as either the altitude or the terrain varies. The direction of the delta cues the pilot as to the direction of corrective action.

Official Gazette of the U.S. Patent and Trademark Office

N95-23565# Civil Aeromedical Inst., Oklahoma City, OK. THE ROLE OF FLIGHT PROGRESS STRIPS IN EN ROUTE AIR TRAFFIC CONTROL: A TIME-SERIES ANALYSIS Final Report MARK B. EDWARDS (Oklahoma Univ., Oklahoma City, OK.), DANA FULLER (Oklahoma Univ., Oklahoma City, OK.), O. U. VORTAC (Oklahoma Univ., Oklahoma City, OK.), and CAROL A. MANNING Jan. 1995 13 p

(DOT/FAA/AM-95/4) Avail: CASI HC A03/MF A01

Paper flight progress strips (FPS's) are currently used in the United States en route air traffic control system to document flight information. Impending automation will replace these paper strips with electronic flight data entries. In this observational study, control actions, communication events, and computer interactions were recorded and analyzed using time-series regression models. Regression models were developed to predict FPS activities (Writing, Manipulating, Looking) at different levels of traffic complexity, for individuals and teams of air traffic controllers. The ability to predict FPS manipulations was modest, but prediction of looking at FPS's was poor. Overall, these data indicate that: (1) flight strip activities were similar for individuals and for the data-side controllers in the team (whose primary responsibility is the strips); and (2) flight strip activity for teams was predictable from the radar-side controller's actions, but not the data-side controller's actions. Author

05

### AIRCRAFT DESIGN, TESTING AND PERFOMANCE

Includes aircraft simulation technology.

#### A95-73437

#### LABS BEHIND BOEING'S NEW 777

ART BROWN Boeing Commercial Airplanes Group, TOM MOORE, MATT MILLER, and MARK LAPIN Aerospace Engineering (Warrendale, Pennsylvania) (ISSN 0736-2536) vol. 14, no. 12 December 1994 p. 17-20

(BTN-95-EIX95142562403) Copyright

Boeing's 777 twinjet transport is innovative in many ways, the most important of which is the extent to which its onboard systems for flight control, navigation, communication, climate control, and passenger comfort are integrated and interdependent. This aircraft has taken systems interdependence to an entirely new level, which could not be achieved without a new type of test laboratory. IASL will conduct all-encompassing integration testing to verify that interdependent aircraft systems function together as intended.

#### A95-73526

### NONLINEAR ANGLE OF TWIST OF ADVANCED COMPOSITE WING BOXES UNDER PURE TORSION

GIULIO ROMEO, GIACOMO FRULLA, and MARIO BUSTO Journal of Aircraft (ISSN 0021-8669) vol. 31, no. 6 November-December 1994 p. 1297-1302 refs

(BTN-95-EIX95152582323) Copyright

This article reports both the theoretical analysis and experimental results performed on advanced composite wing boxes under pure torsion. By taking into account the nonlinear effective shear modulus of skin panels operating during postbuckling, it is possible to obtain good correlation between the theoretical and the experimental behavior. An incomplete diagonal shear stress field is used to calculate the effective shear modulus that can be reduced by up to 50% in comparison to the unbuckled panels. This causes a drastic reduction in the wing box's torsional stiffness. At a shear load triple that of buckling, our results revealed angles of twist up to 50% greater than those predicted by the linear analysis.

Author (EI)

A95-73531\* National Aeronautics and Space Administration. Ames Research Center, Moffett Field, CA.

### NAVIER-STOKES PREDICTION OF LARGE-AMPLITUDE DELTA-WING ROLL OSCILLATIONS

NEAL M. CHADERJIAN National Aeronautics and Space Administration. Ames Research Center, Moffett Field, CA. Journal of Aircraft (ISSN 0021-8669) vol. 31, no. 6 November-December 1994 p. 1333-1340 refs

(BTN-95-EIX95152582329) Copyright

Vertical flow about a 65-deg sweep delta wing at 15-deg angle of attack is numerically simulated for static roll and forced roll oscillations using the time-dependent, three-dimensional, Reynoldsaveraged, Navier-Stokes (RANS) equations. This is a first step towards the development of an experimentally validated computational method for simulating wing rock with the RANS equations. Turbulent computations are presented for static roll angles up through 42 deg. The effects of roll angle on the vortex aerodynamics are discussed, and solution accuracy is evaluated by comparison with experimental data. The effects of grid refinement and zonal boundary condition treatment are assessed at zero roll angle. Computational results for a large-amplitude (Phi(sub max) = 40 deg), high-rate (f = 7 Hz) forced roll motion is also presented. Computed static and dynamic surface-pressure coefficients, rollingmoment coefficients, normal-force coefficients, and streamwise c.p. locations compare very well with experimental data. The static rolling-moment coefficients indicate the wing is statically stable under the present flow conditions. Moreover, the dynamic rollingmoment coefficients indicate that the fluid extracts energy from the wing motion, i.e., the wing is positively damped. The computed and experimental damping energy agree within 3%. Author (EI)

#### A95-73533

### FURTHER ANALYSIS OF HIGH-RATE ROLLING EXPERIMENTS OF A 65-DEG DELTA WING

LARS E. ERICSSON and ERNEST S. HANFF Journal of Aircraft (ISSN 0021-8669) vol. 31, no. 6 November-December 1994 p. 1350-1357 refs

(BTN-95-EIX95152582331) Copyright

Further analyses have been performed of the experimental results obtained in the roll oscillation tests of a 65-deg sharp-edged delta wing at 30-deg inclination of the roll axis in order to uncover the fluid mechanical phenomena causing the unusual, highly nonlinear vehicle dynamics. It was found in an earlier analysis that in addition to the expected effect of convective flow time lag, the test results show highly nonlinear effects on vortex breakdown of the oscillatory rate. The present analysis reveals that these effects are themselves influenced by convective flow time lag. As a result, the past time history of the oscillatory response can in some cases have a strong influence on the final trim condition.

A95-73535\* National Aeronautics and Space Administration. Ames Research Center, Moffett Field, CA.

### FOREBODY FLOW CONTROL ON A FULL-SCALE F/A-18 AIRCRAFT

WENDY R. LANSER National Aeronautics and Space Administration. Ames Research Center, Moffett Field, CA and LARRY A. MEYN Journal of Aircraft (ISSN 0021-8669) vol. 31, no. 6 November-December 1994 p. 1365-1371 refs

(BTN-95-EIX95152582333) Copyright

A full-scale F/A-18 was tested in the 80- by 120-ft Wind Tunnel at NASA Ames Research Center to measure the effectiveness of pneumatic forebody vortex control devices. By altering the forebody vortex flow, yaw control can be maintained to angles of attack greater than 50 deg. Two forebody vortex control devices were tested: (1) a discrete circular jet; and (2) a tangential blowingslot. The tests were conducted for angles of attack between 25-50 deg. and angles of sideslip from - 15 to 15 deg. The Reynolds number based on wing mean aerodynamic chord ranged from 4.5 to 12.0 x 10(exp 6). The time-averaged yawing moments, along with both time-averaged and time-dependent pressures on the forebody of the aircraft, are presented here for various configurations. Of particular interest was the result that the tangentially blowing slot had a greater effect on the yawing moment than the discrete circular jet. Additionally, it was found that blowing very close to the radome apex was not as effective as blowing slightly farther aft on the radome, and that a 16-in.-long slot was more effective than either an 8- or 48-in.-long Author (Ei)

#### 495-73537

### PNEUMATIC CONCEPT FOR TIP-STALL CONTROL OF CRANKED-ARROW WINGS

DHANVADA M. RAO ViGYAN, Inc, Hampton, VA, United States Journal of Aircraft (ISSN 0021-8669) vol. 31, no. 6 November-December 1994 p. 1380-1386 refs (BTN-95-EIX95152582335) Copyright

A novel blowing concept aimed at controlling the tip stall of cranked-arrow wings was experimentally investigated. The concept employs a tangential jet sheet blown spanwise on the tip-panel upper surface, from a chordwise slot located at the leading-edge break. The blown sheet interacts three dimensionally with the external flow, forming a controllable vortex that powerfully influences the tip-panel upper-surface flowfield leading to local lift improvement and stall delay. As a consequence, simultaneous blowing on both the tips alleviates pitch-up, whereas one-side blowing provides roll control; a concurrent overall lift increase occurs in both cases due to vortex augmentation. Low-speed wind-tunnel flow visualizations, pressure measurements, and six-component balance data were acquired on a generic cranked-arrow configuration to verify the concept and obtain preliminary indications of its aerodynamic control potential. Author (EI)

### A95-73540

### DYNAMIC ANALYSIS OF BEARINGLESS TAIL ROTOR BLADES BASED ON NONLINEAR SHELL MODES

OLIVIER A. BAUCHAU Rensselaer Polytechnic Inst, Troy, NY, United States and WUYING CHIANG Journal of Aircraft (ISSN 0021-8669) vol. 31, no. 6 November-December 1994 p. 1402-1410 refs

(BTN-95-EIX95152582338) Copyright

The unique structural features of helicopter bearingless rotors call for the development of design and modeling methodologies for laminated composite flex-structures. Indeed, the flex-structure should be flexible enough to replace the flap, lead-lag, and feathering bearings, while maintaining high strength and stiffness in the axial direction. Laminated composite materials are a material of choice for such an application. Chordwise deformations, transitional zones between different cross sections and localized compressive stresses are all likely to be present in the flex-structure, rendering the validity of a beam model questionable. In this article a nonlinear anisotropic shallow shell model is developed that accommodates transverse shearing deformations, and arbitrarily large displacements and rotations, but strains are assumed to remain small. The displacement-based shell model has six degrees of freedom at each node

05

and allows for an automatic compatibility of the shell and beam models. The model is validated by comparing its predictions with several benchmark problems. A four-bladed composite bearingless tail rotor system is analyzed in detail using the shell model and compared with the predictions of a beam model. Significant differences are observed between the two models, especially in the torsional behavior. Author (EI)

#### A95-73542

### STATIC AEROELASTIC CHARACTERISTICS OF A **COMPOSITE WING**

IN LEE Korea Advanced Inst of Science and Technology, Taejon, Korea, Republic of, SEUNG-HO KIM, and HIROKAZU MIURA Journal of Aircraft (ISSN 0021-8669) vol. 31, no. 6 November-December 1994 p. 1413-1416 refs

(BTN-95-EIX95152582340) Copyright

The effect of fiber orientation on the deformation pattern and aerodynamic coefficients of the cantilevered composite wing is investigated. The wing structure is assumed as a plate-like wing. The finite element method that accounts for the transverse shear deformation has been used for the structural analysis. The vortex lattice method has been applied to the various-shaped thin wings for the aerodynamic analysis. The aerodynamic forces are interpolated to the structural nodal forces by the surface spline method. The deformed shape of a wing and redistributed aerodynamic forces are obtained from an iteration procedure. Various-shaped thin wings are analyzed and the flexibility effect of the laminated composite wing is investigated.

#### A95-73544

### METHOD FOR THE PREDICTION OF THE ONSET OF WING

BRAD S. LIEBST Air Force Inst of Technology, Wright-Patterson Air Force Base, OH, United States and ROBERT C. NOLAN Journal of Aircraft (ISSN 0021-8669) vol. 31, no. 6 November-December 1994 p. 1419-1421 refs (BTN-95-EIX95152582342) Copyright

The rolling oscillations that are commonly referred to as wing rock are actually unstable dutch-roll motions developing into a limit cycle. Dutch-roll motion may consist of considerable yaw, and sideslip at low angle of attack (AOA). The trigger parameter has been developed to predict the onset of wing rock for a swept-wing fighter design. The procedure appears to be accurate within one degree AOA as verified with flight test data.

### A95-73549

### EFFECT OF LEEWARD FLOW DIVIDERS ON THE WING **ROCK OF A DELTA WING**

T. TERRY NG Univ of Toledo, Toledo, OH, United States, TONY SKAFF, and JOHN KOUNTZ Journal of Aircraft (ISSN 0021-8669) vol. 31, no. 6 November-December 1994 p. 1431-1433 refs (BTN-95-EIX95152582347) Copyright

The effects of a flow divider placed on the leeward side of an 80 degree sharp-edged delta wing were studied. Effects of divider geometry, sizes, and placement were investigated. Measurements indicate that the divider increases the rolling moment at sideslip condition for the angle-of-attack range where wing rock is promoted by the divider. Flow visualization shows that this is due to an increase in the vortex position asymmetry. The static stability is increased moderately, but the dynamic stability is reduced correspondingly. The divider therefore enhances the tendency for wing rock. At higher angles of attack where wing rock is suppressed by the divider, the rolling moment at sideslip is reduced by the divider. El

#### A95-73587

### ANALYTICAL SOLUTION FOR CONTROLS, HEATS, AND STATES OF FLIGHT TRAJECTORIES

AHMED Z. AL-GARNI King Fahd Univ of Petroleum and Minerals, Dhahran, Saudi Arabia Journal of Spacecraft and Rockets (ISSN 0022-4650) vol. 31, no. 5 September-October 1994 p. 924-928 refs

(BTN-95-EIX95152583286) Copyright

A new closed-form analytical solution for the nonlinear aerodvnamic and thrust controls in feedback form for high angle of attack is presented. Three cases are presented for each of a given pair of constraints, including analytical solutions for heat rate and heat load and for most of the state variables. Comparisons with numerical results show good agreement. It is suggested that the results obtained for the three cases can be used during several intervals of the trajectory to simulate and approximate the more general case.

#### A95-73589

#### **VALIDATION OF AN EFFECTIVE FLAT CRUCIFORM-SHAPED** SPECIMEN TO STUDY CFRP COMPOSITE LAMINATES UNDER BIAXIAL LOADING

Y. YOUSSEF Universite de Sherbrooke, Sherbrooke, Que, Canada, S. LABONTE, C. ROY, and D. LEFEBVRE Canadian Aeronautics and Space Journal (ISSN 0008-2821) vol. 40, no. 4 December 1994 p. 158-162 refs

(BTN-95-EIX95152584677) Copyright

A global research project covering different topics related to biaxial testing and characterization of composite laminates is being carried out at the Universite de Sherbrooke. Optimization of a specimen design, fabrication procedures and techniques, strain/ stress measuring methods, damage monitoring, and failure theories are some of the aspects being investigated. This paper describes how the optimization of a flat cruciform-shaped specimen has been achieved by a simple testing procedure. Typical results from static biaxial tests demonstrate the effectiveness of the specimen to provide a better understanding of the strength of composite laminates. Author (EI)

### **EVALUATION OF ADVANCED AEROSPACE MATERIALS BY DEPTH SENSING INDENTATION AND SCRATCH METHODS**

R. BERRICHE Materials and Propulsion Lab, Ottawa, Ont, Canada Canadian Aeronautics and Space Journal (ISSN 0008-2821) vol. 40, no. 4 December 1994 p. 163-170 refs (BTN-95-EIX95152584678) Copyright

Depth Sensing Indentation (DSI) instruments have been proven very useful for evaluating the mechanical properties of various materials on a small scale. In this paper, a newly developed DSI instrument called the NanoMechanical Probe (NMP) is described. Methods for measuring various micro-mechanical properties, such as hardness, elastic modulus, coating-substrate adhesion, and fiber-matrix interfacial strength, are reviewed. In addition, the results of recent tests conducted on coatings and other materials for aerospace applications are presented and discussed. Author (EI)

### A95-73591

### IMPROVING PREDICTION: THE INCORPORATION OF SIMPLIFIED ROTOR DYNAMICS IN A MATHEMATICAL **MODEL OF THE BELL 412HP**

KENNETH HUI Flight Research Lab, Ottawa, Ont, Canada and STEWART BAILLIE Canadian Aeronautics and Space Journal (ISSN 0008-2821) vol. 40, no. 4 December 1994 p. 171-177 refs (BTN-95-EIX95152584679) Copyright

The development of a mathematical model of the Flight Research Laboratory (FRL) Bell 412HP helicopter is described. This mathematical model, based on project-dedicated flight test data, will be used to support the flight mechanics research program of the FRL. All models analyzed in this paper were developed using the NRC-modified version of NASA's MMLE3 program: a time domain parameter estimation routine. Because the quasi-steady six degree of freedom rigid body model resulted in a poor representation of the Bell 412HP, a rotor dynamics model has been appended to the six degree of freedom model structure to form a hybrid model. These two modelling approaches, where rotor dynamic effects were included and excluded from the estimation model, were compared for two Bell 412HP flight test cases. The incorporation of simplified rotor dynamic effects in the hybrid model results in a Bell 412HP model with improved prediction capabilities.

Author (EI)

### A95-75098

### H-76B FANTAIL DEMONSTRATER COMPOSITE FAN BLADE FABRICATION

THOMAS FALASCO Boeing Defense & Space Group, Philadelphia, PA, US, EDWARD ZACHAR Boeing Defense & Space Group, Philadelphia, PA, US, and ART LALLO Boeing Defense & Space Group, Philadelphia, PA, US American Helicopter Society, Journal (ISSN 0002-8711) vol. 39, no. 3 July 1994 p. 53-57 (HTN-95-80856) Copyright

The Boeing Sikorsky First Team jointly developed a modified H-76B helicopter as a demonstrater aircraft for the LH Fantail (TM) antitorque system. A significant achievement was the development and fabrication of the occurred composite Fantail (TM) blades in 15 months between program start in 1989 and aircraft completion in March 1990. The Fantail (TM) blade manufacturing concept utilizes a single cure technique which completely eliminates the requirement for multiple cure cycles and air bladers.

Author (Herner)

A95-75099\* National Aeronautics and Space Administration. Langley Research Center, Hampton, VA.

AN ANALYTICAL AND EXPERIMENTAL INVESTIGATION OF THE RESPONSE OF THE CURVED, COMPOSITE FRAME/SKIN SPECIMENS

EDUARDO MOAS Analytical Services and Materials, Inc., Hampton, VA, US, RICHARD L. BOITNOTT U.S. Army Research Laboratory, Hampton, VA, US, and O. HAYDEN GRIFFIN, JR. Virginia Polytechnic Institute, Blacksburg, VA, US American Helicopter Society, Journal (ISSN 0002-8711) vol. 39, no. 3 July 1994 p. 58-66

(Contract(s)/Grant(s): NAG1-343; NAG1-19317) (HTN-95-80857) Copyright

Six-foot diameter, semicircular graphite/epoxy specimens representative of generic aircraft frames were loaded quasi-statistically to determine their load response and failure mechanisms for large deflections that occur in airplanes crashes. These frame/skin specimens consisted of a cylindrical skin section co-cured with a semicircular I-frame. The skin provided the necessary lateral stiffness to keep deformations in the plane of the frame in order to realistically represent deformations as they occur in actual fuselage structures. Various frame laminate stacking sequences and geometries were evaluated by statically loading the specimen until multiple failures occurred. Two analytical methods were compared for modeling the frame/skin specimens: a two-dimensional shell finite element analysis and a one-dimensional, closed-form, curved beam solution derived using an energy method. Flange effectivities were included in the beam analysis to account for the curling phenomenon that occurs in thin flanges of curved beams. Good correlation was obtained between experimental results and the analytical predictions of the linear response of the frames prior to the initial failure. The specimens were found to be useful for evaluating composite frame designs. Author (Herner)

#### A95-75100

AN UNMANNED AIR VEHICLE CONCEPT WITH TIPJET DRIVE ALAN W. SCHWARTZ Naval Surface Warfare Center, Bethesda, MD, US, KENNETH R. READER Naval Surface Warfare Center, Bethesda, MD, US, and ERNEST O. ROGERS Naval Surface Warfare Center, Bethesda, MD, US American Helicopter Society, Journal (ISSN 0002-8711) vol. 39, no. 3 July 1994 p. 67-74 (HTN-95-80858) Copyright

A new concept is developed for an unmanned aerial vehicle (UAV) configured with a tipjet-driven, two-bladed, stoppable rotor and circulation control airfoils. The vehicle's high-aspect ratio wing 'converts' to a tipjet-driven helicopter rotor for vertical takeoff and landing (VTOL). The conceptual design is presented for a 1200-lb Tipjet VTOL UAV that is suitable for performing various Navy UAV missions. Vehicle performance predicitions are included for the key flight regimes of hover, low-speed rotary-wing flight, and conversion

between rotary-wing and fixed-wing flight. Results of standard mission performance analyses indicate that the 1200-lb Tipjet VTOL UAV is a viable candidate vehicle for the designated Navy UAV missions. Moreover, the Tipjet concept is directly applicable to much larger UAVs that will greatly enhance naval warfare capabilities.

Author (Herner)

### A95-75773

EXPERIMENTAL EVALUATION OF A BOX BEAM SPECIFICALLY TAILORED FOR CHORDWISE DEFORMATION LAWRENCE W. REHFIELD Univ of California, Davis, CA, United States, PETER J. ZISCHKA, STEPHEN CHANG, MICHAEL L. FENTRESS, and DAMODAR R. AMBUR AIAA Journal (ISSN 0001-1452) vol. 33, no. 1 January 1995 p. 116-119 refs (BTN-95-EIX95182619088) Copyright

This paper describes an experimental methodology based upon the use of a flexible sling support and load application system that has been created and utilized to evaluate a box beam that incorporates an elastic tailoring technology. The design technique used here for elastically tailoring the composite box beam structure is to produce exaggerated chordwise camber deformation of substantial magnitude to be of practical use in the new composite aircraft wings. The traditional methods such as a four-point bend test to apply constant bending moment with rigid fixtures inhibit the desired chordwise deformation from occurring, hence the need for the new test method. The experimental results for global camber and spanwise bending compliances correlate well with theoretical predictions based on a beamlike model.

Author (EI)

#### A95-76390

### **CYPHER MOVES TOWARD AUTONOMOUS FLIGHT**

STANLEY W. KANDEBO Aviation Week & Space Technology (ISSN 0005-2175) vol. 140, no. 10 March 7, 1994 p. 42-45 (HTN-95-41394) Copyright

Sikorsky aircraft expects to resume flight test of its Cypher unmanned aerial vehicle (UAV) this week following several months of retrofits aimed at advancing the autonomous capabilities of the aircraft. Cypher is a 6.5-ft-diameter, doughnut-shaped UAV driven by two independent coaxial rotors that are powered by a 52-hp, 2-cycle, rotary Aldis engine. A brief discussion of design, performance tests, and other aspects of the aircraft is presented.

#### A95-76582

### COMPARISON OF LINEAR STABILITY RESULTS WITH FLIGHT TRANSITION DATA

J. A. MASAD High Technology Corp, Hampton, VA, United States and M. R. MALIK AIAA Journal (ISSN 0001-1452) vol. 33, no. 1 January 1995 p. 161-163 refs

(BTN-95-EIX95182619097) Copyright

There is a need for an accurate and efficient method of predicting the location of transition on aerodynamic surfaces. Currently, the most common approach is the empirical e(exp N) method which utilizes linear stability theory. In the work described here, the results of the e(exp N) method were compared with the experimental flight data of Fisher and Dougherty for compressible flow past a sharp cone. The comparisons demonstrate the effect of mild heat transfer at subsonic freestream Mach numbers and the effect of compressibility for freestream Mach numbers up to 2.

A95-76635\* National Aeronautics and Space Administration. Langley Research Center, Hampton, VA.

### SUMMARY OF AN ACTIVE FLEXIBLE WING PROGRAM

BOYD PERRY, III National Aeronautics and Space Administration, Langley Research Center, Hampton, VA, STANLEY R. COLE, and GERALD D. MILLER Journal of Aircraft (ISSN 0021-8669) vol. 32, no. 1 January-February 1995 p. 10-15 refs (BTN-95-EIX95182619209) Copyright

This article presents a summary of a NASA/Rockwell Active Flexible Wing program. Major elements of the program are presented. Key program accomplishments included single- and multiple-mode flutter suppression, load alleviation and load control

during rapid roll maneuvers, and multi-input/multi-output multiplefunction active controls tests above the open-loop flutter boundary. Author (EI)

#### A95-76644

### **APPLICATION OF NAVIER-STOKES AEROELASTIC** METHODS TO IMPROVE FIGHTER WING MANEUVER **PERFORMANCE**

DAVID M. SCHUSTER Lockheed Engineering and Sciences Co, Inc, Hampton, VA, United States Journal of Aircraft (ISSN 0021-8669) vol. 32, no. 1 January-February 1995 p. 77-83 refs (BTN-95-EIX95182619218) Copyright

An aeroelastic analysis method, based on three-dimensional Navier-Stokes aerodynamics, has been applied to improve the performance of fighter wings operating at sustained maneuver flight conditions. The scheme reduces the trimmed pressure drag of wings performing high-g maneuvers through a simultaneous application of control surface deflection and aeroelastic twist. The aerodynamic and structural interactions are decoupled by assuming an aeroelastic twist mode shape and optimizing the aerodynamic performance based on this aeroelastic mode. The wing structural stiffness properties are then determined through an inverse scheme based on the aerodynamic loads and desired twist at the maneuver flight condition. The decoupled technique is verified by performing a fully coupled aeroelastic analysis. One of the more important features of this application, over and above improved maneuver flight performance, is that the wing performance at cruise conditions is not compromised. Thus, this method represents a multiple-point wing design capability utilizing computational aerodynamics methods and aeroelastic tailoring. Author (EI)

#### A95-76654

### RESPONSE OF A NONROTATING ROTOR BLADE TO **LATERAL TURBULENCE. PART 1: THEORY**

D. M. TANG Duke Univ, Durham, NC, United States and E. H. DOWELL Journal of Aircraft (ISSN 0021-8669) vol. 32, no. 1 January-February 1995 p. 145-153 refs (BTN-95-EIX95182619228) Copyright

Theoretical simulation of a rotor blade in forward flight by a nonrotating rotor blade in a longitudinal sinusoidal pulsating flow, and the flapping and torsional response of a flexible nonrotating rotor blade model to lateral turbulence, have been investigated. A direct time domain computational method using a modified linear ONERA aerodynamic model and a time-frequency approach using the classical aerodynamic model have been proposed. A theoretical lift comparison between the classical aerodynamic theory and the modified ONERA model is made. The numerical calculations indicate that the statistically quantitative agreement for both flap and torsional variance responses between the linear ONERA and classical aerodynamic models is reasonably good. The effects of random parametric excitation (when the longitudinal flow includes a turbulence component) and parameter variations are discussed. The numerical results are used to confirm the validity of a new experimental method presented as a companion paper. Author (EI)

### A95-76655

### RESPONSE OF A NONROTATING ROTOR BLADE TO **LATERAL TURBULENCE, PART 2: EXPERIMENT**

D. M. TANG Duke Univ, Durham, NC, United States and E. H. DOWELL Journal of Aircraft (ISSN 0021-8669) vol. 32, no. 1 January-February 1995 p. 154-160 refs (BTN-95-EIX95182619229) Copyright

In Part 1 of this work, a theoretical simulation study of rotor blade response to turbulence in forward flight is presented. For verification of this theoretical computational method, a new experimental method based on a special gust field generated by a rotating slotted cylinder with an airfoil (RSC/airfoil) in a wind tunnel is developed to simulate the aerodynamic environment of a rotating rotor blade in forward flight. This gust generator can produce a single harmonic gust wave and also turbulence with uniform power spectral density over a certain frequency band in the lateral and longitudinal

directions. In this article, quantitative comparisons are also made with theoretical results for both random and nonrandom parametric excitation. The quantitative agreement between theory and experiment indicates that this experimental method is useful. Author (EI)

N95-22510# Army Research Lab., Watertown, MA. Materials Directorate.

RATIONALE FOR THE MODULAR AIR-SYSTEM **VULNERABILITY ESTIMATION NETWORK (MAVEN)** METHODOLOGY Final Report, Jan. - Jun. 1994

LISA K. ROACH Sep. 1994 26 p

(Contract(s)/Grant(s): DA PROJ. 1L1-62618-AH-80) (AD-A285797; ARL-TR-581) Avail: CASI HC A03/MF A01

The air community has long had a need for a new vulnerability/ lethality (V/L) methodology, one usable by the triservice community. Current models range from manual calculations of total vulnerable area (Av) to complex models of incendiary functioning, fragment penetration, and fire initiation with component fault tree damage modes. Most, if not all, of these models make use of expected value. or deterministic, methods which do not accurately reflect the actual, observed phenomenology. In addition, technological advances in system design and weapon lethality have outpaced the growth of these models. While the community has tried to come to grips with these more complex systems and phenomenology, clearly, the existing models have not. The purpose of this report is to describe the rationale behind the development of a new stochastic, pointburst vulnerability model for air systems which supports the myriad of analyses the air community must perform, as well as to discuss, in general, the technical requirements which generated this need.

N95-22806\*# National Aeronautics and Space Administration. Flight Research Center, Edwards, CA.

### FLIGHT TEST OF THE X-29A AT HIGH ANGLE OF ATTACK: FLIGHT DYNAMICS AND CONTROLS

JEFFREY E. BAUER, ROBERT CLARKE, and JOHN J. BURKEN Washington Feb. 1995 70 p (Contract(s)/Grant(s): RTOP 505-64-30)

(NASA-TP-3537; H-1984; NAS 1.60:3537) Avail: CASI HC A04/MF

The NASA Dryden Flight Research Center has flight tested two X-29A aircraft at low and high angles of attack. The high-angle-ofattack tests evaluate the feasibility of integrated X-29A technologies. More specific objectives focus on evaluating the high-angle-of-attack flying qualities, defining multiaxis controllability limits, and determining the maximum pitch-pointing capability. A pilot-selectable gain system allows examination of tradeoffs in airplane stability and maneuverability. Basic fighter maneuvers provide qualitative evaluation. Bank angle captures permit qualitative data analysis. This paper discusses the design goals and approach for high-angle-of-attack control laws and provides results from the envelope expansion and handling qualities testing at intermediate angles of attack. Comparisons of the flight test results to the predictions are made where appropriate. The pitch rate command structure of the longitudinal control system is shown to be a valid design for high-angle-of-attack control laws. Flight test results show that wing rock amplitude was overpredicted and aileron and rudder effectiveness were underpredicted. Flight tests show the X-29A airplane to be a good aircraft up to 40 deg angle of attack.

N95-22829\*# National Aeronautics and Space Administration. Flight Research Center, Edwards, CA.

**DIRECT ADAPTIVE PERFORMANCE OPTIMIZATION OF** SUBSONIC TRANSPORTS: A PERIODIC PERTURBATION **TECHNIQUE** 

MARTIN D. ESPANA and GLENN GILYARD Washington Mar. 1995 45 p

(Contract(s)/Grant(s): RTOP 505-69-10)

(NASA-TM-4676; H-2040; NAS 1.15:4676) Avail: CASI HC A03/MF

Aircraft performance can be optimized at the flight condition by using available redundancy among actuators. Effective use of this potential allows improved performance beyond limits imposed by design compromises. Optimization based on nominal models does not result in the best performance of the actual aircraft at the actual flight condition. An adaptive algorithm for optimizing performance parameters, such as speed or fuel flow, in flight based exclusively on flight data is proposed. The algorithm is inherently insensitive to model inaccuracies and measurement noise and biases and can optimize several decision variables at the same time. An adaptive constraint controller integrated into the algorithm regulates the optimization constraints, such as altitude or speed, without requiring and prior knowledge of the autopilot design. The algorithm has a modular structure which allows easy incorporation (or removal) of optimization constraints or decision variables to the optimization problem. An important part of the contribution is the development of analytical tools enabling convergence analysis of the algorithm and the establishment of simple design rules. The fuel-flow minimization and velocity maximization modes of the algorithm are demonstrated on the NASA Dryden B-720 nonlinear flight simulator for the singleand multi-effector optimization cases. Author

N95-22949\*# Old Dominion Univ., Norfolk, VA. Dept. of Aerospace Engineering.

A CFD STUDY OF COMPLEX MISSILE AND STORE CONFIGURATIONS IN RELATIVE MOTION Final Report, period ending 30 Sep. 1994

OKTAY BAYSAL Mar. 1995 6 p

(Contract(s)/Grant(s): NAG1-1150) (NASA-CR-197912: NAS 1 26:197912)

(NASA-CR-197912; NAS 1.26:197912) Avail: CASI HC A02/MF

An investigation was conducted from May 16, 1990 to August 31, 1994 on the development of computational fluid dynamics (CFD) methodologies for complex missiles and the store separation problem. These flowfields involved multiple-component configurations, where at least one of the objects was engaged in relative motion. The two most important issues that had to be addressed were: (1) the unsteadiness of the flowfields (time-accurate and efficient CFD algorithms for the unsteady equations), and (2) the generation of grid systems which would permit multiple and moving bodies in the computational domain (dynamic domain decomposition). The study produced two competing and promising methodologies, and their proof-of-concept cases, which have been reported in the open literature: (1) Unsteady solutions on dynamic, overlapped grids, which may also be perceived as moving, locally-structured grids, and (2) Unsteady solutions on dynamic, unstructured grids. Author

N95-22953\*# National Aeronautics and Space Administration. Langley Research Center, Hampton, VA.

# INTEGRATED AERODYNAMIC/DYNAMIC/STRUCTURAL OPTIMIZATION OF HELICOPTER ROTOR BLADES USING MULTILEVEL DECOMPOSITION

JOANNE L. WALSH, KATHERINE C. YOUNG, JOCELYN I. PRITCHARD (Army Vehicle Structures Lab., Hampton, VA.), HOWARD M. ADELMAN, and WAYNE R. MANTAY (Army Aviation Systems Command, Hampton, VA.) Jan. 1995 52 p (Contract(s)/Grant(s): RTOP 505-63-36-06; DA PROJ. 1L1-6241-A-

47-AB) (NASA-TP-3465; L-17233; NAS 1.60:3465; ARL-TR-518) Avail: CASI HC A04/MF A01

This paper describes an integrated aerodynamic/dynamic/structural (IADS) optimization procedure for helicopter rotor blades. The procedure combines performance, dynamics, and structural analyses with a general-purpose optimizer using multilevel decomposition techniques. At the upper level, the structure is defined in terms of global quantities (stiffness, mass, and average strains). At the lower level, the structure is defined in terms of local quantities (detailed dimensions of the blade structure and stresses). The IADS procedure provides an optimization technique that is compatible with industrial design practices in which the aerodynamic and dynamic designs are performed at a global level and the structural

design is carried out at a detailed level with considerable dialog and compromise among the aerodynamic, dynamic, and structural groups. The IADS procedure is demonstrated for several examples.

Author

N95-23161# National Aerospace Lab., Amsterdam (Netherlands).
REVIEW OF AERONAUTICAL FATIGUE INVESTIGATION IN
THE NETHERLANDS DURING THE PERIOD MARCH 1991MARCH 1993 Technical Paper

J. B. DEJONGE 16 Mar. 1993 33 p See also PB92-223437 (PB95-139184; NLR-TP-93109-U) Avail: CASI HC A03/MF A01

A brief review is given of work performed in the Netherlands in the field of aeronautical fatigue. Where possible, applicable references have been presented.

NTIS

N95-23217\*# Princeton Univ., NJ. Dept. of Mechanical and Aerospace Engineering.

AN INVESTIGATION OF HELICOPTER DYNAMIC COUPLING USING AN ANALYTICAL MODEL Final Report

JEFFREY D. KELLER 7 Mar. 1995 23 p (Contract(s)/Grant(s): NAG2-561)

(NASA-CR-197420; NAS 1.26:197420) Avail: CASI HC A03/MF

À01

Many attempts have been made in recent years to predict the off-axis response of a helicopter to control inputs, and most have had little success. Since physical insight is limited by the complexity of numerical simulation models, this paper examines the off-axis response problem using an analytical model, with the goal of understanding the mechanics of the coupling. A new induced velocity model is extended to include the effects of wake distortion from pitch rate. It is shown that the inclusion of these results in a significant change in the lateral flap response to a steady pitch rate. The proposed inflow model is coupled with the full rotor/body dynamics, and comparisons are made between the model and flight test data for a UH-60 in hover. Results show that inclusion of induced velocity variations due to shaft rate improves correlation in the pitch response to lateral cycle inputs.

N95-23317\*# Mississippi State Univ., Mississippi State, MS. Dept. of Aerospace Engineering.

### THIN TAILORED COMPOSITE WING FOR CIVIL TILTROTOR Abstract Only

MASOUD RAIS-ROHANI In Hampton Univ., 1994 NASA-HU American Society for Engineering Education (ASEE) Summer Faculty Fellowship Program p 99 Dec. 1994 Avail: CASI HC A01/MF A02

The tiltrotor aircraft is a flight vehicle which combines the efficient low speed (i.e., take-off, landing, and hover) characteristics of a helicopter with the efficient cruise speed of a turboprop airplane. A well-known example of such vehicle is the Bell-Boeing V-22 Osprey. The high cruise speed and range constraints placed on the civil tiltrotor require a relatively thin wing to increase the dragdivergence Mach number which translates into lower compressibility drag. It is required to reduce the wing maximum thickness-to-chord ratio t/c from 23% (i.e., V-22 wing) to 18%. While a reduction in wing thickness results in improved aerodynamic efficiency, it has an adverse effect on the wing structure and it tends to reduce structural stiffness. If ignored, the reduction in wing stiffness leads to susceptibility to aeroelastic and dynamic instabilities which may consequently cause a catastrophic failure. By taking advantage of the directional stiffness characteristics of composite materials the wing structure may be tailored to have the necessary stiffness, at a lower thickness, while keeping the weight low. The goal of this study is to design a wing structure for minimum weight subject to structural. dynamic and aeroelastic constraints. The structural constraints are in terms of strength and buckling allowables. The dynamic constraints are in terms of wing natural frequencies in vertical and horizontal bending and torsion. The aeroelastic constraints are in terms of frequency placement of the wing structure relative to those of the rotor system. The wing-rotor-pylon aeroelastic and dynamic interactions are limited in this design study by holding the cruise

speed, rotor-pylon system, and wing geometric attributes fixed. To assure that the wing-rotor stability margins are maintained a more rigorous analysis based on a detailed model of the rotor system will need to ensue following the design study. The skin-stringer-rib type architecture is used for the wing-box structure. The design variables include upper and lower skin ply thicknesses and orientation angles, spar and rib web thicknesses and cap areas, and stringer crosssectional areas. These design variables will allow the maximum tailoring of the structure to meet the design requirements most efficiently. Initial dynamic analysis has been conducted using MSC/ NASTRAN to determine the baseline wing's frequencies and mode shapes. For the design study we intend to use the finite-element based code called WIDOWAC (Wing Design Optimization With Aeroeastic Constraints) that was developed at NASA Langlev in early 1970's for airplane wing structural analysis and preliminary design. Currently, the focus is on modification and validation of this code which will be used for the civil tiltrotor design efforts. Author

N95-23390\* National Aeronautics and Space Administration. Ames Research Center, Moffett Field, CA.

AERODYNAMIC SURFACE DISTENSION SYSTEM FOR HIGH ANGLE OF ATTACK FOREBODY VORTEX CONTROL Patent PETER T. ZELL, inventor (to NASA) 5 Jul. 1994 10 p Filed 8 Feb.

(NASA-CASE-ARC-11979-1; US-PATENT-5,326,050; US-PATENT-APPL-SN-014584; US-PATENT-CLASS-244-75R; US-PATENT-CLASS-244-199; INT-PATENT-CLASS-B64C-5/00) Avail: US Patent and Trademark Office

A deployable system is introduced for assisting flight control under certain flight conditions, such as at high angles of attack, whereby two inflatable membranes are located on the forebody portion of an aircraft on opposite sides thereof. The members form control surfaces for effecting lateral control forces if one is inflated and longitudinal control forces if both are inflated.

Official Gazette of the U.S. Patent and Trademark Office

N95-23395\* National Aeronautics and Space Administration. Ames Research Center, Moffett Field, CA.

### LIFT ENHANCING TABS FOR AIRFOILS Patent

JAMES C. ROSS, inventor (to NASA) 15 Mar. 1994 9 p Filed 8 Feb. 1993

(NASA-CASE-ARC-11990-1; US-PATENT-5,294,080; US-PATENT-APPL-SN-014581; US-PATENT-CLASS-244-215; US-PATENT-CLASS-244-216; INT-PATENT-CLASS-B64C-9/16) Avail: US Patent and Trademark Office

A tab deployable from the trailing edge of a main airfoil element forces flow onto a following airfoil element, such as a flap, to keep the flow attached and thus enhance lift. For aircraft wings with high lift systems that include leading edge slats, the slats may also be provided with tabs to turn the flow onto the following main element.

Official Gazette of the U.S. Patent and Trademark Office

N95-23666 Defence Science and Technology Organisation, Melbourne (Australia). Air Operations Div.

### ENHANCEMENT OF F/A-18 OPERATIONAL FLIGHT MEASUREMENTS: DATA REPORT FOR PHASE 1

B. A. WOODYATT, J. BENNETT, and S. D. HILL Aug. 1994 73 p (DSTO-TR-0049; AR-008-910) Copyright Avail: Issuing Activity (DSTO Aeronautical and Maritime Research Lab., GPO Box 4331, Melbourne, Victoria 3001, Australia)

This report describes the procedures used in the processing of approximately 300 hours of flight maintenance data from the F/A-18's Maintenance Status Display and Recording System (MSDRS). A Flight Path Reconstruction (FPR) program and a modified F/A-18 mathematical model from the US Naval Air Warfare Center Aircraft Division (NAWC-AD) were used to enhance these flight data in resolution and frequency. DSTO's Airframes and Engines Division (AED) will use these enhanced flight data to obtain a representative flight load spectrum. The load spectrum will be used in a full scale

fatigue test of the empennage and aft fuselage of an F/A-18, the Australian contribution to the International Follow-On Structural Test Program (IFOSTP). IFOSTP is a joint collaboration between the Canadian Forces (CF) and the Royal Australian Air Force (RAAF) to appraise structural modifications to the F/A-18 designed to achieve a service life of 6000 hours.

Author

N95-24091# General Accounting Office, Washington, DC. National Security and International Affairs Div.

REPORT TO THE SECRETARY OF DEFENSE. UNMANNED AERIAL VEHICLES: NO MORE HUNTER SYSTEMS SHOULD BE BOUGHT UNTIL PROBLEMS ARE FIXED

Mar. 1995 19 p

(GAO/NSIAD-95-52; B-259256) Avail: CASI HC A03/MF A01; GAO, PO Box 6015, Gaithersburg, MD 20877 HC

The Department of Defense is acquiring the Hunter Short-Range Unmanned Aerial Vehicle (UAV) for use by the Army, Navy and Marine Corps. The Hunter is a pilotless aircraft resembling a small airplane that is controlled from a ground station. It is intended to perform reconnaissance, target acquisition, and other military missions by flying over enemy territory and transmitting video imagery back to ground stations for use by military commanders. This report reviews the Hunter program to determine: (1) whether it has been demonstrated to be logistically supportable; (2) whether performance deficiencies found in prior testing have been resolved; and (3) whether it represents a valid joint-service effort as mandated by Congress.

# 06 AIRCRAFT INSTRUMENTATION

Includes cockpit and cabin display devices; and flight instruments.

#### A95-73438

### FLIGHT-DECK DISPLAYS ON THE BOEING 777

JEAN M. CRANE Boeing Commercial Airplane Group, ERIC S. BANG, and MARTIN C. HARTEL Aerospace Engineering (Warrendale, Pennsylvania) (ISSN 0736-2536) vol. 14, no. 12 December 1994 p. 11-16 (BTN-95-EIX95142562402) Copyright

Two new functions incorporated onto the Boeing 777 flight deck, the electronic checklist function (ECL) and the flight deck communication function (FDCF), can be accessed interactively on multifunctional displays. Using an integrated design approach, wherein the design and operational requirements of both were developed with CCds and a CUI, engineers were able to maximize ease of training and operation. Before the functions could be integrated to the flight deck, decisions regarding where information would be displayed, how pilot would interact with the functions, and where the controls would be located were made. Boeing 777 applied an integrated approach that maintained the existing flight-deck philosophies and did not add new technologies simply for technologies' sake.

### A95-73451

### GROWTH OF MULTIPLE CRACKS AND THEIR LINKUP IN A FUSELAGE LAP JOINT

RIPUDAMAN SINGH Georgia Inst of Technology, Atlanta, GA, United States, JAI H. PARK, and SATYA N. ATLURI AIAA Journal (ISSN 0001-1452) vol. 32, no. 11 November 1994 p. 2260-2268 refs

(BTN-95-EIX95142553047) Copyright

An issue of concern in aging aircraft is the growth of multiple cracks emanating from a row of fastener holes, typically in a pressurized aircraft fuselage lap splice. This multisite damage (MSD), or widespread fatigue damage, if allowed to progress, can suddenly become catastrophic. The understanding of the failure

behavior dictates the level of compromise between safety and economy. The complexity of the structure due to various stiffening elements makes it unamenable to a simple direct analysis. A two-step elastic finite element fatigue analysis combining a conventional finite element method and the Schwartz-Neumann alternating method with analytical solutions is developed to understand fatigue growth of multiple cracks and to obtain a first estimate of the residual life of multiple cracks and to obtain a first estimate of the residual life of stiffened fuselage shell structure with MSD in the riveted lap joint. The analysis procedure is validated by simulating a laboratory fatigue test on a lap joint in a flat coupon. Both the coupon and the shell panel are found to have fatigue lives only up to the first linkup of neighboring crack tips.

#### A95-75716

### CASS: DESIGN FOR SUPPORTABILITY

ANDREW C. MENA Martin Marietta Corp, Daytona Beach, FL, United States IEEE Aerospace and Electronic Systems Magazine (ISSN 0885-8985) vol. 10, no. 1 January 1995 p. 23-27 refs (BTN-95-EIX95172595296) Copyright

All configurations of the CASS test set are designed around a common HYBRID core. The five configurations of CASS provide the heart of all known present and future requirements for Automatic Test Equipment (ATE). Additional testing requirements are fulfilled by CASS through ancillary equipment such as inertial navigation systems, advanced communication bus interfaces, fiber optic data bus, high-speed data bus, and pneumatics capabilities. The high-power device test subsystem, currently in its conceptual phase, is another ancillary addition which can be connected to any RF or CNI configuration to support all high-power RF requirements. Building all capabilities around a common core eliminates many of the problems associated with previously fielded ATE systems. One of the major problems that has been reduced is the negative impact on systems being supported when the test set fails.

#### A95-75717

# CONTAINING MILITARY AUTOTEST COST GROWTH THROUGH THE USE OF COMMERCIAL STANDARD EQUIPMENT ARCHITECTURES

R. E. KNOFF Collins Avionics & Communications Div, Cedar Rapids, IA, United States IEEE Aerospace and Electronic Systems Magazine (ISSN 0885-8985) vol. 10, no. 1 January 1995 p. 19-22

(BTN-95-EIX95172595295) Copyright

The recent past has been stressful for commercial airline Industry: fierce competition has caused the demise of several carriers. The resulting drive to slash operating expenses has bolstered development of avionics industry standards for automated test equipment. Rockwell's Collins Air Transport Division (CATD) has begun to market compliant test gear that airline maintenance departments wishing to acquire modern high performance test systems without the development cost penalty has eagerly received. A similar situation now confronts the military. The various branches can no longer justify the maintenance of independent autotest architectures. This paper describes the CATD implementation of the commercial-standard architecture; shows how we have designed the system to avoid obsolescence; and indicates the considerations that are necessary for adapting it to military scenarios.

Author (EI)

### A95-75718

#### ATE ENABLING TECHNOLOGIES

LARRY V. KIRKLAND OO-ALC/TISA, Hill AFB, UT, United States and JEFFREY S. DEAN IEEE Aerospace and Electronic Systems Magazine (ISSN 0885-8985) vol. 10, no. 1 January 1995 p. 14-18 refs

(BTN-95-EIX95172595294) Copyright

A discussion of the current and emerging core technologies and philosophies that will enable Air Force personnel to quickly, accurately and intuitively diagnose faults in increasingly complex systems.

Author (EI)

### A95-75720

### NEW COMMERCIAL OFF-THE-SHELF TESTERS ARE AUTOMATIC AND INTELLIGENT

HENRY OMAN IEEE Aerospace and Electronic Systems Magazine (ISSN 0885-8985) vol. 10, no. 1 January 1995 p. 3-8 refs (BTN-95-EIX95172595292) Copyright

A typical commercial off-the-shelf (COTS) automatic tester is based on a 60-MHz 486 PC with a 1-Gb hard disk. It uses openarchitecture operating systems. The test engineer can create his own test programs, using packages such as LABVIEW, ATLAS, and SMART. He does not need support from a team of computer programmers. This is the direction in which commercial airlines are going. The COTS tester can have an IEEE Standard 'VXI' box. Into it can be plugged virtual-instrument circuit cards. New automatic-testing technology ranges from multi-media presentations of test advice to the trouble-shooting technician, to 3-D video displays. This technology, plus orders for Department of Defense agencies to use COTS, presents to the armed services these choices: (1) continue buying and using 1980's technology, or (2) go to the lower-cost, high-performance COTS that were shown and described at AUTOTESTCON '93 by the test-equipment industry.

#### A95-76734

### OVERVIEW OF ALLIEDSIGNAL'S AVIONICS DEVELOPMENT IN THE CIS

FRANK M. G. DORENBERG AlliedSignal Commercial Avionics Systems and LEO G. LAFORGE IEEE Aerospace and Electronic Systems Magazine (ISSN 0885-8985) vol. 10, no. 2 February 1995 p. 8-12 refs

(BTN-95-EIX95212641069) Copyright

Comprised of 12 independent countries, the Commonwealth of Independent States (CIS), successor to the Soviet Union, has a large aerospace industry. In pursuing its objectives as a global supplier, AlliedSignal Aerospace has adopted a strategy for conducting business in the CIS which is based upon forming long-term partnerships with domestic suppliers, to jointly develop products and services for this large and growing market. This paper describes the CIS aviation industry and infrastructure, and gives an overview of the development of the ARIA-200 system - a project of AlliedSignal to provide air transports with internationally accepted levels of operational capabilities and state-of-the-art equipment, functionality, and reliability. A description of one such air transport, the BE-200, is given. It is a multirole amphibious aircraft designed primarily for fire fighting.

#### A95-76735

### DESIGN OF WIDE ANGLE HEAD UP DISPLAYS FOR SYNTHETIC VISION

PAUL L. WISELY GEC Marconi Avionic Ltd, Kent, United Kingdom IEEE Aerospace and Electronic Systems Magazine (ISSN 0885-8985) vol. 10, no. 2 February 1995 p. 13-18 refs (BTN-95-EIX95212641070) Copyright

With the current interest by aircraft manufacturers and operators in both enhanced and synthetic vision has come increased interest by industry in designing and producing suitable head up displays to help realize such systems.

Author (EI)

#### A95-76736

### FLIGHT TEST EVALUATION OF A 35 GHZ FORWARD LOOKING ALTIMETER FOR TERRAIN AVOIDANCE

ROBERT C. BECKER Honeywell Technology Cent, Minneapolis, MN, United States and LARRY D. ALMSTED IEEE Aerospace and Electronic Systems Magazine (ISSN 0885-8985) vol. 10, no. 2 February 1995 p. 19-22

(BTN-95-EIX95212641071) Copyright

Honeywell has conducted a series of flight tests of a 35 GHz digital microprocessor controlled forward looking radar altimeter. A Bell 206L Jet Ranger helicopter was used to evaluate the capability of the sensor as a detector of various types of terrain collision hazards. The sensor was composed of a covert, spread spectrum radar altimeter processor driving a 35 GHz converter and antenna

assembly mounted on a steerable platform. Excellent correlation between predicted performance and observed performance was obtained.

Author (EI)

N95-22578\* National Aeronautics and Space Administration. Pasadena Office, CA.

#### VIRTUAL REALITY FLIGHT CONTROL DISPLAY WITH SIX-DEGREE-OF-FREEDOM CONTROLLER AND SPHERICAL ORIENTATION OVERLAY Patent

BRIAN C. BECKMAN, inventor (to NASA) (Jet Propulsion Lab., California Inst. of Tech., Pasadena, CA.) 14 Feb. 1995 14 p Filed 23 Apr. 1993 Supersedes N93-30416 (31 - 11, p 3251)

(Contract(s)/Grant(s): NAS7-918)

(NASA-CASE-NPO-18733-1-CÚ; US-PATENT-5,388,990; US-PATENT-APPL-SN-056503; US-PATENT-CLASS-434-38; US-PATENT-CLASS-434-307R; US-PATENT-CLASS-434-307R; US-PATENT-CLASS-364-578; US-PATENT-CLASS-395-152; US-PATENT-CLASS-345-8) Avail: US Patent and Trademark Office

A virtual reality flight control system displays to the pilot the image of a scene surrounding a vehicle or pod having six degrees of freedom of acceleration or velocity control by the pilot and traveling through inertial space, the image itself including a superimposed figure providing the pilot an instant reference of orientation consisting of superimposed sets of geometric figures whose relative orientations provide the pilot an instantaneous feel or sense of orientation changes with respect to some fixed coordinate system. They include a first set of geometric figures whose orientations are fixed to the pilot's vehicle and a second set of geometric figures whose orientations are fixed with respect to a fixed or interstellar coordinate system. The first set of figures is a first set of orthogonal great circles about the three orthogonal axes of the flight vehicle or pod and centered at and surrounding the pilot's head, while the second set of figures is a second set of orthogonal great circles about the three orthogonal axes of a fixed or interstellar coordinate system, also centered at and surrounding the pilot's head.

Official Gazette of the U.S. Patent and Trademark Office

N95-24030\*# National Aeronautics and Space Administration. Ames Research Center, Moffett Field, CA.

#### TRISTAR 1: EVALUATION METHODS FOR TESTING HEAD-UP DISPLAY (HUD) FLIGHT SYMBOLOGY

R. L. NEWMAN (Crew Systems Consultants, San Marcos, TX.), L. A. HAWORTH, G. K. KESSLER (Naval Air Test Center, Patuxent River, MD.), D. J. EKSUZIAN (Naval Air Development Center, Warminster, PA.), W. R. ERCOLINE (Krug Life Sciences, Inc., Houston, TX.), R. H. EVANS (Air Force Instrument Flight Center, Randolph AFB, TX.), T. C. HUGHES (Aeronautical Systems Div., Wright-Patterson AFB, OH.), and L. F. WEINSTEIN (Krug Life Sciences, Inc., Houston, TX.) Feb. 1995 88 p (Contract(s)/Grant(s): RTOP 505-64-36)

(NASA-TM-4665; A-94141; NAS 1.15:4665; TR-94-A-019; NAWCADPAX-95-10-RTR; AL-CF-TR-1994-0159) Avail: CASI HC A05/MF A01

The first in a series of piloted head-up display (HUD) flight symbology studies (TRISTAR) measuring pilot task performance was conducted at the NASA Ames Research Center by the Tri-Service Flight Symbology Working Group (FSWG). Sponsored by the U.S. Army Aeroflightdynamics Directorate, this study served as a focal point for the FSWG to examine HUD test methodology and flight symbology presentations. HUD climb-dive marker dynamics and climb-dive ladder presentations were examined as pilots performed air-to-air (A/A), air-to-ground (A/G), instrument landing system (ILS), and unusual attitude (UA) recover tasks. Symbolic presentations resembled pitch ladder variations used by the U.S. Air Force (USAF), U.S. Navy (USN), and Royal Air Force (RAF). The study was initiated by the FSWG to address HUD flight symbology deficiencies, standardization, issue identification, and test methodologies. It provided the mechanism by which the USAF, USN, RAF, and USA could integrate organizational ideas and reduce differences for comparisons. Specifically it examined flight symbology

issues collectively identified by each organization and the use of objective and subjective text methodology and flight tasking proposed by the FSWG.

Author

#### 07

#### AIRCRAFT PROPULSION AND POWER

Includes prime propulsion systems and systems components, e.g., gas turbine engines and compressors; and on-board auxiliary power plants for aircraft.

#### A95-75757

### ARTIFICIAL INTELLIGENCE FOR TURBOPROP ENGINE MAINTENANCE

Aerospace Engineering (Warrendale, Pennsylvania) (ISSN 0736-2536) vol. 15, no. 1 January-February 1995 p. 27-31 (BTN-95-EIX95182617812) Copyright

Long-term maintenance operations, causing the unit to out of action, may seem economical - but they result in reduced operating readiness. Offsetting that concern, careless, hurried maintenance reduces margins of safety and reliability. Any tool that improves maintenance without causing a sharp increase in cost is valuable. Artificial intelligence (AI) is one of the tools. Expert system and neural networks are two different areas of AI that show promise for turboprop engine maintenance.

#### A95-76389

#### LYCOMING TO TEST NEW ENGINE CORE

STANLEY W. KANDEBO Aviation Week & Space Technology (ISSN 0005-2175) vol. 140, no. 10 March 7, 1994 p. 32-33 (HTN-95-41393) Copyright

Textron Lycoming plans to develop a new family of engines based on a common core. The core engine for the new Lycoming engine family, designated the 500 series, is an increased efficiency, improved performance derivative based on the core used in the company's T55, ALF502, and LF507 engines. A brief description of engine design, performance, and Textron Lycoming business plans is given.

#### A95-76616

### DERIVATION OF SYSTEM MATRICES FROM NONLINEAR DYNAMIC SIMULATION OF JET ENGINES

N. SUGIYAMA Natl Aerospace Lab, Chofu, Japan Journal of Guidance, Control, and Dynamics (ISSN 0731-5090) vol. 17, no. 6 November-December 1994 p. 1320-1326 refs (BTN-95-EIX95182619139) Copyright

Most multivariable control design methodologies are linear theories and utilize a linearized plant model. Since accuracy of a linearized plant model affects the quality of a control system designed by those methods, a reasonable linearized plant model that adequately simulates the plant must be prepared. This paper describes a derivation method of such a model in the form of ABCD system matrices from nonlinear dynamic simulation. System matrices of a two-spool turbofan engine are derived and compared to the actual engine data. The effect of perturbation size and linearization formula over a linearized model are discussed. A corrected form of the system matrices is introduced to extend the data base to the whole flight envelope.

#### A95-76648

## EROSION OF DUST-FILTERED HELICOPTER TURBINE ENGINES. PART 1: BASIC THEORETICAL CONSIDERATIONS JOHANNES P. VANDERWALT Univ of the Witwatersrand,

JOHANNES P. VANDEHWALT Univ of the Witwatersrand, Johannesburg, South Africa and ALAN NURICK Journal of Aircraft (ISSN 0021-8669) vol. 32, no. 1 January-February 1995 p. 106-111 refs

(BTN-95-EIX95182619222) Copyright

 A theoretical model has been developed for predicting the effects of the erosion of helicopter engines and their performance as a result of ingesting sparse dust concentrations. In such concentrations particle-on-particle interactions are negligible, and most particles have diameters less than 100 micron. These dust distributions may be found in engines fitted with filters comprised of banks of centrifugal separators. The model includes the effects of particle size distribution, particle velocity, and dust concentration.

Author (EI)

#### A95-76649

### EROSION OF DUST-FILTERED HELICOPTER TURBINE ENGINES. PART 2: EROSION REDUCTION

JOHANNES P. VANDERWALT Univ of the Witwatersrand, Johannesburg, South Africa and ALAN NURICK Journal of Aircraft (ISSN 0021-8669) vol. 32, no. 1 January-February 1995 p. 112-117 refs

(BTN-95-EIX95182619223) Copyright

The effects of erosion of filtered and unfiltered dusts ingested by a helicopter gas turbine engine are investigated for the case where particle-on-particle interactions are negligible. The effects of the particle size distribution of the dust in the ingested airstream on engine life are included in the analysis. An erosion reduction factor, which may be used to predict the increase in life of a gas turbine engine in terms of a filtration efficiency factor and the effective particle sizes of the filtered and unfiltered dusts is presented. The method is validated using experimental results obtained on a Turmo 4B gas turbine engine.

Author (EI)

#### A95-76650

### LIFE PREDICTION OF HELICOPTER ENGINES FITTED WITH DUST FILTERS

JOHANNES P. VANDERWALT Univ of the Witwatersrand, Johannesburg, South Africa and ALAN NURICK Journal of Aircraft (ISSN 0021-8669) vol. 32, no. 1 January-February 1995 p. 118-123 refs

(BTN-95-EIX95182619224) Copyright

Engine erosion in environments such as those that may be encountered by helicopters during hover, nap-of-the-Earth flight, dust storms, and generally dusty atmospheres can have significant effects on engine performance and life, resulting from the degradation of the first-stage compressor. Ingestion of dust into a turbine engine may be limited by means of dust filters fitted to the engine intakes. Efficient filtration of the dust results in a sparse dust concentration entering the engine that is comprised essentially of particles that have a diameter of less than 100 micron, and indicated negligible particle-on-particle interactions. The dependence of engine performance on the erosion of the first-stage compressor by sparse dust concentrations may be extended to enable the life of an engine to be predicted for a typical flight in a specific dust environment. The methodology for predicting engine life is presented.

Author (EI)

#### A95-76673

#### A NEW TYPE OF SIMULATOR FOR SIMULATING THE FLOW-FIELD DISTORTION OF ENGINE INLET

CHENGYI PENG Nanjing Univ of Aeronautics & Astronautics, Nanjing, China, JIAJU MA, and JUENFEI YING Tuijin Jishu/Journal of Propulsion Technology (ISSN 1001-4055) no. 6 December 1994 p. 18-22 In CHINESE refs

(BTN-95-EIX95202638963) Copyright

The need of innovation in the art of engine-face flow-field simulation is expounded, and a new type of simulator is presented. The design concept, principle and construction, special features, and test results of the simulator are also discussed. Owing to its capability in simulating the distortion of steady and dynamic pressure as well as the swirling flow-field, it is suitable to research on: (1) their comprehensive influence on the performance of engine or compressor; (2) evaluating the compatibility between engine and its inlet; and (3) the tolerant limit of engine or compressor for distortion.

N95-23088\*# Colorado Univ., Boulder, CO. Dept. of Aerospace Engineering Sciences.

HIGH-PERFORMANCE PARALLEL ANALYSIS OF COUPLED

PROBLEMS FOR AIRCRAFT PROPULSION Progress Report, Jun. 1994 - Jan. 1995

C. A. FELIPPA, C. FARHAT, P.-S. CHEN, U. GUMASTE, M. LEOINNE, and P. STERN Feb. 1995 51 p Original contains color illustrations

(Contract(s)/Grant(s): NAG3-1273)

(NASA-CR-197440; CU-CAS-95-03; NAS 1.26:197440) Avail: CASI HC A04/MF A01 4 functional color pages

This research program deals with the application of highperformance computing methods to the numerical simulation of complete jet engines. The program was initiated in 1993 by applying two-dimensional parallel aeroelastic codes to the interior gas flow problem of a by-pass jet engine. The fluid mesh generation, domain decomposition and solution capabilities were successfully tested. Attention was then focused on methodology for the partitioned analysis of the interaction of the gas flow with a flexible structure and with the fluid mesh motion driven by these structural displacements. The latter is treated by an ALE technique that models the fluid mesh motion as that of a fictitious mechanical network laid along the edges of near-field fluid elements. New partitioned analysis procedures to treat this coupled 3-component problem were developed in 1994. These procedures involved delayed corrections and subcycling, and have been successfully tested on several massively parallel computers. For the global steady-state axisymmetric analysis of a complete engine we have decided to use the NASA-sponsored ENG10 program, which uses a regular FV-multiblock-grid discretization in conjunction with circumferential averaging to include effects of blade forces, loss, combustor heat addition, blockage, bleeds and convective mixing. A load-balancing preprocessor for parallel versions of ENG10 has been developed. It is planned to use the steady-state global solution provided by ENG10 as input to a localized three-dimensional FSI analysis for engine regions where aeroelastic effects may be important.

N95-23222\*# Moller International, Inc., Davis, CA.
EVALUATION OF THERMAL BARRIER AND PS-200 SELFLUBRICATING COATINGS IN AN AIR-COOLED ROTARY
ENGINE Final Contractor Report

PAUL S. MOLLER Cleveland, OH NASA Mar. 1995 39 p (Contract(s)/Grant(s): NAS3-26309; RTOP 324-02-00) (NASA-CR-195445; E-9493; NAS 1.26:195445) Avail: CASI HC A03/MF A01

This project provides an evaluation of the feasibility and desirability of applying a thermal barrier coating overlaid with a wear coating on the internal surfaces of the combustion area of rotary engines. Many experiments were conducted with different combinations of coatings applied to engine components of aluminum, iron and titanium, and the engines were run on a well-instrumented test stand. Significant improvements in specific fuel consumption were achieved and the wear coating, PS-200, which was invented at NASA's Lewis Research Center, held up well under severe test conditions.

N95-23550\*# National Aeronautics and Space Administration. Lewis Research Center, Cleveland, OH.

## SENSITIVITY OF COMBUSTION-ACOUSTIC INSTABILITIES TO BOUNDARY CONDITIONS FOR PREMIXED GAS TURBINE COMBUSTORS

DOUGLAS DARLING, KRISHNAN RADHAKRISHNAN (NYMA, Inc., Brook Park, OH.), and AYO OYEDIRAN (AYT Corp., Brook Park, OH.) Mar. 1995 8 p Presented at the Central/Western States Sections Joint Technical Meeting, San Antonio, TX, 23-26 Apr. 1995; sponsored by the Combustion Institute

(Contract(s)/Grant(s): NAS3-27186; RTOP 537-02-21)

(NASA-TM-106890; E-9530; NAS 1.15:106890) Avail: CASI HC A02/MF A01

Premixed combustors, which are being considered for low NOx engines, are susceptible to instabilities due to feedback between pressure perturbations and combustion. This feedback can cause damaging mechanical vibrations of the system as well as degrade the emissions characteristics and combustion efficiency. In a lean

combustor instabilities can also lead to blowout. A model was developed to perform linear combustion-acoustic stability analysis using detailed chemical kinetic mechanisms. The Lewis Kinetics and Sensitivity Analysis Code, LSENS, was used to calculate the sensitivities of the heat release rate to perturbations in density and temperature. In the present work, an assumption was made that the mean flow velocity was small relative to the speed of sound. Results of this model showed the regions of growth of perturbations to be most sensitive to the reflectivity of the boundary when reflectivities were close to unity.

N95-24053\*# Union Carbide Industrial Gases, Inc., Tonawanda, NY. Linde Div.

AIRBORNE ROTARY AIR SEPARATOR STUDY Interim Report A. ACHARYA, C. F. GOTTZMANN, and J. J. NOWOBILSKI Cleveland, OH NASA Dec. 1990 64 p

(Contract(s)/Grant(s): NAS3-25560)

(NASA-CR-189099; E-9583; NAS 1.26:189099) Avail: CASI HC A04/MF A01

Several air breathing propulsion concepts for future earth-toorbit transport vehicles utilize air collection and enrichment, and subsequent storage of liquid oxygen for later use in the vehicle emission. Work performed during the 1960's established the feasibility of substantially reducing weight and volume of a distillation type air separator system by operating the distillation elements in high 'g' fields obtained by rotating the separator assembly. This contract studied the capability test and hydraulic behavior of a novel structured or ordered distillation packing in a rotating device using air and water. Pressure drop and flood points were measured for different air and water flow rates in gravitational fields of up to 700 g. Behavior of the packing follows the correlations previously derived from tests at normal gravity. The novel ordered packing can take the place of trays in a rotating air separation column with the promise of substantial reduction in pressure drop, volume, and system weight. The results obtained in the program are used to predict design and performance of rotary separators for air collection and enrichment systems of interest for past and present concepts of air breathing propulsion (single or two-stage to orbit) systems.

Author

## 08 AIRCRAFT STABILITY AND CONTROL

Includes aircraft handling qualities; piloting; flight controls; and autopilots.

#### A95-75093

#### IDENTIFICATION OF HIGHER ORDER HELICOPTER DYNAMICS USING LINEAR MODELING METHODS

BIMAL L. APONSO Systems Technologies, Inc., Hawthorne, CA, US, DONALD E. JOHNSTON Systems Technologies, Inc., Hawthorne, CA, US, WALTER A. JOHNSON Systems Technologies, Inc., Hawthorne, CA, US, and RAYMOND E. MAGDELANEO Systems Technologies, Inc., Hawthorne, CA, US American Helicopter Society, Journal (ISSN 0002-8711) vol. 39, no. 3 July 1994 p. 3-11

(Contract(s)/Grant(s): NOOO19-87-C-0195)

(HTN-95-80851) Copyright

The higher order dynamics of the helicopter are dominated by rotor and structural modes. Accurate modeling of these high-order dynamics is essential if high bandwidth, robust control systems are to be implemented in modern helicopters. An analytically based, higher-order linear model has been developed and compared with frequency domain flight data for a Sikorsky CH-53E helicopter at hover. Flight test data showed that the helicopter to be remarkably linear in its responses. The linear model proved capable of modeling the higher-order dynamics of the helicopter in hover with an adequate degree of accuracy. Correlation between the model and flight data for the cyclic response in the pitch and roll axes was improved

by adjusting model parameters specific to the rotor lag degree-offreedom dynamics were different from those predicted by theory. The model was used to identify the dominant high-order modes in the helicopter responses.

#### A95-75094

### EFFECTS OF HIGH ORDER DYNAMICS ON HELICOPTER FLIGHT CONTROL LAW DESIGN

STEVEN J. INGLE Boeing Defense and Space Group, Philadelphia, PA, US and ROBERTO CELI Univ. of Maryland, College Park, MD, US American Helicopter Society, Journal (ISSN 0002-8711) vol. 39, no. 3 July 1994 p. 12-23

(Contract(s)/Grant(s): NSF CDR-88-03012)

(HTN-95-80852) Copyright

The main objective of the study is to assess the effects of incorporating higher order dynamics such as rotor and inflow dynamics when designing a flight control system to satisfy handling qualities specifications such as Aeronautical Design Standard (ADS)-33C. The control methodologies examined are Linear Quadratic Gaussian (LQG), Eigenstructure Assignment (EA), and H(sub infinity). The UH-60 in hover is used as a test case to which a representative subset of the ADS-33C requirements, for a Rate Command Attitude Hold response type, is applied. The results indicate that acceptable controllers can be designed using EA with a rigid body model of the helicopter; however the control activity is high and the controller is not robust. An H(sub infinity) design requires the modeling of higher order dynamics; the resulting controller is higher order but more robust, and the control activity is lower. It was not possible to determine a suitable LQG based controller that would satisfy all the requirements. Author (Herner)

A95-75095\* National Aeronautics and Space Administration. Ames Research Center, Moffett Field, CA.

## INVESTIGATION OF THE EFFECTS OF BANDWIDTH AND TIME DELAY ON HELICOPTER ROLL-AXIS HANDLING QUALITIES

CHRIS L. BLANKEN NASA. Ames Research Center, Moffet Field, CA, US and HEINZ-JURGEN PAUSDER Institut fuer Flumechanik, Braunschweig, Germany American Helicopter Society, Journal (ISSN 0002-8711) vol. 39, no. 3 July 1994 p. 24-33 (HTN-95-80853) Copyright

Several years of cooperative research conducted under the U.S./German Memorandum of Understanding (MOU) in helicopter aeromechanics have recently resulted in a successful handling qualities study. The focus of this cooperative research has been the effect of time delays in a high bandwidth vehicle on handling qualities. The jointly performed study included the use of U.S. ground-based simulation and German in-flight simulation facilities. The NASA-Ames Vertical Motion Simulator (VMS) was used to develop a high bandwidth slalom tracking task which took into consideration the constraints of the facilities. The VMS was used to define a range of the test parameters and to perform initial handling qualities evaluations. The flight tests were conducted using DLR's variable-stability BO 105 S3 Advanced Technology Testing Helicopter System (ATTHeS). Configurations included a rate command and an attitude command response system with added time delays of up to 160 milliseconds over the baseline and band width values between 1.5 and 4.5 rad/sec. Sixty-six evaluations were performed in about 25 hours of flight time during ten days of testing. The results indicate a need to more tightly constrain the allowable roll axis phase delay for the Level 1 and Level 2 requirements in the U.S. Army's specification for helicopter handling qualities Aeronautical Design Standard (ADS)-33C. Author (Herner)

A95-75096\* National Aeronautics and Space Administration. Lewis Research Center, Cleveland, OH.

### INTEGRATED FLIGHT/PROPULSION CONTROL FOR HELICOPTERS

STEPHEN M. ROCK Stanford Univ., Stanford, CA, US and KEN NEIGHBORS Stanford Univ., Stanford, CA, US American Helicopter Society, Journal (ISSN 0002-8711) vol. 39, no. 3 July 1994 p.

34-42 (Contract(s)/Grant(s): NAG3-1177) (HTN-95-80854) Copyright

Presented is a procedure for improving the communication of requirements and specifications in the early design phases of an integrated helicopter/engine control system. The procedure is based on establishing a bound on a transfer matrix that relates blade cyclic and collective inputs to rotor speed variations. This bound becomes a new specification for the propulsion control system designer that embodies the mission-level performance goals of the helicopter. An example application of the procedure is provided for a Blackhawk/ 700 system undergoing vertical accelerations from hover.

Author (Herner)

#### A95-75772

#### FLUTTER OF AN INFINITELY LONG PANEL IN A DUCT

RONALD J. EPSTEIN Duke Univ, Durham, NC, United States, RAMAKRISHNA SRINIVASAN, and EARL H. DOWELL AIAA Journal (ISSN 0001-1452) vol. 33, no. 1 January 1995 p. 109-115 refs

(BTN-95-EIX95182619087) Copyright

The aeroelastic stability is examined of an infinitely long panel of finite width enclosed in a duct such that both the upper and lower surfaces of the panel are exposed to an inviscid and compressible flow. The panel behavior is accounted for by small deflection plate theory, whereas the aerodynamic forces acting on the panel are described by the classical linearized small disturbance potential theory. As such, a self-consistent theoretical model is constructed for the asymptotic behavior of the panel. Two panel boundary conditions are considered; the panel is assumed to be either simply supported or clamped along the side edges. For the simply supported case, rather extensive numerical results have been obtained. The effects of Mach number, air/panel mass ratio, and duct dimension on the flutter velocity are determined.

Author (EI)

#### A95-76603

### KINEMATICS AND AERODYNAMICS OF VELOCITY-VECTOR ROLL

WAYNE C. DURHAM Virginia Polytechnic Inst and State Univ, Blacksburg, VA, United States, FREDERICK H. LUTZE, and WILL-IAM MASON Journal of Guidance, Control, and Dynamics (ISSN 0731-5090) vol. 17, no. 6 November-December 1994 p. 1228-1233 (BTN-95-EIX95182619126) Copyright

The velocity-vector roll is an angular rotation of an airplane about its instantaneous velocity vector, constrained to be performed at a constant angle of attack (AOA), no sideslip, and constant velocity. The body-axis rotations and the constraints are used in the moment equations to determine the aerodynamic moments required to perform the velocity-vector roll. The total aerodynamic moments are analyzed to know the conditions under which their maximum occur. For representative tactical airplanes, it is shown that the conditions for maximum pitching moment are strongly a function of the orientation of the airplane. Maximum required pitching moment occurs at peak roll rate and is achieved at an AOA in excess of 45 deg. The conditions for maximum rolling moment depend on the value of the roll mode time constant. Lastly, results are compared with those obtained using conventional assumptions of zero pitch and yaw rates. Significant improvement is observed, especially in the prediction of maximum pitching-moment requirements.

A95-76606\* National Aeronautics and Space Administration. Ames Research Center, Moffett Field, CA.

H-INFINITY HELICOPTER FLIGHT CONTROL LAW DESIGN WITH AND WITHOUT ROTOR STATE FEEDBACK

MARC D. TAKAHASHI National Aeronautics and Space Administration, Ames Research Center, Moffett Field, CA Journal of Guid-

ance, Control, and Dynamics (ISSN 0731-5090) vol. 17, no. 6 November-December 1994 p. 1245-1251 refs (BTN-95-EIX95182619129) Copyright

An H-infinity formulation to design pitch-roll flight control laws for hovering helicopter is proposed. Using this formulation, control law designs were developed to examine the effect of using rotor state feedback. Two laws developed for an articulated helicopter math model in low-speed flight include a compensator using rigid-body measurements and one using body plus rotor statements. The design with no rotor state feedback has the potential to pass approximately twice as much noise to the actuators near the 1/rev frequency as the design with rotor state feedback. In addition, response of the controller with no rotor state feedback was more sensitive to gain variations. Due to this sensitivity, the design with no rotor state feedback showed more high-frequency oscillation in roll.

=1

A95-76607\* National Aeronautics and Space Administration. Ames Research Center, Moffett Field, CA.

### AUTOMATIC GUIDANCE AND CONTROL FOR HELICOPTER OBSTACLE AVOIDANCE

VICTOR H. L. CHENG National Aeronautics and Space Administration, Ames Research Center, Moffett Field, CA and T. LAM Journal of Guidance, Control, and Dynamics (ISSN 0731-5090) vol. 17, no. 6 November-December 1994 p. 1252-1259 refs (BTN-95-EIX95182619130) Copyright

The helicopter nap-of-the-earth flight problem has previously been discussed in various papers. The concept of automatic guidance involving obstacle avoidance requires a sophisticated obstacle detection system to provide three-dimensional obstacle and terrain data in flight in a hostile and unknown environment. Passive imaging sensors, augmented by selective use of low-detectability active sensors, will likely be needed to maximize covertness and safety. thus necessitating data fusion. The sensor data, limited by intervisibility constraints of the environment, suggest the use of heuristic arguments in flight-path planning over conventional analytic techniques. In addition, explicit consideration of vehicle capability is essential in the autopilot design to assure safe flight in such close proximity to the ground. This paper describes the automatic obstacle avoidance guidance and control functions and the implementation of these functions and a mock obstacle detection system in a graphical simulation for evaluation. Author (EI)

#### A95-76608

### DIRECT-LIFT DESIGN STRATEGY FOR LONGITUDINAL CONTROL OF HYPERSONIC AIRCRAFT

PHUONG VU California Polytechnic State Univ, San Luis Obispo, CA, United States and DANIEL J. BIEZAD Journal of Guidance, Control, and Dynamics (ISSN 0731-5090) vol. 17, no. 6 November-December 1994 p. 1260-1266 refs (BTN-95-EIX95182619131) Copyright

A longitudinal control design called the G-command, alpha follow-up is described that significantly improves the lag between pitch angle and flight-path angle responses associated with hypersonic flight. The design technique relies on classical, successive loop closures to determine the control architecture and introduces a direct-lift control strategy to design dynamic compensation. This dynamic compensation constrains and 'washes out' body-flap input to avoid excessive flap deflection and associated heating while providing angle-of-attack control at the engine inlet. The final design was implemented on a generic hypersonic aircraft simulation at NASA Dryden and evaluated by a NASA test pilot familiar with the SR-71. The pilot flew turning and altitude change maneuvers using the implemented control law and verified the ability to track flight path with ease and precision. Finally, evidence is presented that supports a flying qualities metric for longitudinal, hypersonic flight based on the bandwidth of the flight-path-angle-to-stick-frequency Author (EI) response.

#### A95-76609

### MULTIRATE FLUTTER SUPPRESSION SYSTEM DESIGN FOR A MODEL WING

GREGORY S. MASON Seattle Univ, Seattle, WA, United States and MARTIN C. BERG Journal of Guidance, Control, and Dynamics (ISSN 0731-5090) vol. 17, no. 6 November-December 1994 p. 1267-1274 refs

(BTN-95-EIX95182619132) Copyright

A new methodology for multirate control system design is described. It accommodates a general multiple-input, multiple-output control law structure that allows the sampling rates for the plant sensor output signals, the update rates for the processor states, and the update rates for the plant control input signals to be independently specified. It includes a capability to design for multiple plant conditions so as to achieve robustness to plant parameter variations. Its analysis components include a method for determining conventional gain and phase margins, a method for determining a bound on the smallest destabilizing uncertainty, and a method for determining the maximum root-mean-square (rms) gain of a multirate system. The methodology is demonstrated by application to the design of a multirate flutter suppression system for a model wing.

Author (EI)

#### A95-76630

#### **AUTOMATIC FORMATION FLIGHT CONTROL**

M. PACHTER Air Force Inst of Technology, Wright-Patterson AFB, OH, United States, J. J. D'AZZO, and J. L. DARGAN Journal of Guidance, Control, and Dynamics (ISSN 0731-5090) vol. 17, no. 6 November-December 1994 p. 1380-1383 (BTN-95-EIX95182619153) Copyright

The control design problem of an automatic pilot for formation flight control has been analyzed and decomposed into two uncoupled linear single-input, two-output dynamic tracking control system design problems. This, in turn, results in the efficient design of a PI formation-hold autopilot that uses a mix of separation errors and maneuver errors. The formation flight control problem considered here is significant in view of its direct operational importance: It affords the automation of the coordination of a leader/wingman flight, the design of a robotic wingman, and the automatic control of aircraft during maneuvers such as aerial refueling.

A95-76640\* National Aeronautics and Space Administration. Langley Research Center, Hampton, VA.

### FLUTTER SUPPRESSION CONTROL LAW DESIGN AND TESTING FOR THE ACTIVE FLEXIBLE WING

VIVEK MUKHOPADHYAY National Aeronautics and Space Administration, Langley Research Center, Hampton, VA Journal of Aircraft (ISSN 0021-8669) vol. 32, no. 1 January-February 1995 p. 45-51 refs

(BTN-95-EIX95182619214) Copyright

Design of a control law for simultaneously suppressing the symmetric and antisymmetric flutter modes of a sting-mounted, fixed-in-roll aeroelastic wind-tunnel model is described. The flutter suppression control law was designed using linear quadratic Gaussian theory, and involved control law order reduction, a gain root-locus study, and use of previous experimental results. A 23% increase in the open-loop flutter dynamic pressure was demonstrated during the wind-tunnel test. Rapid roll maneuvers at 11% above the symmetric flutter boundary were also performed when the model was in a free-to-roll configuration.

Author (EI)

A95-76641\* National Aeronautics and Space Administration. Langley Research Center, Hampton, VA.

DESIGN AND MULTIFUNCTION TESTS OF A FREQUENCY DOMAIN-BASED ACTIVE FLUTTER SUPPRESSION SYSTEM

WILLIAM M. ADAMS, JR. National Aeronautics and Space Administration, Langely Research Center, Hampton, VA and DAVID M. CHRISTHILF Journal of Aircraft (ISSN 0021-8669) vol. 32, no. 1 January-February 1995 p. 52-60 refs (BTN-95-EIX95182619215) Copyright

This article describes the process of analysis, design, digital

implementation, and subsonic testing of an active controls flutter suppression system for a full-span, free-to-roll, wind-tunnel model of an advanced fighter concept. A frequency domain representation of the plant was employed, and a robust multiinput/multioutput controller was generated by using optimization techniques to maximize singular value robustness criteria and insensitivity to uncertainty in the flutter frequency. During testing in a fixed-in-roll configuration, simultaneous suppression of both symmetric and antisymmetric flutter was successfully demonstrated. For a free-to-roll configuration, symmetric flutter was suppressed to the limit of the tunnel test envelope. During aggressive rolling maneuvers above the openloop flutter boundary, simultaneous flutter suppression and maneuver load control were demonstrated. Finally, the flutter suppression controller was reoptimized during the test using combined experimental and analytical frequency domain data, resulting in improved stability robustness. The reoptimization, accomplished overnight, shows the potential, with a much faster computer, to apply the design procedure to a tuning-type adaptive active flutter suppression controller. Author (EI)

A95-76642\* National Aeronautics and Space Administration. Langley Research Center, Hampton, VA.

### FLUTTER SUPPRESSION FOR THE ACTIVE FLEXIBLE WING: A CLASSICAL DESIGN

M. R. WASZAK National Aeronautics and Space Administration, Langley Research Center, Hampton, VA and S. SRINATHKUMAR Journal of Aircraft (ISSN 0021-8669) vol. 32, no. 1 January-February 1995 p. 61-67 refs

(BTN-95-EIX95182619216) Copyright

The synthesis and experimental validation of a control law for an active flutter suppression system for the active flexible wing wind-tunnel model is presented. The design was accomplished with traditional root locus methods making extensive use of interactive computer graphics tools and simulation-based analysis. The design approach relied on a fundamental understanding of the flutter mechanism to formulate a very simple control law structure resulting in a filter with an 'inverted notch' characteristic. This unusual filter characteristic was required to compensate for adverse zero locations in the frequency range near flutter. Wind-tunnel tests of the flutter suppression controller demonstrated simultaneous suppression of two flutter modes, significantly increasing the flutter dynamic pressure. The flutter suppression controller was also successfully operated in combination with a rolling maneuver controller to perform flutter suppression during rapid rolling maneuver. Author (EI)

#### A95-76681

### ROBUSTLY STABLE PRELIMINARY CONTROL SYSTEMS DESIGN FOR THE YF-16 CCV AIRCRAFT

IEEE Transactions on Aerospace and Electronic Systems (ISSN 0018-9251) vol. 31, no. 1 January 1995 p. 479-486 refs (BTN-95-EIX95202637608) Copyright

A preliminary control system design for the YF-16 CCV aircraft in its longitudinal mode satisfying its flying qualities specifications is investigated. The design is shown to be robustly stable when the actuator model and the unstable pole in the airframe model of the aircraft are subjected to structured uncertainties. Very recent tools of robust stability analysis are utilized to accomplish this goal.

Author (EI)

N95-22674\*# McDonnell-Douglas Aerospace, Long Beach, CA. Transport Aircraft.

GUIDANCE AND CONTROL REQUIREMENTS FOR HIGH-SPEED ROLLOUT AND TURNOFF (ROTO) Final Report STEVE H. GOLDTHORPE, ALAN C. KERNIK, LARRY S. MCBEE, and ORV W. PRESTON Jan. 1995 127 p

(Contract(s)/Grant(s): NAS1-19703; RTOP 538-04-13-01) (NASA-CR-195026; NAS 1.26:195026) Avail: CASI HC A07/MF A02

This report defines the initial requirements for designing a research high-speed rollout and turnoff (ROTO) guidance and control system applicable to transport class aircraft whose purpose

is to reduce the average runway occupancy time (ROT) for aircraft operations. The requirements will be used to develop a ROTO system for both automatic and manual piloted operation under normal and reduced visibility conditions. Requirements were determined for nose wheel/rudder steering, braking/reverse thrust, and the navigation system with the aid of a non-real time, three degree-of-freedom MD-11 simulation program incorporating airframe and gear dynamics. The requirements were developed for speeds up to 70 knots using 30 ft exit geometries under dry and wet surface conditions. The requirements were generated under the assumptions that the aircraft landing system meets the current Category III touchdown dispersion requirements and that aircraft interarrival spacing is 2 nautical miles. This effort determined that auto-asymmetric braking is needed to assist steering for aft center-of-gravity aircraft. This report shows various time-history plots of the aircraft performance for the ROTO operation. This effort also investigated the state-of-the-art in the measurement of the runway coefficient of friction for various runway conditions.

N95-22908\*# Massachusetts Inst. of Tech., Cambridge, MA. Dept. of Aeronautics and Astronautics.

DESIGN OF HIGH PERFORMANCE MULTIVARIABLE CONTROL SYSTEMS FOR SUPERMANEUVERABLE AIRCRAFT AT HIGH ANGLE OF ATTACK Final Report

LENA VALAVANI 1995 3 p (Contract(s)/Grant(s): NAG1-1088)

(NASA-CR-197661; NAS 1.26:197661) Avail: CASI HC A01/MF A01

The main motivation for the work under the present grant was to use nonlinear feedback linearization methods to further enhance performance capabilities of the aircraft, and robustify its response throughout its operating envelope. The idea was to use these methods in lieu of standard Taylor series linearization, in order to obtain a well behaved linearized plant, in its entire operational regime. Thus, feedback linearization was going to constitute an 'inner loop', which would then define a 'design plant model' to be compensated for robustness and guaranteed performance in an 'outer loop' application of modern linear control methods. The motivation for this was twofold; first, earlier work had shown that by appropriately conditioning the plant through conventional, simple feedback in an 'inner loop', the resulting overall compensated plant design enjoyed considerable enhancement of performance robustness in the presence of parametric uncertainty. Second, the nonlinear techniques did not have any proven robustness properties in the presence of unstructured uncertainty; a definition of robustness (and performance) is very difficult to achieve outside the frequency domain; to date, none is available for the purposes of control system design. Thus, by proper design of the outer loop, such properties could still be 'injected' in the overall system.

N95-22954\*# National Aeronautics and Space Administration. Lewis Research Center, Cleveland, OH.

STABLE H(INFINITY) CONTROLLER DESIGN FOR THE LONGITUDINAL DYNAMICS OF AN AIRCRAFT

HITAY OEZBAY (Ohio State Univ., Columbus, OH.) and SANJAY GARG Feb. 1995 53 p

(Contract(s)/Grant(s): RTOP 505-62-50)

(NASA-TM-106847; E-9421; NAS 1.15:106847) Avail: CASI HC A04/MF A01

This report discusses different approaches to stable H infinity controller design applied to the problem of augmenting the longitudinal dynamics of an aircraft. Stability of the H infinity controller is investigated by analyzing the effects of changes in the performance index weights, and modifications in the measured outputs. The existence of a stable suboptimal controller is also investigated. It is shown that this is equivalent to finding a stable controller, whose infinity norm is less than a specified bound, for an unstable plant which is determined from parametrization of all H infinity controllers. Examples are given for a gust alleviation and a command tracking problem.

N95-23297\*# California Univ., Davis, CA. Dept. of Mechanical and Aeronautical Engineering.

ANALYSIS OF THE LONGITUDINAL HANDLING QUALITIES

#### AND PILOT-INDUCED-OSCILLATION TENDENCIES OF THE HIGH-ANGLE-OF-ATTACK RESEARCH VEHICLE (HARV) **Abstract Only**

RONALD A. HESS In Hampton Univ., 1994 NASA-HU American Society for Engineering Education (ASEE) Summer Faculty Fellowship Program p 79 Dec. 1994

Avail: CASI HC A01/MF A02

The NASA High-Angle-of Attack Research Vehicle (HARV), a modified F-18 aircraft, experienced handling qualities problems in recent flight tests at NASA Dryden Research Center. Foremost in these problems was the tendency of the pilot-aircraft system to exhibit a potentially dangerous phenomenon known as a pilot-induced oscillation (PIO). When they occur, PIO's can severely restrict performance. sharply dimish mission capabilities, and can even result in aircraft loss. A pilot/vehicle analysis was undertaken with the goal of reducing these PIO tendencies and improving the overall vehicle handling qualities with as few changes as possible to the existing feedback/feedforward flight control laws. Utilizing a pair of analytical pilot models developed by the author, a pilot/vehicle analysis of the existing longitudinal flight control system was undertaken. The analysis included prediction of overall handling qualities levels and PIO susceptability. The analysis indicated that improvement in the flight control system was warranted and led to the formulation of a simple control stick command shaping filter. Analysis of the pilot/vehicle system with the shaping filter indicated significant improvements in handling qualities and PIO tendencies could be achieved. A non-real time simulation of the modified control system was undertaken with a realistic, nonlinear model of the current HARV. Special emphasis was placed upon those details of the command filter implementation which could effect safety of flight. The modified system is currently awaiting evaluation in the real-time, pilotin-the-loop, Dual-Maneuvering-Simulator (DMS) facility at Langley.

Author

N95-23314\*# Old Dominion Coll., Norfolk, VA. Dept. of Aerospace Engineering.

INNER LOOP FLIGHT CONTROL FOR THE HIGH-SPEED CIVIL **TRANSPORT Abstract Only** 

BRETT A. NEWMAN In Hampton Univ., 1994 NASA-HU American Society for Engineering Education (ASEE) Summer Faculty Fellowship Program p 96 Dec. 1994

Avail: CASI HC A01/MF A02

High-speed aerospace vehicles which employ high strength, light weight, yet deformable materials may exhibit significant interaction between the rigid-body and vibrational dynamics. Preliminary High-Speed Civil Transport (HSCT) configurations are a prime example. Traditionally, separate control systems have been used to augment the rigid-body and vibrational dynamics. In the HSCT arena, the highly coupled motions may not allow this design freedom. The research activity addresses two specific issues associated with the design and development of an integrated flight control system (FCS) for HSCT configurations, which are discussed next. The HSCT is expected to have a short period instability at subsonic speeds. Flight vehicles with this characteristic (i.e., F-16, F-22, X-29, Space Shuttle) are stabilized with what is called a superaugmented pitch rate loop. One concern is 'Will this stability augmentation logic work for a HSCT?' Studies show that an idealized pitch rate design would be acceptable, but is not realistic. Investigations using a contaminated pitch rate design reveal serious hurdles to overcome in the FCS design. Mounting location for the pitch rate sensor is critical. Results indicate a forward location leads to destabilizing pick-up of aeroelastic modes, while aft locations lead to undesirable coupling of the dominate pitch mode with the first aeroelastic mode. Intermediate locations for the sensor may not be acceptable. The source of the problem is the presence of low frequency aeroelastic modes in HSCT configurations, which are not present in vehicles currently using the superaugmented logic. To say the least, a conventional superaugmented pitch rate loop strategy may have undesirable characteristics. An unconventional strategy, which attempts to eliminate the above deficiencies by blending several pitch rate signals, indicates an improvement in the FCS architecture feasibility, but is still lacking in some respects. The HSCT configu-

ration does not have aerodynamic surfaces in the vicinity of the nose (i.e., no canard or vane). A second concern is 'Can the fuselage bending/torsion aeroelastic modes be effectively augmented without sufficient control input near the vehicle nose?' The superaugmented FCS results above may be suggesting the necessity of a secondary feedback loop to achieve an acceptable integrated FCS. Preliminary analysis of HSCT aeroelastic mode shapes indicate the use of existing wing leading edge devices as a second control input may be lacking in control authority for the rigid-body attitude and aeroelastic modes. An effort is underway to incorporate generic wing leading edge devices and canards into a generic HSCT model for the purpose of assessing additional control authority and it's use in candidate FCS designs. A generic HSCT mathematical model was necessary for the studies above. A HSCT category model is available in NASA-CR-172201. This model describes the linear. longitudinal dynamics about the following flight condition: ascent, W = 730,000 lbs, h = 6,500 ft, M = 0.6. The model incorporates the full rigid-body variable set, as well as eighteen aeroelastic modes. Elevator deflection serves as the control input. Modifications to the model include the incorporation of relaxed static stability (i.e., static margin from -7.3% to +10%) and additional control inputs. Author

N95-23319\*# Saint Louis Univ., Cahokia, IL. Dept. of Aerospace Engineering.

### PRELIMINARY IDENTIFICATION OF BUFFET PROBLEMS IN HIGH SPEED CIVIL TRANSPORT Abstract Only

KRISHNASWAMY RAVINDRA In Hampton Univ., 1994 NASA-HU American Society for Engineering Education (ASEE) Summer Faculty Fellowship Program p 101 Dec. 1994 Avail: CASI HC A01/MF A02

In the present study, some effort is made to identify whether empennage buffet is a relevant factor in the design and operation of the High Speed Civil Transport (HSCT). Based on some results of the only operational supersonic transport. Concorde and the innumerable studies that exist on the tail buffet of high performance airplanes. CFD analyses on the HSCT as well as low speed wind tunnel tests on models, it appears as though buffet will be a factor that needs attention in the proper design of empennage structure. Utilizing the existing empirical relation between the reduced frequency of the leading edge vortices and the geometric parameters, it is estimated that the characteristic frequencies of the vortices from the wing cranks are in the range of certain fundamental frequencies of the wing-fuselage-empennage structure. Buffet is believed to be critical during take-off, climb, descent and landing. Computational and experimental data available in open literature indicate coherent vortex flow structure in the empennage region at supersonic cruise speeds. This raises further concern on the fatigue life of the empennage structure. Three second generation supersonic transport designs taken from open literature are briefly compared with the 'empennage buffet' in mind. Future research efforts relating to buffet studies on the HSCT are summarized. A bibliography pertaining to the present research, including relevant studies on the first generation supersonic transport is presented. The effect of rounded wing leading edges on the present frequency estimates needs further study. The effect of engine exhaust on the flow field in the empennage region also needs further study. Author

## N95-23325\*# Tennessee Univ. Space Inst., Tullahoma, TN. HANDLING QUALITIES OF THE HIGH SPEED CIVIL TRANSPORT Abstract Only

U. PETER SOLIES In Hampton Univ., 1994 NASA-HU American Society for Engineering Education (ASEE) Summer Faculty Fellowship Program p 107 Dec. 1994

Avail: CASI HC A01/MF A02

The low speed handling qualities of a High Speed Civil Transport class aircraft have been investigated by using data of the former Advanced Supersonic Transport (AST) 105. The operation of such vehicles in the airport terminal area is characterized by 'backside' performance. Main objectives of this research effort were: (Q) determination of the nature and magnitude of the speed instability associated with the backside of the thrust required curve; (2)

confirmation of the validity of existing MIL-SPEC handling qualities criteria; (3) safety of operation of the vehicle in the event of autothrottle failure; and (4) correlation of required engine responsiveness with level of speed instability. Preliminary findings comprise the following: (1) The critical velocity for speed instability was determined to be 196 knots, well above the projected approach speed of 155 knots. This puts the vehicle far on the backside of its thrust required curve. While the aircraft can be configured to have static and dynamic stability at this trim point, a significant speed instability emerges, if a pilot or autopilot attempts flight path control with elevator and/or canard control surfaces only. This requires a properly configured autothrottle and/or variable aerodynamic drag devices which can provide speed stability; (2) An AST 105 type vehicle meets MIL-SPEC criteria only in part. While the damping criteria for phugoid and short period motion are met easily, the AST 105 falls short of the required minimum short period frequency, meaning that the HSCT is too sluggish in pitch to meet the military criteria. Obviously the military specification do not consider a vehicle with such high pitch inertia. With regard to speed stability and flight path stability criteria, the vehicle meets levels 2 and 3 of the military requirements, indicating that it would be landed safety with manual controls in case of an autothrottle failure, even though the pilot workload would be high; and (3) This requires quick thrust response to throttle adjustment, however. If the engine responsiveness is slow, the aircraft handling qualities are further deteriorated. Progress has been made in correlating required engine responses dyanmics with the given level of speed instability of the vehicle.

Author (revised)

N95-23389\* National Aeronautics and Space Administration. Ames Research Center, Moffett Field, CA.

#### **ENGINES-ONLY FLIGHT CONTROL SYSTEM Patent**

FRANK W. BURCHAM, inventor (to NASA), GLENN B GILYARD, inventor (to NASA), JOSEPH L. CONLEY, inventor (to NASA), JAMES F. STEWART, inventor (to NASA), and CHARLES G. FULLERTON, inventor (to NASA) 19 Jul. 1994 18 p Filed 28 May 1992

(NASA-CASE-ARC-11944-1; US-PATENT-5,330,131; US-PATENT-APPL-SN-889347; US-PATENT-CLASS-244-75R; US-PATENT-CLASS-244-7R; US-PATENT-CLASS-244-182; US-PATENT-CLASS-244-51; INT-PATENT-CLASS-B64C-19/00) Avail: US Patent and Trademark Office

A backup flight control system for controlling the flightpath of a multi-engine airplane using the main drive engines is introduced. The backup flight control system comprises an input device for generating a control command indicative of a desired flightpath, a feedback sensor for generating a feedback signal indicative of at least one of pitch rate, pitch attitude, roll rate and roll attitude, and a control device for changing the output power of at least one of the main drive engines on each side of the airplane in response to the control command and the feedback signal.

Official Gazette of the U.S. Patent and Trademark Office

N95-23392\*# Georgia Tech Research Inst., Atlanta, GA. Contracting Support Div.

### FLUTTER ANALYSIS OF COMPOSITE BOX BEAMS Final Administrative Report, 21 Sep. 1993 - 20 Sep. 1994

DEWEY H. HODGES and MATTHEW GREENMAN 21 Feb. 1995 14 p

(Contract(s)/Grant(s): NGT-50981)

(NASA-CR-197931; NAS 1.26:197931) Avail: CASI HC A03/MF A01

The dynamic aeroelastic instability of flutter is an important factor in the design of modern high-speed, flexible aircraft. The current trend is toward the creative use of composites to delay flutter. To obtain an optimum design, we need an accurate as well as efficient model. As a first step towards this goal, flutter analysis is carried out for an unswept composite box beam using a linear structural model and Theodorsen's unsteady aerodynamic theory. Structurally, the wing was modeled as a thin-walled box-beam of rectangular cross section. Theodorsen's theory was used to get 2-

D unsteady aerodynamic forces, which were integrated over the span. A free-vibration analysis is carried out. These fundamental modes are used to get the flutter solution using the V-g method. Future work is intended to build on this foundation. Author

N95-23410\*# Minnesota Univ., Minneapolis, MN. Dept. of Aerospace Engineering and Mechanics.

FEEDBACK CONTROL LAWS FOR HIGHLY MANEUVERABLE AIRCRAFT Annual Report, 1 Feb. 1995 - 31 Jan. 1996

WILLIAM L. GARRARD and GARY J. BALAS 31 Jan. 1995 11 p (Contract(s)/Grant(s): NAG1-1380)

(NASA-CR-197944; NAS 1.26:197944) Avail: CASI HC A03/MF

During this year, we concentrated our efforts on the design of controllers for lateral/directional control using mu synthesis. This proved to be a more difficult task than we anticipated and we are still working on the designs. In the lateral-directional control problem, the inputs are pilot lateral stick and pedal commands and the outputs are roll rate about the velocity vector and side slip angle. The control effectors are ailerons, rudder deflection, and directional thrust vectoring vane deflection which produces a yawing moment about the body axis. Our math model does not contain any provision for thrust vectoring of rolling moment. This has resulted in limitations of performance at high angles of attack. During 1994-95, the following tasks for the lateral-directional controllers were accomplished: (1) Designed both inner and outer loop dynamic inversion controllers. These controllers are implemented using accelerometer outputs rather than an a priori model of the vehicle aerodynamics; (2) Used classical techniques to design controllers for the system linearized by dynamics inversion. These controllers acted to control roll rate and Dutch roll response; (3) Implemented the inner loop dynamic inversion and classical controllers on the six DOF simulation; (4) Developed a lateral-directional control allocation scheme based on minimizing required control effort among the ailerons, rudder, and directional thrust vectoring; and (5) Developed mu outer loop controllers combined with classical inner loop controllers.

Derived from text

N95-23671\*# National Aeronautics and Space Administration. Lewis Research Center, Cleveland, OH.

### MOTOR DRIVE TECHNOLOGIES FOR THE POWER-BY-WIRE (PBW) PROGRAM: OPTIONS, TRENDS AND TRADEOFFS

MALIK E. ELBULUK (Akron Univ., Akron, OH.) and M. DAVID KANKAM Mar. 1995 14 p Presented at the National Aerospace and Electronics Conference, Wright-Patterson AFB, OH, 23-27 May 1995; cosponsored by the IEEE and the Aerospace and Electronics Systems Society

(Contract(s)/Grant(s): RTOP 233-02-03)

(NASA-TM-106885; E-9521; NAS 1.15:106885) Avail: CASI HC A03/MF A01

Power-By-Wire (PBW) is a program involving the replacement of hydraulic and pneumatic systems currently used in aircraft with an all-electric secondary power system. One of the largest loads of the all-electric secondary power system will be the motor loads which include pumps, compressors and Electrical Actuators (EA's). Issues of improved reliability, reduced maintenance and efficiency, among other advantages, are the motivation for replacing the existing aircraft actuators with electrical actuators. An EA system contains four major components. These are the motor, the power electronic converters, the actuator and the control system, including the sensors. This paper is a comparative literature review in motor drive technologies, with a focus on the trends and tradeoffs involved in the selection of a particular motor drive technology. The reported research comprises three motor drive technologies. These are the induction motor (IM), the brushless dc motor (BLDCM) and the switched reluctance motor (SRM). Each of the three drives has the potential for application in the PBW program. Many issues remain to be investigated and compared between the three motor drives, using actual mechanical loads expected in the PBW program.

Author

#### 09

#### RESEARCH AND SUPPORT FACILITIES (AIR)

Includes airports, hangars and runways; aircraft repair and overhaul facilities; wind tunnels; shock tube facilities; and engine test blocks.

#### A95-74554

### MEASUREMENT OF PARTICLE EMISSIONS FROM CLEAN ROOM GAS-HANDLING COMPONENTS

R. PERIASAMY Research Triangle Inst, Research Triangle Park, NC, United States, D. S. ENSOR, R. P. DONOVAN, A. C. CLAYTON, and J. RIDDLE Journal of the Electrochemical Society (ISSN 0013-4651) vol. 141, no. 6 June 1994 p. 1649-1653 refs (BTN-94-EIX94381359040) Copyright

Particle emissions from clean room gas-handling components were measured by following a test method developed recently by SEMATECH. Three types of tests, namely, the static, the dynamic, and the impact tests were conducted to determine particle emissions from the components tested. Particles emitted by the components such as valves, point-of-use filters and inline pressure regulators were measured using a condensation nucleus particle counter. The number of particles emitted by the valve was influenced by the actuator pressure used to open and close the test valve. That is, the higher the actuator pressure the higher the number of particles released from the automatic valve. Particle contributions measured from valves, filters, and regulators are presented here. Author (EI)

#### A95-74629

## MEASUREMENT OF MOISTURE AND TOTAL HYDROCARBON CONTRIBUTIONS BY VALVES USED IN CLEAN ROOM GASDELIVERY SYSTEMS

R. PERIASAMY Research Triangle Inst, Research Triangle Park, NC, United States, J. R. NEWSOME, D. S. ENSOR, R. P. DONOVAN, and J. RIDDLE Journal of the Electrochemical Society (ISSN 0013-4651) vol. 141, no. 6 June 1994 p. 1653-1657 refs (BTN-94-EIX94381359041) Copyright

Moisture and total hydrocarbon (THC) emissions from valves used in clean room gas-distribution systems were measured by following two test methods developed recently by SEMATECH. Each test method consists of two types of tests: a purge test and a bakeout test. The apparatus specified in each test method is similar except for the detector. Simply by switching the detectors, the same apparatus may be used for both test methods. We report measurements of THC and moisture made with this apparatus and carried out on both manual and automatic all metal stainless steel valves with either Kel-F or tetrafluoroethylene gaskets, some new (fresh out o the bag) and some used.

#### A95-76584

#### APPLICATION OF A CONTROL-VOLUME-BASED FINITE-ELEMENT FORMULATION TO THE SHOCK TUBE PROBLEM

S. M. H. KARIMIAN Univ of Waterloo, Waterloo, Ont, Canada and G. E. SCHNEIDER AIAA Journal (ISSN 0001-1452) vol. 33, no. 1 January 1995 p. 165-167 refs

(BTN-95-EIX95182619099) Copyright

The performance of a newly developed pressure-based method for incompressible/compressible flow calculation is investigated by solving the shock tube problem, which has served as a benchmark case in literature. It is demonstrated that the present method is capable of solving transient and compressible flows incorporating strong discontinuities.

A95-76637\* National Aeronautics and Space Administration. Langley Research Center, Hampton, VA.

### SIMULATION AND MODEL REDUCTION FOR THE ACTIVE FLEXIBLE WING PROGRAM

CAREY BUTTRILL National Aeronautics and Space Administration, Langley Research Center, Hampton, VA, BARTON BACON, JENNI-FER HEEG, JACOB HOUCK, and DAVID WOOD Journal of Aircraft (ISSN 0021-8669) vol. 32, no. 1 January-February 1995 p. 23-31 refs

(BTN-95-EIX95182619211) Copyright

The simulation methodology used in the Active Flexible Wing wind-tunnel test program is described. An overview of the aeroservoelastic modeling used in building the required batch and hot-bench simulations is presented. Successful hot-bench implementation required that the full mathematical model be significantly reduced while assuring that accuracy be maintained for all combinations of 10 inputs and 56 outputs. The reduction was accomplished by using a method based on internally balanced realizations and by focusing on the linear, aeroelastic portion of the full mathematical model. The error-bound properties of the internally balanced realization significantly contribute to its utility in the model reduction process. The reduction method and the results achieved are described.

A95-76639\* National Aeronautics and Space Administration.
Langley Research Center, Hampton, VA.
ON-LINE ANALYSIS CAPABILITIES DEVELOPED TO
SUPPORT THE ACTIVE FLEXIBLE WING WIND-TUNNEL
TESTS

CAROL D. WIESEMAN National Aeronautics and Space Administration, Langley Research Center, Hampton, VA, SHERWOOD T. HOADLEY, and SANDRA M. MCGRAW Journal of Aircraft (ISSN 0021-8669) vol. 32, no. 1 January-February 1995 p. 39-44 refs (BTN-95-EIX95182619213) Copyright

A variety of on-line analysis tools were developed to support two active flexible wing (AFW) wind-tunnel tests. These tools were developed to verify control law execution, to satisfy analysis requirements of the control law designers, to provide measures of system stability in a real-time environment, and to provide project managers with a quantitative measure of controller performance. Descriptions and purposes of capabilities that were developed are presented in this article along with examples. Procedures for saving and transferring data for near real-time analysis, and descriptions of the corresponding data interface programs, are also presented. Although much of the on-line analysis capabilities described herein are not technically new, the implementation for near real-time analysis to verify and evaluate controller performance is new, and is included in this special Journal of Aircraft issue for completeness in describing the AFW wind-tunnel testing. The on-line analysis tools worked well before, during, and after the wind-tunnel tests, and proved to be a vital and important part of the entire test effort, part of the entire test effort. Author (EI)

N95-23011\*# National Aeronautics and Space Administration. Langley Research Center, Hampton, VA.

DYNAMIC RESPONSE TESTS OF INERTIAL AND OPTICAL
WIND-TUNNEL MODEL ATTITUDE MEASUREMENT DEVICES
R. D. BUEHRLE, C. P. YOUNG, JR. (North Carolina State Univ., Raleigh, NC.), A. W. BURNER, J. S. TRIPP, P. TCHENG, T. D.
FINLEY, and T. G. POPERNACK, JR. Feb. 1995 44 p
(Contract(s)/Grant(s): RTOP 505-59-54-01)
(NASA-TM-109182; NAS 1.15:109182) Avail: CASI HC A03/MF A01

Results are presented for an experimental study of the response of inertial and optical wind-tunnel model attitude measurement systems in a wind-off simulated dynamic environment. This study is part of an ongoing activity at the NASA Langley Research Center to develop high accuracy, advanced model attitude measurement systems that can be used in a dynamic wind-tunnel environment. This activity was prompted by the inertial model attitude sensor response observed during high levels of model vibration which results in a model attitude measurement bias error. Significant bias errors in model attitude measurement were found for the measurement using the inertial device during wind-off dynamic testing of a model system. The amount of bias present during wind-tunnel tests will depend on the amplitudes of the model dynamic response and the modal characteristics of the model system.

Correction models are presented that predict the vibration-induced bias errors to a high degree of accuracy for the vibration modes characterized in the simulated dynamic environment. The optical system results were uncorrupted by model vibration in the laboratory setup.

Author

N95-23192\*# National Aeronautics and Space Administration.
Lewis Research Center, Cleveland, OH.
NASA LOW-SPEED AXIAL COMPRESSOR FOR
FUNDAMENTAL RESEARCH

CHARLES A. WASSERBAUER (Sverdrup Technology, Inc., Brook Park, OH.), HAROLD F. WEAVER, and RICHARD G. SENYITKO (Sverdrup Technology, Inc., Brook Park, OH.) Feb. 1995 13 p (Contract(s)/Grant(s): NAS3-25266; RTOP 505-62-52) (NASA-TM-4635; E-9016; NAS 1.15:4635) Avail: CASI HC A03/MF A01

A low-speed multistage axial compressor built by the NASA Lewis Research Center is described. The purpose of this compressor is to increase the understanding of the complex flow phenomena within multistage axial compressors and to obtain detailed data from a multistage compressor environment for use in developing and verifying models for computational fluid dynamic code assessment. The compressor has extensive pressure instrumentation in both stationary and rotating frames of reference, and has provisions for flow visualization and laser velocimetry. The compressor will accommodate rotational speeds to 1050 rpm and is rated at a pressure ratio of 1.042.

N95-23299\*# Old Dominion Coll., Norfolk, VA. Dept. of Mechanical Engineering.

SYSTEM IDENTIFICATION OF THE LARGE-ANGLE
MAGNETIC SUSPENSION TEST FIXTURE (LAMSTF) Abstract
Only

JEN-KUANG HUANG In Hampton Univ., 1994 NASA-HU American Society for Engineering Education (ASEE) Summer Faculty Fellowship Program p 81 Dec. 1994

Avail: CASI HC A01/MF A02

The Large-Angle Magnetic Suspension Test Fixture (LAMSTF), a laboratory-scale research project to demonstrate the magnetic suspension of objects over wide ranges of attitudes, has been developed. This system represents a scaled model of a planned Large-Gap Magnetic Suspension System (LGMSS). The LAMSTF consists of a small cylindrical permanent magnet suspended element which is levitated above a planar array of five electromagnets mounted in a circular configuration. The cylinder is a rigid body and can be controlled to move in five independent degrees of freedom. Six position variables are sensed indirectly by using infrared lightemitting diodes and light-receiving phototransistors. The motion of the suspended cylinder is in general nonlinear and hence only the linear, time-invariant perturbed motion about an equilibrium state is considered. One of the main challenges in this project is the control of the suspended element over a wide range of orientations. An accurate dynamic model plays an essential role in controller design. The analytical model is first derived and open-loop characteristics discussed. The system is shown to be highly unstable and requires feedback control for system identification. Projection filters are first proposed to identify the state space model from closed-loop input/ output test data in the time domain. This method is then extended to identify linear systems from the frequency test data. A canonical transformation matrix is also derived to transform the identified state space model into the physical coordinate. The LAMSTF system is stabilized by using a linear quadratic regulator (LQR) feedback controller for closed-loop identification. The rate information is obtained by calculating the back difference of the sensed position signals. Only the closed-loop random input/output data are recorded. Preliminary results from numerical simulations demonstrate that the identified system model is fairly accurate from either time domain or frequency-domain data. Experiments will be performed to validate the proposed closed-loop identification algorithms. Author

N95-23304\*# Old Dominion Coll., Norfolk, VA. Dept. of Mechanical Engineering.

OPTIMIZED DESIGN OF A HYPERSONIC NOZZLE Abstract Only

RAMESH KRISHNAMURTHY In Hampton Univ., 1994 NASA-HU American Society for Engineering Education (ASEE) Summer Faculty Fellowship Program p 86 Dec. 1994

Avail: CASI HC A01/MF A02 Conventional procedures for designing nozzles involve the design of an inviscid contour (using the method of characteristics) that is corrected with a displacement thickness calculated from boundary-layer theory. However, nozzles designed using this classical procedure have been shown to exhibit poor flow quality at Mach numbers characteristic of hypersonic applications. The nozzle to be designed will be a part of the NASA HYPULSE facility which is being used for hypervelocity flight research. Thus, the flow quality of the nozzle is a critical question that needs to be addressed. Design of nozzles for hypersonic applications requires a proper assessment of the effects of the thick boundary layer on the inviscid flowfield. Since the flow field is largely supersonic, the parabolized form of the Navier-Stokes (PNS) equations can be used. The requirement of a uniform flow at the exit plane of the nozzle can be used to define an objective function as part of an optimization procedure. The design procedure used in this study involves the coupling of a nonlinear (least-squares) optimization algorithm with an efficient, explicit PNS solver. The thick boundary layers growing on the walls of the nozzle limit the extent of the usable core region (region with uniform flow) for testing models (especially rectangular). In order to maximize the region of uniform flow, it was decided to have the exit plane of this nozzle to be (nearly) rectangular. Thus, an additional constraint on the nozzle shape resulted, namely the nozzle will have a shape transitioning from a circular one at the inlet to that of a rectangle at the exit. In order to provide for a smooth shape transition, the cross sectional contour of the nozzle is defined by a superellipse. The nozzle is taken to be a meter in length. The axial variations of the major and minor radii of the superellipse are governed by cubic splines. The design parameters are the coefficients of the splines associated with the local nozzle wall slopes. Extensive calculations have been made (with a three-dimensional Euler code) to understand the effects of various parameters such as location of the knot points of the spline function, different ways of characterizing the uniformity of the flow in the exit plane, as well as the effect of constraining the area of the nozzle to be invariant. Turbulent flow (measurements indicate that the flow at the nozzle inlet is turbulent) calculations are now being performed (with the inviscibly designed

N95-23309\*# New Jersey Inst. of Tech., Newark, NJ. Dept. of Chemical Engineering, Chemistry and Environmental Science.
DESIGN OF A VARIABLE AREA DIFFUSER FOR A 15-INCH

Author (revised)

MACH 6 OPEN-JET TUNNEL Abstract Only
NORMAN W. LONEY In Hampton Univ., 1994 NASA-HU American
Society for Engineering Education (ASEE) Summer Faculty Fellowship Program p 91 Dec. 1994

Avail: CASI HC A01/MF A02

nozzle contours) to assess the flow quality.

The Langley 15-inch Mach 6 High Temperature Tunnel was recently converted from a Mach 10 Hypersonic Flow Apparatus. This conversion was effected to improve the capability of testing in Mach 6 air at relatively high reservoir temperatures not previously possible at Langley. Elevated temperatures allow the matching of the Mach numbers, Reynolds numbers, and ratio of wall-to-adiabatic-wall temperatures (TW/Taw) between this and the Langley 20-inch Mach 6 CF4 Tunnel. This ratio is also matched for Langley's 31-inch Mach 10 Tunnel and is an important parameter useful in the simulation of slender bodies such as National Aerospace Plane (NASP) configurations currently being studied. Having established the nozzle's operating characteristics, the decision was made to install another test section to provide model injection capability. This test section is an open-jet type, with an injection system capable of injecting a model from retracted position to nozzle centerline between 0.5 and

2 seconds. Preliminary calibrations with the new test section resulted in Tunnel blockage. This blockage phenomenon was eliminated when the conical center body in the diffuser was replaced. The issue then, is to provide a new and more efficient variable area diffuser configuration with the capability to withstand testing of larger models without sending the Tunnel into an unstart condition. Use of the 1-dimensional steady flow equation with due regard to friction and heat transfer was employed to estimate the required area ratios (exit area / throat area) in a variable area diffuser. Correlations between diffuser exit Mach number and area ratios, relative to the stagnation pressure ratios and diffuser inlet Mach number were derived. From these correlations, one can set upper and lower operating pressures and temperatures for a given diffuser throat area. In addition, they will provide appropriate input conditions for the full 3-dimensional computational fluid dynamics (CFD) code for further simulation studies.

N95-24019# Los Alamos National Lab., NM.
NTS-SPILL TEST FACILITY WIND TUNNEL EXHAUST PLUME
CHARACTERIZATION

R. KERR, H. GOLDWIRE, D. SMITH, J. RAWLINGS, T. SCHAFFER, and J. ROBSON Jul. 1994 8 p Presented at the 1994 Chemical Analysis By Laser Interrogation of Proliferation Effluents (CALIOPE ITR) Interim Technical Review, Livermore, CA, 26-28 Apr. 1994 (Contract(s)/Grant(s): W-7405-ENG-48)

(DE95-003630; UCRL-JC-118476; CONF-9404162-14) Avail: CASI HC A02/MF A01

The exhaust plume of the NTS-STF wind tunnel has been characterized to demonstrate its suitability as a target for CALIOPE experiments. Smoke from grenades has been released in multiple quantities and at different positions inside the tunnel. The smoke plumes have been recorded on video tape. The wind velocity profile has also been determined with a moveable array of miniature vane anemometers. These measurements will be used to determine the vapor concentration pathlength as part of the ground truth. DOE

## 10 ASTRONAUTICS

Includes astronautics (general); astrodynamics; ground support systems and facilities (space); launch vehicles and space vehicles; space transportation; spacecraft communications, command and tracking; spacecraft design, testing and performance; spacecraft instrumentation; and spacecraft propulsion and power.

A95-73559
PREDICTING EXHAUST PLUME BOUNDARIES WITH SUPERSONIC EXTERNAL FLOWS

KYLE L. NASH Mevatec Corp, Huntsville, AL, United States, KEVIN W. WHITAKER, and L. MICHAEL FREEMAN Journal of Spacecraft and Rockets (ISSN 0022-4650) vol. 31, no. 5 September-October 1994 p. 773-777 refs

(BTN-95-EIX95152583258) Copyright

Several methods for predicting exhaust plume boundaries with a surrounding external flow currently exist. Unfortunately, these methods are usually cumbersome and often expensive, since they may be computationally intensive. Also, these methods typically provide many flowfield details in addition to the plume boundary location. If only the latter is desired, then calculation of these other details is wasted effort. This concern resulted in the development of a simplified plume boundary prediction method capable of analyzing underexpanded nozzle flow exhausting into a supersonic external flow. This new method is based upon the well-established Latvala method and uses an iterative scheme that employs two-dimensional flowfield assumptions. However, the method is still applicable to axisymmetric plumes, and its simplicity permits efficient operation on personal computers. Predictions of boundaries for axisymmetric plumes surrounded by various high-speed external flows exhibit

excellent agreement with empirical data, and parametric studies indicate that trends are correctly predicted. Author (EI)

#### A95-73564

### FUNCTIONAL DEPENDENCE OF TRAJECTORY DISPERSION ON INITIAL CONDITION ERRORS

ROBERT A. LAFARGE Sandia Natl Lab, Albuquerque, NM, United States and ROY S. BATY Journal of Spacecraft and Rockets (ISSN 0022-4650) vol. 31, no. 5 September-October 1994 p. 806-813 refs

(BTN-95-EIX95152583263) Copyright

This article proposes numerical techniques to approximate dispersion bounds and burst patterns for Monte Carlo trajectory simulations. The algorithms developed approximate trajectory dispersion bounds and burst patterns caused by the errors in initial conditions in 1/100th of the computational expense of full Monte Carlo analyses. The proposed techniques are based on the properties that the six-degree-of-freedom equations of motion produce solutions that vary continuously with initial conditions and preserve the statistical distribution of the initial conditions. The continuity of solutions in initial conditions is studied numerically by performing a stability analysis. Numerical experiments simulating a fuse effectiveness study for two generic re-entry bodies are exhibited. The dispersion bounds and burst patterns predicted using the proposed algorithms are compared to the dispersion bounds and burst patterns predicted using full Monte Carlo simulations. The agreement is excellent. Author (EI)

#### A95-73568

#### **FOURTH-GENERATION MARS VEHICLE CONCEPTS**

BRENT SHERWOOD Boeing Defense & Space Group, Huntsville, AL, United States Journal of Spacecraft and Rockets (ISSN 0022-4650) vol. 31, no. 5 September-October 1994 p. 834-841 refs (BTN-95-EIX95152583267) Copyright

Conceptual designs for fourth-generation crew-carrying Mars transfer and excursion vehicles, fully integrated to state-of-the-art standards, are presented. The resulting vehicle concepts are sized for six crew members, and can support all opposition and conjunction opportunities in or after 2014. The modular, reusable transfer ship is launched to Earth orbit on six 185-ton-class boosters and assembled there robotically. Its dual nuclear-thermal rocket engines use liquid hydrogen propollant. The payload consists of a microgravity habitation system and an expendable lift-to-drag = 1.6 lander capable of aeromaneuvering to sites within +/- 20 deg of the equator. This lander can deliver either an expendable, storable-bipropellant crew-carrying ascent vehicle, or 40 tons of cargo, and it is capable of limited surface mobility to support base buildup. Multiple cargo landers sent ahead on robotic transfer vehicles deliver the supplies and equipment required for long-duration surface missions.

#### A95-73577

### EFFECTS OF SATELLITE BUNCHING ON THE PROBABILITY OF COLLISION IN GEOSYNCHRONOUS ORBIT

V. A. CHOBOTOV Aerospace Corp, El Segundo, CA, United States and C. G. JOHNSON Journal of Spacecraft and Rockets (ISSN 0022-4650) vol. 31, no. 5 September-October 1994 p. 895-899 refs

(BTN-95-EIX95152583276) Copyright

The rapid increase in the satellite population in geostationary Earth orbit is a matter of international concern, in part because of increased collision hazard. Collocated satellite pairs in GEO experience natural drift requiring periodic station-keeping impulses, leading to similar trajectories and close encounters. To assess this risk, a procedure was devised that ranks satellite pairs in GEO according to the highest number of encounters over an extended time interval. Probability of collision was determined by a geometric and a statistical approach. It was found that many pairs of satellites in GEO remain in close proximity and experience many close approaches over time. The top 10 pairs in terms of closest encounters were identified, and mean-time-to-collision based on encounter statistics was determined. Results of the study suggest that the

bunching of active or inactive satellites at certain longitudes is a significant effect to be considered in the assessment of the collision hazard in the geosynchronous ring.

Author (EI)

#### A95-73583

### DYNAMICAL INSTABILITY OF THE AEROGRAVITY ASSIST MANEUVER

COLIN R. MCINNER Univ of Glasgow, Glasgow, United Kingdom Journal of Spacecraft and Rockets (ISSN 0022-4650) vol. 31, no. 5 September-October 1994 p. 916-918 refs (BTN-95-EIX95152583282) Copyright

Fundamental dynamical equations are used to form a single expression for vertical acceleration. It is shown that the AGA (aerogravity assist) maneuver is dynamically unstable with respect to altitude errors. However, this instability can be controlled using feedback linearization. The existence of instability further emphasizes the need for robust guidance during the atmospheric pass.

E

### A95-75725\* National Aeronautics and Space Administration. Langley Research Center, Hampton, VA.

### AERODYNAMICS OF THE SHUTTLE ORBITER AT HIGH ALTITUDES

DIDIER F. G. RAULT National Aeronautics and Space Administration, Langley Research Center, Hampton, VA Journal of Spacecraft and Rockets (ISSN 0022-4650) vol. 31, no. 6 November-December 1994 p. 944-952 refs

(BTN-95-EIX95182617454) Copyright

The high-altitude, high-Knudsen-number aerodynamics of the Shuttle Orbiter are computed from low Earth orbit down to 100 km using three-dimensional direct simulation Monte Carlo and free-molecule codes. Results are compared with the latest Shuttle aerodynamic model, which is based on in-flight accelerometer measurements, and bridging-formula models. Good comparison is observed, except for the normal-force and pitching-moment coefficients. The present results were obtained for a generic Shuttle geometry configuration corresponding to a zero deflection for all control surfaces.

Author (EI)

#### A95-75734

### AERODYNAMIC DESIGN OF PEGASUS: CONCEPT TO FLIGHT WITH COMPUTATIONAL FLUID DYNAMICS

MICHAEL R. MENDENHALL Nielsen Engineering & Research Inc, Mountain View, CA, United States, DANIEL J. LESIEUTRE, STEVEN C. CARUSO, MARNIX F. E. DILLENIUS, and GARY D. KUHN Journal of Spacecraft and Rockets (ISSN 0022-4650) vol. 31, no. 6 November-December 1994 p. 1007-1015 refs (BTN-95-EIX95182617463) Copyright

Pegasus, a three-stage, air-launched, winged space booster, was developed to provide fast and efficient commercial launch services for small satellites. The aerodynamic design and analysis of the vehicle were conducted without wind-tunnel and subscale model testing, using only computational aerodynamic and fluid-dynamic methods. All levels of codes, ranging in complexity from empirical database methods to three-dimensional Navier-Stokes codes, were used in the design. This article describes the design and analysis requirements, the unique and conservative design philosophy, and the analysis methods considered for the various technical areas of interest and concern.

Author (EI)

#### A95-75735

### SOME ASPECTS OF THE AERODYNAMICS OF SEPARATING STRAP-ONS

K. K. BISWAS Vikram Sarabhai Space Cent, Thruvananthapuram, India and C. G. KRISHNAN Journal of Spacecraft and Rockets (ISSN 0022-4650) vol. 31, no. 6 November-December 1994 p. 1016-1020 refs

(BTN-95-EIX95182617464) Copyright

An aerodynamics model for analyzing strap-on separation is proposed. This model comprises both interference aerodynamics and free-body aerodynamics. The interference aerodynamics is

primarily due to the close proximity of core and strap-ons. The free-body aerodynamics is solely due to the body geometry of the strap-ons. Using this aerodynamic model, the dynamics of separating strap-ons has been simulated in a six-degree-of-freedom mode to determine if a collision occurs. This aerodynamic model is very handy for various off-design studies relating to separating strap-ons.

Author (EI)

#### A95-76621

### SHUTTLE ENTRY GUIDANCE REVISITED USING NONLINEAR GEOMETRIC METHODS

KENNETH D. MEASE Univ of California, Irvine, CA, United States and JEAN-PAUL KREMER Journal of Guidance, Control, and Dynamics (ISSN 0731-5090) vol. 17, no. 6 November-December 1994 p. 1350-1356 refs

(BTN-95-EIX95182619144) Copyright

The entry guidance law for the space shuttle orbiter is revisited using nonlinear geometric methods. The shuttle guidance concept is to track a reference drag trajectory that has been designed to lead a specified range and velocity. It is shown that the approach taken in the original derivation of the shuttle entry guidance has much in common with the more recently developed feedback linearization method of differential geometric control. Using the feedback linearization method, however, an alternative, potentially superior, guidance law was formulated. Comparing the two guidance laws based performance domains in state space, taking into account the nonlinear dynamics, the alternative guidance law achieves the desired performance over larger domains in state space; the stability domain of the laws are similar. With larger operating domain for the shuttle or some other entry vehicle, the alternative guidance law should be considered.

#### A95-76758

#### FUEL-OPTIMAL BANK-ANGLE CONTROL FOR LUNAR-RETURN AEROCAPTURE

J. L. MEYER North Carolina State Univ, Raleigh, NC, United States, L. SILVERBERG, and G. D. WALBERG Journal of Spacecraft and Rockets (ISSN 0022-4650) vol. 32, no. 1 January-February 1995 p. 149-155 refs

(BTN-95-EIX95212645706) Copyright

Aerocapture is defined as the deceleration of a spacecraft due to drag produced on it by a planet's atmosphere such that the vehicle is captured into orbit about the planet. This is accomplished by varying the direction of the vehicle's lift vector through bank-angle modulation. This paper examines the application of four optimalcontrol approaches to aerocapture. The first is a minimization of a pseudo fuel cost function, which yields continuous controls. The second is bang-bang control, which minimizes the time associated with bank-angle modulation. Next, an absolute fuel function is minimized, which results in controls in the form of impulses. A fourth approach is a modification to impulsive control, where impulses are approximated by pulses of finite duration. All of the approaches are applied to a single-pass aerocapture problem. The modified impulsive-control approach is applied to a two-pass aerocapture scenario. Recommendations on the practical implementation of these control approaches in the presence of vehicle and atmospheric uncertainties are given. Author (EI)

#### A95-76759

### MINIMUM-MASS DESIGN OF SANDWICH AEROBRAKES FOR A LUNAR TRANSFER VEHICLE

K. N. SHIVAKUMAR North Carolina A&T State Univ, Greensboro, NC, United States and J. C. RIDDICK Journal of Spacecraft and Rockets (ISSN 0022-4650) vol. 32, no. 1 January-February 1995 p. 156-161 refs

(BTN-95-EIX95212645707) Copyright

A structural mass optimization study of a sandwich aerobrake for a lunar transfer vehicle (LTV) was conducted. The proposed spherical aerobrake had a base diameter of 15.2 m and radius of 13.6 m. A hot thermal protection system (TPS) and cold structure were used in the design. Honeycomb sandwich aerobrake structures made up of four

different materials - aluminum alloy, titanium alloy, graphite-epoxy, and graphite-polyimide - were considered. Cases of aerodynamic load, equivalent uniform pressure, and aerodynamic plus thermal load were analyzed. Both linear stress and buckling analyses were conducted for a range of skin and core thicknesses. A graphical optimization procedure was used to determine the skin and core thicknesses of a minimum-mass aerobrake. The design criteria used were material strength, global buckling, and TPS tile deformation. Among them, the TPS deformation criterion was the most critical. The graphite-epoxy aerobrake was the lightest among the four materials studied. Its total mass is about 12.3% of the LTV mass, for supports at 75% span. Equivalent uniform loading produced smaller deformations, stresses, and buckling loads than did the more realistic aerodynamic loading for the same aerobrake configuration. Thermally induced stresses countered the aerodynamically induced stresses and hence had a beneficial effect on the deformation and buckling of the aerobrake. Author (EI)

## N95-23532# Sandia National Labs., Albuquerque, NM. MOVING MASS TRIM CONTROL FOR AEROSPACE VEHICLES

R. D. ROBINETT, B. A. RAINWATER, and S. A. KERR 1994 17 p Presented at the American Institute of Aeronautics and Astronautics Missile Sciences Conference, Monterey, CA, 7-9 Nov. 1994 (Contract(s)/Grant(s): DE-AC04-94AL-85000)

(DE95-002602; SAND-94-2746C; CONF-9411142-4) Avail: CASI HC A03/MF A01

A moving mass trim controller increases the accuracy of axisymmetric, ballistic vehicles. The MMTC is different than other moving mass schemes because it generates an angle-of-attack (AOA) directly from the mass motion. The nonlinear equations of motion for a ballistic vehicle with one moving point mass are derived and provide the basis for a detailed simulation model. The full nonlinear equations are linearized to produce a set of linear, time-varying autopilot equations. These autopilot equations are analyzed and used to develop theoretical design tools for the creation of MMTC's for both fast and slow spinning vehicles. A fast spinning MMTC is designed for a generic artillery rocket that uses principal axis misalignment to generate trim AOA. A slow spinning is designed for a generic reentry vehicle that generates a trim AOA with a center of mass offset and aerodynamic drag. The performance of both MMTC's are evaluated with the detailed simulation.

## N95-23761\*# Honeywell Technology Center, Minneapolis, MN. EMPIRICAL RESULTS ON SCHEDULING AND DYNAMIC BACKTRACKING

MARK S. BODDY and ROBERT P. GOLDMAN In JPL, Third International Symposium on Artificial Intelligence, Robotics, and Automation for Space 1994 p 431-434 Oct. 1994
Avail: CASI HC A01/MF A03

At the Honeywell Technology Center (HTC), we have been working on a scheduling problem related to commercial avionics. This application is large, complex, and hard to solve. To be a little more concrete: 'large' means almost 20,000 activities, 'complex' means several activity types, periodic behavior, and assorted types of temporal constraints, and 'hard to solve' means that we have been unable to eliminate backtracking through the use of search heuristics. At this point, we can generate solutions, where solutions exist, or report failure and sometimes why the system failed. To the best of our knowledge, this is among the largest and most complex scheduling problems to have been solved as a constraint satisfaction problem, at least that has appeared in the published literature. This abstract is a preliminary report on what we have done and how. In the next section, we present our approach to treating scheduling as a constraint satisfaction problem. The following sections present the application in more detail and describe how we solve scheduling problems in the application domain. The implemented system makes use of Ginsberg's Dynamic Backtracking algorithm, with some minor extensions to improve its utility for scheduling. We describe those extensions and the performance of the resulting system. The paper concludes with some general remarks, open questions and plans for future work. Derived from text

N95-23781# Massachusetts Inst. of Tech., Lexington, MA. Lincoin Lab

#### **CALCULATION OF SATELLITE DRAG COEFFICIENTS**

EDWARD M. GAPOSCHKIN 18 Jul. 1994 57 p (Contract(s)/Grant(s): F19628-90-C-0002)

(AD-A285118; MIT-TR-998; ESC-TR-93-293) Avail: CASI HC A04/

MF A01

Calculation of Cd for satellites using accommodation coefficients is reviewed. A phenomenological model for accommodation coefficients due to Hurlbut, Sherman, and Nocilla is used to obtain values for the accommodation coefficients for average satellite materials, thermosphere constituents and temperatures, and satellite velocities using a number of laboratory measurements. There is a significant difference between these results and the traditional method of calculating Cd. These differences contribute as much as 20% error in use of thermosphere models for calculation of satellite

N95-24032\*# Auburn Univ., AL. Dept. of Aerospace Engineering. AERODYNAMIC FLIGHT CONTROL TO INCREASE PAYLOAD CAPABILITY OF FUTURE LAUNCH VEHICLES Final Report, 20 Jan. 1994 - 19 Jan. 1995

JOHN E. COCHRAN, JR. 28 Feb. 1995 9 p

(Contract(s)/Grant(s): NAS8-39131)

(NASA-CR-197704; NAS 1.26:197704) Avail: CASI HC A02/MF A01

The development of new launch vehicles will require that designers use innovative approaches to achieve greater performance in terms of pay load capability. The objective of the work performed under this delivery order was to provide technical assistance to the Contract Officer's Technical Representative (COTR) in the development of ideas and concepts for increasing the payload capability of launch vehicles by incorporating aerodynamic controls. Although aerodynamic controls, such as moveable fins, are currently used on relatively small missiles, the evolution of large launch vehicles has been moving away from aerodynamic control. The COTR reasoned that a closer investigation of the use of aerodynamic controls on large vehicles was warranted. Derived from text

### CHEMISTRY AND MATERIALS

Includes chemistry and materials (general); composite materials; inorganic and physical chemistry; metallic materials; nonmetallic materials; and propellants and fuels.

#### A95-73345

#### MIL-HDBK-5 DESIGN ALLOWABLES FOR FIBRE/METAL LAMINATES: ARALL 2 AND ARALL 3

H. F. WU Alcoa Technical Cent, Alcoa Cent, PA, United States and L. L. WU Journal of Materials Science Letters (ISSN 0261-8028) vol. 13, no. 8 April 15, 1994 p. 582-585 (BTN-94-EIX94371346933) Copyright

Fiber/metal laminates are a new aircraft material showing great potential where both strength and fatigue resistance are required and in certain non-structural application. In view of their comparative weight saving of over 20% in typical applications, fiber/metal laminates can replace monolithic aluminium alloys in over 30% of aircraft structures. Consideration of fiber/metal laminates for aerospace applications will require the generation of these basic strength property design allowables. The work in this article sets a precedent in that fiber/metal laminates represent the first emerging classes of hybrid materials to be incorporated into MIL-HDBK-5 as modified metals.

#### A95-75755 AIRCRAFT STRIPPING AND PAINTING

STUART BIRCH and LINDA E. TREGO Aerospace Engineering (Warrendale, Pennsylvania) (ISSN 0736-2536) January-February 1995 p. 21-23

(BTN-95-EIX95182617810) Copyright

Many researchers are studying different stripping processes and paint that will improve coating duration, decrease maintenance time, and be environmentally friendly. Particularly, FLS Aerospace is assessing two possible solutions for its future needs: Envirostrip, a biodegradable, nontoxic polymer stripper designed to remove paint and primer from metal composites surfaces, and Flashjet, using a dry-ice-particle stream which uses pulse light energy and is fully automated.

#### N95-22689# Oak Ridge National Lab., TN. **EVOLUTION OF OXIDATION AND CREEP DAMAGE MECHANISMS IN HIPED SILICON NITRIDE MATERIALS**

A. A. WERESZCZAK, M. K. FERBER, T. P. KIRKLAND, and K. L. MORE 1994 14 p Presented at the Conference on Plastic Deformation of Ceramics, Snowbird, UT, 7-12 Aug. 1994 (Contract(s)/Grant(s): DE-AC05-84OR-21400)

(DE95-001360; CONF-940865-4) Avail: CASI HC A03/MF A01

Several yttria-fluxed, hot-isostatically pressed (HIPed) silicon nitrides have been tensile creep tested at temperatures representative of gas turbine engines. Creep and oxidation assisted damage mechanisms concurrently evolve when these materials are tested at high temperatures and low stresses (i.e., long exposure times at temperature). Atmospheric creep testing results in creation of oxygen and yttrium gradients across the radial dimension. High concentrations of oxygen and yttrium coincide with dense populations of lenticular-shaped cavities near the surface of crept specimens. The center of the tensile specimens was devoid of oxygen or yttrium; in addition, lenticular cavities were rare. The gradient in lenticularcavity concentration is coincident with the oxygen and yttrium gradients. Stress corrosion cracking (SCC) also occurs in these HIPed silicon nitrides when they are subjected to stress at high temperatures in ambient air. The size of this damage zone increases when the temperature is higher and/or the applied stress is lower. Stress-corrosion cracking initiates at the surface of the tensile specimen and advances radially inwards. What nucleates SCC has not yet been identified, but it is believed to result from a stressconcentrator (e.g., machining damage) at the surface and its growth is a result of coalescence of microcracks and cavities. The higher concentration of oxygen and yttrium in the grain boundaries near the specimen's surface lessens the local high temperature mechanical integrity; this is believed to be associated with the growth of the SCC zone. This SCC zone continues to grow in size during tensile loading until it reaches a critical size which causes fracture. DOF

#### N95-22764# Argonne National Lab., IL. **EVALUATION OF NEUTRON TECHNIQUES FOR ILLICIT** SUBSTANCE DETECTION

C. L. FINK, B. J. MICKLICH, T. J. YULE, P. HUMM, L. SAGALOVSKY, and M. M. MARTIN 1994 5 p Presented at the 13th International Conference on the Application of Accelerators in Research and Industry, Denton, TX, 7-10 Nov. 1994

(Contract(s)/Grant(s): W-31-109-ENG-38)

(DE95-002988; ANL/TD/CP-83462; CONF-941129-9) Avail: CASI HC A01/MF A01

The authors are studying inspection systems based on the use of fast neutrons for detecting illicit substances such as explosives and drugs in luggage and cargo containers. Fast neutron techniques can determine the quantities of light elements such as carbon. nitrogen, and oxygen in a volume element. Illicit substances containing these elements are characterized by distinctive elemental densities or density ratios. They discuss modeling and tomographic reconstruction studies for fast-neutron transmission spectroscopy.

N95-23031\*# Air Force Systems Command, McClellan AFB, CA. Advanced Composites Program Office.

MISHAP RISK CONTROL FOR ADVANCED AEROSPACE/ COMPOSITE MATERIALS

JOHN M. OLSON In NASA. Goddard Space Flight Center, Environmental, Safety, and Health Considerations: Composite Materials in the Aerospace Industry p 107-120 Oct. 1994

Avail: CASI HC A03/MF A03

Although advanced aerospace materials and advanced composites provide outstanding performance, they also present several unique post-mishap environmental, safety, and health concerns. The purpose of this paper is to provide information on some of the unique hazards and concerns associated with these materials when damaged by fire, explosion, or high-energy impact. Additionally, recommended procedures and precautions are addressed as they pertain to all phases of a composite aircraft mishap response, including fire-fighting, investigation, recovery, clean-up, and guidelines are general in nature and not application-specific. The goal of this project is to provide factual and realistic information which can be used to develop consistent and effective procedures and policies to minimize the potential environmental, safety, and health impacts of a composite aircraft mishap response effort.

## N95-23038\*# Air Force Inst. of Tech., Wright-Patterson AFB, OH. MODELING AEROSOL EMISSIONS FROM THE COMBUSTION OF COMPOSITE MATERIALS

J. A. ROOP, D. J. CALDWELL, and K. J. KUHLMANN In NASA. Goddard Space Flight Center, Environmental, Safety, and Health Considerations: Composite Materials in the Aerospace Industry p 219-230 Oct. 1994

Avail: CASI HC A03/MF A03

The use of advanced composite materials (ACM) in the B-2 bomber, composite armored vehicle, and F-22 advanced tactical fighter has rekindled interest concerning the health risk of burned or burning ACM. The objective of this work was to determine smoke production from burning ACM and its toxicity. A commercial version of the UPITT II combustion toxicity method developed at the University of Pittsburgh, and subsequently refined through a US Armyfunded basic research project, was used to established controlled combustion conditions which were selected to evaluate real-world exposure scenarios. Production and yield of toxic species varied with the combustion conditions. Previous work with this method showed that the combustion conditions directly influenced the toxicity of the decomposition products from a variety of materials.

Author

N95-23179\*# Virginia Polytechnic Inst., Blacksburg, VA. Dept. of Engineering Science and Mechanics.

DEVELOPMENT AND VERIFICATION OF A RESIN FILM INFUSION/RESIN TRANSFER MOLDING SIMULATION MODEL FOR FABRICATION OF ADVANCED TEXTILE COMPOSITES Interim Report 99, Jan 1992 - Dec. 1994

JOHN DOUGLAS MACRAE, ALFRED C. LOOS, H. BENSON DEXTER (National Aeronautics and Space Administration. Langley Research Center, Hampton, VA.), JERRY W. DEATON (National Aeronautics and Space Administration. Langley Research Center, Hampton, VA.), and GROGORY H. HASKO (Lockheed Engineering and Sciences Co., Hampton, VA.) Dec. 1994 176 p (Contract(s)/Grant(s): NAG1-343)

(NASA-CR-197439; NAS 1.26:197439; CCMS-95-01; VPI-E-94-09) Avail: CASI HC A09/MF A02

The objective of this study was to develop a two-dimensional computer model for the simulation of the resin transfer molding/resin film infusion processing of advanced composite materials. This computer simulation model is designed to provide aircraft structure and tool designers with a method of predicting the infiltration and curing behavior of a composite material component. For a given specified cure cycle, the computer model can be used to calculate the resin infiltration, resin viscosity, resin advancement, heat transfer within the component/tool assembly during processing and preform compaction. Formulations of the resin flow problem are

given using the finite element/control volume technique based on Darcy's Law of flow through porous media. This technique allows for the efficient numerical calculation of the advancing resin front within the preform materials. The heat transfer in the fabric preform and tooling is analyzed using a transient finite element method which Included the effects of convection on the tooling surfaces. Compaction behavior of the tooling assembly is analyzed using a simplified isotropic form of the plane elasticity equations. All of these solutions were coupled together in a quasi-steady state non-linear fashion inside the computer code. Simulation model verifications were carried out on individual components of the computer model. A verification of the flow model is carried out by a comparison with experiments reported in literature as well as two dimensional visualization studies performed for a center-port injection of a flat plate. The heat transfer model was verified using the experimental results of a thick section composite laminate processing. Verification of the compaction model were limited to the comparison of the final part dimensions. Two computer simulations were performed on two resin infusion cycles of a single blade-stiffened composite panel. The simulation model results of the two cycles were used to assist in the development of an alternative cycle for the composite manufacturing of a three blade stiffened panel. The results demonstrated the importance of a sufficient minimum viscosity region in the cycle in order to allow the resin to completely infiltrate the fabric preform of the structure. Predictions of the viscosities and degree of cure profiles wthin the single blade stiffened panel illustrated the uniformity of these parameters during the curing cycle.

N95-23277\*# lowa State Univ. of Science and Technology, Ames, IA. Dept. of Aerospace Engineering and Engineering Mechanics. IDEALIZED TEXTILE COMPOSITES FOR EXPERIMENTAL/ANALYTICAL CORRELATION Abstract Only

DANIEL O. ADAMS In Hampton Univ., 1994 NASA-HU American Society for Engineering Education (ASEE) Summer Faculty Fellowship Program p 57 Dec. 1994

Avail: CASI HC A01/MF A02

Textile composites are fiber reinforced materials produced by weaving, braiding, knitting, or stitching. These materials offer possible reductions in manufacturing costs compared to conventional laminated composites. Thus, they are attractive candidate materials for aircraft structures. To date, numerous experimental studies have been performed to characterize the mechanical performance of specific textile architectures. Since many materials and architectures are of interest, there is a need for analytical models to predict the mechanical properties of a specific textile composite material. Models of varying sophistication have been proposed based on mechanics of materials, classical laminated plate theory, and the finite element method. These modeling approaches assume an idealized textile architecture and generally consider a single unit cell. Due to randomness of the textile architectures produced using conventional processing techniques, experimental data obtained has been of limited use for verifying the accuracy of these analytical approaches. This research is focused on fabricating woven textile composites with highly aligned and accurately placed fiber tows that closely represent the idealized architectures assumed in analytical models. These idealized textile composites have been fabricated with three types of layer nesting configurations: stacked, diagonal, and split-span. Compression testing results have identified strength variations as a function of nesting. Moire interferometry experiments are being used to determine localized deformations for detailed correlation with model predictions. Author

N95-23300°# Florida Univ., Gainesville, FL. Dept. of Aerospace Engineering, Mechanical and Engineering Science.

INTERLAMINAR SHEAR TEST METHOD DEVELOPMENT FOR LONG TERM DURABILITY TESTING OF COMPOSITES Abstract Only

PETER G. IFJU In Hampton Univ., 1994 NASA-HU American Society for Engineering Education (ASEE) Summer Faculty Fellowship Program p 82 Dec. 1994

Avail: CASI HC A01/MF A02

#### 11 CHEMISTRY AND MATERIALS

The high speed civil transport is a commercial aircraft that is expected to carry 300 passengers at Mach 2.4 over a range of more than 6000 nautical miles. With the existing commercial structural material technology (i.e., aluminum) the performance characteristics of the high speed civil transport would not be realized. Therefore there has been a concerted effort in the development of light weight materials capable of withstanding elevated temperatures for long duration. Thermoplastic composite materials are such candidate materials and the understanding of how these materials perform over the long term under harsh environments is essential to safe and effective design. The matrix dominated properties of thermoplastic composites are most affected by both time and temperature. There is currently an effort to perform short term testing to predict long term behavior of in-plane mechanical properties E22 (transverse modulus of elasticity) and G12 (shear modulus). Out-of-plane properties such as E33, G13, and G23 are inherently more difficult to characterize. This is especially true for the out-of-plane shear modulus G23 and hence there is no existing acceptable standard test method. Since G23 is the most matrix dominated property, it is essential that a test method be developed. A shear test methodology is developed to do just that. The test method, called the double notched specimen, along with the previously developed shear gage was tested at room temperature. Mechanical testing confirmed the attributes of the methodology. A finite element parametric study was conducted for specimen optimization. Moire interferometry, a high sensitivity laser optical method, was used for full-field analysis of the specimen. From this work, material parameters will be determined and thus enable the prediction of long term material behavior of laminates subjected to general loading states. Author (revised)

N95-23496# Advisory Group for Aerospace Research and Development, Neuilly-Sur-Seine (France). Structures and Materials Panel. CORROSION DETECTION AND MANAGEMENT OF ADVANCED AIRFRAME MATERIALS [LA DETECTION DE LA CORROSION ET LA GESTON DES MATERIAUX AVANCES ENTRANT DANS LA CONSTRUCTION DES CELLULES]
Jan. 1995 240 p In ENGLISH and FRENCH Presented at the 79th Meeting of the AGARD Structures and Materials Panel, Seville, Spain, 5-6 Oct. 1994 Original contains color illustrations (AGARD-CP-565; ISBN-92-836-1011-3) Copyright Avail: CASI HC A11/MF A03

A Specialists' Meeting on Corrosion Detection and Management of Advanced Airframe Materials was held to present the current knowledge base of corrosion, degradation, detection and prevention and to identify the research and development issues which must be addressed in order to ensure long service life and low maintenance costs of NATO aircraft. The Meeting concentrated on corrosion detection, test methodology for environmental assessment, mechanistic evaluation, corrosion prevention methods, and materials selection and design to prevent environmental degradation. For individual titles, see N95-23497 through N95-23519.

N95-23497# Defence Research Agency, Farnborough, Hampshire (England). Structural Materials Centre.

### THE CORROSION AND PROTECTION OF ADVANCED ALUMINIUM - LITHIUM AIRFRAME ALLOYS

C. J. E. SMITH, D. L. BARTLETT, and J. A. GRAY In AGARD, Corrosion Detection and Management of Advanced Airframe Materials 9 p Jan. 1995

Copyright Avail: CASI HC A02/MF A03

The corrosion and stress corrosion cracking behavior of 8090-T81 and 2091-T84 sheet and 8090-T8171 plate aluminum-lithium alloys tested under laboratory and marine exposure conditions are compared with aerospace aluminium alloys currently in service. Initial results are also presented on the corrosion performance of a metal matrix composite aluminium alloy. The corrosion protection of aluminium-lithium alloys is discussed and progress on the development of chromate-free systems and their application to advanced aluminium alloys is described.

Author

N95-23500# Naval Air Warfare Center, Warminster, PA. Aircraft

#### CORROSION OF LANDING GEAR STEELS

E. U. LEE, J. KOZOL, J. B. BOODEY, and J. WALDMAN *In* AGARD, Corrosion Detection and Management of Advanced Airframe Materials 12 p Jan. 1995

Copyright Avail: CASI HC A03/MF A03

A study was conducted on the corrosion behavior of landing gear steels, AerMet 100, 300M, AF1410, HYTUF and 4340. This study included investigations of stress corrosion cracking and immersion corrosion in an aqueous 3.5 percent NaCl solution, salt spray corrosion in a fog chamber of atomized aqueous 5 percent NaCl solution, humidity corrosion in an atmosphere of vapor from distilled water and hydrogen embrittlement. AF1410 steel is most resistant to stress corrosion cracking, and it is followed by AerMet 100, 0.20C AF1410, HYTUF, 300M and 4340 steels. The immersion corrosion and salt spray corrosion rates of an AerMet 100 steel are 33-40 percent and 13-20 percent those of a 300M steel. In a humidity chamber, AerMet 100 steel is not corrodible in 110 days, whereas 300M steel is quite susceptible to humidity corrosion. Compared to 300M steel, AerMet 100 steel is less susceptible to hydrogen embrittlement. Author

N95-23508# Belgian Center for Corrosion Study, Brussels (Belgium). Center for Corrosion Study.

#### IN-SITU DETECTION OF SURFACE PASSIVATION OR ACTIVATION AND OF LOCALIZED CORROSION: EXPERIENCES AND PROSPECTIVES IN AIRCRAFT

A. POURBAIX In AGARD, Corrosion Detection and Management of Advanced Airframe Materials 5 p Jan. 1995
Copyright Avail: CASI HC A01/MF A03

The surveillance of the actual conditions of materials in aircrafts and the analysis of the influence of flight or standby conditions require detection methods that give quantitative and instantaneous results and that are related to the real degradation process. Electrochemical methods derived from methods used in laboratory have proven to be of interest. The scientific concepts and the instrumentation are generally easily applicable to field conditions; some effort is necessary to develop relevant sensors. The first example applies to the phosphating of carbon steels before painting. The characterization of surface passivation or reactivity can be of interest before and during the surface conversion processes. The second example applies to the detection of crevice corrosion, as may occur in riveted joints.

N95-23509# Belgian Center for Corrosion Study, Brussels (Belgium). Center for Corrosion Study.

### TEST METHOD AND TEST RESULTS FOR ENVIRONMENTAL ASSESSMENT OF AIRCRAFT MATERIALS

A. POURBAIX In AGARD, Corrosion Detection and Management of Advanced Airframe Materials 4 p Jan. 1995 (Contract(s)/Grant(s): DAJA45-83-C-0011; DAJA45-83-C-0041)

Copyright Avail: CASI HC A01/MF A03

A study was conducted to identify whether life prediction of high strength aluminum alloys for aircrafts can be determined from short term accelerated atmospheric corrosion tests. The method used is a wet and dry method with electrochemical measurements to characterize the formation or destruction of passive layers. The materials tested include high strength steel 4130, precipitation hardening 15-7 Mo-PH steel and aluminum alloys 6061, 7075 and 2024 with different heat treatments and surface conditions. It appears that the ranking of different Al alloys depends on the type of atmosphere (chloride or acid). The method also clearly showed the detrimental effect of chromated cadmium plating on the hydrogen embrittlement of high strength steel. Corrosion processes of aluminum and high strength steels were clearly identified and useful recommendations could be derived from such tests.

N95-23510# Deutsche Aerospace A.G., Munich (Germany).
CORROSION PROTECTION MEASURES FOR CFC/METAL
JOINTS OF FUEL INTEGRAL TANK STRUCTURES OF
ADVANCED MILITARY AIRCRAFT

CLAUS D. HAMM In AGARD, Corrosion Detection and Management of Advanced Airframe Materials 11 p Jan. 1995 Copyright Avail: CASI HC A03/MF A03

Assembly of carbon fiber composites (CFC) and aluminum structures shall be avoided in unprotected conditions. The more noble CFC could cause fatal galvanic corrosion on the aluminum part. Adequate protection methods for electrical isolation of these dissimilar materials shall be adopted. Adhesion of the coatings on both the CFC and aluminum substrate during exposure to the simulated fuel tank environment is an essential requirement for corrosion protection and fuel tightness of the joint. In a sequence of material and functional tests for selection of adequate coatings and associated materials as well as galvanic corrosion and integral tank aspects have been taken into account. Additional to the static panel test for paint adhesion corrosion tests under dynamic loading and corrosive environment were performed. Based on the experience of these investigations the selected combinations of the coatings, sealants and associated materials were applied on structural tank box for final evaluation. This test article represented the section of a fuselage integral fuel tank structure. For simulation of the complete in-service spectrum, during the life of an aircraft structure, static and dynamic loads were induced. The internal tank environment was simulated by water as fuel replacement and by pressurization of the compartment. Resistance of the CFC/aluminum joint to galvanic corrosion and liquid tightness of the selected integral tank concept proved excellent under simulated conditions.

## N95-23513# Air Products and Chemicals, Inc., Allentown, PA. ORGANIC COATING TECHNOLOGY FOR THE PROTECTION OF AIRCRAFT AGAINST CORROSION

CHARLES R. HEGEDUS, STEPHEN J. SPADAFORA, and ANTHONY T. ENG (Naval Air Warfare Center, Warminster, PA.) In AGARD, Corrosion Detection and Management of Advanced Airframe Materials 12 p Jan. 1995 Original contains color illustrations Copyright Avail: CASI HC A03/MF A03

Coating systems on military and commercial aircraft perform a variety of functions. Clearly, the most critical of these is the protection of aircraft structures from environmental degradation. Protective coatings serve as the primary defense against corrosion of aircraft metallic alloys, as well as degradation of other materials such as polymeric composites. Traditional coatings for aircraft include epoxy primers and polyurethane topcoats. Primers normally contain high concentrations of corrosion inhibitors, such as chromates, and they are designed to provide superior adhesion and corrosion protection. Polyurethane topcoats are formulated to enhance protection and durability; they also provide desired optical effects (i.e., anesthetics or camouflage). More recently, alternative coatings have been developed, such as selfpriming topcoats, flexible primers, temporary and multi-functional coatings. These new developments reflect trends in protective coatings technology, changes in aircraft operational requirements/capabilities, and, most dramatically, concerns over environmental protection and worker safety. This issue has created a drive toward coatings with low (possibly zero) concentrations of volatile organic compounds (VOC's) and non-toxic corrosion inhibitors. In turn, these changes have led to concerns over long-term performance, especially protection against corrosion. This paper reviews current organic coatings technology for the protection of aircraft structures and discusses future needs and trends based on advancing technology, environmental concerns, and operational requirements.

N95-23515# Naval Air Warfare Center, Warminster, PA. Aircraft

### CORROSION DETECTION AND MONITORING OF AIRCRAFT STRUCTURES: AN OVERVIEW

V. S. AGARWALA, P. K. BHAGAT (Federal Aviation Administration, Atlantic City, NJ.), and G. L. HARDY (Wright Lab., Wright-Patterson AFB, OH.) In AGARD, Corrosion Detection and Management of

Advanced Airframe Materials 6 p Jan. 1995 Copyright Avail: CASI HC A02/MF A03

Corrosion occurs on both military and civilian aircraft as a result of operation in corrosive environments and utilization of less than optimum corrosion preventive measures during fabrication. For low usage rate systems such as military aircraft, corrosion treatment constitutes a high cost maintenance action because corrosion effects can be life limiting mainly due to the fact that current techniques require extensive material loss for reliable detection of corrosion. For high usage systems such as commercial aircraft. corrosion may constitute a safety problem. A recent study by the U.S. Air Force at Tinker Air Force Base has demonstrated that while off-the-shelf nondestructive inspection equipment has some capability for detecting and quantifying aircraft corrosion, significant improvements in both detection and quantification are still required. Results of this study will be briefly reviewed along with discussions relating to some new and innovative inspection technology for detecting corrosion. New concepts and techniques for corrosion monitoring, i.e., detection of onset of corrosion or breakdown of corrosion protection system, will also be discussed. Advances in electrochemical measurements, thermal imaging, and optical scanning for chemical changes are providing some new research and development opportunities. Finally, concepts relating to damagerevealing chemicals and coatings which may revolutionize the detection and management of corrosion in our systems will be discussed.

#### N95-23516# Deutsche Aerospace A.G., Munich (Germany). EXPERIENCE OF IN-SERVICE CORROSION ON MILITARY AIRCRAFT

H. J. VOSS In AGARD, Corrosion Detection and Management of Advanced Airframe Materials 18 p Jan. 1995
Copyright Avail: CASI HC A03/MF A03

To prevent corrosion of military aircraft the design has to be performed with respect to a careful material selection and an effective surface protection treatment of the materials. Protective treatment on aircraft against moisture, humidity, salty atmosphere, industrial environment, hydraulic fluids, fuel, de-icing fluids, combat chemicals etc. is necessary to meet the operation requirements of the aircraft throughout its operational life. Occurring corrosion detected during maintenance shows that not in every case the requirements above can avoid corrosion problems. This report will show some selected examples of in-service corrosion under investigation of the causes. Inspection and repair methods are shown; further recommendations for corrosion prevention and control to reduce corrosion problems based on practical experiences will be given.

## N95-23517# Naval Air Station, Norfolk, VA. US NAVY OPERATING EXPERIENCE WITH NEW AIRCRAFT CONSTRUCTION MATERIALS

G. T. BROWNE In AGARD, Corrosion Detection and Management of Advanced Airframe Materials 19 p Jan. 1995
Copyright Avail: CASI HC A03/MF A03

This paper addresses the U.S. Navy's experience and problems encountered with new aircraft construction material in the highly corrosive naval operating environment, including: experience with carbon bismaleimide (BMI) and epoxy matrices composite, new aluminum alloys and metal to composite joint repair of honeycomb and monolithic composite structure in fleet activities ashore and afloat; problems experienced with electromagnetic interference (EMI) protection, systems currently in use, and the development of corrosion inhibiting conductive (EMI) sealant; and fastener compatibility for joining carbon composite to metals, H-60 and H-53 helicopter problems, and corrective actions.

## N95-23518# Aerospatiale, Toulouse (France). Avions Div. CORROSION IN SERVICE EXPERIENCE WITH AIRCRAFT IN FRANCE

M. J. FRUSTIE and P. GAUTHIER (CTMS, Toulouse, France.) In AGARD, Corrosion Detection and Management of Advanced Air-

frame Materials 7 p Jan. 1995 In FRENCH Copyright Avail: CASI HC A02/MF A03

The objective of this communication is to present from a comparison of observed corrosions on modern airplanes (Airtbus, ATR) and corrosions on older airplanes (Transall, Caravelli) the progress realized in the control of corrosion, based on the adaption of materials and better performing protection. It's necessary today to adapt the techniques and constraints of the new legislative dispositions concerning the environment which bring to research the new materials and protection system.

N95-23981# Oak Ridge National Lab., TN.

CU DEPOSITION USING A PERMANENT MAGNET ELECTRON CYCLOTRON RESONANCE MICROWAVE PLASMA SOURCE

L. A. BERRY, S. M. GORBATKIN, and R. L. RHOADES 1994 14 p Presented at the International Conference on Metallurgical Coatings and Thin Films, San Diego, CA, 25-29 Apr. 1994

(Contract(s)/Grant(s): DE-AC05-84OR-21400)

(DE94-017768; CONF-940440-5) Avail: CASI HC A03/MF A01

An electron cyclotron resonance (ECR) plasma has been used in conjunction with a solid metal sputter target for Cu deposition over 200-mm diameters. The goal is to develop a deposition process suitable for filling submicron, high aspect ratio features used for ultralarge scale integration. The system uses a permanent magnet for creation of the magnetic field necessary for ECR and is significantly more compact than systems equipped with electromagnets A custom launcher design allows remote microwave injection with the microwave entrance window shielded from the Cu flux. Cu deposition rates up to 100 nm/min were observed and film resistivities were typically in the low to mid 2 micro-ohm-cm range. Based on deposition rate measurements at two radial sample position, uniformities of a few percent over 200-mm diameters should be attainable.

12

#### **ENGINEERING**

Includes engineering (general); communications; electronics and electrical engineering; fluid mechanics and heat transfer; instrumentation and photography; lasers and masers; mechanical engineering; quality assurance and reliability; and structural mechanics.

A95-73439

#### **COMPLIANT INTERLAYER**

G. P. JARRABET Technetics Corp Aerospace Engineering (Warrendale, Pennsylvania) (ISSN 0736-2536) vol. 14, no. 12 December 1994 p. 7-10

(BTN-95-EIX95142562401) Copyright

Although ceramics withstand extremely high temperatures that would destroy most other engineering materials, these are most likely to fail catastrophically; thus, they must be processed and applied carefully to avoid flaws and operating loads that stress them beyond their operating failure. These problems are avoided with the use of a fiber-metal complaint interlayer between the ceramic and the metal, hence reducing thermal cycling stresses that lead to failure. Typical applications include high-temperature gas-turbine engine seals and combustors, and internal-combustion engine components and insulators.

A95-73452

### MECHANICAL SYSTEM RELIABILITY AND RISK ASSESSMENT

T. A. CRUSE Vanderbilt Univ, Nashville, TN, United States, S. MAHADEVAN, Q. HUANG, and S. MEHTA AIAA Journal (ISSN 0001-1452) vol. 32, no. 11 November 1994 p. 2249-2259 refs (BTN-95-EIX95142553046) Copyright

A new methodology is reported for the prediction of the reliability of mechanical structures subject to multiple failure modes, including noncritical damage. The reduction of system reliability due

to accumulated damage is quantitatively estimated by updating the critical system failure states at each level of damage. Correlated design variables are automatically accounted for in the system reliability calculations. Second-order reliability bounds are reported which are unbiased to the ordering of the events. A system risk assessment methodology is also reported that accounts for the cost of multiple types of failure modes and includes the effect of inspection success on reducing the consequences of system failure. Application of the new technology is illustrated for a simplified system model of an aeropropulsion rotor system. However, the methodology is general and is applicable to any engineering system. Author (EI)

A95-73454\* National Aeronautics and Space Administration. Lewis Research Center, Cleveland, OH.

### FLOW STRUCTURE IN THE WAKE OF A WISHBONE VORTEX GENERATOR

B. J. WENDT National Aeronautics and Space Administration, Lewis Research Center, Cleveland, OH and W. R. HINGST AIAA Journal (ISSN 0001-1452) vol. 32, no. 11 November 1994 p. 2234-2240 refs

(BTN-95-EIX95142553044) Copyright

The results of an experimental examination of the vortex structures shed from a low-profile 'wishbone' generator are presented. The vortex generator height relative to the turbulent boundary layer was varied by testing two differently sized models. Measurements of the mean three-dimensional velocity field were conducted in cross-stream planes downstream of the vortex generators. In all cases a counter-rotating vortex pair was observed. Individual vortices were characterized by three descriptors derived from the velocity data: circulation, peak vorticity, and cross-stream location of peak vorticity. Measurements in the cross plane at two axial locations behind the smaller wishbone characterize the downstream development of the vortex pairs. A single region of streamwise velocity deficit is shared by both vortex cores. This is in contrast to conventional generators, where each core coincides with a region of velocity deficit. The measured cross-stream velocities for each case are compared with an Oseen model with matching descriptors. The best comparison occurs with the data from the larger wishbone.

Author (EI)

#### A95-73457

#### SIMULATION OF TURBULENT FLUCTUATIONS

GIOVANNI MENGALI Univ of Pisa, Pisa, Italy and MARCO MICHELI AIAA Journal (ISSN 0001-1452) vol. 32, no. 11 November 1994 p. 2210-2216 refs

(BTN-95-EIX95142553041) Copyright

A simulation technique is used to generate three signals representing the time variation of the velocity components in turbulent flows. This technique makes use of a bank of linear filters driven by non-Gaussian white noises. The filter impulse responses are chosen so as to obtain specified second-order (spectral) characteristics at the filter outputs. Higher order moments can also be accommodated by further specifying the statistical properties of the driving noises. The signals generated in this way may be employed to solve various engineering problems such as, testing the adequacy of measurement methods based on hot-wire anemometry or obtaining gust velocity components suitable for applications in flight simulators.

#### A95-73458

#### MAIN FEATURES OF OVEREXPANDED TRIPLE JETS

GAMAL H. MOUSTAFA Menoufia Univ, Shbien El-Kom, Egypt AlAA Journal (ISSN 0001-1452) vol. 32, no. 11 November 1994 p. 2205-2209 refs

(BTN-95-EIX95142553040) Copyright

The flowfield of an overexpanded triple free jet has been investigated. The flowfield was generated by three Laval nozzles set in a common end wall with equal spacing in a triangular configuration. Total pressure measurements were made for three exit Mach numbers of 1.5, 2, and 2.5 with the range of stagnation pressure from

2.9 to 4.5 atmospheres. The spacing between the nozzles based on the throat diameter was varied as 2.8, 3.6, 4.4, and 6. The triple jet has been compared to a single jet operating at the same initial flow conditions. It is shown that the triple jet in triangular configuration undergoes a transformation in its shape and axis orientation. The triple jet spreads at the base side more than at the top side. The differential spreading rate generates more flow disturbance and, therefore, enhances the mixing process.

Author (EI)

#### A95-73460

### ADAPTIVE FINITE ELEMENT METHOD FOR TURBULENT FLOW NEAR A PROPELLER

DOMINIQUE PELLETIER Ecole Polytechnique de Montreal, Montreal, Que, Canada, FLORIN ILINCA, and JEAN-FRANCOIS HETU AIAA Journal (ISSN 0001-1452) vol. 32, no. 11 November 1994 p. 2186-2193 refs

(BTN-95-EIX95142553038) Copyright

This paper presents an adaptive finite element method based on remeshing to solve incompressible turbulent free shear flow near a propeller. Solutions are obtained in primitive variables using a highly accurate finite element approximation on unstructured grids. Turbulence is modeled by a mixing length formulation. Two general purpose error estimators, which take into account swirl and the variation of the eddy viscosity, are presented and applied to the turbulent wake of a propeller. Predictions compare well with experimental measurements. The proposed adaptive scheme is robust, reliable and cost effective.

Author (EI)

#### A95-73477

### SHOCK TUNNEL MEASUREMENTS OF HYPERVELOCITY BLUNTED CONE DRAG

L. M. PORTER Univ of Queensland, St. Lucia, Australia, A. PAULL, D. J. MEE, and J. M. SIMMONS AIAA Journal (ISSN 0001-1452) vol. 32, no. 12 December 1994 p. 2476-2477 refs (BTN-95-EIX95152577606) Copyright

Presented here are results obtained from an investigation into the effects of nose bluntness on slender cone drag in the hypervelocity flight regime. The results indicate that, for small cone angles, the drag of a blunt cone is reasonably well predicted by the Newtonian sine-square law modified for blunt bodies. This suggests the absence of any real gas effects on the total drag. The effect of nose bluntness at the smaller bluntness ratios is relatively small. This is encouraging for the design of a hypervelocity space plane or a centerbody for an axisymmetric scramjet where a slightly blunted nose is required to reduce stagnation point heating.

#### Δ95-73479

### EFFECTS OF SPATIAL ORDER OF ACCURACY ON THE COMPUTATION OF VORTICAL FLOWFIELDS

J. A. EKATERINARIS Navy-NASA Joint Inst of Aeronautics, Moffett Field, CA, United States AIAA Journal (ISSN 0001-1452) vol. 32, no. 12 December 1994 p. 2471-2474 refs (BTN-95-EIX95152577604) Copyright

A high-order accurate method on general curvilinear meshes was used to improve the numerical solutions of complex, three-dimensional, vortical flowfields over a sharp-edged double-delta wing at high incidence. The inviscid fluxes computed from the flowfield were evaluated using third-, fourth-, and fifth-order upwind-brased formulas. Result showed that a higher order of accuracy enables better convection of vorticity, yields stronger vortices, and produces closer agreement with the measured surface pressures.

#### A95-73486

### EIGENANALYSIS OF UNSTEADY FLOWS ABOUT AIRFOILS, CASCADES, AND WINGS

KENNETH C. HALL Duke Univ, Durham, NC, United States AIAA Journal (ISSN 0001-1452) vol. 32, no. 12 December 1994 p. 2426-2432 refs

(BTN-95-EIX95152577597) Copyright

A general technique for constructing reduced order models of

unsteady aerodynamic flows about two-dimensional isolated airfoils, cascades of airfoils, and three-dimensional wings is developed. The starting point is a time domain computational model of the unsteady small disturbance flow. For illustration purposes, we apply the technique to an unsteady incompressible vortex lattice model. The eigenmodes of the system, which may be though of as aerodynamic states, are computed and subsequently used to construct computationally efficient, reduced order models of the unsteady flowfield. Only a handful of the most dominant eigenmodes are retained in the reduced order model. The effect of the remaining eigenmodes is included approximately using a static correction technique. An important advantage of the present method is that once the eigenmode information has been computed, reduced order models can be constructed for any number of arbitrary modes of airfoil motion very inexpensively. Numerical examples are presented that demonstrate the accuracy and computational efficiency of the present method. Finally, we show how the reduced order model may be incorporated into an aeroelastic flutter model.

Author (EI)

#### A95-73498

### DEVELOPMENT OF AERONAUTICAL MOBILE SATELLITE SERVICES OVER THE PAST THIRTY YEARS

GUANGREN CHEN Civil Aviation Inst of China, Tianjin, China and FUQIN XIONG IEEE Aerospace and Electronic Systems Magazine (ISSN 0885-8985) vol. 9, no. 12 December 1994 p. 25-36 refs (BTN-95-EIX95152569458) Copyright

This paper presents an overview of the development of aeronautical mobile satellite services (AMSS) over the past 30 years. The inherent shortcomings of present air-ground HF communications have hindered the development of civil aviation, but according to the Future Air Navigation Systems (FANS) concept aeronautical satellite communication - including Automatic Dependent Surveillance (ADS) - will be the key to eliminating the shortcomings of HF communication systems. Satellite-based communication and surveillance will significantly improve air traffic control (ATC) over the oceanic and remote terrestrial airspace, and it will benefit civil aviation authorities, airlines as well as passengers. This paper discusses the availability of system elements, and world wide trials, demonstrations and preoperational use of aeronautical satellite communications over past years are described. Future satellite systems possible for aeronautical communications are also discussed. Author (EI)

#### A95-73551

### HYPERSONIC RAREFIED FLOW PAST SPHERES INCLUDING WAKE STRUCTURE

VIRENDRA K. DOGRA VIGYAN, Inc, Hampton, VA, United States, JAMES N. MOSS, RICHARD G. WILMOTH, and JOSEPH M. PRICE Journal of Spacecraft and Rockets (ISSN 0022-4650) vol. 31, no. 5 September-October 1994 p. 713-718 refs (BTN-95-EIX95152583250) Copyright

Results of a numerical study using the direct simulation Monte Carlo method are presented for hypersonic rarefied flow past spheres. The flow conditions considered are those corresponding to low-density wind-tunnel test conditions. The set of the experimental conditions for the calculations encompasses the transitional to near-continuum flow regimes. Comparison of the calculated drag with experimental results shows good agreement to well within the experimental error. Particular attention is focused on the wake structure. Calculations show that the wake is very rarefied with considerable thermal nonequilibrium for all the cases considered. No flow separation is observed in the wake for the near-continuum case where a vortex has been predicted by Navier-Stokes-type calculations.

A95-73553\* National Aeronautics and Space Administration. Ames Research Center, Moffett Field, CA.

### HYPERSONIC NONEQUILIBRIUM NAVIER-STOKES SOLUTIONS OVER AN ABLATING GRAPHITE NOSETIP

Y.-K. CHEN National Aeronautics and Space Administration, Ames

Research Center, Moffett Field, CA and W. D. HENLINE Journal of Spacecraft and Rockets (ISSN 0022-4650) vol.31, no. 5 September-October 1994 p. 728-734 refs

(BTN-95-EIX95152583252) Copyright

The general boundary conditions, including mass and energy balances, of chemically equilibrated or nonequilibrated gas adjacent to ablating surfaces have been derived. A computer procedure based on these conditions was developed and interfaced with the Navier-Stokes solver GASP (General Aerodynamics Simulation Program). A test case with a proposed hypersonic test-vehicle configuration and associated freestream conditions was developed. The solutions of the GASP code with various surface boundary conditions were obtained and compared with those of the ASCC (ABRES Shape Change) code, and the effect of nonequilibrium gas as well as surface chemistry on surface heating and ablation rate were examined.

A95-73554\* National Aeronautics and Space Administration. Ames Research Center, Moffett Field, CA.

#### HYPERSONIC CONVECTIVE HEAT TRANSFER OVER 140-DEG BLUNT CONES IN DIFFERENT GASES

D. A. STEWART National Aeronautics and Space Administration, Ames Research Center, Moffett Field, CA and Y. K. CHEN Journal of Spacecraft and Rockets (ISSN 0022-4650) vol. 31, no. 5 September-October 1994 p. 735-743 refs (BTN-95-EIX95152583253) Copyright

Large-angle blunt cones, with various corner radii, were tested in dissociated air, CO2, and CO2-Ar gas mixtures. These experiments were conducted at angles of attack from 0 to 20 deg. The heating distribution data and how shock-waved geometry were obtained during the cone's exposure to the three gases. The data can be used to partially validate two-dimensional (2-D) axisymmetric and three-dimensional Navier-Stokes solutions of the heating distribution over a 140-deg blunt cone in a simulated Martian atmosphere. The predicted heating distribution over the cones and estimated bow shock standoff distances using a 2-D axisymmetric Navier-Stokes code were compared with test data taken at zero angle of attack.

Author (EI)

A95-73555\* National Aeronautics and Space Administration. Langley Research Center, Hampton, VA.

### APPLICATION OF THE MULTIGRID SOLUTION TECHNIQUE TO HYPERSONIC ENTRY VEHICLES

FRANCIS A. GREENE National Aeronautics and Space Administration, Langley Research Center, Hampton, VA Journal of Spacecraft and Rockets (ISSN 0022-4650) vol. 31, no. 5 September-October 1994 p. 744-750 refs

(BTN-95-EIX95152583254) Copyright

Multigrid techniques have been incorporated into an existing hypersonic flow analysis code, the Langley aerothermodynamic upwind relaxation algorithm. The multigrid scheme is based on the full approximation storage approach and uses full multigrid to obtain a well-defined fine-mesh starting solution. Predictions were obtained using standard transfer operators, and a V cycle was used to control grid sequencing. Computed hypersonic flow solutions, compared with experimental data for a 15-deg blunted sphere-cone and a blended-wing body, are presented. It is shown that the algorithm predicts heating rates accurately, and computes solutions in one-third the computational time of the nonmultigrid algorithm.

A95-73556\* National Aeronautics and Space Administration. Langley Research Center, Hampton, VA.

### HIGHER-ORDER VISCOUS SHOCK-LAYER SOLUTIONS FOR HIGH-ALTITUDE FLOWS

ROOP N. GUPTA National Aeronautics and Space Administration, Langley Research Center, Hampton, VA, ERNEST V. ZOBY, SUDHEER N. NAYANI, and KAM-PUI LEE Journal of Spacecraft and Rockets (ISSN 0022-4650) vol. 31, no. 5 September-October 1994 p. 751-758 refs

(BTN-95-EIX95152583255) Copyright

A higher-order viscous-shock-layer method has been developed and is used to obtain physically consistent results under varying degrees of low-density conditions for perfect-gas and

nonequilibrium flows past slender bodies. The method of solution is a spatial-marching, implicit finite-difference technique, which employs a Vigneron pressure condition in the subsonic nose region. Higher-order body and shock slip conditions are employed with the method to obtain solutions for the low-density flows. Detailed comparisons with the direct simulation Monte Carlo method and Navier-Stokes calculations clearly show that the higher-order terms included in the HVSL equations are required to predict comparable values of surface pressure and heat transfer rate at higher altitude. The deficiency of the standard viscous shock-layer method in predicting low-density flows can not be corrected by the slip conditions alone as considered by earlier researchers. Author (EI)

#### A95-73584

### SUPERSONIC AXISYMMETRIC CONICAL FLOW SOLUTIONS FOR DIFFERENT RATIOS OF SPECIFIC HEATS

BHAVESH B. PATEL Mississippi State Univ, Mississippi State, MS, United States, B. K. HODGE, and KEITH KOENIG Journal of Spacecraft and Rockets (ISSN 0022-4650) vol. 31, no. 5 September-October 1994 p. 918-920 refs (BTN-95-EIX95152583283) Copyright

The aim of this study is to summarize the salient behavioural characteristics of calorically perfect conical supersonic flows for different values of the ratio of specific heats. Although the computation of the conical flow is relatively straightforward, some effort is required to assemble a useful set of information for a variety of values of gamma. Over the range of ratio of specific heats, 1.0(+) less than gamma less than 1.67, the characteristics demonstrate considerable variations.

#### A95-74496

### SEM REPRESENTATION OF THE EARLY AND LATE TIME FIELDS SCATTERED FROM WIRE TARGETS

MICHAEL A. RICHARDS Nichols Research Corp, Shalimar, FL, United States IEEE Transactions on Antennas and Propagation (ISSN 0018-926X) vol. 42, no. 4 April 1994 p. 564-566 refs (BTN-94-EIX94381353142) Copyright

In this communication, the singularity expansion method (SEM) is used to express the field scattered from an arbitrary thin-wire target. Explicit expressions are given for both the class-1 and class-2 representations of the scattered field due to step excitations. Numerical results are given for the early-time transient fields scattered from both a straight wire and a simple swept-wing aircraft model. The results of the SEM computations are compared to fields obtained by Fourier inversion techniques. It is shown that the class-2 representation yields a significant improvement over the class-1 result during the early-time interval, albeit at the expense of a more complex computation.

#### A95-74612

#### FINITE ELEMENT MODEL FOR A FLEXIBLE NON-SYMMETRIC ROTOR ON DISTRIBUTED BEARING: A STABILITY STUDY

A. G. TAYLOR Univ of Alberta, Edmonton, Alberta, Canada and A. CRAGGS Journal of Sound and Vibration (ISSN 0022-460X) vol. 173, no. 1 May 26, 1994 p. 1-21 refs (BTN-94-EIX94381352212) Copyright

A finite element model is presented for a flexible, non-axisymmetric shaft-rotor system supported in distributed bearings. The stability of this model is analyzed over a normal rotation speed range and the results are compared with analytical and numerical studies carried out on rigid and simpler flexible models. The same types of regions of instabilities are found for the finite element, flexible shaft-rotor model, and the role of shear deflection is particularly significant in one of the mechanisms.

Author (EI)

#### A95-74702

### TRANSIENT ANALYSIS OF A CRACKED ROTOR PASSING THROUGH CRITICAL SPEED

A. S. SEKHAR Indian Inst of Technology Madras, Madras, India and B. S. PRABHU Journal of Sound and Vibration (ISSN 0022-460X)

vol. 173, no. 3 June 9, 1994 p. 415-421 refs (BTN-94-EIX94401360022) Copyright

The past several years have seen growing interest in the dynamic behavior of rotor bearing systems with cracked shafts. Vibration monitoring is considered as a possible means of detecting the presence of growth of cracks, which can otherwise lead to catastrophic failure. The transient vibration response of a cracked rotor passing through its critical speed is analyzed in the context of crack detection and monitoring.

#### A95-75516

# FATIGUE STRENGTH OF HIGH-TEMPERATURE ALLOYS UNDER CONDITIONS OF CYCLIC TEMPERATURE VARIATION. COMMUNICATION 1: EXPERIMENTAL PROCEDURE AND RESULTS

V. T. TROSHCHENKO Inst Problem Prochnosti AN Ukrainy, Kiev, Ukraine, B. A. GRYAZNOV, and YU. B. YAMSHANOV Problemy Prochnosti (ISSN 0556-171X) no. 3 March 1994 p. 13-20 In RUSSIAN refs

(BTN-94-EIX94401363884) Copyright

Determination of the serviceability of the material of gasturbine engine blades, one of the most loaded elements of the engine, critical for the reliability of the turbine, is discussed. The NUM-3 setup, intended for studying fatigue strength of high-temperature alloys under conditions simulating service ones, is briefly described. The results of the investigation into the fatigue of alloys EP962 and El698 under isothermal conditions and complex thermal-mechanical loading are presented. The analysis of the findings revealed a number of regularities in the effect of thermal cycling and resulting varying thermal stresses on the fatigue strength of the materials studied.

#### A95-75760

### NUMERICAL STUDY OF SOUND GENERATION DUE TO A SPINNING VORTEX PAIR

DUCK JOO LEE Korea Advanced Inst of Science and Technology, Taejon, Korea, Republic of and SAM OK KOO AIAA Journal (ISSN 0001-1452) vol. 33, no. 1 January 1995 p. 20-26 refs (BTN-95-EIX95182619075) Copyright

A numerical approach for the calculation of an acoustic field is applied to the case of a spinning vortex pair to investigate the sound generation by quadrupole sources in unsteady vortical flows. Based on the unsteady hydrodynamic information from the known incompressible flowfield, the perturbed compressible acoustic terms derived from the Euler equations are calculated. Nonreflecting boundary conditions are developed to obtain highly stable solutions. Calculated results are compared with analytical solutions obtained by the method of matched asymptotic expansions. The possibility of predicting the effect of convective mean flow is also tested. It is concluded that the sound generated by the quadrupole sources of unsteady vortical flows without a sound-generating body or surface can be calculated by using the source terms of hydrodynamic flow fluctuations.

Author (EI)

#### A95-75762

### APPLICATION OF WALL FUNCTIONS TO GENERALIZED NONORTHOGONAL CURVILINEAR COORDINATE SYSTEMS

DOUGLAS L. SONDAK United Technologies Research Cent, East Hartford, CT, United States and RICHARD H. PLETCHER AIAA Journal (ISSN 0001-1452) vol. 33, no. 1 January 1995 p. 33-41 refs

(BTN-95-EIX95182619077) Copyright

A method has been developed for the application of wall functions to generalized curvilinear coordinate systems with nonorthogonal grids. Two test cases have been computed using this method with the k-epsilon turbulence model: flow over a flat plate at 0-deg angle of attack using a nonorthogonal grid at the wall and flow over a prolate hemispheroid with a hemispherical nose cap at 0-deg angle of attack. All results are compared with experimental data. In addition, the hemispheroid results are compared with computations

using the Baldwin-Lomax algebraic turbulence model and the Chien low-Reynolds-number k-epsilon turbulence model. Author (EI)

A95-76484° National Aeronautics and Space Administration. Langley Research Center, Hampton, VA.

## MULTIGRID SOLUTION OF COMPRESSIBLE TURBULENT FLOW ON UNSTRUCTURED MESHES USING A TWO-EQUATION MODEL

D. J. MAVRIPLIS National Aeronautics and Space Administration Langley Research Center, Hampton, VA, United States and L. MATINELLI International Journal for Numerical Methods in Fluids (ISSN 0271-2091) vol. 18, no. 10 May 30, 1994 p. 887-914 refs (BTN-94-EIX94401378794) Copyright

The steady state solution of the system of equations consisting of the full Navier-Stokes equations and two turbulence equations has been obtained using a multigrid strategy of unstructured meshes. The flow equations and turbulence equations are solved in a loosely coupled manner. The flow equations are advanced in time using a multistage Runge-Kutta time-stepping scheme with a stability-bound local time step, while turbulence equations are advanced in a point-implicit scheme with a time step which guarantees stability and positivity. Low-Reynolds-number modifications to the original two-equation model are incorporated in a manner which results in well-behaved equations for arbitrarily small wall distances. A variety of aerodynamic flows are solved, initializing all quantities with uniform freestream values. Rapid and uniform convergence rates for the flow and turbulence equations are observed.

#### A95-76489

## INFLUENCE OF STREAMWISE CURVATURE ON LONGITUDINAL VORTICES IMBEDDED IN TURBULENT BOUNDARY LAYERS

W. J. KIM Univ of Iowa, Iowa City, IA, United States and V. C. PATEL Computers & Fluids (ISSN 0045-7930) vol. 23, no. 5 June 1994 p. 647-673 refs

(BTN-94-EIX94401378820) Copyright

Numerical experiments were conducted to study the fate of artificially introduced vortex pairs in an otherwise two-dimensional turbulent boundary layer, with emphasis on the influence of streamwise surface curvature. The Reynolds-averaged Navier-Stokes equations for three-dimensional turbulent flows, together with a two-layer turbulence model to resolve the near-wall flow, were solved by a numerical method for a configuration for which some measurements are available from recent experiments.

#### A95-76491

### GRID REFINEMENT TEST OF TIME-PERIODIC FLOWS OVER BLUFF BODIES

MOSHE ROSENFELD Tel Aviv Univ, Tel Aviv, Israel Computers & Fluids (ISSN 0045-7930) vol. 23, no. 5 June 1994 p. 693-709 refs (BTN-94-EIX94401378822) Copyright

A grid refinement study of the time-periodic flow over a circular cylinder at Re = 200 is presented. An efficient numerical solution method of the time-dependent incompressible Navier-Stokes equations allowed the solution of the problem on several meshes up to 513 x 513 points. The time-periodic solution was presented in the frequency domain by expanding it into a Fourier series in time. The dependence of the solution on the mesh size has been studied both in the physical and Fourier domains. In the physical domain, very fine meshes are needed to obtain a spatially converged solution, i.e. a solution that varies with the mesh size as the spatial accuracy of the scheme.

#### A95-76585

### SIMULATING HEAT ADDITION VIA MASS ADDITION IN CONSTANT AREA COMPRESSIBLE FLOWS

W. H. HEISER U.S. Air Force Acad, CO, United States, W. B. MCCLURE, and C. W. WOOD AIAA Journal (ISSN 0001-1452) vol. 33, no. 1 January 1995 p. 167-171 refs (BTN-95-EIX95182619100) Copyright

#### 12 ENGINEERING

A study conducted demonstrated the striking similarity between the influence of heat addition and mass addition on compressible flows. These results encourage the belief that relatively modest laboratory experiments employing mass addition can be devised that will reproduce the leading phenomena of heat addition, such as the axial variation of properties, choking, and wall-boundary-layer separation. These suggest that some aspects of the complex behavior of dual-mode ramjet/scramjet combustors could be experimentally evaluated or demonstrated by replacing combustion with less expensive, more easily controlled, and safer mass addition.

NEL

#### A95-76586

### EFFECT OF AMBIENT TURBULENCE INTENSITY ON SPHERE WAKES AT INTERMEDIATE REYNOLDS NUMBERS

J.-S. WU Univ of Michigan, Ann Arbor, MI, United States and G. M. FAETH AIAA Journal (ISSN 0001-1452) vol. 33, no. 1 January 1995 p. 171-173 refs

(BTN-95-EIX95182619101) Copyright

In order to resolve the effects of ambient turbulence intensity variations on sphere wakes at intermediate Reynolds numbers (Re = 125-1560), the effect of Re on vortex shedding, the mean streamwise velocities, and the effects of vortex shedding, wake turbulence, and ambient turbulence on effective turbulent viscosities have been determined.

#### A95-76647

#### TRACKING OF RAINDROPS IN FLOW OVER AN AIRFOIL

JAMES R. VALENTINE Univ of Utah, Salt Lake City, UT, United States and RAND A. DECKER Journal of Aircraft (ISSN 0021-8669) vol. 32, no. 1 January-February 1995 p. 100-105 refs (BTN-95-EIX95182619221) Copyright

The splashback that occurs when raindrops impact an airfoil results in an 'ejecta fog' of small droplets near the leading edge. Acceleration of these droplets by the air flowfield is a momentum sink for the airflow and has been hypothesized to contribute to the degradation of airfoil performance in heavy rain. Presented here is a one-way coupled Lagrangian particle tracking scheme to evaluate droplet concentrations and the associated momentum sink around a NACA 64-210 airfoil section for three rainfall rates. A laminar air flowfield is determined with a standard CFD code and is used as input to the particle tracking algorithm. Raindrops are assumed to be noninteracting, nondeforming, nonevaporating, and nonspinning spheres, and are tracked through the same curvilinear grid used by the airflow code. A simple model is used to simulate impacts and the resulting splashback on the airfoil surface.

### A95-76652

### NATURAL LAMINAR FLOW WING CONCEPT FOR SUPERSONIC TRANSPORTS

BERRY T. GIBSON Northrop Grumman Corp, Pico Rivera, CA, United States and HEINZ A. GERHARDT Journal of Aircraft (ISSN 0021-8669) vol. 32, no. 1 January-February 1995 p. 130-136 refs (BTN-95-EIX95182619226) Copyright

A 'reverse' delta wing, having a straight leading edge and forward-swept trailing edges, is shown to be capable of achieving extended runs of natural laminar flow during supersonic flight. Euler calculations at supersonic Mach number confirm that the flow over a reverse delta wing is nominally two dimensional, in contrast to delta wing flow that exhibits large spanwise flow gradients, particularly near the leading edge. The data suggest that crossflow and attachment line instabilities, the primary modes of transition on swept wings, are minimal on a reverse delta wing. Predicted forces on 2% thick delta wings are in accord with the principles of reciprocal flow theory because lift-curve slope, wave drag, and drag-due-to-lift are nearly identical. The reverse delta wing has a large aerodynamic center shift as Mach number increases from subsonic to supersonic. Subsonic wind-tunnel tests were conducted with a variety of leading-

and trailing-edge flap planforms to assess the longitudinal characteristics of a reverse delta wing. The experimental data show that leading-edge flaps are highly effective at increasing maximum lift and decreasing drag at moderate angles of attack. Trailing-edge flaps were up to 90% as effective as delta wing flaps in generating untrimmed lift increments.

Author (EI)

#### A95-76658

### NEURAL NETWORK PREDICTION OF THREE-DIMENSIONAL UNSTEADY SEPARATED FLOWFIELDS

SCOTT J. SCHRECK U.S. Air Force Acad, CO, United States, WILLIAM E. FALLER, and MARVIN W. LUTTGES Journal of Aircraft (ISSN 0021-8669) vol. 32, no. 1 January-February 1995 p. 178-185 refs

(BTN-95-EIX95182619232) Copyright

Unsteady surface pressures were measured on a wing pitching beyond static stall. Surface pressure measurements confirmed that the pitching wing generated a rapidly evolving, three-dimensional unsteady surface pressure field. Using these data, both linear and nonlinear neural networks were developed. A novel quasilinear activation function enabled extraction of a linear equation system from the weight matrices of the linear network. This equation set was used to predict unsteady surface pressures and unsteady aerodynamic loads. Neural network predictions were compared directly to measured surface pressures and aerodynamic loads. The neural network accurately predicted both temporal and spatial variations for the unsteady separated flowfield as well as for the aerodynamic loads. Consistent results were obtained using either the linear or nonlinear neural network. In addition, fluid mechanics modeled by the linear equation set were consistent with established vorticity dynamics principles. Author (EI)

A95-76660\* National Aeronautics and Space Administration. Ames Research Center, Moffett Field, CA.

### CFD OPTIMIZATION OF A THEORETICAL MINIMUM-DRAG BODY

SAMSON CHEUNG National Aeronautics and Space Administration, Ames Research Center, Moffett Field, CA, PHILIP AARONSON, and THOMAS EDWARDS Journal of Aircraft (ISSN 0021-8669) vol. 32, no. 1 January-February 1995 p. 193-198 refs (BTN-95-EIX95182619234) Copyright

This article describes a methodology behind coupling a fast, parabolized Navier-Stokes flow solver to a nonlinear constrained optimizer. The design parameters, constraints, grid refinement, behavior of the optimizer, and flow physics related to the CFD calculations are discussed. Pressure drag reduction in the supersonic regime of a theoretical minimum-drag body of revolution is performed. Careful selection of design variables allows the optimization process to improve the aerodynamic performance. A calculation including nonlinear and viscous effects produces a different minimum drag geometry than linear theory and results in a drag reduction of approximately 4%. Effect of grid density on the optimization process is also studied. In order to obtain accurate optimization results, CFD calculations must model physical phenomena that contribute to the optimization parameters.

#### A95-76686

### DESCRIPTION OF A GNSS AVAILABILITY MODEL AND ITS USE IN DEVELOPING REQUIREMENTS

WALTER A. POOR MITRE Corp, McLean, VA, United States IEEE Transactions on Aerospace and Electronic Systems (ISSN 0018-9251) vol. 31, no. 1 January 1995 p. 436-446 refs (BTN-95-EIX95-02637603) Copyright

(BTN-95-EIX95202637603) Copyright
The Global Navigation Satellite System (GNSS) Air Traffic
Operations Model (GATOM) calculates a variety of statistical measures of the required services at locations specified by the user. A
description of the current version of the model is presented. Results
of the analysis which addresses Global Positioning System (GPS)
constellations of 24 to 32 satellites as well as augmentation with

baro-altimeter and geostationary satellites conducted with respect to availability during category 1 and nonprecision approaches, are discussed.

N95-22481\*# Eloret Corp., Palo Alto, CA. PARTICLE KINETIC SIMULATION OF HIGH ALTITUDE HYPERVELOCITY FLIGHT Report, 1 Jan. 1989 - 31 Jan. 1994 IAIN BOYD and BRIAN L. HAAS 19 Apr. 1994 9 p (Contract(s)/Grant(s): NCC2-582) (NASA-CR-197383; NAS 1.26:197383) Avail: CASI HC A02/MF

A01 Rarefied flows about hypersonic vehicles entering the upper

atmosphere or through nozzles expanding into a near vacuum may only be simulated accurately with a direct simulation Monte Carlo (DSMC) method. Under this grant, researchers enhanced the models employed in the DSMC method and performed simulations in support of existing NASA projects or missions. DSMC models were developed and validated for simulating rotational, vibrational, and chemical relaxation in high-temperature flows, including effects of quantized anharmonic oscillators and temperature-dependent relaxation rates. State-of-the-art advancements were made in simulating coupled vibration - dissociation - recombination for post-shock flows. Models were also developed to compute vehicle surface temperatures directly in the code rather than requiring isothermal estimates. These codes were instrumental in simulating aerobraking of NASA's Magellan spacecraft during orbital maneuvers to assess heat transfer and aerodynamic properties of the delicate satellite. NASA also depended upon simulations of entry of the Galileo probe into the atmosphere of Jupiter to provide drag and flow field information essential for accurate interpretation of an onboard experiment. Finally, the codes have been used extensively to simulate expanding nozzle flows in low-power thrusters in support of propulsion activities at NASA-Lewis. Detailed comparisons between continuum calculations and DSMC results helped to quantify the limitations of continuum CFD codes in rarefied applications.

N95-22669\*# National Aeronautics and Space Administration. Lewis Research Center, Cleveland, OH.

#### ADDITIONAL IMPROVEMENTS TO THE NASA LEWIS ICE **ACCRETION CODE LEWICE**

WILLIAM B. WRIGHT (NYMA, Inc., Brook Park, OH.) and COLIN S. BIDWELL Mar. 1995 14 p Presented at the 33rd Aerospace Sciences Meeting and Exhibit, Reno, NV, 9-12 Jan. 1995; sponsored byAIAA

(Contract(s)/Grant(s): NAS3-27186: RTOP 505-68-10)

(NASA-TM-106849; E-9425; NAS 1.15:106849; AIAA PAPER 95-0752) Avail: CASI HC A03/MF A01

Due to the feedback of the user community, three major features have been added to the NASA Lewis ice accretion code LEWICE. These features include: first, further improvements to the numerics of the code so that more time steps can be run and so that the code is more stable; second, inclusion and refinement of the roughness prediction model described in an earlier paper; third, inclusion of multi-element trajectory and ice accretion capabilities to LEWICE. This paper will describe each of these advancements in full and make comparisons with the experimental data available. Further refinement of these features and inclusion of additional features will be performed as more feedback is received.

N95-22804\*# National Aeronautics and Space Administration. Ames Research Center, Moffett Field, CA.

#### NONLINEAR SYSTEM GUIDANCE IN THE PRESENCE OF TRANSMISSION ZERO DYNAMICS

G. MEYER, L. R. HUNT, and R. SU Jan. 1995 42 p

(Contract(s)/Grant(s): RTOP 505-64-52)

(NASA-TM-4661; A-95014; NAS 1.15:4661) Avail: CASI HC A03/

An iterative procedure is proposed for computing the commanded state trajectories and controls that guide a possibly multiaxis. time-varying, nonlinear system with transmission zero dynamics through a given arbitrary sequence of control points. The procedure

is initialized by the system inverse with the transmission zero effects nulled out. Then the 'steady state' solution of the perturbation model with the transmission zero dynamics intact is computed and used to correct the initial zero-free solution. Both time domain and frequency domain methods are presented for computing the steady state solutions of the possibly nonminimum phase transmission zero dynamics. The proce-dure is illustrated by means of linear and nonlinear examples. Author

N95-23015\*# National Aeronautics and Space Administration. Langley Research Center, Hampton, VA.

#### MACH 10 COMPUTATIONAL STUDY OF A THREE-**DIMENSIONAL SCRAMJET INLET FLOW FIELD**

SCOTT D. HOLLAND Mar. 1995 32 p (Contract(s)/Grant(s): RTOP 506-40-41-02)

(NASA-TM-4602; L-17348; NAS 1.15:4602) Avail: CASI HC A03/ MF A01

The present work documents the computational results for a combined computational and experimental parametric study of the internal aerodynamics of a generic three-dimensional sidewallcompression scramjet inlet configuration at Mach 10. The threedimensional Navier-Stokes code SCRAMIN was chosen for the computational portion of the study because it uses a well-known and well-proven numerical scheme and has shown favorable comparison with experiment at Mach numbers between 2 and 6. One advantage of CFD was that it provided flow field data for a detailed examination of the internal flow characteristics in addition to the surface properties. The experimental test matrix at mach 10 included three geometric contraction ratios (3, 5, and 9), three Reynolds numbers (0.55 x 10(exp 6) per foot, 1.14 x 10(exp 6) per foot, and 2.15 x 10(exp 6) per foot), and three cowl positions (at the throat and two forward positions). Computational data for two of these configurations (the contraction ratio of 3.  $Re = 2.15 \times 10$  (exp. 6) per foot, at two cowl positions) are presented along with a detailed analysis of the flow interactions in successive computational planes.

N95-23183\*# Tennessee Univ., Tullahoma, TN. Center for Space Transportation and Applied Research.

#### A WALL INTERFERENCE ASSESSMENT/CORRECTION SYSTEM Final Report, Jun. 1991 - Jun. 1994

C. F. LO Jun. 1994 10 p

(Contract(s)/Grant(s): NAG2-733)

(NASA-CR-197421; NAS 1.26:197421) Avail: CASI HC A02/MF

A Wall Signature method originally developed by Hackett has been selected to be adapted for the Ames 12-ft Wind Tunnel WIAC system in the project. This method uses limited measurements of the static pressure at the wall, in conjunction with the solid wall boundary condition, to determine the strength and distribution of singularities representing the test article. The singularities are used in turn for estimating wall interference at the model location. The development and implementation of a working prototype will be completed, delivered and documented with a software manual. The WIAC code will be validated by conducting numerically simulated experiments rather than actual wind tunnel experiments. The simulations will be used to generate both free-air and confined windtunnel flow fields for each of the test articles over a range of test configurations. Specifically, the pressure signature at the test section wall will be computed for the tunnel case to provide the simulated 'measured' data. These data will serve as the input for the WIAC method-Wall Signature method. The performance of the WIAC method then may be evaluated by comparing the corrected parameters with those for the free-air simulation. The following two additional tasks are included: (1) On-line wall interference calculation: The developed wall signature method (modified Hackett's method) for Ames 12-ft Tunnel will be the pre-computed coefficients which facilitate the on-line calculation of wall interference, and (2) Support system effects estimation: The effects on the wall pressure measurements due to the presence of the model support systems will be evaluated. Author

N95-23190\*# Auburn Univ., AL. Dept. of Mechanical Engineering. INFLUENCE OF BACKUP BEARINGS AND SUPPORT STRUCTURE DYNAMICS ON THE BEHAVIOR OF ROTORS WITH ACTIVE SUPPORTS Semiannual Status Report GEORGE T. FLOWERS Feb. 1995 5 p (Contract(s)/Grant(s): NAG3-1507)

(NASA-CR-197438: NAS 1.26:197438) Avail: CASI HC A01/MF À01

This semiannual status report lists specific accomplishments made on the research of the influence of backup bearings and support structure dynamics on the behavior of rotors with active supports. Papers have been presented representing work done on the T-501 engine model; an experimental/simulation study of auxiliary bearing rotordynamics; and a description of a rotordynamical model for a magnetic bearing supported rotor system, including auxiliary bearing effects. A finite element model for a foil bearing has been developed. Additional studies of rotor/bearing/housing dynamics are currently being performed as are studies of the effects of sideloading on auxiliary bearing rotordynamics using the magnetic bearing supported rotor model. Derived from text

N95-23210\*# National Aeronautics and Space Administration. Langley Research Center, Hampton, VA. MACH 10 COMPUTATIONAL STUDY OF A THREE-

**DIMENSIONAL SCRAMJET INLET FLOW FIELD** 

SCOTT D. HOLLAND Mar. 1995 30 p (Contract(s)/Grant(s): RTOP 506-40-41-02)

(NASA-TM-4602; L-17348; NAS 1.15:4602) Avail: CASI HC A03/ MF A01

The present work documents the computational results for a combined computational and experimental parametric study of the internal aerodynamics of a generic three-dimensional sidewallcompression scramjet inlet configuration at Mach 10. The threedimensional Navier-Stokes code SCRAMIN was chosen for the computational portion of the study because it uses a well-known and well-proven numerical scheme and has shown favorable comparison with experiment at Mach numbers between 2 and 6. One advantage of CFD was that it provided flow field data for a detailed examination of the internal flow characteristics in addition to the surface properties. The experimental test matrix at Mach 10 included three geometric contraction ratios (3, 5, and 9), three Reynolds numbers (0.55 x 10(exp 6) per foot, 1.14 x 10(exp 6) per foot, and 2.15 x 10(exp 6) per foot), and three cowl positions (at the throat and two forward positions). Computational data for two of these configurations (the contraction ratio of 3,  $Re = 2.15 \times 10(exp)$ 6) per foot, at two cowl positions) are presented along with a detailed analysis of the flow interactions in successive computational planes. **Author** 

N95-23257\*# Vigyan Research Associates, Inc., Hampton, VA. PERFORMANCE OF THE 0.3-METER TRANSONIC CRYOGENIC TUNNEL WITH AIR, NITROGEN, AND SULFUR **HEXAFLUORIDE MEDIA UNDER CLOSED LOOP AUTOMATIC** 

S. BALAKRISHNA and W. ALLEN KILGORE Jan. 1995 35 p. (Contract(s)/Grant(s): NAS1-19672; RTOP 505-59-50-02) (NASA-CR-195052; NAS 1.26:195052) Avail: CASI HC A03/MF

The NASA Langley 0.3-m Transonic Cryogenic Tunnel was modified in 1994, to operate with any one of the three test gas media viz., air, cryogenic nitrogen gas, or sulfur hexafluoride gas. This document provides the initial test results with respect to the tunnel performance and tunnel control, as a part of the commissioning activities on the microcomputer based controller. The tunnel can provide precise and stable control of temperature to less than or equal to +/- 0.3 K in the range 80-320 K in cyro mode or 300-320 K in air/SF6 mode, pressure to +/- 0.01 psia in the range 15-88 psia and Mach number to +/- O.0015 in the range 0.150 to transonic Mach numbers up to 1.000. A new heat exchanger has been included in the tunnel circuit and is performing adequately. The tunnel airfoil testing benefits considerably by precise control of tunnel states and helps

in generating high quality aerodynamic test data from the 0.3-m Author

N95-23287\*# Illinois Univ., Chicago, IL. HOLOGRAPHIC INTERFEROMETRIC TOMOGRAPHY FOR **RECONSTRUCTING FLOW FIELDS Abstract Only** 

SOYOUNG S. CHA In Hampton Univ., 1994 NASA-HU American Society for Engineering Education (ASEE) Summer Faculty Fellowship Program p 68 Dec. 1994

Avail: CASI HC A01/MF A02

Holographic interferometric tomography is a technique for instantaneously capturing and quantitatively reconstructing threedimensional flow fields. It has a very useful application potential for high-speed aerodynamics. However, three major challenging tasks need to be accomplished before its practical applications. First, fluid flows are mostly unsteady or at least non repeatable. Consequently, a means for Instantaneously recording three-dimensional flow fields. that is, a simple holographic technique for simultaneously recording multi-directional projections, needs to be developed. Second, while holographic interferometry provides enormous data storage capabilities, expeditious data extraction from complicated interferograms is very important for timely near real-time applications. Third, unlike medical applications, flow tomography does not provide complete data sets but instead involves ill-posed reconstruction problems of incomplete projection and limited angular scanning. During this summer research period, new experimental techniques and corresponding hardware were developed and tested to address the above mentioned tasks. The first task was achieved by diffuser illumination. This concept allows instantaneous capture of many projections with a conventional setup for single-projection recording. For the second task, a phase-shifting technique was incorporated. This technique allows one to acquire multiple phase-stepped interferograms for a single projection and thus to extract phase information from intensity data almost at real-time. For the third task, the research that has been extensively conducted previously was utilized. In this research period, a complete experimental setup that provides the above three major capabilities was designed, built, and tested by integrating all the techniques. A simple laboratory experiment for simulating wind-tunnel testing was then conducted. A test flow was produced by employing a relatively simple device that generated a gravity-driven flow. The flow was then experimentally investigated to check the viability of the holographic interferometric tomographic technique before wind-tunnel application. Author

N95-23290\*# Rochester Univ., NY. Dept. of Imaging and Photographic Technology.

SCIENTIFIC AND TECHNICAL PHOTOGRAPHY AT NASA LANGLEY RESEARCH CENTER Abstract Only

ANDREW DAVIDHAZY In Hampton Univ., 1994 NASA-HU American Society for Engineering Education (ASEE) Summer Faculty Fellowship Program Dec. 1994

Avail: CASI HC A01/MF A02

As part of my assignment connected with the Scientific and Technical Photography & Lab (STPL) at the NASA Langley Research Center I conducted a series of interviews and observed the day to day operations of the STPL with the ultimate objective of becoming exposed first hand to a scientific and technical photo/ imaging department for which my school prepares its graduates. I was also asked to share my observations with the staff in order that these comments and observations might assist the STPL to better serve its customers. Meetings with several individuals responsible for various wind tunnels and with a group that provides photo-optical instrumentation services at the Center gave me an overview of the services provided by the Lab and possible areas for development. In summary form these are some of the observations that resulted from the interviews and daily contact with the STPL facility. (1) The STPL is perceived as a valuable and almost indispensable service group within the organization. This comment was invariably made by everyone. Everyone also seemed to support the idea that the STPL continue to provide its current level of service and quality. (2) The STPL generally is not perceived to be a highly technically oriented

group but rather as a provider of high quality photographic illustration and documentation services. In spite of the importance and high marks assigned to the STPL there are several observations that merit consideration and evaluation for possible inclusion into the STPL's scope of expertise and future operating practices. (1) While the care and concern for artistic rendition of subjects is seen as laudable and sometimes valuable, the time that this often requires is seen as interfering with keeping the tunnels operating at maximum productivity. Tunnel managers would like to shorten down-time due to photography, have services available during evening hours and on short notice. It may be of interest to the STPL that tunnel managers are incorporating ever greater imaging capabilities in their facilities. To some extent this could mean a reduced demand for traditional photographic services. (2) The photographic archive is seen as a Center resource. Archiving of images, as well as data, is a matter of concern to the investigators. The early holdings of the Photographic Archives are quickly deteriorating. The relative inaccessibility of the material held in the archives is problematic. (3) In certain cases delivery or preparation of digital image files instead of, or along with, hardcopy is already being perceived by the STPL's customers as desirable. The STPL should make this option available, and the fact that it has, or will have this capability widely known. (4) The STPL needs to continue to provide expert advice and technical imaging support in terms of application information to users of traditional photographic and new electronic imaging systems. Cooperative demo projects might be undertaken to maintain or improve the capabilities of the Lab. (5) STPL personnel do not vet have significant electronic imaging or electronic communication skills and improvements in this is an area could potentially have a positive impact on the Center. (6) High speed photographic or imaging services are often mentioned by the STPL as being of primary importance to their mission but the lab supports very few projects calling for high speed imaging services. Much high speed equipment is in poor state of repair. It is interesting to note that when the operation of lasers, digital imaging or quantitative techniques are requested these are directed to another NASA department. Could joint activities be initiated to solve problems? (7). The STPL could acquire more technical assignments if examples of the areas where they posses expertise would be circulated around the center. The fact that the STPL owns high speed video capability could be 'advertised' among its customer base if there truly was an interest in building up a customer base in this area. The STPL could participate in events like TOPS as an exhibitor, as well as a documenter, of the event.

N95-23311\*# Arizona Univ., Tucson, AZ. Dept. of Aerospace and Mechanical Engineering.

RESIDUAL STRENGTH OF THIN PANELS WITH CRACKS Abstract Only

ERDOGAN MADENCI In Hampton Univ., 1994 NASA-HU American Society for Engineering Education (ASEE) Summer Faculty Fellowship Program p 93 Dec. 1994

Avail: CASI HC A01/MF A02

The previous design philosophies involving safe life, fail-safe and damage tolerance concepts become inadequate for assuring the safety of aging aircraft structures. For example, the failure mechanism for the Aloha Airline accident involved the coalescence of undetected small cracks at the rivet holes causing a section of the fuselage to peel open during flight. Therefore, the fuselage structure should be designed to have sufficient residual strength under worst case crack configurations and in-flight load conditions. Residual strength is interpreted as the maximum load carrying capacity prior to unstable crack growth. Internal pressure and bending moment constitute the two major components of the external loads on the fuselage section during flight. Although the stiffeners in the form of stringers, frames and tear straps sustain part of the external loads, the significant portion of the load is taken up by the skin. In the presence of a large crack in the skin, the crack lips bulge out with considerable yielding; thus, the geometric and material nonlinearities must be included in the analysis for predicting residual strength. Also, these nonlinearities do not permit the decoupling of in-plane

and out-of-plane bending deformations. The failure criterion combining the concepts of absorbed specific energy and strain energy density addresses the aforementioned concerns. The critical absorbed specific energy (local toughness) for the material is determined from the global specimen response and deformation geometry based on the uniaxial tensile test data and detailed finite element modeling of the specimen response. The use of the local toughness and stress-strain response at the continuum level eliminates the size effect. With this critical parameter and stress-strain response, the finite element analysis of the component by using STAGS along with the application of this failure criterion provides the stable crack growth calculations for residual strength predictions.

N95-23377\* National Aeronautics and Space Administration. Ames Research Center, Moffett Field, CA.

### SYSTEM FOR DETERMINING AERODYNAMIC IMBALANCE Patent

GARY B. CHURCHILL, inventor (to NASA) and BENNY K. CHEUNG, inventor (to NASA) 4 Oct. 1994 7 p Filed 7 Aug. 1992 (NASA-CASE-ARC-11913-1; US-PATENT-5,352,090; US-PATENT-APPL-SN-926117; US-PATENT-CLASS-416-61; US-PATENT-CLASS-416-34; INT-PATENT-CLASS-B64C-11/00) Avail: US Patent and Trademark Office

A system is provided for determining tracking error in a propeller or rotor driven aircraft by determining differences in the aerodynamic loading on the propeller or rotor blades of the aircraft. The system includes a microphone disposed relative to the blades during the rotation thereof so as to receive separate pressure pulses produced by each of the blades during the passage thereof by the microphone. A low pass filter filters the output signal produced by the microphone, the low pass filter having an upper cut-off frequency set below the frequency at which the blades pass by the microphone. A sensor produces an output signal after each complete revolution of the blades, and a recording display device displays the outputs of the low pass filter and sensor so as to enable evaluation of the relative magnitudes of the pressure pulses produced by passage of the blades by the microphone during each complete revolution of the blades.

Official Gazette of the U.S. Patent and Trademark Office

N95-23423\*# Sverdrup Technology, Inc., Brook Park, OH. THREE-DIMENSIONAL NAVIER-STOKES ANALYSIS AND REDESIGN OF AN IMBEDDED BELLMOUTH NOZZLE IN A TURBINE CASCADE INLET SECTION

P. W. GIEL and J. R. SIRBAUGH In NASA. Marshall Space Flight Center, Eleventh Workshop for Computational Fluid Dynamic Applications in Rocket Propulsion p 1239-1257 Jul. 1993

Avail: CASI HC A03/MF A10

Verification of proposed turbopump blading performance will involve evaluation of candidate blades in cascade test facilities. It is necessary to be able to predict the flow fields within these cascades for the results to be applicable to actual engine environments. This work presents the results of a study to predict the flow field for the NASA Lewis Transonic Turbine Blade Cascade Facility, which is similar to those used to evaluate rocket propulsion turbines. A pitchwise nonuniform total pressure distribution was observed at the blade row leading edge plane. A CFD analysis was used to show that the cause of the flow nonuniformity was a pair of vortices that originated in an embedded bellmouth inlet. Further CFD analysis was used to verify that a redesigned inlet section resulted in a flow with acceptable uniformity. A computational analysis was chosen because physical accessibility to the inlet section was limited, and because a computational approach also allows one to examine design changes cheaper and more quickly than an experimental approach would. The PARC code, a general purpose, three-dimensional, Navier-Stokes code with multiblock solution capability, was chosen for the present study. Results are presented detailing the computational requirements needed to accurately predict flows of this nature. Calculations of the original geometry showed total pressure loss regions consistent in strength and in location to experimental measurements. An examination of the results shows that the distortions are caused by a pair of vortices that originate as

a result of the interaction of the flow with the imbedded bellmouth. Computations were performed for an inlet geometry which eliminated the imbedded bellmouth by bridging the region between it and the upstream wall. This analysis indicated that eliminating the imbedded bellmouth eliminates the troublesome pair of vortices, resulting in a flow with much greater pitchwise uniformity. Author

N95-23425\*# MCAT Inst., Moffett Field, CA.
THREE-DIMENSIONAL UNSTEADY FLOW CALCULATIONS IN
AN ADVANCED GAS GENERATOR TURBINE

AKIL A. RANGWALLA In NASA. Marshall Space Flight Center, Eleventh Workshop for Computational Fluid Dynamic Applications in Rocket Propulsion p 1287-1320 Jul. 1993

Avail: CASI HC A03/MF A10

This paper deals with the application of a three-dimensional, unsteady Navier-Stokes code for predicting the unsteady flow in a single stage of an advanced gas generator turbine. The numerical method solves the three-dimensional thin-layer Navier-Stokes equations, using a system of overlaid grids, which allow for relative motion between the rotor and stator airfoils. Results in the form of time averaged pressures and pressure amplitudes on the airfoil surfaces will be shown. In addition, instantaneous contours of pressure. Mach number, etc. will be presented in order to provide a greater understanding of the inviscid as well as the viscous aspects of the flowfield. Also, relevant secondary flow features such as cross-plane velocity vectors and total pressure contours will be presented. Prior work in two-dimensions has indicated that for the advanced designs, the unsteady interactions can play a significant role in turbine performance. These interactions affect not only the stage efficiency but can substantially alter the time-averaged features of the flow. This work is a natural extension of the work done in two-dimensions and hopes to address some of the issues raised by the two-dimensional calculations. These calculations are being performed as an integral part of an actual design process and demonstrate the value of unsteady rotor-stator interaction calculations in the design of turbomachines.

N95-23429°# Virginia Polytechnic Inst. and State Univ., Blacksburg, VA. Dept. of Mechanical Engineering.

### SUPERSONIC FLOW AND SHOCK FORMATION IN TURBINE TIP GAPS

JOHN MOORE In NASA. Marshall Space Flight Center, Eleventh Workshop for Computational Fluid Dynamic Applications in Rocket Propulsion p 1423-1433 Jul. 1993

Avail: CASI HC A03/MF A10

Shock formation due to overexpansion of supersonic flow at the inlet to the tip clearance gap of a turbomachine has been studied. As the flow enters the tip gap, it accelerates around the blade pressureside corner creating a region of minimum static pressure. The 'free streamline' separates from the wall at the comer; and, for Mach numbers greater than about 1.3, it curves back to intersect the blade tip. At this point, the freestream flow is abruptly turned parallel to the surface, giving rise to an oblique shock. The results are consistent with compressible sharp-edged orifice flow calculations found in the literature and with the theory of oblique shock wave formation in supersonic flow over a wedge. For freestream Mach numbers of 1.4 to 1.8, wave angles are 43 to 54 deg, and turning angles are 9 to 20 deg; as the Mach number increases, the angle of turn also increases. It appears that in a turbine, after separating from the inlet comer, the flow reattaches on the blade tip and an oblique shock is formed at 0.4-1.4 tip gap heights into the clearance gap. The resulting shock-boundary layer interaction may contribute to further enhancement of already high heat transfer to the blade tip in this region. This in turn could lead to higher blade temperatures and adversely affect blade life and turbine efficiency.

N95-23435\*# Pratt and Whitney Aircraft, West Palm Beach, FL. AERODYNAMIC DESIGN AND ANALYSIS OF A HIGHLY LOADED TURBINE EXHAUST

F. W. HUBER, X. A. MONTESDEOCA, and R. J. ROWEY In NASA. Marshall Space Flight Center, Eleventh Workshop for Computational Fluid Dynamic Applications in Rocket Propulsion p 1535-1553 Jul. 1993

Avail: CASI HC A03/MF A10

The aerodynamic design and analysis of a turbine exhaust volute manifold is described. This turbine exhaust system will be used with an advanced gas generator oxidizer turbine designed for very high specific work. The elevated turbine stage loading results in increased discharge Mach number and swirl velocity which, along with the need for minimal circumferential variation of fluid properties at the turbine exit, represent challenging volute design requirements. The design approach, candidate geometries analyzed, and steady state/unsteady CFD analysis results are presented. Author

N95-23436\*# Rockwell International Corp., Canoga Park, CA. Rocketdyne Div.

#### CFD ANALYSIS OF TURBOPUMP VOLUTES

EDWARD P. ASCOLI, DANIEL C. CHAN, ARMEN DARIAN, WAYNE W. HSU, and KEN TRAN In NASA. Marshall Space Flight Center, Eleventh Workshop for Computational Fluid Dynamic Applications in Rocket Propulsion p 1555-1578 Jul. 1993

Avail: CASI HC A03/MF A10

An effort is underway to develop a procedure for the regular use of CFD analysis in the design of turbopump volutes. Airflow data to be taken at NASA Marshall will be used to validate the CFD code and overall procedure. Initial focus has been on preprocessing (geometry creation, translation, and grid generation). Volute geometries have been acquired electronically and imported into the CATIA CAD system and RAGGS (Rockwell Automated Grid Generation System) via the IGES standard. An initial grid topology has been identified and grids have been constructed for turbine inlet and discharge volutes. For CFD analysis of volutes to be used regularly, a procedure must be defined to meet engineering design needs in a timely manner. Thus, a compromise must be established between making geometric approximations, the selection of grid topologies, and possible CFD code enhancements. While the initial grid developed approximated the volute tongue with a zero thickness, final computations should more accurately account for the geometry in this region. Additionally, grid topologies will be explored to minimize skewness and high aspect ratio cells that can affect solution accuracy and slow code convergence. Finally, as appropriate, code modifications will be made to allow for new grid topologies in an effort to expedite the overall CFD analysis process.

## N95-23438\*# Pratt and Whitney Aircraft, West Palm Beach, FL. PHASE 2: HGM AIR FLOW TESTS IN SUPPORT OF HEX VANE INVESTIGATION

G. B. COX, JR., L. L. STEELE, and D. W. EISENHART In NASA. Marshall Space Flight Center, Eleventh Workshop for Computational Fluid Dynamic Applications in Rocket Propulsion p 1607-1618 Jul. 1993

(Contract(s)/Grant(s): NAS8-36801)

Avail: CASI HC A03/MF A10

Following the start of SSME certification testing for the Pratt and Whitney Alternate Turbopump Development (ATD) High Pressure Oxidizer Turbopump (HPOTP), cracking of the leading edge of the inner HEX vane was experienced. The HEX vane, at the inlet of the oxidizer bowl in the Hot Gas Manifold (HGM), accepts the HPOTP turbine discharge flow and turns it toward the Gaseous Oxidizer Heat Exchanger (GOX HEX) coil. The cracking consistently initiated over a specific circumferential region of the hex vane, with other circumferential locations appearing with increased run time. Since cracking had not to date been seen with the baseline HPOTP. a fluid-structural interaction involving the ATD HPOTP turbine exit flowfield and the HEX inner vane was suspected. As part of NASA contract NAS8-36801, Pratt and Whitney conducted air flow tests of the ATD HPOTP turbine turnaround duct flowpath in the MSFC Phase 2 HGM air flow model. These tests included HEX vane strain gages and additional fluctuating pressure gages in the turnaround duct and HEX vane flowpath area. Three-dimensional flow probe measurements at two stations downstream of the turbine simulator exit plane were also made. Modifications to the HPOTP turbine

simulator investigated the effects on turbine exit flow profile and velocity components, with the objective of reproducing flow conditions calculated for the actual ATD HPOTP hardware. Testing was done at the MSFC SSME Dynamic Fluid Air Flow (Dual-Leg) Facility, at air supply pressures between 50 and 250 psia. Combinations of turbine exit Mach number and pressure level were run to investigate the effect of flow regime. Information presented includes: (1) Descriptions of turbine simulator modifications to produce the desired flow environment; (2) Types and locations for instrumentation added to the flow model for improved diagnostic capability; (3) Evaluation of the effect of changes to the turbine simulator flowpath on the turbine exit flow environment; and (4) Comparison of the experimental turbine exit flow environment to the environment calculated for the ATD HPOTP.

N95-23440\*# Rockwell International Corp., Canoga Park, CA. Rocketdyne Div.

### IMPELLER FLOW FIELD CHARACTERIZATION WITH A LASER TWO-FOCUS VELOCIMETER

L. A. BROZOWSKI, T. V. FERGUSON, and L. ROJAS In NASA. Marshall Space Flight Center, Eleventh Workshop for Computational Fluid Dynamic Applications in Rocket Propulsion p 1635-1688 Jul. 1993

(Contract(s)/Grant(s): NAS8-38864)

Avail: CASI HC A04/MF A10

Use of Computational Fluid Dynamics (CFD) codes, prevalent in the rocket engine turbomachinery industry, necessitates data of sufficient quality and quantity to benchmark computational codes. Existing data bases for typical rocket engine configurations, in particular impellers, are limited. In addition, traditional data acquisition methods have several limitations: typically transducer uncertainties are 0.5% of transducer full scale and traditional pressure probes are unable to provide flow characteristics in the circumferential (blade-to-blade) direction. Laser velocimetry circumvents these limitations by providing +0.5% uncertainty in flow velocity and +0.5% uncertainty in flow angle. The percent of uncertainty in flow velocity is based on the measured value, not full range capability. The laser electronics multiple partitioning capability allows data acquired between blades as the impeller rotates, to be analyzed separately, thus providing blade-to-blade flow characterization. Unlike some probes, the non-intrusive measurements made with the laser velocimeter does not disturb the flow. To this end,, and under Contract (NAS8-38864) to the National Aeronautics and Space Administration (NASA) at Marshall Space Flight Center (MSFC), an extensive test program was undertaken at Rocketdyne. Impellers from two different generic rocket engine pump configurations were examined. The impellers represent different spectrums of pump design: the Space Shuttle Main Engine (SSME) high pressure fuel turbopump (HPFTP) impeller was designed in the 1 1970's the Consortium for CFD application in Propulsion Technology Pump Stage Technology Team (Pump Consortium) optimized impeller was designed with the aid of modern computing techniques. The tester configuration for each of the impellers consisted of an axial inlet, an inducer, a diffuser, and a crossover discharge. While the tested configurations were carefully chosen to be representative of generic rocket engine pumps, several features of both testers were intentionally atypical. A crossover discharge, downstream of the impeller, rather than a volute discharge was used to minimize asymmetric flow conditions that might be reflected in the impeller discharge flow data. Impeller shroud wear ring radial clearances were purposely close to minimize leakage flow, thus increasing confidence in using the inlet data as an input to CFD programs. The empirical study extensively examined the flow fields of the two impellers via performance of laser two-focus velocimeter surveys in an axial plane upstream of the impellers and in multiple radial planes downstream of the impellers. Both studies were performed at the impeller design flow coefficients. Inlet laser surveys that provide CFD code inlet boundary conditions were performed in one axial plane, with ten radial locations surveyed. Three wall static pressures, positioned circumferentially around the impeller inlet, were used to identify asymmetrical pressure distributions in the inlet survey plane. The impeller discharge flow characterization consisted of three radial planes for the SSME HPFTP impeller and two radial planes for the Pump Consortium optimized impeller. Housing wall static pressures were placed to correspond to the radial locations surveyed with the laser velocimeter. Between five and thirteen axial stations across the discharge channel width were examined in each radial plane during the extensive flow mapping. The largely successful empirical flow characterization of two different impellers resulted in a substantial contribution to the limited existing data base, and yielded accurate data for CFD code benchmarking.

N95-23444\*# Pennsylvania State Univ., University Park, PA. Dept. of Aerospace Engineering.

## NUMERICAL COMPUTATION OF AERODYNAMICS AND HEAT TRANSFER IN A TURBINE CASCADE AND A TURN-AROUND DUCT USING ADVANCED TURBULENCE MODELS

B. LAKSHMINARAYANA and J. LUO In NASA. Marshall Space Flight Center, Eleventh Workshop for Computational Fluid Dynamic Applications in Rocket Propulsion p 1773-1806 Jul. 1993 Avail: CASI HC A03/MF A10

The objective of this research is to develop turbulence models to predict the flow and heat transfer fields dominated by the curvature effect such as those encountered in turbine cascades and turnaround ducts. A Navier-Stokes code has been developed using an explicit Runge-Kutta method with a two layer k-epsilon/ARSM (Algebraic Reynolds Stress Model), Chien's Low Reynolds Number (LRN) k-epsilon model and Coakley's LRN q-omega model. The near wall pressure strain correlation term was included in the ARSM. The formulation is applied to Favre-averaged N-S equations and no thin-layer approximations are made in either the mean flow or turbulence transport equations. Anisotropic scaling of artificial dissipation terms was used. Locally variable timestep was also used to improve convergence. Detailed comparisons were made between computations and data measured in a turbine cascade by Arts et al. at Von Karman Institute. The surface pressure distributions and wake profiles were predicted well by all the models. The blade heat transfer is predicted well by k-epsilon/ARSM model, as well as the k-epsilon model. It's found that the onset of boundary layer transition on both surfaces is highly dependent upon the level of local freestream turbulence intensity, which is strongly influenced by the streamline curvature. Detailed computation of the flow in the turn around duct has been carried out and validated against the data by Monson as well as Sandborn. The computed results at various streamwise locations both on the concave and convex sides are compared with flow and turbulence data including the separation zone on the inner well. The k-epsilon/ARSM model yielded relatively better results than the two-equation turbulence models. A detailed assessment of the turbulence models has been made with regard to their applicability to curved flows. Author

N95-23446\*# Pennsylvania State Univ., University Park, PA. Propulsion Engineering Research Center.

### CONVERGENCE ACCELERATION OF IMPLICIT SCHEMES IN THE PRESENCE OF HIGH ASPECT RATIO GRID CELLS

B. E. O. BUELOW, S. VENKATESWARAN, and C. L. MERKLE In NASA. Marshall Space Flight Center, Eleventh Workshop for Computational Fluid Dynamic Applications in Rocket Propulsion p 1829-1855 Jul. 1993

Avail: CASI HC A03/MF A10

The performance of Navier-Stokes codes are influenced by several phenomena. For example, the robustness of the code may be compromised by the lack of grid resolution, by a need for more precise initial conditions or because all or part of the flowfield lies outside the flow regime in which the algorithm converges efficiently. A primary example of the latter effect is the presence of extended low Mach number and/or low Reynolds number regions which cause convergence deterioration of time marching algorithms. Recent research into this problem by several workers including the present authors has largely negated this difficulty through the introduction of

time-derivative preconditioning. In the present paper, we employ the preconditioned algorithm to address convergence difficulties arising from sensitivity to grid stretching and high aspect ratio grid cells. Strong grid stretching is particularly characteristic of turbulent flow calculations where the grid must be refined very tightly in the dimension normal to the wall, without a similar refinement in the tangential direction. High aspect ratio grid cells also arise in problems that involve high aspect ratio domains such as combustor coolant channels. In both situations, the high aspect ratio cells can lead to extreme deterioration in convergence. It is the purpose of the present paper to address the reasons for this adverse response to grid stretching and to suggest methods for enhancing convergence under such circumstances. Numerical algorithms typically possess a maximum allowable or optimum value for the time step size, expressed in non-dimensional terms as a CFL number or vonNeumann number (VNN). In the presence of high aspect ratio cells, the smallest dimension of the grid cell controls the time step size causing it to be extremely small, which in turn results in the deterioration of convergence behavior. For explicit schemes, this time step limitation cannot be exceeded without violating stability restrictions of the scheme. On the other hand, for implicit schemes, which are typically unconditionally stable, there appears to be room for improvement through careful tailoring of the time step definition based on results of linear stability analyses. In the present paper, we focus on the central-differenced alternating direction implicit (ADI) scheme. The understanding garnered from this analyses can then be applied to other implicit schemes. In order to systematically study the effects of aspect ratio and the methods of mitigating the associated problems, we use a two pronged approach. We use stability analyses as a tool for predicting numerical convergence behavior and numerical experiments on simple model problems to verify predicted trends. Based on these analyses, we determine that efficient convergence may be obtained at all aspect ratios by getting a combination of things right. Primary among these are the proper definition of the time step size, proper selection of viscous preconditioner and the precise treatment of boundary conditions. These algorithmic improvements are then applied to a variety of test cases to demonstrate uniform convergence at all aspect ratios.

Author

N95-23447\*# National Aeronautics and Space Administration. Lewis Research Center, Cleveland, OH.

### A TIME-ACCURATE FINITE VOLUME METHOD VALID AT ALL FLOW VELOCITIES

S.-W. KIM In NASA. Marshall Space Flight Center, Eleventh Workshop for Computational Fluid Dynamic Applications in Rocket Propulsion p 1857-1887 Jul. 1993

Avail: CASI HC A03/MF A10

A finite volume method to solve the Navier-Stokes equations at all flow velocities (e.g., incompressible, subsonic, transonic, supersonic and hypersonic flows) is presented. The numerical method is based on a finite volume method that incorporates a pressurestaggered mesh and an incremental pressure equation for the conservation of mass. Comparison of three generally accepted time-advancing schemes, i.e., Simplified Marker-and-Cell (SMAC), Pressure-Implicit-Splitting of Operators (PISO), and Iterative-Time-Advancing (ITA) scheme, are made by solving a lid-driven polar cavity flow and self-sustained oscillatory flows over circular and square cylinders. Calculated results show that the ITA is the most stable numerically and yields the most accurate results. The SMAC is the most efficient computationally and is as stable as the ITA. It is shown that the PISO is the most weakly convergent and it exhibits an undesirable strong dependence on the time-step size. The degenerated numerical results obtained using the PISO are attributed to its second corrector step that cause the numerical results to deviate further from a divergence free velocity field. The accurate numerical results obtained using the ITA is attributed to its capability to resolve the nonlinearity of the Navier-Stokes equations. The present numerical method that incorporates the ITA is used to solve an unsteady transitional flow over an oscillating airfoil and a chemically reacting flow of hydrogen in a vitiated supersonic airstream.

The turbulence fields in these flow cases are described using multiple-time-scale turbulence equations. For the unsteady transitional over an oscillating airfoil, the fluid flow is described using ensemble-averaged Navier-Stokes equations defined on the Lagrangian-Eulerian coordinates. It is shown that the numerical method successfully predicts the large dynamic stall vortex (DSV) and the trailing edge vortex (TEV) that are periodically generated by the oscillating airfoil. The calculated streaklines are in very good comparison with the experimentally obtained smoke picture. The calculated turbulent viscosity contours show that the transition from laminar to turbulent state and the relaminarization occur widely in space as well as in time. The ensemble-averaged velocity profiles are also in good agreement with the measured data and the good comparison indicates that the numerical method as well as the multipletime-scale turbulence equations successfully predict the unsteady transitional turbulence field. The chemical reactions for the hydrogen in the vitiated supersonic airstream are described using 9 chemical species and 48 reaction-steps. Consider that a fast chemistry can not be used to describe the fine details (such as the instability) of chemically reacting flows while a reduced chemical kinetics can not be used confidently due to the uncertainty contained in the reaction mechanisms. However, the use of a detailed finite rate chemistry may make it difficult to obtain a fully converged solution due to the coupling between the large number of flow, turbulence, and chemical equations. The numerical results obtained in the present study are in good agreement with the measured data. The good comparison is attributed to the numerical method that can yield strongly converged results for the reacting flow and to the use of the multiple-time-scale turbulence equations that can accurately describe the mixing of the fuel and the oxidant. Author

N95-23466\*# Institute for Computer Applications in Science and Engineering, Hampton, VA.

#### A STUDY OF THE VORTEX FLOW OVER 76/40-DEG DOUBLE-DELTA WING Final Report

N. G. VERHAAGEN (Technische Hogeschool, Delft, Netherlands.), L. N. JENKINS (National Aeronautics and Space Administration. Langley Research Center, Hampton, VA.), S. B. KERN (Naval Air Warfare Center, Warminster, PA.), and A. E. WASHBURN (Vigyan Research Associates, Inc., Hampton, VA.) NASA Feb. 1995 34 p (Contract(s)/Grant(s): NAS1-19480; RTOP 505-90-52-01)

(NASA-CR-195032; NAS 1.26:195032; ICASE-95-5; AIAÁ PAPER 95-0560) Avail: CASI HC A03/MF A01

A low-speed wind-tunnel study of the flow about a 76/40-deg double-delta wing is described for angles of attack ranging from -10 to 25 deg and Reynolds numbers ranging from 0.5 to 1.5 Million. The study was conducted to provide data for the purpose of understanding the vortical flow behavior and for validating Computational Fluid Dynamics methods. Flow visualization tests have provided insight into the effect of the angle of attack and Reynolds number of the vortex-dominated flow both on and off of the surface of the double-delta wing. Upper surface pressure recordings from pressure orifices and Pressure Sensitive Paint have provided data on the pressures induced by the vortices. Flowfield surveys were carried out at an angle of attack of 10 deg by using a thin 5-hole probe. Numerical solutions of the compressible thin-layer Navier-Stokes equations were conducted and compared to the experimental data.

N95-23505# Defence Research Agency, Farnborough, Hampshire (England). Structural Materials Centre.

### NON-DESTRUCTIVE DETECTION OF CORROSION FOR LIFE MANAGEMENT

DAVID A: BRUCE In AGARD, Corrosion Detection and Management of Advanced Airframe Materials 8 p Jan. 1995
Copyright Avail: CASI HC A02/MF A03

In recent years, aircraft operators have been driven to increased use of Non-Destructive Evaluation (NDE) to ensure airworthiness during life extensions for ageing aircraft or as an integral part of a damage tolerant lifting philosophy. Major airframe static and fatigue tests are routinely used to highlight problem areas on

airframes where design limitations or changes of usage may lead to early failures. The results of such tests become progressively less reliable as the age of the airframe increases and the operating conditions diverge from those under which the tests were conducted. Increased inspection, whether by visual or other means is usually the only alternative to wholesale refurbishment or replacement of aircraft or components. Almost all of the development to date of NDE techniques for corrosion detection and characterization has been concentrated on existing airframe materials, principally Aluminum alloys and steels. The current capabilities of corrosion detection techniques will be reviewed and current research aimed at areas where there is a requirement for improved detection capability will be described. New materials, such as Polymer Matrix Composites, will experience different types of 'corrosive' deterioration. The capability of NDE methods to detect material degradation in new composite materials will be discussed. Finally, reliance on NDE, choice of NDE technique and optimal scheduling of inspections all require an assessment of the reliability of NDE methods. It will be shown that a range of NDE techniques with differing capabilities and characteristics will be required to ensure compatibility with maintenance schedules if full use is to be made of NDE for life management of structures which may be subject to corrosion.

## N95-23507# National Aerospace Lab., Amsterdam (Netherlands). EDDY CURRENT DETECTION OF PITTING CORROSION AROUND FASTENER HOLES

J. H. HEIDA and W. G. J. THART In AGARD, Corrosion Detection and Management of Advanced Airframe Materials 10 p Jan. 1995 Sponsored by Royal Netherlands Air Force Copyright Avail: CASI HC A02/MF A03

An evaluation of the eddy current technique for the detection and depth assessment of corrosion around fastener holes in F-16 lower wing skins is described. The corrosion type in this structure is pitting corrosion at the countersink edge of the fastener holes. Due to a corrosion clean-up limit of only 1.5 - 2.5 percent, a maximum thickness reduction in the range of 0.08 - 0.32 mm is allowed (depending on local skin thickness). This specifies the needed sensitivity for in-service corrosion inspection. In the evaluation use was made of specimens cut out of the F-16 lower wing skin structure. In total twelve specimens were exposed to an accelerated corrosion test (EXCO-test). Eddy current inspection of the specimens with installed fasteners was performed with a standard eddy scope and four different eddy current probes. After the eddy current inspection cross-sections of the twelve-specimens were made to determine the extent of pitting corrosion at the countersink edges. After evaluation of the inspection results the following conclusions can be drawn: for in-service detection of countersink edge corrosion standard visual inspection is the preferred technique regarding the simplicity, sensitivity and reliability of inspection; and for the purpose of depth assessment the eddy current technique is capable of detecting countersink edge corrosion with a depth from about 0.1 mm. Due to the corrosion clean-up limit of only 1.5 - 2.5 percent (0.08 - 0.32 mm), however, the eddy current technique is considered not applicable for in-service depth assessment of countersink edge corrosion in F-16 lower wing skins. Author

N95-23512# National Aeronautics and Space Administration. Langley Research Center, Hampton, VA.

## NEW NONDESTRUCTIVE TECHNIQUES FOR THE DETECTION AND QUANTIFICATION OF CORROSION IN AIRCRAFT STRUCTURES

W. P. WINFREE, K. E. CRAMER, P. H. JOHNSTON, and M. NAMKUNG In AGARD, Corrosion Detection and Management of Advanced Airframe Materials 6 p Jan. 1995
Copyright Avail: CASI HC A02/MF A03

An overview is presented of several techniques under development at NASA Langley Research Center for detection and quantification of corrosion in aircraft structures. The techniques have been developed as part of the NASA Airframe Structural Integrity Program. The techniques focus on the detection of subsurface corrosion in thin laminated structures. Results are presented on specimens

with both manufactured defects, for calibration of the techniques, and on specimens removed from aircraft.

Author

N95-23602# Advisory Group for Aeronautical Research and Development, Oxford (England). Structures and Materials Panel. POD ASSESSMENT OF NDI PROCEDURES USING A ROUND ROBIN TEST [LES TESTS COMPARATIFS INTERLABORATOIRES POUR L'EVALUATION DE LA PROBABILITE DE DETECTION (POD) DES PROCEDURES NDI]

Jan. 1995 40 p

(AGARD-R-809; ISBN-92-836-1010-5) Copyright Avail: CASI HC A03/MF A01

Under the auspices of the AGARD Structures and Materials Panel R&D Cooperation Program, a round-robin NDI demonstration has been carried out. Six laboratories in four NATO countries participated in the project. The aim of the project was to determine the sensitivity and reliability of NDI procedures presently employed by the participating laboratories and to establish whether or not the procedures would be adequate for the implementation of a damage-tolerance based maintenance approach or whether improved methods are required.

N95-23630\*# Pennsylvania State Univ., State College, PA. Propulsion Engineering Research Center.

### CAVITATION MODELING IN EULER AND NAVIER-STOKES

MANISH DESHPANDE, JINZHANG FENG, and CHARLES L. MERKLE In NASA. Marshall Space Flight Center, Eleventh Workshop for Computational Fluid Dynamic Applications in Rocket Propulsion, Part 1 p 377-401 Jul. 1993

Avail: CASI HC A03/MF A10

Many previous researchers have modeled sheet cavitation by means of a constant pressure solution in the cavity region coupled with a velocity potential formulation for the outer flow. The present paper discusses the issues involved in extending these cavitation models to Euler or Navier-Stokes codes. The approach taken is to start from a velocity potential model to ensure our results are compatible with those of previous researchers and available experimental data, and then to implement this model in both Euler and Navier-Stokes codes. The model is then augmented in the Navier-Stokes code by the inclusion of the energy equation which allows the effect of subcooling in the vicinity of the cavity interface to be modeled to take into account the experimentally observed reduction in cavity pressures that occurs in cryogenic fluids such as liquid hydrogen. Although our goal is to assess the practicality of implementing these cavitation models in existing three-dimensional, turbomachinery codes, the emphasis in the present paper will center on two-dimensional computations, most specifically isolated airfoils and cascades. Comparisons between velocity potential, Euler and Navier-Stokes implementations indicate they all produce consistent predictions. Comparisons with experimental results also indicate that the predictions are qualitatively correct and give a reasonable first estimate of sheet cavitation effects in both cryogenic and noncryogenic fluids. The impact on CPU time and the code modifications required suggests that these models are appropriate for incorporation in current generation turbomachinery codes.

N95-23652\*# National Aeronautics and Space Administration.

Marshall Space Flight Center, Huntsville, AL.

## VALIDATION OF A COMPUTATIONAL FLUID DYNAMICS (CFD) CODE FOR SUPERSONIC AXISYMMETRIC BASE FLOW

P. KEVIN TUCKER In its Eleventh Workshop for Computational Fluid Dynamic Applications in Rocket Propulsion, Part 1 p 879-901

Avail: CASI HC A03/MF A10

The ability to accurately and efficiently calculate the flow structure in the base region of bodies of revolution in supersonic flight is a significant step in CFD code validation for applications ranging from base heating for rockets to drag for protectives. The FDNS code is used to compute such a flow and the results are

compared to benchmark quality experimental data. Flowfield calculations are presented for a cylindrical afterbody at M = 2.46 and angle of attack a = O. Grid independent solutions are compared to mean velocity profiles in the separated wake area and downstream of the reattachment point. Additionally, quantities such as turbulent kinetic energy and shear layer growth rates are compared to the data. Finally, the computed base pressures are compared to the measured values. An effort is made to elucidate the role of turbulence models in the flowfield predictions. The level of turbulent eddy viscosity, and its origin, are used to contrast the various turbulence models and compare the results to the experimental data.

N95-23662# Technion - Israel Inst. of Tech., Haifa (Israel), Faculty of Aerospace Engineering.

REVIEW OF SOME RESULTS OF THE AUTHOR'S FATIGUE INVESTIGATIONS WITH APPLICATIONS IN ENGINEERING AND MATERIAL SCIENCE

A. BUCH Apr. 1994 61 p (TAE-698) Avail: CASI HC A04/MF A01

This document deals with research results mainly connected with the problem of fatigue calculations and various aspects of fatigue. It contains the following topics: Correlation between fatigue limits and ultimate tensile strength, Fatigue properties of pure metals, Analytical approach to notch-size effects in fatigue of aircraft sheet materials, Torsional fatigue life of axle shafts under program loading, Fatigue properties of aircraft lugs with interference fit. Comparison of various aircraft loading test results with the aid of Relative-Miner-Rule. The Relative Method in the case of Local-Strain-Approach, and Prediction of fatigue life. CASI

N95-23670\*# Clemson Univ., SC. Radar Systems Lab. MAXIMUM-LIKELIHOOD SPECTRAL ESTIMATION AND ADAPTIVE FILTERING TECHNIQUES WITH APPLICATION TO AIRBORNE DOPPLER WEATHER RADAR Thesis Technical Report No. 20

JONATHAN Y. LAI 28 Nov. 1994 88 p (Contract(s)/Grant(s): NAG1-928)

(NASA-CR-197699; NAS 1.26:197699; TR-112894-3570P) Avail: CASI HC A05/MF-A01

This dissertation focuses on the signal processing problems associated with the detection of hazardous windshears using airborne Doppler radar when weak weather returns are in the presence of strong clutter returns. In light of the frequent inadequacy of spectral-processing oriented clutter suppression methods, we model a clutter signal as multiple sinusoids plus Gaussian noise, and propose adaptive filtering approaches that better capture the temporal characteristics of the signal process. This idea leads to two research topics in signal processing: (1) signal modeling and parameter estimation, and (2) adaptive filtering in this particular signal environment. A high-resolution, low SNR threshold maximum likelihood (ML) frequency estimation and signal modeling algorithm is devised and proves capable of delineating both the spectral and temporal nature of the clutter return. Furthermore, the Least Mean Square (LMS) -based adaptive filter's performance for the proposed signal model is investigated, and promising simulation results have testified to its potential for clutter rejection leading to more accurate estimation of windspeed thus obtaining a better assessment of the windshear hazard.

N95-23792\*# Technology Integration and Development Group, Inc., Bedford, MA.

**GEARBOX VIBRATION DIAGNOSTIC ANALYZER Final Report** 

Cleveland, OH NASA Apr. 1992 19 p

(Contract(s)/Grant(s): NAS3-26134; RTOP 505-63-36)

(NASA-CR-189141; E-9589; NAS 1.26:189141; TII-R9201-001-RD) Avail: CASI HC A03/MF A01

This report describes the Gearbox Vibration Diagnostic Analyzer installed in the NASA Lewis Research Center's 500 HP Helicopter Transmission Test Stand to monitor gearbox testing. The vibration of the gearbox is analyzed using diagnostic algorithms to calculate a parameter indicating damaged components.

N95-24189\*# Toledo Univ., OH. Dept. of Mechanical Engineer-

UŠER'S GUIDE FOR ECAP2D: AN EULER UNSTEADY AERODYNAMIC AND AEROELASTIC ANALYSIS PROGRAM FOR TWO DIMENSIONAL OSCILLATING CASCADES, **VERSION 1.0** 

T. S. R. REDDY Cleveland, OH NASA Apr. 1995 71 p. (Contract(s)/Grant(s): NAG3-1137; RTOP 538-06-13) (NASA-CR-189146; E-9552; NAS 1.26:189146) Avail: CASI HC A04/MF A01

This guide describes the input data required for using ECAP2D (Euler Cascade Aeroelastic Program-Two Dimensional). ECAP2D can be used for steady or unsteady aerodynamic and aeroelastic analysis of two dimensional cascades. Euler equations are used to obtain aerodynamic forces. The structural dynamic equations are written for a rigid typical section undergoing pitching (torsion) and plunging (bending) motion. The solution methods include harmonic oscillation method, influence coefficient method, pulse response method, and time integration method. For harmonic oscillation method, example inputs and outputs are provided for pitching motion and plunging motion. For the rest of the methods, input and output for pitching motion only are given.

#### 13 **GEOSCIENCES**

Includes geosciences (general); earth resources; energy production and conversion; environment pollution; geophysics; meteorology and climatology; and oceanography.

#### A95-73517 PILOT WEATHER ADVISOR SYSTEM

SHASHI SETH VIGYAN, Inc. Hampton, VA, United States and NORMAN L. CRABILL Journal of Aircraft (ISSN 0021-8669) vol. 31, no. 6 November-December 1994 p. 1240-1243 refs (BTN-95-EIX95152582314) Copyright

We are currently developing a system called the Pilot Weather Advisor, which will shortly provide pilots with graphical weather depictions using color laptop computers, and eventually will be a part of an advanced technology flight management system. Through the use of broadcast satellite communications the PWxA system provides near real-time graphic depictions of weather information in the cockpit of aircraft in flight. The purpose of this system is to improve the safety and utility of general aviation and commercial aircraft operations. The concept of providing pilots with graphic depictions of weather conditions, overlaid on maps with geographical and navigational information, is extremely powerful. We have demonstrated the feasibility of using satellite communications to provide significant amounts of weather data to aircraft in flight. We have also demonstrated the usefulness of providing weather data in graphic form which increases efficiency and decreases pilot workload.

Author (EI)

#### A95-73521 **POLAR PATROL BALLOON**

JUN NISHIMURA Inst of Space and Astronautical Science, Tokyo, Japan, NOBUYUKI YAJIMA, HIROMITSU AKIYAMA, and S. KOKUBUN Journal of Aircraft (ISSN 0021-8669) vol. 31, no. 6 November-December 1994 p. 1264-1267 refs (BTN-95-EIX95152582318) Copyright

From late December of 1990 to early January of 1991, the National Institute of Polar Research, in collaboration with the Institute of Space and Astronautical Science, launched two large zeropressure balloons from Syowa Station, which is the Japanese research base in Antarctica. The balloon launched on December 25 returned near Syowa Station after 15 days of flight, keeping a consent altitude of about 30 km. It finally accomplished almost a one and half circumpolar flight. The total flight duration was about 40

days. This article will describe the balloon system and the flight behavior of the balloon. Author (EI)

A95-75031\* National Aeronautics and Space Administration. Goddard Space Flight Center, Greenbelt, MD.

### TRAJECTORY MODELING OF EMISSIONS FROM LOWER STRATOSPHERIC AIRCRAFT

LYNN C. SPARLING Hughes STX, Lanham, MD, US, MARK R. SCHOEBERL NASA. Goddard Space Flight Center, Greenbelt, MD, US, ANNE R. DOUGLASS NASA. Goddard Space Flight Center, Greenbelt, MD, US, CLARK J. WEAVER Applied Research Corporation, Landover, MD, US, PAUL A. NEWMAN NASA. Goddard Space Flight Center, Greenbelt, MD, US, and LESLIE R. LAIT Hughes STX, Lanham, MD, US Journal of Geophysical Research (ISSN 0148-0227) vol. 100, no. D1 January 20, 1995 p. 1427-1438 (HTN-95-41219) Copyright

A series of isentropic trajectory calculations has been performed for emissions by stratospheric aircraft moving across the northern midlatitude oceanic flight corridors. Emission of exhaust is simulated by the daily initialization of air parcels along a flight path on the 500 K isentropic surface. Parcels are tracked during the first three weeks of each January from 1980 to 1994 in order to determine the interannual variability in the spatial distribution of the exhaust and the likelihood of exposure to cold temperatures. Few parcels emitted along these flight paths at this time of year had experienced nitric acid trihydrate (NAT) formation temperatures, except for the particularly cold Januarys 1986, 1987, and 1992. Large zonal fluctuations in the distribution of the emissions are typical for this time year and are strongly dependent on flight path. An extended 6month (January-June) run in which parcels were released daily along the New York-London route shows that emissions in the flight corridor increase at a time-averaged rate which is nearly twice the rate at which the zonal average increases. In addition, local fluctuations of pollutant density can be several times higher than the zonal average and can persist for several weeks. A rapid buildup of emissions occurred during the summer months. These elevated emission levels must be considered in the interpretation of environmental impact assessments based on two-dimensional transport models. Author (Herner).

#### A95-75035

## THUNDERCLOUD ELECTRIC FIELD MODELING FOR THE IONOSPHERE-EARTH REGION. 1: DEPENDENCE ON CLOUD CHARGE DISTRIBUTION

PETER I. Y. VELINOV Bulgarian Academy of Sciences, Sofia, Bulgaria and PETER T. TONEV Bulgarian Academy of Sciences, Sofia, Bulgaria Journal of Geophysical Research (ISSN 0148-0227) vol. 100, no. D1 January 20, 1995 p. 1477-1485 Research sponsored by the Bulgarian National Science Foundation (HTN-95-41223) Copyright

The transmission of DC electric fields by thunderclouds with charge distributions is investigated analytically for the region between the ionosphere and the Earth surface. In such a way the hitherto existing presentations of thunderclouds by electric charge centers (monopole presentation) are generalized to much more adequate three-dimensional model charge regions. A modified ellipsoidal Gaussian profile for the charge distribution of the electrified cloud is accepted. The electrical conductivities are approximated by piecewise exponential functions of altitude. An assumption is made that the geomagnetic field lines in the lower and middle atmosphere are straight and vertical. Analytical solutions to Maxwell equations for the electric potential U and field E are obtained. The effect of the spatial distribution of the charge on E is investigated. The variations of the electric fields at the ionospheric and surface levels, which are caused by different charge distributions, horizontal sizes, and heights of the electrified clouds, are analyzed.

Author (Herner)

#### A95-75532 A NEW GENERATION OF INSTRUMENTS FOR FLYING LABORATORIES

A. V. LITINETSKIJ, V. V. VOLKOV, and YU. A. SEREGIN Meteorologiia i Gidrologiia (ISSN 0130-2906) no. 3 March 1994 p. 103-109 In RUSSIAN refs

(BTN-94-EIX94401363947) Copyright

Technical possibilities of the measurement-computational complexes 'Cyclon-1' and 'Cyclon-2' designed for airplanes-meteolaboratories and timely airplanes carrying out the works on cloud seeding to bring about additional precipitation are analyzed. The complexes have been installed on the AN-26 and YaK-40 airplanes, and passed the flying tests. Technical characteristics of the complexes are presented and the prospects of their improvement are discussed.

#### A95-75976

#### POSSIBLE EFFECTS OF CO2 INCREASE ON THE HIGH-SPEED CIVIL TRANSPORT IMPACT ON OZONE

G. PITARI Univ. degliStudi, L'Aquila, Italy and G. VISCONTI Univ. degliStudi, L'Aquila, Italy Journal of Geophysical Research (ISSN 0148-0227) vol. 99, no. D8 August 20, 1994 p. 16,879-16,896 Research sponsored by the Italian Space Agency and the Commission of European Communities

(HTN-95-60779) Copyright

The role of heterogeneous chemistry on the potential impact on ozone of a commercial fleet of high speed civil transport aircraft (HSCT) has been recently studied with assessment models. Here an attempt is made to model the effects of the carbon dioxide increase which is predicted in the furture atmosphere when HSCT should be operational. For this purpose we have first used a three-dimensional model for the radiative and dynamical calculations and then a photochemical two-dimensional model including an explicit gasparticle interaction in the process of aerosol formation. The denoxification and denitrification associated with the formation of nitric acid trihydrate (NAT) aerosols is shown to significantly affect the partition of chemical families. The radiative perturbation introduced by the CO2 increase is shown to perturb the stratospheric dynamics in such a way that the lower stratospheric residual circulation is enhanced. This has the effect of reducing by about 15% the stratospheric residence time of odd nitrogen injected by the aircraft, so that the overall perturbation of stratospheric chemistry due to HSCT is mitigated with respect to the reference case in which CO2 is kept at the present level. Another effect is found to be produced by the stratospheric temperature cooling following the CO2 increase. Our model predicts a large enhancement of the surface area density of NAT aerosols in the arctic region, so that the additional denitrification produces a further decrease of the relative role of the NO(X) catalytic cycle for ozone destruction in the lower stratosphere. For this reason, the CIO and OH decreases associated with the HSCT-induced NO(X) increase are found to be dominant in the ozone budget, thus producing a global ozone increase in the case of 500 ppmv CO2 (+0.27% for mach 2.4 and NO(X), emission index 15). The balance between the different tendencies of C1O, NO(X), and OH cycles is found to be closer in the reference case of 335 ppmv CO2, where a small column ozone depletion by HSCT is predicted (-0.53% globally). Author (Herner)

A95-76265\* National Aeronautics and Space Administration. Ames Research Center, Moffett Field, CA.

## ESTIMATES OF TOTAL ORGANIC AND INORGANIC CHLORINE IN THE LOWER STRATOSPHERE FROM IN SITU AND FLASK MEASUREMENTS DURING AASE 2

E. L. WOODBRIDGE National Oceanic and Atmospheric Administration, Boulder, CO, US, J. W. ELKINS National Oceanic and Atmospheric Administration, Boulder, CO, US, D. W. FAHEY National Oceanic and Atmospheric Administration, Boulder, CO, US, L. E. HEIDT National Center for Atmospheric Research, Boulder, CO, US, S. SOLOMON National Oceanic and Atmospheric Administration, Boulder, CO, US, T. J. BARING Colorado Univ., Boulder, CO, US, T. M. GILPIN National Center for Atmospheric Research, Boulder, CO, US, W. H. POLLACK National Center for Atmospheric Research, Boulder, CO, US, S. M. SCHAUFFLER National Center for Atmospheric Research, Boulder, CO, US, E. L. ATLAS National

Center for Atmospheric Research, Boulder, CO, US et al. Journal of Geophysical Research (ISSN 0148-0227) vol. 100, no. D2 February 20, 1995 p. 3057-3064 Research sponsored by NASA. Ames Research Center and JPL

(HTN-95-A0861) Copyright

Aircraft sampling has provided extensive in situ and flask measurements of organic chlorine species in the lower stratosphere. The recent Airborne Arctic Stratospheric Expedition 2 (AASE 2) included two independent measurements of organic chlorine species using whole air sample and real-time techniques. From the whole air sample measurements we derive directly the burden of total organic chlorine (CCI(y)) in the lower stratosphere. From the more limited real-time measurements we estimate the CCI(v) burden using mixing ratios and growth rates of the principal CCI(y) species in the troposphere in conjunction with results from a two-dimensional photochemical model. Since stratospheric chlorine is tropospheric in origin and tropospheric mixing ratios are increasing, it is necessary to establish the average age of a stratospheric air parcel to assess its total chlorine (Cl(sub Total)) abundance. Total inorganic chlorine (Cl(y)) in the parcel is then estimated by the simple difference, CI(y) = CI(sub Total) - CCI(y). The consistency of the results from these two quite different techniques suggests that we can determine the CCI(y) and CI(y) in the lower stratosphere with confidence. Such estimates of organic and inorganic chlorine are crucial in evaluating the photochemistry controlling chlorine partitioning and hence ozone loss processes in the lower stratosphere. Author (Herner)

A95-76266\* National Aeronautics and Space Administration. Ames Research Center, Moffett Field, CA.

### IN SITU OBSERVATIONS IN AIRCRAFT EXHAUST PLUMES IN THE LOWER STRATOSPHERE AT MIDLATITUDES

D. W. FAHEY National Oceanic and Atmospheric Administration, Boulder, CO, US, E. R. KEIM National Oceanic and Atmospheric Administration, Boulder, CO, US, E. L. WOODBRIDGE National Oceanic and Atmospheric Administration, Boulder, CO, US, R. S. GAO National Oceanic and Atmospheric Administration, Boulder, CO, US, K. A. BOERING Harvard Univ., Cambridge, MA, US, B. C. DAUBE Harvard Univ., Cambridge, MA, US, S. C. WOFSY Harvard Univ., Cambridge, MA, US, R. P. LOHMANN Pratt & Whitney, East Harford, CT, US, E. J. HINTSA Harvard Univ., Cambridge, MA, US, A. E. DESSLER Harvard Univ., Cambridge, MA, US et al. Journal of Geophysical Research (ISSN 0148-0227) vol. 100, no. D2 February 20, 1995 p. 3065-3074 Research sponsored by NASA. Ames Research Center, JPL, and NAS-NRC (HTN-95-A0862) Copyright

Instrumentation on the NASA ER-2 high-altitude aircraft has been used to observe engine exhaust from the same aircraft while operating in the lower stratosphere. Encounters with the exhaust plume occurred approximately 10 min after emission with spatial scales near 2 km and durations of up to 10 s. Measurements include total reactive nitrogen, NO(y), the component species NO and NO2, CO2, H2O, CO, N2O, condensation nuclei, and meteorological parameters. The integrated amounts of CO2 and H2O during the encounters are consistent with the stoichiometry of fuel combustion (1:1 molar). Emission indices (EI) for NO(x) (= NO + NO2), CO, and N2O are calculated using simultaneous measurements of CO2. El values for NO(x) near 4 g/(kg fuel) are in good agreement with values scaled from limited ground-based tests of the ER-2 engine. Non-NO(x) species comprise less than about 20% of emitted reactive nitrogen, consistent with model evaluations. In addition to demonstrating the feasibility of aircraft plume detection, these results increase confidence in the projection of emissions from current and proposed supersonic aircraft fleets and hence in the assessment of potential long-term changes in the atmosphere. Author (Hemer)

A95-76267\* National Aeronautics and Space Administration.
Goddard Space Flight Center, Greenbelt, MD.
SENSITIVITY OF TWO-DIMENSIONAL MODEL PREDICTIONS
OF OZONE RESPONSE TO STRATOSPHERIC AIRCRAFT: AN

#### **UPDATE**

DAVID B. CONSIDINE Applied Research Corp., Landover, MD, US, ANNE R. DOUGLASS NASA. Goddard Space Flight Center, Greenbelt, MD, US, and CHARLES H. JACKMAN NASA. Goddard Space Flight Center, Greenbelt, MD, US Journal of Geophysical Research (ISSN 0148-0227) vol. 100, no. D2 February 20, 1995 p. 3075-3090

(HTN-95-A0863) Copyright

The Goddard Space Flight Center (GSFC) two-dimensional model of stratospheric photochemistry and dynamics has been used to calculate the O3 response to stratospheric aircraft (high-speed civil transport (HSCT)) emissions. The sensitivity of the model O3 response was examined for systematic variations of five parameters and two reaction rates over a wide range, expanding on calculations by various modeling groups for the NASA High Speed Research Program and the World Meteorological Organization. In all, 448 model runs were required to test the effects of variations in the latitude, altitude, and magnetitude of the aircraft emissions perturbation, the background chlorine levels, the background sulfate aerosol surface area densities, and the rates of two key reactions. No deviation from previous conclusions concerning the response of O3 to HSCTs was found in this more exhaustive exploration of parameter space. Maximum O3 depletions occur for high-altitude, low altitude HSCT perturbations. Small increases in global total O3 can occur for low-altitude, high-altitude injections. Decreasing aerosol surface area densities and background chlorine levels increases the sensitivity of model O3 to the HSCT perturbations. The location of the aircraft emissions is the most important determinant of the model response. Response to the location of the HSCT emissions is not changed qualitatively by changes in background chlorine and aerosol loading. The response is also not very sensitive to changes in the rates of the reactions NO + HO2 yields NO2 + OH and HO2 + O3 yields OH + 2O2 over the limits of their respective uncertainties. Finally, levels of lower stratospheric HO(sub x) generally decrease when the HSCT perturbation is included, even though there are large increases in H2O due to the perturbation. Author (Herner)

#### A95-76394

### DIURNAL VARIATION OF LEE VORTICES IN TAIWAN AND THE SURROUNDING AREA

WEN-YIH SUN Purdue University, West Lafayette, IN, US and JIUN-DAR CHERN Purdue University, West Lafayette, IN, US Journal of the Atmospheric Sciences (ISSN 0022-4928) vol. 50, no. 20 October 15, 1993 p. 3404-3430

(Contract(s)/Grant(s): NSF ATMS-86-11729; NSF ATMS-89-07881) (HTN-95-91363) Copyright

Lee vortices have been frequently observed in the wake of mesoscale mountains under a low Froude number flow regime. During the Taiwan Area Mesoscale Experiment (TAMEX), a cyclonic vortex was observed to the lee of Taiwan by a P-3 aircraft. In this paper a numerical simulation is carried out to study this event. It is shown that the numerical results are capable of recapturing the detailed features as observed by airplane and surface analysis. The simulated surface pressure, wind field, and lee vortex are in good agreement with observations. The diurnal oscillation of cloudiness and precipitation in Taiwan is also consistent with the observations under undisturbed conditions during the TAMEX period. Under a prevailing southwesterly - to - westerly summer monsoon flow, numerical results demonstrate that the observed cyclonic vortex initially develops to the southeast of Taiwan after sunset, then drifts northeastward. The diurnal forcing not only generates land/sea breezes but also controls the vortex shedding. A sensitivity test without diurnal forcing indicates that the intrinsic vortex shedding period of Taiwan island is about 54 hours under the same initial condition. Due to the influence of diurnal forcing, however, the vortex shedding period becomes 24 hours, with the cyclonic vortex forming at 1700 LST and the anticyclonic vortex forming at 0500 LST. Moreover, the diurnal effect also influences the propagation of vortices, especially near the surface. The results of a vorticity budget study show that the tilting term is important to generate vorticity over

the Central Mountain Range. However, the stretching and advection terms are responsible for carrying and enhancing the vorticity to the lee side and are directly related to the initial development of the vortex. Each term in the vorticity budget is quite complicated due to the existence of clouds, boundary-layer forcing, and the circulation of land/sea breezes.

Author (Herner)

#### A95-76657

### REAL-TIME ESTIMATION OF ATMOSPHERIC TURBULENCE SEVERITY FROM IN-SITU AIRCRAFT MEASUREMENTS

LARRY B. CORNMAN Natl Cent for Atmospheric Research, Boulder, CO, United States, CORINNE S. MORSE, and GARY CUNNING Journal of Aircraft (ISSN 0021-8669) vol. 32, no. 1 January-February 1995 p. 171-177 refs

(BTN-95-EIX95182619231) Copyright

The quality of atmospheric turbulence detection and forecast information for the operational meteorology and aviation communities is directly linked to the quality of real-time measurements. Currently, the only direct data are subjective, qualitative, and intermittent pilot reports. This article describes techniques, suitable for real-time application on commercial transport aircraft, to generate quantitative and comprehensive turbulence measurements. These algorithms build on standard methods used in the analysis of aircraft response to turbulence, but are specifically designed to address the limitations of the available on-board data and computational resources.

#### A95-76737

#### 2 MICRON LIDAR FOR LASER-BASED REMOTE SENSING: FLIGHT DEMONSTRATION AND APPLICATION SURVEY

THOMAS J. WAGENER Honeywell Technology Cent, Bloomington, MN, United States, NICK DEMMA, JEFFREY D. KMETEC, and TRACY S. KUBO IEEE Aerospace and Electronic Systems Magazine (ISSN 0885-8985) vol. 10, no. 2 February 1995 p. 23-28 refs

(BTN-95-EIX95212641072) Copyright

A flight test of a diode-pumped solid-state 2 micron Doppler Light Detection And Ranging (LIDAR) system was conducted onboard the NASA Ames DC-8 Airborne Laboratory. This was the first ever airborne demonstration of a 2 micron diode-pumped solid-state Doppler LIDAR. The LIDAR performance was verified by comparing the true-airspeed (TAS) estimate with that found using the pneumatic air data system; excellent agreement was found. The capabilities of this pulsed 2 micron Doppler LIDAR system include high bandwidth air data determination without the need for extensive forebody calibration, remote wind profiling as far as several kilometers away from the aircraft, eye-safe laser transmission at 2 micron, and diode-pumped solid-state design for compact construction and reliable performance.

#### A95-77000

# A COMPARISON OF SOME AERODYNAMIC RESISTANCE METHODS USING MEASUREMENTS OVER COTTON AND GRASS FROM THE 1991 CALIFORNIA OZONE DEPOSITION EXPERIMENT

J. PADRO Atmospheric Environment Service, Downsview, Ontorio, Canada, W. J. MASSMAN USDA/Forest Service, Fort Collins, CO, US, R. H. SHAW Univ. of California, Davis, CA, US, A. DELANY NCAR, Boulder, CO, US, and S. P. ONCLEY NCAR, Boulder, CO, US Boundary-Layer Meteorology (ISSN 0006-8314) vol. 71, no. 4 December 1994 p. 327-339

(HTN-95-11295) Copyright

Measurements of dry deposition velocities (V(sub d)) of O3 (using the eddy correlation technique) made over a cotton field and senescent grass near Fresno California during July and August 1991 were used to test some dry deposition velocity models. Over the cotton field, the observed maximum daytime V(sub d) was about

0.8 cm/s and the average nighttime value was about 0.2 cm/s. Over the grass, daytime values averaged about 0.2 cm/s and nighttime values about 0.05 cm/s. Application of a site-specific model known as ADOM (Acid Deposition and Oxidant Model) over the cotton field generally overestimated the observations except for a few hours in the afternoon when the observations were underestimated. The overestimation was attributed to inadequacies in the surface resistance formulation and the underestimation to uncertainties in the aerodynamic formulation. Unlike previous studies which focused on the role of surface resistance, we perform additional tests using a large variety of aerodynamic resistance formulae, in addition to those in ADOM, to determine their influence on the modelled V(sub d) of O3 over cotton. Over grass, ADOM considerably overestimated the observations but showed improvement when other surface resistance formulations were applied. Author (Herner)

#### A95-77009

### GEOID LINEATIONS OF 1000 KM WAVELENGTH OVER THE CENTRAL PACIFIC

A. CAZENAVE GRGS-CNES, Toulouse, France, B. PARSONS Univ. of Oxford, Oxford, UK, and P. CALCAGNO GRGS-CNES, Toulouse, France Geophysical Research Letters (ISSN 0094-8276) vol. 22, no. 2 Jannuary 15, 1995 p. 97-100 Research sponsored by the Centre National d'Etudes Spatiales

(HTN-95-11304) Copyright

Altimeter profiles of the ERS-1 and Topex-Poseidon satellites have been used to compute a geoid surface from which we have extracted medium-wavelenth geoid anomalies over the central Pacific. In this region, the geoid shows prominent elongated anomalies of 20-40 cm in amplitude, with a spacing of approx. 1000 km and oriented N60 deg W. In the south central Pacific, the Polynesian hotspot swells seem to be located on the linear geoid highs. However, the latter extend much farther eastward, preceeding the active hotspots. To the north, other goold lines are visible but they do not coincide with known tectonic features. The wavelet transform applied to raw geoid data clearly detects a strong signal at the 1000-1200 km wavelength. The amplitude of the lineations increases with age, by a factor of 3 between 10 and 50 my. Analysis of seafloor topography corrected for age and sediments reveals topography anomalies correlated with the geoid lineations. Admittance and coherence calculations give high coherence (0.9) in the 1000-1200 km waveband and admittance values of 1.5 m/km at 10 my and 3 m/ km at 60 my. The mechanism producing the lineations is unclear. Their characteristics however are not incompatible with a convective origin. Author (Herner)

#### A95-77334

### TRANSPORT OF EXHAUST PRODUCTS IN THE NEAR TRAIL OF A JET ENGINE UNDER ATMOSPHERIC CONDITIONS

B. KARCHER Universitat Muenchen, Freising, Germany Journal of Geophysical Research (ISSN 0148-0227) vol. 99, no. D7 July 20, 1994 p. 14,509-14,517 Research sponsored by the Bundesministerium fuer Forschung und Technologie, Germany

(HTN-95-91421) Copyright

The transport of exhaust effluents and the possibility of water ice contrail formation are investigated under the specific fluid dynamical conditions in the near exhaust trail of a subsonic jet aircraft at cruise altitude. By means of a computational model describing the two-dimensional turbulent mixing of a single jet of hot exhaust gas with the atmosphere, representative results are discussed on the temperature and saturation ratio evolutions of air parcels in the jet flow field as well as on radial distributions of exhaust effluents undergoing chemical reactions behind the nozzle exit with prescribed, typical net reaction rates. The results underline the importance of a simultaneous treatment of spatially resolved jet expansion together with microphysical and chemical processes, because this coupling leads to distinct concentration patterns for various classes of chemical reactants and is essential for the detailed prediction of contrails. Author (Herner)

N95-23009\*# National Aeronautics and Space Administration. Langley Research Center, Hampton, VA.

COMPENDIUM OF NASA DATA BASE FOR THE GLOBAL TROPOSPHERIC EXPERIMENT'S PACIFIC EXPLORATORY MISSION WEST-A (PEM WEST-A)

G. L. GREGORY and A. D. SCOTT, JR. Feb. 1995 140 p (Contract(s)/Grant(s): RTOP 464-54-03-70)

(NASA-TM-109177; NAS 1.15:109177) Ávail: CASI HC A07/MF

This compendium describes aircraft data that are available from NASA's Pacific Exploratory Mission West-A (PEM West-A). PEM West is a component of the International Global Atmospheric Chemistry's (IGAC) East Asia/North Pacific Regional Study (APARE) project. The PEM- West program encompassed two expeditions to study contrasting meteorological regimes in the Pacific. Objectives of PEM West are to investigate the atmospheric chemistry of ozone over the northwest Pacific - natural budgets and the impact of anthropogenic sources; and to investigate sulfur chemistry - continental versus marine sulfur sources. PEM West-A was conducted in September 1991 during which the predominance of tropospheric air is from the mid-Pacific (marine) regions, but (at times) is modified/ mixed with Asian continental outflow. PEM West-B was conducted during February 1994, a period characterized by maximum continental outflow. PEM-B data (not included) will become public domain during the Summer of 1995. PEM West-A flight experiments were based at Japan, Hong Kong, and Guam. This document provides a representation of NASA DC-8 aircraft data that are available from NASA Langley's Distributed Active Archive Center (DAAC), which include numerous data such as meteorological observations, modeling products, results from surface studies, satellite observations, and sonde releases.

N95-23259\*# National Aeronautics and Space Administration. Lewis Research Center, Cleveland, OH.

### DESIGN OF A GAAS/GE SOLAR ARRAY FOR UNMANNED AERIAL VEHICLES

DAVID A. SCHEIMAN (NYMA, Inc., Brook Park, OH.), DAVID J. BRINKER, DAVID J. BENTS, and ANTHONY J. COLOZZA (NYMA, Inc., Brook Park, OH.) Mar. 1995 6 p Presented at the First World Conference on Photovoltaic Energy Conversion, Waikoloa, HI, 5-9 Dec. 1994; cosponsored by IEEE, PVSEC-Japan, and PVSEC-Europe

(Contract(s)/Grant(s): NAS3-27186; RTOP 233-02-0A) (NASA-TM-106870; E-9489; NAS 1.15:106870) Avail: CASI HC

Unmanned Aerial Vehicles (UAV) are being proposed for many applications including surveillance, mapping and atmospheric studies. These applications require a lightweight, low speed, medium to long duration airplane. Due to the weight, speed, and altitude constraints imposed on such aircraft, solar array generated electric power is a viable alternative to air-breathing engines. Development of such aircraft is currently being funded under the Environmental Research Aircraft and Sensor Technology (ERAST) program. NASA Lewis Research Center (LeRC) is currently building a Solar Electric Airplane to demonstrate UAV technology. This aircraft utilizes high efficiency Applied Solar Energy Corporation (ASEC) GaAs/Ge space solar cells. The cells have been provided by the Air Force through the ManTech Office. Expected completion of the plane is early 1995, with the airplane currently undergoing flight testing using battery power.

N95-23766\* Woods Hole Oceanographic Inst., MA. Dept. of Applied Ocean Physics and Engineering.

ASSIMILATION OF ALTIMETER DATA IN A QUASI-GEOSTROPHIC MODEL OF THE GULF STREAM SYSTEM: A DYNAMICAL PERSPECTIVE Ph.D. Thesis - MIT

ANTONIETTA CAPOTONDI Jun. 1993 243 p Limited Reproducibility: More than 20% of this document may be affected by microfiche quality

(Contract(s)/Grant(s): JPL-958208)

(NASA-CR-196313; NAS 1.26:196313; AD-A279436; WHOI-93-29)

Avail: Issuing Activity (Defense Technical Information Center (DTIC))

The dynamical aspects involved in the assimilation of altimeter data in a numerical ocean model have been investigated. The model used for this study is a quasi-geostrophic model of the Gulf Stream region. The data that have been assimilated are maps of sea surface height which have been obtained as the superposition of sea surface height variability deduced from the Geosat altimeter measurements and a mean field constructed from historical hydrographic data. The method used for assimilating the data is the nudging technique. Nudging has been implemented in such a way as to achieve a high degree of convergence of the surface model fields toward the observations. We have analyzed the mechanisms of the model adjustment, and the final statistical equilibrium characteristics of the model simulation when the surface data are assimilated. Since the surface data are the superposition of a mean component and an eddy component, in order to understand the relative role of these two components in determining the characteristics of the final statistical steady state, we have considered two different experiments: in the first experiment only the climatological mean field is assimilated, while in the second experiment the total surface streamfunction field (mean + eddies) has been used. We have found that the mean component of the surface data determines, to a large extent, the structure of the flow field in the subsurface layers, while the eddy field, as well as the inflow/outflow conditions at the open boundaries, affect its intensity. In particular, if surface eddies are not assimilated only a weak flow develops in the two deeper model layers where no inflow/outflow is prescribed at the boundaries.

## N95-23940\*# Consiglio Nazionale delle Ricerche, Rome (Italy). MAX-91: POLARIMETRIC SAR RESULTS ON MONTESPERTOLI SITE

S. BARONTI, S. LUCIANI (Tor Vergata Univ., Rome, Italy.), S. MORETTI (Florence Univ., Italy.), S. PALOSCIA, G. SCHIAVON (Tor Vergata Univ., Rome, Italy.), and S. SIGISMONDI (Florence Univ., Italy.) In JPL, Summaries of the 4th Annual JPL Airborne Geoscience Workshop. Volume 3: AIRSAR Workshop p 5-8 25 Oct. 1993 Sponsored by Italian Space Agency

Avail: CASI HC A01/MF A01

The polarimetric Synthetic Aperture Radar (SAR) is a powerful sensor for high resolution ocean and land mapping and particularly for monitoring hydrological parameters in large watersheds. There is currently much research in progress to assess the SAR operational capability as well as to estimate the accuracy achievable in the measurements of geophysical parameters with the presently available airborne and spaceborne sensors. An important goal of this research is to improve our understanding of the basic mechanisms that control the interaction of electro-magnetic waves with soil and vegetation. This can be done both by developing electromagnetic models and by analyzing statistical relations between backscattering and ground truth data. A systematic investigation, which aims at a better understanding of the information obtainable from the multifrequency polarimetric SAR to be used in agro-hydrology, is in progress by our groups within the framework of SIR-C/X-SAR Project and has achieved a most significant milestone with the NASA/JPL Aircraft Campaign named MAC-91. Indeed this experiment allowed us to collect a large and meaningful data set including multi-temporal multi-frequency polarimetric SAR measurements and ground truth. This paper presents some significant results obtained over an agricultural flat area within the Montespertoli site, where intensive ground measurements were carried out. The results are critically discussed with special regard to the information associated with polarimetric data.

N95-23947\*# Naval Research Lab., Washington, DC. Remote Sensing Div.

### STATISTICS OF MULTI-LOOK AIRSAR IMAGERY: A COMPARISON OF THEORY WITH MEASUREMENTS

J. S. LEE, K. W. HOPPEL, and S. A. MANGO In JPL, Summaries of the 4th Annual JPL Airborne Geoscience Workshop. Volume 3: AIRSAR Workshop p 33-36 25 Oct. 1993

Avail: CASI HC A01/MF A01

The intensity and amplitude statistics of SAR images, such as L-Band HH for SEASAT and SIR-B, and C-Band VV for ERS-1 have been extensively investigated for various terrain, ground cover and ocean surfaces. Less well-known are the statistics between multiple channels of polarimetric of interferometric SAR's, especially for the multi-look processed data. In this paper, we investigate the probability density functions (PDF's) of phase differences, the magnitude of complex products and the amplitude ratios, between polarization channels (i.e. HH, HV, and VV) using 1-look and 4-look AIRSAR polarimetric data. Measured histograms are compared with theoretical PDF's which were recently derived based on a complex Gaussian model.

N95-23948\*# New South Wales Univ., Kensington (Australia). Center for Remote Sensing and GIS.

### AIRSAR DEPLOYMENT IN AUSTRALIA, SEPTEMBER 1993: MANAGEMENT AND OBJECTIVES

A. K. MILNE and I. J. TAPLEY (Commonwealth Scientific and Industrial Research Organization, Wembley, Australia.) In JPL, Summaries of the 4th Annual JPL Airborne Geoscience Workshop. Volume 3: AIRSAR Workshop p 37-40 25 Oct. 1993

Avail: CASI HC A01/MF A01

Past co-operation between the NASA Earth Science and Applications Division and the CSIRO and Australian university researchers has led to a number of mutually beneficial activities. These include the deployment of the C-130 aircraft with TIMS, AIS, and NS001 sensors in Australia in 1985; collaboration between scientists from the USA and Australia in soils research which has extended for the past decade; and in the development of imaging spectroscopy where DSIRO and NASA have worked closely together and regularly exchanged visiting scientists. In May this year TIMS was flown in eastern Australia on board a CSIRO-owned aircraft together with a CSIRO-designed CO2 laser spectrometer. The Science Investigation Team for the Shuttle Imaging Radar (SIRC-C) Program includes one Australian Principal Investigator and ten Australian co-investigators who will work on nine projects related to studying land and near-shore surfaces after the Shuttle flight scheduled for April 1994. This long-term continued joint collaboration was progressed further with the deployment of AIRSAR downunder in September 1993. During a five week period, the DC-8 aircraft flew in all Australian states and collected data from some 65 individual test sites. Derived from text

15

#### MATHEMATICAL AND COMPUTER SCIENCES

Includes mathematical and computer sciences (general); computer operations and hardware; computer programming and software; computer systems; cybernetics; numerical analysis; statistics and probability; systems analysis; and theoretical mathematics.

A95-73471

## PRECONDITIONED DOMAIN DECOMPOSITION SCHEME FOR THREE-DIMENSIONAL AERODYNAMIC SENSITIVITY ANALYSIS

MOHAMED E. ELESHAKY Old Dominion Univ, Norfolk, VA, United States and OKTAY BAYSAL AIAA Journal (ISSN 0001-1452) vol. 32, no. 12 December 1994 p. 2489-2491 refs (BTN-95-EIX95152577612) Copyright

A preconditioned domain decomposition scheme is introduced for the solution of 3-D aerodynamic sensitivity equation. To reduce the memory requirement and ensure its convergence, this scheme uses the restarting GMRES procedure with preconditioners to solve the effective sensitivity equation of the boundary-interface cells in the SADD scheme. It is found that the commonly used preconditioners do not provide a converged solution for the present approach. However, excluding the dense matrices and the effect of cross terms between boundary interfaces produces an efficient and effective

preconditioning matrix. Excluding only the dense matrix and using the complete LU factorization of the coefficient matrix of the boundary-interface cells produce a more effective preconditioning matrix with 58% increase in the computer memory requirement.

#### A95-76588

### OBSERVATIONS ON USING EXPERIMENTAL DATA AS BOUNDARY CONDITIONS FOR COMPUTATIONS

PAUL D. ORKWIS Univ of Cincinnati, Cincinnati, OH, United States, CHUNG-JEN TAM, and PETER J. DISIMILE AIAA Journal (ISSN 0001-1452) vol. 33, no. 1 January 1995 p. 176-178 refs (BTN-95-EIX95182619103) Copyright

Many computational efforts have been undertaken to simulate experiments of open cavity flows. These computations have attempted to match the conditions of the experiment by employing the same nondimensional flowfield parameters and identical geometries. However, without intimate knowledge of the experimental procedures and apparatus, it is impossible of match all of the boundary conditions for these flow fields. In this paper, a procedure to determine the computational boundary conditions from an experimental supersonic open cavity flow field study is presented. The approach produces valid quantitative and qualitative field and surface property information that can be used to uncover the dynamic mechanisms that drive open cavity flow fields.

#### A95-76592

### AEROELASTIC VEHICLE MULTIVARIABLE CONTROL SYNTHESIS WITH ANALYTICAL ROBUSTNESS EVALUATION

BRETT NEWMAN Old Dominion Univ, Norfolk, VA, United States and DAVID K. SCHMIDT Journal of Guidance, Control, and Dynamics (ISSN 0731-5090) vol. 17, no. 6 November-December 1994 p. 1145-1153 refs

(BTN-95-EIX95182619115) Copyright

An aeroelastic vehicle model is briefly presented and deficiencies in the vehicle dynamics are noted. A new approach to model-following control synthesis is briefly discussed and applied to the vehicle model. A conventional or classical control synthesis approach is also considered for the purposes of comparison. The resulting compensators and closed-loop systems are analyzed with an analytical model to expose sources of system characteristics that limit the closed-loop system stability robustness. It is shown, that major among these critical characteristics are the frequency and damping of the vehicle first aeroelastic mode dipole; and closed-form expressions for these terms are presented as functions of the vehicle stability derivatives and vibrational characteristics.

#### A95-76598

### FUNCTIONAL AGILITY METRICS AND OPTIMAL TRAJECTORY ANALYSIS

GEORGE W. RYAN, III Univ of Kansas, Lawrence, KS, United States and DAVID R. DOWNING Journal of Guidance, Control, and Dynamics (ISSN 0731-5090) vol. 17, no. 6 November-December 1994 p. 1193-1197 refs

(BTN-95-EIX95182619121) Copyright

This paper examines several functional fighter agility metrics using optimal and nonoptimal maneuvers for a generic F-18-type aircraft to investigate the sensitivity of these metrics to the control strategy used to test them. The maneuvers tested are 180 deg heading changes. The metrics tested are the combat cycle time, the dynamic speed turn agility plots, and the relative energy state metric. Significant improvements in the measured agility metrics are possible if an optimal control strategy is used to test them. For example. reductions in combat cycle time of 60% with subsequent reductions in speed bleed rate of 80% are possible if an optimal maneuver is flown instead of a typical flight test maneuver. The specific agility improvements are vehicle airframe and control system dependent. However, the techniques used in this study are applicable to any aircraft and could provide insight into flight control system design and design tactics for maximizing performance during air combat engagements. Author (EI)

A95-76602

#### **MULTIVARIABLE STABILITY AND ROBUSTNESS OF** SEQUENTIALLY DESIGNED FEEDBACK SYSTEMS

BRETT NEWMAN Old Dominion Univ. Norfolk, VA, United States and DAVID K. SCHMIDT Journal of Guidance, Control, and Dynamics (ISSN 0731-5090) vol. 17, no. 6 November-December 1994 p. 1219-1227 refs

(BTN-95-EIX95182619125) Copyright

In sequential loop closure, the importance of evaluating the stability and stability robustness at the intermediate loop closures is well known. However, knowledge concerning how the intermediate loop closures, as well as the final loop closures, contribute to the stability and stability robustness of the overall feedback system holds special significance to the analysis and design of multivariable feedback systems. An analysis of the complete feedback system reveals the multivariable Nyquist contributions from the intermediate loop closures. It is also shown that the results greatly simplify if frequency separation exists between the intermediate loops. The analysis is presented with a two-step loop closure procedure using 'inner' and 'outer' loops that can be generalized to multistep situations. The control of the longitudinal dynamics of an aircraft is addressed to further clarify and demonstrate the results. Author (EI)

#### A95-76626

#### ATTAINABLE MOMENTS FOR THE CONSTRAINED CONTROL **ALLOCATION PROBLEM**

WAYNE C. DURHAM Virginia Polytechnic Inst and State Univ, Blacksburg, VA, United States Journal of Guidance, Control, and Dynamics (ISSN 0731-5090) vol. 17, no. 6 November-December 1994 p. 1371-1373 refs

(BTN-95-EIX95182619149) Copyright

Modern tactical aircraft are being designed with more than the classical set of control effectors. The effective allocation, or blending, of these controls to achieve specific objectives is the control allocation problem. A means of determining the subset of attainable moments that will yield a description of the boundary that contains the necessary information for the determination of controls in the allocation problem is therefore needed. Here, an algorithm is presented that is computationally simple, requiring only the inversion of a 2 x 2 matrix and a subsequent multiplication of an m-dimensional control vector (where m is the number of controls) by the control effectiveness matrix to calculate the coordinates of each vertex in moment space.

A95-76638\* National Aeronautics and Space Administration. Langley Research Center, Hampton, VA.

#### MULTIPLE-FUNCTION DIGITAL CONTROLLER SYSTEM FOR **ACTIVE FLEXIBLE WING WIND-TUNNEL MODEL**

SHERWOOD T. HOADLEY National Aeronautics and Space Administration, Langley Research Center, Hampton, VA and SANDRA M. MCGRAW Journal of Aircraft (ISSN 0021-8669) vol. 32, no. 1 January-February 1995 p. 32-38 refs (BTN-95-EIX95182619212) Copyright

A real-time multiple-function digital controller system was developed for the Active Flexible Wing program, which demonstrated through wind-tunnel tests that digital control can be used with great versatility to perform a multifunction task such as suppressing flutter and reducing loads during rolling maneuvers. The digital controller system (DCS) allowed simultaneous execution of two control laws: (1) flutter suppression and (2) either roll trim or a rolling maneuver load control. The DCS operated within, but independently of, a slower host operating system environment, at regulated speeds up to 200 Hz. It also coordinated the acquisition, storage, and transfer of data for near real-time controller performance evaluation and both open- and closed-loop plant estimation. It synchronized the operation of four different processing units, allowing flexibility in the number, form, functionality, and order of control laws, and variability in selection of sensors and actuators employed. Most importantly, the DCS enabled successful demonstration of active flutter suppression to conditions approximately 26% (in dynamic pressure) above the open-loop boundary in cases when the model was fixed-in-roll,

and up to 23% when it was free-to-roll. Aggressive roll maneuvers with load control were achieved above the flutter boundary. The purpose of this article is to present the development, validation, and wind-tunnel testing of this multiple-function digital controller system. Author (EI)

N95-23308\*# Kansas Univ., Lawrence, KS. Dept. of Aerospace Engineering.

ON-LINE, ADAPTIVE STATE ESTIMATOR FOR ACTIVE NOISE **CONTROL Abstract Only** 

TAE W. LIM In Hampton Univ., 1994 NASA-HU American Society for Engineering Education (ASEE) Summer Faculty Fellowship Program p 90 Dec. 1994 Avail: CASI HC A01/MF A02

Dynamic characteristics of airframe structures are expected to vary as aircraft flight conditions change. Accurate knowledge of the changing dynamic characteristics is crucial to enhancing the performance of the active noise control system using feedback control. This research investigates the development of an adaptive, on-line state estimator using a neural network concept to conduct active noise control. In this research, an algorithm has been developed that can be used to estimate displacement and velocity responses at any locations on the structure from a limited number of acceleration measurements and input force information. The algorithm employs band-pass filters to extract from the measurement signal the frequency contents corresponding to a desired mode. The filtered signal is then used to train a neural network which consists of a linear neuron with three weights. The structure of the neural network is designed as simple as possible to increase the sampling frequency as much as possible. The weights obtained through neural network training are then used to construct the transfer function of a mode in z-domain and to identify modal properties of each mode. By using the identified transfer function and interpolating the mode shape obtained at sensor locations, the displacement and velocity responses are estimated with reasonable accuracy at any locations on the structure. The accuracy of the response estimates depends on the number of modes incorporated in the estimates and the number of sensors employed to conduct mode shape interpolation. Computer simulation demonstrates that the algorithm is capable of adapting to the varying dynamic characteristics of structural properties. Experimental implementation of the algorithm on a DSP (digital signal processing) board for a plate structure is underway. The algorithm is expected to reach the sampling frequency range of about 10 kHz to 20 kHz which needs to be maintained for a typical active noise control application. **Author** 

N95-23419\*# Mississippi State Univ., Mississippi State, MS. Center for Computational Field Simulation.

#### TIGER: A USER-FRIENDLY INTERACTIVE GRID **GENERATION SYSTEM FOR COMPLICATED TURBOMACHINERY AND AXIS-SYMMETRIC** CONFIGURATIONS

MING H. SHIH and BHARAT K. SONI In NASA. Marshall Space Flight Center, Eleventh Workshop for Computational Fluid Dynamic Applications in Rocket Propulsion p 1149-1161 Jul. 1993 Sponsored by NASA. Lewis Research Center Avail: CASI HC A03/MF A10

The issue of time efficiency in grid generation is addressed by developing a user friendly graphical interface for interactive/automatic construction of structured grids around complex turbomachinery/axis-symmetric configurations. The accuracy of geometry modeling and its fidelity is accomplished by adapting the nonuniform rational b-spline (NURBS) representation. A customized interactive grid generation code, TIGER, has been developed to facilitate the grid generation process for complicated internal, external, and internal-external turbomachinery fields simulations. The FORMS Library is utilized to build user-friendly graphical interface. The algorithm allows a user to redistribute grid points interactively on curves/surfaces using NURBS formulation with accurate geometric definition. TIGER's features include multiblock, multiduct/shroud, multiblade row, uneven blade count, and patched/overlapping block

interfaces. It has been applied to generate grids for various complicated turbomachinery geometries, as well as rocket and missile configurations.

Author (revised)

N95-23603# Civil Aeromedical Inst., Oklahoma City, OK. DEVELOPMENT OF QUALIFICATION GUIDELINES FOR PERSONAL COMPUTER-BASED AVIATION TRAINING DEVICES Final Report

KEVIN W. WILLIAMS and ROBERT E. BLANCHARD Feb. 1995 28 p.

(DOT/FAA/AM-95/6) Avail: CASI HC A03/MF A01

Recent advances in the capabilities of personal computers have resulted in an increase in the number of flight simulation programs made available as Personal Computer-Based Aviation Training Devices (PCATD's). The potential benefits of PCATD's have been recognized by researchers and software/hardware developers alike. The purpose of this report is twofold: (1) present a conceptual approach based upon human learning principles and available flight training data for use in the development and evaluation of PCATD's; and (2) provide a detailed technical plan for an initial effort to develop and test guidelines for assessing the use of PCATD's in a training curriculum of a flight school conducted in accordance with the regulations stated in FAR Part 141. Author

#### 16

#### **PHYSICS**

Includes physics (general); acoustics; atomic and molecular physics; nuclear and high-energy physics; optics; plasma physics; solid-state physics; and thermodynamics and statistical physics.

## A95-73538 STRUCTURAL ACOUSTIC CALCULATIONS IN THE LOW-FREQUENCY RANGE

S. DEROSA CIRA SpA, Capua, Italy, G. PEZZULLO, L. LECCE, and F. MARULO Journal of Aircraft (ISSN 0021-8669) vol. 31, no. 6 November-December 1994 p. 1387-1394 refs (BTN-95-EIX95152582336) Copyright

The structural acoustic research activities pursued at the Aircraft Design Institute in collaboration with the Italian Aerospace Research Center during the last 5 yr are collected and summarized in this article. The fluid-structural interaction is approached from several viewpoints, paying attention to the theoretical analysis of the problem, as well as to its practical and realistic applications. The research results are presented with a view to outline both the future necessary developments of the theoretical approach, mainly looking at the possible extension of the deterministic approach, and the actual numerical-experimental comparisons that have been completed for gaining a necessary confidence level of the methodologies when facing real design problems.

#### A95-75494

### EFFECTS OF AMB PARAMETERS ON THE DYNAMIC STABILITY OF THE ROTOR

HONGLI WANG Tianjin Univ, Tianjin, China and ZHIQIANG WU Applied Mathematics and Mechanics (English Edition) (ISSN 0253-4827) vol. 15, no. 4 April 1994 p. 347-351 refs (BTN-94-EIX94381353450) Copyright

The motion equation of the rotor suspended by active magnetic bearing (AMB) was derived in which the nonlinear characteristics of the force was taken into account. Then the response equation was also derived, and based on the response equation, the functions of jump range and the effects of AMB parameters were discussed. It is shown that the jumps will appear as the eccentricity of the rotor is suitably chosen. In addition, the smaller the gap of the magnetic field, the smaller the ratio of the characteristic currents, or the larger the linearized range of the magnetic force. These results can be

used to improve the properties of electromagnetic bearings and controlling them.

N95-22675\*# Cambridge Acoustical Associates, Inc., Cambridge, MA

### THE USE OF COWL CAMBER AND TAPER TO REDUCE ROTOR/STATOR INTERACTION NOISE Final Report

R. MARTINEZ Cleveland, OH NASA Feb. 1995 89 p (Contract(s)/Grant(s): NAS3-27229; RTOP 535-03-10) (NASA-CR-195421; E-9364; NAS 1.26:195421) Avail: CASI HC A05/MF A01

The project had two specific technical objectives: (1) to develop a realistic three-dimensional model of tonal noise due to rotor/stator interaction, as the input field for predictions of diffraction and dissipation by a lined cowl; and (2) to determine whether the generator curve of that cowl, or duct, could be 'steered' to yield substantially lower values of propulsor noise along the engine's fore and aft open sectors. The more general and important aim of their research is to provide the commercial aircraft industry with a useful predictive tool to help it meet its noise-reduction goals. The work has produced a tractable and yet realistic model of rotor/stator interaction noise. The blades in the fan stage are radially divergent, twisted, and of realistically wide chords to match the high frequencies and speeds of the sound-production process. The resulting three-dimensional acoustic nearfield insonifies the interior wall of the diffracting cowl, whose shape, incidentally, does not affect fore or aft noise significantly (but other factors do).

N95-23178\*# National Aeronautics and Space Administration.
Lewis Research Center, Cleveland, OH.
SUPERSONIC LET NOISE REPUICTIONS PREDICTED WITH

### SUPERSONIC JET NOISE REDUCTIONS PREDICTED WITH INCREASED JET SPREADING RATE

MILO D. DAHL and PHILIP J. MORRIS (Pennsylvania State Univ., University Park, PA.) Mar. 1995 8 p Presented at the Joint Fluids Engineering Conference, Hilton Head, SC, 13-18 Aug. 1995; cosponsored by the ASME and the Japan Society of Mechanical Engineers

(Contract(s)/Grant(s): RTOP 505-62-52)

(NASA-TM-106872; E-9491; NAS 1.15:106872) Avail: CASI HC A02/MF A01

In this paper, predictions are made of noise radiation from single, supersonic, axisymmetric jets. We examine the effects of changes in operating conditions and the effects of simulated enhanced mixing that would increase the spreading rate of the jet shear layer on radiated noise levels. The radiated noise in the downstream direction is dominated by mixing noise and it is well described by the instability wave noise radiation analysis. A numerical prediction scheme is used for the mean flow providing an efficient method to obtain the mean flow development for various operating conditions and to simulate the enhanced mixing. Using far field radiated noise measurements as a reference, the calculations predict that enhanced jet spreading results in a reduction of radiated noise.

Author

N95-23503# Institute for Aerospace Research, Ottawa (Ontario). Structures, Materials and Propulsion Lab.

### DOUBLE PASS RETROREFLECTION FOR CORROSION DETECTION IN AIRCRAFT STRUCTURES

J. P. KOMOROWSKI, S. KRISHNAKUMAR, R. W. GOULD, N. C. BELLINGER, F. KARPALA (Diffracto Ltd., Windsor, Ontario.), and O. L. HAGENIERS (Diffracto Ltd., Windsor, Ontario.) *In* AGARD, Corrosion Detection and Management of Advanced Airframe Materials 12 p Jan. 1995

Copyright Avail: CASI HC A03/MF A03

An optical double pass retroreflection surface inspection technique (D Sight) used for visualizing surface distortions, depressions or pertrusions has been adapted as a rapid, enhanced visual inspection method inspection of large external aircraft surfaces. A project to fully characterize the D Sight indications of corrosion damage in lap splices is currently active. Over 150 large transport aircraft fuselage lap splice specimens have been collected. D Sight

Aircraft Inspection System - (DAIS) 250C has been developed and tested both in the laboratory and in the field. In laboratory tests lap splices retrieved from retired aircraft and subjected to accelerated corrosion and lap splices naturally corroded in-service were inspected with DAIS, eddy current, X-ray, shadow moire and subjected to tear down. It has been shown that the DAIS 250C is capable of locating corrosion pillowing indicative of a thickness loss as low as 2 percent. The first field trial of the DAIS 250C was based on two service bulletins requiring inspection of longitudinal and circumferential lap splices on the 737-200 aircraft from BS 259.5 to BS 1016. The DAIS 250C inspection, including analysis and report, took 36 man-hours. The recommended technique in the SB was close visual inspection and the time required according to the service bulletins, was 278 man-hours.

N95-24076# Los Alamos National Lab., NM.
PHONON CHARACTERISTICS OF HIGH (T SUB C)
SUPERCONDUCTORS FROM NEUTRON DOPPLER
BROADENING MEASUREMENTS

W. J. TRELA, G. H. KWEI, J. E. LYNN, and K. MEGGERS (Kiel Univ., Germany.) 1994 9 p Presented at the 1994 Fall Meeting of the Materials Research Society (MRS), Boston, MA, 28 Nov. - 2 Dec. 1994

(Contract(s)/Grant(s): W-7405-ENG-36)

(DE95-003703; LA-UR-94-3872; CONF-941144-14) Avail: CASI

Statistical information on the phonon frequency spectrum of materials can be measured by neutron transmission techniques if they contain nuclei with low energy resonances, narrow enough to be Doppler-broadened, in their neutron cross sections. The authors have carried out some measurements using this technique for materials of the lanthanum barium cuprate class, La(2-x)Ba(x)CuO4. Two samples with slightly different concentrations of oxygen, one being superconductive, the other not, were examined. Pure lanthanum cuprate was also measured. Lanthanum, barium and copper all have relatively low energy narrow resonances. Thus it should be possible to detect differences in the phonons carried by different kinds of atom in the lattice. Neutron cross section measurements have been made with high energy resolution and statistical precision on the 59 m flight path of LANSCE, the pulsed spallation neutron source at Los Alamos National Laboratory. Measurements on all three materials were made over a range of temperatures from 15 to 300 K, with small steps through the critical temperature region near 27 K. No significant changes in the mean phonon energy of the lanthanum atoms were observed near the critical temperature of the super-conducting material. It appears however that the mean phonon energy of lanthanum in the superconductor is considerably higher than that in the non-superconductors. The samples used in this series of experiments were too thin in barium and copper to determine anything significant about their phonon spectra.

N95-23168# Defense Advanced Research Projects Agency, Arlington, VA.

TECHNOLOGY REINVESTMENT PROJECT'S FOCUS AREA: AFFORDABLE POLYMER MATRIX COMPOSITES FOR AIRFRAME STRUCTURES

1994 202 p Workshops held in Seattle, WA, 16 Nov. 1994; and Oakland, CA, 18 Nov. 1994

(PB95-136032) Avail: CASI HC A10/MF A03

The mission of the Technology Reinvestment Project (TRP) is to stimulate the transition to a growing, integrated, national industrial capability that provides the most advanced, affordable military systems and the most competitive commercial products. Programs are structured to expand high quality employment opportunities in dual-use technologies that demonstrably enhance U.S. competitiveness and national security. The publication contains the transparencies from the TRP workshops held in Seattle, WA and Oakland, CA in November, 1994. It includes general sessions on TRP, Technology Development, Regional Technology Alliances, and

Manufacturing Education and Training, as well as the break out session on Affordable Polymer Matrix Composites for Airframe Structures. Also included are registration forms for both workshops.

NTIS

N95-23284\*# Arkansas Univ., Pine Bluff, AR. Dept. of Mathematics and Computer Science.

AUTOMATION TECHNOLOGY USING GEOGRAPHIC INFORMATION SYSTEM (GIS) Abstract Only

CYNTHIA L. BROOKS In Hampton Univ., 1994 NASA-HU American Society for Engineering Education (ASEE) Summer Faculty Fellowship Program p 64 Dec. 1994

Avail: CASI HC A01/MF A02

Airport Surface Movement Area is but one of the actions taken to increase the capacity and safety of existing airport facilities. The System Integration Branch (SIB) has designed an integrated system consisting of an electronic moving display in the cockpit, and includes display of taxi routes which will warn controllers and pilots of the position of other traffic and warning information automatically. Although, this system has in test simulation proven to be accurate and helpful; the initial process of obtaining an airport layout of the taxi-routes and designing each of them is a very tedious and timeconsuming process. Other methods of preparing the display maps are being researched. One such method is the use of the Geographical Information System (GIS). GIS is an integrated system of computer hardware and software linking topographical, demographic and other resource data that is being referenced. The software can support many areas of work with virtually unlimited information compatibility due to the system's open architecture. GIS will allow us to work faster with increased efficiency and accuracy while providing decision making capabilities. GIS is currently being used at the Langley Research Center with other applications and has been validated as an accurate system for that task. GIS usage for our task will involve digitizing aerial photographs of the topology for each taxirunway and identifying each position according to its specific spatial coordinates. The information currently being used can be integrated with the GIS system, due to its ability to provide a wide variety of user interfaces. Much more research and data analysis will be needed before this technique will be used, however we are hopeful this will lead to better usage of man-power and technological capabilities for the future.

N95-23320\*# College of William and Mary, Williamsburg, VA. Dept. of Mathematics.

PREPARATION OF COURSE MATERIALS: ELEMENTARY MATHEMATICS OF POWERED FLIGHT Abstract Only

GEORGE T. RUBLEIN In Hampton Univ., 1994 NASA-HU American Society for Engineering Education (ASEE) Summer Faculty Fellowship Program p 102 Dec. 1994

Avail: CASI HC A01/MF A02

Non-science students at William and Mary will soon be required to take a mathematics course in order to earn a bachelor's degree. A standard menu of technique courses is the usual way in which universities provide for this requirement: Trigonometry, probability, geometry for teachers, and the like. In this work, we attempt to break away from these largely unsuccessful choices. Our intent is to prepare material that sets a variety of simple mathematical procedures in the context of a commonly experienced part of students' lives: riding in commercial airplanes. The work, begun last summer at Langley, is now close to completion and trial in upcoming fall term at William and Mary. As of this writing, the narrative is complete for 12 to 14 projected sections. We have prepared material on wind triangles, wind roses, navigation maps, drag induced loss of velocity for unpowered missiles (tennis balls), luggage and its effect on center of gravity, localized magnetic declination and VOR orientation, geometry of great circles, terminal velocity for falling bodies, pressure vessels: tires and balloons and blimps, global structure of declination lines, map projections (mercator, azimuthal equidistant, Lambert), ears and their reaction to altitude change. The next

section will treat lift, drag and thrust. The last will treat control surfaces. The entire approach avoids any effort to investigate mathematical topics that arise in the solution of problems. And by the same token, we avoid any organized attempt to explain aeronautical engineering, even on an elementary level. We look only at enoughmathematics to do a problem and we select only engineering topics that permit some kind of (elementary) mathematical analysis. In the end, we will think of the material as successful if two things happen: Students must come away with some confidence that even lay people can quantify parts of their surroundings. Other potential instructors must be willing to gain enough familiarity with the physical content of the material so that it can be used at other universities. Author

N95-23872\*# National Aeronautics and Space Administration. Ames Research Center, Moffett Field, CA. **AVIRIS AND TIMS DATA PROCESSING AND DISTRIBUTION** AT THE LAND PROCESSES DISTRIBUTED ACTIVE ARCHIVE

G. R. MAH and J. MYERS In JPL, Summaries of the 4th Annual JPL Airborne Geoscience Workshop, Volume 1: AVIRIS Workshop p 109-112 25 Oct. 1993

Avail: CASI HC A01/MF A03

The U.S. Government has initiated the Global Change Research program, a systematic study of the Earth as a complete system. NASA's contribution of the Global Change Research Program is the Earth Observing System (EOS), a series of orbital sensor platforms and an associated data processing and distribution system. The EOS Data and Information System (EOSDIS) is the archiving, production, and distribution system for data collected by the EOS space segment and uses a multilayer architecture for processing, archiving, and distributing EOS data. The first layer consists of the spacecraft ground stations and processing facilities that receive the raw data from the orbiting platforms and then separate the data by individual sensors. The second layer consists of Distributed Active Archive Centers (DAAC) that process, distribute, and archive the sensor data. The third laver consists of a user science processing network. The EOSDIS is being developed in a phased implementation. The initial phase, Version 0, is a prototype of the operational system. Version 0 activities are based upon existing systems and are designed to provide an EOSDIS-like capability for information management and distribution. An important science support task is the creation of simulated data sets for EOS instruments from precursor aircraft or satellite data. The Land Processes DAAC, at the EROS Data Center (EDC), is responsible for archiving and processing EOS precursor data from airborne instruments such as the Thermal Infrared Multispectral Scanner (TIMS), the Thematic Mapper Simulator (TMS), and Airborne Visible and Infrared Imaging Spectrometer (AVIRIS). AVIRIS, TIMS, and TMS are flown by the NASA-Ames Research Center ARC) on an ER-2. The ER-2 flies at 65000 feet and can carry up to three sensors simultaneously. Most jointly collected data sets are somewhat boresighted and roughly registered. The instrument data are being used to construct data sets that simulate the spectral and spatial characteristics of the Advanced Spaceborne Thermal Emission and Reflection Radiometer (ASTER) instrument scheduled to be flown on the first EOS-AM spacecraft. The ASTER is designed to acquire 14 channels of land science data in the visible and near-IR (VNIR). shortwave-IR (SWIR), and thermal-IR (TIR) regions from 0.52 micron to 11.65 micron at high spatial resolutions of 15 m to 90 m. Stereo data will also be acquired in the VNIR region in a single band. The AVIRIS and TMS cover the ASTER VNIR and SWIR bands, and the TIMS covers the TIR bands. Simulated ASTER data sets have been generated over Death Valley, California, Cuprite, Nevada, and the Drum Mountains, Utah using a combination of AVIRIS, TIMS, amd TMS data, and existing digital elevation models (DEM) for the topographic information.

## 19 **GENERAL**

N95-23276\*# Hampton Univ., VA. Dept. of Architecture. 1994 NASA-HU AMERICAN SOCIETY FOR ENGINEERING **EDUCATION (ASEE) SUMMER FACULTY FELLOWSHIP PROGRAM Abstracts Only** 

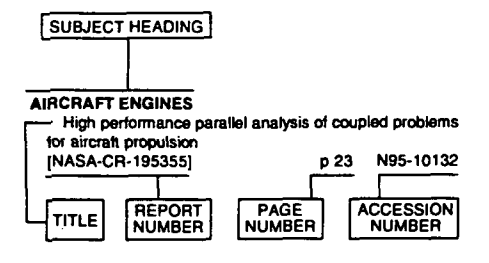
JOHN H. SPENCER, comp. and DEBORAH B. YOUNG, comp. (Old Dominion Coll., Norfolk, VA.) Dec. 1994 155 p Program held in Hampton, VA, 6 Jun. - 12 Aug. 1994

(Contract(s)/Grant(s): NGT-47-020-800)

(NASA-CR-194972; NAS 1.26:194972) Avail: CASI HC A08/MF

Since 1964, the National Aeronautics and Space Administration (NASA) has supported a program of summer faculty fellowships for engineering and science educators. In a series of collaborations between NASA research and development centers and nearby universities, engineering faculty members spend 10 weeks working with professional peers on research. The Summer Faculty Program Committee of the American Society for Engineering Education supervises the programs. Objectives: (1) To further the professional knowledge of qualified engineering and science faculty members: (2) To stimulate and exchange ideas between participants and NASA; (3) To enrich and refresh the research and teaching activities of participants' institutions; (4) To contribute to the research objectives of the NASA center. For individual titles, see N95-23277 through N95-23333.

## Typical Subject Index Listing



The subject heading is a key to the subject content of the document. The title is used to provide a description of the subject matter. When the title is insufficiently descriptive of document content, a title extension is added, separated from the title by three hyphens. The accession number and the page number are included in each entry to assist the user in locating the abstract in the abstract section. If applicable, a report number is also included as an aid in identifying the document. Under any one subject heading, the accession numbers are arranged in sequence.

### ABLATION

Hypersonic nonequilibrium Navier-Stokes solutions over an ablating graphite nosetip 1BTN-95-EIX951525832521 p 305 A95-73553

### ACCELERATED LIFE TESTS

Interlaminar shear test method development for long term durability testing of composites

p 301 N95-23300 Eddy current detection of pitting corrosion around fastener holes p 315 N95-23507

Test method and test results environmental p 302 N95-23509 assessment of aircraft materials ACCELERATION (PHYSICS)

Dynamical instability of the aerogravity assist maneuver

[BTN-95-EIX95152583282] p 298 A95-73583

**ACCELEROMETERS** Covariance analysis of strapdown INS considering gyrocompass characteristics

BTN-95-EIX95202637592 n 279 A95-76697 **ACCIDENT PREVENTION** 

### Mishap risk control for advanced aerospace/composite materials

p 301 N95-23031

## **ACCOMMODATION COEFFICIENT**

Calculation of satellite drag coefficients p 300 N95-23781 IAD-A2851181

### ACOUSTIC EMISSION

Mach wave emission from a high-temperature supersonic iet

IBTN-95-EIX951525775861 p 264 A95-73496 ACOUSTIC MEASUREMENT

Structural acoustic calculations in the low-frequency

p 323 A95-73538 | BTN-95-EIX95152582336 | ACTIVE CONTROL

Grid refinement test of time-periodic flows over bluff hodies [BTN-94-EIX94401378822] p 307 A95-76491

Summary of an active flexible wing program

p 283 A95-76635 IBTN-95-FIX951826192091 Simulation and model reduction for the active flexible

IBTN-95-EIX951826192111 p 295 A95-76637 Multiple-function digital controller system for active flexible wing wind-tunnel model

[BTN-95-EIX95182619212] p 322 A95-76638 On-line analysis capabilities developed to support the active flexible wing wind-tunnel tests

IBTN-95-EIX95182619213 | p 296 A95-76639 Flutter suppression control law design and testing for the active flexible wing

|BTN-95-EIX95182619214| p 292 A95-76640 Design and multifunction tests a frequency domain-based active flutter suppression system

p 292 A95-76641 IBTN-95-EIX951826192151 Rolling maneuver load alleviation using active controls IBTN-95-EIX951826192171 p 270 A95-76643 Active control of panel vibrations induced by a boundary

INASA-CR-197867 I p 273 N95-23182 On-line, adaptive state estimator for active noise p 322 N95-23308 control

Supersonic laminar flow control research NASA-CR-197938) p 275 N95-23669

### **ACTIVE SATELLITES**

Effects of satellite bunching on the probability of collision geosynchronous orbit

1BTN-95-EIX951525832761 p 298 A95-73577

### ACTUATORS

Motor drive technologies for the power-by-wire (PBW) program: Options, trends and tradeoffs

NASA-TM-106885 p 295 N95-23671

ADAPTIVE CONTROL Adaptive finite element method for turbulent flow near

p 305 A95-73460 [BTN-95-EIX95142553038] Direct adaptive performance optimization of subsonic

transports: A periodic perturbation technique INASA-TM-46761 p 284 N95-22829

### ADAPTIVE FILTERS

Maximum-likelihood spectral estimation and adaptive filtering techniques with application to airborne Doppler weather radar

p 316 N95-23670

[NASA-CR-197699]

## ADHESION TESTS

Evaluation of advanced aerospace materials by depth sensing indentation and scratch methods

[BTN-95-EIX95152584678] p 282 A95-73590 Corrosion protection measures for CFC/metal joints of

fuel integral tank structures of advanced military aircraft p 303 N95-23510

### ADHESIVE BONDING

Evaluation of advanced aerospace materials by depth sensing indentation and scratch methods

[BTN-95-EIX95152584678] p 282 A95-73590

### **AEROACOUSTICS**

Analysis of a higher harmonic control test to reduce blade vortex interaction noise

[BTN-95-EIX95152582330] p 265 A95-73532 Numerical study of sound generation due to a spinning

[BTN-95-EIX95182619075] p 307 A95-75760 Aeroacoustic model for weak shock waves based on

p 269 A95-75761 IBTN-95-FIX951826190761

Supersonic jet noise reductions predicted with increased iet spreading rate

NASA-TM-106872) p 323 N95-23178

### AEROBRAKING

Minimum-mass design of sandwich aerobrakes for a lunar transfer vehicle BTN-95-EIX95212645707 | p 299 A95-76759

## **AEROCAPTURE**

Fuel-optimal bank-angle control for lunar-return aerocapture [BTN-95-EIX95212645706] p 299 A95-76758

## AERODYNAMIC BALANCE

System for determining aerodynamic imbalance NASA-CASE-ARC-11913-1 p 311 N95-23377

### **AERODYNAMIC BRAKES**

Minimum-mass design of sandwich aerobrakes for a unar transfer vehicle

p 299 A95-76759 IBTN-95-EIX95212645707 I

## AFRODYNAMIC CHARACTERISTICS

Aerodynamic characteristics of a hypersonic viscous p 266 A95-73552 |BTN-95-EIX95152583251|

Aerodynamic characteristics of a canard-controlled missile at high angles of attack

|BTN-95-EIX95152583257| p 267 A95-73558 Aerodynamic characteristics external store configurations at low speeds

|BTN-95-EIX95182619230| p 271 A95-76656 Thin tailored composite wing for civil tiltrotor

p 285 N95-23317

Aerodynamic flight control to increase payload capability of future launch vehicles INASA-CR-1977041

p 300 N95-24032

### **AERODYNAMIC COEFFICIENTS**

Navier-Stokes prediction of large-amplitude delta-wing roll oscillations

[BTN-95-EIX95152582329] p 281 A95-73531 Analytic prediction of lift for delta wings with partial

[BTN-95-EIX95152582345] p 266 A95-73547

Drag function modeling for air traffic simulation p 279 A95-76631 [BTN-95-EIX95182619154]

Unsteady ground effects on aerodynamic coefficients IBTN-95-EIX951826192331 p 271 A95-76659

Calculation of satellite drag coefficients

p 300 N95-23781 IAD-A2851181

### **AERODYNAMIC CONFIGURATIONS**

Aerodynamic shape optimization using preconditioned conjugate gradient methods

|BTN-95-EIX95142553033| p 263 A95-73465 Base drag prediction on missile configurations

p 266 A95-73557 IBTN-95-EIX951525832561 Aerodynamic characteristics of a canard-controlled

missile at high angles of attack [BTN-95-EIX95152583257] p 267 A95-73558 Impeller flow field characterization with a laser two-focus

p 313 N95-23440 velocimeter AERODYNAMIC DRAG

Analytic prediction of lift for delta wings with partial [BTN-95-EIX95152582345] p 266 A95-73547

Base drag prediction on missile configurations [BTN-95-EIX95152583256] p 266 A9 p 266 A95-73557 Improved version of the Naval Surface Warfare Center

eroprediction code (AP93) p 267 A95-73561 IBTN-95-EIX951525832601

Drag function modeling for air traffic simulation

p 279 A95-76631 [BTN-95-EIX95182619154] Application of Navier-Stokes aeroelastic methods to improve fighter wing maneuver performance

|BTN-95-EIX95182619218| p 284 A95-76644 Numerical investigation of supersonic flows around a spiked blunt body

[BTN-95-EIX95212645690] p 271 A95-76742 A comparison of some aerodynamic resistance methods using measurements over cotton and grass from the 1991

California ozone deposition experiment IHTN-95-112951 p.319 A95-77000 Calculation of satellite drag coefficients

p 300 N95-23781 IAD-A2851181

## **AERODYNAMIC FORCES**

Static aeroelastic characteristics of a composite wing p 282 A95-73542 [BTN-95-EIX95152582340] Flutter of an infinitely long panel in a duct

### BTN-95-EIX95182619087 p 291 A95-75772 **AERODYNAMIC HEAT TRANSFER**

Numerical computation of aerodynamics and heat transfer in a turbine cascade and a turn-around duct using p 313 N95-23444 advanced turbulence models

### AERODYNAMIC HEATING

Hypersonic convective heat transfer over 140-deg blunt

cones in different gases [BTN-95-EIX95152583253] p 306 A95-73554

Convective and radiative heat transfer analysis for the	Higher-order viscous shock-layer solutions for	AERONAUTICAL SATELLITES
fire 2 forebody	high-altitude flows	Development of aeronautical mobile satellite services
BTN-95-EIX95182617460  p 268 A95-75731	[BTN-95-EIX95152583255] p 306 A95-73556	over the past thirty years 1BTN-95-EIX95152569458   p 305 A95-73498
AERODYNAMIC INTERFERENCE Wing vertical position effects on wing-body carryover	Aerodynamic characteristics of a canard-controlled missile at high angles of attack	AEROSERVOELASTICITY
for noncircular missiles	[BTN-95-EIX95152583257] p 267 A95-73558	Simulation and model reduction for the active flexible
BTN-95-EIX95182617462  p 268 A95-75733	Improved version of the Naval Surface Warfare Center	wing program  BTN-95-EIX95182619211  p 295 A95-76637
Some aspects of the aerodynamics of separating strap-ons	aeroprediction code (AP93)	AEROSOLS
[BTN-95-EIX95182617464] p 298 A95-75735	[BTN-95-EIX95152583260] p 267 A95-73561 Functional dependence of trajectory dispersion on initial	Modeling aerosol emissions from the combustion of
A wall interference assessment/correction system	condition errors	composite materials p 301 N95-23038
[NASA-CR-197421] p 309 N95-23183 <b>AERODYNAMIC LOADS</b>	[BTN-95-EIX95152583263] p 298 A95-73564	AEROSPACE ENGINEERING Research and Technology, 1994
Design constraints in the payload-range diagram of	Supersonic axisymmetric conical flow solutions for	[NASA-TM-106764] p 262 N95-24025
ultrahigh capacity transport airplanes	different ratios of specific heats [BTN-95-EIX95152583283] p 306 A95-73584	AEROSPACE INDUSTRY  Overview of AlliedSignat's avionics development in the
[BTN-95-EIX95152582319] p 276 A95-73522 Hypersonic rarefied flow past spheres including wake	Analytical solution for controls, heats, and states of flight	CIS
structure	trajectories	[BTN-95-EIX95212641069] p 287 A95-76734
[BTN-95-EIX95152583250] p 305 A95-73551	[BTN-95-EIX95152583286] p 282 A95-73587 Aerodynamics of the Shuttle Orbiter at high altitudes	AEROSPACE VEHICLES  Application of the multigrid solution technique to
Summary of an active flexible wing program   BTN-95-EIX95182619209   p 283 A95-76635	[BTN-95-EIX95182617454] p 298 A95-75725	hypersonic entry vehicles
Rolling maneuver load alleviation using active controls	Some aspects of the aerodynamics of separating	[BTN-95-EIX95152583254] p 306 A95-73555
[BTN-95-EIX95182619217] p 270 A95-76643	strap-ons	Integrated design of hypersonic waveriders including inlets and tailfins
Minimum-mass design of sandwich aerobrakes for a lunar transfer vehicle	[BTN-95-EIX95182617464] p 298 A95-75735 Comparison of linear stability results with flight transition	[BTN-95-EIX95212645692] p 271 A95-76744
[BTN-95-EIX95212645707] p 299 A95-76759	data	Moving mass trim control for aerospace vehicles
System for determining aerodynamic imbalance	[BTN-95-EIX95182619097] p 283 A95-76582	[DE95-002602] p 299 N95-23532
[NASA-CASE-ARC-11913-1] p 311 N95-23377 Review of some results of the author's fatigue	Aeroelastic vehicle multivariable control synthesis with	AEROTHERMOCHEMISTRY Hypersonic nonequilibrium Navier-Stokes solutions over
investigations with applications in engineering and material	analytical robustness evaluation [BTN-95-EIX95182619115] p 321 A95-76592	an ablating graphite nosetip
science	Functional agility metrics and optimal trajectory	[BTN-95-EIX95152583252] p 305 A95-73553
TAE-698   p 316 N95-23662 AERODYNAMIC NOISE	analysis	AEROTHERMODYNAMICS
Numerical study of sound generation due to a spinning	[BTN-95-EIX95182619121] p 321 A95-76598	Hypersonic nonequilibrium Navier-Stokes solutions over an ablating graphite nosetip
vortex pair	Analytical solution and parameter estimation of projectile dynamics	[BTN-95-EIX95152583252] p 305 A95-73553
[BTN-95-EIX95182619075] p 307 A95-75760 Supersonic jet noise reductions predicted with increased	[BTN-95-EIX95212645695] p 272 A95-76747	Hypersonic convective heat transfer over 140-deg blunt
jet spreading rate	Calculation of wing-alone aerodynamics to high angles	cones in different gases [BTN-95-EIX95152583253] p 306 A95-73554
[NASA-TM-106872] p 323 N95-23178	of attack [BTN-95-EIX95212645713] p 261 A95-76765	AFTERBODIES
ARRODYNAMIC STABILITY  Analytical study of the neutral stability of a model	Mach 10 computational study of a three-dimensional	Experimental investigation of the flowfield about an
hypersonic boundary layer	scramjet inlet flow field	upswept afterbody
[BTN-95-EIX95152577589] p 263 A95-73493	[NASA-TM-4602] p 310 N95-23210	[BTN-95-EIX95152582321] p 265 A95-73524 Supersonic near-wake afterbody boattailing effects on
Navier-Stokes prediction of large-amplitude delta-wing roll oscillations	Aerodynamic design optimization with sensitivity analysis and computational fluid dynamics	axisymmetric bodies
[BTN-95-EIX95152582329] p 281 A95-73531	[NASA-CR-197419] p 274 N95-23218	[BTN-95-EIX95182617465] p 268 A95-75736
Further analysis of high-rate rolling experiments of a	Aerodynamic surface distension system for high angle	Experimental results for a hypersonic nozzle/afterbody
65-deg delta wing	of attack forebody vortex control	flow field
	of attack forebody vortex control [NASA-CASE-ARC-11979-1] p 286 N95-23390	
65-deg delta wing  BTN-95-EIX95152582331  p 281 A95-73533 The influence of atternate inter-blade connections on ground resonance	of attack forebody vortex control	flow field   NASA-TM-4638   p 274 N95-23250 Validation of a Computational Fluid Dynamics (CFD) code for supersonic axisymmetric base flow
65-deg delta wing  BTN-95-EIX95152582331  p 281 A95-73533 The inlluence of alternate inter-blade connections on ground resonance  HTN-95-80859  p 267 A95-75101	of attack forebody vortex control [NASA-CASE-ARC-11979-1] p 286 N95-23390 Aerodynamic design and analysis of a highly loaded turbine exhaust p 312 N95-23435 Numerical computation of aerodynamics and heat	flow field [NASA-TM-4638] p 274 N95-23250 Validation of a Computational Fluid Dynamics (CFD) code for supersonic axisymmetric base flow p 315 N95-23652
65-deg delta wing   BTN-95-EIX95152582331   p 281 A95-73533   The influence of atternate inter-blade connections on ground resonance   HTN-95-80859   p 267 A95-75101   Dynamic investigation of the angular motion of a rotating body-parachute system	of attack forebody vortex control [NASA-CASE-ARC-11979-1] p 286 N95-23390 Aerodynamic design and analysis of a highly loaded turbine exhaust Numerical computation of aerodynamics and heat transfer in a turbine cascade and a turn-around duct using	flow field   NASA-TM-4638   p 274 N95-23250 Validation of a Computational Fluid Dynamics (CFD) code for supersonic axisymmetric base flow
65-deg delta wing  BTN-95-EIX95152582331  p 281 A95-73533   The influence of atternate inter-blade connections on ground resonance  HTN-95-80859  p 267 A95-75101   Dynamic investigation of the angular motion of a rotating body-parachute system  BTN-95-EIX95182619220  p 270 A95-76646	of attack forebody vortex control [NASA-CASE-ARC-11979-1] p 286 N95-23390 Aerodynamic design and analysis of a highly loaded turbine exhaust p 312 N95-23435 Numerical computation of aerodynamics and heat	flow field    NASA-TM-4638   p 274 N95-23250    Validation of a Computational Fluid Dynamics (CFD)   code for supersonic axisymmetric base flow   p 315 N95-23652    AGING (MATERIALS)   N95-23652    Oklahoma City air logistics center (USAF) aging aircraft corrosion program   p 262 N95-23519
65-deg delta wing   BTN-95-EIX95152582331   p 281 A95-73533   The influence of atternate inter-blade connections on ground resonance   HTN-95-80859   p 267 A95-75101   Dynamic investigation of the angular motion of a rotating body-parachute system	of attack forebody vortex control [NASA-CASE-ARC-11979-1] p 286 N95-23390 Aerodynamic design and analysis of a highly loaded turbine exhaust p 312 N95-23435 Numerical computation of aerodynamics and heat transfer in a turbine cascade and a turn-around duct using advanced turbulence models p 313 N95-23444 NTS-spill test facility wind tunnel exhaust plume characterization	flow field  [NASA-TM-4638]  Validation of a Computational Fluid Dynamics (CFD) code for supersonic axisymmetric base flow  p 315  N95-23652  AGING (MATERIALS)  Oklahoma City air logistics center (USAF) aging aircraft corrosion program  p 262  N95-23519  AGRICULTURE
65-deg delta wing  BTN-95-EIX95152582331  p 281 A95-73533 The influence of atternate inter-blade connections on ground resonance  HTN-95-80859  p 267 A95-75101 Dynamic investigation of the angular motion of a rotating body-parachute system  BTN-95-EIX95182619220  p 270 A95-76646 AERODYNAMIC STALLING Computation of the poststall behavior of a circulation controlled airfoil	of attack forebody vortex control [NASA-CASE-ARC-11979-1] p 286 N95-23390 Aerodynamic design and analysis of a highly loaded turbine exhaust p 312 N95-23435 Numerical computation of aerodynamics and heat transfer in a turbine cascade and a turn-around duct using advanced turbulence models p 313 N95-23444 NTS-spill test facility wind tunnel exhaust plume characterization [DE95-003630] p 297 N95-24019	flow field    NASA-TM-4638   p 274 N95-23250    Validation of a Computational Fluid Dynamics (CFD)   code for supersonic axisymmetric base flow   p 315 N95-23652    AGING (MATERIALS)   N95-23652    Oklahoma City air logistics center (USAF) aging aircraft corrosion program   p 262 N95-23519
65-deg delta wing   BTN-95-EIX95152582331  p 281 A95-73533  The influence of alternate inter-blade connections on ground resonance  HTN-95-B0859  p 267 A95-75101  Dynamic investigation of the angular motion of a rotating body-parachute system  BTN-95-EIX95182619220  p 270 A95-76646  AERODYNAMIC STALLING  Computation of the poststall behavior of a circulation controlled airfoil  BTN-95-EIX95152582320  p 264 A95-73523	of attack forebody vortex control [NASA-CASE-ARC-11979-1] p 286 N95-23390 Aerodynamic design and analysis of a highly loaded turbine exhaust p 312 N95-23435 Numerical computation of aerodynamics and heat transfer in a turbine cascade and a turn-around duct using advanced turbulence models p 313 N95-23444 NTS-spill test facility wind tunnel exhaust plume characterization	flow field  [NASA-TM-4638]  Validation of a Computational Fluid Dynamics (CFD) code for supersonic axisymmetric base flow  p 315  N95-23652  AGING (MATERIALS)  Oklahoma City air logistics center (USAF) aging aircraft corrosion program  p 262  N95-23519  AGRICULTURE  MAX-91: Polarimetric SAR results on Montespertoli site  p 320  N95-23940  AIR
65-deg delta wing  BTN-95-EIX95152582331  p 281 A95-73533 The influence of atternate inter-blade connections on ground resonance  HTN-95-80859  p 267 A95-75101 Dynamic investigation of the angular motion of a rotating body-parachute system  BTN-95-EIX95182619220  p 270 A95-76646 AERODYNAMIC STALLING Computation of the poststall behavior of a circulation controlled airfoil  BTN-95-EIX95152582320  p 264 A95-73523 Moving wall effect in relation to other dynamic stall flow mechanisms	of attack forebody vortex control [NASA-CASE-ARC-11979-1] p 286 N95-23390 Aerodynamic design and analysis of a highly loaded turbine exhaust p 312 N95-23435 Numerical computation of aerodynamics and heat transfer in a turbine cascade and a turn-around duct using advanced turbulence models p 313 N95-23444 NTS-spill test facility wind tunnel exhaust plume characterization [DE95-003630] p 297 N95-24019 AEROELASTICITY Eigenanalysis of unsteady flows about airfoils, cascades, and wings	flow field  [NASA-TM-4638]  Validation of a Computational Fluid Dynamics (CFD) code for supersonic axisymmetric base flow  p 315  N95-23652  AGING (MATERIALS)  Oklahoma City air logistics center (USAF) aging aircraft corrosion program  p 262  N95-23519  AGRICULTURE  MAX-91: Polarimetric SAR results on Montespertoli site  p 320  N95-23940  AIR  Airborne rotary air separator study
65-deg delta wing  BTN-95-EIX95152582331  p 281 A95-73533 The influence of atternate inter-blade connections on ground resonance  HTN-95-80859  p 267 A95-75101 Dynamic investigation of the angular motion of a rotating body-parachute system  BTN-95-EIX95182619220  p 270 A95-76646 AERODYNAMIC STALLING Computation of the poststall behavior of a circulation controlled airfoil  BTN-95-EIX95152582320  p 264 A95-73523 Moving wall effect in relation to other dynamic stall flow mechanisms  BTN-95-EIX95152582324  p 265 A95-73527	of attack forebody vortex control [NASA-CASE-ARC-11979-1] p 286 N95-23390 Aerodynamic design and analysis of a highly loaded turbine exhaust p 312 N95-23435 Numerical computation of aerodynamics and heat transfer in a turbine cascade and a turn-around duct using advanced turbulence models p 313 N95-23444 NTS-spill test facility wind tunnel exhaust plurne characterization [DE95-003630] p 297 N95-24019  AEROELASTICITY  Eigenanalysis of unsteady flows about airfoils, cascades, and wings [BTN-95-EIX95152577597] p 305 A95-73486	flow field  [NASA-TM-4638]  Validation of a Computational Fluid Dynamics (CFD) code for supersonic axisymmetric base flow p 315  N95-23652  AGING (MATERIALS)  Oklahoma City air logistics center (USAF) aging aircraft corrosion program p 262  N95-23519  AGRICULTURE  MAX-91: Polarimetric SAR results on Montespertoli site p 320  N95-23940  AIR  Airborne rotary air separator study [NASA-CR-189099] p 290  N95-24053
65-deg delta wing   BTN-95-EIX95152582331   p 281 A95-73533   The influence of atternate inter-blade connections on ground resonance   HTN-95-80859   p 267 A95-75101   Dynamic investigation of the angular motion of a rotating body-parachute system   BTN-95-EIX95182619220   p 270 A95-76646   AERODYNAMIC STALLING   Computation of the poststall behavior of a circulation controlled airtiol     BTN-95-EIX95152582320   p 264 A95-73523     Moving wall effect in relation to other dynamic stall flow mechanisms     BTN-95-EIX95152582324   p 265 A95-73527     AERODYNAMICS	of attack forebody vortex control [NASA-CASE-ARC-11979-1] p 286 N95-23390 Aerodynamic design and analysis of a highly loaded turbine exhaust p 312 N95-23435 Numerical computation of aerodynamics and heat transfer in a turbine cascade and a turn-around duct using advanced turbulence models p 313 N95-23444 NTS-spill test facility wind tunnel exhaust plume characterization [DE95-003630] p 297 N95-24019  AEROELASTICITY Eigenanalysis of unsteady flows about airfoits, cascades, and wings [BTN-95-EIX95152577597] p 305 A95-73486 Efficient sensitivity analysis for rotary-wing aeromechanical problems	flow field  [NASA-TM-4638]  Validation of a Computational Fluid Dynamics (CFD) code for supersonic axisymmetric base flow  p 315  N95-23652  AGING (MATERIALS)  Oklahoma City air logistics center (USAF) aging aircraft corrosion program  p 262  N95-23519  AGRICULTURE  MAX-91: Polarimetric SAR results on Montespertoli site  p 320  N95-23940  AIR  Airborne rotary air separator study [NASA-CR-189099]  INASA-CR-1890999]  P 290  N95-24053  AIR BREATHING ENGINES  Computational study of plume-induced separation on a
65-deg delta wing   BTN-95-EIX95152582331  p 281 A95-73533  The influence of alternate inter-blade connections on ground resonance  HTN-95-B0859  p 267 A95-75101  Dynamic investigation of the angular motion of a rotating body-parachute system   p 270 A95-76646  AERODYNAMIC STALLING  Computation of the poststall behavior of a circulation controlled airfoil    BTN-95-EIX95152582320  p 264 A95-73523  Moving wall effect in relation to other dynamic stall flow mechanisms    BTN-95-EIX95152582324  p 265 A95-73527  AERODYNAMICS  Mechanical system reliability and risk assessment    BTN-95-EIX95142553046  p 304 A95-73452	of attack forebody vortex control [NASA-CASE-ARC-11979-1] p 286 N95-23390 Aerodynamic design and analysis of a highly loaded turbine exhaust p 312 N95-23435 Numerical computation of aerodynamics and heat transfer in a turbine cascade and a turn-around duct using advanced turbulence models p 313 N95-23444 NTS-spill test facility wind tunnel exhaust plurne characterization [DE95-003630] p 297 N95-24019  AEROELASTICITY  Eigenanalysis of unsteady flows about airfoils, cascades, and wings [BTN-95-EIX95152577597] p 305 A95-73486 Efficient sensitivity analysis for rotary-wing aeromechanical problems [BTN-95-EIX95152577585] p 264 A95-73497	flow field    NASA-TM-4638
65-deg delta wing   BTN-95-EIX95152582331   p 281 A95-73533   The influence of alternate inter-blade connections on ground resonance   HTN-95-80859   p 267 A95-75101   Dynamic investigation of the angular motion of a rotating body-parachute system   BTN-95-EIX95182619220   p 270 A95-76646   AERODYNAMIC STALLING   Computation of the poststall behavior of a circulation controlled airfoil   BTN-95-EIX95152582320   p 264 A95-73523   Moving wall effect in relation to other dynamic stall flow mechanisms   BTN-95-EIX95152582324   p 265 A95-73527   AERODYNAMICS   Mechanical system reliability and risk assessment   BTN-95-EIX95142553046   p 304 A95-73452   Simulation of turbulent fluctuations	of attack forebody vortex control [NASA-CASE-ARC-119-1] p 286 N95-23390 Aerodynamic design and analysis of a highly loaded turbine exhaust p 312 N95-23435 Numerical computation of aerodynamics and heat transfer in a turbine cascade and a turn-around duct using advanced turbulence models p 313 N95-23444 NTS-spill test facility wind tunnel exhaust plume characterization [DE95-003630] p 297 N95-24019 AEROELASTICITY  Eigenanalysis of unsteady flows about airfoils, cascades, and wings [BTN-95-EIX95152577587] p 305 A95-73486 Efficient sensitivity analysis for rotary-wing aeromechanical problems [BTN-95-EIX95152577586] p 264 A95-73497 Limit cycle phenomena in computational transonic	flow field  [NASA-TM-4638]  Validation of a Computational Fluid Dynamics (CFD) code for supersonic axisymmetric base flow p 315  N95-23652  AGING (MATERIALS)  Oklahoma City air logistics center (USAF) aging aircraft corrosion program p 262  N95-23519  AGRICULTURE  MAX-91: Potarimetric SAR results on Montespertolisite p 320  N95-23940  AIR  Airborne rotary air separator study [NASA-CR-189099] p 290  N95-24053  AIR BREATHING ENGINES  Computational study of plume-induced separation on a hypersonic powered model [BTN-95-EIX95152582346] p 266  A95-73548
65-deg delta wing  BTN-95-EIX95152582331  p 281 A95-73533   The influence of alternate inter-blade connections on ground resonance  HTN-95-80859  p 267 A95-75101   Dynamic investigation of the angular motion of a rotating body-parachute system  BTN-95-EIX95182619220  p 270 A95-76646   AERODYNAMIC STALLING   Computation of the poststall behavior of a circulation controlled airfoil  BTN-95-EIX95152582320  p 264 A95-73523   Moving wall effect in relation to other dynamic stall flow mechanisms  BTN-95-EIX95142553041  p 265 A95-73452   BERODYNAMICS   Mechanical system reliability and risk assessment  BTN-95-EIX95142553046  p 304 A95-73452   Simulation of turbulent fluctuations  BTN-95-EIX95142553041  p 304 A95-73457	of attack forebody vortex control [NASA-CASE-ARC-11979-1] p 286 N95-23390 Aerodynamic design and analysis of a highly loaded turbine exhaust p 312 N95-23435 Numerical computation of aerodynamics and heat transfer in a turbine cascade and a turn-around duct using advanced turbulence models p 313 N95-23444 NTS-spill test facility wind tunnel exhaust plurne characterization [DE95-003630] p 297 N95-24019  AEROELASTICITY  Eigenanalysis of unsteady flows about airfoils, cascades, and wings [BTN-95-EIX95152577597] p 305 A95-73486 Efficient sensitivity analysis for rotary-wing aeromechanical problems [BTN-95-EIX95152577585] p 264 A95-73497	flow field    NASA-TM-4638
65-deg delta wing   BTN-95-EIX95152582331   p 281 A95-73533   The influence of alternate inter-blade connections on ground resonance   HTN-95-80859   p 267 A95-75101   Dynamic investigation of the angular motion of a rotating body-parachute system   BTN-95-EIX95182619220   p 270 A95-76646   AERODYNAMIC STALLING   Computation of the poststall behavior of a circulation controlled airfoil   BTN-95-EIX95152582320   p 264 A95-73523   Moving wall effect in relation to other dynamic stall flow mechanisms   BTN-95-EIX95152582324   p 265 A95-73527   AERODYNAMICS   Mechanical system reliability and risk assessment   BTN-95-EIX95142553046   p 304 A95-73457   Simulation of turbulent fluctuations   BTN-95-EIX95142553041   p 304 A95-73457   Laplace interaction law for the computation of viscous airfoil flow in low- and high-speed aerodynamics	of attack forebody vortex control [NASA-CASE-ARC-11979-1] p 286 N95-23390 Aerodynamic design and analysis of a highly loaded turbine exhaust p 312 N95-23435 Numerical computation of aerodynamics and heat transfer in a turbine cascade and a turn-around duct using advanced turbulence models p 313 N95-23444 NTS-spill test facility wind tunnel exhaust plume characterization [DE95-003630] p 297 N95-24019  AEROELASTICITY Eigenanalysis of unsteady flows about airfoils, cascades, and wings [BTN-95-EIX95152577597] p 305 A95-73486 Efficient sensitivity analysis for rotary-wing aeromechanical problems [BTN-95-EIX95152577585] p 264 A95-73497 Limit cycle phenomena in computational transonic aeroelasticity [BTN-95-EIX95152582317] p 264 A95-73520 Static aeroelastic characteristics of a composite wing	flow field  [NASA-TM-4638]  Validation of a Computational Fluid Dynamics (CFD) code for supersonic axisymmetric base flow p 315  N95-23652  AGING (MATERIALS)  Oklahoma City air logistics center (USAF) aging aircraft corrosion program p 262  N95-23519  AGRICULTURE  MAX-91: Polarimetric SAR results on Montespertolisite p 320  N95-23940  AIR  Airborne rotary air separator study [NASA-CR-189099] p 290  N95-24053  AIR BREATHING ENGINES  Computational study of plume-induced separation on a hypersonic powered model [BTN-95-EIX95152582346] p 266  A95-73548  Airborne rotary air separator study [NASA-CR-189099] p 290  N95-24053  AIR COOLING
65-deg delta wing   BTN-95-EIX95152582331   p 281 A95-73533   The influence of atternate inter-blade connections on ground resonance   HTN-95-80859   p 267 A95-75101   Dynamic investigation of the angular motion of a rotating body-parachute system   BTN-95-EIX95182619220   p 270 A95-76646   AERODYNAMIC STALLING   Computation of the poststall behavior of a circulation controlled airfoil   BTN-95-EIX95152582320   p 264 A95-73523   Moving wall effect in relation to other dynamic stall flow mechanisms   BTN-95-EIX95152582324   p 265 A95-73527   AERODYNAMICS   Mechanical system reliability and risk assessment   BTN-95-EIX95142553046   p 304 A95-73452   Simulation of turbulent fluctuations   BTN-95-EIX95142553041   p 304 A95-73457   Laplace interaction law for the computation of viscous airfoil flow in low- and high-speed aerodynamics   BTN-95-EIX95142553037   p 263 A95-73461	of attack forebody vortex control [NASA-CASE-ARC-11979-1] p 286 N95-23390 Aerodynamic design and analysis of a highly loaded turbine exhaust p 312 N95-23435 Numerical computation of aerodynamics and heat transfer in a turbine cascade and a turn-around duct using advanced turbulence models p 313 N95-23444 NTS-spill test facility wind tunnel exhaust plume characterization [DE95-003630] p 297 N95-24019  AEROELASTICITY  Eigenanalysis of unsteady flows about airfoils, cascades, and wings [BTN-95-EIX95152577597] p 305 A95-73486 Efficient sensitivity analysis for rotary-wing aeromechanical problems [BTN-95-EIX95152577585] p 264 A95-73497 Limit cycle phenomena in computational transonic aeroelasticity [BTN-95-EIX95152582317] p 264 A95-73520 Static aeroelastic characteristics of a composite wing [BTN-95-EIX95152582340] p 282 A95-73542	flow field  [NASA-TM-4638]  Validation of a Computational Fluid Dynamics (CFD) code for supersonic axisymmetric base flow p 315  N95-23652  AGING (MATERIALS)  Oklahoma City air logistics center (USAF) aging aircraft corrosion program p 262  N95-23519  AGRICULTURE  MAX-91: Potarimetric SAR results on Montespertoli site p 320  N95-23940  AIR  Airborne rotary air separator study [NASA-CR-189099] p 290  N95-24053  AIR BREATHING ENGINES  Computational study of plume-induced separation on a hypersonic powered model [BTN-95-EIX95152582346] p 266  A95-73548  Airborne rotary air separator study [NASA-CR-189099]  P 290  N95-24053  AIR COOLING  Evaluation of thermal barrier and PS-200 self-lubricating
65-deg delta wing    BTN-95-EIX95152582331   p 281 A95-73533   The influence of alternate inter-blade connections on ground resonance   HTN-95-B0859   p 267 A95-75101   Dynamic investigation of the angular motion of a rotating body-parachute system   BTN-95-EIX95182619220   p 270 A95-76646   AERODYNAMIC STALLING   Computation of the poststall behavior of a circulation controlled airfoil     BTN-95-EIX95152582320   p 264 A95-73523     Moving wall effect in relation to other dynamic stall flow mechanisms     BTN-95-EIX95152582324   p 265 A95-73527     AERODYNAMICS   p 304 A95-73452     Simulation of turbulent fluctuations     BTN-95-EIX95142553046   p 304 A95-73452     Simulation of turbulent fluctuations     BTN-95-EIX95142553041   p 304 A95-73457     Laplace interaction law for the computation of viscous airfoil flow in low- and high-speed aerodynamics     BTN-95-EIX95142553037   p 263 A95-73461     Preconditioned domain decomposition scheme for	of attack forebody vortex control [NASA-CASE-ARC-11979-1] p 286 N95-23390 Aerodynamic design and analysis of a highly loaded turbine exhaust p 312 N95-23435 Numerical computation of aerodynamics and heat transfer in a turbine cascade and a turn-around duct using advanced turbulence models p 313 N95-23444 NTS-spill test facility wind tunnel exhaust plurne characterization [DE95-003630] p 297 N95-24019  AEROELASTICITY  Eigenanalysis of unsteady flows about airfoils, cascades, and wings [BTN-95-EIX95152577597] p 305 A95-73486 Efficient sensitivity analysis for rotary-wing aeromechanical problems [BTN-95-EIX95152577585] p 264 A95-73497 Limit cycle phenomena in computational transonic aeroelasticity [BTN-95-EIX95152582317] p 264 A95-73520 Static aeroelastic characteristics of a composite wing [BTN-95-EIX95152582340] p 282 A95-73542 Flutter of an infinitely long panel in a duct	flow field  [NASA-TM-4638]  Validation of a Computational Fluid Dynamics (CFD) code for supersonic axisymmetric base flow p 315  N95-23652  AGING (MATERIALS)  Oklahoma City air logistics center (USAF) aging aircraft corrosion program p 262  N95-23519  AGRICULTURE  MAX-91: Polarimetric SAR results on Montespertolisite p 320  N95-23940  AIR  Airborne rotary air separator study [NASA-CR-189099] p 290  N95-24053  AIR BREATHING ENGINES  Computational study of plume-induced separation on a hypersonic powered model [BTN-95-EIX95152582346] p 266  A95-73548  Airborne rotary air separator study [NASA-CR-189099] p 290  N95-24053  AIR COOLING
65-deg delta wing   BTN-95-EIX95152582331   p 281 A95-73533   The influence of alternate inter-blade connections on ground resonance   HTN-95-80859   p 267 A95-75101   Dynamic investigation of the angular motion of a rotating body-parachute system   BTN-95-EIX95182619220   p 270 A95-76646   AERODYNAMIC STALLING   Computation of the poststall behavior of a circulation controlled airtiol   BTN-95-EIX95152582320   p 264 A95-73523   Moving wall effect in relation to other dynamic stall flow mechanisms   BTN-95-EIX95152582324   p 265 A95-73527   AERODYNAMICS   Mechanical system reliability and risk assessment   BTN-95-EIX95142553046   p 304 A95-73452   Simulation of turbulent fluctuations   BTN-95-EIX95142553041   p 304 A95-73457   Laplace interaction law for the computation of viscous airfoil flow in low- and high-speed aerodynamics   BTN-95-EIX95142553037   p 263 A95-73461   Preconditioned domain decomposition scheme for three-dimensional aerodynamic sensitivity analysis   BTN-95-EIX95152577612   p 321 A95-73471	of attack forebody vortex control [NASA-CASE-ARC-11979-1] p 286 N95-23390 Aerodynamic design and analysis of a highly loaded turbine exhaust p 312 N95-23435 Numerical computation of aerodynamics and heat transfer in a turbine cascade and a turn-around duct using advanced turbulence models p 313 N95-23444 NTS-spill test facility wind tunnel exhaust plume characterization [DE95-003630] p 297 N95-24019 AEROELASTICITY  Eigenanalysis of unsteady flows about airfoils, cascades, and wings [BTN-95-EIX95152577597] p 305 A95-73486 Efficient sensitivity analysis for rotary-wing aeromechanical problems [BTN-95-EIX95152577585] p 264 A95-73497 Limit cycle phenomena in computational transonic aeroelasticity [BTN-95-EIX95152582317] p 264 A95-73520 Static aeroelastic characteristics of a composite wing [BTN-95-EIX95152582340] p 282 A95-73542 Flutter of an infinitely long panel in a duct [BTN-95-EIX95182619087] p 291 A95-75772 Aeroelastic vehicle multivariable control synthesis with	flow field  [NASA-TM-4638]  Palidation of a Computational Fluid Dynamics (CFD) code for supersonic axisymmetric base flow  p 315  N95-23652  AGING (MATERIALS)  Oklahoma City air logistics center (USAF) aging aircraft corrosion program  p 262  N95-23519  AGRICULTURE  MAX-91: Polarimetric SAR results on Montespertolisite  p 320  N95-23940  AIR  Airborne rotary air separator study [NASA-CR-189099]  p 290  N95-24053  AIR BREATHING ENGINES  Computational study of plume-induced separation on a hypersonic powered model [BTN-95-EIX95152582346]  p 266  A95-73548  Airborne rotary air separator study [NASA-CR-189099]  p 290  N95-24053  AIR COOLING  Evaluation of thermal barrier and PS-200 self-lubricating coatings in an air-cooled rotary engine [NASA-CR-189445]  p 289  N95-23222  AIR FILTERS
65-deg delta wing   BTN-95-EIX95152582331   p 281 A95-73533   The influence of alternate inter-blade connections on ground resonance   HTN-95-80859   p 267 A95-75101   Dynamic investigation of the angular motion of a rotating body-parachute system   BTN-95-EIX95182619220   p 270 A95-76646   AERODYNAMIC STALLING   Computation of the poststall behavior of a circulation controlled airfoil   BTN-95-EIX95152582320   p 264 A95-73523   Moving wall effect in relation to other dynamic stall flow mechanisms   BTN-95-EIX95152582324   p 265 A95-73527   AERODYNAMICS   Mechanical system reliability and risk assessment   BTN-95-EIX95142553046   p 304 A95-73452   Simulation of turbulent fluctuations   BTN-95-EIX95142553041   p 304 A95-73457   Laplace interaction law for the computation of viscous airfoil flow in low- and high-speed aerodynamics   BTN-95-EIX95142553037   p 263 A95-73461   P reconditioned domain decomposition scheme for three-dimensional aerodynamic sensitivity analysis   BTN-95-EIX95152577612   p 321 A95-73471   Shock tunnet measurements of hypervelocity blunted	of attack forebody vortex control [NASA-CASE-ARC-11979-1] p 286 N95-23390 Aerodynamic design and analysis of a highly loaded turbine exhaust p 312 N95-23435 Numerical computation of aerodynamics and heat transfer in a turbine cascade and a turn-around duct using advanced turbulence models p 313 N95-23444 NTS-spill test facility wind tunnel exhaust plurne characterization [DE95-003630] p 297 N95-24019  AEROELASTICITY  Eigenanalysis of unsteady flows about airfoils, cascades, and wings [BTN-95-EIX95152577597] p 305 A95-73486 Efficient sensitivity analysis for rotary-wing aeromechanical problems [BTN-95-EIX95152577585] p 264 A95-73497 Limit cycle phenomena in computational transonic aeroelasticity [BTN-95-EIX95152582340] p 264 A95-73520 Static aeroelastic characteristics of a composite wing [BTN-95-EIX95152582340] p 282 A95-73542 Flutter of an infinitely long panel in a duct [BTN-95-EIX95182619087] p 291 A95-75772 Aeroelastic vehicle multivariable control synthesis with analytical robustness evaluation	flow field  [NASA-TM-4638]  Validation of a Computational Fluid Dynamics (CFD)  code for supersonic axisymmetric base flow  p 315  N95-23652  AGING (MATERIALS)  Oklahoma City air logistics center (USAF) aging aircraft corrosion program  p 262  N95-23519  AGRICULTURE  MAX-91: Polarimetric SAR results on Montespertoli site  p 320  N95-23940  AIR  Airborne rotary air separator study  [NASA-CR-189099]  p 290  N95-24053  AIR BREATHING ENGINES  Computational study of plume-induced separation on a hypersonic powered model  [BTN-95-EIX95152582346]  p 266  A95-73548  Airborne rotary air separator study  [NASA-CR-189099]  p 290  N95-24053  AIR COOLING  Evaluation of thermal barrier and PS-200 self-lubricating coatings in an air-cooled rotary engine  [NASA-CR-195445]  p 289  N95-23222  AIR FILTERS  Erosion of dust-filtered heticopter turbine engines. Part
65-deg delta wing   BTN-95-EIX95152582331   p 281 A95-73533   The influence of alternate inter-blade connections on ground resonance   HTN-95-80859   p 267 A95-75101   Dynamic investigation of the angular motion of a rotating body-parachute system   BTN-95-EIX95182619220   p 270 A95-76646   AERODYNAMIC STALLING   Computation of the poststall behavior of a circulation controlled airfoil   BTN-95-EIX95152582320   p 264 A95-73523   Moving wall effect in relation to other dynamic stall flow mechanisms   BTN-95-EIX95152582324   p 265 A95-73527   AERODYNAMICS   Mechanical system reliability and risk assessment   BTN-95-EIX95142553046   p 304 A95-73452   Simulation of turbulent fluctuations   BTN-95-EIX95142553041   p 304 A95-73457   Laplace interaction law for the computation of viscous airfoil flow in low- and high-speed aerodynamics   BTN-95-EIX95142553037   p 263 A95-73461   Preconditioned domain decomposition scheme for three-dimensional aerodynamic sensitivity analysis   BTN-95-EIX95152577612   p 321 A95-73471   Shock tunnel measurements of hypervelocity blunted cone drag   BTN-95-EIX95152577606   p 305 A95-73477	of attack forebody vortex control [NASA-CASE-ARC-11979-1] p 286 N95-23390 Aerodynamic design and analysis of a highly loaded turbine exhaust p 312 N95-23435 Numerical computation of aerodynamics and heat transfer in a turbine cascade and a turn-around duct using advanced turbulence models p 313 N95-23444 NTS-spill test facility wind tunnel exhaust plume characterization [DE95-003630] p 297 N95-24019 AEROELASTICITY  Eigenanalysis of unsteady flows about airfoils, cascades, and wings [BTN-95-EIX95152577597] p 305 A95-73486 Efficient sensitivity analysis for rotary-wing aeromechanical problems [BTN-95-EIX95152577585] p 264 A95-73497 Limit cycle phenomena in computational transonic aeroelasticity [BTN-95-EIX95152582317] p 264 A95-73520 Static aeroelastic characteristics of a composite wing [BTN-95-EIX95152582340] p 282 A95-73542 Flutter of an infinitely long panel in a duct [BTN-95-EIX95182619087] p 291 A95-75772 Aeroelastic vehicle multivariable control synthesis with	flow field  [NASA-TM-4638]  Validation of a Computational Fluid Dynamics (CFD) code for supersonic axisymmetric base flow p 315  N95-23652  AGING (MATERIALS)  Oklahoma City air logistics center (USAF) aging aircraft corrosion program p 262  N95-23519  AGRICULTURE  MAX-91: Polarimetric SAR results on Montespertolisite p 320  N95-23940  AIR  Airborne rotary air separator study [NASA-CR-189099] p 290  N95-24053  AIR BREATHING ENGINES  Computational study of plume-induced separation on a hypersonic powered model [BTN-95-EIX95152582346] p 266  A95-73548  Airborne rotary air separator study [NASA-CR-189099]  N95-24053  AIR COOLING  Evaluation of thermal barrier and PS-200 self-lubricating coatings in an air-cooled rotary engine [NASA-CR-189445]  P 289  N95-23222  AIR FILTERS
65-deg delta wing   BTN-95-EIX95152582331   p 281 A95-73533   The influence of alternate inter-blade connections on ground resonance   HTN-95-80859   p 267 A95-75101   Dynamic investigation of the angular motion of a rotating body-parachute system   BTN-95-EIX95182619220   p 270 A95-76646   AERODYNAMIC STALLING   Computation of the poststall behavior of a circulation controlled airtiol   BTN-95-EIX95152582320   p 264 A95-73523   Moving wall effect in relation to other dynamic stall flow mechanisms   BTN-95-EIX95152582324   p 265 A95-73527   AERODYNAMICS   Mechanical system reliability and risk assessment   BTN-95-EIX95142553046   p 304 A95-73452   Simulation of turbulent fluctuations   BTN-95-EIX95142553041   p 304 A95-73457   Laplace interaction law for the computation of viscous airfoil flow in low- and high-speed aerodynamics   BTN-95-EIX95142553037   p 263 A95-73461   Preconditioned domain decomposition scheme for three-dimensional aerodynamic sensitivity analysis   BTN-95-EIX95152577612   p 321 A95-73471   Shock tunnel measurements of hypervelocity blunted cone drag   BTN-95-EIX95152577606   p 305 A95-73477   Eigenanalysis of unsteady flows about airfoils, cascades,	of attack forebody vortex control [NASA-CASE-ARC-11979-1] p 286 N95-23390 Aerodynamic design and analysis of a highly loaded turbine exhaust p 312 N95-23435 Numerical computation of aerodynamics and heat transfer in a turbine cascade and a turn-around duct using advanced turbulence models p 313 N95-23444 NTS-spill test facility wind tunnel exhaust plurne characterization [DE95-003630] p 297 N95-24019  AEROELASTICITY  Eigenanalysis of unsteady flows about airfoils, cascades, and wings [BTN-95-EIX95152577597] p 305 A95-73486 Efficient sensitivity analysis for rotary-wing aeromechanical problems [BTN-95-EIX95152577585] p 264 A95-73497 Limit cycle phenomena in computational transonic aeroelasticity [BTN-95-EIX95152582340] p 264 A95-73520 Static aeroelastic characteristics of a composite wing [BTN-95-EIX95152582340] p 282 A95-73542 Flutter of an infinitely long panel in a duct [BTN-95-EIX95182619087] p 291 A95-75772 Aeroelastic vehicle multivariable control synthesis with analytical robustness evaluation [BTN-95-EIX95182619115] p 321 A95-76592 Analytical hypersonic-vehicle model with dynamic analysis	flow field  [NASA-TM-4638]  Validation of a Computational Fluid Dynamics (CFD)  code for supersonic axisymmetric base flow  p 315  N95-23652  AGING (MATERIALS)  Oklahoma City air logistics center (USAF) aging aircraft corrosion program  p 262  N95-23519  AGRICULTURE  MAX-91: Potarimetric SAR results on Montespertoliste  p 320  N95-23940  AIR  Airborne rotary air separator study [NASA-CR-189099]  p 290  N95-24053  AIR BREATHING ENGINES  Computational study of plume-induced separation on a hypersonic powered model [BTN-95-EIX95152582346]  p 266  A95-73548  Airborne rotary air separator study [NASA-CR-189099]  p 290  N95-24053  AIR COOLING  Evaluation of thermal barrier and PS-200 self-lubricating coatings in an air-cooled rotary engine [NASA-CR-195445]  p 289  N95-23222  AIR FILTERS  Erosion of dust-filtered helicopter turbine engines. Part 2: Erosion reduction  [BTN-95-EIX95182619223]  p 289  A95-76649  Life prediction of helicopter engines fitted with dust
65-deg delta wing   BTN-95-EIX95152582331   p 281 A95-73533   The influence of alternate inter-blade connections on ground resonance   HTN-95-80859   p 267 A95-75101   Dynamic investigation of the angular motion of a rotating body-parachute system   BTN-95-EIX95182619220   p 270 A95-76646   AERODYNAMIC STALLING   Computation of the poststall behavior of a circulation controlled airfoil   BTN-95-EIX95152582320   p 264 A95-73523   Moving wall effect in relation to other dynamic stall flow mechanisms   BTN-95-EIX95152582324   p 265 A95-73527   AERODYNAMICS   Mechanical system reliability and risk assessment   BTN-95-EIX95142553046   p 304 A95-73452   Simulation of turbulent fluctuations   BTN-95-EIX95142553041   p 304 A95-73457   Laplace interaction law for the computation of viscous airfoil flow in low- and high-speed aerodynamics   BTN-95-EIX95142553037   p 263 A95-73461   P 260 A95-73461   P 260 A95-73461   P 260 A95-73461   P 260 A95-73461   P 261 A95-73461   P 262 A95-73461   P 263 A95	of attack forebody vortex control [NASA-CASE-ARC-11979-1] p 286 N95-23390 Aerodynamic design and analysis of a highly loaded turbine exhaust p 312 N95-23435 Numerical computation of aerodynamics and heat transfer in a turbine cascade and a turn-around duct using advanced turbulence models p 313 N95-23444 NTS-spill test facility wind tunnel exhaust plurne characterization [DE95-003630] p 297 N95-24019  AEROELASTICITY Eigenanalysis of unsteady flows about airfoits, cascades, and wings [BTN-95-EIX95152577597] p 305 A95-73486 Efficient sensitivity analysis for rotary-wing aeromechanical problems [BTN-95-EIX95152577585] p 264 A95-73497 Limit cycle phenomena in computational transonic aeroelasticity [BTN-95-EIX95152582317] p 264 A95-73520 Static aeroelastic characteristics of a composite wing [BTN-95-EIX95182582340] p 282 A95-73542 Flutter of an infinitely long panel in a duct [BTN-95-EIX95182619087] p 291 A95-75772 Aeroelastic vehicle multivariable control synthesis with analytical control synthesis with analytical aeropropulsive/aeroelastic hypersonic-vehicle model with dynamic analysis [BTN-95-EIX95182619115] p 321 A95-76615	flow field  [NASA-TM-4638]  Validation of a Computational Fluid Dynamics (CFD) code for supersonic axisymmetric base flow p 315 N95-23652  AGING (MATERIALS)  Oklahoma City air logistics center (USAF) aging aircraft corrosion program p 262 N95-23519  AGRICULTURE  MAX-91: Polarimetric SAR results on Montespertolisite p 320 N95-23940  AIR  Airborne rotary air separator study [NASA-CR-189099]  AIR BREATHING ENGINES  Computational study of plume-induced separation on a hypersonic powered model [BTN-95-EIX95152582346]  [BTN-95-EIX95152582346]  Airborne rotary air separator study [NASA-CR-189099]  P 290 N95-24053  AIR COOLING  Evaluation of thermal barrier and PS-200 self-lubricating coatings in an air-cooled rotary engine [NASA-CR-195445]  P 289 N95-23222  AIR FILTERS  Erosion of dust-filtered helicopter turbine engines. Part 2: Erosion reduction [BTN-95-EIX95182619223]  Life prediction of helicopter engines fitted with dust filters
65-deg delta wing   BTN-95-EIX95152582331   p 281 A95-73533   The influence of atternate inter-blade connections on ground resonance   HTN-95-80859   p 267 A95-75101   Dynamic investigation of the angular motion of a rotating body-parachute system   BTN-95-EIX95182619220   p 270 A95-76646   AERODYNAMIC STALLING   Computation of the poststall behavior of a circulation controlled airfoil   BTN-95-EIX95152582320   p 264 A95-73523   Moving wall effect in relation to other dynamic stall flow mechanisms   BTN-95-EIX95152582324   p 265 A95-73527   AERODYNAMICS   Mechanical system reliability and risk assessment   BTN-95-EIX95142553046   p 304 A95-73452   Simulation of turbulent fluctuations   BTN-95-EIX95142553041   p 304 A95-73457   Laplace interaction law for the computation of viscous airfoil flow in low- and high-speed aerodynamics   BTN-95-EIX95142553037   p 263 A95-73461   Preconditioned domain decomposition scheme for three-dimensional aerodynamic sensitivity analysis   BTN-95-EIX95152577612   p 321 A95-73471   Shock tunnel measurements of hypervelocity blunted cone drag   BTN-95-EIX95152577606   p 305 A95-73477   Eigenanalysis of unsteady flows about airfoils, cascades, and wings   BTN-95-EIX95152577597   p 305 A95-73486	of attack forebody vortex control [NASA-CASE-ARC-11979-1] p 286 N95-23390 Aerodynamic design and analysis of a highly loaded turbine exhaust p 312 N95-23435 Numerical computation of aerodynamics and heat transfer in a turbine cascade and a turn-around duct using advanced turbulence models p 313 N95-23444 NTS-spill test facility wind tunnel exhaust plurne characterization [DE95-003630] p 297 N95-24019  AEROELASTICITY  Eigenanalysis of unsteady flows about airfoils, cascades, and wings [BTN-95-EIX95152577597] p 305 A95-73486 Efficient sensitivity analysis for rotary-wing aeromechanical problems [BTN-95-EIX95152577585] p 264 A95-73497 Limit cycle phenomena in computational transonic aeroelasticity [BTN-95-EIX95152582340] p 264 A95-73520 Static aeroelastic characteristics of a composite wing [BTN-95-EIX95152582340] p 282 A95-73542 Flutter of an infinitely long panel in a duct [BTN-95-EIX95182619087] p 291 A95-75772 Aeroelastic vehicle multivariable control synthesis with analytical robustness evaluation [BTN-95-EIX95182619115] p 321 A95-76592 Analytical hypersonic-vehicle model with dynamic analysis	flow field  [NASA-TM-4638]  Validation of a Computational Fluid Dynamics (CFD) code for supersonic axisymmetric base flow p 315  N95-23652  AGING (MATERIALS)  Oklahoma City air logistics center (USAF) aging aircraft corrosion program p 262  N95-23519  AGRICULTURE  MAX-91: Polarimetric SAR results on Montespertolisite p 320  N95-23940  AIR  Airborne rotary air separator study [NASA-CR-189099] p 290  N95-24053  AIR BREATHING ENGINES  Computational study of plume-induced separation on a hypersonic powered model [BTN-95-EIX95152582346] p 266  A95-73548  Airborne rotary air separator study [NASA-CR-189099] p 290  N95-24053  AIR COOLING  Evaluation of thermal barrier and PS-200 self-lubricating coatings in an air-cooled rotary engine [NASA-CR-195445] p 289  N95-23222  AIR FILTERS  Erosion of dust-filtered helicopter turbine engines. Part 2: Erosion reduction [BTN-95-EIX95182619223] p 289 A95-76649  Life prediction of helicopter engines fitted with dust filters [BTN-95-EIX95182619224] p 289 A95-76650
65-deg delta wing   BTN-95-EIX95152582331   p 281 A95-73533   The influence of alternate inter-blade connections on ground resonance   HTN-95-80859   p 267 A95-75101   Dynamic investigation of the angular motion of a rotating body-parachute system   BTN-95-EIX95182619220   p 270 A95-76646   AERODYNAMIC STALLING   Computation of the poststall behavior of a circulation controlled airfoil   BTN-95-EIX95152582320   p 264 A95-73523   Moving wall effect in relation to other dynamic stall flow mechanisms   BTN-95-EIX95152582324   p 265 A95-73527   AERODYNAMICS   Mechanical system reliability and risk assessment   BTN-95-EIX95142553046   p 304 A95-73452   Simulation of turbulent fluctuations   BTN-95-EIX95142553041   p 304 A95-73457   Laplace interaction law for the computation of viscous airfoil flow in low- and high-speed aerodynamics   BTN-95-EIX95142553037   p 263 A95-73461   P reconditioned domain decomposition scheme for three-dimensional aerodynamic sensitivity analysis   BTN-95-EIX95152577612   p 321 A95-73471   Shock tunnel measurements of hypervelocity blunted cone drag   BTN-95-EIX95152577606   p 305 A95-73477   Eigenanalysis of unsteady flows about airfoils, cascades, and wings   BTN-95-EIX95152577597   p 305 A95-73486   Progress in high-lift aerodynamic calculations   BTN-95-EIX95152582315   p 264 A95-73518	of attack forebody vortex control [NASA-CASE-ARC-11979-1] p 286 N95-23390 Aerodynamic design and analysis of a highly loaded turbine exhaust p 312 N95-23435 Numerical computation of aerodynamics and heat transfer in a turbine cascade and a turn-around duct using advanced turbulence models p 313 N95-23444 NTS-spill test facility wind tunnel exhaust plurne characterization [DE95-003630] p 297 N95-24019 AEROELASTICITY Eigenanalysis of unsteady flows about airfoits, cascades, and wings [BTN-95-EIX95152577597] p 305 A95-73486 Efficient sensitivity analysis for rotary-wing aeromechanical problems [BTN-95-EIX95152577585] p 264 A95-73497 Limit cycle phenomena in computational transonic aeroelasticity [BTN-95-EIX95152582317] p 264 A95-73520 Static aeroelastic characteristics of a composite wing [BTN-95-EIX95152582340] p 282 A95-73542 Flutter of an infinitely long panel in a duct [BTN-95-EIX95182619087] p 291 A95-75772 Aeroelastic vehicle multivariable control synthesis with analytical aroustness evaluation [BTN-95-EIX95182619115] p 321 A95-76592 Analytical aeropropulsive/aeroelastic hypersonic-vehicle model with dynamic analysis [BTN-95-EIX95182619118] p 269 A95-76615 Application of transonic small disturbance theory to the active (lexible wing model [BTN-95-EIX95182619210] p 270 A95-76636	flow field  [NASA-TM-4638]  Validation of a Computational Fluid Dynamics (CFD) code for supersonic axisymmetric base flow p 315 N95-23652  AGING (MATERIALS)  Oklahoma City air logistics center (USAF) aging aircraft corrosion program p 262 N95-23519  AGRICULTURE  MAX-91: Polarimetric SAR results on Montespertolisite p 320 N95-23940  AIR  Airborne rotary air separator study [NASA-CR-189099]  AIR BREATHING ENGINES  Computational study of plume-induced separation on a hypersonic powered model [BTN-95-EIX95152582346]  [BTN-95-EIX95152582346]  Airborne rotary air separator study [NASA-CR-189099]  P 290 N95-24053  AIR COOLING  Evaluation of thermal barrier and PS-200 self-lubricating coatings in an air-cooled rotary engine [NASA-CR-195445]  P 289 N95-23222  AIR FILTERS  Erosion of dust-filtered helicopter turbine engines. Part 2: Erosion reduction [BTN-95-EIX95182619223]  Life prediction of helicopter engines fitted with dust filters
BTN-95-EIX95152582331   p 281 A95-73533     The influence of atternate inter-blade connections on ground resonance   HTN-95-80859   p 267 A95-75101     Dynamic investigation of the angular motion of a rotating body-parachute system   BTN-95-EIX95182619220   p 270 A95-76646     AERODYNAMIC STALLING   Computation of the poststall behavior of a circulation controlled airfoil   BTN-95-EIX95152582320   p 264 A95-73523     Moving wall effect in relation to other dynamic stall flow mechanisms   BTN-95-EIX95152582324   p 265 A95-73527     AERODYNAMICS   Mechanical system reliability and risk assessment   BTN-95-EIX95142553046   p 304 A95-73452     Simulation of turbulent fluctuations   BTN-95-EIX95142553041   p 304 A95-73457     Laplace interaction law for the computation of viscous airfoil flow in low- and high-speed aerodynamics   BTN-95-EIX95142553037   p 263 A95-73461     Preconditioned domain decomposition scheme for three-dimensional aerodynamic sensitivity analysis   BTN-95-EIX95152577612   p 321 A95-73471     Shock tunnel measurements of hypervelocity blunted cone drag   BTN-95-EIX95152577606   p 305 A95-73477     Eigenanalysis of unsteady flows about airfoils, cascades, and wings   BTN-95-EIX95152582315   p 264 A95-73518     Unstructured grid solutions to a wing/pylon/store	of attack forebody vortex control [NASA-CASE-ARC-1199-1] p 286 N95-23390 Aerodynamic design and analysis of a highly loaded turbine exhaust p 312 N95-23435 Numerical computation of aerodynamics and heat transfer in a turbine cascade and a turn-around duct using advanced turbulence models p 313 N95-23444 NTS-spill test facility wind tunnel exhaust plume characterization [DE95-003630] p 297 N95-24019  AEROELASTICITY Eigenanalysis of unsteady flows about airfoits, cascades, and wings [BTN-95-EIX95152577587] p 305 A95-73486 Efficient sensitivity analysis for rotary-wing aeromechanical problems [BTN-95-EIX95152577586] p 264 A95-73497 Limit cycle phenomena in computational transonic aeroelasticity [BTN-95-EIX95152582317] p 264 A95-73520 Static aeroelastic characteristics of a composite wing [BTN-95-EIX95152582340] p 282 A95-73542 Flutter of an infinitely long panel in a duct [BTN-95-EIX95182619917] p 291 A95-75772 Aeroelastic vehicle multivariable control synthesis with analytical robustness evaluation [BTN-95-EIX95182619115] p 321 A95-76592 Analytical aeroelastic model with dynamic analysis [BTN-95-EIX95182619138] p 269 A95-76615 Application of transonic small disturbance theory to the active flexible wing model [BTN-95-EIX95182619210] p 270 A95-76636 Application of Navier-Stokes aeroelastic methods to	flow field [NASA-TM-4638]  Validation of a Computational Fluid Dynamics (CFD) code for supersonic axisymmetric base flow p 315 N95-23652  AGING (MATERIALS) Oklahoma City air logistics center (USAF) aging aircraft corrosion program p 262 N95-23519  AGRICULTURE MAX-91: Polarimetric SAR results on Montespertolisite p 320 N95-23940  AIR Airborne rotary air separator study [NASA-CR-189099] p 290 N95-24053  AIR BREATHING ENGINES Computational study of plume-induced separation on a hypersonic powered model [BTN-95-EIX95152582346] p 266 A95-73548 Airborne rotary air separator study [NASA-CR-189099] p 290 N95-24053  AIR COOLING Evaluation of thermal barrier and PS-200 self-lubricating coatings in an air-cooled rotary engine [NASA-CR-195445] p 289 N95-23222  AIR FILTERS Erosion of dust-filtered helicopter turbine engines. Part 2: Erosion reduction [BTN-95-EIX95182619223] p 289 A95-76649 Life prediction of helicopter engines fitted with dust filters [BTN-95-EIX95182619224] p 289 A95-76650 Airborne rotary air separator study [NASA-CR-189099] p 290 N95-24053
65-deg delta wing   BTN-95-EIX95152582331   p 281 A95-73533   The influence of alternate inter-blade connections on ground resonance   HTN-95-80859   p 267 A95-75101   Dynamic investigation of the angular motion of a rotating body-parachute system   BTN-95-EIX95182619220   p 270 A95-76646   AERODYNAMIC STALLING   Computation of the poststall behavior of a circulation controlled airfoil   BTN-95-EIX95152582320   p 264 A95-73523   Moving wall effect in relation to other dynamic stall flow mechanisms   BTN-95-EIX95152582324   p 265 A95-73527   AERODYNAMICS   Mechanical system reliability and risk assessment   BTN-95-EIX95142553046   p 304 A95-73452   Simulation of turbulent fluctuations   BTN-95-EIX95142553041   p 304 A95-73457   Laplace interaction law for the computation of viscous airfoil flow in low- and high-speed aerodynamics   BTN-95-EIX95142553037   p 263 A95-73461   P reconditioned domain decomposition scheme for three-dimensional aerodynamic sensitivity analysis   BTN-95-EIX95152577612   p 321 A95-73471   Shock tunnel measurements of hypervelocity blunted cone drag   BTN-95-EIX95152577606   p 305 A95-73477   Eigenanalysis of unsteady flows about airfoils, cascades, and wings   BTN-95-EIX95152577597   p 305 A95-73486   Progress in high-lift aerodynamic calculations   BTN-95-EIX95152582315   p 264 A95-73518   Unstructured grid solutions to a wing/pylon/store configuration   BTN-95-EIX95152582322   p 265 A95-73525	of attack forebody vortex control [NASA-CASE-ARC-11979-1] p 286 N95-23390 Aerodynamic design and analysis of a highly loaded turbine exhaust p 312 N95-23435 Numerical computation of aerodynamics and heat transfer in a turbine cascade and a turn-around duct using advanced turbulence models p 313 N95-23444 NTS-spill test facility wind tunnel exhaust plurne characterization [DE95-003630] p 297 N95-24019 AEROELASTICITY Eigenanalysis of unsteady flows about airfoits, cascades, and wings [BTN-95-EIX95152577597] p 305 A95-73486 Efficient sensitivity analysis for rotary-wing aeromechanical problems [BTN-95-EIX95152577585] p 264 A95-73497 Limit cycle phenomena in computational transonic aeroelasticity [BTN-95-EIX95152582317] p 264 A95-73520 Static aeroelastic characteristics of a composite wing [BTN-95-EIX95152582340] p 282 A95-73542 Flutter of an infinitely long panel in a duct [BTN-95-EIX95182619087] p 291 A95-75772 Aeroelastic vehicle multivariable control synthesis with analytical aroustness evaluation [BTN-95-EIX95182619115] p 321 A95-76592 Analytical aeropropulsive/aeroelastic hypersonic-vehicle model with dynamic analysis [BTN-95-EIX95182619118] p 269 A95-76615 Application of transonic small disturbance theory to the active (lexible wing model [BTN-95-EIX95182619210] p 270 A95-76636	flow field  [NASA-TM-4638]  Validation of a Computational Fluid Dynamics (CFD) code for supersonic axisymmetric base flow p 315  N95-23652  AGING (MATERIALS)  Oklahoma City air logistics center (USAF) aging aircraft corrosion program p 262  N95-23519  AGRICULTURE  MAX-91: Polarimetric SAR results on Montespertolisite p 320  N95-23940  AIR  Airborne rotary air separator study [NASA-CR-189099] p 290  N95-24053  AIR BREATHING ENGINES  Computational study of plume-induced separation on a hypersonic powered model [BTN-95-EIX95152582346] P 266  A95-73548  Airborne rotary air separator study [NASA-CR-189099]  INASA-CR-189099]  AIR COOLING  Evaluation of thermal barrier and PS-200 self-lubricating coatings in an air-cooled rotary engine [NASA-CR-195445]  Erosion of dust-filtered helicopter turbine engines. Part 2: Erosion reduction [BTN-95-EIX95182619223]  D 289  A95-76649  Life prediction of helicopter engines fitted with dust filters [BTN-95-EIX95182619224]  P 289  A95-76650  Airborne rotary air separator study [NASA-CR-189099]  P 290  N95-24053  AIR FLOW  Simulation of transverse gas injection in turbulent
BTN-95-EIX95152582331   p 281 A95-73533     The influence of alternate inter-blade connections on ground resonance   HTN-95-80859   p 267 A95-75101     Dynamic investigation of the angular motion of a rotating body-parachute system   BTN-95-EIX95182619220   p 270 A95-76646     AERODYNAMIC STALLING   Computation of the poststall behavior of a circulation controlled airfoil   BTN-95-EIX95152582320   p 264 A95-73523   Moving wall effect in relation to other dynamic stall flow mechanisms   BTN-95-EIX95152582324   p 265 A95-73527     AERODYNAMICS   Mechanical system reliability and risk assessment   BTN-95-EIX95142553046   p 304 A95-73457     ABTN-95-EIX95142553046   p 304 A95-73457   Laplace interaction law for the computation of viscous airfoil flow in low- and high-speed aerodynamics   BTN-95-EIX95142553037   p 263 A95-73461   P reconditioned domain decomposition scheme for three-dimensional aerodynamic sensitivity analysis   BTN-95-EIX95152577612   p 321 A95-73471   Shock tunnet measurements of hypervelocity blunted cone drag   BTN-95-EIX95152577606   p 305 A95-73477   Eigenanalysis of unsteady flows about airfoils, cascades, and wings   BTN-95-EIX95152577597   p 305 A95-73486   Progress in high-litt aerodynamic calculations   BTN-95-EIX95152582315   p 264 A95-73518   Unstructured grid solutions to a wing/pylon/store configuration   BTN-95-EIX95152582322   p 265 A95-73525   Moving wall effect in relation to other dynamic stall flow	of attack forebody vortex control [NASA-CASE-ARC-11979-1] p 286 N95-23390 Aerodynamic design and analysis of a highly loaded turbine exhaust p 312 N95-23435 Numerical computation of aerodynamics and heat transfer in a turbine cascade and a turn-around duct using advanced turbulence models p 313 N95-23444 NTS-spill test facility wind tunnel exhaust plume characterization [DE95-003630] p 297 N95-24019  AEROELASTICITY Eigenanalysis of unsteady flows about airfoits, cascades, and wings [BTN-95-EIX95152577597] p 305 A95-73486 Efficient sensitivity analysis for rotary-wing aeromechanical problems [BTN-95-EIX95152577585] p 264 A95-73497 Limit cycle phenomena in computational transonic aeroelasticity [BTN-95-EIX95152582317] p 264 A95-73542 Flutter of an infinitely long panel in a duct [BTN-95-EIX95182619087] p 291 A95-75772 Aeroelastic vehicle multivariable control synthesis with analytical robustness evaluation [BTN-95-EIX95182619115] p 321 A95-76592 Analytical aeroelastic characteristics of a composite wing [BTN-95-EIX95182619115] p 321 A95-76592 Analytical robustness evaluation [BTN-95-EIX95182619118] p 269 A95-76615 Application of transonic small disturbance theory to the active flexible wing model [BTN-95-EIX9518261910] p 270 A95-76636 Application of Navier-Stokes aeroelastic methods to improve fighter wing maneuver performance [BTN-95-EIX95182619218] p 284 A95-76644 High-performance parallel analysis of coupled problems	flow field [NASA-TM-4638]  Validation of a Computational Fluid Dynamics (CFD) code for supersonic axisymmetric base flow p 315  N95-23652  AGING (MATERIALS)  Oklahoma City air logistics center (USAF) aging aircraft corrosion program p 262  N95-23519  AGRICULTURE  MAX-91: Polarimetric SAR results on Montespertolisite p 320  N95-23940  AIR  Airborne rotary air separator study [NASA-CR-189099] p 290  N95-24053  AIR BREATHING ENGINES  Computational study of plume-induced separation on a hypersonic powered model [BTN-95-EIX95152582346] p 266  A95-73548  Airborne rotary air separator study [NASA-CR-189099] p 290  N95-24053  AIR COOLING  Evaluation of thermal barrier and PS-200 self-lubricating coatings in an air-cooled rotary engine [NASA-CR-195445] p 289  N95-23222  AIR FILTERS  Erosion of dust-filtered helicopter turbine engines. Part 2: Erosion reduction [BTN-95-EIX95182619223] p 289  A95-76649  Life prediction of helicopter engines fitted with dust filters [BTN-95-EIX95182619224] p 289  A95-76650  Airborne rotary air separator study [NASA-CR-189099] p 290  N95-24053  AIR FLOW
Page	of attack forebody vortex control [NASA-CASE-ARC-11979-1] p 286 N95-23390 Aerodynamic design and analysis of a highly loaded turbine exhaust p 312 N95-23435 Numerical computation of aerodynamics and heat transfer in a turbine cascade and a turn-around duct using advanced turbulence models p 313 N95-23444 NTS-spill test facility wind tunnel exhaust plurne characterization [DE95-003630] p 297 N95-24019 AEROELASTICITY  Eigenanalysis of unsteady flows about airfoils, cascades, and wings [BTN-95-EIX95152577597] p 305 A95-73486 Efficient sensitivity analysis for rotary-wing aeromechanical problems [BTN-95-EIX95152577585] p 264 A95-73497 Limit cycle phenomena in computational transonic aeroelasticity [BTN-95-EIX95152582340] p 264 A95-73520 Static aeroelastic characteristics of a composite wing [BTN-95-EIX95152582340] p 282 A95-73542 Flutter of an infinitely long panel in a duct [BTN-95-EIX95182619087] p 291 A95-75772 Aeroelastic vehicle multivariable control synthesis with analytical robustness evaluation [BTN-95-EIX95182619115] p 321 A95-76592 Analytical aeropropulsive/aeroelastic hypersonic-vehicle model with dynamic analysis [BTN-95-EIX95182619115] p 269 A95-76615 Application of transonic small disturbance theory to the active flexible wing model [BTN-95-EIX95182619210] p 270 A95-76636 Application of Navier-Stokes aeroelastic methods to improve lighter wing maneuver performance [BTN-95-EIX95182619218] p 284 A95-76644 High-performance parallel analysis of coupled problems for aircraft propulsion	flow field [NASA-TM-4638] p 274 N95-23250  Validation of a Computational Fluid Dynamics (CFD) code for supersonic axisymmetric base flow p 315 N95-23652  AGING (MATERIALS) Oklahoma City air logistics center (USAF) aging aircraft corrosion program p 262 N95-23519  AGRICULTURE MAX-91: Polarimetric SAR results on Montespertolisite p 320 N95-23940  AIR Airborne rotary air separator study [NASA-CR-189099] p 290 N95-24053  AIR BREATHING ENGINES Computational study of plume-induced separation on a hypersonic powered model [BTN-95-EIX95152582346] p 266 A95-73548 Airborne rotary air separator study [NASA-CR-189099] p 290 N95-24053  AIR COOLING Evaluation of thermal barrier and PS-200 self-lubricating coatings in an air-cooled rotary engine [NASA-CR-195445] p 289 N95-23222  AIR FILTERS Erosion of dust-filtered helicopter turbine engines. Part 2: Erosion of dust-filtered helicopter turbine engines. Part 2: Erosion of dust-filtered helicopter turbine engines. Part 2: Erosion reduction [BTN-95-EIX95182619223] p 289 A95-76649 Life prediction of helicopter engines fitted with dust filters [BTN-95-EIX95182619224] p 289 A95-76650 Airborne rotary air separator study [NASA-CR-189099] p 290 N95-24053  AIR FLOW Simulation of transverse gas injection in turbulent supersonic air flows [BTN-95-EIX95182619080] p 269 A95-75765 Tracking of raindrops in flow over an airfoil
BTN-95-EIX95152582331   p 281 A95-73533     The influence of alternate inter-blade connections on ground resonance   HTN-95-80859   p 267 A95-75101     Dynamic investigation of the angular motion of a rotating body-parachute system   BTN-95-EIX95182619220   p 270 A95-76646     AERODYNAMIC STALLING   Computation of the poststall behavior of a circulation controlled airfoil   BTN-95-EIX95152582320   p 264 A95-73523     Moving wall effect in relation to other dynamic stall flow mechanisms   BTN-95-EIX95152582324   p 265 A95-73527     AERODYNAMICS   p 265 A95-73527     ABRODYNAMICS   p 265 A95-73527     ABRODYNAMICS   p 265 A95-73527     ABRODYNAMICS   p 265 A95-73527     ABRODYNAMICS   p 304 A95-73457     BTN-95-EIX95142553046   p 304 A95-73457     Laplace interaction law for the computation of viscous airfoil flow in low- and high-speed aerodynamics     BTN-95-EIX95142553037   p 263 A95-73461     P reconditioned domain decomposition scheme for three-dimensional aerodynamic sensitivity analysis     BTN-95-EIX95152577612   p 321 A95-73471     Shock tunnel measurements of hypervelocity blunted cone drag   BTN-95-EIX95152577606   p 305 A95-73477     Eigenanalysis of unsteady flows about airfoils, cascades, and wings   BTN-95-EIX95152577597   p 305 A95-73486     Progress in high-lift aerodynamic calculations   BTN-95-EIX95152582315   p 264 A95-73518     Unstructured grid solutions to a wing/pylon/store configuration   BTN-95-EIX95152582322   p 265 A95-73525     Moving wall effect in relation to other dynamic stall flow mechanisms   BTN-95-EIX95152582324   p 265 A95-73527     Navier-Stokes prediction of large-amplitude delta-wing   BTN-95-EIX95152582324   p 265 A95-73527     Navier-Stokes prediction of large-amplitude delta-wing   BTN-95-EIX95152582324   p 265 A95-73527     Navier-Stokes prediction of large-amplitude delta-wing	of attack forebody vortex control [NASA-CASE-ARC-11979-1] p 286 N95-23390 Aerodynamic design and analysis of a highly loaded turbine exhaust p 312 N95-23435 Numerical computation of aerodynamics and heat transfer in a turbine cascade and a turn-around duct using advanced turbulence models p 313 N95-23444 NTS-spill test facility wind tunnel exhaust plume characterization [DE95-003630] p 297 N95-24019  AEROELASTICITY Eigenanalysis of unsteady flows about airfoils, cascades, and wings [BTN-95-EIX95152577597] p 305 A95-73486 Efficient sensitivity analysis for rotary-wing aeromechanical problems [BTN-95-EIX95152577585] p 264 A95-73497 Limit cycle phenomena in computational transonic aeroelasticity [BTN-95-EIX95152582317] p 264 A95-73542 Flutter of an infinitely long panel in a duct [BTN-95-EIX95182619087] p 291 A95-75772 Aeroelastic vehicle multivariable control synthesis with analytical robustness evaluation [BTN-95-EIX95182619115] p 321 A95-76592 Analytical aeroelastic smodel with dynamic analysis [BTN-95-EIX95182619115] p 321 A95-76615 Application of transonic small disturbance theory to the active flexible wing model [BTN-95-EIX9518261910] p 270 A95-76636 Application of Navier-Stokes aeroelastic methods to improve fighter wing maneuver performance [BTN-95-EIX95182619210] p 284 A95-76644 High-performance parallel analysis of coupled problems for aircraft propulsion [NASA-CR-197440] p 289 N95-23088	flow field [NASA-TM-4638]  Validation of a Computational Fluid Dynamics (CFD) code for supersonic axisymmetric base flow p 315  N95-23652  AGING (MATERIALS) Oklahoma City air logistics center (USAF) aging aircraft corrosion program p 262  N95-23519  AGRICULTURE MAX-91: Polarimetric SAR results on Montespertolisite p 320  N95-23940  AIR Airborne rotary air separator study [NASA-CR-189099] p 290  N95-24053  AIR BREATHING ENGINES Computational study of plume-induced separation on a hypersonic powered model [BTN-95-EIX95152582346] P 266  Ajrborne rotary air separator study [NASA-CR-189099] p 290  N95-24053  AIR COOLING Evaluation of thermal barrier and PS-200 self-lubricating coatings in an air-cooled rotary engine [NASA-CR-195445] Erosion of dust-filtered helicopter turbine engines. Part 2: Erosion of dust-filtered helicopter turbine engines. Part 2: Erosion of dust-filtered helicopter engines fitted with dust filters [BTN-95-EIX95182619223] p 289  A95-76649 Life prediction of helicopter engines fitted with dust filters [BTN-95-EIX95182619224] p 289  A95-76650 Airborne rotary air separator study [NASA-CR-189099] p 290  N95-24053  AIR FLOW Simulation of transverse gas injection in turbulent supersonic air flows [BTN-95-EIX95182619080] p 269  A95-76647
BTN-95-EIX95152582331   p 281 A95-73533   The influence of alternate inter-blade connections on ground resonance   HTN-95-80859   p 267 A95-75101   Dynamic investigation of the angular motion of a rotating body-parachute system   BTN-95-EIX95182619220   p 270 A95-76646   AERODYNAMIC STALLING   Computation of the poststall behavior of a circulation controlled airfoil   BTN-95-EIX95152582320   p 264 A95-73523   Moving wall effect in relation to other dynamic stall flow mechanisms   BTN-95-EIX95152582324   p 265 A95-73527   AERODYNAMICS   Mechanical system reliability and risk assessment   BTN-95-EIX95142553046   p 304 A95-73452   Simulation of turbulent fluctuations   BTN-95-EIX95142553041   p 304 A95-73457   Laplace interaction law for the computation of viscous airfoil flow in low- and high-speed aerodynamics   BTN-95-EIX95142553037   p 263 A95-73461   Preconditioned domain decomposition scheme for three-dimensional aerodynamic sensitivity analysis   BTN-95-EIX95152577612   p 321 A95-73471   Shock tunnel measurements of hypervelocity blunted cone drag   BTN-95-EIX95152577606   p 305 A95-73477   Eigenanalysis of unsteady flows about airfoils, cascades, and wings   BTN-95-EIX95152577597   p 305 A95-73486   Progress in high-lift aerodynamic calculations   BTN-95-EIX95152582315   p 264 A95-73518   Unstructured grid solutions to a wing/pylon/store configuration   BTN-95-EIX95152582322   p 265 A95-73525   Moving wall effect in relation to other dynamic stall flow mechanisms   BTN-95-EIX95152582324   p 265 A95-73527   Navier-Stokes prediction of large-amplitude delta-wing roll oscillations	of attack forebody vortex control [NASA-CASE-ARC-11979-1] p 286 N95-23390 Aerodynamic design and analysis of a highly loaded turbine exhaust p 312 N95-23435 Numerical computation of aerodynamics and heat transfer in a turbine cascade and a turn-around duct using advanced turbulence models p 313 N95-23444 NTS-spill test facility wind tunnel exhaust plurne characterization [DE95-003630] p 297 N95-24019  AEROELASTICITY Eigenanalysis of unsteady flows about airfoils, cascades, and wings [BTN-95-EIX95152577597] p 305 A95-73486 Efficient sensitivity analysis for rotary-wing aeromechanical problems [BTN-95-EIX95152577585] p 264 A95-73497 Limit cycle phenomena in computational transonic aeroelasticity [BTN-95-EIX95152582317] p 264 A95-73520 Static aeroelastic characteristics of a composite wing [BTN-95-EIX95152582340] p 282 A95-73542 Flutter of an infinitely long panel in a duct [BTN-95-EIX95182619087] p 291 A95-75772 Aeroelastic vehicle multivariable control synthesis with analytical robustness evaluation [BTN-95-EIX95182619115] p 321 A95-76592 Analytical aeropropulsive/aeroelastic hypersonic-vehicle model with dynamic analysis [BTN-95-EIX95182619115] p 269 A95-76615 Application of transonic small disturbance theory to the active flexible wing modet [BTN-95-EIX95182619210] p 270 A95-76636 Application of Navier-Stokes aeroelastic methods to improve fighter wing maneuver performance [BTN-95-EIX95182619218] p 284 A95-76644 High-performance parallel analysis of coupled problems for aircraft propulsion [NASA-CR-197931] p 294 N95-23392	flow field [NASA-TM-4638]  Validation of a Computational Fluid Dynamics (CFD) code for supersonic axisymmetric base flow p 315 N95-23652  AGING (MATERIALS)  Oklahoma City air logistics center (USAF) aging aircraft corrosion program p 262 N95-23519  AGRICULTURE  MAX-91: Polarimetric SAR results on Montespertolisite p 320 N95-23940  AIR  Airborne rotary air separator study [NASA-CR-189099]  AIR BREATHING ENGINES  Computational study of plume-induced separation on a hypersonic powered model [BTN-95-EIX95152582346] p 266 A95-73548  Airborne rotary air separator study [NASA-CR-189099]  AIR COOLING  Evaluation of thermal barrier and PS-200 self-lubricating coatings in an air-cooled rotary engine [NASA-CR-1895445]  AIR FILTERS  Erosion of dust-filtered helicopter turbine engines. Part 2: Erosion reduction [BTN-95-EIX95182619223]  Life prediction of helicopter engines fitted with dust filters [BTN-95-EIX95182619224]  Airborne rotary air separator study [NASA-CR-189099]  APS-76650  AIR FLOW  Simulation of transverse gas injection in turbulent supersonic air flows [BTN-95-EIX95182619221]  CFD analysis of turbopoump volutes
65-deg delta wing   BTN-95-EIX95152582331   p 281 A95-73533   The influence of alternate inter-blade connections on ground resonance   HTN-95-80859   p 267 A95-75101   Dynamic investigation of the angular motion of a rotating body-parachute system   BTN-95-EIX95152619220   p 270 A95-76646   AERODYNAMIC STALLING   Computation of the poststall behavior of a circulation controlled airfoil   BTN-95-EIX95152582320   p 264 A95-73523   Moving wall effect in relation to other dynamic stall flow mechanisms   BTN-95-EIX95152582324   p 265 A95-73527   AERODYNAMICS   Mechanical system reliability and risk assessment   BTN-95-EIX95142553046   p 304 A95-73452   Simulation of turbulent fluctuations   BTN-95-EIX95142553041   p 304 A95-73452   Simulation of turbulent fluctuations   BTN-95-EIX95142553041   p 263 A95-73451   Laplace interaction law for the computation of viscous airfoil flow in low- and high-speed aerodynamics   BTN-95-EIX95142553037   p 263 A95-73461   P Peconditioned domain decomposition scheme for three-dimensional aerodynamic sensitivity analysis   BTN-95-EIX95152577612   p 321 A95-73471   Shock tunnel measurements of hypervelocity blunted cone drag   BTN-95-EIX95152577606   p 305 A95-73477   Eigenanalysis of unsteady flows about airfoils, cascades, and wings   BTN-95-EIX95152582315   p 264 A95-73518   Unstructured grid solutions to a wing/pylon/store configuration   BTN-95-EIX95152582322   p 265 A95-73525   Moving wall effect in relation to other dynamic stall flow mechanisms   BTN-95-EIX95152582324   p 265 A95-73527   Navier-Stokes prediction of large-amplitude delta-wing roll oscillations   BTN-95-EIX95152582329   p 281 A95-73531	of attack forebody vortex control [NASA-CASE-ARC-11979-1] p 286 N95-23390 Aerodynamic design and analysis of a highly loaded turbine exhaust p 312 N95-23435 Numerical computation of aerodynamics and heat transfer in a turbine cascade and a turn-around duct using advanced turbulence models p 313 N95-23444 NTS-spill test facility wind tunnel exhaust plurne characterization [DE95-003630] p 297 N95-24019 AEROELASTICITY Eigenanalysis of unsteady flows about airfoits, cascades, and wings [BTN-95-EIX95152577597] p 305 A95-73486 Efficient sensitivity analysis for rotary-wing aeromechanical problems [BTN-95-EIX95152577585] p 264 A95-73497 Limit cycle phenomena in computational transonic aeroelasticity [BTN-95-EIX95152582317] p 264 A95-73520 Static aeroelastic characteristics of a composite wing [BTN-95-EIX95152582340] p 282 A95-73542 Flutter of an infinitely long panel in a duct [BTN-95-EIX95182619087] p 291 A95-75772 Aeroelastic vehicle multivariable control synthesis with analytical analytical aeropropulsive/aeroelastic hypersonic-vehicle model with dynamic analysis [BTN-95-EIX95182619115] p 321 A95-76592 Analytical aeropropulsive/aeroelastic hypersonic-vehicle model with dynamic analysis [BTN-95-EIX95182619138] p 269 A95-76615 Application of transonic small disturbance theory to the active flexible wing model [BTN-95-EIX95182619210] p 270 A95-76636 Application of Navier-Stokes aeroelastic methods to improve fighter wing maneuver performance [BTN-95-EIX95182619218] p 284 A95-76644 High-performance parallel analysis of coupled problems for aircraft propulsion [NASA-CR-197440] p 289 N95-23088 Flutter analysis of composite box beams [NASA-CR-1977440] p 289 N95-23392 User's guide for ECAP2D: An Euler unsteady	flow field [NASA-TM-4638]  Validation of a Computational Fluid Dynamics (CFD) code for supersonic axisymmetric base flow p 315  N95-23652  AGING (MATERIALS) Oklahoma City air logistics center (USAF) aging aircraft corrosion program p 262  N95-23519  AGRICULTURE MAX-91: Polarimetric SAR results on Montespertolisite p 320  N95-23940  AIR Airborne rotary air separator study [NASA-CR-189099] p 290  N95-24053  AIR BREATHING ENGINES Computational study of plume-induced separation on a hypersonic powered model [BTN-95-EIX95152582346] P 266  Ajrborne rotary air separator study [NASA-CR-189099] p 290  N95-24053  AIR COOLING Evaluation of thermal barrier and PS-200 self-lubricating coatings in an air-cooled rotary engine [NASA-CR-195445] Erosion of dust-filtered helicopter turbine engines. Part 2: Erosion of dust-filtered helicopter turbine engines. Part 2: Erosion of dust-filtered helicopter engines fitted with dust filters [BTN-95-EIX95182619223] p 289  A95-76649 Life prediction of helicopter engines fitted with dust filters [BTN-95-EIX95182619224] p 289  A95-76650 Airborne rotary air separator study [NASA-CR-189099] p 290  N95-24053  AIR FLOW Simulation of transverse gas injection in turbulent supersonic air flows [BTN-95-EIX95182619080] p 269  A95-76647
BTN-95-EIX95152582331   p 281 A95-73533   The influence of alternate inter-blade connections on ground resonance   HTN-95-80859   p 267 A95-75101   Dynamic investigation of the angular motion of a rotating body-parachute system   BTN-95-EIX95182619220   p 270 A95-76646   AERODYNAMIC STALLING   Computation of the poststall behavior of a circulation controlled airfoil   BTN-95-EIX95152582320   p 264 A95-73523   Moving wall effect in relation to other dynamic stall flow mechanisms   BTN-95-EIX95152582324   p 265 A95-73527   AERODYNAMICS   Mechanical system reliability and risk assessment   BTN-95-EIX95142553046   p 304 A95-73452   Simulation of turbulent fluctuations   BTN-95-EIX95142553041   p 304 A95-73457   Laplace interaction law for the computation of viscous airfoil flow in low- and high-speed aerodynamics   BTN-95-EIX95142553037   p 263 A95-73461   Preconditioned domain decomposition scheme for three-dimensional aerodynamic sensitivity analysis   BTN-95-EIX95152577612   p 321 A95-73471   Shock tunnel measurements of hypervelocity blunted cone drag   BTN-95-EIX95152577606   p 305 A95-73477   Eigenanalysis of unsteady flows about airfoils, cascades, and wings   BTN-95-EIX95152582315   p 264 A95-73518   Unstructured grid solutions to a wing/pylon/store configuration   BTN-95-EIX95152582321   p 265 A95-73525   Moving wall effect in relation to other dynamic stall flow mechanisms   BTN-95-EIX95152582329   p 265 A95-73527   Navie-Stokes prediction of large-amplitude delta-wing roll oscillations   BTN-95-EIX95152582329   p 281 A95-7351   Further analysis of high-rate rolling experiments of a 65-deg delta wing	of attack forebody vortex control [NASA-CASE-ARC-11979-1] p 286 N95-23390 Aerodynamic design and analysis of a highly loaded turbine exhaust p 312 N95-23435 Numerical computation of aerodynamics and heat transter in a turbine cascade and a turn-around duct using advanced turbulence models p 313 N95-23444 NTS-spill test facility wind tunnel exhaust plurne characterization [DE95-003630] p 297 N95-24019 AEROELASTICITY  Eigenanalysis of unsteady flows about airfoils, cascades, and wings [BTN-95-EIX95152577597] p 305 A95-73486 Efficient sensitivity analysis for rotary-wing aeromechanical problems [BTN-95-EIX95152577585] p 264 A95-73497 Limit cycle phenomena in computational transonic aeroelasticity [BTN-95-EIX95152582340] p 264 A95-73520 Static aeroelastic characteristics of a composite wing [BTN-95-EIX95152582340] p 282 A95-73542 Flutter of an infinitely long panel in a duct [BTN-95-EIX95182619087] p 291 A95-75772 Aeroelastic vehicle multivariable control synthesis with analytical robustness evaluation [BTN-95-EIX95182619115] p 321 A95-76592 Analytical aeropropulsive/aeroelastic hypersonic-vehicle model with dynamic analysis [BTN-95-EIX95182619115] p 269 A95-76615 Application of transonic small disturbance theory to the active flexible wing model [BTN-95-EIX951826191138] p 269 A95-76636 Application of Navier-Stokes aeroelastic methods to improve lighter wing maneuver performance [BTN-95-EIX95182619210] p 270 A95-76644 High-performance parallel analysis of coupled problems for aircraft propulsion [NASA-CR-197931] p 294 N95-23088 Flutter analysis of composite box beams [NASA-CR-197931] p 294 N95-23392 User's guide for ECAP2D: An Euler unsteady aerodynamic and aeroelastic analysis program for two dimensional oscillating cascades, version 1.0	flow field [NASA-TM-4638] p 274 N95-23250  Validation of a Computational Fluid Dynamics (CFD) code for supersonic axisymmetric base flow p 315 N95-23652  AGING (MATERIALS) Oklahoma City air logistics center (USAF) aging aircraft corrosion program p 262 N95-23519  AGRICULTURE MAX-91: Potarimetric SAR results on Montespertolisite p 320 N95-23940  AIR Airborne rotary air separator study [NASA-CR-189099] p 290 N95-24053  AIR BREATHING ENGINES Computational study of plume-induced separation on a hypersonic powered model [BTN-95-EIX95152582346] p 266 A95-73548 Airborne rotary air separator study [NASA-CR-189099] p 290 N95-24053  AIR COOLING Evaluation of thermal barrier and PS-200 self-lubricating coatings in an air-cooled rotary engine [NASA-CR-195445] p 289 N95-23222  AIR FILTERS Erosion of dust-filtered helicopter turbine engines. Part 2: Erosion of dust-filtered helicopter turbine engines. Part 2: Erosion reduction [BTN-95-EIX95182619223] p 289 A95-76649 Life prediction of helicopter engines fitted with dust filters [BTN-95-EIX95182619224] p 289 A95-76650 Airborne rotary air separator study [NASA-CR-189099] p 290 N95-24053  AIR FLOW Simulation of transverse gas injection in turbulent supersonic air flows [BTN-95-EIX95182619080] p 269 A95-75765 Tracking of raindrops in flow over an airtoil [BTN-95-EIX95182619221] p 308 A95-76647 CFD analysis of turbopump volutes p 312 N95-23436 Phase 2: HGM air flow tests in support of HEX vane investigation p 312 N95-23438
65-deg delta wing IBTN-95-EIX95152582331   p 281 A95-73533 The influence of alternate inter-blade connections on ground resonance IHTN-95-80859   p 267 A95-75101 Dynamic investigation of the angular motion of a rotating body-parachute system IBTN-95-EIX95162619220   p 270 A95-76646 AERODYNAMIC STALLING  Computation of the poststall behavior of a circulation controlled airfoil IBTN-95-EIX95152582320   p 264 A95-73523 Moving wall effect in relation to other dynamic stall flow mechanisms [BTN-95-EIX95152582324   p 265 A95-73527 AERODYNAMICS  Mechanical system reliability and risk assessment IBTN-95-EIX95142553046   p 304 A95-73452 Simulation of turbulent fluctuations [IBTN-95-EIX95142553041   p 304 A95-73457 Laplace interaction law for the computation of viscous airfoil flow in low- and high-speed aerodynamics IBTN-95-EIX951425530371   p 263 A95-73461 Preconditioned domain decomposition scheme for three-dimensional aerodynamic sensitivity analysis IBTN-95-EIX95152577612   p 321 A95-73471 Shock tunnel measurements of hypervelocity blunted cone drag [IBTN-95-EIX95152577606]   p 305 A95-73477 Eigenanalysis of unsteady flows about airfoils, cascades, and wings [IBTN-95-EIX95152577597]   p 305 A95-73486 Progress in high-lift aerodynamic calculations [IBTN-95-EIX95152582321]   p 264 A95-73518 Unstructured grid solutions to a wing/pylon/store configuration [IBTN-95-EIX95152582321]   p 265 A95-73527 Navier-Stokes prediction of large-amplitude delta-wing roll oscillations [IBTN-95-EIX95152582329]   p 281 A95-73531 Further analysis of high-rate rolling experiments of a 65-deg delta wing [IBTN-95-EIX95152582331]   p 281 A95-73533	of attack forebody vortex control [NASA-CASE-ARC-11979-1] p 286 N95-23390 Aerodynamic design and analysis of a highly loaded turbine exhaust p 312 N95-23435 Numerical computation of aerodynamics and heat transfer in a turbine cascade and a turn-around duct using advanced turbulence models p 313 N95-23444 NTS-spill test facility wind tunnel exhaust plurne characterization [DE95-003630] p 297 N95-24019 AEROELASTICITY Eigenanalysis of unsteady flows about airfoits, cascades, and wings [BTN-95-EIX95152577597] p 305 A95-73486 Efficient sensitivity analysis for rotary-wing aeromechanical problems [BTN-95-EIX95152577585] p 264 A95-73497 Limit cycle phenomena in computational transonic aeroelasticity [BTN-95-EIX95152582317] p 264 A95-73542 Static aeroelastic characteristics of a composite wing [BTN-95-EIX95152582340] p 282 A95-73542 Flutter of an infinitely long panel in a duct [BTN-95-EIX95182619087] p 291 A95-75772 Aeroelastic vehicle multivariable control synthesis with analytical aeropropulsive/aeroelastic hypersonic-vehicle model with dynamic analysis [BTN-95-EIX95182619115] p 321 A95-76592 Analytical aeropropulsive/aeroelastic hypersonic-vehicle model with dynamic analysis [BTN-95-EIX95182619138] p 269 A95-76615 Application of transonic small disturbance theory to the active flexible wing model [BTN-95-EIX95182619210] p 270 A95-76636 Application of Navier-Stokes aeroelastic methods to improve lighter wing maneuver performance [BTN-95-EIX951826192118] p 284 A95-76644 High-performance parallel analysis of coupled problems for aircraft propulsion [NASA-CR-197440] p 289 N95-23088 Flutter analysis of composite box beams [NASA-CR-197440] p 299 N95-23088 Flutter analysis of composite box beams [NASA-CR-197931] p 294 N95-23392 User's guide for ECAP2D: An Euler unsteady aerodynamic and aeroelastic analysis program for two dimensional oscillating cascades, version 1.0 [NASA-CR-1879416] p 316 N95-24189	flow field [NASA-TM-4638]  P 274 N95-23250  Validation of a Computational Fluid Dynamics (CFD) code for supersonic axisymmetric base flow p 315 N95-23652  AGING (MATERIALS)  Oklahoma City air logistics center (USAF) aging aircraft corrosion program p 262 N95-23519  AGRICULTURE  MAX-91: Polarimetric SAR results on Montespertolisite p 320 N95-23940  AIR  Airborne rotary air separator study [NASA-CR-189099]  AIR BREATHING ENGINES  Computational study of plume-induced separation on a hypersonic powered model [BTN-95-EIX95152582346]  Evaluation of thermal barrier and PS-200 self-lubricating coatings in an air-cooled rotary engine [NASA-CR-189099]  P 289 N95-23222  AIR FILTERS  Erosion of dust-filtered helicopter turbine engines. Part 2: Erosion reduction [BTN-95-EIX95182619223]  Life prediction of helicopter engines fitted with dust filters [BTN-95-EIX95182619224]  P 289 A95-76649  Life prediction of helicopter engines fitted with dust filters [BTN-95-EIX95182619224]  P 289 A95-76650  Airborne rotary air separator study [NASA-CR-189099]  P 290 N95-24053  AIR FLOW  Simulation of transverse gas injection in turbulent supersonic air flows [BTN-95-EIX95182619280]  P 269 A95-75765  Tracking of raindrops in flow over an airfoil [BTN-95-EIX95182619221]  CFD analysis of turbopump volutes  P 312 N95-23438  Phase 2: HGM air flow tests in support of HEX vane investigation  AIR INTAKES
BTN-95-EIX95152582331   p 281 A95-73533   The influence of alternate inter-blade connections on ground resonance   HTN-95-80859   p 267 A95-75101   Dynamic investigation of the angular motion of a rotating body-parachute system   BTN-95-EIX95182619220   p 270 A95-76646   AERODYNAMIC STALLING   Computation of the poststall behavior of a circulation controlled airfoil   BTN-95-EIX95152582320   p 264 A95-73523   Moving wall effect in relation to other dynamic stall flow mechanisms   BTN-95-EIX95152582324   p 265 A95-73527   AERODYNAMICS   Mechanical system reliability and risk assessment   BTN-95-EIX95142553046   p 304 A95-73452   Simulation of turbulent fluctuations   BTN-95-EIX95142553041   p 304 A95-73457   Laplace interaction law for the computation of viscous airfoil flow in low- and high-speed aerodynamics   BTN-95-EIX95142553037   p 263 A95-73461   Preconditioned domain decomposition scheme for three-dimensional aerodynamic sensitivity analysis   BTN-95-EIX95152577612   p 321 A95-73471   Shock tunnel measurements of hypervelocity blunted cone drag   BTN-95-EIX95152577606   p 305 A95-73477   Eigenanalysis of unsteady flows about airfoils, cascades, and wings   BTN-95-EIX95152582315   p 264 A95-73518   Unstructured grid solutions to a wing/pylon/store configuration   BTN-95-EIX95152582321   p 265 A95-73525   Moving wall effect in relation to other dynamic stall flow mechanisms   BTN-95-EIX95152582329   p 265 A95-73527   Navie-Stokes prediction of large-amplitude delta-wing roll oscillations   BTN-95-EIX95152582329   p 281 A95-7351   Further analysis of high-rate rolling experiments of a 65-deg delta wing	of attack forebody vortex control [NASA-CASE-ARC-11979-1] p 286 N95-23390 Aerodynamic design and analysis of a highly loaded turbine exhaust p 312 N95-23435 Numerical computation of aerodynamics and heat transter in a turbine cascade and a turn-around duct using advanced turbulence models p 313 N95-23444 NTS-spill test facility wind tunnel exhaust plurne characterization [DE95-003630] p 297 N95-24019 AEROELASTICITY  Eigenanalysis of unsteady flows about airfoils, cascades, and wings [BTN-95-EIX95152577597] p 305 A95-73486 Efficient sensitivity analysis for rotary-wing aeromechanical problems [BTN-95-EIX95152577585] p 264 A95-73497 Limit cycle phenomena in computational transonic aeroelasticity [BTN-95-EIX95152582340] p 264 A95-73520 Static aeroelastic characteristics of a composite wing [BTN-95-EIX95152582340] p 282 A95-73542 Flutter of an infinitely long panel in a duct [BTN-95-EIX95182619087] p 291 A95-75772 Aeroelastic vehicle multivariable control synthesis with analytical robustness evaluation [BTN-95-EIX95182619115] p 321 A95-76592 Analytical aeropropulsive/aeroelastic hypersonic-vehicle model with dynamic analysis [BTN-95-EIX95182619115] p 269 A95-76615 Application of transonic small disturbance theory to the active flexible wing model [BTN-95-EIX951826191138] p 269 A95-76636 Application of Navier-Stokes aeroelastic methods to improve lighter wing maneuver performance [BTN-95-EIX95182619210] p 270 A95-76644 High-performance parallel analysis of coupled problems for aircraft propulsion [NASA-CR-197931] p 294 N95-23088 Flutter analysis of composite box beams [NASA-CR-197931] p 294 N95-23392 User's guide for ECAP2D: An Euler unsteady aerodynamic and aeroelastic analysis program for two dimensional oscillating cascades, version 1.0	flow field [NASA-TM-4638] p 274 N95-23250  Validation of a Computational Fluid Dynamics (CFD) code for supersonic axisymmetric base flow p 315 N95-23652  AGING (MATERIALS) Oklahoma City air logistics center (USAF) aging aircraft corrosion program p 262 N95-23519  AGRICULTURE MAX-91: Potarimetric SAR results on Montespertolisite p 320 N95-23940  AIR Airborne rotary air separator study [NASA-CR-189099] p 290 N95-24053  AIR BREATHING ENGINES Computational study of plume-induced separation on a hypersonic powered model [BTN-95-EIX95152582346] p 266 A95-73548 Airborne rotary air separator study [NASA-CR-189099] p 290 N95-24053  AIR COOLING Evaluation of thermal barrier and PS-200 self-lubricating coatings in an air-cooled rotary engine [NASA-CR-195445] p 289 N95-23222  AIR FILTERS Erosion of dust-filtered helicopter turbine engines. Part 2: Erosion of dust-filtered helicopter turbine engines. Part 2: Erosion reduction [BTN-95-EIX95182619223] p 289 A95-76649  Life prediction of helicopter engines fitted with dust filters [BTN-95-EIX95182619224] p 289 A95-76650  Airborne rotary air separator study [NASA-CR-189099] p 290 N95-24053  AIR FLOW Simulation of transverse gas injection in turbulent supersonic air flows [BTN-95-EIX95182619080] p 269 A95-75765  Tracking of raindrops in flow over an airtoil [BTN-95-EIX95182619221] p 308 A95-76647  CFD analysis of turbopump volutes p 312 N95-23438  Phase 2: HGM air flow tests in support of HEX vane investigation p 312 N95-23438

AIR JETS	AIRCRAFT CONFIGURATIONS	Euler Technology Assessment program for preliminary
Simulation of transverse gas injection in turbulent supersonic air flows	Unstructured grid solutions to a wing/pylon/store	aircraft design employing SPLITFLOW code with Cartesian unstructured grid method
[BTN-95-EIX95182619080] p 269 A95-75765	configuration [BTN-95-EIX95152582322] p 265 A95-73525	[NASA-CR-4649] p 273 N95-22917
AIR LAUNCHING	AIRCRAFT CONSTRUCTION MATERIALS	Euler technology assessment for preliminary aircraft
Aerodynamic design of pegasus: Concept to flight with	MIL-HDBK-5 design allowables for fibre/metal	design employing OVERFLOW code with multiblock
computational fluid dynamics	laminates: ARALL 2 and ARALL 3	structured-grid method
[BTN-95-EIX95182617463] p 298 A95-75734	[BTN-94-EIX94371346933] p 300 A95-73345	[NASA-CR-4651] p 273 N95-23095
AIR LAW	Evaluation of advanced aerospace materials by depth sensing indentation and scratch methods	Control of flow separation in airfoil/wing design applications p 274 N95-23294
Oceanic operations: An authoritative guide to oceanic operations	[BTN-95-EIX95152584678] p 282 A95-73590	Thin tailored composite wing for civil tiltrotor
[FAA-AFS-550] p 277 N95-24065	H-76B fantail demonstrater composite fan blade	p 285 N95-23317
AIR NAVIGATION	fabrication	AIRCRAFT ENGINES
Development of aeronautical mobile satellite services	[HTN-95-80856] p 283 A95-75098	Artificial intelligence for turboprop engine maintenance
over the past thirty years	Mishap risk control for advanced aerospace/composite materials p 301 N95-23031	[BTN-95-EIX95182617812] p 288 A95-75757
[BTN-95-EIX95152569458] p 305 A95-73498	Technology reinvestment project's focus area:	Lycoming to test new engine core [HTN-95-41393] p 288 A95-76389
Real-time navigation using the global positioning	Affordable polymer matrix composites for airframe	A new type of simulator for simulating the flow-field
system (BTN-95-EIX95172595298) p 279 A95-75714	structures	distortion of engine inlet
(BTN-95-EIX95172595298) p 279 A95-75714  Cueing light configuration for aircraft navigation	(PB95-136032) p 324 N95-23168	[BTN-95-EIX95202638963] p 289 A95-76673
[NASA-CASE-ARC-11982-1] p 280 N95-23393	Development and verification of a resin film	High-performance parallel analysis of coupled problems
Oceanic operations: An authoritative guide to oceanic	infusion/resin transfer molding simulation model for fabrication of advanced textile composites	for aircraft propulsion [NASA-CR-197440] p 289 N95-23088
operations	[NASA-CR-197439] p 301 N95-23179	[NASA-CR-197440] p 289 N95-23088 Engines-only flight control system
[FAA-AFS-550] p 277 N95-24065	Test method and test results for environmental	(NASA-CASE-ARC-11944-1) p 294 N95-23389
AIR POLLUTION	assessment of aircraft materials p 302 N95-23509	AIRCRAFT FUELS
In situ observations in aircraft exhaust plumes in the	US Navy operating experience with new aircraft	Trajectory modeling of emissions from lower
lower stratosphere at midlatitudes	construction materials p 303 N95-23517	stratospheric aircraft
[HTN-95-A0862] p 318 A95-76266	Review of some results of the author's fatigue investigations with applications in engineering and material	[HTN-95-41219] p 317 A95-75031
Transport of exhaust products in the near trail of a jet engine under atmospheric conditions	science	In situ observations in aircraft exhaust plumes in the lower stratosphere at midlatitudes
[HTN-95-91421] p 319 A95-77334	[TAE-698] p 316 N95-23662	[HTN-95-A0862] p 318 A95-76266
AIR SAMPLING	AIRCRAFT CONTROL	Sensitivity of two-dimensional model predictions of
Estimates of total organic and inorganic chlorine in the	Cypher moves toward autonomous flight	ozone response to stratospheric aircraft: An update
lower stratosphere from in situ and flask measurements	[HTN-95-41394] p 283 A95-76390	[HTN-95-A0863] p 318 A95-76267
during AASE 2	Functional agility metrics and optimal trajectory analysis	AIRCRAFT GUIDANCE
[HTN-95-A0861] p 317 A95-76265	[BTN-95-EIX95182619121] p 321 A95-76598	Analytical solution for controls, heats, and states of flight trajectories
AIR TRAFFIC CONTROL  Development of aeronautical mobile satellite services	Multiaxis pilot ratings for damaged aircraft	[BTN-95-EIX95152583286] p 282 A95-73587
over the past thirty years	[BTN-95-EIX95182619128] p 269 A95-76605	Guidance and control requirements for high-speed
[BTN-95-EIX95152569458] p 305 A95-73498	Direct-lift design strategy for longitudinal control of	Rollout and Turnoff (ROTO)
Description of a GNSS availability model and its use in	hypersonic aircraft	[NASA-CR-195026] p 292 N95-22674
developing requirements	[BTN-95-EIX95182619131] p 291 A95-76608 Attainable moments for the constrained control	Nonlinear system guidance in the presence of
[BTN-95-EIX95202637603] p 308 A95-76686	allocation problem	transmission zero dynamics [NASA-TM-4661] p 309 N95-22804
The role of flight progress strips in en route air traffic	[BTN-95-EIX95182619149] p 322 A95-76626	AIRCRAFT HAZARDS
control: A time-series analysis [DOT/FAA/AM-95/4] p 280 N95-23565	Automatic formation flight control	Thundercloud electric field modeling for the
AIR TRAFFIC CONTROLLERS (PERSONNEL)	[BTN-95-EIX95182619153] p 292 A95-76630	ionosphere-Earth region. 1: Dependence on cloud charge
The role of flight progress strips in en route air traffic	Multiple-function digital controller system for active flexible wing wind-tunnel model	distribution
control: A time-series analysis	[BTN-95-EIX95182619212] p 322 A95-76638	[HTN-95-41223] p 317 A95-75035 AIRCRAFT ICING
[DOT/FAA/AM-95/4] p 280 N95-23565	Robustly stable preliminary control systems design for	Effect of curvature in the numerical simulation of an
AIR TRANSPORTATION	the YF-16 CCV aircraft	electrothermal de-icer pad
Maintenance challenges and trends	[BTN-95-EIX95202637608] p 292 A95-76681	[BTN-95-EIX95182619219] p 276 A95-76645
[BTN-95-EIX95182617808] p 261 A95-75753	Guidance and control requirements for high-speed Rollout and Turnoff (ROTO)	Aerodynamics of a finite wing with simulated ice
Report of proceedings: Aviation Accident Investigation Symposium. Volume 2: Participant presentations	[NASA-CR-195026] p 292 N95-22674	[BTN-95-EIX95182619227] p 270 A95-76653 Additional improvements to the NASA Lewis ice
[PB94-917007] p 277 N95-23598	Nonlinear system guidance in the presence of	accretion code LEWICE
Oceanic operations: An authoritative guide to oceanic	transmission zero dynamics	[NASA-TM-106849] p 309 N95-22669
operations	[NASA-TM-4661] p 309 N95-22804	Collaborative research on aircraft icing and charging
[FAA-AFS-550] p 277 N95-24065	Flight test of the X-29A at high angle of attack: Flight	processes in ice
AIRBORNE RADAR 2 micron LIDAR for laser-based remote sensing: Flight	dynamics and controls [NASA-TP-3537] p 284 N95-22806	[AD-A285102] p 276 N95-23201
demonstration and application survey	Design of high performance multivariable control	AIRCRAFT INDUSTRY Report of proceedings: Aviation Accident Investigation
[BTN-95-EIX95212641072] p 319 A95-76737	systems for supermaneuverable aircraft at high angle of	Symposium. Volume 2: Participant presentations
MAX-91: Polarimetric SAR results on Montespertoli	attack	[PB94-917007] p 277 N95-23598
site p 320 N95-23940	[NASA-CR-197661] p 293 N95-22908	AIRCRAFT INSTRUMENTS
AIRCRAFT ACCIDENT INVESTIGATION	Stable H(infinity) controller design for the longitudinal dynamics of an aircraft	Flight-deck displays on the Boeing 777
Report of proceedings: Aviation Accident Investigation Symposium. Volume 2: Participant presentations	[NASA-TM-106847] p 293 N95-22954	[BTN-95-EIX95142562402] p 286 A95-73438 Flight test evaluation of a 35 GHz forward looking
(PB94-917007) p 277 N95-23598	Analysis of the longitudinal handling qualities and	altimeter for terrain avoidance
Aircraft accident report. Runway overrun following	pilot-induced-oscillation tendencies of the	[BTN-95-EIX95212641071] p 287 A95-76736
rejected takeoff. Continental airlines flight 795, McDonnell	High-Angle-of-Attack Research Vehicle (HARV)	AIRCRAFT LANDING
Douglas MD-82, N18835, LaGuardia Airport, Flushing, NY,	p 293 N95-23297	Progress in high-lift aerodynamic calculations
2 March 1994 [PB95-910401] p 277 N95-23609	Handling qualities of the High Speed Civil Transport p 294 N95-23325	[BTN-95-EIX95152582315] p 264 A95-73518
Aviation Accident Investigation Symposium. Volume 1:	Feedback control laws for highly maneuverable	AIRCRAFT MAINTENANCE Maintenance challenges and trends
Industry recommendations and Safety Board responses	aircraft	[BTN-95-EIX95182617808] p 261 A95-75753
[PB94-917005] p 278 N95-24105	[NASA-CR-197944] p 295 N95-23410	Maintenance programs
AIRCRAFT ACCIDENTS	AIRCRAFT DESIGN	[BTN-95-EIX95182617809] p 261 A95-75754
Mishap risk control for advanced aerospace/composite	Flight-deck displays on the Boeing 777 [BTN-95-EIX95142562402] p 286 A95-73438	Aircraft stripping and painting
materials p 301 N95-23031 Aircraft accident report. Runway overrun following	Structural acoustic calculations in the low-frequency	[BTN-95-EIX95182617810] p 300 A95-75755 Condition monitoring and diagnostics
rejected takeoff. Continental airlines flight 795, McDonnell	range	[BTN-95-EIX95182617811] p 261 A95-75756
Douglas MD-82, N18835, LaGuardia Airport, Flushing, NY,	[BTN-95-EIX95152582336] p 323 A95-73538	Artificial intelligence for turboprop engine maintenance
2 March 1994	Flow study of supersonic wing-necelle configuration	(BTN-95-EIX95182617812) p 288 A95-75757
[PB95-910401] p 277 N95-23609	[BTN-95-EIX95152582344] p 266 A95-73546	POD assessment of NDI procedures using a round robin
Aircraft fires, smoke toxicity, and survival: An overview [DOT/FAA/AM-95/8] p 277 N95-24024	An analytical and experimental investigation of the response of the curved, composite frame/skin	test [AGARD-R-809] p 315 N95-23602
A review of civil aviation fatal accidents in which	specimens	Enhancement of F/A-18 operational flight
lost/disoriented was a cause/factor: 1981-1990	[HTN-95-80857] p 283 A95-75099	measurements: Data report for phase 1
[DOT/FAA/AM-95/1] p 278 N95-24071	An unmanned air vehicle concept with tipjet drive	[DSTO-TR-0049] p 286 N95-23666
AIRCRAFT APPROACH SPACING	[HTN-95-80858] p 283 A95-75100	AIRCRAFT MANEUVERS
Guidance and control requirements for high-speed	Integrated design of hypersonic waveriders including	Functional agility metrics and optimal trajectory
Rollout and Turnoff (ROTO) [NASA-CR-195026] p 292 N95-22674	inlets and tailfins [BTN-95-EIX95212645692] p 271 A95-76744	analysis [BTN-95-EIX95182619121] p 321 A95-76598
114 (DA-O) 1000E01 P 282 1195-22074	(= 00-EINOUE IEUTOUSE) P 2/ 1 MSD-/0/44	10 00 FINOS (050 19 15 1) h 05 1 M30-10330

AIRCRAFT MODELS		SUBJECT INDEX
Kinematics and aerodynamics of velocity-vector roll	AIRCRAFT SPECIFICATIONS	Effect of underwing frost on a transport aircraft airfoil
[BTN-95-EIX95182619126] p 291 A95-76603	Integrated flight/propulsion control for helicopters	at flight Reynolds number
Optimal lateral-escape maneuvers for microburst encounters during final approach	[HTN-95-80854] p 290 A95-75096 AIRCRAFT STABILITY	[BTN-95-EIX95152582334] p 276 A95-73536 Postinstability behavior of a two-dimensional airfoil with
[BTN-95-EIX95182619127] p 276 A95-76604	Postinstability behavior of a two-dimensional airfoil with	a structural nonlinearity
Multiaxis pilot ratings for damaged aircraft	a structural nonlinearity	[BTN-95-EIX95152582337] p 266 A95-73539 Turbulent transonic airfoil flow simulation using a
[8TN-95-EIX95182619128] p 269 A95-76605 Automatic formation flight control	[BTN-95-EIX95152582337] p 266 A95-73539 Method for the prediction of the onset of wing rock	pressure-based algorithm
[BTN-95-EIX95182619153] p 292 A95-76630	[BTN-95-EIX95152582342] p 282 A95-73544	[BTN-95-EIX95182619078] p 269 A95-75763
Rolling maneuver load alleviation using active controls [BTN-95-EIX95182619217] p 270 A95-76643	Effect of leeward flow dividers on the wing rock of a	Viscous-inviscid interaction method for unsteady low-speed airfoil flows
Application of Navier-Stokes aeroelastic methods to	delta wing {BTN-95-EIX95152582347} p 282 A95-73549	[BTN-95-EIX95182619093] p 269 A95-75778
improve fighter wing maneuver performance IBTN-95-EIX951826192181 p 284 A95-76644	System for determining aerodynamic imbalance	Tracking of raindrops in flow over an airfoil [BTN-95-EIX95182619221] p 308 A95-76647
[BTN-95-EIX95182619218] p 284 A95-76644 AIRCRAFT MODELS	[NASA-CASE-ARC-11913-1] p 311 N95-23377	Response of a nonrotating rotor blade to lateral
SEM representation of the early and late time fields	Aerodynamic flight control to increase payload capability of future launch vehicles	turbulence. Part 2: Experiment IBTN-95-EIX951826192291 p 284 A95-76655
scattered from wire targets (BTN-94-EIX94381353142) p 306 A95-74496	[NASA-CR-197704] p 300 N95-24032	[BTN-95-EIX95182619229] p 284 A95-76655 AIRFRAME MATERIALS
Some aspects of the aerodynamics of separating	AIRCRAFT STRUCTURES	Technology reinvestment project's focus area:
strap-ons (BTN-95-EIX95182617464) p 298 A95-75735	MIL-HDBK-5 design allowables for fibre/metal laminates: ARALL 2 and ARALL 3	Affordable polymer matrix composites for airframe structures
Aeroelastic vehicle multivariable control synthesis with	[BTN-94-EIX94371346933] p 300 A95-73345	[PB95-136032] p 324 N95-23168
analytical robustness evaluation	Experimental evaluation of a box beam specifically	Corrosion detection and management of advanced airframe materials
(BTN-95-EIX95182619115) p 321 A95-76592 Orag function modeling for air traffic simulation	tailored for chordwise deformation {BTN-95-EIX95182619088} p 283 A95-75773	[AGARD-CP-565] p 302 N95-23496
[BTN-95-EIX95182619154] p 279 A95-76631	Review of aeronautical fatigue investigation in the	The corrosion and protection of advanced aluminium -
An investigation of helicopter dynamic coupling using an analytical model	Netherlands during the period March 1991-March 1993 [PB95-139184] p 285 N95-23161	lithium airframe alloys p 302 N95-23497 Non-destructive detection of corrosion for life
[NASA-CR-197420] p 285 N95-23217	Double pass retroreflection for corrosion detection in	management p 314 N95-23505
Inner loop flight control for the High-Speed Civil Transport p 293 N95-23314	aircraft structures p 323 N95-23503	New nondestructive techniques for the detection and quantification of corrosion in aircraft structures
AIRCRAFT NOISE	Non-destructive detection of corrosion for life management p 314 N95-23505	p 315 N95-23512
The use of cowl camber and taper to reduce rotor/stator interaction noise	Health and usage monitoring systems: Corrosion	AIRFRAMES An analytical and experimental investigation of the
(NASA-CR-195421) p 323 N95-22675	surveillance p 262 N95-23506	response of the curved, composite frame/skin
AIRCRAFT PARTS	New nondestructive techniques for the detection and quantification of corrosion in aircraft structures	specimens
Review of some results of the author's fatigue investigations with applications in engineering and material	p 315 N95-23512	[HTN-95-80857] p 283 A95-75099 Integrated design of hypersonic waveriders including
science	Organic coating technology for the protection of aircraft	inlets and tailfins
[TAE-698] p 316 N95-23662 AIRCRAFT PERFORMANCE	against corrosion p 303 N95-23513 Corrosion detection and monitoring of aircraft structures:	[BTN-95-EIX95212645692] p 271 A95-76744 Oklahoma City air logistics center (USAF) aging aircraft
An unmanned air vehicle concept with tipjet drive	An overview p 303 N95-23515	corrosion program p 262 N95-23519
[HTN-95-80858] p 283 A95-75100 Multiaxis pilot ratings for damaged aircraft	Experience of in-service corrosion on military aircraft	AIRLINE OPERATIONS  Development of aeronautical mobile satellite services
[BTN-95-EIX95182619128] p 269 A95-76605	p 303 N95-23516 US Navy operating experience with new aircraft	over the past thirty years
Drag function modeling for air traffic simulation [BTN-95-EIX95182619154] p 279 A95-76631	construction materials p 303 N95-23517	(BTN-95-EIX95152569458) p 305 A95-73498 Containing military autotest cost growth through the use
Application of Navier-Stokes aeroelastic methods to	Oklahoma City air logistics center (USAF) aging aircraft corrosion program p 262 N95-23519	of commercial standard equipment architectures
Improve fighter wing maneuver performance (BTN-95-EIX95182619218) p 284 A95-76644	AIRCRAFT WAKES	(BTN-95-EIX95172595295) p 287 A95-75717
Tracking of raindrops in flow over an airfoil	Unsteady ground effects on aerodynamic coefficients of finite wings with camber	Maintenance challenges and trends [BTN-95-EIX95182617808] p 261 A95-75753
[BTN-95-EIX95182619221] p 308 A95-76647	[BTN-95-EIX95182619233] p 271 A95-76659 AIRFIELD SURFACE MOVEMENTS	Maintenance programs
Guidance and control requirements for high-speed Rollout and Turnoff (ROTO)	Automation technology using Geographic Information	[BTN-95-EIX95182617809] p 261 A95-75754 Aircraft accident report, Runway overrun following
[NASA-CR-195026] p 292 N95-22674	System (GIS) p 324 N95-23284 AIRFOIL OSCILLATIONS	rejected takeoff. Continental airlines flight 795, McDonnell
Direct adaptive performance optimization of subsonic transports: A periodic perturbation technique	Computation of oscillating airfoil flows with one- and	Douglas MD-82, N18835, LaGuardia Airport, Flushing, NY, 2 March 1994
[NASA-TM-4676] p 284 N95-22829	two-equation turbulence models	[PB95-910401] p 277 N95-23609
Design of high performance multivariable control systems for supermaneuverable aircraft at high angle of	[BTN-95-EIX95152577588] p 263 A95-73494 AIRFOIL PROFILES	The airline quality report, 1994 [NIAR-94-11] p 277 N95-24012
attack	Forebody flow control on a full-scale F/A-18 aircraft	AIRPORTS
[NASA-CR-197661] p 293 N95-22908	[BTN-95-EIX95152582333] p 281 A95-73535 Effect of curvature in the numerical simulation of an	Evaluation of neutron techniques for illicit substance
AIRCRAFT POWER SUPPLIES  Motor drive technologies for the power-by-wire (PBW)	electrothermal de-icer pad	detection [DE95-002988] p 300 N95-22764
program: Options, trends and tradeoffs	[BTN-95-EIX95182619219] p 276 A95-76645 Control of flow separation in airfoil/wing design	Automation technology using Geographic Information
[NASA-TM-106885] p 295 N95-23671 AIRCRAFT PRODUCTION	applications p 274 N95-23294	System (GIS) p 324 N95-23284
Automatic riveting cell for commercial aircraft floor grid	AIRFOILS  Two-equation turbulence model for unsteady separated	AIRSPACE Oceanic operations: An authoritative guide to oceanic
assembly	flows around airfoils	operations
[BTN-95-EIX95182617807] p 261 A95-75752  AIRCRAFT RELIABILITY	[BTN-95-EIX95142553054] p 262 A95-73444 Laplace interaction law for the computation of viscous	[FAA-AFS-550] p 277 N95-24065  ALGORITHMS
Labs behind Boeing's new 777	airfoil flow in low- and high-speed aerodynamics	Efficient sensitivity analysis for rotary-wing
[BTN-95-EIX95142562403] p 280 A95-73437 Oklahoma City air logistics center (USAF) aging aircraft	[BTN-95-EIX95142553037] p 263 A95-73461 Aerodynamic shape optimization using preconditioned	aeromechanical problems [BTN-95-EIX95152577585] p 264 A95-73497
corrosion program p 262 N95-23519	conjugate gradient methods	Application of the multigrid solution technique to
AIRCRAFT SAFETY	(BTN-95-EIX95142553033) p 263 A95-73465 Eigenanalysis of unsteady flows about airfoils, cascades,	hypersonic entry vehicles
Maintenance programs [BTN-95-EIX95182617809] p 261 A95-75754	and wings	[BTN-95-EIX95152583254] p 306 A95-73555 Functional dependence of trajectory dispersion on initial
Additional improvements to the NASA Lewis ice	[BTN-95-EIX95152577597] p 305 A95-73486 Computation of oscillating airfoil flows with one- and	condition errors
accretion code LEWICE [NASA-TM-106849] p 309 N95-22669	two-equation turbulence models	[BTN-95-EIX95152583263] p 298 A95-73564 Optimization of contoured hypersonic scramjet inlets
Handling qualities of the High Speed Civil Transport	[BTN-95-EIX95152577588] p 263 A95-73494	with a least-squares parabolized Navier-Stokes
p 294 N95-23325	Flow visualization studies on sidewall effects in two-dimensional transonic airfuil testing	procedure [HTN-95-20976] p 261 A95-74042
Report of proceedings: Aviation Accident Investigation Symposium. Volume 2: Participant presentations	[BTN-95-EIX95152582313] p 264 A95-73516	Real-time estimation of atmospheric turbulence severity
[PB94-917007] p 277 N95-23598	Progress in high-lift aerodynamic calculations [BTN-95-EIX95152582315] p 264 A95-73518	from in-situ aircraft measurements
Aircraft fires, smoke toxicity, and survival: An overview [DOT/FAA/AM-95/8] p 277 N95-24024	Computation of the poststall behavior of a circulation	[BTN-95-EIX95182619231] p 319 A95-76657 Aerodynamic design optimization with sensitivity analysis
[DOT/FAA/AM-95/8] p 277 N95-24024 A multibody/finite element analysis approach for	controlled airfoil {BTN-95-EIX95152582320} p 264 A95-73523	and computational fluid dynamics
modeling of crash dynamic responses	Separation control on high-lift airfoils via micro-vortex	(NASA-CR-197419) p 274 N95-23218
[NIAR-94-3] p 277 N95-24050 Aviation Accident Investigation Symposium. Volume 1:	generators [BTN-95-EIX95152582326] p 265 A95-73529	On-line, adaptive state estimator for active noise control p 322 N95-23308
Industry recommendations and Safety Board responses	Study of an airfoil with a flap and spoiler	Empirical results on scheduling and dynamic
[PB94-917005] p 278 N95-24105	[BTN-95-EIX95152582327] p 265 A95-73530	backtracking p 299 N95-23761

ALTERNATING DIRECTION IMPLICIT METHODS
Convergence acceleration of implicit schemes in the presence of high aspect ratio grid cells
p 313 N95-23446
Assimilation of altimeter data in a quasi-geostrophic model of the Gulf Stream system: A dynamical perspective
Parspective
Geoid lineations of 1000 km wavelength over the central Pacific
[HTN-95-11304] p 319 A95-77009
Corrosion protection measures for CFC/metal joints of fuel integral tank structures of advanced military aircraft p 303 N95-23510
ALUMINUM ALLOYS  Test method and test results for environmental assessment of aircraft materials p 302 N95-23509  ALUMINUM-LITHIUM ALLOYS
The corrosion and protection of advanced aluminium - lithium airframe alloys p 302 N95-23497
ANGLE OF ATTACK  Aerodynamic characteristics of a canard-controlled missile at high angles of attack
[BTN-95-EIX95152583257] p 267 A95-73558
Improved version of the Naval Surface Warfare Center
aeroprediction code (AP93)   BTN-95-EIX951525832601 p 267 A95-73561
Transient structure of vortex breakdown on a delta wing
[BTN-95-EIX95182619073] p 268 A95-75758
Kinematics and aerodynamics of velocity-vector roll
[BTN-95-EIX95182619126] p 291 A95-76603 Review and development of base pressure and base
heating correlations in supersonic flow
[BTN-95-EIX95212645688] p 271 A95-76740
Numerical investigation of supersonic flows around a spiked blunt body
[BTN-95-EIX95212645690] p 271 A95-76742
Calculation of wing-alone aerodynamics to high angles
of attack [BTN-95-EIX95212645713] p 261 A95-76765
Wing pressure distributions from subsonic tests of a high-wing transport model in the Langley 14- by 22-Foot
Subsonic Wind Tunnel [NASA-TM-4583] p 272 N95-22802
Flight test of the X-29A at high angle of attack: Flight dynamics and controls
[NASA-TP-3537] p 284 N95-22806
An assessment of viscous effects in computational
simulation of benign and burst vortex flows on generic fighter wind-tunnel models using TEAM code
[NASA-CR-4650] p 273 N95-23185
Aerodynamic surface distension system for high angle of attack forebody vortex control
[NASA-CASE-ARC-11979-1] p 286 N95-23390
ANNUAL VARIATIONS
Possible effects of CO2 increase on the high-speed civil transport impact on ozone
[HTN-95-60779] p 317 A95-75976
ANTIAIRCRAFT MISSILES
Switched bias proportional navigation for homing guidance against highly maneuvering targets
[BTN-95-EIX95182619145] p 279 A95-76622
Preparation of course materials: Elementary
mathematics of powered flight p 324 N95-23320 APPROACH
Optimal lateral-escape maneuvers for microburst encounters during final approach
BTN-95-EIX95182619127  p 276 A95-76604 APPROXIMATION
Adaptive finite element method for turbulent flow near a propeller
[BTN-95-EIX95142553038] p 305 A95-73460 Application of the multigrid solution technique to
hypersonic entry vehicles
[BTN-95-EIX95152583254] p 306 A95-73555 Multiple site fatigue damage in fuselage skin splices:
Experimental simulation and theoretical prediction
[BTN-95-EIX95152584676] p 276 A95-73588 Application of a control-volume-based finite-element
formulation to the shock tube problem [BTN-95-EIX95182619099] p 295 A95-76584

intelligent |BTN-95-EIX95172595292|

p 287 A95-75720

ALTERNATING DIRECTION IMPLICIT METHODS	ARGON
Convergence acceleration of implicit schemes in the	Hypersonic convec
presence of high aspect ratio grid cells	cones in different ga
p 313 N95-23446	BTN-95-EIX9515258
ALTIMETERS	ARTIFICIAL INTELLIG
Assimilation of altimeter data in a quasi-geostrophic	New commercial o
model of the Gulf Stream system: A dynamical	intelligent
perspective	[BTN-95-EIX9517259
[NASA-CR-196313] p 320 N95-23766	Artificial intelligence
ALTIMETRY	[BTN-95-EIX951826
Geoid lineations of 1000 km wavelength over the central	ARTIFICIAL SATELLI
Pacific	Calculation of sate [AD-A285118]
[HTN-95-11304] p 319 A95-77009	ASCENT PROPULSIO
ALUMINUM	Fourth-generation
Corrosion protection measures for CFC/metal joints of	BTN-95-EIX9515258
fuel integral tank structures of advanced military aircraft	ASCENT TRAJECTOR
p 303 N95-23510	Dynamical instab
ALUMINUM ALLOYS	maneuver
Test method and test results for environmental	BTN-95-EIX9515258
assessment of aircraft materials p 302 N95-23509	ASPECT RATIO
ALUMINUM-LITHIUM ALLOYS	Calculation of wing
The corrosion and protection of advanced aluminium	of attack
lithium airframe alloys p 302 N95-23497	IBTN-95-EIX9521264
ANGLE OF ATTACK	ASSIMILATION
Aerodynamic characteristics of a canard-controlled	Assimilation of al
missile at high angles of attack	model of the Gu
[BTN-95-EIX95152583257] p 267 A95-73558	perspective
Improved version of the Naval Surface Warfare Center	[NASA-CR-196313]
aeroprediction code (AP93)	ATLANTIC OCEAN
[BTN-95-EIX95152583260] p 267 A95-73561	Oceanic operation
Transient structure of vortex breakdown on a delta	operations
wing	[FAA-AFS-550] ATMOSPHERIC CHEM
[BTN-95-EIX95182619073] p 268 A95-75758	Possible effects of
Kinematics and aerodynamics of velocity-vector roll	
[BTN-95-EIX95182619126] p 291 A95-76603	transport impact on ( 1HTN-95-60779)
Review and development of base pressure and base	Compendium of
heating correlations in supersonic flow	Tropospheric Experi
[BTN-95-EIX95212645688] p 271 A95-76740	West-A (PEM West-A
Numerical investigation of supersonic flows around a	[NASA-TM-109177]
spiked blunt body	ATMOSPHERIC COMP
[BTN-95-EIX95212645690] p 271 A95-76742	Possible effects of
Calculation of wing-alone aerodynamics to high angles	transport impact on o
of attack	[HTN-95-60779]
[BTN-95-EIX95212645713] p 261 A95-76765	Compendium of
Wing pressure distributions from subsonic tests of a	Tropospheric Expe
high-wing transport model in the Langley 14- by 22-Foot	West-A (PEM West-A
Subsonic Wind Tunnel	[NASA-TM-109177]
[NASA-TM-4583] p 272 N95-22802	ATMOSPHERIC EFFE
Flight test of the X-29A at high angle of attack: Flight	Test method and
dynamics and controls [NASA-TP-3537] p 284 N95-22806	assessment of aircra
·	ATMOSPHERIC ENTR Application of the
An assessment of viscous effects in computational	hypersonic entry veh
simulation of benign and burst vortex flows on generic fighter wind-tunnel models using TEAM code	BTN-95-EIX9515258
[NASA-CR-4650] p 273 N95-23185	ATMOSPHERIC MODE
Aerodynamic surface distension system for high angle	Hypersonic convec
of attack forebody vortex control	cones in different gas
[NASA-CASE-ARC-11979-1] p 286 N95-23390	[BTN-95-EIX9515256
ANNUAL VARIATIONS	Thundercloud ele
Possible effects of CO2 increase on the high-speed civil	ionosphere-Earth reg
transport impact on ozone	distribution
[HTN-95-60779] p 317 A95-75976	[HTN-95-41223]
ANTIAIRCRAFT MISSILES	Possible effects of
Switched bias proportional navigation for homing	
	transport impact on o
guidance against highly maneuvering targets	[HTN-95-60779]
guidance against highly maneuvering targets [BTN-95-EIX95182619145] p 279 A95-76622	[HTN-95-60779] Estimates of total (
guidance against highly maneuvering targets [BTN-95-EIX95182619145] p 279 A95-76622 APPLICATIONS OF MATHEMATICS	[HTN-95-60779] Estimates of total of lower stratosphere to
guidance against highly maneuvering targets [BTN-95-EIX95182619145] p 279 A95-76622 APPLICATIONS OF MATHEMATICS Preparation of course materials: Elementary	[HTN-95-60779] Estimates of total of lower stratosphere from during AASE 2
guidance against highly maneuvering targets [BTN-95-EIX95182619145] p 279 APPLICATIONS OF MATHEMATICS Preparation of course materials: Elementary mathematics of powered flight p 324 N95-23320	[HTN-95-60779] Estimates of total of lower stratosphere to during AASE 2 [HTN-95-A0861]
guidance against highly maneuvering targets [BTN-95-EIX95182619145] p 279 A95-76622  APPLICATIONS OF MATHEMATICS Preparation of course materials: Elementary mathematics of powered flight p 324 N95-23320  APPROACH	[HTN-95-60779] Estimates of total of lower stratosphere from the during AASE 2 [HTN-95-A0861] Sensitivity of two-
guidance against highly maneuvering largets [BTN-95-EIX95182619145] p 279 A95-76622 APPLICATIONS OF MATHEMATICS Preparation of course materials: Elementary mathematics of powered flight p 324 N95-23320 APPROACH Optimal lateral-escape maneuvers for microburst	[HTN-95-60779] Estimates of total of lower stratosphere from during AASE 2 [HTN-95-A0861] Sensitivity of two-ozone response to significant strategies.
guidance against highly maneuvering largets [BTN-95-EIX95182619145] p 279  APPLICATIONS OF MATHEMATICS Preparation of course materials: Elementary mathematics of powered flight p 324  APPROACH Optimal lateral-escape maneuvers for microburst encounters during final approach	HTN-95-60779] Estimates of total clower stratosphere to during AASE 2 HTN-95-A0861] Sensitivity of two-ozone response to st HTN-95-A0863]
guidance against highly maneuvering largets [BTN-95-EIX95182619145] p 279 A95-76622  APPLICATIONS OF MATHEMATICS Preparation of course materials: Elementary mathematics of powered flight p 324 N95-23320  APPROACH Optimal lateral-escape maneuvers for microburst encounters during final approach [BTN-95-EIX95182619127] p 276 A95-76604	[HTN-95-60779] Estimates of total clower stratosphere frequency of the during AASE 2 [HTN-95-A0861] Sensitivity of two-ozone response to sight [HTN-95-A0863] Diurnal variation
guidance against highly maneuvering targets   BTN-95-EIX95182619145  p 279 A95-76622 APPLICATIONS OF MATHEMATICS  Preparation of course materials: Elementary mathematics of powered flight p 324 N95-23320 APPROACH  Optimal lateral-escape maneuvers for microburst encounters during final approach   BTN-95-EIX95182619127   p 276 A95-76604 APPROXIMATION	[HTN-95-60779] Estimates of total lower stratosphere frequency of two-ozone response to st [HTN-95-A0863] Diurnal variation surrounding area
guidance against highly maneuvering targets   BTN-95-EIX95182619145  p 279 A95-76622 APPLICATIONS OF MATHEMATICS  Preparation of course materials: Elementary mathematics of powered flight p 324 N95-23320 APPROACH  Optimal lateral-escape maneuvers for microburst encounters during final approach   BTN-95-EIX95182619127   p 276 A95-76604 APPROXIMATION  Adaptive finite element method for turbulent flow near	[HTN-95-60779] Estimates of total oliver stratosphere for during AASE 2 [HTN-95-A0861] Sensitivity of two-ozone response to st [HTN-95-A0863] Diurnal variation surrounding area [HTN-95-91363]
guidance against highly maneuvering largets [BTN-95-EIX95182619145] p 279  APPLICATIONS OF MATHEMATICS Preparation of course materials: Elementary mathematics of powered flight p 324  APPROACH Optimal lateral-escape maneuvers for microburst encounters during final approach [BTN-95-EIX95182619127] p 276  APPROXIMATION Adaptive finite element method for turbulent flow near a propeller	[HTN-95-60779] Estimates of total clower stratosphere to during AASE 2 [HTN-95-A0861] Sensitivity of two-ozone response to si [HTN-95-A0863] Diurnal variation surrounding area [HTN-95-91363] Assimilation of alti
guidance against highly maneuvering targets   BTN-95-EIX95182619145  p 279 A95-76622 APPLICATIONS OF MATHEMATICS  Preparation of course materials: Elementary mathematics of powered flight p 324 N95-23320 APPROACH  Optimal lateral-escape maneuvers for microburst encounters during final approach   BTN-95-EIX95182619127   p 276 A95-76604 APPROXIMATION  Adaptive finite element method for turbulent flow near a propeller   BTN-95-EIX95142553038   p 305 A95-73460	[HTN-95-60779] Estimates of total clower stratosphere for during AASE 2 [HTN-95-A0861] Sensitivity of two-ozone response to si [HTN-95-A0863] Diurnal variation surrounding area [HTN-95-91363] Assimilation of altimodel of the Gu
guidance against highly maneuvering targets   BTN-95-EIX95182619145  p 279 A95-76622 APPLICATIONS OF MATHEMATICS  Preparation of course materials: Elementary mathematics of powered flight p 324 N95-23320 APPROACH  Optimal lateral-escape maneuvers for microburst encounters during final approach   BTN-95-EIX95182619127  p 276 A95-76604 APPROXIMATION  Adaptive finite element method for turbulent flow near a propeller   BTN-95-EIX95142553038  p 305 A95-73460 Application of the multigrid solution technique to	[HTN-95-60779] Estimates of total olower stratosphere for during AASE 2 [HTN-95-A0861] Sensitivity of two-ozone response to st [HTN-95-A0863] Diurnal variation surrounding area [HTN-95-91363] Assimilation of altimodel of the Guperspective
guidance against highly maneuvering targets   BTN-95-EIX95182619145  p 279 A95-76622 APPLICATIONS OF MATHEMATICS   Preparation of course materials: Elementary mathematics of powered flight p 324 N95-23320 APPROACH   Optimal lateral-escape maneuvers for microburst encounters during final approach   BTN-95-EIX95182619127   p 276 A95-76604 APPROXIMATION   Approximation   Approximation   Propeller   BTN-95-EIX95142553038   p 305 A95-73460   Application of the multigrid solution technique to hypersonic entry vehicles	[HTN-95-60779] Estimates of total clower stratosphere frequency of the during AASE 2 [HTN-95-A0861] Sensitivity of two-ozone response to st [HTN-95-A0863] Diurnal variation surrounding area [HTN-95-91363] Assimilation of altimodel of the Guperspective [NASA-CR-196313]
guidance against highly maneuvering targets   BTN-95-EIX95182619145  p 279 A95-76622 APPLICATIONS OF MATHEMATICS  Preparation of course materials: Elementary mathematics of powered flight p 324 N95-23320 APPROACH  Optimal lateral-escape maneuvers for microburst encounters during final approach   BTN-95-EIX95182619127   p 276 A95-76604 APPROXIMATION  Adaptive finite element method for turbulent flow near a propeller   BTN-95-EIX95142553038   p 305 A95-73460 Application of the multigrid solution technique to hypersonic entry vehicles   BTN-95-EIX95152583254   p 306 A95-73555	[HTN-95-60779] Estimates of total clower stratosphere to during AASE 2 [HTN-95-A0861] Sensitivity of two-ozone response to si [HTN-95-A0863] Diurnal variation surrounding area [HTN-95-91363] Assimilation of altimodel of the Gu perspective [NASA-CR-196313] ATMOSPHERIC TURB
guidance against highly maneuvering targets   BTN-95-EIX95182619145  p 279 A95-76622 APPLICATIONS OF MATHEMATICS   Preparation of course materials: Elementary mathematics of powered flight p 324 N95-23320 APPROACH   Optimal lateral-escape maneuvers for microburst encounters during final approach   BTN-95-EIX95182619127   p 276 A95-76604 APPROXIMATION   Approximation   Approximation   Propeller   BTN-95-EIX95142553038   p 305 A95-73460   Application of the multigrid solution technique to hypersonic entry vehicles	[HTN-95-60779] Estimates of total clower stratosphere for during AASE 2 [HTN-95-A0861] Sensitivity of two-ozone response to st [HTN-95-A0863] Diurnal variation surrounding area [HTN-95-91363] Assimilation of altimodel of the Gu perspective [NASA-CR-196313] ATMOSPHERIC TURB Response of a strategictory and the surrounding area [HTN-95-91363]
guidance against highly maneuvering targets   BTN-95-EIX95182619145  p 279 A95-76622 APPLICATIONS OF MATHEMATICS  Preparation of course materials: Elementary mathematics of powered flight p 324 N95-23320 APPROACH  Optimal lateral-escape maneuvers for microburst encounters during final approach   BTN-95-EIX95182619127  p 276 A95-76604 APPROXIMATION  Adaptive finite element method for turbulent flow near a propeller   BTN-95-EIX95142553038  p 305 A95-73460 Application of the multigrid solution technique to hypersonic entry vehicles   BTN-95-EIX95152583254   p 306 A95-73555   BTN-95-EIX95152583254   p 306 A95-73555	[HTN-95-60779] Estimates of total clower stratosphere frequency of the during AASE 2 [HTN-95-A0861] Sensitivity of two-ozone response to st [HTN-95-A0863] Diurnal variation surrounding area [HTN-95-91363] Assimilation of alt model of the Guperspective [NASA-CR-196313] ATMOSPHERIC TURB Response of a sturbulence. Part 2: Estimates of the control of th
guidance against highly maneuvering targets   BTN-95-EIX95182619145  p 279 A95-76622 APPLICATIONS OF MATHEMATICS  Preparation of course materials: Elementary mathematics of powered flight p 324 N95-23320 APPROACH  Optimal lateral-escape maneuvers for microburst encounters during final approach   BTN-95-EIX95182619127  p 276 A95-76604 APPROXIMATION  Adaptive finite element method for turbulent flow near a propeller   BTN-95-EIX95142553038  p 305 A95-73460 Application of the multigrid solution technique to hypersonic entry vehicles   BTN-95-EIX95152583254  p 306 A95-73555 Multiple site fatigue damage in fuselage skin splices: Experimental simulation and theoretical prediction	HTN-95-60779   Estimates of total clower stratosphere treduring AASE 2   HTN-95-A0861   Sensitivity of two-ozone response to st   HTN-95-A0863   Diurnal variation surrounding area   HTN-95-91363   Assimilation of altimodel of the Guperspective   NASA-CR-196313   ATMOSPHERIC TURB Response of a turbulence, Part 2:   BTN-95-EIX9518261
guidance against highly maneuvering targets   BTN-95-EIX95182619145  p 279 A95-76622 APPLICATIONS OF MATHEMATICS  Preparation of course materials: Elementary mathematics of powered flight p 324 N95-23320 APPROACH  Optimal lateral-escape maneuvers for microburst encounters during final approach   BTN-95-EIX95182619127  p 276 A95-76604 APPROXIMATION  Adaptive finite element method for turbulent flow near a propeller   BTN-95-EIX95142553038  p 305 A95-73460 Application of the multigrid solution technique to hypersonic entry vehicles   BTN-95-EIX95152583254  p 306 A95-73555 Multiple site fatigue damage in fuselage skin splices: Experimental simulation and theoretical prediction   BTN-95-EIX95152584676  p 276 A95-73588 Application of a control-volume-based finite-element formulation to the shock tube problem	[HTN-95-60779] Estimates of total lower stratosphere treduring AASE 2 [HTN-95-A0861] Sensitivity of two-ozone response to si [HTN-95-A0863] Diurnal variation surrounding area [HTN-95-91363] Assimilation of altimodel of the Guperspective [NASA-CR-196313] ATMOSPHERIC TURB Response of a sturbulence. Part 2: E. [BTN-95-EIX9518261
guidance against highly maneuvering targets   BTN-95-EIX95182619145  p 279 A95-76622 APPLICATIONS OF MATHEMATICS  Preparation of course materials: Elementary mathematics of powered flight p 324 N95-23320 APPROACH  Optimal lateral-escape maneuvers for microburst encounters during final approach   BTN-95-EIX95182619127  p 276 A95-76604 APPROXIMATION  Adaptive finite element method for turbulent flow near a propeller   BTN-95-EIX95142553038  p 305 A95-73460 Application of the multigrid solution technique to hypersonic entry vehicles   BTN-95-EIX95152583254  p 306 A95-73555 Multiple site fatigue damage in fuselage skin splices: Experimental simulation and theoretical prediction   BTN-95-EIX95152584676  p 276 A95-73588 Application of a control-volume-based finite-element formulation to the shock tube problem   BTN-95-EIX95182619099  p 295 A95-76584	[HTN-95-60779] Estimates of total clower stratosphere for during AASE 2 [HTN-95-A0861] Sensitivity of two-ozone response to st [HTN-95-A0863] Diurnal variation surrounding area [HTN-95-91363] Assimilation of alt model of the Gu perspective [NASA-CR-196313] ATMOSPHERIC TURB Response of a sturbulence. Part 2: E. [BTN-95-E1X9518261] Real-time estimatic from in-situ aircraft m
guidance against highly maneuvering targets   BTN-95-EIX95182619145  p 279 A95-76622 APPLICATIONS OF MATHEMATICS  Preparation of course materials: Elementary mathematics of powered flight p 324 N95-23320 APPROACH  Optimal lateral-escape maneuvers for microburst encounters during final approach   BTN-95-EIX95182619127  p 276 A95-76604 APPROXIMATION  Adaptive finite element method for turbulent flow near a propeller   BTN-95-EIX95142553038  p 305 A95-73460 Application of the multigrid solution technique to hypersonic entry vehicles   BTN-95-EIX95152583254  p 306 A95-73555 Multiple site fatigue damage in fuselage skin splices: Experimental simulation and theoretical prediction   BTN-95-EIX951525832564 p 276 A95-73588 Application of a control-volume-based finite-element formulation to the shock tube problem   BTN-95-EIX951626180999   p 295 A95-76584 ARAMID FIBER COMPOSITES	[HTN-95-60779] Estimates of total clower stratosphere frequency of two-ozone response to state [HTN-95-A0861] Sensitivity of two-ozone response to state [HTN-95-A0863] Diurnal variation surrounding area [HTN-95-91363] Assimilation of altimodel of the Guperspective [NASA-CR-196313] ATMOSPHERIC TURB Response of a sturbulence. Part 2: E: [BTN-95-EIX9518261] Real-time estimatio from in-situ aircraft m [BTN-95-EIX9518261]
guidance against highly maneuvering targets   BTN-95-EIX95182619145  p 279 A95-76622 APPLICATIONS OF MATHEMATICS  Preparation of course materials: Elementary mathematics of powered flight p 324 N95-23320 APPROACH  Optimal lateral-escape maneuvers for microburst encounters during final approach   BTN-95-EIX95182619127  p 276 A95-76604 APPROXIMATION  Adaptive finite element method for turbulent flow near a propeller   BTN-95-EIX9514253038  p 305 A95-73460 Application of the multigrid solution technique to hypersonic entry vehicles   BTN-95-EIX95152583254  p 306 A95-73555 Multiple site fatigue damage in fuselage skin splices: Experimental simulation and theoretical prediction   BTN-95-EIX95152584676  p 276 A95-73588 Application of a control-volume-based finite-element formulation to the shock tube problem   BTN-95-EIX95182619099  p 295 A95-76584 ARAMID FIBER COMPOSITES  MIL-HDBK-5 design allowables for fibre/metal	HTN-95-60779   Estimates of total clower stratosphere frequiring AASE 2   HTN-95-A0861   Sensitivity of two-ozone response to st   HTN-95-A0863   Diurnal variation surrounding area   HTN-95-91363   Assimilation of altimodel of the Gu perspective   NASA-CR-196313   ATMOSPHERIC TURB Response of a st turbulence. Part 2: E   BTN-95-EIX9518261   Real-time estimatic from in-situ aircraft in   BTN-95-EIX9518261
guidance against highly maneuvering targets [BTN-95-EIX95182619145] p 279 A95-76622 APPLICATIONS OF MATHEMATICS  Preparation of course materials: Elementary mathematics of powered flight p 324 N95-23320 APPROACH  Optimal lateral-escape maneuvers for microburst encounters during final approach [BTN-95-EIX95182619127] p 276 A95-76604 APPROXIMATION  Adaptive finite element method for turbulent flow near a propeller [BTN-95-EIX95142553038] p 305 A95-73460 Application of the multigrid solution technique to hypersonic entry vehicles [BTN-95-EIX95152583254] p 306 A95-73555 Multiple site fatigue damage in fuselage skin splices: Experimental simulation and theoretical prediction [BTN-95-EIX95152584676] p 276 A95-73588 Application of a control-volume-based finite-element formulation to the shock tube problem [BTN-95-EIX95182619099] p 295 A95-76584 ARAMID FIBER COMPOSITES MIL-HDBK-5 design allowables for fibre/metal saminates: ARALL 2 and ARALL 3	[HTN-95-60779] Estimates of total clower stratosphere for during AASE 2 [HTN-95-A0861] Sensitivity of two-ozone response to st [HTN-95-0863] Diurnal variation surrounding area [HTN-95-91363] Assimilation of alt model of the Gu perspective [NASA-CR-196313] ATMOSPHERIC TURB Response of a sturbulence. Part 2: E: [BTN-95-EIX9518261 Real-time estimatic from in-situ aircraft m [BTN-95-EIX9518261 ATTITUDE (INCLINAT Dynamic response response of serior of the sturbulence of a sturbulenc
guidance against highly maneuvering targets   BTN-95-EIX95182619145  p 279 A95-76622 APPLICATIONS OF MATHEMATICS  Preparation of course materials: Elementary mathematics of powered flight p 324 N95-23320 APPROACH  Optimal lateral-escape maneuvers for microburst encounters during final approach   BTN-95-EIX95182619127  p 276 A95-76604 APPROXIMATION  Adaptive finite element method for turbulent flow near a propeller   BTN-95-EIX9518263038  p 305 A95-73460 Application of the multigrid solution technique to hypersonic entry vehicles   BTN-95-EIX95152583254  p 306 A95-73555 Multiple site fatigue damage in fuselage skin splices: Experimental simulation and theoretical prediction   BTN-95-EIX951525832564  p 376 A95-73588 Application of a control-volume-based finite-element formulation to the shock tube problem   BTN-95-EIX95182619099  p 295 A95-76584 ARAMID FIBER COMPOSITES   MIL-HDBK-5 design allowables for fibre/metal laminates: ARALL 2 and ARALL 3   BTN-94-EIX94371346933  p 300 A95-73345	[HTN-95-60779] Estimates of total clower stratosphere from the during AASE 2 [HTN-95-A0861] Sensitivity of two-ozone response to si [HTN-95-A0863] Diurnal variation surrounding area [HTN-95-91363] Assimilation of alt model of the Guperspective [NASA-CR-196313] ATMOSPHERIC TURB Response of a sturbulence. Part 2: E. [BTN-95-EIX951826: Real-time estimatio from in-situ aircraft m [BTN-95-EIX951826: ATTITUDE (INCLINAT Dynamic respons wind-tunnel model at the diagram of the control of th
guidance against highly maneuvering targets [BTN-95-EIX95182619145] p 279 A95-76622 APPLICATIONS OF MATHEMATICS  Preparation of course materials: Elementary mathematics of powered flight p 324 N95-23320 APPROACH  Optimal lateral-escape maneuvers for microburst encounters during final approach [BTN-95-EIX95182619127] p 276 A95-76604 APPROXIMATION  Adaptive finite element method for turbulent flow near a propeller [BTN-95-EIX95142553038] p 305 A95-73460 Application of the multigrid solution technique to hypersonic entry vehicles [BTN-95-EIX95152583254] p 306 A95-73555 Multiple site fatigue damage in fuselage skin splices: Experimental simulation and theoretical prediction [BTN-95-EIX95152584676] p 276 A95-73588 Application of a control-volume-based finite-element formulation to the shock tube problem [BTN-95-EIX95182619099] p 295 A95-76584 ARAMID FIBER COMPOSITES MIL-HDBK-5 design allowables for fibre/metal saminates: ARALL 2 and ARALL 3	[HTN-95-60779] Estimates of total clower stratosphere for during AASE 2 [HTN-95-A0861] Sensitivity of two-ozone response to st [HTN-95-0863] Diurnal variation surrounding area [HTN-95-91363] Assimilation of alt model of the Gu perspective [NASA-CR-196313] ATMOSPHERIC TURB Response of a sturbulence. Part 2: E: [BTN-95-EIX9518261 Real-time estimatic from in-situ aircraft m [BTN-95-EIX9518261 ATTITUDE (INCLINAT Dynamic response response of serior of the sturbulence of a sturbulenc

	77.0.1
ARGON	ATTITUDE INDICATORS
Hypersonic convective heat transfer over 140-deg blunt	Dynamic response tests of inertial and optical
cones in different gases	wind-tunnel model attitude measurement devices
[BTN-95-EIX95152583253] ρ 306 A95-73554	[NASA-TM-109182] p 296 N95-23011
ARTIFICIAL INTELLIGENCE  New commercial off-the-shell testers are automatic and	AUSTRALIA AIRSAR deployment in Australia, September 1993:
intelligent	Management and objectives p 321 N95-23948
[BTN-95-EIX95172595292] p 287 A95-75720	AUTOMATED PILOT ADVISORY SYSTEM
Artificial intelligence for turboprop engine maintenance [BTN-95-EIX95182617812] p 288 A95-75757	Differential GPS and system integration of the Low
ARTIFICIAL SATELLITES	Visibility Landing and Surface Operations (LVLASO) demonstration p 280 N95-23318
Calculation of satellite drag coefficients	AUTOMATIC CONTROL
[AD-A285118] p 300 N95-23781	Automatic riveting cell for commercial aircraft floor grid
ASCENT PROPULSION SYSTEMS Fourth-generation Mars vehicle concepts	assembly [BTN-95-EIX95182617807] p 261 A95-75752
[BTN-95-EIX95152583267] p 298 A95-73568	Cypher moves toward autonomous flight
ASCENT TRAJECTORIES	[HTN-95-41394] p 283 A95-76390
Dynamical instability of the aerogravity assist	Automatic guidance and control for helicopter obstacle
maneuver [BTN-95-EIX95152583282] p 298 A95-73583	avoidance  BTN-95-EIX95182619130  p 291 A95-76607
ASPECT RATIO	Nonlinear system guidance in the presence of
Calculation of wing-alone aerodynamics to high angles	transmission zero dynamics
of attack  BTN-95-EIX95212645713  p 261 A95-76765	[NASA-TM-4661] p 309 N95-22804
BTN-95-EIX95212645713  p 261 A95-76765 ASSIMILATION	Performance of the 0.3-meter transonic cryogenic tunnel with air, nitrogen, and sulfur hexafluoride media under
Assimilation of altimeter data in a quasi-geostrophic	closed loop automatic control
model of the Gulf Stream system: A dynamical	[NASA-CR-195052] p 310 N95-23257
perspective  NASA-CR-196313  p 320 N95-23766	AUTOMATIC FLIGHT CONTROL
ATLANTIC OCEAN	Automatic formation flight control   BTN-95-EIX95182619153   p 292 A95-76630
Oceanic operations: An authoritative guide to oceanic	AUTOMATIC PILOTS
operations	Automatic guidance and control for helicopter obstacle
[FAA-AFS-550] p 277 N95-24065 ATMOSPHERIC CHEMISTRY	avoidance [BTN-95-EIX95182619130] p 291 A95-76607
Possible effects of CO2 increase on the high-speed civil	Automatic formation flight control
transport impact on ozone	[BTN-95-EIX95182619153] p 292 A95-76630
[HTN-95-60779] p 317 A95-75976	AUTOMATIC TEST EQUIPMENT
Compendium of NASA data base for the Global Tropospheric Experiment's Pacific Exploratory Mission	CASS: Design for supportability [BTN-95-EIX95172595296] p 287 A95-75716
West-A (PEM West-A)	Containing military autotest cost growth through the use
[NASA-TM-109177] p 320 N95-23009	of commercial standard equipment architectures
ATMOSPHERIC COMPOSITION  Possible effects of CO2 increase on the high-speed civil	[BTN-95-EIX95172595295] p 287 A95-75717
transport impact on ozone	ATE enabling technologies [BTN-95-EIX95172595294] p 287 A95-75718
[HTN-95-60779] p 317 A95-75976	New commercial off-the-shelf testers are automatic and
Compendium of NASA data base for the Global	intelligent
Tropospheric Experiment's Pacific Exploratory Mission West-A (PEM West-A)	[BTN-95-EIX95172595292] p 287 A95-75720 AUTOMATION
[NASA-TM-109177] p 320 N95-23009	New commercial off-the-shelf testers are automatic and
ATMOSPHERIC EFFECTS	intelligent
Test method and test results for environmental assessment of aircraft materials p 302 N95-23509	[BTN-95-EIX95172595292] p 287 A95-75720 The role of flight progress strips in en route air traffic
ATMOSPHERIC ENTRY	control: A time-series analysis
Application of the multigrid solution technique to	[DOT/FAA/AM-95/4] p 280 N95-23565
hypersonic entry vehicles [BTN-95-EIX95152583254] p 306 A95-73555	AUTONOMOUS NAVIGATION
ATMOSPHERIC MODELS	Cypher moves toward autonomous flight [HTN-95-41394] p 283 A95-76390
Hypersonic convective heat transfer over 140-deg blunt	AUXILIARY POWER SOURCES
cones in different gases [BTN-95-EIX95152583253] p 306 A95-73554	Motor drive technologies for the power-by-wire (PBW)
[BTN-95-EIX95152583253] p 306 A95-73554 Thundercloud electric field modeling for the	program: Options, trends and tradeoffs [NASA-TM-106885] p 295 N95-23671
ionosphere-Earth region. 1: Dependence on cloud charge	AVIONICS
distribution	Labs behind Boeing's new 777
[HTN-95-41223] p 317 A95-75035 Possible effects of CO2 increase on the high-speed civil	[BTN-95-EIX95142562403] p 280 A95-73437 CASS: Design for supportability
transport impact on ozone	[BTN-95-EIX95172595296] p 287 A95-75716
[HTN-95-60779] p 317 A95-75976	Containing military autotest cost growth through the use
Estimates of total organic and inorganic chlorine in the	of commercial standard equipment architectures
lower stratosphere from in situ and flask measurements during AASE 2	[BTN-95-EIX95172595295] p 287 A95-75717 ATE enabling technologies
[HTN-95-A0861] p 317 A95-76265	[BTN-95-EIX95172595294] p 287 A95-75718
Sensitivity of two-dimensional model predictions of	New commercial off-the-shelf testers are automatic and
ozone response to stratospheric aircraft: An update	intelligent   BTN-95-EIX95172595292   p 287 A95-75720
[HTN-95-A0863] p 318 A95-76267 Diurnal variation of lee vortices in Taiwan and the	Overview of AlliedSignal's avionics development in the
surrounding area	CIS
[HTN-95-91363] p 318 A95-76394	[BTN-95-EIX95212641069] p 287 A95-76734
Assimilation of altimeter data in a quasi-geostrophic	Design of wide angle head up displays for synthetic vision
model of the Gulf Stream system: A dynamical	[BTN-95-EIX95212641070] p 287 A95-76735
perspective [NASA-CR-196313] p 320 N95-23766	AXIAL LOADS
ATMOSPHERIC TURBULENCE	Validation of an effective flat cruciform-shaped specimen to study CFRP composite laminates under biaxial
Response of a nonrotating rotor blade to lateral	loading
turbulence. Part 2: Experiment [BTN-95-EIX95182619229] p 284 A95-76655	[BTN-95-EIX95152584677] p 282 A95-73589
[BTN-95-EIX95182619229] p 284 A95-76655 Real-time estimation of atmospheric turbulence severity	AXISYMMETRIC BODIES
from in-situ aircraft measurements	Supersonic near-wake afterbody boattailing effects on axisymmetric bodies
[BTN-95-EIX95182619231] p 319 A95-76657	[BTN-95-EIX95182617465] p 268 A95-75736
ATTITUDE (INCLINATION)	AXISYMMETRIC FLOW
Dynamic response tests of inertial and optical wind-tunnel model attitude measurement devices	Supersonic axisymmetric conical flow solutions for different ratios of specific heats
[NASA-TM-109182] p 296 N95-23011	[BTN-95-EIX95152583283] p 306 A95-73584
ATTITUDE CONTROL	Supersonic jet noise reductions predicted with increased

p 299 N95-23532

jet spreading rate (NASA-TM-106872)

Moving mass trim control for aerospace vehicles [DE95-002602] p 299 N95-2

p 323 N95-23178

Active control of panel vibrations induced by a boundary TIGER: A user-friendly interactive grid generation system Pneumatic concept for tip-stall control of cranked-arrow for complicated turbomachinery and axis-symmetric layer flow p 273 N95-23182 INASA-CR-197867 I [BTN-95-EIX95152582335] p 281 A95-73537 configurations p 322 N95-23419 Validation of a Computational Fluid Dynamics (CFD) BOUNDARY LAYER SEPARATION **BLUFF BODIES** code for supersonic axisymmetric base flow Computation of the poststall behavior of a circulation Grid refinement test of time-periodic flows over bluff p 315 N95-23652 controlled airfoil p 264 A95-73523 IBTN-95-EIX951525823201 [BTN-94-EIX94401378822] p 307 A95-76491 Experimental investigation of the flowfield about an **BLUNT BODIES** В upswept afterbody Shock tunnel measurements of hypervelocity blunted cone drag [BTN-95-EIX95152582321] p 265 A95-73524 **BACKWASH** Separation control on high-lift airfoils via micro-vortex IBTN-95-EIX951525776061 p 305 A95-73477 Sidewash on the vertical tail in subsonic and supersonic Zonally decoupled direct simulation Monte Carlo nenerators flows BTN-95-EIX95152582326 | p 265 A95-73529 solutions of hypersonic blunt-body wake flows |BTN-95-EIX95152582316| p 264 A95-73519 Study of an airfoil with a flap and spoiler IBTN-95-EIX951525823271 p 26: p 268 A95-75729 IBTN-95-EIX951826174581 p 265 A95-73530 BAFFLES Numerical investigation of supersonic flows around a Coupled FEM-BEM approach for mean flow effects on Computational study of plume-induced separation on a spiked blunt body vibro-acoustic behavior of planar structures [BTN-95-EIX95212645690] typersonic powered model p 271 A95-76742 |BTN-95-EIX95152577587| p 263 A95-73495 **BO-105 HELICOPTER** [BTN-95-EIX95152582346] p 266 A95-73548 **BALLISTIC TRAJECTORIES** Scaling of incipient separation in supersonic/transonic Analysis of a higher harmonic control test to reduce blade vortex interaction noise Analytical solution and parameter estimation of projectile peed laminar flows dynamics [BTN-95-EIX95212645695] |BTN-95-EIX95182619104| p 269 A95-76589 BTN-95-EIX95152582330 | p 265 A95-73532 p 272 A95-76747 Aerodynamics of a finite wing with simulated ice **BODIES OF REVOLUTION** BALLISTIC VEHICLES p 270 A95-76653 BTN-95-EIX95182619227 | CFD optimization of a theoretical minimum-drag body Moving mass trim control for aerospace vehicles [DE95-002602] p 299 N95p 308 A95-76660 Control of flow separation in airfoil/wing design BTN-95-EIX951826192341 p 299 N95-23532 p 274 N95-23294 applications **BODY-WING CONFIGURATIONS** BÁLLISTICS BOUNDARY LAYER STABILITY Improved version of the Naval Surface Warfare Center Analytical solution and parameter estimation of projectile eroprediction code (AP93) Supersonic laminar flow control research dynamics [NASA-CR-197938] p 275 N95-23669 IBTN-95-EIX951525832601 p 267 A95-73561 IBTN-95-EIX952126456951 p 272 A95-76747 BOUNDARY LAYER TRANSITION Wing vertical position effects on wing-body carryover **BALLOON FLIGHT** Hypersonic rarefied flow past spheres including wake for noncircular missiles Polar Patrol Balloon structure IBTN-95-EIX951826174621 p 268 A95-75733 [BTN-95-EIX95152582318] p 316 A95-73521 |BTN-95-EIX95152583250| p 305 A95-73551 **BOEING AIRCRAFT** BANDWIDTH Scaling of incipient separation in supersonic/transonic H-76B fantail demonstrater composite fan blade Identification of higher order helicopter dynamics using speed laminar flows fabrication linear modeling methods p 269 A95-76589 [HTN-95-80856] p 283 A95-75098 |BTN-95-EIX95182619104| 1HTN-95-808511 p 290 A95-75093 Crossflow instability control on a swept-wing: Preliminary tudies p 274 N95-23283 **BOEING 737 AIRCRAFT** Investigation of the effects of bandwidth and time delay Differential GPS and system integration of the Low on helicopter roll-axis handling qualities High-lift flow-physics flight experiments on a subsonic civil transport aircraft (B737-100) p 275 N95-23333 Visibility Landing and Surface Operations (LVLASO) p 290 A95-75095 [HTN-95-80853] p 280 N95-23318 demonstration **BARIUM OXIDES BOEING 777 AIRCRAFT** Supersonic laminar flow control research Phonon characteristics of high (T sub c) superconductors Labs behind Boeing's new 777 INASA-CR-1979381 p 275 N95-23669 from neutron Doppler broadening measurements BOUNDARY LAYERS [BTN-95-EIX95142562403] p 280 A95-73437 [DE95-003703] p 324 N95-24076 Laplace interaction law for the computation of viscous Flight-deck displays on the Boeing 777 BASE FLOW airfoil flow in low- and high-speed aerodynamics [BTN-95-EIX95142553037] p 263 A9 [BTN-95-EIX95142562402] p 286 A95-73438 Base drag prediction on missile configurations p 263 A95-73461 BOMBS (ORDNANCE) p 266 A95-73557 |BTN-95-EIX95152583256| Simulating heat addition via mass addition in constant Aerodynamic characteristics of external store Validation of a Computational Fluid Dynamics (CFD) configurations at low speeds [BTN-95-EIX95182619230] area compressible flows code for supersonic axisymmetric base flow p 307 A95-76585 [BTN-95-EIX95182619100] p 271 A95-76656 p 315 N95-23652 BOOSTER ROCKET ENGINES Scaling of incipient separation in supersonic/transonic **BASE HEATING** Aerodynamic design of pegasus: Concept to flight with computational fluid dynamics speed laminar flows Review and development of base pressure and base [BTN-95-EIX95182619104] p 269 A95-76589 heating correlations in supersonic flow [BTN-95-EIX95182617463] p 298 A95-75734 Optimized design of a hypersonic nozzle |BTN-95-EIX95212645688| p 271 A95-76740 p 297 N95-23304 Some aspects of the aerodynamics of separating **BASE PRESSURE** BOX BEAMS strap-ons Review and development of base pressure and base IBTN-95-EIX95182617464 I Experimental evaluation of a box beam specifically p 298 A95-75735 heating correlations in supersonic flow ailored for chordwise deformation **BOUNDARY CONDITIONS** |BTN-95-EIX95212645688| p 271 A95-76740 Determination of wall boundary conditions [BTN-95-EIX95182619088] p 283 A95-75773 BEACONS Flutter analysis of composite box beams high-speed-ratio direct simulation Monte Carlo Cueing light configuration for aircraft navigation p 294 N95-23392 [NASA-CR-197931] calculations NASA-CASE-ARC-11982-11 p 280 N95-23393 [BTN-95-EIX95182617457] BUFFETING p 267 A95-75728 BEARINGLESS ROTORS Preliminary identification of buffet problems in high speed Observations on using experimental data as boundary p 294 N95-23319 Dynamic analysis of bearingless tail rotor blades based onditions for computations civil transport on nonlinear shell modes o 321 A95-76588 [BTN-95-EIX95182619103] BUNCHING p 281 A95-73540 [BTN-95-EIX95152582338] Sensitivity of combustion-acoustic instabilities to boundary conditions for premixed gas turbine Effects of satellite bunching on the probability of collision BEARINGS in geosynchronous orbit Finite element model for a flexible non-symmetric rotor |BTN-95-EIX95152583276| p 298 A95-73577 combustors on distributed bearing: A stability study BURGER EQUATION (NASA-TM-106890) p 289 N95-23550 Aeroacoustic model for weak shock waves based on p 306 A95-74612 |BTN-94-EIX94381352212| **BOUNDARY ELEMENT METHOD Burgers** equation Coupled FEM-BEM approach for mean flow effects on BELL AIRCRAFT Improving prediction: The incorporation of simplified vibro-acoustic behavior of planar structures [BTN-95-EIX95182619076] p 269 A95-75761 p 263 A95-73495 rotor dynamics in a mathematical model of the bell JBTN-95-FIX951525775871 BOUNDARY LAYER CONTROL 412HP [BTN-95-EIX95152584679] p 282 A95-73591 Flow structure in the wake of a wishbone vortex generator BEND TESTS CALIBRATING |BTN-95-EIX95142553044| p 304 A95-73454 Experimental evaluation of a box beam specifically Design of a variable area diffuser for a 15-inch Mach Separation control on high-lift airfoils via micro-vortex tailored for chordwise deformation p 297 N95-23309 6 open-jet tunnel generators [BTN-95-EIX95182619088] p 283 A95-75773 CALIFORNIA [BTN-95-EIX95152582326] p 265 A95-73529 BENDING A comparison of some aerodynamic resistance methods Forebody flow control on a full-scale F/A-18 aircraft [BTN-95-EIX95152582333] p 281 A95-73535 Experimental evaluation of a box beam specifically using measurements over cotton and grass from the 1991 California ozone deposition experiment tailored for chordwise deformation Supersonic laminar flow control research |BTN-95-EIX95182619088| p 283 A95-75773 p 319 A95-77000 IHTN-95-112951 p 275 N95-23669 I NASA-CR-197938 I BLADE SLAP NOISE **BOUNDARY LAYER EQUATIONS** Sensitivity of acoustic predictions to variation of input The use of cowl camber and taper to reduce rotor/stator An approximate theoretical method for modeling the parameters interaction noise static thrust performance of non-axisymmetric IHTN-95-808551 p 267 A95-75097 [NASA-CR-195421] p 323 N95-22675 two-dimensional convergent-divergent nozzles **BLADE TIPS** CAMBERED WINGS p 273 N95-23193 I NASA-CR-195050 I Supersonic flow and shock formation in turbine tip Unsteady ground effects on aerodynamic coefficients **BOUNDARY LAYER FLOW** p 312 N95-23429 gaps of finite wings with camber Analytical study of the neutral stability of a model [BTN-95-EIX95182619233] **BLADE-VORTEX INTERACTION** p 271 A95-76659 hypersonic boundary layer p 263 A95-73493 **CANARD CONFIGURATIONS** Analysis of a higher harmonic control test to reduce [BTN-95-EIX95152577589] Aerodynamic characteristics of a canard-controlled missile at high angles of attack blade vortex interaction noise Flow visualization studies on sidewall effects in [BTN-95-EIX95152582330] p 265 A95-73532 two-dimensional transonic airfoil testing IBTN-95-EIX951525832571 p 267 A95-73558 [BTN-95-EIX95152582313] p 264 A95-73516 BLOWING Forebody flow control on a full-scale F/A-18 aircraft Flow study of supersonic [BTN-95-EIX95152582344] acelle configuration Inner loop flight control for the High-Speed Civil

Transport

p 293 N95-23314

p 266 A95-73546

[BTN-95-EIX95152582333]

p 281 A95-73535

p 297 A95-73559

p 267 A95-73560

external flows

[BTN-95-EIX95152583258]

IBTN-95-EIX95152583259 I

impinging on an inclined plate

Three-dimensional structure of a supersonic iet

CARBON DIOXIDE			
Hypersonic convective heat transfe	r over	140-0	deg blunt
cones in different gases			
[BTN-95-EIX95152583253]			5-73554
Possible effects of CO2 increase or	the h	ap-st	eed civil
transport impact on ozone [HTN-95-60779]	p 317		5-75976
CARBON FIBER REINFORCED PLAS		AS	0.75976
Mishap risk control for advanced as		ce/cr	omnosite
materials	p 301		5-23031
CARBON FIBERS	,		
Corrosion protection measures for	CFC/I	netal	joints of
fuel integral tank structures of advan-			
	p 303	N9	5-23510
CARBON STEELS		•	
In-situ detection of surface passivat			
of localized corrosion: Experiences aircraft			5-23508
CARGO	P 001		3-20000
Evaluation of neutron techniques	for ith	cit su	bstance
detection			
(DE95-002988)	p 300	N9	5-22764
CARIBBEAN REGION			
Oceanic operations: An authoritation	ve gun	te to	oceanic
operations [FAA-AFS-550]	0 277	, NIC	5-24065
CASCADE FLOW	pzii	143	3-24003
Eigenanalysis of unsteady flows abo	ut airfo	ils. ca	ascades.
and wings			
[BTN-95-EIX95152577597]			5-73486
Numerical computation of aero			
transfer in a turbine cascade and a tur			
advanced turbulence models User's guide for ECAP2D: A			15-23444 Insteady
aerodynamic and aeroelastic analys			
dimensional oscillating cascades, ver			10. 140
[NASA-CR-189146]			5-24189
CASES (CONTAINERS)			
NASA low-speed axial compress	sor for	func	lamental
research			
NASA-TM-4635	p 296	N9	5-23192
CAVITATION FLOW  Cavitation modeling in Euler and N	avior S	toko	codec
Cavitation modeling in Edici and re			5-23630
CAVITIES	<b>F</b> • • •		
Cavitation modeling in Euler and N	avier-S	toke	s codes
	p 315	N9	5-23630
CAVITY FLOW		4	
Observations on using experiment conditions for computations	ai data	ast	юundary
BTN-95-EIX95182619103	p 321	Δα	5-76588
A time-accurate finite volume met			
velocities			5-23447
CERAMIC COATINGS			
Compliant interlayer			
	p 304	A9	5-73439
[BTN-95-EIX95142562401]			
CERAMICS			
CERAMICS Compliant interlayer	n 304	ΔQ	5-73439
CERAMICS Compliant interlayer [BTN-95-EIX95142562401]	p 304	A9	5-73439
CERAMICS Compliant interlayer [BTN-95-EIX95142562401] CHANGE DETECTION	•		
CERAMICS  Compliant interlayer [BTN-95-EIX95142562401]  CHANGE DETECTION  Real-time estimation of atmospheric from in-situ aircraft measurements	turbu	lence	severity
CERAMICS Compliant interlayer [BTN-95-EIX95142562401] CHANGE DETECTION Real-time estimation of atmospheric from in-situ aircraft measurements [BTN-95-EIX95182619231]	turbu	lence	
CÉRAMICS Compliant interlayer [BTN-95-EIX95142562401] CHANGE DETECTION Real-time estimation of atmospheric from in-situ aircraft measurements [BTN-95-EIX95182619231] CHARGE DISTRIBUTION	turbu p 319	lence	severity 5-76657
CERAMICS Compliant interlayer [BTN-95-EIX95142562401] CHANGE DETECTION Real-time estimation of atmospheric from in-situ aircraft measurements [BTN-95-EIX95182619231] CHARGE DISTRIBUTION Thundercloud electric field in	p 319	lence A9	severity 5-76657 or the
CERAMICS Compliant interlayer [BTN-95-EIX95142562401] CHANGE DETECTION Real-time estimation of atmospheristrom in-situ aircraft measurements [BTN-95-EIX95182619231] CHARGE DISTRIBUTION Thundercloud electric field in ionosphere-Earth region. 1: Depender	p 319	lence A9	severity 5-76657 or the
CÉRAMICS Compliant interlayer [BTN-95-EIX95142562401] CHANGE DETECTION Real-time estimation of atmospheric from in-situ aircraft measurements [BTN-95-EIX95182619231] CHARGE DISTRIBUTION Thundercloud electric field n ionosphere-Earth region. 1: Depender distribution	p 319 nodelinace on	lence A9 ig 1 cloui	severity 5-76657 or the d charge
CERAMICS Compliant interlayer [BTN-95-EIX95142562401] CHANGE DETECTION Real-time estimation of atmospheristrom in-situ aircraft measurements [BTN-95-EIX95182619231] CHARGE DISTRIBUTION Thundercloud electric field in ionosphere-Earth region. 1: Depender	p 319 nodelinace on	lence A9 ig 1 cloui	severity 5-76657 or the
CÉRAMICS Compliant interlayer [BTN-95-EIX95142562401] CHANGE DETECTION Real-time estimation of atmospheric from in-situ aircraft measurements [BTN-95-EIX95182619231] CHARGE DISTRIBUTION Thundercloud electric field in ionosphere-Earth region. 1: Depender distribution [HTN-95-41223]	p 319 nodelinace on p 317	A9 Ig 1 Cloud	severity 5-76657 or the d charge
CERAMICS Compliant interlayer [BTN-95-EIX95142562401] CHANGE DETECTION Real-time estimation of atmospheric from in-situ aircraft measurements [BTN-95-EIX95182619231] CHARGE DISTRIBUTION Thundercloud electric field n ionosphere-Earth region. 1: Depender distribution [HTN-95-41223] CHARGE TRANSFER Collaborative research on aircraft processes in ice	p 319 nodelimice on p 317 icing	lence A9 Ig f cloud A9	severity 5-76657 for the dicharge 5-75035 charging
CERAMICS Compliant interlayer [BTN-95-EIX95142562401] CHANGE DETECTION Real-time estimation of atmospheris [BTN-95-EIX95182619231] CHARGE DISTRIBUTION Thundercloud electric field in ionosphere-Earth region. 1: Depender distribution [HTN-95-41223] CHARGE TRANSFER Collaborative research on aircraft processes in ice [AD-8285102]	p 319 nodelimice on p 317 icing	lence A9 Ig f cloud A9	severity 5-76657 or the d charge
CERAMICS Compliant interlayer [BTN-95-EIX95142562401] CHANGE DETECTION Real-time estimation of atmospheric [BTN-95-EIX95182619231] CHARGE DISTRIBUTION Thundercloud electric field in ionosphere-Earth region. 1: Depender distribution [HTN-95-41223] CHARGE TRANSFER Collaborative research on aircraft processes in ice [AD-A285102] CHEMICAL COMPOSITION	p 319 nodelinace on p 317 icing	lence A9 Ig 1 cloud A9 and C	severity 5-76657 for the dicharge 5-75035 charging 5-23201
CERAMICS Compliant interlayer [BTN-95-EIX95142562401] CHANGE DETECTION Real-time estimation of atmospheric from in-situ aircraft measurements [BTN-95-EIX95182619231] CHARGE DISTRIBUTION Thundercloud electric field in conosphere-Earth region. 1: Depender distribution [HTN-95-41223] CHARGE TRANSFER Collaborative research on aircraft processes in ice [AD-A285102] CHEMICAL COMPOSITION Possible effects of CO2 increase on	p 319 nodelinace on p 317 icing	lence A9 Ig 1 cloud A9 and C	severity 5-76657 for the dicharge 5-75035 charging 5-23201
CERAMICS Compliant interlayer [BTN-95-EIX95142562401] CHANGE DETECTION Real-time estimation of atmospheris [BTN-95-EIX95182619231] CHARGE DISTRIBUTION Thundercloud electric field in ionosphere-Earth region. 1: Depender distribution [HTN-95-41223] CHARGE TRANSFER Collaborative research on aircraft processes in ice [AD-A285102] CHEMICAL COMPOSITION Possible effects of CO2 increase on transport impact on ozone	p 319 nodelimee on p 317 icing p 276 the hi	lence A9 Ig 1 cloud A9 and 6 N9 gh-sp	severity 5-76657 or the dicharge 5-75035 charging 5-23201 seed civil
CERAMICS Compliant interlayer [BTN-95-EIX95142562401] CHANGE DETECTION Real-time estimation of atmospheric from in-situ aircraft measurements [BTN-95-EIX95182619231] CHARGE DISTRIBUTION Thundercloud electric field in ionosphere-Earth region. 1: Depender distribution [HTN-95-41223] CHARGE TRANSFER Collaborative research on aircraft processes in ice [AD-A285102] CHEMICAL COMPOSITION Possible effects of CO2 increase on transport impact on ozone [HTN-95-60779]	p 319 nodelimee on p 317 icing p 276 the hi	lence A9 Ig 1 cloud A9 and 6 N9 gh-sp	severity 5-76657 for the dicharge 5-75035 charging 5-23201
CERAMICS Compliant interlayer [BTN-95-EIX95142562401] CHANGE DETECTION Real-time estimation of atmospheric from in-situ aircraft measurements [BTN-95-EIX95182619231] CHARGE DISTRIBUTION Thundercloud electric field in onosphere-Earth region. 1: Depender distribution [HTN-95-41223] CHARGE TRANSFER Collaborative research on aircraft processes in ice [AD-A285102] CHEMICAL COMPOSITION Possible effects of CO2 increase on transport impact on ozone [HTN-95-60779] CHEMICAL EXPLOSIONS	p 319 modelimace on p 317 icing p 276 the hi	ence A9 A9 Cloud A9 A9 A9 A9 A9	severity 5-76657 for the dicharge 5-75035 charging 5-23201 seed civil
CERAMICS Compliant interlayer [BTN-95-EIX95142562401] CHANGE DETECTION Real-time estimation of atmospheric from in-situ aircraft measurements [BTN-95-EIX95182619231] CHARGE DISTRIBUTION Thundercloud electric field in ionosphere-Earth region. 1: Depender distribution [HTN-95-41223] CHARGE TRANSFER Collaborative research on aircraft processes in ice [AD-A285102] CHEMICAL COMPOSITION Possible effects of CO2 increase on transport impact on ozone [HTN-95-60779]	p 319 modelimace on p 317 icing p 276 the hi	ence A9 A9 Cloud A9 A9 A9 A9 A9	severity 5-76657 for the dicharge 5-75035 charging 5-23201 seed civil
CERAMICS Compliant interlayer [BTN-95-EIX95142562401] CHANGE DETECTION Real-time estimation of atmospheric ffrom in-situ aircraft measurements [BTN-95-EIX95182619231] CHARGE DISTRIBUTION Thundercloud electric field in ionosphere-Earth region. 1: Depended distribution [HTN-95-41223] CHARGE TRANSFER Collaborative research on aircraft processes in ice [AD-A285102] CHEMICAL COMPOSITION Possible effects of CO2 increase on transport impact on ozone [HTN-95-60779] CHEMICAL EXPLOSIONS E valuation of neutron techniques detection [DE95-002988]	p 319 nodelimice on p 317 icing p 276 the hi p 317 for illi	dence A9 A9 Colour A9 A9 A9 A9 A9 A9 A9 A9	severity 5-76657 for the dicharge 5-75035 charging 5-23201 seed civil
CERAMICS Compliant interlayer [BTN-95-EIX95142562401] CHANGE DETECTION Real-time estimation of atmospheric from in-situ aircraft measurements [BTN-95-EIX95182619231] CHARGE DISTRIBUTION Thundercloud electric field nonosphere-Earth region. 1: Depender distribution [HTN-95-41223] CHARGE TRANSFER Collaborative research on aircraft processes in ice [AD-A285102] CHEMICAL COMPOSITION Possible effects of CO2 increase on transport impact on ozone [HTN-95-60779] CHEMICAL EXPLOSIONS Evaluation of neutron techniques detection [DE95-002988] CHLORINE COMPOUNDS	p 319 nodelir nce on p 317 icing p 276 the hi p 317 for illi p 300	lence A9 Cloud A9	severity 5-76657 for the dicharge 5-75035 charging 5-23201 seed civil 5-75976 ubstance 5-22764
CERAMICS Compliant interlayer [BTN-95-EIX95142562401] CHANGE DETECTION Real-time estimation of atmospheris (FOR in-5itu aircraft measurements [BTN-95-EIX95182619231] CHARGE DISTRIBUTION Thundercloud electric field in ionosphere-Earth region. 1: Depender distribution [HTN-95-41223] CHARGE TRANSFER Collaborative research on aircraft processes in ice [AD-A285102] CHEMICAL COMPOSITION Possible effects of CO2 increase on transport impact on ozone [HTN-95-60779] CHEMICAL EXPLOSIONS Evaluation of neutron techniques detection [DE95-002988] CHLORINE COMPOUNDS Estimates of total organic and inore	p 319 nodelir nce on p 317 icing p 276 the hi p 317 for illi p 300	lence A9	severity 5-76657 for the dicharge 5-75035 charging 5-23201 seed civit 5-75976 sbstance 5-22764 ne in the
CERAMICS Compliant interlayer [BTN-95-EIX95142562401] CHANGE DETECTION Real-time estimation of atmospheric Iform in-situ aircraft measurements [BTN-95-EIX95182619231] CHARGE DISTRIBUTION Thundercloud electric field in onosphere-Earth region. 1: Depender distribution [HTN-95-41223] CHARGE TRANSFER Collaborative research on aircraft processes in ice [AD-A285102] CHEMICAL COMPOSITION Possible effects of CO2 increase on transport impact on ozone [HTN-95-60779] CHEMICAL EXPLOSIONS E valuation of neutron techniques detection [DE95-002988] CHLORINE COMPOUNDS Estimates of total organic and inore lower stratosphere from in situ and in	p 319 nodelir nce on p 317 icing p 276 the hi p 317 for illi p 300	lence A9	severity 5-76657 for the dicharge 5-75035 charging 5-23201 seed civit 5-75976 sbstance 5-22764 ne in the
CERAMICS Compliant interlayer [BTN-95-EIX95142562401] CHANGE DETECTION Real-time estimation of atmospheris [FOR 1975-EIX95182619231] CHARGE DISTRIBUTION Thundercloud electric field nonosphere-Earth region. 1: Depender distribution [HTN-95-41223] CHARGE TRANSFER Collaborative research on aircraft processes in ice [AD-A285102] CHEMICAL COMPOSITION Possible effects of CO2 increase on transport impact on ozone [HTN-95-60779] CHEMICAL EXPLOSIONS Evaluation of neutron techniques detection [DE95-002988] CHLORINE COMPOUNDS Estimates of total organic and inortower stratosphere from in situ and during AASE 2	p 319 nodelir nce on p 317 icing p 276 the hi p 317 for illi p 300 ganic c	dence A9	severity 5-76657 or the dicharge 5-75035 charging 5-23201 seed civil 6-75976 sbstance 5-22764 ne in the
CERAMICS Compliant interlayer [BTN-95-EIX95142562401] CHANGE DETECTION Real-time estimation of atmospheris [BTN-95-EIX95182619231] CHARGE DISTRIBUTION Thundercloud electric field in ionosphere-Earth region. 1: Depender distribution [HTN-95-41223] CHARGE TRANSFER Collaborative research on aircraft processes in ice [AD-A285102] CHEMICAL COMPOSITION Possible effects of CO2 increase on transport impact on ozone [HTN-95-60779] CHEMICAL EXPLOSIONS Evaluation of neutron techniques detection [DE95-002988] CHLORINE COMPOUNDS Estimates of total organic and inor lower stratosphere from in situ and in during AASE 2 [HTN-95-A0861]	p 319 nodelir nce on p 317 icing p 276 the hi p 317 for illi p 300 ganic c	dence A9	severity 5-76657 for the dicharge 5-75035 charging 5-23201 seed civit 5-75976 sbstance 5-22764 ne in the
CERAMICS Compliant interlayer [BTN-95-EIX95142562401] CHANGE DETECTION Real-time estimation of atmospheris [BTN-95-EIX95182619231] CHARGE DISTRIBUTION Thundercloud electric field in ionosphere-Earth region. 1: Depender distribution [HTN-95-41223] CHARGE TRANSFER Collaborative research on aircraft processes in ice [AD-A285102] CHEMICAL COMPOSITION Possible effects of CO2 increase on transport impact on ozone [HTN-95-60779] CHEMICAL EXPLOSIONS Evaluation of neutron techniques detection [DE95-002988] CHLORINE COMPOUNDS Estimates of total organic and inor lower stratosphere from in situ and in during AASE 2 [HTN-95-A0861]	p 319 nodelir nce on p 317 icing p 276 the hi p 317 for illi p 300 ganic c lask n	dence A9 A9 A9 A9 A9 A9 A9 A9 Cit su N9 Chlorineasu	severity 5-76657 or the dicharge 5-75035 charging 5-23201 seed civit 5-75976 sbstance 5-22764 the in the greenents
CERAMICS Compliant interlayer [BTN-95-EIX95142562401] CHANGE DETECTION Real-time estimation of atmospheris [FOR 1975-EIX95182619231] CHARGE DISTRIBUTION Thundercloud electric field in ionosphere-Earth region. 1: Depender distribution [HTN-95-41223] CHARGE TRANSFER Collaborative research on aircraft processes in ice [AD-A285102] CHEMICAL COMPOSITION Possible effects of CO2 increase on transport impact on ozone [HTN-95-60779] CHEMICAL EXPLOSIONS Evaluation of neutron techniques detection [DE95-002988] CHLORINE COMPOUNDS Estimates of total organic and inoratower stratosphere from in situ and in during AASE 2 [HTN-95-A0861] CIVIL AVIATION Development of aeronautical mobilover the past thirty years	p 319 nodelir nce on p 317 icing p 276 the hi p 317 for illi p 300 ganic c lask n	ence A9	severity 5-76657 or the dicharge 5-75035 charging 5-23201 seed civil 5-75976 sbstance 5-22764 ne in the greenents 5-76265 services
CERAMICS Compliant interlayer [BTN-95-EIX95142562401] CHANGE DETECTION Real-time estimation of atmospheris from in-situ aircraft measurements [BTN-95-EIX95182619231] CHARGE DISTRIBUTION Thundercloud electric field in ionosphere-Earth region. 1: Depended distribution [HTN-95-41223] CHARGE TRANSFER Collaborative research on aircraft processes in ice [AD-A285102] CHEMICAL COMPOSITION Possible effects of CO2 increase on transport impact on ozone [HTN-95-60779] CHEMICAL EXPLOSIONS Evaluation of neutron techniques detection [DE95-002988] CHLORINE COMPOUNDS Estimates of total organic and inor- lower stratosphere from in situ and in during AASE 2 [HTN-95-A0861] CIVIL AVIATION Development of aeronautical mobi- over the past thirty years [BTN-95-EIX95152569458]	p 315 and delir mode on p 317 icing p 276 the hi p 317 for illi p 300 ganic c ganic c p 317	g 1 cloud A9 g 1 cloud A9 g 1 cloud A9 g 1 A9 c 1 A9 c 1 A9 d 1 A9 d 1 A9 d 1 A9	severity 5-76657 or the dicharge 5-75035 charging 5-23201 seed civil 5-75976 substance 5-22764 ne in the greenents 5-76265 services 5-73498
CERAMICS Compliant interlayer [BTN-95-EIX95142562401] CHANGE DETECTION Real-time estimation of atmospheric from in-situ aircraft measurements [BTN-95-EIX95182619231] CHARGE DISTRIBUTION Thundercloud electric field nonosphere-Earth region. 1: Depender distribution [HTN-95-41223] CHARGE TRANSFER Collaborative research on aircraft processes in ice [AD-A285102] CHEMICAL COMPOSITION Possible effects of CO2 increase on transport impact on ozone [HTN-95-60779] CHEMICAL COMPOSITION Evaluation of neutron techniques detection [DE95-002988] CHLORINE COMPOUNDS Estimates of total organic and inortower stratosphere from in situ and it during AASE 2 [HTN-95-A0861] CIVIL AVIATION Development of aeronautical mobiover the past thirty years [BTN-95-EIX95152569458] Containing military autotest cost groups are considered to company of the containing military autotest cost groups are considered to containing military autotest cost groups.	p 315 p 317 for illi p 300 ganic c p 317 le sate p 305 with th	g 1 cloud A9 and color N9 A9 ccit st. N9 ccit st. N9 ccit st. A9 ccit st. A9 ccit st. A9 ccit st. A9 ccit st.	severity 5-76657 or the dicharge 5-75035 charging 5-23201 seed civil 5-75976 substance 5-22764 ne in the greenents 5-76265 services 5-73498
CERAMICS Compliant interlayer [BTN-95-EIX95142562401] CHANGE DETECTION Real-time estimation of atmospheristrom in-situ aircraft measurements [BTN-95-EIX95182619231] CHARGE DISTRIBUTION Thundercloud electric field in ionosphere-Earth region. 1: Depender distribution [HTN-95-41223] CHARGE TRANSFER Collaborative research on aircraft processes in ice [AD-A285102] CHEMICAL COMPOSITION Possible effects of CO2 increase on transport impact on ozone [HTN-95-60779] CHEMICAL EXPLOSIONS Evaluation of neutron techniques detection [DE95-002988] CHLORINE COMPOUNDS Estimates of total organic and inordower stratosphere from in situ and induring AASE 2 [HTN-95-A0861] CIVIL AVIATION Development of aeronautical mobilioner of the past thirty years [BTN-95-EIX95152569458] Containing military autotest cost gree of commercial standard equipment aid	p 319 nodelirince on p 317 icing p 276 the hi p 317 for illi p 300 ganic c glask n p 317	dence A9 A9 A9 A9 A9 A9 A9 A9 Cit st N9 Chlorineasu A9 A9 Colorineasu A9 A9 Colorineasu A9 Color	severity 5-76657 or the dicharge 5-75035 charging 5-23201 seed civil 5-75976 substance 5-22764 ne in the greenents 5-76265 services 5-73498

Maintenance challenges and trends [BTN-95-EIX95182617808]

Maintenance programs

[BTN-95-EIX95182617809]

1PB95-9104011

p 261 A95-75753

p 261 A95-75754

	COMPUTATIONAL FLUID DYNAMICS
Possible effects of CO2 increase on the high-speed civil transport impact on ozone	COMMONWEALTH OF INDEPENDENT STATES Overview of AlhedSignal's avionics development in the
[HTN-95-60779] p 317 A95-75976 Inner loop flight control for the High-Speed Civil	CIS  BTN-95-EIX95212641069  p 287 A95-76734
Transport p 293 N95-23314 Handling qualities of the High Speed Civil Transport	COMPONENT RELIABILITY  Mechanical system reliability and risk assessment
p 294 N95-23325 The airline quality report, 1994 I NIAR-94-111 p 277 N95-24012	[BTN-95-EIX95142553046] p 304 A95-73452 COMPOSITE MATERIALS
[NIAR-94-11] p 277 N95-24012 Oceanic operations: An authoritative guide to oceanic operations	Modeling aerosol emissions from the combustion of composite materials p 301 N95-23038
[FAA-AFS-550] p 277 N95-24065 A review of civil aviation fatal accidents in which	Review of aeronautical fatigue investigation in the Netherlands during the period March 1991-March 1993
lost/disoriented was a cause/factor: 1981-1990 IDOT/FAA/AM-95/1  p 278 N95-24071	PB95-139184   p 285 N95-23161   COMPOSITE STRUCTURES
CLEAN ROOMS  Measurement of particle emissions from clean room	Nonlinear angle of twist of advanced composite wing boxes under pure torsion
gas-handling components [BTN-94-EIX94381359040] p 295 A95-74554	[BTN-95-EIX95152582323] p 281 A95-73526 Static aeroelastic characteristics of a composite wing
Measurement of moisture and total hydrocarbon contributions by valves used in clean room gas-delivery	[BTN-95-EIX95152582340] p 282 A95-73542 H-76B fantail demonstrater composite fan blade
systems  BTN-94-EIX94381359041  p 295 A95-74629	fabrication [HTN-95-80856] p 283 A95-75098
CLOUD COVER Diurnal variation of lee vortices in Taiwan and the	Experimental evaluation of a box beam specifically tailored for chordwise deformation
surrounding area [HTN-95-91363] p 318 A95-76394 CLOUD SEEDING	[BTN-95-EIX95182619088] p 283 A95-75773 Mishap risk control for advanced aerospace/composite
A new generation of instruments for flying laboratories [BTN-94-EIX94401363947] p 317 A95-75532	materials p 301 N95-23031  Development and verification of a resin film
CLUTTER  Maximum-likelihood spectral estimation and adaptive	infusion/resin transfer molding simulation model for fabrication of advanced textile composites [NASA-CR-197439] p 301 N95-23179
filtering techniques with application to airborne Doppler weather radar	Thin tailored-composite wing for civil tiltrotor p 285 N95-23317
[NASA-CR-197699] p 316 N95-23670 COATING	US Navy operating experience with new aircraft
Organic coating technology for the protection of aircraft against corrosion p 303 N95-23513	construction materials p 303 N95-23517  COMPRESSIBLE BOUNDARY LAYER  Effects of expansions on a supersonic boundary layer:
Corrosion in service experience with aircraft in France p 303 N95-23518	Surface pressure measurements [BTN-95-EIX95142553036] p 263 A95-73462
COCKPITS Flight-deck displays on the Boeing 777 [BTN-95-EIX95142562402] p 286 A95-73438	COMPRESSIBLE FLOW  Computation of oscillating airfoil flows with one- and
Differential GPS and system integration of the Low Visibility Landing and Surface Operations (LVLASO)	two-equation turbulence models [BTN-95-EIX95152577588] p 263 A95-73494
demonstration p 280 N95-23318 COLLISION AVOIDANCE	Supersonic axisymmetric conical flow solutions for different ratios of specific heats
Automatic guidance and control for helicopter obstacle avoidance	[BTN-95-EIX95152583283] p 306 A95-73584 Multigrid solution of compressible turbulent flow on
[BTN-95-EIX95182619130] p 291 A95-76607 Flight test evaluation of a 35 GHz forward looking	unstructured meshes using a two-equation model [BTN-94-EIX94401378794] p 307 A95-76484
altimeter for terrain avoidance [BTN-95-EIX95212641071  p 287 A95-76736	Comparison of linear stability results with flight transition data
COLLISIONS  Effects of satellite bunching on the probability of collision in geosynchronous orbit	[BTN-95-EIX95182619097] p 283 A95-76582 Application of a control-volume-based finite-element
[BTN-95-EIX95152583276] p 298 A95-73577  COMBUSTION	formulation to the shock tube problem [BTN-95-EIX95182619099] p 295 A95-76584
Modeling aerosol emissions from the combustion of composite materials p 301 N95-23038	An approximate theoretical method for modeling the static thrust performance of non-axisymmetric
COMBUSTION CHAMBERS Simulating heat addition via mass addition in constant	NASA-CR-195050   p 273 N95-23193
area compressible flows [BTN-95-EIX95182619100] p 307 A95-76585	COMPRESSOR BLADES  NASA low-speed axial compressor for fundamental
Sensitivity of combustion-acoustic instabilities to boundary conditions for premixed gas turbine	research [NASA-TM-4635] p 296 N95-23192 COMPRESSORS
combustors [NASA-TM-106890] p 289 N95-23550 COMBUSTION EFFICIENCY	Static pressure distribution in the inlet of a helicopter turbine compressor
Sensitivity of combustion-acoustic instabilities to boundary conditions for premixed gas turbine	[BTN-95-EIX95152582339] p 266 A95-73541 COMPUTATIONAL FLUID DYNAMICS
combustors [NASA-TM-106890] p 289 N95-23550	Adaptive finite element method for turbulent flow near a propeller
COMBUSTION PRODUCTS Aircraft fires, smoke toxicity, and survival: An overview	[BTN-95-EIX95142553038] p 305 A95-73460 Laplace interaction law for the computation of viscous
[DOT/FAA/AM-95/8] p 277 N95-24024 COMBUSTION STABILITY	airfoil flow in low- and high-speed aerodynamics [BTN-95-EIX95142553037] p 263 A95-73461
Sensitivity of combustion-acoustic instabilities to boundary conditions for premixed gas turbine	Effects of spatial order of accuracy on the computation of vortical flowfields
combustors [NASA-TM-106890] p 289 N95-23550	[BTN-95-EIX95152577604] p 305 A95-73479 Eigenanalysis of unsteady flows about airfoils, cascades.
COMMERCIAL AIRCRAFT  Automatic riveting cell for commercial aircraft floor grid assembly	and wings [BTN-95-EIX95152577597] p 305 A95-73486 Progress in bigh-lift perodynamic calculations
(BTN-95-EIX95182617807) p 261 A95-75752 Maintenance challenges and trends	Progress in high-lift aerodynamic calculations [BTN-95-EIX95152582315] p 264 A95-73518 Higher-order viscous shock-layer solutions for
[BTN-95-EIX95182617808] p 261 A95-75753 Maintenance programs	high-alitude flows [BTN-95-EIX95152583255] p 306 A95-73556
[BTN-95-EIX95182617809] p 261 A95-75754 Preparation of course materials: Elementary	Base drag prediction on missile configurations [BTN-95-EIX95152583256] p 266 A95-73557
mathematics of powered flight p 324 N95-23320 Aircraft accident report. Runway overrun following	Predicting exhaust plume boundaries with supersonic external flows

Aircraft accident report. Runway overrun following

p 277 N95-23609

rejected takeoff. Continental airlines flight 795, McDonnell

Douglas MD-82, N18835, LaGuardia Airport, Flushing, NY,

Optimization of contoured hypersonic scramjet inlet with a least-squares parabolized Navier-Stoke
procedure
[HTN-95-20976] p 261 A95-7404; Zonally decoupled direct simulation Monte Carle
solutions of hypersonic blunt-body wake flows [BTN-95-EIX95182617458] p 268 A95-75729
Convective and radiative heat transfer analysis for the fire 2 forebody
[BTN-95-EIX95182617460] p 268 A95-7573
Aerodynamic design of pegasus: Concept to flight with computational fluid dynamics
[BTN-95-EIX95182617463] p 298 A95-75734 Application of wall functions to generalized
nonorthogonal curvilinear coordinate systems [BTN-95-EIX95182619077] p 307 A95-75762
Turbulent transonic airfoil flow simulation using a pressure-based algorithm
[BTN-95-EIX95182619078] p 269 A95-75763
Simulation of transverse gas injection in turbulen supersonic air flows
[BTN-95-EIX95182619080] p 269 A95-75765 Viscous-inviscid interaction method for unsteady
low-speed airfoil flows [BTN-95-EIX95182619093] p 269 A95-75778
Multigrid solution of compressible turbulent flow or
unstructured meshes using a two-equation model  BTN-94-EIX94401378794  p 307 A95-76484
Grid refinement test of time-periodic flows over bluff bodies
[BTN-94-EIX94401378822] p 307 A95-76491 Comparison of linear stability results with flight transition
data  BTN-95-EIX95182619097  p 283 A95-76582
Application of a control-volume-based finite-element
formulation to the shock tube problem [BTN-95-EIX95182619099] p 295 A95-76584
CFD optimization of a theoretical minimum-drag body [BTN-95-EIX95182619234] p 308 A95-76660
Simulation on the 3-D turbulent flow in the passages of finocyl grain
BTN-95-EIX95202638962   p 279 A95-76674 Particle kinetic simulation of high altitude hypervelocity
flight [NASA-CR-197383] p 309 N95-22481
Euler Technology Assessment program for preliminary
aircraft design employing SPLITFLOW code with Cartesian unstructured grid method
[NASA-CR-4649] p 273 N95-22917 A CFD study of complex missile and store configurations
in relative motion [NASA-CR-197912] p 285 N95-22949
Mach 10 computational study of a three-dimensional scramjet inlet flow field
[NASA-TM-4602] p 309 N95-23015 Euler technology assessment for preliminary aircraft
design employing OVERFLOW code with multiblock
structured-grid method [NASA-CR-4651] p 273 N95-23095
An assessment of viscous effects in computational simulation of benign and burst vortex flows on generic
fighter wind-tunnel models using TEAM code [NASA-CR-4650] p 273 N95-23185
Mach 10 computational study of a three-dimensional scramjet inlet flow field
[NASA-TM-4602] p 310 N95-23210
Aerodynamic design optimization with sensitivity analysis and computational fluid dynamics
NASA-CR-197419 p 274 N95-23218 TIGER: A user-friendly interactive grid generation system
for complicated turbomachinery and axis-symmetric configurations p 322 N95-23419
Three-dimensional Navier-Stokes analysis and redesign of an imbedded bellmouth nozzle in a turbine cascade
inlet section p 311 N95-23423 Supersonic flow and shock formation in turbine tip
gaps p 312 N95-23429
CFD analysis of turbopump volutes p 312 N95-23436
Convergence acceleration of implicit schemes in the presence of high aspect ratio grid cells
p 313 N95-23446 A time-accurate finite volume method valid at all flow
velocities p 314 N95-23447
A study of the vortex flow over 76/40-deg double-delta wing
NASA-CR-195032 p 314 N95-23466 Validation of a Computational Fluid Dynamics (CFD)
code for supersonic axisymmetric base flow p 315 N95-23652
Supersonic laminar flow control research NASA-CR-197938 p 275 N95-23669
OMPUTATIONAL GRIDS
Adaptive finite element method for turbulent flow near

Laplace interaction law for the computation of viscous airfoil flow in low- and high-speed aerodynamics p 263 A95-73461 | BTN-95-EIX95142553037 | Effects of spatial order of accuracy on the computation of vortical flowfields IBTN-95-FIX951525776041 p 305 A95-73479 Eigenanalysis of unsteady flows about airfoils, cascades, p 305 A95-73486 IRTN-95.FIX951525775971 Progress in high-lift aerodynamic calculations p 264 A95-73518 IBTN-95-EIX951525823151 Unstructured grid solutions to a wing/pylon/store configuration IBTN-95-EIX951525823221 p 265 A95-73525 Navier-Stokes prediction of large-amplitude delta-wing roll oscillations |BTN-95-EIX95152582329| p 281 A95-73531 Application of the multigrid solution technique to hypersonic entry vehicles [BTN-95-EIX95152583254] p 306 A95-73555 Application of wall functions to generalized nonorthogonal curvilinear coordinate systems |BTN-95-EIX95182619077| p 307 A95-75762 Viscous-inviscid interaction method for unsteady low-speed airfoil flows [BTN-95-EIX95182619093] p 269 A95-75778 Grid refinement test of time-periodic flows over bluff bodies p 307 A95-76491 [BTN-94-EIX94401378822] Observations on using experimental data as boundary conditions for computations [BTN-95-EIX95182619103] p 321 A95-76588 CFD optimization of a theoretical minimum-drag body [BTN-95-EIX95182619234] p 308 A95-76660 A CFD study of complex missile and store configurations in relative motion NASA-CR-1979121 p 285 N95-22949 Mach 10 computational study of a three-dimensional scramiet inlet flow field INASA-TM-46021 p 310 N95-23210 TIGER: A user-friendly interactive grid generation system for complicated turbomachinery and axis-symmetric configurations p 322 N95-23419 CFD analysis of turbopump volutes p 312 N95-23436 Convergence acceleration of implicit schemes in the presence of high aspect ratio grid cells p 313 N95-23446 COMPUTER AIDED DESIGN Functional agility metrics and optimal trajectory analysis IBTN-95-EIX951826191211 p 321 A95-76598 Euler Technology Assessment program for preliminary aircraft design employing SPLITFLOW code with Cartesian unstructured grid method [NASA-CR-4649] p 273 N95-22917 Euler technology assessment for preliminary aircraft design employing OVERFLOW code with multiblock structured-grid method INASA-CR-4651 I p 273 N95-23095 Control of flow separation in airfoil/wing design p 274 N95-23294 applications Thin tailored composite wing for civil tiltrotor p 285 N95-23317 CFD analysis of turbopump volutes p 312 N95-23436 **COMPUTER GRAPHICS** Pilot Weather Advisor system BTN-95-EIX95152582314 p 316 A95-73517 COMPUTER PROGRAMS Unstructured grid solutions to a wing/pylon/store IBTN-95-EIX951525823221 p 265 A95-73525 Improved version of the Naval Surface Warfare Center aeroprediction code (AP93) p 267 A95-73561 IBTN-95-EIX95152583260 I Multiple site fatigue damage in fuselage skin splices: Experimental simulation and theoretical prediction [BTN-95-EIX95152584676] p 276 A95-73588 Aerodynamic design of pegasus: Concept to flight with computational fluid dynamics [BTN-95-EIX95182617463] p 298 A95-75734 CFD optimization of a theoretical minimum-drag body IBTN-95-EIX951826192341 p 308 A95-76660 NASA Lewis ice Additional improvements to the accretion code LEWICE p 309 N95-22669 I NASA-TM-106849 I Automation technology using Geographic Information System (GIS) p 324 N95-23284 Residual strength of thin panels with cracks p 311 N95-23311 CFD analysis of turbopump volutes p 312 N95-23436

Enhanced analysis and users manual for radial-inflow

p 275 N95-23462

turbine conceptual design code RTD

I NASA-CR-1954541

User's guide for ECAP2D: An Euler unsteady aerodynamic and aeroelastic analysis program for two dimensional oscillating cascades, version 1.0 p 316 N95-24189 INASA-CR-1891461 COMPUTER SYSTEMS DESIGN CASS: Design for supportability p 287 A95-75716 IRTN-95-FIX951725952961 Containing military autotest cost growth through the use of commercial standard equipment architectures p 287 A95-75717 IRTN-95-FIX951725952951 ATE enabling technologies p 287 A95-75718 [BTN-95-EIX95172595294] New commercial off-the-shelf testers are automatic and intelligent p 287 A95-75720 [BTN-95-EIX95172595292] On-line, adaptive state estimator for active noise ontrol p 322 N95-23308 control COMPUTER SYSTEMS PERFORMANCE CASS: Design for supportability [BTN-95-EIX95172595296] p 287 A95-75716 COMPUTERIZED SIMULATION Navier-Stokes prediction of large-amplitude delta-wing roll oscillations [BTN-95-EIX95152582329] p 281 A95-73531 Aerodynamic characteristics of a hypersonic viscous optimized waverider at high altitudes p 266 A95-73552 IBTN-95-EIX951525832511 Hypersonic convective heat transfer over 140-deg blunt cones in different gases [BTN-95-EIX95152583253] p 306 A95-73554 Predicting exhaust plume boundaries with supersonic external flows [BTN-95-EIX95152583258] p 297 A95-73559 Improving prediction: The incorporation of simplified rotor dynamics in a mathematical model of the bell IBTN-95-EIX951525846791 p 282 A95-73591 New commercial off-the-shelf testers are automatic and intelligent IBTN-95-EIX951725952921 p 287 A95-75720 Determination of wall boundary conditions high-speed-ratio direct simulation Monte Carlo calculations [BTN-95-EIX95182617457] p 267 A95-75728 Zonally decoupled direct simulation Monte Carlo solutions of hypersonic blunt-body wake flows p 268 A95-75729 [BTN-95-EIX95182617458] Simulating heat addition via mass addition in constant area compressible flows p 307 A95-76585 [BTN-95-EIX95182619100] Functional agility metrics and optimal trajectory IRTN-95-FIX951826191211 p 321 A95-76598 Response of a nonrotating rotor blade to lateral rbulence. Part 2: Experiment IBTN-95-EIX951826192291 p 284 A95-76655 Unsteady ground effects on aerodynamic coefficients of finite wings with camber .IBTN-95-EIX951826192331 p 271 A95-76659 Particle kinetic simulation of high altitude hypervelocity flight INASA-CR-1973831 p 309 N95-22481 High-performance parallel analysis of coupled problems for aircraft propulsion [NASA-CR-197440] p 289 N95-23088 Development and verification of a resin film infusion/resin transfer molding simulation model for fabrication of advanced textile composites [NASA-CR-197439] p 301 N95-23179 A wall interference assessment/correction system p 309 N95-23183 |NASA-CR-197421| Design of a variable area diffuser for a 15-inch Mach p 297 N95-23309 6 open-jet tunnel Development of qualification guidelines for personal computer-based aviation training devices p 323 N95-23603 DOT/FAA/AM-95/6 CONCENTRATION (COMPOSITION) Time-of-flight mass spectrometer for impulse facilities [BTN-95-EIX95142553057] p 262 A95-73441 Erosion of dust-filtered helicopter turbine engines. Part Basic theoretical considerations p 288 A95-76648 [BTN-95-EIX95182619222] CONCORDE AIRCRAFT Preliminary identification of buffet problems in high speed p 294 N95-23319 civil transport CONDUCTIVE HEAT TRANSFER Effect of curvature in the numerical simulation of an electrothermal de-icer pad |BTN-95-EIX95182619219| p 276 A95-76645 CONFERENCES Corrosion detection and management of advanced airframe materials p 302 N95-23496 IAGARD-CP-565 Report of proceedings: Aviation Accident Investigation Symposium. Volume 2: Participant presentations IPB94-9170071 p 277 N95-23598

a propeller

[BTN-95-EIX95142553038]

p 305 A95-73460

Aviation Accident Investigation Symposium. Volume 1: Industry recommendations and Safety Board responses (PB94-917005) p 278 N95-24105
CONGRESSIONAL REPORTS  Report to the Secretary of Defense. Unmanned aerial vehicles: No more Hunter systems should be bought until
problems are fixed [GAO/NSIAD-95-52] p 286 N95-24091
CONICAL FLOW  Supersonic axisymmetric conical flow solutions for
different ratios of specific heats [BTN-95-EIX95152583283] p 306 A95-73584  CONJUGATE GRADIENT METHOD
Aerodynamic shape optimization using preconditioned conjugate gradient methods
BTN-95-EIX95142553033  p 263 A95-73465  CONSERVATION LAWS
A time-accurate finite volume method valid at all flow velocities p 314 N95-23447
CONSTRAINTS  Empirical results on scheduling and dynamic backtracking p 299 N95-23761
CONTAMINATION  Measurement of moisture and total hydrocarbon
contributions by valves used in clean room gas-delivery systems
BTN-94-EIX94381359041  p 295 A95-74629
Hypersonic rarefied flow past spheres including wake structure
[BTN-95-EIX95152583250] p 305 A95-73551 CONTRAILS
Transport of exhaust products in the near trail of a jet engine under atmospheric conditions
[HTN-95-91421] p 319 A95-77334 CONTROL EQUIPMENT
Engines-only flight control system [NASA-CASE-ARC-11944-1] p 294 N95-23389
Investigation of the effects of bandwidth and time delay
on helicopter roll-axis handling qualities [HTN-95-80853] p 290 A95-75095
CONTROL STABILITY  Multivariable stability and robustness of sequentially
designed feedback systems  BTN-95-EIX95182619125  p 322 A95-76602
Robustly stable preliminary control systems design for the YF-16 CCV aircraft [BTN-95-EIX95202637608] p 292 A95-76681
Stable H(infinity) controller design for the longitudinal dynamics of an aircraft
[NASA-TM-106847 ] p 293 N95-22954  CONTROL SURFACES  Comparison of linear stability results with flight transition
data  BTN-95-EIX95182619097  p 283 A95-76582
Attainable moments for the constrained control allocation problem
[8TN-95-EIX95182619149] p 322 A95-76626 Rolling maneuver load alleviation using active controls
BTN-95-EIX95182619217  p 270 A95-76643 Aerodynamic surface distension system for high angle
of attack forebody vortex control [NASA-CASE-ARC-11979-1] p 286 N95-23390
CONTROL SYSTEMS DESIGN Effects of high order dynamics on helicopter flight control
law design  HTN-95-80852  p 290 A95-75094
Integrated flight/propulsion control for helicopters [HTN-95-80854] p 290 A95-75096
Multivariable stability and robustness of sequentially designed feedback systems
[BTN-95-EIX95182619125] p 322 A95-76602 H-infinity helicopter flight control law design with and
without rotor state feedback  BTN-95-EIX95182619129  p 291 A95-76606 Direct-lift design strategy for longitudinal control of
hypersonic aircraft [BTN-95-EIX95182619131] p 291 A95-76608 Multirate flutter suppression system design for a model
wing [BTN-95-EIX95182619132] p 292 A95-76609 Derivation of system matrices from nonlinear dynamic
simulation of jet engines (BTN-95-EIX95182619139) p 288 A95-76616
Attainable moments for the constrained control allocation problem [BTN-95-EIX95182619149] p 322 A95-76626
Automatic formation flight control  [BTN-95-EiX95182619153] p 292 A95-76630
Flutter suppression control law design and testing for the active flexible wing
p 292 A95-76640 Design and multifunction tests of a frequency
domain-based active flutter suppression system [BTN-95-EIX95182619215] p 292 A95-76641

: S	FI class (BTN
5	IBTN Ro IBTN
ı	Ro IBTN Ro the Y
i	İBIN
r 1	syste attac INAS
	St dyna
5	dyna   NAS Sy Susp
5 v 7	INAS
: 	Fe aircri   NAS CONTI
	Sh
) ) )	geon IBTN Sw
•	guida (BTN Str
	dyna I NAS CONTE
t I	Fli
	dyna [ NAS Ar
,	pilot- High
, 5	CONT
,	Mu flexib (BTN Or activ (BTN
) ; ; ;	activ (BTN
 	Str dyna I NAS
3	CONVI
1	Fu 65-dd 1BTN CONVE Hy cone 1BTN Co fire 2 1BTN
? 1	Cone
) ;	Co fire 2
} <del>?</del>	CONVE
)	three (BTN
1	An trajed (BTN
5	Co prese
	CONVE
! !	ATB [
i	static two-c   NAS
} 	COOLI Ba
) ;	COPPE Cu
) 	COPPE
,	Ph from
)	CORR

	CRACK PROPAGATION
Flutter suppression for the active flexible wing: A classical design	Double pass retroreflection for corrosion detection in aircraft structures p 323 N95-23503
[BTN-95-EIX95182619216] p 292 A95-76642	Non-destructive detection of corrosion for life
Rolling maneuver load alleviation using active controls [BTN-95-EIX95182619217] p 270 A95-76643	management p 314 N95-23505
Robustly stable preliminary control systems design for	Health and usage monitoring systems: Corrosion surveillance p 262 N95-23506
the YF-16 CCV aircraft	Eddy current detection of pitting corrosion around
[BTN-95-EIX95202637608] p 292 A95-76681  Design of high performance multivariable control	fastener holes p 315 N95-23507
systems for supermaneuverable aircraft at high angle of	In-situ detection of surface passivation or activation and of localized corrosion: Experiences and prospectives in
attack  NASA-CR-197661  p 293 N95-22908	aircraft p 302 N95-23508
Stable H(infinity) controller design for the longitudinal	Test method and test results for environmental assessment of aircraft materials p 302 N95-23509
dynamics of an aircraft [NASA-TM-106847] p 293 N95-22954	New nondestructive techniques for the detection and
System identification of the Large-Angle Magnetic	quantification of corrosion in aircraft structures p 315 N95-23512
Suspension Test Fixture (LAMSTF) p 296 N95-23299 Engines-only (light control system	Corrosion detection and monitoring of aircraft structures:
[NASA-CASE-ARC-11944-1] p 294 N95-23389	An overview p 303 N95-23515
Feedback control laws for highly maneuverable aircraft	Experience of in-service corrosion on military aircraft p 303 N95-23516
NASA-CR-197944   p 295 N95-23410	US Navy operating experience with new aircraft
Shuttle entry guidance revisited using nonlinear	construction materials p 303 N95-23517 Corrosion in service experience with aircraft in France
geometric methods  BTN-95-EIX95182619144  p 299 A95-76621	p 303 N95-23518
[BTN-95-EIX95182619144] p 299 A95-76621 Switched bias proportional navigation for homing	Oktahoma City air logistics center (USAF) aging aircraft corrosion program p 262 N95-23519
guidance against highly maneuvering targets [BTN-95-EIX95182619145] p 279 A95-76622	corrosion program p 262 N95-23519 CORROSION PREVENTION
[BTN-95-EIX95182619145] p 279 A95-76622 Stable H(infinity) controller design for the longitudinal	Corrosion detection and management of advanced
dynamics of an aircraft	airtrame materials [AGARD-CP-565] p 302 N95-23496
(NASA-TM-106847) p 293 N95-22954 CONTROLLABILITY	The corrosion and protection of advanced aluminium -
Flight test of the X-29A at high angle of attack: Flight	lithium airframe alloys p 302 N95-23497 Corrosion protection measures for CFC/metal joints of
dynamics and controls [NASA-TP-3537] p 284 N95-22806	fuel integral tank structures of advanced military aircraft
Analysis of the longitudinal handling qualities and pilot-induced-oscillation tendencies of the	p 303 N95-23510
pilot-induced-oscillation tendencies of the High-Angle-of-Attack Research Vehicle (HARV)	Organic coating technology for the protection of aircraft against corrosion p 303 N95-23513
p 293 N95-23297	Corrosion detection and monitoring of aircraft structures:
Multiple-function digital controller system for active	An overview p 303 N95-23515 Experience of in-service corrosion on military aircraft
flexible wing wind-tunnel model [BTN-95-EIX95182619212] p 322 A95-76638	p 303 N95-23516
On-line analysis capabilities developed to support the	US Navy operating experience with new aircraft construction materials p 303 N95-23517
active flexible wing wind-tunnel tests [BTN-95-EIX95182619213] p 296 A95-76639	Corrosion in service experience with aircraft in France p 303 N95-23518
Stable H(infinity) controller design for the longitudinal	CORROSION RESISTANCE
dynamics of an aircraft [NASA-TM-106847] p 293 : N95-22954	In-situ detection of surface passivation or activation and of localized corrosion: Experiences and prospectives in
ONVECTIVE FLOW	aircraft p 302 N95-23508
Further analysis of high-rate rolling experiments of a 65-deg delta wing	CORROSION TESTS Corrosion detection and management of advanced
BTN-95-EIX95152582331  p 281 A95-73533	airframe materials
Hypersonic convective heat transfer over 140-deg blunt	[AGARD-CP-565] p 302 N95-23496 Corrosion of landing gear steels p 302 N95-23500
cones in different gases [BTN-95-EIX95152583253] p 306 A95-73554	Eddy current detection of pitting corrosion around fastener holes p 315 N95-23507
Convective and radiative heat transfer analysis for the	Test method and test results for environmental
fire 2 forebody [BTN-95-EIX95182617460] p 268 A95-75731	assessment of aircraft materials p 302 N95-23509 Corrosion protection measures for CFC/metal joints of
ONVERGENCE	fuel integral tank structures of advanced military aircraft
Preconditioned domain decomposition scheme for three-dimensional aerodynamic sensitivity analysis	p 303 N95-23510 New nondestructive techniques for the detection and
[BTN-95-EIX95152577612] p 321 A95-73471	quantification of corrosion in aircraft structures.
Analytical solution for controls, heats, and states of flight trajectories	p 315 N95-23512 US Navy operating experience with new aircraft
[BTN-95-EIX95152583286] p 282 A95-73587	construction materials p 303 N95-23517
Convergence acceleration of implicit schemes in the presence of high aspect ratio grid cells	COST REDUCTION  Containing military autotest cost growth through the use
p 313 N95-23446 ONVERGENT-DIVERGENT NOZZLES	of commercial standard equipment architectures
Main features of overexpanded triple jets	[BTN-95-EIX95172595295] p 287 A95-75717 Maintenance challenges and trends
[BTN-95-EIX95142553040] p 304 A95-73458 An approximate theoretical method for modeling the	[BTN-95-EIX95182617808] p 261 A95-75753
static thrust performance of non-axisymmetric	A comparison of some aerodynamic resistance methods
two-dimensional convergent-divergent nozzles [NASA-CR-195050] p 273 N95-23193	using measurements over cotton and grass from the 1991 California ozone deposition experiment
OOLING FINS	[HTN-95-11295] p 319 A95-77000
Base drag prediction on missile configurations [BTN-95-EIX95152583256] p 266 A95-73557	COUNTER ROTATION  Flow structure in the wake of a wishbone vortex
OPPER	generator
Cu deposition using a permanent magnet electron cyclotron resonance microwave plasma source	[BTN-95-EIX95142553044] p 304 A95-73454 COWLINGS
[DE94-017768] p 304 N95-23981	The use of cowl camber and taper to reduce rotor/stator
Phonon characteristics of high (T sub c) superconductors	interaction noise [NASA-CR-195421] p 323 N95-22675
from neutron Doppler broadening measurements	CRACK PROPAGATION
[DE95-003703] p 324 N95-24076 CORROSION	Growth of multiple cracks and their linkup in a fuselage lap joint
Corrosion detection and management of advanced airframe materials	[BTN-95-EIX95142553047] p 286 A95-73451
[AGARD-CP-565] p 302 N95-23496	Multiple site fatigue damage in fuselage skin splices: Experimental simulation and theoretical prediction
The corrosion and protection of advanced aluminium - lithium airframe alloys p 302 N95-23497	[BTN-95-EIX95152584676] p 276 A95-73588
Corrosion of landing gear steels p 302 N95-23500	Residual strength of thin panels with cracks p 311 N95-23311

CRACKS	DATA ACQUISITION	Analytic prediction of lift for delta wings with partial
Growth of multiple cracks and their linkup in a fuselage lap joint	Condition monitoring and diagnostics [BTN-95-EIX95182617811] p 261 A95-75756	leading-edge thrust  BTN-95-EIX95152582345  p 266 A95-73547
[BTN-95-EIX95142553047] p 286 A95-73451	DATA BASES	Effect of leeward flow dividers on the wing rock of a
Multiple site fatigue damage in fuselage skin splices: Experimental simulation and theoretical prediction	Compendium of NASA data base for the Global Tropospheric Experiment's Pacific Exploratory Mission	delta wing [BTN-95-EIX95152582347] p 282 A95-73549
[BTN-95-EIX95152584676] p 276 A95-73588	West-A (PEM West-A)	Wing vertical position effects on wing-body carryover
Transient analysis of a cracked rotor passing through critical speed	[NASA-TM-109177] p 320 N95-23009	for noncircular missiles [BTN-95-EIX95182617462] p 268 A95-75733
[BTN-94-EIX94401360022] p 306 A95-74702	Impeller flow field characterization with a laser two-focus velocimeter p 313 N95-23440	Transient structure of vortex breakdown on a delta
Residual strength of thin panels with cracks	DATA LINKS	wing [BTN-95-EIX95182619073] p 268 A95-75758
CRASHES	Differential GPS and system integration of the Low Visibility Landing and Surface Operations (LVLASO)	Natural laminar flow wing concept for supersonic
Aircraft fires, smoke toxicity, and survival: An overview [DOT/FAA/AM-95/8] p 277 N95-24024	demonstration p 280 N95-23318	transports 1BTN-95-EIX951826192261 p 308 A95-76652
A multibody/finite element analysis approach for	DATA PROCESSING On-line analysis capabilities developed to support the	A study of the vortex flow over 76/40-deg double-delta
modeling of crash dynamic responses   NIAR-94-3   p 277 N95-24050	active flexible wing wind-tunnel tests	wing [NASA-CR-195032] p 314 N95-23466
CRASHWORTHINESS	[BTN-95-EIX95182619213] p 296 A95-76639 Enhancement of F/A-18 operational flight	DEPOSITION
A multibody/finite element analysis approach for modeling of crash dynamic responses	measurements: Data report for phase 1	A comparison of some aerodynamic resistance methods using measurements over cotton and grass from the 1991
[NIAR-94-3] p 277 N95-24050	[DSTO-TR-0049] p 286 N95-23666	California ozone deposition experiment
CREEP PROPERTIES  Evolution of oxidation and creep damage mechanisms	Calculation of satellite drag coefficients [AD-A285118] p 300 N95-23781	[HTN-95-11295] p 319 A95-77000 Cu deposition using a permanent magnet electron
in HIPed silicon nitride materials	AVIRIS and TIMS data processing and distribution at	cyclotron resonance microwave plasma source
DE95-001360  p 300 N95-22689 CREEP TESTS	the land processes distributed active archive center p 325 N95-23872	[DE94-017768] p 304 N95-23981 DEPTH
Evolution of oxidation and creep damage mechanisms	DATA STORAGE	Evaluation of advanced aerospace materials by depth
in HIPed silicon nitride materials [DE95-001360] p 300 N95-22689	Holographic interferometric tomography for reconstructing flow fields p 310 N95-23287	sensing indentation and scratch methods [BTN-95-EIX95152584678] p 282 A95-73590
CRITICAL VELOCITY	AVIRIS and TIMS data processing and distribution at	DESIGN ANALYSIS
Transient analysis of a cracked rotor passing through critical speed	the land processes distributed active archive center p 325 N95-23872	Mechanical system reliability and risk assessment [BTN-95-EIX95142553046] p 304 A95-73452
BTN-94-EIX94401360022  p 306 A95-74702	DATA TRANSFER (COMPUTERS)	Efficient sensitivity analysis for rotary-wing
Flow structure in the wake of a wishbone vortex	AVIRIS and TIMS data processing and distribution at	aeromechanical problems [BTN-95-EIX95152577585] p 264 A95-73497
generator	the land processes distributed active archive center p 325 N95-23872	Design constraints in the payload-range diagram of
[BTN-95-EIX95142553044] p 304 A95-73454 Experimental investigation of the flowfield about an	DEFECTS	ultrahigh capacity transport airplanes [BTN-95-EIX95152582319] p 276 A95-73522
upswept afterbody	New nondestructive techniques for the detection and quantification of corrosion in aircraft structures	Structural acoustic calculations in the low-frequency
[BTN-95-EIX95152582321] p 265 A95-73524 Crossflow instability control on a swept-wing: Preliminary	p 315 N95-23512	range [BTN-95-EIX95152582336] p 323 A95-73538
studies p 274 N95-23283	DEFENSE PROGRAM Report to the Secretary of Defense. Unmanned aerial	Aerodynamic design of pegasus: Concept to flight with
CRYOGENIC FLUIDS Cavitation modeling in Euler and Navier-Stokes codes	vehicles: No more Hunter systems should be bought until	computational fluid dynamics [BTN-95-EIX95182617463] p 298 A95-75734
p 315 N95-23630	problems are fixed [GAO/NSIAD-95-52] p 286 N95-24091	Euler technology assessment for preliminary aircraft design employing OVERFLOW code with multiblock
CURING  Development and verification of a resin film	DEFORMATION	structured-grid method
infusion/resin transfer molding simulation model for	Dynamic analysis of bearingless tail rotor blades based on nonlinear shell modes	[NASA-CR-4651] p 273 N95-23095
fabrication of advanced textile composites [NASA-CR-197439] p 301 N95-23179	[BTN-95-EIX95152582338] p 281 A95-73540	Aerodynamic design optimization with sensitivity analysis and computational fluid dynamics
CURVATURE	Static aeroelastic characteristics of a composite wing [BTN-95-EIX95152582340] p 282 A95-73542	[NASA-CR-197419] p 274 N95-23218
Influence of streamwise curvature on longitudinal vortices imbedded in turbulent boundary layers	DEGRADATION	Design of a GaAs/Ge solar array for unmanned aerial vehicles
[BTN-94-EIX94401378820] p 307 A95-76489	Evolution of oxidation and creep damage mechanisms in HIPed silicon nitride materials	[NASA-TM-106870] p 320 N95-23259
Effect of curvature in the numerical simulation of an electrothermal de-icer pad	[DE95-001360] p 300 N95-22689	Inner loop flight control for the High-Speed Civil Transport p 293 N95-23314
[BTN-95-EIX95182619219] p 276 A95-76645	Non-destructive detection of corrosion for life management p 314 N95-23505	Enhanced analysis and users manual for radial-inflow
CYCLOTRON RESONANCE  Cu deposition using a permanent magnet electron	In-situ detection of surface passivation or activation and	turbine conceptual design code RTD [NASA-CR-195454] p 275 N95-23462
cyclotron resonance microwave plasma source	of localized corrosion: Experiences and prospectives in aircraft p 302 N95-23508	DETECTION
[DE94-017768] p 304 N95-23981	Oklahoma City air logistics center (USAF) aging aircraft	Evaluation of neutron techniques for illicit substance detection
n	corrosion program p 262 N95-23519 DEGREES OF FREEDOM	[DE95-002988] p 300 N95-22764
D	Functional dependence of trajectory dispersion on initial	Health and usage monitoring systems: Corrosion surveillance p 262 N95-23506
DAMAGE	condition errors [BTN-95-EIX95152583263] p 298 A95-73564	In-situ detection of surface passivation or activation and
Multiaxis pilot ratings for damaged aircraft [BTN-95-EIX95182619128] p 269 A95-76605	Improving prediction: The incorporation of simplified rotor dynamics in a mathematical model of the bell	of localized corrosion: Experiences and prospectives in aircraft p 302 N95-23508
Rationale for the Modular Air-system Vulnerability	412HP	New nondestructive techniques for the detection and
Estimation Network (MAVEN) methodology [AD-A285797] p 284 N95-22510	[BTN-95-EIX95152584679] p 282 A95-73591 Identification of higher order helicopter dynamics using	quantification of corrosion in aircraft structures p 315 N95-23512
Residual strength of thin panels with cracks	linear modeling methods	Corrosion detection and monitoring of aircraft structures:
p 311 N95-23311	[HTN-95-80851] p 290 A95-75093 <b>DEICERS</b>	An overview p 303 N95-23515
Double pass retroreflection for corrosion detection in aircraft structures p 323 N95-23503	Effect of curvature in the numerical simulation of an	Experience of in-service corrosion on military aircraft p 303 N95-23516
POD assessment of NDI procedures using a round robin	electrothermal de-icer pad [BTN-95-EIX95182619219] p 276 A95-76645	DETERIORATION
test [AGARD-R-809] p 315 N95-23602	DEICING	Non-destructive detection of corrosion for life management p 314 N95-23505
DAMAGE ASSESSMENT	Effect of curvature in the numerical simulation of an electrothermal de-icer pad	DIAGNOSIS
Mechanical system reliability and risk assessment [BTN-95-EIX95142553046] p 304 A95-73452	[BTN-95-EIX95182619219] p 276 A95-76645	Condition monitoring and diagnostics [BTN-95-EIX95182617811] p 261 A95-75756
Validation of an effective flat cruciform-shaped specimen	DELTA WINGS Effects of spatial order of accuracy on the computation	DIFFERENTIAL EQUATIONS
to study CFRP composite laminates under biaxial loading	of vortical flowfields	Three-dimensional structure of a supersonic jet impinging on an inclined plate
BTN-95-EIX95152584677  p 282 A95-73589	[BTN-95-EIX95152577604] p 305 A95-73479 Unstructured grid solutions to a wing/pylon/store	[BTN-95-EIX95152583259] p 267 A95-73560
POD assessment of NDI procedures using a round robin test	configuration	DIGITAL SYSTEMS  Multiple-function digital controller system for active
[AGARD-R-809] p 315 N95-23602	[BTN-95-EIX95152582322] p 265 A95-73525 Navier-Stokes prediction of large-amplitude delta-wing	flexible wing wind-tunnel model
Aircraft accident report. Runway overrun following	roll oscillations  BTN-95-EIX95152582329  p 281 A95-73531	[BTN-95-EIX95182619212] p 322 A95-76638 DIRECT LIFT CONTROLS
rejected takeoff. Continental airlines flight 795, McDonnell Douglas MD-82, N18835, LaGuardia Airport, Flushing, NY,	Further analysis of high-rate rolling experiments of a	Direct-lift design strategy for longitudinal control of
2 March 1994 [PB95-910401] p 277 N95-23609	65-deg delta wing  BTN-95-EIX95152582331  p 281 A95-73533	hypersonic aircraft [BTN-95-EIX95182619131] p 291 A95-76608
	,	, p 231 N33-70000

DIRECTIONAL CONTROL	DURABILITY	EDDY CURRENTS
Feedback control laws for highly maneuverable	Interlaminar shear test method development for long	Eddy current detection of pitting corrosion around
aircraft [NASA-CR-197944] p 295 N95-23410	term durability testing of composites p 301 N95-23300	fastener holes p 315 N95-23507
DISCONTINUITY p 295 N95-234 TO	DUST p 301 1495-23300	EDDY VISCOSITY  Adaptive finite element method for turbulent flow near
Application of a control-volume-based finite-element	Erosion of dust-filtered helicopter turbine engines. Part	a propeller
formulation to the shock tube problem	Basic theoretical considerations	[BTN-95-EIX95142553038] p 305 A95-73460
BTN-95-EIX95182619099  p 295 A95-76584	[BTN-95-EIX95182619222] p 288 A95-76648	EDUCATION
DISORIENTATION	Erosion of dust-filtered helicopter turbine engines. Part 2: Erosion reduction	ATE enabling technologies {BTN-95-EIX95172595294} p 287 A95-75718
A review of civil aviation fatal accidents in which lost/disonented was a cause/factor: 1981-1990	[BTN-95-EIX95182619223] p 289 A95-76649	1994 NASA-HU American Society for Engineering
DOT/FAA/AM-95/1  p 278 N95-24071	Life prediction of helicopter engines fitted with dust	Education (ASEE) Summer Faculty Fellowship Program
DISPERSIONS	filters	[NASA-CR-194972] p 325 N95-23276
Functional dependence of trajectory dispersion on initial	[BTN-95-EIX95182619224] p 289 A95-76650	Preparation of course materials: Elementary
condition errors	DUST COLLECTORS  Erosion of dust-filtered helicopter turbine engines. Part	mathematics of powered flight p 324 N95-23320 EIGENVALUES
[BTN-95-EIX95152583263] p 298 A95-73564	2: Erosion reduction	Eigenanalysis of unsteady flows about airfoils, cascades,
DISPLAY DEVICES	[BTN-95-EIX95182619223] p 289 A95-76649	and wings
Flight-deck displays on the Boeing 777 [BTN-95-EIX95142562402] p 286 A95-73438	Life prediction of helicopter engines fitted with dust	[BTN-95-EIX95152577597] p 305 A95-73486
	filters	ELASTIC BENDING
Virtual reality flight control display with six-degree-of-freedom controller and spherical orientation	[BTN-95-EIX95182619224] p. 289 A95-76650	Residual strength of thin panels with cracks
overlay	DYNAMIC CHARACTERISTICS  Analytical aeropropulsive/aeroelastic	p 311 N95-23311 Thin tailored composite wing for civil tiltrotor
[NASA-CASE-NPO-18733-1-CU] p 288 N95-22578	hypersonic-vehicle model with dynamic analysis	p 285 N95-23317
Automation technology using Geographic Information	[BTN-95-EIX95182619138] p 269 A95-76615	ELECTRIC FIELDS
System (GIS) p 324 N95-23284	DYNAMIC LOADS	Thundercloud electric field modeling for the
Differential GPS and system integration of the Low	Enhancement of F/A-18 operational flight	ionosphere-Earth region. 1: Dependence on cloud charge
Visibility Landing and Surface Operations (LVLASO) demonstration p 280 N95-23318	measurements: Data report for phase 1	distribution
demonstration p 280 N95-23318  DISTILLATION	DSTO-TR-0049  p 286 N95-23666   DYNAMIC MODELS	[HTN-95-41223] p 317 A95-75035 ELECTRIC MOTORS
Airborne rotary air separator study	Flutter analysis of composite box beams	Motor drive technologies for the power-by-wire (PBW)
[NASA-CR-189099] p 290 N95-24053	[NASA-CR-197931] p 294 N95-23392	program: Options, trends and tradeoffs
DISTRIBUTED PROCESSING	DYNAMIC RESPONSE	[NASA-TM-106885] p 295 N95-23671
AVIRIS and TIMS data processing and distribution at	Effects of AMB parameters on the dynamic stability of	ELECTRIFICATION
the land processes distributed active archive center	the rotor IBTN-94-EIX94381353450 i p 323 A95-75494	Collaborative research on aircraft icing and charging
p 325 N95-23872	[BTN-94-EIX94381353450] p 323 A95-75494 Response of a nonrotating rotor blade to lateral	processes in ice   AD-A285102   p 276 N95-23201
DISTRIBUTION FUNCTIONS	turbulence. Part 1: Theory	ELECTROCHEMICAL CORROSION
Determination of wall boundary conditions for high-speed-ratio direct simulation Monte Carlo	[BTN-95-EIX95182619228] p 284 A95-76654	Corrosion protection measures for CFC/metal joints of
calculations	Dynamic response tests of inertial and optical	fuel integral tank structures of advanced military aircraft
[BTN-95-EIX95182617457] p 267 A95-75728	wind-tunnel model attitude measurement devices	p 303 N95-23510
DIURNAL VARIATIONS	[NASA-TM-109182] p 296 N95-23011 Influence of backup bearings and support structure	ELECTROCHEMISTRY
Diurnal variation of lee vortices in Taiwan and the	dynamics on the behavior of rotors with active supports	Health and usage monitoring systems: Corrosion surveillance p 262 N95-23506
surrounding area	[NASA-CR-197438] p 310 N95-23190	In-situ detection of surface passivation or activation and
[HTN-95-91363] p 318 A95-76394	A multibody/finite element analysis approach for	of localized corrosion: Experiences and prospectives in
A comparison of some aerodynamic resistance methods using measurements over cotton and grass from the 1991	modeling of crash dynamic responses	aircraft p 302 N95-23508
California ozone deposition experiment	[NIAR-94-3] p 277 N95-24050	Test method and test results for environmental
[HTN-95-11295] p 319 A95-77000	DYNAMIC STABILITY  Dynamical instability of the aerogravity assist	assessment of aircraft materials p 302 N95-23509
DIVIDERS	maneuver	US Navy operating experience with new aircraft
Effect of leeward flow dividers on the wing rock of a	[BTN-95-EIX95152583282] p 298 A95-73583	construction materials p 303 N95-23517
delta wing	Effects of AMB parameters on the dynamic stability of	ELECTROMAGNETS
[BTN-95-EIX95152582347] p 282 A95-73549	the rotor	Cu deposition using a permanent magnet electron
DOPPLER RADAR 2 micron LIDAR for laser-based remote sensing: Flight	[BTN-94-EIX94381353450] p 323 A95-75494	cyclotron resonance microwave plasma source I DE94-017768 i p 304 N95-23981
demonstration and application survey	Handling qualities of the High Speed Civil Transport p 294 N95-23325	[DE94-017768] p 304 N95-23981 ELECTRONIC EQUIPMENT
[BTN-95-EIX95212641072] p 319 A95-76737	DYNAMIC STRUCTURAL ANALYSIS	Differential GPS and system integration of the Low
Maximum-likelihood spectral estimation and adaptive	Postinstability behavior of a two-dimensional airfoil with	Visibility Landing and Surface Operations (LVLASO)
filtering techniques with application to airborne Doppler	a structural nonlinearity	demonstration p 280 N95-23318
weather radar	[BTN-95-EIX95152582337] p 266 A95-73539	ELECTRONIC EQUIPMENT TESTS
[NASA-CR-197699] p 316 N95-23670	Integrated aerodynamic/dynamic/structural optimization of helicopter rotor blades using multilevel	CASS: Design for supportability [BTN-95-EIX95172595296] p 287 A95-75716
Shock tunnel measurements of hypervelocity blunted	decomposition	ENERGY BUDGETS
cone drag	[NASA-TP-3465] p 285 N95-22953	Diurnal variation of lee vortices in Taiwan and the
[BTN-95-EIX95152577606] p 305 A95-73477	Thin tailored composite wing for civil tiltrotor	surrounding area
Separation control on high-lift airfoils via micro-vortex	p 285 N95-23317	[HTN-95-91363] p 318 A95-76394
generators	Flutter analysis of composite box beams [NASA-CR-197931] p 294 N95-23392	ENGINE AIRFRAME INTEGRATION  Flow study of supersonic wing-nacelle configuration
BTN-95-EIX95152582326  p 265 A95-73529	DYNAMIC TESTS	IBTN-95-EIX95152582344    p 266   A95-73546
DRAG REDUCTION	Measurement of particle emissions from clean room	Integrated flight/propulsion control for helicopters
Effect of underwing frost on a transport aircraft airfoil at flight Reynolds number	gas-handling components	[HTN-95-80854] p 290 A95-75096
(BTN-95-EIX95152582334) p 276 A95-73536	[BTN-94-EIX94381359040] p 295 A95-74554	ENGINE ANALYZERS
Numerical investigation of supersonic flows around a		Gearbox vibration diagnostic analyzer
spiked blunt body	DYNAMICAL SYSTEMS	
	Nonlinear system guidance in the presence of	[NASA-CR-189141] p 316 N95-23792
[BTN-95-EIX95212645690] p 271 A95-76742	Nonlinear system guidance in the presence of transmission zero dynamics	[NASA-CR-189141] p 316 N95-23792 ENGINE DESIGN
DROP SIZE	Nonlinear system guidance in the presence of transmission zero dynamics	[NASA-CR-189141] p 316 N95-23792
DROP SIZE Study of the droplet spray characteristics of a subsonic	Nonlinear system guidance in the presence of transmission zero dynamics [NASA-TM-4661] p 309 N95-22804	[NASA-CR-189141] p 316 N95-23792 ENGINE DESIGN Lycoming to test new engine core [HTN-95-41393] p 288 A95-76389 Aerodynamic design and analysis of a highly loaded
DROP SIZE Study of the droplet spray characteristics of a subsonic wind tunnel	Nonlinear system guidance in the presence of transmission zero dynamics	[NASA-CR-189141] p 316 N95-23792  ENGINE DESIGN  Lycoming to test new engine core [HTN-95-41393] p 288 A95-76389  Aerodynamic design and analysis of a highly loaded turbine exhaust p 312 N95-23435
DROP SIZE Study of the droplet spray characteristics of a subsonic wind tunnel [BTN-95-EIX95182619235] p 271 A95-76661	Nonlinear system guidance in the presence of transmission zero dynamics [NASA-TM-4661] p 309 N95-22804	INASA-CR-189141   p 316 N95-23792 ENGINE DESIGN Lycoming to test new engine core [HTN-95-41393] p 288 A95-76389 Aerodynamic design and analysis of a highly loaded turbine exhaust Phase 2: HGM air flow tests in support of HEX vane
DROP SIZE Study of the droplet spray characteristics of a subsonic wind tunnel [BTN-95-EIX95182619235] p 271 A95-76661 DROPS (LIQUIDS)	Nonlinear system guidance in the presence of transmission zero dynamics [NASA-TM-4661] p 309 N95-22804   E  EARTH ORBITS  Effects of satellite bunching on the probability of collision	[NASA-CR-189141] p 316 N95-23792 ENGINE DESIGN Lycoming to test new engine core [HTN-95-41393] p 288 A95-76389 Aerodynamic design and analysis of a highly loaded turbine exhaust p 312 N95-23435 Phase 2: HGM air flow tests in support of HEX vane investigation p 312 N95-23438
DROP SIZE Study of the droplet spray characteristics of a subsonic wind tunnel [BTN-95-EIX95182619235] p 271 A95-76661	Nonlinear system guidance in the presence of transmission zero dynamics [NASA-TM-4661] p 309 N95-22804   E  EARTH ORBITS  Effects of satellite bunching on the probability of collision in geosynchronous orbit	INASA-CR-189141   p 316 N95-23792 ENGINE DESIGN Lycoming to test new engine core [HTN-95-41393] p 288 A95-76389 Aerodynamic design and analysis of a highly loaded turbine exhaust Phase 2: HGM air flow tests in support of HEX vane
Study of the droplet spray characteristics of a subsonic wind tunnel [BTN-95-EIX95182619235] p 271 A95-76661  DROPS (LIQUIDS) Study of the droplet spray characteristics of a subsonic	Nonlinear system guidance in the presence of transmission zero dynamics [NASA-TM-4661] p 309 N95-22804   E  EARTH ORBITS  Effects of satellite bunching on the probability of collision in geosynchronous orbit [BTN-95-EIX95152583276] p 298 A95-73577	[NASA-CR-189141] p 316 N95-23792  ENGINE DESIGN Lycoming to test new engine core [HTN-95-41393] p 288 A95-76389 Aerodynamic design and analysis of a highly loaded turbine exhaust p 312 N95-23435 Phase 2: HGM air flow tests in support of HEX vane investigation p 312 N95-23438  ENGINE INLETS A new type of simulator for simulating the flow-field distortion of engine inlet
Study of the droplet spray characteristics of a subsonic wind tunnel [BTN-95-EIX95182619235] p 271 A95-76661  DROPS (LIQUIDS) Study of the droplet spray characteristics of a subsonic wind tunnel [BTN-95-EIX95182619235] p 271 A95-76661  DRUGS	Nonlinear system guidance in the presence of transmission zero dynamics   NASA-TM-4661   p 309 N95-22804   E  EARTH ORBITS  Effects of satellite bunching on the probability of collision in geosynchronous orbit  BTN-95-EIX95152583276   p 298 A95-73577  EARTH SURFACE	[NASA-CR-189141] p 316 N95-23792  ENGINE DESIGN Lycoming to test new engine core [HTN-95-41393] p 288 A95-76389 Aerodynamic design and analysis of a highly loaded turbine exhaust p 312 N95-23435 Phase 2: HGM air flow tests in support of HEX vane investigation p 312 N95-23438  ENGINE INLETS A new type of simulator for simulating the flow-field distortion of engine inlet [BTN-95-EIX95202638963] p 289 A95-76673
Study of the droplet spray characteristics of a subsonic wind tunnel [BTN-95-EIX95182619235] p 271 A95-76661  DROPS (LIQUIDS) Study of the droplet spray characteristics of a subsonic wind tunnel [BTN-95-EIX95182619235] p 271 A95-76661  DRUGS Evaluation of neutron techniques for illicit substance	Nonlinear system guidance in the presence of transmission zero dynamics [NASA-TM-4661] p 309 N95-22804   E  EARTH ORBITS  Effects of satellite bunching on the probability of collision in geosynchronous orbit [BTN-95-EIX95152583276] p 298 A95-73577  EARTH SURFACE Thundercloud electric field modeling for the	INASA-CR-189141   p 316 N95-23792 ENGINE DESIGN Lycoming to test new engine core [HTN-95-41393   p 288 A95-76389 Aerodynamic design and analysis of a highly loaded turbine exhaust p 312 N95-23435 Phase 2: HGM air flow tests in support of HEX vane investigation p 312 N95-23438 ENGINE INLETS A new type of simulator for simulating the flow-field distortion of engine inlet [BTN-95-EIX95202638963] p 289 A95-76673 Integrated design of hypersonic waveriders including
Study of the droplet spray characteristics of a subsonic wind tunnel [BTN-95-EIX95182619235] p 271 A95-76661  DROPS (LIQUIDS) Study of the droplet spray characteristics of a subsonic wind tunnel [BTN-95-EIX95182619235] p 271 A95-76661  DRUGS Evaluation of neutron techniques for illicit substance detection	Nonlinear system guidance in the presence of transmission zero dynamics   NASA-TM-4661   p 309 N95-22804   E  EARTH ORBITS  Effects of satellite bunching on the probability of collision in geosynchronous orbit  BTN-95-EIX95152583276   p 298 A95-73577  EARTH SURFACE	INASA-CR-189141   p 316 N95-23792  ENGINE DESIGN Lycoming to test new engine core [HTN-95-41393] p 288 A95-76389 Aerodynamic design and analysis of a highly loaded turbine exhaust p 312 N95-23435 Phase 2: HGM air flow tests in support of HEX vane investigation p 312 N95-23438  ENGINE INLETS A new type of simulator for simulating the flow-field distortion of engine inlet [BTN-95-EIX95202638963] p 289 A95-76673 Integrated design of hypersonic waveriders including inlets and tailflins
Study of the droplet spray characteristics of a subsonic wind tunnel [BTN-95-EIX95182619235] p 271 A95-76661  DROPS (LIQUIDS) Study of the droplet spray characteristics of a subsonic wind tunnel [BTN-95-EIX95182619235] p 271 A95-76661  DRUGS Evaluation of neutron techniques for illicit substance detection [DE95-002988] p 300 N95-22764	Nonlinear system guidance in the presence of transmission zero dynamics [NASA-TM-4661] p 309 N95-22804   E  EARTH ORBITS  Effects of satellite bunching on the probability of collision in geosynchronous orbit [BTN-95-EIX95152583276] p 298 A95-73577  EARTH SURFACE  Thundercloud electric field modeling for the ionosphere-Earth region. 1: Dependence on cloud charge	INASA-CR-189141   p 316 N95-23792 ENGINE DESIGN Lycoming to test new engine core [HTN-95-41393   p 288 A95-76389 Aerodynamic design and analysis of a highly loaded turbine exhaust p 312 N95-23435 Phase 2: HGM air flow tests in support of HEX vane investigation p 312 N95-23438 ENGINE INLETS A new type of simulator for simulating the flow-field distortion of engine inlet [BTN-95-EIX95202638963] p 289 A95-76673 Integrated design of hypersonic waveriders including
Study of the droplet spray characteristics of a subsonic wind tunnel [BTN-95-EIX95182619235] p 271 A95-76661  DROPS (LIQUIDS) Study of the droplet spray characteristics of a subsonic wind tunnel [BTN-95-EIX95182619235] p 271 A95-76661  DRUGS Evaluation of neutron techniques for illicit substance detection	Nonlinear system guidance in the presence of transmission zero dynamics [NASA-TM-4661] p 309 N95-22804   E  EARTH ORBITS  Effects of satellite bunching on the probability of collision in geosynchronous orbit [BTN-95-EIX95152583276] p 298 A95-73577  EARTH SURFACE  Thundercloud electric field modeling for the ionosphere-Earth region. 1: Dependence on cloud charge distribution [HTN-95-41223] p 317 A95-75035  MAX-91: Polarimetric SAR results on Montespertoli	INASA-CR-189141   p 316 N95-23792  ENGINE DESIGN Lycoming to test new engine core [HTN-95-41393] p 288 A95-76389 Aerodynamic design and analysis of a highly loaded turbine exhaust p 312 N95-23435 Phase 2: HGM air flow tests in support of HEX vane investigation p 312 N95-23438  ENGINE INLETS A new type of simulator for simulating the flow-field distortion of engine inlet [BTN-95-EIX95202638963] p 289 A95-76673 Integrated design of hypersonic waveriders including inlets and tailfins [BTN-95-EIX95212645692] p 271 A95-76744  ENGINE MONITORING INSTRUMENTS Gearbox vibration diagnostic analyzer
Study of the droplet spray characteristics of a subsonic wind tunnel [BTN-95-EIX95182619235] p 271 A95-76661  DROPS (LIQUIDS) Study of the droplet spray characteristics of a subsonic wind tunnel [BTN-95-EIX95182619235] p 271 A95-76661  DRUGS Evaluation of neutron techniques for illicit substance detection [DE95-002988] p 300 N95-22764  DUCTED FLOW Flutter of an infinitely long panel in a duct [BTN-95-EIX95182619087] p 291 A95-75772	Nonlinear system guidance in the presence of transmission zero dynamics [NASA-TM-4661] p 309 N95-22804  E  EARTH ORBITS  Effects of satellite bunching on the probability of collision in geosynchronous orbit [BTN-95-EIX95152583276] p 298 A95-73577  EARTH SURFACE  Thundercloud electric field modeling for the ionosphere-Earth region. 1: Dependence on cloud charge distribution [HTN-95-41223] p 317 A95-75035 MAX-91: Polarimetric SAR results on Montespertolisite p 320 N95-23940	[NASA-CR-189141] p 316 N95-23792  ENGINE DESIGN Lycoming to test new engine core [HTN-95-41393] p 288 A95-76389 Aerodynamic design and analysis of a highly loaded turbine exhaust p 312 N95-23435 Phase 2: HGM air flow tests in support of HEX vane investigation p 312 N95-23438  ENGINE INLETS A new type of simulator for simulating the flow-field distortion of engine inlet [BTN-95-EIX95202638963] p 289 A95-76673 Integrated design of hypersonic waveriders including inlets and tailfins [BTN-95-EIX95212645692] p 271 A95-76744  ENGINE MONITORING INSTRUMENTS Gearbox vibration diagnostic analyzer [NASA-CR-189141] p 316 N95-23792
Study of the droplet spray characteristics of a subsonic wind tunnel [BTN-95-EIX95182619235] p 271 A95-76661  DROPS (LIQUIDS) Study of the droplet spray characteristics of a subsonic wind tunnel [BTN-95-EIX95182619235] p 271 A95-76661  DRUGS Evaluation of neutron techniques for illicit substance detection [DE95-002988] p 300 N95-22764  DUCTED FLOW Flutter of an infinitely long panel in a duct [BTN-95-EIX95182619087] p 291 A95-75772  DUCTS	Nonlinear system guidance in the presence of transmission zero dynamics [NASA-TM-4661] p 309 N95-22804  E  EARTH ORBITS  Effects of satellite bunching on the probability of collision in geosynchronous orbit [BTN-95-EIX95152583276] p 298 A95-73577  EARTH SURFACE  Thundercloud electric field modeling for the ionosphere-Earth region. 1: Dependence on cloud charge distribution [HTN-95-41223] p 317 A95-75035 MAX-91: Polarimetric SAR results on Montespertolisite p 320 N95-23940  ECONOMIC ANALYSIS	INASA-CR-189141   p 316 N95-23792  ENGINE DESIGN Lycoming to test new engine core [HTN-95-41393] p 288 A95-76389 Aerodynamic design and analysis of a highly loaded turbine exhaust p 312 N95-23435 Phase 2: HGM air flow tests in support of HEX vane investigation p 312 N95-23438  ENGINE INLETS A new type of simulator for simulating the flow-field distortion of engine inlet [BTN-95-EIX95202638963] p 289 A95-76673 Integrated design of hypersonic waveriders including inlets and tailfins [BTN-95-EIX95212645692] p 271 A95-76744  ENGINE MONITORING INSTRUMENTS Gearbox vibration diagnostic analyzer [NASA-CR-189141] p 316 N95-23792  ENGINE NOISE
Study of the droplet spray characteristics of a subsonic wind tunnel [BTN-95-EIX95182619235] p 271 A95-76661  DROPS (LIQUIDS)  Study of the droplet spray characteristics of a subsonic wind tunnel [BTN-95-EIX95182619235] p 271 A95-76661  DRUGS  Evaluation of neutron techniques for illicit substance detection [DE95-002988] p 300 N95-22764  DUCTED FLOW  Flutter of an infinitely long panel in a duct [BTN-95-EIX95182619087] p 291 A95-75772  DUCTS  The use of cowl camber and taper to reduce rotor/stator	Nonlinear system guidance in the presence of transmission zero dynamics [NASA-TM-4661] p 309 N95-22804  E  EARTH ORBITS  Effects of satellite bunching on the probability of collision in geosynchronous orbit [BTN-95-EIX95152583276] p 298 A95-73577  EARTH SURFACE  Thundercloud electric field modeling for the ionosphere-Earth region. 1: Dependence on cloud charge distribution [HTN-95-41223] p 317 A95-75035 MAX-91: Polarimetric SAR results on Montespertolisite p 320 N95-23940  ECONOMIC ANALYSIS  Design constraints in the payload-range diagram of	INASA-CR-189141   p 316 N95-23792  ENGINE DESIGN Lycoming to test new engine core [HTN-95-41393]
Study of the droplet spray characteristics of a subsonic wind tunnel [BTN-95-EIX95182619235] p 271 A95-76661  DROPS (LIQUIDS) Study of the droplet spray characteristics of a subsonic wind tunnel [BTN-95-EIX95182619235] p 271 A95-76661  DRUGS Evaluation of neutron techniques for illicit substance detection [DE95-002988] p 300 N95-22764  DUCTED FLOW Flutter of an infinitely long panel in a duct [BTN-95-EIX95182619087] p 291 A95-75772  DUCTS	Nonlinear system guidance in the presence of transmission zero dynamics [NASA-TM-4661] p 309 N95-22804  E  EARTH ORBITS  Effects of satellite bunching on the probability of collision in geosynchronous orbit [BTN-95-EIX95152583276] p 298 A95-73577  EARTH SURFACE  Thundercloud electric field modeling for the ionosphere-Earth region. 1: Dependence on cloud charge distribution [HTN-95-41223] p 317 A95-75035 MAX-91: Polarimetric SAR results on Montespertolisite p 320 N95-23940  ECONOMIC ANALYSIS	INASA-CR-189141   p 316 N95-23792  ENGINE DESIGN Lycoming to test new engine core [HTN-95-41393] p 288 A95-76389 Aerodynamic design and analysis of a highly loaded turbine exhaust p 312 N95-23435 Phase 2: HGM air flow tests in support of HEX vane investigation p 312 N95-23438  ENGINE INLETS A new type of simulator for simulating the flow-field distortion of engine inlet [BTN-95-EIX95202638963] p 289 A95-76673 Integrated design of hypersonic waveriders including inlets and tailfins [BTN-95-EIX95212645692] p 271 A95-76744  ENGINE MONITORING INSTRUMENTS Gearbox vibration diagnostic analyzer [NASA-CR-189141] p 316 N95-23792  ENGINE NOISE

Supersonic jet noise reductions predicted with increased	Euler Technology Assessment program for preliminary	Enhancement of F/A-18 operational flight
jet spreading rate   NASA-TM-106872   p 323 N95-23178	aircraft design employing SPLITFLOW code with Cartesian unstructured grid method	measurements: Data report for phase 1 (DSTO-TR-0049) p 286 N95-23666
ENGINE PARTS	NASA-CR-4649   p 273 N95-22917	FABRICATION
Compliant interlayer	Euler technology assessment for preliminary aircraft	Idealized textile composites for experimental/analytical
IBTN-95-EIX951425624011 p 304 A95-73439 Influence of backup bearings and support structure	design employing OVERFLOW code with multiblock	correlation p 301 N95-23277 FAIL-SAFE SYSTEMS
dynamics on the behavior of rotors with active supports	structured-grid method [NASA-CR-4651] p 273 N95-23095	Residual strength of thin panels with cracks
[NASA-CR-197438] p 310 N95-23190	An assessment of viscous effects in computational	p 311 N95-23311
Evaluation of thermal barrier and PS-200 self-lubricating coatings in an air-cooled rotary engine	simulation of benign and burst vortex flows on generic	FAILURE ANALYSIS  New failure detection approach and its application to
[NASA-CR-195445] p 289 N95-23222	fighter wind-tunnel models using TEAM code [NASA-CR-4650] p 273 N95-23185	GPS autonomous integrity monitoring
ENGINE TESTS	Convergence acceleration of implicit schemes in the	[BTN-95-EIX95202637613] p 279 A95-76676
Phase 2: HGM air flow tests in support of HEX vane investigation p 312 N95-23438	presence of high aspect ratio grid cells	Handling qualities of the High Speed Civil Transport p 294 N95-23325
investigation p 312 N95-23438 Impeller flow field characterization with a laser two-focus	p 313 N95-23446	FAILURE MODES
velocimeter p 313 N95-23440	Cavitation modeling in Euler and Navier-Stokes codes p 315 N95-23630	Mechanical system reliability and risk assessment
ENGINEERING	User's guide for ECAP2D: An Euler unsteady	[BTN-95-EIX95142553046] p 304 A95-73452 Residual strength of thin panels with cracks
1994 NASA-HU American Society for Engineering Education (ASEE) Summer Faculty Fellowship Program	aerodynamic and aeroelastic analysis program for two	p 311 N95-23311
[NASA-CR-194972] p 325 N95-23276	dimensional oscillating cascades, version 1.0	FAN BLADES
ENTHALPY	[NASA-CR-189146] p 316 N95-24189 EUROPEAN AIRBUS	H-76B fantail demonstrater composite fan blade
Shock tunnel measurements of hypervelocity blunted cone drag	Automatic riveting cell for commercial aircraft floor grid	fabrication [HTN-95-80856] p 283 A95-75098
[BTN-95-EIX95152577606] p 305 A95-73477	assembly	FAST NEUTRONS
ENTRY GUIDANCE (STS)	[BTN-95-EIX95182617807] p 261 A95-75752	Evaluation of neutron techniques for illicit substance
Shuttle entry guidance revisited using nonlinear geometric methods	SEM representation of the early and late time fields	detection [DE95-002988] p 300 N95-22764
[BTN-95-EIX95182619144] p 299 A95-76621	scattered from wire targets	FASTENERS
ENVIRONMENT EFFECTS	[BTN-94-EIX94381353142] p 306 A95-74496	Eddy current detection of pitting corrosion around
Modeling aerosol emissions from the combustion of composite materials p 301 N95-23038	EXHAUST DIFFUSERS	fastener holes p 315 N95-23507  FATIGUE (MATERIALS)
ENVIRONMENT PROTECTION	Design of a variable area diffuser for a 15-inch Mach 6 open-jet tunnel p 297 N95-23309	Growth of multiple cracks and their linkup in a fuselage
Aircraft stripping and painting	EXHAUST EMISSION	lap joint
[BTN-95-EIX95182617810] p 300 A95-75755	Trajectory modeling of emissions from lower	[BTN-95-EIX95142553047] p 286 A95-73451
Corrosion in service experience with aircraft in France p 303 N95-23518	stratospheric aircraft IHTN-95-41219 p 317 A95-75031	Validation of an effective flat cruciform-shaped specimen to study CFRP composite laminates under biaxial
ENVIRONMENT SIMULATION	[HTN-95-41219] p 317 A95-75031 EXHAUST GASES	loading
Hypersonic convective heat transfer over 140-deg blunt	Predicting exhaust plume boundaries with supersonic	[BTN-95-EIX95152584677] p 282 A95-73589
cones in different gases [BTN-95-EIX95152583253] p 306 A95-73554	external flows	Evaluation of advanced aerospace materials by depth sensing indentation and scratch methods
EQUATIONS OF MOTION	[BTN-95-EIX95152583258] p 297 A95-73559	[BTN-95-EIX95152584678] p 282 A95-73590
Functional dependence of trajectory dispersion on initial	In situ observations in aircraft exhaust plumes in the lower stratosphere at midiatitudes	Review of aeronautical fatigue investigation in the
condition errors [BTN-95-EIX95152583263] p 298 A95-73564	[HTN-95-A0862] p 318 A95-76266	Netherlands during the period March 1991-March 1993 [PB95-139184] p 285 N95-23161
Analytical solution and parameter estimation of projectile	Sensitivity of two-dimensional model predictions of	Review of some results of the author's fatigue
dynamics	ozone response to stratospheric aircraft: An update [HTN-95-A0863] p 318 A95-76267	investigations with applications in engineering and material
[BTN-95-EIX95212645695] p 272 A95-76747 Moving mass trim control for aerospace vehicles	NTS-spill test facility wind tunnel exhaust plume	science
[DE95-002602] p 299 N95-23532	characterization	[TAE-698] p 316 N95-23662 FATIGUE LIFE
EQUATIONS OF STATE	[DE95-003630] p 297 N95-24019	Growth of multiple cracks and their linkup in a fuselage
Application of a control-volume-based finite-element formulation to the shock tube problem	EXHAUST SYSTEMS Aerodynamic design and analysis of a highly loaded	tap joint
[BTN-95-EIX95182619099] p 295 A95-76584	turbine exhaust p 312 N95-23435	[BTN-95-EIX95142553047] p 286 A95-73451
On-line, adaptive state estimator for active noise	EXHAUST VELOCITY	Review of some results of the author's fatigue investigations with applications in engineering and material
control p 322 N95-23308 EROSION	Aerodynamic design and analysis of a highly loaded turbine exhaust p 312 N95-23435	science
Erosion of dust-filtered helicopter turbine engines. Part	EXPANSION	[TAE-698] p 316 N95-23662
1: Basic theoretical considerations	Effects of expansions on a supersonic boundary layer:	FATIGUE TESTS Growth of multiple cracks and their linkup in a fuselage
BTN-95-EIX95182619222   p 288 A95-76648 Erosion of dust-filtered helicopter turbine engines. Part	Surface pressure measurements	lap joint
2: Erosion reduction	[BTN-95-EIX95142553036] p 263 A95-73462 EXPERT SYSTEMS	[BTN-95-EIX95142553047] p 286 A95-73451
[BTN-95-EIX95182619223] p 289 A95-76649	Artificial intelligence for turboprop engine maintenance	Validation of an effective flat cruciform-shaped specimen to study CFRP composite laminates under biaxial
Life prediction of helicopter engines fitted with dust filters	[BTN-95-EIX95182617812] p 288 A95-75757	loading
[BTN-95-EIX95182619224] p 289 A95-76650	EXPOSURE The corrosion and protection of advanced aluminium -	[BTN-95-EIX95152584677] p 282 A95-73589
ERROR ANALYSIS	lithium airframe alloys p 302 N95-23497	Evaluation of advanced aerospace materials by depth
Enhancing filter robustness in cascaded GPS-INS integrations	Corrosion protection measures for CFC/metal joints of	sensing indentation and scratch methods [BTN-95-EIX95152584678] p 282 A95-73590
[BTN-95-EIX95142555475] p 278 A95-73435	fuel integral tank structures of advanced military aircraft p 303 N95-23510	Fatigue strength of high-temperature alloys under
Covariance analysis of strapdown INS considering	EXTERNAL STORE SEPARATION	conditions of cyclic temperature variation. Communication
gyrocompass characteristics	A CFD study of complex missile and store configurations	1: Experimental procedure and results [BTN-94-EIX94401363884] p 307 A95-75516
BTN-95-EIX95202637592  p 279 A95-76697 ERROR CORRECTING CODES	in relative motion [NASA-CR-197912] p 285 N95-22949	FAULT DETECTION
Improved version of the Naval Surface Warfare Center	EXTERNAL STORES	Evaluation of advanced aerospace materials by depth
aeroprediction code (AP93)	Aerodynamic characteristics of external store	sensing indentation and scratch methods
[BTN-95-EIX95152583260] p 267 A95-73561	configurations at low speeds [BTN-95-EIX95182619230] p 271 A95-76656	[BTN-95-EIX95152584678] p 282 A95-73590 ATE enabling technologies
ESTIMATING Improving prediction: The incorporation of simplified	EXTRACTION	[BTN-95-EIX95172595294] p 287 A95-75718
rotor dynamics in a mathematical model of the bell	On-line, adaptive state estimator for active noise	Condition monitoring and diagnostics
412HP	control p 322 N95-23308 EXTREMELY HIGH FREQUENCIES	[BTN-95-EIX95182617811] p 261 A95-75756
[BTN-95-EIX95152584679] p 282 A95-73591  Real-time estimation of atmospheric turbulence severity	Flight test evaluation of a 35 GHz forward looking	New failure detection approach and its application to GPS autonomous integrity monitoring
from in-situ aircraft measurements	altimeter for terrain avoidance	[BTN-95-EIX95202637613] p 279 A95-76676
[BTN-95-EIX95182619231] p 319 A95-76657	[BTN-95-EIX95212641071] p 287 A95-76736	FAULT TREES
Rationale for the Modular Air-system Vulnerability	F	Rationale for the Modular Air-system Vulnerability
Estimation Network (MAVEN) methodology (AD-A285797) p 284 N95-22510	Г	Estimation Network (MAVEN) methodology {AD-A285797} p 284 N95-22510
EULER EQUATIONS OF MOTION	F-18 AIRCRAFT	FEASIBILITY ANALYSIS
Limit cycle phenomena in computational transonic	Forebody flow control on a full-scale F/A-18 aircraft	Inner loop flight control for the High-Speed Civil
aeroelasticity  BTN-95-EIX95152582317  p 264 A95-73520	(BTN-95-EIX95152582333) p 281 A95-73535	Transport p 293 N95-23314 FEEDBACK CONTROL
Aeroacoustic model for weak shock waves based on	Analysis of the longitudinal handling qualities and pilot-induced-oscillation tendencies of the	Dynamical instability of the aerogravity assist
Burgers equation	High-Angle-of-Attack Research Vehicle (HARV)	maneuver
[BTN-95-EIX95182619076] p 269 A95-75761	p 293 N95-23297	[BTN-95-EIX95152583282] p 298 A95-73583

Analytical solution for controls, heats, and states of flight	FINITE VOLUME METHOD	Identification of higher order helicopter dynamics using
trajectories	A time-accurate finite volume method valid at all flow	linear modeling methods
[BTN-95-EIX95152583286] p 282 A95-73587	velocities p 314 N95-23447	[HTN-95-80851] p 290 A95-75093
Real-time navigation using the global positioning	FINS	Effects of high order dynamics on helicopter flight control
system	Integrated design of hypersonic waveriders including	law design
[BTN-95-EIX95172595298] p 279 A95-75714	inlets and tailfins	[HTN-95-80852] p 290 A95-75094
Aeroelastic vehicle multivariable control synthesis with	BTN-95-EIX95212645692  p 271 A95-76744 FIRES	Investigation of the effects of bandwidth and time delay on helicopter roll-axis handling qualities
analytical robustness evaluation [BTN-95-EIX95182619115] p 321 A95-76592	Rationale for the Modular Air-system Vulnerability	[HTN-95-80853] p 290 A95-75095
Multivariable stability and robustness of sequentially	Estimation Network (MAVEN) methodology	Integrated flight/propulsion control for helicopters
designed feedback systems	[AD-A285797] p 284 N95-22510	[HTN-95-80854] p 290 A95-75096
[BTN-95-EIX95182619125] p 322 A95-76602	Aircraft fires, smoke toxicity, and survival: An overview	Cypher moves toward autonomous flight
H-infinity helicopter flight control law design with and	[DOT/FAA/AM-95/8] p 277 N95-24024	[HTN-95-41394] p 283 A95-76390
without rotor state feedback	FLAPS (CONTROL SURFACES) Study of an airfoil with a flap and spoiler	Functional agility metrics and optimal trajectory
[BTN-95-EIX95182619129] p 291 A95-76606 Performance of the 0.3-meter transonic cryogenic tunnel	[BTN-95-EIX95152582327] p 265 A95-73530	analysis [BTN-95-EIX95182619121] p 321 A95-76598
with air, nitrogen, and sulfur hexalluoride media under	FLAT PLATES	H-infinity helicopter flight control law design with and
closed loop automatic control	Coupled FEM-BEM approach for mean flow effects on	without rotor state feedback
[NASA-CR-195052] p 310 N95-23257	vibro-acoustic behavior of planar structures	[BTN-95-EIX95182619129] p 291 A95-76606
System identification of the Large-Angle Magnetic	BTN-95-EIX95152577587  p 263 A95-73495	Automatic guidance and control for helicopter obstacle
Suspension Test Fixture (LAMSTF) p 296 N95-23299	Three-dimensional structure of a supersonic jet	avoidance IBTN-95-EIX95182619130 I p 291 A95-76607
On-line, adaptive state estimator for active noise control p 322 N95-23308	impinging on an inclined plate [BTN-95-EIX95152583259] p 267 A95-73560	[BTN-95-EIX95182619130] p 291 A95-76607 Direct-lift design strategy for longitudinal control of
Feedback control laws for highly maneuverable	Crossflow instability control on a swept-wing: Preliminary	hypersonic aircraft
aircraft	studies p 274 N95-23283	[BTN-95-EIX95182619131] p 291 A95-76608
[NASA-CR-197944] p 295 N95-23410	FLAT SURFACES	Shuttle entry guidance revisited using nonlinear
IBER COMPOSITES	Validation of an effective flat cruciform-shaped specimen	geometric methods
Validation of an effective flat cruciform-shaped specimen	to study CFRP composite laminates under biaxial	[BTN-95-EIX95182619144] p 299 A95-76621
to study CFRP composite laminates under biaxial	loading  BTN-95-EIX95152584677  p 282 A95-73589	Attainable moments for the constrained control
loading IBTN-95-EIX95152584677   p 282 A95-73589	FLEXIBLE WINGS	allocation problem [BTN-95-EIX95182619149] p 322 A95-76626
Corrosion protection measures for CFC/metal joints of	Experimental evaluation of a box beam specifically	Application of Navier-Stokes aeroelastic methods to
fuel integral tank structures of advanced military aircraft	tailored for chordwise deformation	improve fighter wing maneuver performance
p 303 N95-23510	[BTN-95-EIX95182619088] p 283 A95-75773	[BTN-95-EIX95182619218] p 284 A95-76644
IELD OF VIEW	Summary of an active flexible wing program	Robustly stable preliminary control systems design for
Design of wide angle head up displays for synthetic	[BTN-95-EIX95182619209] p 283 A95-76635	the YF-16 CCV aircraft
VISION	Application of transonic small disturbance theory to the active flexible wing model	[BTN-95-EIX95202637608] p 292 A95-76681 Virtual reality flight control display with
[BTN-95-EIX95212641070] p 287 A95-76735	[BTN-95-EIX95182619210] p 270 A95-76636	Virtual reality flight control display with six-degree-of-freedom controller and spherical orientation
Method for the prediction of the onset of wing rock	Simulation and model reduction for the active flexible	overlay
[BTN-95-EIX95152582342] p 282 A95-73544	wing program	[NASA-CASE-NPO-18733-1-CU] p 288 N95-22578
Design and multifunction tests of a frequency	BTN-95-EIX95182619211  p 295 A95-76637	Flight test of the X-29A at high angle of attack: Flight
domain-based active flutter suppression system	Multiple-function digital controller system for active	dynamics and controls
[BTN-95-EIX95182619215] p 292 A95-76641	flexible wing wind-tunnel model	[NASA-TP-3537] p 284 N95-22806
Application of Navier-Stokes aeroelastic methods to improve fighter wing maneuver performance	BTN-95-EIX95182619212  p 322 A95-76638 On-line analysis capabilities developed to support the	Analysis of the longitudinal handling qualities and pilot-induced-oscillation tendencies of the
BTN-95-EIX95182619218  p 284 A95-76644	active flexible wing wind-tunnel tests	High-Angle-of-Attack Research Vehicle (HARV)
An assessment of viscous effects in computational	BTN-95-EIX95182619213  p 296 A95-76639	p 293 N95-23297
simulation of benign and burst vortex flows on generic	Flutter suppression control law design and testing for	Inner loop flight control for the High-Speed Civil
fighter wind-tunnel models using TEAM code	the active flexible wing	Transport p 293 N95-23314
[NASA-CR-4650] p 273 N95-23185	[BTN-95-EIX95182619214] p 292 A95-76640	Differential GPS and system integration of the Low
ILTRATION	Flutter suppression for the active flexible wing: A classical design	Visibility Landing and Surface Operations (LVLASO)
Erosion of dust-filtered helicopter turbine engines. Part 1: Basic theoretical considerations	[BTN-95-EIX95182619216] p 292 A95-76642	demonstration p 280 N95-23318 Engines-only flight control system
IBTN-95-EIX951826192221 p 288 A95-76648	Rolling maneuver load alleviation using active controls	[NASA-CASE-ARC-11944-1] p 294 N95-23389
Erosion of dust-filtered helicopter turbine engines. Part	[BTN-95-EIX95182619217] p 270 A95-76643	Aerodynamic surface distension system for high angle
2: Erosion reduction	Response of a nonrotating rotor blade to lateral	of attack forebody vortex control
[BTN-95-EIX95182619223] p 289 A95-76649	turbulence. Part 1: Theory	[NASA-CASE-ARC-11979-1] p 286 N95-23390
Life prediction of helicopter engines fitted with dust	[BTN-95-EIX95182619228] p 284 A95-76654 Flutter analysis of composite box beams	Feedback control laws for highly maneuverable aircraft
filters  BTN-95-EIX95182619224  p 289 A95-76650	[NASA-CR-197931] p 294 N95-23392	[NASA-CR-197944] p 295 N95-23410
INITE DIFFERENCE THEORY	FLIGHT ALTITUDE	Aerodynamic flight control to increase payload capability
Higher-order viscous shock-layer solutions for	Aerodynamic characteristics of a hypersonic viscous	of future launch vehicles
high-altitude flows	optimized waverider at high altitudes	[NASA-CR-197704] p 300 N95-24032
[BTN-95-EIX95152583255] p 306 A95-73556	[BTN-95-EIX95152583251] p 266 A95-73552	FLIGHT CREWS
Aeroacoustic model for weak shock waves based on Burgers equation	FLIGHT CHARACTERISTICS Polar Patrol Balloon	Aircraft accident report. Runway overrun following rejected takeoff. Continental airlines flight 795, McDonnell
[BTN-95-EIX95182619076] p 269 A95-75761	[BTN-95-EIX95152582318] p 316 A95-73521	Douglas MD-82, N18835, LaGuardia Airport, Flushing, NY,
INITE ELEMENT METHOD	Analytical solution for controls, heats, and states of flight	2 March 1994
Adaptive finite element method for turbulent flow near	trajectories	[PB95-910401] p 277 N95-23609
a propeller .	[BTN-95-EIX95152583286] p 282 A95-73587	FLIGHT HAZARDS
[BTN-95-EIX95142553038] p 305 A95-73460	Real-time estimation of atmospheric turbulence severity	Thundercloud electric field modeling for the
Coupled FEM-BEM approach for mean flow effects on	from in-situ aircraft measurements [BTN-95-EIX95182619231] p 319 A95-76657	ionosphere-Earth region. 1: Dependence on cloud charge distribution
vibro-acoustic behavior of planar structures  BTN-95-EIX95152577587  p 263 A95-73495	· · · · · · · · · · · · · · · · · · ·	[HTN-95-41223] p 317 A95-75035
Static aeroelastic characteristics of a composite wing	Flight test of the X-29A at high angle of attack: Flight dynamics and controls	Optimal lateral-escape maneuvers for microburst
[BTN-95-EIX95152582340] p 282 A95-73542	[NASA-TP-3537] p 284 N95-22806	encounters during final approach
Thermal force modeling for global positioning system	Analysis of the longitudinal handling qualities and	[BTN-95-EIX95182619127] p 276 A95-76604
satellites using the finite element method	pilot-induced-oscillation tendencies of the	FLIGHT INSTRUMENTS
[BTN-95-EIX95152583270] p 278 A95-73571	High-Angle-of-Attack Research Vehicle (HARV)	Design of wide angle head up displays for synthetic
Finite element model for a flexible non-symmetric rotor on distributed bearing: A stability study	p 293 N95-23297	vision (BTN-95-EIX95212641070) p 287 A95-76735
BTN-94-EIX94381352212  p 306 A95-74612	Preparation of course materials: Elementary	TRISTAR 1: Evaluation methods for testing head-up
Application of a control-volume-based finite-element	mathematics of powered flight p 324 N95-23320	display (HUD) flight symbology
formulation to the shock tube problem	Handling qualities of the High Speed Civil Transport p 294 N95-23325	[NASA-TM-4665] p 288 N95-24030
[BTN-95-EIX95182619099] p 295 A95-76584	p 294 N95-23325 FLIGHT CONDITIONS	FLIGHT MANAGEMENT SYSTEMS
Effect of curvature in the numerical simulation of an	Direct adaptive performance optimization of subsonic	Pilot Weather Advisor system
electrothermal de-icer pad	transports: A periodic perturbation technique	[BTN-95-EIX95152582314] p 316 A95-73517 FLIGHT MECHANICS
[BTN-95-EIX95182619219] p 276 A95-76645 Idealized textile composites for experimental/analytical	[NASA-TM-4676] p 284 N95-22829	Functional dependence of trajectory dispersion on initial
correlation p 301 N95-23277	Control of flow separation in airfoil/wing design	condition errors
Residual strength of thin panels with cracks	applications p 274 N95-23294	[BTN-95-EIX95152583263] p 298 A95-73564
p 311 N95-23311	FLIGHT CONTROL	Aerodynamics of the Shuttle Orbiter at high altitudes
A multibody/finite element analysis approach for	Dynamical instability of the aerogravity assist	[BTN-95-EIX95182617454] p 298 A95-75725
modeling of crash dynamic responses	maneuver	Kinematics and aerodynamics of velocity-vector roll

[BTN-95-EIX95152583282]

p 298 A95-73583

[BTN-95-EIX95182619126]

modeling of crash dynamic responses [NIAR-94-3] p 277 N95-24050

p 291 A95-76603

FLIGHT OPERATIONS	Supersonic near-wake afterbody boattailing effects on	FLUID BOUNDARIES
Pilot Weather Advisor system [BTN-95-EIX95152582314] p 316 A95-73517	axisymmetric bodies [BTN-95-EIX95182617465] p 268 A95-75736	Predicting exhaust plume boundaries with supersonic external flows
Guidance and control requirements for high-speed	Transient structure of vortex breakdown on a delta	[BTN-95-EIX95152583258] p 297 A95-73559
Rollout and Turnoff (ROTO)	wing	FLUID DYNAMICS
[NASA-CR-195026] p 292 N95-22674	[BTN-95-EIX95182619073] p 268 A95-75758	Possible effects of CO2 increase on the high-speed civil
Oceanic operations: An authoritative guide to oceanic	Observations on using experimental data as boundary	transport impact on ozone
operations [FAA-AFS-550] p 277 N95-24065	conditions for computations	[HTN-95-60779] p 317 A95-75976
FLIGHT PATHS	[BTN-95-EIX95182619103] p 321 A95-76588	Transport of exhaust products in the near trail of a jet engine under atmospheric conditions
Trajectory modeling of emissions from lower	Simple method of supersonic flow visualization using watertable	[HTN-95-91421] p 319 A95-77334
stratosphenc aircraft	BTN-95-EIX95182619105  p 269 A95-76590	High-lift flow-physics flight experiments on a subsonic
[HTN-95-41219] p 317 A95-75031 Optimal lateral-escape maneuvers for microburst	Tracking of raindrops in flow over an airfoil	civil transport aircraft (B737-100) p 275 N95-23333
encounters during final approach	[BTN-95-EIX95182619221] p 308 A95-76647	FLUID FLOW
[BTN-95-EIX95182619127] p 276 A95-76604	Aerodynamics of a finite wing with simulated ice	Holographic interferometric tomography for reconstructing flow fields p 310 N95-23287
Analytical solution and parameter estimation of projectile	[BTN-95-EIX95182619227] p 270 A95-76653	Phase 2: HGM air flow tests in support of HEX vane
dynamics	Neural network prediction of three-dimensional unsteady separated flowfields	investigation p 312 N95-23438
[BTN-95-EIX95212645695] p 272 A95-76747 Nonlinear system guidance in the presence of	BTN-95-EIX95182619232  p 308 A95-76658	A time-accurate finite volume method valid at all flow
transmission zero dynamics	Flow visualization studies of VTOL aircraft models during	velocities p 314 N95-23447
(NASA-TM-4661) p 309 N95-22804	Hover in ground effect	FLUID-SOLID INTERACTIONS
Engines-only flight control system	[NASA-TM-108860] p 272 N95-22666	Structural acoustic calculations in the low-frequency
[NASA-CASE-ARC-11944-1] p 294 N95-23389 FLIGHT RECORDERS	A CFD study of complex missile and store configurations	range  BTN-95-EIX95152582336  p 323 A95-73538
The role of flight progress strips in en route air traffic	in relative motion [NASA-CR-197912] p 285 N95-22949	FLUTTER
control: A time-series analysis	Mach 10 computational study of a three-dimensional	Postinstability behavior of a two-dimensional airfoil with
[DOT/FAA/AM-95/4] p 280 N95-23565	scramjet inlet flow field	a structural nonlinearity
FLIGHT SAFETY	[NASA-TM-4602] p 309 N95-23015	[BTN-95-EIX95152582337] p 266 A95-73539
Automatic guidance and control for helicopter obstacle avoidance	Experimental results for a hypersonic nozzle/afterbody flow field	Flutter of an infinitely long panel in a duct
[BTN-95-EIX95182619130] p 291 A95-76607	[NASA-TM-4638] p 274 N95-23250	[BTN-95-EIX95182619087] p 291 A95-75772
Additional improvements to the NASA Lewis ice	Holographic interferometric tomography for	Multirate flutter suppression system design for a model wing
accretion code LEWICE	reconstructing flow fields p 310 N95-23287	[BTN-95-EIX95182619132] p 292 A95-76609
[NASA-TM-106849] p 309 N95-22669 Oklahoma City air logistics center (USAF) aging aircraft	Three-dimensional unsteady flow calculations in an advanced gas generator turbine p 312 N95-23425	Summary of an active flexible wing program
corrosion program p 262 N95-23519	advanced gas generator turbine p 312 N95-23425 A study of the vortex flow over 76/40-deg double-delta	[BTN-95-EIX95182619209] p 283 A95-76635
A multibody/finite element analysis approach for	wing	Multiple-function digital controller system for active
modeling of crash dynamic responses	[NASA-CR-195032] p 314 N95-23466	flexible wing wind-tunnel model [BTN-95-EIX95182619212] p 322 A95-76638
NIAR-94-3   p 277 N95-24050   FLIGHT SIMULATION	Validation of a Computational Fluid Dynamics (CFD)	Flutter suppression control law design and testing for
Virtual reality flight control display with	code for supersonic axisymmetric base flow p 315 N95-23652	the active flexible wing
six-degree-of-freedom controller and spherical orientation	FLOW MEASUREMENT	BTN-95-EIX95182619214  p 292 A95-76640
overlay	Time-of-flight mass spectrometer for impulse facilities	Flutter suppression for the active flexible wing: A
[NASA-CASE-NPO-18733-1-CU] p 288 N95-22578	[BTN-95-EIX95142553057] p 262 A95-73441	classical design [BTN-95-EIX95182619216] p 292 A95-76642
Direct adaptive performance optimization of subsonic transports: A periodic perturbation technique	Flow structure in the wake of a wishbone vortex generator	[BTN-95-EIX95182619216] p 292 A95-76642 Flutter analysis of composite box beams
[NASA-TM-4676] p 284 N95-22829	BTN-95-EIX95142553044  p 304 A95-73454	[NASA-CR-197931] p 294 N95-23392
Review of aeronautical fatigue investigation in the	Real-time estimation of atmospheric turbulence severity	FLUTTER ANALYSIS
Netherlands during the period March 1991-March 1993	from in-situ aircraft measurements	Application of transonic small disturbance theory to the
[PB95-139184] p 285 N95-23161	[BTN-95-EIX95182619231] p 319 A95-76657 Impeller flow field characterization with a laser two-focus	active flexible wing model
Development of qualification guidelines for personal computer-based aviation training devices	velocimeter p 313 N95-23440	[BTN-95-EIX95182619210] p 270 A95-76636
[DOT/FAA/AM-95/6] p 323 N95-23603	FLOW STABILITY	Flutter analysis of composite box beams [NASA-CR-197931] p 294 N95-23392
FLIGHT SIMULATORS	A time-accurate finite volume method valid at all flow	FOIL BEARINGS
Simulation of turbulent fluctuations	velocities p 314 N95-23447 FLOW VELOCITY	Influence of backup bearings and support structure
[BTN-95-EIX95142553041] p 304 A95-73457	Flow structure in the wake of a wishbone vortex	dynamics on the behavior of rotors with active supports
FLIGHT TESTS	generator	[NASA-CR-197438] p 310 N95-23190
Flight test evaluation of a 35 GHz forward looking altimeter for terrain avoidance	[BTN-95-EIX95142553044] p 304 A95-73454	FOREBODIES Forebody flow control on a full-scale F/A-18 aircraft
[BTN-95-EIX95212641071] p 287 A95-76736	Simulation of turbulent fluctuations	(BTN-95-EIX95152582333) p 281 A95-73535
2 micron LIDAR for laser-based remote sensing: Flight	[BTN-95-EIX95142553041] p 304 A95-73457 Effects of expansions on a supersonic boundary layer:	Convective and radiative heat transfer analysis for the
demonstration and application survey	Surface pressure measurements	fire 2 forebody
[BTN-95-EIX95212641072] p 319 A95-76737	[BTN-95-EIX95142553036] p 263 A95-73462	[BTN-95-EIX95182617460] p 268 A95-75731
Flight test of the X-29A at high angle of attack: Flight dynamics and controls	Supersonic axisymmetric conical flow solutions for	Review and development of base pressure and base heating correlations in supersonic flow
[NASA-TP-3537] p 284 N95-22806		
[14A3A-17-3337] D 204 1433-22000	different ratios of specific heats IBTN-95-EIX951525832831 p 306 A95-73584	[BTN-95-EIX95212645688] p 271 A95-76740
High-lift flow-physics flight experiments on a subsonic	[BTN-95-EIX95152583283] p 306 A95-73584 Real-time estimation of atmospheric turbulence severity	
High-lift flow-physics flight experiments on a subsonic civil transport aircraft (B737-100) p 275 N95-23333	[BTN-95-EIX95152583283] p 306 A95-73584 Real-time estimation of atmospheric turbulence severity from in-situ aircraft measurements	[BTN-95-EIX95212645688] p 271 A95-76740 Aerodynamic surface distension system for high angle of attack forebody vortex control
High-lift flow-physics flight experiments on a subsonic civil transport aircraft (B737-100) p 275 N95-23333 TRISTAR 1: Evaluation methods for testing head-up	[BTN-95-EIX95152583283] p 306 A95-73584 Real-time estimation of atmospheric turbulence severity from in-situ aircraft measurements [BTN-95-EIX95182619231] p 319 A95-76657	BTN-95-EIX95212645688  p 271 A95-76740 Aerodynamic surface distension system for high angle of attack forebody vortex control  NASA-CASE-ARC-11979-1  p 286 N95-23390
High-lift flow-physics flight experiments on a subsonic civil transport aircraft (B737-100) p 275 N95-23333 TRISTAR 1: Evaluation methods for testing head-up display (HUD) flight symbology	[BTN-95-EIX95152583283] p 306 A95-73584 Real-time estimation of atmospheric turbulence severity from in-situ aircraft measurements [BTN-95-EIX95182619231] p 319 A95-76657 Phase 2: HGM air flow tests in support of HEX vane	[BTN-95-EIX95212645688] p 271 A95-76740 Aerodynamic surface distension system for high angle of attack forebody vortex control [NASA-CASE-ARC-11979-1] p 286 N95-23390 FRAGMENTS
High-lift flow-physics flight experiments on a subsonic civil transport aircraft (B737-100) p 275 N95-2333 TRISTAR 1: Evaluation methods for testing head-up display (HUD) flight symbology [NASA-TM-4665] p 288 N95-24030	[BTN-95-EIX95152583283] p 306 A95-73584 Real-time estimation of atmospheric turbulence severity from in-situ estirati measurements [BTN-95-EIX95182619231] p 319 A95-76657 Phase 2: HGM air flow tests in support of HEX vane investigation p 312 N95-23438	[BTN-95-EIX95212645688] p 271 A95-76740 Aerodynamic surface distension system for high angle of attack forebody vortex control [NASA-CASE-ARC-11979-1] p 286 N95-23390 FRAGMENTS Rationale for the Modular Air-system Vulnerability
High-lift flow-physics flight experiments on a subsonic civil transport aircraft (B737-100) p 275 N95-23333 TRISTAR 1: Evaluation methods for testing head-up display (HUD) flight symbology [NASA-TM-4665] p 288 N95-24030 FLIGHT TRAINING	[BTN-95-EIX95152583283] p 306 A95-73584 Real-time estimation of atmospheric turbulence severity from in-situ aircraft measurements [BTN-95-EIX95182619231] p 319 A95-76657 Phase 2: HGM air flow tests in support of HEX vane investigation p 312 N95-23438 Impeller flow field characterization with a laser two-focus velocimeter p 313 N95-23440	[BTN-95-EIX95212645688] p 271 A95-76740 Aerodynamic surface distension system for high angle of attack forebody vortex control [NASA-CASE-ARC-11979-1] p 286 N95-23390 FRAGMENTS
High-lift flow-physics flight experiments on a subsonic civil transport aircraft (B737-100) p 275 N95-2333 TRISTAR 1: Evaluation methods for testing head-up display (HUD) flight symbology [NASA-TM-4665] p 288 N95-24030 FLIGHT TRAINING Development of qualification guidelines for personal computer-based aviation training devices	[BTN-95-EIX95152583283] p 306 A95-73584 Real-time estimation of atmospheric turbulence severity from in-situ aircraft measurements [BTN-95-EIX95182619231] p 319 A95-76657 Phase 2: HGM air flow tests in support of HEX vane investigation p 312 N95-23438 Impeller flow field characterization with a laser two-focus velocimeter p 313 N95-23440 A time-accurate finite volume method valid at all flow	[BTN-95-EIX95212645688] p 271 A95-76740 Aerodynamic surface distension system for high angle of attack forebody vortex control [NASA-CASE-ARC-11979-1] p 286 N95-23390 FRAGMENTS Rationale for the Modular Air-system Vulnerability Estimation Network (MAVEN) methodology
High-lift flow-physics flight experiments on a subsonic civil transport aircraft (B737-100) p 275 N95-23333 TRISTAR 1: Evaluation methods for testing head-up display (HUD) flight symbology [NASA-TM-4665] p 288 N95-24030 FLIGHT TRAINING Development of qualification guidelines for personal computer-based aviation training devices [DOT/FAA/AM-95/6] p 323 N95-23603	[BTN-95-EIX95152583283] p 306 A95-73584 Real-time estimation of atmospheric turbulence severity from in-situ aircraft measurements [BTN-95-EIX95182619231] p 319 A95-76657 Phase 2: HGM air flow tests in support of HEX vane investigation p 312 N95-234438 Impeller flow field characterization with a laser two-focus velocimeter p 313 N95-23440 A time-accurate finite volume method valid at all flow velocities p 314 N95-23447	[BTN-95-EIX95212645688] p 271 A95-76740 Aerodynamic surface distension system for high angle of attack forebody vortex control [NASA-CASE-ARC-11979-1] p 286 N95-23390 FRAGMENTS Rationale for the Modular Air-system Vulnerability Estimation Network (MAVEN) methodology [AD-A285797] p 284 N95-22510 FREE FLOW Aerodynamic shape optimization using preconditioned
High-lift flow-physics flight experiments on a subsonic civil transport aircraft (B737-100) p 275 N95-23333 TRISTAR 1: Evaluation methods for testing head-up display (HUD) flight symbology [NASA-TM-4665] p 288 N95-24030 FLIGHT TRAINING Development of qualification guidelines for personal computer-based aviation training devices [DOT/FAA/AM-95/6] p 323 N95-23603 FLOORS	[BTN-95-EIX95152583283] p 306 A95-73584 Real-time estimation of atmospheric turbulence severity from in-situ aircraft measurements [BTN-95-EIX95182619231] p 319 A95-76657 Phase 2: HGM air flow tests in support of HEX vane investigation p 312 N95-23438 Impeller flow field characterization with a laser two-focus velocimeter p 313 N95-23440 A time-accurate finite volume method valid at all flow	BTN-95-EIX95212645688   p 271 A95-76740   Aerodynamic surface distension system for high angle of attack forebody vortex control   NASA-CASE-ARC-11979-1   p 286 N95-23390   FRAGMENTS   Rationale for the Modular Air-system Vulnerability Estimation Network (MAVEN) methodology   AD-A285797   p 284 N95-22510   FREE FLOW   Aerodynamic shape optimization using preconditioned conjugate gradient methods
High-lift flow-physics flight experiments on a subsonic civil transport aircraft (B737-100) p 275 N95-23333 TRISTAR 1: Evaluation methods for testing head-up display (HUD) flight symbology [NASA-TM-4665] p 288 N95-24030 FLIGHT TRAINING Development of qualification guidelines for personal computer-based aviation training devices [DOT/FAA/AM-95/6] p 323 N95-23603 FLOORS Automatic riveting cell for commercial aircraft floor grid	[BTN-95-EIX95152583283] p 306 A95-73584 Real-time estimation of atmospheric turbulence severity from in-situ aircraft measurements [BTN-95-EIX95182619231] p 319 A95-76657 Phase 2: HGM air flow tests in support of HEX vane investigation p 312 N95-23438 Impeller flow field characterization with a laser two-focus velocimeter p 313 N95-23440 A time-accurate finite volume method valid at all flow velocities p 314 N95-23447 FLOW VISUALIZATION Flow visualization studies on sidewall effects in two-dimensional transonic airfoil testing	BTN-95-EIX95212645688   p 271 A95-76740   Aerodynamic surface distension system for high angle of attack forebody vortex control   NASA-CASE-ARC-11979-1   p 286 N95-23390
High-lift flow-physics flight experiments on a subsonic civil transport aircraft (B737-100) p 275 N95-23333 TRISTAR 1: Evaluation methods for testing head-up display (HUD) flight symbology [NASA-TM-4665] p 288 N95-24030 FLIGHT TRAINING Development of qualification guidelines for personal computer-based aviation training devices [DOT/FAA/AM-95/6] p 323 N95-23603 FLOORS	[BTN-95-EIX95152583283] p 306 A95-73584 Real-time estimation of atmospheric turbulence severity from in-situ aircraft measurements [BTN-95-EIX95182619231] p 319 A95-76657 Phase 2: HGM air flow tests in support of HEX vane investigation p 312 N95-23438 Impeller flow field characterization with a laser two-focus velocimeter p 313 N95-23440 A time-accurate finite volume method valid at all flow velocities p 314 N95-23447 FLOW VISUALIZATION Flow visualization studies on sidewall effects in two-dimensional transonic airfoil testing [BTN-95-EIX95152582313] p 264 A95-73516	BTN-95-EIX95212645688   p 271 A95-76740   Aerodynamic surface distension system for high angle of attack forebody vortex control   NASA-CASE-ARC-11979-1   p 286 N95-23390   FRAGMENTS   Rationale for the Modular Air-system Vulnerability Estimation Network (MAVEN) methodology   AD-A285797   p 284 N95-22510   FREE FLOW   Aerodynamic shape optimization using preconditioned conjugate gradient methods
High-lift flow-physics flight experiments on a subsonic civil transport aircraft (B737-100) p 275 N95-23333 TRISTAR 1: Evaluation methods for testing head-up display (HUD) flight symbology [NASA-TM-4665] p 288 N95-24030 FLIGHT TRAINING  Development of qualification guidelines for personal computer-based aviation training devices [DOT/FAA/AM-95/6] p 323 N95-23603 FLOORS  Automatic riveting cell for commercial aircraft floor grid assembly	[BTN-95-EIX95152583283] p 306 A95-73584 Real-time estimation of atmospheric turbulence severity from in-situ aircraft measurements [BTN-95-EIX95182619231] p 319 A95-76657 Phase 2: HGM air flow tests in support of HEX vane investigation p 312 N95-23438 Impeller flow field characterization with a laser two-focus velocimeter p 313 N95-23440 A time-accurate finite volume method valid at all flow velocities p 314 N95-23447 FLOW VISUALIZATION Flow visualization studies on sidewall effects in two-dimensional transonic airfoil testing [BTN-95-EIX95152582313] p 264 A95-73516 Experimental investigation of the flowfield about an	BTN-95-EIX95212645688   p 271 A95-76740   Aerodynamic surface distension system for high angle of attack forebody vortex control [NASA-CASE-ARC-11979-1]   p 286 N95-23390   FRAGMENTS   Rationale for the Modular Air-system Vulnerability Estimation Network (MAVEN) methodology [AD-A285797]   p 284 N95-22510   FREE FLOW   Aerodynamic shape optimization using preconditioned conjugate gradient methods   BTN-95-EIX95142553033   p 263 A95-73465   Unstructured grid solutions to a wing/pylon/store configuration   BTN-95-EIX95152582322   p 265 A95-73525
High-lift flow-physics flight experiments on a subsonic civil transport aircraft (B737-100) p 275 N95-23333 TR/STAR 1: Evaluation methods for testing head-up display (HUD) flight symbology [NASA-TM-4665] p 288 N95-24030 FLIGHT TRAINING  Development of qualification guidelines for personal computer-based aviation training devices [DOT/FAA/AM-95/6] p 323 N95-23603 FLOORS  Automatic riveting cell for commercial aircraft floor grid assembly [BTN-95-EIX95182617807] p 261 A95-75752 FLOW CHARACTERISTICS Impeller flow field characterization with a laser two-focus	[BTN-95-EIX95152583283] p 306 A95-73584 Real-time estimation of atmospheric turbulence severity from in-situ aircraft measurements [BTN-95-EIX95182619231] p 319 A95-76657 Phase 2: HGM air flow tests in support of HEX vane investigation p 312 N95-23438 Impeller flow field characterization with a laser two-focus velocimeter p 313 N95-23440 A time-accurate finite volume method valid at all flow velocities p 314 N95-23447 FLOW VISUALIZATION Flow visualization studies on sidewall effects in two-dimensional transonic airfoil testing [BTN-95-EIX95152582313] p 264 A95-73516	BTN-95-EIX95212645688   p 271 A95-76740   Aerodynamic surface distension system for high angle of attack forebody vortex control   NASA-CASE-ARC-11979-1   p 286 N95-23390   FRAGMENTS   Rationale for the Modular Air-system Vulnerability Estimation Network (MAVEN) methodology   AD-A285797   p 284 N95-22510   FREE FLOW   Aerodynamic shape optimization using preconditioned conjugate gradient methods   BTN-95-EIX95142553033   p 263 A95-73465   Unstructured grid solutions to a wing/pylon/store configuration   BTN-95-EIX95152582322   p 265 A95-73525   Hypersonic nonequilibrium Navier-Stokes solutions over
High-lift flow-physics flight experiments on a subsonic civil transport aircraft (B737-100) p 275 N95-23333 TRISTAR 1: Evaluation methods for testing head-up display (HUD) flight symbology [NASA-TM-4665] p 288 N95-24030 FLIGHT TRAINING  Development of qualification guidelines for personal computer-based aviation training devices [DOT/FAA/AM-95/6] p 323 N95-23603 FLOORS  Automatic riveting cell for commercial aircraft floor grid assembly [BTN-95-EIX95182617807] p 261 A95-75752 FLOW CHARACTERISTICS Impeller flow field characterization with a laser two-focus velocimeter p 313 N95-23440	[BTN-95-EIX95152583283] p 306 A95-73584 Real-time estimation of atmospheric turbulence severity from in-situ aircraft measurements [BTN-95-EIX95182619231] p 319 A95-76657 Phase 2: HGM air flow tests in support of HEX vane investigation p 312 N95-23438 Impeller flow field characterization with a laser two-focus velocimeter p 313 N95-23440 A time-accurate finite volume method valid at all flow velocities p 314 N95-23447 FLOW VISUALIZATION Flow visualization studies on sidewall effects in two-dimensional transonic airfoil testing [BTN-95-EIX95152582313] p 264 A95-73516 Experimental investigation of the flowfield about an upswept afterbody	BTN-95-EIX95212645688   p 271 A95-76740   Aerodynamic surface distension system for high angle of attack forebody vortex control {NASA-CASE-ARC-11979-1} p 286 N95-23390   FRAGMENTS   Rationale for the Modular Air-system Vulnerability Estimation Network (MAVEN) methodology   AD-A285797   p 284 N95-22510   FREE FLOW   Aerodynamic shape optimization using preconditioned conjugate gradient methods   BTN-95-EIX95142553033   p 263 A95-73465   Unstructured grid solutions to a wing/pylon/store configuration   BTN-95-EIX95152582322   p 265 A95-73525   Hypersonic nonequilibrium Navier-Stokes solutions over an ablating graphite nosetip
High-lift flow-physics flight experiments on a subsonic civil transport aircraft (B737-100) p 275 N95-23333 TRISTAR 1: Evaluation methods for testing head-up display (HUD) flight symbology [NASA-TM-4665] p 288 N95-24030 FLIGHT TRAINING Development of qualification guidelines for personal computer-based aviation training devices [DOT/FAA/AM-95/6] p 323 N95-23603 FLOORS Automatic riveting cell for commercial aircraft floor grid assembly [BTN-95-EIX95182617807] p 261 A95-75752 FLOW CHARACTERISTICS Impeller flow field characterization with a laser two-focus velocimeter p 313 N95-23440 FLOW DISTORTION	[BTN-95-EIX95152583283] p 306 A95-73584 Real-time estimation of atmospheric turbulence severity from in-situ aircraft measurements [BTN-95-EIX95182619231] p 319 A95-76657 Phase 2: HGM air flow tests in support of HEX vane investigation p 312 N95-23438 Impeller flow field characterization with a laser two-focus velocimeter p 313 N95-23440 A time-accurate finite volume method valid at all flow velocities p 314 N95-23447 FLOW VISUALIZATION Flow visualization studies on sidewall effects in two-dimensional transonic airfoil testing [BTN-95-EIX95152582313] p 264 A95-73516 Experimental investigation of the flowfield about an upswept afterbody [BTN-95-EIX95152582321] p 265 A95-73524 Simple method of supersonic flow visualization using watertable	BTN-95-EIX95212645688   p 271 A95-76740   Aerodynamic surface distension system for high angle of attack forebody vortex control {NASA-CASE-ARC-11979-1 } p 286 N95-23390   FRAGMENTS   Rationale for the Modular Air-system Vulnerability Estimation Network (MAVEN) methodology [AD-A285797] p 284 N95-22510   FREE FLOW   Aerodynamic shape optimization using preconditioned conjugate gradient methods [BTN-95-EIX95142553033] p 263 A95-73465   Unstructured grid solutions to a wing/pylon/store configuration [BTN-95-EIX95152582322] p 265 A95-73525   Hypersonic nonequilibrium Navier-Stokes solutions over an ablating graphite nosetip [BTN-95-EIX95152583252] p 305 A95-73553
High-lift flow-physics flight experiments on a subsonic civil transport aircraft (B737-100) p 275 N95-23333 TRISTAR 1: Evaluation methods for testing head-up display (HUD) flight symbology [NASA-TM-4665] p 288 N95-24030 FLIGHT TRAINING Development of qualification guidelines for personal computer-based aviation training devices [DOT/FAA/AM-95/6] p 323 N95-23603 FLOORS Automatic riveting cell for commercial aircraft floor grid assembly [BTN-95-EIX95182617807] p 261 A95-75752 FLOW CHARACTERISTICS Impeller flow field characterization with a laser two-focus velocimeter p 313 N95-23440 FLOW DISTORTION A new type of simulator for simulating the flow-field	[BTN-95-EIX95152583283] p 306 A95-73584 Real-time estimation of atmospheric turbulence severity from in-situ aircraft measurements [BTN-95-EIX95182619231] p 319 A95-76657 Phase 2: HGM air flow tests in support of HEX vane investigation p 312 N95-23438 Impeller flow field characterization with a laser two-focus velocimeter p 313 N95-23440 A time-accurate finite volume method valid at all flow velocities p 314 N95-23447 FLOW VISUALIZATION Flow visualization studies on sidewall effects in two-dimensional transonic airfoil testing [BTN-95-EIX95152582313] p 264 A95-73516 Experimental investigation of the flowfield about an upswept afterbody [BTN-95-EIX95152582321] p 265 A95-73524 Simple method of supersonic flow visualization using watertable [BTN-95-EIX95182619105] p 269 A95-76590	BTN-95-EIX95212645688   p 271 A95-76740   Aerodynamic surface distension system for high angle of attack forebody vortex control {NASA-CASE-ARC-11979-1} p 286 N95-23390   FRAGMENTS   Rationale for the Modular Air-system Vulnerability Estimation Network (MAVEN) methodology   AD-A285797   p 284 N95-22510   FREE FLOW   Aerodynamic shape optimization using preconditioned conjugate gradient methods   BTN-95-EIX95142553033   p 263 A95-73465   Unstructured grid solutions to a wing/pylon/store configuration   BTN-95-EIX95152582322   p 265 A95-73525   Hypersonic nonequilibrium Navier-Stokes solutions over an ablating graphite nosetip
High-lift flow-physics flight experiments on a subsonic civil transport aircraft (B737-100) p 275 N95-23333 TRISTAR 1: Evaluation methods for testing head-up display (HUD) flight symbology [NASA-TM-4665] p 288 N95-24030 FLIGHT TRAINING Development of qualification guidelines for personal computer-based aviation training devices [DOT/FAA/AM-95/6] p 323 N95-23603 FLOORS Automatic riveting cell for commercial aircraft floor grid assembly [BTN-95-EIX95182617807] p 261 A95-75752 FLOW CHARACTERISTICS Impeller flow field characterization with a laser two-focus velocimeter p 313 N95-23440 FLOW DISTORTION	BTN-95-EIX95152583283   p 306 A95-73584   Real-time estimation of atmospheric turbulence severity from in-situ aircraft measurements     BTN-95-EIX95182619231   p 319 A95-76657     Phase 2: HGM air flow tests in support of HEX vane investigation   p 312 N95-23438     Impeller flow field characterization with a laser two-focus velocimeter   p 313 N95-23440     A time-accurate finite volume method valid at all flow velocities   p 314 N95-23447     FLOW VISUALIZATION   Flow visualization studies on sidewall effects in two-dimensional transonic airfoil testing     BTN-95-EIX95152582313   p 264 A95-73516     Experimental investigation of the flowfield about an upswept afterbody     BTN-95-EIX95152582321   p 265 A95-73524     Simple method of supersonic flow visualization using watertable     BTN-95-EIX95182619105   p 269 A95-76590     Aerodynamic characteristics of external store	BTN-95-EIX95212645688   p 271 A95-76740   Aerodynamic surface distension system for high angle of attack forebody vortex control {NASA-CASE-ARC-11979-1} p 286 N95-23390   FRAGMENTS   Rationale for the Modular Air-system Vulnerability Estimation Network (MAVEN) methodology   AD-A285797   p 284 N95-22510   FREE FLOW   Aerodynamic shape optimization using preconditioned conjugate gradient methods   BTN-95-EIX95142553033   p 263 A95-73465   Unstructured grid solutions to a wing/pylon/store configuration   BTN-95-EIX95152582322   p 265 A95-73525   Hypersonic nonequilibrium Navier-Stokes solutions over an ablating graphite nosetip   BTN-95-EIX95152583252   p 305 A95-73553   Comparison of linear stability results with flight transition
High-lift flow-physics flight experiments on a subsonic civil transport aircraft (B737-100) p 275 N95-23333 TRISTAR 1: Evaluation methods for testing head-up display (HUD) flight symbology [NASA-TM-4665] p 288 N95-24030 FLIGHT TRAINING Development of qualification guidelines for personal computer-based aviation training devices [DOT/FAA/AM-95/6] p 323 N95-23603 FLOORS Automatic riveting cell for commercial aircraft floor grid assembly [BTN-95-EIX95182617807] p 261 A95-75752 FLOW CHARACTERISTICS Impeller flow field characterization with a laser two-focus velocimeter p 313 N95-23440 FLOW DISTORTION A new type of simulator for simulating the flow-field distortion of engine inlet [BTN-95-EIX95202638963] p 289 A95-76673 FLOW DISTRIBUTION	BTN-95-EIX95152583283   p 306 A95-73584   Real-time estimation of atmospheric turbulence severity from in-situ aircraft measurements   BTN-95-EIX95182619231   p 319 A95-76657   Phase 2: HGM air flow tests in support of HEX vane investigation p 312 N95-23438   Impeller flow field characterization with a laser two-focus velocimeter p 313 N95-23440   A time-accurate finite volume method valid at all flow velocities p 314 N95-23447   FLOW VISUALIZATION   Flow visualization studies on sidewall effects in two-dimensional transonic airfoil testing   BTN-95-EIX95152582313   p 264 A95-73516   Experimental involvy   BTN-95-EIX95152582321   p 265 A95-73524   Simple method of supersonic flow visualization using watertable   BTN-95-EIX95182619105   p 269 A95-76590   Aerodynamic characteristics of external store configurations at low speeds   BTN-95-EIX95182619230   p 271 A95-76656	BTN-95-EIX95212645688   p 271 A95-76740   Aerodynamic surface distension system for high angle of attack forebody vortex control {NASA-CASE-ARC-11979-1} p 286 N95-23390   FRAGMENTS   Rationale for the Modular Air-system Vulnerability Estimation Network (MAVEN) methodology   AD-A285797   p 284 N95-22510   FREE FLOW   Aerodynamic shape optimization using preconditioned conjugate gradient methods   BTN-95-EIX95142553033   p 263 A95-73465   Unstructured grid solutions to a wing/pylon/store configuration   BTN-95-EIX95152582322   p 265 A95-73525   Hypersonic nonequilibrium Navier-Stokes solutions over an ablating graphite nosetip   BTN-95-EIX95152583252   p 305 A95-73553   Comparison of linear stability results with flight transition data   BTN-95-EIX95182619097   p 283 A95-76582   FREE JETS
High-lift flow-physics flight experiments on a subsonic civil transport aircraft (B737-100) p 275 N95-23333  TRISTAR 1: Evaluation methods for testing head-up display (HUD) flight symbology [NASA-TM-4665] p 288 N95-24030  FLIGHT TRAINING  Development of qualification guidelines for personal computer-based aviation training devices [DOT/FAA/AM-95/6] p 323 N95-23603  FLOORS  Automatic riveting cell for commercial aircraft floor grid assembly [BTN-95-EIX95182617807] p 261 A95-75752  FLOW CHARACTERISTICS Impeller flow field characterization with a laser two-focus velocimeter p 313 N95-23440  FLOW DISTORTION  A new type of simulator for simulating the flow-field distortion of engine inlet [BTN-95-EIX95202638963] p 289 A95-76673  FLOW DISTRIBUTION  Experimental investigation of the flowfield about an	[BTN-95-EIX95152583283] p 306 A95-73584 Real-time estimation of atmospheric turbulence severity from in-situ aircraft measurements [BTN-95-EIX95182619231] p 319 A95-76657 Phase 2: HGM air flow tests in support of HEX vane investigation p 312 N95-23438 Impeller flow field characterization with a laser two-focus velocimeter p 313 N95-23440 A time-accurate finite volume method valid at all flow velocities p 314 N95-23447 FLOW VISUALIZATION Flow visualization studies on sidewall effects in two-dimensional transonic airfoil testing [BTN-95-EIX95152582313] p 264 A95-73516 Experimental investigation of the flowfield about an upswept afterbody [BTN-95-EIX95152582321] p 265 A95-73524 Simple method of supersonic flow visualization using watertable [BTN-95-EIX95182619105] p 269 A95-76590 Aerodynamic characteristics of external store configurations at low speeds [BTN-95-EIX95182619230] p 271 A95-76656 Flow visualization studies of VTOL aircraft models during	BTN-95-EIX95212645688   p 271 A95-76740   Aerodynamic surface distension system for high angle of attack forebody vortex control [NASA-CASE-ARC-11979-1]   p 286 N95-23390   FRAGMENTS   Rationale for the Modular Air-system Vulnerability Estimation Network (MAVEN) methodology [AD-A285797]   p 284 N95-22510   FREE FLOW   Aerodynamic shape optimization using preconditioned conjugate gradient methods [BTN-95-EIX95142553033]   p 263 A95-73465   Unstructured grid solutions to a wing/pylon/store configuration [BTN-95-EIX95152582322]   p 265 A95-73525   Hypersonic nonequilibrium Navier-Stokes solutions over an ablating graphite nosetip [BTN-95-EIX95152583252]   p 305 A95-73553   Comparison of linear stability results with flight transition data [BTN-95-EIX95182619097]   p 283 A95-76582   FREE JETS   Main features of overexpanded triple jets
High-lift flow-physics flight experiments on a subsonic civil transport aircraft (B737-100) p 275 N95-23333 TRISTAR 1: Evaluation methods for testing head-up display (HUD) flight symbology [NASA-TM-4665] p 288 N95-24030 FLIGHT TRAINING Development of qualification guidelines for personal computer-based aviation training devices [DOT/FAA/AM-95/6] p 323 N95-23603 FLOORS Automatic riveting cell for commercial aircraft floor grid assembly [BTN-95-EIX95182617807] p 261 A95-75752 FLOW CHARACTERISTICS Impeller flow field characterization with a laser two-focus velocimeter p 313 N95-23440 FLOW DISTORTION A new type of simulator for simulating the flow-field distortion of engine inlet [BTN-95-EIX95202638963] p 289 A95-76673 FLOW DISTRIBUTION Experimental investigation of the flowfield about an upswept afterbooy	[BTN-95-EIX95152583283] p 306 A95-73584 Real-time estimation of atmospheric turbulence severity from in-situ aircraft measurements [BTN-95-EIX95182619231] p 319 A95-76657 Phase 2: HGM air flow tests in support of HEX vane investigation p 312 N95-23438 Impeller flow field characterization with a laser two-focus velocimeter p 313 N95-23440 A time-accurate finite volume method valid at all flow velocities p 314 N95-23447 FLOW VISUALIZATION Flow visualization studies on sidewall effects in two-dimensional transonic airfoil testing [BTN-95-EIX951525823213] p 264 A95-73516 Experimental investigation of the flowfield about an upswept afterbody [BTN-95-EIX95152582321] p 265 A95-73524 Simple method of supersonic flow visualization using watertable [BTN-95-EIX95182619105] p 269 A95-76590 Aerodynamic characteristics of external store configurations at low speeds [BTN-95-EIX95182619230] p 271 A95-76656 Flow visualization studies of VTOL aircraft models during Hover in ground effect	BTN-95-EIX95212645688   p 271 A95-76740   Aerodynamic surface distension system for high angle of attack forebody vortex control {NASA-CASE-ARC-11979-1} p 286 N95-23390   FRAGMENTS   Rationale for the Modular Air-system Vulnerability Estimation Network (MAVEN) methodology [AD-A285797] p 284 N95-22510   FREE FLOW   Aerodynamic shape optimization using preconditioned conjugate gradient methods [BTN-95-EIX95142553033] p 263 A95-73465   Unstructured grid solutions to a wing/pylon/store configuration [BTN-95-EIX95152582322] p 265 A95-73525   Hypersonic nonequilibrium Navier-Stokes solutions over an ablating graphite nosetip [BTN-95-EIX95152583252] p 305 A95-73553   Comparison of linear stability results with flight transition data [BTN-95-EIX95182619097] p 283 A95-76582   FREE JETS   Main features of overexpanded triple jets [BTN-95-EIX95142553040] p 304 A95-73458
High-lift flow-physics flight experiments on a subsonic civil transport aircraft (B737-100) p 275 N95-23333 TRISTAR 1: Evaluation methods for testing head-up display (HUD) flight symbology [NASA-TM-4665] p 288 N95-24030 FLIGHT TRAINING Development of qualification guidelines for personal computer-based aviation training devices [DOT/FAA/AM-95/6] p 323 N95-23603 FLOORS Automatic riveting cell for commercial aircraft floor grid assembly [BTN-95-EIX95182617807] p 261 A95-75752 FLOW CHARACTERISTICS Impeller flow field characterization with a laser two-focus velocimeter p 313 N95-23440 FLOW DISTORTION A new type of simulator for simulating the flow-field distortion of engine inlet [BTN-95-EIX95202638963] p 289 A95-76673 FLOW DISTRIBUTION Experimental investigation of the flowfield about an upswept afterbody [BTN-95-EIX95122582321] p 265 A95-73524	BTN-95-EIX95152583283   p 306 A95-73584   Real-time estimation of atmospheric turbulence severity from in-situ aircraft measurements   BTN-95-EIX95182619231   p 319 A95-76657   Phase 2: HGM air flow tests in support of HEX vane investigation p 312 N95-23438   Impeller flow field characterization with a laser two-focus velocimeter p 313 N95-23440   A time-accurate finite volume method valid at all flow velocities p 314 N95-23447   FLOW VISUALIZATION   Flow visualization studies on sidewall effects in two-dimensional transonic airfoil testing   BTN-95-EIX95152582313   p 264 A95-73516   Experimental investigation of the flowfield about an upswept afterbody   BTN-95-EIX95152582321   p 265 A95-73524   Simple method of supersonic flow visualization using watertable   BTN-95-EIX95182619105   p 269 A95-76590   Aerodynamic characteristics of external store configurations at low speeds   BTN-95-EIX95182619230   p 271 A95-76656   Flow visualization studies of VTOL aircraft models during Hover in ground effect   NASA-TM-108860   p 272 N95-22666	BTN-95-EIX95212645688   p 271 A95-76740   Aerodynamic surface distension system for high angle of attack forebody vortex control {NASA-CASE-ARC-11979-1} p 286 N95-23390   FRAGMENTS   Rationale for the Modular Air-system Vulnerability Estimation Network (MAVEN) methodology   AD-A285797   p 284 N95-22510   FREE FLOW   Aerodynamic shape optimization using preconditioned conjugate gradient methods   BTN-95-EIX95142553033   p 263 A95-73465   Unstructured grid solutions to a wing/pylon/store configuration   BTN-95-EIX95152582322   p 265 A95-73525   Hypersonic nonequalitiorium Navier-Stokes solutions over an ablating graphite nosetip   BTN-95-EIX95152583252   p 305 A95-73553   Comparison of linear stability results with flight transition data   BTN-95-EIX95182619097   p 283 A95-76582   FREE JETS   Main features of overexpanded triple jets   BTN-95-EIX95142553040   p 304 A95-73458   FREQUENCY RESPONSE
High-lift flow-physics flight experiments on a subsonic civil transport aircraft (B737-100) p 275 N95-23333 TRISTAR 1: Evaluation methods for testing head-up display (HUD) flight symbology [NASA-TM-4665] p 288 N95-24030 FLIGHT TRAINING Development of qualification guidelines for personal computer-based aviation training devices [DOT/FAA/AM-95/6] p 323 N95-23603 FLOORS Automatic riveting cell for commercial aircraft floor grid assembly [BTN-95-EIX95182617807] p 261 A95-75752 FLOW CHARACTERISTICS Impeller flow field characterization with a laser two-focus velocimeter p 313 N95-23440 FLOW DISTORTION A new type of simulator for simulating the flow-field distortion of engine inlet [BTN-95-EIX95202638963] p 289 A95-76673 FLOW DISTRIBUTION Experimental investigation of the flowfield about an upswept afterbooy	[BTN-95-EIX95152583283] p 306 A95-73584 Real-time estimation of atmospheric turbulence severity from in-situ aircraft measurements [BTN-95-EIX95182619231] p 319 A95-76657 Phase 2: HGM air flow tests in support of HEX vane investigation p 312 N95-23438 Impeller flow field characterization with a laser two-focus velocimeter p 313 N95-23440 A time-accurate finite volume method valid at all flow velocities p 314 N95-23447 FLOW VISUALIZATION Flow visualization studies on sidewall effects in two-dimensional transonic airfoil testing [BTN-95-EIX951525823213] p 264 A95-73516 Experimental investigation of the flowfield about an upswept afterbody [BTN-95-EIX95152582321] p 265 A95-73524 Simple method of supersonic flow visualization using watertable [BTN-95-EIX95182619105] p 269 A95-76590 Aerodynamic characteristics of external store configurations at low speeds [BTN-95-EIX95182619230] p 271 A95-76656 Flow visualization studies of VTOL aircraft models during Hover in ground effect	BTN-95-EIX95212645688   p 271 A95-76740   Aerodynamic surface distension system for high angle of attack forebody vortex control {NASA-CASE-ARC-11979-1} p 286 N95-23390   FRAGMENTS   Rationale for the Modular Air-system Vulnerability Estimation Network (MAVEN) methodology [AD-A285797] p 284 N95-22510   FREE FLOW   Aerodynamic shape optimization using preconditioned conjugate gradient methods [BTN-95-EIX95142553033] p 263 A95-73465   Unstructured grid solutions to a wing/pylon/store configuration [BTN-95-EIX95152582322] p 265 A95-73525   Hypersonic nonequilibrium Navier-Stokes solutions over an ablating graphite nosetip [BTN-95-EIX95152583252] p 305 A95-73553   Comparison of linear stability results with flight transition data [BTN-95-EIX95182619097] p 283 A95-76582   FREE JETS   Main features of overexpanded triple jets [BTN-95-EIX95142553040] p 304 A95-73458

**HEAT TRANSFER** SUBJECT INDEX

GROUND EFFECT (AERODYNAMICS) GAS-SOLID INTERACTIONS FREQUENCY STABILITY Sensitivity of combustion-acoustic instabilities Three-dimensional structure of a supersonic jet The influence of alternate inter-blade connections on impinging on an inclined plate boundary conditions for premixed gas turbine nround resonance p 267 A95-73560 IHTN-95-808591 combustors IBTN-95-EIX951525832591 [NASA-TM-106890] p 289 N95-23550 Stability derivatives of a flapped plate in unsteady ground Gearbox vibration diagnostic analyzer FROST p 316 N95-23792 INASA-CR-1891411 IRTN-95-FIX951826192251 Effect of underwing frost on a transport aircraft airfoil GENERAL OVERVIEWS Unsteady ground effects on aerodynamic coefficients at flight Reynolds number Aircraft fires, smoke toxicity, and survival: An overview IDOT/FAA/AM-95/8 p 277 N95-24024 [BTN-95-EIX95152582334] p 276 A95-73536 of finite wings with camber FUEL CONSUMPTION IBTN-95-FIX951826192331 GEOGRAPHIC INFORMATION SYSTEMS Fuel-optimal bank-angle control for lunar-return Flow visualization studies of VTOL aircraft models during Pilot Weather Advisor system [BTN-95-EIX95152582314] aerocapture Hover in ground effect p 316 A95-73517 [BTN-95-EIX95212645706] p 299 A95-76758 INASA-TM-108860 I Automation technology using Geographic Information FUSELAGES GROUND RESONANCE System (GIS) n 324 N95-23284 The influence of alternate inter-blade connections on Growth of multiple cracks and their linkup in a fuselage GEOIDS ground resonance lap joint Geoid lineations of 1000 km wavelength over the central |BTN-95-EIX95142553047| p 286 A95-73451 HTN-95-808591 Pacific GUIDANCE (MOTION) Efficient sensitivity analysis for rotary-wing IHTN-95-11304 I n 319 A95-77009 Moving mass trim control for aerospace vehicles aeromechanical problems GEOMETRIC DILUTION OF PRECISION LDE95.0026021 IBTN-95-EIX951525775851 p 264 A95-73497 On the exact solutions of pseudorange equations **GULF OF MEXICO** Experimental investigation of the flowfield about an BTN-95-EIX95142555477 | p 278 A95-73433 Oceanic operations: An authoritative guide to oceanic upswept afterbody GEOSYNCHRONOUS ORBITS operations [BTN-95-EIX95152582321] p 265 A95-73524 Effects of satellite bunching on the probability of collision IFAA-AFS-5501 Multiple site fatigue damage in fuselage skin splices: Experimental simulation and theoretical prediction in geosynchronous orbit IBTN-95-EIX951525832761 **GULF STREAM** n 298 A95-73577 Assimilation of altimeter data in a quasi-geostrophic |BTN-95-EIX95152584676| p 276 A95-73588 GERMANIUM ALLOYS model of the Gulf Stream system: A dynamical An analytical and experimental investigation of the Design of a GaAs/Ge solar array for unmanned aerial perspective response of the curved, composite frame/skin vehicles INASA-CR-1963131 NASA-TM-106870) p 320 N95-23259 **GUST LOADS** IHTN-95-808571 p 283 A95-75099 GLOBAL POSITIONING SYSTEM Response of a nonrotating rotor blade to lateral Residual strength of thin panels with cracks On the exact solutions of pseudorange equations turbulence Part 2: Experiment IBTN-95-EIX951425554771 p 278 A95-73433 p 311 N95-23311 |BTN-95-EIX95182619229| Enhancing filter robustness in cascaded GPS-INS Review of aeronautical fatigue investigation in the Netherlands during the period March 1991-March 1993 integrations G |BTN-95-EIX95142555475| p 278 A95-73435 Thermal force modeling for global positioning system satellites using the finite element method GYROCOMPASSES GALLIUM ARSENIDES Covariance analysis of strapdown INS considering [BTN-95-EIX95152583270] p 278 A95-73571 Design of a GaAs/Ge solar array for unmanned aerial gyrocompass characteristics Real-time navigation using the global positioning IBTN-95-FIX952026375921 INASA-TM-106870 system p 320 N95-23259 [BTN-95-EIX95172595298] p 279 A95-75714 GAS DYNAMICS н New failure detection approach and its application to Measurement of particle emissions from clean room GPS autonomous integrity monitoring gas-handling components p 279 A95-76676 [BTN-95-EIX95202637613] H-INFINITY CONTROL IBTN-94-EIX943813590401 p 295 A95-74554 H-infinity helicopter flight control law design with and Description of a GNSS availability model and its use in Measurement of moisture and total hydrocarbon without rotor state feedback developing requirements contributions by valves used in clean room gas-delivery [BTN-95-EIX95182619129] [BTN-95-EIX95202637603] p 308 A95-76686 Stable H(infinity) controller design for the longitudinal Differential GPS and system integration of the Low IBTN-94-FIX943813590411 p 295 A95-74629 dynamics of an aircraft Visibility Landing and Surface Operations (LVLASO) High-performance parallel analysis of coupled problems [NASA-TM-106847] p 280 N95-23318 demonstration for aircraft propulsion Feedback control laws for highly maneuverable GRAPHICAL USER INTERFACE | NASA-CR-197440 | p 289 N95-23088 aircraft TIGER: A user-friendly interactive orid generation system GAS FLOW (NASA-CR-197944) for complicated turbomachinery and axis-symmetric High-performance parallel analysis of coupled problems HARDNESS p 322 N95-23419 configurations for aircraft propulsion Evaluation of advanced aerospace materials by depth [NASA-CR-197440] GRAPHITE p 289 N95-23088 sensing indentation and scratch methods [BTN-95-EIX95152584678] p.2 Hypersonic nonequilibrium Navier-Stokes solutions over GAS GENERATORS an ablating graphite nosetip Three-dimensional unsteady flow calculations in an HARMONIC CONTROL IBTN-95-FIX951525832521 p.305 A95-73553 advanced gas generator turbine p 312 N95-23425 GRAPHITE-EPOXY COMPOSITES GAS HEATING blade vortex interaction noise An analytical and experimental investigation of the Hypersonic nonequilibrium Navier-Stokes solutions over BTN-95-EIX95152582330 | response of the curved, composite frame/skin an ablating graphite nosetip HAZARDS specimens [BTN-95-EIX95152583252] p 305 A95-73553 HTN-95-80857 I p 283 A95-75099 GAS INJECTION materials GRASSLANDS HEAD-UP DISPLAYS Simulation of transverse gas injection in turbulent A comparison of some aerodynamic resistance methods supersonic air flows using measurements over cotton and grass from the 1991 [BTN-95-EIX95182619080] p 269 A95-75765 California ozone deposition experiment |BTN-95-EIX95212641070| GAS JETS p 319 A95-77000 Mach wave emission from a high-temperature | HTN-95-11295 | supersonic jet |BTN-95-EIX95152577586| GRAVITATIONAL EFFECTS display (HUD) flight symbology [NASA-TM-4665] Airborne rotary air separator study p 264 A95-73496 GAS MIXTURES [NASA-CR-189099] p 290 N95-24053 **HEAT EXCHANGERS** Hypersonic convective heat transfer over 140-deg blunt GRID GENERATION (MATHEMATICS) cones in different gases CFD optimization of a theoretical minimum-drag body [BTN-95-EIX95152583253] p 306 A95-73554 [BTN-95-EIX95182619234] p 308 A95-76660 GAS STREAMS Euler Technology Assessment program for preliminary investigation HEAT OF SOLUTION Experimental results for a hypersonic nozzle/afterbody aircraft design employing SPLITFLOW code with Cartesian flow field unstructured arid method [NASA-TM-4638] p 274 N95-23250 [NASA-CR-4649] trajectories p 273 N95-22917 GAS TURBINE ENGINES BTN-95-EIX951525832861 A CFD study of complex missile and store configurations Fatigue strength of high-temperature alloys under HEAT RESISTANT ALLOYS in relative motion conditions of cyclic temperature variation. Communication [NASA-CR-197912] p 285 N95-22949 1: Experimental procedure and results High-performance parallel analysis of coupled problems p 307 A95-75516 |BTN-94-EIX94401363884| for aircraft propulsion Erosion of dust-filtered helicopter turbine engines. Part p 289 N95-23088 [NASA-CR-197440]

Euler technology assessment for preliminary aircraft design employing OVERFLOW code with multiblock

TIGER: A user-friendly interactive grid generation system

for complicated turbomachinery and axis-symmetric

CFD analysis of turbopump volutes

p 273 N95-23095

p 322 N95-23419

p 312 N95-23436

structured-grid method

INASA-CR-46511

2: Erosion reduction

NASA-TM-1068901

I DE95-001360 I

GAS TURBINES

combustors

|BTN-95-EIX951826192231

in HIPed silicon nitride materials

Evolution of oxidation and creep damage mechanisms

Sensitivity of combustion-acoustic instabilities to

boundary conditions for premixed gas turbine

p 289 A95-76649

p 300 N95-22689

p 289 N95-23550

p 282 A95-73590 Analysis of a higher harmonic control test to reduce p 265 A95-73532 Mishap risk control for advanced aerospace/composite p 301 N95-23031 Design of wide angle head up displays for synthetic p 287 A95-76735 TRISTAR 1: Evaluation methods for testing head-up p 288 N95-24030 Base drag prediction on missile configurations [BTN-95-EJX95152583256] p 266 A9 p 266 A95-73557 Phase 2: HGM air flow tests in support of HEX vane p 312 N95-23438 Analytical solution for controls, heats, and states of flight p 282 A95-73587 Fatigue strength of high-temperature alloys under conditions of cyclic temperature variation. Communication 1: Experimental procedure and results. BTN-94-EIX94401363884] p 307 A95-75516 HEAT TRANSFER Comparison of linear stability results with flight transition p 283 A95-76582 [BTN-95-EIX95182619097] Application of a control-volume-based finite-element formulation to the shock tube problem BTN-95-EIX951826190991 p 295 A95-76584 Simulating heat addition via mass addition in constant rea compressible flows IBTN-95-FIX951826191001 p 307 A95-76585 Δ-15

p 267 A95-75101

p 270 A95-76651

p 271 A95-76659

n 272 N95-22666

p 267 A95-75101

p 299 N95-23532

p 277 N95-24065

p.320 N95-23766

p 284 A95-76655

p 285 N95-23161

p 279 A95-76697

p 291 A95-76606

p 293 N95-22954

p 295 N95-23410

Development and verification of a resin film	HIGH SPEED	HYPERSONIC AIRCRAFT
infusion/resin transfer molding simulation model for	Possible effects of CO2 increase on the high-speed civil	Direct-lift design strategy for longitudinal control
fabrication of advanced textile composites [NASA-CR-197439] p 301 N95-23179	transport impact on ozone LHTN-95-607791 p 317 A95-75976	hypersonic aircraft IBTN-95-EIX95182619131 p 291 A95-7660
[NASA-CR-197439] p 301 N95-23179 HELICOPTER CONTROL	[HTN-95-60779] p 317 A95-75976 Inner loop flight control for the High-Speed Civil	HYPERSONIC BOUNDARY LAYER
Identification of higher order helicopter dynamics using	Transport p 293 N95-23314	Analytical study of the neutral stability of a mode
linear modeling methods	HIGH STRENGTH STEELS	hypersonic boundary layer
[HTN-95-80851] p 290 A95-75093	Test method and test results for environmental	[BTN-95-EIX95152577589] p 263 A95-7349
Effects of high order dynamics on helicopter flight control law design	assessment of aircraft materials p 302 N95-23509	HYPERSONIC FLIGHT  Shock tunnel measurements of hypervelocity blunte
[HTN-95-80852] p 290 A95-75094	HIGH TEMPERATURE Evolution of oxidation and creep damage mechanisms	cone drag
Investigation of the effects of bandwidth and time delay	in HIPed silicon nitride materials	[BTN-95-EIX95152577606] p 305 A95-7347
on helicopter roll-axis handling qualities	[DE95-001360] p 300 N95-22689	Analytical solution for controls, heats, and states of flight
[HTN-95-80853] p 290 A95-75095	Design of a variable area diffuser for a 15-inch Mach	trajectories IBTN-95-EIX951525832861 p 282 A95-7358
Integrated flight/propulsion control for helicopters [HTN-95-80854] p 290 A95-75096	6 open-jet tunnel p 297 N95-23309	BTN-95-EIX95152583286  p 282 A95-7358   Direct-lift design strategy for longitudinal control of
H-infinity helicopter flight control law design with and	HIGH TEMPERATURE GASES  Mach wave emission from a high-temperature	hypersonic aircraft
without rotor state feedback	supersonic jet	[BTN-95-EIX95182619131] p 291 A95-7660
BTN-95-EIX95182619129  p 291 A95-76606	[BTN-95-EIX95152577586] p 264 A95-73496	Particle kinetic simulation of high altitude hypervelocit
Automatic guidance and control for helicopter obstacle avoidance	Phase 2: HGM air flow tests in support of HEX vane	flight [NASA-CR-197383] p 309 N95-2248
BTN-95-EIX95182619130  p 291 A95-76607	investigation p 312 N95-23438 HIGH TEMPERATURE SUPERCONDUCTORS	HYPERSONIC FLOW
An investigation of helicopter dynamic coupling using	Phonon characteristics of high (T sub c) superconductors	Time-of-flight mass spectrometer for impulse facilitie
an analytical model	from neutron Doppler broadening measurements	[BTN-95-EIX95142553057] p 262 A95-7344
[NASA-CR-197420] p 285 N95-23217	[DE95-003703] p 324 N95-24076	Analytical study of the neutral stability of a mode
HELICOPTER DESIGN	HIGHLY MANEUVERABLE AIRCRAFT	hypersonic boundary layer [BTN-95-EIX95152577589] p 263 A95-7349:
Integrated flight/propulsion control for helicopters [HTN-95-80854] p 290 A95-75096	Feedback control laws for highly maneuverable aircraft	[BTN-95-EIX95152577589] p 263 A95-7349: Hypersonic rarefied flow past spheres including wake
H-76B fantail demonstrater composite fan blade	[NASA-CR-197944] p 295 N95-23410	structure
fabrication	HISTORIES	[BTN-95-EIX95152583250] p 305 A95-7355
[HTN-95-80856] p 283 A95-75098	Development of aeronautical mobile satellite services	Application of the multigrid solution technique to
HELICOPTER ENGINES	over the past thirty years [BTN-95-EIX95152569458] p 305 A95-73498	hypersonic entry vehicles
Erosion of dust-filtered helicopter turbine engines. Part	HOLES (MECHANICS)	[BTN-95-EIX95152583254] p 306 A95-73555
1: Basic theoretical considerations  BTN-95-EIX95182619222  p 288 A95-76648	Eddy current detection of pitting corrosion around	Zonally decoupled direct simulation Monte Carlo solutions of hypersonic blunt-body wake flows
Erosion of dust-filtered helicopter turbine engines. Part	fastener holes p 315 N95-23507	BTN-95-EIX95182617458  p 268 A95-75729
2: Erosion reduction	POD assessment of NDI procedures using a round robin	Scaling of incipient separation in supersonic/transonic
[BTN-95-EIX95182619223] p 289 A95-76649	lest  AGARD-R-809  p 315 N95-23602	speed laminar flows
Life prediction of helicopter engines fitted with dust	HOLOGRAPHIC INTERFEROMETRY	[BTN-95-EIX95182619104] p 269 A95-76589
filters	Holographic interferometric tomography for	Review and development of base pressure and base
[BTN-95-EIX95182619224] p 289 A95-76650 HELICOPTER PERFORMANCE	reconstructing flow fields p 310 N95-23287	heating correlations in supersonic flow [BTN-95-EIX95212645688] p 271 A95-76740
Investigation of the effects of bandwidth and time delay	HOMING Switched bias proportional navigation for homing	Numerical analysis of hypersonic low-density scramje
on helicopter roll-axis handling qualities	guidance against highly maneuvering targets	inlet flow
[HTN-95-80853] p 290 A95-75095	[BTN-95-EIX95182619145] p 279 A95-76622	[BTN-95-EIX95212645694] p 272 A95-76746
The influence of alternate inter-blade connections on	HONEYCOMB STRUCTURES	Laser velocimetry seed-particle behavior in shear layers
ground resonance [HTN-95-80859] p 267 A95-75101	Minimum-mass design of sandwich aerobrakes for a	at Mach 12 [BTN-95-EIX95212645712] p 272 A95-76764
HELICOPTER PROPELLER DRIVE	lunar transfer vehicle [BTN-95-EIX95212645707] p 299 A95-76759	Experimental results for a hypersonic nozzle/afterbody
Gearbox vibration diagnostic analyzer	HORIZONTAL FLIGHT	flow field
[NASA-CR-189141] p 316 N95-23792	Response of a nonrotating rotor blade to lateral	[NASA-TM-4638] p 274 N95-23250
HELICOPTERS	turbulence. Part 1: Theory	Design of a variable area diffuser for a 15-inch Mach
Static pressure distribution in the inlet of a helicopter	BTN-95-EIX95182619228  p 284 A95-76654 <b>HOT ISOSTATIC PRESSING</b>	6 open-jet tunnel p 297 N95-23309
turbine compressor [BTN-95-EIX95152582339] p 266 A95-73541	Evolution of oxidation and creep damage mechanisms	HYPERSONIC HEAT TRANSFER  Hypersonic convective heat transfer over 140-deg blun
Improving prediction: The incorporation of simplified	in HIPed silicon nitride materials	cones in different gases
rotor dynamics in a mathematical model of the bell	[DE95-001360] p 300 N95-22689 HOYERING	[BTN-95-EIX95152583253] p 306 A95-73554
412HP	H-infinity helicopter flight control law design with and	HYPERSONIC INLETS
[BTN-95-EIX95152584679] p 282 A95-73591	without rotor state feedback	Optimization of contoured hypersonic scramjet inlets
Sensitivity of acoustic predictions to variation of input parameters	[BTN-95-EIX95182619129] p 291 A95-76606	with a least-squares parabolized Navier-Stokes procedure
[HTN-95-80855] p 267 A95-75097	Flow visualization studies of VTOL aircraft models during	[HTN-95-20976] p 261 A95-74042
The influence of alternate inter-blade connections on	Hover in ground effect [NASA-TM-108860] p 272 N95-22666	Numerical analysis of hypersonic low-density scramje
ground resonance	HUBS	inlet flow
[HTN-95-80859] p 267 A95-75101	NASA low-speed axial compressor for fundamental	[BTN-95-EIX95212645694] p 272 A95-76746
An investigation of helicopter dynamic coupling using an analytical model	research	HYPERSONIC NOZZLES Optimized design of a hypersonic nozzle
[NASA-CR-197420] p 285 N95-23217	(NASA-TM-4635) p 296 N95-23192 HUMAN FACTORS ENGINEERING	p 297 N95-23304
Thin tailored composite wing for civil tiltrotor	TRISTAR 1: Evaluation methods for testing head-up	HYPERSONIC SPEED
p 285 N95-23317	display (HUD) flight symbology	Mach 10 computational study of a three-dimensional
HEURISTIC METHODS	[NASA-TM-4665] p 288 N95-24030	scramjet inlet flow field
Automatic guidance and control for helicopter obstacle	HUMIDITY	[NASA-TM-4602] p 309 N95-23015
avoidance  BTN-95-EiX95182619130  p 291 A95-76607	Corrosion of landing gear steels p 302 N95-23500 HYDRAULIC ANALOGIES	Mach 10 computational study of a three-dimensional scramjet inlet flow field
HIGH ALTITUDE	Simple method of supersonic flow visualization using	INASA-TM-46021 p 310 N95-23210
Aerodynamic characteristics of a hypersonic viscous	watertable	Design of a variable area diffuser for a 15-inch Mach
optimized waverider at high altitudes	[BTN-95-EIX95182619105] p 269 A95-76590 HYDROCARBONS	6 open-jet tunnel p 297 N95-23309
[BTN-95-EIX95152583251] p 266 A95-73552	Measurement of moisture and total hydrocarbon	HYPERSONIC VEHICLES
Higher-order viscous shock-layer solutions for	contributions by valves used in clean room gas-delivery	Computational study of plume-induced separation on a
high-altitude flows [BTN-95-EIX95152583255] p 306 A95-73556	systems	hypersonic powered model [BTN-95-EIX95152582346] p 266 A95-73548
Aerodynamics of the Shuttle Orbiter at high altitudes	[BTN-94-EIX94381359041] p 295 A95-74629	Application of the multigrid solution technique to
[BTN-95-EIX95182617454] p 298 A95-75725	HYDRODYNAMICS  Numerical study of sound generation due to a spinning	hypersonic entry vehicles
Particle kinetic simulation of high altitude hypervelocity	vortex pair	[BTN-95-EIX95152583254] p 306 A95-73555
flight	[BTN-95-EIX95182619075] p 307 A95-75760	Analytical aeropropulsive/aeroelastic
[NASA-CR-197383] p 309 N95-22481	HYDROGRAPHY	hypersonic-vehicle model with dynamic analysis [BTN-95-EIX95182619138] p 269 A95-76615
HIGH ASPECT RATIO  Convergence acceleration of implicit schemes in the	Assimilation of altimeter data in a quasi-geostrophic model of the Gulf Stream system: A dynamical	Integrated design of hypersonic waveriders including
presence of high aspect ratio grid cells	perspective	inlets and tailfins
p 313 N95-23446	[NASA-CR-196313] p 320 N95-23766	[BTN-95-EIX95212645692] p 271 A95-76744
HIGH RESOLUTION	HYPERBOLIC DIFFERENTIAL EQUATIONS  On the exact solutions of pseudorange equations	Particle kinetic simulation of high altitude hypervelocity
MAX-91: Polarimetric SAR results on Montespertoli		flight

JET AIRCRAFT NOISE SUBJECT INDEX

HYPERSONIC WAKES Simulation on the 3-D turbulent flow in the passages Zonally decoupled direct simulation Monte Carlo of finocyl grain IBTN-95-EIX952026389621 IAGARD-R-8091 solutions of hypersonic blunt-body wake flows p 279 A95-76674 p 268 A95-75729 [BTN-95-EIX95182617458] INDENTATION INTAKE SYSTEMS HYPERSONIC WIND TUNNELS Evaluation of advanced aerospace materials by depth sensing indentation and scratch methods Time-of-flight mass spectrometer for impulse facilities urbine compressor |BTN-95-EIX95152584678| p 282 A95-73590 1BTN-95-EIX95142553057 | IBTN-95-EIX951525823391 p 262 A95-73441 INDUCTION MOTORS INTEGRAL EQUATIONS Optimized design of a hypersonic nozzle Motor drive technologies for the power-by-wire (PBW) program: Options, trends and tradeoffs p 297 N95-23304 **HYPERSONICS** p 295 N95-23671 NASA-TM-106885| Computational study of plume-induced separation on a INERTIAL NAVIGATION INTEGRATED CIRCUITS hypersonic powered model Enhancing filter robustness in cascaded GPS-INS [BTN-95-EIX95152582346] p 266 A95-73548 Aerodynamic characteristics of a hypersonic viscous 18TN-95-EIX951425554751 p 278 A95-73435 DE94-0177681 optimized waverider at high altitudes Covariance analysis of strapdown INS considering [BTN-95-EIX95152583251] p 266 A95-73552 gyrocompass characteristics Hypersonic nonequilibrium Navier-Stokes solutions over IBTN-95-FIX952026375921 p 279 A95-76697 an ablating graphite nosetip INERTIAL PLATFORMS p 305 A95-73553 [BTN-95-EIX95152583252] Dynamic response tests of inertial and optical wind-tunnel model attitude measurement devices HYSTERESIS Computation of oscillating airfoil flows with one- and INASA-TM-1091821 p 296 N95-23011 for noncircular missiles two-equation turbulence models INFILTRATION |BTN-95-EIX95152577588| p 263 A95-73494 IRTN-95-FIX951826174621 Development and verification of a resin film INTERLAYERS infusion/resin transfer molding simulation model for Compliant interlayer fabrication of advanced textile composites |BTN-95-EIX95142562401| [NASA-CR-197439] p 301 N95-23179 INTERNAL FLOW INFORMATION SYSTEMS Collaborative research on aircraft icing and charging Automation technology using Geographic Information IRTN-95-EIX95142553040 I p 324 N95-23284 System (GIS) processes in ice AD-A2851021 INFRARED IMAGERY p 276 N95-23201 scramjet inlet flow field AVIRIS and TIMS data processing and distribution at IMAGE ANALYSIS INASA-TM-4602 I the land processes distributed active archive center Scientific and technical photography at NASA Langley p 325 N95-23872 Research Center p 310 N95-23290 research Statistics of multi-look AIRSAR imagery: A comparison INFRARED LASERS INASA-TM-46351 2 micron LIDAR for laser-based remote sensing: Flight of theory with measurements p 320 N95-23947 demonstration and application survey IBTN-95-EIX95212641072 | **IMAGE PROCESSING** p 319 A95-76737 Simple method of supersonic flow visualization using INFRARED SPECTRA watertable velocimeter BTN-95-EIX951826191051 AVIRIS and TIMS data processing and distribution at p 269 A95-76590 INTERNAL PRESSURE the land processes distributed active archive center AVIRIS and TIMS data processing and distribution at the land processes distributed active archive center p 325 N95-23872 INGESTION (ENGINES) p 325 N95-23872 INTERNATIONAL TRADE Erosion of dust-filtered helicopter turbine engines. Part Statistics of multi-look AIRSAR imagery: A comparison of theory with measurements IMAGING TECHNIQUES 1: Basic theoretical considerations p 320 N95-23947 IBTN-95-EIX951826192221 p 288 A95-76648 IRTN-95-FIX952126410691 Erosion of dust-filtered helicopter turbine engines. Part Scientific and technical photography at NASA Langley 2. Fresion reduction Research Center p 310 N95-23290 [BTN-95-EIX95182619223] p 289 A95-76649 AIRSAR deployment in Australia, September 1993: IBTN-95-EIX951525832671 Management and objectives Life prediction of helicopter engines fitted with dust p 321 N95-23948 INTERPOLATION fitters [BTN-95-EIX95182619224] p 289 A95-76650 Measurement of particle emissions from clean room INLET FLOW gas-handling components [BTN-95-EIX95182619099] |BTN-94-EIX94381359040| p 295 A95-74554 Static pressure distribution in the inlet of a helicopter IN SITU MEASUREMENT turbine compressor control In situ observations in aircraft exhaust plumes in the [BTN-95-EIX95152582339] p 266 A95-73541 INVISCID FLOW lower stratosphere at midlatitudes A new type of simulator for simulating the flow-field IHTN-95-A08621 distortion of engine inlet p 318 A95-76266 conjugate gradient methods Real-time estimation of atmospheric turbulence severity IBTN-95-EIX952026389631 p 289 A95-76673 IBTN-95-EIX951425530331 from in-situ aircraft measurements Numerical analysis of hypersonic low-density scramjet [BTN-95-EIX95182619231] p 319 A95-76657 of vortical flowfields IN-FLIGHT MONITORING Enhancement of F/A-18 p 272 A95-76746 IBTN-95-EIX952126456941 IBTN-95-EIX951525776041 operational flight Flow visualization studies of VTOL aircraft models during measurements: Data report for phase 1 Hover in ground effect IDSTO-TR-00491 p 286 N95-23666 [BTN-95-EIX95152582316] [NASA-TM-108860] p 272 N95-22666 INCENDIARY AMMUNITION Mach 10 computational study of a three-dimensional Rationale for the Modular Air-system Vulnerability scramjet inlet flow field Estimation Network (MAVEN) methodology IBTN-95-EIX951525823221 [NASA-TM-4602] p 309 N95-23015 p 284 N95-22510 1AD-A2857971 Mach 10 computational study of a three-dimensional INCOMPRESSIBLE FLOW cramjet inlet flow field Two-equation turbulence model for unsteady separated I NASA-TM-46021 p 310 N95-23210 flows around airfoils ION CYCLOTRON RADIATION |BTN-95-EIX95142553054| Three-dimensional Navier-Stokes analysis and redesign p 262 A95-73444 of an imbedded bellmouth nozzle in a turbine cascade Adaptive finite element method for turbulent flow near p 311 N95-23423 inlet section a propeller IDE94-0177681 [BTN-95-EIX95142553038] Supersonic flow and shock formation in turbine tip p 305 A95-73460 IONOSPHERES Eigenanalysis of unsteady flows about airfoils, cascades, gans p 312 N95-23429 INORGANIC COMPOUNDS and wings |BTN-95-EIX95152577597| p 305 A95-73486 Estimates of total organic and inorganic chlorine in the distribution Progress in high-lift aerodynamic calculations [BTN-95-EIX95152582315] p 264 AS lower stratosphere from in situ and flask measurements [HTN-95-41223] p 264 A95-73518 durino AASE 2 ISENTROPIC PROCESSES Sidewash on the vertical tail in subsonic and supersonic 1HTN-95-A08611 p 317 A95-76265 stratospheric aircraft INSPECTION IBTN-95-EIX951525823161 p 264 A95-73519 Double pass retroreflection for corrosion detection in IHTN-95-412191 Postinstability behavior of a two-dimensional airfoil with ITERATIVE SOLUTION aircraft structures p 323 N95-23503 a structural nonlinearity Non-destructive detection of corrosion for life |BTN-95-EIX95152582337| p 266 A95-73539 p 314 N95-23505 management Grid refinement test of time-periodic flows over bluff [BTN-95-EIX95152577612] Health and usage monitoring systems: Corrosion bodies p 262 N95-23506 surveillance p 307 A95-76491 IBTN-94-EIX944013788221 Eddy current detection of pitting corrosion around Aerodynamic characteristics of configurations at low speeds external store fastener holes p 315 N95-23507 Corrosion detection and monitoring of aircraft structures: (BTN-95-EIX95182619230) p 271 A95-76656 p 303 N95-23515

An overview

Experience of in-service corrosion on military aircraft

p 303 N95-23516

Study of the droplet spray characteristics of a subsonic

p 27.1 A95-76661

wind tunnel

|BTN-95-EIX95182619235|

POD assessment of NDI procedures using a round robin p 315 N95-23602 Static pressure distribution in the inlet of a helicopter p 266 A95-73541 Coupled FEM-BEM approach for mean flow effects on vibro-acoustic behavior of planar structures [BTN-95-EIX95152577587] p 263 p 263 A95-73495 Cu deposition using a permanent magnet electron cyclotron resonance microwave plasma source p 304 N95-23981 INTEGRATED LIBRARY SYSTEMS AVIRIS and TIMS data processing and distribution at the land processes distributed active archive center p 325 N95-23872 INTERACTIONAL AFRODYNAMICS Wing vertical position effects on wing-body carryover p 268 A95-75733 p 304 A95-73439 Main features of overexpanded triple jets p 304 A95-73458 Mach 10 computational study of a three-dimensional p 309 N95-23015 NASA low-speed axial compressor for fundamental p 296 N95-23192 CFD analysis of turbopump volutes p 312 N95-23436 impeller flow field characterization with a laser two-focus p 313 N95-23440 Residual strength of thin panels with cracks p 311 N95-23311 Overview of AlliedSignal's avionics development in the p 287 A95-76734 INTERPLANETARY SPACECRAFT Fourth-generation Mars vehicle concepts p 298 A95-73568 Application of a control-volume-based finite-element formulation to the shock tube problem p 295 A95-76584 On-line, adaptive state estimator for active noise ontrol p 322 N95-23308 Aerodynamic shape optimization using preconditioned p 263 A95-73465 Effects of spatial order of accuracy on the computation p 305 A95-73479 Sidewash on the vertical tail in subsonic and supersonic p 264 A95-73519 Unstructured grid solutions to a wing/pylon/store p 265 A95-73525 Three-dimensional structure of a supersonic jet impinging on an inclined plate [BTN-95-EIX95152583259] p 267 A95-73560 Cu deposition using a permanent magnet electron cyclotron resonance microwave plasma source p 304 N95-23981 Thundercloud electric field modeling onosphere-Earth region. 1: Dependence on cloud charge p 317 A95-75035 Trajectory modeling of emissions from lower p 317 A95-75031 Preconditioned domain decomposition scheme for three-dimensional aerodynamic sensitivity analysis p 321 A95-73471

JET AIRCRAFT NOISE

Supersonic jet noise reductions predicted with increased jet spreading rate p 323 N95-23178 NASA-TM-1068721

·		
JET ENGINES	LAMINATES	LEAST SQUARES METHOD
Transport of exhaust products in the near trail of a jet	MIL-HDBK-5 design allowables for fibre/metal	Optimization of contoured hypersonic scramjet inlets with a least-squares parabolized Navier-Stokes
engine under atmospheric conditions [HTN-95-91421] p 319 A95-77334	laminates: ARALL 2 and ARALL 3 [BTN-94-EIX94371346933] p 300 A95-73345	procedure parabolized Navier Stokes
High-performance parallel analysis of coupled problems	Dynamic analysis of bearingless tail rotor blades based	[HTN-95-20976] p 261 A95-74042
for aircraft propulsion [NASA-CR-197440] p 289 N95-23088	on nonlinear shell modes	LEE WAVES  Diurnal variation of lee vortices in Taiwan and the
JET EXHAUST	[BTN-95-EIX95152582338] p 281 A95-73540 Validation of an effective flat cruciform-shaped specimen	surrounding area
Transport of exhaust products in the near trail of a jet engine under atmospheric conditions	to study CFRP composite laminates under biaxial	[HTN-95-91363] p 318 A95-76394 LENGTH
[HTN-95-91421] p 319 A95-77334	loading	Numerical investigation of supersonic flows around a
JET FLOW	BTN-95-EIX95152584677  p 282 A95-73589	spiked blunt body  BTN-95-EIX95212645690  p 271 A95-76742
Pneumatic concept for tip-stall control of cranked-arrow wings	Interlaminar shear test method development for long term durability testing of composites	BTN-95-EIX95212645690  p 271 A95-76742 LENTICULAR BODIES
[BTN-95-EIX95152582335] p 281 A95-73537	p 301 N95-23300	Evolution of oxidation and creep damage mechanisms
JET IMPINGEMENT	New nondestructive techniques for the detection and quantification of corrosion in aircraft structures	in HIPed silicon nitride materials [DE95-001360] p 300 N95-22689
Three-dimensional structure of a supersonic jet impinging on an inclined plate	p 315 N95-23512	LIFE (DURABILITY)
[BTN-95-EIX95152583259] p 267 A95-73560	LANDING AIDS	Test method and test results for environmental assessment of aircraft materials p 302 N95-23509
JET MIXING FLOW Supersonic jet noise reductions predicted with increased	Guidance and control requirements for high-speed Rollout and Turnoff (ROTO)	LIFT
jet spreading rate	[NASA-CR-195026] p 292 N95-22674	Laplace interaction law for the computation of viscous
[NASA-TM-106872] p 323 N95-23178	LANDING GEAR	airfoil flow in low- and high-speed aerodynamics [BTN-95-EIX95142553037] p 263 A95-73461
••	Corrosion of landing gear steels p 302 N95-23500  LANTHANUM OXIDES	Progress in high-lift aerodynamic calculations
K	Phonon characteristics of high (T sub c) superconductors	[BTN-95-EIX95152582315] p 264 A95-73518 Separation control on high-lift airfoils via micro-vortex
K-EPSILON TURBULENCE MODEL	trom neutron Doppler broadening measurements [DE95-003703] p 324 N95-24076	generators
Computation of the poststall behavior of a circulation	LAP JOINTS	[BTN-95-EIX95152582326] p 265 A95-73529 Study of an airfoil with a flap and spoiler
controlled airfoil	Growth of multiple cracks and their linkup in a fuselage	[BTN-95-EIX95152582327] p 265 A95-73530
[BTN-95-EIX95152582320] p 264 A95-73523 Application of wall functions to generalized	lap joint [BTN-95-EIX95142553047] . p 286 A95-73451	Pneumatic concept for tip-stall control of cranked-arrow
nonorthogonal curvilinear coordinate systems	LAPLACE TRANSFORMATION	wings  BTN-95-EIX95152582335  p 281 A95-73537
[BTN-95-EIX95182619077] p 307 A95-75762	Laplace interaction law for the computation of viscous	High-lift flow-physics flight experiments on a subsonic
Numerical computation of aerodynamics and heat transfer in a turbine cascade and a turn-around duct using	airfoil flow in low- and high-speed aerodynamics [BTN-95-EIX95142553037] p 263 A95-73461	civil transport aircraft (B737-100) p 275 N95-23333
advanced turbulence models p 313 N95-23444	LASER APPLICATIONS	Lift enhancing tabs for airfoils [NASA-CASE-ARC-11990-1] p 286 N95-23395
KALMAN FILTERS	2 micron LIDAR for laser-based remote sensing: Flight	LIFTOFF (LAUNCHING)
Enhancing filter robustness in cascaded GPS-INS integrations	demonstration and application survey [BTN-95-EIX95212641072] p 319 A95-76737	Fourth-generation Mars vehicle concepts
[BTN-95-EIX95142555475] p 278 A95-73435	LASER DOPPLER VELOCIMETERS	[BTN-95-EIX95152583267] p 298 A95-73568 LINEAR EQUATIONS
Real-time navigation using the global positioning	Laser velocimetry seed-particle behavior in shear layers	Analytical study of the neutral stability of a model
system  BTN-95-EIX95172595298  p 279 A95-75714	at Mach 12 [BTN-95-EIX95212645712] p 272 A95-76764	hypersonic boundary layer [BTN-95-EIX95152577589] p 263 A95-73493
New failure detection approach and its application to	Impeller flow field characterization with a laser two-focus	Neural network prediction of three-dimensional unsteady
GPS autonomous integrity monitoring	velocimeter p 313 N95-23440	separated flowfields
BTN-95-EIX95202637613  p 279 A95-76676 KNUDSEN FLOW	LASER SPECTROMETERS AIRSAR deployment in Australia, September 1993:	[BTN-95-EIX95182619232] p 308 A95-76658 LINEAR QUADRATIC GAUSSIAN CONTROL
Hypersonic rarefied flow past spheres including wake	Management and objectives p 321 N95-23948	Effects of high order dynamics on helicopter flight control
structure [BTN-95-EIX95152583250] p 305 A95-73551	LATERAL CONTROL Pneumatic concept for tip-stall control of cranked-arrow	law design
Aerodynamic characteristics of a hypersonic viscous	wings	[HTN-95-80852] p 290 A95-75094 Flutter suppression control law design and testing for
optimized waverider at high altitudes	[BTN-95-EIX95152582335] p 281 A95-73537	the active flexible wing
[BTN-95-EIX95152583251] p 266 A95-73552 Aerodynamics of the Shuttle Orbiter at high altitudes	H-infinity helicopter flight control law design with and without rotor state feedback	[BTN-95-EIX95182619214] p 292 A95-76640
[BTN-95-EIX95182617454] p 298 A95-75725	[BTN-95-EIX95182619129] p 291 A95-76606	LINEAR QUADRATIC REGULATOR  Aeroelastic vehicle multivariable control synthesis with
Numerical analysis of hypersonic low-density scramjet	Fuel-optimal bank-angle control for lunar-return	analytical robustness evaluation
inlet flow  BTN-95-EIX95212645694  p 272 A95-76746	aerocapture [BTN-95-EIX95212645706] p 299 A95-76758	[BTN-95-EIX95182619115] p 321 A95-76592 System identification of the Large-Angle Magnetic
KUTTA-JOUKOWSKI CONDITION	Aerodynamic surface distension system for high angle	Suspension Test Fixture (LAMSTF) p 296 N95-23299
Laplace interaction law for the computation of viscous airfoil flow in low- and high-speed aerodynamics	of attack forebody vortex control [NASA-CASE-ARC-11979-1] p 286 N95-23390	LINEAR VIBRATION
BTN-95-EIX95142553037  p 263 A95-73461	Feedback control laws for highly maneuverable	Active control of panel vibrations induced by a boundary layer flow
	aircraft	[NASA-CR-197867] p 273 N95-23182
L	[NASA-CR-197944] p 295 N95-23410  LAUNCH VEHICLES	Comparison of linear etablish regults with flight transition
	Aerodynamic flight control to increase payload capability	Comparison of linear stability results with flight transition data
Labs behind Boeing's new 777	of future faunch vehicles [NASA-CR-197704] p 300 N95-24032	[BTN-95-EIX95182619097] p 283 A95-76582
[BTN-95-EIX95142562403] p 280 A95-73437	Airborne rotary air separator study	LINEARIZATION  Dynamical instability of the aerogravity assist
LAMINAR BOUNDARY LAYER	[NASA-CR-189099] p 290 N95-24053	maneuver
Review and development of base pressure and base heating correlations in supersonic flow	LAVAL NUMBER Main features of overexpanded triple jets	[BTN-95-EIX95152583282] p 298 A95-73583
[BTN-95-EIX95212645688] p 271 A95-76740	(BTN-95-EIX95142553040) p 304 A95-73458	Design of high performance multivariable control systems for supermaneuverable aircraft at high angle of
LAMINAR FLOW	LEADING EDGE FLAPS	attack
Effect of ambient turbulence intensity on sphere wakes at intermediate Reynolds numbers	Natural faminar flow wing concept for supersonic transports	NASA-CR-197661   p 293 N95-22908   LIQUID CRYSTALS
[BTN-95-EIX95182619101] p 308 A95-76586	[BTN-95-EIX95182619226] p 308 A95-76652	Flow visualization studies on sidewall effects in
Scaling of incipient separation in supersonic/transonic	Wing pressure distributions from subsonic tests of a	two-dimensional transonic airfoil testing
speed laminar flows [BTN-95-EIX95182619104] p 269 A95-76589	high-wing transport model in the Langley 14- by 22-Foot Subsonic Wind Tunnel	[BTN-95-EIX95152582313] p 264 A95-73516 LIQUID NITROGEN
High-lift flow-physics flight experiments on a subsonic	[NASA-TM-4583] p 272 N95-22802	Performance of the 0.3-meter transonic cryogenic tunnel
civil transport aircraft (8737-100) p 275 N95-23333	LEADING EDGE SLATS	with air, nitrogen, and sulfur hexafluoride media under
Supersonic laminar flow control research (NASA-CR-197938) p 275 N95-23669	Lift enhancing tabs for airfoils [NASA-CASE-ARC-11990-1] p 286 N95-23395	closed loop automatic control [NASA-CR-195052] p 310 N95-23257
LAMINAR FLOW AIRFOILS	LEADING EDGE THRUST	LIQUID ROCKET PROPELLANTS
Natural laminar flow wing concept for supersonic	Analytic prediction of lift for delta wings with partial	Fourth-generation Mars vehicle concepts
transports  BTN-95-EIX95182619226  p 308 A95-76652	leading-edge thrust [BTN-95-EIX95152582345] p 266 A95-73547	[BTN-95-EIX95152583267] p 298 A95-73568 LOAD CARRYING CAPACITY
LAMINAR WAKES	LEADING EDGES	An analytical and experimental investigation of the
Effect of ambient turbulence intensity on sphere wakes	Pneumatic concept for tip-stall control of cranked-arrow	response of the curved, composite frame/skin
at intermediate Reynolds numbers [BTN-95-EIX95182619101] p 308 A95-76586	wings  BTN-95-EIX95152582335  p 281 A95-73537	specimens [HTN-95-80857] p 283 A95-75099
	·	

SUBJECT INDEX		MATTEMATICAL MODELS
LOAD TESTS	Performance of the 0.3-meter transonic cryogenic tunnel	Effects of expansions on a supersonic boundary layer:
Experimental evaluation of a box beam specifically	with air, nitrogen, and sulfur hexafluoride media under	Surface pressure measurements
tailored for chordwise deformation	closed loop automatic control	[BTN-95-EIX95142553036] p 263 A95-73462
BTN-95-EIX95182619088  p 283 A95-75773  LOADING MOMENTS	[NASA-CR-195052] p 310 N95-23257 Design of a variable area diffuser for a 15-inch Mach	Aerodynamic shape optimization using preconditioned
Rolling maneuver load alleviation using active controls	6 open-jet tunnel p 297 N95-23309	conjugate gradient methods 18TN-95-EIX951425530331 p 263 A95-73465
[BTN-95-EIX95182619217] p 270 A95-76643	MACHINE TOOLS	Analytical study of the neutral stability of a model
LONGITUDINAL CONTROL	Automatic riveting cell for commercial aircraft floor grid	hypersonic boundary layer
H-infinity helicopter flight control law design with and	assembly  BTN-95-EIX95182617807  p 261 A95-75752	[BTN-95-EIX95152577589] p 263 A95-73493
without rotor state feedback [BTN-95-EIX95182619129] p 291 A95-76606	MAGNETIC BEARINGS	Efficient sensitivity analysis for rotary-wing aeromechanical problems
Direct-lift design strategy for longitudinal control of	Effects of AMB parameters on the dynamic stability of	[BTN-95-EIX95152577585] p 264 A95-73497
hypersonic aircraft	the rotor  BTN-94-EIX94381353450  p 323 A95-75494	Limit cycle phenomena in computational transonic
[BTN-95-EIX95182619131] p 291 A95-76608	Influence of backup bearings and support structure	aeroelasticity
Robustly stable preliminary control systems design for the YF-16 CCV aircraft	dynamics on the behavior of rotors with active supports	[BTN-95-EIX95152582317] p 264 A95-73520
[BTN-95-EIX95202637608] p 292 A95-76681	[NASA-CR-197438] p 310 N95-23190	Hypersonic rarelied flow past spheres including wake structure
Analysis of the longitudinal handling qualities and	MAGNETIC EFFECTS  Effects of AMB parameters on the dynamic stability of	[BTN-95-EIX95152583250] p 305 A95-73551
pilot-induced-oscillation tendencies of the	the rotor	Aerodynamic characteristics of a hypersonic viscous
High-Angle-of-Attack Research Vehicle (HARV) p 293 N95-23297	[BTN-94-EIX94381353450] p 323 A95-75494	optimized waverider at high altitudes
Aerodynamic surface distension system for high angle	MAGNETIC SUSPENSION	[BTN-95-EIX95152583251] p 266 A95-73552
of attack forebody vortex control	System identification of the Large-Angle Magnetic Suspension Test Fixture (LAMSTF) p 296 N95-23299	Hypersonic nonequilibrium Navier-Stokes solutions over an ablating graphite nosetip
NASA-CASE-ARC-11979-1   p 286 N95-23390   LOW DENSITY FLOW	MAN MACHINE SYSTEMS	[BTN-95-EIX95152583252] p 305 A95-73553
Higher-order viscous shock-layer solutions for	Flight-deck displays on the Boeing 777	Hypersonic convective heat transfer over 140-deg blunt
high-altitude flows	[BTN-95-EIX95142562402] p 286 A95-73438  MANAGEMENT INFORMATION SYSTEMS	cones in different gases
[BTN-95-EIX95152583255] p 306 A95-73556	AVIRIS and TIMS data processing and distribution at	[BTN-95-EIX95152583253] p 306 A95-73554
Numerical analysis of hypersonic low-density scramjet inlet flow	the land processes distributed active archive center	Application of the multigrid solution technique to hypersonic entry vehicles
BTN-95-EIX95212645694  p 272 A95-76746	p 325 N95-23872	[BTN-95-EIX95152583254] p 306 A95-73555
LOW SPEED	MANAGEMENT PLANNING	Higher-order viscous shock-layer solutions for
Aerodynamic characteristics of a canard-controlled	Maintenance programs [BTN-95-EIX95182617809] p 261 A95-75754	high-altitude flows
missile at high angles of attack   BTN-95-EIX95152583257   p 267 A95-73558	MANEUVERABILITY	[BTN-95-EIX95152583255] p 306 A95-73556
Viscous-inviscid interaction method for unsteady	Dynamical instability of the aerogravity assist	Base drag prediction on missile configurations [BTN-95-EIX95152583256] p 266 A95-73557
low-speed airfoil flows	maneuver [BTN-95-EIX95152583282] p 298 A95-73583	Aerodynamic characteristics of a canard-controlled
[BTN-95-EIX95182619093] p 269 A95-75778	Multiaxis pilot ratings for damaged aircraft	missile at high angles of attack
Aerodynamic characteristics of external store configurations at low speeds	[BTN-95-EIX95182619128] p 269 A95-76605	BTN-95-EIX95152583257  p 267 A95-73558
[BTN-95-EIX95182619230] p 271 A95-76656	Solutions of generalized proportional navigation with	Predicting exhaust plume boundaries with supersonic
NASA low-speed axial compressor for fundamental	maneuvering and nonmaneuvering targets [BTN-95-EIX95202637606] p 279 A95-76683	external flows [BTN-95-EIX95152583258] p 297 A95-73559
research [NASA-TM-4635] p 296 N95-23192	MANIFOLDS	Three-dimensional structure of a supersonic jet
Handling qualities of the High Speed Civil Transport	Aerodynamic design and analysis of a highly loaded	impinging on an inclined plate
p 294 N95-23325	turbine exhaust p 312 N95-23435	[BTN-95-EIX95152583259] p 267 A95-73560
LOW TURBULENCE	Phase 2: HGM air flow tests in support of HEX vane investigation p 312 N95-23438	Functional dependence of trajectory dispersion on initial condition errors
Separation control on high-lift airfoils via micro-vortex generators	MANUALS	[BTN-95-EIX95152583263] p 298 A95-73564
[BTN-95-EIX95152582326] p 265 A95-73529	Rationale for the Modular Air-system Vulnerability	Thermal force modeling for global positioning system
LOW VISIBILITY	Estimation Network (MAVEN) methodology	satellites using the finite element method
Differential GPS and system integration of the Low	[AD-A285797] p 284 N95-22510	BTN-95-EIX95152583270  p 278 A95-73571 Supersonic axisymmetric conical flow solutions for
Visibility Landing and Surface Operations (LVLASO) demonstration p 280 N95-23318	MANUFACTURING Automatic riveting cell for commercial aircraft floor grid	different ratios of specific heats
LUMBAR REGION	assembly	[BTN-95-EIX95152583283] p 306 A95-73584
A multibody/finite element analysis approach for	[BTN-95-EIX95182617807] p 261 A95-75752	Improving prediction: The incorporation of simplified rotor dynamics in a mathematical model of the bell
modeling of crash dynamic responses [NIAR-94-3] p 277 N95-24050	MAPS	412HP
LUNAR SPACECRAFT	Automation technology using Geographic Information System (GIS) p 324 N95-23284	[BTN-95-EIX95152584679] p 282 A95-73591
Minimum-mass design of sandwich aerobrakes for a	MARITIME SATELLITES	Finite element model for a flexible non-symmetric rotor
lunar transfer vehicle	Development of aeronautical mobile satellite services	on distributed bearing: A stability study [BTN-94-EIX94381352212] p 306 A95-74612
[BTN-95-£IX95212645707] p 299 A95-76759	over the past thirty years	Flutter of an infinitely long panel in a duct
M	[BTN-95-EIX95152569458] p 305 A95-73498	[BTN-95-EIX95182619087] p 291 A95-75772
IVI	MARKET RESEARCH The airline quality report, 1994	Observations on using experimental data as boundary
MACH NUMBER	[NIAR-94-11] p 277 N95-24012	conditions for computations [BTN-95-EIX95182619103] p 321 A95-76588
Main features of overexpanded triple jets	MARS (PLANET)	Aeroelastic vehicle multivariable control synthesis with
[BTN-95-EIX95142553040] p 304 A95-73458	Fourth-generation Mars vehicle concepts [BTN-95-EIX95152583267] p 298 A95-73568	analytical robustness evaluation
Analytical study of the neutral stability of a model hypersonic boundary layer	MARS EXPLORATION	[BTN-95-EIX95182619115] p 321 A95-76592 Analytical aeropropulsive/aeroelastic
[BTN-95-EIX95152577589] p 263 A95-73493	Fourth-generation Mars vehicle concepts	hypersonic-vehicle model with dynamic analysis
Mach wave emission from a high-temperature	[BTN-95-EIX95152583267] p 298 A95-73568	[BTN-95-EIX95182619138] p 269 A95-76615
supersonic jet [BTN-95-EIX95152577586] p 264 A95-73496	MASS FLOW	Drag function modeling for air traffic simulation
Improved version of the Naval Surface Warfare Center	Simulating heat addition via mass addition in constant area compressible flows	BTN-95-EIX95182619154  p 279 A95-76631 Application of transonic small disturbance theory to the
aeroprediction code (AP93)	[BTN-95-EIX95182619100] p 307 A95-76585	active flexible wing model
[BTN-95-EIX95152583260] p 267 A95-73561	MASS SPECTROMETERS	[BTN-95-EIX95182619210] p 270 A95-76636
Flutter of an infinitely long panel in a duct [BTN-95-EIX95182619087] p 291 A95-75772	Time-of-flight mass spectrometer for impulse facilities	Simulation and model reduction for the active flexible wing program
Scaling of incipient separation in supersonic/transonic	[BTN-95-EIX95142553057] p 262 A95-73441  MASS TRANSFER	[BTN-95-EIX95182619211] p 295 A95-76637
speed laminar flows	Simulating heat addition via mass addition in constant	Erosion of dust-filtered helicopter turbine engines. Part
BTN-95-EIX95182619104  p 269 A95-76589 Natural laminar flow wing concept for supersonic	area compressible flows	1: Basic theoretical considerations {BTN-95-EIX95182619222} p 288 A95-76648
transports	[BTN-95-EIX95182619100] p 307 A95-76585	(BTN-95-EIX95182619222) p 288 A95-76648 Stability derivatives of a flapped plate in unsteady ground
[BTN-95-EIX95182619226] p 308 A95-76652	MATERIALS HANDLING  Measurement of particle emissions from clean room	effect
Numerical investigation of supersonic flows around a	Measurement of particle emissions from clean room gas-handling components	[BTN-95-EIX95182619225] p 270 A95-76651
spiked blunt body [BTN-95-EIX95212645690] p 271 A95-76742	[BTN-94-EIX94381359040] p 295 A95-74554	Response of a nonrotating rotor blade to lateral turbulence. Part 1: Theory
Calculation of wing-alone aerodynamics to high angles	MATHEMATICAL MODELS	[BTN-95-EIX95182619228] p 284 A95-76654
of attack	On the exact solutions of pseudorange equations	Response of a nonrotating rotor blade to lateral
[BTN-95-EIX95212645713] p 261 A95-76765	[BTN-95-EIX95142555477] p 278 A95-73433 Mechanical system reliability and risk assessment	turbulence. Part 2: Experiment
Wing pressure distributions from subsonic tests of a high-wing transport model in the Langley 14- by 22-Foot	[BTN-95-EIX95142553046] p 304 A95-73452	[BTN-95-EIX95182619229] p 284 A95-76655 Aerodynamic characteristics of external store
Subsonic Wind Tunnel	Simulation of turbulent fluctuations	configurations at low speeds
[NASA-TM-4583] p 272 N95-22802	[BTN-95-EIX95142553041] p 304 A95-73457	[BTN-95-EIX95182619230] p 271 A95-76656
		· · · · · · · · · · · · · · · · · · ·

SUBJECT INDEX

Neural network prediction of three-dimensional unsteady	METEOROLOGICAL PARAMETERS	Aerodynamic characteristics of a hypersonic viscous
separated flowfields	Compendium of NASA data base for the Global	optimized waverider at high altitudes
[BTN-95-EIX95182619232] p 308 A95-76658	Tropospheric Experiment's Pacific Exploratory Mission	[BTN-95-EIX95152583251] p 266 A95-73552
Unsteady ground effects on aerodynamic coefficients	West-A (PEM West-A)	Higher-order viscous shock-layer solutions for
of finite wings with camber	[NASA-TM-109177] p 320 N95-23009	high-altitude flows  BTN-95-EIX95152583255  p 306 A95-73556
BTN-95-EIX95182619233  p 271 A95-76659	METEOROLOGICAL RADAR	Functional dependence of trajectory dispersion on initial
CFD optimization of a theoretical minimum-drag body	Maximum-likelihood spectral estimation and adaptive filtering techniques with application to airborne Doppler	condition errors
[BTN-95-EIX95182619234] p 308 A95-76660	weather radar	[BTN-95-EIX95152583263] p 298 A95-73564
A comparison of some aerodynamic resistance methods using measurements over cotton and grass from the 1991	[NASA-CR-197699] p 316 N95-23670	Determination of wall boundary conditions for
California ozone deposition experiment	METEOROLOGICAL SATELLITES	high-speed-ratio direct simulation Monte Carlo
[HTN-95-11295] p 319 A95-77000	Calculation of satellite drag coefficients	calculations IBTN-95-EIX951826174571 p 267 A95-75728
Particle kinetic simulation of high altitude hypervelocity	[AD-A285118] p 300 N95-23781	[BTN-95-EIX95182617457] p 267 A95-75728 Zonally decoupled direct simulation Monte Carlo
flight	METEOROLOGY	solutions of hypersonic blunt-body wake flows
[NASA-CR-197383] p 309 N95-22481	A new generation of instruments for flying laboratories	[BTN-95-EIX95182617458] p 268 A95-75729
Modeling aerosol emissions from the combustion of	[BTN-94-EIX94401363947] p 317 A95-75532	Numerical analysis of hypersonic low-density scramjet
composite materials p 301 N95-23038	MICROBURSTS (METEOROLOGY) Optimal lateral-escape maneuvers for microburst	inlet flow
Supersonic jet noise reductions predicted with increased jet spreading rate	encounters during final approach	[BTN-95-EIX95212645694] p 272 A95-76746
[NASA-TM-106872] p 323 N95-23178	[BTN-95-EIX95182619127] p 276 A95-76604	Particle kinetic simulation of high altitude hypervelocity flight
Development and verification of a resin film	MICROWAVES	[NASA-CR-197383] p 309 N95-22481
infusion/resin transfer molding simulation model for	Cu deposition using a permanent magnet electron	MOON-EARTH TRAJECTORIES
fabrication of advanced textile composites	cyclotron resonance microwave plasma source	Fuel-optimal bank-angle control for lunar-return
[NASA-CR-197439] p 301 N95-23179	[DE94-017768] p 304 N95-23981	aerocapture
An approximate theoretical method for modeling the	MIMO (CONTROL SYSTEMS)  Multirate flutter suppression system design for a model	[BTN-95-EIX95212645706] p 299 A95-76758
static thrust performance of non-axisymmetric	wing	MULTIGRID METHODS  Application of the multigrid solution technique to
two-dimensional convergent-divergent nozzles	[BTN-95-EIX95182619132] p 292 A95-76609	hypersonic entry vehicles
[NASA-CR-195050] p 273 N95-23193 An investigation of helicopter dynamic coupling using	Design and multifunction tests of a frequency	[BTN-95-EIX95152583254] p 306 A95-73555
an analytical model	domain-based active flutter suppression system	MULTIPHASE FLOW
[NASA-CR-197420] p 285 N95-23217	[BTN-95-EIX95182619215] p 292 A95-76641	Effect of ambient turbulence intensity on sphere wakes
Idealized textile composites for experimental/analytical	MINIMUM DRAG	at intermediate Reynolds numbers
correlation p 301 N95-23277	CFD optimization of a theoretical minimum-drag body	[BTN-95-EIX95182619101] p 308 A95-76586 MULTIVARIABLE CONTROL
Inner loop flight control for the High-Speed Civil	[BTN-95-EIX95182619234] p 308 A95-76660 Control of flow separation in airfoil/wing design	Aeroelastic vehicle multivariable control synthesis with
Transport p 293 N95-23314	applications p 274 N95-23294	analytical robustness evaluation
Preparation of course materials: Elementary	MISSILE BODIES	[BTN-95-EIX95182619115] p 321 A95-76592
mathematics of powered flight p 324 N95-23320	Wing vertical position effects on wing-body carryover	Multivariable stability and robustness of sequentially
Aerodynamic design and analysis of a highly loaded turbine exhaust p 312 N95-23435	for noncircular missiles	designed feedback systems
turbine exhaust p 312 N95-23435  Phase 2: HGM air flow tests in support of HEX vane	[BTN-95-EIX95182617462] p 268 A95-75733	[BTN-95-EIX95182619125] p 322 A95-76602 Derivation of system matrices from nonlinear dynamic
investigation p 312 N95-23438	MISSILE CONFIGURATIONS  Base drag prediction on missile configurations	simulation of jet engines
Moving mass trim control for aerospace vehicles	[BTN-95-EIX95152583256] p 266 A95-73557	[BTN-95-EIX95182619139] p 288 A95-76616
[DE95-002602] p 299 N95-23532	Aerodynamic characteristics of a canard-controlled	Design of high performance multivariable control
Assimilation of altimeter data in a quasi-geostrophic	missile at high angles of attack	systems for supermaneuverable aircraft at high angle of
model of the Gulf Stream system: A dynamical	[BTN-95-EIX95152583257] p 267 A95-73558	attack [NASA-CR-197661] p 293 N95-22908
perspective	MISSILE CONTROL  Switched bias proportional navigation for homing	[NASA-CR-197661] p 293 N95-22908
[NASA-CR-196313] p 320 N95-23766 Statistics of multi-look AIRSAR imagery: A comparison	guidance against highly maneuvering targets	N
of theory with measurements p 320 N95-23947.	[BTN-95-EIX95182619145] p 279 A95-76622	17
· · · · · · · · · · · · · · · · · · ·	Moving mass trim control for aerospace vehicles	NAP-OF-THE-FARTH NAVIGATION
A multibody/finite element analysis approach for modeling of crash dynamic responses	Moving mass trim control for aerospace vehicles [DE95-002602] p 299 N95-23532	NAP-OF-THE-EARTH NAVIGATION Automatic guidance and control for helicopter obstacle
A multibody/finite element analysis approach for modeling of crash dynamic responses   NIAR-94-3   p 277 N95-24050	Moving mass trim control for aerospace vehicles [DE95-002602] p 299 N95-23532  MISSILE TRAJECTORIES	Automatic guidance and control for helicopter obstacle avoidance
A multibody/finite element analysis approach for modeling of crash dynamic responses	Moving mass trim control for aerospace vehicles [DE95-002602] p 299 N95-23532	Automatic guidance and control for helicopter obstacle avoidance [BTN-95-EIX95182619130] p 291 A95-76607
A multibody/finite element analysis approach for modeling of crash dynamic responses [NIAR-94-3] p 277 N95-24050   INTRIX MATERIALS US Navy operating experience with new aircraft	Moving mass trim control for aerospace vehicles [DE95-002602] p 299 N95-23532 MISSILE TRAJECTORIES  A CFD study of complex missile and store configurations in relative motion [NASA-CR-197912] p 285 N95-22949	Automatic guidance and control for helicopter obstacle avoidance [BTN-95-EIX95182619130] p 291 A95-76607 NASA PROGRAMS
A multibody/finite element analysis approach for modeling of crash dynamic responses   NIAR-94-3  p 277 N95-24050     ATRIX MATERIALS   US Navy operating experience construction materials   with new aircraft p 303 N95-23517	Moving mass trim control for aerospace vehicles [DE95-002602] p 299 N95-23532  MISSILE TRAJECTORIES  A CFD study of complex missile and store configurations in relative motion  [NASA-CR-197912] p 285 N95-22949  MISSILES	Automatic guidance and control for helicopter obstacle avoidance [BTN-95-EIX95182619130] p 291 A95-76607  NASA PROGRAMS 1994 NASA-HU American Society for Engineering
A multibody/finite element analysis approach for modeling of crash dynamic responses [NIAR-94-3] p 277 N95-24050   IATRIX MATERIALS US Navy operating experience construction materials p 303 N95-23517   IAXIMUM LIKELIHOOD ESTIMATES	Moving mass trim control for aerospace vehicles [DE95-002602] p 299 N95-23532 MISSILE TRAJECTORIES  A CFD study of complex missile and store configurations in relative motion [NASA-CR-197912] p 285 N95-22949 MISSILES  Aerodynamic characteristics of a canard-controlled	Automatic guidance and control for helicopter obstacle avoidance (BTN-95-EIX95182619130) p 291 A95-76607 NASA PROGRAMS 1994 NASA-HU American Society for Engineering Education (ASEE) Summer Faculty Fellowship Program
A multibody/finite element analysis approach for modeling of crash dynamic responses   NIAR-94-3  p 277 N95-24050     ATRIX MATERIALS   US Navy operating experience construction materials   with new aircraft p 303 N95-23517	Moving mass trim control for aerospace vehicles [DE95-002602] p 299 N95-23532  MISSILE TRAJECTORIES  A CFD study of complex missile and store configurations in relative motion [NASA-CR-197912] p 285 N95-22949  MISSILES  Aerodynamic characteristics of a canard-controlled missile at high angles of attack	Automatic guidance and control for helicopter obstacle avoidance  [BTN-95-EIX95182619130] p 291 A95-76607  NASA PROGRAMS  1994 NASA-HU American Society for Engineering Education (ASEE) Summer Faculty Fellowship Program [NASA-CR-194972] p 325 N95-23276  Research and Technology, 1994
A multibody/finite element analysis approach for modeling of crash dynamic responses [NIAR-94-3] p 277 N95-24050   ATRIX MATERIALS US Navy operating experience with new aircraft construction materials [NIAXIMUM LIKELIHOOD ESTIMATES] Maximum-likelihood spectral estimation and adaptive	Moving mass trim control for aerospace vehicles [DE95-002602] p 299 N95-23532  MISSILE TRAJECTORIES  A CFD study of complex missile and store configurations in relative motion [NASA-CR-197912] p 285 N95-22949  MISSILES  Aerodynamic characteristics of a canard-controlled missile at high angles of attack [BTN-95-EIX95152583257] p 267 A95-73558	Automatic guidance and control for helicopter obstacle avoidance [BTN-95-EIX95182619130] p 291 A95-76607  NASA PROGRAMS  1994 NASA-HU American Society for Engineering Education (ASEE) Summer Faculty Fellowship Program [NASA-CR-194972] p 325 N95-23276 Research and Technology, 1994 [NASA-TM-106764] p 262 N95-24025
A multibody/finite element analysis approach for modeling of crash dynamic responses [NIAR-94-3] p 277 N95-24050 IATRIX MATERIALS  US Navy operating experience with new aircraft p 303 N95-23517 IAXIMUM LIKELIHOOD ESTIMATES  Maximum-likelihood spectral estimation and adaptive filtering techniques with application to airborne Doppler weather radar [NASA-CR-197699] p 316 N95-23670	Moving mass trim control for aerospace vehicles [DE95-002602] p 299 N95-23532  MISSILE TRAJECTORIES  A CFD study of complex missile and store configurations in relative motion [NASA-CR-197912] p 285 N95-22949  MISSILES  Aerodynamic characteristics of a canard-controlled missile at high angles of attack	Automatic guidance and control for helicopter obstacle avoidance [BTN-95-EIX95182619130] p 291 A95-76607  NASA PROGRAMS 1994 NASA-HU American Society for Engineering Education (ASEE) Summer Faculty Fellowship Program [NASA-CR-194972] p 325 N95-23276 Research and Technology, 1994 [NASA-TM-106764] p 262 N95-24025  NASTRAN
A multibody/finite element analysis approach for modeling of crash dynamic responses [NIAR-94-3] p 277 N95-24050 NATRIX MATERIALS  US Navy operating experience with new aircraft p 303 N95-23517 NATIONAL PROPERTIES Maximum-likelinood spectral estimation and adaptive filtering techniques with application to airborne Doppler weather radar [NASA-CR-197699] p 316 N95-23670 NPS-23670 NPS-2	Moving mass trim control for aerospace vehicles [DE95-002602] p 299 N95-23532  MISSILE TRAJECTORIES  A CFD study of complex missile and store configurations in relative motion [NASA-CR-197912] p 285 N95-22949  MISSILES  Aerodynamic characteristics of a canard-controlled missile at high angles of attack [BTN-95-EIX95152583257] p 267 A95-73558  Wing vertical position effects on wing-body carryover for noncircular missiles [BTN-95-EIX95182617462] p 268 A95-75733	Automatic guidance and control for helicopter obstacle avoidance  [BTN-95-EIX95182619130] p 291 A95-76607  NASA PROGRAMS  1994 NASA-HU American Society for Engineering Education (ASEE) Summer Faculty Fellowship Program [NASA-CR-194972] p 325 N95-23276  Research and Technology. 1994  [NASA-TM-106764] p 262 N95-24025  NASTRAN  Thin tailored composite wing for civil tiltrotor
A multibody/finite element analysis approach for modeling of crash dynamic responses   NISA-94-3  p 277 N95-24050     ATRIX MATERIALS	Moving mass trim control for aerospace vehicles [DE95-002602] p 299 N95-23532 MISSILE TRAJECTORIES  A CFD study of complex missile and store configurations in relative motion [NASA-CR-197912] p 285 N95-22949 MISSILES  Aerodynamic characteristics of a canard-controlled missile at high angles of attack [BTN-95-EIX95152583257] p 267 A95-73558 Wing vertical position effects on wing-body carryover for noncircular missiles [BTN-95-EIX95182617462] p 268 A95-75733 Supersonic near-wake afterbody boattailing effects on	Automatic guidance and control for helicopter obstacle avoidance  [BTN-95-EIX95182619130] p 291 A95-76607  NASA PROGRAMS  1994 NASA-HU American Society for Engineering Education (ASEE) Summer Faculty Fellowship Program [NASA-CR-194972] p 325 N95-23276  Research and Technology, 1994  [NASA-TM-106764] p 262 N95-24025  NASTRAN  Thin tailored composite wing for civil tiltrotor p 285 N95-23317
A multibody/finite element analysis approach for modeling of crash dynamic responses [NIAR-94-3] p 277 N95-24050 IATRIX MATERIALS  US Navy operating experience with new aircraft construction materials p 303 N95-23517 IAXIMUM LIKELIHOOD ESTIMATES  Maximum-likelihood spectral estimation and adaptive filtering techniques with application to airborne Doppler weather radar [NASA-CR-197699] p 316 N95-23670 IECHANICAL PROPERTIES Idealized textile composites for experimental/analytical correlation p 301 N95-23277	Moving mass trim control for aerospace vehicles [DE95-002602] p 299 N95-23532  MISSILE TRAJECTORIES A CFD study of complex missile and store configurations in relative motion [NASA-CR-197912] p 285 N95-22949  MISSILES Aerodynamic characteristics of a canard-controlled missile at high angles of attack [BTN-95-EIX95152583257] p 267 A95-73558 Wing vertical position effects on wing-body carryover for noncircular missiles [BTN-95-EIX95182617462] p 268 A95-75733 Supersonic near-wake afterbody boattailing effects on axisymmetric bodies	Automatic guidance and control for helicopter obstacle avoidance  [BTN-95-EIX95182619130] p 291 A95-76607  NASA PROGRAMS  1994 NASA-HU American Society for Engineering Education (ASEE) Summer Faculty Fellowship Program [NASA-CR-194972] p 325 N95-23276  Research and Technology. 1994  [NASA-TM-106764] p 262 N95-24025  NASTRAN  Thin tailored composite wing for civil tiltrotor
A multibody/finite element analysis approach for modeling of crash dynamic responses [NIAR-94-3] p 277 N95-24050 IATRIX MATERIALS  US Navy operating experience with new aircraft p 303 N95-23517 IAXIMUM LIKELIHOOD ESTIMATES  Maximum-likelihood spectral estimation and adaptive filtering techniques with application to airborne Doppler weather radar [NASA-CR-197699] p 316 N95-23670 IECHANICAL PROPERTIES Idealized textile composites for experimental/analytical correlation p 301 N95-23277 IESOMETEOROLOGY	Moving mass trim control for aerospace vehicles [DE95-002602] p 299 N95-23532 MISSILE TRAJECTORIES  A CFD study of complex missile and store configurations in relative motion [NASA-CR-197912] p 285 N95-22949 MISSILES  Aerodynamic characteristics of a canard-controlled missile at high angles of attack [BTN-95-EIX95152583257] p 267 A95-73558 Wing vertical position effects on wing-body carryover for noncircular missiles [BTN-95-EIX95182617462] p 268 A95-75733 Supersonic near-wake afterbody boattailing effects on axisymmetric bodies [BTN-95-EIX95182617465] p 268 A95-75736	Automatic guidance and control for helicopter obstacle avoidance [BTN-95-EIX95182619130] p 291 A95-76607  NASA PROGRAMS 1994 NASA-HU American Society for Engineering Education (ASEE) Summer Faculty Fellowship Program [NASA-CR-194972] p 235 N95-23276 Research and Technology, 1994 [NASA-TM-106764] p 262 N95-24025  NASTRAN Thin tailored composite wing for civil tiltrotor p 285 N95-23317  NAVIER-STOKES EQUATION
A multibody/finite element analysis approach for modeling of crash dynamic responses [NIAR-94-3] p 277 N95-24050 NATRIX MATERIALS  US Navy operating experience with new aircraft p 303 N95-23517 NATRIX MATERIALS  AXIMUM LIKELIHOOD ESTIMATES  Maximum-likelihood spectral estimation and adaptive filtering techniques with application to airborne Doppler weather radar  [NASA-CR-197699] p 316 N95-23670 NP5-23670 NP5-23277 NP5-232	Moving mass trim control for aerospace vehicles [DE95-002602] p 299 N95-23532  MISSILE TRAJECTORIES  A CFD study of complex missile and store configurations in relative motion  INASA-CR-197912] p 285 N95-22949  MISSILES  Aerodynamic characteristics of a canard-controlled missile at high angles of attack [BTN-95-EIX95152583257] p 267 A95-73558  Wing vertical position effects on wing-body carryover for noncircular missiles [BTN-95-EIX95182617462] p 268 A95-75733  Supersonic near-wake afterbody boattailing effects on axisymmetric bodies [BTN-95-EIX95182617465] p 268 A95-75736  MOBILE COMMUNICATION SYSTEMS	Automatic guidance and control for helicopter obstacle avoidance [BTN-95-EIX95182619130] p 291 A95-76607  NASA PROGRAMS 1994 NASA-HU American Society for Engineering Education (ASEE) Summer Faculty Fellowship Program [NASA-CR-194972] Research and Technology, 1994 [NASA-TM-106764] p 262 N95-23276  NASTRAN Thin tailored composite wing for civil tiltrotor p 285 N95-23317  NAVIER-STOKES EQUATION Preconditioned domain decomposition scheme for three-dimensional aerodynamic sensitivity analysis [BTN-95-EIX95152577612] p 321 A95-73471
A multibody/finite element analysis approach for modeling of crash dynamic responses [NIAR-94-3] p 277 N95-24050 IATRIX MATERIALS  US Navy operating experience with new aircraft p 303 N95-23517 IAXIMUM LIKELIHOOD ESTIMATES  Maximum-likelihood spectral estimation and adaptive filtering techniques with application to airborne Doppler weather radar [NASA-CR-197699] p 316 N95-23670 IECHANICAL PROPERTIES Idealized textile composites for experimental/analytical correlation p 301 N95-23277 IESOMETEOROLOGY	Moving mass trim control for aerospace vehicles [DE95-002602] p 299 N95-23532 MISSILE TRAJECTORIES  A CFD study of complex missile and store configurations in relative motion [NASA-CR-197912] p 285 N95-22949 MISSILES  Aerodynamic characteristics of a canard-controlled missile at high angles of attack [BTN-95-EIX95152583257] p 267 A95-73558 Wing vertical position effects on wing-body carryover for noncircular missiles [BTN-95-EIX95182617462] p 268 A95-75733 Supersonic near-wake afterbody boattailing effects on axisymmetric bodies [BTN-95-EIX95182617465] p 268 A95-75736	Automatic guidance and control for helicopter obstacle avoidance  [BTN-95-EIX95182619130] p 291 A95-76607  NASA PROGRAMS  1994 NASA-HU American Society for Engineering Education (ASEE) Summer Faculty Fellowship Program [NASA-CR-194972] p 325 N95-23276 Research and Technology, 1994 [NASA-TM-106764] p 262 N95-24025  NASTRAN  Thin tailored composite wing for civil tiltrotor p 285 N95-23317  NAVIER-STOKES EQUATION  Preconditioned domain decomposition scheme for three-dimensional aerodynamic sensitivity analysis [BTN-95-EIX95152577612] p 321 A95-73471 Effects of spatial order of accuracy on the computation
A multibody/finite element analysis approach for modeling of crash dynamic responses [NIAR-94-3] p 277 N95-24050 NATRIX MATERIALS  US Navy operating experience with new aircraft construction materials p 303 N95-23517 NATION CONTROL OF CONTROL	Moving mass trim control for aerospace vehicles [DE95-002602] p 299 N95-23532 MISSILE TRAJECTORIES  A CFD study of complex missile and store configurations in relative motion [NASA-CR-197912] p 285 N95-22949 MISSILES  Aerodynamic characteristics of a canard-controlled missile at high angles of attack [BTN-95-EIX95152583257] p 267 A95-73558 Wing vertical position effects on wing-body carryover for noncircular missiles [BTN-95-EIX95182617462] p 268 A95-75733 Supersonic near-wake afterbody boattailing effects on axisymmetric bodies [BTN-95-EIX95182617465] p 268 A95-75736 MOBILE COMMUNICATION SYSTEMS  Development of aeronautical mobile sateflite services over the past thirty years [BTN-95-EIX95152569458] p 305 A95-73498	Automatic guidance and control for helicopter obstacle avoidance  [BTN-95-EIX95182619130] p 291 A95-76607  NASA PROGRAMS  1994 NASA-HU American Society for Engineering Education (ASEE) Summer Faculty Fellowship Program [NASA-CR-194972] p 325 N95-23276  Research and Technology, 1994  [NASA-TM-106764] p 262 N95-24025  NASTRAN  Thin tailored composite wing for civil tiltrotor p 285 N95-23317  NAVIER-STOKES EQUATION  Preconditioned domain decomposition scheme for three-dimensional aerodynamic sensitivity analysis [BTN-95-EIX95152577612] p 321 A95-73471  Effects of spatial order of accuracy on the computation of vortical flowfields
A multibody/finite element analysis approach for modeling of crash dynamic responses [NIAR-94-3] p 277 N95-24050 NATRIX MATERIALS  US Navy operating experience with new aircraft construction materials p 303 N95-23517 NATION CONTROL OF CONTROL	Moving mass trim control for aerospace vehicles [DE95-002602] p 299 N95-23532  MISSILE TRAJECTORIES  A CFD study of complex missile and store configurations in relative motion  INASA-CR-197912] p 285 N95-22949  MISSILES  Aerodynamic characteristics of a canard-controlled missile at high angles of attack  [BTN-95-EIX95152583257] p 267 A95-73558  Wing vertical position effects on wing-body carryover for noncircular missiles  [BTN-95-EIX95182617462] p 268 A95-75733  Supersonic near-wake afterbody boattailing effects on axisymmetric bodies  [BTN-95-EIX95182617465] p 268 A95-75736  MOBILE COMMUNICATION SYSTEMS  Development of aeronautical mobile sateflite services over the past thirty years  [BTN-95-EIX95152569458] p 305 A95-73498  MODULUS OF ELASTICITY	Automatic guidance and control for helicopter obstacle avoidance [BTN-95-EIX95182619130] p 291 A95-76607  NASA PROGRAMS 1994 NASA-HU American Society for Engineering Education (ASEE) Summer Faculty Fellowship Program [NASA-CR-194972] p 235 N95-23276 Research and Technology, 1994 [NASA-TM-106764] p 262 N95-24025  NASTRAN Thin tailored composite wing for civil tiltrotor p 285 N95-23317  NAVIER-STOKES EQUATION Preconditioned domain decomposition scheme for three-dimensional aerodynamic sensitivity analysis [BTN-95-EIX95152577612] p 321 A95-73471 Effects of spatial order of accuracy on the computation of vortical flowfields [BTN-95-EIX95152577604] p 305 A95-73479
A multibody/finite element analysis approach for modeling of crash dynamic responses [NIAR-94-3] p 277 N95-24050 IATRIX MATERIALS  US Navy operating experience with new aircraft construction materials p 303 N95-23517 IAXIMUM LIKELIHOOD ESTIMATES  Maximum-likelihood spectral estimation and adaptive filtering techniques with application to airborne Doppler weather radar [NASA-CR-197699] p 316 N95-23670 IECHANICAL PROPERTIES Idealized textile composites for experimental/analytical correlation p 301 N95-23277 IESOMETEOROLOGY  Diurnal variation of lee vortices in Taiwan and the surrounding area [HTN-95-91363] p 318 A95-76394 IETAL COATINGS  Cu deposition using a permanent magnet electron cyclotron resonance microwave plasma source	Moving mass trim control for aerospace vehicles [DE95-002602] p 299 N95-23532  MISSILE TRAJECTORIES  A CFO study of complex missile and store configurations in relative motion [NASA-CR-197912] p 285 N95-22949  MISSILES  Aerodynamic characteristics of a canard-controlled missile at high angles of attack [BTN-95-EIX95152583257] p 267 A95-73558  Wing vertical position effects on wing-body carryover for noncircular missiles [BTN-95-EIX95182617462] p 268 A95-75733  Supersonic near-wake atterbody boattailing effects on axisymmetric bodies [BTN-95-EIX95182617465] p 268 A95-75736  MOBILE COMMUNICATION SYSTEMS  Development of aeronautical mobile sateflite services over the past thirty years [BTN-95-EIX95152569458] p 305 A95-73498  MODULUS OF ELASTICITY  Evaluation of advanced aerospace materials by depth	Automatic guidance and control for helicopter obstacle avoidance  [BTN-95-EIX95182619130] p 291 A95-76607  NASA PROGRAMS  1994 NASA-HU American Society for Engineering Education (ASEE) Summer Faculty Fellowship Program [NASA-CR-194972] p 325 N95-23276 Research and Technology, 1994 [NASA-TM-106764] p 262 N95-24025  NASTRAN  Thin tailored composite wing for civil titrotor p 285 N95-23317  NAVIER-STOKES EQUATION  Preconditioned domain decomposition scheme for three-dimensional aerodynamic sensitivity analysis [BTN-95-EIX95152577612] p 321 A95-73471  Effects of spatial order of accuracy on the computation of vortical flowfields [BTN-95-EIX95152577604] p 305 A95-73479 Computation of oscillating airfoil flows with one- and
A multibody/finite element analysis approach for modeling of crash dynamic responses [NIAR-94-3] p 277 N95-24050 IATRIX MATERIALS  US Navy operating experience with new aircraft p. 303 N95-23517 IAXIMUM LIKELIHOOD ESTIMATES  Maximum-likelihood spectral estimation and adaptive filtering techniques with application to airborne Doppler weather radar [NASA-CR-197699] p 316 N95-23670 IECHANICAL PROPERTIES Idealized textile composites for experimental/analytical correlation p 301 N95-23277 IESOMETEOROLOGY  Diurnal variation of lee vortices in Taiwan and the surrounding area [HTN-95-91363] p 318 A95-76394 IETAL COATINGS  Cu deposition using a permanent magnet electron cyclotron resonance microwave plasma source [DE94-017768] p 304 N95-23981	Moving mass trim control for aerospace vehicles [DE95-002602] p 299 N95-23532  MISSILE TRAJECTORIES  A CFD study of complex missile and store configurations in relative motion [NASA-CR-197912] p 285 N95-22949  MISSILES  Aerodynamic characteristics of a canard-controlled missile at high angles of attack [BTN-95-EIX995152583257] p 267 A95-73558  Wing vertical position effects on wing-body carryover for noncircular missiles [BTN-95-EIX95182617462] p 268 A95-75733  Supersonic near-wake afterbody boattailing effects on axisymmetric bodies [BTN-95-EIX95182617465] p 268 A95-75736  MOBILE COMMUNICATION SYSTEMS  Development of aeronautical mobile satellite services over the past thirty years [BTN-95-EIX95152569458] p 305 A95-73498  MODULUS OF ELASTICITY  Evaluation of advanced aerospace materials by depth sensing indentation and scratch methods	Automatic guidance and control for helicopter obstacle avoidance [BTN-95-EIX95182619130] p 291 A95-76607  NASA PROGRAMS 1994 NASA-HU American Society for Engineering Education (ASEE) Summer Faculty Fellowship Program [NASA-CR-194972] p 235 N95-23276 Research and Technology, 1994 [NASA-TM-106764] p 262 N95-24025  NASTRAN Thin tailored composite wing for civil tiltrotor p 285 N95-23317  NAVIER-STOKES EQUATION Preconditioned domain decomposition scheme for three-dimensional aerodynamic sensitivity analysis [BTN-95-EIX95152577612] p 321 A95-73471 Effects of spatial order of accuracy on the computation of vortical flowfields [BTN-95-EIX95152577604] p 305 A95-73479
A multibody/finite element analysis approach for modeling of crash dynamic responses [NIAR-94-3] p 277 N95-24050 NATRIX MATERIALS  US Navy operating experience with new aircraft p 303 N95-23517 NATIONAL ELEMENTS (STATE) NATIONAL ELEMENT (STATE) N	Moving mass trim control for aerospace vehicles [DE95-002602] p 299 N95-23532  MISSILE TRAJECTORIES  A CFD study of complex missile and store configurations in relative motion  INASA-CR-197912] p 285 N95-22949  MISSILES  Aerodynamic characteristics of a canard-controlled missile at high angles of attack [BTN-95-EIX95152583257] p 267 A95-73558  Wing vertical position effects on wing-body carryover for noncircular missiles [BTN-95-EIX95182617462] p 268 A95-75733  Supersonic near-wake afterbody boattailing effects on axisymmetric bodies [BTN-95-EIX95182617465] p 268 A95-75736  MOBILE COMMUNICATION SYSTEMS  Development of aeronautical mobile sateflite services over the past thirty years [BTN-95-EIX95152569458] p 305 A95-73498  MODULUS OF ELASTICITY  Evaluation of advanced aerospace materials by depth sensing indentation and scratch methods [BTN-95-EIX95152584678] p 282 A95-73590	Automatic guidance and control for helicopter obstacle avoidance  [BTN-95-EIX95182619130] p 291 A95-76607  NASA PROGRAMS  1994 NASA-HU American Society for Engineering Education (ASEE) Summer Faculty Fellowship Program [NASA-CR-194972] p 325 N95-23276 Research and Technology, 1994 [NASA-TM-106764] p 262 N95-24025  NASTRAN  Thin tailored composite wing for civil tiltrotor p 285 N95-23317  NAVIER-STOKES EQUATION  Preconditioned domain decomposition scheme for three-dimensional aerodynamic sensitivity analysis [BTN-95-EIX95152577612] p 321 A95-73471 Effects of spatial order of accuracy on the computation of vortical flowfields  [BTN-95-EIX95152577604] p 305 A95-73479 Computation of oscillating airfoil flows with one- and two-equation turbulence models [BTN-95-EIX95152577588] p 263 A95-73494 Computation of the poststall behavior of a circulation
A multibody/finite element analysis approach for modeling of crash dynamic responses [NIAR-94-3] p 277 N95-24050 IATRIX MATERIALS  US Navy operating experience with new aircraft construction materials p 303 N95-23517 IAXIMUM LIKELIHOOD ESTIMATES  Maximum-likelihood spectral estimation and adaptive filtering techniques with application to airborne Doppler weather radar [NASA-CR-197699] p 316 N95-23670 IECHANICAL PROPERTIES Idealized textile composites for experimental/analytical correlation p 301 N95-23277 IESOMETEOROLOGY  Diurnal variation of lee vortices in Taiwan and the surrounding area [HTN-95-91363] p 318 A95-76394 IETAL COATINGS  Cu deposition using a permanent magnet electron cyclotron resonance microwave plasma source [DE94-017768] p 304 N95-23981 IETAL FATIGUE  Multiple site fatigue damage in fuselage skin splices:	Moving mass trim control for aerospace vehicles [DE95-002602] p 299 N95-23532  MISSILE TRAJECTORIES  A CFD study of complex missile and store configurations in relative motion [NASA-CR-197912] p 285 N95-22949  MISSILES  Aerodynamic characteristics of a canard-controlled missile at high angles of attack [BTN-95-EIX995152583257] p 267 A95-73558  Wing vertical position effects on wing-body carryover for noncircular missiles [BTN-95-EIX95182617462] p 268 A95-75733  Supersonic near-wake afterbody boattailing effects on axisymmetric bodies [BTN-95-EIX95182617465] p 268 A95-75736  MOBILE COMMUNICATION SYSTEMS  Development of aeronautical mobile satellite services over the past thirty years [BTN-95-EIX95152569458] p 305 A95-73498  MODULUS OF ELASTICITY  Evaluation of advanced aerospace materials by depth sensing indentation and scratch methods	Automatic guidance and control for helicopter obstacle avoidance  [BTN-95-EIX95182619130] p 291 A95-76607  NASA PROGRAMS  1994 NASA-HU American Society for Engineering Education (ASEE) Summer Faculty Fellowship Program [NASA-CR-194972] p 325 N95-23276  Research and Technology, 1994  [NASA-TM-106764] p 262 N95-24025  NASTRAN  Thin tailored composite wing for civil tiltrotor p 285 N95-23317  NAVIER-STOKES EQUATION  Preconditioned domain decomposition scheme for three-dimensional aerodynamic sensitivity analysis  [BTN-95-EIX95152577604] p 321 A95-73471  Effects of spatial order of accuracy on the computation of vortical flowfields  [BTN-95-EIX95152577604] p 305 A95-73479  Computation of oscillating airfoil flows with one- and two-equation turbulence models  [BTN-95-EIX95152577588] p 263 A95-73494  Computation of the poststall behavior of a circulation controlled airfoil
A multibody/finite element analysis approach for modeling of crash dynamic responses [NIAR-94-3] p 277 N95-24050 IATRIX MATERIALS  US Navy operating experience with new aircraft construction materials  Maximum-likelinood spectral estimation and adaptive filtering techniques with application to airborne Doppler weather radar [NASA-CR-197699] p 316 N95-23670 IECHANICAL PROPERTIES Idealized textile composites for experimental/analytical correlation p 301 N95-23277 IESOMETEOROLOGY  Diurnal variation of lee vortices in Taiwan and the surrounding area [HTN-95-91363] p 318 A95-76394 IETAL COATINGS  Cu deposition using a permanent magnet electron cyclotron resonance microwave plasma source [DE94-017768] p 304 N95-23981 IETAL FATIGUE Multiple site tatigue damage in fuselage skin splices: Experimental simulation and theoretical prediction	Moving mass trim control for aerospace vehicles [DE95-002602] p 299 N95-23532  MISSILE TRAJECTORIES A CFD study of complex missile and store configurations in relative motion [NASA-CR-197912] p 285 N95-22949  MISSILES Aerodynamic characteristics of a canard-controlled missile at high angles of attack [BTN-95-EIX95152583257] p 267 A95-73558 Wing vertical position effects on wing-body carryover for noncircular missiles [BTN-95-EIX95182617462] p 268 A95-75733 Supersonic near-wake afterbody boattailing effects on axisymmetric bodies [BTN-95-EIX95182617465] p 268 A95-75736  MOBILE COMMUNICATION SYSTEMS Development of aeronautical mobile satellite services over the past thirty years [BTN-95-EIX95152569458] p 305 A95-73498  MODULUS OF ELASTICITY Evaluation of advanced aerospace materials by depth sensing indentation and scratch methods [BTN-95-EIX95152584678] p 282 A95-73590 Interlaminar shear test method development for long term durability testing of composites	Automatic guidance and control for helicopter obstacle avoidance [BTN-95-EIX95182619130] p 291 A95-76607  NASA PROGRAMS 1994 NASA-HU American Society for Engineering Education (ASEE) Summer Faculty Fellowship Program [NASA-CR-194972] p 235 N95-23276 Research and Technology, 1994 [NASA-TM-106764] p 262 N95-24025  NASTRAN Thin tailored composite wing for civil tiltrotor p 285 N95-23317  NAVIER-STOKES EQUATION Preconditioned domain decomposition scheme for three-dimensional aerodynamic sensitivity analysis [BTN-95-EIX95152577612] p 321 A95-73471 Effects of spatial order of accuracy on the computation of vortical flowriedds [BTN-95-EIX95152577604] p 305 A95-73479 Computation of oscillating airfoil flows with one- and two-equation turbulence models [BTN-95-EIX95152577588] p 263 A95-73494 Computation of the poststall behavior of a circulation controlled airfoil [BTN-95-EIX95152582320] p 264 A95-73523
A multibody/finite element analysis approach for modeling of crash dynamic responses [NIAR-94-3] p 277 N95-24050 IATRIX MATERIALS  US Navy operating experience with new aircraft p. 303 N95-23517 IAXIMUM LIKELIHOOD ESTIMATES  Maximum-likelihood spectral estimation and adaptive filtering techniques with application to airborne Doppler weather radar [NASA-CR-197699] p 316 N95-23670 IECHANICAL PROPERTIES Idealized textile composites for experimental/analytical correlation p 301 N95-23277 IESOMETEOROLOGY  Diurnal variation of fee vortices in Taiwan and the surrounding area [HTN-95-91363] p 318 A95-76394 IETAL COATINGS  Cu deposition using a permanent magnet electron cyclotron resonance microwave plasma source [DE94-017768] p 304 N95-23981 IETAL FATIGUE  Multiple site fatigue damage in fuselage skin splices: Experimental simulation and theoretical prediction [BTN-95-EIX95152584676] p 276 A95-73588	Moving mass trim control for aerospace vehicles [DE95-002602] p 299 N95-23532  MISSILE TRAJECTORIES  A CFO study of complex missile and store configurations in relative motion [NASA-CR-197912] p 285 N95-22949  MISSILES  Aerodynamic characteristics of a canard-controlled missile at high angles of attack [BTN-95-EIX95152583257] p 267 A95-73558  Wing vertical position effects on wing-body carryover for noncircular missiles [BTN-95-EIX95182617462] p 268 A95-75733  Supersonic near-wake afterbody boattailing effects on axisymmetric bodies [BTN-95-EIX95182617465] p 268 A95-75736  MOBILE COMMUNICATION SYSTEMS  Development of aeronautical mobile satellite services over the past thirty years [BTN-95-EIX95152569458] p 305 A95-73498  MODULUS OF ELASTICITY  Evaluation of advanced aerospace materials by depth sensing indentation and scratch methods [BTN-95-EIX9515256478] p 282 A95-73590 Intertaminar shear test method development for long term durability testing of composites	Automatic guidance and control for helicopter obstacle avoidance  [BTN-95-EIX95182619130] p 291 A95-76607  NASA PROGRAMS  1994 NASA-HU American Society for Engineering Education (ASEE) Summer Faculty Fellowship Program [NASA-CR-194972] p 325 N95-23276  Research and Technology, 1994 [NASA-TM-106764] p 262 N95-24025  NASTRAN  Thin tailored composite wing for civil tiltrotor p 285 N95-23317  NAVIER-STOKES EQUATION  Preconditioned domain decomposition scheme for three-dimensional aerodynamic sensitivity analysis [BTN-95-EIX95152577612] p 321 A95-73471  Effects of spatial order of accuracy on the computation of vortical flowfields  [BTN-95-EIX95152577604] p 305 A95-73479  Computation of oscillating airfoil flows with one- and two-equation turbulence models  [BTN-95-EIX95152577588] p 263 A95-73494  Computation of the poststall behavior of a circulation controlled airfoil  [BTN-95-EIX95152582320] p 264 A95-73523  Navier-Stokes prediction of large-amplitude delta-wing
A multibody/finite element analysis approach for modeling of crash dynamic responses [NIAR-94-3] p 277 N95-24050 IATRIX MATERIALS  US Navy operating experience with new aircraft construction materials  Maximum-likelinood spectral estimation and adaptive filtering techniques with application to airborne Doppler weather radar [NASA-CR-197699] p 316 N95-23670 IECHANICAL PROPERTIES Idealized textile composites for experimental/analytical correlation p 301 N95-23277 IESOMETEOROLOGY  Diurnal variation of lee vortices in Taiwan and the surrounding area [HTN-95-91363] p 318 A95-76394 IETAL COATINGS  Cu deposition using a permanent magnet electron cyclotron resonance microwave plasma source [DE94-017768] p 304 N95-23981 IETAL FATIGUE Multiple site tatigue damage in fuselage skin splices: Experimental simulation and theoretical prediction	Moving mass trim control for aerospace vehicles [DE95-002602] p 299 N95-23532  MISSILE TRAJECTORIES  A CFD study of complex missile and store configurations in relative motion [NASA-CR-197912] p 285 N95-22949  MISSILES  Aerodynamic characteristics of a canard-controlled missile at high angles of attack [BTN-95-EIX95152583257] p 267 A95-73558  Wing vertical position effects on wing-body carryover for noncircular missiles [BTN-95-EIX95182617462] p 268 A95-75733  Supersonic near-wake afterbody boattaiting effects on axisymmetric bodies [BTN-95-EIX95182617465] p 268 A95-75736  MOBILE COMMUNICATION SYSTEMS  Development of aeronautical mobile satellite services over the past thirty years [BTN-95-EIX95152569458] p 305 A95-73498  MODULUS OF ELASTICITY  Evaluation of advanced aerospace materials by depth sensing indentation and scratch methods [BTN-95-EIX95152584678] p 282 A95-73590 Interfaminar shear test method development for long term durability testing of composites  MOISTURE  Measurement of moisture and total hydrocarbon	Automatic guidance and control for helicopter obstacle avoidance [BTN-95-EIX95182619130] p 291 A95-76607  NASA PROGRAMS 1994 NASA-HU American Society for Engineering Education (ASEE) Summer Faculty Fellowship Program [NASA-CR-194972] p 235 N95-23276 Research and Technology, 1994 [NASA-TM-106764] p 262 N95-24025  NASTRAN Thin tailored composite wing for civil tiltrotor p 285 N95-23317  NAVIER-STOKES EQUATION Preconditioned domain decomposition scheme for three-dimensional aerodynamic sensitivity analysis [BTN-95-EIX95152577612] p 321 A95-73471 Effects of spatial order of accuracy on the computation of vortical flowriedds [BTN-95-EIX95152577604] p 305 A95-73479 Computation of oscillating airfoil flows with one- and two-equation turbulence models [BTN-95-EIX95152577588] p 263 A95-73494 Computation of the poststall behavior of a circulation controlled airfoil [BTN-95-EIX95152582320] p 264 A95-73523
A multibody/finite element analysis approach for modeling of crash dynamic responses [NIAR-94-3] p 277 N95-24050 IATRIX MATERIALS  US Navy operating experience with new aircraft p 303 N95-23517 IAXIMUM LIKELIHOOD ESTIMATES  Maximum-likelihood spectral estimation and adaptive filtering techniques with application to airborne Doppler weather radar [NASA-CR-197699] p 316 N95-23670 IECHANICAL PROPERTIES Idealized textile composites for experimental/analytical correlation p 301 N95-23277 IECHANICAL PROPERTIES IDEALIZED FOR STATE OF S	Moving mass trim control for aerospace vehicles [DE95-002602] p 299 N95-23532  MISSILE TRAJECTORIES  A CFD study of complex missile and store configurations in relative motion [NASA-CR-197912] p 285 N95-22949  MISSILES  Aerodynamic characteristics of a canard-controlled missile at high angles of attack [BTN-95-EIX95152583257] p 267 A95-73558  Wing vertical position effects on wing-body carryover for noncircular missiles [BTN-95-EIX95182617462] p 268 A95-75733  Supersonic near-wake afterbody boattailing effects on axisymmetric bodies [BTN-95-EIX95182617465] p 268 A95-75736  MOBILE COMMUNICATION SYSTEMS  Development of aeronautical mobile sateflite services over the past thirty years [BTN-95-EIX95152569458] p 305 A95-73498  MODULUS OF ELASTICITY  Evaluation of advanced aerospace materials by depth sensing indentation and scratch methods [BTN-95-EIX95152584678] p 282 A95-73590 Intertaminar shear test method development for long term durability testing of composites  MOISTURE  Measurement of moisture and total hydrocarbon contributions by valves used in clean room gas-delivery	Automatic guidance and control for helicopter obstacle avoidance  [BTN-95-EIX95182619130] p 291 A95-76607  NASA PROGRAMS  1994 NASA-HU American Society for Engineering Education (ASEE) Summer Faculty Fellowship Program [NASA-CR-194972] p 325 N95-23276  Research and Technology, 1994 [NASA-TM-106764] p 262 N95-24025  NASTRAN  Thin tailored composite wing for civil tiltrotor p 285 N95-23317  NAVIER-STOKES EQUATION  Preconditioned domain decomposition scheme for three-dimensional aerodynamic sensitivity analysis [BTN-95-EIX95152577612] p 321 A95-73471  Effects of spatial order of accuracy on the computation of vortical flowfields  [BTN-95-EIX95152577604] p 305 A95-73479  Computation of oscillating airfoil flows with one- and two-equation turbulence models  [BTN-95-EIX95152577588] p 263 A95-73494  Computation of the poststall behavior of a circulation controlled airfoil  [BTN-95-EIX95152582320] p 264 A95-73523  Navier-Stokes prediction of large-amplitude delta-wing roll oscillations  [BTN-95-EIX95152582329] p 281 A95-73531  Computational study of plume-induced separation on a
A multibody/finite element analysis approach for modeling of crash dynamic responses [NIAR-94-3] p 277 N95-24050 IATRIX MATERIALS  US Navy operating experience with new aircraft construction materials p 303 N95-23517 IAXIMUM LIKELIHOOD ESTIMATES  Maximum-likelihood spectral estimation and adaptive filtering techniques with application to airborne Doppler weather radar  [NASA-CR-197699] p 316 N95-23670 IECHANICAL PROPERTIES Idealized textile composites for experimental/analytical correlation p 301 N95-23277 IESOMETEOROLOGY  Diurnal variation of lee vortices in Taiwan and the surrounding area [HTN-95-91363] p 318 A95-76394 IETAL COATINGS  Cu deposition using a permanent magnet electron cyclotron resonance microwave plasma source [DE94-017768] p 304 N95-23981 IETAL FATIGUE  Multiple site fatigue damage in fuselage skin splices: Experimental simulation and theoretical prediction [BTN-95-EIX95152584676] p 276 A95-73588 Fatigue strength of high-temperature alloys under conditions of cyclic temperature variation. Communication 1: Experimental procedure and results [BTN-94-EIX94401363884] p 307 A95-75516	Moving mass trim control for aerospace vehicles [DE95-002602] p 299 N95-23532  MISSILE TRAJECTORIES  A CFO study of complex missile and store configurations in relative motion [NASA-CR-197912] p 285 N95-22949  MISSILES  Aerodynamic characteristics of a canard-controlled missile at high angles of attack [BTN-95-EIX95152583257] p 267 A95-73558  Wing vertical position effects on wing-body carryover for noncircular missiles [BTN-95-EIX95182617462] p 268 A95-75733  Supersonic near-wake atterbody boattailing effects on axisymmetric bodies [BTN-95-EIX95182617465] p 268 A95-75736  MOBILE COMMUNICATION SYSTEMS  Development of aeronautical mobile sateflite services over the past thirty years [BTN-95-EIX95152569458] p 305 A95-73498  MODULUS OF ELASTICITY  Evaluation of advanced aerospace materials by depth sensing indentation and scratch methods [BTN-95-EIX95152569458] p 282 A95-73590 Interlaminar shear test method development for long term durability testing of composites  p 301 N95-23300  MOISTURE  Measurement of moisture and total hydrocarbon contributions by valves used in clean room gas-delivery systems	Automatic guidance and control for helicopter obstacle avoidance  [BTN-95-EIX95182619130] p 291 A95-76607  NASA PROGRAMS  1994 NASA-HU American Society for Engineering Education (ASEE) Summer Faculty Fellowship Program [NASA-CR-194972] p 325 N95-23276  Research and Technology, 1994  [NASA-TM-106764] p 262 N95-24025  NASTRAN  Thin tailored composite wing for civil tiltrotor p 285 N95-23317  NAVIER-STOKES EQUATION  Preconditioned domain decomposition scheme for three-dimensional aerodynamic sensitivity analysis  [BTN-95-EIX95152577612] p 321 A95-73471  Effects of spatial order of accuracy on the computation of vortical flowfields  [BTN-95-EIX95152577604] p 305 A95-73479  Computation of oscillating airfoil flows with one- and two-equation turbulence models  [BTN-95-EIX95152577588] p 263 A95-73494  Computation of the poststall behavior of a circulation controlled airfoil  [BTN-95-EIX95152582320] p 264 A95-73523  Navier-Stokes prediction of large-amplitude delta-wing roll oscillations  [BTN-95-EIX95152582329] p 281 A95-73531  Computational study of plume-induced separation on a hypersonic powered model
A multibody/finite element analysis approach for modeling of crash dynamic responses [NIAR-94-3] p 277 N95-24050 IATRIX MATERIALS  US Navy operating experience with new aircraft construction materials p 303 N95-23517 IAXIMUM LIKELIHOOD ESTIMATES  Maximum-likelihood spectral estimation and adaptive filtering techniques with application to airborne Doppler weather radar [NASA-CR-197699] p 316 N95-23670 IECHANICAL PROPERTIES Idealized textile composites for experimental/analytical correlation p 301 N95-23277 IESOMETEOROLOGY  Diurnal variation of lee vortices in Taiwan and the surrounding area [HTN-95-91363] p 318 A95-76394 IETAL COATINGS  Cu deposition using a permanent magnet electron cyclotron resonance microwave plasma source [DE94-017768] p 304 N95-23981 IETAL FATIGUE  Multiple site fatigue damage in fuselage skin splices: Experimental simulation and theoretical prediction [BTN-95-EIX95152584676] p 276 A95-73588 Fatigue strength of high-temperature alloys under conditions of cyclic temperature variation. Communication 1: Experimental procedure and results [BTN-94-EIX94401363884] p 307 A95-75516 IETAL FIBERS	Moving mass trim control for aerospace vehicles [DE95-002602] p 299 N95-23532  MISSILE TRAJECTORIES  A CFO study of complex missile and store configurations in relative motion [NASA-CR-197912] p 285 N95-22949  MISSILES  Aerodynamic characteristics of a canard-controlled missile at high angles of attack [BTN-95-EIX95152583257] p 267 A95-73558  Wing vertical position effects on wing-body carryover for noncircular missiles [BTN-95-EIX95182617462] p 268 A95-75733  Supersonic near-wake afterbody boattailing effects on axisymmetric bodies [BTN-95-EIX95182617465] p 268 A95-75736  MOBILE COMMUNICATION SYSTEMS  Development of aeronautical mobile satellite services over the past thirty years [BTN-95-EIX95152569458] p 305 A95-73498  MODULUS OF ELASTICITY  Evaluation of advanced aerospace materials by depth sensing indentation and scratch methods [BTN-95-EIX95152584678] p 282 A95-73590 Interfaminar shear test method development for long term durability testing of composites  p 301 N95-23300  MOISTURE  Measurement of moisture and total hydrocarbon contributions by valves used in clean room gas-delivery systems	Automatic guidance and control for helicopter obstacle avoidance [BTN-95-EIX95182619130] p 291 A95-76607  NASA PROGRAMS 1994 NASA-HU American Society for Engineering Education (ASEE) Summer Faculty Fellowship Program [NASA-CR-194972] p 325 N95-23276 Research and Technology, 1994 [NASA-TM-106764] p 262 N95-24025  NASTRAN Thin tailored composite wing for civil tiltrotor p 285 N95-23317  NAVIER-STOKES EQUATION Preconditioned domain decomposition scheme for three-dimensional aerodynamic sensitivity analysis [BTN-95-EIX95152577612] p 321 A95-73471 Effects of spatial order of accuracy on the computation of vortical flowrields [BTN-95-EIX95152577604] p 305 A95-73479 Computation of oscillating airfoil flows with one- and two-equation turbulence models [BTN-95-EIX95152577588] p 263 A95-73494 Computation of the poststall behavior of a circulation controlled airfoil [BTN-95-EIX95152582320] p 264 A95-73523 Navier-Stokes prediction of large-amplitude delta-wing roll oscillations [BTN-95-EIX95152582329] p 281 A95-73531 Computational study of plume-induced separation on a hypersonic powered model [BTN-95-EIX95152582346] p 266 A95-73548
A multibody/finite element analysis approach for modeling of crash dynamic responses [NIAR-94-3] p 277 N95-24050 IATRIX MATERIALS  US Navy operating experience with new aircraft construction materials  Maximum-likelinood spectral estimation and adaptive filtering techniques with application to airborne Doppler weather radar [NASA-CR-197699] p 316 N95-23570 IECHANICAL PROPERTIES Idealized textile composites for experimental/analytical correlation p 301 N95-23277 IESOMETEOROLOGY  Diurnal variation of lee vortices in Taiwan and the surrounding area [HTN-95-91363] p 318 A95-76394 IETAL COATINGS  Cu deposition using a permanent magnet electron cyclotron resonance microwave plasma source [DE94-017768] p 304 N95-23981 IETAL FATIGUE Multiple site tatigue damage in fuselage skin splices: Experimental simulation and theoretical prediction [BTN-95-EIX95152584676] p 276 A95-73588 Fatigue strength of high-temperature alloys under conditions of cyclic temperature variation. Communication 1: Experimental procedure and results [BTN-94-EIX94401363884] p 307 A95-75516 IETAL FIBERS Comptiant interlayer	Moving mass trim control for aerospace vehicles [DE95-002602] p 299 N95-23532  MISSILE TRAJECTORIES  A CFD study of complex missile and store configurations in relative motion [NASA-CR-197912] p 285 N95-22949  MISSILES  Aerodynamic characteristics of a canard-controlled missile at high angles of attack [BTN-95-EIX95152583257] p 267 A95-73558  Wing vertical position effects on wing-body carryover for noncircular missiles [BTN-95-EIX95182617462] p 268 A95-75733  Supersonic near-wake afterbody boattailing effects on axisymmetric bodies [BTN-95-EIX95182617465] p 268 A95-75736  MOBILE COMMUNICATION SYSTEMS  Development of aeronautical mobile satellite services over the past thirty years [BTN-95-EIX95152569458] p 305 A95-73498  MODULUS OF ELASTICITY  Evaluation of advanced aerospace materials by depth sensing indentation and scratch methods [BTN-95-EIX95152584678] p 282 A95-73590 Interfaminar shear test method development for long term durability testing of composites  MOISTURE  Measurement of moisture and total hydrocarbon contributions by valves used in clean room gas-delivery systems [BTN-94-EIX94381359041] p 295 A95-74629	Automatic guidance and control for helicopter obstacle avoidance  [BTN-95-EIX95182619130] p 291 A95-76607  NASA PROGRAMS  1994 NASA-HU American Society for Engineering Education (ASEE) Summer Faculty Fellowship Program [NASA-CR-194972] p 325 N95-23276  Research and Technology, 1994 [NASA-TM-106764] p 262 N95-24025  NASTRAN  Thin tailored composite wing for civil tiltrotor p 285 N95-23317  NAVIER-STOKES EQUATION  Preconditioned domain decomposition scheme for three-dimensional aerodynamic sensitivity analysis [BTN-95-EIX95152577612] p 321 A95-73471  Effects of spatial order of accuracy on the computation of vortical flowfields  [BTN-95-EIX95152577604] p 305 A95-73479  Computation of oscillating airfoil flows with one- and two-equation turbulence models  [BTN-95-EIX95152577588] p 263 A95-73494  Computation of the poststall behavior of a circulation controlled airfoil  [BTN-95-EIX95152582320] p 264 A95-73523  Navier-Stokes prediction of large-amplitude delta-wing roll oscillations  [BTN-95-EIX95152582329] p 281 A95-73531  Computational study of plume-induced separation on a hypersonic powered model  [BTN-95-EIX95152582346] p 266 A95-73548  Hypersonic rarefied flow past spheres including wake
A multibody/finite element analysis approach for modeling of crash dynamic responses [NIAR-94-3] p 277 N95-24050 IATRIX MATERIALS  US Navy operating experience with new aircraft construction materials p 303 N95-23517 IAXIMUM LIKELIHOOD ESTIMATES  Maximum-likelihood spectral estimation and adaptive filtering techniques with application to airborne Doppler weather radar  [NASA-CR-197699] p 316 N95-23670 IECHANICAL PROPERTIES Idealized textile composites for experimental/analytical correlation p 301 N95-23277 IESOMETEOROLOGY  [BEGNATION DIATRIA STATE OF THE STA	Moving mass trim control for aerospace vehicles [DE95-002602] p 299 N95-23532  MISSILE TRAJECTORIES  A CFD study of complex missile and store configurations in relative motion [NASA-CR-197912] p 285 N95-22949  MISSILES  Aerodynamic characteristics of a canard-controlled missile at high angles of attack [BTN-95-EIX95152583257] p 267 A95-73558  Wing vertical position effects on wing-body carryover for noncircular missiles [BTN-95-EIX95182617462] p 268 A95-75733  Supersonic near-wake afterbody boattaiting effects on axisymmetric bodies [BTN-95-EIX95182617465] p 268 A95-75736  MOBILE COMMUNICATION SYSTEMS  Development of aeronautical mobile satellite services over the past thirty years [BTN-95-EIX95152569458] p 305 A95-73498  MODULUS OF ELASTICITY  Evaluation of advanced aerospace materials by depth sensing indentation and scratch methods [BTN-95-EIX95152584678] p 282 A95-73590 Interfaminar shear test method development for long term durability testing of composites  MOISTURE  Measurement of moisture and total hydrocarbon contributions by valves used in clean room gas-delivery systems  [BTN-94-EIX94381359041] p 295 A95-74629  MOISTURE CONTENT  Study of the droplet spray characteristics of a subsonic wind turnel	Automatic guidance and control for helicopter obstacle avoidance  [BTN-95-EIX95182619130] p 291 A95-76607  NASA PROGRAMS  1994 NASA-HU American Society for Engineering Education (ASEE) Summer Faculty Fellowship Program [NASA-CR-194972] p 325 N95-23276  Research and Technology, 1994  [NASA-TM-106764] p 262 N95-24025  NASTRAN  Thin tailored composite wing for civil tiltrotor p 285 N95-23317  NAVIER-STOKES EQUATION  Preconditioned domain decomposition scheme for three-dimensional aerodynamic sensitivity analysis  [BTN-95-EIX95152577612] p 321 A95-73471  Effects of spatial order of accuracy on the computation of vortical flowfields  [BTN-95-EIX95152577604] p 305 A95-73479  Computation of oscillating airfoil flows with one- and two-equation turbulence models  [BTN-95-EIX95152577588] p 263 A95-73494  Computation of the poststall behavior of a circulation controlled airfoil  [BTN-95-EIX95152582320] p 264 A95-73523  Navier-Stokes prediction of large-amplitude delta-wing roll oscillations  [BTN-95-EIX95152582329] p 281 A95-73531  Computational study of plume-induced separation on a hypersonic powered model  [BTN-95-EIX95152582346] p 266 A95-73548  Hypersonic rarefied flow past spheres including wake structure
A multibody/finite element analysis approach for modeling of crash dynamic responses [NIAR-94-3] p 277 N95-24050 IATRIX MATERIALS  US Navy operating experience with new aircraft construction materials p 303 N95-23517 IAXIMUM LIKELIHOOD ESTIMATES  Maximum-likelihood spectral estimation and adaptive filtering techniques with application to airborne Doppler weather radar [NASA-CR-197699] p 316 N95-23670 IECHANICAL PROPERTIES Idealized textile composites for experimental/analytical correlation p 301 N95-23277 IESOMETEOROLOGY  Diurnal variation of lee vortices in Taiwan and the surrounding area [HTN-95-91363] p 318 A95-76394 IETAL COATINGS  Cu deposition using a permanent magnet electron cyclotron resonance microwave plasma source [DE94-017768] p 304 N95-23981 IETAL FATIGUE  Multiple site fatigue damage in fuselage skin splices: Experimental simulation and theoretical prediction [BTN-95-EIX95152584676] p 276 A95-73588 Fatigue strength of high-temperature alloys under conditions of cyclic temperature variation. Communication 1: Experimental procedure and results [BTN-94-EIX94401363884] p 307 A95-75516 ETAL FIBERS  Compliant interlayer [BTN-95-EIX95142562401] p 304 A95-73439 ETAL MATRIX COMPOSITES	Moving mass trim control for aerospace vehicles [DE95-002602] p 299 N95-23532  MISSILE TRAJECTORIES  A CFD study of complex missile and store configurations in relative motion [NASA-CR-197912] p 285 N95-22949  MISSILES  Aerodynamic characteristics of a canard-controlled missile at high angles of attack [BTN-95-EIX95152583257] p 267 A95-73558 Wing vertical position effects on wing-body carryover for noncircular missiles [BTN-95-EIX95182617462] p 268 A95-75733 Supersonic near-wake afterbody boattailing effects on axisymmetric bodies [BTN-95-EIX95182617465] p 268 A95-75736 MOBILE COMMUNICATION SYSTEMS  Development of aeronautical mobile satellite services over the past thirty years [BTN-95-EIX95152569458] p 305 A95-73498 MODULUS OF ELASTICITY  Evaluation of advanced aerospace materials by depth sensing indentation and scratch methods [BTN-95-EIX95152584678] p 282 A95-73590 Interlaminar shear test method development for long term durability testing of composites p 301 N95-23300 MOISTURE  Measurement of moisture and total hydrocarbon contributions by valves used in clean room gas-delivery systems [BTN-94-EIX94381359041] p 295 A95-74629 MOISTURE CONTENT  Study of the droplet spray characteristics of a subsonic wind tunnel [BTN-95-EIX95182619235] p 271 A95-76661	Automatic guidance and control for helicopter obstacle avoidance  [BTN-95-EIX95182619130] p 291 A95-76607  MASA PROGRAMS  1994 NASA-HU American Society for Engineering Education (ASEE) Summer Faculty Fellowship Program [NASA-CR-194972] p 325 N95-23276  Research and Technology, 1994 [NASA-TM-106764] p 262 N95-24025  MASTRAN  Thin tailored composite wing for civil tiltrotor p 285 N95-23317  NAVIER-STOKES EQUATION  Preconditioned domain decomposition scheme for three-dimensional aerodynamic sensitivity analysis [BTN-95-EIX95152577612] p 321 A95-73471  Effects of spatial order of accuracy on the computation of vortical flowfields  [BTN-95-EIX95152577604] p 305 A95-73479  Computation of oscillating airfoil flows with one- and two-equation turbulence models  [BTN-95-EIX95152577588] p 263 A95-73494  Computation of the poststall behavior of a circulation controlled airfoil  [BTN-95-EIX95152582320] p 264 A95-73523  Navier-Stokes prediction of large-amplitude delta-wing roll oscillations  [BTN-95-EIX95152582329] p 281 A95-73531  Computational study of plume-induced separation on a hypersonic powered model  [BTN-95-EIX95152582346] p 266 A95-73548  Hypersonic rarefied flow past spheres including wake structure  [BTN-95-EIX95152583250] p 305 A95-73551
A multibody/finite element analysis approach for modeling of crash dynamic responses [NIAR-94-3] p 277 N95-24050 IATRIX MATERIALS  US Navy operating experience with new aircraft construction materials p 303 N95-23517 IAXIMUM LIKELIHOOD ESTIMATES  Maximum-likelihood spectral estimation and adaptive filtering techniques with application to airborne Doppler weather radar  [NASA-CR-197699] p 316 N95-23670 IECHANICAL PROPERTIES Idealized textile composites for experimental/analytical correlation p 301 N95-23277 IESOMETEOROLOGY  [BEGNATION DIATRIA STATE OF THE STA	Moving mass trim control for aerospace vehicles [DE95-002602] p 299 N95-23532  MISSILE TRAJECTORIES  A CFO study of complex missile and store configurations in relative motion  [NASA-CR-197912] p 285 N95-22949  MISSILES  Aerodynamic characteristics of a canard-controlled missile at high angles of attack  [BTN-95-EIX95152583257] p 267 A95-73558  Wing vertical position effects on wing-body carryover for noncircular missiles  [BTN-95-EIX95182617462] p 268 A95-75733  Supersonic near-wake afterbody boattailing effects on axisymmetric bodies  [BTN-95-EIX95182617465] p 268 A95-75736  MOBILE COMMUNICATION SYSTEMS  Development of aeronautical mobile satellite services over the past thirty years  [BTN-95-EIX95152569458] p 305 A95-73498  MODULUS OF ELASTICITY  Evaluation of advanced aerospace materials by depth sensing indentation and scratch methods  [BTN-95-EIX95152584678] p 282 A95-73590  Interlaminar shear test method development for long term durability testing of composites  MOISTURE  Measurement of moisture and total hydrocarbon contributions by valves used in clean room gas-delivery systems  [BTN-94-EIX94381359041] p 295 A95-74629  MOISTURE CONTENT  Study of the droplet spray characteristics of a subsonic wind tunnel  [BTN-95-EIX95182619235] p 271 A95-76661	Automatic guidance and control for helicopter obstacle avoidance  (BTN-95-EIX95182619130) p 291 A95-76607  NASA PROGRAMS  1994 NASA-HU American Society for Engineering Education (ASEE) Summer Faculty Fellowship Program [NASA-CR-194972] p 325 N95-23276 Research and Technology, 1994 [NASA-TM-106764] p 262 N95-24025  NASTRAN  Thin tailored composite wing for civil tiltrotor p 285 N95-23317  NAVIER-STOKES EQUATION  Preconditioned domain decomposition scheme for three-dimensional aerodynamic sensitivity analysis [BTN-95-EIX95152577612] p 321 A95-73471 Effects of spatial order of accuracy on the computation of vortical flowfields  [BTN-95-EIX95152577604] p 305 A95-73479 Computation of oscillating airfoil flows with one- and two-equation turbulence models  [BTN-95-EIX95152577588] p 263 A95-73494 Computation of the poststall behavior of a circulation controlled airfoil [BTN-95-EIX95152582320] p 264 A95-73523 Navier-Stokes prediction of large-amplitude delta-wing roll oscillations  [BTN-95-EIX95152582329] p 281 A95-73531 Computational study of plume-induced separation on a hypersonic powered model [BTN-95-EIX95152582346] p 266 A95-73548 Hypersonic rarefied flow past spheres including wake structure  [BTN-95-EIX95152582320] p 305 A95-73551 Hypersonic nonequilibrium Navier-Stokes solutions over
A multibody/finite element analysis approach for modeling of crash dynamic responses [NIAR-94-3] p 277 N95-24050 IATRIX MATERIALS  US Navy operating experience with new aircraft construction materials p 303 N95-23517 IAXIMUM LIKELIHOOD ESTIMATES  Maximum-likelihood spectral estimation and adaptive filtering techniques with application to airborne Doppler weather radar [NASA-CR-197699] p 316 N95-23670 IECHANICAL PROPERTIES Idealized textile composites for experimental/analytical correlation p 301 N95-23277 IESOMETEOROLOGY  Diurnal variation of lee vortices in Taiwan and the surrounding area [HTN-95-91363] p 318 A95-76394 IETAL COATINGS  Cu deposition using a permanent magnet electron cyclotron resonance microwave plasma source [DE94-017768] p 304 N95-23981 IETAL FATIGUE Multiple site fatigue damage in fuselage skin splices: Experimental simulation and theoretical prediction [BTN-95-EIX95152584676] p 276 A95-73588 Fatigue strength of high-temperature alloys under conditions of cyclic temperature variation. Communication 1: Experimental procedure and results [BTN-94-EIX9401363884] p 307 A95-75516 IETAL FIBERS  Compliant interlayer [BTN-95-EIX95142562401] p 304 A95-73439 IETAL FIBERS  Compliant interlayer allowables for fibre/metal	Moving mass trim control for aerospace vehicles [DE95-002602] p 299 N95-23532  MISSILE TRAJECTORIES  A CFD study of complex missile and store configurations in relative motion [NASA-CR-197912] p 285 N95-22949  MISSILES  Aerodynamic characteristics of a canard-controlled missile at high angles of attack [BTN-95-EIX95152583257] p 267 A95-73558  Wing vertical position effects on wing-body carryover for noncircular missiles [BTN-95-EIX95182617462] p 268 A95-75733  Supersonic near-wake afterbody boaltailing effects on axisymmetric bodies [BTN-95-EIX95182617465] p 268 A95-75736  MOBILE COMMUNICATION SYSTEMS  Development of aeronautical mobile satellite services over the past thirty years [BTN-95-EIX95152569458] p 305 A95-73498  MODULUS OF ELASTICITY  Evaluation of advanced aerospace materials by depth sensing indentation and scratch methods [BTN-95-EIX95152569458] p 282 A95-73590 Interlaminar shear test method development for long term durability testing of composites p 301 N95-23300  MOISTURE  Measurement of moisture and total hydrocarbon contributions by valves used in clean room gas-delivery systems [BTN-94-EIX94381359041] p 295 A95-74629  MOISTURE  Study of the droplet spray characteristics of a subsonic wind tunnel [BTN-95-EIX95182619235] p 271 A95-76661  MOLECULES  Determination of wall boundary conditions for	Automatic guidance and control for helicopter obstacle avoidance  (BTN-95-EIX95182619130) p 291 A95-76607  MASA PROGRAMS  1994 NASA-HU American Society for Engineering Education (ASEE) Summer Faculty Fellowship Program [NASA-CR-194972] p 325 N95-23276  Research and Technology, 1994 [NASA-TM-106764] p 262 N95-24025  MASTRAN  Thin tailored composite wing for civil tiltrotor p 285 N95-23317  NAVIER-STOKES EQUATION  Preconditioned domain decomposition scheme for three-dimensional aerodynamic sensitivity analysis [BTN-95-EIX95152577612] p 321 A95-73471  Effects of spatial order of accuracy on the computation of vortical flowrields  [BTN-95-EIX95152577604] p 305 A95-73479  Computation of oscillating airfoil flows with one- and two-equation turbulence models  [BTN-95-EIX95152577588] p 263 A95-73494  Computation of the poststall behavior of a circulation controlled airfoil  [BTN-95-EIX95152582320] p 264 A95-73523  Navier-Stokes prediction of large-amplitude delta-wing roll oscillations  [BTN-95-EIX95152582329] p 281 A95-73531  Computational study of plume-induced separation on a hypersonic powered model  [BTN-95-EIX95152582346] p 266 A95-73548  Hypersonic rarefied flow past spheres including wake structure  [BTN-95-EIX95152583250] p 305 A95-73551
A multibody/finite element analysis approach for modeling of crash dynamic responses [NIAR-94-3] p 277 N95-24050 IATRIX MATERIALS  US Navy operating experience with new aircraft construction materials p 303 N95-23517 IAXIMUM LIKELIHOOD ESTIMATES  Maximum-likelinood spectral estimation and adaptive filtering techniques with application to airborne Doppler weather radar  [NASA-CR-197699] p 316 N95-23670 IECHANICAL PROPERTIES  Idealized textile composites for experimental/analytical correlation p 301 N95-23277 IESOMETEOROLOGY  Diurnal variation of lee vortices in Taiwan and the surrounding area [HTN-95-91363] p 318 A95-76394 IETAL COATINGS  Cu deposition using a permanent magnet electron cyclotron resonance microwave plasma source [DE94-017768] p 304 N95-23981 IETAL FATIGUE  Multiple site fatigue damage in fuselage skin splices: Experimental simulation and theoretical prediction [BTN-95-EIX95192584676] p 276 A95-73588 Fatigue strength of high-temperature alloys under conditions of cyclic temperature variation. Communication 1: Experimental procedure and results [BTN-94-EIX94401363884] p 307 A95-75516 IETAL FIBERS  Comptiant interlayer [BTN-95-EIX95142562401] p 304 A95-73439 IETAL MATRIX COMPOSITES  MIL-HDBK-5 design allowables for fibre/metal laminates: ARALL 2 and ARALL 3	Moving mass trim control for aerospace vehicles [DE95-002602] p 299 N95-23532  MISSILE TRAJECTORIES  A CFO study of complex missile and store configurations in relative motion  [NASA-CR-197912] p 285 N95-22949  MISSILES  Aerodynamic characteristics of a canard-controlled missile at high angles of attack  [BTN-95-EIX95152583257] p 267 A95-73558  Wing vertical position effects on wing-body carryover for noncircular missiles  [BTN-95-EIX95182617462] p 268 A95-75733  Supersonic near-wake afterbody boattailing effects on axisymmetric bodies  [BTN-95-EIX95182617465] p 268 A95-75736  MOBILE COMMUNICATION SYSTEMS  Development of aeronautical mobile satellite services over the past thirty years  [BTN-95-EIX95152569458] p 305 A95-73498  MODULUS OF ELASTICITY  Evaluation of advanced aerospace materials by depth sensing indentation and scratch methods  [BTN-95-EIX95152584678] p 282 A95-73590  Interlaminar shear test method development for long term durability testing of composites  MOISTURE  Measurement of moisture and total hydrocarbon contributions by valves used in clean room gas-delivery systems  [BTN-94-EIX94381359041] p 295 A95-74629  MOISTURE CONTENT  Study of the droplet spray characteristics of a subsonic wind tunnel  [BTN-95-EIX95182619235] p 271 A95-76661	Automatic guidance and control for helicopter obstacle avoidance  [BTN-95-EIX95182619130] p 291 A95-76607  NASA PROGRAMS  1994 NASA-HU American Society for Engineering Education (ASEE) Summer Faculty Fellowship Program [NASA-CR-194972] p 325 N95-23276  Research and Technology, 1994 [NASA-TM-106764] p 262 N95-24025  NASTRAN  Thin tailored composite wing for civil tiltrotor p 285 N95-23317  NAVIER-STOKES EQUATION  Preconditioned domain decomposition scheme for three-dimensional aerodynamic sensitivity analysis [BTN-95-EIX95152577612] p 321 A95-73471  Effects of spatial order of accuracy on the computation of vortical flowfields  [BTN-95-EIX95152577604] p 305 A95-73479  Computation of oscillating airfoil flows with one- and two-equation turbulence models  [BTN-95-EIX95152577588] p 263 A95-73494  Computation of the poststall behavior of a circulation controlled airfoil  [BTN-95-EIX95152582320] p 264 A95-73523  Navier-Stokes prediction of large-amplitude delta-wing roll oscillations  [BTN-95-EIX95152582329] p 281 A95-73531  Computational study of plume-induced separation on a hypersonic powered model  [BTN-95-EIX95152582346] p 266 A95-73548  Hypersonic rarefied flow past spheres including wake structure  [BTN-95-EIX95152583250] p 305 A95-73551  Hypersonic nonequilibrium Navier-Stokes solutions over an ablating graphite nosetip
A multibody/finite element analysis approach for modeling of crash dynamic responses [NIAR-94-3] p 277 N95-24050    IATRIX MATERIALS  US Navy operating experience with new aircraft construction materials  Maximum-likelinood spectral estimation and adaptive filtering techniques with application to airborne Doppler weather radar [NASA-CR-197699] p 316 N95-23570    IECHANICAL PROPERTIES   Idealized textile composites for experimental/analytical correlation p 301 N95-23277    IESOMETEOROLOGY   Diurnal variation of lee vortices in Taiwan and the surrounding area [HTN-95-91363] p 318 A95-76394    IETAL COATINGS   Cu deposition using a permanent magnet electron cyclotron resonance microwave plasma source [DE94-017768] p 304 N95-23981    IETAL FATIGUE   Multiple site fatigue damage in fuselage skin splices: Experimental simulation and theoretical prediction [BTN-95-EIX95152584676] p 276 A95-73588    Fatigue strength of high-temperature alloys under conditions of cyclic temperature variation. Communication 1: Experimental procedure and results [BTN-94-EIX94401363884] p 307 A95-75516    ETAL FIBERS   Comptiant interlayer [BTN-95-EIX95142562401] p 304 A95-73439    ETAL MATRIX COMPOSITES   MIL-HOBK-5 design allowables for fibre/metal laminates: ARALL 2 and ARALL 3    BTN-94-EIX94371346933] p 300 A95-73345    ETEOROLOGICAL BALLOONS   Polar Patrol Balloon	Moving mass trim control for aerospace vehicles [DE95-002602] p 299 N95-23532  MISSILE TRAJECTORIES  A CFD study of complex missile and store configurations in relative motion [NASA-CR-197912] p 285 N95-22949  MISSILES  Aerodynamic characteristics of a canard-controlled missile at high angles of attack [BTN-95-EIX95152583257] p 267 A95-73558 Wing vertical position effects on wing-body carryover for noncircular missiles [BTN-95-EIX95182617462] p 268 A95-75733 Supersonic near-wake afterbody boattailing effects on axisymmetric bodies [BTN-95-EIX95182617465] p 268 A95-75736 MOBILE COMMUNICATION SYSTEMS  Development of aeronautical mobile satellite services over the past thirty years [BTN-95-EIX95152569458] p 305 A95-73498 MODULUS OF ELASTICITY  Evaluation of advanced aerospace materials by depth sensing indentation and scratch methods [BTN-95-EIX95152584678] p 282 A95-73590 Interlaminar shear test method development for long term durability testing of composites  MOISTURE  Measurement of moisture and total hydrocarbon contributions by valves used in clean room gas-delivery systems  [BTN-94-EIX94381359041] p 295 A95-74629 MOISTURE CONTENT  Study of the droplet spray characteristics of a subsonic wind tunnel [BTN-95-EIX95182619235] p 271 A95-76661 MOLECULES  Determination of wall boundary conditions for high-speed-ratio direct simulation Monte Carlo	Automatic guidance and control for helicopter obstacle avoidance  (BTN-95-EIX95182619130) p 291 A95-76607  NASA PROGRAMS  1994 NASA-HU American Society for Engineering Education (ASEE) Summer Faculty Fellowship Program [NASA-CR-194972] p 325 N95-23276  Research and Technology, 1994 [NASA-TM-106764] p 262 N95-24025  NASTRAN  Thin tailored composite wing for civil tiltrotor p 285 N95-23317  NAVIER-STOKES EQUATION  Preconditioned domain decomposition scheme for three-dimensional aerodynamic sensitivity analysis [BTN-95-EIX95152577612] p 321 A95-73471  Effects of spatial order of accuracy on the computation of vortical flowfields  [BTN-95-EIX95152577604] p 305 A95-73479  Computation of oscillating airfoil flows with one- and two-equation turbulence models  [BTN-95-EIX9515258238] p 263 A95-73494  Computation of the poststall behavior of a circulation controlled airfoil  [BTN-95-EIX95152582329] p 264 A95-73523  Navier-Stokes prediction of large-amplitude delta-wing roll oscillations  [BTN-95-EIX95152582329] p 281 A95-73531  Computational study of plume-induced separation on a hypersonic powered model  [BTN-95-EIX95152582346] p 266 A95-73548  Hypersonic rarefied flow past spheres including wake structure  [BTN-95-EIX95152582350] p 305 A95-73551  Hypersonic nonequilibrium Navier-Stokes solutions over an ablating graphite nosetip  [BTN-95-EIX95152582352] p 305 A95-73553  Hypersonic convective heat transfer over 140-deg blunt cones in different gases
A multibody/finite element analysis approach for modeling of crash dynamic responses [NIAR-94-3] p 277 N95-24050 IATRIX MATERIALS  US Navy operating experience with new aircraft construction materials p 303 N95-23517 IAXIMUM LIKELIHOOD ESTIMATES  Maximum-likelihood spectral estimation and adaptive filtering techniques with application to airborne Doppler weather radar  [NASA-CR-197699] p 316 N95-23670 IECHANICAL PROPERTIES Idealized textile composites for experimental/analytical correlation p 301 N95-23277 IESOMETEOROLOGY  Diurnal variation of lee vortices in Taiwan and the surrounding area [HTN-95-91363] p 318 A95-76394 IETAL COATINGS  Cu deposition using a permanent magnet electron cyclotron resonance microwave plasma source [DE94-017768] p 304 N95-23981 IETAL FATIGUE  Multiple site fatigue damage in fuselage skin splices: Experimental simulation and theoretical prediction [BTN-95-EIX95152584676] p 276 A95-73588 Fatigue strength of high-temperature alloys under conditions of cyclic temperature variation. Communication 1: Experimental procedure and results [BTN-94-EIX9401363884] p 307 A95-75516 IETAL FIBERS  Compliant interlayer  [BTN-95-EIX95142562401] p 304 A95-73439 IETAL MATRIX COMPOSITES  MIL-HDBK-5 design allowables for fibre/metal laminates: ARALL 2 and ARALL 3  [BTN-94-EIX94371346933] p 300 A95-73345 IETEOROLOGICAL BALLOONS  Polar Partal Balloon  [BTN-95-EIX95152582318] p 316 A95-73521	Moving mass trim control for aerospace vehicles [DE95-002602] p 299 N95-23532  MISSILE TRAJECTORIES  A CFO study of complex missile and store configurations in relative motion [NASA-CR-197912] p 285 N95-22949  MISSILES  Aerodynamic characteristics of a canard-controlled missile at high angles of attack [BTN-95-EIX95152583257] p 267 A95-73558  Wing vertical position effects on wing-body carryover for noncircular missiles [BTN-95-EIX95182617462] p 268 A95-75733 Supersonic near-wake afterbody boattailing effects on axisymmetric bodies [BTN-95-EIX95182617465] p 268 A95-75736  MOBILE COMMUNICATION SYSTEMS  Development of aeronautical mobile satellite services over the past thirty years [BTN-95-EIX95152569458] p 305 A95-73498  MODULUS OF ELASTICITY  Evaluation of advanced aerospace materials by depth sensing indentation and scratch methods [BTN-95-EIX95152584678] p 282 A95-73590 Intertaminar shear test method development for long term durability testing of composites  MOISTURE  Measurement of moisture and total hydrocarbon contributions by valves used in clean room gas-delivery systems  [BTN-94-EIX94381359041] p 295 A95-74629  MOISTURE CONTENT  Study of the droplet spray characteristics of a subsonic wind tunnel [BTN-95-EIX95182619235] p 271 A95-76661  MOLECULES  Determination of wall boundary conditions for high-speed-ratio direct simulation Monte Carlo calculations  [BTN-95-EIX95182617457] p 267 A95-75728	Automatic guidance and control for helicopter obstacle avoidance [BTN-95-EIX95182619130] p 291 A95-76607  MASA PROGRAMS 1994 NASA-HU American Society for Engineering Education (ASEE) Summer Faculty Fellowship Program [NASA-CR-194972] p 325 N95-23276 Research and Technology, 1994 [NASA-TM-106764] p 262 N95-24025  MASTRAN Thin tailored composite wing for civil tiltrotor p 285 N95-23317  NAVIER-STOKES EQUATION Preconditioned domain decomposition scheme for three-dimensional aerodynamic sensitivity analysis [BTN-95-EIX95152577612] p 321 A95-73471 Effects of spatial order of accuracy on the computation of vortical flowfields [BTN-95-EIX95152577604] p 305 A95-73479 Computation of oscillating airfoil flows with one- and two-equation turbulence models [BTN-95-EIX95152577588] p 263 A95-73494 Computation of the poststall behavior of a circulation controlled airfoil [BTN-95-EIX95152582320] p 264 A95-73523 Navier-Stokes prediction of large-amplitude delta-wing roll oscillations [BTN-95-EIX95152582329] p 281 A95-73531 Computational study of plume-induced separation on a hypersonic powered model [BTN-95-EIX95152582346] p 266 A95-73548 Hypersonic rarefied flow past spheres including wake structure [BTN-95-EIX95152583250] p 305 A95-73551 Hypersonic convective heat transfer over 140-deg blunt cones in different gases [BTN-95-EIX95152583253] p 306 A95-73554
A multibody/finite element analysis approach for modeling of crash dynamic responses [NIAR-94-3] p 277 N95-24050 IATRIX MATERIALS  US Navy operating experience with new aircraft construction materials p 303 N95-23517 IAXIMUM LIKELIHOOD ESTIMATES  Maximum-likelihood spectral estimation and adaptive filtering techniques with application to airborne Doppler weather radar [NASA-CR-197699] p 316 N95-23670 IECHANICAL PROPERTIES Idealized textile composites for experimental/analytical correlation p 301 N95-23277 IESOMETEOROLOGY  Diurnal variation of lee vortices in Taiwan and the surrounding area [HTN-95-91363] p 318 A95-76394 IETAL COATINGS  Cu deposition using a permanent magnet electron cyclotron resonance microwave plasma source [DE94-017768] p 304 N95-23981 IETAL FATIGUE Multiple site fatigue damage in fuselage skin splices: Experimental simulation and theoretical prediction [BTN-95-EIX95152584676] p 276 A95-73588 Fatigue strength of high-temperature alloys under conditions of cyclic temperature variation. Communication 1: Experimental procedure and results [BTN-94-EIX94401363884] p 307 A95-75516 IETAL FIBERS  Compliant interlayer [BTN-95-EIX95142562401] p 304 A95-73439 IETAL MATRIX COMPOSITES  MIL-HDBK-5 design allowables for fibre/metal laminates: ARALL 2 and ARALL 3 [BTN-94-EIX94371346933] p 300 A95-73345 IETOROLOGICAL BALLOONS Polar Patrol Balloon [BTN-95-EIX95152582318] p 316 A95-73521 IETOROLOGICAL INSTRUMENTS	Moving mass trim control for aerospace vehicles [DE95-002602] p 299 N95-23532  MISSILE TRAJECTORIES  A CFO study of complex missile and store configurations in relative motion  [NASA-CR-197912] p 285 N95-22949  MISSILES  Aerodynamic characteristics of a canard-controlled missile at high angles of attack  [BTN-95-EIX95152583257] p 267 A95-73558  Wing vertical position effects on wing-body carryover for noncircular missiles  [BTN-95-EIX95182617462] p 268 A95-75733  Supersonic near-wake afterbody boattailing effects on axisymmetric bodies  [BTN-95-EIX95182617465] p 268 A95-75736  MOBILE COMMUNICATION SYSTEMS  Development of aeronautical mobile satellite services over the past thirty years  [BTN-95-EIX9515259458] p 305 A95-73498  MODULUS OF ELASTICITY  Evaluation of advanced aerospace materials by depth sensing indentation and scratch methods  [BTN-95-EIX95152584678] p 282 A95-73590  Interlaminar shear test method development for long term durability testing of composites  measurement of moisture and total hydrocarbon contributions by valves used in clean room gas-delivery systems  [BTN-94-EIX94381359041] p 295 A95-74629  MOISTURE  Measurement of moisture and total hydrocarbon contributions by valves used in clean room gas-delivery systems  [BTN-94-EIX94381359041] p 295 A95-74629  MOISTURE CONTENT  Study of the droplet spray characteristics of a subsonic wind tunnel  [BTN-95-EIX95182619235] p 271 A95-76661  MOLECULES  Determination of wall boundary conditions for high-speed-ratio direct simulation Monte Carlo calculations  [BTN-95-EIX95182617457] p 267 A95-75728  MONTE CARLO METHOD  Hypersonic rarefied flow past spheres including wake	Automatic guidance and control for helicopter obstacle avoidance  (BTN-95-EIX95182619130] p 291 A95-76607  NASA PROGRAMS  1994 NASA-HU American Society for Engineering Education (ASEE) Summer Faculty Fellowship Program [NASA-CR-194972] p 325 N95-23276  Research and Technology, 1994 [NASA-TM-106764] p 262 N95-24025  NASTRAN  Thin tailored composite wing for civil tiltrotor p 285 N95-23317  NAVIER-STOKES EQUATION  Preconditioned domain decomposition scheme for three-dimensional aerodynamic sensitivity analysis [BTN-95-EIX95152577612] p 321 A95-73471  Effects of spatial order of accuracy on the computation of vortical flowfields [BTN-95-EIX95152577604] p 305 A95-73479  Computation of oscillating airfoil flows with one- and two-equation turbulence models [BTN-95-EIX95152577588] p 263 A95-73494  Computation of the poststall behavior of a circulation controlled airfoil [BTN-95-EIX95152582320] p 264 A95-73523  Navier-Stokes prediction of large-amplitude delta-wing roll oscillations [BTN-95-EIX95152582329] p 281 A95-73531  Computational study of plume-induced separation on a hypersonic powered model [BTN-95-EIX9515258236] p 266 A95-73548  Hypersonic rarefied flow past spheres including wake structure [BTN-95-EIX95152583250] p 305 A95-73551  Hypersonic nonequilibrium Navier-Stokes solutions over an ablating graphite nosetip [BTN-95-EIX95152583253] p 306 A95-73554  Application of the multigrid solution technique to
A multibody/finite element analysis approach for modeling of crash dynamic responses [NIAR-94-3] p 277 N95-24050 IATRIX MATERIALS  US Navy operating experience with new aircraft construction materials p 303 N95-23517 IAXIMUM LIKELIHOOD ESTIMATES  Maximum-likelihood spectral estimation and adaptive filtering techniques with application to airborne Doppler weather radar [NASA-CR-197699] p 316 N95-23670 IECHANICAL PROPERTIES  Idealized textile composites for experimental/analytical correlation p 301 N95-23277 IESOMETEOROLOGY  Diurnal variation of lee vortices in Taiwan and the surrounding area [HTN-95-91363] p 318 A95-76394 IETAL COATINGS  Cu deposition using a permanent magnet electron cyclotron resonance microwave plasma source [DE94-017768] p 304 N95-23981 IETAL FATIGUE Multiple site fatigue damage in fuselage skin spices: Experimental simulation and theoretical prediction [BTN-95-EIX95152584676] p 276 A95-73588 Fatigue strength of high-temperature alloys under conditions of cyclic temperature variation. Communication 1: Experimental procedure and results [BTN-94-EIX9401363884] p 307 A95-73516 IETAL FIBERS  Compliant interlayer [BTN-95-EIX95142562401] p 304 A95-73439 IETAL MATRIX COMPOSITES MIL-HDBK-5 design allowables for fibre/metal laminates: ARALL 2 and ARALL 3 [BTN-94-EIX94371346933] p 300 A95-73345 IETEOROLOGICAL BALLOONS  Polar Patrol Balloon [BTN-95-EIX95152582518] p 316 A95-73521 IETEOROLOGICAL INSTRUMENTS  A new generation of instruments for flying laboratories	Moving mass trim control for aerospace vehicles [DE95-002602] p 299 N95-23532  MISSILE TRAJECTORIES  A CFD study of complex missile and store configurations in relative motion [NASA-CR-197912] p 285 N95-22949  MISSILES  Aerodynamic characteristics of a canard-controlled missile at high angles of attack [BTN-95-EIX95152583257] p 267 A95-73558  Wing vertical position effects on wing-body carryover for noncircular missiles [BTN-95-EIX95182617462] p 268 A95-75733  Supersonic near-wake afterbody boaltailing effects on axisymmetric bodies [BTN-95-EIX95182617465] p 268 A95-75736  MOBILE COMMUNICATION SYSTEMS  Development of aeronautical mobile satellite services over the past thirty years [BTN-95-EIX95152569458] p 305 A95-73498  MODULUS OF ELASTICITY  Evaluation of advanced aerospace materials by depth sensing indentation and scratch methods [BTN-95-EIX95152569458] p 282 A95-73590  Interlaminar shear test method development for long term durability testing of composites p 301 N95-23300  MOISTURE  Measurement of moisture and total hydrocarbon contributions by valves used in clean room gas-delivery systems  [BTN-94-EIX94381359041] p 295 A95-74629  MOISTURE ONTENT  Study of the droplet spray characteristics of a subsonic wind tunnel [BTN-95-EIX95182619235] p 271 A95-76661  MOLECULES  Determination of wall boundary conditions for high-speed-ratio direct simulation Monte Carlo calculations [BTN-95-EIX95182617457] p 267 A95-75728  MONTE CARLO METHOD  Hypersonic rarefied flow past spheres including wake structure	Automatic guidance and control for helicopter obstacle avoidance  (BTN-95-EIX95182619130] p 291 A95-76607  NASA PROGRAMS  1994 NASA-HU American Society for Engineering Education (ASEE) Summer Faculty Fellowship Program [NASA-CR-194972] p 325 N95-23276  Research and Technology, 1994 [NASA-TM-106764] p 262 N95-24025  NASTRAN  Thin tailored composite wing for civil tiltrotor p 285 N95-23317  NAVIER-STOKES EQUATION  Preconditioned domain decomposition scheme for three-dimensional aerodynamic sensitivity analysis [BTN-95-EIX95152577612] p 321 A95-73471  Effects of spatial order of accuracy on the computation of vortical flowfields  [BTN-95-EIX95152577604] p 305 A95-73479  Computation of oscillating airfoil flows with one- and two-equation turbulence models  [BTN-95-EIX95152587588] p 263 A95-73494  Computation of the poststall behavior of a circulation controlled airfoil  [BTN-95-EIX95152582320] p 264 A95-73523  Navier-Stokes prediction of large-amplitude delta-wing roll oscillations  [BTN-95-EIX95152582329] p 281 A95-73531  Computational study of plume-induced separation on a hypersonic powered model  [BTN-95-EIX95152582329] p 266 A95-73548  Hypersonic rarefied flow past spheres including wake structure  [BTN-95-EIX95152582350] p 305 A95-73551  Hypersonic nonequilibrium Navier-Stokes solutions over an ablating graphite nosetip  [BTN-95-EIX95152583252] p 305 A95-73554  Application of the multigrid solution technique to hypersonic entry vehicles
A multibody/finite element analysis approach for modeling of crash dynamic responses [NIAR-94-3] p 277 N95-24050 IATRIX MATERIALS  US Navy operating experience with new aircraft construction materials p 303 N95-23517 IAXIMUM LIKELIHOOD ESTIMATES  Maximum-likelihood spectral estimation and adaptive filtering techniques with application to airborne Doppler weather radar [NASA-CR-197699] p 316 N95-23670 IECHANICAL PROPERTIES Idealized textile composites for experimental/analytical correlation p 301 N95-23277 IESOMETEOROLOGY  Diurnal variation of lee vortices in Taiwan and the surrounding area [HTN-95-91363] p 318 A95-76394 IETAL COATINGS  Cu deposition using a permanent magnet electron cyclotron resonance microwave plasma source [DE94-017768] p 304 N95-23981 IETAL FATIGUE Multiple site fatigue damage in fuselage skin splices: Experimental simulation and theoretical prediction [BTN-95-EIX95152584676] p 276 A95-73588 Fatigue strength of high-temperature alloys under conditions of cyclic temperature variation. Communication 1: Experimental procedure and results [BTN-94-EIX94401363884] p 307 A95-75516 IETAL FIBERS  Compliant interlayer [BTN-95-EIX95142562401] p 304 A95-73439 IETAL MATRIX COMPOSITES  MIL-HDBK-5 design allowables for fibre/metal laminates: ARALL 2 and ARALL 3 [BTN-94-EIX94371346933] p 300 A95-73345 IETOROLOGICAL BALLOONS Polar Patrol Balloon [BTN-95-EIX95152582318] p 316 A95-73521 IETOROLOGICAL INSTRUMENTS	Moving mass trim control for aerospace vehicles [DE95-002602] p 299 N95-23532  MISSILE TRAJECTORIES  A CFO study of complex missile and store configurations in relative motion  [NASA-CR-197912] p 285 N95-22949  MISSILES  Aerodynamic characteristics of a canard-controlled missile at high angles of attack  [BTN-95-EIX95152583257] p 267 A95-73558  Wing vertical position effects on wing-body carryover for noncircular missiles  [BTN-95-EIX95182617462] p 268 A95-75733  Supersonic near-wake afterbody boattailing effects on axisymmetric bodies  [BTN-95-EIX95182617465] p 268 A95-75736  MOBILE COMMUNICATION SYSTEMS  Development of aeronautical mobile satellite services over the past thirty years  [BTN-95-EIX9515259458] p 305 A95-73498  MODULUS OF ELASTICITY  Evaluation of advanced aerospace materials by depth sensing indentation and scratch methods  [BTN-95-EIX95152584678] p 282 A95-73590  Interlaminar shear test method development for long term durability testing of composites  measurement of moisture and total hydrocarbon contributions by valves used in clean room gas-delivery systems  [BTN-94-EIX94381359041] p 295 A95-74629  MOISTURE  Measurement of moisture and total hydrocarbon contributions by valves used in clean room gas-delivery systems  [BTN-94-EIX94381359041] p 295 A95-74629  MOISTURE CONTENT  Study of the droplet spray characteristics of a subsonic wind tunnel  [BTN-95-EIX95182619235] p 271 A95-76661  MOLECULES  Determination of wall boundary conditions for high-speed-ratio direct simulation Monte Carlo calculations  [BTN-95-EIX95182617457] p 267 A95-75728  MONTE CARLO METHOD  Hypersonic rarefied flow past spheres including wake	Automatic guidance and control for helicopter obstacle avoidance  (BTN-95-EIX95182619130] p 291 A95-76607  NASA PROGRAMS  1994 NASA-HU American Society for Engineering Education (ASEE) Summer Faculty Fellowship Program [NASA-CR-194972] p 325 N95-23276  Research and Technology, 1994 [NASA-TM-106764] p 262 N95-24025  NASTRAN  Thin tailored composite wing for civil tiltrotor p 285 N95-23317  NAVIER-STOKES EQUATION  Preconditioned domain decomposition scheme for three-dimensional aerodynamic sensitivity analysis [BTN-95-EIX95152577612] p 321 A95-73471  Effects of spatial order of accuracy on the computation of vortical flowfields [BTN-95-EIX95152577604] p 305 A95-73479  Computation of oscillating airfoil flows with one- and two-equation turbulence models [BTN-95-EIX95152577588] p 263 A95-73494  Computation of the poststall behavior of a circulation controlled airfoil [BTN-95-EIX95152582320] p 264 A95-73523  Navier-Stokes prediction of large-amplitude delta-wing roll oscillations [BTN-95-EIX95152582329] p 281 A95-73531  Computational study of plume-induced separation on a hypersonic powered model [BTN-95-EIX9515258236] p 266 A95-73548  Hypersonic rarefied flow past spheres including wake structure [BTN-95-EIX95152583250] p 305 A95-73551  Hypersonic nonequilibrium Navier-Stokes solutions over an ablating graphite nosetip [BTN-95-EIX95152583253] p 306 A95-73554  Application of the multigrid solution technique to

Mach wave emission from a

supersonic jet

|BTN-95-EIX95152577586|

high-temperature

p 264 A95-73496

NOZZLE FLOW Higher-order viscous shock-layer solutions for NOISE PREDICTION Predicting exhaust plume boundaries with supersonic Analysis of a higher harmonic control test to reduce blade vortex interaction noise high-altitude flows |BTN-95-EIX95152583255| p 306 A95-73556 p 297 A95-73559 |BTN-95-EIX95152582330| p 265 A95-73532 [BTN-95-EIX95152583258] Optimization of contoured hypersonic scramjet inlets NOISE PREDICTION (AIRCRAFT) Simulation on the 3-D turbulent flow in the passages a least-squares parabolized Navier-Stokes Supersonic jet noise reductions predicted with increased procedure of finocyl grain [HTN-95-20976] p 261 A95-74042 jet spreading rate [BTN-95-E1X95202638962] p 279 A95-76674 Convective and radiative heat transfer analysis for the [NASA-TM-106872] p 323 N95-23178 An approximate theoretical method for modeling the NOISE REDUCTION static thrust performance of non-axisymmetric two-dimensional convergent-divergent nozzles fire 2 forebody p 268 A95-75731 Analysis of a higher harmonic control test to reduce IBTN-95-FIX951826174601 blade vortex interaction noise Turbulent transonic airfoil flow simulation using a p 273 N95-23193 INASA-CR-1950501 IBTN-95-EIX95152582330 I p 265 A95-73532 pressure-based algorithm Experimental results for a hypersonic nozzle/afterbody The use of cowl camber and taper to reduce rotor/stator | BTN-95-EIX95182619078 | p 269 A95-75763 flow field Simulation of transverse gas injection in turbulent interaction noise INASA-TM-46381 p 274 N95-23250 [NASA-CR-195421] p 323 N95-22675 supersonic air flows NOZZŁE WALLS | BTN-95-EIX95182619080 | p 269 A95-75765 Supersonic jet noise reductions predicted with increased Supersonic laminar flow control research Viscous-inviscid interaction method for unsteady jet spreading rate p 275 N95-23669 INASA-CR-1979381 [NASA-TM-106872] p 323 N95-23178 low-speed airfoil flows IBTN-95-EIX951826190931 p 269 A95-75778 On-line, adaptive state estimator for active noise Influence of streamwise curvature on longitudinal vortices imbedded in turbulent boundary layers p 322 N95-23308 control NONDESTRUCTIVE TESTS [BTN-94-EIX94401378820] p 307 A95-76489 OBLIQUE SHOCK WAVES Double pass retroreflection for corrosion detection in Scaling of incipient separation in supersonic/transonic Grid refinement test of time-periodic flows over bluff p 323 N95-23503 aircraft structures speed laminar flows bodies Non-destructive detection of corrosion for life p 269 A95-76589 BTN-94-EIX944013788221 p 307 A95-76491 [BTN-95-EIX95182619104] p 314 N95-23505 management Supersonic flow and shock formation in turbine tip Numerical investigation of supersonic flows around a New nondestructive techniques for the detection and p 312 N95-23429 spiked blunt body quantification of corrosion in aircraft structures IBTN-95-EIX952126456901 p 271 A95-76742 OBSTACLE AVOIDANCE p 315 N95-23512 An assessment of viscous effects in computational Optimal lateral-escape maneuvers for microburst POD assessment of NDI procedures using a round robin encounters during final approach simulation of benign and burst vortex flows on generic test fighter wind-tunnel models using TEAM code IBTN-95-EIX951826191271 p 276 A95-76604 IAGARD-R-8091 p 315 N95-23602 INASA-CFI-46501 p 273 N95-23185 Automatic guidance and control for helicopter obstacle NONEQUILIBRIUM FLOW Mach 10 computational study of a three-dimensional Hypersonic nonequilibrium Navier-Stokes solutions over p 291 A95-76607 scramiet inlet flow field [BTN-95-EIX95182619130] an ablating graphite posetio [NASA-TM-4602] OCEAN BOTTOM p 310 N95-23210 [BTN-95-EIX95152583252] p 305 A95-73553 Numerical computation of aerodynamics and heat Geoid lineations of 1000 km wavelength over the central Higher-order viscous shock-layer solutions for transfer in a turbine cascade and a turn-around duct using Pacific advanced turbulence models p 313 N95-23444
Convergence acceleration of implicit schemes in the high-attitude flows HTN-95-11304 IBTN-95-EIX951525832551 p 306 A95-73556 OCEAN MODELS NONINTRUSIVE MEASUREMENT presence of high aspect ratio grid cells Assimilation of altimeter data in a quasi-geostrophic p 313 N95-23446 Impeller flow field characterization with a laser two-focus model of the Gulf Stream system: A dynamical perspective A time-accurate finite volume method valid at all flow velocimeter p 313 N95-23440 p 320 N95-23766 p 314 N95-23447 [NASA-CR-196313] velocities **NONLINEAR EQUATIONS** Cavitation modeling in Euler and Navier-Stokes codes OCEAN SURFACE Neural network prediction of three-dimensional unsteady Assimilation of altimeter data in a quasi-geostrophic parated flowfields p 315 N95-23630 NAVIGATION model of the Gulf Stream system: A dynamical [BTN-95-EIX95182619232] p 308 A95-76658 Switched bias proportional navigation for homing Moving mass trim control for aerospace vehicles guidance against highly maneuvering targets |BTN-95-EIX95182619145| p 279 A95-76622 IDE95-0026021 INASA-CR-1963131 n 320 N95-23766 p 299 N95-23532 ON-LINE SYSTEMS **NONLINEAR FEEDBACK** New failure detection approach and its application to On-line analysis capabilities developed to support the Design of high performance multivariable control GPS autonomous integrity monitoring active flexible wing wind-tunnel tests systems for supermaneuverable aircraft at high angle of p 296 A95-76639 BTN-95-EIX95202637613 p 279 A95-76676 BTN-95-EIX95182619213 Solutions of generalized proportional navigation with On-line, adaptive state estimator for active noise INASA-CR-1976611 p 293 N95-22908 maneuvering and nonmaneuvering targets p 322 N95-23308 control **NONLINEAR SYSTEMS** p 279 A95-76683 BTN-95-EIX95202637606 ONE DIMENSIONAL FLOW Nonlinear system guidance in the presence of NAVIGATION AIDS Simulating heat addition via mass addition in constant area compressible flows transmission zero dynamics Cueing light configuration for aircraft navigation
[NASA-CASE-ARC-11982-1] p 280 N95-23393
TRISTAR 1: Evaluation methods for testing head-up p 309 N95-22804 [NASA-TM-4661] IRTN-95-FIX951826191001 p 307 A95-76585 NONLINEARITY OPERATING COSTS Analytical solution for controls, heats, and states of flight display (HUD) flight symbology Design constraints in the payload-range diagram of ultrahigh capacity transport airplanes [BTN-95-EIX95152582319] INASA-TM-46651 p 288 N95-24030 IBTN-95-EIX951525832861 NAVIGATION SATELLITES p 282 A95-73587 p 276 A95-73522 NORTHERN HEMISPHERE Description of a GNSS availability model and its use in Containing military autotest cost growth through the use Trajectory modeling of emissions from lower stratospheric aircraft developing requirements |BTN-95-EIX95202637603| of commercial standard equipment architectures [BTN-95-EIX95172595295] p 287 A95-75717 p 308 A95-76686 [HTN-95-41219] p 317 A95-75031 **NEAR INFRARED RADIATION** OPTICAL MEASUREMENT 2 micron LIDAR for laser-based remote sensing: Flight NOSE CONES Dynamic response tests of inertial and optical lemonstration and application survey Shock tunnel measurements of hypervelocity blunted vind-tunnel model attitude measurement devices p 296 N95-23011 |BTN-95-EIX952126410721 p 319 A95-76737 cone drag [NASA-TM-109182] [BTN-95-EIX95152577606] AVIRIS and TIMS data processing and distribution at p 305 A95-73477 OPTICAL RADAR the land processes distributed active archive center 2 micron LIDAR for laser-based remote sensing: Flight NOSE TIPS demonstration and application survey p 325 N95-23872 Hypersonic nonequilibrium Navier-Stokes solutions over NEAR WAKES |BTN-95-EIX95212641072| p 319 A95-76737 an ablating graphite nosetip Supersonic near-wake afterbody boattailing effects on [BTN-95-EIX95152583252] OPTIMAL CONTROL p 305 A95-73553 Aeroelastic vehicle multivariable control synthesis with axisymmetric bodies [BTN-95-EIX95182617465] p 268 A95-75736 analytical robustness evaluation Interlaminar shear test method development for long **NETHERLANDS** term durability testing of composites IBTN-95-EIX951826191151 p 321 A95-76592 Review of aeronautical fatigue investigation in the Functional agility metrics and optimal trajectory p 301 N95-23300 Netherlands during the period March 1991-March 1993 **NOZZLE DESIGN** I PB95-1391841 p 285 N95-23161 IRTN-95-FIX951826191211 p 321 A95-76598 An approximate theoretical method for modeling the Design and multifunction tests of a frequency NEURAL NETS static thrust performance of non-axisymmetric two-dimensional convergent-divergent nozzles Artificial intelligence for turboprop engine maintenan domain-based active flutter suppression system IRTN-95-FIX951826178121 p 288 A95-75757 IBTN-95-FIX951826192151 p 292 A95-76641 p 273 N95-23193 [NASA-CR-195050] Fuel-optimal bank-angle control for lunar-return Neural network prediction of three-dimensional unsteady Optimized design of a hypersonic nozzle eparated flowfields perocanture p 297 N95-23304 IBTN-95-FIX951826192321 IBTN-95-EIX952126457061 p 299 A95-76758 p 308 A95-76658 Design of a variable area diffuser for a 15-inch Mach On-line, adaptive state estimator for active nois Active control of panel vibrations induced by a boundary 6 open-jet tunnel p 297 N95-23309 p 322 N95-23308 laver flow Three-dimensional Navier-Stokes analysis and redesign [NASA-CR-197867] p 273 N95-23182 **NEUTRONS** of an imbedded bellmouth nozzle in a turbine cascade PTIMIZATION Phonon characteristics of high (T sub c) superconductors p 311 N95-23423 from neutron Doppler broadening measure inlet section Aerodynamic shape optimization using preconditioned NOZZLE EFFICIENCY p.324 N95-24076 conjugate gradient methods IDE95-0037031 p 263 A95-73465 An approximate theoretical method for modeling the BTN-95-EIX95142553033 | NOISE (SOUND)

static thrust performance of non-axisymmetric

p 273 N95-23193

two-dimensional convergent-divergent nozzles

[NASA-CR-195050]

p 267 A95-73561

Improved version of the Naval Surface Warfare Center

aeroprediction code (AP93)

|BTN-95-EIX95152583260|

Optimization of contoured hypersonic scramjet inlets	PANEL METHOD (FLUID DYNAMICS)	Containing military autotest cost growth through the use
with a least-squares parabolized Navier-Stokes	Viscous-inviscid interaction method for unsteady	of commercial standard equipment architectures (BTN-95-FIX95172595295) p 287 A95-75717
procedure [HTN-95-20976] p 261 A95-74042	low-speed airfoil flows	[BTN-95-EIX95172595295] p 287 A95-75/17 Flight test evaluation of a 35 GHz forward looking
CFD optimization of a theoretical minimum-drag body	[BTN-95-EIX95182619093] p 269 A95-75778	altimeter for terrain avoidance
[BTN-95-EIX95182619234] p 308 A95-76660	PANELS  Shutter of an infinitely long panel in a dust	[BTN-95-EIX95212641071] p 287 A95-76736
Direct adaptive performance optimization of subsonic	Flutter of an infinitely long panel in a duct [BTN-95-EIX95182619087] p 291 A95-75772	Performance of the 0.3-meter transonic cryogenic tunnel
transports: A periodic perturbation technique	Active control of panel vibrations induced by a boundary	with air, nitrogen, and sulfur hexafluoride media under
[NASA-TM-4676] p 284 N95-22829	layer flow	closed loop automatic control
Integrated aerodynamic/dynamic/structural	[NASA-CR-197867] p 273 N95-23182	[NASA-CR-195052] p 310 N95-23257
optimization of helicopter rotor blades using multilevel	Residual strength of thin panels with cracks	Report to the Secretary of Defense. Unmanned aerial
decomposition	p 311 N95-23311	vehicles: No more Hunter systems should be bought until problems are fixed
[NASA-TP-3465] p 285 N95-22953 Aerodynamic design optimization with sensitivity analysis	PARACHUTE DESCENT	[GAO/NSIAD-95-52] p 286 N95-24091
and computational fluid dynamics	Dynamic investigation of the angular motion of a rotating	PERIODIC VARIATIONS
[NASA-CR-197419] p 274 N95-23218	body-parachute system	Grid refinement test of time-periodic flows over bluff
ORBIT CALCULATION	[BTN-95-EIX95182619220] p 270 A95-76646	bodies
Thermal force modeling for global positioning system	PARACHUTES	[BTN-94-EIX94401378822] p 307 A95-76491
satellites using the finite element method	Dynamic investigation of the angular motion of a rotating	PERMANENT MAGNETS
[BTN-95-EIX95152583270] p 278 A95-73571	body-parachute system [BTN-95-EIX95182619220] p 270 A95-76646	Cu deposition using a permanent magnet electron
Aerodynamics of the Shuttle Orbiter at high altitudes [BTN-95-EIX95182617454] p 298 A95-75725	PARALLEL PROCESSING (COMPUTERS)	cyclotron resonance microwave plasma source [DE94-017768] p 304 N95-23981
ORBIT PERTURBATION	High-performance parallel analysis of coupled problems	PERSONAL COMPUTERS
Thermal force modeling for global positioning system	for aircraft propulsion	New commercial off-the-shelf testers are automatic and
satellites using the finite element method	[NASA-CR-197440] p 289 N95-23088	intelligent
BTN-95-EIX95152583270  p 278 A95-73571	PARAMETER IDENTIFICATION	[BTN-95-EIX95172595292] p 287 A95-75720
ORBIT TRANSFER VEHICLES	Improving prediction: The incorporation of simplified	Development of qualification guidelines for personal
Minimum-mass design of sandwich aerobrakes for a	rotor dynamics in a mathematical model of the bell	computer-based aviation training devices
lunar transfer vehicle	412HP	DOT/FAA/AM-95/6   p 323 N95-23603   PERSONNEL
[BTN-95-EIX95212645707] p 299 A95-76759 ORGANIC COMPOUNDS	[BTN-95-EIX95152584679] p 282 A95-73591	CASS: Design for supportability
Estimates of total organic and inorganic chlorine in the	Analytical solution and parameter estimation of projectile dynamics	IBTN-95-EIX951725952961 p 287 A95-75716
lower stratosphere from in situ and flask measurements	IBTN-95-EIX95212645695   p 272 A95-76747	ATE enabling technologies
during AASE 2	PARTICLE EMISSION	[BTN-95-EIX95172595294] p 287 A95-75718
[HTN-95-A0861] p 317 A95-76265	Measurement of particle emissions from clean room	PERTURBATION
ORGANIC MATERIALS	gas-handling components	Direct adaptive performance optimization of subsonic
Organic coating technology for the protection of aircraft against corrosion p 303 N95-23513	[BTN-94-EIX94381359040] p 295 A95-74554	transports: A periodic perturbation technique [NASA-TM-4676] p 284 N95-22829
OSCILLATIONS p 303 1495-23513	PARTICLE IMAGE VELOCIMETRY	PERTURBATION THEORY
Further analysis of high-rate rolling experiments of a	Transient structure of vortex breakdown on a delta	Analytical study of the neutral stability of a model
65-deg delta wing	wing [BTN-95-EIX95182619073] p 268 A95-75758	hypersonic boundary layer
[BTN-95-EIX95152582331] p 281 A95-73533	Laser velocimetry seed-particle behavior in shear layers	[BTN-95-EIX95152577589] p 263, A95-73493
Postinstability behavior of a two-dimensional airfoil with	at Mach 12	Application of transonic small disturbance theory to the
a structural nonlinearity	[BTN-95-EIX95212645712] p 272 A95-76764	active flexible wing model
[BTN-95-EIX95152582337] p 266 A95-73539 OXIDATION	PARTICLE SIZE DISTRIBUTION	[BTN-95-EIX95182619210] p 270 A95-76636
. Evolution of oxidation and creep damage mechanisms	Erosion of dust-filtered helicopter turbine engines. Part	PHASE LOCKED SYSTEMS
in HIPed silicon nitride materials	1: Basic theoretical considerations	Real-time navigation using the global positioning
[DE95-001360] p 300 N95-22689	[BTN-95-EIX95182619222] p 288 A95-76648	system  BTN-95-EIX95172595298  p 279 A95-75714
OXYGEN	PARTICLE TRAJECTORIES	PHASE SHIFT
Evolution of oxidation and creep damage mechanisms	Tracking of raindrops in flow over an airfoil	Real-time navigation using the global positioning
in HIPed silicon nitride materials [DE95-001360] p 300 N95-22689	[BTN-95-EIX95182619221] p 308 A95-76647	system
[DE95-001360] p 300 N95-22689 OZONE	Study of the droplet spray characteristics of a subsonic wind tunnel	[BTN-95-EIX95172595298] p 279 A95-75714
Sensitivity of two-dimensional model predictions of	[BTN-95-EIX95182619235] p 271 A95-76661	PHONONS
ozone response to stratospheric aircraft: An update	PARTICULATES	Phonon characteristics of high (T sub c) superconductors
[HTN-95-A0863] p 318 A95-76267	Laser velocimetry seed-particle behavior in shear layers	from neutron Doppler broadening measurements
A comparison of some aerodynamic resistance methods	at Mach 12	[DE95-003703] p 324 N95-24076
using measurements over cotton and grass from the 1991	[BTN-95-EIX95212645712] p 272 A95-76764	PHOTOCHEMICAL REACTIONS  Possible effects of CO2 increase on the high-speed civil
California ozone deposition experiment [HTN-95-11295] p 319 A95-77000	PASSENGERS	transport impact on ozone
Compendium of NASA data base for the Global	A multibody/finite element analysis approach for modeling of crash dynamic responses	[HTN-95-60779] p 317 A95-75976
Tropospheric Experiment's Pacific Exploratory Mission	[NIAR-94-3] p 277 N95-24050	Estimates of total organic and inorganic chlorine in the
West-A (PEM West-A)	PASSIVITY	lower stratosphere from in situ and flask measurements
[NASA-TM-109177] p 320 N95-23009	In-situ detection of surface passivation or activation and	during AASE 2
OZONE DEPLETION	of localized corrosion: Experiences and prospectives in	[HTN-95-A0861] p 317 A95-76265
Trajectory modeling of emissions from lower stratospheric aircraft	aircraft p 302 N95-23508	PHOTOGRAPHS
[HTN-95-41219] p 317 A95-75031	PAYLOADS  Design constraints in the payload-range diagram of	Simple method of supersonic flow visualization using watertable
Possible effects of CO2 increase on the high-speed civil	ultrahigh capacity transport airplanes	[BTN-95-EIX95182619105] p 269 A95-76590
transport impact on ozone	[BTN-95-EIX95152582319] p 276 A95-73522	Scientific and technical photography at NASA Langley
[HTN-95-60779] p 317 A95-75976	Dynamic investigation of the angular motion of a rotating	Research Center p 310 N95-23290
Estimates of total organic and inorganic chlorine in the	body-parachute system	PHOTOGRAPHY
lower stratosphere from in situ and flask measurements	[BTN-95-EIX95182619220] p 270 A95-76646	Scientific and technical photography at NASA Langley
during AASE 2 [HTN-95-A0861] p 317 A95-76265	Aerodynamic flight control to increase payload capability	Research Center p 310 N95-23290
In situ observations in aircraft exhaust plumes in the	of future taunch vehicles [NASA-CR-197704] p 300 N95-24032	PILOT INDUCED OSCILLATION
lower stratosphere at midlatitudes	PENETRATION	Analysis of the longitudinal handling qualities and
[HTN-95-A0862] p 318 A95-76266	Rationale for the Modular Air-system Vulnerability	pilot-induced-oscillation tendencies of the High-Angle-of-Attack Research Vehicle (HARV)
Sensitivity of two-dimensional model predictions of	Estimation Network (MAVEN) methodology	p 293 N95-23297
ozone response to stratospheric aircraft: An update	[AD-A285797] p 284 N95-22510	PILOT PERFORMANCE
[HTN-95-A0863] p 318 A95-76267	PERFORMANCE PREDICTION  Multipuis sites rations for damaged sizeraft	TRISTAR 1: Evaluation methods for testing head-up
n	Multiaxis pilot ratings for damaged aircraft [BTN-95-EIX95182619128] p 269 A95-76605	display (HUD) flight symbology
Р	Drag function modeling for air traffic simulation	[NASA-TM-4665] p 288 N95-24030
	[BTN-95-EIX95182619154] p 279 A95-76631	A review of civil aviation fatal accidents in which
PACIFIC OCEAN  Coold linestings of 1000 km wayslandth over the central	Life prediction of helicopter engines fitted with dust	lost/disoriented was a cause/factor: 1981-1990
Geoid lineations of 1000 km wavelength over the central Pacific	filters	[DOT/FAA/AM-95/1] p 278 N95-24071
[HTN-95-11304] p 319 A95-77009	[BTN-95-EIX95182619224] p 289 A95-76650	PILOTLESS AIRCRAFT  Design of a GaAs/Ge solar array for unmanned aerial
Oceanic operations: An authoritative guide to oceanic	An approximate theoretical method for modeling the static thrust performance of non-axisymmetric	vehicles
operations	two-dimensional convergent-divergent nozzles	[NASA-TM-106870] p 320 N95-23259
[FAA-AFS-550] p 277 N95-24065	[NASA-CR-195050] p 273 N95-23193	Report to the Secretary of Defense. Unmanned aerial
PAINTS	PERFORMANCE TESTS	vehicles: No more Hunter systems should be bought until
Aircraft stripping and painting	Labs behind Boeing's new 777	problems are fixed
[BTN-95-EIX95182617810] p 300 A95-75755	[BTN-95-EIX95142562403] p 280 A95-73437	[GAO/NSIAD-95-52] p 286 N95-24091

SOBJECT INDEX		71101201112 007111112
PITCH (INCLINATION)	POTENTIAL FLOW	PRESSURE EFFECTS
Identification of higher order helicopter dynamics using	Viscous-inviscid interaction method for unsteady	Main features of overexpanded triple jets
linear modeling methods	low-speed airfoil flows	[BTN-95-EIX95142553040] p 304 A95-73458
(HTN-95-80851) p 290 A95-75093	[BTN-95-EIX95182619093] p 269 A95-75778 Study of the droplet spray characteristics of a subsonic	Effects of expansions on a supersonic boundary layer:
Sensitivity of acoustic predictions to variation of input parameters	wind tunnel	Surface pressure measurements [BTN-95-EIX95142553036] p 263 A95-73462
[HTN-95-80855] p 267 A95-75097	[BTN-95-EIX95182619235] p 271 A95-76661	Experimental investigation of the flowfield about an
PITCHING MOMENTS	POWERED MODELS	upswept afterbody
Kinematics and aerodynamics of velocity-vector roll	Computational study of plume-induced separation on a	[BTN-95-EIX95152582321] p 265 A95-73524
[BTN-95-EIX95182619126] p 291 A95-76603	hypersonic powered model  BTN-95-EIX95152582346  p 266 A95-73548	PRESSURE GRADIENTS
PITTING	BTN-95-EIX95152582346  p 266 A95-73548 PRECIPITATION (METEOROLOGY)	Turbulent transonic airfoil flow simulation using a
Eddy current detection of pitting corrosion around	Diurnal variation of lee vortices in Taiwan and the	pressure-based algorithm [BTN-95-EIX95182619078] p 269 A95-75763
fastener holes p 315 N95-23507 PLANFORMS	surrounding area	[BTN-95-EIX95182619078] p 269 A95-75763 Simulating heat addition via mass addition in constant
A study of the vortex flow over 76/40-deg double-delta	[HTN-95-91363] p 318 A95-76394	area compressible flows
wing	PRECONDITIONING	[BTN-95-EIX95182619100] p 307 A95-76585
[NASA-CR-195032] p 314 N95-23466	Aerodynamic shape optimization using preconditioned conjugate gradient methods	PRESSURE MEASUREMENT
PLASMAS (PHYSICS)	BTN-95-EIX95142553033  p 263 A95-73465	Separation control on high-lift airfoils via micro-vortex
Cu deposition using a permanent magnet electron	PREDICTION ANALYSIS TECHNIQUES	generators
cyclotron resonance microwave plasma source {DE94-017768} p 304 N95-23981	Analytic prediction of lift for delta wings with partial	[BTN-95-EIX95152582326] . p 265 A95-73529
[DE94-017768] p 304 N95-23981 PLATE THEORY	leading-edge thrust	PRESSURE OSCILLATIONS  Active control of panel vibrations induced by a boundary
Idealized textile composites for experimental/analytical	[BTN-95-EIX95152582345] p 266 A95-73547 Aerodynamic characteristics of a hypersonic viscous	layer flow
correlation p 301 N95-23277	optimized waverider at high altitudes	[NASA-CR-197867] p 273 N95-23182
PLATES (STRUCTURAL MEMBERS)	[BTN-95-EIX95152583251] p 266 A95-73552	PRESSURE PULSES
Stability derivatives of a flapped plate in unsteady ground	Base drag prediction on missile configurations	System for determining aerodynamic imbalance
effect	BTN-95-EIX95152583256  p 266 A95-73557	[NASA-CASE-ARC-11913-1] p 311 N95-23377
[BTN-95-EIX95182619225] p 270 A95-76651	Aerodynamic characteristics of a canard-controlled	PRESSURE SENSORS
PLUMES  Production exhaust plume boundaries with supersonic	missile at high angles of attack [BTN-95-EIX95152583257] p 267 A95-73558	Impeller flow field characterization with a laser two-focus velocimeter p 313 N95-23440
Predicting exhaust plume boundaries with supersonic external flows	Predicting exhaust plume boundaries with supersonic	velocimeter p 313 N95-23440 PRIMERS (COATINGS)
[BTN-95-EIX95152583258] p 297 A95-73559	external flows	Organic coating technology for the protection of aircraft
In situ observations in aircraft exhaust plumes in the	[BTN-95-EIX95152583258] p 297 A95-73559	against corrosion p 303 N95-23513
lower stratosphere at midlatitudes	Improved version of the Naval Surface Warfare Center	PROBABILITY DENSITY FUNCTIONS
[HTN-95-A0862] p 318 A95-76266	aeroprediction code (AP93)  BTN-95-EIX95152583260  p 267 A95-73561	Statistics of multi-look AIRSAR imagery: A comparison
NTS-spill test facility wind tunnel exhaust plume	Multiple site fatigue damage in fuselage skin splices:	of theory with measurements p 320 N95-23947
characterization (DE95-003630) p 297 N95-24019	Experimental simulation and theoretical prediction	PROBABILITY THEORY
PNEUMATIC CONTROL	[BTN-95-EIX95152584676] p 276 A95-73588	Effects of satellite bunching on the probability of collision in geosynchronous orbit
Forebody flow control on a full-scale F/A-18 aircraft	Improving prediction: The incorporation of simplified	[BTN-95-EIX95152583276] p 298 A95-73577
[BTN-95-EIX95152582333] p 281 A95-73535	rotor dynamics in a mathematical model of the bell 412HP	PROBLEM SOLVING
Pneumatic concept for tip-stall control of cranked-arrow	[BTN-95-EIX95152584679] p 282 A95-73591	On the exact solutions of pseudorange equations
wings	Comparison of linear stability results with flight transition	[BTN-95-EIX95142555477] p 278 A95-73433
[BTN-95-EIX95152582335] p 281 A95-73537	data	Application of a control-volume-based finite-element
POLAR REGIONS Oceanic operations: An authoritative guide to oceanic	[BTN-95-EIX95182619097] p 283 A95-76582	formulation to the shock tube problem [BTN-95-EIX95182619099] p 295 A95-76584
operations	Real-time estimation of atmospheric turbulence severity from in-situ aircraft measurements	Empirical results on scheduling and dynamic
[FAA-AFS-550] p 277 N95-24065	[BTN-95-EIX95182619231] p 319 A95-76657	backtracking p 299 N95-23761
POLARIMETRY	Neural network prediction of three-dimensional unsteady	PROCEDURES
MAX-91: Polarimetric SAR results on Montespertoli	separated flowfields	Scientific and technical photography at NASA Langley
site p 320 N95-23940	[BTN-95-EIX95182619232] p 308 A95-76658	Research Center p 310 N95-23290
Statistics of multi-look AIRSAR imagery: A comparison of theory with measurements p 320 N95-23947	Additional improvements to the NASA Lewis ice accretion code LEWICE	PRODUCT DEVELOPMENT
POLICIES p 320 N93-23947	[NASA-TM-106849] p 309 N95-22669	New commercial off-the-shelf testers are automatic and intelligent
Mishap risk control for advanced aerospace/composite	Development and verification of a resin film	[BTN-95-EIX95172595292] p 287 A95-75720
materials p 301 N95-23031	infusion/resin transfer molding simulation model for	PROGRAM VERIFICATION (COMPUTERS)
POLLUTION MONITORING	fabrication of advanced textile composites [NASA-CR-197439] p 301 N95-23179	Response of a nonrotating rotor blade to lateral
Modeling aerosol emissions from the combustion of	[NASA-CR-197439] p 301 N95-23179 PREDICTIONS	turbulence. Part 2: Experiment
composite materials p 301 N95-23038	The use of cowl camber and taper to reduce rotor/stator	[BTN-95-EIX95182619229] p 284 A95-76655
POLLUTION TRANSPORT  Trajectory modeling of emissions from lower	interaction noise	PROPELLANT GRAINS Simulation on the 3-D turbulent flow in the passages
stratospheric aircraft	[NASA-CR-195421] p 323 N95-22675	of finocyl grain
[HTN-95-41219] p 317 A95-75031	PREMIXED FLAMES  Sensitivity of combustion-acoustic instabilities to	[BTN-95-EIX95202638962] p 279 A95-76674
Transport of exhaust products in the near trail of a jet	boundary conditions for premixed gas turbine	PROPELLER BLADES
engine under atmospheric conditions	combustors	System for determining aerodynamic imbalance
[HTN-95-91421] p 319 A95-77334	[NASA-TM-106890] p 269 N95-23550	[NASA-CASE-ARC-11913-1] p 311 N95-23377
POLYMER MATRIX COMPOSITES  Validation of an effective flat cruciform-shaped specimen	PRESSURE	PROPELLERS  Adaptive finite element method for turbulent flow near
to study CFRP composite laminates under biaxial	Effects of expansions on a supersonic boundary layer: Surface pressure measurements	a propeller
loading	(BTN-95-EIX95142553036) p 263 A95-73462	(BTN-95-EIX95142553038) p 305 A95-73460
[BTN-95-EIX95152584677] p 282 A95-73589	Neural network prediction of three-dimensional unsteady	PROPULSION
Mishap risk control for advanced aerospace/composite	separated flowfields	Analytical aeropropulsive/aeroelastic
materials p 301 N95-23031	[BTN-95-EIX95182619232] p 308 A95-76658	hypersonic-vehicle model with dynamic analysis
Technology reinvestment project's focus area: Affordable polymer matrix composites for airframe	PRESSURE DISTRIBUTION	[BTN-95-EIX95182619138] p 269 A95-76615 Airborne rotary air separator study
structures	Aerodynamics of a finite wing with simulated ice	[NASA-CR-189099] p 290 N95-24053
(PB95-136032) p 324 N95-23168	[BTN-95-EIX95182619227] p 270 A95-76653 Aerodynamic characteristics of external store	PROPULSION SYSTEM CONFIGURATIONS
POPULATIONS	Aerodynamic characteristics of external store configurations at low speeds	Mechanical system reliability and risk assessment
Effects of satellite bunching on the probability of collision	[BTN-95-EIX95182619230] p 271 A95-76656	[BTN-95-EIX95142553046] p 304 A95-73452
in geosynchronous orbit [BTN-95-EIX95152583276] p 298 A95-73577	Neural network prediction of three-dimensional unsteady	Integrated flight/propulsion control for helicopters [HTN-95-80854] p 290 A95-75096
POSITION (LOCATION)	separated flowfields	An unmanned air vehicle concept with tipjet drive
Description of a GNSS availability model and its use in	[BTN-95-EIX95182619232] p 308 A95-76658	[HTN-95-80858] p 283 A95-75100
developing requirements	Wing pressure distributions from subsonic tests of a	PROTECTIVE COATINGS
[BTN-95-EIX95202637603] p 308 A95-76686	high-wing transport model in the Langley 14- by 22-Foot Subsonic Wind Tunnel	Evaluation of advanced aerospace materials by depth
POSITION ERRORS  Department instability of the agreement assist	[NASA-TM-4583] p 272 N95-22802	sensing indentation and scratch methods [BTN-95-EIX95152584678] p 282 A95-73590
Dynamical instability of the aerogravity assist maneuver	Three-dimensional unsteady flow calculations in an	Evaluation of thermal barrier and PS-200 self-lubricating
BTN-95-EIX95152583282  p 298 A95-73583	advanced gas generator turbine p 312 N95-23425	coatings in an air-cooled rotary engine
POSITION INDICATORS	PRESSURE DRAG	[NASA-CR-195445] p 289 N95-23222
TRISTAR 1: Evaluation methods for testing head-up	Application of Navier-Stokes aeroelastic methods to	Corrosion protection measures for CFC/metal joints of
display (HUD) flight symbology (NASA-TM-4665) p 288 N95-24030	improve fighter wing maneuver performance [BTN-95-EIX95182619218] p 284 A95-76644	fuel integral tank structures of advanced military aircraft p 303 N95-23510
(14.00% (14.000) p 200 (1430-24030	[2 00 E02.02010210] p 204 M30-70044	p 000 1100-20010

PROTON RESONANCE	Fatings of soul control of the	Design of a variable area diffuser for a 15-inch Mach
Phonon characteristics of high (T sub c) superconductors	Estimates of total organic and inorganic chlorine in the lower stratosphere from in situ and flask measurements	6 open-jet tunnel p 297 N95-23309
		RISK
from neutron Doppler broadening measurements	during AASE 2	Mechanical system reliability and risk assessment
[DE95-003703] p 324 N95-24076	[HTN-95-A0861] p 317 A95-76265	
PUMP IMPELLERS	Real-time estimation of atmospheric turbulence severity	, —
Impeller flow field characterization with a laser two-focus	from in-situ aircraft measurements	RIVETED JOINTS
velocimeter p 313 N95-23440	[BTN-95-EIX95182619231] p 319 A95-76657	Growth of multiple cracks and their linkup in a fuselage
	RECOMMENDATIONS	lap joint
^	Aviation Accident Investigation Symposium, Volume 1:	[BTN-95-EIX95142553047] p 286 A95-73451
Q	Industry recommendations and Safety Board responses	RIVETING
	[PB94-917005] p 278 N95-24105	Automatic riveting cell for commercial aircraft floor grid
QUADRUPOLES		assembly
	RECONSTRUCTION	
Numerical study of sound generation due to a spinning	Holographic interferometric tomography for	
vortex pair	reconstructing flow fields p 310 N95-23287	ROBOTICS
[BTN-95-EIX95182619075] p 307 A95-75760	RECTANGULAR WINGS	Fourth-generation Mars vehicle concepts
QUALITY	Aerodynamics of a finite wing with simulated ice	[BTN-95-EIX95152583267] p 298 A95-73568
The airline quality report, 1994	[BTN-95-EIX95182619227] p 270 A95-76653	ROBOTS
[NIAR-94-11] p 277 N95-24012	REENTRY TRAJECTORIES	Automatic riveting cell for commercial aircraft floor grid
		assembly
QUANTITATIVE ANALYSIS	Shuttle entry guidance revisited using nonlinear	[BTN-95-EIX95182617807] p 261 A95-75752
Simple method of supersonic flow visualization using	geometric methods	
watertable ·	[BTN-95-EIX95182619144] p 299 A95-76621	ROBUSTNESS (MATHEMATICS)
[BTN-95-EIX95182619105] p 269 A95-76590	REENTRY VEHICLES	Enhancing filter robustness in cascaded GPS-INS
Evaluation of neutron techniques for illicit substance	Functional dependence of trajectory dispersion on initial	integrations
detection	condition errors	[BTN-95-EIX95142555475] p 278 A95-73435
	[BTN-95-EIX95152583263] p 298 A95-73564	Identification of higher order helicopter dynamics using
[DE95-002988] p 300 N95-22764	Moving mass trim control for aerospace vehicles	linear modeling methods
	DE95-002602  p 299 N95-23532	[HTN-95-80851] p 290 A95-75093
R		Aeroelastic vehicle multivariable control synthesis with
n	REFRACTORY MATERIALS	analytical robustness evaluation
	Compliant interlayer	IBTN-95-EIX95182619115  p 321 A95-76592
RADAR DATA	[BTN-95-EIX95142562401] p 304 A95-73439	•
Statistics of multi-look AIRSAR imagery: A comparison	REINFORCING FIBERS	Multivariable stability and robustness of sequentially
of theory with measurements p 320 N95-23947	Compliant interlayer	designed feedback systems
· · · · · · · · · · · · · · · · · · ·	[BTN-95-EIX95142562401] p 304 A95-73439	[BTN-95-EIX95182619125] p 322 A95-76602
RADAR IMAGERY	REMOTE CONTROL	Robustly stable preliminary control systems design for
Statistics of multi-look AIRSAR imagery: A comparison	Cypher moves toward autonomous flight	the YF-16 CCV aircraft
of theory with measurements p 320 N95-23947	[HTN-95-41394] p 283 A95-76390	[BTN-95-EIX95202637608] p 292 A95-76681
AIRSAR deployment in Australia, September 1993:		Design of high performance multivariable control
Management and objectives p 321 N95-23948	REMOTE SENSING	systems for supermaneuverable aircraft at high angle of
RADAR MAPS	AVIRIS and TIMS data processing and distribution at	
	the land processes distributed active archive center	attack
Differential GPS and system integration of the Low	p 325 N95-23872	[NASA-CR-197661] p 293 N95-22908
Visibility Landing and Surface Operations (LVLASO)	AIRSAR deployment in Australia, September 1993:	ROCKET ENGINES
demonstration p 280 N95-23318	Management and objectives p 321 N95-23948	Fourth-generation Mars vehicle concepts
MAX-91: Polarimetric SAR results on Montespertoli	REMOTELY PILOTED VEHICLES	[BTN-95-EIX95152583267] p 298 A95-73568
site p 320 N95-23940	An unmanned air vehicle concept with tipjet drive	Impeller flow field characterization with a laser two-focus
RADIAL FLOW	[HTN-95-80858] p 283 A95-75100	velocimeter p 313 N95-23440
Enhanced analysis and users manual for radial-inflow	Cypher moves toward autonomous flight	ROLL
turbine conceptual design code RTD	[HTN-95-41394] p 283 A95-76390	Navier-Stokes prediction of large-amplitude delta-wing
	RESEARCH	roll oscillations
[NASA-CR-195454] p 275 N95-23462		[BTN-95-EIX95152582329] p 281 A95-73531
RADIATIVE HEAT TRANSFER	1994 NASA-HU American Society for Engineering	Further analysis of high-rate rolling experiments of a
Convective and radiative heat transfer analysis for the	Education (ASEE) Summer Faculty Fellowship Program	
fire 2 forebody	[NASA-CR-194972] p 325 N95-23276	65-deg delta wing
[BTN-95-EIX95182617460] p 268 A95-75731	Research and Technology, 1994	[BTN-95-EIX95152582331] p 281 A95-73533
Possible effects of CO2 increase on the high-speed civil	(NASA-TM-106764) p 262 N95-24025	Method for the prediction of the onset of wing rock
	RESEARCH AIRCRAFT	[BTN-95-EIX95152582342] p 282 A95-73544
transport impact on ozone	Analysis of the longitudinal handling qualities and	Investigation of the effects of bandwidth and time delay
[HTN-95-60779] p 317 A95-75976	pilot-induced-oscillation tendencies of the	on helicopter roll-axis handling qualities
RADIO ALTIMETERS	High-Angle-of-Attack Research Vehicle (HARV)	[HTN-95-80853] p 290 A95-75095
Flight test evaluation of a 35 GHz forward looking	p 293 N95-23297	
altimeter for terrain avoidance	RESEARCH VEHICLES	Kinematics and aerodynamics of velocity-vector roll
[BTN-95-EIX95212641071] p 287 A95-76736	·	[BTN-95-EIX95182619126] p 291 A95-76603
RADIO FREQUENCIES	Differential GPS and system integration of the Low	Multiple-function digital controller system for active
CASS: Design for supportability	Visibility Landing and Surface Operations (LVLASO)	flexible wing wind-tunnel model
	demonstration p 280 N95-23318	[BTN-95-EIX95182619212] p 322 A95-76638
[BTN-95-EIX95172595296] p 287 A95-75716	RESIDUAL STRENGTH	Rolling maneuver load alleviation using active controls
RAINDROPS	Residual strength of thin panels with cracks	
Tracking of raindrops in flow over an airfoil	p 311 N95-23311	[BTN-95-EIX95182619217] p 270 A95-76643
[BTN-95-EIX95182619221] p 308 A95-76647	RESIN TRANSFER MOLDING	Feedback control laws for highly maneuverable
RANDOM ERRORS	Development and verification of a resin film	aircraft
Functional dependence of trajectory dispersion on initial	infusion/resin transfer molding simulation model for	[NASA-CR-197944] p 295 N95-23410
condition errors	fabrication of advanced textile composites	ROLLING MOMENTS
[BTN-95-EIX95152583263] p 298 A95-73564	[NASA-CR-197439] p 301 N95-23179	Effect of leeward flow dividers on the wing rock of a
RAREFIED GAS DYNAMICS	RESONANT FREQUENCIES	delta wing
	Phonon characteristics of high (T sub c) superconductors	[BTN-95-EIX95152582347] p 282 A95-73549
Hypersonic rarefied flow past spheres including wake		·
structure	from neutron Doppler broadening measurements	Kinematics and aerodynamics of velocity-vector roll
[BTN-95-ElX95152583250] p 305 A95-73551	[DE95-003703] p 324 N95-24076	[BTN-95-EIX95182619126] p 291 A95-76603
Particle kinetic simulation of high altitude hypervelocity	RETROREFLECTION	ROTARY ENGINES
flight	Double pass retroreflection for corrosion detection in	Evaluation of thermal barrier and PS-200 self-lubricating
[NASA-CR-197383] p 309 N95-22481	aircraft structures p 323 N95-23503	coatings in an air-cooled rotary engine
• • • • • • • • • • • • • • • • • • • •	REVERSED FLOW	[NASA-CR-195445] p 289 N95-23222
RATINGS The circles quelity report 1004	Aerodynamic characteristics of external store	ROTARY WING AIRCRAFT
The airline quality report, 1994	configurations at low speeds	
[NIAR-94-11] p 277 N95-24012	[BTN-95-EIX95182619230] p 271 A95-76656	An unmanned air vehicle concept with tipjet drive
RATIOS	REYNOLDS EQUATION	[HTN-95-80858] p 283 A95-75100
Supersonic axisymmetric conical flow solutions for	Influence of streamwise curvature on longitudinal	Cypher moves toward autonomous flight
different ratios of specific heats	vortices imbedded in turbulent boundary layers	[HTN-95-41394] p 283 A95-76390
[BTN-95-EIX95152583283] p 306 A95-73584		System for determining aerodynamic imbalance
REACTION KINETICS	[BTN-94-EIX94401378820] p 307 A95-76489	[NASA-CASE-ARC-11913-1] p 311 N95-23377
_	REYNOLDS NUMBER	
Sensitivity of combustion-acoustic instabilities to	Effect of underwing frost on a transport aircraft airfoil	ROTARY WINGS
boundary conditions for premixed gas turbine	at flight Reynolds number	Efficient sensitivity analysis for rotary-wing
combustors	[BTN-95-EIX95152582334] p 276 A95-73536	aeromechanical problems
[NASA-TM-106890] p 289 N95-23550	Effect of ambient turbulence intensity on sphere wakes	[BTN-95-EIX95152577585] p 264 A95-73497
REAL TIME OPERATION	at intermediate Reynolds numbers	Dynamic analysis of bearingless tail rotor blades based
Pilot Weather Advisor system	[BTN-95-EIX95182619101] p 308 A95-76586	on nonlinear shell modes
[BTN-95-EIX95152582314] p 316 A95-73517		[BTN-95-EIX95152582338] p 281 A95-73540
	Wing pressure distributions from subsonic tests of a	· · · · · · · · · · · · · · · · · · ·
Real-time navigation using the global positioning	high-wing transport model in the Langley 14- by 22-Foot	Sensitivity of acoustic predictions to variation of input
system	Subsonic Wind Tunnel	parameters
[BTN-95-EIX95172595298] p 279 A95-75714	[NASA-TM-4583] p 272 N95-22802	[HTN-95-80855] p 267 A95-75097

SUBJECT INDEX
The influence of alternate inter-blade connections on
ground resonance
[HTN-95-80859] p 267 A95-75101
Response of a nonrotating rotor blade to lateral turbulence. Part 1: Theory
[BTN-95-EIX95182619228] p 284 A95-76654
Response of a nonrotating rotor blade to lateral
turbulence. Part 2: Experiment  BTN-95-EIX95182619229  p 284 A95-76655
Integrated aerodynamic/dynamic/structural
optimization of helicopter rotor blades using multilevel
decomposition
[NASA-TP-3465] p 285 N95-22953 System for determining aerodynamic imbalance
[NASA-CASE-ARC-11913-1] p 311 N95-23377
ROTATING BODIES
Dynamic investigation of the angular motion of a rotating
body-parachute system [BTN-95-EIX95182619220] p 270 A95-76646
ROTATING SHAFTS
Transient analysis of a cracked rotor passing through
critical speed   BTN-94-EIX94401360022   p 306 A95-74702
ROTATION
Dynamic investigation of the angular motion of a rotating
body-parachute system  BTN-95-E X95182619220  p 270 A95-76646
BTN-95-EIX95182619220  p 270 A95-76646 ROTOR AERODYNAMICS
Efficient sensitivity analysis for rotary-wing
aeromechanical problems
[BTN-95-EIX95152577585] p 264 A95-73497
Effects of high order dynamics on helicopter flight control law design
[HTN-95-80852] p 290 A95-75094
Sensitivity of acoustic predictions to variation of input
parameters }HTN-95-80855} p 267 A95-75097
The influence of alternate inter-blade connections on
ground resonance
(HTN-95-80859) p 267 A95-75101
Response of a nonrotating rotor blade to lateral turbulence. Part 2: Experiment
BTN-95-EIX95182619229  p 284 A95-76655
ROTOR BLADES
Response of a nonrotating rotor blade to lateral turbulence. Part 2: Experiment
[BTN-95-EIX95182619229] p 284 A95-76655
ROTOR BLADES (TURBOMACHINERY)
Efficient sensitivity analysis for rotary-wing aeromechanical problems
BTN-95-EIX95152577585  p 264 A95-73497
Analysis of a higher harmonic control test to reduce
blade vortex interaction noise (BTN-95-EIX95152582330) p 265 A95-73532
[BTN-95-EIX95152582330] p 265 A95-73532 Enhanced analysis and users manual for radial-inflow
turbine conceptual design code RTD
[NASA-CR-195454] p 275 N95-23462
ROTOR BODY INTERACTIONS  An investigation of helicopter dynamic coupling using
an analytical model
NASA-CR-197420  p 285 N95-23217
ROTOR DYNAMICS Improving prediction: The incorporation of simplified
rotor dynamics in a mathematical model of the bell
412HP  BTN-95-EIX95152584679  p 282 A95-73591
Transient analysis of a cracked rotor passing through
critical speed
[BTN-94-EIX94401360022] p 306 A95-74702 Identification of higher order helicopter dynamics using
linear modeling methods
[HTN-95-80851] p 290 A95-75093
Effects of high order dynamics on helicopter flight control law design
[HTN-95-80852] p 290 A95-75094
Integrated flight/propulsion control for helicopters
[HTN-95-80854] p 290 A95-75096
HTN-95-80854   p 290 A95-75096 Effects of AMB parameters on the dynamic stability of the rotor  BTN-94-EIX94381353450   p 323 A95-75494
[HTN-95-80854] p 290 A95-75096 Effects of AMB parameters on the dynamic stability of the rotor [BTN-94-EIX94381353450] p 323 A95-75494 Influence of backup bearings and support structure
[HTN-95-80854] p 290 A95-75096 Effects of AMB parameters on the dynamic stability of the rotor [BTN-94-EIX94381353450] p 323 A95-75494 Influence of backup bearings and support structure dynamics on the behavior of rotors with active supports
[HTN-95-80854] p 290 A95-75096 Effects of AMB parameters on the dynamic stability of the rotor [BTN-94-EIX94381353450] p 323 A95-75494 Influence of backup bearings and support structure dynamics on the behavior of rotors with active supports [NASA-CR-197438] p 310 N95-23190 Evaluation of thermal barrier and PS-200 self-lubricating
[HTN-95-80854] p 290 A95-75096 Effects of AMB parameters on the dynamic stability of the rotor [BTN-94-EIX94381353450] p 323 A95-75494 Influence of backup bearings and support structure dynamics on the behavior of rotors with active supports [NASA-CR-197438] p 310 N95-23190 Evaluation of thermal barrier and PS-200 self-lubricating coatings in an air-cooled rotary engine
[HTN-95-80854] p 290 A95-75096 Effects of AMB parameters on the dynamic stability of the rotor [BTN-94-EIX94381353450] p 323 A95-75494 Influence of backup bearings and support structure dynamics on the behavior of rotors with active supports [NASA-CR-197438] p 310 N95-23190 Evaluation of thermal barrier and PS-200 self-lubricating coatings in an air-cooled rotary engine [NASA-CR-195445] p 289 N95-23222
[HTN-95-80854] p 290 A95-75096 Effects of AMB parameters on the dynamic stability of the rotor [BTN-94-EIX94381353450] p 323 A95-75494 Influence of backup bearings and support structure dynamics on the behavior of rotors with active supports [NASA-CR-197438] p 310 N95-23190 Evaluation of thermal barrier and PS-200 self-lubricating coatings in an air-cooled rotary engine [NASA-CR-195445] p 289 N95-23222 ROTOR SYSTEMS RESEARCH AIRCRAFT H-76B fantail demonstrater composite fan blade
[HTN-95-80854] p 290 A95-75096 Effects of AMB parameters on the dynamic stability of the rotor [BTN-94-EIX94381353450] p 323 A95-75494 Influence of backup bearings and support structure dynamics on the behavior of rotors with active supports [NASA-CR-197438] p 310 N95-23190 Evaluation of thermal barrier and PS-200 self-lubricating coatings in an air-cooled rotary engine [NASA-CR-195445] p 289 N95-23222 ROTOR SYSTEMS RESEARCH AIRCRAFT

Finite element model for a flexible non-symmetric rotor

p 306 A95-74612

[BTN-95-EIX95152577612]

p 321 A95-73471

on distributed bearing: A stability study |BTN-94-EIX94381352212|

ROTORS

s on	Tr
101 teral	critic (BTN Eff
654	the r
teral	Inf dyna
655 tural	NAS
evel 1953	RUNG! Eft
377	of vo
iting	Nu trans adva
646	RUNW Gu
ugh	Rollo I NAS RUNW
702	Air rejec
iting	Doug 2 Ma
646 ving	(PB9
497	
ntrol	SABOT An dyna
094 nput	SAFET
097 on	Mis
101	SAFET Co An o
teral	SAFET
655	(BTN
teral 655	lost/e
ving	Av Indus (PB9
497	SALT E
luce 532	Co
flow	SANDY
462	lunar (BTN SATEL
sing 217	De over
ified	BTN Pik
bell 591	(BTN SATEL Ca
ugh	AD-
702 sing	Th satel
093 ntrol	BTN SCALE Ae
094	missi (BTN
096 y of	SCALII Sc
494	Spee (BTN
ture orts	SCANA SE scatt
190 iting	SCHEE

al speed SA-CR-1974381 SA-CR-195026 | AYS rch 1994 5-910401 [ erials Y FACTORS verview 4-917005 BATHS SPRAY TESTS transfer vehicle LITE DRAG A2851181 LITE ORBITS MODELS NG LAWS d laminar flows DULING

sensitivity analysis for rotary-wing ansient analysis of a cracked rotor passing through Efficient aeromechanical problems p 264 A95-73497 N-94-EIX944013600221 p 306 A95-74702 [BTN-95-EIX95152577585] fects of AMB parameters on the dynamic stability of SEPARATED FLOW Two-equation turbulence model for unsteady separated I-94-EIX94381353450| p 323 A95-75494 lows around airfoils p 262 A95-73444 luence of backup bearings and support structure [BTN-95-EIX95142553054] mics on the behavior of rotors with active supports Computation of oscillating airfoil flows with one- and p 310 N95-23190 two-equation turbulence models in tailored composite wing for civil tiltrotor p 263 A95-73494 [BTN-95-EIX95152577588] p 285 N95-23317 Computational study of plume-induced separation on a E-KUTTA METHOD hypersonic powered model [BTN-95-EIX95152582346] lects of spatial order of accuracy on the computation p 266 A95-73548 Simulating heat addition via mass addition in constant N-95-EIX95152577604 | p 305 A95-73479 area compressible flows imerical computation of aerodynamics and heat p 307 A95-76585 [BTN-95-EIX95182619100] ster in a turbine cascade and a turn-around duct using Scaling of incipient separation in supersonic/transonic p 313 N95-23444 nced turbulence models speed laminar flows AY CONDITIONS |BTN-95-EIX95182619104| p 269 A95-76589 idance and control requirements for high-speed Neural network prediction of three-dimensional unsteady out and Turnoff (ROTO) separated flowfields p 292 N95-22674 [BTN-95-EIX95182619232] p 308 A95-76658 rcraft accident report. Runway overrun following SERVICE LIFE ted takeoff. Continental airlines flight 795, McDonnell Life prediction of helicopter engines fitted with dust glas MD-82, N18835, LaGuardia Airport, Flushing, NY, filters IBTN-95-EIX951826192241 p 289 A95-76650 p 277 N95-23609 Oklahoma City air logistics center (USAF) aging aircraft corrosion program p 262 N95-23519 SHADOWGRAPH PHOTOGRAPHY Simple method of supersonic flow visualization using watertable PROJECTILES BTN-95-EIX95182619105 p 269 A95-76590 alytical solution and parameter estimation of projectile SHAFTS (MACHINE ELEMENTS) Finite element model for a flexible non-symmetric rotor I-95-EIX95212645695 | p 272 A95-76747 on distributed bearing: A stability study p 306 A95-74612 [BTN-94-EIX94381352212] shap risk control for advanced aerospace/composite SHALLOW SHELLS p 301 N95-23031 Dynamic analysis of bearingless tail rotor blades based on nonlinear shell modes rrosion detection and monitoring of aircraft structures: [BTN-95-EIX95152582338] p 303 N95-23515 Y MANAGEMENT Finite element model for a flexible non-symmetric rotor intenance programs on distributed bearing: A stability study I-95-EIX95182617809 | p 261 A95-75754 [BTN-94-EIX94381352212] p 306 A95-74612 review of civil aviation fatal accidents in which SHEAR FLOW disoriented was a cause/factor: 1981-1990 /FAA/AM-95/1] Adaptive finite element method for turbulent flow near p 278 N95-24071 a propeller iation Accident Investigation Symposium. Volume 1: BTN-95-EIX95142553038 | p 305 A95-73460 stry recommendations and Safety Board responses SHEAR LAYERS p 278 N95-24105 Laser velocimetry seed-particle behavior in shear layers at Mach 12 rrosion of landing gear steels p 302 N95-23500 [BTN-95-EIX95212645712] p 272 A95-76764 SHEAR STRAIN rrosion of landing gear steels p 302 N95-23500 Finite element model for a flexible non-symmetric rotor WICH STRUCTURES on distributed bearing: A stability study nimum-mass design of sandwich aerobrakes for a IBTN-94-EIX943813522121 p 306 A95-74612 SHEAR STRENGTH I-95-EIX95212645707 p 299 A95-76759 Interlaminar shear test method development for long LITE COMMUNICATION term durability testing of composites velopment of aeronautical mobile satellite services p 301 N95-23300 the past thirty years SHEAR STRESS i-95-EIX95152569458 j p 305 A95-73498 Nonlinear angle of twist of advanced composite wing ot Weather Advisor system I-95-EIX95152582314] p 316 A95-73517 [BTN-95-EIX95152582323] p 281 A95-73526 High-lift flow-physics flight experiments on a subsonic culation of satellite drag coefficients p 275 N95-23333 civil transport aircraft (B737-100) p 300 N95-23781 SHOCK HEATING Application of the multigrid solution technique to ermal force modeling for global positioning system hypersonic entry vehicles lites using the finite element method [BTN-95-EIX95152583254] p 306 A95-73555 1-95-EIX951525832701 p 278 A95-73571 SHOCK LAYERS Higher-order viscous shock-layer solutions for rodynamic characteristics of a canard-controlled high-altitude flows ile at high angles of attack BTN-95-EIX95152583255 | p 306 A95-73556 p 267 A95-73558 SHOCK TUBES Application of a control-volume-based finite-element aling of incipient separation in supersonic/transonic formulation to the shock tube problem p 295 A95-76584 BTN-95-EIX95182619099 | I-95-EIX951826191041 p 269 A95-76589 SHOCK TUNNELS IING ELECTRON MICROSCOPY Shock tunnel measurements of hypervelocity blunted M representation of the early and late time fields cone drag (BTN-95-EIX95152577606) ered from wire targets p 305 A95-73477 N-94-EIX943813531421 p 306 A95-74496 SHOCK WAVE INTERACTION Flow study of supersonic wing-nacelle configuration Empirical results on scheduling and dynamic p 266 A95-73546 [BTN-95-EIX95152582344] backtracking p 299 N95-23761 Scaling of incipient separation in supersonic/transonic SECONDARY FLOW speed laminar flows Three-dimensional unsteady flow calculations in an |BTN-95-EIX95182619104| p 269 A95-76589 advanced gas generator turbine p 312 N95-23425 Mach 10 computational study of a three-dimensional scramjet inlet flow field [NASA-TM-4602] Preconditioned domain decomposition scheme for p 310 N95-23210 three-dimensional aerodynamic sensitivity analysis

p 312 N95-23429

Supersonic flow and shock formation in turbine tip

SHOCK WAVE PROPAGATION	SOLAR ARRAYS	SPECTRAL SENSITIVITY
Aeroacoustic model for weak shock waves based on Burgers equation	Design of a GaAs/Ge solar array for unmanned aerial vehicles	Sensitivity of acoustic predictions to variation of input parameters
[BTN-95-EIX95182619076] p 269 A95-75761	[NASA-TM-106870] p 320 N95-23259	[HTN-95-80855] p 267 A95-75097 SPECTRUM ANALYSIS
SHOCK WAVES Flow study of supersonic wing-nacelle configuration	SOLAR CELLS  Design of a GaAs/Ge solar array for unmanned aerial	Phonon characteristics of high (T sub c) superconductors
IBTN-95-EIX95152582344   p 266 A95-73546 Application of the multigrid solution technique to	vehicles .	from neutron Doppler broadening measurements (DE95-003703) p 324 N95-24076
hypersonic entry vehicles	[NASA-TM-106870] p 320 N95-23259 SOLID LUBRICANTS	SPHERES
[BTN-95-EIX95152583254] p 306 A95-73555 Three-dimensional structure of a supersonic jet	Evaluation of thermal barrier and PS-200 self-lubricating coatings in an air-cooled rotary engine	Hypersonic rarefied flow past spheres including wake structure
impinging on an inclined plate	[NASA-CR-195445] p 289 N95-23222	[BTN-95-EIX95152583250] p 305 A95-73551 SPHERICAL COORDINATES
Supersonic axisymmetric conical flow solutions for	SOLID PROPELLANT ROCKET ENGINES Simulation on the 3-D turbulent flow in the passages	Application of wall functions to generalized
different ratios of specific heats [BTN-95-EIX95152583283] p 306 A95-73584	of finocyl grain	nonorthogonal curvilinear coordinate systems [BTN-95-EIX95182619077] p 307 A95-75762
Aeroacoustic model for weak shock waves based on	[BTN-95-EIX95202638962] p 279 A95-76674 SOLID STATE LASERS	SPHERICAL WAVES
Burgers equation [BTN-95-EIX95182619076] p 269 A95-75761	2 micron LIDAR for laser-based remote sensing: Flight	Effect of ambient turbulence intensity on sphere wakes at intermediate Reynolds numbers
Observations on using experimental data as boundary conditions for computations	demonstration and application survey [BTN-95-EIX95212641072] p 319 A95-76737	[BTN-95-EIX95182619101] p 308 A95-76586 SPIKES (AERODYNAMIC CONFIGURATIONS)
[BTN-95-EIX95182619103] p 321 A95-76588	SONIC BOOMS  Aeroacoustic model for weak shock waves based on	Numerical investigation of supersonic flows around a
SHUTTLE IMAGING RADAR AIRSAR deployment in Australia, September 1993:	Burgers equation	spiked blunt body  BTN-95-EIX95212645690  p 271 A95-76742
Management and objectives p 321 N95-23948 SIDESLIP	[BTN-95-EIX95182619076] p 269 A95-75761 SOUND FIELDS	SPINE A multibody/finite element analysis approach for
Method for the prediction of the onset of wing rock	Numerical study of sound generation due to a spinning	modeling of crash dynamic responses
[BTN-95-EIX95152582342] p 282 A95-73544 Effect of leeward flow dividers on the wing rock of a	vortex pair [BTN-95-EIX95182619075] p 307 A95-75760	[NIAR-94-3] p 277 N95-24050 SPLASHING
delta wing	SOUND WAVES	Tracking of raindrops in flow over an airfoil
[BTN-95-EIX95152582347] p 282 A95-73549 Wing pressure distributions from subsonic tests of a	Coupled FEM-BEM approach for mean flow effects on vibro-acoustic behavior of planar structures	BTN-95-ĒIX95182619221  p 308 A95-76647 <b>SPLICING</b>
high-wing transport model in the Langley 14- by 22-Foot Subsonic Wind Tunnel	[BTN-95-EIX95152577587] p 263 A95-73495	Multiple site fatigue damage in fuselage skin splices: Experimental simulation and theoretical prediction
[NASA-TM-4583] p 272 N95-22802	Mach wave emission from a high-temperature supersonic jet	[BTN-95-EIX95152584676] p 276 A95-73588
SIGNAL PROCESSING Simulation of turbulent fluctuations	[BTN-95-EIX95152577586] p 264 A95-73496 SPACE PROCESSING	SPOILERS Study of an airfoil with a flap and spoiler
[BTN-95-EIX95142553041] p 304 A95-73457	Fourth-generation Mars vehicle concepts	[BTN-95-EIX95152582327] p 265 A95-73530
Maximum-likelihood spectral estimation and adaptive filtering techniques with application to airborne Doppler	[BTN-95-EIX95152583267] p 298 A95-73568  SPACE SHUTTLE MAIN ENGINE	SPRAY CHARACTERISTICS Study of the droplet spray characteristics of a subsonic
weather radar {NASA-CR-197699} p 316 N95-23670	Phase 2: HGM air flow tests in support of HEX vane investigation p 312 N95-23438	wind tunnel [BTN-95-EIX95182619235] p 271 A95-76661
SIKORSKY AIRCRAFT	SPACE SHUTTLE ORBITERS	STABILITY
H-76B fantail demonstrater composite fan blade fabrication	Aerodynamics of the Shuttle Orbiter at high altitudes [BTN-95-EIX95182617454] p 298 A95-75725	Comparison of linear stability results with flight transition data
[HTN-95-80856] p 283 A95-75098 Cypher moves toward autonomous flight	Shuttle entry guidance revisited using nonlinear	[BTN-95-EIX95182619097] p 283 A95-76582 Thin tailored composite wing for civil tiltrotor
[HTN-95-41394] p 283 A95-76390	geometric methods [BTN-95-EIX95182619144] p 299 A95-76621	p 285 N95-23317
SILICON  Cu deposition using a permanent magnet electron	SPACECRAFT CONSTRUCTION MATERIALS  Evaluation of advanced aerospace materials by depth	STABILITY DERIVATIVES  Attainable moments for the constrained control
cyclotron resonance microwave plasma source  DE94-017768  p 304 N95-23981	sensing indentation and scratch methods	allocation problem [BTN-95-EIX95182619149] p 322 A95-76626
SILICON NITRIDES	BTN-95-EIX95152584678  p 282 A95-73590 SPACECRAFT CONTROL	Stability derivatives of a flapped plate in unsteady ground
Evolution of oxidation and creep damage mechanisms in HIPed silicon nitride materials	Fuel-optimal bank-angle control for lunar-return aerocapture	effect  BTN-95-EIX95182619225  p 270 A95-76651
[DE95-001360] p 300 N95-22689 SIMULATION	[BTN-95-EIX95212645706] p 299 A95-76758	STABILITY TESTS Functional dependence of trajectory dispersion on initial
Simulation and model reduction for the active flexible	SPACECRAFT LAUNCHING Fourth-generation Mars vehicle concepts	condition errors
wing program  BTN-95-EIX95182619211  p 295 A95-76637	BTN-95-EIX95152583267  p 298 A95-73568 SPACECRAFT MODELS	BTN-95-EIX95152583263  p 298 A95-73564 STABILIZERS (FLUID DYNAMICS)
Holographic interferometric tomography for reconstructing flow fields p 310 N95-23287	Thermal force modeling for global positioning system	Integrated design of hypersonic waveriders including
SIMULATORS	satellites using the finite element method [BTN-95-EIX95152583270] p 278 A95-73571	inlets and tailfins  BTN-95-EIX95212645692  p 271 A95-76744
A new type of simulator for simulating the flow-field distortion of engine inlet	SPACECRAFT REENTRY Shuttle entry guidance revisited using nonlinear	STAGNATION PRESSURE  Main features of overexpanded triple jets
[BTN-95-EIX95202638963] p 289 A95-76673	geometric methods	[BTN-95-EIX95142553040] p 304 A95-73458
SINGULARITY (MATHEMATICS)  A wall interference assessment/correction system	[BTN-95-EIX95182619144] p 299 A95-76621 SPACECRAFT TRAJECTORIES	STATE ESTIMATION  New failure detection approach and its application to
[NASA-CR-197421] p 309 N95-23183 SITTING POSITION	Effects of satellite bunching on the probability of collision in geosynchronous orbit	GPS autonomous integrity monitoring [BTN-95-EIX95202637613] p 279 A95-76676
A multibody/finite element analysis approach for	[BTN-95-EIX95152583276] p 298 A95-73577	STATIC CHARACTERISTICS
modeling of crash dynamic responses [NIAR-94-3] p 277 N95-24050	SPACING  Main features of overexpanded triple jets	Static aeroelastic characteristics of a composite wing [BTN-95-EIX95152582340] p 282 A95-73542
SKIN (STRUCTURAL MEMBER)  Multiple site fatigue damage in fuselage skin splices:	[BTN-95-EIX95142553040] p 304 A95-73458 SPALLATION	STATIC PRESSURE Static pressure distribution in the inlet of a helicopter
Experimental simulation and theoretical prediction	Phonon characteristics of high (T sub c) superconductors	turbine compressor
[BTN-95-EIX95152584676] p 276 A95-73588 An analytical and experimental investigation of the	from neutron Doppler broadening measurements (DE95-003703) p 324 N95-24076	[BTN-95-EIX95152582339] p 266 A95-73541 Aerodynamic characteristics of external store
response of the curved, composite frame/skin specimens	SPATIAL DISTRIBUTION	configurations at low speeds [BTN-95-EIX95182619230] p 271 A95-76656
[HTN-95-80857] p 283 A95-75099	Thundercloud electric field modeling for the ionosphere-Earth region. 1: Dependence on cloud charge	STATIC STABILITY
SLENDER CONES Shock tunnel measurements of hypervelocity blunted	distribution [HTN-95-41223] p 317 A95-75035	Handling qualities of the High Speed Civil Transport p 294 N95-23325
cone drag	SPATIAL FILTERING	STATIC TESTS
[BTN-95-EIX95152577606] p 305 A95-73477 SLOTS	Simulation of turbulent fluctuations [BTN-95-EIX95142553041] p 304 A95-73457	Validation of an effective flat cruciform-shaped specimen to study CFRP composite laminates under biaxial
Forebody flow control on a full-scale F/A-18 aircraft [BTN-95-EIX95152582333] p 281 A95-73535	SPECIFIC HEAT Supersonic axisymmetric conical flow solutions for	loading [BTN-95-EIX95152584677] p 282 A95-73589
Pneumatic concept for tip-stall control of cranked-arrow	different ratios of specific heats	Corrosion protection measures for CFC/metal joints of
wings  BTN-95-EIX95152582335  p 281 A95-73537	[BTN-95-EIX95152583283] p 306 A95-73584 Review and development of base pressure and base	fuel integral tank structures of advanced military aircraft p 303 N95-23510
SMOKE  Modeling aerosol emissions from the combustion of	heating correlations in supersonic flow [BTN-95-EIX95212645688] p 271 A95-76740	STATIC THRUST  An approximate theoretical method for modeling the
composite materials p 301 N95-23038	SPECIFICATIONS	static thrust performance of non-axisymmetric
Aircraft fires, smoke toxicity, and survival: An overview [DOT/FAA/AM-95/8] p 277 N95-24024	Handling qualities of the High Speed Civil Transport p 294 N95-23325	two-dimensional convergent-divergent nozzles [NASA-CR-195050] p 273 N95-23193

p 323 N95-23503

Double pass retroreflection for corrosion detection in

aircraft structures

STATISTICAL ANALYSIS	Analytical aeropropulsive/aeroelastic	Mach 10 computational study of a three-dimensional
Effects of satellite bunching on the probability of collision	hypersonic-vehicle model with dynamic analysis	scramjet inlet flow field INASA-TM-4602 I p 309 N95-23015
in geosynchronous orbit [BTN-95-EIX95152583276] p 298 A95-73577	[BTN-95-EIX95182619138] p 269 A95-76615 Active control of panel vibrations induced by a boundary	[NASA-TM-4602] p 309 N95-23015 Mach 10 computational study of a three-dimensional
On-line, adaptive state estimator for active noise	layer flow	scramiet inlet flow field
control p 322 N95-23308	[NASA-CR-197867] p 273 N95-23182	[NASA-TM-4602] p 310 N95-23210
POD assessment of NDI procedures using a round robin	Gearbox vibration diagnostic analyzer	SUPERSONIC DRAG
test	[NASA-CR-189141] p 316 N95-23792	CFD optimization of a theoretical minimum-drag body
[AGARD-R-809] p 315 N95-23602	SUBSONIC FLOW  Sidewash on the vertical tail in subsonic and supersonic	[BTN-95-EIX95182619234] p 308 A95-76660
STATORS	flows	SUPERSONIC FLOW
Enhanced analysis and users manual for radial-inflow turbine conceptual design code RTD	[BTN-95-EIX95152582316] p 264 A95-73519	Main features of overexpanded triple jets [BTN-95-EIX95142553040] p 304 A95-73458
[NASA-CR-195454] p 275 N95-23462	Analytic prediction of lift for delta wings with partial	Sidewash on the vertical tail in subsonic and supersonic
STEADY FLOW	leading-edge thrust	flows
Aerodynamic design and analysis of a highly loaded	[BTN-95-EIX95152582345] p 266 A95-73547 Higher-order viscous shock-layer solutions for	BTN-95-EIX95152582316  p 264 A95-73519
turbine exhaust p 312 N95-23435	high-altitude flows	Predicting exhaust plume boundaries with supersonic
STEELS	BTN-95-EIX95152583255  p 306 A95-73556	external flows
Corrosion of landing gear steels p 302 N95-23500 STIFFNESS	Comparison of linear stability results with flight transition	[BTN-95-EIX95152583258] p 297 A95-73559
Dynamic analysis of bearingless tail rotor blades based	data  BTN-95-EIX95182619097  p 283 A95-76582	Supersonic axisymmetric conical flow solutions for different ratios of specific heats
on nonlinear shell modes	Study of the droplet spray characteristics of a subsonic	[BTN-95-EIX95152583283] p 306 A95-73584
[BTN-95-EIX95152582338] p 281 A95-73540	wind tunnel	Supersonic near-wake afterbody boattailing effects on
Finite element model for a flexible non-symmetric rotor	BTN-95-EIX95182619235  p 271 A95-76661	axisymmetric bodies
on distributed bearing: A stability study	Wing pressure distributions from subsonic tests of a	[BTN-95-EIX95182617465] p 268 A95-75736
BTN-94-EIX94381352212  p 306 A95-74612	high-wing transport model in the Langley 14- by 22-Foot Subsonic Wind Tunnel	Simulating heat addition via mass addition in constant
Integrated aerodynamic/dynamic/structural optimization of helicopter rotor blades using multilevel	[NASA-TM-4583] p 272 N95-22802	area compressible flows [BTN-95-EIX95182619100] p 307 A95-76585
decomposition	SUBSONIC FLUTTER	Observations on using experimental data as boundary
[NASA-TP-3465] p 285 N95-22953	Design and multifunction tests of a frequency	conditions for computations
STRAIN MEASUREMENT	domain-based active flutter suppression system	[BTN-95-EIX95182619103] p 321 A95-76588
Shock tunnel measurements of hypervelocity blunted	[BTN-95-EIX95182619215] p 292 A95-76641 SUBSONIC SPEED	Scaling of incipient separation in supersonic/transonic
Cone drag	Computation of the poststall behavior of a circulation	speed laminar flows
[BTN-95-EIX95152577606] p 305 A95-73477 STRATOSPHERE	controlled airfoil	[BTN-95-EIX95182619104] p 269 A95-76589
Trajectory modeling of emissions from lower	[BTN-95-EIX95152582320] p 264 A95-73523	Simple method of supersonic flow visualization using watertable
stratospheric aircraft	Aerodynamic characteristics of a canard-controlled	[BTN-95-EIX95182619105] p 269 A95-76590
[HTN-95-41219] p 317 A95-75031	missile at high angles of attack [BTN-95-EIX95152583257] p 267 A95-73558	CFD optimization of a theoretical minimum-drag body
Possible effects of CO2 increase on the high-speed civil	Inner loop flight control for the High-Speed Civil	[BTN-95-EIX95182619234] p 308 A95-76660
transport impact on ozone [HTN-95-60779] p 317 A95-75976	Transport p 293 N95-23314	Review and development of base pressure and base
[HTN-95-60779] p 317 A95-75976 Estimates of total organic and inorganic chlorine in the	High-lift flow-physics flight experiments on a subsonic	heating correlations in supersonic flow
lower stratosphere from in situ and flask measurements	civil transport aircraft (B737-100) p 275 N95-23333	[BTN-95-EIX95212645688] p 271 A95-76740
during AASE 2	SUBSONIC WIND TUNNELS	Numerical investigation of supersonic flows around a spiked blunt body
[HTN-95-A0861] p 317 A95-76265	Study of the droplet spray characteristics of a subsonic	[BTN-95-EIX95212645690] p 271 A95-76742
In situ observations in aircraft exhaust plumes in the	wind tunnel [BTN-95-EIX95182619235] p 271 A95-76661	Supersonic flow and shock formation in turbine tip
lower stratosphere at midlatitudes [HTN-95-A0862] p 318 A95-76266	SUBSTRATES	gaps p 312 N95-23429
Sensitivity of two-dimensional model predictions of	Evaluation of advanced aerospace materials by depth	Validation of a Computational Fluid Dynamics (CFD)
ozone response to stratospheric aircraft: An update	sensing indentation and scratch methods	code for supersonic axisymmetric base flow
[HTN-95-A0863] p 318 A95-76267	[BTN-95-EIX95152584678] p 282 A95-73590	p 315 N95-23652 Supersonic laminar flow control research
STRESS CORROSION CRACKING	SUCTION  Applytic production of lift for dollar usings with postiol	[NASA-CR-197938] p 275 N95-23669
The corrosion and protection of advanced aluminium -	Analytic prediction of lift for delta wings with partial leading-edge thrust	SUPERSONIC INLETS
lithium airframe alloys p 302 N95-23497	[BTN-95-EIX95152582345] p 266 A95-73547	Mach 10 computational study of a three-dimensional
Corrosion of landing gear steels p 302 N95-23500 STRESS INTENSITY FACTORS	SULFUR	scramjet inlet flow field
Multiple site fatigue damage in fuselage skin splices:	Compendium of NASA data base for the Global	[NASA-TM-4602] p 310 N95-23210
Experimental simulation and theoretical prediction	Tropospheric Experiment's Pacific Exploratory Mission	Supersonic flow and shock formation in turbine tip gaps p 312 N95-23429
[BTN-95-EIX95152584676] p 276 A95-73588 STRIPPING	West-A (PEM West-A) [NASA-TM-109177] p 320 N95-23009	SUPERSONIC JET FLOW
Aircraft stripping and painting	SULFUR HEXAFLUORIDE	Mach wave emission from a high-temperature
[BTN-95-EIX95182617810] p 300 A95-75755	Performance of the 0.3-meter transonic cryogenic tunnel	supersonic jet
STRUCTURAL ANALYSIS	with air, nitrogen, and sulfur hexafluoride media under	[BTN-95-EIX95152577586] p 264 A95-73496
Static aeroelastic characteristics of a composite wing	closed loop automatic control INASA-CR-195052] p 310 N95-23257	Three-dimensional structure of a supersonic jet
[BTN-95-EIX95152582340] p 282 A95-73542 STRUCTURAL DESIGN	[NASA-CR-195052] p 310 N95-23257 SUPERSONIC AIRCRAFT	impinging on an inclined plate [BTN-95-EIX95152583259] p 267 A95-73560
Minimum-mass design of sandwich aerobrakes for a	Mach wave emission from a high-temperature	Simulation of transverse gas injection in turbulent
lunar transfer vehicle	supersonic jet	supersonic air flows
BTN-95-EIX95212645707  p 299 A95-76759	[BTN-95-EIX95152577586] p 264 A95-73496	[BTN-95-EIX95182619080] p 269 A95-75765
Integrated aerodynamic/dynamic/structural	Flow study of supersonic wing-nacelle configuration	Supersonic jet noise reductions predicted with increased
optimization of helicopter rotor blades using multilevel decomposition	[BTN-95-EIX95152582344] p 266 A95-73546	jet spreading rate {NASA-TM-106872} p 323 N95-23178
[NASA-TP-3465] p 285 N95-22953	SUPERSONIC AIRFOILS  Natural laminar flow wing concept for supersonic	SUPERSONIC SPEED
STRUCTURAL FAILURE	transports	Simple method of supersonic flow visualization using
An analytical and experimental investigation of the	[BTN-95-EIX95182619226] p 308 A95-76652	watertable
response of the curved, composite frame/skin	SUPERSONIC BOUNDARY LAYERS	[BTN-95-EIX95182619105] p 269 A95-76590
specimens [HTN-95-80857] p 283 A95-75099	Effects of expansions on a supersonic boundary layer:	SUPERSONIC TRANSPORTS  Natural laminar flow wing concept for supersonic
STRUCTURAL STABILITY	Surface pressure measurements IBTN-95-EIX951425530361 p 263 A95-73462	transports
Finite element model for a flexible non-symmetric rotor	,	[BTN-95-EIX95182619226] p 308 A95-76652
on distributed bearing: A stability study	SUPERSONIC COMBUSTION Simulating heat addition via mass addition in constant	Inner loop flight control for the High-Speed Civil
[BTN-94-EIX94381352212] p 306 A95-74612	area compressible flows	Transport p 293 N95-23314
Flutter of an infinitely long panel in a duct [BTN-95-EIX95182619087] p 291 A95-75772	[BTN-95-EiX95182619100] p 307 A95-76585	Preliminary identification of buffet problems in high speed civil transport p 294 N95-23319
STRUCTURAL STRAIN	SUPERSONIC COMBUSTION RAMJET ENGINES	Handling qualities of the High Speed Civil Transport
Dynamic analysis of bearingless tail rotor blades based	Computational study of plume-induced separation on a	p 294 N95-23325
on nonlinear shell modes	hypersonic powered model [BTN-95-E X95152582346] p 266 A95-73548	SUPERSONIC WIND TUNNELS
[BTN-95-EIX95152582338] p 281 A95-73540	Optimization of contoured hypersonic scramjet inlets	Supersonic laminar flow control research [NASA-CR-197938] p 275 N95-23669
STRUCTURAL VIBRATION  Coupled FEM-BEM approach for mean flow effects on	with a least-squares parabolized Navier-Stokes	SUPPORT SYSTEMS
vibro-acoustic behavior of planar structures	procedure	CASS: Design for supportability
[BTN-95-EIX95152577587] p 263 A95-73495	[HTN-95-20976] p 261 A95-74042	[BTN-95-EIX95172595296] p 287 A95-75716
Transient analysis of a cracked rotor passing through	Numerical analysis of hypersonic low-density scramjet	SURFACE DISTORTION

p 272 A95-76746

inlet flow |BTN-95-EIX95212645694|

p 306 A95-74702

[BTN-94-EIX94401360022]

-	_	
	_	

SURFACE LAYERS	1	TEXTILES
Effects of expansions on a supersonic boundary layer:		Development and verification of a resin film
Surface pressure measurements [BTN-95-EIX95142553036] p 263 A95-73462	TABS (CONTROL SURFACES)	infusion/resin transfer molding simulation model for fabrication of advanced textile composites
BTN-95-EIX95142553036  p 263 A95-73462 SURFACE PROPERTIES	Aerodynamic characteristics of a canard-controlled	[NASA-CR-197439] p 301 N95-23179
Aerodynamic shape optimization using preconditioned	missile at high angles of attack	THEMATIC MAPPING
conjugate gradient methods	[BTN-95-EIX95152583257] p 267 A95-73558	AVIRIS and TIMS data processing and distribution at
	Lift enhancing tabs for airloits	
[BTN-95-EIX95142553033] p 263 A95-73465 Guidance and control requirements for high-speed	[NASA-CASE-ARC-11990-1] p 286 N95-23395	the land processes distributed active archive center p 325 N95-23872
Rollout and Turnoff (ROTO)	TAIL ASSEMBLIES	
	Sidewash on the vertical tail in subsonic and supersonic	THEODORSEN TRANSFORMATION
[NASA-CR-195026] p 292 N95-22674	flows	Flutter analysis of composite box beams INASA-CR-197931 p 294 N95-23392
SURFACE REACTIONS	[BTN-95-EIX95152582316] p 264 A95-73519	
Hypersonic nonequilibrium Navier-Stokes solutions over	Preliminary identification of buffet problems in high speed	THERMAL ANALYSIS
an ablating graphite nosetip	civil transport p 294 N95-23319	Effect of curvature in the numerical simulation of an
[BTN-95-EIX95152583252] p 305 A95-73553	TAIL ROTORS	electrothermal de-icer pad
In-situ detection of surface passivation or activation and	Dynamic analysis of bearingless tail rotor blades based	[BTN-95-EIX95182619219] p 276 A95-76645
of localized corrosion: Experiences and prospectives in	on nonlinear shell modes	THERMAL CONTROL COATINGS
aircraft p 302 N95-23508	[BTN-95-EIX95152582338] p 281 A95-73540	Evaluation of thermal barrier and PS-200 self-lubricating
SURFACE TEMPERATURE	· · · · · · · · · · · · · · · · · · ·	coatings in an air-cooled rotary engine
Particle kinetic simulation of high altitude hypervelocity	TAIWAN	[NASA-CR-195445] p 289 N95-23222
flight	Diurnal variation of lee vortices in Taiwan and the	THERMAL CYCLING TESTS
[NASA-CR-197383] p 309 N95-22481	surrounding area	Fatigue strength of high-temperature alloys under
SURFACE TREATMENT	[HTN-95-91363] p 318 A95-76394	conditions of cyclic temperature variation. Communication
Experience of in-service corrosion on military aircraft	TAKEOFF	Experimental procedure and results
p 303 N95-23516	Progress in high-lift aerodynamic calculations	[BTN-94-EIX94401363884] p 307 A95-75516
SURVIVAL	[BTN-95-EIX95152582315] p 264 A95-73518	THERMAL EMISSION
Aircraft fires, smoke toxicity, and survival: An overview	Effect of underwing frost on a transport aircraft airfoil	AVIRIS and TIMS data processing and distribution at
[DOT/FAA/AM-95/8] p 277 N95-24024	at flight Reynolds number	the land processes distributed active archive center
SWEPT FORWARD WINGS	[BTN-95-EIX95152582334] p 276 A95-73536	p 325 N95-23872
Natural laminar flow wing concept for supersonic	Aircraft accident report. Runway overrun following	THERMAL ENVIRONMENTS
transports	rejected takeoff. Continental airlines flight 795, McDonnell	Thermal force modeling for global positioning system
[BTN-95-EIX95182619226] p 308 A95-76652	Douglas MD-82, N18835, LaGuardia Airport, Flushing, NY,	satellites using the finite element method
Flight test of the X-29A at high angle of attack: Flight	2 March 1994	[BTN-95-EIX95152583270] p 278 A95-73571
dynamics and controls	[PB95-910401] p 277 N95-23609	THERMAL FATIGUE
[NASA-TP-3537] p 284 N95-22806	TAPERING	Fatique strength of high-temperature alloys under
SWEPT WINGS	The use of cowl camber and taper to reduce rotor/stator	conditions of cyclic temperature variation. Communication
Limit cycle phenomena in computational transonic	interaction noise	1: Experimental procedure and results
aeroelasticity	[NASA-CR-195421] p 323 N95-22675	[BTN-94-EIX94401363884] p 307 A95-75516
[BTN-95-EIX95152582317] p 264 A95-73520	TARGETS	THERMAL PROTECTION
Method for the prediction of the anset of wing rock	SEM representation of the early and late time fields	Minimum-mass design of sandwich aerobrakes for a
[BTN-95-EIX95152582342] p 282 A95-73544	scattered from wire targets	lunar transfer vehicle
Aerodynamics of a finite wing with simulated ice	[BTN-94-EIX94381353142] p 306 A95-74496	[BTN-95-EIX95212645707] p 299 A95-76759
[BTN-95-EIX95182619227] p 270 A95-76653	TECHNOLOGY ASSESSMENT	THERMAL RADIATION
Crossflow instability control on a swept-wing: Preliminary	Euler Technology Assessment program for preliminary	Thermal force modeling for global positioning system
studies p 274 N95-23283	aircraft design employing SPLITFLOW code with Cartesian	satellites using the finite element method
SWIRLING	unstructured grid method	[BTN-95-EIX95152583270] p 278 A95-73571
Aerodynamic design and analysis of a highly loaded	[NASA-CR-4649] p 273 N95-22917	THERMAL STRESSES
turbine exhaust p 312 N95-23435	Euler technology assessment for preliminary aircraft	Minimum-mass design of sandwich aerobrakes for a
SYMBOLS	design employing OVERFLOW code with multiblock	lunar transfer vehicle
TRISTAR 1: Evaluation methods for testing head-up	structured-grid method	[BTN-95-EIX95212645707] p 299 A95-76759
display (HUD) flight symbology	[NASA-CR-4651] p 273 N95-23095	THERMOSPHERE
[NASA-TM-4665] p 288 N95-24030	Motor drive technologies for the power-by-wire (PBW)	Calculation of satellite drag coefficients
SYNTHETIC APERTURE RADAR	program: Options, trends and tradeoffs	[AD-A285118] p 300 N95-23781
MAX-91: Polarimetric SAR results on Montespertoli	[NASA-TM-106885] p 295 N95-23671	THIN WINGS
site p 320 N95-23940	Report to the Secretary of Defense. Unmanned aerial	Static aeroelastic characteristics of a composite wing
Statistics of multi-look AIRSAR imagery: A comparison	vehicles: No more Hunter systems should be bought until	[BTN-95-EIX95152582340] p 282 A95-73542
of theory with measurements p 320 N95-23947	problems are fixed	Unsteady ground effects on aerodynamic coefficients
AIRSAR deployment in Australia, September 1993:	[GAO/NSIAD-95-52] p 286 N95-24091	of finite wings with camber
Management and objectives p 321 N95-23948	TECHNOLOGY TRANSFER	[BTN-95-EIX95182619233] p 271 A95-76659
SYSTEM FAILURES	Technology reinvestment project's focus area:	Thin tailored composite wing for civil tiltrotor
Mechanical system reliability and risk assessment	Affordable polymer matrix composites for airframe	p 285 N95-23317
[BTN-95-EIX95142553046] p 304 A95-73452	structures	THREE DIMENSIONAL FLOW
SYSTEM IDENTIFICATION	[PB95-136032] p 324 N95-23168	Effects of spatial order of accuracy on the computation
System identification of the Large-Angle Magnetic	Research and Technology, 1994	of vortical flowfields
Suspension Test Fixture (LAMSTF) p 296 N95-23299	[NASA-TM-106764] p 262 N95-24025	[BTN-95-EIX95152577604] p 305 A95-73479
SYSTEMS ANALYSIS	TECHNOLOGY UTILIZATION	Influence of streamwise curvature on longitudinal
CASS: Design for supportability	ATE enabling technologies	vortices imbedded in turbulent boundary layers
[BTN-95-EIX95172595296] p 287 A95-75716	[BTN-95-EIX95172595294] p 287 A95-75718	[BTN-94-EIX94401378820] p 307 A95-76489
Aerodynamic design of pegasus: Concept to flight with	Technology reinvestment project's focus area:	Comparison of linear stability results with flight transition
computational fluid dynamics	Affordable polymer matrix composites for airframe	data
[BTN-95-EIX95182617463] p 298 A95-75734	structures	[BTN-95-EIX95182619097] p 283 A95-76582
SYSTEMS ENGINEERING	[PB95-136032] p 324 N95-23168	Neural network prediction of three-dimensional unsteady
Aeroelastic vehicle multivariable control synthesis with	TEMPERATE REGIONS	separated flowfields
analytical robustness evaluation	In situ observations in aircraft exhaust plumes in the	[BTN-95-EIX95182619232] p 308 A95-76658
[BTN-95-EIX95182619115] p 321 A95-76592	lower stratosphere at midiatitudes	Unsteady ground effects on aerodynamic coefficients
Inner loop flight control for the High-Speed Civil	[HTN-95-A0862] p 318 A95-76266	of finite wings with camber
Transport p 293 N95-23314	TENSILE CREEP	[BTN-95-EIX95182619233] p 271 A95-76659
Aerodynamic design and analysis of a highly loaded	Evolution of oxidation and creep damage mechanisms	Study of the droplet spray characteristics of a subsonic
	in HIPed silicon nitride materials	wind tunnel
· · · · · · · · · · · · · · · · · · ·	[DE95-001360] p 300 N95-22689	[BTN-95-EIX95182619235] p 271 A95-76661
SYSTEMS INTEGRATION Labe behind Reging's new 777	TENSILE STRENGTH	Simulation on the 3-D turbulent flow in the passages
Labs behind Boeing's new 777	Review of some results of the author's fatigue	of finocyt grain
[BTN-95-EIX95142562403] p 280 A95-73437	investigations with applications in engineering and material	[BTN-95-EIX95202638962] p 279 A95-76674
Automation technology using Geographic Information	science	
System (GIS) p 324 N95-23284	[TAE-698] p 316 N95-23662	Mach 10 computational study of a three-dimensional
Differential GPS and system integration of the Low	TEST CHAMBERS	scramjet inlet flow field
Visibility Landing and Surface Operations (LVLASO)	Design of a variable area diffuser for a 15-inch Mach	[NASA-TM-4602] p 309 N95-23015
demonstration p 280 N95-23318	6 open-jet tunnel p 297 N95-23309	Mach 10 computational study of a three-dimensional
SYSTEMS SIMULATION	TEST FACILITIES	scramjet inlet flow field
Derivation of system matrices from nonlinear dynamic	Labs behind Boeing's new 777	[NASA-TM-4602] p 310 N95-23210
simulation of jet engines	[BTN-95-EIX95142562403] p 280 A95-73437	Holographic interferometric tomography for
[BTN-95-EIX95182619139] p 288 A95-76616	NASA low-speed axial compressor for fundamental	reconstructing flow fields p 310 N95-23287
SYSTEMS STABILITY	research	Three-dimensional unsteady flow calculations in an
Dynamical instability of the aerogravity assist	[NASA-TM-4635] p 296 N95-23192	advanced gas generator turbine p 312 N95-23425
maneuver	System identification of the Large-Angle Magnetic	Phase 2: HGM air flow tests in support of HEX vane
[BTN-95-EIX95152583282] p 298 A95-73583	Suspension Test Fixture (LAMSTF) p 296 N95-23299	investigation p 312 N95-23438

THREE DIMENSIONAL MODELS	TRAJECTORIES	Wing pressure distributions from subsonic tests of a
Three-dimensional structure of a supersonic jet impinging on an inclined plate	Functional dependence of trajectory dispersion on initial condition errors	high-wing transport model in the Langley 14- by 22-Foot Subsonic Wind Tunnel
[BTN-95-EIX95152583259] p 267 A95-73560	[BTN-95-EIX95152583263] p 298 A95-73564	[NASA-TM-4583] p 272 N95-22802
Neural network prediction of three-dimensional unsteady	TRAJECTORY ANALYSIS	Handling qualities of the High Speed Civil Transport
separated flowfields	Trajectory modeling of emissions from lower stratospheric aircraft	p 294 N95-23325
BTN-95-EIX95182619232  p 308 A95-76658 THREE DIMENSIONAL MOTION	[HTN-95-41219] p 317 A95-75031	High-lift flow-physics flight experiments on a subsonic civil transport aircraft (B737-100) p 275 N95-23333
Preconditioned domain decomposition scheme for	Functional agility metrics and optimal trajectory	TRANSVERSE OSCILLATION
three-dimensional aerodynamic sensitivity analysis	analysis	Coupled FEM-BEM approach for mean flow effects on
[BTN-95-EIX95152577612] p 321 A95-73471	BTN-95-EIX95182619121   p 321 A95-76598 Analytical solution and parameter estimation of projectile	vibro-acoustic behavior of planar structures IBTN-95-EIX95152577587   p 263 A95-73495
THROATS  Design of a variable area diffuser for a 15-inch Mach	dynamics	[BTN-95-EIX95152577587] p 263 A95-73495 TROPOSPHERE
6 open-jet tunnel p 297 N95-23309	BTN-95-EIX95212645695  p 272 A95-76747	Compendium of NASA data base for the Global
THRUST CONTROL	TRAJECTORY CONTROL  Dynamical instability of the aerogravity assist	Tropospheric Experiment's Pacific Exploratory Mission
Analytical solution for controls, heats, and states of flight	maneuver	West-A (PEM West-A) INASA-TM-1091771 p 320 N95-23009
trajectories  BTN-95-EIX95152583286  p 282 A95-73587	[BTN-95-EIX95152583282] p 298 A95-73583	[NASA-TM-109177] p 320 N95-23009 TURBINE BLADES .
THUNDERSTORMS	Analytical solution for controls, heats, and states of flight trajectories	Fatigue strength of high-temperature alloys under
Thundercloud electric field modeling for the	BTN-95-EIX95152583286  p 282 A95-73587	conditions of cyclic temperature variation. Communication
ionosphere-Earth region. 1: Dependence on cloud charge distribution	Functional agility metrics and optimal trajectory	1: Experimental procedure and results  BTN-94-EIX94401363884  p 307 A95-75516
[HTN-95-41223] p 317 A95-75035	analysis [BTN-95-EIX95182619121] p 321 A95-76598	Supersonic flow and shock formation in turbine tip
Collaborative research on aircraft icing and charging	Nonlinear system guidance in the presence of	gaps p 312 N95-23429
processes in ice	transmission zero dynamics	TURBINE ENGINES
[AD-A285102] p 276 N95-23201	[NASA-TM-4661] p 309 N95-22804	Erosion of dust-filtered helicopter turbine engines. Part
FIME DEPENDENCE  Grid refinement test of time-periodic flows over bluff	TRAJECTORY OPTIMIZATION  Analytical solution for controls, heats, and states of flight	1: Basic theoretical considerations  BTN-95-EIX95182619222  p 288 A95-76648
bodies	trajectories	Life prediction of helicopter engines fitted with dust
[BTN-94-EIX94401378822] p 307 A95-76491	[BTN-95-EIX95152583286] p 282 A95-73587	filters
TIME LAG	Optimal lateral-escape maneuvers for microburst encounters during final approach	(BTN-95-EIX95182619224) p 289 A95-76650
Investigation of the effects of bandwidth and time delay on helicopter roll-axis handling qualities	[BTN-95-EIX95182619127] p 276 A95-76604	TURBINE PUMPS  CFD analysis of turbopump volutes
[HTN-95-80853] p 290 A95-75095	TRANSFER FUNCTIONS	p 312 N95-23436
TIME OF FLIGHT SPECTROMETERS	On-line, adaptive state estimator for active noise control p 322 N95-23308	Phase 2: HGM air flow tests in support of HEX vane
Time-of-flight mass spectrometer for impulse facilities [BTN-95-EIX95142553057] p 262 A95-73441	control p 322 N95-23308 TRANSIENT RESPONSE	investigation p 312 N95-23438
TIME SERIES ANALYSIS	Transient analysis of a cracked rotor passing through	TURBINES  Static pressure distribution in the inlet of a helicopter
The role of flight progress strips in en route air traffic	critical speed	turbine compressor
control: A time-series analysis	[BTN-94-EIX94401360022] p 306 A95-74702 TRANSITION FLOW	[BTN-95-EIX95152582339] p 266 A95-73541
DOT/FAA/AM-95/4  p 280 N95-23565  TOMOGRAPHY	Computation of oscillating airfoil flows with one- and	Three-dimensional unsteady flow calculations in an
Evaluation of neutron techniques for illicit substance	two-equation turbulence models	advanced gas generator turbine p 312 N95-23425 Aerodynamic design and analysis of a highly loaded
detection	[BTN-95-EIX95152577588] p 263 A95-73494 Crossflow instability control on a swept-wing: Preliminary	turbine exhaust p 312 N95-23435
DE95-002988  p 300 N95-22764	studies p 274 N95-23283	CFD analysis of turbopump volutes
FOPOGRAPHY Geoid lineations of 1000 km wavelength over the central	TRANSITION TEMPERATURE	p 312 N95-23436
Pacific Pacific	Phonon characteristics of high (T sub c) superconductors	Numerical computation of aerodynamics and heat transfer in a turbine cascade and a turn-around duct using
HTN-95-11304  p 319 A95-77009	from neutron Doppler broadening measurements [DE95-003703] p 324 N95-24076	advanced turbulence models p 313 N95-23444
AVIRIS and TIMS data processing and distribution at	TRANSONIC FLOW	Enhanced analysis and users manual for radial-inflow
the land processes distributed active archive center p 325 N95-23872	Aerodynamic shape optimization using preconditioned	turbine conceptual design code RTD [NASA-CR-195454] p 275 N95-23462
TOPOLOGY	conjugate gradient methods [BTN-95-EIX95142553033] p 263 A95-73465	[NASA-CR-195454] p 275 N95-23462 TURBOCOMPRESSORS
CFD analysis of turbopump volutes	Flow visualization studies on sidewall effects in	NASA low-speed axial compressor for fundamental
p 312 N95-23436 FORSION	two-dimensional transonic airfoil testing	research (NASA-TM-4635) p 296 N95-23192
Nonlinear angle of twist of advanced composite wing	[BTN-95-EIX95152582313] p 264 · A95-73516	[NASA-TM-4635] p 296 N95-23192 TURBOFAN ENGINES
boxes under pure torsion	Improved version of the Naval Surface Warfare Center aeroprediction code (AP93)	Lycoming to test new engine core
[BTN-95-EIX95152582323] p 281 A95-73526	[BTN-95-EIX95152583260] p 267 A95-73561	[HTN-95-41393] p 288 A95-76389
ORSIONAL VIBRATION Application of Navier-Stokes aeroelastic methods to	Turbulent transonic airfoil flow simulation using a	Derivation of system matrices from nonlinear dynamic simulation of jet engines
improve fighter wing maneuver performance	pressure-based algorithm	[BTN-95-EIX95182619139] p 288 A95-76616
[BTN-95-EIX95182619218] p 284 A95-76644	[BTN-95-EIX95182619078] p 269 A95-75763	TURBOJET ENGINE CONTROL
OXICITY  Modeling aerosol emissions from the combustion of	Scaling of incipient separation in supersonic/transonic speed laminar flows	Derivation of system matrices from nonlinear dynamic simulation of jet engines
composite materials p 301 N95-23038	[BTN-95-EIX95182619104] p 269 A95-76589	[BTN-95-EIX95182619139] p 288 A95-76616
Aircraft fires, smoke toxicity, and survival: An overview	TRANSONIC FLUTTER	TURBOPROP ENGINES
[DOT/FAA/AM-95/8] p 277 N95-24024 TRACKING (POSITION)	Limit cycle phenomena in computational transonic aeroelasticity	Artificial intelligence for turboprop engine maintenance [BTN-95-EIX95182617812] p 288 A95-75757
Solutions of generalized proportional navigation with	[BTN-95-EIX95152582317] p 264 A95-73520	Lycoming to test new engine core
maneuvering and nonmaneuvering targets	Application of transonic small disturbance theory to the	[HTN-95-41393] p 288 A95-76389
[BTN-95-EIX95202637606] p 279 A95-76683	active flexible wing model	TURBOSHAFTS Lycoming to test new engine core
Natural laminar flow wing concept for supersonic	[BTN-95-EIX95182619210] p 270 A95-76636 Rolling maneuver load alleviation using active controls	[HTN-95-41393] p 288 A95-76389
transports	[BTN-95-EIX95182619217] p 270 A95-76643	TURBULENCE
[BTN-95-EIX95182619226] p 308 A95-76652 Wing pressure distributions from subsonic tests of a	TRANSONIC WIND TUNNELS	Navier-Stokes prediction of large-amplitude delta-wing roll oscillations
high-wing transport model in the Langley 14- by 22-Foot	Performance of the 0.3-meter transonic cryogenic tunnel with air, nitrogen, and sulfur hexafluoride media under	[BTN-95-EIX95152582329] p 281 A95-73531
Subsonic Wind Tunnel	closed loop automatic control	Flow study of supersonic wing-nacelle configuration
NASA-TM-4583   p 272 N95-22802   TRAILING EDGES	[NASA-CR-195052] p 310 N95-23257	[BTN-95-EIX95152582344] p 266 A95-73546 Observations on using experimental data as boundary
Computation of the poststall behavior of a circulation	Three-dimensional Navier-Stokes analysis and redesign	conditions for computations
controlled airfoil	of an imbedded belimouth nozzle in a turbine cascade inlet section p 311 N95-23423	[BTN-95-EIX95182619103] p 321 A95-76588
[BTN-95-EIX95152582320] p 264 A95-73523	TRANSPORT AIRCRAFT	Response of a nonrotating rotor blade to lateral turbulence. Part 1: Theory
Lift enhancing tabs for airfoils  NASA-CASE-ARC-11990-1  p 286 N95-23395	Design constraints in the payload-range diagram of	BTN-95-EIX95182619228  p 284 A95-76654
RAINING DEVICES	ultrahigh capacity transport airplanes	TURBULENCE EFFECTS
Virtual reality flight control display with	[BTN-95-EIX95152582319] p 276 A95-73522 Effect of underwing frost on a transport aircraft airfoil	Effect of ambient turbulence intensity on sphere wakes
six-degree-of-freedom controller and spherical orientation overlay	at flight Reynolds number	at intermediate Reynolds numbers [BTN-95-EIX95182619101] p 308 A95-76586
[NASA-CASE-NPO-18733-1-CU] p 288 N95-22578	[BTN-95-EIX95152582334] p 276 A95-73536	TURBULENCE MODELS
Development of qualification guidelines for personal	Possible effects of CO2 increase on the high-speed civil	Two-equation turbulence model for unsteady separated
computer-based aviation training devices	transport impact on ozone	flows around airfoils [BTN-95-EIX95142553054] p 262 A95-73444
[DOT/FAA/AM-95/6] p 323 N95-23603	[HTN-95-60779] p 317 A95-75976	D 114-33-CIA3314E333341   D 20E A33-13444

### **TURBULENT BOUNDARY LAYER**

Flow structure in the wake of a wishbone vortex

nenerator |BTN-95-EIX95142553044| p 304 A95-73454 Adaptive finite element method for turbulent flow near a propelter IBTN-95-EIX951425530381 p 305 A95-73460 Laplace interaction law for the computation of viscous airfoil flow in low- and high-speed aerodynamics p 263 A95-73461 IBTN-95-EIX951425530371 Computation of oscillating airfoil flows with one- and two-equation turbulence models [BTN-95-EIX95152577588] p 263 A95-73494 Progress in high-lift aerodynamic calculations p 264 A95-73518 IBTN-95-EIX951525823151 Computation of the poststall behavior of a circulation controlled airfoil |BTN-95-EIX951525823201 p 264 A95-73523 Transport of exhaust products in the near trail of a jet ngine under atmospheric conditions p 319 A95-77334 1HTN-95-914211 Numerical computation of aerodynamics and heat transfer in a turbine cascade and a turn-around duct using advanced turbulence models p 313 N95-23444 TURBULENT BOUNDARY LAYER Flow structure in the wake of a wishbone vortex generator BTN-95-EIX95142553044 p 304 A95-73454 Effects of expansions on a supersonic boundary layer: Surface pressure measurements |BTN-95-EIX95142553036| n 263 A95-73462 Influence of streamwise curvature on longitudinal vortices imbedded in turbulent boundary layers p 307 A95-76489 [BTN-94-EIX94401378820] Review and development of base pressure and base heating correlations in supersonic flow IBTN-95-EIX952126456881 p 271 A95-76740 TURBULENT DIFFUSION Transport of exhaust products in the near trail of a let ngine under atmospheric conditions IHTN-95-914211 p 319 A95-77334 Two-equation turbulence model for unsteady separated flows around airfoils (BTN-95-EIX95142553054) p 262 A95-73444 Flow structure in the wake of a wishbone vortex generator IBTN-95-EIX95142553044 I p 304 A95-73454 Simulation of turbulent fluctuations p 304 A95-73457 IBTN-95-EIX951425530411 Adaptive finite element method for turbulent flow near a propeller [BTN-95-EIX95142553038] p 305 A95-73460 Laplace interaction law for the computation of viscous airfoil flow in low- and high-speed aerodynamics p 263 A95-73461 |BTN-95-EIX95142553037| Effects of expansions on a supersonic boundary layer: Surface pressure measurements p 263 A95-73462 IRTN-95-EIX951425530361 Computation of oscillating airfoil flows with one- and p 263 A95-73494 IRTN-95-EIX95152577588 I Mach wave emission from a high-temperature supersonic jet [BTN-95-EIX95152577586] p 264 A95-73496 Base drag prediction on missile configurations p 266 A95-73557 IRTN-95-EIX951525832561 Turbulent transonic airfoil flow simulation using a pressure-based algorithm p 269 A95-75763 IBTN-95-EIX951826190781 Simulation of transverse gas injection in turbulent supersonic air flows |BTN-95-EIX95182619080| p 269 A95-75765 Multigrid solution of compressible turbulent flow on instructured meshes using a two-equation model p 307 A95-76484 |BTN-94-EIX94401378794| Influence of streamwise curvature on longitudinal vortices imbedded in turbulent boundary layers BTN-94-EIX944013788201 p 307 A95-76489 Effect of ambient turbulence intensity on sphere wakes at intermediate Reynolds numbers p 308 A95-76586 |BTN-95-EIX95182619101| Real-time estimation of atmospheric turbulence severity from in-situ aircraft measurements IRTN-95-EIX95182619231 I p 319 A95-76657 Simulation on the 3-D turbulent flow in the passages of finocyl grain [BTN-95-EIX95202638962] p 279 A95-76674 Crossflow instability control on a swept-wing: Preliminary p 274 N95-23283 High-lift flow-physics flight experiments on a subsonic civil transport aircraft (B737-100) p 275 N95-23333 Numerical computation of aerodynamics and heat transfer in a turbine cascade and a turn-around duct using advanced turbulence models p 313 N95-23444

Convergence acceleration of implicit schemes in the presence of high aspect ratio grid cells p 313 N95-23446 TURBULENT WAKES Flow structure in the wake of a wishbone vortex generator [BTN-95-EIX95142553044] p 304 A95-73454 Adaptive finite element method for turbulent flow near a propelle p 305 A95-73460 IRTN-95-FIX951425530381 TURNING FLIGHT Efficient sensitivity analysis for rotary-wing aeromechanical problems p 264 A95-73497 IRTN-95-FIX951525775851 Functional agility metrics and optimal trajectory analysis IBTN-95-EIX95182619121 I n 321 A95-76598 Optimal lateral-escape maneuvers for microburst encounters during final approach IBTN-95-EIX951826191271 p 276 A95-76604 TVD SCHEMES Three-dimensional structure of a supersonic jet impinging on an inclined plate IBTN-95-EIX951525832591 p 267 A95-73560 TWISTED WINGS Nonlinear angle of twist of advanced composite wing boxes under pure torsion n 281 A95-73526 IRTN-95-FIX951525823231 TWISTING Application of Navier-Stokes aeroelastic methods to rove fighter wing maneuver performance IBTN-95-EIX951826192181 p 284 A95-76644 TWO DIMENSIONAL BOUNDARY LAYER Influence of streamwise curvature on longitudinal vortices imbedded in turbulent boundary layers [BTN-94-EIX94401378820] p 307 A95-76489 IBTN-94-EIX944013788201 TWO DIMENSIONAL FLOW Predicting exhaust plume boundaries with supersonic external flows [BTN-95-EIX95152583258] p 297 A95-73559 Comparison of linear stability results with flight transition IBTN-95-EIX95182619097 I p 283 A95-76582 Observations on using experimental data as boundary conditions for computations [BTN-95-EIX95182619103] p 321 A95-76588 Study of the droplet spray characteristics of a subsonic IBTN-95-EIX95182619235 I p 271 A95-76661 User's guide for ECAP2D: An Euler unsteady aerodynamic and aeroelastic analysis program for two dimensional oscillating cascades, version 1.0 [NASA-CR-189146] p 316 N95-24189 TWO DIMENSIONAL MODELS Predicting exhaust plume boundaries with supersonic IBTN-95-EIX951525832581 p 297 A95-73559 Sensitivity of two-dimensional model predictions of onse to stratospheric aircraft: An update p 318 A95-76267 IHTN-95-A08631 Observations on using experimental data as boundary conditions for computati IBTN-95-EIX951826191031 p 321 A95-76588 TWO PHASE FLOW Simulation of transverse gas injection in turbulent supersonic air flows p 269 A95-75765 [BTN-95-EIX95182619080]

### UNIVERSITIES

1994 NASA-HU American Society for Engineering Education (ASEE) Summer Faculty Fellowship Program p 325 N95-23276

### UNSTEADY AERODYNAMICS

IRTN-95-EIX951525775971

Neural network prediction of three-dimensional unsteady

IBTN-95-EIX951826192321 p 308 A95-76658 Unsteady ground effects on aerodynamic coefficients of finite wings with camber

p 271 A95-76659 IBTN-95-EIX951826192331

Flutter analysis of composite box beams [NASA-CR-197931] User's quide for ECAP2D: p 294 N95-23392 An Euler unsteady

aerodynamic and aeroelastic analysis program for two dimensional oscillating cascades, version 1.0 [NASA-CR-189146] p 316 N95-24189

**UNSTEADY FLOW** 

Two-equation turbulence model for unsteady separated flows around airfoils

IBTN-95-EIX951425530541 p 262 A95-73444 Eigenanalysis of unsteady flows about airfoils, cascades,

p 305 A95-73486

Computation of oscillating airfoil flows with one- and two-equation turbulence models

p 263 A95-73494 IBTN-95-EIX951525775881 Limit cycle phenomena in computational transonic aeroelasticity

p 264 A95-73520 BTN-95-EIX951525823171 Moving wall effect in relation to other dynamic stall flow mechanisms n 265 A95-73527

BTN-95-EIX95152582324 | Numerical study of sound generation due to a spinning vortex pair p 307 A95-75760 BTN-95-EIX95182619075 |

Viscous-inviscid interaction method for unsteady low-speed airfoil flows p 269 A95-75778

[BTN-95-EIX95182619093] Stability derivatives of a flapped plate in unsteady ground offect

p 270 A95-76651 [BTN-95-EIX95182619225] Response of a nonrotating rotor blade to lateral turbulence. Part 1: Theory

RTN-95.FIX951826192281 n 284 A95-76654 Neural network prediction of three-dimensional unsteady separated flowfields

|BTN-95-EIX951826192321 p 308 A95-76658 Unsteady ground effects on aerodynamic coefficients of finite wings with camber

IBTN-95-FIX951826192331 p 271 A95-76659 A CFD study of complex missile and store configurations in relative motion

INASA-CR-1979121 p 285 N95-22949 interferometric Holographic tomography p 310 N95-23287 reconstructing flow fields Three-dimensional unsteady flow calculations in an advanced gas generator turbine p 312 N95-23425 Aerodynamic design and analysis of a highly loaded

p 312 N95-23435 turbine exhaust A time-accurate finite volume method valid at all flow p 314 N95-23447 velocities

### UPPER ATMOSPHERE

Particle kinetic simulation of high altitude hypervelocity

INASA-CR-197383] p 309 N95-22481

UPWIND SCHEMES (MATHEMATICS)

Application of the multigrid solution technique to hypersonic entry vehicles IRTN-95-EIX951525832541 p 306 A95-73555

USER MANUALS (COMPUTER PROGRAMS)

Enhanced analysis and users manual for radial-inflow

turbine conceptual design code RTD p 275 N95-23462 INASA-CR-1954541 User's guide for ECAP2D: An Euler unsteady aerodynamic and aeroelastic analysis program for two

dimensional oscillating cascades, version 1.0 p 316 N95-24189 INASA-CR-1891461

USER REQUIREMENTS

Real-time navigation using the global positioning n 279 A95-75714 I RTN-95-EIX95172595298 I

## V-22 AIRCRAFT

VALVES

Thin tailored composite wing for civil tiltrotor p 285 N95-23317

Measurement of moisture and total hydrocarbon

# contributions by valves used in clean room gas-delivery

p 295 A95-74629 IBTN-94-EIX94381359041 I

### VANES Phase 2: HGM air flow tests in support of HEX vane

investigation p 312 N95-23438 VAPORS NTS-spill test facility wind tunnel exhaust plume

### characterization IDE95-0036301 p 297 N95-24019

VARIATIONS

### Simulation of turbulent fluctuations BTN-95-EIX95142553041

p 304 A95-73457 A comparison of some aerodynamic resistance methods

using measurements over cotton and grass from the 1991 California ozone deposition experiment IHTN-95-112951 p 319 A95-77000

## VELOCITY DISTRIBUTION

Determination of wall boundary high-speed-ratio direct simulation conditions for Monte Carlo calculations [BTN-95-EIX95182617457] p 267 A95-75728

### **VELOCITY MEASUREMENT**

Impeller flow field characterization with a laser two-focus velocimeter p 313 N95-23440

Flow visualization studies of VTOL aircraft models during Hover in ground effect [NASA-TM-108860] p 272 N95-22666 VERTICAL TAKEOFF Flow visualization studies of VTOL aircraft models during Hover in ground effect [NASA-TM-108860] p 272 N95-22666 VERTICAL TAKEOFF AIRCRAFT Cypher moves toward autonomous flight [HTN-95-41394] p 283 A95-76390 Flow visualization studies of VTOL aircraft models during Hover in ground effect [NASA-TM-108860] p 272 N95-22666 VIGNAS-TM-108860] p 273 A95-76699 Summary of an active flexible wing program [BTN-95-EIX95182619213] p 283 A95-76638 Flutter suppression control law design and testing for the active flexible wing ind-tunnel model [BTN-95-EIX95182619212] p 322 A95-76640 Design and multiflunction tests of a frequency domain-based active flutter suppression system [BTN-95-EIX95182619212] p 292 A95-76641 Design and multiflunction tests of a frequency domain-based active flutter suppression system [BTN-95-EIX95182619215] p 292 A95-76642 Active control of panel vibrations induced by a boundary layer flow [NASA-CR-197867] p 273 N95-23182 VIGNAS-CR-197867] p 273 N95-23182 VIGNAS-CR-197867] p 274 A95-76644 VIKING LANDER SPACECRAFT Fourth-generation Mars vehicle concepts [BTN-95-EIX95152583267] p 288 A95-76644 VIKING LANDER SPACECRAFT Fourth-generation Mars vehicle concepts [BTN-95-EIX95152583267] p 288 N95-22578 VIRTUAL REALITY Virtual reality flight control display with six-degree-of-freedom controller and spherical orientation overlay [NASA-CR-197439] p 279 A95-73664 VIKING LANDER SPACECRAFT Fourth-generation Mars vehicle concepts [BTN-95-EIX95152583257] p 289 A95-73664 VIKING LANDER SPACECRAFT PO-18733-1-CU p 288 N95-22578 VIRTUAL REALITY Virtual reality flight control display with six-degree-of-freedom controller and spherical orientation overlay [NASA-CR-197439] p 266 A95-73568 VIRTUAL REALITY VIRTUAL REALITY P 280 A95		
pozone response to stratospheric aircraft: An update   HTN-95-A0863  p 318 A95-76267   VERTICAL LANDING   Flow visualization studies of VTOL aircraft models during Hover in ground effect   NASA-TM-108860  p 272 N95-22666   VERTICAL TAKEOFF   Flow visualization studies of VTOL aircraft models during Hover in ground effect   NASA-TM-108860  p 272 N95-22666   VERTICAL TAKEOFF AIRCRAFT   Cypher moves toward autonomous flight   HTN-95-41394  p 283 A95-76390   Flow visualization studies of VTOL aircraft models during Hover in ground effect   NASA-TM-108860  p 272 N95-22666   VIBRATION DAMPING   P 274 N95-22666   VIBRATION DAMPING   P 275 N95-22666   VIBRATION DAMPING   P 276 N95-22666   VIBRATION DAMPING   P 277 N95-22666   VIBRATION DAMPING   P 278 A95-76639   Summary of an active flexible wing program   BTN-95-EIX951826192012  p 282 A95-76638   Flutter suppression control law design and testing for the active flexible wing wind-tunnel model   BTN-95-EIX95182619212  p 322 A95-76640   Design and multifunction tests of a frequency domain-based active flutter suppression system   BTN-95-EIX95182619211   P 292 A95-76641   D 293 A95-76641   D 293 A95-76641   P 294 A95-76642   P 295 A95-76641   P 296 A95-76644   P 296 A95-76644   P 296 A95-76644   P 297 A95-76644   P 297 A95-73568   P 297 A95		4-4 (5-654
HTN-95-0863	DZONE response to stratospheric airc	nodel predictions of
FILTER LANDING Flow visualization studies of VTOL aircraft models during Hover in ground effect (NASA-TM-108860) p 272 N95-22666 VERTICAL TAKEOFF Flow visualization studies of VTOL aircraft models during Hover in ground effect (NASA-TM-108860) p 272 N95-22666 VERTICAL TAKEOFF AIRCRAFT Cypher moves toward autonomous flight (NASA-TM-108860) p 283 A95-76390 Flow visualization studies of VTOL aircraft models during Hover in ground effect (NASA-TM-108860) p 283 A95-76390 Flow visualization studies of VTOL aircraft models during Hover in ground effect (NASA-TM-108860) p 272 N95-22666 VIBRATION DAMPING Multirate flutter suppression system design for a model wing (MBRATION DAMPING) p 283 A95-76639 Summary of an active flexible wing program (BTN-95-EIX95182619212) p 292 A95-76638 Flutter suppression control law design and testing for the active flexible wing wind-tunnel model (BTN-95-EIX95182619212) p 292 A95-76640 Design and multifunction tests of a frequency domain-based active flutter suppression system (BTN-95-EIX95182619215) p 292 A95-76641 Flutter suppression for the active flexible wing: A classical design (BTN-95-EIX95182619216) p 292 A95-76642 Network (MSA-CR-197867) p 273 N95-23182 VIBRATION MODE Application of Navier-Stokes aeroelastic methods to improve tighter wing maneuver performance (BTN-95-EIX95182619218) p 284 A95-76644 VIKING LANDER SPACECRAFT Fourth-generation Mars vehicle concepts (BTN-95-EIX95182619218) p 288 N95-22578 VIBRATION MODE Application of Navier-Stokes aeroelastic methods to improve tighter wing maneuver performance (BTN-95-EIX95182619218) p 284 A95-76644 VIKING LANDER SPACECRAFT Fourth-generation Mars vehicle concepts (BTN-95-EIX95182619218) p 289 A95-73568 (BTN-95-EIX95182619218) p 289 A95-73558 (BTN-95-EIX95182619234) p 308 A95-73556 (BTN-95-EIX95182619234) p 308 A95-73556 (BTN-95-EIX95182		
Hover in ground effect   NASA-TM-108860   p 272 N95-22666   VERTICAL TAKEOFF   Flow visualization studies of VTOL aircraft models during Hover in ground effect   NASA-TM-108860   p 272 N95-22666   VERTICAL TAKEOFF AIRCRAFT   Cypher moves toward autonomous flight   HTN-95-41394   p 283 A95-76390   Flow visualization studies of VTOL aircraft models during Hover in ground effect   NASA-TM-108860   p 272 N95-22666   VERTICAL TAKEOFF AIRCRAFT   P 272 N95-22666   VIRPATION DAMPING   p 272 N95-22666   VIRPATION DAMPING   p 272 N95-22666  VIRPATION DAMPING   Multirate flutter suppression system design for a model wing   STM-95-EIX95182619132   p 292 A95-76609   Summary of an active flexible wing program   BTN-95-EIX95182619212   p 322 A95-76638   Flutter suppression control law design and testing for the active flexible wing ind-tunnel model   BTN-95-EIX95182619212   p 322 A95-76641   D 292 A95-76641   Flutter suppression for the active flexible wing: A classical design   BTN-95-EIX95182619215   p 292 A95-76642   Active control of panel vibrations induced by a boundary layer flow   NASA-CR-197867   p 273 N95-23182   VIRPATION MODE   Application of Navier-Stokes aeroelastic methods to improve lighter wing maneuver performance   BTN-95-EIX95182619218   p 284 A95-76644   VIKING LANDER SPACECRAFT   Fourth-generation Mars vehicle concepts   BTN-95-EIX95182583267   p 298 A95-73568   VIRPATION MODE   Application of Navier-Stokes aeroelastic methods to improve lighter wing maneuver performance   BTN-95-EIX95182583267   p 298 A95-73568   VIRPATION MODE   Application of Navier-Stokes aeroelastic methods to improve lighter wing maneuver performance   BTN-95-EIX95182583257   p 298 A95-73568   VIRPATION MODE   Application of Navier-Stokes aeroelastic methods to improve lighter wing method of the model wing   p 298 A95-73568   P 298 A95-73568   VIRPATION MODE   Application of Navier-Stokes a	VERTICAL LANDING	•
NASA-TM-108860   p 272 N95-22666   VERTICAL TAKEOFF   Flow visualization studies of VTOL aircraft models during Hover in ground effect   NASA-TM-108860   p 272 N95-22666   VERTICAL TAKEOFF AIRCRAFT   Cypher moves toward autonomous flight   HTN-95-41394   p 283 A95-76390   Flow visualization studies of VTOL aircraft models during Hover in ground effect   NASA-TM-108860   p 272 N95-22666   VIBRATION DAMPING   p 272 N95-22666   VIBRATION DAMPING   p 273 N95-22666   VIBRATION DAMPING   p 292 A95-76609   Summary of an active flexible wing program   BTN-95-EIX95182619132   p 292 A95-76635   Multiple-function digital controller system for active flexible using wind-tunnel model   BTN-95-EIX95182619212   p 322 A95-76636   Flutter suppression control law design and testing to the active flexible wing   BTN-95-EIX95182619212   p 322 A95-76640   Design and multifunction tests of a frequency domain-based active flutter suppression system   BTN-95-EIX95182619215   p 292 A95-76641   Flutter suppression for the active flexible wing: A classical design and multifunction tests of a frequency domain-based active flutter suppression system   BTN-95-EIX95182619215   p 292 A95-76641   Flutter suppression for the active flexible wing: A classical design   BTN-95-EIX95182619216   p 292 A95-76642   Active control of panel vibrations induced by a boundary layer flow   NASA-CR-197867   p 273 N95-23182   VIBRATION MODE   P 274 N95-23182   VIBRATION MODE   P 275 N95-23182   VIBRATION MODE   P 276 A95-76644   VIKING LANDER SPACECRAFT   p 284 A95-76644   VIKING LANDER SPACECRAFT   P 284 A95-76644   VIKING LANDER SPACECRAFT   P 285 N95-22578   VIBRATION ACCASE-NPO-18733-1-CU   p 288 N95-22578   VISCOSITY   VITUAL REALITY   VITUAL reality flight control display with six-degree-ol-freedom controller and spherical orientation overlay   NASA-CR-197439   p 301 N95-23179   VISCOSITY   D 266 A95-73556   VISCOSITY   D 266 A95-73556   VISCOSITY   D 267 A95-73660   An assessment of viscous shock-layer solutions for high-altitude flows   BTN-95-EIX95		ircraft models during
VERTICAL TAKEOFF Flow visualization studies of VTOL aircraft models during Hover in ground effect [NASA-TM-108860] p 272 N95-22666 VERTICAL TAKEOFF AIRCRAFT Cypher moves toward autonomous flight [HTN-95-41394] p 283 A95-76390 Flow visualization studies of VTOL aircraft models during Hover in ground effect [NASA-TM-108860] p 272 N95-22666 VIBRATION DAMPING Multrate flutter suppression system design for a model wing [BTN-95-EIX95182619132] p 292 A95-76609 Summary of an active flexible wing program [BTN-95-EIX95182619209] p 283 A95-76635 Multiple-function digital controller system for active flexible wing wind-tunnel model [BTN-95-EIX95182619212] p 322 A95-76638 Flutter suppression control law design and testing for the active flexible wing [BTN-95-EIX95182619214] p 292 A95-76640 Design and multifunction tests of a frequency domain-based active flutter suppression system [BTN-95-EIX95182619215] p 292 A95-76641 Flutter suppression for the active flexible wing: A classical design [BTN-95-EIX95182619216] p 292 A95-76641 Flutter suppression for the active flexible wing: A classical design [BTN-95-EIX95182619216] p 292 A95-76642 Active control of panel vibrations induced by a boundary layer flow [NASA-CR-197867] p 273 N95-23182 VIRINATION MODE Application of Navier-Stokes aeroetastic methods to improve tighter wing maneuver performance [BTN-95-EIX95182619218] p 284 A95-76644 VIKING LANDER SPACECRAFT Fourth-generation Mars vehicle concepts [BTN-95-EIX95182583267] p 298 A95-73568 VIRITUAL REALITY Virtual reality flight control display with six-degree-ol-freedom controller and spherical orientation overlay [NASA-CASE-NPO-18733-1-CU] p 288 N95-22578 VISCOSITY Development and verification of a resin film infusion/resin transfer molding simulation model for abrication of advanced textile composites [NASA-CR-197439] p 301 N95-23179 VISCOSITY Development and verification of a resin film infusion/resin transfer molding simulation model for unsteady [BTN-95-EIX95152583255] p 306 A95-73556 Viscous-inviscid interaction method for		
Flow visualization studies of VTOL aircraft models during Hover in ground effect [NASA-TM-108860] p 272 N95-22666 VERTICAL TAKEOFF AIRCRAFT Cypher moves toward autonomous flight [HTN-95-41394] p 283 A95-76390 Flow visualization studies of VTOL aircraft models during Hover in ground effect [NASA-TM-108860] p 272 N95-22666 VIBRATION DAMPING Multrate flutter suppression system design for a model wing [BTN-95-EIX95182619132] p 292 A95-76609 Summary of an active flexible wing program [BTN-95-EIX95182619209] p 283 A95-76635 Multiple-function digital controller system for active flexible wing wind-tunnel model [BTN-95-EIX95182619212] p 322 A95-76635 Multiple-function digital controller system for active flexible wing wind-tunnel model [BTN-95-EIX95182619212] p 292 A95-76641 Flutter suppression control law design and testing to the active flexible wing [BTN-95-EIX95182619212] p 292 A95-76641 Platter suppression for the active flexible wing: A classical design and multifunction tests of a frequency domain-based active flutter suppression system [BTN-95-EIX95182619215] p 292 A95-76641 Flutter suppression for the active flexible wing: A classical design [BTN-95-EIX95182619216] p 292 A95-76642 Active control of panel vibrations induced by a boundary layer flow [NASA-CR-197867] p 273 N95-23182 VIBRATION MODE Application of Navier-Stokes aeroelastic methods to improve lighter wing maneuver performance [BTN-95-EIX95182619218] p 284 A95-76644 VIKING LANDER SPACECRAFT Fourth-generation Mars vehicle concepts BTN-95-EIX95182619218] p 284 A95-76644 VIKING LANDER SPACECRAFT Fourth-generation Mars vehicle concepts BTN-95-EIX95192583267] p 288 N95-22578 ISS-18259192 p 286 A95-73568 VIRTUAL reality flight control display with six-degree-ol-freedom controller and spherical orientation overlay [NASA-CA-SE-NPO-187331-CU] p 286 N95-2379 P 286 A95-73568 VIRTUAL REALITY Virtual reality flight control display with six-degree-ol-freedom controller and spherical orientation overlay p 265 A95-73556 Viscous-invision interaction method for unstea		p 272 N95-22666
Hover in ground effect   NASA-TM-108860    p 272 N95-22666   VERTICAL TAKEOFF AIRCRAFT   Cypher moves toward autonomous flight   HTN-95-41394    p 283 A95-76390   Flow visualization studies of VTOL aircraft models during   Hover in ground effect   NASA-TM-108860    p 272 N95-22666   VIBRATION DAMPING   Multirate flutter suppression system design for a model wing   BTN-95-EIX95182619132    p 292 A95-76609   Summary of an active flexible wing program   BTN-95-EIX95182619120    p 283 A95-76639   Multiple-function digital controller system for active flexible wing wind-funnel model   BTN-95-EIX95182619212    p 322 A95-76638   Multiple-function digital controller system for active flexible wing wind-funnel model   BTN-95-EIX95182619212    p 322 A95-76638   Flutter suppression control law design and testing for the active flexible wing   BTN-95-EIX95182619214    p 292 A95-76640   Design and multifunction tests of a frequency domain-based active flutter suppression system   BTN-95-EIX95182619215    p 292 A95-76641   Flutter suppression for the active flexible wing: A classical design   BTN-95-EIX95182619216    p 292 A95-76642   Active control of panel vibrations induced by a boundary layer flow   NASA-CR-197867    p 273 N95-23182   VIBRATION MODE   Application of Navier-Stokes aeroelastic methods to improve tighter wing maneuver performance   BTN-95-EIX95182619218    p 284 A95-76644   VIKING LANDER SPACECRAFT   Fourth-generation Mars vehicle concepts   BTN-95-EIX951826192191    p 288 N95-73568   VIBRATION MODE   Application of Navier-Stokes aeroelastic methods to improve tighter wing maneuver performance   BTN-95-EIX95182619271    p 298 A95-73568   VIBRATION MODE   Application of valver-Stokes aeroelastic methods to improve tighter wing-time and vehicle concepts   BTN-95-EIX95182619271    p 280 A95-73568   VIBRATION MODE   P 280 A95-73568   P 280 A95-73568 A95-73568   P 280 A95-73568 A95-73568   P 280 A95-73569 A95-73578   D 280 A95-73569 A95-73569 A95-73569 A95-73569 A95-73569   P 280 A95-73551 A96-90-90-90-90-90-90-		inamata mandala di mina
NASA-TM-108860  p 272 N95-22666   VERTICAL TAKEOFF AIRCRAFT   Cypher moves toward autonomous flight   HTN-95-41394  p 283 A95-76390   Flow visualization studies of VTOL aircraft models during Hover in ground effect   NASA-TM-108860  p 272 N95-22666   VIBRATION DAMPING   Multirate flutter suppression system design for a model wing   BTN-95-EIX95182619132  p 292 A95-76639   Summary of an active flexible wing program   BTN-95-EIX95182619209  p 283 A95-76635   Multiple-function digital controller system for active flexible wing wind-tunnel model   BTN-95-EIX95182619209  p 283 A95-76635   Flutter suppression control law design and testing for the active flexible wing   BTN-95-EIX95182619212  p 322 A95-76638   Flutter suppression control law design and testing for the active flexible wing   BTN-95-EIX95182619214  p 292 A95-76640   Design and multifunction tests of a frequency domain-based active flutter suppression system   BTN-95-EIX95182619215  p 292 A95-76642   Active control of panel vibrations induced by a boundary layer flow   NASA-CR-197867  p 273 N95-23182   VIBRATION MODE   Application of Navier-Stokes aeroelastic methods to improve lighter wing maneuver performance   BTN-95-EIX95182619218  p 284 A95-76644   VIKING LANDER SPACECRAFT   Fourth-generation Mars vehicle concepts   BTN-95-EIX95182619218  p 298 A95-73568   VIKING LANDER SPACECRAFT   Fourth-generation Mars vehicle concepts   BTN-95-EIX95182530267  p 298 A95-73568   VIKING LANDER SPACECRAFT   Fourth-generation Mars vehicle concepts   BTN-95-EIX95182530257  p 298 A95-73568   VIKING LANDER SPACECRAFT   Fourth-generation Mars vehicle concepts   BTN-95-EIX95182530257  p 298 A95-73568   VIKING LANDER SPACECRAFT   Fourth-generation Mars vehicle concepts   BTN-95-EIX95182530257  p 298 A95-73568   VIKING LANDER SPACECRAFT   Fourth-generation Mars vehicle concepts   BTN-95-EIX95182530257  p 298 A95-73568   VIKING LANDER SPACECRAFT   Fourth-generation Mars vehicle concepts   BTN-95-EIX95182530257  p 298 A95-73568   VIKING LANDER SPACECRAFT   Fourth-generatio		ircran models during
Cypher moves toward autonomous flight   HTN-95-41394		p 272 N95-22666
HTN-95-41394   p 283 A95-76390   Flow visualization studies of VTOL aircraft models during Hover in ground effect [NASA-TM-108860]   p 272 N95-22666   VIBRATION DAMPING   Multirate flutter suppression system design for a model wing [BTN-95-EIX95182619129]   p 292 A95-76609   Summary of an active flexible wing program [BTN-95-EIX95182619209]   p 283 A95-76638   Multiple-function digital controller system for active flexible wing wind-tunnel model [BTN-95-EIX95182619212]   p 322 A95-76638   Flutter suppression control law design and testing for the active flexible wing [BTN-95-EIX95182619212]   p 292 A95-76640   Design and multifunction tests of a frequency domain-based active flutter suppression system [BTN-95-EIX95182619215]   p 292 A95-76641   Flutter suppression for the active flexible wing: A classical design [BTN-95-EIX95182619216]   p 292 A95-76642   Active control of panel vibrations induced by a boundary layer flow [NASA-CR-197867]   p 273 N95-23182   VIBRATION MODE   Application of Navier-Stokes aeroelastic methods to improve fighter wing maneuver performance [BTN-95-EIX95182619218]   p 284 A95-76644   VIBRATION MODE   Application of Navier-Stokes aeroelastic methods to improve fighter wing maneuver performance [BTN-95-EIX95182619218]   p 284 A95-76644   VIBRATION MODE   Application of Navier-Stokes aeroelastic methods to improve fighter wing maneuver performance [BTN-95-EIX95152583267]   p 298 A95-73568   VIBRATION MODE   Application of Navier-Stokes aeroelastic methods to improve fighter wing maneuver performance [BTN-95-EIX95152583267]   p 298 A95-73568   VIBRATION MODE   Application of Marier Performance   BTN-95-EIX95152583267]   p 298 A95-73568   VIBRATION MODE   Application of Marier Performance   BTN-95-EIX95152583251]   p 266 A95-73568   VIBRATION MODE   Application of Marier Performance   BTN-95-EIX95152583251]   p 266 A95-73568   VIBRATION MODE   Application of Marier Performance   BTN-95-EIX95152583255]   p 306 A95-73568   VIBRATION MODE   Application of Marier Performance   BTN-95-EIX9518	VERTICAL TAKEOFF AIRCRAFT	
Flow visualization studies of VTOL aircraft models during Hover in ground effect [NASA-TM-108860] p 272 N95-22666 VIBRATION DAMPING  Multrate flutter suppression system design for a model wing [BTN-95-EIX95182619132] p 292 A95-76609 Summary of an active flexible wing program [BTN-95-EIX95182619209] p 283 A95-76635 Multiple-function digital controller system for active flexible wing wind-tunnel model [BTN-95-EIX95182619212] p 322 A95-76638 Flutter suppression control law design and testing for the active flexible wing [BTN-95-EIX95182619212] p 322 A95-76640 Design and multifunction tests of a frequency domain-based active flutter suppression system [BTN-95-EIX95182619215] p 292 A95-76641 Flutter suppression for the active flexible wing: A classical design [BTN-95-EIX95182619216] p 292 A95-76642 Active control of panel vibrations induced by a boundary layer flow [NASA-CR-197867] p 273 N95-23182 VIBRATION MODE Application of Navier-Stokes aeroelastic methods to improve tighter wing maneuver performance [BTN-95-EIX95182619218] p 284 A95-76644 VIKING LANDER SPACECRAFT Fourth-generation Mars vehicle concepts [BTN-95-EIX95182583267] p 298 A95-73568 VIBRATION Application of Navier-Stokes aeroelastic methods to improve tighter wing maneuver performance [BTN-95-EIX95152583267] p 288 A95-73568 VIRTUAL REALITY Virtual reality flight control display with six-degree-of-freedom controller and spherical orientation overlay [NASA-CASE-NPO-18733-1-CU] p 288 N95-22578 VISCOUSTTY  Development and verification of a resin film infusion/resin transfer molding simulation model for fabrication of advanced textile composites [NASA-CR-197439] p 301 N95-23179 VISCOUS FLOW  Laplace interaction law for the computation of viscous airfoil flow in low- and high-speed aerodynamics [BTN-95-EIX95152583255] p 306 A95-73560 A95-73560 A95-73560 P 308-875758 Viscous-inviscid interaction method for unsteady low-speed airfoil flows [BTN-95-EIX95152619031] p 268 A95-73560 A95-73560 P 308-73556 Viscous-inviscid interaction method for unsteady low-speed a		
Hover in ground effect [NASA-TM-108860] p 272 N95-22666 VIBRATION DAMPING  Multrate flutter suppression system design for a model wing [BTN-95-EIX95182619132] p 292 A95-76609 Summary of an active flexible wing program [BTN-95-EIX95182619209] p 283 A95-76635 Multiple-function digital controller system for active flexible wing wind-tunnel model [BTN-95-EIX95182619212] p 322 A95-76638 Flutter suppression control law design and testing for the active flexible wing [BTN-95-EIX95182619214] p 292 A95-76640 Design and multifunction tests of a frequency domain-based active flutter suppression system [BTN-95-EIX95182619215] p 292 A95-76640 Flutter suppression for the active flexible wing: A classical design [BTN-95-EIX95182619216] p 292 A95-76642 Active control of panel vibrations induced by a boundary layer flow [ISTN-95-EIX95182619216] p 292 A95-76642 Active control of panel vibrations induced by a boundary layer flow [ISTN-95-EIX95182619216] p 294 A95-76644 VIBRATION MODE  Application of Navier-Stokes aeroetastic methods to improve fighter wing maneuver performance [BTN-95-EIX95182619218] p 284 A95-7368 VIBRATION MODE  Application of Navier-Stokes aeroetastic methods to improve fighter wing maneuver performance [BTN-95-EIX95182619218] p 284 A95-7368 VIBRATION MODE  Application of Navier-Stokes aeroetastic methods to improve fighter wing maneuver performance [BTN-95-EIX95182619218] p 288 A95-7368 VIBRATION MODE  Application of Navier-Stokes aeroetastic methods to improve fighter wing maneuver performance [BTN-95-EIX95182619218] p 288 A95-7368 VIBRATION MODE  Tyrical reality flight control display with six-degree-of-freedom controller and spherical orientation overlay  Development and verification of a resin film infusion/resin transfer molding simulation model for fabrication of advanced textile composites [BTN-95-EIX95142553037] p 268 A95-7356 VIBROUS FLOW  Laplace interaction law for the computation of viscous airfoil flow in low- and high-speed aerodynamics [BTN-95-EIX95162619073] p 268 A95-73556 VIBROUS-EIX95162619		
NASA-TM-10860  p 272 N95-22666   VIBRATION DAMPING   Multrate flutter suppression system design for a model wing   BTN-95-EIX95182619132  p 292 A95-76609   Summary of an active flexible wing program   BTN-95-EIX95182619209  p 283 A95-76635   Multiple-function digital controller system for active flexible wing wind-tunnel model   BTN-95-EIX95182619212  p 322 A95-76638   Flutter suppression control law design and testing for the active flexible wing   BTN-95-EIX95182619212  p 322 A95-76640   Design and multifunction tests of a frequency domain-based active flutter suppression system   BTN-95-EIX95182619215  p 292 A95-76641   Flutter suppression for the active flexible wing: A classical design   BTN-95-EIX95182619215  p 292 A95-76641   Active control of panel vibrations induced by a boundary layer flow   NASA-CR-197867  p 273 N95-23182   VIBRATION MODE   Application of Navier-Stokes aeroelastic methods to improve fighter wing maneuver performance   BTN-95-EIX95182619218  p 284 A95-76644   VIKING LANDER SPACECRAFT   Fourth-generation Mars vehicle concepts   BTN-95-EIX9518258267  p 298 A95-73568   VIRTUAL REALITY   Virtual reality flight control display with six-degree-of-freedom controller and spherical orientation overlay   NASA-CASE-NPO-18733-1-CU  p 288 N95-22578   VISCOSITY   Development and verification of a resin film infusion/resin transfer molding simulation model for fabrication of advanced textile composites   NASA-CR-197439  p 301 N95-23179   N95-23179   N95-23179   N95-23185   N95-0485182583251  p 266 A95-73556   N95-04851825932551  p 268 A95-73568   BTN-95-EIX951825832551  p 269 A95-73578   N95-23185   N95-04851825932571   p 269 A95-73568   N95-04851825932571   p 269 A95-73556   N95-04851825932571   p 269 A95-73556   N95-04851825932571   p 269 A95-73578   N95-04851825932571   p 269 A95-73556   N95-04851825932	Flow visualization studies of VTOL a	ircraft models during
Multrate flutter suppression system design for a model wing    BTN-95-EIX95182619132  p 292 A95-76609   Summary of an active flexible wing program     BTN-95-EIX95182619209  p 283 A95-76635   Multiple-function digital controller system for active flexible wing wind-tunnel model     BTN-95-EIX95182619212  p 322 A95-76638     Flutter suppression control law design and testing for the active flexible wing     BTN-95-EIX95182619214  p 292 A95-76640     Design and multifunction tests of a frequency domain-based active flutter suppression system     BTN-95-EIX95182619215  p 292 A95-76641     Flutter suppression for the active flexible wing: A classical design     BTN-95-EIX95182619216  p 292 A95-76642     Active control of panel vibrations induced by a boundary layer flow     NASA-CR-197867  p 273 N95-23182     VIBRATION MODE     Application of Navier-Stokes aeroelastic methods to improve fighter wing maneuver performance     BTN-95-EIX95182619218  p 284 A95-76644     VIKING LANDER SPACECRAFT     Fourth-generation Mars vehicle concepts     BTN-95-EIX95182619218  p 284 A95-73568     WIRTUAL REALITY     Virtual reality flight control display with six-degree-of-freedom controller and spherical orientation overlay     NASA-CASE-NPO-18733-1-CU  p 288 N95-22578     VISCOSITY     Development and verification of a resin film infusion/resin transfer molding simulation model for fabrication of advanced textile composites     NASA-CR-197439  p 301 N95-23179     VISCOUS FLOW     Laplace interaction law for the computation of viscous airfoil flow in low- and high-speed aerodynamics     BTN-95-EIX95152583255  p 306 A95-73566     APS-73566     APS-73567     Aerodynamic characteristics of a hypersonic viscous optimized waverider at high allitudes     BTN-95-EIX95152583255  p 306 A95-73556     Aerodynamic characteristics of a hypersonic viscous optimized waverider at high allitudes     BTN-95-EIX95152583255  p 308 A95-73566     An assessment of viscous shock-layer solutions for high-allitude flows     BTN-95-EIX95162619093  p 269 A95		n 272 NGS 22666
Multirate flutter suppression system design for a model wing [BTN-95-EIX95182619132] p 292 A95-76609 Summary of an active flexible wing program [BTN-95-EIX95182619209] p 283 A95-76635 Multiple-function digital controller system for active flexible wing wind-tunnel model [BTN-95-EIX95182619212] p 322 A95-76638 Flutter suppression control law design and testing for the active flexible wing [BTN-95-EIX95182619214] p 292 A95-76640 Design and multifunction tests of a frequency domain-based active flutter suppression system [BTN-95-EIX95182619215] p 292 A95-76641 Flutter suppression for the active flexible wing: A classical design [BTN-95-EIX95182619215] p 292 A95-76642 Active control of panel vibrations induced by a boundary layer flow [NASA-CR-197867] p 273 N95-23182 VIBRATION MODE Application of Navier-Stokes aeroelastic methods to improve fighter wing maneuver performance [BTN-95-EIX95182619218] p 284 A95-76644 VIKING LANDER SPACECRAFT Fourth-generation Mars vehicle concepts [BTN-95-EIX95182583267] p 298 A95-73568 VIBTUAL REALITY Virtual reality flight control display with six-degree-of-freedom controller and spherical orientation overlay [NASA-CASE-NPO-18733-1-CU] p 288 N95-22578 VISCOSITY Development and verification of a resin film infusion/resin transfer molding simulation model for fabrication of advanced textile composites [NASA-CR-197439] p 301 N95-23179 VISCOUS FLOW Laplace interaction law for the computation of viscous airfoil flow in low- and high-speed aerodynamics [BTN-95-EIX95182583255] p 306 A95-7356 (PTN-95-EIX95182619073] p 263 A95-73660 An assessment of viscous shock-layer solutions for ingh-altitude flows [BTN-95-EIX95182619073] p 268 A95-7356 (PTSUAL SIGNALS Cueing light configuration for aircraft navigation (NASA-CR-4650) p 273 N95-23185 (PTSUAL SIGNALS Cueing light configuration for aircraft navigation (NASA-CR-4650) p 273 N95-23185 (PTSUAL SIGNALS Cueing light configuration for aircraft navigation (NASA-CR-4650) p 273 N95-23185 (PTSUAL SIGNALS Cueing light configuration for aircraft navigati	•	p 272 1455-22000
BTN-95-EIX95182619132   p 292 A95-76609   Summary of an active flexible wing program   BTN-95-EIX95182619209   p 283 A95-76635   Multiple-function digital controller system for active flexible wing wind-tunnel model   BTN-95-EIX95182619212   p 322 A95-76638   Flutter suppression control law design and testing for the active flexible wing   BTN-95-EIX95182619214   p 292 A95-76640   Design and multifunction tests of a frequency domain-based active flutter suppression system   BTN-95-EIX95182619215   p 292 A95-76641   Flutter suppression for the active flexible wing: A classical design   BTN-95-EIX95182619215   p 292 A95-76642   Active control of panel vibrations induced by a boundary layer flow   INASA-CR-197867   p 273 N95-23182   VIBRATION MODE   Application of Navier-Stokes aeroelastic methods to improve fighter wing maneuver performance   BTN-95-EIX95182619218   p 284 A95-76644   VIRING LANDER SPACECRAFT   Fourth-generation Mars vehicle concepts   BTN-95-EIX95182589367   p 298 A95-73568   VIRTUAL REALITY   Virtual reality flight control display with six-degree-of-freedom controller and spherical orientation overlay   INASA-CR-197439   p 301 N95-22578   VISCOSITY   Development and verification of a resin film infusion/resin transfer molding simulation model for fabrication of advanced textile composites   INASA-CR-197439   p 301 N95-23179   VISCOUS FLOW   Laplace interaction law for the computation of viscous airfoil flow in low- and high-speed aerodynamics   BTN-95-EIX951825832551   p 266 A95-73552   VISCOUS-invisciol interaction method for unsteady low-speed airfoil flows   BTN-95-EIX951826892551   p 306 A95-73566   VISCOUS-invisciol interaction method for unsteady low-speed airfoil flows   BTN-95-EIX951826892551   p 306 A95-73566   VISCOUS-invisciol interaction method for unsteady low-speed airfoil flows   BTN-95-EIX951826892341   p 308 A95-73660   An assessment of viscous effects in compulational simulation of benign and burst vortex flows on generic (ighter wind-tunnel models using TEAM code   p 273 N95		design for a model
Summary of an active flexible wing program   BTN-95-EIX95182619209  p 283 A95-76635   Multiple-function digital controller system for active flexible wing wind-tunnel model   BTN-95-EIX95182619212  p 322 A95-76638   Flutter suppression control law design and testing for the active flexible wing   BTN-95-EIX95182619214  p 292 A95-76640   Design and multifunction tests of a frequency domain-based active flutter suppression system   BTN-95-EIX95182619215  p 292 A95-76641   Flutter suppression for the active flexible wing: A classical design   BTN-95-EIX95182619215  p 292 A95-76642   Active control of panel vibrations induced by a boundary layer flow   NASA-CR-197867  p 273 N95-23182   VIBRATION MODE   Application of Navier-Stokes aeroelastic methods to improve fighter wing maneuver performance   BTN-95-EIX95182619218  p 284 A95-76644   VIKING LANDER SPACECRAFT   Fourth-generation Mars vehicle concepts   BTN-95-EIX95182619218  p 298 A95-73568   VIRTUAL REALITY   Virtual reality flight control display with six-degree-of-freedom controller and spherical orientation overlay   NASA-CASE-NPO-18733-1-CU  p 288 N95-22578   VISCOSITY   Development and verification of a resin film infusion/resin transfer molding simulation model for fabrication of advanced textile composites   NASA-CR-197439  p 301 N95-23179   VISCOUS FLOW   Laplace interaction law for the computation of viscous airfoil flow in low- and high-speed aerodynamic poptimized waverider at high allitudes   BTN-95-EIX95182593255  p 306 A95-73556   Viscous-inviscid interaction method for unsteady low-speed airfoil flows   BTN-95-EIX95182619033  p 269 A95-75560   Viscous-inviscid interaction method for unsteady low-speed airfoil flows   BTN-95-EIX95182619033  p 269 A95-75560   Viscous-inviscid interaction for aircraft navigation   NASA-CASE-ARC-11982-1  p 280 N95-23185   VISCOUS-Inviscid interaction for aircraft navigation   NASA-CASE-ARC-11982-1  p 280 N95-2393   VISCOUS-Inviscid interaction for aircraft navigation   NASA-CASE-ARC-11982-1  p 268 A95-7558   VISCOUS-I		
Multiple-function digital controller system for active flexible wing wind-tunnel model [BTN-95-EIX95182619212] p 322 A95-76638 Flutter suppression control law design and testing for the active flexible wing [BTN-95-EIX95182619214] p 292 A95-76640 Design and multifunction tests of a frequency domain-based active flutter suppression system [BTN-95-EIX95182619215] p 292 A95-76641 Flutter suppression for the active flexible wing: A classical design [BTN-95-EIX95182619216] p 292 A95-76642 Active control of panel vibrations induced by a boundary layer flow [NASA-CR-197867] p 273 N95-23182 //IBRATION MODE Application of Navier-Stokes aeroelastic methods to improve fighter wing maneuver performance [BTN-95-EIX95182619218] p 284 A95-76644 //IKING LANDER SPACECRAFT Fourth-generation Mars vehicle concepts [BTN-95-EIX95182619218] p 284 A95-73668 //IRTUAL REALITY // Virtual reality flight control display with six-degree-of-freedom controller and spherical orientation overlay [NASA-CASE-NPO-18733-1-CU] p 288 N95-22578 //ISCOSITY  Development and verification of a resin film infusion/resin transfer molding simulation model for fabrication of advanced textile composites [NASA-CR-197439] p 301 N95-23179 //ISCOUS FLOW  Laplace interaction law for the computation of viscous airfoil flow in low- and high-speed aerodynamics [BTN-95-EIX951825593255] p 266 A95-73561 Viscous-inviscid interaction method for unsteady low-speed airfoil flows [BTN-95-EIX9518263939] p 269 A95-75786 //ISCOUS-inviscid interaction method for unsteady low-speed airfoil flows [BTN-95-EIX95182619033] p 269 A95-75786 //ISCOLS-INVISCOUS effects in computational simulation of benign and burst vortex flows on generic fighter wind-tunnel models using TEAM code [NASA-CR-4650] p 273 N95-23185 //ISCOLS-INSP-EIX95182619033] p 269 A95-75758 //ISCOLS-INVISCOUS effects in computational simulation of benign and burst vortex flows on generic fighter wind-tunnel models using TEAM code [NASA-CR-4650] p 273 N95-23185 //ISUAL SIGNALS Cueing light configuration for aircraft naviga		
Multiple-function digital controller system for active flexible wing wind-tunnel model [BTN-95-EIX95182619212] p 322 A95-76638 Flutter suppression control law design and testing for the active flexible wing [BTN-95-EIX95182619214] p 292 A95-76640 Design and multifunction tests of a frequency domain-based active flutter suppression system [BTN-95-EIX95182619215] p 292 A95-76641 Flutter suppression for the active flexible wing: A classical design [BTN-95-EIX95182619216] p 292 A95-76642 Active control of panel vibrations induced by a boundary layer flow [INASA-CR-197867] p 273 N95-23182 VIBRATION MODE Application of Navier-Stokes aeroelastic methods to improve fighter wing maneuver performance [BTN-95-EIX95182619218] p 284 A95-76644 VIKING LANDER SPACECRAFT Fourth-generation Mars vehicle concepts [BTN-95-EIX95182619218] p 284 A95-76644 VIKING LANDER SPACECRAFT Fourth-generation Mars vehicle concepts [BTN-95-EIX95152583267] p 298 A95-73568 VIRTUAL REALITY Virtual reality flight control display with six-degree-of-freedom controller and spherical orientation overlay [INASA-CASE-NPO-18733-1-CU] p 288 N95-22578 VISCOSITY Development and verification of a resin film infusion/resin transfer molding simulation model for fabrication of advanced textile composites [NASA-CR-197439] p 301 N95-23179 VISCOUS FLOW Laplace interaction law for the computation of viscous airfoil flow in low- and high-speed aerodynamics [BTN-95-EIX95152583251] p 266 A95-73552 VISCOUS FLOW Laplace interaction shock-layer solutions for high-altitude flows [BTN-95-EIX95152583251] p 266 A95-73556 Viscous-inviscid interaction method for unsteady low-speed airfoil flows [BTN-95-EIX9515263255] p 306 A95-73556 Viscous-inviscid interaction method for unsteady low-speed airfoil flows [BTN-95-EIX9515263255] p 306 A95-73556 Viscous-inviscid interaction method for unsteady low-speed airfoil flows [BTN-95-EIX95162619031] p 269 A95-73556 Viscous-inviscid interaction method or unsteady low-speed airfoil flows [BTN-95-EIX9516261903] p 269 A95-73556 Viscous-inviscid	Summary of an active flexible wing	program
IBXN-95-EIX95182619212  p 322 A95-76638		
BTN-95-EIX95182619212  p 322 A95-76638     Flutter suppression control law design and testing for the active flexible wing   BTN-95-EIX95182619214  p 292 A95-76640     Design and multifunction tests of a frequency domain-based active flutter suppression system   BTN-95-EIX95182619215  p 292 A95-76641     Flutter suppression for the active flexible wing: A classical design   BTN-95-EIX95182619216  p 292 A95-76642     Active control of panel vibrations induced by a boundary layer flow   NASA-CR-197867  p 273 N95-23182     INFANCION MODE   P 273 N95-23182     Application of Navier-Stokes aeroelastic methods to improve fighter wing maneuver performance   BTN-95-EIX95182619218  p 284 A95-76644     WIKING LANDER SPACECRAFT   Fourth-generation Mars vehicle concepts   BTN-95-EIX95152583267  p 298 A95-73568     WIRTUAL REALITY   Virtual reality flight control display with six-degree-of-freedom controller and spherical orientation overlay   NASA-CASE-NPO-18733-1-CU  p 288 N95-22578     VISCOSITY   Development and verification of a resin film infusion/resin transfer molding simulation model for fabrication of advanced textile composites   NASA-CR-197439  p 301 N95-23179     VISCOUS FLOW   Laplace interaction law for the computation of viscous airfoil flow in low- and high-speed aerodynamics   BTN-95-EIX95152593251  p 266 A95-73561     Aerodynamic characteristics of a hypersonic viscous optimized waverider at high allitudes   BTN-95-EIX95152593251  p 266 A95-73552     Higher-order viscous shock-layer solutions for high-altitude flows   BTN-95-EIX95182619234  p 308 A95-76660     BTN-95-EIX95182619033  p 269 A95-75780   CFD optimization of a theoretical minimum-drag body   BTN-95-EIX95182619234  p 308 A95-76660     NASA-CASE-ARC-11982-1  p 260 A95-75560   NSC-2393   NSS-23185   NSS-23185   NSS-23185   NSS-23185   NSS-23185   NSS-23185   NSS-23185   NSS-2333   P 268 A95-75758   NSS-23185   NSS-2333   P 268 A95-75758   NSS-2333	Multiple-function digital controller	system for active
Flutter suppression control law design and testing for the active flexible wing [BTN-95-EIX95182619214] p 292 A95-76640 Design and multifunction tests of a frequency domain-based active flutter suppression system [BTN-95-EIX95182619215] p 292 A95-76641 Flutter suppression for the active flexible wing: A classical design [BTN-95-EIX95182619216] p 292 A95-76642 Active control of panel vibrations induced by a boundary layer flow [NASA-CR-197867] p 273 N95-23182 VIBRATION MODE  Application of Navier-Stokes aeroelastic methods to improve lighter wing maneuver performance [BTN-95-EIX95182619218] p 284 A95-76644 VIKING LANDER SPACECRAFT  Fourth-generation Mars vehicle concepts [BTN-95-EIX95152583267] p 298 A95-73568 VIRTUAL REALITY  Virtual reality flight control display with six-degree-of-freedom controller and spherical orientation overlay [NASA-CASE-NPO-18733-1-CU] p 288 N95-22578 VISCOSITY  Development and verification of a resin film infusion/resin transfer molding simulation model for fabrication of advanced textile composites [NASA-CR-197439] p 301 N95-23179 VISCOUS FLOW  Laplace interaction law for the computation of viscous airfoil flow in low- and high-speed aerodynamics (PIXNS-0EIX95152583251) p 266 A95-73552 Higher-order viscous shock-layer solutions for high-altitude flows [BTN-95-EIX95152583255] p 306 A95-73556 Viscous-inviscid interaction method for unsteady low-speed airfoil flows [BTN-95-EIX95152619234] p 269 A95-75778 CFD optimization of a theoretical minimum-drag body [BTN-95-EIX95152619234] p 269 A95-75786 CFD optimization of a theoretical minimum-drag body [BTN-95-EIX95152619234] p 269 A95-75550 Viscous-inviscid interaction method for unsteady low-speed airfoil flows [BTN-95-EIX9515263255] p 306 A95-73556 Viscous-inviscid interaction for aircraft navigation [NASA-CASE-ARC-11982-1] p 269 A95-75788 CFD optimization of a theoretical minimum-drag body [BTN-95-EIX95152619031] p 269 A95-75780 VISCOUS Flows on generic fighter wind-tunnel models using TEAM code [NASA-CR-4650] p 273 N95-23185 VISCOUS Flows	IBTN-95-FIX951826192121	n 322 A05,76638
the active flexible wing   BTN-95-EIX95182619214  p 292 A95-76640   Design and multifunction tests of a frequency domain-based active flutter suppression system   BTN-95-EIX95182619215  p 292 A95-76641   Flutter suppression for the active flexible wing: A classical design   BTN-95-EIX95182619216  p 292 A95-76642   Active control of panel vibrations induced by a boundary layer flow   INASA-CR-197867  p 273 N95-23182   VIBRATION MODE   Application of Navier-Stokes aeroelastic methods to improve tighter wing maneuver performance   BTN-95-EIX95182619218  p 284 A95-76644   VIKING LANDER SPACECRAFT   Fourth-generation Mars vehicle concepts   BTN-95-EIX95182619218  p 288 A95-73568   VIRTUAL REALITY   Virtual reality flight control display with six-degree-of-freedom controller and spherical orientation overlay   INASA-CASE-NPO-18733-1-CU  p 288 N95-22578   VISCOUSTY   Development and verification of a resin film infusion/resin transfer molding simulation model for fabrication of advanced textile composites   NASA-CR-197439  p 301 N95-23179   VISCOUS FLOW   Laplace interaction law for the computation of viscous airfoil flow in low- and high-speed aerodynamics   BTN-95-EIX95142553037  p 263 A95-73461   Aerodynamic characteristics of a hypersonic viscous optimized waverider at high allitudes   BTN-95-EIX95152583251  p 266 A95-73552   Viscous-inviscid interaction method for unsteady low-speed airfoil flows   BTN-95-EIX95182619234  p 306 A95-735660   An assessment of viscous shock-layer solutions for high-altitude flows   BTN-95-EIX95182619234  p 308 A95-76660   An assessment of viscous effects in computational simulation of benign and burst vortex flows on generic fighter wind-tunnel models using TEAM code   NASA-CR-4650  p 273 N95-23185   Viscous-inviscid interaction for aircraft navigation   NASA-CASE-ARC-11982-1  p 268 A95-75788   VISCOUS BREAKOOWN   Transient structure of vortex breakdown on a delta wing   BTN-95-EIX95182619234  p 268 A95-75758   VISCOUS Generators   P 268 A95-75758   VISCOUS Generators   P 269 A95-734		
BTN-95-EIX95182619214   p 292 A95-76640   Design and multifunction tests of a frequency domain-based active flutter suppression system   BTN-95-EIX95182619215   p 292 A95-76641   Flutter suppression for the active flexible wing: A classical design   BTN-95-EIX95182619216   p 292 A95-76642   Active control of panel vibrations induced by a boundary layer flow   NASA-CR-197867   p 273 N95-23182   VIBRATION MODE   Application of Navier-Stokes aeroelastic methods to improve fighter wing maneuver performance   BTN-95-EIX95182619218   p 284 A95-76644   VIKING LANDER SPACECRAFT   Fourth-generation Mars vehicle concepts   BTN-95-EIX95182619218   p 298 A95-7368   VIRTUAL REALITY   Virtual reality flight control display with six-degree-of-freedom controller and spherical orientation overlay   NASA-CASE-NPO-18733-1-CU   p 288 N95-22578   VISCOSITY   Development and verification of a resin film infusion/resin transfer molding simulation model for fabrication of advanced textile composites   NASA-CR-197439   p 301 N95-23179   VISCOUS FLOW   Laplace interaction law for the computation of viscous airfoil flow in low- and high-speed aerodynamics   BTN-95-EIX95142553037   p 263 A95-73461   Aerodynamic characteristics of a hypersonic viscous optimized waverider at high allitudes   BTN-95-EIX95152583255   p 306 A95-73556   Viscous-inviscid interaction method for unsteady low-speed airfoil flows   BTN-95-EIX95182619033   p 269 A95-75778   CFD optimization of a theoretical minimum-drag body   BTN-95-EIX95182619033   p 269 A95-75778   CFD optimization of a theoretical minimum-drag body   BTN-95-EIX95182619033   p 269 A95-75560   Viscous-inviscid interaction method for unsteady low-speed airfoil flows   BTN-95-EIX95182619033   p 269 A95-75578   CFD optimization of a theoretical minimum-drag body   BTN-95-EIX95182619033   p 269 A95-75580   Viscous-inviscid interaction for aircraft navigation   NASA-CASE-ARC-11982-1   p 260 N95-23185   VISCOUS PREAKDOWN   Transient structure of vortex breakdown on a delta wing   BTN-95-EIX95142553044	the active flexible wing	sign and testing to
domain-based active flutter suppression system [BTN-95-EIX95182619215] p 292 A95-76641 Flutter suppression for the active flexible wing: A classical design [BTN-95-EIX95182619216] p 292 A95-76642 Active control of panel vibrations induced by a boundary layer flow [NASA-CR-197867] p 273 N95-23182 VIBRATION MODE  Application of Navier-Stokes aeroelastic methods to improve fighter wing maneuver performance [BTN-95-EIX95182619218] p 284 A95-76644 VIKING LANDER SPACECRAFT Fourth-generation Mars vehicle concepts [BTN-95-EIX95182619218] p 298 A95-73568 VIRTUAL REALITY Virtual reality flight control display with six-degree-ol-freedom controller and spherical orientation overlay [NASA-CASE-NPO-18733-1-CU] p 288 N95-22578 VISCOSITY Development and verification of a resin film infusion/resin transfer molding simulation model for fabrication of advanced textile composites [NASA-CR-197439] p 301 N95-23179 VISCOUS FLOW Laplace interaction law for the computation of viscous airfoil flow in low- and high-speed aerodynamics [BTN-95-EIX95142553037] p 263 A95-73661 Aerodynamic characteristics of a hypersonic viscous optimized waverider at high altitudes [BTN-95-EIX95152583251] p 266 A95-73552 Higher-order viscous shock-layer solutions for high-altitude flows [BTN-95-EIX95182619093] p 269 A95-75778 CFD optimization of a theoretical minimum-drag body (BTN-95-EIX95182619093] p 269 A95-75778 CFD optimization of a theoretical minimum-drag body (BTN-95-EIX95182619093] p 269 A95-75786 CFD optimization of a theoretical minimum-drag body (BTN-95-EIX95182619031] p 280 N95-23185 VISCOUS-FLOW  Transient structure of vortex breakdown on a delta wing [BTN-95-EIX95182619073] p 268 A95-7558 Flow structure in the wake of a wishbone vortex generator [BTN-95-EIX95142553044] p 304 A95-73454 Separation control on high-lift airfoils via micro-vortex generator		p 292 A95-76640
BTN-95-EIX95182619215   p. 292 A95-76641 Flutter suppression for the active flexible wing: A classical design   BTN-95-EIX95182619216   p. 292 A95-76642 Active control of panel vibrations induced by a boundary layer flow   INASA-CR-197867   p. 273 N95-23182 VIBRATION MODE   Application of Navier-Stokes aeroelastic methods to improve fighter wing maneuver performance   BTN-95-EIX95182619218   p. 284 A95-76644 VIKING LANDER SPACECRAFT   p. 284 A95-76644 VIKING LANDER SPACECRAFT   p. 298 A95-73568 VIRTUAL REALITY   Virtual reality flight control display with six-degree-of-freedom controller and spherical orientation overlay   INASA-CASE-NPO-18733-1-CU   p. 288 N95-22578 VISCOSITY   p. 288 N95-22578 VISCOSITY   p. 298 N95-23179 VISCOUS FLOW   Laplace interaction law for the computation of viscous airfoil flow in low- and high-speed aerodynamics   BTN-95-EIX95142553037   p. 263 A95-73461   Aerodynamic characteristics of a hypersonic viscous optimized waverider at high allitudes   BTN-95-EIX95152583251   p. 266 A95-73552   Nigha-altitude flows   BTN-95-EIX95182619093   p. 269 A95-75778   D. 269 N95-23185 VISCOUS-Inviscid interaction method for unsteady low-speed airfoil flows   BTN-95-EIX95182619093   p. 269 A95-75778   CFD optimization of a theoretical minimum-drag body   BTN-95-EIX95182619093   p. 269 A95-7556 VISCOUS-Inviscid interaction method for unsteady low-speed airfoil flows   BTN-95-EIX95182619031   p. 269 A95-75578   CFD optimization of a theoretical minimum-drag body   BTN-95-EIX95182619031   p. 269 A95-7558   VISCOUS-Inviscid interaction for aircraft navigation   NASA-CASE-ARC-11982-1   p. 280 N95-23185   VISUAL SIGNALS   p. 268 A95-75758   VISUAL SIGNALS   p. 268 A95-75758   VISUAL SIGNALS   p. 268 A95-75758   VISUAL		
Flutter suppression for the active flexible wing: A classical design   BTN-95-EIX95182619216   p 292 A95-76642 Active control of panel vibrations induced by a boundary layer flow   INASA-CR-197867   p 273 N95-23182 / INASA-CR-197867   p 284 A95-76644 / INASA-CR-19786   p 284 A95-76644 / INASA-CR-19786   p 284 A95-76644 / INASA-CR-19786   p 284 A95-76644 / INASA-CR-1978   p 298 A95-73568 / INASA-CR-1978   p 298 N95-22578 / INASA-CR-1978   p 298 N95-22578 / INASA-CR-1978   p 298 N95-22578 / INASA-CR-197439   p 281 N95-23179 / INASA-CR-197439   p 301 N95-23179 / INASA-CR-197439   p 306 A95-73461   Aerodynamic characteristics of a hypersonic viscous airfoil flow in low- and high-speed aerodynamics   IBTN-95-EIX95152553251   p 266 A95-73552   Higher-order viscous shock-layer solutions for high-altitude flows   IBTN-95-EIX95152563251   p 266 A95-73556 / Viscous-inviscid interaction method for unsteady low-speed airfoil flows   IBTN-95-EIX9515263255   p 306 A95-73556 / INASA-CR-1982619033   p 269 A95-7578   CFD optimization of a theoretical minimum-drag body   IBTN-95-EIX95152619234   p 308 A95-73556 / INASA-CR-4650   p 273 N95-23185 / INASA-CR-4650   p 273 N95-23185 / INASA-CR-4650   p 273 N95-23185 / INASA-CR-4650   p 273 N95-2333 /		
classical design [BTN-95-EIX95182619216] p 292 A95-76642 Active control of panel vibrations induced by a boundary layer flow [NASA-CR-197867] p 273 N95-23182 VIBRATION MODE  Application of Navier-Stokes aeroelastic methods to improve tighter wing maneuver performance [BTN-95-EIX95182619218] p 284 A95-76644 VIKING LANDER SPACECRAFT Fourth-generation Mars vehicle concepts [BTN-95-EIX95182583267] p 298 A95-73568 VIRTUAL REALITY Virtual reality flight control display with six-degree-ol-freedom controller and spherical orientation overlay [NASA-CASE-NPO-18733-1-CU] p 288 N95-22578 VISCOSITY Development and verification of a resin film infusion/resin transfer molding simulation model for fabrication of advanced textile composites [NASA-CR-197439] p 301 N95-23179 VISCOUS FLOW Laplace interaction law for the computation of viscous airfoil flow in low- and high-speed aerodynamics [BTN-95-EIX95182583251] p 266 A95-73561 Negh-altitude flows [BTN-95-EIX95152583255] p 266 A95-73552 Viscous-inviscid interaction method for unsteady low-speed airfoil flows [BTN-95-EIX95182619093] p 269 A95-75778 CFD optimization of a theoretical minimum-drag body [BTN-95-EIX95182619093] p 269 A95-75778 CFD optimization of a theoretical minimum-drag body [BTN-95-EIX95182619093] p 269 A95-75778 CFD optimization of a theoretical minimum-drag body [BTN-95-EIX95182619093] p 269 A95-75778 CFD optimization of a theoretical minimum-drag body [BTN-95-EIX95182619093] p 269 A95-75788 Cueing light configuration for aircraft navigation [NASA-CR-4650] p 273 N95-23185 VISUAL SIGNALS Cueing light configuration for aircraft navigation [NASA-CASE-ARC-11982-1] p 260 A95-73558 Flow structure in the wake of a wishbone vortex generator [BTN-95-EIX95182619073] p 268 A95-7558 Flow structure in the wake of a wishbone vortex generator [BTN-95-EIX95182653044] p 304 A95-73454 Separation control on high-lift airfoils via micro-vortex generator		
BTN-95-EIX95182619216   p 292 A95-76642 Active control of panel vibrations induced by a boundary layer flow   NASA-CR-197867   p 273 N95-23182   VIBRATION MODE   Application of Navier-Stokes aeroelastic methods to improve tighter wing maneuver performance   BTN-95-EIX95182619218   p 284 A95-76644   VIKING LANDER SPACECRAFT   Fourth-generation Mars vehicle concepts   BTN-95-EIX95152583267   p 298 A95-73568   VIRTUAL REALITY   Virtual reality flight control display with six-degree-of-freedom controller and spherical orientation overlay   NASA-CASE-NPO-18733-1-CU   p 288 N95-22578   VISCOSITY   Development and verification of a resin film infusion/resin transfer molding simulation model for fabrication of advanced textile composites   NASA-CR-197439   p 301 N95-23179   VISCOUS FLOW   Laplace interaction law for the computation of viscous airfoil flow in low- and high-speed aerodynamics   BTN-95-EIX95142553037   p 263 A95-73461   Aerodynamic characteristics of a hypersonic viscous optimized waverider at high allitudes   BTN-95-EIX95182593251   p 266 A95-73552   Higher-order viscous shock-layer solutions for high-altitude flows   BTN-95-EIX95182619093   p 269 A95-75778   CFD optimization of a theoretical minimum-drag body   BTN-95-EIX95182619093   p 269 A95-75778   CFD optimization of a theoretical minimum-drag body   BTN-95-EIX95182619093   p 269 A95-75778   CFD optimization of a theoretical minimum-drag body   BTN-95-EIX95182619093   p 269 A95-75778   CFD optimization of a theoretical minimum-drag body   BTN-95-EIX95182619093   p 269 A95-75778   CFD optimization of a theoretical minimum-drag body   BTN-95-EIX95182619033   p 269 A95-75778   CFD optimization of a theoretical minimum-drag body   BTN-95-EIX95182619033   p 269 A95-75778   CFD optimization of a theoretical minimum-drag body   BTN-95-EIX95182619033   p 269 A95-7578   CFT optimization of a theoretical minimum-drag body   BTN-95-EIX95182619073   p 268 A95-75758   CFT optimization of a theoretical minimum-drag body   BTN-95-EIX95182619073   p 268 A95-7575		We Hexible Willy. A
INASA-CR-197867   p 273 N95-23182   NASA-CR-197867   p 273 N95-23182   NBRATION MODE   Application of Navier-Stokes aeroelastic methods to improve fighter wing maneuver performance   g8TN-95-EIX95182619218   p 284 A95-76644   WIKING LANDER SPACECRAFT   Fourth-generation Mars vehicle concepts   IBTN-95-EIX9518258267   p 298 A95-73568   NBTUAL REALITY   Wirtual reality flight control display with six-degree-ol-freedom controller and spherical orientation overlay   NASA-CASE-NPO-18733-1-CU   p 288 N95-22578   NBSA-CR-197439   p 301 N95-23779   P 301 N95-23179   P 301 N95-23185   P 301 N95-23393   P 3		p 292 A95-76642
NASA-CR-197867   p 273 N95-23182     IBRATION MODE	Active control of panel vibrations in	duced by a boundary
Application of Navier-Stokes aeroelastic methods to improve tighter wing maneuver performance [BTN-95-EIX95182619218] p 284 A95-76644  VIKING LANDER SPACECRAFT Fourth-generation Mars vehicle concepts [BTN-95-EIX95152583267] p 298 A95-73568  VIRTUAL REALITY Virtual reality flight control display with six-degree-of-freedom controller and spherical orientation overlay [NASA-CASE-NPO-18733-1-CU] p 288 N95-22578  VISCOSITY Development and verification of a resin film infusion/resin transfer molding simulation model for fabrication of advanced textile composites [NASA-CR-197439] p 301 N95-23179  VISCOUS FLOW Laplace interaction law for the computation of viscous airfoil flow in low- and high-speed aerodynamics [BTN-95-EIX95152553037] p 263 A95-73461 Aerodynamic characteristics of a hypersonic viscous optimized waverider at high allitudes [BTN-95-EIX95152583251] p 266 A95-73552 Higher-order viscous shock-layer solutions for high-allitude flows [BTN-95-EIX95152583255] p 306 A95-73556 Viscous-inviscid interaction method for unsteady low-speed airfoil flows [BTN-95-EIX95152619031] p 269 A95-75778 CFD optimization of a theoretical minimum-drag body [BTN-95-EIX95152619031] p 269 A95-75778 CFD optimization of a theoretical minimum-drag body [BTN-95-EIX95152619031] p 269 A95-75788 CFD optimization of a theoretical minimum-drag body [BTN-95-EIX95152619031] p 269 A95-75788 CFD optimization of a theoretical minimum-drag body [BTN-95-EIX95152619031] p 269 A95-75788 CFD optimization of a theoretical minimum-drag body [BTN-95-EIX95152619031] p 269 A95-75788 CFD optimization of a theoretical minimum-drag body [BTN-95-EIX95152619031] p 269 A95-75788 CFD optimization of a theoretical minimum-drag body [BTN-95-EIX95152619031] p 269 A95-75788 CFD optimization of a theoretical minimum-drag body [BTN-95-EIX95152619031] p 269 A95-75788 (BTN-95-EIX95152619031] p 269 A95-75788 (BTN-95-EIX95152619031] p 269 A95-75788 (BTN-95-EIX95152619073] p 268 A95-75758 (BTN-95-EIX95152619073] p 268 A95-75758 (BTN-95-EIX95152612553044] p 304 A95-73454 Sep		070 4105 00100
Application of Navier-Stokes aeroelastic methods to improve tighter wing maneuver performance [BTN-95-EIX95182619218] p 284 A95-76644 VIKING LANDER SPACECRAFT Fourth-generation Mars vehicle concepts [BTN-95-EIX95182583267] p 298 A95-73568 VIRTUAL REALITY Virtual reality flight control display with six-degree-ol-freedom controller and spherical orientation overlay [NASA-CASE-NPO-18733-1-CU] p 288 N95-22578 VISCOSITY Development and verification of a resin film infusion/resin transfer molding simulation model for fabrication of advanced textile composites [NASA-CR-197439] p 301 N95-23179 VISCOUS FLOW Laplace interaction law for the computation of viscous airfoil flow in low- and high-speed aerodynamics [BTN-95-EIX95142553037] p 263 A95-73461 Aerodynamic characteristics of a hypersonic viscous optimized waverider at high altitudes [BTN-95-EIX95152583251] p 266 A95-73552 Higher-order viscous shock-layer solutions for high-altitude flows [BTN-95-EIX95182619093] p 269 A95-75778 CFD optimization of a theoretical minimum-drag body [BTN-95-EIX95182619034] p 308 A95-76660 An assessment of viscous effects in computational simulation of benign and burst vortex flows on generic fighter wind-tunnel models using TEAM code [NASA-CR-4650] p 273 N95-23185 VISUAL SIGNALS Cueing light configuration for aircraft navigation [NASA-CR-4650] p 273 N95-23185 VISUAL SIGNALS Cueing light configuration for aircraft navigation [NASA-CR-4650] p 268 A95-75758 (PATEX BREAKDOWN) Transient structure of vortex breakdown on a delta wing [BTN-95-EIX95182619073] p 268 A95-75758 (PORTEX BREAKDOWN) Transient structure in the wake of a wishbone vortex generator [BTN-95-EIX95142553044] p 304 A95-73454 Separation control on high-lift airfoils via micro-vortex generators		p 273 N95-23182
mprove tighter wing maneuver performance (BTN-95-EIX95182619218) p 284 A95-76644  VIKING LANDER SPACECRAFT Fourth-generation Mars vehicle concepts (BTN-95-EIX95152583267) p 298 A95-73568  VIRTUAL REALITY Virtual reality flight control display with six-degree-of-freedom controller and spherical orientation overlay (INASA-CASE-NPO-18733-1-CU) p 288 N95-22578  VISCOSITY Development and verification of a resin film infusion/resin transfer molding simulation model for fabrication of advanced textile composites (NASA-CR-19749) p 301 N95-23179  VISCOUS FLOW Laplace interaction law for the computation of viscous airfoil flow in low- and high-speed aerodynamics (BTN-95-EIX95142553037) p 263 A95-73461 Aerodynamic characteristics of a hypersonic viscous optimized waverider at high allitudes (BTN-95-EIX95152583251) p 266 A95-73552 Higher-order viscous shock-layer solutions for high-altitude flows (BTN-95-EIX95182619093) p 269 A95-75778 CFD optimization of a theoretical minimum-drag body (BTN-95-EIX95182619093) p 269 A95-76660 An assessment of viscous effects in computational simulation of benign and burst vortex flows on generic fighter wind-tunnel models using TEAM code (NASA-CR-4650) p 273 N95-23185  VISUAL SIGNALS Cueing light configuration for aircraft navigation (NASA-CR-4650) p 268 A95-7558  VISTONEL SIGNALS Cueing light configuration for aircraft navigation (NASA-CR-4650) p 268 A95-7558  VISTONEL SIGNALS Cueing light configuration for aircraft navigation (NASA-CR-4650) p 268 A95-7558  VISTONEL SIGNALS Cueing light configuration for aircraft navigation (NASA-CR-4650) p 268 A95-7558  VISTONEL SIGNALS Cueing light configuration for aircraft navigation (NASA-CR-4650) p 268 A95-7558  VISTONEL SIGNALS Cueing light configuration for aircraft navigation (NASA-CR-4650) p 268 A95-7558  VISTONEL SIGNALS Cueing light configuration for aircraft navigation (NASA-CR-4650) p 268 A95-7558  VISTONEL SIGNALS Cueing light configuration for aircraft navigation (NASA-CR-4650) p 268 A95-75758  VISTONEL SIGNALS Cueing light configuration f		elastic methods to
BTN-95-EIX95182619218   p 284 A95-76644   WIKING LANDER SPACECRAFT   Fourth-generation Mars vehicle concepts   BTN-95-EIX95152583267   p 298 A95-73568   WIRTUAL REALITY   Virtual reality flight control display with six-degree-of-freedom controller and spherical orientation overlay   INASA-CASE-NPO-18733-1-CU   p 288 N95-22578   INASA-CASE-NPO-18733-1-CU   p 280 N95-23179   P 301 N95-23185		
Fourth-generation Mars vehicle concepts   BTN-95-EIX95152583267   p 298 A95-73568   PTTUAL REALITY   Virtual reality flight control display with six-degree-of-freedom controller and spherical orientation overlay   NASA-CASE-NPO-18733-1-CU   p 288 N95-22578   NSCOSITY   p 288 N95-22578   NSCOSITY   p 288 N95-22578   P 267 NSCOSITY   p 287 N95-23179   P 267 NSCOSITY   p 268 NSS-73461   P 268 NSS-73552   P 268 NSS-73552   P 268 NSS-73552   P 268 NSS-73552   P 269		
BTN-95-EIX95152583267   p 298 A95-73568 WIRTUAL REALITY   Virtual reality   flight   control   display   with   six-degree-of-freedom controller and spherical orientation   overlay   [NASA-CASE-NPO-18733-1-CU]   p 288 N95-22578   VISCOSITY   Development   and   verification   of   a   resin   film   infusion/resin   transfer   molding   simulation   model   for   fabrication   of   a   resin   film   infusion/resin   transfer   molding   simulation   model   for   fabrication   of   a   resin   film   infusion/resin   transfer   molding   simulation   model   for   fabrication   of   a   resin   film   infusion/resin   transfer   molding   simulation   model   for   fabrication   of   a   resin   film   model   for   fabrication   of   a   resin   film   model   for   fabrication   of   a   a   a   a   a   a   a   a   a		
VIRTUAL REALITY  Virtual reality flight control display with Six-degree-of-freedom controller and spherical orientation overlay  [NASA-CASE-NPO-18733-1-CU] p 288 N95-22578  VISCOSITY  Development and verification of a resin film infusion/resin transfer molding simulation model for fabrication of advanced textile composites  [NASA-CR-197439] p 301 N95-23179  VISCOUS FLOW  Laplace interaction law for the computation of viscous airfoil flow in low- and high-speed aerodynamics  [BTN-95-EIX95142553037] p 263 A95-73661  Aerodynamic characteristics of a hypersonic viscous optimized waverider at high allitudes  [BTN-95-EIX95152583251] p 266 A95-73552  Higher-order viscous shock-layer solutions for high-allitude flows  [BTN-95-EIX95152583255] p 306 A95-73556  Viscous-inviscid interaction method for unsteady low-speed airfoil flows  [BTN-95-EIX95182619031] p 269 A95-75778  CFD optimization of a theoretical minimum-drag body (BTN-95-EIX95182619234] p 308 A95-76660  An assessment of viscous effects in computational simulation of benign and burst vortex flows on generic fighter wind-tunnel models using TEAM code  [NASA-CR-4650] p 273 N95-23185  VISIONALS  Cueing light configuration for aircraft navigation  [NASA-CASE-ARC-11982-1] p 280 N95-2393  VORTEX BREAKDOWN  Transient structure of vortex breakdown on a delta wing  [BTN-95-EIX95182619073] p 268 A95-75758  Flow structure in the wake of a wishbone vortex generator  [BTN-95-EIX95142553044] p 304 A95-73454  Separation control on high-lift airfoils via micro-vortex generators		
Virtual reality flight control display with six-degree-of-freedom controller and spherical orientation overlay [NASA-CASE-NPO-18733-1-CU] p 288 N95-22578 //SCOSITY Development and verification of a resin film infusion/resin transfer molding simulation model for flabrication of advanced textile composites [NASA-CR-197439] p 301 N95-23179 //SCOUS FLOW  Laplace interaction law for the computation of viscous airfoil flow in low- and high-speed aerodynamics [BTN-95-EIX95142553037] p 263 A95-73461 Aerodynamic characteristics of a hypersonic viscous optimized waverider at high alltitudes [BTN-95-EIX95152583251] p 266 A95-73552 Higher-order viscous shock-layer solutions for high-altitude flows [BTN-95-EIX95152583255] p 306 A95-73556 Viscous-inviscid interaction method for unsteady low-speed airfoil flows [BTN-95-EIX95182619093] p 269 A95-75778 CFD optimization of a theoretical minimum-drag body [BTN-95-EIX95182619093] p 269 A95-76660 An assessment of viscous effects in computational simulation of benign and burst vortex flows on generic fighter wind-tunnel models using TEAM code [NASA-CR-4650] p 273 N95-23185 //SUAL SIGNALS Cueing light configuration for aircraft navigation [NASA-CASE-ARC-11982-1] p 260 N95-2393 //ORTEX BREAKDOWN  Transient structure of vortex breakdown on a delta wing [BTN-95-EIX95182619073] p 268 A95-75758 //ORTEX GENERATORS  Flow structure in the wake of a wishbone vortex generator [BTN-95-EIX95142553044] p 304 A95-73454 Separation control on high-lift airfoils via micro-vortex generator	Fourth-generation Mars vehicle cor	
six-degree-ol-freedom controller and spherical orientation overlay [NASA-CASE-NPO-18733-1-CU] p 288 N95-22578 /ISCOSITY  Development and verification of a resin film infusion/resin transfer molding simulation model for fabrication of advanced textile composites [NASA-CR-197439] p 301 N95-23179 /ISCOUS FLOW  Laplace interaction law for the computation of viscous airfoil flow in low- and high-speed aerodynamics [BTN-95-EIX9514255037] p 263 A95-73461 Aerodynamic characteristics of a hypersonic viscous optimized waverider at high allitudes [BTN-95-EIX95152583251] p 266 A95-73552 Higher-order viscous shock-layer solutions for high-altitude flows [BTN-95-EIX95152583251] p 306 A95-73556 Viscous-inviscid interaction method for unsteady low-speed airfoil flows [BTN-95-EIX95152619234] p 269 A95-75778 CFD optimization of a theoretical minimum-drag body [BTN-95-EIX95152619234] p 308 A95-76660 An assessment of viscous effects in computational simulation of benign and burst vortex flows on generic fighter wind-tunnel models using TEAM code [NASA-CR-4650] p 273 N95-23185 /ISUAL SIGNALS Cueing light configuration for aircraft navigation [NASA-CASE-ARC-11982-1] p 260 N95-2393 /ORTEX BREAKDOWN  Transient structure of vortex breakdown on a delta wing [BTN-95-EIX95182619073] p 268 A95-75758 Flow structure in the wake of a wishbone vortex generator [BTN-95-EIX95142553044] p 304 A95-73454 Separation control on high-lift airfoils via micro-vortex generators	Fourth-generation Mars vehicle coi [BTN-95-EIX95152583267]	
NASA-CASE-NPO-18733-1-CU   p 288 N95-22578     INSCOSITY	Fourth-generation Mars vehicle coi  BTN-95-EIX95152583267   VIRTUAL REALITY	p 298 A95-73568
Development and verification of a resin film infusion/resin transfer molding simulation model for fabrication of advanced textile composites [NASA-CR-197439] p 301 N95-23179 [VISCOUS FLOW]  Laplace interaction law for the computation of viscous airfoil flow in low- and high-speed aerodynamics [BTN-95-EIX95142553037] p 263 A95-73461 Aerodynamic characteristics of a hypersonic viscous optimized waverider at high allitudes [BTN-95-EIX95152583251] p 266 A95-73552 Higher-order viscous shock-layer solutions for high-altitude flows [BTN-95-EIX95152583251] p 306 A95-73556 Viscous-inviscid interaction method for unsteady low-speed airfoil flows [BTN-95-EIX95152619031] p 269 A95-75778 CFD optimization of a theoretical minimum-drag body [BTN-95-EIX95182619034] p 308 A95-76660 An assessment of viscous effects in computational simulation of benign and burst vortex flows on generic flighter wind-tunnel models using TEAM code [NASA-CR-4650] p 273 N95-23185 (ISUAL SIGNALS Cueing light configuration for aircraft navigation [NASA-CASE-ARC-11982-1] p 280 N95-2393 (ORTEX BREAKDOWN Transient structure of vortex breakdown on a delta wing [BTN-95-EIX95182619073] p 268 A95-75758 Flow structure in the wake of a wishbone vortex generator [BTN-95-EIX95142553044] p 304 A95-73454 Separation control on high-lift airfoils via micro-vortex generators	Fourth-generation Mars vehicle col  BTN-95-EIX95152583267   VIRTUAL REALITY Virtual reality flight control	p 298 A95-73568 ol display with
Development and verification of a resin film infusion/resin transfer molding simulation model for fabrication of advanced textile composites (NASA-CR-197439) p 301 N95-23179 // INSCOUS FLOW  Laplace interaction law for the computation of viscous airfoil flow in low- and high-speed aerodynamics (BTN-95-EIX95142553037) p 263 A95-73461 Aerodynamic characteristics of a hypersonic viscous optimized waverider at high allitudes (BTN-95-EIX95152583251) p 266 A95-73552 Higher-order viscous shock-layer solutions for high-allitude flows (BTN-95-EIX95152583255) p 306 A95-73556 Viscous-inviscid interaction method for unsteady low-speed airfoil flows (BTN-95-EIX95152619234) p 308 A95-736660 An assessment of viscous effects in computational simulation of benign and burst vortex flows on generic fighter wind-tunnel models using TEAM code (NASA-CR-4650) p 273 N95-23185 // ISJAL SIGNALS Cueing light configuration for aircraft navigation (NASA-CASE-ARC-1982-1) p 268 A95-75758 // ISJAL SIGNALS Cueing light configuration for aircraft navigation (NASA-CASE-ARC-1982-1) p 268 A95-75758 // ISJAL SIGNALS Cueing light configuration for aircraft navigation (NASA-CASE-ARC-1982-1) p 268 A95-75758 // ISJAL SIGNALS Cueing light configuration for aircraft navigation (NASA-CASE-ARC-1982-1) p 268 A95-75758 // ISJAL SIGNALS Cueing light configuration for aircraft navigation (NASA-CASE-ARC-1982-1) p 268 A95-75758 // ISJAL SIGNALS Cueing light configuration for aircraft navigation (NASA-CASE-ARC-1982-1) p 268 A95-75758 // ISJAL SIGNALS Cueing light configuration for aircraft navigation (NASA-CASE-ARC-1982-1) p 268 A95-75758 // ISJAL SIGNALS Cueing light configuration for aircraft navigation (NASA-CASE-ARC-1982-1) p 268 A95-75758 // ISJAL SIGNALS Cueing light configuration for aircraft navigation (NASA-CASE-ARC-1982-1) p 268 A95-75758 // ISJAL SIGNALS Cueing light configuration for aircraft navigation (NASA-CASE-ARC-1982-1) p 268 A95-75758 // ISJAL SIGNALS Cueing light configuration for aircraft navigation (NASA-CASE-ARC-1982-1) p 268 A95-75758 // I	Fourth-generation Mars vehicle cor  BTN-95-EIX95152583267   VIRTUAL REALITY Virtual reality flight control six-degree-of-freedom controller and overlay	p 298 A95-73568 of display with spherical orientation
infusion/resin transfer molding simulation model for fabrication of advanced textile composites [NASA-CR-197439] p 301 N95-23179 //SCOUS FLOW  Laplace interaction law for the computation of viscous airfoil flow in low- and high-speed aerodynamics [BTN-95-EIX95142553037] p 263 A95-73461 Aerodynamic characteristics of a hypersonic viscous optimized waverider at high allitudes [BTN-95-EIX95152583251] p 266 A95-73552 Higher-order viscous shock-layer solutions for high-altitude flows [BTN-95-EIX95152583255] p 306 A95-73556 Viscous-inviscid interaction method for unsteady low-speed airfoil flows [BTN-95-EIX95182619093] p 269 A95-75778 CFD optimization of a theoretical minimum-drag body [BTN-95-EIX95182619034] p 308 A95-76660 An assessment of viscous effects in computational simulation of benign and burst vortex flows on generic fighter wind-tunnel models using TEAM code [NASA-CR-4650] p 273 N95-23185 //SUAL SIGNALS Cueing light configuration for aircraft navigation [NASA-CR-4650] p 280 N95-23393 //ORTEX BREAKDOWN  Transient structure of vortex breakdown on a delta wing [BTN-95-EIX95182619073] p 268 A95-75758 //ORTEX GENERATORS  Flow structure in the wake of a wishbone vortex generator [BTN-95-EIX95142553044] p 304 A95-73454 Separation control on high-lift airfoils via micro-vortex generators	Fourth-generation Mars vehicle col  BTN-95-EIX95152583267   VIRTUAL REALITY Virtual reality flight control six-degree-of-freedom controller and overlay  NASA-CASE-NPO-18733-1-CU	p 298 A95-73568 of display with spherical orientation
flabrication of advanced textile composites  NASA-CR-197439	Fourth-generation Mars vehicle cor   BTN-95-EIX95152583267   VIRTUAL REALITY Virtual reality flight control six-degree-of-freedom controller and overlay [NASA-CASE-NPO-18733-1-CU   VISCOSITY	p 298 A95-73568 of display with spherical orientation p 288 N95-22578
NASA-CR-197439   p 301 N95-23179     NSCOUS FLOW     Laplace interaction law for the computation of viscous airfoil flow in low- and high-speed aerodynamics     BTN-95-EIX95142553037   p 263 A95-73461     Aerodynamic characteristics of a hypersonic viscous optimized waverider at high altitudes     BTN-95-EIX95152583251   p 266 A95-73552     Higher-order viscous shock-layer solutions for high-altitude flows     BTN-95-EIX95152583255   p 306 A95-73556     Viscous-inviscid interaction method for unsteady low-speed airfoil flows     BTN-95-EIX95182619093   p 269 A95-7578     CFD optimization of a theoretical minimum-drag body     BTN-95-EIX95182619234   p 308 A95-76660     An assessment of viscous effects in computational simulation of benign and burst vortex flows on generic fighter wind-tunnel models using TEAM code     NASA-CR-4650   p 273 N95-23185     ISUAL SIGNALS   Cueing light configuration for aircraft navigation     NASA-CASE-ARC-11982-1   p 280 N95-2393     INSA-CR-455182619073   p 268 A95-75758     ORTEX BREAKDOWN   Transient structure of vortex breakdown on a delta wing     BTN-95-EIX95182619073   p 268 A95-75758     ORTEX GENERATORS   Flow structure in the wake of a wishbone vortex generator     BTN-95-EIX95142553044   p 304 A95-73454     Separation control on high-lift airfoils via micro-vortex generators	Fourth-generation Mars vehicle col  BTN-95-EIX95152583267   VIRTUAL REALITY Virtual reality flight control six-degree-of-freedom controller and overlay  NASA-CASE-NPO-18733-1-CU   ////////////////////////////////////	p 298 A95-73568 of display with spherical orientation p 288 N95-22578 of a resin film
Laplace interaction law for the computation of viscous airfoil flow in low- and high-speed aerodynamics [BTN-95-EIX95142550037] p 263 A95-73461 Aerodynamic characteristics of a hypersonic viscous optimized waverider at high allitudes [BTN-95-EIX95152583251] p 266 A95-73552 Higher-order viscous shock-layer solutions for high-altitude flows [BTN-95-EIX95152583255] p 306 A95-73556 Viscous-inviscid interaction method for unsteady low-speed airfoil flows [BTN-95-EIX95182619033] p 269 A95-75778 CFD optimization of a theoretical minimum-drag body [BTN-95-EIX95182619034] p 308 A95-76660 An assessment of viscous effects in computational simulation of benign and burst vortex flows on generic fighter wind-tunnel models using TEAM code [NASA-CR-4650] p 273 N95-23185 VISUAL SIGNALS Cueing light configuration for aircraft navigation [NASA-CASE-ARC-11982-1] p 280 N95-2393 VORTEX BREAKDOWN  Transient structure of vortex breakdown on a delta wing [BTN-95-EIX95182619073] p 268 A95-75758 Flow structure in the wake of a wishbone vortex generator [BTN-95-EIX95142553044] p 304 A95-73454 Separation control on high-lift airfoils via micro-vortex generators	Fourth-generation Mars vehicle col  BTN-95-EIX95152583267   VIRTUAL REALITY Virtual reality flight control six-degree-of-freedom controller and overlay  NASA-CASE-NPO-18733-1-CU   VISCOSITY Development and verification influsion/resin transfer molding si	p 298 A95-73568 of display with spherical orientation p 288 N95-22578 of a resin film mulation model for
airfoil flow in low- and high-speed aerodynamics   BTN-95-EIX95142553037   p 263 A95-73461 Aerodynamic characteristics of a hypersonic viscous optimized waverider at high altitudes   BTN-95-EIX95152583251   p 266 A95-73552   Higher-order viscous shock-layer solutions for high-altitude flows   BTN-95-EIX95152583255   p 306 A95-73556   Viscous-inviscid interaction method for unsteady low-speed airfoil flows   BTN-95-EIX95182619093   p 269 A95-7578   CFD optimization of a theoretical minimum-drag body   BTN-95-EIX951826190234   p 308 A95-76660   An assessment of viscous effects in computational simulation of benign and burst vortex flows on generic fighter wind-tunnel models using TEAM code   NASA-CR-4650   p 273 N95-23185   VISUAL SIGNALS   Cueing light configuration for aircraft navigation   NASA-CASE-ARC-11982-1   p 280 N95-2393   VORTEX BREAKDOWN   Transient structure of vortex breakdown on a delta wing   BTN-95-EIX95182619073   p 268 A95-75758   VORTEX GENERATORS   Flow structure in the wake of a wishbone vortex generator   BTN-95-EIX95142553044   p 304 A95-73454   Separation control on high-lift airfoils via micro-vortex generators	Fourth-generation Mars vehicle cor  BTN-95-EIX95152583267   VIRTUAL REALITY Virtual reality flight control six-degree-of-freedom controller and overlay [NASA-CASE-NPO-18733-1-CU   VISCOSITY Development and verification influsion/resin transfer molding si fabrication of advanced textile compo [NASA-CR-197439]	p 298 A95-73568 of display with spherical orientation p 288 N95-22578 of a resin film mulation model for sistes
BTN-95-EIX95142553037   p 263 A95-73461 Aerodynamic characteristics of a hypersonic viscous optimized waverider at high allitudes  BTN-95-EIX95152583251   p 266 A95-73552   Higher-order viscous shock-layer solutions for high-allitude flows  BTN-95-EIX95152583255   p 306 A95-73556   Viscous-inviscid interaction method for unsteady low-speed airfoil flows  BTN-95-EIX95182619093   p 269 A95-75778  CFD optimization of a theoretical minimum-drag body  BTN-95-EIX95182619234   p 308 A95-76660  An assessment of viscous effects in computational simulation of benign and burst vortex flows on generic fighter wind-tunnel models using TEAM code   NASA-CR-4650   p 273 N95-23185   VISUAL SIGNALS   Cueing light configuration for aircraft navigation   NASA-CASE-ARC-1982-1   p 280 N95-2393   VORTEX BREAKDOWN   Transient structure of vortex breakdown on a delta wing   BTN-95-EIX95182619073   p 268 A95-75758   VORTEX GENERATORS   P 304 A95-73454   Separation control on high-lift airfoils via micro-vortex generators	Fourth-generation Mars vehicle col   BTN-95-EIX95152583267   VIRTUAL REALITY   Virtual reality flight control six-degree-of-freedom controller and overlay   INASA-CASE-NPO-18733-1-CU   VISCOSITY   Development and verification infusion/resin transfer molding si fabrication of advanced textile compo   INASA-CR-197439   VISCOUS FLOW	p 298 A95-73568 ol display with spherical orientation p 288 N95-22578 of a resin film mulation model for sites p 301 N95-23179
Aerodynamic characteristics of a hypersonic viscous optimized waverider at high altitudes  [BTN-95-EIX95152583251] p 266 A95-73552  Higher-order viscous shock-layer solutions for high-altitude flows  [BTN-95-EIX95152583255] p 306 A95-73556  Viscous-inviscid interaction method for unsteady low-speed airfoil flows  [BTN-95-EIX95182619093] p 269 A95-75778  CFD optimization of a theoretical minimum-drag body [BTN-95-EIX95182619034] p 308 A95-76660  An assessment of viscous effects in computational simulation of benign and burst vortex flows on generic fighter wind-tunnel models using TEAM code [NASA-CR-4650] p 273 N95-23185  //ISUAL SIGNALS  Cueing light configuration for aircraft navigation [NASA-CASE-ARC-11982-1] p 280 N95-2393  //ORTEX BREAKDOWN  Transient structure of vortex breakdown on a delta wing [BTN-95-EIX95182619073] p 268 A95-75758  //ORTEX GENERATORS  Flow structure in the wake of a wishbone vortex generator [BTN-95-EIX95142553044] p 304 A95-73454  Separation control on high-lift airfoils via micro-vortex generators	Fourth-generation Mars vehicle cor  BTN-95-EINS95152883267   VIRTUAL REALITY Virtual reality flight control six-degree-of-freedom controller and overlay  NASA-CASE-NPO-18733-1-CU   VISCOSITY Development and verification infusion/resin transfer molding si fabrication of advanced textile compo  NASA-CR-197439   VISCOUS FLOW Laplace interaction law for the con	p 298 A95-73568 of display with spherical orientation p 288 N95-22578 of a resin film mulation model for sistes p 301 N95-23179 equitation of viscous
optimized waverider at high altitudes   BTN-95-EIX95152583251   p 266 A95-73552   higher-order viscous shock-layer solutions for high-altitude flows   BTN-95-EIX95152583255   p 306 A95-73556   Viscous-inviscid interaction method for unsteady low-speed airfoil flows   BTN-95-EIX95182619093   p 269 A95-7578   CFD optimization of a theoretical minimum-drag body   BTN-95-EIX95182619234   p 308 A95-76660   An assessment of viscous effects in computational simulation of benign and burst vortex flows on generic fighter wind-tunnel models using TEAM code   NASA-CR-4650   p 273 N95-23185   VISUAL SIGNALS   Cueing light configuration for aircraft navigation   NASA-CASE-ARC-11982-1   p 280 N95-23393   VORTEX BREAKDOWN   p 280 N95-23393   CORTEX GENERATORS   p 268 A95-75758   VORTEX GENERATORS   p 268 A95-75758   VORTEX GENERATORS   Flow structure in the wake of a wishbone vortex generator   BTN-95-EIX95142553044   p 304 A95-73454   Separation control on high-lift airfoils via micro-vortex generators	Fourth-generation Mars vehicle cor  BTN-95-EIX95152583267   VIRTUAL REALITY  Virtual reality flight control six-degree-of-freedom controller and overlay  INASA-CASE-NPO-18733-1-CU   //ISCOSITY  Development and verification infusion/resin transfer molding si fabrication of advanced textile compo  INASA-CR-197439   //ISCOUS FLOW  Laplace interaction law for the con airfoil flow in low- and high-speed aei	p 298 A95-73568 of display with spherical orientation p 288 N95-22578 of a resin film mulation model for sistes p 301 N95-23179 exputation of viscous rodynamics
Higher-order viscous shock-layer solutions for high-altitude flows  [BTN-95-EIX95152583255] p 306 A95-73556  Viscous-inviscid interaction method for unsteady low-speed airfoil flows  [BTN-95-EIX95182619093] p 269 A95-75778  CFD optimization of a theoretical minimum-drag body [BTN-95-EIX95182619234] p 308 A95-76660  An assessment of viscous effects in computational simulation of benign and burst vortex flows on generic fighter wind-tunnel models using TEAM code [NASA-CR-4650] p 273 N95-23185  // INSULA SIGNALS  Cueing light configuration for aircraft navigation [NASA-CASE-ARC-1982-1] p 280 N95-23393  // ORTEX BREAKDOWN  Transient structure of vortex breakdown on a delta wing [BTN-95-EIX95182619073] p 268 A95-75758  // ORTEX GENERATORS  Flow structure in the wake of a wishbone vortex generator [BTN-95-EIX95142553044] p 304 A95-73454  Separation control on high-lift airfoils via micro-vortex generators	Fourth-generation Mars vehicle col   BTN-95-EIX95152583267   VIRTUAL REALITY   Virtual reality flight control six-degree-of-freedom controller and overlay   NASA-CASE-NPO-18733-1-CU   VISCOSITY   Development and verification infusion/resin transfer molding sifabrication of advanced textile compo   INASA-CR-197439   VISCOUS FLOW   Laplace interaction law for the conairfoil flow in low- and high-speed ae   BTN-95-EIX95-142553037	p 298 A95-73568 ol display with spherical orientation p 288 N95-22578 of a resin film mulation model for sites p 301 N95-23179 uputation of viscous rodynamics p 263 A95-73461
Higher-order viscous shock-layer solutions for high-altitude flows  [BTN-95-EIX95152583255] p 306 A95-73556  Viscous-inviscid interaction method for unsteady low-speed airfoil flows  [BTN-95-EIX95182619093] p 269 A95-75778  CFD optimization of a theoretical minimum-drag body [BTN-95-EIX95182619234] p 308 A95-76660  An assessment of viscous effects in computational simulation of benign and burst vortex flows on generic fighter wind-tunnel models using TEAM code [NASA-CR-4650] p 273 N95-23185  // INSULA SIGNALS  Cueing light configuration for aircraft navigation [NASA-CASE-ARC-1982-1] p 280 N95-23393  // ORTEX BREAKDOWN  Transient structure of vortex breakdown on a delta wing [BTN-95-EIX95182619073] p 268 A95-75758  // ORTEX GENERATORS  Flow structure in the wake of a wishbone vortex generator [BTN-95-EIX95142553044] p 304 A95-73454  Separation control on high-lift airfoils via micro-vortex generators	Fourth-generation Mars vehicle col   BTN-95-EIX95152583267   VIRTUAL REALITY	p 298 A95-73568 ol display with spherical orientation p 288 N95-22578 of a resin film mulation model for sites p 301 N95-23179 exputation of viscous rodynamics p 263 A95-73461 hypersonic viscous
[BTN-95-EIX95152583255] p 306 A95-73556 Viscous-inviscid interaction lows peed airtoil flows [BTN-95-EIX95182619093] p 269 A95-7578 CFD optimization of a theoretical minimum-drag body (BTN-95-EIX95182619234] p 308 A95-76660 An assessment of viscous effects in computational simulation of benign and burst vortex flows on generic fighter wind-tunnel models using TEAM code [NASA-CR-4650] p 273 N95-23185 //ISUAL SIGNALS Cueing light configuration for aircraft navigation [NASA-CASE-ARC-1982-1] p 280 N95-23393 //ORTEX BREAKDOWN Transient structure of vortex breakdown on a delta wing [BTN-95-EIX95182619073] p 268 A95-75758 //ORTEX GENERATORS Flow structure in the wake of a wishbone vortex generator [BTN-95-EIX95142553044] p 304 A95-73454 Separation control on high-lift airfoils via micro-vortex generators	Fourth-generation Mars vehicle col   BTN-95-EIX95152583267   VIRTUAL REALITY   Virtual reality flight control six-degree-of-freedom controller and overlay   NASA-CASE-NPO-18733-1-CU   VISCOSITY   Development and verification infusion/resin transfer molding sifabrication of advanced textile compote [NASA-CR-197439] / INSCOUS FLOW   Laplace interaction law for the control flow in low- and high-speed ae   BTN-95-EIX95142553037   Aerodynamic characteristics of a optimized waverider at high attitudes   BTN-95-EIX95152583251	p 298 A95-73568 of display with spherical orientation p 288 N95-22578 of a resin film mulation model for sites p 301 N95-23179 reputation of viscous rodynamics p 263 A95-73461 hypersonic viscous p 266 A95-73552
Viscous-inviscid interaction method for unsteady low-speed airfoil flows  [BTN-95-EIX95182619093] p 269 A95-75778  CFD optimization of a theoretical minimum-drag body [BTN-95-EIX95182619234] p 308 A95-76660  An assessment of viscous effects in computational simulation of benign and burst vortex flows on generic fighter wind-tunnel models using TEAM code [NASA-CR-4650] p 273 N95-23185  //ISUAL SIGNALS  Cueing light configuration for aircraft navigation [NASA-CASE-ARC-11982-1] p 280 N95-2393  //ORTEX BREAKDOWN  Transient structure of vortex breakdown on a delta wing [BTN-95-EIX95182619073] p 268 A95-75758  //ORTEX GENERATORS  Flow structure in the wake of a wishbone vortex generator [BTN-95-EIX95142553044] p 304 A95-73454  Separation control on high-lift airfoils via micro-vortex generators	Fourth-generation Mars vehicle col   BTN-95-EIX95152583267   VIRTUAL REALITY   Virtual reality flight control   Six-degree-of-freedom controller and overlay   NASA-CASE-NPO-18733-1-CU   VISCOSITY   Development and verification infusion/resin transfer molding sifabrication of advanced textile compo   NASA-CR-197439   VISCOUS FLOW   Laplace interaction law for the conairful flow in low- and high-speed aer   BTN-95-EIX95142553037   Aerodynamic characteristics of a optimized waverider at high altitudes   BTN-95-EIX951425530251   Higher-order viscous shock-lay	p 298 A95-73568 of display with spherical orientation p 288 N95-22578 of a resin film mulation model for sites p 301 N95-23179 reputation of viscous rodynamics p 263 A95-73461 hypersonic viscous p 266 A95-73552
low-speed airfoil flows  BTN-95-EIX95182619093  p 269 A95-75778 CFD optimization of a theoretical minimum-drag body  BTN-95-EIX95182619234] p 308 A95-76660 An assessment of viscous effects in computational simulation of benign and burst vortex flows on generic fighter wind-tunnel models using TEAM code  NASA-CR-4650  p 273 N95-23185  ISUAL SIGNALS	Fourth-generation Mars vehicle cor   BTN-95-EIX95152883267   VIRTUAL REALITY Virtual reality flight control is vehicle reality flight control in vehicle reality flight control influsion/resin transfer molding signification of advanced textile compour (NASA-CR-197439) VISCOUS FLOW Laplace interaction law for the containful flow in low- and high-speed aer   BTN-95-EIX9514255037   Aerodynamic characteristics of a optimized waverider at high altitudes   BTN-95-EIX95152883251   Higher-order viscous shock-lay high-altitude flows	p 298 A95-73568 ol display with spherical orientation p 288 N95-22578 of a resin film mulation model for sistes p 301 N95-23179 nputation of viscous rodynamics p 263 A95-73461 hypersonic viscous p 266 A95-73552 ver solutions for
CFD optimization of a theoretical minimum-drag body [BTN-95-EIX95182619234] p 308 A95-76660 An assessment of viscous ettects in computational simulation of benign and burst vortex flows on generic fighter wind-tunnel models using TEAM code [NASA-CR-4650] p 273 N95-23185 //ISUAL SIGNALS Cueing light configuration for aircraft navigation [NASA-CASE-ARC-11982-1] p 280 N95-23393 //ORTEX BREAKDOWN Transient structure of vortex breakdown on a delta wing [BTN-95-EIX95182619073] p 268 A95-75758 //ORTEX GENERATORS Flow structure in the wake of a wishbone vortex generator [BTN-95-EIX95142553044] p 304 A95-73454 Separation control on high-lift airfoils via micro-vortex generators	Fourth-generation Mars vehicle col   BTN-95-EIX95152583267   VIRTUAL REALITY   Virtual reality flight control six-degree-of-freedom controller and overlay   NASA-CASE-NPO-18733-1-CU   VISCOSITY   Development and verification infusion/resin transfer molding sifabrication of advanced textile compote [ANSA-CR-197439] / INSCOUS FLOW   Laplace interaction law for the control info in low- and high-speed aer   BTN-95-EIX95142553037   Aerodynamic characteristics of a optimized waverider at high altitudes   BTN-95-EIX95152583251   Higher-order viscous shock-lay high-altitude flows   BTN-95-EIX95152583255	p 298 A95-73568 ol display with spherical orientation p 288 N95-22578 of a resin film mulation model for sites p 301 N95-23179 uputation of viscous rodynamics p 263 A95-73461 hypersonic viscous p 266 A95-73552 ver solutions for p 306 A95-73556
BTN-95-EIX95182619234  p 308 A95-76660 An assessment of viscous effects in computational simulation of benign and burst vortex flows on generic fighter wind-tunnel models using TEAM code [NASA-CR-4650] p 273 N95-23185 //ISUAL SIGNALS  Cueing light configuration for aircraft navigation [NASA-CASE-ARC-11982-1] p 280 N95-23393 //ORTEX BREAKDOWN  Transient structure of vortex breakdown on a delta wing [BTN-95-EIX95182619073] p 268 A95-75758 //ORTEX GENERATORS Flow structure in the wake of a wishbone vortex generator [BTN-95-EIX95142553044] p 304 A95-73454 Separation control on high-lift airfoils via micro-vortex generators	Fourth-generation Mars vehicle col   BTN-95-EIX95152583267   VIRTUAL REALITY   Virtual reality flight control six-degree-of-freedom controller and overlay   INASA-CASE-NPO-18733-1-CU   VISCOSITY   Development and verification infusion/resin transfer molding si fabrication of advanced textile compo   INASA-CR-197439   VISCOUS FLOW   Laplace interaction law for the conairfoil flow in low- and high-speed aer   BTN-95-EIX95142553037   Aerodynamic characteristics of a optimized waverider at high altitudes   BTN-95-EIX95152583251   Higher-order viscous shock-lay high-altitude flows   IBTN-95-EIX95152583255   Viscous-inviscid interaction met	p 298 A95-73568 ol display with spherical orientation p 288 N95-22578 of a resin film mulation model for sites p 301 N95-23179 uputation of viscous rodynamics p 263 A95-73461 hypersonic viscous p 266 A95-73552 ver solutions for p 306 A95-73556
An assessment of viscous effects in computational simulation of benign and burst vortex flows on generic fighter wind-tunnel models using TEAM code [NASA-CR-4650] p 273 N95-23185 / ISUAL SIGNALS  Cueing light configuration for aircraft navigation [NASA-CASE-ARC-1982-1] p 280 N95-2393 / ORTEX BREAKDOWN  Transient structure of vortex breakdown on a delta wing [BTN-95-EIX95182619073] p 268 A95-75758 / ORTEX GENERATORS Flow structure in the wake of a wishbone vortex generator [BTN-95-EIX95142553044] p 304 A95-73454 Separation control on high-lift airfoils via micro-vortex generators	Fourth-generation Mars vehicle col   BTN-95-EIX95152583267   VIRTUAL REALITY   Virtual reality flight control six-degree-of-freedom controller and overlay   NASA-CASE-NPO-18733-1-CU   VISCOSITY   Development and verification infusion/resin transfer molding sitabrication of advanced textile compote   NASA-CR-197439   VISCOUS FLOW   Laplace interaction law for the control flow in low- and high-speed aer   BTN-95-EIX95142553037   Aerodynamic characteristics of a optimized waverider at high altitudes   BTN-95-EIX95152583251   Higher-order viscous shock-lay high-altitude flows   BTN-95-EIX95152583255   Viscous-inviscid interaction met low-speed airfoil flows   BTN-95-EIX95-EIX95162619993   BTN-95-EIX95-EIX95162619993	p 298 A95-73568 ol display with spherical orientation p 288 N95-22578 of a resin film mulation model for sites p 301 N95-23179 nputation of viscous rodynamics p 263 A95-73461 hypersonic viscous p 266 A95-73552 ver solutions for p 306 A95-73556 hod for unsteady
simulation of benign and burst vortex flows on generic fighter wind-tunnel models using TEAM code [NASA-CR-4650] p 273 N95-23185 /ISUAL SIGNALS  Cueing light configuration for aircraft navigation [NASA-CASE-ARC-11982-1] p 280 N95-23393 /ORTEX BREAKDOWN  Transient structure of vortex breakdown on a delta wing [BTN-95-EIX95182619073] p 268 A95-75758 /ORTEX GENERATORS Flow structure in the wake of a wishbone vortex generator [BTN-95-EIX95142553044] p 304 A95-73454 Separation control on high-lift airfoils via micro-vortex generators	Fourth-generation Mars vehicle col   BTN-95-EIX95152583267   VIRTUAL REALITY Virtual reality flight control   six-degree-of-freedom controller and overlay   INASA-CASE-NPO-18733-1-CU   VISCOSITY Development and verification infusion/resin transfer molding si fabrication of advanced textile compo   INASA-CR-197439   VISCOUS FLOW Laplace interaction law for the con airfoil flow in low- and high-speed aei   IBTN-95-EIX95142553037   Aerodynamic characteristics of a optimized waverider at high altitudes   IBTN-95-EIX95152583251   Higher-order viscous shock-lay high-altitude flows   IBTN-95-EIX95152583255   Viscous-inviscid interaction met low-speed airfoil flows   IBTN-95-EIX9515283251   CFD optimization of a theoretical   CFD optimization of a theoretical	p 298 A95-73568 ol display with spherical orientation p 288 N95-22578 of a resin film mulation model for osites p 301 N95-23179 nputation of viscous rodynamics p 263 A95-73561 hypersonic viscous p 266 A95-73552 ver solutions for p 306 A95-73556 hod for unsteady p 269 A95-75778 minimum-drag body
fighter wind-tunnel models using TEAM code [NASA-CR-4650] p 273 N95-23185 [NSUAL SIGNALS]  Cueing light configuration for aircraft navigation [NASA-CASE-ARC-11982-1] p 280 N95-23393 (ORTEX BREAKDOWN)  Transient structure of vortex breakdown on a delta wing [BTN-95-EIX95182619073] p 268 A95-75758 (ORTEX GENERATORS)  Flow structure in the wake of a wishbone vortex generator [BTN-95-EIX95142553044] p 304 A95-73454 Separation control on high-lift airfoils via micro-vortex generators	Fourth-generation Mars vehicle cor   BTN-95-EIX95152583267   Virtual reality flight control six-degree-of-freedom controller and overlay   INASA-CASE-NPO-18733-1-CU   VISCOSITY Development and verification infusion/resin transfer molding sifabrication of advanced textile compound infusion flows FLOW Laplace interaction law for the conditional flow in low- and high-speed ae   BTN-95-EIX95142553037   Aerodynamic characteristics of a optimized waverider at high altitudes   BTN-95-EIX95152583251   Higher-order viscous shock-lay high-altitude flows   BTN-95-EIX95152583255   Viscous-inviscid interaction met low-speed airfoil flows   BTN-95-EIX95182619993   CFD optimization of a theoretical   BTN-95-EIX95182619934	p 298 A95-73568 ol display with spherical orientation p 288 N95-22578 of a resin film mulation model for sites p 301 N95-23179 noutation of viscous rodynamics p 263 A95-73461 hypersonic viscous p 266 A95-73552 ver solutions for p 306 A95-73556 hod for unsteady p 269 A95-7778 minimum-drag body p 308 A95-76660
NASA-CR-4650   p 273 N95-23185	Fourth-generation Mars vehicle col   BTN-95-EIX95152583267   VIRTUAL REALITY  Virtual reality flight control six-degree-of-freedom controller and overlay   NASA-CASE-NPO-18733-1-CU   VISCOSITY  Development and verification infusion/resin transfer molding sitabrication of advanced textile compc   NASA-CR-197439   VISCOUS FLOW  Laplace interaction law for the condification in low- and high-speed aei   BTN-95-EIX95142553037   Aerodynamic characteristics of a optimized waverider at high altitudes   BTN-95-EIX95152583251   Higher-order viscous shock-lay high-altitude flows   BTN-95-EIX95152583255   Viscous-inviscid interaction met low-speed airfoil flows   BTN-95-EIX9518261993   CFD optimization of a theoretical   BTN-95-EIX95182619234   An assessment of viscous effectives   An assessment   An assessment of viscous effectives   An assessment   A	p 298 A95-73568 ol display with spherical orientation p 288 N95-22578 of a resin film mulation model for sites p 301 N95-23179 noutation of viscous rodynamics p 263 A95-73461 hypersonic viscous p 266 A95-73552 ver solutions for p 306 A95-73556 hod for unsteady p 269 A95-75778 minimum-drag body p 308 A95-7660
Cueing light configuration for aircraft navigation [NASA-CASE-ARC-11982-1] p 280 N95-23393 / ORTEX BREAKDOWN Transient structure of vortex breakdown on a delta wing [BTN-95-EIX95182619073] p 268 A95-75758 / ORTEX GENERATORS Flow structure in the wake of a wishbone vortex generator [BTN-95-EIX95142553044] p 304 A95-73454 Separation control on high-lift airfoils via micro-vortex generators	Fourth-generation Mars vehicle col   BTN-95-EIX95152583267   VIRTUAL REALITY   Virtual reality flight control six-degree-of-freedom controller and overlay   INASA-CASE-NPO-18733-1-CU   VISCOSITY   Development and verification infusion/resin transfer molding si fabrication of advanced textile compo   INASA-CR-197439   VISCOSITY   VISCOSITY   Development and verification infusion/resin transfer molding si fabrication of advanced textile compo   INASA-CR-197439   VISCOSITY   VISCOSITY	p 298 A95-73568 ol display with spherical orientation p 288 N95-22578 of a resin film mulation model for osites p 301 N95-23179 nputation of viscous rodynamics p 263 A95-7356 hypersonic viscous p 266 A95-73552 ver solutions for p 306 A95-7356 hod for unsteady p 308 A95-76660
NASA-ČAŠE-ARC-11982-1   p 280 N95-23393     NORTEX BREAKDOWN	Fourth-generation Mars vehicle col   BTN-95-EIX95152583267   VIRTUAL REALITY  Virtual reality flight control   six-degree-of-freedom controller and overlay   INASA-CASE-NPO-18733-1-CU   VISCOSITY  Development and verification infusion/resin transfer molding si fabrication of advanced textile compty   NASA-CR-197439   VISCOUS FLOW  Laplace interaction law for the control   atfoil flow in low- and high-speed aet   BTN-95-EIX95142553037   Aerodynamic characteristics of a poptimized waverider at high altitudes   BTN-95-EIX95152583251   Higher-order viscous shock-lay high-altitude flows   BTN-95-EIX95152583255   Viscous-inviscid interaction met low-speed airfoil flows   BTN-95-EIX95182619093   CFD optimization of a theoretical   BTN-95-EIX95182619034   An assessment of viscous effects   An assessment of viscous effects   An assessment of viscous effects   Ighter-wind-tunnel models using TEA   INASA-CR-4650	p 298 A95-73568 ol display with spherical orientation p 288 N95-22578 of a resin film mulation model for sites p 301 N95-23179 nputation of viscous rodynamics p 263 A95-73461 hypersonic viscous p 266 A95-73552 rer solutions for p 306 A95-73556 hod for unsteady p 269 A95-7578 minimum-drag body p 308 A95-76660 ts in computational ex flows on generic M code
Transient structure of vortex breakdown on a delta wing   BTN-95-EIX95182619073   p 268 A95-75758 / ORTEX GENERATORS   Flow structure in the wake of a wishbone vortex generator   BTN-95-EIX95142553044   p 304 A95-73454   Separation control on high-lift airfoils via micro-vortex generators	Fourth-generation Mars vehicle col   BTN-95-EIX95152583267   VIRTUAL REALITY   Virtual reality flight control six-degree-of-freedom controller and overlay   INASA-CASE-NPO-18733-1-CU   VISCOSITY   Development and verification infusion/resin transfer molding si fabrication of advanced textile compo   INASA-CR-197439   VISCOUS FLOW   Laplace interaction law for the condition   Iow in low- and high-speed aer   BTN-95-EIX95142553037   Aerodynamic characteristics of a optimized waverider at high altitudes   BTN-95-EIX95152583251   Higher-order viscous shock-lay high-altitude flows   BTN-95-EIX95152583255   Viscous-inviscid interaction met low-speed airtoit flows   BTN-95-EIX95182619093   CFD optimization of a theoretical   BTN-95-EIX95182619093   CFD optimization of a theoretical   BTN-95-EIX95182619034   An assessment of viscous effective wind-tunnel models using TEA   INASA-CR-4650   VISUAL SIGNALS	p 298 A95-73568 ol display with spherical orientation p 288 N95-22578 of a resin film mulation model for sistes p 301 N95-23179 nputation of viscous rodynamics p 263 A95-7356 hypersonic viscous p 266 A95-73552 ver solutions for unsteady p 306 A95-7556 hod for unsteady p 269 A95-75778 minimum-drap body p 308 A95-76660 tis in computational ex flows on generic M code p 273 N95-23185
Transient structure of vortex breakdown on a delta wing    BTN-95-EIX95182619073    p 268 A95-75758 /OHTEX GENERATORS   p 268 A95-75758 /Flow structure in the wake of a wishbone vortex generator  BTN-95-EIX95142553044    p 304 A95-73454   Separation control on high-lift airfoils via micro-vortex generators	Fourth-generation Mars vehicle col   BTN-95-EIX95152583267   VIRTUAL REALITY   Virtual reality flight control   Virtual reality flight   Virtual reality flig	p 298 A95-73568 ol display with spherical orientation p 288 N95-22578 of a resin film mulation model for sites p 301 N95-23179 nputation of viscous rodynamics p 263 A95-73461 hypersonic viscous p 266 A95-73552 ver solutions for p 306 A95-73556 hod for unsteady p 308 A95-7578 minimum-drag body p 308 A95-76660 ts in computational visitions on generic M code p 273 N95-23185 ft navigation
wing  BTN-95-EIX95182619073  p 268 A95-75758 /ORTEX GENERATORS Flow structure in the wake of a wishbone vortex generator  BTN-95-EIX95142553044  p 304 A95-73454 Separation control on high-lift airfoils via micro-vortex generators	Fourth-generation Mars vehicle col   BTN-95-EIX95152583267   VIRTUAL REALITY   Virtual reality flight control   Virtual reality flight   Virtual real	p 298 A95-73568 ol display with spherical orientation p 288 N95-22578 of a resin film mulation model for sites p 301 N95-23179 nputation of viscous rodynamics p 263 A95-73461 hypersonic viscous p 266 A95-73552 ver solutions for p 306 A95-73556 hod for unsteady p 308 A95-7578 minimum-drag body p 308 A95-76660 ts in computational visitions on generic M code p 273 N95-23185 ft navigation
Flow structure in the wake of a wishbone vortex generator [BTN-95-EIX95142553044] p 304 A95-73454 Separation control on high-lift airfoils via micro-vortex generators	Fourth-generation Mars vehicle col   BTN-95-EIX95152583267   VIRTUAL REALITY Virtual reality flight control six-degree-of-freedom controller and overlay   NASA-CASE-NPO-18733-1-CU   VISCOSITY  Development and verification infusion/resin transfer molding sifabrication of advanced textile compote   NASA-CR-197439   VISCOUS FLOW  Laplace interaction law for the control flow in low- and high-speed aeright   Size   Nasa-CR-197439   VISCOUS FLOW  Laplace interaction law for the control flow in low- and high-speed aeright   Size   Nasa-CR-197439   VISCOUS FLOW  Laplace interaction law for the control flow in low- and high-speed aeright   Size   Size   Size     BTN-95-EIX95142553037   Aerodynamic characteristics of a optimized waverider at high altitudes   BTN-95-EIX95152583255   Viscous-inviscid interaction met low-speed airol flows     BTN-95-EIX95182619093     CFD optimization of a theoretical   BTN-95-EIX95182619034     An assessment of viscous effective wind-tunnel models using TEA   NASA-CR-4650     NASA-CR-4650     VISUAL SIGNALS     Cueing light configuration for aircraft   NASA-CASE-ARC-11982-1     VORTEX BREAKDOWN	p 298 A95-73568 ol display with spherical orientation p 288 N95-22578 of a resin film mulation model for sites p 301 N95-23179 nputation of viscous rodynamics p 263 A95-73461 hypersonic viscous p 266 A95-73552 ter solutions for p 306 A95-73556 hod for unsteady p 269 A95-7578 minimum-drag body p 308 A95-76660 test in computational ex flows on generic M code p 273 N95-23185 ft navigation p 280 N95-23393
Flow structure in the wake of a wishbone vortex generator [BTN-95-EIX95142553044] p 304 A95-73454 Separation control on high-lift airfoils via micro-vortex generators	Fourth-generation Mars vehicle col   BTN-95-EIX95152583267   VIRTUAL REALITY Virtual reality flight control six-degree-of-freedom controller and overlay   INASA-CASE-NPO-18733-1-CU   VISCOSITY Development and verification infusion/resin transfer molding sifabrication of advanced textile compo   INASA-CR-197439   VISCOSITY Development and verification infusion/resin transfer molding sifabrication of advanced textile compo   INASA-CR-197439   VISCOUS FLOW   Laplace interaction law for the con airfoil flow in low- and high-speed aer   IBTN-95-EIX95142553037   Aerodynamic characteristics of a optimized waverider at high altitudes   IBTN-95-EIX951425832251   Higher-order viscous shock-lay high-altitude flows   IBTN-95-EIX95152632255   Viscous-inviscid interaction met low-speed airfoil flows   IBTN-95-EIX95182619031   CFD optimization of a theoretical   IBTN-95-EIX95182619234   An assessment of viscous effects in the latitude of latitude	p 298 A95-73568 ol display with spherical orientation p 288 N95-22578 of a resin film mulation model for sites p 301 N95-23179 nputation of viscous rodynamics p 263 A95-73461 hypersonic viscous p 266 A95-73552 ter solutions for p 306 A95-73556 hod for unsteady p 269 A95-7578 minimum-drag body p 308 A95-76660 test in computational ex flows on generic M code p 273 N95-23185 ft navigation p 280 N95-23393
generator   BTN-95-EIX95142553044   p 304 A95-73454   Separation control on high-lift airfoils via micro-vortex generators	Fourth-generation Mars vehicle col   BTN-95-EIX95152583267   VIRTUAL REALITY   Virtual reality flight control six-degree-of-freedom controller and overlay   NASA-CASE-NPO-18733-1-CU   VISCOSITY   Development and verification infusion/resin transfer molding sitabrication of advanced textile compote   NASA-CR-197439   VISCOUS FLOW   Laplace interaction law for the control flow in low- and high-speed aer   BTN-95-EIX95142553037   Aerodynamic characteristics of a optimized waverider at high altitudes   BTN-95-EIX95152583251   Higher-order viscous shock-lay high-altitude flows   BTN-95-EIX95152583255   Viscous-inviscid interaction met low-speed airfoil flows   BTN-95-EIX95182619234   An assessment of viscous effect simulation of benign and burst vorte fighter wind-tunnel models using TEA   NASA-CR-4650   VISUAL SIGNALS   Cueing light configuration for aircra   NASA-CASE-ARC-11982-1   VORTEX BREAKDOWN   Transient structure of vortex breaking   BTN-95-EIX95182619273	p 298 A95-73568 ol display with spherical orientation p 288 N95-22578 of a resin film mulation model for sites p 301 N95-23179 nputation of viscous rodynamics p 263 A95-73461 hypersonic viscous p 266 A95-73552 rer solutions for p 306 A95-73556 hod for unsteady p 269 A95-7778 minimum-drag body p 308 A95-76660 ots in computational ext flows on generic M code p 273 N95-23185 ft navigation p 280 N95-23393 kdown on a delta
[BTN-95-EIX95142553044] p 304 A95-73454 Separation control on high-lift airfoils via micro-vortex generators	Fourth-generation Mars vehicle col   BTN-95-EIX95152583267   VIRTUAL REALITY Virtual reality flight control six-degree-of-freedom controller and overlay   INASA-CASE-NPO-18733-1-CU   VISCOSITY Development and verification infusion/resin transfer molding sifabrication of advanced textile compo   INASA-CR-197439   VISCOUS FLOW Laplace interaction law for the con airfoil flow in low- and high-speed aer   BTN-95-EIX95142553037   Aerodynamic characteristics of a optimized waverider at high altitudes   BTN-95-EIX951425832251   Higher-order viscous shock-lay high-altitude flows   BTN-95-EIX9515263255   Viscous-inviscid interaction met low-speed airfoil flows   BTN-95-EIX95182619093   CFD optimization of a theoretical   BTN-95-EIX95182619234   An assessment of viscous effects of the product of the production of the product of the production of the produc	p 298 A95-73568 ol display with spherical orientation p 288 N95-22578 ol a resin film mulation model for sites p 301 N95-23179 reputation of viscous rodynamics p 266 A95-73552 rer solutions for unsteady p 306 A95-73556 hod for unsteady p 308 A95-76660 ts in computational set flows on generic M code p 273 N95-23185 ft navigation p 280 N95-23393 kdown on a detta
Separation control on high-lift airfoils via micro-vortex generators	Fourth-generation Mars vehicle col   BTN-95-EIX95152583267   VIRTUAL REALITY  Virtual reality flight control is vicegree-of-freedom controller and overlay   INASA-CASE-NPO-18733-1-CU   VISCOSITY  Development and verification infusion/resin transfer molding si fabrication of advanced textile compty   INASA-CR-197439   VISCOUS FLOW  Laplace interaction law for the condition infusion infusi	p 298 A95-73568 ol display with spherical orientation p 288 N95-22578 ol a resin film mulation model for sites p 301 N95-23179 reputation of viscous rodynamics p 266 A95-73552 rer solutions for unsteady p 306 A95-73556 hod for unsteady p 308 A95-76660 ts in computational set flows on generic M code p 273 N95-23185 ft navigation p 280 N95-23393 kdown on a detta
generators	Fourth-generation Mars vehicle col   BTN-95-EIX95152583267   VIRTUAL REALITY  Virtual reality flight control six-degree-of-freedom controller and overlay   NASA-CASE-NPO-18733-1-CU   VISCOSITY  Development and verification infusion/resin transfer molding sitabrication of advanced textile compty [NASA-CR-197439   VISCOUS FLOW  Laplace interaction law for the control infolion in low- and high-speed aeightn-95-EIX95142553037   Aerodynamic characteristics of a optimized waverider at high altitudes   BTN-95-EIX95152583251   Higher-order viscous shock-lay high-altitude flows   BTN-95-EIX95152583255   Viscous-inviscid interaction met low-speed airfoil flows   BTN-95-EIX95182619234   JRTN-95-EIX95182619234   An assessment of viscous effect simulation of benign and burst vorte fighter wind-tunnel models using TEA   NASA-CR-4650   VISUAL SIGNALS  Cueing light configuration for aircra   NASA-CR-4650   VISUAL	p 298 A95-73568 ol display with spherical orientation p 288 N95-22578 of a resin film mulation model for sites p 301 N95-23179 nputation of viscous rodynamics p 263 A95-73461 hypersonic viscous p 266 A95-73552 ver solutions for p 306 A95-73556 hod for unsteady p 269 A95-75778 minimum-drag body p 308 A95-76660 ts in computational ex flows on generic M code p 273 N95-23185 ft navigation p 280 N95-23393 kdown on a delta p 268 A95-75758 a wishbone vortex
[BTN-95-EIX95152582326] D 265 A95-73529	Fourth-generation Mars vehicle col   BTN-95-EIX95152583267   VIRTUAL REALITY Virtual reality flight control   six-degree-of-freedom controller and overlay   NASA-CASE-NPO-18733-1-CU   VISCOSITY Development and verification infusion/resin transfer molding si fabrication of advanced textile compo     NASA-CR-197439   VISCOUS FLOW Laplace interaction law for the con airfoil flow in low- and high-speed ae     BTN-95-EIX95142553037     Aerodynamic characteristics of a optimized waverider at high altitudes     BTN-95-EIX95142553037     Aerodynamic characteristics of a optimized waverider at high altitudes     BTN-95-EIX95152832251     Higher-order viscous shock-lay high-altitude flows     BTN-95-EIX95182632351     Viscous-inviscid interaction met low-speed airfoil flows     BTN-95-EIX95182619031     CFD optimization of a theoretical     BTN-95-EIX95182619234     An assessment of viscous effect     An assessment of viscous effect     BTN-95-EIX95182619234     An assessment of viscous effect     BTN-95-EIX95182619231     CFD optimization of a theoretical     BTN-95-EIX95182619234     STN-95-EIX95182619234     An assessment of viscous effect     BTN-95-EIX95182619234     An assessment of viscous effect     BTN-95-EIX95182619234     An assessment of viscous effect     BTN-95-EIX95182619234     An assessment of viscous effect     BTN-95-EIX95182619073     CORTEX BREAKDOWN     Transient structure of vortex breaking     BTN-95-EIX95182619073     CORTEX GENERATORS     Flow structure in the wake of generator     BTN-95-EIX95182553044	p 298 A95-73568 ol display with spherical orientation p 288 N95-22578 ol a resin film mulation model for sistes p 301 N95-23179 reputation of viscous rodynamics p 263 A95-73461 hypersonic viscous p 266 A95-73552 ver solutions for p 306 A95-73556 hod for unsteady p 308 A95-7660 ts in computational viscous minimum-drag body p 308 A95-7660 ts in computational visitous on generic M code p 273 N95-23185 ft navigation p 280 N95-23393 kdown on a delta p 268 A95-75758 a wishbone vortex p 304 A95-73454
ORTEX LATTICE METHOD	Fourth-generation Mars vehicle col   BTN-95-EIX95152583267   VIRTUAL REALITY  Virtual reality flight control six-degree-of-freedom controller and overlay   NASA-CASE-NPO-18733-1-CU   VISCOSITY  Development and verification infusion/resin transfer molding sitabrication of advanced textile compty   NASA-CR-197439   VISCOUS FLOW  Laplace interaction law for the control info in low and high-speed aeightn-95-EIX95142553037   Aerodynamic characteristics of a optimized waverider at high altitudes   BTN-95-EIX95152583251   Higher-order viscous shock-lay high-altitude flows   BTN-95-EIX95152583251   Viscous-inviscid interaction met low-speed airfoil flows   BTN-95-EIX95182619234   An assessment of viscous effecting   BTN-95-EIX95182619234   An assessment of viscous effecting   NASA-CR-4650   VISUAL SIGNALS  Cueing light configuration for aircra   NASA-CR-4650   VISUAL SIGNALS  Cueing light configuration fo	p 298 A95-73568 ol display with spherical orientation p 288 N95-22578 of a resin film mulation model for sites p 301 N95-23179 nputation of viscous rodynamics p 263 A95-73461 hypersonic viscous p 266 A95-73552 ver solutions for p 306 A95-73556 hod for unsteady p 269 A95-7578 minimum-drag body p 308 A95-76660 ts in computational ex flows on generic M code p 273 N95-23185 ff navigation p 280 N95-23393 kdown on a delta p 268 A95-75758 a wishbone vortex p 304 A95-73454 olis via micro-vortex

Sidewash on the vertical tail in subsonic and supersonic

Static aeroelastic characteristics of a composite win [BTN-95-EIX95152582340] p 282 A95-7354

p 264 A95-73519

p 282 A95-73542

[BTN-95-EIX95152582316]

ORTICES	
Flow structure in the wake of a generator	wishbone vortex
	304 A95-73454
of vortical flowfields	
[BTN-95-EIX95152577604] Experimental investigation of the f	305 A95-73479 Sowfield about an
upswept afterbody	265 A95-73524
Navier-Stokes prediction of large-am	
	281 A95-73531
Forebody flow control on a full-sca [BTN-95-EIX95152582333] p	le F/A-18 aircraft 281 A95-73535
Pneumatic concept for tip-stall contro	
• • • • • • • • • • • • • • • • • • • •	281 A95-73537
Effect of leeward flow dividers on the delta wing	ne wing rock of a
[BTN-95-EIX95152582347] p Transient structure of vortex breaks	282 A95-73549
wing	
BTN-95-EIX95182619073  p Numerical study of sound generation	268 A95-75758 due to a spinning
vortex pair  BTN-95-EIX95182619075  p	307 A95-75760
Diurnal variation of lee vortices in	
	318 A95-76394
Influence of streamwise curvature vortices imbedded in turbulent boundar	
[BTN-94-EIX94401378820] p Euler technology assessment for p	307 A95-76489
design employing OVERFLOW code	
	273 N95-23095
<ul> <li>An assessment of viscous effects simulation of benign and burst vortex</li> </ul>	
fighter wind-tunnel models using TEAM	
Crossflow instability control on a swep	t-wing: Preliminary
studies p Preliminary identification of buffet prob	274 N95-23283 lems in high speed
civil transport p Aerodynamic surface distension syst	294 N95-23319 em for high angle
of attack forebody vortex control	286 N95-23390
Three-dimensional Navier-Stokes ana	lysis and redesign
of an imbedded bellmouth nozzle in a inlet section p	311 N95-23423
A study of the vortex flow over 76/40 wing	-deg double-delta
[NASA-CR-195032] p	314 N95-23466
ULNERABILITY  Rationale for the Modular Air-syst	
Estimation Network (MAVEN) methodol AD-A285797   p	ogy 284 N95-22510
w	
AKES	
Experimental investigation of the fupswept afterbody	lowfield about an
[BTN-95-EIX95152582321] p	265 A95-73524
Separation control on high-lift airfoils generators	
[BTN-95-EIX95152582326] p Hypersonic rarefied flow past sphere	265 A95-73529
structure	-
ALL FLOW	305 A95-73551
Main features of overexpanded triple [BTN-95-EIX95142553040] p	jets 304 A95-73458
Effects of expansions on a superson	
Surface pressure measurements [BTN-95-EIX95142553036] p	263 A95-73462
Charles of the standard according to the	

p 265	A95-73524
airloils via	micro-vorte
- 265	A95-73529
•	cluding wake
р 305	A95-73551
triple jets	
	airfoils via p 265 spheres inc p 305

visualization studies two-dimensional transonic airfoil testing [BTN-95-EIX95152582313] p 264 A95-73516 Moving wall effect in relation to other dynamic stall flow

p 265 A95-73527 [BTN-95-EIX95152582324] Application of wall functions to generalized nonorthogonal curvilinear coordinate systems

[BTN-95-EIX95182619077] p 307 A95-75762 Observations on using experimental data as boundary conditions for computations [BTN-95-EIX95182619103] p 321 A95-76588

A wall interference assessment/correction system p 309 N95-23183 [NASA-CR-197421] WALL PRESSURE

A wall interference assessment/correction system [NASA-CR-197421] p 309 N95-23183

WIND TUNNEL TESTS Study of the droplet spray characteristics of a subsonic wind tunnel p 271 A95-76661 IBTN-95-EIX951826192351 Airborne rotary air separator study p 290 N95-24053 INASA-CR-1890991 WATER TABLES Simple method of supersonic flow visualization using watertable [BTN-95-EIX95182619105] p 269 A95-76590 WAVE SCATTERING SEM representation of the early and late time fields scattered from wire targets p 306 A95-74496 | BTN-94-EIX94381353142 | WAVELENGTHS Geoid lineations of 1000 km wavelength over the central Pacific [HTN-95-11304] p 319 A95-77009 WAVERIDERS Aerodynamic characteristics of a hypersonic viscous optimized waverider at high altitudes |BTN-95-EIX95152583251| p 266 A95-73552 Integrated design of hypersonic waveriders including inlets and taillins |BTN-95-EIX95212645692| p 271 A95-76744 **WEAPON SYSTEMS** Improved version of the Naval Surface Warfare Center aeroprediction code (AP93) |BTN-95-EIX95152583260| n 267 A95-73561 WEAR TESTS Evaluation of thermal barrier and PS-200 self-lubricating coatings in an air-cooled rotary engine [NASA-CR-195445] p 289 N95-23222 WEATHER FORECASTING Pilot Weather Advisor system [BTN-95-EIX95152582314] p 316 A95-73517 WEIGHT REDUCTION Minimum-mass design of sandwich aerobrakes for a tunar transfer vehicle p 299 A95-76759 IRTN-95-FIX952126457071 WEIGHTING FUNCTIONS On-line, adaptive state estimator for active noise control p 322 N95-23308 WENTZEL-KRAMER-BRILLOUIN METHOD Analytical study of the neutral stability of a model hypersonic boundary layer |BTN-95-EIX95152577589| p 263 A95-73493 WIND SHEAR Optimal lateral-escape maneuvers for microburst ncounters during final approach IBTN-95-EIX95182619127 | p 276 A95-76604 Maximum-likelihood spectral estimation and adaptive filtering techniques with application to airborne Doppler weather radar [NASA-CR-197699] p 316 N95-23670 WIND TUNNEL APPARATUS Time-of-flight mass spectrometer for impulse facilities [BTN-95-EIX95142553057] p 262 A95-73441 WIND TUNNEL MODELS Application of transonic small disturbance theory to the IBTN-95-EIX951826192101 n 270 A95-76636 Multiple-function digital controller system for active flexible wing wind-tunnel model [BTN-95-EIX95182619212] p 322 A95-76638 Flutter suppression control law design and testing for the active flexible wing |BTN-95-EIX95182619214| p 292 A95-76640 Design and multifunction tests of a frequency domain-based active flutter suppression system [BTN-95-EIX95182619215] p 292 A95-76641 Flutter suppression for the active flexible wing: A classical design [BTN-95-EIX95182619216] p 292 A95-76642 Dynamic response tests of inertial and optical wind-tunnel model attitude measurement devices | NASA-TM-109182 | p 296 N95-23011 WIND TUNNEL NOZZLES Optimized design of a hypersonic nozzle p 297 N95-23304 Three-dimensional Navier-Stokes analysis and redesign of an imbedded bellmouth nozzle in a turbine cascade p 311 N95-23423 Supersonic laminar flow control research [NASA-CR-197938] p 275 p 275 N95-23669

WIND TUNNEL TESTS

[BTN-95-EIX95152582326]

blade vortex interaction noise

BTN-95-EIX95152582330 |

generators

Main features of overexpanded triple jets [BTN-95-EIX95142553040] p 304 A95-73458

Separation control on high-lift airfoils via micro-vortex

Analysis of a higher harmonic control test to reduce

Forebody flow control on a full-scale F/A-18 aircraft | BTN-95-EIX95152582333 | p 281 A95-73535

p 265 A95-73529

p 265 A95-73532

p 281 A95-73535

Effect of underwing frost on a transport aircraft airfoil at flight Reynolds number p 276 A95-73536 IBTN-95-FIX951525823341 Pneumatic concept for tip-stall control of cranked-arrow p 281 A95-73537 IBTN-95-EIX951525823351 Flow study of supersonic wing-nacelle configuration |BTN-95-EIX95152582344| p 266 A95-73546 Computational study of plume-induced separation on a hypersonic powered model IBTN-95-EIX951525823461 p 266 A95-73548 Base drag prediction on missile configurations p 266 A95-73557 IBTN-95-EIX951525832561 Aerodynamic characteristics of a canard-controlled missile at high angles of attack IBTN-95-EIX95152583257 I p 267 A95-73558 Some aspects of the aerodynamics of separating IBTN-95-EIX951826174641 n 298 A95-75735 Comparison of linear stability results with flight transition |BTN-95-EIX95182619097| p 283 A95-76582 Effect of ambient turbulence intensity on sphere wakes at intermediate Reynolds numbers p 308 A95-76586 IBTN-95-EIX951826191011 Observations on using experimental data as boundary conditions for computations p 321 A95-76588 IBTN-95-EIX951826191031 Simulation and model reduction for the active flexible ing program IBTN-95-EIX951826192111 p 295 A95-76637 On-line analysis capabilities developed to support the active flexible wing wind-tunnel tests p 296 A95-76639 IBTN-95-EIX95182619213 | Flutter suppression control law design and testing for the active flexible wind BTN-95-EIX95182619214 | p 292 A95-76640 Design and multifunction tests of a frequency domain-based active flutter suppression.system IBTN-95-EIX951826192151 p 292 A95-76641 Flutter suppression for the active flexible wing: A classical design [BTN-95-EIX95182619216] p 292 A95-76642 Rolling maneuver load alleviation using active controls [BTN-95-EIX95182619217] p 270 A95-76643 Dynamic investigation of the angular motion of a rotating body-parachute system [BTN-95-EIX95182619220] p 270 A95-76646 Natural laminar flow wing concept for supersonic transports [BTN-95-EIX95182619226] p 308 A95-76652 Aerodynamic characteristics of external store configurations at low speeds IBTN-95-EIX951826192301 n 271 A95-76656 Study of the droplet spray characteristics of a subsonic IBTN-95-EIX951826192351 p 271 A95-76661 Laser velocimetry seed-particle behavior in shear layers IBTN-95-EIX952126457121 p 272 A95-76764 Wing pressure distributions from subsonic tests of a high-wing transport model --- in the Langley 14- by 22-Foot Subsonic Wind Tunnel [NASA-TM-4583] p 272 N95-22802 Dynamic response tests of inertial and optical wind-tunnel model attitude measurement devices |NASA-TM-109182| p 296 N95-23011 Experimental results for a hypersonic nozzle/afterbody flow field p 274 N95-23250 INASA-TM-46381 Performance of the 0.3-meter transpric cryogenic tunnel with air, nitrogen, and sulfur hexafluoride media under closed loop automatic control INASA-CR-1950521 p 310 N95-23257 Crossflow instability control on a swept-wing: Preliminary studies p 274 N95-23283 Preliminary identification of buffet problems in high speed ivil transport p 294 N95-23319 A study of the vortex flow over 76/40-deg double-delta wing p 314 N95-23466 I NASA-CR-195032 I WIND TUNNEL WALLS A wall interference assessment/correction system INASA-CR-197421 | p 309 N95-23183 WIND TUNNELS

NTS-spill test facility wind tunnel exhaust plume

NTS-spill test facility wind tunnel exhaust plume

Stability derivatives of a flapped plate in unsteady ground

p 297 N95-24019

p 297 N95-24019

p 270 A95-76651

WING LOADING Summary of an active flexible wing program [BTN-95-EIX95182619209] p 283 A95-76635 Multiple-function digital controller system for active flexible wing wind-tunnel model [BTN-95-EIX95182619212] Rolling maneuver load alleviation using active controls p 270 A95-76643 |BTN-95-EIX95182619217| Aerodynamics of a finite wing with simulated ice LBTN-95-FIX95182619227 L p 270 A95-76653 WING NACELLE CONFIGURATIONS Flow study of supersonic wing-nacelle configuration |BTN-95-EIX95152582344| p 266 A95-73546 Eigenanalysis of unsteady flows about airfoils, cascades, and wings p 305 A95-73486 [BTN-95-EIX95152577597] Sidewash on the vertical tail in subsonic and supersonic p 264 A95-73519 IBTN-95-EIX951525823161 Nonlinear angle of twist of advanced composite wing boxes under pure torsion [BTN-95-EIX95152582323] p 281 A95-73526 Moving wall effect in relation to other dynamic stall flow mechanisms IBTN-95-EIX951525823241 p 265 A95-73527 Study of an airfoil with a flap and spoiler p 265 A95-73530 [BTN-95-EIX95152582327] Effect of underwing frost on a transport aircraft airfoil at flight Revnolds number [BTN-95-EIX95152582334] p 276 A95-73536 Pneumatic concept for tip-stall control of cranked-arrow IBTN-95-EIX951525823351 p 281 A95-73537 Method for the prediction of the onset of wing rock | BTN-95-EIX95152582342 | p 282 A95-73544 Multirate flutter suppression system design for a model [BTN-95-EIX95182619132] p 292 A95-76609 Application of Navier-Stokes aeroelastic methods to improve fighter wing maneuver performance p 284 A95-76644 1BTN-95-EIX951826192181 Calculation of wing-alone aerodynamics to high angles of attack [BTN-95-EIX95212645713] p 261 A95-76765 Wing pressure distributions from subsonic tests of a high-wing transport model --- in the Langley 14- by 22-Foot Subsonic Wind Tunnel p 272 . N95-22802 INASA-TM-45831 Control of flow separation in airfoil/wing design oplications p 274 N95-23294 applications High-lift flow-physics flight experiments on a subsonic p 275 N95-23333 civil transport aircraft (B737-100) Lift enhancing tabs for airfoils p 286 N95-23395 INASA-CASE-ARC-11990-11 WIRE SEM representation of the early and late time fields scattered from wire targets [BTN-94-EIX94381353142] p 306 A95-74496 WOVEN COMPOSITES Idealized textile composites for experimental/analytical corretation p 301 N95-23277 X X RAY INSPECTION POD assessment of NDI procedures using a round robin [AGARD-R-809] p 315 N95-23602 X-29 AIRCRAFT Flight test of the X-29A at high angle of attack: Flight

dynamics and controls [NASA-TP-3537] p 284 N95-22806

YAW Forebody flow control on a full-scale F/A-18 aircraft p 281 A95-73535 [BTN-95-EIX95152582333] Method for the prediction of the onset of wing rock [BTN-95-EIX95152582342] p 282 A95-73544 Feedback control laws for highly maneuverable aircraft [NASA-CR-197944] p 295 N95-23410 YAWING MOMENTS

Forebody flow control on a full-scale F/A-18 aircraft p 281 A95-73535 BTN-95-EIX95152582333] YE-16 AIRCRAFT

Robustly stable preliminary control systems design for the YF-16 CCV aircraft |BTN-95-EIX95202637608| p 292 A95-76681

Evolution of oxidation and creep damage mechanisms in HIPed silicon nitride materials [DE95-001360] p 300 N95-22689

characterization

characterization

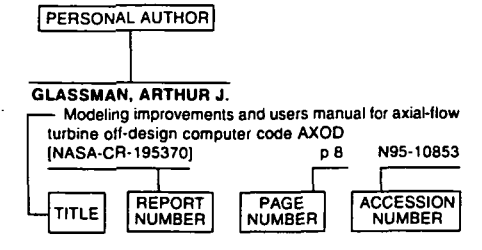
I DE95-003630 I

IBTN-95-EIX951826192251

WING FLAPS

WIND VELOCITY

## **Typical Personal Author Index Listing**



Listings in this index are arranged alphabetically by personal author. The title of the document is used to provide a brief description of the subject matter. The report number helps to indicate the type of document (e.g., NASA report, translation, NASA contractor report). The page and accession numbers are located beneath and to the right of the title. Under any one author's name the accession numbers are arranged in sequence.

### AARONSON, PHILIP

CFD optimization of a theoretical minimum-drag body IBTN-95-EIX95182619234 p 308 A95-76660

## AREL JONATHAN

On the exact solutions of pseudorange equations |BTN-95-EIX95142555477| p 278 A95-73433

### ABUSALI, P. A. M.

Thermal force modeling for global positioning system satellites using the finite element method [BTN-95-EIX95152583270] p 278 A95-73571

### ACHARYA, A.

Airborne rotary air separator study

### [NASA-CR-189099] p 290 N95-24053

ADAMS, DANIEL O. Idealized textile composites for experimental/analytical

### correlation

p 301 N95-23277 ADAMS, WILLIAM M., JR.

Design and multifunction tests of a frequency domain-based active flutter suppression system [BTN-95-EIX95182619215] p 292 A95-76641

### ADELMAN, HOWARD M.

Integrated aerodynamic/dynamic/structural optimization of helicopter rotor blades using multilevel

decomposition INASA-TP-34651 p 285 N95-22953 AGARWALA, V. S.

### Corrosion detection and monitoring of aircraft structures

p 303 N95-23515 An overview AKIYAMA, HIROMITSU

Polar Patrol Balloon IBTN-95-EIX95152582318 I p 316 A95-73521

## AL-GARNI, AHMED Z.

Analytical solution for controls, heats, and states of flight

(BTN-95-FIX95152583286) p 282 A95-73587

### ALIGHANBARI, H.

Postinstability behavior of a two-dimensional airfoil with structural nonlinearity IBTN-95-FIX951525823371 p 266 A95-73539

## ALMSTED, LARRY D.

Flight test evaluation of a 35 GHz forward looking altimeter for terrain avoidance

[BTN-95-EIX95212641071] p 287 A95-76736

### AMBUR, DAMODAR R.

Experimental evaluation of a box beam specifically tailored for chordwise deformation [BTN-95-EIX95182619088] n 283 A95-75773

### ANDERSON, MARK R.

Drag function modeling for air traffic simulation p 279 A95-76631

### APONSO, BIMAL L.

Identification of higher order helicopter dynamics using linear modeling methods

p 290 A95-75093

p 312 N95-23436

p 263 A95-73495

n 317 A95-76265

p:286 A95-73451

### IHTN-95-80851 I

APPLIN, ZACHARY T. Wing pressure distributions from subsonic tests of a high-wing transport model

NASA-TM-45831 p 272 N95-22802

### ARNETTE, STEPHEN A.

Effects of expansions on a supersonic boundary laver: Surface pressure measurements [BTN-95-EIX95142553036] p 263 A95-73462

ARNOLD, F.

Laplace interaction law for the computation of viscous airfoil flow in low- and high-speed aerodynamics

[BTN-95-EIX95142553037] p 263 A95-73461

### ASCOLI, EDWARD P.

CFD analysis of turbopump volutes

### ASLAN A R

characteristics of external store Aerodynamic configurations at low speeds

IBTN-95-EIX951826192301 p 271 A95-76656 ATALLA, NOUREDDINE Coupled FEM-BEM approach for mean flow effects on vibro-acoustic behavior of planar structures

BTN-95-EIX95152577587 ATLAS, E. L.

Estimates of total organic and inorganic chlorine in the lower stratosphere from in situ and flask measurements during AASE 2

### [HTN-95-A0861]

ATLURI, SATYA N. Growth of multiple cracks and their linkup in a fuselage

IBTN-95-EIX951425530471 AUSLENDER, A. H.

Optimization of contoured hypersonic scramjet inlets with a least-squares parabolized procedure Navier-Stokes p 261 A95-74042

HTN-95-20976 I

AYDIN, N. H. Aerodynamic characteristics of external store

configurations at low speeds [BTN-95-EIX95182619230] p 271 A95-76656

### BACON, BARTON

Simulation and model reduction for the active flexible ng program

## BAILLIE, STEWART

IBTN-95-FIX951826192111 p 295 A95-76637

Improving prediction: The incorporation of simplified

rotor dynamics in a mathematical model of the bell

## IBTN-95-EIX951525846791

p 282 A95-73591 BALAKRISHNA, S.

Performance of the 0.3-meter transonic cryogenic tunnel with air, nitrogen, and sulfur hexafluoride media under closed loop automatic control [NASA-CR-195052] p 310 N95-23257

### BALAS, GARY J.

Feedback control laws for highly maneuverable

### INASA-CR-1979441 BANG, ERIC S.

### Flight-deck displays on the Boeing 777 p 286 A95-73438 IBTN-95-EIX951425624021

BARING, T. J. Estimates of total organic and inorganic chlorine in the lower stratosphere from in situ and flask measurements

[HTN-95-A0861]

p 317 A95-76265

p 295 N95-23410

### BARONTI, S.

MAX-91: Polarimetric SAR results on Montespertoli p 320 N95-23940

### BARTLETT, D. L.

The corrosion and protection of advanced aluminium p 302 N95-23497 lithium airframe alloys

BATY, ROY S. Functional dependence of trajectory dispersion on initial

condition errors |BTN-95-EIX95152583263| p 298 A95-73564

BAUCHAU, OLIVIER A. Dynamic analysis of bearingless tail rotor blades based

on nonlinear shell modes IBTN-95-FIX951525823381 p 281 A95-73540

BAUER, JEFFREY E.

Flight test of the X-29A at high angle of attack: Flight dynamics and controls p 284 N95-22806

BAYSAL, OKTAY Aerodynamic shape optimization using preconditioned conjugate gradient methods

IBTN-95-EIX951425530331 p 263 A95-73465 Preconditioned domain decomposition scheme for ree-dimensional aerodynamic sensitivity analysis

IRTN-95-EIX951525776121 p 321 A95-73471 A CFD study of complex missile and store configurations

INASA-CR-1979121 D 285 N95-22949 Aerodynamic design optimization with sensitivity analysis and computational fluid dynamics INASA-CR-1974191 p 274 N95-23218

### BECKER, ROBERT C.

Flight test evaluation of a 35 GHz forward looking altimeter for terrain avoidance

BTN-95-EIX95212641071 ) p 287 A95-76736

## BECKMAN, BRIAN C.

flight control with reality display Virtual six-degree-of-freedom controller and spherical orientation p 288 N95-22578

[NASA-CASE-NPO-18733-1-CU] BELLINGER, N. C.

Double pass retroreflection for corrosion detection in p 323 N95-23503 aircraft structures

### BENDIKSEN, ODDVAR O.

Limit cycle phenomena in computational transonic [BTN-95-EIX951525823171 p 264 A95-73520

BENNETT, J. of F/A-18 operational flight

### Enhancement measurements: Data report for phase 1 IDSTO-TR-00491 p 286 N95-23666

BENNETT, ROBERT M. Application of transonic small disturbance theory to the

tive flexible wing model [BTN-95-EIX95182619210] p 270 A95-76636

### RENTS DAVID J. Design of a GaAs/Ge solar array for unmanned aerial

vehicles p 320 N95-23259

### BERG. MARTIN C. Multirate flutter suppression system design for a model

IBTN-95-EIX951826191321 p 292 A95-76609 BERRICHE, R.

Evaluation of advanced aerospace materials by depth sensing indentation and scratch methods

### [BTN-95-EIX95152584678] p 282 A95-73590 BERRY, L. A.

Cu deposition using a permanent magnet electron cyclotron resonance microwave plasma source [DE94-017768] p 304 N95-23981

### BHAGAT, P. K. Corrosion detection and monitoring of aircraft structures:

p 303 N95-23515 An overview RHAT THONSERS

Mach wave emission from a high-temperature IBTN-95-EIX951525775861 p 264 A95-73496

### BIBER, KASIM Flow study of supersonic wing-nacelle configuration [BTN-95-EIX95152582344] p 266 A95-73546

BIDWELL, COLIN S.	BROWN, ART	Effects of high order dynamics on helicopter flight control
Additional improvements to the NASA Lewis ice	Labs behind Boeing's new 777	law design LHTN-95-808521 p 290 A95-75094
accretion code LEWICE [NASA-TM-106849] p 309 N95-22669	BTN-95-EIX95142562403  p 280 A95-73437 BROWNE, G. T.	[HTN-95-80852] p 290 A95-75094 CHA, SOYOUNG S.
BIEZAD, DANIEL J.	US Navy operating experience with new aircraft	Holographic interferometric tomography for
Direct-lift design strategy for longitudinal control of	construction materials p 303 N95-23517	reconstructing flow fields p 310 N95-23287
hypersonic aircraft  BTN-95-EIX95182619131  p 291 A95-76608	BROZOWSKI, L. A. Impeller flow field characterization with a laser two-focus	CHADERJIAN, NEAL M.  Navier-Stokes prediction of large-amplitude delta-wing
BIRCH, STUART	velocimeter p 313 N95-23440	roll oscillations
Aircraft stripping and painting	BRUCE, DAVID A.	[BTN-95-EIX95152582329] p 281 A95-73531
[BTN-95-EIX95182617810] p 300 A95-75755	Non-destructive detection of corrosion for life	CHAFFEE, JAMES
BISWAS, K. K.  Some aspects of the aerodynamics of separating	management p 314 N95-23505 BUCH, A.	On the exact solutions of pseudorange equations [BTN-95-EIX95142555477] p 278 A95-73433
strap-ons	Review of some results of the author's fatigue	CHAN, DANIEL C.
BTN-95-EIX95182617464  p 298 A95-75735	investigations with applications in engineering and material	CFD analysis of turbopump volutes
BLANCHARD, ROBERT E.  Development of qualification guidelines for personal	science [TAE-698] p 316 N95-23662	p 312 N95-23436 CHANG, KEUN-SHIK
computer-based aviation training devices	BUEHRLE, R. D.	Three-dimensional structure of a supersonic jet
[DOT/FAA/AM-95/6] p 323 N95-23603	Dynamic response tests of inertial and optical	impinging on an inclined plate
BLANKEN, CHRIS L. Investigation of the effects of bandwidth and time delay	wind-tunnel model attitude measurement devices [NASA-TM-109182] p 296 N95-23011	[BTN-95-EIX95152583259] ρ 267 A95-73560 CHANG, STEPHEN
on helicopter roll-axis handling qualities	BUELOW, B. E. O.	Experimental evaluation of a box beam specifically
[HTN-95-80853] p 290 A95-75095	Convergence acceleration of implicit schemes in the	tailored for chordwise deformation
BODDY, MARK S.	presence of high aspect ratio grid cells p 313 N95-23446	[BTN-95-EIX95182619088] p 283 A95-75773
Empirical results on scheduling and dynamic backtracking p 299 N95-23761	BURCHAM, FRANK W.	CHATURVEDI, ARVIND K.  Aircraft fires, smoke toxicity, and survival: An overview
BOERING, K. A.	Engines-only flight control system	[DOT/FAA/AM-95/8] p 277 N95-24024
In situ observations in aircraft exhaust plumes in the	[NASA-CASE-ARC-11944-1] p 294 N95-23389	CHAVEZ, FRANK R.
lower stratosphere at midlatitudes [HTN-95-A0862] p 318 A95-76266	BURGREEN, GREG W.  Aerodynamic shape optimization using preconditioned	Analytical aeropropulsive/aeroelastic hypersonic-vehicle model with dynamic analysis
BOITNOTT, RICHARD L.	conjugate gradient methods	[BTN-95-EIX95182619138] p 269 A95-76615
An analytical and experimental investigation of the	[BTN-95-EIX95142553033] p 263 A95-73465	CHEN, GUANGREN
response of the curved, composite frame/skin	BURKEN, JOHN J.  Flight test of the X-29A at high angle of attack: Flight	Development of aeronautical mobile satellite services
specimens [HTN-95-80857] p 283 A95-75099	dynamics and controls	over the past thirty years [BTN-95-EIX95152569458] p 305 A95-73498
BOODEY, J. B.	NASA-TP-3537   p 284 N95-22806	CHEN, PS.
Corrosion of landing gear steels p 302 N95-23500	BURLEY, CASEY L.	High-performance parallel analysis of coupled problems
BOOTH, EARL R., JR.  Analysis of a higher harmonic control test to reduce	Sensitivity of acoustic predictions to variation of input parameters	for aircraft propulsion [NASA-CR-197440] p 289 N95-23088
blade vortex interaction noise	[HTN-95-80855] p 267 A95-75097	CHEN, Y. K.
[BTN-95-EIX95152582330] p 265 A95-73532	BURNER, A. W.	Hypersonic convective heat transfer over 140-deg blunt
BOSE, B. Simple method of supersonic flow visualization using	Dynamic response tests of inertial and optical wind-tunnel model attitude measurement devices	cones in different gases (BTN-95-EIX95152583253) p 306 A95-73554
watertable	[NASA-TM-109182] p 296 N95-23011	CHEN, YK.
[BTN-95-EIX95182619105] p 269 A95-76590	BUSTO, MARIO	Hypersonic nonequilibrium Navier-Stokes solutions over
BOWEN, BRENT D. The sisting quality report 1004	Nonlinear angle of twist of advanced composite wing boxes under pure torsion	an ablating graphite nosetip (BTN-95-EIX95152583252) p 305 A95-73553
The airline quality report, 1994 [NIAR-94-11] p 277 N95-24012	[BTN-95-EIX95152582323] p 281 A95-73526	[BTN-95-EIX95152583252] p 305 A95-73553 CHENG, VICTOR H. L.
BOWER, DANIEL R.	BUTTRILL, CAREY	Automatic guidance and control for helicopter obstacle
BOWER, DANIEL R.  Analytical study of the neutral stability of a model	Simulation and model reduction for the active flexible	Automatic guidance and control for helicopter obstacle avoidance
BOWER, DANIEL R.  Analytical study of the neutral stability of a model hypersonic boundary layer	BUTTRILL, CAREY Simulation and model reduction for the active flexible wing program	Automatic guidance and control for helicopter obstacle avoidance [BTN-95-EIX95182619130] p 291 A95-76607
BOWER, DANIEL R.  Analytical study of the neutral stability of a model	Simulation and model reduction for the active flexible	Automatic guidance and control for helicopter obstacle avoidance
BOWER, DANIEL R.  Analytical study of the neutral stability of a model hypersonic boundary layer [BTN-95-EIX95152577589] p 263 A95-73493 BOYD, D DOUGLAS, JR.  Analysis of a higher harmonic control test to reduce	Simulation and model reduction for the active flexible wing program [BTN-95-EIX95182619211] p 295 A95-76637	Automatic guidance and control for helicopter obstacle avoidance   BTN-95-EIX95182619130   p 291 A95-76607 CHERN, JIUN-DAR Diurnal variation of lee vortices in Taiwan and the surrounding area
BOWER, DANIEL R.  Analytical study of the neutral stability of a model hypersonic boundary layer  [BTN-95-EIX95152577589] p 263 A95-73493  BOYD, D. DOUGLAS, JR.  Analysis of a higher harmonic control test to reduce blade vortex interaction noise	Simulation and model reduction for the active flexible wing program [BTN-95-EIX95182619211] p 295 A95-76637	Automatic guidance and control for helicopter obstacle avoidance  [BTN-95-EIX95182619130] p 291 A95-76607  CHERN, JIUN-DAR  Diurnal variation of lee vortices in Taiwan and the surrounding area  [HTN-95-91363] p 318 A95-76394
BOWER, DANIEL R.  Analytical study of the neutral stability of a model hypersonic boundary layer [BTN-95-EIX95152577589] p 263 A95-73493 BOYD, D DOUGLAS, JR.  Analysis of a higher harmonic control test to reduce	Simulation and model reduction for the active flexible wing program [BTN-95-EIX95182619211] p 295 A95-76637	Automatic guidance and control for helicopter obstacle avoidance   BTN-95-EIX95182619130   p 291 A95-76607 CHERN, JIUN-DAR Diurnal variation of lee vortices in Taiwan and the surrounding area
BOWER, DANIEL R.  Analytical study of the neutral stability of a model hypersonic boundary layer  [BTN-95-EIX95152577589] p 263 A95-73493  BOYD, D. DOUGLAS, JR.  Analysis of a higher harmonic control test to reduce blade vortex interaction noise  [BTN-95-EIX95152582330] p 265 A95-73532  BOYD, IAIN  Particle kinetic simulation of high altitude hypervelocity	Simulation and model reduction for the active flexible wing program [BTN-95-EIX95182619211] p 295 A95-76637  C  CAI, TIMIN Simulation on the 3-D turbulent flow in the passages	Automatic guidance and control for helicopter obstacle avoidance  [BTN-95-EIX95182619130] p 291 A95-76607  CHERN, JIUN-DAR  Diurnal variation of lee vortices in Taiwan and the surrounding area  [HTN-95-91363] p 318 A95-76394  CHEUNG, BENNY K.  System for determining aerodynamic imbalance  [NASA-CASE-ARC-11913-1] p 311 N95-23377
BOWER, DANIEL R.  Analytical study of the neutral stability of a model hypersonic boundary layer  [BTN-95-EIX95152577589] p 263 A95-73493  BOYD, D. DOUGLAS, JR.  Analysis of a higher harmonic control test to reduce blade vortex interaction noise  [BTN-95-EIX95152582330] p 265 A95-73532  BOYD, IAIN  Particle kinetic simulation of high altitude hypervelocity flight	Simulation and model reduction for the active flexible wing program [BTN-95-EIX95182619211] p 295 A95-76637	Automatic guidance and control for helicopter obstacle avoidance  [BTN-95-EIX95182619130] p 291 A95-76607  CHERN, JIUN-DAR  Diurnal variation of lee vortices in Taiwan and the surrounding area  [HTN-95-91363] p 318 A95-76394  CHEUNG, BENNY K.  System for determining aerodynamic imbalance  [NASA-CASE-ARC-11913-1] p 311 N95-23377  CHEUNG, SAMSON
BOWER, DANIEL R.  Analytical study of the neutral stability of a model hypersonic boundary layer  [BTN-95-EIX95152577589] p 263 A95-73493  BOYD, D. DOUGLAS, JR.  Analysis of a higher harmonic control test to reduce blade vortex interaction noise  [BTN-95-EIX95152582330] p 265 A95-73532  BOYD, IAIN  Particle kinetic simulation of high altitude hypervelocity	Simulation and model reduction for the active flexible wing program  [BTN-95-EIX95182619211] p 295 A95-76637  C  CAI, TIMIN  Simulation on the 3-D turbulent flow in the passages of finocyl grain  [BTN-95-EIX95202638962] p 279 A95-76674  CALCAGNO, P.	Automatic guidance and control for helicopter obstacle avoidance [BTN-95-EIX95182619130] p 291 A95-76607  CHERN, JIUN-DAR  Diurnal variation of lee vortices in Taiwan and the surrounding area [HTN-95-91363] p 318 A95-76394  CHEUNG, BENNY K.  System for determining aerodynamic imbalance [NASA-CASE-ARC-11913-1] p 311 N95-23377  CHEUNG, SAMSON  CFD optimization of a theoretical minimum-drag body
BOWER, DANIEL R.  Analytical study of the neutral stability of a model hypersonic boundary layer  [BTN-95-EIX95152577589] p 263 A95-73493  BOYD, D. DOUGLAS, JR.  Analysis of a higher harmonic control test to reduce blade vortex interaction noise  [BTN-95-EIX95152582330] p 265 A95-73532  BOYD, IAIN  Particle kinetic simulation of high altitude hypervelocity flight  [NASA-CR-197383] p 309 N95-22481  BOZKURT, Y.  Aerodynamic characteristics of external store	Simulation and model reduction for the active flexible wing program [BTN-95-EIX95182619211] p 295 A95-76637  C  CAI, TIMIN Simulation on the 3-D turbulent flow in the passages of finocyl grain [BTN-95-EIX95202638962] p 279 A95-76674  CALCAGNO, P. Geoid lineations of 1000 km wavelength over the central	Automatic guidance and control for helicopter obstacle avoidance  [BTN-95-EIX95182619130] p 291 A95-76607  CHERN, JIUN-DAR  Diurnal variation of lee vortices in Taiwan and the surrounding area [HTN-95-91363] p 318 A95-76394  CHEUNG, BENNY K.  System for determining aerodynamic imbalance [NASA-CASE-ARC-11913-1] p 311 N95-23377  CHEUNG, SAMSON  CFD optimization of a theoretical minimum-drag body [BTN-95-EIX95182619234] p 308 A95-76660  CHIANG, WUYING
BOWER, DANIEL R.  Analytical study of the neutral stability of a model hypersonic boundary layer [BTN-95-EIX95152577589] p 263 A95-73493 BOYD, D. DOUGLAS, JR.  Analysis of a higher harmonic control test to reduce blade vortex interaction noise [BTN-95-EIX9515258230] p 265 A95-73532 BOYD, IAIN  Particle kinetic simulation of high altitude hypervelocity flight [NASA-CR-197383] p 309 N95-22481 BOZKURT, Y.  Aerodynamic characteristics of external store configurations at low speeds	Simulation and model reduction for the active flexible wing program  [BTN-95-EIX95182619211] p 295 A95-76637  C  CAI, TIMIN  Simulation on the 3-D turbulent flow in the passages of finocyl grain  [BTN-95-EIX95202638962] p 279 A95-76674  CALCAGNO, P.  Geoid lineations of 1000 km wavelength over the central Pacific	Automatic guidance and control for helicopter obstacle avoidance  [BTN-95-EIX95182619130] p 291 A95-76607  CHERN, JIUN-DAR  Diurnal variation of lee vortices in Taiwan and the surrounding area  [HTN-95-91363] p 318 A95-76394  CHEUNG, BENNY K.  System for determining aerodynamic imbalance  [NASA-CASE-ARC-11913-1] p 311 N95-23377  CHEUNG, SAMSON  CFD optimization of a theoretical minimum-drag body  [BTN-95-EIX95182619234] p 308 A95-76660  CHIANG, WUYING  Dynamic analysis of bearingless tail rotor blades based
BOWER, DANIEL R.  Analytical study of the neutral stability of a model hypersonic boundary layer  [BTN-95-EIX95152577589] p 263 A95-73493  BOYD, D. DOUGLAS, JR.  Analysis of a higher harmonic control test to reduce blade vortex interaction noise  [BTN-95-EIX95152582330] p 265 A95-73532  BOYD, IAIN  Particle kinetic simulation of high altitude hypervelocity flight  [NASA-CR-197383] p 309 N95-22481  BOZKURT, Y.  Aerodynamic characteristics of external store	Simulation and model reduction for the active flexible wing program [BTN-95-EIX95182619211] p 295 A95-76637  C  CAI, TIMIN Simulation on the 3-D turbulent flow in the passages of finocyl grain [BTN-95-EIX95202638962] p 279 A95-76674 CALCAGNO, P. Geoid lineations of 1000 km wavelength over the central Pacific [HTN-95-11304] p 319 A95-77009 CALDWELL, D. J.	Automatic guidance and control for helicopter obstacle avoidance  [BTN-95-EIX95182619130] p 291 A95-76607  CHERN, JIUN-DAR  Diurnal variation of lee vortices in Taiwan and the surrounding area [HTN-95-91363] p 318 A95-76394  CHEUNG, BENNY K.  System for determining aerodynamic imbalance [NASA-CASE-ARC-11913-1] p 311 N95-23377  CHEUNG, SAMSON  CFD optimization of a theoretical minimum-drag body [BTN-95-EIX95182619234] p 308 A95-76660  CHIANG, WUYING
BOWER, DANIEL R.  Analytical study of the neutral stability of a model hypersonic boundary layer [BTN-95-EIX95152577589] p 263 A95-73493 BOYD, D. DOUGLAS, JR.  Analysis of a higher harmonic control test to reduce blade vortex interaction noise [BTN-95-EIX9515258230] p 265 A95-73532 BOYD, IAIN  Particle kinetic simulation of high altitude hypervelocity flight [NASA-CR-197383] p 309 N95-22481 BOZKURT, Y.  Aerodynamic characteristics of external store configurations at low speeds [BTN-95-EIX95182619230] p 271 A95-76656 BRAGG, M. B.  Effect of underwing frost on a transport aircraft airfoil	Simulation and model reduction for the active flexible wing program  [BTN-95-EIX95182619211] p 295 A95-76637  C  CAI, TIMIN  Simulation on the 3-D turbulent flow in the passages of finocyl grain  [BTN-95-EIX95202638962] p 279 A95-76674  CALCAGNO, P.  Geoid lineations of 1000 km wavelength over the central Pacific  [HTN-95-11304] p 319 A95-77009  CALDWELL, D. J.  Modeling aerosol emissions from the combustion of	Automatic guidance and control for helicopter obstacle avoidance  [BTN-95-EIX95182619130] p 291 A95-76607  CHERN, JIUN-DAR  Diurnal variation of lee vortices in Taiwan and the surrounding area  [HTN-95-91363] p 318 A95-76394  CHEUNG, BENNY K.  System for determining aerodynamic imbalance  [NASA-CASE-ARC-11913-1] p 311 N95-23377  CHEUNG, SAMSON  CFD optimization of a theoretical minimum-drag body  [BTN-95-EIX95182619234] p 308 A95-76660  CHIANG, WUYING  Dynamic analysis of bearingless tail rotor blades based on nonlinear shell modes  [BTN-95-EIX95152582338] p 281 A95-73540  CHIU, CHYN-SHAN
BOWER, DANIEL R.  Analytical study of the neutral stability of a model hypersonic boundary layer [BTN-95-EIX95152577589] p 263 A95-73493 BOYD, D. DOUGLAS, JR.  Analysis of a higher harmonic control test to reduce blade vortex interaction noise [BTN-95-EIX95152582330] p 265 A95-73532 BOYD, IAIN  Particle kinetic simulation of high altitude hypervelocity flight [NASA-CR-197383] p 309 N95-22481 BOZKURT, Y.  Aerodynamic characteristics of external store configurations at low speeds [BTN-95-EIX95182619230] p 271 A95-76656 BRAGG, M. B.  Effect of underwing frost on a transport aircraft airfoil at flight Reynolds number	Simulation and model reduction for the active flexible wing program [BTN-95-EIX95182619211] p 295 A95-76637  C  CAI, TIMIN Simulation on the 3-D turbulent flow in the passages of finocyl grain [BTN-95-EIX95202638962] p 279 A95-76674 CALCAGNO, P. Geoid lineations of 1000 km wavelength over the central Pacific [HTN-95-11304] p 319 A95-77009 CALDWELL, D. J.	Automatic guidance and control for helicopter obstacle avoidance  [BTN-95-EIX95182619130] p 291 A95-76607  CHERN, JIUN-DAR  Diurnal variation of lee vortices in Taiwan and the surrounding area [HTN-95-91363] p 318 A95-76394  CHEUNG, BENNY K.  System for determining aerodynamic imbalance [NASA-CASE-ARC-11913-1] p 311 N95-23377  CHEUNG, SAMSON  CFD optimization of a theoretical minimum-drag body [BTN-95-EIX95182619234] p 308 A95-76660  CHIANG, WUYING  Dynamic analysis of bearingless tail rotor blades based on nonlinear shell modes [BTN-95-EIX95152582338] p 281 A95-73540  CHIJ, CHYN-SHAN  Sidewash on the vertical tail in subsonic and supersonic
BOWER, DANIEL R.  Analytical study of the neutral stability of a model hypersonic boundary layer  [BTN-95-EIX95152577589] p 263 A95-73493  BOYD, D. DOUGLAS, JR.  Analysis of a higher harmonic control test to reduce blade vortex interaction noise  [BTN-95-EIX95152582330] p 265 A95-73532  BOYD, IAIN  Particle kinetic simulation of high altitude hypervelocity flight  [NASA-CR-197383] p 309 N95-22481  BOZKURT, Y.  Aerodynamic characteristics of external store configurations at low speeds  [BTN-95-EIX95182619230] p 271 A95-76656  BRAGG, M. B.  Effect of underwing frost on a transport aircraft airfoil at flight Reynolds number  [BTN-95-EIX95152582334] p 276 A95-73536	Simulation and model reduction for the active flexible wing program  [BTN-95-EIX95182619211] p 295 A95-76637   C  CAI, TIMIN  Simulation on the 3-D turbulent flow in the passages of finocyl grain  [BTN-95-EIX95202638962] p 279 A95-76674  CALCAGNO, P.  Geoid lineations of 1000 km wavelength over the central Pacific  [HTN-95-11304] p 319 A95-77009  CALDWELL, D. J.  Modeling aerosol emissions from the combustion of composite materials p 301 N95-23038  CAPOTONDI, ANTONIETTA  Assimilation of altimeter data in a quasi-geostrophic	Automatic guidance and control for helicopter obstacle avoidance  [BTN-95-EIX95182619130] p 291 A95-76607  CHERN, JIUN-DAR  Diurnal variation of lee vortices in Taiwan and the surrounding area  [HTN-95-91363] p 318 A95-76394  CHEUNG, BENNY K.  System for determining aerodynamic imbalance  [NASA-CASE-ARC-11913-1] p 311 N95-23377  CHEUNG, SAMSON  CFD optimization of a theoretical minimum-drag body  [BTN-95-EIX95182619234] p 308 A95-76660  CHIANG, WUYING  Dynamic analysis of bearingless tail rotor blades based on nonlinear shell modes  [BTN-95-EIX95152582338] p 281 A95-73540  CHIU, CHYN-SHAN  Sidewash on the vertical tail in subsonic and supersonic flows
BOWER, DANIEL R.  Analytical study of the neutral stability of a model hypersonic boundary layer [BTN-95-EIX95152577589] p 263 A95-73493 BOYD, D. DOUGLAS, JR.  Analysis of a higher harmonic control test to reduce blade vortex interaction noise [BTN-95-EIX95152582330] p 265 A95-73532 BOYD, IAIN  Particle kinetic simulation of high altitude hypervelocity flight [NASA-CR-197383] p 309 N95-22481 BOZKURT, Y.  Aerodynamic characteristics of external store configurations at low speeds [BTN-95-EIX95182619230] p 271 A95-76656 BRAGG, M. B.  Effect of underwing frost on a transport aircraft airfoil at flight Reynolds number [BTN-95-EIX95152582334] p 276 A95-73536 Aerodynamics of a finite wing with simulated ice [BTN-95-EIX95182619227] p 270 A95-76653	Simulation and model reduction for the active flexible wing program  [BTN-95-EIX95182619211] p 295 A95-76637   C  CAI, TIMIN  Simulation on the 3-D turbulent flow in the passages of finocyl grain  [BTN-95-EIX95202638962] p 279 A95-76674  CALCAGNO, P.  Geoid lineations of 1000 km wavelength over the central Pacific  [HTN-95-11304] p 319 A95-77009  CALDWELL, D. J.  Modeling aerosol emissions from the combustion of composite materials p 301 N95-23038  CAPOTONDI, ANTONIETTA  Assimilation of altimeter data in a quasi-geostrophic model of the Gulf Stream system: A dynamical	Automatic guidance and control for helicopter obstacle avoidance  [BTN-95-EIX95182619130] p 291 A95-76607  CHERN, JIUN-DAR  Diurnal variation of lee vortices in Taiwan and the surrounding area [HTN-95-91363] p 318 A95-76394  CHEUNG, BENNY K.  System for determining aerodynamic imbalance [NASA-CASE-ARC-11913-1] p 311 N95-23377  CHEUNG, SAMSON  CFD optimization of a theoretical minimum-drag body [BTN-95-EIX95182619234] p 308 A95-76660  CHIANG, WUYING  Dynamic analysis of bearingless tail rotor blades based on nonlinear shell modes [BTN-95-EIX95152582338] p 281 A95-73540  CHIU, CHYN-SHAN  Sidewash on the vertical tail in subsonic and supersonic flows [BTN-95-EIX95152582316] p 264 A95-73519  CHOBOTOV, V. A.
BOWER, DANIEL R.  Analytical study of the neutral stability of a model hypersonic boundary layer [BTN-95-EIX95152577589] p 263 A95-73493 BOYD, D. DOUGLAS, JR.  Analysis of a higher harmonic control test to reduce blade vortex interaction noise [BTN-95-EIX95152582330] p 265 A95-73532 BOYD, IAIN  Particle kinetic simulation of high altitude hypervelocity flight [NASA-CR-197383] p 309 N95-22481 BOZKURT, Y.  Aerodynamic characteristics of external store configurations at low speeds [BTN-95-EIX95182619230] p 271 A95-76656 BRAGG, M. B.  Effect of underwing frost on a transport aircraft airfoil at flight Reynolds number [BTN-95-EIX95152582334] p 276 A95-73536 Aerodynamics of a finite wing with simulated ice [BTN-95-EIX95182619227] p 270 A95-76653 BRAGG, MICHAEL B.	Simulation and model reduction for the active flexible wing program  [BTN-95-EIX95182619211] p 295 A95-76637   C  CAI, TIMIN  Simulation on the 3-D turbulent flow in the passages of finocyl grain  [BTN-95-EIX95202638962] p 279 A95-76674  CALCAGNO, P.  Geoid lineations of 1000 km wavelength over the central Pacific  [HTN-95-11304] p 319 A95-77009  CALDWELL, D. J.  Modeling aerosol emissions from the combustion of composite materials p 301 N95-23038  CAPOTONDI, ANTONIETTA  Assimilation of altimeter data in a quasi-geostrophic	Automatic guidance and control for helicopter obstacle avoidance  [BTN-95-EIX95182619130] p 291 A95-76607  CHERN, JIUN-DAR  Diurnal variation of lee vortices in Taiwan and the surrounding area  [HTN-95-91363] p 318 A95-76394  CHEUNG, BENNY K.  System for determining aerodynamic imbalance [NASA-CASE-ARC-11913-1] p 311 N95-23377  CHEUNG, SAMSON  CFD optimization of a theoretical minimum-drag body [BTN-95-EIX95182619234] p 308 A95-76660  CHIANG, WUYING  Dynamic analysis of bearingless tail rotor blades based on nonlinear shell modes [BTN-95-EIX95152582338] p 281 A95-73540  CHIU, CHYN-SHAN  Sidewash on the vertical tail in subsonic and supersonic flows [BTN-95-EIX95152582316] p 264 A95-73519  CHOBOTOV, V. A.  Effects of satellite bunching on the probability of collision
BOWER, DANIEL R.  Analytical study of the neutral stability of a model hypersonic boundary layer  [BTN-95-EIX95152577589] p 263 A95-73493  BOYD, D. DOUGLAS, JR.  Analysis of a higher harmonic control test to reduce blade vortex interaction noise  [BTN-95-EIX95152582330] p 265 A95-73532  BOYD, IAIN  Particle kinetic simulation of high altitude hypervelocity flight  [NASA-CR-197383] p 309 N95-22481  BOZKURT, Y.  Aerodynamic characteristics of external store configurations at low speeds  [BTN-95-EIX95182619230] p 271 A95-76656  BRAGG, M. B.  Effect of underwing frost on a transport aircraft airfoil at flight Reynolds number  [BTN-95-EIX95182619227] p 270 A95-73536  Aerodynamics of a finite wing with simulated ice  [BTN-95-EIX95182619227] p 270 A95-76653  BRAGG, MICHAEL B.  Study of the droplet spray characteristics of a subsonic	Simulation and model reduction for the active flexible wing program  [BTN-95-EIX95182619211] p 295 A95-76637  C  CAI, TIMIN  Simulation on the 3-D turbulent flow in the passages of finocyl grain  [BTN-95-EIX95202638962] p 279 A95-76674  CALCAGNO, P.  Geoid lineations of 1000 km wavelength over the central Pacific  [HTN-95-11304] p 319 A95-77009  CALDWELL, D. J.  Modeling aerosol emissions from the combustion of composite materials p 301 N95-23038  CAPOTONDI, ANTONIETTA  Assimilation of altimeter data in a quasi-geostrophic model of the Gulf Stream system: A dynamical perspective  [NASA-CR-196313] p 320 N95-23766  CARBONARO, MARIO C.	Automatic guidance and control for helicopter obstacle avoidance [BTN-95-EIX95182619130] p 291 A95-76607  CHERN, JIUN-DAR  Diurnal variation of lee vortices in Taiwan and the surrounding area [HTN-95-91363] p 318 A95-76394  CHEUNG, BENNY K.  System for determining aerodynamic imbalance [NASA-CASE-ARC-11913-1] p 311 N95-23377  CHEUNG, SAMSON  CFD optimization of a theoretical minimum-drag body [BTN-95-EIX95182619234] p 308 A95-76660  CHIANG, WUYING  Dynamic analysis of bearingless tail rotor blades based on nonlinear shell modes [BTN-95-EIX95152582338] p 281 A95-73540  CHIU, CHYN-SHAN  Sidewash on the vertical tail in subsonic and supersonic flows [BTN-95-EIX95152582316] p 264 A95-73519  CHOBOTOV, V. A.  Effects of satellite bunching on the probability of collision in geosynchronous orbit
BOWER, DANIEL R.  Analytical study of the neutral stability of a model hypersonic boundary layer [BTN-95-EIX95152577589] p 263 A95-73493 BOYD, D. DOUGLAS, JR.  Analysis of a higher harmonic control test to reduce blade vortex interaction noise [BTN-95-EIX95152582330] p 265 A95-73532 BOYD, IAIN  Particle kinetic simulation of high altitude hypervelocity flight [NASA-CR-197383] p 309 N95-22481 BOZKURT, Y.  Aerodynamic characteristics of external store configurations at low speeds [BTN-95-EIX95182619230] p 271 A95-76656 BRAGG, M. B.  Effect of underwing frost on a transport aircraft airfoil at flight Reynolds number [BTN-95-EIX95152582334] p 276 A95-73536 Aerodynamics of a finite wing with simulated ice [BTN-95-EIX95182619227] p 270 A95-76653 BRAGG, MICHAEL B.	Simulation and model reduction for the active flexible wing program  [BTN-95-EIX95182619211] p 295 A95-76637  C  CAI, TIMIN  Simulation on the 3-D turbulent flow in the passages of finocyl grain  [BTN-95-EIX95202638962] p 279 A95-76674  CALCAGNO, P.  Geoid lineations of 1000 km wavelength over the central Pacific  [HTN-95-11304] p 319 A95-77009  CALDWELL, D. J.  Modeling aerosol emissions from the combustion of composite materials p 301 N95-23038  CAPOTONDI, ANTONIETTA  Assimilation of altimeter data in a quasi-geostrophic model of the Gulf Stream system: A dynamical perspective  [NASA-CR-196313] p 320 N95-23766  CARBONARO, MARIO C.  Experimental investigation of the flowfield about an	Automatic guidance and control for helicopter obstacle avoidance  [BTN-95-EIX95182619130] p 291 A95-76607  CHERN, JIUN-DAR  Diurnal variation of lee vortices in Taiwan and the surrounding area  [HTN-95-91363] p 318 A95-76394  CHEUNG, BENNY K.  System for determining aerodynamic imbalance [NASA-CASE-ARC-11913-1] p 311 N95-23377  CHEUNG, SAMSON  CFD optimization of a theoretical minimum-drag body [BTN-95-EIX95182619234] p 308 A95-76660  CHIANG, WUYING  Dynamic analysis of bearingless tail rotor blades based on nonlinear shell modes [BTN-95-EIX95152582338] p 281 A95-73540  CHIU, CHYN-SHAN  Sidewash on the vertical tail in subsonic and supersonic flows [BTN-95-EIX95152582316] p 264 A95-73519  CHOBOTOV, V. A.  Effects of satellite bunching on the probability of collision
BOWER, DANIEL R.  Analytical study of the neutral stability of a model hypersonic boundary layer  [BTN-95-EIX95152577589] p 263 A95-73493  BOYD, D. DOUGLAS, JR.  Analysis of a higher harmonic control test to reduce blade vortex interaction noise  [BTN-95-EIX95152582330] p 265 A95-73532  BOYD, IAIN  Particle kinetic simulation of high altitude hypervelocity flight  [NASA-CR-197383] p 309 N95-22481  BOZKURT, Y.  Aerodynamic characteristics of external store configurations at low speeds  [BTN-95-EIX95182619230] p 271 A95-76656  BRAGG, M. B.  Effect of underwing frost on a transport aircraft airfoil at flight Reynolds number  [BTN-95-EIX95182619231] p 276 A95-73536  Aerodynamics of a finite wing with simulated ice  [BTN-95-EIX95182619227] p 270 A95-76653  BRAGG, MICHAEL B.  Study of the droplet spray characteristics of a subsonic wind tunnel  [BTN-95-EIX95182619235] p 271 A95-76661  BRAZA, M.	Simulation and model reduction for the active flexible wing program  [BTN-95-EIX95182619211] p 295 A95-76637   C  CAI, TIMIN  Simulation on the 3-D turbulent flow in the passages of finocyl grain  [BTN-95-EIX95202638962] p 279 A95-76674  CALCAGNO, P.  Geoid lineations of 1000 km wavelength over the central Pacific  [HTN-95-11304] p 319 A95-77009  CALDWELL, D. J.  Modelling aerosol emissions from the combustion of composite materials p 301 N95-23038  CAPOTONDI, ANTONIETTA  Assimilation of altimeter data in a quasi-geostrophic model of the Gulf Stream system: A dynamical perspective  [NASA-CR-196313] p 320 N95-23766  CARBONARO, MARIO C.  Experimental investigation of the flowfield about an upswept afterbody	Automatic guidance and control for helicopter obstacle avoidance [BTN-95-EIX95182619130] p 291 A95-76607  CHERN, JIUN-DAR  Diurnal variation of lee vortices in Taiwan and the surrounding area [HTN-95-91363] p 318 A95-76394  CHEUNG, BENNY K.  System for determining aerodynamic imbalance [NASA-CASE-ARC-11913-1] p 311 N95-23377  CHEUNG, SAMSON  CFD optimization of a theoretical minimum-drag body [BTN-95-EIX95182619234] p 308 A95-76660  CHIANG, WUYING  Dynamic analysis of bearingless tail rotor blades based on nonlinear shell modes [BTN-95-EIX95152582338] p 281 A95-73540  CHIU, CHYN-SHAN  Sidewash on the vertical tail in subsonic and supersonic flows [BTN-95-EIX95152582316] p 264 A95-73519  CHOBOTOV, V. A.  Effects of satellite bunching on the probability of collision in geosynchronous orbit [BTN-95-EIX95152583276] p 298 A95-73577  CHOW, PAO-LIU  Active control of panel vibrations induced by a boundary
BOWER, DANIEL R.  Analytical study of the neutral stability of a model hypersonic boundary layer [BTN-95-EIX95152577589] p 263 A95-73493 BOYD, D. DOUGLAS, JR.  Analysis of a higher harmonic control test to reduce blade vortex interaction noise [BTN-95-EIX95152582330] p 265 A95-73532 BOYD, IAIN  Particle kinetic simulation of high altitude hypervelocity flight [NASA-CR-197383] p 309 N95-22481 BOZKURT, Y.  Aerodynamic characteristics of external store configurations at low speeds [BTN-95-EIX95182619230] p 271 A95-76656 BRAGG, M. B.  Effect of underwing frost on a transport aircraft airfoil at flight Reynolds number [BTN-95-EIX95152582334] p 276 A95-73536 Aerodynamics of a finite wing with simulated ice [BTN-95-EIX95182619227] p 270 A95-76653 BRAGG, MICHAEL B.  Study of the droplet spray characteristics of a subsonic wind tunnel [BTN-95-EIX95182619235] p 271 A95-76661 BRAZA, M.  Two-equation turbulence model for unsteady separated	Simulation and model reduction for the active flexible wing program [BTN-95-EIX95182619211] p 295 A95-76637  C  CAI, TIMIN  Simulation on the 3-D turbulent flow in the passages of finocyl grain [BTN-95-EIX95202638962] p 279 A95-76674  CALCAGNO, P.  Geoid lineations of 1000 km wavelength over the central Pacific [HTN-95-11304] p 319 A95-77009  CALDWELL, D. J.  Modeling aerosol emissions from the combustion of composite materials p 301 N95-23038  CAPOTONDI, ANTONIETTA  Assimilation of altimeter data in a quasi-geostrophic model of the Gulf Stream system: A dynamical perspective [NASA-CR-196313] p 320 N95-23766  CARBONARO, MARIO C.  Experimental investigation of the flowfield about an upswept afterbody [BTN-95-EIX95152582321] p 265 A95-73524  CARTER, DALE	Automatic guidance and control for helicopter obstacle avoidance [BTN-95-EIX95182619130] p 291 A95-76607  CHERN, JIUN-DAR  Diurnal variation of lee vortices in Taiwan and the surrounding area [HTN-95-91363] p 318 A95-76394  CHEUNG, BENNY K.  System for determining aerodynamic imbalance [NASA-CASE-ARC-11913-1] p 311 N95-23377  CHEUNG, SAMSON  CFD optimization of a theoretical minimum-drag body [BTN-95-EIX95182619234] p 308 A95-76660  CHIANG, WUYING  Dynamic analysis of bearingless tail rotor blades based on nonlinear shell modes [BTN-95-EIX95152582338] p 281 A95-73540  CHIU, CHYN-SHAN  Sidewash on the vertical tail in subsonic and supersonic flows [BTN-95-EIX95152582316] p 264 A95-73519  CHOBOTOV, V. A.  Effects of satellite bunching on the probability of collision in geosynchronous orbit [BTN-95-EIX95152583276] p 298 A95-73577  CHOW, PAO-LIU  Active control of panel vibrations induced by a boundary layer flow
BOWER, DANIEL R.  Analytical study of the neutral stability of a model hypersonic boundary layer  [BTN-95-EIX95152577589] p 263 A95-73493  BOYD, D. DOUGLAS, JR.  Analysis of a higher harmonic control test to reduce blade vortex interaction noise  [BTN-95-EIX95152582330] p 265 A95-73532  BOYD, IAIN  Particle kinetic simulation of high altitude hypervelocity flight  [NASA-CR-197383] p 309 N95-22481  BOZKURT, Y.  Aerodynamic characteristics of external store configurations at low speeds  [BTN-95-EIX95182619230] p 271 A95-76656  BRAGG, M. B.  Effect of underwing frost on a transport aircraft airfoil at flight Reynolds number  [BTN-95-EIX95182619231] p 276 A95-73536  Aerodynamics of a finite wing with simulated ice  [BTN-95-EIX95182619227] p 270 A95-76653  BRAGG, MICHAEL B.  Study of the droplet spray characteristics of a subsonic wind tunnel  [BTN-95-EIX95182619235] p 271 A95-76661  BRAZA, M.	Simulation and model reduction for the active flexible wing program  [BTN-95-EIX95182619211] p 295 A95-76637   CAI, TIMIN  Simulation on the 3-D turbulent flow in the passages of finocyl grain  [BTN-95-EIX95202638962] p 279 A95-76674  CALCAGNO, P.  Geoid lineations of 1000 km wavelength over the central Pacific  [HTN-95-11304] p 319 A95-77009  CALDWELL, D. J.  Modeling aerosol emissions from the combustion of composite materials p 301 N95-23038  CAPOTONDI, ANTONIETTA  Assimilation of altimeter data in a quasi-geostrophic model of the Gulf Stream system: A dynamical perspective  [NASA-CR-196313] p 320 N95-23766  CARBONARO, MARIO C.  Experimental investigation of the flowfield about an upswept afterbody  [BTN-95-EIX95152582321] p 265 A95-73524  CARTER, DALE  Flow visualization studies of VTOL aircraft models during	Automatic guidance and control for helicopter obstacle avoidance [BTN-95-EIX95182619130] p 291 A95-76607  CHERN, JIUN-DAR  Diurnal variation of lee vortices in Taiwan and the surrounding area [HTN-95-91363] p 318 A95-76394  CHEUNG, BENNY K.  System for determining aerodynamic imbalance [NASA-CASE-ARC-11913-1] p 311 N95-23377  CHEUNG, SAMSON  CFD optimization of a theoretical minimum-drag body [BTN-95-EIX95182619234] p 308 A95-76660  CHIANG, WUYING  Dynamic analysis of bearingless tail rotor blades based on nonlinear shell modes [BTN-95-EIX95152582338] p 281 A95-73540  CHIU, CHYN-SHAN  Sidewash on the vertical tail in subsonic and supersonic flows [BTN-95-EIX95152582316] p 264 A95-73519  CHOBOTOV, V. A.  Effects of satellite bunching on the probability of collision in geosynchronous orbit [BTN-95-EIX95152583276] p 298 A95-73577  CHOW, PAO-LIU  Active control of panel vibrations induced by a boundary
BOWER, DANIEL R.  Analytical study of the neutral stability of a model hypersonic boundary layer [BTN-95-EIX95152577589] p 263 A95-73493 BOYD, D. DOUGLAS, JR.  Analysis of a higher harmonic control test to reduce blade vortex interaction noise [BTN-95-EIX95152582330] p 265 A95-73532 BOYD, IAIN  Particle kinetic simulation of high altitude hypervelocity flight [NASA-CR-197383] p 309 N95-22481 BOZKURT, Y.  Aerodynamic characteristics of external store configurations at low speeds [BTN-95-EIX95182619230] p 271 A95-76656 BRAGG, M. B.  Effect of underwing frost on a transport aircraft airfoil at flight Reynolds number [BTN-95-EIX95182619231] p 276 A95-73536 Aerodynamics of a finite wing with simulated ice [BTN-95-EIX95182619227] p 270 A95-76653 BRAGG, MICHAEL B.  Study of the droplet spray characteristics of a subsonic wind tunnel [BTN-95-EIX95182619235] p 271 A95-76661 BRAZA, M.  Two-equation turbulence model for unsteady separated flows around airfoils [BTN-95-EIX95142553054] p 262 A95-73444 BRENTNER, KENNETTH S.	Simulation and model reduction for the active flexible wing program [BTN-95-EIX95182619211] p 295 A95-76637  C  CAI, TIMIN  Simulation on the 3-D turbulent flow in the passages of finocyl grain [BTN-95-EIX95202638962] p 279 A95-76674  CALCAGNO, P.  Geoid lineations of 1000 km wavelength over the central Pacific [HTN-95-11304] p 319 A95-77009  CALDWELL, D. J.  Modeling aerosol emissions from the combustion of composite materials p 301 N95-23038  CAPOTONDI, ANTONIETTA  Assimilation of altimeter data in a quasi-geostrophic model of the Gulf Stream system: A dynamical perspective [NASA-CR-196313] p 320 N95-23766  CARBONARO, MARIO C.  Experimental investigation of the flowfield about an upswept afterbody [BTN-95-EIX95152582321] p 265 A95-73524  CARTER, DALE  Flow visualization studies of VTOL aircraft models during Hover in ground effect	Automatic guidance and control for helicopter obstacle avoidance  [BTN-95-EIX95182619130] p 291 A95-76607  CHERN, JIUN-DAR  Diurnal variation of lee vortices in Taiwan and the surrounding area [HTN-95-91363] p 318 A95-76394  CHEUNG, BENNY K.  System for determining aerodynamic imbalance [NASA-CASE-ARC-11913-1] p 311 N95-23377  CHEUNG, SAMSON  CFD optimization of a theoretical minimum-drag body [BTN-95-EIX95182619234] p 308 A95-76660  CHIANG, WUYING  Dynamic analysis of bearingless tail rotor blades based on nonlinear shell modes [BTN-95-EIX95152582338] p 281 A95-73540  CHIU, CHYN-SHAN  Sidewash on the vertical tail in subsonic and supersonic flows [BTN-95-EIX95152582316] p 264 A95-73519  CHOBOTOV, V. A.  Effects of satellite bunching on the probability of collision in geosynchronous orbit [BTN-95-EIX95152583276] p 298 A95-73577  CHOW, PAO-LIU  Active control of panel vibrations induced by a boundary layer flow [NASA-CR-197867] p 273 N95-23182  CHRISTHILF, DAVID M.  Design and multifunction tests of a frequency
BOWER, DANIEL R.  Analytical study of the neutral stability of a model hypersonic boundary layer [BTN-95-EIX95152577589] p 263 A95-73493 BOYD, D. DOUGLAS, JR.  Analysis of a higher harmonic control test to reduce blade vortex interaction noise [BTN-95-EIX95152582330] p 265 A95-73532 BOYD, IAIN  Particle kinetic simulation of high altitude hypervelocity flight [NASA-CR-197383] p 309 N95-22481 BOZKURT, Y.  Aerodynamic characteristics of external store configurations at low speeds [BTN-95-EIX95182619230] p 271 A95-76656 BRAGG, M. B.  Effect of underwing frost on a transport aircraft airfoil at flight Reynolds number [BTN-95-EIX95152582334] p 276 A95-73536 Aerodynamics of a finite wing with simulated ice [BTN-95-EIX95182619227] p 270 A95-76653 BRAGG, MICHAEL B. Study of the droplet spray characteristics of a subsonic wind tunnel [BTN-95-EIX95182619235] p 271 A95-76661 BRAZA, M.  Two-equation turbulence model for unsteady separated flows around airfoils [BTN-95-EIX95142553054] p 262 A95-73444 BRENTNER, KENNETH S.  Sensitivity of acoustic predictions to variation of input	Simulation and model reduction for the active flexible wing program  [BTN-95-EIX95182619211] p 295 A95-76637   CAI, TIMIN  Simulation on the 3-D turbulent flow in the passages of finocyl grain  [BTN-95-EIX95202638962] p 279 A95-76674  CALCAGNO, P.  Geoid lineations of 1000 km wavelength over the central Pacific  [HTN-95-11304] p 319 A95-77009  CALDWELL, D. J.  Modeling aerosol emissions from the combustion of composite materials p 301 N95-23038  CAPOTONDI, ANTONIETTA  Assimilation of altimeter data in a quasi-geostrophic model of the Gulf Stream system: A dynamical perspective  [NASA-CR-196313] p 320 N95-23766  CARBONARO, MARIO C.  Experimental investigation of the flowfield about an upswept afterbody  [BTN-95-EIX95152582321] p 265 A95-73524  CARTER, DALE  Flow visualization studies of VTOL aircraft models during Hover in ground effect  [NASA-TM-108860] p 272 N95-22666  CARUSO, STEVEN C.	Automatic guidance and control for helicopter obstacle avoidance  [BTN-95-EIX95182619130] p 291 A95-76607  CHERN, JIUN-DAR  Diurnal variation of lee vortices in Taiwan and the surrounding area  [HTN-95-91363] p 318 A95-76394  CHEUNG, BENNY K.  System for determining aerodynamic imbalance  [NASA-CASE-ARC-11913-1] p 311 N95-23377  CHEUNG, SAMSON  CFD optimization of a theoretical minimum-drag body  [BTN-95-EIX95182619234] p 308 A95-76600  CHIANG, WUYING  Dynamic analysis of bearingless tail rotor blades based on nonlinear shell modes  [BTN-95-EIX95152582338] p 281 A95-73540  CHIU, CHYN-SHAN  Sidewash on the vertical tail in subsonic and supersonic flows  [BTN-95-EIX95152582316] p 264 A95-73519  CHOBOTOV, V. A.  Effects of satellite bunching on the probability of collision in geosynchronous orbit  [BTN-95-EIX95152583276] p 298 A95-73577  CHOW, PAO-LIU  Active control of panel vibrations induced by a boundary layer flow  [NASA-CR-197867] p 273 N95-23182  CHRISTHILF, DAVID M.  Design and multifunction tests of a frequency domain-based active flutter suppression system
BOWER, DANIEL R.  Analytical study of the neutral stability of a model hypersonic boundary layer [BTN-95-EIX95152577589] p 263 A95-73493 BOYD, D. DOUGLAS, JR.  Analysis of a higher harmonic control test to reduce blade vortex interaction noise [BTN-95-EIX95152582330] p 265 A95-73532 BOYD, IAIN  Particle kinetic simulation of high altitude hypervelocity flight [NASA-CR-197383] p 309 N95-22481 BOZKURT, Y.  Aerodynamic characteristics of external store configurations at low speeds [BTN-95-EIX95182619230] p 271 A95-76656 BRAGG, M. B.  Effect of underwing frost on a transport aircraft airfoil at flight Reynolds number [BTN-95-EIX95182619231] p 276 A95-73536 Aerodynamics of a finite wing with simulated ice [BTN-95-EIX95182619227] p 270 A95-76653 BRAGG, MICHAEL B.  Study of the droplet spray characteristics of a subsonic wind tunnel [BTN-95-EIX95182619235] p 271 A95-76661 BRAZA, M.  Two-equation turbulence model for unsteady separated flows around airfoils [BTN-95-EIX95142553054] p 262 A95-73444 BRENTNER, KENNETTH S.	Simulation and model reduction for the active flexible wing program [BTN-95-EIX95182619211] p 295 A95-76637  C  CAI, TIMIN  Simulation on the 3-D turbulent flow in the passages of finocyl grain [BTN-95-EIX95202638962] p 279 A95-76674  CALCAGNO, P.  Geoid lineations of 1000 km wavelength over the central Pacific [HTN-95-11304] p 319 A95-77009  CALDWELL, D. J.  Modeling aerosol emissions from the combustion of composite materials p 301 N95-23038  CAPOTONDI, ANTONIETTA  Assimilation of altimeter data in a quasi-geostrophic model of the Gulf Stream system: A dynamical perspective [NASA-CR-196313] p 320 N95-23766  CARBONARO, MARIO C.  Experimental investigation of the flowfield about an upswept afterbody [BTN-95-EIX95152582321] p 265 A95-73524  CARTER, DALE  Flow visualization studies of VTOL aircraft models during Hover in ground effect [NASA-TM-108860] p 272 N95-22666  CARUSO, STEVEN C.  Aerodynamic design of pegasus: Concept to flight with	Automatic guidance and control for helicopter obstacle avoidance [BTN-95-EIX95182619130] p 291 A95-76607  CHERN, JIUN-DAR  Diurnal variation of lee vortices in Taiwan and the surrounding area [HTN-95-91363] p 318 A95-76394  CHEUNG, BENNY K.  System for determining aerodynamic imbalance [NASA-CASE-ARC-11913-1] p 311 N95-23377  CHEUNG, SAMSON  CFD optimization of a theoretical minimum-drag body [BTN-95-EIX95182619234] p 308 A95-76660  CHIANG, WUYING  Dynamic analysis of bearingless tail rotor blades based on nonlinear shell modes [BTN-95-EIX95152582338] p 281 A95-73540  CHIU, CHYN-SHAN  Sidewash on the vertical tail in subsonic and supersonic flows [BTN-95-EIX95152582316] p 264 A95-73519  CHOBOTOV, V. A.  Effects of satellite bunching on the probability of collision in geosynchronous orbit [BTN-95-EIX95152583276] p 298 A95-73577  CHOW, PAO-LIU  Active control of panel vibrations induced by a boundary layer flow [NASA-CR-197867] p 273 N95-23182  CHRISTHILF, DAVID M.  Design and multifunction tests of a frequency domain-based active flutter suppression system [BTN-95-EIX95182619215] p 292 A95-76641  CHUNG, CHAN H.
BOWER, DANIEL R.  Analytical study of the neutral stability of a model hypersonic boundary layer [BTN-95-EIX95152577589] p 263 A95-73493 BOYD, D. DOUGLAS, JR.  Analysis of a higher harmonic control test to reduce blade vortex interaction noise [BTN-95-EIX95152582330] p 265 A95-73532 BOYD, IAIN  Particle kinetic simulation of high altitude hypervelocity flight [NASA-CR-197383] p 309 N95-22481 BOZKURT, Y.  Aerodynamic characteristics of external store configurations at low speeds [BTN-95-EIX95182619230] p 271 A95-76656 BRAGG, M. B.  Effect of underwing frost on a transport aircraft airfoil at flight Reynolds number [BTN-95-EIX95152582334] p 276 A95-73536 Aerodynamics of a finite wing with simulated ice [BTN-95-EIX95182619227] p 270 A95-76653 BRAGG, MICHAEL B.  Study of the droplet spray characteristics of a subsonic wind tunnel [BTN-95-EIX95182619235] p 271 A95-76661 BRAZA, M.  Two-equation turbulence model for unsteady separated flows around airfoils [BTN-95-EIX9514255054] p 262 A95-73444 BRENTNER, KENNETH S.  Sensitivity of acoustic predictions to variation of input parameters [HTN-95-80855] p 267 A95-75097 BRIOGES, DAVID H.	Simulation and model reduction for the active flexible wing program  [BTN-95-EIX95182619211] p 295 A95-76637  C  CAI, TIMIN  Simulation on the 3-D turbulent flow in the passages of finocyl grain  [BTN-95-EIX95202638962] p 279 A95-76674  CALCAGNO, P.  Geoid lineations of 1000 km wavelength over the central Pacific  [HTN-95-11304] p 319 A95-77009  CALDWELL, D. J.  Modeling aerosol emissions from the combustion of composite materials p 301 N95-23038  CAPOTONDI, ANTONIETTA  Assimilation of altimeter data in a quasi-geostrophic model of the Gulf Stream system: A dynamical perspective  [NASA-CR-196313] p 320 N95-23766  CARBONARO, MARIO C.  Experimental investigation of the flowfield about an upswept afterbody  [BTN-95-EIX95152582321] p 265 A95-73524  CARTER, DALE  Flow visualization studies of VTOL aircraft models during Hover in ground effect  [NASA-TM-108860] p 272 N95-22666  CARUSO, STEVEN C.  Aerodynamic design of pegasus: Concept to flight with computational fluid dynamics	Automatic guidance and control for helicopter obstacle avoidance  [BTN-95-EIX95182619130] p 291 A95-76607  CHERN, JIUN-DAR  Diurnal variation of lee vortices in Taiwan and the surrounding area [HTN-95-91363] p 318 A95-76394  CHEUNG, BENNY K.  System for determining aerodynamic imbalance [NASA-CASE-ARC-11913-1] p 311 N95-23377  CHEUNG, SAMSON  CFD optimization of a theoretical minimum-drag body [BTN-95-EIX95182619234] p 308 A95-76660  CHIANG, WUYING  Dynamic analysis of bearingless tail rotor blades based on nonlinear shell modes [BTN-95-EIX95152582338] p 281 A95-73540  CHIU, CHYN-SHAN  Sidewash on the vertical tail in subsonic and supersonic flows [BTN-95-EIX95152582316] p 264 A95-73519  CHOBOTOV, V. A.  Effects of satellite bunching on the probability of collision in geosynchronous orbit [BTN-95-EIX95152583276] p 298 A95-73577  CHOW, PAO-LIU  Active control of panel vibrations induced by a boundary layer flow [NASA-CR-197867] p 273 N95-23182  CHRISTHILF, DAVID M.  Design and multifunction tests of a frequency domain-based active flutter suppression system [BTN-95-EIX95182619215] p 292 A95-76641  CHUNG, CHAN H.  Numerical analysis of hypersonic low-density scramjet
BOWER, DANIEL R.  Analytical study of the neutral stability of a model hypersonic boundary layer [BTN-95-EIX95152577589] p 263 A95-73493 BOYD, D. DOUGLAS, JR.  Analysis of a higher harmonic control test to reduce blade vortex interaction noise [BTN-95-EIX9515258230] p 265 A95-73532 BOYD, IAIN  Particle kinetic simulation of high altitude hypervelocity flight [NASA-CR-197383] p 309 N95-22481 BOZKURT, Y.  Aerodynamic characteristics of external store configurations at low speeds [BTN-95-EIX95182619230] p 271 A95-76656 BRAGG, M. B.  Effect of underwing frost on a transport aircraft airfoil at flight Reynolds number [BTN-95-EIX95152582334] p 276 A95-73536 Aerodynamics of a finite wing with simulated ice [BTN-95-EIX95152582334] p 270 A95-76653 BRAGG, MICHAEL B.  Study of the droplet spray characteristics of a subsonic wind tunnel [BTN-95-EIX95182619235] p 271 A95-76661 BRAZA, M.  Two-equation turbulence model for unsteady separated flows around airfoils [BTN-95-EIX95142553054] p 262 A95-73444 BRENTNER, KENNETH S.  Sensitivity of acoustic predictions to variation of input parameters [HTN-95-80855] p 267 A95-75097 BRIDGES, DAVID H.  Crossflow instability control on a swept-wing: Preliminary	Simulation and model reduction for the active flexible wing program [BTN-95-EIX95182619211] p 295 A95-76637  C  CAI, TIMIN  Simulation on the 3-D turbulent flow in the passages of finocyl grain [BTN-95-EIX95202638962] p 279 A95-76674  CALCAGNO, P.  Geoid lineations of 1000 km wavelength over the central Pacific [HTN-95-11304] p 319 A95-77009  CALDWELL, D. J.  Modeling aerosol emissions from the combustion of composite materials p 301 N95-23038  CAPOTONDI, ANTONIETTA  Assimilation of altimeter data in a quasi-geostrophic model of the Gulf Stream system: A dynamical perspective [NASA-CR-196313] p 320 N95-23766  CARBONARO, MARIO C.  Experimental investigation of the flowfield about an upswept afterbody [BTN-95-EIX95152582321] p 265 A95-73524  CARTER, DALE  Flow visualization studies of VTOL aircraft models during Hover in ground effect [NASA-TM-108860] p 272 N95-22666  CARUSO, STEVEN C.  Aerodynamic design of pegasus: Concept to flight with	Automatic guidance and control for helicopter obstacle avoidance [BTN-95-EIX95182619130] p 291 A95-76607  CHERN, JIUN-DAR  Diurnal variation of lee vortices in Taiwan and the surrounding area [HTN-95-91363] p 318 A95-76394  CHEUNG, BENNY K.  System for determining aerodynamic imbalance [NASA-CASE-ARC-11913-1] p 311 N95-23377  CHEUNG, SAMSON  CFD optimization of a theoretical minimum-drag body [BTN-95-EIX95182619234] p 308 A95-76660  CHIANG, WUYING  Dynamic analysis of bearingless tail rotor blades based on nonlinear shell modes [BTN-95-EIX95182619238] p 281 A95-73540  CHIU, CHYN-SHAN  Sidewash on the vertical tail in subsonic and supersonic flows [BTN-95-EIX95152582316] p 264 A95-73519  CHOBOTOV, V. A.  Effects of satellite bunching on the probability of collision in geosynchronous orbit [BTN-95-EIX95152583276] p 298 A95-73577  CHOW, PAO-LIU  Active control of panel vibrations induced by a boundary layer flow [NASA-CR-197867] p 273 N95-23182  CHRISTHILEF, DAVID M.  Design and multifunction tests of a frequency domain-based active flutter suppression system [BTN-95-EIX95182619215] p 292 A95-76641  CHUNG, CHAN H.  Numerical analysis of hypersonic low-density scramjet inlet flow
BOWER, DANIEL R.  Analytical study of the neutral stability of a model hypersonic boundary layer [BTN-95-EIX95152577589] p 263 A95-73493 BOYD, D. DOUGLAS, JR.  Analysis of a higher harmonic control test to reduce blade vortex interaction noise [BTN-95-EIX95152582330] p 265 A95-73532 BOYD, IAIN  Particle kinetic simulation of high altitude hypervelocity flight [NASA-CR-197383] p 309 N95-22481 BOZKURT, Y.  Aerodynamic characteristics of external store configurations at low speeds [BTN-95-EIX95182619230] p 271 A95-76656 BRAGG, M. B.  Effect of underwing frost on a transport aircraft airfoil at flight Reynolds number [BTN-95-EIX95152582334] p 276 A95-73536 Aerodynamics of a finite wing with simulated ice [BTN-95-EIX95182619227] p 270 A95-76653 BRAGG, MICHAEL B. Study of the droplet spray characteristics of a subsonic wind tunnel [BTN-95-EIX95182619235] p 271 A95-76661 BRAZA, M.  Two-equation turbulence model for unsteady separated flows around airfoils [BTN-95-EIX95142553054] p 262 A95-73444 BRENTNER, KENNETH S.  Sensitivity of acoustic predictions to variation of input parameters [HTN-95-80855] p 267 A95-75097 BRIDGES, DAVID H.  Crossflow instability control on a swept-wing: Preliminary studies	Simulation and model reduction for the active flexible wing program  [BTN-95-EIX95182619211] p 295 A95-76637  C  CAI, TIMIN  Simulation on the 3-D turbulent flow in the passages of finocyl grain  [BTN-95-EIX95202638962] p 279 A95-76674  CALCAGNO, P.  Geoid lineations of 1000 km wavelength over the central Pacific  [HTN-95-11304] p 319 A95-77009  CALDWELL, D. J.  Modeling aerosol emissions from the combustion of composite materials p 301 N95-23038  CAPOTONDI, ANTONIETTA  Assimilation of altimeter data in a quasi-geostrophic model of the Gulf Stream system: A dynamical perspective  [NASA-CR-196313] p 320 N95-23766  CARBONARO, MARIO C.  Experimental investigation of the flowfield about an upswept afterbody  [BTN-95-EIX95152582321] p 265 A95-73524  CARTER, DALE  Flow visualization studies of VTOL aircraft models during Hover in ground effect  [NASA-TM-108860] p 272 N95-22666  CARUSO, STEVEN C.  Aerodynamic design of pegasus: Concept to flight with computational fluid dynamics  [BTN-95-EIX95182617463] p 298 A95-75734  CAUDRON, F.  Experimental investigation of the flowfield about an	Automatic guidance and control for helicopter obstacle avoidance  [BTN-95-EIX95182619130] p 291 A95-76607  CHERN, JIUN-DAR  Diurnal variation of lee vortices in Taiwan and the surrounding area [HTN-95-91363] p 318 A95-76394  CHEUNG, BENNY K.  System for determining aerodynamic imbalance [NASA-CASE-ARC-11913-1] p 311 N95-23377  CHEUNG, SAMSON  CFD optimization of a theoretical minimum-drag body [BTN-95-EIX95182619234] p 308 A95-76660  CHIANG, WUYING  Dynamic analysis of bearingless tail rotor blades based on nonlinear shell modes [BTN-95-EIX95152582338] p 281 A95-73540  CHIU, CHYN-SHAN  Sidewash on the vertical tail in subsonic and supersonic flows [BTN-95-EIX95152582316] p 264 A95-73519  CHOBOTOV, V. A.  Effects of satellite bunching on the probability of collision in geosynchronous orbit [BTN-95-EIX95152583276] p 298 A95-73577  CHOW, PAO-LIU  Active control of panel vibrations induced by a boundary layer flow [NASA-CR-197867] p 273 N95-23182  CHRISTHILF, DAVID M.  Design and multifunction tests of a frequency domain-based active flutter suppression system [BTN-95-EIX95182619215] p 292 A95-76641  CHUNG, CHAN H.  Numerical analysis of hypersonic low-density scramjet
BOWER, DANIEL R.  Analytical study of the neutral stability of a model hypersonic boundary layer [BTN-95-EIX95152577589] p 263 A95-73493 BOYD, D. DOUGLAS, JR.  Analysis of a higher harmonic control test to reduce blade vortex interaction noise [BTN-95-EIX95152582330] p 265 A95-73532 BOYD, IAIN  Particle kinetic simulation of high altitude hypervelocity flight [NASA-CR-197383] p 309 N95-22481 BOZKURT, Y.  Aerodynamic characteristics of external store configurations at low speeds [BTN-95-EIX95182619230] p 271 A95-76656 BRAGG, M. B.  Effect of underwing frost on a transport aircraft airfoil at flight Reynolds number [BTN-95-EIX95152582334] p 276 A95-73536 Aerodynamics of a finite wing with simulated ice [BTN-95-EIX95152582334] p 270 A95-76653 BRAGG, MICHAEL B.  Study of the droplet spray characteristics of a subsonic wind tunnel [BTN-95-EIX95182619235] p 271 A95-76661 BRAZA, M.  Two-equation turbulence model for unsteady separated flows around airfoils [BTN-95-EIX95142553054] p 262 A95-73444 BRENTNER, KENNETH S.  Sensitivity of acoustic predictions to variation of input parameters [HTN-95-80855] p 267 A95-75097 BRIDGES, DAVID H.  Crossflow instability control on a swept-wing: Preliminary studies BRINKER, DAVID J.  Design of a GaAs/Ge solar array for unmanned aerial	Simulation and model reduction for the active flexible wing program  [BTN-95-EIX95182619211] p 295 A95-76637  C  CAI, TIMIN  Simulation on the 3-D turbulent flow in the passages of finocyl grain  [BTN-95-EIX95202638962] p 279 A95-76674  CALCAGNO, P.  Geoid lineations of 1000 km wavelength over the central Pacific  [HTN-95-11304] p 319 A95-77009  CALDWELL, D. J.  Modeling aerosol emissions from the combustion of composite materials p 301 N95-23038  CAPOTONDI, ANTONIETTA  Assimilation of altimeter data in a quasi-geostrophic model of the Gulf Stream system: A dynamical perspective  [NASA-CR-196313] p 320 N95-23766  CARBONARO, MARIO C.  Experimental investigation of the flowfield about an upswept afterbody  [BTN-95-EIX95152582321] p 265 A95-73524  CARTER, DALE  Flow visualization studies of VTOL aircraft models during Hover in ground effect  [NASA-TM-108860] p 272 N95-22666  CARUSO, STEVEN C.  Aerodynamic design of pegasus: Concept to flight with computational fluid dynamics  [BTN-95-EIX95182617463] p 298 A95-75734  CAUDRON, F.  Experimental investigation of the flowfield about an upswept afterbody	Automatic guidance and control for helicopter obstacle avoidance  (BTN-95-EIX95182619130] p 291 A95-76607  CHERN, JIUN-DAR  Diurnal variation of lee vortices in Taiwan and the surrounding area  [HTN-95-91363] p 318 A95-76394  CHEUNG, BENNY K.  System for determining aerodynamic imbalance  [NASA-CASE-ARC-11913-1] p 311 N95-23377  CHEUNG, SAMSON  CFD optimization of a theoretical minimum-drag body  [BTN-95-EIX95182619234] p 308 A95-76660  CHIANG, WUYING  Dynamic analysis of bearingless tail rotor blades based on nonlinear shell modes  [BTN-95-EIX95182619238] p 281 A95-73540  CHIU, CHYN-SHAN  Sidewash on the vertical tail in subsonic and supersonic flows  [BTN-95-EIX95152582338] p 281 A95-73519  CHOBOTOV, V. A.  Effects of satellite bunching on the probability of collision in geosynchronous orbit  [BTN-95-EIX95152583276] p 298 A95-73577  CHOW, PAO-LIU  Active control of panel vibrations induced by a boundary layer flow  [NASA-CR-197867] p 273 N95-23182  CHRISTHILF, DAVID M.  Design and multifunction tests of a frequency domain-based active flutter suppression system  [BTN-95-EIX95182619215] p 292 A95-76641  CHUNG, CHAN H.  Numerical analysis of hypersonic low-density scramjet inlet flow  [BTN-95-EIX95212645694] p 272 A95-76746  CHURCHILL, GARY B.  System for determining aerodynamic imbalance
BOWER, DANIEL R.  Analytical study of the neutral stability of a model hypersonic boundary layer [BTN-95-EIX95152577589] p 263 A95-73493 BOYD, D. DOUGLAS, JR.  Analysis of a higher harmonic control test to reduce blade vortex interaction noise [BTN-95-EIX95152582330] p 265 A95-73532 BOYD, IAIN  Particle kinetic simulation of high altitude hypervelocity flight [NASA-CR-197383] p 309 N95-22481 BOZKURT, Y.  Aerodynamic characteristics of external store configurations at low speeds [BTN-95-EIX95182619230] p 271 A95-76656 BRAGG, M. B.  Effect of underwing frost on a transport aircraft airfoil at flight Reynolds number [BTN-95-EIX95152582334] p 276 A95-73536 Aerodynamics of a finite wing with simulated ice [BTN-95-EIX95182619227] p 270 A95-76653 BRAGG, MICHAEL B.  Study of the droplet spray characteristics of a subsonic wind tunnel [BTN-95-EIX95182619235] p 271 A95-76661 BRAZA, M.  Two-equation turbulence model for unsteady separated flows around airfoils [BTN-95-EIX95142553054] p 262 A95-73444 BRENTNER, KENNETH S.  Sensitivity of acoustic predictions to variation of input parameters [HTN-95-80855] p 267 A95-75097 BRIGGES, DAVID H.  Crossflow instability control on a swept-wing: Preliminary studies  BRINKER, DAVID J.  Design of a GaAs/Ge solar array for unmanned aerial vehicles	Simulation and model reduction for the active flexible wing program  [BTN-95-EIX95182619211] p 295 A95-76637  CAI, TIMIN  Simulation on the 3-D turbulent flow in the passages of finocyl grain  [BTN-95-EIX95202638962] p 279 A95-76674  CALCAGNO, P.  Geoid lineations of 1000 km wavelength over the central Pacific  [HTN-95-11304] p 319 A95-77009  CALDWELL, D. J.  Modeling aerosol emissions from the combustion of composite materials p 301 N95-23038  CAPOTONDI, ANTONIETTA  Assimilation of altimeter data in a quasi-geostrophic model of the Gulf Stream system: A dynamical perspective  [NASA-CR-196313] p 320 N95-23766  CARBONARO, MARIO C.  Experimental investigation of the flowfield about an upswept afterbody  [BTN-95-EIX95152582321] p 265 A95-73524  CARTER, DALE  Flow visualization studies of VTOL aircraft models during Hover in ground effect  [NASA-TM-108860] p 272 N95-22666  CARUSO, STEVEN C.  Aerodynamic design of pegasus: Concept to flight with computational fluid dynamics  [BTN-95-EIX95182617463] p 298 A95-75734  CAUDRON, F.  Experimental investigation of the flowfield about an upswept afterbody  [BTN-95-EIX95152582321] p 265 A95-73524	Automatic guidance and control for helicopter obstacle avoidance [BTN-95-EIX95182619130] p 291 A95-76607  CHERN, JIUN-DAR  Diurnal variation of lee vortices in Taiwan and the surrounding area [HTN-95-91363] p 318 A95-76394  CHEUNG, BENNY K.  System for determining aerodynamic imbalance [NASA-CASE-ARC-11913-1] p 311 N95-23377  CHEUNG, SAMSON  CFD optimization of a theoretical minimum-drag body [BTN-95-EIX95182619234] p 308 A95-76660  CHIANG, WUYING  Dynamic analysis of bearingless tail rotor blades based on nonlinear shell modes [BTN-95-EIX95152582338] p 281 A95-73540  CHIU, CHYN-SHAN  Sidewash on the vertical tail in subsonic and supersonic flows [BTN-95-EIX95152582338] p 264 A95-73519  CHOBOTOV, V. A.  Effects of satellite bunching on the probability of collision in geosynchronous orbit [BTN-95-EIX95152583276] p 298 A95-73577  CHOW, PAO-LIU  Active control of panel vibrations induced by a boundary layer flow [NASA-CR-197867] p 273 N95-23182  CHRISTHILF, DAVID M.  Design and multifunction tests of a frequency domain-based active flutter suppression system [BTN-95-EIX95182619215] p 292 A95-76641  CHUNG, CHAN H.  Numerical analysis of hypersonic low-density scramjet inlet flow [BTN-95-EIX95212645694] p 272 A95-76746  CHURCHILL, GARY B.  System for determining aerodynamic imbalance [NASA-CASE-ARC-11913-1] p 311 N95-23377
BOWER, DANIEL R.  Analytical study of the neutral stability of a model hypersonic boundary layer [BTN-95-EIX95152577589] p 263 A95-73493 BOYD, D. DOUGLAS, JR.  Analysis of a higher harmonic control test to reduce blade vortex interaction noise [BTN-95-EIX95152582330] p 265 A95-73532 BOYD, IAIN  Particle kinetic simulation of high altitude hypervelocity flight [NASA-CR-197383] p 309 N95-22481 BOZKURT, Y.  Aerodynamic characteristics of external store configurations at low speeds [BTN-95-EIX95182619230] p 271 A95-76656 BRAGG, M. B.  Effect of underwing frost on a transport aircraft airfoil at flight Reynolds number [BTN-95-EIX95152582334] p 276 A95-73536 Aerodynamics of a finite wing with simulated ice [BTN-95-EIX95182619227] p 270 A95-76653 BRAGG, MICHAEL B.  Study of the droplet spray characteristics of a subsonic wind tunnel [BTN-95-EIX95182619235] p 271 A95-76661 BRAZA, M.  Two-equation turbulence model for unsteady separated flows around airfoils [BTN-95-EIX95142553054] p 262 A95-73444 BRENTNER, KENNETH S.  Sensitivity of acoustic predictions to variation of input parameters [HTN-95-80855] p 267 A95-75097 BRIDGES, DAVID H.  Crossflow instability control on a swept-wing: Preliminary studies  BRINKER, DAVID J.  Design of a GaAs/Ge solar array for unmanned aerial vehicles [NASA-TM-106870] p 320 N95-23259	Simulation and model reduction for the active flexible wing program  [BTN-95-EIX95182619211] p 295 A95-76637  C  CAI, TIMIN  Simulation on the 3-D turbulent flow in the passages of finocyl grain  [BTN-95-EIX95202638962] p 279 A95-76674  CALCAGNO, P.  Geoid lineations of 1000 km wavelength over the central Pacific  [HTN-95-11304] p 319 A95-77009  CALDWELL, D. J.  Modeling aerosol emissions from the combustion of composite materials p 301 N95-23038  CAPOTONDI, ANTONIETTA  Assimilation of altimeter data in a quasi-geostrophic model of the Gulf Stream system: A dynamical perspective  [NASA-CR-196313] p 320 N95-23766  CARBONARO, MARIO C.  Experimental investigation of the flowfield about an upswept afterbody  [BTN-95-EIX95152582321] p 265 A95-73524  CARTER, DALE  Flow visualization studies of VTOL aircraft models during Hover in ground effect  [NASA-TM-108860] p 272 N95-22666  CARUSO, STEVEN C.  Aerodynamic design of pegasus: Concept to flight with computational fluid dynamics  [BTN-95-EIX95182617463] p 298 A95-75734  CAUDRON, F.  Experimental investigation of the flowfield about an upswept afterbody	Automatic guidance and control for helicopter obstacle avoidance  [BTN-95-EIX95182619130] p 291 A95-76607  CHERN, JIUN-DAR  Diurnal variation of lee vortices in Taiwan and the surrounding area  [HTN-95-91363] p 318 A95-76394  CHEUNG, BENNY K.  System for determining aerodynamic imbalance  [NASA-CASE-ARC-11913-1] p 311 N95-23377  CHEUNG, SAMSON  CFD optimization of a theoretical minimum-drag body  [BTN-95-EIX95182619234] p 308 A95-76660  CHIANG, WUYING  Dynamic analysis of bearingless tail rotor blades based on nonlinear shell modes  [BTN-95-EIX95152582338] p 281 A95-73540  CHIU, CHYN-SHAN  Sidewash on the vertical tail in subsonic and supersonic flows  [BTN-95-EIX95152582316] p 264 A95-73519  CHOBOTOV, V. A.  Effects of satellite bunching on the probability of collision in geosynchronous orbit  [BTN-95-EIX95152583276] p 298 A95-73577  CHOW, PAO-LIU  Active control of panel vibrations induced by a boundary layer flow  [NASA-CR-197667] p 273 N95-23182  CHRISTHILF, DAVID M.  Design and multifunction tests of a frequency domain-based active flutter suppression system  [BTN-95-EIX95182619215] p 292 A95-76641  CHUNG, CHAN H.  Numerical analysis of hypersonic low-density scramjet inlet flow  [BTN-95-EIX95212645694] p 272 A95-76746  CHURCHILL, GARY B.  System for determining aerodynamic imbalance  [NASA-CASE-ARC-11913-1] p 311 N95-23377  CLARKE, ROBERT
BOWER, DANIEL R.  Analytical study of the neutral stability of a model hypersonic boundary layer [BTN-95-EIX95152577589] p 263 A95-73493 BOYD, D. DOUGLAS, JR.  Analysis of a higher harmonic control test to reduce blade vortex interaction noise [BTN-95-EIX95152582330] p 265 A95-73532 BOYD, IAIN  Particle kinetic simulation of high altitude hypervelocity flight [NASA-CR-197383] p 309 N95-22481 BOZKURT, Y.  Aerodynamic characteristics of external store configurations at low speeds [BTN-95-EIX95182619230] p 271 A95-76656 BRAGG, M. B.  Effect of underwing frost on a transport aircraft airfoil at flight Reynolds number [BTN-95-EIX95152582334] p 276 A95-73536 Aerodynamics of a finite wing with simulated ice [BTN-95-EIX95182619227] p 270 A95-76653 BRAGG, MICHAEL B.  Study of the droplet spray characteristics of a subsonic wind tunnel [BTN-95-EIX95182619235] p 271 A95-76661 BRAZA, M.  Two-equation turbulence model for unsteady separated flows around airfoils [BTN-95-EIX95142553054] p 262 A95-73444 BRENTNER, KENNETH S.  Sensitivity of acoustic predictions to variation of input parameters [HTN-95-80855] p 267 A95-75097 BRIGGES, DAVID H.  Crossflow instability control on a swept-wing: Preliminary studies p 274 N95-23283 BRINKER, DAVID J.  Design of a GaAs/Ge solar array for unmarnned aerial vehicles [NASA-TM-106870] p 320 N95-23259 BROOKS, CYNTHIA L.  Automation technology using Geographic Information	Simulation and model reduction for the active flexible wing program  [BTN-95-EIX95182619211] p 295 A95-76637  CAI, TIMIN  Simulation on the 3-D turbulent flow in the passages of finocyl grain  [BTN-95-EIX95202638962] p 279 A95-76674  CALCAGNO, P.  Geoid lineations of 1000 km wavelength over the central Pacific  [HTN-95-11304] p 319 A95-77009  CALDWELL, D. J.  Modeling aerosol emissions from the combustion of composite materials p 301 N95-23038  CAPOTONDI, ANTONIETTA  Assimilation of altimeter data in a quasi-geostrophic model of the Gulf Stream system: A dynamical perspective  [NASA-CR-196313] p 320 N95-23766  CARBONARO, MARIO C.  Experimental investigation of the flowfield about an upswept afterbody  [BTN-95-EIX95152582321] p 265 A95-73524  CARTER, DALE  Flow visualization studies of VTOL aircraft models during Hover in ground effect  [NASA-TM-108860] p 272 N95-22666  CARUSO, STEVEN C.  Aerodynamic design of pegasus: Concept to flight with computational fluid dynamics  [BTN-95-EIX95182617463] p 298 A95-75734  CAUDRON, F.  Experimental investigation of the flowfield about an upswept afterbody  [BTN-95-EIX95182617463] p 298 A95-75734  CAUDRON, F.  Experimental investigation of the flowfield about an upswept afterbody  [BTN-95-EIX95152582321] p 265 A95-73524  CAZENAVE, A.  Geoid lineations of 1000 km wavelength over the central Pacific	Automatic guidance and control for helicopter obstacle avoidance [BTN-95-EIX95182619130] p 291 A95-76607  CHERN, JIUN-DAR  Diurnal variation of lee vortices in Taiwan and the surrounding area [HTN-95-91363] p 318 A95-76394  CHEUNG, BENNY K.  System for determining aerodynamic imbalance [NASA-CASE-ARC-11913-1] p 311 N95-23377  CHEUNG, SAMSON  CFD optimization of a theoretical minimum-drag body [BTN-95-EIX95182619234] p 308 A95-76660  CHIANG, WUYING  Dynamic analysis of bearingless tail rotor blades based on nonlinear shell modes [BTN-95-EIX95152582338] p 281 A95-73540  CHIU, CHIVN-SHAN  Sidewash on the vertical tail in subsonic and supersonic flows [BTN-95-EIX95152582338] p 264 A95-73519  CHOBOTOV, V. A.  Effects of satellite bunching on the probability of collision in geosynchronous orbit [BTN-95-EIX95152583276] p 298 A95-73577  CHOW, PAO-LIU  Active control of panel vibrations induced by a boundary layer flow [NASA-CR-197867] p 273 N95-23182  CHING, CHAN H.  Design and multifunction tests of a frequency domain-based active flutter suppression system [BTN-95-EIX95182619215] p 292 A95-76641  CHUNG, CHAN H.  Numerical analysis of hypersonic low-density scramjet inlet flow [BTN-95-EIX9512645694] p 272 A95-76746  CHURCHILL, GARY B.  System for determining aerodynamic imbalance [NASA-CASE-ARC-11913-1] p 311 N95-23377  CLARKE, ROBERT  Flight test of the X-29A at high angle of attack: Flight dynamics and controls
BOWER, DANIEL R.  Analytical study of the neutral stability of a model hypersonic boundary layer [BTN-95-EIX95152577589] p 263 A95-73493 BOYD, D. DOUGLAS, JR.  Analysis of a higher harmonic control test to reduce blade vortex interaction noise [BTN-95-EIX95152582330] p 265 A95-73532 BOYD, IAIN  Particle kinetic simulation of high altitude hypervelocity flight [NASA-CR-197383] p 309 N95-22481 BOZKURT, Y.  Aerodynamic characteristics of external store configurations at low speeds [BTN-95-EIX95182619230] p 271 A95-76656 BRAGG, M. B.  Effect of underwing frost on a transport aircraft airfoil at flight Reynolds number [BTN-95-EIX95152582334] p 276 A95-73536 Aerodynamics of a finite wing with simulated ice [BTN-95-EIX95182619227] p 270 A95-76653 BRAGG, MICHAEL B.  Study of the droplet spray characteristics of a subsonic wind tunnel [BTN-95-EIX95182619235] p 271 A95-76661 BRAZA, M.  Two-equation turbulence model for unsteady separated flows around airfoils [BTN-95-EIX95142553054] p 262 A95-73444 BRENTNER, KENNETH S.  Sensitivity of acoustic predictions to variation of input parameters [HTN-95-80855] p 267 A95-75097 BRIDGES, DAVID H.  Crossflow instability control on a swept-wing: Preliminary studies [NASA-TM-106870] p 320 N95-23283 BRINKER, DAVID J.  Design of a GaAs/Ge solar array for unmanned aerial vehicles [NASA-TM-106870] p 320 N95-23259 BROOKS, CYNTHIA L.  Automation technology using Geographic Information System (GIS)	Simulation and model reduction for the active flexible wing program  [BTN-95-EIX95182619211] p 295 A95-76637  C  CAI, TIMIN  Simulation on the 3-D turbulent flow in the passages of finocyl grain  [BTN-95-EIX95202638962] p 279 A95-76674  CALCAGNO, P.  Geoid lineations of 1000 km wavelength over the central Pacific  [HTN-95-11304] p 319 A95-77009  CALDWELL, D. J.  Modeling aerosol emissions from the combustion of composite materials p 301 N95-23038  CAPOTONDI, ANTONIETTA  Assimilation of altimeter data in a quasi-geostrophic model of the Gulf Stream system: A dynamical perspective  [NASA-CR-196313] p 320 N95-23766  CARBONARO, MARIO C.  Experimental investigation of the flowfield about an upswept afterbody  [BTN-95-EIX95152582321] p 265 A95-73524  CARTER, DALE  Flow visualization studies of VTOL aircraft models during Hover in ground effect  [NASA-TM-108860] p 272 N95-22666  CARLSO, STEVEN C.  Aerodynamic design of pegasus: Concept to flight with computational fluid dynamics  [BTN-95-EIX95182617463] p 298 A95-75734  CAUDRON, F.  Experimental investigation of the flowfield about an upswept afterbody  [BTN-95-EIX95152582321] p 265 A95-73524  CAZENAVE, A.  Geoid lineations of 1000 km wavelength over the central Pacitic  [HTN-95-11304] p 319 A95-77009	Automatic guidance and control for helicopter obstacle avoidance  [BTN-95-EIX95182619130] p 291 A95-76607  CHERN, JIUN-DAR  Diurnal variation of lee vortices in Taiwan and the surrounding area  [HTN-95-91363] p 318 A95-76394  CHEUNG, BENNY K.  System for determining aerodynamic imbalance  [NASA-CASE-ARC-11913-1] p 311 N95-23377  CHEUNG, SAMSON  CFD optimization of a theoretical minimum-drag body  [BTN-95-EIX95182619234] p 308 A95-76660  CHIANG, WUYING  Dynamic analysis of bearingless tail rotor blades based on nonlinear shell modes  [BTN-95-EIX95152582338] p 281 A95-73540  CHIU, CHYN-SHAN  Sidewash on the vertical tail in subsonic and supersonic flows  [BTN-95-EIX95152582316] p 264 A95-73519  CHOBOTOV, V. A.  Effects of satellite bunching on the probability of collision in geosynchronous orbit  [BTN-95-EIX95152583276] p 298 A95-73577  CHOW, PAO-LIU  Active control of panel vibrations induced by a boundary layer flow  [NASA-CR-197667] p 273 N95-23182  CHRISTHILF, DAVID M.  Design and multifunction tests of a frequency domain-based active flutter suppression system  [BTN-95-EIX95182619215] p 292 A95-76641  CHUNG, CHAN H.  Numerical analysis of hypersonic low-density scramjet intel flow  [NSA-CASE-ARC-11913-1] p 311 N95-23377  CLARKE, ROBERT  Flight test of the X-29A at high angle of attack: Flight dynamics and controls  [NASA-TP-3537] p 284 N95-22806
BOWER, DANIEL R. Analytical study of the neutral stability of a model hypersonic boundary layer [BTN-95-EIX95152577589] p 263 A95-73493 BOYD, D. DOUGLAS, JR. Analysis of a higher harmonic control test to reduce blade vortex interaction noise [BTN-95-EIX95152582330] p 265 A95-73532 BOYD, IAIN Particle kinetic simulation of high altitude hypervelocity flight [NASA-CR-197383] p 309 N95-22481 BOZKURT, Y. Aerodynamic characteristics of external store configurations at low speeds [BTN-95-EIX95182619230] p 271 A95-76656 BRAGG, M. B. Effect of underwing frost on a transport aircraft airfoil at flight Reynolds number [BTN-95-EIX95152582334] p 276 A95-73536 Aerodynamics of a finite wing with simulated ice [BTN-95-EIX95162619227] p 270 A95-76653 BRAGG, MICHAEL B. Study of the droplet spray characteristics of a subsonic wind tunnel [BTN-95-EIX95182619235] p 271 A95-76661 BRAZA, M. Two-equation turbulence model for unsteady separated flows around airfoils [BTN-95-EIX95142553054] p 262 A95-73444 BRENTNER, KENNETH S. Sensitivity of acoustic predictions to variation of input parameters [HTN-95-80855] p 267 A95-75097 BRIDGES, DAVID H. Crossflow instability control on a swept-wing: Preliminary studies BRINKER, DAVID J. Design of a GaAs/Ge solar array for unmanned aerial vehicles [NASA-TM-106870] p 320 N95-23259 BROOKS, CYNTHIAL Automation technology using Geographic Information System (GIS) p 324 N95-23284	Simulation and model reduction for the active flexible wing program  [BTN-95-EIX95182619211] p 295 A95-76637  C  CAI, TIMIN  Simulation on the 3-D turbulent flow in the passages of finocyl grain  [BTN-95-EIX95202638962] p 279 A95-76674  CALCAGNO, P.  Geoid lineations of 1000 km wavelength over the central Pacific  [HTN-95-11304] p 319 A95-77009  CALDWELL, D. J.  Modeling aerosol emissions from the combustion of composite materials p 301 N95-23038  CAPOTONDI, ANTONIETTA  Assimilation of altimeter data in a quasi-geostrophic model of the Gulf Stream system: A dynamical perspective  [NASA-CR-196313] p 320 N95-23766  CARBONARO, MARIO C.  Experimental investigation of the flowfield about an upswept afterbody  [BTN-95-EIX95152582321] p 265 A95-73524  CARTER, DALE  Flow visualization studies of VTOL aircraft models during Hover in ground effect  [NASA-TM-108860] p 272 N95-22666  CARUSO, STEVEN C.  Aerodynamic design of pegasus: Concept to flight with computational fluid dynamics  [BTN-95-EIX95152582321] p 298 A95-75734  CAUDRON, F.  Experimental investigation of the flowfield about an upswept afterbody  [BTN-95-EIX95152582321] p 265 A95-73524  CAUDRON, F.  Experimental investigation of the flowfield about an upswept afterbody  [BTN-95-EIX95152582321] p 265 A95-73524  CAZENAVE, A.  Geoid lineations of 1000 km wavelength over the central Pacitic  [HTN-95-11304] p 319 A95-77009  CELI, ROBERTO	Automatic guidance and control for helicopter obstacle avoidance [BTN-95-EIX95182619130] p 291 A95-76607  CHERN, JIUN-DAR  Diurnal variation of lee vortices in Taiwan and the surrounding area [HTN-95-91363] p 318 A95-76394  CHEUNG, BENNY K.  System for determining aerodynamic imbalance [NASA-CASE-ARC-11913-1] p 311 N95-23377  CHEUNG, SAMSON  CFD optimization of a theoretical minimum-drag body [BTN-95-EIX95182619234] p 308 A95-76660  CHIANG, WUYING  Dynamic analysis of bearingless tail rotor blades based on nonlinear shell modes [BTN-95-EIX95182619238] p 281 A95-73540  CHIU, CHYN-SHAN  Sidewash on the vertical tail in subsonic and supersonic flows [BTN-95-EIX95152582316] p 264 A95-73519  CHOBOTOV, V. A.  Effects of satellite bunching on the probability of collision in geosynchronous orbit [BTN-95-EIX95152583276] p 298 A95-73577  CHOW, PAO-LIU  Active control of panel vibrations induced by a boundary layer flow [NASA-CR-197867] p 273 N95-23182  CHRISTHILF, DAVID M.  Design and multifunction tests of a frequency domain-based active flutter suppression system [BTN-95-EIX95182619215] p 292 A95-76641  CHUNG, CHAN H.  Numerical analysis of hypersonic low-density scramjet inlet flow [BTN-95-EIX9512645694] p 272 A95-76746  CHURCHILL, GARY B.  System for determining aerodynamic imbalance [NASA-CASE-ARC-11913-1] p 311 N95-23377  CLARKE, ROBERT  Flight test of the X-29A at high angle of attack: Flight dynamics and controls [NASA-TP-3537] p 284 N95-22806
BOWER, DANIEL R.  Analytical study of the neutral stability of a model hypersonic boundary layer [BTN-95-EIX95152577589] p 263 A95-73493 BOYD, D. DOUGLAS, JR.  Analysis of a higher harmonic control test to reduce blade vortex interaction noise [BTN-95-EIX95152582330] p 265 A95-73532 BOYD, IAIN  Particle kinetic simulation of high altitude hypervelocity flight [NASA-CR-197383] p 309 N95-22481 BOZKURT, Y.  Aerodynamic characteristics of external store configurations at low speeds [BTN-95-EIX95182619230] p 271 A95-76656 BRAGG, M. B.  Effect of underwing frost on a transport aircraft airfoil at flight Reynolds number [BTN-95-EIX95152582334] p 276 A95-73536 Aerodynamics of a finite wing with simulated ice [BTN-95-EIX95182619227] p 270 A95-76653 BRAGG, MICHAEL B.  Study of the droplet spray characteristics of a subsonic wind tunnel [BTN-95-EIX95182619235] p 271 A95-76661 BRAZA, M.  Two-equation turbulence model for unsteady separated flows around airfoils [BTN-95-EIX95142553054] p 262 A95-73444 BRENTNER, KENNETH S.  Sensitivity of acoustic predictions to variation of input parameters [HTN-95-80855] p 267 A95-75097 BRIDGES, DAVID H.  Crossflow instability control on a swept-wing: Preliminary studies [NASA-TM-106870] p 320 N95-23283 BRINKER, DAVID J.  Design of a GaAs/Ge solar array for unmanned aerial vehicles [NASA-TM-106870] p 320 N95-23259 BROOKS, CYNTHIA L.  Automation technology using Geographic Information System (GIS)	Simulation and model reduction for the active flexible wing program  [BTN-95-EIX95182619211] p 295 A95-76637  C  CAI, TIMIN  Simulation on the 3-D turbulent flow in the passages of finocyl grain  [BTN-95-EIX95202638962] p 279 A95-76674  CALCAGNO, P.  Geoid lineations of 1000 km wavelength over the central Pacific  [HTN-95-11304] p 319 A95-77009  CALDWELL, D. J.  Modeling aerosol emissions from the combustion of composite materials p 301 N95-23038  CAPOTONDI, ANTONIETTA  Assimilation of altimeter data in a quasi-geostrophic model of the Gulf Stream system: A dynamical perspective  [NASA-CR-196313] p 320 N95-23766  CARBONARO, MARIO C.  Experimental investigation of the flowfield about an upswept afterbody  [BTN-95-EIX95152582321] p 265 A95-73524  CARTER, DALE  Flow visualization studies of VTOL aircraft models during Hover in ground effect  [NASA-TM-108860] p 272 N95-22666  CARLSO, STEVEN C.  Aerodynamic design of pegasus: Concept to flight with computational fluid dynamics  [BTN-95-EIX95182617463] p 298 A95-75734  CAUDRON, F.  Experimental investigation of the flowfield about an upswept afterbody  [BTN-95-EIX95152582321] p 265 A95-73524  CAZENAVE, A.  Geoid lineations of 1000 km wavelength over the central Pacitic  [HTN-95-11304] p 319 A95-77009	Automatic guidance and control for helicopter obstacle avoidance  [BTN-95-EIX95182619130] p 291 A95-76607  CHERN, JIUN-DAR  Diurnal variation of lee vortices in Taiwan and the surrounding area  [HTN-95-91363] p 318 A95-76394  CHEUNG, BENNY K.  System for determining aerodynamic imbalance  [NASA-CASE-ARC-11913-1] p 311 N95-23377  CHEUNG, SAMSON  CFD optimization of a theoretical minimum-drag body  [BTN-95-EIX95182619234] p 308 A95-76660  CHIANG, WUYING  Dynamic analysis of bearingless tail rotor blades based on nonlinear shell modes  [BTN-95-EIX95152582338] p 281 A95-73540  CHIU, CHYN-SHAN  Sidewash on the vertical tail in subsonic and supersonic flows  [BTN-95-EIX95152582316] p 264 A95-73519  CHOBOTOV, V. A.  Effects of satellite bunching on the probability of collision in geosynchronous orbit  [BTN-95-EIX95152583276] p 298 A95-73577  CHOW, PAO-LIU  Active control of panel vibrations induced by a boundary layer flow  [NASA-CR-197667] p 273 N95-23182  CHRISTHILF, DAVID M.  Design and multifunction tests of a frequency domain-based active flutter suppression system  [BTN-95-EIX95182619215] p 292 A95-76641  CHUNG, CHAN H.  Numerical analysis of hypersonic low-density scramjet intel flow  [NSA-CASE-ARC-11913-1] p 311 N95-23377  CLARKE, ROBERT  Flight test of the X-29A at high angle of attack: Flight dynamics and controls  [NASA-TP-3537] p 284 N95-22806

p 318 A95-76267

p 284 A95-76654

p 284 A95-76655

p 291 A95-75772

p 321 A95-76598

p 291 A95-76603

p 322 A95-76626

p 268 A95-75736

p 276 A95-73588

p 280 N95-23565

p 308 A95-76660

p 312 N95-23438

p 305 A95-73479

p 263 A95-73494

p 269 A95-75778

p 288 N95-24030

p 279 A95-75714

p 295 N95-23671

p 321 A95-73471

p 317 A95-76265

p 303 N95-23513

Scientific and technical photography at NASA Langley

Research Center

p 310 N95-23290

Sensitivity of two-dimensional model predictions of COCHRAN, JOHN E., JR. DAVIDSON, LARS ozone response to stratospheric aircraft: An update Aerodynamic flight control to increase payload capability Turbulent transonic airfoil flow simulation using a [HTN-95-A0863] of future launch vehicles oressure-based algorithm INASA-CR-1977041 p 300 N95-24032 | BTN-95-EIX95182619078 | p 269 A95-75763 DOWELL, E. H. Response of a nonrotating rotor blade to lateral COLE, STANLEY R. DAVIS, SANFORD S. turbulence. Part 1: Theory IBTN-95-EIX95182619228 | Summary of an active flexible wing program Aeroacoustic model for weak shock waves based on p 283 A95-76635 |BTN-95-EIX95182619209| Burgers equation Response of a nonrotating rotor blade to lateral COLLINS, FRANK G. p 269 A95-75761 [BTN-95-EIX95182619076] Determination of wall boundary conditions for urbulence. Part 2: Experiment DAWSON, JONATHAN A. IRTN-95-EIX951826192291 high-speed-ratio direct simulation Monte Carlo Effects of expansions on a supersonic boundary layer: DOWELL, EARL H. calculations Surface pressure measurements |BTN-95-EIX95182617457| p 267 A95-75728 Flutter of an infinitely long panel in a duct [BTN-95-EIX95182619087] p 291 IBTN-95-EIX951425530361 p 263 A95-73462 COLLINS, WILLIAM E. DEAN, JEFFREY S. DOWNING, DAVID R. A review of civil aviation fatal accidents in which ATE enabling technologies [BTN-95-EIX95172595294] lost/disoriented was a cause/factor: 1981-1990 Functional agility metrics and optimal trajectory p 287 A95-75718 IDOT/FAA/AM-95/11 p 278 N95-24071 analysis DEATON, JERRY W. |BTN-95-EIX95182619121| COLOZZA, ANTHONY J. Development and verification of a resin film DURHAM, WAYNE C.

Kinematics and aerodynamics of velocity-vector roll Design of a GaAs/Ge solar array for unmanned aerial infusion/resin transfer molding simulation model for vehicles fabrication of advanced textile composites [NASA-TM-106870] p 320 N95-23259 |BTN-95-EIX95182619126| INASA-CR-1974391 p 301 N95-23179 Attainable moments for the constrained control allocation problem CONLEY, JOSEPH L DECKER, RAND A. Engines-only flight control system [NASA-CASE-ARC-11944-1] Tracking of raindrops in flow over an airfoil |BTN-95-EIX95182619149| p 294 N95-23389 |BTN-95-EIX95182619221| p 308 A95-76647 CONSIDINE, DAVID B. DUTTON, J. C. DEJONGE, J. B. Supersonic near-wake afterbody boattailing effects on Sensitivity of two-dimensional model predictions of Review of aeronautical fatigue investigation in the Netherlands during the period March 1991-March 1993 axisymmetric bodies [BTN-95-EIX95182617465] ozone response to stratospheric aircraft. An update p 318 A95-76267 IHTN-95-A08631 p 285 N95-23161 CORNMAN, LARRY B. [PB95-139184] Real-time estimation of atmospheric turbulence severity DELANY, A. from in-situ aircraft measurements A comparison of some aerodynamic resistance methods [BTN-95-EIX95182619231] p 319 A95-76657 using measurements over cotton and grass from the 1991 EASTAUGH, GRAEME F. COUILLAUD, STEPHANE California ozone deposition experiment Flow visualization studies of VTOL aircraft models during p 319 A95-77000 Multiple site fatigue damage in fuselage skin splices: IHTN-95-112951 Experimental simulation and theoretical prediction Hover in ground effect DEMMA, NICK [NASA-TM-108860] IBTN-95-EIX951525846761 p 272 N95-22666 2 micron LIDAR for laser-based remote sensing: Flight EDWARDS, MARK B. COX, G. B., JR. demonstration and application survey Phase 2: HGM air flow tests in support of HEX vane IBTN-95-EIX952126410721 n 319 A95-76737 The role of flight progress strips in en route air traffic p 312 N95-23438 control: A time-series analysis investigation DEROSA, S. CRABILL, NORMAN L. [DOT/FAA/AM-95/4] Structural acoustic calculations in the low-frequency Pilot Weather Advisor system EDWARDS, THOMAS [BTN-95-EIX95152582314] p 316 A95-73517 [BTN-95-EIX95152582336] CFD optimization of a theoretical minimum-drag body p 323 A95-73538 CRAGGS, A. IBTN-95-EIX95182619234 | DESHPANDE, MANISH Finite element model for a flexible non-symmetric rotor EISENHART, D. W. Cavitation modeling in Euler and Navier-Stokes codes on distributed bearing: A stability study p 315 N95-23630 Phase 2: HGM air flow tests in support of HEX vane [BTN-94-EIX94381352212] p 306 A95-74612 nvestigation DESSLER, A. E. CRAMER, K. E. EKATERINARIS, J. A. In situ observations in aircraft exhaust plumes in the New nondestructive techniques for the detection and Effects of spatial order of accuracy on the computation lower stratosphere at midlatitudes quantification of corrosion in aircraft structures IHTN-95-A08621 of vortical flowfields p 318 A95-76266 p 315 N95-23512 [BTN-95-EIX95152577604] DEWITT, KENNETH J. CRANE, JEAN M. Computation of oscillating airfoil flows with one- and Effect of curvature in the numerical simulation of an Flight-deck displays on the Boeing 777 electrothermal de-icer pad two-equation turbulence models p 286 A95-73438 [BTN-95-EIX95142562402] (BTN-95-EIX95152577588) p 276 A95-76645 IRTN-95-FIX951826192191 CRUSE, T. A. EKATERINARIS, JOHN A. Numerical analysis of hypersonic low-density scramjet Mechanical system reliability and risk assessment Viscous-inviscid interaction method for unsteady IBTN-95-EIX951425530461 p 304 A95-73452 inlet flow CUERNO, CRISTINA [BTN-95-EIX95212645694] p 272 A95-76746 tow-speed airfoil flows IRTN-95-EIX951826190931 Design constraints in the payload-range diagram of DEXTER, H. BENSON EKSUZIAN, D. J. ultrahigh capacity transport airplanes [BTN-95-EIX95152582319] Development and verification of a resin film TRISTAR 1: Evaluation methods for testing head-up infusion/resin transfer molding simulation model for p 276 A95-73522 display (HUD) flight symbology [NASA-TM-4665] **CUNNING, GARY** fabrication of advanced textile composites p 301 N95-23179 INASA-CR-1974391 Real-time estimation of atmospheric turbulence severity EL-SHERIEF, HOSSNY from in-situ aircraft measurements DILLENIUS, MARNIX F. E. IBTN-95-EIX951826192311 p 319 A95-76657 Aerodynamic design of pegasus: Concept to flight with Real-time navigation using the global positioning computational fluid dynamics system [BTN-95-EIX95182617463] [BTN-95-EIX95172595298] p 298 A95-75734 D ELBULUK, MALIK E. DISIMILE, PETER J. Observations on using experimental data as boundary Motor drive technologies for the power-by-wire (PBW) D'AZZO, J. J. conditions for computations program: Options, trends and tradeoffs Automatic formation flight control IBTN-95-EIX95182619103] [NASA-TM-106885] p 321 A95-76588 [BTN-95-EIX95182619153] p 292 A95-76630 DOGRA, VIRENDRA K. ELESHAKY, MOHAMED E. Hypersonic rarefied flow past spheres including wake Preconditioned domain decomposition scheme for New failure detection approach and its application to structure three-dimensional aerodynamic sensitivity analysis GPS autonomous integrity monitoring [BTN-95-EIX95152583250] p 305 A95-73551 IBTN-95-EIX95152577612 | p 279 A95-76676 IBTN-95-EIX952026376131 Zonally decoupled direct simulation Monte Carlo ELKINS, J. W. DAHL MILO D solutions of hypersonic blunt-body wake flows Estimates of total organic and inorganic chlorine in the Supersonic jet noise reductions predicted with increased [BTN-95-EIX95182617458] p 268 A95-75729 lower stratosphere from in situ and flask measurements jet spreading rate DOHERR, KARL-FRIEDRICH durina AASE 2 p 323 N95-23178 INASA-TM-1068721 Analytical solution and parameter estimation of projectile [HTN-95-A0861] DARGAN, J. L. dynamics ENG. ANTHONY T. Automatic formation flight control BTN-95-EIX952126456951 p 272 A95-76747 Organic coating technology for the protection of aircraft IBTN-95-EIX95182619153 J p 292 A95-76630 DONOVAN, R. P. against corrosion DARIAN, ARMEN Measurement of particle emissions from clean room CFD analysis of turbopump volutes ENSOR, D. S. gas-handling components IBTN-94-EIX943813590401 p 312 N95-23436 Measurement of particle emissions from clean room p 295 A95-74554 gas-handling components DARLING, DOUGLAS Measurement of moisture and total hydrocarbon Sensitivity of combustion-acoustic instabilities to oundary conditions for premixed gas turbine IRTN-94-FIX943813590401 contributions by valves used in clean room gas-delivery boundary systems combustors |BTN-94-EIX94381359041| p 295 A95-74629 [NASA-TM-106890] p 289 N95-23550 DORENBERG, FRANK M. G. IBTN-94-EIX94381359041 | DAUBE, B. C. Overview of AlliedSignal's avionics development in the In situ observations in aircraft exhaust plumes in the EPSTEIN, RONALD J. p 287 A95-76734 lower stratosphere at midlatitudes [BTN-95-EIX95212641069] 1HTN-95-A08621 p 318 A95-76266 DOUGLASS, ANNE R. pswept afterbody Trajectory modeling of emissions from stratospheric aircraft DAVIDHAZY, ANDREW lowe

[HTN-95-41219]

p 317 A95-75031

•		
ERCOLINE, W. R.	FRULLA, GIACOMO	GRASSO, F.
TRISTAR 1: Evaluation methods for testing head-up display (HUD) flight symbology	Nonlinear angle of twist of advanced composite wing boxes under pure torsion	Simulation of transverse gas injection in turbulent supersonic air flows
[NASA-TM-4665] p 288 N95-24030	BTN-95-EIX95152582323  p 281 A95-73526	[BTN-95-EIX95182619080] p 269 A95-75765
ERICSSON, LARS E.	FRUSTIE, M. J.	GRAY, J. A.
Moving wall effect in relation to other dynamic stall flow mechanisms	Corrosion in service experience with aircraft in France p 303 N95-23518	The corrosion and protection of advanced aluminium - lithium airframe alloys p 302 N95-23497
BTN-95-EIX95152582324  p 265 A95-73527	FUJII, KOZO	GREENDYKE, ROBERT B.
Further analysis of high-rate rolling experiments of a	Numerical investigation of supersonic flows around a spiked blunt body	Convective and radiative heat transfer analysis for the
65-deg delta wing  BTN-95-EIX95152582331  p 281 A95-73533	[BTN-95-EIX95212645690] p 271 A95-76742	fire 2 forebody [BTN-95-EIX95182617460] p 268 A95-75731
ESPANA, MARTIN D.	FULLER, DANA	GREENE, FRANCIS A.
Direct adaptive performance optimization of subsonic	The role of flight progress strips in en route air traffic control: A time-series analysis	Application of the multigrid solution technique to
transports: A periodic perturbation technique [NASA-TM-4676] p 284 N95-22829	[DOT/FAA/AM-95/4] p 280 N95-23565	hypersonic entry vehicles [BTN-95-EIX95152583254] p 306 A95-73555
EST, BRIAN E.	FULLERTON, CHARLES G.	GREENMAN, MATTHEW
Wing vertical position effects on wing-body carryover	Engines-only flight control system [NASA-CASE-ARC-11944-1] p 294 N95-23389	Flutter analysis of composite box beams
for noncircular missiles  BTN-95-EIX95182617462  p 268 A95-75733	,,,,,,,,,,,,,,,,,,,,,,,,,,,,,,,,,,,,,,,	[NASA-CR-197931] p 294 N95-23392 GREGORY, G. L.
EVANS, R. H.	G	Compendium of NASA data base for the Global
TRISTAR 1: Evaluation methods for testing head-up		Tropospheric Experiment's Pacific Exploratory Mission
display (HUD) flight symbology {NASA-TM-4665} p 288 N95-24030	GALLY, THOMAS A.  Control of flow separation in airfoil/wing design	West-A (PEM West-A) [NASA-TM-109177] p 320 N95-23009
(1/10/1/1/1/1005) p 200 1/105/24000	applications p 274 N95-23294	GRIFFIN, O. HAYDEN, JR.
F	GAO, R. S.	An analytical and experimental investigation of the
•	In situ observations in aircraft exhaust plumes in the lower stratosphere at midlatitudes	response of the curved, composite frame/skin specimens
FAETH, G. M.	[HTN-95-A0862] p 318 A95-76266	[HTN-95-80857] p 283 A95-75099
Effect of ambient turbulence intensity on sphere wakes	GAPOSCHKIN, EDWARD M. Calculation of satellite drag coefficients	GRYAZNOV, B. A.
at intermediate Reynolds numbers [BTN-95-EIX95182619101] p 308 A95-76586	[AD-A285118] p 300 N95-23781	Fatigue strength of high-temperature alloys under conditions of cyclic temperature variation. Communication
FAHEY, D. W.	GARG, SANJAY	Experimental procedure and results
Estimates of total organic and inorganic chlorine in the	Stable H(infinity) controller design for the longitudinal dynamics of an aircraft	[BTN-94-EIX94401363884] p 307 A95-75516
lower stratosphere from in situ and flask measurements during AASE 2	[NASA-TM-106847] p 293 N95-22954	GUMASTE, U.  High-performance parallel analysis of coupled problems
[HTN-95-A0861] p 317 A95-76265	GARRARD, WILLIAM L.  Feedback control laws for highly maneuverable	for aircraft propulsion
In situ observations in aircraft exhaust plumes in the lower stratosphere at midlatitudes	aircraft	[NASA-CR-197440] p 289 N95-23088
[HTN-95-A0862] p 318 A95-76266	[NASA-CR-197944] p 295 N95-23410	GUPTA, ROOP N.  Higher-order viscous shock-layer solutions for
FALASCO, THOMAS	GAUTHIER, P.  Corrosion in service experience with aircraft in France	high-altitude flows
H-76B fantail demonstrater composite fan blade fabrication	p 303 N95-23518	[BTN-95-EIX95152583255] p 306 A95-73556
[HTN-95-80856] p 283 A95-75098	GENTRY, GARL L., JR.  Wing pressure distributions from subsonic tests of a	u
FALLER, WILLIAM E.	high-wing transport model	н
Neural network prediction of three-dimensional unsteady separated flowlields	[NASA-TM-4583] p 272 N95-22802	HAAS, BRIAN L.
BTN-95-EIX95182619232  p 308 A95-76658	GERHARDT, HEINZ A.  Natural laminar flow wing concept for supersonic	Particle kinetic simulation of high altitude hypervelocity
BTN-95-EIX95182619232  p 308 A95-76658 FARHAT, C.	Natural laminar flow wing concept for supersonic transports	Particle kinetic simulation of high altitude hypervelocity flight [NASA-CR-197383] p 309 N95-22481
BTN-95-EIX95182619232  p 308 A95-76658 FARHAT, C. High-performance parallel analysis of coupled problems	Natural laminar flow wing concept for supersonic transports [BTN-95-EIX95182619226] p 308 A95-76652	flight  NASA-CR-197383  p 309 N95-22481   HAGENIERS, O. L.
BTN-95-EIX95182619232   p 308 A95-76658 FARHAT, C. High-performance parallel analysis of coupled problems for aircraft propulsion   NASA-CR-197440   p 289 N95-23088	Natural laminar flow wing concept for supersonic transports	flight [NASA-CR-197383] p 309 N95-22481 HAGENIERS, O. L. Double pass retroreflection for corrosion detection in
BTN-95-EIX95182619232   p 308 A95-76658 FARHAT, C. High-performance parallel analysis of coupled problems for aircraft propulsion [NASA-CR-197440 ] p 289 N95-23088 FELIPPA, C. A.	Natural laminar flow wing concept for supersonic transports  [BTN-95-EIX95182619226] p 308 A95-76652  GIBSON, BERRY T.  Natural laminar flow wing concept for supersonic transports	flight [NASA-CR-197383] p 309 N95-22481  MAGENIERS, O. L.  Double pass retroreflection for corrosion detection in aircraft structures p 323 N95-23503  MALL, KENNETH C.
BTN-95-EIX95182619232   p 308 A95-76658 FARHAT, C. High-performance parallel analysis of coupled problems for aircraft propulsion   NASA-CR-197440   p 289 N95-23088	Natural laminar flow wing concept for supersonic transports  [BTN-95-EIX95182619226] p 308 A95-76652  GIBSON, BERRY T.  Natural laminar flow wing concept for supersonic	flight  NASA-CR-197383   p 309 N95-22481  HAGENIERS, O. L  Double pass retroreflection for corrosion detection in aircraft structures p 323 N95-23503  HALL, KENNETH C.  Eigenanalysis of unsteady flows about airfoils. cascades.
BTN-95-EIX95182619232   p 308 A95-76658 FARHAT, C. High-performance parallel analysis of coupled problems for aircraft propulsion   NASA-CR-197440   p 289 N95-23088 FELIPPA, C. A. High-performance parallel analysis of coupled problems for aircraft propulsion   NASA-CR-197440   p 289 N95-23088	Natural laminar flow wing concept for supersonic transports  [BTN-95-EIX95182619226] p 308 A95-76652  GIBSON, BERRY T.  Natural laminar flow wing concept for supersonic transports  [BTN-95-EIX95182619226] p 308 A95-76652  GIEL, P. W.  Three-dimensional Navier-Stokes analysis and redesign	flight [NASA-CR-197383] p 309 N95-22481  MAGENIERS, O. L.  Double pass retroreflection for corrosion detection in aircraft structures p 323 N95-23503  MALL, KENNETH C.
BTN-95-EIX95182619232   p 308 A95-76658 FARHAT, C. High-performance parallel analysis of coupled problems for aircraft propulsion [NASA-CR-197440   p 289 N95-23088 FELIPPA, C. A. High-performance parallel analysis of coupled problems for aircraft propulsion [NASA-CR-197440   p 289 N95-23088 FENG, JINZHANG	Natural laminar flow wing concept for supersonic transports [BTN-95-EIX95182619226] p 308 A95-76652 GIBSON, BERRY T.  Natural laminar flow wing concept for supersonic transports [BTN-95-EIX95182619226] p 308 A95-76652 GIEL. P. W.  Three-dimensional Navier-Stokes analysis and redesign of an imbedded belimouth nozzle in a turbine cascade	flight   NASA-CR-197383   p 309 N95-22481   MAGENIERS, O. L   Double pass retroreflection for corrosion detection in aircraft structures p 323 N95-23503   MALL, KENNETH C.   Eigenanalysis of unsteady flows about airfoils. cascades. and wings   BTN-95-EIX95152577597   p 305 A95-73486   HAMM, CLAUS D.
BTN-95-EIX95182619232   p 308 A95-76658	Natural laminar flow wing concept for supersonic transports  [BTN-95-EIX95182619226] p 308 A95-76652  GIBSON, BERRY T.  Natural laminar flow wing concept for supersonic transports  [BTN-95-EIX95182619226] p 308 A95-76652  GIEL, P. W.  Three-dimensional Navier-Stokes analysis and redesign of an imbedded bellmouth nozzle in a turbine cascade inlet section p 311 N95-23423  GILPIN, T. M.	flight  [NAS-CR-197383] p 309 N95-22481  MAGENIERS, O. L  Double pass retroreflection for corrosion detection in aircraft structures p 323 N95-23503  MALL, KENNETH C.  Eigenanalysis of unsteady flows about airfoils, cascades, and wings  [BTN-95-EIX95152577597] p 305 A95-73486  MAMM, CLAUS D.  Corrosion protection measures for CFC/metal joints of
BTN-95-EIX95182619232   p 308 A95-76658	Natural laminar flow wing concept for supersonic transports  [BTN-95-EIX95182619226] p 308 A95-76652  GIBSON, BERRY T.  Natural laminar flow wing concept for supersonic transports  [BTN-95-EIX95182619226] p 308 A95-76652  GIEL, P. W.  Three-dimensional Navier-Stokes analysis and redesign of an imbedded bellmouth nozzle in a turbine cascade inlet section p 311 N95-23423  GILPIN, T. M.  Estimates of total organic and inorganic chlorine in the	flight   NASA-CR-197383   p 309 N95-22481   MAGENIERS, O. L   Double pass retroreflection for corrosion detection in aircraft structures p 323 N95-23503   MALL, KENNETH C.   Eigenanalysis of unsteady flows about airfoils. cascades, and wings   BTN-95-EIX95152577597   p 305 A95-73486   MAMM, CLAUS D.   Corrosion protection measures for CFC/metal joints of fuel integral tank structures of advanced military aircraft p 303 N95-23510
BTN-95-EIX95182619232   p 308 A95-76658 FARHAT, C. High-performance parallel analysis of coupled problems for aircraft propulsion [NASA-CR-197440   p 289 N95-23088 FELIPPA, C. A. High-performance parallel analysis of coupled problems for aircraft propulsion [NASA-CR-197440   p 289 N95-23088 FENG, JINZHANG Cavitation modeling in Euler and Navier-Stokes codes p 315 N95-23630 FENTRESS, MICHAEL L Experimental evaluation of a box beam specifically	Natural laminar flow wing concept for supersonic transports  [BTN-95-EIX95182619226] p 308 A95-76652  GIBSON, BERRY T.  Natural laminar flow wing concept for supersonic transports  [BTN-95-EIX95182619226] p 308 A95-76652  GIEL, P. W.  Three-dimensional Navier-Stokes analysis and redesign of an imbedded bellmouth nozzle in a turbine cascade inlet section p 311 N95-23423  GILPIN, T. M.  Estimates of total organic and inorganic chlorine in the lower stratosphere from in situ and flask measurements during AASE 2	flight [NASA-CR-197383] p 309 N95-22481  MAGENIERS, O. L.  Double pass retroreflection for corrosion detection in aircraft structures p 323 N95-23503  MALL, KENNETH C.  Eigenanalysis of unsteady flows about airfoils, cascades, and wings [BTN-95-EIX95152577597] p 305 A95-73486  MAMM, CLAUS D.  Corrosion protection measures for CFC/metal joints of fuel integral tank structures of advanced military aircraft p 303 N95-23510  HAMMADI, MUNIR AL
BTN-95-EIX95182619232   p 308 A95-76658	Natural laminar flow wing concept for supersonic transports [BTN-95-EIX95182619226] p 308 A95-76652  GIBSON, BERRY T.  Natural laminar flow wing concept for supersonic transports [BTN-95-EIX95182619226] p 308 A95-76652  GIEL, P. W.  Three-dimensional Navier-Stokes analysis and redesign of an imbedded belimouth nozzle in a turbine cascade inlet section p 311 N95-23423  GILPIN, T. M.  Estimates of total organic and inorganic chlorine in the lower stratosphere from in situ and flask measurements during AASE 2  [HTN-95-A0861] p 317 A95-76265	flight  [NASA-CR-197383]  P 309  N95-22481  HAGENIERS, O. L.  Double pass retroreflection for corrosion detection in aircraft structures  p 323  N95-23503  HALL, KENNETH C.  Eigenanalysis of unsteady flows about airfoils, cascades, and wings  [BTN-95-EIX95152577597]  p 305  A95-73486  HAMM, CLAUS D.  Corrosion protection measures for CFC/metal joints of fuel integral tank structures of advanced military aircraft  p 303  N95-23510  HAMMADI, MUNIR AL  Study of an airfoil with a flap and spoiler  [BTN-95-EIX95152582327]  p 265  A95-73530
BTN-95-EIX95182619232   p 308 A95-76658   FARHAT, C.   High-performance parallel analysis of coupled problems for aircraft propulsion   NASA-CR-197440   p 289 N95-23088   FELIPPA, C. A.   High-performance parallel analysis of coupled problems for aircraft propulsion   NASA-CR-197440   p 289 N95-23088   FENG, JINZHANG   p 289 N95-23088   FENG, JINZHANG   Cavitation modeling in Euler and Navier-Stokes codes p 315 N95-23630   FENTRESS, MICHAEL L   Experimental evaluation of a box beam specifically tailored for chordwise deformation   BTN-95-EIX95182619088   p 283 A95-75773   FERBER, M. K.	Natural laminar flow wing concept for supersonic transports  [BTN-95-EIX95182619226] p 308 A95-76652  GIBSON, BERRY T.  Natural laminar flow wing concept for supersonic transports  [BTN-95-EIX95182619226] p 308 A95-76652  GIEL, P. W.  Three-dimensional Navier-Stokes analysis and redesign of an imbedded bellmouth nozzle in a turbine cascade inlet section p 311 N95-23423  GILPIN, T. M.  Estimates of total organic and inorganic chlorine in the lower stratosphere from in situ and flask measurements during AASE 2  [HTN-95-A0861] p 317 A95-76265  GILYARD, GLENN  Direct adaptive performance optimization of subsonic	flight [NASA-CR-197383] p 309 N95-22481  MAGENIERS, O. L.  Double pass retroreflection for corrosion detection in aircraft structures p 323 N95-23503  MALL, KENNETH C.  Eigenanalysis of unsteady flows about airfoils, cascades, and wings [BTN-95-EIX95152577597] p 305 A95-73486  HAMM, CLAUS D.  Corrosion protection measures for CFC/metal joints of fuel integral tank structures of advanced military aircraft p 303 N95-23510  HAMMADI, MUNIR AL  Study of an airfoil with a flap and spoiler [BTN-95-EIX95152582327] p 265 A95-73530  HANFF, ERNEST S.
BTN-95-EIX95182619232   p 308 A95-76658	Natural laminar flow wing concept for supersonic transports  [BTN-95-EIX95182619226] p 308 A95-76652  GIBSON, BERRY T.  Natural laminar flow wing concept for supersonic transports  [BTN-95-EIX95182619226] p 308 A95-76652  GIEL, P. W.  Three-dimensional Navier-Stokes analysis and redesign of an imbedded bellmouth nozzle in a turbine cascade inlet section p 311 N95-23423  GILPIN, T. M.  Estimates of total organic and inorganic chlorine in the lower stratosphere from in situ and flask measurements during AASE 2  [HTN-95-A0861] p 317 A95-76265  GILYARD, GLENN  Direct adaptive performance optimization of subsonic transports: A periodic perturbation technique	flight  [NASA-CR-197383]  P 309  N95-22481  HAGENIERS, O. L.  Double pass retroreflection for corrosion detection in aircraft structures  p 323  N95-23503  HALL, KENNETH C.  Eigenanalysis of unsteady flows about airfoils, cascades, and wings  [BTN-95-EIX95152577597]  p 305  A95-73486  HAMM, CLAUS D.  Corrosion protection measures for CFC/metal joints of fuel integral tank structures of advanced military aircraft  p 303  N95-23510  HAMMADI, MUNIR AL  Study of an airfoil with a flap and spoiler  [BTN-95-EIX95152582327]  p 265  A95-73530
BTN-95-EIX95182619232   p 308 A95-76658   FARHAT, C.   High-performance parallel analysis of coupled problems for aircraft propulsion   NASA-CR-197440   p 289 N95-23088   FELIPPA, C. A.   High-performance parallel analysis of coupled problems for aircraft propulsion   NASA-CR-197440   p 289 N95-23088   FENG, JINZHANG   p 289 N95-23088   FENG, JINZHANG   Cavitation modeling in Euler and Navier-Stokes codes p 315 N95-23630   FENTRESS, MICHAEL L   Experimental evaluation of a box beam specifically tailored for chordwise deformation   BTN-95-EIX95182619088   p 283 A95-75773   FERBER, M. K.   Evolution of oxidation and creep damage mechanisms in HIPed silicon nitride materials   DE95-001360   p 300 N95-22689	Natural laminar flow wing concept for supersonic transports  [BTN-95-EIX95182619226] p 308 A95-76652  GIBSON, BERRY T.  Natural laminar flow wing concept for supersonic transports  [BTN-95-EIX95182619226] p 308 A95-76652  GIEL, P. W.  Three-dimensional Navier-Stokes analysis and redesign of an imbedded bellmouth nozzle in a turbine cascade inlet section p 311 N95-23423  GILPIN, T. M.  Estimates of total organic and inorganic chlorine in the lower stratosphere from in situ and flask measurements during AASE 2  [HTN-95-A0861] p 317 A95-76265  GILYARD, GLENN  Direct adaptive performance optimization of subsonic	flight  [NASA-CR-197383] p 309 N95-22481  MAGENIERS, O. L  Double pass retroreflection for corrosion detection in aircraft structures p 323 N95-23503  MALL, KENNETH C.  Eigenanalysis of unsteady flows about airfoils. cascades. and wings  [BTN-95-EIX95152577597] p 305 A95-73486  HAMM, CLAUS D.  Corrosion protection measures for CFC/metal joints of fuel integral tank structures of advanced military aircraft p 300 N95-23510  HAMMADI, MUNIR AL  Study of an airfoil with a flap and spoiler  [BTN-95-EIX95152582327] p 265 A95-73530  HANFF, ERNEST S.  Further analysis of high-rate rolling experiments of a 65-deg delta wing  [BTN-95-EIX95152582331] p 281 A95-73533
BTN-95-EIX95182619232   p 308 A95-76658   FARHAT, C.   High-performance parallel analysis of coupled problems for aircraft propulsion   NASA-CR-197440   p 289 N95-23088   FELIPPA, C. A.   High-performance parallel analysis of coupled problems for aircraft propulsion   NASA-CR-197440   p 289 N95-23088   FENG, JINZHANG   p 289 N95-23088   FENG, JINZHANG   Cavitation modeling in Euler and Navier-Stokes codes p 315 N95-23630   FENTRESS, MICHAEL L   Experimental evaluation of a box beam specifically tailored for chordwise deformation   BTN-95-EIX95182619088   p 283 A95-75773   FERBER, M. K.   Evolution of oxidation and creep damage mechanisms in HIPed silicon nitride materials   DE95-001360   p 300 N95-22689   FERGUSON, T. V.	Natural laminar flow wing concept for supersonic transports  [BTN-95-EIX95182619226] p 308 A95-76652  GIBSON, BERRY T.  Natural laminar flow wing concept for supersonic transports  [BTN-95-EIX95182619226] p 308 A95-76652  GIEL, P. W.  Three-dimensional Navier-Stokes analysis and redesign of an imbedded bellmouth nozzle in a turbine cascade inlet section p 311 N95-23423  GILPIN, T. M.  Estimates of total organic and inorganic chlorine in the lower stratosphere from in situ and flask measurements during AASE 2  [HTN-95-A0861] p 317 A95-76265  GILYARD, GLENN  Direct adaptive performance optimization of subsonic transports: A periodic perturbation technique [NASA-TM-4676] p 284 N95-22829  GILYARD, GLENN B  Engines-only flight control system	flight [NASA-CR-197383] p 309 N95-22481  MAGENIERS, O. L.  Double pass retroreflection for corrosion detection in aircraft structures p 323 N95-23503  MALL, KENNETH C.  Eigenanalysis of unsteady flows about airfoils, cascades, and wings [BTN-95-EIX95152577597] p 305 A95-73486  MAMM, CLAUS D.  Corrosion protection measures for CFC/metal joints of fuel integral tank structures of advanced military aircraft p 303 N95-23510  HAMMADI, MUNIR AL  Study of an airfoil with a flap and spoiler [BTN-95-EIX95152582327] p 265 A95-73530  HANFF, ERNEST S.  Further analysis of high-rate rolling experiments of a 65-deg delta wing [BTN-95-EIX95152582331] p 281 A95-73533  HANGE, CRAIG
BTN-95-EIX95182619232   p 308  A95-76658   FARHAT, C.   High-performance parallel analysis of coupled problems for aircraft propulsion   NASA-CR-197440   p 289  N95-23088   FELIPPA, C. A.   High-performance parallel analysis of coupled problems for aircraft propulsion   NASA-CR-197440   p 289  N95-23088   FENG, JINZHANG   p 289  N95-23088   FENG, JINZHANG   Cavitation modeling in Euler and Navier-Stokes codes p 315  N95-23630   FENTRESS, MICHAEL L   Experimental evaluation of a box beam specifically tailored for chordwise deformation   BTN-95-EIX95182619088   p 283  A95-75773   FERBER, M. K.   Evolution of oxidation and creep damage mechanisms in HIPed silicon nitride materials   DE95-001360   p 300  N95-22689   FERGUSON, T. V.   Impeller flow field characterization with a laser two-focus velocimeter	Natural laminar flow wing concept for supersonic transports [BTN-95-EIX95182619226] p 308 A95-76652  GIBSON, BERRY T.  Natural laminar flow wing concept for supersonic transports [BTN-95-EIX95182619226] p 308 A95-76652  GIEL, P. W.  Three-dimensional Navier-Stokes analysis and redesign of an imbedded belimouth nozzle in a turbine cascade inlet section p 311 N95-23423  GILPIN, T. M.  Estimates of total organic and inorganic chlorine in the lower stratosphere from in situ and flask measurements during AASE 2  [HTN-95-A0861] p 317 A95-76265  GILYARD, GLENN  Direct adaptive performance optimization of subsonic transports: A periodic perturbation technique [NASA-TM-4676] p 284 N95-22829  GILYARD, GLENN B  Engines-only flight control system [NASA-CASE-ARC-11944-1] p 294 N95-23389	flight  [NASA-CR-197383] p 309 N95-22481  MAGENIERS, O. L  Double pass retroreflection for corrosion detection in aircraft structures p 323 N95-23503  MALL, KENNETH C.  Eigenanalysis of unsteady flows about airfoils. cascades. and wings  [BTN-95-EIX95152577597] p 305 A95-73486  HAMM, CLAUS D.  Corrosion protection measures for CFC/metal joints of fuel integral tank structures of advanced military aircraft p 303 N95-23510  HAMMADI, MUNIR AL  Study of an airfoil with a flap and spoiler  [BTN-95-EIX95152582327] p 265 A95-73530  HANFF, ERNEST S.  Further analysis of high-rate rolling experiments of a 65-deg delta wing  [BTN-95-EIX95152582331] p 281 A95-73533  HANGE, CRAIG  Flow visualization studies of VTOL aircraft models during Hover in ground effect
BTN-95-EIX95182619232   p 308 A95-76658   FARHAT, C.   High-performance parallel analysis of coupled problems for aircraft propulsion   NASA-CR-197440   p 289 N95-23088   FELIPPA, C. A. High-performance parallel analysis of coupled problems for aircraft propulsion   NASA-CR-197440   p 289 N95-23088   FENG, JINZHANG   p 289 N95-23088   FENG, JINZHANG   Cavitation modeling in Euler and Navier-Stokes codes p 315 N95-23630   FENTRESS, MICHAEL L   Experimental evaluation of a box beam specifically tailored for chordwise deformation   BTN-95-EIX95182619088   p 283 A95-75773   FERBER, M. K.   Evolution of oxidation and creep damage mechanisms in HIPed silicon nitride materials   DE95-001360   p 300 N95-22689   FERGUSON, T. V.   Impeller flow field characterization with a laser two-focus velocimeter   p 313 N95-23440   FINK, C. L.	Natural laminar flow wing concept for supersonic transports  [BTN-95-EIX95182619226] p 308 A95-76652  GIBSON, BERRY T.  Natural laminar flow wing concept for supersonic transports  [BTN-95-EIX95182619226] p 308 A95-76652  GIEL, P. W.  Three-dimensional Navier-Stokes analysis and redesign of an imbedded bellmouth nozzle in a turbine cascade inlet section p 311 N95-23423  GILPIN, T. M.  Estimates of total organic and inorganic chlorine in the lower stratosphere from in situ and flask measurements during AASE 2  [HTN-95-A0861] p 317 A95-76265  GILYARD, GLENN  Direct adaptive performance optimization of subsonic transports: A periodic perturbation technique [NASA-TM-4676] p 284 N95-22829  GILYARD, GLENN B  Engines-only flight control system  [NASA-CASE-ARC-11944-1] p 294 N95-23389  GLASSMAN, ARTHUR J.  Enhanced analysis and users manual for radial-inflow	flight   INASA-CR-197383   p 309 N95-22481   MAGENIERS, O. L   Double pass retrorellection for corrosion detection in aircraft structures p 323 N95-23503   MALL, KENNETH C.
BTN-95-EIX95182619232   p 308 A95-76658 FARHAT, C. High-performance parallel analysis of coupled problems for aircraft propulsion   NASA-CR-197440   p 289 N95-23088 FELIPPA, C. A. High-performance parallel analysis of coupled problems for aircraft propulsion   NASA-CR-197440   p 289 N95-23088 FENG, JINZHANG   p 289 N95-23088 FENG, JINZHANG   Cavitation modeling in Euler and Navier-Stokes codes p 315 N95-23630 FENTRESS, MICHAEL L   Experimental evaluation of a box beam specifically tailored for chordwise deformation   BTN-95-EIX95182619088   p 283 A95-75773 FERBER, M. K.   Evolution of oxidation and creep damage mechanisms in HiPed silicon nitride materials   DE95-001360   p 300 N95-22689 FERGUSON, T. V.   Impeller flow field characterization with a laser two-focus velocimeter   p 313 N95-23440 FINK, C. L.   Evaluation of neutron fechniques for illicit substance detection	Natural laminar flow wing concept for supersonic transports [BTN-95-EIX95182619226] p 308 A95-76652  GIBSON, BERRY T.  Natural laminar flow wing concept for supersonic transports [BTN-95-EIX95182619226] p 308 A95-76652  GIEL, P. W.  Three-dimensional Navier-Stokes analysis and redesign of an imbedded belimouth nozzle in a turbine cascade inlet section p 311 N95-23423  GILPIN, T. M.  Estimates of total organic and inorganic chlorine in the lower stratosphere from in situ and flask measurements during AASE 2  [HTN-95-A0861] p 317 A95-76265  GILYARD, GLENN  Direct adaptive performance optimization of subsonic transports: A periodic perturbation technique [NASA-TM-4676] p 284 N95-22829  GILYARD, GLENN B  Engines-only flight control system [NASA-CASE-ARC-11944-1] p 294 N95-23389  GLASSMAN, ARTHUR J.  Enhanced analysis and users manual for radial-inflow turbine conceptual design code RTD	flight  [NASA-CR-197383]  P 309 N95-22481  MAGENIERS, O. L.  Double pass retroreflection for corrosion detection in aircraft structures  P 323 N95-23503  MALL, KENNETH C.  Eigenanalysis of unsteady flows about airfoils, cascades, and wings  [BTN-95-EIX95152577597]  P 305 A95-73486  HAMM, CLAUS D.  Corrosion protection measures for CFC/metal joints of fuel integral tank structures of advanced military aircraft  P 303 N95-23510  HAMMADI, MUNIR AL  Study of an airfoil with a flap and spoiler  [BTN-95-EIX95152582327]  P 265 A95-73530  HANFF, ERNEST S.  Further analysis of high-rate rolling experiments of a 65-deg delta wing  [BTN-95-EIX95152582331]  P 281 A95-73533  HANGE, CRAIG  Flow visualization studies of VTOL aircraft models during Hover in ground effect  [NASA-TM-108860]  P 272 N95-22666  HARDY, G. L.  Corrosion detection and monitoring of aircraft structures:
BTN-95-EIX95182619232   p 308 A95-76658	Natural laminar flow wing concept for supersonic transports  [BTN-95-EIX95182619226] p 308 A95-76652  GIBSON, BERRY T.  Natural laminar flow wing concept for supersonic transports  [BTN-95-EIX95182619226] p 308 A95-76652  GIEL, P. W.  Three-dimensional Navier-Stokes analysis and redesign of an imbedded bellmouth nozzle in a turbine cascade inlet section p 311 N95-23423  GILPIN, T. M.  Estimates of total organic and inorganic chlorine in the lower stratosphere from in situ and flask measurements during AASE 2  [HTN-95-A0861] p 317 A95-76265  GILYARD, GLENN  Direct adaptive performance optimization of subsonic transports: A periodic perturbation technique [NASA-TM-4676] p 284 N95-22829  GILYARD, GLENN B  Engines-only flight control system  [NASA-CASE-ARC-11944-1] p 294 N95-23389  GLASSMAN, ARTHUR J.  Enhanced analysis and users manual for radial-inflow turbine conceptual design code RTD  [NASA-CR-195442] p 275 N95-23462  GOLDMAN, ROBERT P.	flight   INASA-CR-197383   p 309 N95-22481   MAGENIERS, O. L   Double pass retrorellection for corrosion detection in aircraft structures p 323 N95-23503   MALL, KENNETH C.
BTN-95-EIX95182619232   p 308 A95-76658 FARHAT, C. High-performance parallel analysis of coupled problems for aircraft propulsion   NASA-CR-197440   p 289 N95-23088 FELIPPA, C. A. High-performance parallel analysis of coupled problems for aircraft propulsion   NASA-CR-197440   p 289 N95-23088 FENG, JINZHANG   p 289 N95-23088 FENG, JINZHANG   Cavitation modeling in Euler and Navier-Stokes codes p 315 N95-23630 FENTRESS, MICHAEL L. Experimental evaluation of a box beam specifically tailored for chordwise deformation   BTN-95-EIX95182619088   p 283 A95-75773 FERBER, M. K. Evolution of oxidation and creep damage mechanisms in HIPed silicon nitride materials   DE95-001360   p 300 N95-22689 FERGUSON, T. V. Impeller flow field characterization with a laser two-focus velocimeter p 313 N95-23440 FINK, C. L. Evaluation of neutron techniques for illicit substance detection   DE95-002988   p 300 N95-22764 FINLEY, DENNIS B. Euler Technology Assessment program for preliminary	Natural laminar flow wing concept for supersonic transports  [BTN-95-EIX95182619226] p 308 A95-76652  GIBSON, BERRY T.  Natural laminar flow wing concept for supersonic transports  [BTN-95-EIX95182619226] p 308 A95-76652  GIEL, P. W.  Three-dimensional Navier-Stokes analysis and redesign of an imbedded belimouth nozzle in a turbine cascade inlet section p 311 N95-23423  GILPIN, T. M.  Estimates of total organic and inorganic chlorine in the lower stratosphere from in situ and flask measurements during AASE 2  [HTN-95-A0861] p 317 A95-76265  GILYARD, GLENN  Direct adaptive performance optimization of subsonic transports: A periodic perturbation technique  [NASA-TM-4676] p 284 N95-22829  GILYARD, GLENN B  Engines-only flight control system  [NASA-CASE-ARC-11944-1] p 294 N95-23389  GLASSMAN, ARTHUR J.  Enhanced analysis and users manual for radial-inflow turbine conceptual design code RTD  [NASA-CR-195454] p 275 N95-23462  GOLDMAN, ROBERT P.  Empirical results on scheduling and dynamic	flight  [NASA-CR-197383]  P 309 N95-22481  MAGENIERS, O. L.  Double pass retroreflection for corrosion detection in aircraft structures  P 323 N95-23503  MALL, KENNETH C.  Eigenanalysis of unsteady flows about airfoils, cascades, and wings  [BTN-95-EIX95152577597]  P 305 A95-73486  HAMM, CLAUS D.  Corrosion protection measures for CFC/metal joints of fuel integral tank structures of advanced military aircraft  P 303 N95-23510  HAMMADI, MUNIR AL  Study of an airfoil with a flap and spoiler  [BTN-95-EIX95152582327]  P 265 A95-73530  HANFF, ERNEST S.  Further analysis of high-rate rolling experiments of a 65-deg delta wing  [BTN-95-EIX95152582331]  P 281 A95-73533  HANGE, CRAIG  Flow visualization studies of VTOL aircraft models during Hover in ground effect  [NASA-TM-108860]  P 272 N95-22666  HARDY, G. L.  Corrosion detection and monitoring of aircraft structures: An overview  P 303 N95-23515  HARRIS, BRENDA W.  An assessment of viscous effects in computational
BTN-95-EIX95182619232   p 308 A95-76658   FARHAT, C.   High-performance parallel analysis of coupled problems for aircraft propulsion   NASA-CR-197440   p 289 N95-23088   FELIPPA, C. A. High-performance parallel analysis of coupled problems for aircraft propulsion   NASA-CR-197440   p 289 N95-23088   FENG, JINZHANG   p 289 N95-23088   FENG, JINZHANG   Cavitation modeling in Euler and Navier-Stokes codes p 315 N95-23630   FENG, JINZHANG   Cavitation modeling in Euler and Navier-Stokes codes p 315 N95-23630   FENTRESS, MICHAEL L   Experimental evaluation of a box beam specifically tailored for chordwise deformation   BTN-95-EIX95182619088   p 283 A95-75773   FERBER, M. K.   Evolution of oxidation and creep damage mechanisms in HIPed silicon nitride materials   DE95-001360   p 300 N95-22689   FERGUSON, T. V.   Impeller flow field characterization with a laser two-focus velocimeter   p 313 N95-23440   FINK, C. L   Evaluation of neutron techniques for illicit substance detection   DE95-002988   p 300 N95-22764   FINLEY, DENNIS B.   Euler Technology Assessment program for preliminary aircraft design employing SPLITFLOW code with Cartesian	Natural laminar flow wing concept for supersonic transports  [BTN-95-EIX95182619226] p 308 A95-76652  GIBSON, BERRY T.  Natural laminar flow wing concept for supersonic transports  [BTN-95-EIX95182619226] p 308 A95-76652  GIEL, P. W.  Three-dimensional Navier-Stokes analysis and redesign of an imbedded bellmouth nozzle in a turbine cascade inlet section p 311 N95-23423  GILPIN, T. M.  Estimates of total organic and inorganic chlorine in the lower stratosphere from in situ and flask measurements during AASE 2  [HTN-95-A0861] p 317 A95-76265  GILYARD, GLENN  Direct adaptive performance optimization of subsonic transports: A periodic perturbation technique [NASA-TM-4676] p 284 N95-22829  GILYARD, GLENN B  Engines-only flight control system  [NASA-CASE-ARC-11944-1] p 294 N95-23389  GLASSMAN, ARTHUR J.  Enhanced analysis and users manual for radial-inflow turbine conceptual design code RTD  INASA-CR-195454] p 275 N95-23462  GOLDMAN, ROBERT P.  Empirical results on scheduling and dynamic backtracking p 299 N95-23761	flight  INASA-CR-197383   p 309 N95-22481  HAGENIERS, O. L  Double pass retrorellection for corrosion detection in aircraft structures p 323 N95-23503  HALL, KENNETH C.  Eigenanalysis of unsteady flows about airfoils, cascades, and wings  [BTN-95-EIX95152577597] p 305 A95-73486  HAMM, CLAUS D.  Corrosion protection measures for CFC/metal joints of fuel integral tank structures of advanced military aircraft p 303 N95-23510  HAMMADI, MUNIR AL  Study of an airfoil with a flap and spoiler  [BTN-95-EIX95152582327] p 265 A95-73530  HANFF, ERNEST S.  Further analysis of high-rate rolling experiments of a 65-deg delta wing  [BTN-95-EIX95152582331] p 281 A95-73533  HANGE, CRAIG  Flow visualization studies of VTOL aircraft models during Hover in ground effect  [NASA-TM-108860] p 272 N95-22666  HARDY, G. L  Corrosion detection and monitoring of aircraft structures: An overview p 303 N95-23515  HARRIS, BRENDA W.  An assessment of viscous effects in computational simulation of benign and burst vortex flows on generic
BTN-95-EIX95182619232   p 308 A95-76658 FARHAT, C. High-performance parallel analysis of coupled problems for aircraft propulsion   NASA-CR-197440   p 289 N95-23088 FELIPPA, C. A. High-performance parallel analysis of coupled problems for aircraft propulsion   NASA-CR-197440   p 289 N95-23088 FENG, JINZHANG   p 289 N95-23088 FENG, JINZHANG   Cavitation modeling in Euler and Navier-Stokes codes p 315 N95-23630 FENTRESS, MICHAEL L. Experimental evaluation of a box beam specifically tailored for chordwise deformation   BTN-95-EIX95182619088   p 283 A95-75773 FERBER, M. K. Evolution of oxidation and creep damage mechanisms in HIPed silicon nitride materials   DE95-001360   p 300 N95-22689 FERGUSON, T. V. Impeller flow field characterization with a laser two-focus velocimeter p 313 N95-23440 FINK, C. L. Evaluation of neutron techniques for illicit substance detection   DE95-002988   p 300 N95-22764 FINLEY, DENNIS B. Euler Technology Assessment program for preliminary	Natural laminar flow wing concept for supersonic transports  [BTN-95-EIX95182619226] p 308 A95-76652  GIBSON, BERRY T.  Natural laminar flow wing concept for supersonic transports  [BTN-95-EIX95182619226] p 308 A95-76652  GIEL, P. W.  Three-dimensional Navier-Stokes analysis and redesign of an imbedded belimouth nozzle in a turbine cascade inlet section p 311 N95-23423  GILPIN, T. M.  Estimates of total organic and inorganic chlorine in the lower stratosphere from in situ and flask measurements during AASE 2  [HTN-95-A0861] p 317 A95-76265  GILYARD, GLENN  Direct adaptive performance optimization of subsonic transports: A periodic perturbation technique  [NASA-TM-4676] p 284 N95-22829  GILYARD, GLENN B  Engines-only flight control system  [NASA-CASE-ARC-11944-1] p 294 N95-23389  GLASSMAN, ARTHURJ  Enhanced analysis and users manual for radial-inflow turbine conceptual design code RTD  [NASA-CR-195454] p 275 N95-23462  GOLDMAN, ROBERT P.  Empirical results on scheduling and dynamic backtracking p 299 N95-23761  GOLDTHORPE, STEVE H.  Guidance and control requirements for high-speed	flight  [NASA-CR-197383]  P 309 N95-22481  MAGENIERS, O. L.  Double pass retroreflection for corrosion detection in aircraft structures  P 323 N95-23503  MALL, KENNETH C.  Eigenanalysis of unsteady flows about airfoils, cascades, and wings  [BTN-95-EIX95152577597]  P 305 A95-73486  HAMM, CLAUS D.  Corrosion protection measures for CFC/metal joints of fuel integral tank structures of advanced military aircraft  P 303 N95-23510  HAMMADI, MUNIR AL  Study of an airfoil with a flap and spoiler  [BTN-95-EIX95152582327]  P 265 A95-73530  HANFF, ERNEST S.  Further analysis of high-rate rolling experiments of a 65-deg delta wing  [BTN-95-EIX95152582331]  P 281 A95-73533  HANGE, CRAIG  Flow visualization studies of VTOL aircraft models during Hover in ground effect  [NASA-TM-108860]  P 272 N95-22666  HARDY, G. L.  Corrosion detection and monitoring of aircraft structures: An overview  P 303 N95-23515  HARRIS, BRENDA W.  An assessment of viscous effects in computational simulation of benign and burst vortex flows on generic fighter wind-tunnel models using TEAM code [NASA-CR-4650]  P 273 N95-23185
BTN-95-EIX95182619232   p 308 A95-76658 FARHAT, C. High-performance parallel analysis of coupled problems for aircraft propulsion   NASA-CR-197440   p 289 N95-23088	Natural laminar flow wing concept for supersonic transports  [BTN-95-EIX95182619226] p 308 A95-76652  GIBSON, BERRY T.  Natural laminar flow wing concept for supersonic transports  [BTN-95-EIX95182619226] p 308 A95-76652  GIEL, P. W.  Three-dimensional Navier-Stokes analysis and redesign of an imbedded bellmouth nozzle in a turbine cascade inlet section p 311 N95-23423  GILPIN, T. M.  Estimates of total organic and inorganic chlorine in the lower stratosphere from in situ and flask measurements during AASE 2  IHTN-95-A0861  p 317 A95-76265  GILYARD, GLENN  Direct adaptive performance optimization of subsonic transports: A periodic perturbation technique  [NASA-TM-4676] p 284 N95-22829  GILYARD, GLENN B  Engines-only flight control system  [NASA-CASE-ARC-11944-1] p 294 N95-23389  GLASSMAN, ARTHUR J.  Enhanced analysis and users manual for radial-inflow turbine conceptual design code RTD  [NASA-CR-195454] p 275 N95-23462  GOLDMAN, ROBERT P.  Empirical results on scheduling and dynamic backtracking p 299 N95-23761  GOLDTHORPE, STEVE H.  Guidance and control requirements for high-speed Rollout and Turnoff (ROTO)	flight   INASA-CR-197383   p 309 N95-22481   MAGENIERS, O. L   Double pass retrorellection for corrosion detection in aircraft structures p 323 N95-23503   MALL, KENNETH C.
BTN-95-EIX95182619232   p 308  A95-76658   FARHAT, C.   High-performance parallel analysis of coupled problems for aircraft propulsion   NASA-CR-197440   p 289  N95-23088   FELIPPA, C. A.   High-performance parallel analysis of coupled problems for aircraft propulsion   NASA-CR-197440   p 289  N95-23088   FENG, JINZHANG   p 289  N95-23088   FENG, JINZHANG   Cavitation modeling in Euler and Navier-Stokes codes p 315  N95-23630   N95-23630   FENTRESS, MICHAEL L   Experimental evaluation of a box beam specifically tailored for chordwise deformation   BTN-95-EIX95182619088   p 283  A95-75773   FERBER, M. K.   Evolution of oxidation and creep damage mechanisms in HiPed silicon nitride materials   DE95-001360   p 300  N95-22689   FERGUSON, T. V.   Impeller flow field characterization with a laser two-focus velocimeter	Natural laminar flow wing concept for supersonic transports  [BTN-95-EIX95182619226] p 308 A95-76652  GIBSON, BERRY T.  Natural laminar flow wing concept for supersonic transports  [BTN-95-EIX95182619226] p 308 A95-76652  GIEL, P, W.  Three-dimensional Navier-Stokes analysis and redesign of an imbedded bellmouth nozzle in a turbine cascade inlet section p 311 N95-23423  GILPIN, T. M.  Estimates of total organic and inorganic chlorine in the lower stratosphere from in situ and flask measurements during AASE 2  [HTN-95-A0861] p 317 A95-76265  GILYARD, GLENN  Direct adaptive performance optimization of subsonic transports: A periodic perturbation technique  [NASA-TM-4676] p 284 N95-22829  GILYARD, GLENN B  Engines-only flight control system  [NASA-CASE-ARC-11944-1] p 294 N95-23389  GLASSMAN, ARTHUR J.  Enhanced analysis and users manual for radial-inflow turbine conceptual design code RTD  [NASA-CR-195454] p 275 N95-23462  GOLDMAN, ROBERT P.  Empirical results on scheduling and dynamic backtracking p 299 N95-23761  GOLDTHORPE, STEVE H.  Guidance and control requirements for high-speed Rollout and Turnoff (ROTO)  [NASA-CR-195026] p 292 N95-22674	flight  [NASA-CR-197383]  P 309 N95-22481  MAGENIERS, O. L.  Double pass retroreflection for corrosion detection in aircraft structures  P 323 N95-23503  MALL, KENNETH C.  Eigenanalysis of unsteady flows about airfoils, cascades, and wings  [BTN-95-EIX95152577597]  P 305 A95-73486  HAMM, CLAUS D.  Corrosion protection measures for CFC/metal joints of fuel integral tank structures of advanced military aircraft  P 303 N95-23510  HAMMADI, MUNIR AL  Study of an airfoil with a flap and spoiler  [BTN-95-EIX95152582327]  P 265 A95-73530  HANFF, ERNEST S.  Further analysis of high-rate rolling experiments of a 65-deg delta wing  [BTN-95-EIX95152582331]  P 281 A95-73533  HANGE, CRAIG  Flow visualization studies of VTOL aircraft models during Hover in ground effect  [NASA-TM-108860]  P 272 N95-22666  HARDY, G. L.  Corrosion detection and monitoring of aircraft structures: An overview  P 303 N95-23515  HARRIS, BRENDA W.  An assessment of viscous effects in computational simulation of benign and burst vortex flows on generic fighter wind-tunnel models using TEAM code [NASA-CR-4650]  P 273 N95-23185
BTN-95-EIX95182619232   p 308 A95-76658   FARHAT, C.	Natural laminar flow wing concept for supersonic transports  [BTN-95-EIX95182619226] p 308 A95-76652  GIBSON, BERRY T.  Natural laminar flow wing concept for supersonic transports  [BTN-95-EIX95182619226] p 308 A95-76652  GIEL, P. W.  Three-dimensional Navier-Stokes analysis and redesign of an imbedded belimouth nozzle in a turbine cascade inlet section p 311 N95-23423  GILPIN, T. M.  Estimates of total organic and inorganic chlorine in the lower stratosphere from in situ and flask measurements during AASE 2  [HTN-95-A0861] p 317 A95-76265  GILYARD, GLENN  Direct adaptive performance optimization of subsonic transports: A periodic perturbation technique  [NASA-TM-4676] p 284 N95-22829  GILYARD, GLENN B  Engines-only flight control system  [NASA-CASE-ARC-11944-1] p 294 N95-23389  GLASSMAN, ARTHUR J.  Enhanced analysis and users manual for radial-inflow turbine conceptual design code RTD  [NASA-CR-195454]  GOLDMAN, ROBERT P.  Empirical results on scheduling and dynamic backtracking p 299 N95-23761  GOLDTHORPE, STEVE H.  Guidance and control requirements for high-speed Rollout and Turnoff (ROTO)  [NASA-CR-195026] p 292 N95-22674  GOLDWIRE, H.  NTS-spill test facility wind tunnel exhaust plume	flight   INASA-CR-197383   p 309 N95-22481   MAGENIERS, O. L   Double pass retrorellection for corrosion detection in aircraft structures p 323 N95-23503   MALL, KENNETH C.
BTN-95-EIX95182619232   p 308 A95-76658   FARHAT, C. L. Evaluation of neutron techniques for blems in HIPed silicon nitride materials   p 309 N95-23640   p 309 N95-23689   p 300 N95-23640	Natural laminar flow wing concept for supersonic transports  [BTN-95-EIX95182619226] p 308 A95-76652  GIBSON, BERRY T.  Natural laminar flow wing concept for supersonic transports  [BTN-95-EIX95182619226] p 308 A95-76652  GIEL, P, W.  Three-dimensional Navier-Stokes analysis and redesign of an imbedded bellmouth nozzle in a turbine cascade inlet section p 311 N95-23423  GILPIN, T. M.  Estimates of total organic and inorganic chlorine in the lower stratosphere from in situ and flask measurements during AASE 2  [HTN-95-A0861] p 317 A95-76265  GILYARD, GLENN  Direct adaptive performance optimization of subsonic transports: A periodic perturbation technique [NASA-TM-4676] p 284 N95-22829  GILYARD, GLENN B  Engines-only flight control system  [NASA-CASE-ARC-11944-1] p 294 N95-23389  GLASSMAN, ARTHUR J.  Enhanced analysis and users manual for radial-inflow turbine conceptual design code RTD  [NASA-CR-195454] p 275 N95-23462  GOLDMAN, ROBERT P.  Empirical results on scheduling and dynamic backtracking p 299 N95-23761  GOLDTHORPE, STEVE H.  Guidance and control requirements for high-speed Rollout and Turnoff (ROTO)  [NASA-CR-195026] p 292 N95-22674  GOLDWIRE, H.  NTS-spill test facility wind tunnel exhaust plume characterization  [DE95-003630] p 297 N95-24019	flight  [NASA-CR-197383]  P 309 N95-22481  MAGENIERS, O. L.  Double pass retrorellection for corrosion detection in aircraft structures  P 323 N95-23503  MALL, KENNETH C.  Eigenanalysis of unsteady flows about airfoils, cascades, and wings  [BTN-95-EIX95152577597]  P 305 A95-73486  MAMM, CLAUS D.  Corrosion protection measures for CFC/metal joints of fuel integral tank structures of advanced military aircraft  P 303 N95-23510  HAMMADI, MUNIR AL  Study of an airfoil with a flap and spoiler  [BTN-95-EIX95152582327]  P 265 A95-73530  HANFF, ERNEST S.  Further analysis of high-rate rolling experiments of a 65-deg delta wing  [BTN-95-EIX95152582331]  P 281 A95-73533  HANGE, CRAIG  Flow visualization studies of VTOL aircraft models during Hover in ground effect  [NASA-TM-108860]  P 272 N95-22666  HARDY, G. L.  Corrosion detection and monitoring of aircraft structures: An overview  An assessment of viscous effects in computational simulation of beingin and burst vortex flows on generic fighter wind-tunnel models using TEAM code  [NASA-CR-4650]  P 273 N95-23185  HARTIN C.  Flight-deck displays on the Boeing 777  [BTN-95-EIX95142562402]  P 286 A95-73438  HARTUNG, LIN C.  Convective and radiative heat transfer analysis for the
BTN-95-EIX95182619232   p 308 A95-76658 FARHAT, C. High-performance parallel analysis of coupled problems for aircraft propulsion [NASA-CR-197440   p 289 N95-23088 FELIPPA, C. A. High-performance parallel analysis of coupled problems for aircraft propulsion [NASA-CR-197440   p 289 N95-23088 FENG, JINZHANG Cavitation modeling in Euler and Navier-Stokes codes p 315 N95-23630 FENG, JINZHANG Cavitation modeling in Euler and Navier-Stokes codes p 315 N95-23630 FENTRESS, MICHAEL L Experimental evaluation of a box beam specifically tailored for chordwise deformation [BTN-95-EIX95182619088   p 283 A95-75773 FERBER, M. K. Evolution of oxidation and creep damage mechanisms in HIPed silicon nitride materials [DE95-001360] p 300 N95-22689 FERGUSON, T. V. Impeller flow field characterization with a laser two-focus velocimeter p 313 N95-23440 FINK, C. L Evaluation of neutron techniques for illicit substance detection [DE95-002988] p 300 N95-22764 FINLEY, DENNIS B. Euler Technology Assessment program for preliminary aircraft design employing SPLITFLOW code with Cartesian unstructured grid method [NASA-CR-4649] p 273 N95-22917 FINLEY, T. D. Dynamic response tests of inertial and optical wind-tunnel model attitude measurement devices [NASA-TM-109182] p 296 N95-23011 FLOWERS, GEORGE T. Influence of backup bearings and support structure dynamics on the behavior of rotors with active supports	Natural laminar flow wing concept for supersonic transports  [BTN-95-EIX95182619226] p 308 A95-76652  GIBSON, BERRY T.  Natural laminar flow wing concept for supersonic transports  [BTN-95-EIX95182619226] p 308 A95-76652  GIEL, P. W.  Three-dimensional Navier-Stokes analysis and redesign of an imbedded belimouth nozzle in a turbine cascade inlet section p 311 N95-23423  GILPIN, T. M.  Estimates of total organic and inorganic chlorine in the lower stratosphere from in situ and flask measurements during AASE 2  [HTN-95-A0861] p 317 A95-76265  GILYARD, GLENN  Direct adaptive performance optimization of subsonic transports: A periodic perturbation technique  [NASA-TM-4676] p 284 N95-22829  GILYARD, GLENN B  Engines-only flight control system  [NASA-CASE-ARC-11944-1] p 294 N95-23389  GLASSMAN, ARTHUR J.  Enhanced analysis and users manual for radial-inflow turbine conceptual design code RTD  [NASA-CR-195454] p 275 N95-23462  GOLDMAN, ROBERT P.  Empirical results on scheduling and dynamic backtracking p 299 N95-23761  GOLDTHORPE, STEVE H.  Guidance and control requirements for high-speed Rollout and Turnoff (ROTO)  [NASA-CR-195026] p 292 N95-22674  GOLDWIRE, H.  NTS-spill test facility wind tunnel exhaust plume characterization  [DE95-003630] p 297 N95-24019  GORBATKIN, S. M.	flight  [NASA-CR-197383]  [NASA-TM-108860]  [NASA-CR-197384]  [NASA-TM-10860]  [NASA-CR-197384]  [NASA-CR-197385]  [NASA-CR-197385]  [NASA-CR-197385]  [NASA-CR-197383]  [NASR
BTN-95-EIX95182619232   p 308 A95-76658   FARHAT, C. L.   Evaluation of neutron techniques for illicit substance detection   DE95-002988   p 300 N95-23440   FERGUSON, T. V.   Impeller flow field characterization with a laser two-focus velocimeter   p 300 N95-23440   p 300 N95-23689   p 300 N95-23689   p 300 N95-23689   p 300 N95-23630   p 300 N95-236	Natural laminar flow wing concept for supersonic transports  [BTN-95-EIX95182619226] p 308 A95-76652  GIBSON, BERRY T.  Natural laminar flow wing concept for supersonic transports  [BTN-95-EIX95182619226] p 308 A95-76652  GIEL, P, W.  Three-dimensional Navier-Stokes analysis and redesign of an imbedded bellmouth nozzle in a turbine cascade inlet section p 311 N95-23423  GILPIN, T. M.  Estimates of total organic and inorganic chlorine in the lower stratosphere from in situ and flask measurements during AASE 2  [HTN-95-A0861] p 317 A95-76265  GILYARD, GLENN  Direct adaptive performance optimization of subsonic transports: A periodic perturbation technique [NASA-TM-4676] p 284 N95-22829  GILYARD, GLENN B  Engines-only flight control system  [NASA-CASE-ARC-11944-1] p 294 N95-23389  GLASSMAN, ARTHUR J.  Enhanced analysis and users manual for radial-inflow turbine conceptual design code RTD  [NASA-CR-195454] p 275 N95-23462  GOLDMAN, ROBERT P.  Empirical results on scheduling and dynamic backtracking p 299 N95-23761  GOLDTHORPE, STEVE H.  Guidance and control requirements for high-speed Rollout and Turnoff (ROTO)  [NASA-CR-195026] p 292 N95-22674  GOLDWIRE, H.  NTS-spill test facility wind tunnel exhaust plume characterization  [DE95-003630] p 297 N95-24019	flight  [NASA-CR-197383]  P 309 N95-22481  HAGENIERS, O. L.  Double pass retrorellection for corrosion detection in aircraft structures  P 323 N95-23503  HALL, KENNETH C.  Eigenanalysis of unsteady flows about airfoils, cascades, and wings  [BTN-95-EIX95152577597]  P 305 A95-73486  HAMM, CLAUS D.  Corrosion protection measures for CFC/metal joints of fuel integral tank structures of advanced military aircraft  P 303 N95-23510  HAMMADI, MUNIR AL  Study of an airfoil with a flap and spoiler  [BTN-95-EIX95152582327]  P 265 A95-73530  HANFF, ERNEST S.  Further analysis of high-rate rolling experiments of a 65-deg delta wing  [BTN-95-EIX95152582331]  P 281 A95-73533  HANGE, CRAIG  Flow visualization studies of VTOL aircraft models during Hover in ground effect  [NASA-TM-108860]  P 272 N95-22666  HARDY, G. L.  Corrosion detection and monitoring of aircraft structures: An overview  An assessment of viscous effects in computational simulation of beingin and burst vortex flows on generic fighter wind-tunnel models using TEAM code  [NASA-CR-4650]  P 273 N95-23185  HARTLIN C.  Flight-deck displays on the Boeing 777  [BTN-95-EIX95142562402]  P 286 A95-73438  HARTUNG, LIN C.  Convective and radiative heat transfer analysis for the fire 2 forebody  [BTN-95-EIX95182617460]  P 268 A95-75731
BTN-95-EIX95182619232   p 308 A95-76658   FARHAT, C.	Natural laminar flow wing concept for supersonic transports  [BTN-95-EIX95182619226] p 308 A95-76652  GIBSON, BERRY T.  Natural laminar flow wing concept for supersonic transports  [BTN-95-EIX95182619226] p 308 A95-76652  GIEL, P. W.  Three-dimensional Navier-Stokes analysis and redesign of an imbedded bellmouth nozzle in a turbine cascade inlet section p 311 N95-23423  GILPIN, T. M.  Estimates of total organic and inorganic chlorine in the lower stratosphere from in situ and flask measurements during AASE 2  [HTN-95-A0861] p 317 A95-76265  GILYARD, GLENN  Direct adaptive performance optimization of subsonic transports: A periodic perturbation technique  [NASA-TM-4676] p 284 N95-22829  GILYARD, GLENN B  Engines-only flight control system  [NASA-CASE-ARC-11944-1] p 294 N95-23389  GLASSMAN, ARTHUR J.  Enhanced analysis and users manual for radial-inflow turbine conceptual design code RTD  [NASA-CR-195454] p 275 N95-23462  GOLDMAN, ROBERT P.  Empirical results on scheduling and dynamic backtracking p 299 N95-23761  GOLDTHORPE, STEVE H.  Guidance and control requirements for high-speed Rollout and Turnoff (ROTO)  INASA-CR-195026] p 292 N95-22674  GOLDWIRE, H.  NTS-spill test facility wind tunnel exhaust plume characterization  [DE95-003630] p 297 N95-24019  GORBATKIN, S. M.  Cu deposition using a permanent magnet electron cyclotror resonance microwave plasma source  [DE94-017768] p 304 N95-23981	flight  INASA-CR-197383   p 309 N95-22481  MAGENIERS, O. L  Double pass retrorellection for corrosion detection in aircraft structures p 323 N95-23503  MALL, KENNETH C.  Eigenanalysis of unsteady flows about airfoils, cascades, and wings  (BTN-95-EIX95152577597   p 305 A95-73486  MAMM, CLAUS D.  Corrosion protection measures for CFC/metal joints of fuel integral tank structures of advanced military aircraft p 303 N95-23510  HAMMADI, MUNIR AL  Study of an airfoil with a flap and spoiler  [BTN-95-EIX95152582327   p 265 A95-73530  HANFF, ERNEST S.  Further analysis of high-rate rolling experiments of a 65-deg delta wing  [BTN-95-EIX95152582331   p 281 A95-73533  HANGE, CRAIG  Flow visualization studies of VTOL aircraft models during Hover in ground effect  [NASA-TM-108860   p 272 N95-22666  HARDY, G. L  Corrosion detection and monitoring of aircraft structures: An overview p 303 N95-23515  HARRIS, BRENDA W.  An assessment of viscous effects in computational simulation of benign and burst vortex flows on generic fighter wind-tunnel models using TEAM code [NASA-CR-4650] p 273 N95-23185  HARTEL, MARTIN C.  Flight-deck displays on the Boeing 777  [BTN-95-EIX95142562402   p 286 A95-73438  HARTUNG, LIN C.  Convective and radiative heat transfer analysis for the fire 2 forebody  [BTN-95-EIX95182617460   p 268 A95-75731  HASKO, GROGORY H.  Development and verification of a resin film infusion/resin transfer molding simulation model for
BTN-95-EIX95182619232   p 308 A95-76658   FARHAT, C.   High-performance parallel analysis of coupled problems for aircraft propulsion   NASA-CR-197440   p 289 N95-23088   FELIPPA, C. A. High-performance parallel analysis of coupled problems for aircraft propulsion   NASA-CR-197440   p 289 N95-23088   FENG, JINZHANG   p 289 N95-23088   FENG, JINZHANG   Cavitation modeling in Euler and Navier-Stokes codes p 315 N95-23630   FENTRESS, MICHAEL L Experimental evaluation of a box beam specifically tailored for chordwise deformation   BTN-95-EIX95182619088   p 283 A95-75773   FERBER, M. K. Evolution of oxidation and creep damage mechanisms in HIPed silicon nitride materials   DE95-001360   p 300 N95-22689   FERGUSON, T. V. Impeller flow field characterization with a laser two-focus velocimeter p 313 N95-23440   FINK, C. L. Evaluation of neutron techniques for illicit substance detection   DE95-002988   p 300 N95-22764   FINLEY, DENNIS B. Euler Technology Assessment program for preliminary aircraft design employing SPLITFLOW code with Cartesian unstructured grid method   NASA-CR-4649   p 273 N95-22917   FINLEY, T. D. Dynamic response tests of inertial and optical wind-tunnel model attitude measurement devices   INASA-TM-109182   p 296 N95-23011   FLOWERS, GEORGE T. Influence of backup bearings and support structure dynamics on the behavior of rotors with active supports   INASA-CR-197438   p 310 N95-23190   FREEMAN, L. MICHAEL   Predicting exhaust plume boundaries with supersonic external flows	Natural laminar flow wing concept for supersonic transports  [BTN-95-EIX95182619226] p 308 A95-76652  GIBSON, BERRY T.  Natural laminar flow wing concept for supersonic transports  [BTN-95-EIX95182619226] p 308 A95-76652  GIEL, P. W.  Three-dimensional Navier-Stokes analysis and redesign of an imbedded bellmouth nozzle in a turbine cascade intel section p 311 N95-23423  GILPIN, T. M.  Estimates of total organic and inorganic chlorine in the lower stratosphere from in situ and flask measurements during AASE 2  IHTN-95-A0861  p 317 A95-76265  GILYARD, GLENN  Direct adaptive performance optimization of subsonic transports: A periodic perturbation technique [NASA-TM-4676] p 284 N95-22829  GILYARD, GLENN B  Engines-only flight control system [NASA-CASE-ARC-11944-1] p 294 N95-23389  GLASSMAN, ARTHUR J.  Enhanced analysis and users manual for radial-inflow turbine conceptual design code RTD [NASA-CR-195454] p 275 N95-23462  GOLDMAN, ROBERT P.  Empirical results on scheduling and dynamic backtracking p 299 N95-23761  GOLDTHORPE, STEVE H.  Guidance and control requirements for high-speed Rollout and Turnoff (ROTO)  INASA-CR-195026] p 292 N95-22674  GOLDWIRE, H.  NTS-spill test facility wind tunnel exhaust plume characterization [DE95-003630] p 297 N95-24019  GORBATKIN, S. M.  Cu deposition using a permanent magnet electron cyclotron resonance microwave plasma source [DE94-017768] p 304 N95-23981	flight  [NASA-CR-197383]  P 309 N95-22481  HAGENIERS, O. L.  Double pass retrorellection for corrosion detection in aircraft structures  P 323 N95-23503  HALL, KENNETH C.  Eigenanalysis of unsteady flows about airfoils, cascades, and wings  [BTN-95-EIX95152577597]  P 305 A95-73486  HAMM, CLAUS D.  Corrosion protection measures for CFC/metal joints of fuel integral tank structures of advanced military aircraft p 303 N95-23510  HAMMADI, MUNIR AL  Study of an airfoil with a flap and spoiler  [BTN-95-EIX95152582327]  P 265 A95-73530  HANFF, ERNEST S.  Further analysis of high-rate rolling experiments of a 65-deg delta wing  [BTN-95-EIX95152582331]  P 281 A95-73533  HANGE, CRAIG  Flow visualization studies of VTOL aircraft models during Hover in ground effect  [NASA-TM-108860]  P 272 N95-22666  HARDY, G. L.  Corrosion detection and monitoring of aircraft structures: An overview  An assessment of viscous effects in computational simulation of beingin and burst vortex flows on generic fighter wind-tunnel models using TEAM code  [NASA-CR-4650]  P 273 N95-23185  HARTLING, LIN C.  Flight-deck displays on the Boeing 777  [BTN-95-EIX95142562402]  P 286 A95-73438  HARTUNG, LIN C.  Convective and radiative heat transfer analysis for the fire 2 forebody  [BTN-95-EIX95182617460]  P 268 A95-75731  HASKO, GROGORY H.  Development and verification of a resin film infusion/resin transfer molding simulation model for fabrication of advanced textile composites
BTN-95-EIX95182619232   p 308 A95-76658   FARHAT, C.	Natural laminar flow wing concept for supersonic transports  [BTN-95-EIX95182619226] p 308 A95-76652  GIBSON, BERRY T.  Natural laminar flow wing concept for supersonic transports  [BTN-95-EIX95182619226] p 308 A95-76652  GIEL, P. W.  Three-dimensional Navier-Stokes analysis and redesign of an imbedded bellmouth nozzle in a turbine cascade inlet section p 311 N95-23423  GILPIN, T. M.  Estimates of total organic and inorganic chlorine in the lower stratosphere from in situ and flask measurements during AASE 2  [HTN-95-A0861] p 317 A95-76265  GILYARD, GLENN  Direct adaptive performance optimization of subsonic transports: A periodic perturbation technique  [NASA-TM-4676] p 284 N95-22829  GILYARD, GLENN B  Engines-only flight control system  [NASA-CASE-ARC-11944-1] p 294 N95-23389  GLASSMAN, ARTHUR J.  Enhanced analysis and users manual for radial-inflow turbine conceptual design code RTD  [NASA-CR-195454] p 275 N95-23462  GOLDMAN, ROBERT P.  Empirical results on scheduling and dynamic backtracking p 299 N95-23761  GOLDTHORPE, STEVE H.  Guidance and control requirements for high-speed Rollout and Turnoff (ROTO)  INASA-CR-195026] p 292 N95-22674  GOLDWIRE, H.  NTS-spill test facility wind tunnel exhaust plume characterization  [DE95-003630] p 297 N95-24019  GORBATKIN, S. M.  Cu deposition using a permanent magnet electron cyclotror resonance microwave plasma source  [DE94-017768] p 304 N95-23981	flight  INASA-CR-197383   p 309 N95-22481  MAGENIERS, O. L  Double pass retrorellection for corrosion detection in aircraft structures p 323 N95-23503  MALL, KENNETH C.  Eigenanalysis of unsteady flows about airfoils, cascades, and wings  (BTN-95-EIX95152577597   p 305 A95-73486  MAMM, CLAUS D.  Corrosion protection measures for CFC/metal joints of fuel integral tank structures of advanced military aircraft p 303 N95-23510  HAMMADI, MUNIR AL  Study of an airfoil with a flap and spoiler  [BTN-95-EIX95152582327   p 265 A95-73530  HANFF, ERNEST S.  Further analysis of high-rate rolling experiments of a 65-deg delta wing  [BTN-95-EIX95152582331   p 281 A95-73533  HANGE, CRAIG  Flow visualization studies of VTOL aircraft models during Hover in ground effect  [NASA-TM-108860   p 272 N95-22666  HARDY, G. L  Corrosion detection and monitoring of aircraft structures: An overview p 303 N95-23515  HARRIS, BRENDA W.  An assessment of viscous effects in computational simulation of benign and burst vortex flows on generic fighter wind-tunnel models using TEAM code [NASA-CR-4650] p 273 N95-23185  HARTEL, MARTIN C.  Flight-deck displays on the Boeing 777  [BTN-95-EIX95142562402   p 286 A95-73438  HARTUNG, LIN C.  Convective and radiative heat transfer analysis for the fire 2 forebody  [BTN-95-EIX95182617460   p 268 A95-75731  HASKO, GROGORY H.  Development and verification of a resin film infusion/resin transfer molding simulation model for
BTN-95-EIX95182619232   p 308 A95-76658   FARHAT, C. High-performance parallel analysis of coupled problems for aircraft propulsion   NASA-CR-197440   p 289 N95-23088   FELIPPA, C. A. High-performance parallel analysis of coupled problems for aircraft propulsion   NASA-CR-197440   p 289 N95-23088   FENG, JINZHANG   p 289 N95-23088   FENG, JINZHANG   Cavitation modeling in Euler and Navier-Stokes codes p 315 N95-23630   Experimental evaluation of a box beam specifically tailored for chordwise deformation   BTN-95-EIX95182619088   p 283 A95-75773   FERBER, M. K.   Evolution of oxidation and creep damage mechanisms in HIPed silicon nitride materials   DE95-001360   p 300 N95-22689   FERGUSON, T. V.   Impeller flow field characterization with a laser two-focus velocimeter   p 313 N95-23440   FINK, C. L.   Evaluation of neutron techniques for illicit substance detection   DE95-002988   p 300 N95-22764   FINLEY, DENNIS B.   Euler Technology Assessment program for preliminary aircraft design employing SPLITFLOW code with Cartesian unstructured grid method   NASA-CR-4649   p 273 N95-22917   FINLEY, T. D.   Dynamic response tests of inertial and optical wind-tunnel model attitude measurement devices   INASA-TM-109182   p 296 N95-23011   FLOWERS, GEORGE T.   Influence of backup bearings and support structure dynamics on the behavior of rotors with active supports   INASA-CR-197438   p 310 N95-23190   FREEMAN, L MICHAEL   Predicting exhaust plume boundaries with supersonic external flows   BTN-95-EIX95152583258   p 297 A95-73559   FRINK, NEAL T.   Unstructured grid solutions to a wing/pylon/store	Natural laminar flow wing concept for supersonic transports  [BTN-95-EIX95182619226] p 308 A95-76652  GIBSON, BERRY T.  Natural laminar flow wing concept for supersonic transports  [BTN-95-EIX95182619226] p 308 A95-76652  GIEL, P. W.  Three-dimensional Navier-Stokes analysis and redesign of an imbedded bellmouth nozzle in a turbine cascade intel section p 311 N95-23423  GILPIN, T. M.  Estimates of total organic and inorganic chlorine in the lower stratosphere from in situ and flask measurements during AASE 2  IHTN-95-A0861  p 317 A95-76265  GILYARD, GLENN  Direct adaptive performance optimization of subsonic transports: A periodic perturbation technique [NASA-TM-4676] p 284 N95-22829  GILYARD, GLENN B  Engines-only flight control system [NASA-CASE-ARC-11944-1] p 294 N95-23389  GLASSMAN, ARTHUR J.  Enhanced analysis and users manual for radial-inflow turbine conceptual design code RTD [NASA-CR-195454] p 275 N95-23462  GOLDMAN, ROBERT P.  Empirical results on scheduling and dynamic backtracking p 299 N95-23761  GOLDTHORPE, STEVE H.  Guidance and control requirements for high-speed Rollout and Turnoff (ROTO)  INASA-CR-195026] p 292 N95-22674  GOLDWIRE, H.  NTS-spill test facility wind tunnel exhaust plume characterization [DE95-003630] p 297 N95-24019  GORBATKIN, S. M.  Cu deposition using a permanent magnet electron cyclotron resonance microwave plasma source [DE94-017768] p 304 N95-23981  GOTTZMANN, C. F.  Airborne rotary air separator study [NASA-CR-189099] p 290 N95-24053	flight  [NASA-CR-197383]  P 309 N95-22481  HAGENIERS, O. L.  Double pass retrorellection for corrosion detection in aircraft structures  P 323 N95-23503  HALL, KENNETH C.  Eigenanalysis of unsteady flows about airfoils, cascades, and wings  [BTN-95-EIX95152577597]  P 305 A95-73486  HAMM, CLAUS D.  Corrosion protection measures for CFC/metal joints of fuel integral tank structures of advanced military aircraft p 303 N95-23510  HAMMADI, MUNIR AL  Study of an airfoil with a flap and spoiler  [BTN-95-EIX95152582327]  P 265 A95-73530  HANFF, ERNEST S.  Further analysis of high-rate rolling experiments of a 65-deg delta wing  [BTN-95-EIX95152582331]  P 281 A95-73533  HANGE, CRAIG  Flow visualization studies of VTOL aircraft models during Hover in ground effect  [NASA-TM-108860]  P 272 N95-22666  HARDY, G. L.  Corrosion detection and monitoring of aircraft structures: An overview  P 303 N95-23515  HARRIS, BRENDA W.  An assessment of viscous effects in computational simulation of beingin and burst vortex flows on generic fighter wind-tunnel models using TEAM code  [NASA-CR-4650]  P 273 N95-23185  HARTLING, LIN C.  Flight-deck displays on the Boeing 777  [BTN-95-EIX95142562402]  P 286 A95-73438  HARTUNG, LIN C.  Convective and radiative heat transfer analysis for the fire 2 forebody  [BTN-95-EIX95182617460]  P 268 A95-75731  HASKO, GROGORY H.  Development and verification of a resin film infusion/resin transfer molding simulation model for fabrication of advanced textile composites  [NASA-CR-197439]  P 301 N95-23179  HAWORTH, L A.  TRISTAR 1: Evaluation methods for testing head-up
BTN-95-EIX95182619232   p 308 A95-76658   FARHAT, C. High-performance parallel analysis of coupled problems for aircraft propulsion   NASA-CR-197440   p 289 N95-23088   FELIPPA, C. A. High-performance parallel analysis of coupled problems for aircraft propulsion   NASA-CR-197440   p 289 N95-23088   FENG, JINZHANG   p 289 N95-23088   FENG, JINZHANG   Cavitation modeling in Euler and Navier-Stokes codes p 315 N95-23630   ENG, JINZHANG   Cavitation modeling in Euler and Navier-Stokes codes p 315 N95-23630   ENG, JINZHANG   p 283 A95-7573   FENTRESS, MICHAEL L   Experimental evaluation of a box beam specifically tailored for chordwise deformation   BTN-95-EIX95182619088   p 283 A95-7573   FERBER, M. K.   Evolution of oxidation and creep damage mechanisms in HIPed silicon nitride materials   DE95-001360   p 300 N95-22689   FERGUSON, T. V.   Impeller flow field characterization with a laser two-focus velocimeter   p 313 N95-23440   FINK, C. L   Evaluation of neutron techniques for illicit substance detection   DE95-002988   p 300 N95-22764   FINLEY, DENNIS B.   Euler Technology Assessment program for preliminary aircraft design employing SPLITFLOW code with Cartesian unstructured grid method   INASA-CR-4649   p 273 N95-22917   FINLEY, T. D.   Dynamic response tests of inertial and optical wind-tunnel model attitude measurement devices   INASA-CR-4649   p 296 N95-23011   FLOWERS, GEORGE T.   Influence of backup bearings and support structure dynamics on the behavior of rotors with active supports   INASA-CR-197438   p 310 N95-23190   FREEMAN, L. MICHAEL   Predicting exhaust plume boundaries with supersonic external flows   BTN-95-EIX95152583258   p 297 A95-73559   FRINK, NEAL T.	Natural laminar flow wing concept for supersonic transports  [BTN-95-EIX95182619226] p 308 A95-76652  GIBSON, BERRY T.  Natural laminar flow wing concept for supersonic transports  [BTN-95-EIX95182619226] p 308 A95-76652  GIEL, P. W.  Three-dimensional Navier-Stokes analysis and redesign of an imbedded bellmouth nozzle in a turbine cascade inlet section p 311 N95-23423  GILPIN, T. M.  Estimates of total organic and inorganic chlorine in the lower stratosphere from in situ and flask measurements during AASE 2  IHTN-95-A0861  p 317 A95-76265  GILYARD, GLENN  Direct adaptive performance optimization of subsonic transports: A periodic perturbation technique [NASA-TM-4676] p 284 N95-22829  GILYARD, GLENN B  Engines-only flight control system [NASA-CASE-ARC-11944-1] p 294 N95-23389  GLASSMAN, ARTHUR J.  Enhanced analysis and users manual for radial-inflow turbine conceptual design code RTD [NASA-CR-195454] p 275 N95-23462  GOLDMAN, ROBERT P.  Empirical results on scheduling and dynamic backtracking p 299 N95-23761  GOLDMAN, ROBERT P.  Empirical results on scheduling and dynamic backtracking p 299 N95-23761  GOLDWIRE, H.  NTS-spill test facility wind tunnel exhaust plume characterization [DE95-003630] p 297 N95-24019  GORBATKIN, S. M.  Cu deposition using a permanent magnet electron cyclotron resonance microwave plasma source [DE94-017768] p 304 N95-23981  GOTTZMANN, C. F.  Airborne rotary air separator study [NASA-CR-189099] p 290 N95-24053	flight   NASA-CR-197383   p 309 N95-22481   NASA-CR-197383   p 309 N95-22481   MAGENIERS, O. L   Double pass retrorellection for corrosion detection in aircraft structures p 323 N95-23503   ALL, KENNETH C.   Eigenanalysis of unsteady flows about airfoils, cascades, and wings   BTN-95-EIX95152577597   p 305 A95-73486   HAMM, CLAUS D.   Double pass retrorection measures for CFC/metal joints of fuel integral tank structures of advanced military aircraft p 303 N95-23510   HAMMADI, MUNIR AL   Study of an airfoil with a flap and spoiler   BTN-95-EIX95152582327   p 265 A95-73530   HAMFF, ERNEST S.   Further analysis of high-rate rolling experiments of a 65-deg delta wing   BTN-95-EIX95152582331   p 281 A95-73533   HANGE, CRAIG   Flow visualization studies of VTOL aircraft models during Hover in ground effect   NASA-TM-108860   p 272 N95-22666   HARDY, G. L   Corrosion detection and monitoring of aircraft structures: An overview p 303 N95-23515   HARRIS, BRENDA W.   An assessment of viscous effects in computational simulation of benign and burst vortex flows on generic fighter wind-tunnel models using TEAM code   NASA-CR-4650   p 273 N95-23185   HARRIS, BRENDA W.   Flight-deck displays on the Boeing 777   BTN-95-EIX95142562402   p 286 A95-73438   HARTUNG, LIN C.   Convective and radiative heat transfer analysis for the fire 2 torebody   BTN-95-EIX95182617460   p 268 A95-75731   HASKO, GROGORY H.   Development and verification of a resin film infusion/resin transfer molding simulation model for fabrication of advanced textile composites   NASA-CR-197439   p 301 N95-23179   HAWORTH, L. A.

IE, HONGQING	HOUCK, JACOB
Simulation on the 3-D turbulent flow in the passages of finocyl grain	Simulation and model reduction for the active flexible wing program
BTN-95-EIX95202638962  p 279 A95-76674  EADLEY, DEAN E.	BTN-95-EIX95182619211  p 295 A95-76637 HSU, SHIH-CHE
The airline quality report, 1994 [NIAR-94-11] p 277 N95-24012	Solutions of generalized proportional navigation with maneuvering and nonmaneuvering targets
REBBAR, SHESHAGIRI Aerodynamic characteristics of a canard-controlled	[BTN-95-EIX95202637606] p 279 A95-76683
missile at high angles of attack	HSU, WAYNE W. CFD analysis of turbopump volutes
BTN-95-EIX95152583257  p 267 A95-73558  EEG, JENNIFER	p 312 N95-23436
Simulation and model reduction for the active flexible	HUANG, J. R.  Effect of curvature in the numerical simulation of an
wing program [BTN-95-EIX95182619211] p 295 A95-76637	electrothermal de-icer pad
EGEDUS, CHARLES R.	BTN-95-EIX95182619219  p 276 A95-76645 HUANG, JEN-KUANG
Organic coating technology for the protection of aircraft against corrosion p 303 N95-23513	System identification of the Large-Angle Magnetic Suspension Test Fixture (LAMSTF) p 296 N95-23299
IEIDA, J. H.	HUANG, Q.
Eddy current detection of pitting corrosion around fastener holes p 315 N95-23507	Mechanical system reliability and risk assessment [BTN-95-EIX95142553046] p 304 A95-73452
IEIDT, L. E.	HUBER, F. W.
Estimates of total organic and inorganic chlorine in the lower stratosphere from in situ and flask measurements	Aerodynamic design and analysis of a highly loaded turbine exhaust p 312 N95-23435
during AASE 2 [HTN-95-A0861] p 317 A95-76265	HUEBNER, L. D.
HEINRICH, D. C.	Computational study of plume-induced separation on a hypersonic powered model
Effect of underwing frost on a transport aircraft airfoil at flight Reynolds number	[BTN-95-EIX95152582346] p 266 A95-73548
[BTN-95-EIX95152582334] p 276 A95-73536	HUGHES, T. C. TRISTAR 1: Evaluation methods for testing head-up
IEISER, W. H. Simulating heat addition via mass addition in constant	display (HUD) flight symbology
area compressible flows	[NASA-TM-4665] p 288 N95-24030 HUI, FRANK C. L.
(BTN-95-EIX95182619100) p 307 A95-76585 #ENLINE, W. D.	Experimental results for a hypersonic nozzle/afterbody
Hypersonic nonequilibrium Navier-Stokes solutions over	flow field [NASA-TM-4638] p 274 N95-23250
an ablating graphite nosetip [BTN-95-EIX95152583252] p 305 A95-73553	HUI, KENNETH
IERRIN, J. L.	Improving prediction: The incorporation of simplified rotor dynamics in a mathematical model of the bell
Supersonic near-wake afterbody boattailing effects on axisymmetric bodies	412HP [BTN-95-EIX95152584679] p 282 A95-73591
[BTN-95-EIX95182617465] p 268 A95-75736	HUMM, P.
IESS, RONALD A.  Analysis of the longitudinal handling qualities and	Evaluation of neutron techniques for illicit substance detection
pilot-induced-oscillation tendencies of the High-Angle-of-Attack Research Vehicle (HARV)	(DE95-002988) p 300 N95-22764
p 293 N95-23297	HUNT, L. R.  Nonlinear system guidance in the presence of
IETU, JEAN-FRANÇOIS  Adaptive finite element method for turbulent flow near	transmission zero dynamics
a propeller	[NASA-TM-4661] p 309 N95-22804 HUNTER, CRAIG A.
[BTN-95-EIX95142553038] p 305 A95-73460	An approximate theoretical method for modeling the
Numerical investigation of supersonic flows around a	static thrust performance of non-axisymmetric two-dimensional convergent-divergent nozzles
spiked blunt body  BTN-95-EIX95212645690  p 271 A95-76742	[NASA-CR-195050] p 273 N95-23193 HYMER, T.
ILL, S. D. Enhancement of F/A-18 operational flight	Base drag prediction on missile configurations
measurements: Data report for phase 1	[BTN-95-EIX95152583256] p 266 A95-73557 Improved version of the Naval Surface Warfare Center
[DSTO-TR-0049] p 286 N95-23666 INGST, W. R.	aeroprediction code (AP93)
Flow structure in the wake of a wishbone vortex	[BTN-95-EIX95152583260] p 267 A95-73561
generator [BTN-95-EIX95142553044] p 304 A95-73454	1
INTSA, E. J.	•
In situ observations in aircraft exhaust plumes in the lower stratosphere at midlatitudes	IFJU, PETER G. Interlaminar shear test method development for long
[HTN-95-A0862]. p 318 A95-76266	term durability testing of composites
OADLEY, SHERWOOD T.  Multiple-function digital controller system for active	p 301 N95-23300 ILINCA, FLORIN
flexible wing wind-tunnel model  BTN-95-EIX95182619212   p 322 A95-76638	Adaptive finite element method for turbulent flow near
On-line analysis capabilities developed to support the	a propeller [BTN-95-EIX95142553038] p 305 A95-73460
active flexible wing wind-tunnel tests [BTN-95-EIX95182619213] p 296 A95-76639	INGER, GEORGE R.  Scaling of incipient separation in supersonic/transonic
Rolling maneuver load alleviation using active controls	speed laminar flows
[BTN-95-EIX95182619217] p 270 A95-76643  ODGE, B. K.	[BTN-95-EIX95182619104] p 269 A95-76589 INGLE, STEVEN J.
Supersonic axisymmetric conical flow solutions for	Effects of high order dynamics on helicopter flight control law design
different ratios of specific heats  BTN-95-EIX95152583283  p 306 A95-73584	
	[HTN-95-80852] p 290 A95-75094
ODGES, DEWEY H.	
ODGES, DEWEY H. Flutter analysis of composite box beams [NASA-CR-197931] p 294 N95-23392 OLLAND, SCOTT D.	HTN-95-80852
ODGES, DEWEY H. Fiutter analysis of composite box beams [NASA-CR-197931] p 294 N95-23392 OLLAND, SCOTT D. Mach 10 computational study of a three-dimensional scramjet inlet flow field	HTN-95-80852   p 290 A95-75094  J  JACKMAN, CHARLES H. Sensitivity of two-dimensional model predictions of
ODGES, DEWEY H. Flutter analysis of composite box beams [NASA-CR-197931] p 294 N95-23392  OLLAND, SCOTT D. Mach 10 computational study of a three-dimensional scramjet inlet flow field [NASA-TM-4602] p 309 N95-23015	JACKMAN, CHARLES H. Sensitivity of two-dimensional model predictions of ozone response to stratospheric aircraft: An update [HTN-95-A0863] p 318 A95-76267
ODGES, DEWEY H. Flutter analysis of composite box beams [NASA-CR-197931] p 294 N95-23392  OLLAND, SCOTT D.  Mach 10 computational study of a three-dimensional scramjet inlet flow field [NASA-TM-4602] p 309 N95-23015  Mach 10 computational study of a three-dimensional scramjet inlet flow field	JACKMAN, CHARLES H. Sensitivity of two-dimensional model predictions of ozone response to stratospheric aircraft: An update
ODGES, DEWEY H. Flutter analysis of composite box beams [NASA-CR-197931] p 294 N95-23392  OLLAND, SCOTT D.  Mach 10 computational study of a three-dimensional scramjet inlet flow field [NASA-TM-4602] p 309 N95-23015  Mach 10 computational study of a three-dimensional	JACKMAN, CHARLES H. Sensitivity of two-dimensional model predictions of ozone response to stratospheric aircraft: An update [HTN-95-A0863] p 318 A95-76267 JARRABET, G. P.

p 269 A95-76605

[BTN-95-EIX95182619128]

p 320 N95-23947

of theory with measurements

JENKINS, L. N. A study of the vortex flow over 76/40-deg double-delta wing p 314 N95-23466 [NASA-CR-195032] JIN. G. Two-equation turbulence model for unsteady separated flows around airfoils [BTN-95-EIX95142553054] p 262 A95-73444 JOHNSON, C. G. Effects of satellite bunching on the probability of collision in geosynchronous orbit [BTN-95-EIX95152583276] p 298 A95-73577 JOHNSON, WALTER A. Identification of higher order helicopter dynamics using linear modeling methods p 290 A95-75093 IHTN-95-808511 JOHNSON, WALTER J. Cueing light configuration for aircraft navigation [NASA-CASE-ARC-11982-1] p 280 N9: p 280 N95-23393 JOHNSTON, DONALD E. Identification of higher order helicopter dynamics using linear modeling methods IHTN-95-808511 p 290 A95-75093 JOHNSTON, P. H. New nondestructive techniques for the detection and quantification of corrosion in aircraft structures p 315 N95-23512 K KAISER, MARY K. Cueing light configuration for aircraft navigation [NASA-CASE-ARC-11982-1] p 280 N95-23393 KANDA, HIROSHI Flow visualization studies on sidewall effects in wo-dimensional transonic airfoil testing p 264 A95-73516 IBTN-95-EIX951525823131 KANDEBO, STANLEY W. Lycoming to test new engine core [HTN-95-41393] p 288 A95-76389 Cypher moves toward autonomous flight IHTN-95-413941 p 283 A95-76390 KANKAM, M. DAVID Motor drive technologies for the power-by-wire (PBW) program: Options, trends and tradeoffs p 295 N95-23671 INASA-TM-1068851 KARATSINIDES, SPIRO P. Enhancing filter robustness in cascaded GPS-INS integrations [BTN-95-EIX95142555475] p 278 A95-73435 KARCHER. B. Transport of exhaust products in the near trail of a jet engine under atmospheric conditions [HTN-95-91421] p 319 A95-77334 KARIMIAN, S. M. H. Application of a control-volume-based finite-element formulation to the shock tube problem [BTN-95-EIX95182619099] p 295 A95-76584 KARPALA, F. Double pass retroreflection for corrosion detection in aircraft structures p 323 N95-23503 KEENER FARL R. Experimental results for a hypersonic nozzle/afterbody flow field [NASA-TM-4638] p 274 N95-23250 KEIM. E. R. In situ observations in aircraft exhaust plumes in the lower stratosphere at midlatitudes [HTN-95-A0862] p 318 A95-76266 KEITH, THEO G., JR. Effect of curvature in the numerical simulation of an electrothermal de-icer pad [BTN-95-EIX95182619219] p 276 A95-76645 KELLER, JEFFREY D. An investigation of helicopter dynamic coupling using an analytical model [NASA-CR-197420] p 285 N95-23217 KERN, S. B. A study of the vortex flow over 76/40-deg double-delta [NASA-CR-195032] p 314 N95-23466 KERNIK, ALAN C. Guidance and control requirements for high-speed Rollout and Turnoff (ROTO) [NASA-CR-195026] p 292 N95-22674 KERR, R. NTS-spill test facility wind tunnel exhaust plume characterization [DE95-003630] p 297 N95-24019 KERR, S. A. Moving mass trim control for aerospace vehicles I DE95-002602 I p 299 N95-23532

KRISHNAMURTHY, RAMESH LEE, JANG GYU KESSLER, G. K. Covariance analysis of strapdown INS considering TRISTAR 1: Evaluation methods for testing head-up Optimized design of a hypersonic nozzle display (HUD) flight symbology p 297 N95-23304 gyrocompass characteristics p 279 A95-76697 [NASA-TM-4665] IRTN-95-FIX952026375921 p 288 N95-24030 KRISHNAN, C. G. LEE, KAM-PUI KHODADOUST, A. Some aspects of the aerodynamics of separating viscous shock-layer solutions for Aerodynamics of a finite wing with simulated ice strap-ons Higher-order IBTN-95-EIX95182619227 | p 270 A95-76653 IBTN-95-EIX951826174641 p 298 A95-75735 high-altitude flows |BTN-95-EIX95152583255| p 306 A95-73556 KHODADOUST, ABDOLLAH KUBE, ROLAND Analysis of a higher harmonic control test to reduce LEFEBVRE, D. Study of the droplet spray characteristics of a subsonic blade vortex interaction noise Validation of an effective flat cruciform-shaped specimen and tunnet p 265 A95-73532 to study CFRP composite laminates under biaxial IBTN-95-EIX95152582330 I IBTN-95-EIX951826192351 p 271 A95-76661 KUBO, TRACY S. KILGORE, W. ALLEN 2 micron LIDAR for laser-based remote sensing: Flight p 282 A95-73589 IRTN-95-FIX951525846771 Performance of the 0.3-meter transonic cryogenic tunnel demonstration and application survey with air, nitrogen, and sulfur hexafluoride media under LECINNE. M. IBTN-95-EIX952126410721 p 319 A95-76737 High-performance parallel analysis of coupled problems closed loop automatic control KUHLMANN, K. J. [NASA-CR-195052] for aircraft propulsion p 310 N95-23257 Modeling aerosol emissions from the combustion of p 289 N95-23088 KIM. KYOUNG-HO INASA-CR-1974401 composite materials p 301 N95-23038 Three-dimensional structure of a supersonic jet LESIEUTRE, DANIEL J. KUHN, GARY D. Aerodynamic design of pegasus: Concept to flight with impinging on an inclined plate Aerodynamic design of pegasus: Concept to flight with [BTN-95-EIX95152583259] computational fluid dynamics p 267 A95-73560 computational fluid dynamics p 298 A95-75734 IRTN-95-EIX951826174631 KIM. S.-W. p 298 A95-75734 [BTN-95-EIX95182617463] LEVIN, D. A time-accurate finite volume method valid at all flow KWEI, G. H. Dynamic investigation of the angular motion of a rotating p 314 N95-23447 velocities Phonon characteristics of high (T sub c) superconductors body-parachute system KIM SELING-HO from neutron Doppler broadening measurements IRTN-95-FIX951826192201 p 270 A95-76646 Static aeroelastic characteristics of a composite wing p 324 N95-24076 IDE95-0037031 |BTN-95-EIX95152582340| p 282 A95-73542 LIEBST, BRAD S. Method for the prediction of the onset of wing rock KIM, SUK C. [BTN-95-EIX95152582342] p 282 A95-73544 Numerical analysis of hypersonic low-density scramjet LIM. TAE W. inlet flow [BTN-95-EIX95212645694] LABONTE, S. On-line, adaptive state estimator for active noise p 272 A95-76746 Validation of an effective flat cruciform-shaped specimen p 322 N95-23308 control KIM, W. J. study CFRP composite laminates under biaxial LIN. CHING-FANG Influence of streamwise curvature on longitudinal loading New failure detection approach and its application to vortices imbedded in turbulent boundary lavers IBTN-95-EIX95152584677 I p 282 A95-73589 GPS autonomous integrity monitoring [BTN-95-EIX95202637613] [BTN-94-EIX94401378820] p 307 A95-76489 LAFARGE, ROBERT A. p 279 A95-76676 KINARD, TIM A. An assessment of viscous effects in computational Functional dependence of trajectory dispersion on initial LIN. I. J. simulation of benign and burst vortex flows on generic condition errors Sidewash on the vertical tail in subsonic and supersonic [BTN-95-EIX95152583263] p 298 A95-73564 fighter wind-tunnel models using TEAM code flows NASA-CR-46501 p 273 N95-23185 LAFORGE, LEO G. [BTN-95-EIX95152582316] p 264 A95-73519 KIRKLAND LARRY V Overview of AlliedSignal's avionics development in the LIN, J. -C. ATE enabling technologies Transient structure of vortex breakdown on a delta |BTN-95-EIX95172595294| p 287 A95-75718 [BTN-95-EIX95212641069] p 287 A95-76734 wing |BTN-95-EIX95182619073| KIRKLAND, T. P. LAI, JONATHAN Y. p 268 A95-75758 Evolution of oxidation and creep damage mechanisms Maximum-likelihood spectral estimation and adaptive LIN. JOHN C. in HIPed silicon nitride materials filtering techniques with application to airborne Doppler Separation control on high-lift airfoils via micro-vortex IDE95-0013601 p 300 N95-22689 weather radar generators KMETEC, JEFFREY D. INASA-CR-1976991 p 316 N95-23670 BTN-95-EIX95152582326 p 265 A95-73529 2 micron LIDAR for laser-based remote sensing: Flight LAIT, LESLIE R. LIN, SHEAM-CHYUN demonstration and application survey Trajectory modeling of emissions from lower Integrated design of hypersonic waveriders including [BTN-95-EIX95212641072] p 319 A95-76737 stratospheric aircraft inlets and tailfins KNOFF, R. E. IHTN-95-412191 p 317 A95-75031 |BTN-95-EIX95212645692| p 271 A95-76744 Containing military autotest cost growth through the use LAKSHMINARAYANA, B. LINTON, SAMUEL W. of commercial standard equipment architectures Numerical computation of aerodynamics and heat Computation of the poststall behavior of a circulation [BTN-95-EIX95172595295] p 287 A95-75717 transfer in a turbine cascade and a turn-around duct using controlled airfoil KNOX, E. C. advanced turbulence models p 264 A95-73523 BTN-95-EIX951525823201 Determination of wall boundary conditions for high-speed-ratio direct simulation Monte Carlo LALLO, ART LITINETSKIJ, A. V. H-76B fantail demonstrater composite fan blade A new generation of instruments for flying laboratories calculations fabrication |BTN-94-EIX94401363947| A95-75532 |BTN-95-EIX95182617457| p 267 A95-75728 [HTN-95-80856] p 283 A95-75098 KOENIG, KEITH LIU, CHING SHI LAM, T. Supersonic axisymmetric conical flow solutions for Analytical study of the neutral stability of a model Automatic guidance and control for helicopter obstacle hypersonic boundary layer different ratios of specific heats BTN-95-EIX95152583283 | avoidance BTN-95-EIX95152577589 | p 263 A95-73493 p 306 A95-73584 IRTN-95-FIX951826191301 p 291 A95-76607 KOKUBUN. S. LIU. YU Polar Patrol Balloon LAMB, J. PARKER Simulation on the 3-D turbulent flow in the passages IBTN-95-EIX951525823181 p 316 A95-73521 Review and development of base pressure and base of finocyl grain |BTN-95-EIX95202638962| heating correlations in supersonic flow KOMOROWSKI, J. P. p 279 A95-76674 p 271 A95-76740 IBTN-95-EIX952126456881 Double pass retroreflection for corrosion detection in p 323 N95-23503 aircraft structures LANSER, WENDY R. A wall interference assessment/correction system Forebody flow control on a full-scale F/A-18 aircraft [NASA-CR-197421] p 309 N95-23183 KOO. SAM OK [BTN-95-EIX95152582333] p 281 A95-73535 Supersonic laminar flow control research Numerical study of sound generation due to a spinning p 275 N95-23669 INASA-CR-1979381 vortex pair LAPIN, MARK [BTN-95-EIX95182619075] p 307 A95-75760 LOHMANN, R. P. Labs behind Boeing's new 777 [BTN-95-EIX95142562403] p 280 A95-73437 In situ observations in aircraft exhaust plumes in the lower stratosphere at midlatitudes Ontimization of contoured hypersonic scramiet inlets HTN-95-A08621 with a least-squares parabolized Navier-Stokes p 318 A95-76266 Structural acoustic calculations in the low-frequency LONEY, NORMAN W. procedure Design of a variable area diffuser for a 15-inch Mach IHTN-95-209761 p 261 A95-74042 [BTN-95-EIX95152582336] p 323 A95-73538 p 297 N95-23309 6 open-jet tunnel LOOS, ALFRED C. KOUNTZ, JOHN LEE, B. H. K. Effect of leeward flow dividers on the wing rock of a Postinstability behavior of a two-dimensional airfoil with Development and verification of a resin film delta wing a structural nonlinearity |BTN-95-EIX95152582347| p 282 A95-73549 infusion/resin transfer molding simulation model for (BTN-95-EIX95152582337) p 266 A95-73539 KOUSEN, KENNETH A. fabrication of advanced textile composites LEE, DUCK JOO p 301 N95-23179 NASA-CR-197439| Limit cycle phenomena in computational transonic Numerical study of sound generation due to a spinning eroelasticity LUCIANI. S. vortex pair [BTN-95-EIX95152582317] MAX-91: Polarimetric SAR results on Montespertoli p 264 A95-73520 IBTN-95-EIX951826190751 p 307 A95-75760 KÖZOL, J. p 320 N95-23940 LEE, E. U. Corrosion of landing gear steels p 302 N95-23500 LUO. J. Corrosion of landing gear steels p 302 N95-23500 KREMER, JEAN-PAUL Numerical computation of aerodynamics and heat Shuttle entry guidance revisited using nonlinear geometric methods transfer in a turbine cascade and a turn-around duct using LEE. IN Static aeroelastic characteristics of a composite wing p 313 N95-23444 advanced turbulence models p 282 A95-73542 [BTN-95-EIX95152582340] BTN-95-EIX95182619144 p 299 A95-76621 LUO. YU-SHAN KRISHNAKUMAR, S. Integrated design of hypersonic waveriders including LEE. J. S. Statistics of multi-look AIRSAR imagery: A comparison inlets and tailfins Double pass retroreflection for corrosion detection in

aircraft structures

p 323 N95-23503

of theory with measurements

p 320 N95-23947

|BTN-95-EIX95212645692|

p 271 A95-76744

LUTTGES, MARVIN W.	
Neural network prediction of three-	dimensional unsteady
separated flowfields  BTN-95-EIX95182619232	p 308 A95-76658
LUTZE, FREDERICK H.	h 200 Ma2-10020
Kinematics and aerodynamics	of velocity-vector roll
18TN-95-EIX95182619126)	p 291 A95-76603
LYNN, J. E.	
Phonon characteristics of high (T s	
from neutron Doppler broadening m [DE95-003703]	p 324 N95-24076
[5235-005705]	p 324 1433-24070
M	
IÁI	
MA, DEREN	
A multibody/finite element an	alysis approach for
modeling of crash dynamic respons	es
[NIAR-94/3]	p 277 N95-24050
MA, JIAJU  A new type of simulator for sim	ulating the flow-field
distortion of engine inlet	waing the now-held
BTN-95-EIX95202638963	p 289 A95-76673
MACRAE, JOHN DOUGLAS	
Development and verification	
infusion/resin transfer molding : fabrication of advanced textile comp	
[NASA-CR-197439]	p 301 N95-23179
MADENCI, ERDOGAN	•
Residual strength of thin panels v	
	p 311 N95-23311
MAGDELANEO, RAYMOND E.	
Identification of higher order helic linear modeling methods	opter dynamics using
[HTN-95-80851]	p 290 A95-75093
MAGI, V.	•
Simulation of transverse gas in	rjection in turbulent
supersonic air flows	
[BTN-95-EIX95182619080]	p 269 A95-75765
MAH, G. R. AVIRIS and TIMS data processing	no and distribution at
the land processes distributed active	
	p 325 N95-23872
MAHADEVAN, S.	
Mechanical system reliability and	
[BTN-95-EIX95142553046]	p 304 A95-73452
MALIK, M. R.  Comparison of linear stability resul	ts with flight transition
data	is with hight transition
[BTN-95-EIX95182619097]	p 283 A95-76582
MANGO, S. A.	
Statistics of multi-look AIRSAR in	
of theory with measurements	p 320 N95-23947
MANNING, CAROL A.  The role of flight progress strips	in en route air traffic
control: A time-series analysis	o route as build
[DOT/FAA/AM-95/4]	p 280 N95-23565
MANTAY, WAYNE R.	
	ic/dynamic/structural
optimization of helicopter rotor bla decomposition	ades using multilevel
[NASA-TP-3465]	p 285 N95-22953
MARCOLINI, MICHAEL A.	
Sensitivity of acoustic predictions	to variation of input
parameters	- 067 ADE 75007
(HTN-95-80855) MARGASON, RICHARD J.	p 267 A95-75097
Flow visualization studies of VTOL	aircraft models during
Hover in ground effect	
NASA-TM-108860	p 272 N95-22666
MARTIN, M. M.	
Evaluation of neutron techniques	s for illicit substance
detection [DE95-002988]	p 300 N95-22764
MARTINEZ-VAL, RODRIGO	, , , ,
Design constraints in the paylo	ad-range diagram of
ultrahigh capacity transport airplane	s
[BTN-95-EIX95152582319]	p 276 A95-73522
MARTINEZ, R.	to radiuse sates/atatas
The use of cowl camber and taper interaction noise	to reduce rotor/stator
[NASA-CR-195421]	p 323 N95-22675
MARULO, F.	
Structural acoustic calculations in	n the low-frequency
range	- 000 405 70500
[BTN-95-EIX95152582336]	p 323 A95-73538
MASAD, J. A.  Comparison of linear stability result	is with flight transition
data Companyon or linear stability result	
	p 283 A95-76582

MASON GREGORY S.

IRTN-95-FIX951826191321

Multirate flutter suppression system design for a model

p 292 A95-76609

MASON, WILLIAM		
Kinematics and aerodynamics   BTN-95-EIX95182619126   MASSMAN, W. J.	of veloci p 291	ty-vector roll A95-76603
A comparison of some aerodynam		
using measurements over cotton an California ozone deposition experin	nent	
HTN-95-11295  IATHEW, JOSEPH	p 319	A95-77000
Study of an airfoil with a flap and		
BTN-95-EIX95152582327  WATINELLI, L.	p 265	A95-73530
Multigrid solution of compress		
unstructured meshes using a two-e [BTN-94-EIX94401378794]		A95-76484
MATSUNO, KENICHI Flow visualization studies on	sidewall	effects in
two-dimensional transonic airfoil tes	sting	
BTN-95-EIX95152582313  Waurice, M. S.	p 264	A95-73516
Laser velocimetry seed-particle b	ehavior in	shear layers
at Mach 12 [BTN-95-EIX95212645712]	p 272	A95-76764
MAVRIPLIS, D. J.	المعادية	ant flaw on
Multigrid solution of compressib unstructured meshes using a two-e	quation m	odel
[BTN-94-EIX94401378794] ICBEE, LARRY S.	p 307	A95-76484
Guidance and control require	ments for	high-speed
Rollout and Turnoff (ROTO) [NASA-CR-195026]	p 292	N95-22674
ACCLURE, W. B.	·	
Simulating heat addition via mass area compressible flows	s addition	in constant
[BTN-95-EIX95182619100]	p 307	A95-76585
MCGHEE, R. J.  Effect of underwing frost on a to	ransport a	ircraft airfoil
at flight Reynolds number [BTN-95-EIX95152582334]	n 276	A95-73536
ACGHEE, ROBERT J.	•	
Separation control on high-lift air generators	rfoils via	micro-vortex
(BTN-95-EIX95152582326)	p 265	A95-73529
MCGRAW, SANDRA M.  Multiple-function digital controlle	er system	for active
flexible wing wind-tunnel model [BTN-95-EIX95182619212]	p 322	A95-76638
On-line analysis capabilities deve	eloped to	
active flexible wing wind-tunnel test {BTN-95-EIX95182619213}		A95-76639
CINNER, COLIN R.		
Dynamical instability of the maneuver		
[BTN-95-EIX95152583282] MCINVILLE, R.	p 298	A95-73583
Improved version of the Naval Su	ırface Wa	rfare Center
aeroprediction code (AP93) [BTN-95-EIX95152583260]	p 267	A95-73561
MCINVILLE, R. M.	·	
Calculation of wing-alone aerodyl of attack	namics to	high angles
[BTN-95-EIX95212645713] WEASE, KENNETH D.	p 261	A95-76765
Shuttle entry guidance revisit	ed using	nonlinear
geometric methods [BTN-95-EIX95182619144]	p 299	A95-76621
MEE, D. J. Shock tunnel measurements of		oite blemtad
cone drag	•	•
[BTN-95-EIX95152577606] MEGGERS, K.	p 305	A95-73477
Phonon characteristics of high (T s		
from neutron Doppler broadening n [DE95-003703]		N95-24076
MEHTA, S.  Mechanical system reliability and	rick seco	tnemes
[BTN-95-EIX95142553046]		A95-73452
MENA, ANDREW C.  CASS: Design for supportability		
(BTN-95-EIX95172595296) MENDENHALL, MICHAEL R.	p 287	A95-75716
Aerodynamic design of pegasus:	Concept	to flight with
computational fluid dynamics [BTN-95-EIX95182617463]	p 298	A95-75734
MENDOZA, JOEL	•	
Flow study of supersonic wing [BTN-95-EIX95152582344]		A95-73546
MENGALI, GIOVANNI Simulation of turbulent fluctuation	ns	
[BTN-95-EIX95142553041]		A95-73457
MENTER, F. R.  Computation of oscillating airfoil	flows wi	th one- and

p 263 A95-73494

Hover in ground effect [NASA-TM-108860]

vo-equation turbulence models

[BTN-95-EIX95152577588]

```
MOURTOS, NIKOS J.
MERKLE, C. L.
    Convergence acceleration of implicit schemes in the
  presence of high aspect ratio grid cells
                                    p 313 N95-23446
MERKLE, CHARLES L.
    Cavitation modeling in Euler and Navier-Stokes codes
                                    p 315 N95-23630
MEYER, G.
    Nonlinear system guidance in the presence of
  transmission zero dynamics
                                    p 309 N95-22804
  NASA-TM-4661
MEYER, J. L.
    Fuel-optimal bank-angle control for lunar-return
  aerocapture
|BTN-95-EIX95212645706|
                                    p 299 A95-76758
MEYN, LARRY A.
  Forebody flow control on a full-scale F/A-18 aircraft [BTN-95-EIX95152582333] p 281 A95-73535
MICHELI, MARCO
  Simulation of turbulent fluctuations 
[BTN-95-EIX95142553041]
                                    p 304 A95-73457
MICKLICH, B. J.
    Evaluation of neutron techniques for illicit substance
  detection
                                    p 300 N95-22764
  DE95-0029881
MILLER, GERALD D.
    Summary of an active flexible wing program
  IBTN-95-EIX951826192091
                                    p 283 A95-76635
MILLER, MATT
    Labs behind Boeing's new 777
  BTN-95-EIX95142562403]
                                    p 280 A95-73437
MILNE, A. K.
    AIRSAR deployment in Australia, September 1993:
                                    p 321 N95-23948
  Management and objectives
MITCHELTREE, ROBERT A.
    Zonally decoupled direct simulation Monte Carlo
  solutions of hypersonic blunt-body wake flows
                                    p 268 A95-75729
  |BTN-95-EIX95182617458|
MIURA, HIROKAZU
    Static aeroelastic characteristics of a composite wing
  [BTN-95-EIX95152582340]
                                    p 282 A95-73542
MOAS, EDUARDO
   An analytical and experimental investigation of the
  response of the curved, composite frame/skin
  specimens
  IHTN-95-808571
                                    p 283 A95-75099
MOLLER, PAUL S.
    Evaluation of thermal barrier and PS-200 self-lubricating
  coatings in an air-cooled rotary engine
                                    p 289 N95-23222
  INASA-CR-1954451
MONTESDEOCA, X. A.
    Aerodynamic design and analysis of a highly loaded
                                    p 312 N95-23435
MOORE, F. G.
  Base drag prediction on missile configurations
[BTN-95-EIX95152583256] p 266 A9
                                    p 266 A95-73557
    Improved version of the Naval Surface Warfare Center
  aeroprediction code (AP93)
                                    p 267 A95-73561
  IBTN-95-EIX951525832601
    Calculation of wing-alone aerodynamics to high angles
  IBTN-95-FIX952126457131
                                    p 261 A95-76765
MOORE JOHN
   Supersonic flow and shock formation in turbine tip
                                    p 312 N95-23429
MOORE, TOM
   Labs behind Roeing's new 777
  |BTN-95-EIX95142562403|
                                    p 280 A95-73437
MORE, K. L.
    Evolution of oxidation and creep damage mechanisms
  in HIPed silicon nitride materials
  [DE95-001360]
                                    p 300 N95-22689
MORETTI, S.
   MAX-91: Polarimetric SAR results on Montespertoli
                                    p 320 N95-23940
MORRIS, PHILIP J.
    Supersonic jet noise reductions predicted with increased
  iet spreading rate
  [NASA-TM-106872]
                                    p 323 N95-23178
MORSE, CORINNE S.
    Real-time estimation of atmospheric turbulence severity
  from in-situ aircraft measurements
  [BTN-95-EIX95182619231]
                                    p 319 A95-76657
MOSS, JAMES N.
    Hypersonic rarefied flow past spheres including wake
  structure
  [BTN-95-EIX95152583250]
                                    p 305 A95-73551
    Zonally decoupled direct simulation Monte Carlo
  solutions of hypersonic blunt-body wake flows
  [BTN-95-EIX95182617458]
                                    p 268 A95-75729
MOURTOS, NIKOS J.
    Flow visualization studies of VTOL aircraft models during
```

p 272 N95-22666

•	•	
MOUSTAFA, GAMAL H.	NUHAIT, A. O.	PARSONS, B.
Main features of overexpanded triple jets	Stability derivatives of a flapped plate in unsteady ground	Geoid lineations of 1000 km wavelength over the central
[BTN-95-EIX95142553040] p 304 A95-73458	effect	Pacific [HTN-95-11304] p 319 A95-77009
MUILENBURG, DENNIS A.  Euler technology assessment for preliminary aircraft	[BTN-95-EIX95182619225] p 270 A95-76651 Unsteady ground effects on aerodynamic coefficients	PATEL, BHAVESH B.
design employing OVERFLOW code with multiblock	of finite wings with camber	Supersonic axisymmetric conical flow solutions for
structured-grid method	[BTN-95-EIX95182619233] p 271 A95-76659	different ratios of specific heats
[NASA-CR-4651] p 273 N95-23095	NURICK, ALAN	[BTN-95-EIX95152583283] p 306 A95-73584
MUKHOPADHYAY, VIVEK	Static pressure distribution in the inlet of a helicopter turbine compressor	PATEL, V. C. Influence of streamwise curvature on longitudinal
Flutter suppression control law design and testing for the active flexible wing	[BTN-95-EIX95152582339] p 266 A95-73541	vortices imbedded in turbulent boundary layers
BTN-95-EIX95182619214  p 292 A95-76640	Erosion of dust-filtered helicopter turbine engines. Part	[BTN-94-EIX94401378820] p 307 A95-76489
MUNOZ, TOMAS	1: Basic theoretical considerations	PAULL, A.
Design constraints in the payload-range diagram of	[BTN-95-EIX95182619222] p 288 A95-76648 Erosion of dust-filtered helicopter turbine engines. Part	Shock tunnel measurements of hypervelocity blunted
ultrahigh capacity transport airplanes	2: Erosion reduction	cone drag [BTN-95-EIX95152577606] p 305 A95-73477
[BTN-95-EIX95152582319] p 276 A95-73522 MYERS, J.	[BTN-95-EIX95182619223] p 289 A95-76649	PAUSDER, HEINZ-JURGEN
AVIRIS and TIMS data processing and distribution at	Life prediction of helicopter engines fitted with dust	Investigation of the effects of bandwidth and time delay
the land processes distributed active archive center	filters   BTN-95-EIX95182619224   p 289 A95-76650	on helicopter roll-axis handling qualities 1HTN-95-808531 p 290 A95-75095
p 325 N95-23872	[B114-33-E1X33102013224] p 203 x03-70030	[HTN-95-80853] p 290 A95-75095 PELLETIER, DOMINIQUE
	0	Adaptive finite element method for turbulent flow near
N	0	a propeller
• •	OBERKAMPF, WILLIAM L.	[BTN-95-EIX95142553038] p 305 A95-73460
NAGAMATSU, HENRY T.	Review and development of base pressure and base	PENG, CHENGYI  A new type of simulator for simulating the flow-field
Numerical analysis of hypersonic low-density scramjet	heating correlations in supersonic flow	distortion of engine inlet
inlet flow   BTN-95-EIX95212645694   p 272 A95-76746	BTN-95-EIX95212645688  p 271 A95-76740 <b>OEZBAY, HITAY</b>	[BTN-95-EIX95202638963] p 289 A95-76673
BTN-95-EIX95212645694  p 272 A95-76746 NAMKUNG, M.	Stable H(infinity) controller design for the longitudinal	PEREZ, EMILIO
New nondestructive techniques for the detection and	dynamics of an aircraft	Design constraints in the payload-range diagram of ultrahigh capacity transport airplanes
quantification of corrosion in aircraft structures	[NASA-TM-106847] p 293 N95-22954	[BTN-95-EIX95152582319] p 276 A95-73522
p 315 N95-23512	OLSON, JOHN M.  Mishap risk control for advanced aerospace/composite	PERIASAMY, R.
NASH, KYLE L.	materials p 301 N95-23031	Measurement of particle emissions from clean room
Predicting exhaust plume boundaries with supersonic external flows	OLSSON, ERIK	gas-handling components [BTN-94-EIX94381359040] p 295 A95-74554
[BTN-95-EIX95152583258] p 297 A95-73559	Turbulent transonic airfoil flow simulation using a	Measurement of moisture and total hydrocarbon
NAYANI, SUDHEER N.	pressure-based algorithm [BTN-95-EIX95182619078] p 269 A95-75763	contributions by valves used in clean room gas-delivery
Higher-order viscous shock-layer solutions for	OMAN, HENRY	systems IBTN-94-EIX943813590411 p 295 A95-74629
high-altitude flows [BTN-95-EIX95152583255] p 306 A95-73556	New commercial off-the-shelf testers are automatic and	[BTN-94-EIX94381359041] p 295 A95-74629 PERRY, BOYD, III
NEIGHBORS, KEN	intelligent	Summary of an active flexible wing program
Integrated flight/propulsion control for helicopters	[BTN-95-EIX95172595292] p 287 A95-75720 ONCLEY, S. P.	[BTN-95-EIX95182619209] p 283 A95-76635
[HTN-95-80854] p 290 A95-75096	A comparison of some aerodynamic resistance methods	PEZZULLO, G. Structural acoustic calculations in the low-frequency
NELSON, H. F.	using measurements over cotton and grass from the 1991	range
Wing vertical position effects on wing-body carryover for noncircular missiles	California ozone deposition experiment	[BTN-95-EIX95152582336] p 323 A95-73538
[BTN-95-EIX95182617462] p 268 A95-75733	[HTN-95-11295] p 319 A95-77000 ORKWIS, PAUL D.	PIRZADEH, SHAHYAR
NEWMAN, BRETT	Observations on using experimental data as boundary	Unstructured grid solutions to a wing/pylon/store
Aeroelastic vehicle multivariable control synthesis with	conditions for computations	configuration [BTN-95-EIX95152582322] p 265 A95-73525
analytical robustness evaluation [BTN-95-EIX95182619115] p 321 A95-76592	[BTN-95-EIX95182619103] p 321 A95-76588	PITARI, G.
Multivariable stability and robustness of sequentially	OYEDIRAN, AYO Sensitivity of combustion-acoustic instabilities to	Possible effects of CO2 increase on the high-speed civil
designed feedback systems	boundary conditions for premixed gas turbine	transport impact on ozone [HTN-95-60779] p 317 A95-75976
[BTN-95-EIX95182619125] p 322 A95-76602	combustors	PLATZER, MAX F.
NEWMAN, BRETT A.	[NASA-TM-106890] p 289 N95-23550 OZCAN, O.	Aerodynamic characteristics of a canard-controlled
Inner loop flight control for the High-Speed Civil Transport p 293 N95-23314	Aerodynamic characteristics of external store	missile at high angles of attack [BTN-95-EIX95152583257] p 267 A95-73558
NEWMAN, PAUL A.	configurations at low speeds	[BTN-95-EIX95152583257] p 267 A95-73558 Viscous-inviscid interaction method for unsteady
Trajectory modeling of emissions from lower	[BTN-95-EIX95182619230] p 271 A95-76656	low-speed airfoil flows
stratospheric aircraft	B	[BTN-95-EIX95182619093] p 269 A95-75778
[HTN-95-41219] p 317 A95-75031	P	PLETCHER, RICHARD H.
NEWMAN, R. L. TRISTAR 1: Evaluation methods for testing head-up	BACHTED 44	Application of wall functions to generalized nonorthogonal curvilinear coordinate systems
display (HUD) flight symbology	PACHTER, M. Automatic formation flight control	[BTN-95-EIX95182619077] p 307 A95-75762
[NASA-TM-4665] p 288 N95-24030	[BTN-95-EIX95182619153] p 292 A95-76630	POLLACK, W. H.
NEWSOME, J. R.  Measurement of moisture and total hydrocarbon	PADRO, J.	Estimates of total organic and inorganic chlorine in the lower stratosphere from in situ and flask measurements
contributions by valves used in clean room gas-delivery	A comparison of some aerodynamic resistance methods using measurements over cotton and grass from the 1991	during AASE 2
systems	California ozone deposition experiment	[HTN-95-A0861] p 317 A95-76265
[BTN-94-EIX94381359041] p 295 A95-74629	[HTN-95-11295] p 319 A95-77000	PONTON, MICHAEL K.
NG, T. TERRY  Effect of leeward flow dividers on the wing rock of a	PAL, A. K.	Mach wave emission from a high-temperature supersonic jet
delta wing	Simple method of supersonic flow visualization using watertable	[BTN-95-EIX95152577586] p 264 A95-73496
[BTN-95-EIX95152582347] p 282 A95-73549	[BTN-95-EIX95182619105] p 269 A95-76590	POOR, WALTER A.
NICOLAS, JEAN	PALOSCIA, S.	Description of a GNSS availability model and its use in
Coupled FEM-BEM approach for mean flow effects on vibro-acoustic behavior of planar structures	MAX-91: Polarimetric SAR results on Montespertoli	developing requirements [BTN-95-EIX95202637603] p 308 A95-76686
[BTN-95-EIX95152577587] p 263 A95-73495	site p 320 N95-23940	POPERNACK, T. G., JR.
NIESER, DONALD E.	PARIKH, PARESH Unstructured grid solutions to a wing/pylon/store	Dynamic response tests of inertial and optical
Oklahoma City air logistics center (USAF) aging aircraft	configuration	wind-tunnel model attitude measurement devices
corrosion program p 262 N95-23519 NIESL, GEORG H.	[BTN-95-EIX95152582322] p 265 A95-73525	[NASA-TM-109182] p 296 N95-23011 PORTER, L. M.
Analysis of a higher harmonic control test to reduce	PARK, CHAN GOOK	Shock tunnel measurements of hypervelocity blunted
blade vortex interaction noise	Covariance analysis of strapdown INS considering	cone drag
[BTN-95-EIX95152582330] p 265 A95-73532	gyrocompass characteristics [BTN-95-EIX95202637592] p 279 A95-76697	[BTN-95-EIX95152577606] p 305 A95-73477
NISHIMURA, JUN Polar Patrol Balloon	PARK, HEUNG WON	POTOTZKY, ANTHONY S.  Rolling maneuver load alleviation using active controls
[BTN-95-EIX95152582318] p 316 A95-73521	Covariance analysis of strapdown INS considering	[BTN-95-EIX95182619217] p 270 A95-76643
NOLAN, ROBERT C.	gyrocompass characteristics	POURBAIX, A.
Method for the prediction of the onset of wing rock	[BTN-95-EIX95202637592] p 279 A95-76697	In-situ detection of surface passivation or activation and
BTN-95-EIX95152582342  p 282 A95-73544 NOWOBILSKI, J. J.	PARK, JAI H.  Growth of multiple cracks and their linkup in a fusetage	of localized corrosion: Experiences and prospectives in aircraft p 302 N95-23508
Airborne rotary air separator study	tap joint	Test method and test results for environmental

p 264 A95-73516

p 276 N95-23201

p 279 A95-76631

p 297 N95-24019

p 317 A95-76265

p 320 N95-23259

p 320 N95-23940

p 321 A95-76592

p 322 A95-76602

p 269 A95-76615

p 272 A95-76764

aeropropulsive/aeroelastic

Flow visualization studies on sidewall effects in

Collaborative research on aircraft icing and charging

NTS-spill test facility wind tunnel exhaust plume

Estimates of total organic and inorganic chlorine in the lower stratosphere from in situ and flask measurements

Design of a GaAs/Ge solar array for unmanned aerial

MAX-91: Polarimetric SAR results on Montespertoli

Analytical solution and parameter estimation of projectile

Aeroelastic vehicle multivariable control synthesis with

Multivariable stability and robustness of sequentially designed feedback systems

Laser velocimetry seed-particle behavior in shear layers

hypersonic-vehicle model with dynamic analysis

Drag function modeling for air traffic simulation

two-dimensional transonic airfoil testing IBTN-95-EIX95152582313 | p

SATO, MAMORU

SAUNDERS, C. P.

processes in ice

AD-A285102 |

SCHAFFER, T.

SCHAB, DANIEL E.

characterization

[DE95-003630] SCHAUFFLER, S. M.

during AASE 2

SCHIAVON, G.

dynamics

| HTN-95-A0861 |

SCHEIMAN, DAVID A.

INASA-TM-1068701

SCHILLING, HARTMUT

SCHMIDT, DAVID K.

Analytical

at Mach 12

|BTN-95-EIX95212645695|

[BTN-95-EIX95182619125]

|BTN-95-EIX95182619138| SCHMISSEUR, J. D.

[BTN-95-EIX95212645712]

analytical robustness evaluation |BTN-95-EIX95182619115|

[BTN-95-EIX95182619154]

PRABHU, B. S.  Transient analysis of a cracked in	rotor nas	sina Ibrawa
critical speed		
BTN-94-EIX94401360022  PRESTON, ORV W.	p 306	A95-7470
Guidance and control requireme Rollout and Turnoff (ROTO)	ents for	high-spee
INASA-CR-1950261	p 292	N95-2267
PRICE, JOSEPH M.  Hypersonic rarefied flow past spi	norae inc	ludina wak
structure		=
BTN-95-EIX95152583250  PRICE, S. J.	p 305	A95-7355
Postinstability behavior of a two-d	ımension	al airfoil wit
a structural nonlinearity  BTN-95-EIX95152582337	p 266	A95-7353
PRITCHARD, JOCELYN I. Integrated aerodynam	ic/dunam	ic/structurs
optimization of helicopter rotor bla		
decomposition [NASA-TP-3465]	p 285	N95-2295
. <u>_</u>		
R		
RADHAKRISHNAN, KRISHNAN		
Sensitivity of combustion-acou boundary conditions for prem		tabilities t as turbin
combustors	•	N95-2355
[NASA-TM-106890] RAINWATER, B. A.	p 209	1490-2300
Moving mass trim control for aero   DE95-002602		hicles N95-2353
RAIS-ROHANI, MASOUD	•	
Thin tailored composite wing for o		or N95-2331
AJ, PRADEEP		
An assessment of viscous effect simulation of benign and burst von	tex flows	on generi
fighter wind-tunnel models using TE [NASA-CR-4650]		N95-2318
ANGWALLA, AKIL A.		
Three-dimensional unsteady flo advanced gas generator turbine		ations in a N95-2342
ANKIN, JAMES M. Differential GPS and system inte	aration	of the Lov
Visibility Landing and Surface O	peration	s (LVLASO
demonstration	p 280	N95-2331
Pneumatic concept for tip-stall cor wings	trol of cr	anked-arrov
[BTN-95-EIX95152582335]	p 281	A95-7353
AULT, DIDIER F. G. Aerodynamic characteristics of a	hyperso	nic viscou
optimized waverider at high altitudes [BTN-95-EIX95152583251]	•	A95-7355
Aerodynamics of the Shuttle Orb		
BTN-95-EIX95182617454     AVINDRA, KRISHNASWAMY	p 298	A95-7572
Preliminary identification of buffet p		
civil transport	p 294	N95-23319
Switched bias proportional na- guidance against highly maneuvering		for homin
[BTN-95-EIX95182619145]		A95-7662
AWLINGS, J. NTS-spill test facility wind tur	inel exh	aust plume
characterization [DE95-003630]	D 297	N95-2401
EADER, KENNETH R.	•	
An unmanned air vehicle concept [HTN-95-80858]		t drive A95-7510
EDDY, T. S. R. User's guide for ECAP2D: A		r unstead
aerodynamic and aeroelastic analys	sis progr	am for two
dimensional oscillating cascades, ve [NASA-CR-189146]		N95-2418
EHFIELD, LAWRENCE W.		
Experimental evaluation of a b tailored for chordwise deformation		
BTN-95-EIX95182619088  HOADES, R. L.	p 283	A95-7577
Cu deposition using a permaner		
cyclotron resonance microwave plas	ma sour	Ce C

[DE94-017768]

RIDDICK, J. C.

RICHARDS, MICHAEL A.

lunar transfer vehicle [BTN-95-EIX95212645707]

scattered from wire targets. [BTN-94-EIX94381353142] p 304 N95-23981

p 306 A95-74496

p 299 A95-76759

SEM representation of the early and late time fields

Minimum-mass design of sandwich aerobrakes for a

RIDDLE, J. Measurement of particle emissions	from	clean room
gas-handling components	p 295	A95-74554
Measurement of moisture and	total I	nydrocarbor
contributions by valves used in clean systems		
[BTN-94-EIX94381359041] ROACH, LISA K.	p 295	A95-74629
Rationale for the Modular Air-sy Estimation Network (MAVEN) methodo (AD-A285797)		_
ROBINETT, R. D.		
•		hicles N95-23532
ROBINSON, STEPHEN K.  Separation control on high-lift airfoi	ls via r	micro-vortex
generators [BTN-95-EIX95152582326]	p 265	A95-73529
ROBSON, J. NTS-spill test facility wind tunne	el exha	aust plume
characterization		N95-24019
ROCHE, NIGEL R.	,	
Automatic riveting cell for commercial assembly	al aircra	aft floor grid
BTN-95-EIX95182617807  ROCK, STEPHEN M.	p 261	A95-75752
Integrated (light/propulsion control for		
(HTN-95-80854) ROCKWELL, D.	p 290	A95-75096
Transient structure of vortex break wing	down	on a delta
	p <b>26</b> 8	A95-75758
An unmanned air vehicle concept wi		
[HTN-95-80858] ROGERS, STUART E.	p 283	A95-75100
Progress in high-lift aerodynamic cal [BTN-95-EIX95152582315]		ns A95-73518
ROJAS, L. Impeller flow field characterization wit		
		N95-23440
Nonlinear angle of twist of advance	ed com	posite wing
boxes under pure torsion [BTN-95-EIX95152582323]	281	A95-73526
ROOP, J. A.  Modeling aerosol emissions from the	the cor	mbustion of
		N95-23038
The influence of alternate inter-blace ground resonance	te con	nections on
[HTN-95-80859]	267	A95-75101
ROSENFELD, MOSHE Grid refinement test of time-periodi	c flows	over bluff
bodies [BTN-94-EIX94401378822]	307	A95-76491
ROSS, JAMES C. Lift enhancing tabs for airfoils		
	286	N95-23395
Aerodynamic design and analysis of		
ROY, C.		N95-23435
Validation of an effective flat cruciform to study CFRP composite laminat loading	n-shape es un	d specimen der biaxial
[BTN-95-EIX95152584677]	282	A95-73589
RUBLEIN, GEORGE T. Preparation of course mater		Elementary
RYAN, GEORGE W., III		N95-23320
analysis	optimal	
[BTN-95-EIX95182619121]	p 321	A95-76598
S		
SAGALOVSKY, L.		
Evaluation of neutron techniques for detection	or illicit	substance

SCHNEIDER, G. E. g Application of a control-volume-based finite-element formulation to the shock tube problem 6 p 295 A95-76584 [BTN-95-EIX95182619099] SCHOEBERL, MARK R. Trajectory modeling of emissions from lower stratospheric aircraft [HTN-95-41219] p 317 A95-75031 SCHRECK, SCOTT J. Neural network prediction of three-dimensional unsteady separated flowfields |BTN-95-EIX95182619232| p 308 A95-76658 SCHULTZ, KLAUS-J. Analysis of a higher harmonic control test to reduce blade vortex interaction noise [BTN-95-EIX95152582330] p 265 A95-73532 SCHUSTER, DAVID M. 5 Application of Navier-Stokes aeroelastic methods to improve fighter wing maneuver performance |BTN-95-EIX95182619218| p 284 A95-76644 SCHUTZ, BOB E. Thermal force modeling for global positioning system satellites using the finite element method [BTN-95-EIX95152583270] p 2 p 278 A95-73571 SCHWARTZ, ALAN W. An unmanned air vehicle concept with tipjet drive [HTN-95-80858] p 283 A95-7 p 283 A95-75100 Compendium of NASA data base for the Global Tropospheric Experiment's Pacific Exploratory Mission West-A (PEM West-A) INASA-TM-1091771 p.320 N95-23009 SEINER, JOHN M. Mach wave emission from a high-temperature supersonic jet [BTN-95-EIX95152577586] p 264 A95-73496 SEKHAR, A. S. Transient analysis of a cracked rotor passing through p 306 A95-74702 [DE95-002988] BTN-94-EIX944013600221 p 300 N95-22764 SELA, N. M. SAMIMY, MO The influence of alternate inter-blade connections on Effects of expansions on a supersonic boundary layer: Surface pressure measurements ground resonance IBTN-95-EIX951425530361 p 263 A95-73462 [HTN-95-80859] p 267 A95-75101 SENYITKO, RICHARD G. SANDERS, DONALD C. Aircraft fires, smoke toxicity, and survival: An overview | DOT/FAA/AM-95/8 | p 277 N95-24024 NASA low-speed axial compressor for fundamental p 277 N95-24024 research p 296 N95-23192 [NASA-TM-4635] Switched bias proportional navigation for homing SEREGIN, YU. A. A new generation of instruments for flying laboratories [BTN-94-EIX94401363947] p 317 A95-75532 guidance against highly maneuvering targets [BTN-95-EIX95182619145] p 279 A95-76622

	•	
SETH, SHASHI	SONI, BHARAT K.	TAM, CHUNG-JEN
Pilot Weather Advisor system	TIGER: A user-friendly interactive grid generation system	Observations on using experimental data as boundary conditions for computations
[BTN-95-EIX95152582314] p 316 A95-73517 SGARD, FRANCK	for complicated turbomachinery and axis-symmetric configurations p 322 N95-23419	IBTN-95-EIX95182619103  p 321 A95-76588
Coupled FEM-BEM approach for mean flow effects on	SPADAFORA, STEPHEN J.	TANG, D. M.
vibro-acoustic behavior of planar structures	Organic coating technology for the protection of aircraft	Response of a nonrotating rotor blade to lateral
[BTN-95-EIX95152577587] p 263 A95-73495	against corrosion p 303 N95-23513 SPAID, FRANK W.	turbulence. Part 1: Theory [BTN-95-EIX95182619228] p 284 A95-76654
SHABIBI, ABDULLAH AL Study of an airfoil with a flap and spoiler	Experimental results for a hypersonic nozzle/afterbody	Response of a nonrotating rotor blade to lateral
BTN-95-EIX95152582327  p 265 A95-73530	flow field	turbulence. Part 2: Experiment
SHAW, R. H.	[NASA-TM-4638] p 274 N95-23250	[BTN-95-EIX95182619229] p 284 A95-76655
A comparison of some aerodynamic resistance methods	SPARLING, LYNN C.  Trajectory modeling of emissions from lower	TAPLEY, I. J.
using measurements over cotton and grass from the 1991	stratospheric aircraft	AIRSAR deployment in Australia, September 1993: Management and objectives p 321 N95-23948
California ozone deposition experiment [HTN-95-11295] p 319 A95-77000	[HTN-95-41219] p 317 A95-75031	TAYLOR, A. G.
SHERWOOD, BRENT	SPENCE, ANNE MARIE	Finite element model for a flexible non-symmetric rotor
Fourth-generation Mars vehicle concepts	Efficient sensitivity analysis for rotary-wing aeromechanical problems	on distributed bearing: A stability study
[BTN-95-EIX95152583267] p 298 A95-73568	[BTN-95-EIX95152577585] . p 264 A95-73497	[BTN-94-EIX94381352212] p 306 A95-74612
SHIH, MING H. TIGER: A user-friendly interactive grid generation system	SPENCER, JOHN H.	TCHENG, P.  Dynamic response tests of inertial and optical
for complicated turbomachinery and axis-symmetric	1994 NASA-HU American Society for Engineering	wind-tunnel model attitude measurement devices
configurations p 322 N95-23419	Education (ASEE) Summer Faculty Fellowship Program [NASA-CR-194972] p 325 N95-23276	[NASA-TM-109182] p 296 N95-23011
SHIVAKUMAR, K. N.	SPLETTSTOESSER, WOLF R.	THART, W. G. J.
Minimum-mass design of sandwich aerobrakes for a	Analysis of a higher harmonic control test to reduce	Eddy current detection of pitting corrosion around
lunar transfer vehicle [BTN-95-EIX95212645707] p 299 A95-76759	blade vortex interaction noise 1BTN-95-EIX951525823301 p 265 A95-73532	fastener holes p 315 N95-23507 THIELE, F.
SHPUND, Z.	[BTN-95-EIX95152582330] p 265 A95-73532 SRINATHKUMAR, S.	Laplace interaction law for the computation of viscous
Dynamic investigation of the angular motion of a rotating	Flutter suppression for the active flexible wing: A	airfoil flow in low- and high-speed aerodynamics
body-parachute system	classical design	[BTN-95-EIX95142553037] p 263 A95-73461
[BTN-95-EIX95182619220] p 270 A95-76646	[BTN-95-EIX95182619216] p 292 A95-76642	TONEV, PETER T.
SIGISMONDI, S.  MAX-91: Polarimetric SAR results on Montespertoli	SRINIVASAN, RAMAKRISHNA Flutter of an infinitely long panel in a duct	Thundercloud electric field modeling for the ionosphere-Earth region. 1: Dependence on cloud charge
site p 320 N95-23940	[BTN-95-EIX95182619087] p 291 A95-75772	distribution
SILVA, WALTER A.	STALKER, R. J.	[HTN-95-41223] p 317 A95-75035
Application of transonic small disturbance theory to the	Time-of-flight mass spectrometer for impulse facilities	TRAN, KEN
active flexible wing model	[BTN-95-EIX95142553057] p 262 A95-73441	CFD analysis of turbopump volutes p 312 N95-23436
[BTN-95-EIX95182619210] p 270 A95-76636 SILVERBERG, L.	STEELE, L. L. Phase 2: HGM air flow tests in support of HEX vane	TRAUB. LANCE W.
Fuel-optimal bank-angle control for lunar-return	investigation p 312 N95-23438	Analytic prediction of lift for delta wings with partial
aerocapture	STERN, P.	leading-edge thrust
[BTN-95-EIX95212645706] p 299 A95-76758	High-performance parallel analysis of coupled problems	[BTN-95-EIX95152582345] p 266 A95-73547
SIMMONS, J. M.  Shock tunnel measurements of hypervelocity blunted	for aircraft propulsion [NASA-CR-197440] p 289 N95-23088	TREGO, LINDA E.
cone drag	STEWART, D. A.	Maintenance challenges and trends [BTN-95-EIX95182617808] p 261 A95-75753
[BTN-95-EIX95152577606] p 305 A95-73477	Hypersonic convective heat transfer over 140-deg blunt	Maintenance programs
SIMON, DAN	cones in different gases	[BTN-95-EIX95182617809] p 261 A95-75754
Real-time navigation using the global positioning	[BTN-95-EIX95152583253] p 306 A95-73554	Aircraft stripping and painting
system  BTN-95-EIX95172595298  p 279 A95-75714	STEWART, JAMES F. Engines-only flight control system	[BTN-95-EIX95182617810] p 300 A95-75755
SIMPSON, DAVID L.	[NASA-CASE-ARC-11944-1] p 294 N95-23389	TREIBER, DAVID A.  Euler technology assessment for preliminary aircraft
Multiple site fatigue damage in fuselage skin splices:	STRAZNICKY, PAUL V.	design employing OVERFLOW code with multiblock
Experimental simulation and theoretical prediction	Multiple site fatigue damage in fuselage skin splices:	structured-grid method
[BTN-95-EIX95152584676] p 276 A95-73588 SINGH, RIPUDAMAN	Experimental simulation and theoretical prediction [BTN-95-EIX95152584676] p 276 A95-73588	[NASA-CR-4651] p 273 N95-23095
Growth of multiple cracks and their linkup in a fuselage	STREBY, OLIVIER	TRELA, W. J.  Phonon characteristics of high (T sub c) superconductors
lap joint	Analysis of a higher harmonic control test to reduce	from neutron Doppler broadening measurements
[BTN-95-EIX95142553047] p 286 A95-73451	blade vortex interaction noise	[DE95-003703] p 324 N95-24076
SIRBAUGH, J. R. Three-dimensional Navier-Stokes analysis and redesign	[BTN-95-EIX95152582330] p 265 A95-73532	TRIPP, J. S.
of an imbedded bellmouth nozzle in a turbine cascade .	SU, R.  Nonlinear system guidance in the presence of	Dynamic response tests of inertial and optical wind-tunnel model attitude measurement devices
inlet section p 311 N95-23423	transmission zero dynamics	[NASA-TM-109182] p 296 N95-23011
SKAFF, TONY	[NASA-TM-4661] p 309 N95-22804	TROSHCHENKO, V. T.
Effect of leeward flow dividers on the wing rock of a delta wing	SUDANI, NORIKAZU	Fatigue strength of high-temperature alloys under
[BTN-95-EIX95152582347] p 282 A95-73549	Flow visualization studies on sidewall effects in two-dimensional transonic airfoil testing	conditions of cyclic temperature variation. Communication  1: Experimental procedure and results
SKINNER, K. A.	[BTN-95-EIX95152582313] p 264 A95-73516	[BTN-94-EIX94401363884] p 307 A95-75516
Time-of-flight mass spectrometer for impulse facilities	SUGIYAMA, N.	TUCKER, P. KEVIN
[BTN-95-EIX95142553057] p 262 A95-73441 SMART, J. D.	Derivation of system matrices from nonlinear dynamic	Validation of a Computational Fluid Dynamics (CFD)
Health and usage monitoring systems: Corrosion	simulation of jet engines  BTN-95-EIX95182619139  p 288 A95-76616	code for supersonic axisymmetric base flow p 315 N95-23652
surveillance p 262 N95-23506	SUN, WEN-YIH	TUNCER, ISMAIL H.
SMITH, C. J. E.  The corrosion and protection of advanced aluminium -	Diurnal variation of lee vortices in Taiwan and the	Viscous-inviscid interaction method for unsteady
lithium airframe alloys p 302 N95-23497	surrounding area	low-speed airfoil flows
SMITH, D.	[HTN-95-91363] p 318 A95-76394 SWAIM, ROBERT L	[BTN-95-EIX95182619093] p 269 A95-75778
NTS-spill test facility wind tunnel exhaust plume	Multiaxis pilot ratings for damaged aircraft	
characterization [DE95-003630] p 297 N95-24019	[BTN-95-EIX95182619128] p 269 A95-76605	U
SMITH, EDMUND H.	SWAMY, K. N.	UNAL, M. F.
Aerodynamic characteristics of a canard-controlled	Switched bias proportional navigation for homing guidance against highly maneuvering targets	Aerodynamic characteristics of external store
missile at high angles of attack [BTN-95-EIX95152583257] p 267 A95-73558	[BTN-95-EIX95182619145] p 279 A95-76622	configurations at low speeds
SOLIES, U. PETER	, , , , , , , , , , , , , , , , , , , ,	[BTN-95-EIX95182619230] p 271 A95-76656
Handling qualities of the High Speed Civil Transport	T	W
p 294 N95-23325	•	. <b>V</b>
SOLOMON, S.  Estimates of total organic and inorganic chlorine in the	TAKAHASHI, MARC D.	VALAREZO, W. O.
lower stratosphere from in situ and flask measurements	H-infinity helicopter flight control law design with and	Effect of underwing frost on a transport aircraft airfoil
during AASE 2	without rotor state feedback	at flight Reynolds number
[HTN-95-A0861] p 317 A95-76265	[BTN-95-EIX95182619129] p 291 A95-76606	[BTN-95-EIX95152582334] p 276 A95-73536
SONDAK, DOUGLAS L.  Application of wall functions to generalized	TAKALLU, M. A.  Wing pressure distributions from subsonic tests of a	VALAREZO, WALTER O.  Separation control on high-lift airloits via micro-vortex
nonorthogonal curvilinear coordinate systems	high-wing transport model	generators
[BTN-95-EIX95182619077] p 307 A95-75762	[NASA-TM-4583] p 272 N95-22802	[BTN-95-EIX95152582326] p 265 A95-73529

VALAVANI LENA Design of high performance multivariable control systems for supermaneuverable aircraft at high angle of attack INASA-CR-197661 I n 293 N95-22908 VALENTINE, JAMES R. Tracking of raindrops in flow over an airfoil |BTN-95-EIX95182619221| p 308 A95-76647 VANDAM. CORNELIS P. High-lift flow-physics flight experiments on a subsonic transport aircraft (B737-100) p 275 N95-23333 VANDERWALT, JOHANNES P. Static pressure distribution in the inlet of a helicopter turbine compressor IBTN-95-FIX951525823391 p 266 A95-73541 Erosion of dust-filtered helicopter turbine engines. Part Basic theoretical considerations n 288 A95-76648 IBTN-95-EIX951826192221 Erosion of dust-filtered belicopter turbine engines. Part Erosion reduction IRTN-95-FIX951826192231 n 289 A95-76649 Life prediction of helicopter engines fitted with dust filters IBTN-95-EIX951826192241 p 289 A95-76650 VELINOV, PETER I. Y. Thundercloud electric field modeling for the ionosphere-Earth region. 1: Dependence on cloud charge p 317 A95-75035 IHTN-05-412231 VENKATESWARAN, S. Convergence acceleration of implicit schemes in the presence of high aspect ratio grid cells p 313 N95-23446 VERHAAGEN, N. G. A study of the vortex flow over 76/40-deg double-delta INASA-CR-1950321 p.314 N95-23466 VIGUE. YVONNE Thermal force modeling for global positioning system satellites using the finite element method [BTN-95-EIX95152583270] p 278 A95-73571 Possible effects of CO2 increase on the high-speed civil transport impact on ozone [HTN-95-60779] p 317 A95-75976 Optimal lateral-escape maneuvers for microburst encounters during final approach [BTN-95-EIX95182619127] p 276 A95-76604 VOLKOV, V. V. A new generation of instruments for flying laboratories |BTN-94-EIX94401363947| p 317 A95-75532 VORTAC, O. U. The role of flight progress strips in en route air traffic control: A time-series analysis IDOT/FAA/AM-95/41 VOSS. H. J. Experience of in-service corrosion on military aircraft p 303 N95-23516 VU, PHUONG Direct-lift design strategy for longitudinal control of hypersonic aircraft |BTN-95-EIX95182619131| p 291 A95-76608 WAGENER, THOMAS J. 2 micron LIDAR for laser-based remote sensing: Flight demonstration and application survey p 319 A95-76737 [BTN-95-EIX95212641072] WALBERG, G. D. Fuel-optimal bank-angle control for lunar-return aerocapture IBTN-95-EIX952126457061 p 299 A95-76758

WALDMAN, J. Corrosion of landing gear steels p 302 N95-23500 WALSH, JOANNE L. Integrated aerodynamic/dynamic/structural optimization of helicopter rotor blades using multilevel decomposition [NASA-TP-3465] p 285 N95-22953 WANG, HONGLI

the rotor [BTN-94-EIX94381353450] p 323 A95-75494 WARDWELL DOUG Flow visualization studies of VTOL aircraft models during Hover in ground effect [NASA-TM-108860] p 272 N95-22666 WASHBURN, A. E.

Effects of AMB parameters on the dynamic stability of

A study of the vortex flow over 76/40-deg double-delta p 314 N95-23466 [NASA-CR-195032]

WASSERBALIER CHARLES A NASA low-speed axial compressor for fundamental

INASA-TM-46351 p 296 N95-23192 WASZAK M R

Flutter suppression for the active flexible wing: A classical design

IBTN-95-EIX951826192161 p 292 A95-76642 WEAVER, CLARK J.

Trajectory modeling of emissions from lower stratospheric aircraft p 317 A95-75031 WEAVER, HAROLD F.

NASA low-speed axial compressor for fundamental esearch

INASA-TM-46351 p 296 N95-23192 WEETMAN, D. C.

Health and usage monitoring systems: Corrosion p 262 N95-23506 surveillance WEINSTEIN, L. F.

TRISTAR 1: Evaluation methods for testing head-up display (HUD) flight symbology [NASA-TM-4665] n 288 N95-24030

WEISS, SUSANNE Analytical solution and parameter estimation of projectile

dynamics |BTN-95-EIX95212645695| p 272 A95-76747 WENDT, B. J.

Flow structure in the wake of a wishbone vortex renerator [BTN-95-EIX95142553044]

p 304 A95-73454 WERESZCZAK, A. A.

Evolution of oxidation and creep damage mechanisms in HIPed silicon nitride materials I DE95-001360 I p 300 N95-22689

WHITAKER, KEVIN W. Predicting exhaust plume boundaries with supersonic external flows

[BTN-95-EIX95152583258] p 297 A95-73559 WIESEMAN, CAROL D.

On-line analysis capabilities developed to support the active flexible wing wind-tunnel tests. BTN-95-EIX95182619213|

WILCOX, F. Base drag prediction on missile configurations

[BTN-95-EIX95152583256] p 266 A95-73557 WILLIAMS KEVIN W

Development of qualification guidelines for personal computer-based aviation training devices

DOT/FAA/AM-95/61 p 323 N95-23603 WILMOTH, RICHARD G.

Hypersonic rarefied flow past spheres including wake structure [BTN-95-EIX95152583250] p 305 A95-73551

Zonally decoupled direct simulation Monte Carlo solutions of hypersonic blunt-body wake flows [BTN-95-EIX95182617458] p 268 A95-75729

WINFREE, W. P. New nondestructive techniques for the detection and quantification of corrosion in aircraft structures

n 315 N95-23512 WISELY, PAUL L. Design of wide angle head up displays for synthetic

[BTN-95-EIX95212641070] p 287 A95-76735 WOFSY, S. C.

In situ observations in aircraft exhaust plumes in the lower stratosphere at midlatitudes [HTN-95-A0862] p 318 A95-76266

Simulating heat addition via mass addition in constant

area compressible flows BTN-95-EIX95182619100] p 307 A95-76585 WOOD, DAVID

Simulation and model reduction for the active flexible wing program |BTN-95-EIX951826192111

p 295 A95-76637 WOODBRIDGE, E. L.

Estimates of total organic and inorganic chlorine in the lower stratosphere from in situ and flask measurements during AASE 2 p 317 A95-76265 1HTN-95-A08611

In situ observations in aircraft exhaust plumes in the lower stratosphere at midiatitudes

I HTN-95-A0862 I p 318 A95-76266 WOODS-VEDELER, JESSICA A.

Rolling maneuver load alleviation using active controls [BTN-95-EIX95182619217] p 270 A95-76643 p 270 A95-76643 WOODYATT, B. A.

Enhancement of F/A-18 operational flight measurements: Data report for phase 1 p 286 N95-23666 WRIGHT, WILLIAM B.

Additional improvements to the NASA Lewis ice accretion code LEWICE p 309 N95-22669 INASA-TM-1068491

MIL-HDBK-5 design allowables for fibre/metal laminates: ARALL 2 and ARALL 3

[BTN-94-EIX94371346933] p 300 A95-73345 Effect of ambient turbulence intensity on sphere wakes at intermediate Reynolds numbers p 308 A95-76586 BTN-95-EIX95182619101 | WU. L. L. MIL-HDBK-5 design allowables for fibre/metal laminates: ARALL 2 and ARALL 3 IBTN-94-EIX943713469331 p 300 A95-73345 WU. XINPING Simulation on the 3-D turbulent flow in the passages of finocyl grain [BTN-95-EIX95202638962] p 279 A95-76674 WU. ZHIQIANG Effects of AMB parameters on the dynamic stability of IRTN-94-FIX943813534501 n 323 A95-75494

X

**XIONG, FUQIN** Development of aeronautical mobile satellite services

over the past thirty years [BTN-95-EIX95152569458] n 305 A95-73498

YAJIMA, NOBUYUKI Polar Patrol Balloon

|BTN-95-EIX95152582318| p 316 A95-73521

YAMAUCHI, MASAFUMI

Numerical investigation of supersonic flows around a spiked blunt body

[BTN-95-EIX95212645690] p 271 A95-76742 YAMSHANOV, YU. B.

Fatigue strength of high-temperature alloys under conditions of cyclic temperature variation. Communication

1: Experimental procedure and results n 307 A95-75516 IRTN-94-FIX944013638841 YING, JUENFEI

A new type of simulator for simulating the flow-field distortion of engine inlet IBTN-95-FIX952026389631 n 289 A95-76673

YOUNG, C. P., JR. Dynamic response tests of inertial and optical

wind-tunnel model attitude measurement device n 296 N95-23011 INASA-TM-1091821

YOUNG DEBORAH B. 1994 NASA-HU American Society for Engineering Education (ASEE) Summer Faculty Fellowship Program

p 325 N95-23276 INASA-CR-1949721 YOUNG, KATHERINE C. Integrated aerodynamic/dynamic/structural

optimization of helicopter rotor blades using multilevel decomposition p 285 N95-22953 [NASA-TP-3465]

YOUSSEF, Y. Validation of an effective flat cruciform-shaped specimen to study CFRP composite laminates under biaxial

IBTN-95-EIX951525846771 p 282 A95-73589

YUAN, PIN-JAR

Solutions of generalized proportional navigation with maneuvering and nonmaneuvering targets [BTN-95-EIX95202637606] p 27 p 279 A95-76683

YULE, T. J. Evaluation of neutron techniques for illicit substance

detection [DE95-002988] p 300 N95-22764

Z

ZACHAR, EDWARD H-76B fantail demonstrater composite fan blade fabrication

IHTN-95-808561 p 283 A95-75098 ZEDAN, M. F.

Stability derivatives of a flapped plate in unsteady ground

[BTN-95-EIX95182619225] p 270 A95-76651 ZELL PETER T.

Aerodynamic surface distension system for high angle attack forebody vortex control p 286 N95-23390 [NASA-CASE-ARC-11979-1]

ZHOU, GANG Turbulent transonic airfoil flow simulation using a pressure-based algorithm |BTN-95-EIX95182619078| p 269 A95-75763

PERSONAL AUTHOR INDEX ZISCHKA, PETER J.

Experimental evaluation of a box beam specifically tailored for chordwise deformation | BTN-95-EIX95182619088 | p 283 A95-7573

ZOBY, ERNEST V. Higher-order viscous shock-layer solutions for high-altitude flows | BTN-95-EIX95152583255 | p 306 A95-73556

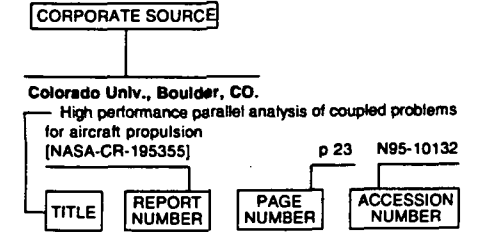
SOURC

July 1995

# CORPORATE SOURCE INDEX

# AERONAUTICAL ENGINEERING / A Continuing Bibliography (Supplement 319)

# **Typical Corporate Source** Index Listing



Listings in this index are arranged alphabetically by corporate source. The title of the document is used to provide a brief description of the subject matter. The page number and the accession number are included in each entry to assist the user in locating the abstract in the abstract section. If applicable, a report number is also included as an aid in identifying the document.

#### Advisory Group for Aeronautical Research and Development, Oxford (England).

POD assessment of NDI procedures using a round robin test

[AGARD-R-809]

p 315 N95-23602

#### Advisory Group for Aerospace Research and Development, Neuilly-Sur-Seine (France).

Corrosion detection and management of advanced airframe materials

(AGARD-CP-565)

p 302 N95-23496

# Aerospatiale, Toulouse (France).

Corrosion in service experience with aircraft in France p 303 N95-23518

#### Force inst. of Tech., Wright-Patterson AFB, OH. Modeling aerosol emissions from the combustion of composite materials p 301 N95-23038

### Air Force Systems Command, McClellan AFB, CA.

Mishap risk control for advanced aerospace/composite p 301 N95-23031

## Air Products and Chemicals, Inc., Allentown, PA.

Organic coating technology for the protection of aircraft p 303 N95-23513 against corrosion

# Argonne National Lab., IL.

Evaluation of neutron techniques for illicit substance detection

p 300 N95-22764 I DE95-0029881

### Arizona Univ., Tucson, AZ.

Residual strength of thin panels with cracks

p 311 N95-23311

## Arkansas Univ., Pine Bluff, AR.

Automation technology using Geographic Information System (GIS) p 324 N95-23284

## Army Research Lab., Watertown, MA.

Rationale for the Modular Air-system Vulnerability Estimation Network (MAVEN) methodology p 284 N95-22510 I AD-A285797 I

#### Auburn Univ., AL.

surveillance

Influence of backup bearings and support structure dynamics on the behavior of rotors with active supports INASA-CR-1974381 p 310 N95-23190

Aerodynamic flight control to increase payload capability of future launch vehicles

|NASA-CR-197704| p 300 N95-24032 AVRO International Aerospace, Woodford (England). Health and usage monitoring systems: Corrosion

# В

#### Belgian Center for Corrosion Study, Brussels (Belgium).

In-situ detection of surface passivation or activation and of localized corrosion: Experiences and prospectives in p 302 N95-23508 aircraft

Test method and test results for environmental p 302 N95-23509 assessment of aircraft materials

## Boeing Defense and Space Group, Seattle, WA.

Euler technology assessment for preliminary aircraft design employing OVERFLOW code with multiblock structured-grid method [NASA-CR-4651]

p 273 N95-23095

## C

#### California Univ., Davis, CA.

Analysis of the longitudinal handling qualities and pilot-induced-oscillation tendencies ٥f High-Angle-of-Attack Research Vehicle (HARV)

p 293 N95-23297

p 262 N95-23506

High-lift flow-physics flight experiments on a subsonic civil transport aircraft (B737-100) p 275 N95-23333

# Cambridge Acoustical Associates, Inc., Cambridge,

The use of cowl camber and taper to reduce rotor/stator interaction noise INASA-CR-1954211

p 323 N95-22675

#### Civil Aeromedical Inst., Oklahoma City, OK. The role of flight progress strips in en route air traffic

IDOT/FAA/AM-95/41 p 280 N95-23565

Development of qualification guidelines for personal computer-based aviation training devices

IDOT/FAA/AM-95/6] p 323 N95-23603

Aircraft fires, smoke toxicity, and survival: An overview [DOT/FAA/AM-95/8] p 277 N95-24024 p 277 N95-24024 A review of civil aviation fatal accidents in which

lost/disoriented was a cause/factor: 1981-1990 [DOT/FAA/AM-95/1] p 278 N95-24071

# Clemson Univ., SC.

Maximum-likelihood spectral estimation and adaptive filtering techniques with application to airborne Doppler weather radar

[NASA-CR-197699] p 316 N95-23670

# College of William and Mary, Williamsburg, VA.

Preparation of course materials: Elementary mathematics of powered flight p 324 N95-23320

## Colorado Univ., Boulder, CO.

High-performance parallel analysis of coupled problems for aircraft propulsion [NASA-CR-197440] p 289 N95-23088

Consiglio Nazionale delle Ricerche, Rome (Italy). MAX-91: Polarimetric SAR results on Montespertoli p 320 N95-23940

#### Defence Research Agency, Farnborough, Hampshire (England).

The corrosion and protection of advanced aluminium lithium airframe alloys p 302 N95-23497

corrosion for life p 314 N95-23505 Non-destructive detection of management

# Defence Science and Technology Organisation,

Melbourne (Australia). Enhancement of F/A-18

operational measurements: Data report for phase 1 p 286 N95-23666 IDSTO-TR-00491

# Defense Advanced Research Projects Agency,

# Arlington, VA.

Technology reinvestment project's focus Affordable polymer matrix composites for airframe structures p 324 N95-23168 IPB95-1360321

## Department of the Air Force, Tinker AFB, OK.

Oklahoma City air logistics center (USAF) aging aircraft p 262 N95-23519 corrosion program

## Deutsche Aerospace A.G., Munich (Germany).

Corrosion protection measures for CFC/metal joints of fuel integral tank structures of advanced military aircraft p 303 N95-23510

Experience of in-service corrosion on military aircraft p 303 N95-23516

## E

## Eloret Corp., Palo Alto, CA.

Particle kinetic simulation of high altitude hypervelocity

[NASA-CR-197383]

# p 309 N95-22481

## Federal Aviation Administration, Washington, DC.

Oceanic operations: An authoritative guide to oceanic operations p 277 N95-24065

#### [FAA-AFS-550] Florida Univ., Gainesville, FL.

Interlaminar shear test method development for long term durability testing of composites

p 301 N95-23300

# G

# General Accounting Office, Washington, DC.

Report to the Secretary of Defense. Unmanned aerial vehicles: No more Hunter systems should be bought until problems are fixed [GAO/NSIAD-95-52] p 286 N95-24091

## Georgia Tech Research Inst., Atlanta, GA.

Flutter analysis of composite box beams [NASA-CR-197931] p 294

p 294 N95-23392

## Н

Hampton Univ., VA. 1994 NASA-HU American Society for Engineering Education (ASEE) Summer Faculty Fellowship Program INASA-CR-1949721 p 325 N95-23276

Honeywell Technology Center, Minneapolis, MN.

Empirical results on scheduling and dynamic acktracking p 299 N95-23761 backtracking

# Illinois Univ., Chicago, IL.

Holographic interferometric tomography for p 310 N95-23287 reconstructing flow fields p 310 N95-23287 istitute for Aerospace Research, Ottawa (Ontario). Double pass retroreflection for corrosion detection in

p 323 N95-23503 aircraft structures Institute for Computer Applications in Science and

Engineering, Hampton, VA.
A study of the vortex flow over 76/40-deg double-delta

[NASA-CR-195032] p 314 N95-23466 Iowa State Univ. of Science and Technology, Ames, IA.

Idealized textile composites for experimental/analytical p 301 N95-23277 correlation

Jet Propulsion Lab., California Inst. of Tech. Pasadena, CA.

Estimates of total organic and inorganic chlorine in the lower stratosphere from in situ and flask measurements during AASE 2

IHTN-95-A0861 I p 317 A95-76265 In situ observations in aircraft exhaust plumes in the lower stratosphere at midlatitudes

[HTN-95-A0862] p 318 A95-76266 flight control Virtual reality display six-degree-of-freedom controller and spherical orientation overlay

INASA-CASE-NPO-18733-1-CU| p 288 N95-22578 Joint Inst. for Advancement of Flight Sciences, Hampton, VA.

An approximate theoretical method for modeling the static thrust performance of non-axisymmetric two-dimensional convergent-divergent nozzles [NASA-CR-195050] p 273 N95-23193

Kansas Univ., Lawrence, KS.

On-line, adaptive state estimator for active noise p 322 N95-23308

Lockheed Aeronautical Systems Co., Marietta, GA.

An assessment of viscous effects in computational simulation of benign and burst vortex flows on generic fighter wind-tunnel models using TEAM code INASA-CR-46501 p 273 N95-23185

Lockheed-Fort Worth Co., Fort Worth, TX. Euler Technology Assessment program for preliminary aircraft design employing SPLITFLOW code with Cartesian unstructured grid method

INASA-CR-46491 p 273 N95-22917 Los Alamos National Lab., NM.

NTS-spill test facility wind tunnel exhaust plume characterization

IDE95-0036301 p 297 N95-24019 Phonon characteristics of high (T sub c) superconductors from neutron Doppler broadening measurements [DE95-003703] p 324 N95-24076

Manchester Univ. (England).

Collaborative research on aircraft icing and charging processes in ice

IAD-A2851021 p 276 N95-23201 Massachusetts Inst. of Tech., Cambridge, MA.

Design of high performance multivariable control systems for supermaneuverable aircraft at high angle of INASA-CR-197661 I p 293 N95-22908

Massachusetts Inst. of Tech., Lexington, MA.

Calculation of satellite drag coefficients IAD-A2851181 p 300 N95-23781

MCAT Inst., Moffett Field, CA.

Three-dimensional unsteady flow calculations in an advanced gas generator turbine p 312 N95-23425 McDonnell-Douglas Aerospace, Long Beach, CA.

Guidance and control requirements for high-speed Rollout and Turnoff (ROTO)

[NASA-CR-195026] p 292 N95-22674

Minnesota Univ., Minneapolis, MN.

Feedback control laws for highly maneuverable aircraft

[NASA-CR-197944] p 295 N95-23410

Mississippi State Univ., Mississippi State, MS.

Crossflow instability control on a swept-wing: Preliminary tudies p 274 N95-23283 studies

Thin tailored composite wing for civil tiltrotor

p 285 N95-23317

TIGER: A user-friendly interactive grid generation system for complicated turbomachinery and axis-symmetric p 322 N95-23419 configurations

Moller International, Inc., Davis, CA. Evaluation of thermal barrier and PS-200 self-lubricating

coatings in an air-cooled rotary engine [NASA-CR-195445] p 289 N95-23222

National Aeronautics and Space Administration. Ames Research Center, Moffett Field, CA.

Progress in high-lift aerodynamic calculations IBTN-95-EIX951525823151 p 264 A95-73518

Navier-Stokes prediction of large-amplitude delta-wing rofl oscillations

BTN-95-EIX95152582329 p 281 A95-73531 Forebody flow control on a full-scale F/A-18 aircraft | BTN-95-EIX95152582333 | p 281 A95-73535

Hypersonic nonequilibrium Navier-Stokes solutions over an ablating graphite nosetip

p 305 A95-73553 BTN-95-EIX951525832521 Hypersonic convective heat transfer over 140-deg blunt cones in different gases

p 306 A95-73554 IBTN-95-EIX951525832531 Investigation of the effects of bandwidth and time delay on helicopter roll-axis handling qualities

p 290 A95-75095 HTN-95-80853 Aeroacoustic model for weak shock waves based on **Rurgers** equation

[BTN-95-EIX95182619076] p 269 A95-75761 Estimates of total organic and inorganic chlorine in the

lower stratosphere from in situ and flask measurements during AASE 2 IHTN-95-A0861 I p 317 A95-76265

In situ observations in aircraft exhaust plumes in the ver stratosphere at midlatitudes

p 318 A95-76266 1HTN-95-A08621 H-infinity helicopter flight control law design with and without rotor state feedback

p 291 A95-76606 BTN-95-EIX95182619129 | Automatic guidance and control for helicopter obstacle

[BTN-95-EIX95182619130] p 291 A95-76607

CFD optimization of a theoretical minimum-drag body p 308 A95-76660 BTN-95-EIX95182619234 | Flow visualization studies of VTOL aircraft models during Hover in ground effect

INASA-TM-1088601 p 272 N95-22666 Nonlinear system guidance in the presence of transmission zero dynamics

INASA-TM-4661 p 309 N95-22804 Experimental results for a hypersonic nozzle/afterbody

| NASA-TM-4638 | p 274 N95-23250 System for determining aerodynamic imbalance

INASA-CASE-ARC-11913-1 p 311 N95-23377 Engines-only flight control system

INASA-CASE-ARC-11944-1] p 294 N95-23389 Aerodynamic surface distension system for high angle of attack forebody vortex control [NASA-CASE-ARC-11979-1] p 286 N95-23390

Cueing light configuration for aircraft navigation p 280 N95-23393 [NASA-CASE-ARC-11982-1]

Lift enhancing tabs for airfoils [NASA-CASE-ARC-11990-1] p 286 N95-23395 AVIRIS and TIMS data processing and distribution at the land processes distributed active archive center

p 325 N95-23872 TRISTAR 1: Evaluation methods for testing head-up display (HUD) flight symbology [NASA-TM-4665] p 288 N95-24030

National Aeronautics and Space Administration. Flight Research Center, Edwards, CA.

Flight test of the X-29A at high angle of attack: Flight dynamics and controls

[NASA-TP-3537] p 284 N95-22806 Direct adaptive performance optimization of subsonic transports: A periodic perturbation technique p 284 N95-22829 INASA-TM-46761

National Aeronautics and Space Administration. Goddard Space Flight Center, Greenbelt, MD.

Trajectory model stratospheric aircraft modeling of emissions from [HTN-95-41219] p 317 A95-75031

Sensitivity of two-dimensional model predictions of ozone response to stratospheric aircraft: An update p 318 A95-76267 IHTN-95-A08631

National Aeronautics and Space Administration. Langley Research Center, Hampton, VA.

Mach wave emission from a high-temperature supersonic iet

[BTN-95-EIX95152577586] p 264 A95-73496 Separation control on high-lift airfoils via micro-vortex

BTN-95-EIX95152582326] p 265 A95-73529 Analysis of a higher harmonic control test to reduce blade vortex interaction noise

[BTN-95-EIX95152582330] p 265 A95-73532 Computational study of plume-induced separation on a

BTN-95-EIX951525823461 p 266 A95-73548 Aerodynamic characteristics of a hypersonic viscous optimized wavender at high altitudes

p 266 A95-73552 [BTN-95-EIX95152583251] Application of the multigrid solution technique to rsonic entry vehicles

IRTN-95-EIX95152583254 I p 306 A95-73555 Higher-order viscous shock-layer solutions for altitude flows

IBTN-95-EIX951525832551 p 306 A95-73556 Optimization of contoured hypersonic scramjet inlets a least-squares parabolized Navier-Stokes procedure

[HTN-95-20976] p 261 A95-74042 Sensitivity of acoustic predictions to variation of input narameters

p 267 A95-75097 IHTN-95-808551 An analytical and experimental investigation of the response of the curved composite frame/skin

specimens p 283 A95-75099 [HTN-95-80857] Aerodynamics of the Shuttle Orbiter at high altitudes p 298 A95-75725 [BTN-95-EIX95182617454] Zonally decoupled direct simulation Monte Carlo

solutions of hypersonic blunt-body wake flows |BTN-95-EIX95182617458| p 268 A95-75729 Multigrid solution of compressible turbulent flow on

unstructured meshes using a two-equation model p 307 A95-76484 |BTN-94-EIX94401378794| Summary of an active flexible wing program

n 283 A95-76635 |BTN-95-EIX95182619209| Application of transonic small disturbance theory to the ctive flexible wing model

IBTN-95-EIX951826192101 p 270 A95-76636 Simulation and model reduction for the active flexible ring program

IBTN-95-EIX951826192111 p 295 A95-76637 Multiple-function digital controller system for active

flexible wing wind-tunnel model IBTN-95-EIX951826192121 p 322 A95-76638 On-line analysis capabilities developed to support the

ctive flexible wing wind-tunnel tests p 296 A95-76639 IRTN-95-FIX951826192131 Flutter suppression control law design and testing for

the active flexible wing p 292 A95-76640 [BTN-95-EIX951826192141 Design and multifunction tests of a

domain-based active flutter suppression system p 292 A95-76641 IBTN-95-EIX95182619215 I Flutter suppression for the active flexible wing: A

classical design [BTN-95-EIX95182619216] p 292 A95-76642 Rolling maneuver load alleviation using active controls IBTN-95-EIX951826192171 p 270 A95-76643

Wing pressure distributions from subsonic tests of a high-wing transport model NASA-TM-45831 p 272 N95-22802

aerodynamic/dynamic/structural integrated optimization of helicopter rotor blades using multilevel decomposition p 285 N95-22953 INASA-TP-34651

Compendium of NASA data base for the Global Tropospheric Experiment's Pacific Exploratory Mission West-A (PEM West-A) p 320 N95-23009 INASA-TM-1091771

Dynamic response tests of inertial and optical wind-tunnel model attitude measurement devices INASA-TM-1091821

Mach 10 computational study of a three-dimensional scramiet inlet flow field [NASA-TM-4602] p 309 N95-23015 Mach 10 computational study of a three-dimensional

scramjet inlet flow field INASA-TM-4602] p 310 N95-23210 New nondestructive techniques for the detection and

quantification of corrosion in aircraft structures p 315 N95-23512

National Aeronautics and Space Administration. Lewis Research Center, Cleveland, OH. Flow structure in the wake of a wishbone vortex

generator [BTN-95-EIX95142553044] p 304 A95-73454

Integrated flight/propulsion control for helicopters p 290 A95-75096 [HTN-95-80854] Numerical analysis of hypersonic low-density scramjet

inlet flow IBTN-95-EIX952126456941 p 272 A95-76746

Additional improvements to the NASA Lewis ice accretion code LEWICE

INASA-TM-1068491 p 309 N95-22669 Stable H(infinity) controller design for the longitudinal dynamics of an aircraft INASA-TM-106847] p 293 N95-22954

Supersonic jet noise reductions predicted with increased jet spreading rate

NASA-TM-106872] p 323 N95-23178 NASA low-speed axial compressor for fundamental research

p 296 N95-23192 INASA-TM-46351 Design of a GaAs/Ge solar array for unmanned aerial vehicle INASA-TM-1068701 p 320 N95-23259

velocities

combustors

INASA-TM-1068901

INASA-TM-1068851

INASA-TM-1067641

Pasadena Office, CA.

IPB95-1391841

fastener holes

[PB94-917007]

2 March 1994

IPB95-910401 I

Naval Air Station, Norfolk, VA.

Management and objectives

Oak Ridge National Lab., TN.

[DE95-001360]

LDF94-017768 L

Transport

in relative motion INASA-CR-1979121

INASA-CR-1974191

in HIPed silicon nitride materials

Old Dominion Coll., Norfolk, VA.

and computational fluid dynamics

advanced turbulence models

presence of high aspect ratio grid cells

Pennsylvania State Univ., State College, PA.

Pennsylvania State Univ., University Park, PA.

Naval Air Warfare Center, Warminster, PA.

DC.

Virtual reality flight

INASA-CASE-NPO-18733-1-CU

A time-accurate finite volume method valid at all flow

Sensitivity of combustion-acoustic instabilities to

Motor drive technologies for the power-by-wire (PBW)

Validation of a Computational Fluid Dynamics (CFD)

six-degree-of-freedom controller and spherical orientation

National Aerospace Lab., Amsterdam (Netherlands).
Review of aeronautical fatigue investigation in the
Netherlands during the period March 1991-March 1993

National Transportation Safety Board, Washington,

Symposium. Volume 2: Participant presentations

Eddy current detection of pitting corrosion around astener holes p 315 N95-23507

Report of proceedings: Aviation Accident Investigation

Aircraft accident report. Runway overrun following

Aviation Accident Investigation Symposium. Volume 1: Industry recommendations and Safety Board responses |PB94-917005| p 278 N95-24105

US Navy operating experience with new aircraft construction materials p 303 N95-23517

Corrosion of landing gear steels p 302 N95-23500 Corrosion detection and monitoring of aircraft structures:

Statistics of multi-look AIRSAR imagery: A comparison

Design of a variable area diffuser for a 15-inch Mach

AIRSAR deployment in Australia, September 1993:

Evolution of oxidation and creep damage mechanisms

Cu deposition using a permanent magnet electron cyclotron resonance microwave plasma source

System identification of the Large-Angle Magnetic

inner loop flight control for the High-Speed Civil

Aerodynamic design optimization with sensitivity analysis

Old Dominion Univ., Norfolk, VA.

A CFD study of complex missile and store configurations

P

Cavitation modeling in Euler and Navier-Stokes codes

Numerical computation of aerodynamics and heat

Convergence acceleration of implicit schemes in the

transfer in a turbine cascade and a turn-around duct using

Suspension Test Fixture (LAMSTF) p 296 N95-23299 Optimized design of a hypersonic nozzle

p 303 N95-23515

Naval Research Lab., Washington, DC.

Statistics of multi-lab.

of theory with measurements p 320 N95-23947 New Jersey Inst. of Tech., Newark, NJ.

6 open-jet tunnel p 297 N95-23309 New South Wales Univ., Kensington (Australia).

0

rejected takeoff, Continental airlines flight 795, McDonnell Douglas MD-82, N18835, LaGuardia Airport, Flushing, NY,

control

program: Options, trends and tradeoffs

National Aeronautics and Space Administration.

Marshall Space Flight Center, Huntsville, AL.

National Aeronautics and Space Administration.

code for supersonic axisymmetric base flow

Research and Technology, 1994

boundary conditions for premixed gas turbine

p 314 N95-23447

p 289 N95-23550

p 295 N95-23671

p 262 N95-24025

p 315 N95-23652

p 288 N95-22578

p 285 N95-23161

p 277 N95-23598

p 277 N95-23609

p 321 N95-23948

p 300 N95-22689

p 304 N95-23981

p 297 N95-23304

p 293 N95-23314

p 285 N95-22949

p 274 N95-23218

p 315 N95-23630

p 313 N95-23444

p 313 N95-23446

display

n 273 N95-23182

p 277 N95-24012

p 277 N95-24050

p 320 N95-23766

A multibody/finite element analysis approach for

Assimilation of altimeter data in a quasi-geostrophic

model of the Gulf Stream system: A dynamical

layer flow INASA-CR-1978671

INASA-CR-1963131

INIAR-94-111

(NIAR-94.31

Wichita State Univ., Wichita, KS.

The airline quality report, 1994

modeling of crash dynamic responses

Woods Hole Oceanographic Inst., MA.

Aerodynamic design and analysis of a highly loaded	
rbine exhaust p 312 N95-23435	Wayne State Univ., Detroit, Ml.
Phase 2: HGM air flow tests in support of HEX vane	Active control of panel vibrations induced by a boundary

Phase 2: HGM air flow tests in support of HEX vane p 312 N95-23438 investigation Princeton Univ., NJ.

Pratt and Whitney Aircraft, West Palm Beach, FL.

An investigation of helicopter dynamic coupling using an analytical model

[NASA-CR-197420] p 285 N95-23217

#### Rochester Univ., NY.

Scientific and technical photography at NASA Langley

#### Saint Cloud State Coll., MN.

Visibility Landing and Surface Operations (LVLASO) demonstration p 280 N95-23318

Saint Louis Univ., Cahokia, IL.

civil transport

Moving mass trim control for aerospace vehicles [DE95-002602] p 299 N95-23532

of an imbedded bellmouth nozzle in a turbine cascade

#### Technion - Israel Inst. of Tech., Haifa (Israel).

A wall interference assessment/correction system [NASA-CR-197421] p 309 N95-23183

Tennessee Univ. Space Inst., Tullahoma, TN.

Texas A&M Univ., College Station, TX.

applications p 274 N95-23294

Toledo Univ., OH.

Enhanced analysis and users manual for radial-inflow

#### Union Carbide Industrial Gases, Inc., Tonawanda, NY. Airborne rotary air separator study

[NASA-CR-189099] p 290 N95-24053

## Vigyan Research Associates, Inc., Hampton, VA.

ith air, nitrogen, and sulfur hexafluoride media under closed loop automatic control [NASA-CR-195052] p 310 N95-23257

fabrication of advanced textile composites

Supersonic flow and shock formation in turbine tip p 312 N95-23429

# R

Research Center p 310 N95-23290 Rockwell International Corp., Canoga Park, CA.

CFD analysis of turbopump volutes

p.312 N95-23436 Impeller flow field characterization with a laser two-focus p 313 N95-23440 velocimeter

Differential GPS and system integration of the Low

Preliminary identification of buffet problems in high speed p 294 N95-23319

Sandia National Labs., Albuquerque, NM.

Sverdrup Technology, Inc., Brook Park, OH.

Three-dimensional Navier-Stokes analysis and redesign

inlet section p 311 N95-23423

Review of some results of the author's fatigue investigations with applications in engineering and material

p 316 N95-23662 ITAF-6981 Technology Integration and Development Group, Inc.,

Gearbox vibration diagnostic analyzer

[NASA-CR-189141] p 316 N95-23792 Tennessee Univ., Tullahoma, TN.

Supersonic laminar flow control research [NASA-CR-197938] p 275 p 275 N95-23669

Handling qualities of the High Speed Civil Transport p 294 N95-23325

Control of flow separation in airfoil/wing design

turbine conceptual design code RTD p 275 N95-23462

[NASA-CR-195454] p 275 N95-23462 User's guide for ECAP2D: An Euler unsteady aerodynamic and aeroelastic analysis program for two dimensional oscillating cascades, version 1.0 [NASA-CR-189146] p 316 N95-24189

Performance of the 0.3-meter transonic cryogenic tunnel

Virginia Polytechnic Inst., Blacksburg; VA.

Development and verification of a resin film infusion/resin transfer molding simulation model for [NASA-CR-197439] p 301 N95-23179

Virginia Polytechnic Inst. and State Univ., Blacksburg,

**C-3** 

# FOREIGN TECHNOLOGY INDEX

# AERONAUTICAL ENGINEERING / A Continuing Bibliography (Supplement 319)

# **Typical Foreign Technology** Index Listing

COUNTRY OF INTELLECTUAL ORIGIN FRANCE Numerical study of Gortler instability: Application to the design of a quiet supersonic wind tunnel [PB94-184801] N95-10844 TITLE NUMBER NUMBER NUMBER

Listings in this index are arranged alphabetically by country of intellectual origin. The title of the document is used to provide a brief description of the subject matter. The page number and accession number are included in each entry to assist the user in locating the abstract in the abstract section. If applicable, a report number is also included as an aid in identifying the document

## AUSTRALIA

Time-of-flight mass spectrometer for impulse facilities |BTN-95-EIX95142553057| p 262 A95-73441 Shock tunnel measurements of hypervelocity blunted

[BTN-95-EIX95152577606] p 305 A95-73477

Enhancement of F/A-18 operational flight measurements: Data report for phase 1

[DSTO-TR-0049] p 286 N95-23666 AIRSAR deployment in Australia, September 1993: Management and objectives D 321 N95-23948

BELGIUM Experimental investigation of the flowfield about an upswept afterbody

B

[BTN-95-EIX95152582321] p 265 A95-73524 In-situ detection of surface passivation or activation and of localized corrosion: Experiences and prospectives in aircraft p 302 N95-23508

Test method and test results for environmental assessment of aircraft materials BULGARIA

Thundercloud electric field modeling for the ionosphere-Earth region. 1: Dependence on cloud charge

[HTN-95-412231 p 317 A95-75035

#### CANADA

Adaptive finite element method for turbulent flow near

[BTN-95-EIX95142553038] p 305 A95-73460

Coupled FEM-BEM approach for mean flow effects on vibro-acoustic behavior of planar structures

IBTN-95-EIX951525775871 p 263 A95-73495 Postinstability behavior of a two-dimensional airfoil with

a structural nonlinearity BTN-95-EIX95152582337 p 266 A95-73539

Multiple site fatigue damage in fuselage skin splices: Experimental simulation and theoretical prediction

p 276 A95-73588 |BTN-95-EIX95152584676| Validation of an effective flat cruciform-shaped specimen to study CFRP composite laminates under biaxial

IBTN-95-FIX95152584677 I p 282 A95-73589 Evaluation of advanced aerospace materials by depth

ensing indentation and scratch methods IRTN-95-FIX951525846781 p 282 A95-73590 Improving prediction: The incorporation of simplified

rotor dynamics in a mathematical model of the bell [BTN-95-EIX95152584679]

Finite element model for a flexible non-symmetric rotor on distributed bearing: A stability study BTN-94-EIX943813522121 p 306 A95-74612

Application of a control-volume-based finite-element formulation to the shock tube problem p 295 A95-76584

BTN-95-EIX95182619099] A comparison of some aerodynamic resistance methods using measurements over cotton and grass from the 1991 California ozone deposition experiment

IHTN-95-112951 p 319 A95-77000 Double pass retroreflection for corrosion detection in

p 323 N95-23503 aircraft structures CHINA

Development of aeronautical mobile satellite services over the past thirty years [BTN-95-EIX95152569458]

p 305 A95-73498 Effects of AMB parameters on the dynamic stability of the rotor

|BTN-94-EIX94381353450| p 323 A95-75494 A new type of simulator for simulating the flow-field distortion of engine inlet

[BTN-95-EIX95202638963] p 289 A95-76673 Simulation on the 3-D turbulent flow in the passages

of finocyl grain [BTN-95-EIX95202638962] p 279 A95-76674

## E

Main features of overexpanded triple jets [BTN-95-EIX95142553040] p 304 A95-73458

## FRANCE

Two-equation turbulence model for unsteady separated lows around airfoils

IBTN-95-EIX951425530541 p 262 A95-73444 Geoid lineations of 1000 km wavelength over the central

Pacific [HTN-95-11304] Corrosion detection and management of advanced

airframe materials I AGARD-CP-565 I p 302 N95-23496

Corrosion in service experience with aircraft in France p 303 N95-23518

# G

#### GERMANY

Laplace interaction law for the computation of viscous airfoil flow in low- and high-speed aerodynamics p 263 A95-73461 IBTN-95-EIX951425530371

Analytical solution and parameter estimation of projectile

p 272 A95-76747 [BTN-95-EIX95212645695] Transport of exhaust products in the near trail of a jet engine under atmospheric conditions p 319 A95-77334 [HTN-95-91421]

Corrosion protection measures for CFC/metal joints of fuel integral tank structures of advanced military aircraft p 303 N95-23510

Experience of in-service corrosion on military aircraft p 303 N95-23516

Transient analysis of a cracked rotor passing through critical speed |BTN-94-EIX94401360022|

Some aspects of the aerodynamics of separating

p 298 A95-75735 IBTN-95-EIX951826174641 Simple method of supersonic flow visualization using watertable

p 269 A95-76590 |BTN-95-EIX95182619105| Switched bias proportional navigation for homing

guidance against highly maneuvering targets [BTN-95-EIX95182619145] p 279 p 279 A95-76622 RELAND

The influence of alternate inter-blade connections on ground resonance [HTN-95-80859] p 267 A95-75101

#### ISRAEL Grid refinement test of time-periodic flows over bluff

bodies IBTN-94-EIX94401378822 I p 307 A95-76491

Dynamic investigation of the angular motion of a rotating [BTN-95-EIX95182619220] p 270 A95-76646

Review of some results of the author's fatigue investigations with applications in engineering and material science

[TAE-698] p 316 N95-23662

ITALY

Simulation of turbulent fluctuations

p 304 A95-73457 [BTN-95-EIX95142553041] Structural acoustic calculations in the low-frequency

p 323 A95-73538 [BTN-95-EIX95152582336]

Simulation of transverse gas injection in turbulent supersonic air flows

[BTN-95-EIX95182619080] p 269 A95-75765 Possible effects of CO2 increase on the high-speed civil

transport impact on ozone p 317 A95-75976 IHTN-95-607791

MAX-91: Polarimetric SAR results on Montespertoli p 320 N95-23940

## J

Flow visualization studies on sidewall effects in vo-dimensional transonic airfoil testing p 264 A95-73516 IBTN-95-EIX951525823131

Polar Patrol Balloon p 316 A95-73521 BTN-95-EIX95152582318 |

Derivation of system matrices from nonlinear dynamic simulation of jet engines (BTN-95-EIX95182619139) p 288 A95-76616

Numerical investigation of supersonic flows around a spiked blunt body

IBTN-95-EIX952126456901 p 271 A95-76742

#### KOREA, REPUBLIC OF

Static aeroelastic characteristics of a composite wing [BTN-95-EIX95152582340] p 282 A95-73542 Numerical study of sound generation due to a spinning

[BTN-95-EIX95182619075] p 307 A95-75760 Covariance analysis of strapdown INS considering gyrocompass characteristics BTN-95-EIX95202637592 | p 279 A95-76697

#### **NETHERLANDS**

N

#### **NETHERLANDS**

Optimal lateral-escape maneuvers for microburst ncounters during final approach

IBTN-95-EIX951826191271 p 276 A95-76604 Review of aeronautical fatigue investigation in the Netherlands during the period March 1991-March 1993 | PB95-139184 | p 285 N95-23161

Eddy current detection of pitting corrosion around fastener holes p 315 N95-23507

0

#### OMAN

Study of an airfoil with a flap and spoiler | BTN-95-EIX95152582327 | p 265 A95-73530

#### RUSSIA

A new generation of instruments for flying laboratories BTN-94-EIX94401363947 p 317 A95-75532 [BTN-94-EIX94401363947]

S

#### SAUDI ARABIA

Analytical solution for controls, heats, and states of flight

IBTN-95-EIX951525832861 p 282 A95-73587 Stability derivatives of a flapped plate in unsteady ground effect

[BTN-95-EIX95182619225] p 270 A95-76651 Unsteady ground effects on aerodynamic coefficients of finite wings with camber [BTN-95-EIX95182619233] p 271 A95-76659

SOUTH AFRICA

Static pressure distribution in the inlet of a helicopter turbine compressor IBTN-95-EIX951525823391 p 266 A95-73541

Analytic prediction of lift for delta wings with partial eading-edge thrust IBTN-95-EIX951525823451

p 266 A95-73547 Erosion of dust-filtered helicopter turbine engines. Part 1: Basic theoretical considerations

IBTN-95-FIX951826192221 p 288 A95-76648 Erosion of dust-filtered helicopter turbine engines. Part

2: Erosion reduction [BTN-95-EIX95182619223] p 289 A95-76649 Life prediction of helicopter engines fitted with dust filters

|BTN-95-EIX95182619224| p 289 A95-76650 SPAIN Design constraints in the payload-range diagram of

ultrahigh capacity transport airplanes p 276 A95-73522 [BTN-95-EIX95152582319]

SWEDEN Turbulent transonic airfoil flow simulation using a pressure-based algorithm {BTN-95-EIX95182619078} p 269 A95-75763

#### TAIWAN, PROVINCE OF CHINA

[BTN-95-EIX95182619230]

Sidewash on the vertical tail in subsonic and supersonic (BTN-95-EIX95152582316) p 264 A95-73519 Solutions of generalized proportional navigation with maneuvering and nonmaneuvering targets |BTN-95-EIX95202637606| p 279 A95-76683 Integrated design of hypersonic waveriders including inlets and tailfins |BTN-95-EIX95212645692| p 271 A95-76744 TURKEY Aerodynamic characteristics of external store configurations at low speeds

U

#### UKRAINE

Fatigue strength of high-temperature alloys under conditions of cyclic temperature variation. Communication : Experimental procedure and results

p 307 A95-75516 IBTN-94-EIX94401363884 I

UNITED KINGDOM

Dynamical instability of the aerogravity assist IBTN-95-FIX95152583282 I p 298 A95-73583 Design of wide angle head up displays for synthetic

IBTN-95-EIX952126410701

p 287 A95-76735

p 271 A95-76656

Collaborative research on aircraft icing and charging processes in ice AD-A285102

p 276 N95-23201 The corrosion and protection of advanced aluminium

p 302 N95-23497 lithium airframe alloys Non-destructive detection of corrosion for life p 314 N95-23505 management Health and usage monitoring systems: Corrosion

p 262 N95-23506 POD assessment of NDI procedures using a round robin

[AGARD-R-809] p 315 N95-23602

# Typical Contract Number Index Listing

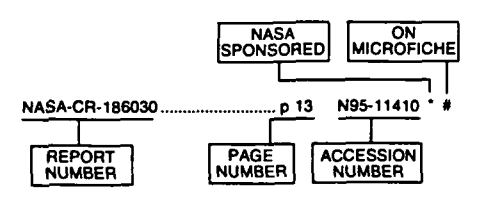
N00014-82-K-0185	p	22	N95-10231
CONTRACT	PAGE	[*	CCESSION
NUMBER	NUMBER		NUMBER

Listings in this index are arranged alphanumerically by contract number. Under each contract number the accession numbers denoting documents that have been produced as a result of research done under the contract are shown. The accession number denotes the number by which the citation is identified in the abstract section. Preceding the accession number is the page number on which the citation may be found.

AF-AFOSR-0376-91	p 276	N95-23201
DA PROJ. 1L1-6241-A-47-AB	p 285	N95-22953
DA PROJ. 1L1-62618-AH-80	p 284	N95-22510
DAJA45-83-C-0011	p 302	N95-23509
DAJA45-83-C-0041	D 305	N95-23509
DE-AC04-94AL-85000	p 299	N95-23532
DE-AC05-84OR-21400	p 300	N95-22689
	p 304	N95-23981
F19628-90-C-0002	p 300	N95-23781
JPL-958208	p 320	N95-23766
NAG1-1088	p 293	N95-22908
NAG1-1150	p 285	N95-22949
NAG1-1175	p 273	N95-23182
NAG1-1188	p 274	N95-23218
NAG1-1380	p 295	N95-23410
NAG1-19317	p 283	A95-75099
NAG1-343	p 283	A95-75099
	p 301	N95-23179
NAG1-928	p 316	N95-23670
NAG2-561	p 285	N95-23217
NAG2-733 NAG2-881	p 309 p 275	N95-23183
NAG3-1137	p 316	N95-23669 N95-24189
NAG3-1165	p 275	N95-24169 N95-23462
NAG3-1177	p 290	A95-75096
NAG3-1273	p 289	N95-23088
NAG3-1507	p 310	N95-23190
NAS1-18762	D 273	N95-23095
NAS1-19000	p 273	N95-22917
	p 273	N95-23185
NAS1-19480	p 314	N95-23466
NAS1-19672	p 310	N95-23257
NAS1-19703	p 292	N95-22674
NAS3-25266	p 296	N95-23192
NAS3-25560	p 290	N95-24053
NAS3-26134	p 316	N95-23792
NAS3-26309	p 289	N95-23222
NAS3-27186	p 309	N95-22669
	p 320	N95-23259
NAS3-27229	p 289	N95-23550
	p 323	N95-22675
NAS7-918 NAS8-36801	p 288 p 312	N95-22578 N95-23438
NAS8-38864	p 313	N95-23440
NAS8-39131	p 300	N95-23440 N95-24032
NCC1-14	D 273	N95-24032 N95-23193
NCC1-24	D 273	N95-23193
NCC2-582	p 309	N95-22481
NGT-47-020-800	p 325	N95-23276
NGT-50981	p 294	N95-23392
NOOO19-87-C-0195	p 290	A95-75093

NSF ATMS-86-11729	p 318	A95-76394
NSF ATMS-89-07881	p 318	A95-76394
NSF CDR-88-03012	p 290	A95-75094
RTOP 233-02-0A	p 320	N95-23259
RTOP 233-02-03	p 295	N95-23671
RTOP 324-02-00	p 289	N95-23222
RTOP 464-54-03-70	p 320	N95-23009
RTOP 505-59-10-13	p 272	N95-22802
RTOP 505-59-50-02	p 310	N95-23257
RTOP 505-59-54-01	p 296	N95-23011
RTOP 505-62-50	p 293	N95-22954
RTOP 505-62-52	p 323	N95-23178
	p 296	N95-23192
RTOP 505-63-36-06	p 285	N95-22953
RTOP 505-63-36	p 316	N95-23792
RTOP 505-64-30	p 284	N95-22806
RTOP 505-64-36	p 288	N95-24030
RTOP 505-64-52	p 309	N95-22804
RTOP 505-68-10	p 309	N95-22669
RTOP 505-68-30-03	p 273	N95-22917
	p 273	N95-23095
	p 273	N95-23185
RTOP 505-68-32	p 272	N95-22666
RTOP 505-69-10	p 284	N95-22829
RTOP 505-69-50	p 275	N95-23462
RTOP 505-70-62	p 274	N95-23250
RTOP 505-90-52-01	p 314	N95-23466
RTOP 506-40-41-02	p 309	N95-23015
	p 310	N95-23210
RTOP 535-03-10	p 323	N95-22675
RTOP 537-02-21	p 289	N95-23550
RTOP 537-07-20	p 273	N95-23193
RTOP 538-04-13-01	p 292	N95-22674
RTOP 538-06-13	p 316	N95-24189
W-31-109-ENG-38	p 300	N95-22764
W-7405-ENG-36	p 324	N95-24076
W-7405-ENG-48	p 297	N95-24019

# Typical Report Number Index Listing



Listings in this index are arranged alphanumerically by report number. The page number indicates the page on which the citation is located. The accession number denotes the number by which the citation is identified. An asterisk (\*) indicates that the item is a NASA report. A pound sign (#) indicates that the item is available on microfiche.

A-94119	p 274	N95-23250 * #
A-94141	p 288	N95-24030 * #
A-95014	p 309	N95-22804 * #
A-95025	p 272	N95-22666 * #
AD-A279436	p 320	N95-23766 *
AD-A285102	p 276	N95-23201 #
	p 300	
AD-A285797	p 284	N95-22510 #
AGARD-CP-565	p 302	N95-23496 #
AGARD-R-809	p 315	N95-23602 #
AIAA PAPER 95-0560	p 314	N95-23466 * #
AIAA PAPER 95-0752	p 309	N95-22669 * #
	•	
AL-CF-TR-1994-0159	n 288	N95-24030 * #
7.2.2 100 . 0	p 200	7100 21000 #
ANL/TD/CP-83462	p 300	N95-22764 #
ANL/10/CP-83462	p 300	N95-22/04 #
AR-008-910	p 286	N95-23666
ARL-TR-518	p 285	N95-22953 * #
ARL-TR-581	p 284	N95-22510 #
B-259256	p 286	N95-24091 #
BTN-94-EIX94371346933	p 300	A95-73345
BTN-94-EIX94381352212	p 306	A95-74612
BTN-94-EIX94381353142	p 306	A95-74496
	p 323	A95-75494
T : 1 - : - : - : - : - : - : - : - : - :		A95-74554
BTN-94-EIX94381359040	p 295	
BTN-94-EIX94381359041	p 295	A95-74629
BTN-94-EIX94401360022	p 306	A95-74702
BTN-94-EIX94401363884	p 307	
		A95-75516
BTN-94-EIX94401363947	p 317	A95-75516 A95-75532
BTN-94-EIX94401363947 BTN-94-EIX94401378794	p 317 p 307	
	p 307	A95-75532
BTN-94-EIX94401378794 BTN-94-EIX94401378820	p 307 p 307	A95-75532 A95-76484 A95-76489
BTN-94-EIX94401378794BTN-94-EIX94401378820BTN-94-EIX94401378822	p 307 p 307 p 307	A95-75532 A95-76484 A95-76489 A95-76491
BTN-94-EIX94401378794	p 307 p 307 p 307 p 263	A95-75532 A95-76484 * A95-76489 A95-76491 A95-73465
BTN-94-EIX94401378794 BTN-94-EIX94401378820 BTN-94-EIX94401378822 BTN-95-EIX95142553033 BTN-95-EIX95142553036	p 307 p 307 p 307 p 263 p 263	A95-75532 A95-76484 A95-76489 A95-76491 A95-73465 A95-73462
BTN-94-EIX94401378794 BTN-94-EIX94401378820 BTN-94-EIX94401378822 BTN-95-EIX95142553033 BTN-95-EIX95142553036 BTN-95-EIX95142553037	p 307 p 307 p 307 p 263 p 263 p 263	A95-75532 A95-76484 A95-76489 A95-76491 A95-73465 A95-73462 A95-73461
BTN-94-EIX94401378794 BTN-94-EIX94401378820 BTN-95-EIX94401378822 BTN-95-EIX95142553033 BTN-95-EIX95142553036 BTN-95-EIX95142553037 BTN-95-EIX95142553038	p 307 p 307 p 307 p 263 p 263 p 263 p 305	A95-75532 A95-76484 * A95-76489 A95-76491 A95-73465 A95-73462 A95-73461 A95-73460
BTN-94-EIX94401378794 BTN-94-EIX94401378820 BTN-94-EIX94401378822 BTN-95-EIX95142553033 BTN-95-EIX95142553036 BTN-95-EIX95142553037 BTN-95-EIX95142553038 BTN-95-EIX95142553038	p 307 p 307 p 307 p 263 p 263 p 263 p 305 p 304	A95-75532 A95-76484 * A95-76489 A95-76491 A95-73465 A95-73462 A95-73461 A95-73460 A95-73458
BTN-94-EIX94401378794 BTN-94-EIX94401378820 BTN-94-EIX94401378822 BTN-95-EIX95142553033 BTN-95-EIX95142553036 BTN-95-EIX95142553037 BTN-95-EIX95142553038 BTN-95-EIX95142553040 BTN-95-EIX95142553041	p 307 p 307 p 307 p 263 p 263 p 263 p 305 p 304 p 304	A95-75532 A95-76484 • A95-76489 A95-76491 A95-73465 A95-73462 A95-73461 A95-73450 A95-73458 A95-73457
BTN-94-EIX94401378794 BTN-94-EIX94401378820 BTN-94-EIX94401378822 BTN-95-EIX95142553033 BTN-95-EIX95142553036 BTN-95-EIX95142553037 BTN-95-EIX95142553040 BTN-95-EIX95142553041 BTN-95-EIX95142553044	p 307 p 307 p 307 p 263 p 263 p 263 p 305 p 304 p 304 p 304	A95-75532 A95-76489 A95-76489 A95-76481 A95-73465 A95-73461 A95-73461 A95-73460 A95-73457 A95-73454
BTN-94-EIX94401378794 BTN-94-EIX94401378820 BTN-94-EIX94401378822 BTN-95-EIX95142553033 BTN-95-EIX95142553036 BTN-95-EIX95142553037 BTN-95-EIX95142553038 BTN-95-EIX95142553040 BTN-95-EIX95142553041 BTN-95-EIX95142553044	p 307 p 307 p 307 p 263 p 263 p 263 p 305 p 304 p 304 p 304 p 304	A95-75532 A95-76484 A95-76489 A95-76491 A95-73465 A95-73461 A95-73461 A95-73460 A95-73454 A95-73454 A95-73454 A95-73455
BTN-94-EIX94401378794 BTN-94-EIX94401378820 BTN-94-EIX94401378822 BTN-95-EIX95142553033 BTN-95-EIX95142553036 BTN-95-EIX95142553037 BTN-95-EIX95142553040 BTN-95-EIX95142553041 BTN-95-EIX95142553044	p 307 p 307 p 307 p 263 p 263 p 263 p 305 p 304 p 304 p 304	A95-75532 A95-76489 A95-76489 A95-76481 A95-73465 A95-73461 A95-73461 A95-73460 A95-73457 A95-73454
BTN-94-EIX94401378794 BTN-94-EIX94401378820 BTN-94-EIX94401378822 BTN-95-EIX95142553033 BTN-95-EIX95142553036 BTN-95-EIX95142553038 BTN-95-EIX95142553040 BTN-95-EIX95142553041 BTN-95-EIX95142553044 BTN-95-EIX95142553044	p 307 p 307 p 307 p 263 p 263 p 263 p 305 p 304 p 304 p 304 p 304	A95-75532 A95-76484 A95-76489 A95-76491 A95-73465 A95-73461 A95-73461 A95-73460 A95-73454 A95-73454 A95-73454 A95-73455
BTN-94-EIX94401378794 BTN-94-EIX94401378820 BTN-94-EIX94401378822 BTN-95-EIX95142553033 BTN-95-EIX95142553036 BTN-95-EIX95142553037 BTN-95-EIX95142553030 BTN-95-EIX95142553040 BTN-95-EIX95142553041 BTN-95-EIX95142553044 BTN-95-EIX95142553044 BTN-95-EIX95142553047 BTN-95-EIX95142553047	p 307 p 307 p 307 p 263 p 263 p 263 p 305 p 304 p 304 p 304 p 304 p 286 p 262	A95-75532 A95-76484 A95-76489 A95-76481 A95-73465 A95-73462 A95-73461 A95-73458 A95-73457 A95-73454 A95-73454 A95-73454
BTN-94-EIX94401378794 BTN-94-EIX94401378820 BTN-95-EIX9401378822 BTN-95-EIX95142553033 BTN-95-EIX95142553036 BTN-95-EIX95142553038 BTN-95-EIX95142553040 BTN-95-EIX95142553041 BTN-95-EIX95142553044 BTN-95-EIX95142553044 BTN-95-EIX95142553044 BTN-95-EIX95142553045 BTN-95-EIX95142553045	p 307 p 307 p 307 p 263 p 263 p 263 p 305 p 304 p 304 p 304 p 304 p 286 p 262 p 262	A95-75532 A95-76489 A95-76489 A95-76489 A95-73465 A95-73461 A95-73461 A95-73460 A95-73457 A95-73457 A95-73454 A95-73454 A95-73454 A95-73444 A95-73444
BTN-94-EIX94401378794 BTN-94-EIX94401378820 BTN-94-EIX94401378822 BTN-95-EIX95142553033 BTN-95-EIX95142553036 BTN-95-EIX95142553036 BTN-95-EIX95142553040 BTN-95-EIX95142553041 BTN-95-EIX95142553044 BTN-95-EIX95142553047 BTN-95-EIX95142553047 BTN-95-EIX95142553047 BTN-95-EIX95142553047 BTN-95-EIX95142553054 BTN-95-EIX95142553054	p 307 p 307 p 307 p 263 p 263 p 263 p 305 p 304 p 304 p 304 p 304 p 286 p 262 p 262 p 278	A95-75532 A95-76484 A95-76489 A95-76491 A95-73465 A95-73461 A95-73460 A95-73450 A95-73457 A95-73454 A95-73454 A95-73451 A95-73451 A95-73444 A95-73441 A95-73441
BTN-94-EIX94401378794 BTN-94-EIX94401378820 BTN-95-EIX9401378822 BTN-95-EIX95142553033 BTN-95-EIX95142553036 BTN-95-EIX95142553038 BTN-95-EIX95142553040 BTN-95-EIX95142553041 BTN-95-EIX95142553044 BTN-95-EIX95142553044 BTN-95-EIX95142553044 BTN-95-EIX95142553045 BTN-95-EIX95142553045	p 307 p 307 p 307 p 263 p 263 p 263 p 305 p 304 p 304 p 304 p 304 p 286 p 262 p 278 p 278	A95-75532 A95-76489 A95-76489 A95-76489 A95-73465 A95-73462 A95-73461 A95-73458 A95-73457 A95-73454 A95-73451 A95-73451 A95-73451 A95-73444 A95-73443 A95-73433
BTN-94-EIX94401378794 BTN-94-EIX94401378820 BTN-94-EIX94401378822 BTN-95-EIX95142553033 BTN-95-EIX95142553036 BTN-95-EIX95142553036 BTN-95-EIX95142553040 BTN-95-EIX95142553041 BTN-95-EIX95142553044 BTN-95-EIX95142553047 BTN-95-EIX95142553047 BTN-95-EIX95142553047 BTN-95-EIX95142553047 BTN-95-EIX95142553054 BTN-95-EIX95142553054	p 307 p 307 p 307 p 263 p 263 p 263 p 305 p 304 p 304 p 304 p 304 p 286 p 262 p 262 p 278	A95-75532 A95-76484 A95-76489 A95-76491 A95-73465 A95-73461 A95-73460 A95-73450 A95-73457 A95-73454 A95-73454 A95-73451 A95-73451 A95-73444 A95-73441 A95-73441
BTN-94-EIX94401378794 BTN-94-EIX94401378820 BTN-94-EIX94401378822 BTN-95-EIX95142553033 BTN-95-EIX95142553036 BTN-95-EIX95142553037 BTN-95-EIX95142553038 BTN-95-EIX95142553040 BTN-95-EIX95142553041 BTN-95-EIX95142553044 BTN-95-EIX95142553047 BTN-95-EIX95142553047 BTN-95-EIX95142553054 BTN-95-EIX95142553054 BTN-95-EIX95142553054 BTN-95-EIX95142553055	p 307 p 307 p 307 p 263 p 263 p 263 p 305 p 304 p 304 p 304 p 304 p 286 p 262 p 278 p 278	A95-75532 A95-76489 A95-76489 A95-76489 A95-73465 A95-73462 A95-73461 A95-73458 A95-73457 A95-73454 A95-73451 A95-73451 A95-73451 A95-73444 A95-73443 A95-73433

BTN-95-EIX95142562403		p 280	A95-73437
-,			
BTN-95-EIX95152569458		p 305	A95-73498
BTN-95-EIX95152577585		p 264	A95-73497
BTN-95-EIX95152577586		p 264	A95-73496 °
	••••••		
BTN-95-EIX95152577587		p 263	A95-73495
BTN-95-EIX95152577588		p 263	A95-73494
BTN-95-EIX95152577589		p 263	A95-73493
BTN-95-EIX95152577597			
	•••••	p 305	A95-73486
BTN-95-EIX95152577604	•••••	p 305	A95-73479
BTN-95-EIX95152577606		p 305	A95-73477
BTN-95-EIX95152577612		p 321	A95-73471
BTN-95-EIX95152582313		p 264	A95-73516
BTN-95-EIX95152582314			
	•••••	p 316	A95-73517
BTN-95-EIX95152582315		p 264	A95-73518 °
BTN-95-EIX95152582316		p 264	A95-73519
BTN-95-EIX95152582317		p 264	A95-73520
BTN-95-EIX95152582318		p 316	A95-73521
BTN-95-EIX95152582319		•	
		p 276	A95-73522
BTN-95-EIX95152582320	•••••	p 264	A95-73523
BTN-95-EIX95152582321		p 265	A95-73524
BTN-95-EIX95152582322		p 265	A95-73525
BTN-95-EIX95152582323		p 281	A95-73526
BTN-95-EIX95152582324	••••••		
		p 265	A95-73527
BTN-95-EIX95152582326	•••••	p 265	A95-73529 °
BTN-95-EIX95152582327		p 265	A95-73530
BTN-95-EIX95152582329		p 281	A95-73531 *
BTN-95-EIX95152582330		p 265	A95-73532 *
BTN-95-EIX95152582331			
	•••••••	p 281	A95-73533
BTN-95-EIX95152582333		p 281	A95-73535 *
BTN-95-EIX95152582334		p 276	A95-73536
BTN-95-EIX95152582335		p 281	A95-73537
BTN-95-EIX95152582336		p 323	A95-73538
BTN-95-EIX95152582337		p 266	A95-73539
BTN-95-EIX95152582338	•••••	p 281	A95-73540
BTN-95-EIX95152582339		p 266	A95-73541
BTN-95-EIX95152582340	***********	p 282	A95-73542
BTN-95-EIX95152582342		p 282	A95-73544
BTN-95-EIX95152582344		p 266	A95-73546
BTN-95-EIX95152582345			A95-73547
	•••••	p 266	
BTN-95-EIX95152582346	•••••	p 266	A95-73548 *
BTN-95-EIX95152582347		p 282	A95-73549
BTN-95-EIX95152583250		p 305	A95-73551
BTN-95-EIX95152583251		p 266	A95-73552 *
BTN-95-EIX95152583252		p 305	A95-73553 *
BTN-95-EIX95152583253			
BTN-95-EIX95152583253	•••••	p 306	A95-73554 *
BTN-95-EIX95152583254		p 306 p 306	A95-73554 * A95-73555 *
BTN-95-EIX95152583254 BTN-95-EIX95152583255		p 306 p 306 p 306	A95-73554 * A95-73555 * A95-73556 *
BTN-95-EIX95152583254 BTN-95-EIX95152583255 BTN-95-EIX95152583256		p 306 p 306 p 306 p 266	A95-73554 * A95-73555 * A95-73556 * A95-73557
BTN-95-EIX95152583254 BTN-95-EIX95152583255 BTN-95-EIX95152583256 BTN-95-EIX95152583257		p 306 p 306 p 306 p 266 p 267	A95-73554 * A95-73555 * A95-73556 * A95-73557 A95-73558
BTN-95-EIX95152583254 BTN-95-EIX95152583255 BTN-95-EIX95152583256 BTN-95-EIX95152583257 BTN-95-EIX95152583258		p 306 p 306 p 306 p 266 p 267 p 297	A95-73554 * A95-73556 * A95-73557 A95-73558 A95-73559
BTN-95-EIX95152583254 BTN-95-EIX95152583255 BTN-95-EIX95152583256 BTN-95-EIX95152583257		p 306 p 306 p 306 p 266 p 267	A95-73554 * A95-73555 * A95-73556 * A95-73557 A95-73558
BTN-95-EIX95152583254 BTN-95-EIX95152583255 BTN-95-EIX95152583256 BTN-95-EIX95152583257 BTN-95-EIX95152583258		p 306 p 306 p 306 p 266 p 267 p 297 p 267	A95-73554 * A95-73555 * A95-73556 * A95-73557 A95-73558 A95-73559 A95-73560
BTN-95-EIX95152583255 BTN-95-EIX95152583255 BTN-95-EIX95152583256 BTN-95-EIX95152583257 BTN-95-EIX95152583259 BTN-95-EIX95152583259 BTN-95-EIX95152583250		p 306 p 306 p 306 p 266 p 267 p 297 p 267 p 267	A95-73554 * A95-73555 * A95-73556 * A95-73557 A95-73558 A95-73559 A95-73560 A95-73561
BTN-95-EIX95152583254 BTN-95-EIX95152583255 BTN-95-EIX95152583256 BTN-95-EIX95152583257 BTN-95-EIX95152583258 BTN-95-EIX95152583258 BTN-95-EIX95152583260 BTN-95-EIX95152583263		p 306 p 306 p 306 p 266 p 267 p 297 p 267 p 267 p 298	A95-73554 * A95-73555 * A95-73556 * A95-73557 A95-73559 A95-73560 A95-73561 A95-73564
BTN-95-EIX95152583254 BTN-95-EIX95152583255 BTN-95-EIX95152583256 BTN-95-EIX95152583257 BTN-95-EIX95152583258 BTN-95-EIX95152583259 BTN-95-EIX95152583260 BTN-95-EIX95152583263		p 306 p 306 p 306 p 266 p 267 p 267 p 267 p 267 p 267 p 298 p 298	A95-73554 * A95-73555 * A95-73556 * A95-73557 A95-73559 A95-73560 A95-73561 A95-73564 A95-73568
BTN-95-EIX95152583254 BTN-95-EIX95152583255 BTN-95-EIX95152583256 BTN-95-EIX95152583257 BTN-95-EIX95152583259 BTN-95-EIX95152583259 BTN-95-EIX95152583260 BTN-95-EIX95152583267 BTN-95-EIX95152583267		p 306 p 306 p 306 p 266 p 267 p 297 p 267 p 267 p 298 p 298 p 278	A95-73554 * A95-73555 * A95-73557 A95-73557 A95-73558 A95-73569 A95-73561 A95-73564 A95-73568 A95-73571
BTN-95-EIX95152583254 BTN-95-EIX95152583255 BTN-95-EIX95152583256 BTN-95-EIX95152583257 BTN-95-EIX95152583259 BTN-95-EIX95152583259 BTN-95-EIX95152583263 BTN-95-EIX95152583263 BTN-95-EIX95152583270 BTN-95-EIX95152583270		p 306 p 306 p 306 p 266 p 267 p 297 p 267 p 298 p 298 p 278 p 298	A95-73554 * A95-73555 * A95-73556 * A95-73557 A95-73558 A95-73560 A95-73561 A95-73564 A95-73571 A95-73577
BTN-95-EIX95152583254 BTN-95-EIX95152583255 BTN-95-EIX95152583256 BTN-95-EIX95152583257 BTN-95-EIX95152583258 BTN-95-EIX95152583259 BTN-95-EIX95152583260 BTN-95-EIX95152583267 BTN-95-EIX95152583267 BTN-95-EIX95152583267 BTN-95-EIX95152583276 BTN-95-EIX95152583276		p 306 p 306 p 306 p 266 p 267 p 297 p 267 p 267 p 298 p 298 p 278	A95-73554 * A95-73555 * A95-73557 A95-73557 A95-73558 A95-73569 A95-73561 A95-73564 A95-73568 A95-73571
BTN-95-EIX95152583254 BTN-95-EIX95152583255 BTN-95-EIX95152583256 BTN-95-EIX95152583257 BTN-95-EIX95152583259 BTN-95-EIX95152583259 BTN-95-EIX95152583263 BTN-95-EIX95152583263 BTN-95-EIX95152583270 BTN-95-EIX95152583270		p 306 p 306 p 306 p 266 p 267 p 297 p 267 p 298 p 298 p 298 p 298 p 298 p 298 p 306	A95-73554 * A95-73555 * A95-73556 * A95-73557 A95-73558 A95-73560 A95-73561 A95-73564 A95-73571 A95-73577
BTN-95-EIX95152583254 BTN-95-EIX95152583255 BTN-95-EIX95152583256 BTN-95-EIX95152583257 BTN-95-EIX95152583258 BTN-95-EIX95152583259 BTN-95-EIX95152583260 BTN-95-EIX95152583267 BTN-95-EIX95152583267 BTN-95-EIX95152583267 BTN-95-EIX95152583276 BTN-95-EIX95152583276		p 306 p 306 p 306 p 266 p 267 p 297 p 267 p 298 p 298 p 278 p 298 p 298	A95-73554 • A95-73555 • A95-73557 • A95-73558 • A95-73550 • A95-73560 • A95-73561 • A95-73564 • A95-73571 • A95-73571 • A95-73583
BTN-95-EIX95152583254 BTN-95-EIX95152583255 BTN-95-EIX95152583256 BTN-95-EIX95152583257 BTN-95-EIX95152583259 BTN-95-EIX95152583259 BTN-95-EIX95152583260 BTN-95-EIX95152583267 BTN-95-EIX95152583267 BTN-95-EIX95152583276 BTN-95-EIX95152583278 BTN-95-EIX95152583288		p 306 p 306 p 306 p 266 p 267 p 297 p 267 p 267 p 298 p 298 p 278 p 298 p 298 p 298 p 298 p 298 p 298 p 298	A95-73554 * A95-73556 * A95-73556 * A95-73556 * A95-73558 * A95-73550 * A95-73561 * A95-73561 * A95-73564 * A95-73567 * A95-73577 * A95-73584 * A95-73584 * A95-73587
BTN-95-EIX95152583254 BTN-95-EIX95152583255 BTN-95-EIX95152583256 BTN-95-EIX95152583257 BTN-95-EIX95152583258 BTN-95-EIX95152583259 BTN-95-EIX95152583260 BTN-95-EIX95152583263 BTN-95-EIX95152583267 BTN-95-EIX95152583270 BTN-95-EIX95152583276 BTN-95-EIX95152583282 BTN-95-EIX95152583286 BTN-95-EIX95152583286		p 306 p 306 p 306 p 266 p 267 p 297 p 267 p 298 p 298 p 298 p 298 p 298 p 298 p 298 p 298 p 297	A95-73554 * A95-73556 * A95-73556 * A95-73557 * A95-73559 * A95-73560 * A95-73560 * A95-73564 * A95-73564 * A95-7357 * A95-73577 * A95-73583 * A95-73587 * A95-73587 * A95-73588 *
BTN-95-EIX95152583254 BTN-95-EIX95152583255 BTN-95-EIX95152583256 BTN-95-EIX95152583257 BTN-95-EIX95152583259 BTN-95-EIX95152583259 BTN-95-EIX95152583260 BTN-95-EIX95152583267 BTN-95-EIX95152583270 BTN-95-EIX95152583270 BTN-95-EIX95152583278 BTN-95-EIX95152583283 BTN-95-EIX95152583283 BTN-95-EIX95152583283 BTN-95-EIX95152583283 BTN-95-EIX95152583286		p 306 p 306 p 306 p 266 p 267 p 297 p 267 p 298 p 298 p 298 p 298 p 306 p 306 p 306 p 282 p 276 p 282	A95-73554 • A95-73556 • A95-73556 • A95-73556 • A95-73559 A95-73560 A95-73561 A95-73561 A95-73561 A95-73571 A95-73583 A95-73583 A95-73588 A95-73588 A95-73589
BTN-95-EIX95152583254 BTN-95-EIX95152583255 BTN-95-EIX95152583256 BTN-95-EIX95152583257 BTN-95-EIX95152583259 BTN-95-EIX95152583260 BTN-95-EIX95152583260 BTN-95-EIX95152583267 BTN-95-EIX95152583267 BTN-95-EIX95152583270 BTN-95-EIX95152583270 BTN-95-EIX95152583286 BTN-95-EIX95152583286 BTN-95-EIX95152583286 BTN-95-EIX95152583286 BTN-95-EIX951525836677 BTN-95-EIX95152584677		p 306 p 306 p 306 p 267 p 297 p 267 p 298 p 298 p 298 p 298 p 298 p 306 p 282 p 282 p 282 p 282	A95-73554 • A95-73556 • A95-73556 • A95-73556 A95-73559 A95-73560 A95-73561 A95-73568 A95-73571 A95-73583 A95-73584 A95-73587 A95-73589 A95-73589 A95-73590
BTN-95-EIX95152583255 BTN-95-EIX95152583255 BTN-95-EIX95152583256 BTN-95-EIX95152583257 BTN-95-EIX95152583259 BTN-95-EIX95152583259 BTN-95-EIX95152583260 BTN-95-EIX95152583263 BTN-95-EIX95152583270 BTN-95-EIX95152583276 BTN-95-EIX95152583276 BTN-95-EIX95152583283 BTN-95-EIX95152583283 BTN-95-EIX95152583283 BTN-95-EIX95152584676 BTN-95-EIX95152584676		p 306 p 306 p 306 p 266 p 267 p 297 p 267 p 298 p 298 p 298 p 298 p 306 p 282 p 276 p 282 p 282 p 282	A95-73554 * A95-73556 * A95-73556 * A95-73556 * A95-73557 * A95-73559 * A95-73560 * A95-73561 * A95-73564 * A95-73564 * A95-7357 * A95-7357 * A95-7357 * A95-73581 * A95-73588 * A95-73588 * A95-73589 * A95-73590 * A95-73590 * A95-73590 * A95-73591
BTN-95-EIX95152583254 BTN-95-EIX95152583255 BTN-95-EIX95152583256 BTN-95-EIX95152583257 BTN-95-EIX95152583259 BTN-95-EIX95152583260 BTN-95-EIX95152583260 BTN-95-EIX95152583267 BTN-95-EIX95152583267 BTN-95-EIX95152583270 BTN-95-EIX95152583270 BTN-95-EIX95152583286 BTN-95-EIX95152583286 BTN-95-EIX95152583286 BTN-95-EIX95152583286 BTN-95-EIX951525836677 BTN-95-EIX95152584677		p 306 p 306 p 306 p 267 p 297 p 267 p 298 p 298 p 298 p 298 p 298 p 306 p 282 p 282 p 282 p 282	A95-73554 • A95-73556 • A95-73556 • A95-73556 A95-73559 A95-73560 A95-73561 A95-73568 A95-73571 A95-73583 A95-73584 A95-73587 A95-73589 A95-73589 A95-73590
BTN-95-EIX95152583255 BTN-95-EIX95152583255 BTN-95-EIX95152583256 BTN-95-EIX95152583257 BTN-95-EIX95152583259 BTN-95-EIX95152583259 BTN-95-EIX95152583260 BTN-95-EIX95152583263 BTN-95-EIX95152583270 BTN-95-EIX95152583276 BTN-95-EIX95152583276 BTN-95-EIX95152583283 BTN-95-EIX95152583283 BTN-95-EIX95152583283 BTN-95-EIX95152584676 BTN-95-EIX95152584676		p 306 p 306 p 366 p 267 p 297 p 267 p 298 p 298 p 298 p 298 p 298 p 306 p 306 p 282 p 276 p 282 p 282 p 282 p 282	A95-73554 • A95-73556 • A95-73556 • A95-73556 • A95-73558 • A95-73560 A95-73560 A95-73564 A95-73564 A95-7357 A95-73583 A95-73584 A95-73588 A95-73589 A95-73599 A95-73591 A95-75720
BTN-95-EIX95152583254 BTN-95-EIX95152583255 BTN-95-EIX95152583256 BTN-95-EIX95152583257 BTN-95-EIX95152583258 BTN-95-EIX95152583260 BTN-95-EIX95152583260 BTN-95-EIX95152583260 BTN-95-EIX95152583260 BTN-95-EIX95152583270 BTN-95-EIX95152583270 BTN-95-EIX95152583270 BTN-95-EIX95152583282 BTN-95-EIX95152583283 BTN-95-EIX95152583283 BTN-95-EIX95152583283 BTN-95-EIX95152584678		p 306 p 306 p 366 p 267 p 297 p 267 p 298 p 298 p 298 p 298 p 382 p 362 p 276 p 282 p 282 p 282 p 287 p 287	A95-73554 * A95-73556 * A95-73556 * A95-73556 * A95-73558 * A95-73559 * A95-73560 * A95-73561 * A95-73561 * A95-73561 * A95-73561 * A95-73571 * A95-73583 * A95-73584 * A95-73589 * A95-73589 * A95-73589 * A95-73590 * A95-73590 * A95-75718
BTN-95-EIX95152583255 BTN-95-EIX95152583255 BTN-95-EIX95152583256 BTN-95-EIX95152583257 BTN-95-EIX95152583259 BTN-95-EIX95152583259 BTN-95-EIX95152583260 BTN-95-EIX95152583263 BTN-95-EIX95152583267 BTN-95-EIX95152583276 BTN-95-EIX95152583278 BTN-95-EIX95172595292		p 306 p 306 p 306 p 266 p 267 p 297 p 267 p 298 p 298 p 298 p 298 p 298 p 282 p 283	A95-73554 * A95-73556 * A95-73556 * A95-73556 * A95-73557 * A95-73559 * A95-73560 * A95-73560 * A95-73561 * A95-7357 * A95-7357 * A95-7357 * A95-73581 * A95-73582 * A95-73583 * A95-73589 * A95-73589 * A95-73589 * A95-73580 * A95-757590 * A95-75718 * A95-75718 * A95-75718 * A95-75718 *
BTN-95-EIX95152583254 BTN-95-EIX95152583255 BTN-95-EIX95152583256 BTN-95-EIX95152583257 BTN-95-EIX95152583257 BTN-95-EIX95152583259 BTN-95-EIX95152583259 BTN-95-EIX95152583260 BTN-95-EIX95152583267 BTN-95-EIX95152583270 BTN-95-EIX95152583270 BTN-95-EIX95152583283 BTN-95-EIX95152583283 BTN-95-EIX95152583283 BTN-95-EIX95152583283 BTN-95-EIX95152584677 BTN-95-EIX95152584679 BTN-95-EIX95152584679 BTN-95-EIX95152584679 BTN-95-EIX95172595294 BTN-95-EIX95172595292		p 306 p 306 p 306 p 266 p 267 p 297 p 267 p 298 p 298 p 298 p 298 p 298 p 308 p 276 p 282 p 282 p 282 p 282 p 287 p 287 p 287 p 287 p 287	A95-73554 * A95-73556 * A95-73556 * A95-73556 * A95-73550 * A95-73580 * A95-73560 * A95-73564 * A95-73564 * A95-7357 * A95-73583 * A95-73583 * A95-73584 * A95-73587 * A95-73589 * A95-73589 * A95-73590 * A95-73591 * A95-75716 * A95-75716
BTN-95-EIX95152583254 BTN-95-EIX95152583255 BTN-95-EIX95152583256 BTN-95-EIX95152583257 BTN-95-EIX95152583258 BTN-95-EIX95152583260 BTN-95-EIX95152583260 BTN-95-EIX95152583260 BTN-95-EIX95152583260 BTN-95-EIX95152583270 BTN-95-EIX95152583270 BTN-95-EIX95152583270 BTN-95-EIX95152583282 BTN-95-EIX95152583283 BTN-95-EIX95152583283 BTN-95-EIX95152584678 BTN-95-EIX95152584678 BTN-95-EIX95152584678 BTN-95-EIX95172595292 BTN-95-EIX95172595292 BTN-95-EIX95172595292		p 306 p 306 p 306 p 266 p 267 p 297 p 267 p 298 p 298 p 298 p 298 p 298 p 298 p 298 p 298 p 276 p 282 p 282 p 282 p 287 p 287	A95-73554 * A95-73556 * A95-73556 * A95-73556 * A95-73559 * A95-73560 * A95-73561 * A95-73561 * A95-73561 * A95-73561 * A95-73571 * A95-73571 * A95-73583 * A95-73584 * A95-73588 * A95-73589 * A95-73589 * A95-73590 * A95-73591 * A95-75716 * A95-75716 * A95-75716 * A95-75716 * A95-75716 * A95-75714 *
BTN-95-EIX95152583254 BTN-95-EIX95152583255 BTN-95-EIX95152583256 BTN-95-EIX95152583256 BTN-95-EIX95152583259 BTN-95-EIX95152583259 BTN-95-EIX95152583260 BTN-95-EIX95152583267 BTN-95-EIX95152583267 BTN-95-EIX95152583276 BTN-95-EIX95152583276 BTN-95-EIX95152583288 BTN-95-EIX95152583288 BTN-95-EIX95152584677 BTN-95-EIX95152584678 BTN-95-EIX95152584678 BTN-95-EIX95152584679 BTN-95-EIX95152584679 BTN-95-EIX95152584679 BTN-95-EIX95152584678 BTN-95-EIX95152584678 BTN-95-EIX95152584678 BTN-95-EIX95172595294 BTN-95-EIX95172595294 BTN-95-EIX95172595294 BTN-95-EIX95172595295 BTN-95-EIX95172595296 BTN-95-EIX95172595298 BTN-95-EIX95172595298		p 306 p 306 p 266 p 267 p 267 p 267 p 298 p 298 p 298 p 298 p 298 p 282 p 282 p 282 p 282 p 282 p 287 p 287 p 287 p 287 p 287 p 287 p 287	A95-73554 * A95-73556 * A95-73556 * A95-73557 * A95-73559 * A95-73560 * A95-73560 * A95-73561 * A95-73561 * A95-7357 * A95-7357 * A95-7357 * A95-73581 * A95-73582 * A95-73589 * A95-73589 * A95-73580 * A95-73580 * A95-73580 * A95-75750 * A95-75710 * A95-75710 * A95-75711 * A95-75714 * A95-75712 *
BTN-95-EIX95152583254 BTN-95-EIX95152583255 BTN-95-EIX95152583256 BTN-95-EIX95152583257 BTN-95-EIX95152583258 BTN-95-EIX95152583260 BTN-95-EIX95152583260 BTN-95-EIX95152583260 BTN-95-EIX95152583260 BTN-95-EIX95152583270 BTN-95-EIX95152583270 BTN-95-EIX95152583270 BTN-95-EIX95152583282 BTN-95-EIX95152583283 BTN-95-EIX95152583283 BTN-95-EIX95152584678 BTN-95-EIX95152584678 BTN-95-EIX95152584678 BTN-95-EIX95172595292 BTN-95-EIX95172595292 BTN-95-EIX95172595292		p 306 p 306 p 266 p 267 p 297 p 267 p 298 p 278 p 298 p 298 p 298 p 298 p 282 p 282 p 282 p 287 p 287	A95-73554 * A95-73556 * A95-73556 * A95-73556 * A95-73559 * A95-73560 * A95-73561 * A95-73561 * A95-73561 * A95-73561 * A95-73571 * A95-73571 * A95-73583 * A95-73584 * A95-73588 * A95-73589 * A95-73589 * A95-73590 * A95-73591 * A95-75716 * A95-75716 * A95-75716 * A95-75716 * A95-75716 * A95-75714 *
BTN-95-EIX95152583254 BTN-95-EIX95152583255 BTN-95-EIX95152583256 BTN-95-EIX95152583256 BTN-95-EIX95152583259 BTN-95-EIX95152583259 BTN-95-EIX95152583260 BTN-95-EIX95152583267 BTN-95-EIX95152583267 BTN-95-EIX95152583276 BTN-95-EIX95152583276 BTN-95-EIX95152583288 BTN-95-EIX95152583288 BTN-95-EIX95152584677 BTN-95-EIX95152584678 BTN-95-EIX95152584678 BTN-95-EIX95152584679 BTN-95-EIX95152584679 BTN-95-EIX95152584679 BTN-95-EIX95152584678 BTN-95-EIX95152584678 BTN-95-EIX95152584678 BTN-95-EIX95172595294 BTN-95-EIX95172595294 BTN-95-EIX95172595294 BTN-95-EIX95172595295 BTN-95-EIX95172595296 BTN-95-EIX95172595298 BTN-95-EIX95172595298		p 306 p 306 p 266 p 267 p 267 p 267 p 298 p 298 p 298 p 298 p 298 p 282 p 282 p 282 p 282 p 282 p 287 p 287 p 287 p 287 p 287 p 287 p 287	A95-73554 * A95-73556 * A95-73556 * A95-73557 * A95-73559 * A95-73560 * A95-73560 * A95-73561 * A95-73561 * A95-7357 * A95-7357 * A95-7357 * A95-73581 * A95-73582 * A95-73589 * A95-73589 * A95-73580 * A95-73580 * A95-73580 * A95-75750 * A95-75710 * A95-75710 * A95-75711 * A95-75714 * A95-75712 *
BTN-95-EIX95152583254 BTN-95-EIX95152583256 BTN-95-EIX95152583257 BTN-95-EIX95152583257 BTN-95-EIX95152583257 BTN-95-EIX95152583260 BTN-95-EIX95152583260 BTN-95-EIX95152583260 BTN-95-EIX95152583270 BTN-95-EIX95152583270 BTN-95-EIX95152583270 BTN-95-EIX95152583270 BTN-95-EIX95152583280 BTN-95-EIX95152583280 BTN-95-EIX95152583286 BTN-95-EIX95152584678 BTN-95-EIX95152584678 BTN-95-EIX95172595294 BTN-95-EIX95172595294 BTN-95-EIX95172595294 BTN-95-EIX95172595294 BTN-95-EIX95172595298 BTN-95-EIX95182617458		P 306 P 306 P 266 P 267 P 267 P 267 P 298 P 298 P 298 P 306 P 282 P 282	A95-73554 * A95-73556 * A95-73556 * A95-73556 * A95-73559 A95-73560 A95-73560 A95-73564 A95-73564 A95-73577 A95-73587 A95-73588 A95-73588 A95-73589 A95-73591 A95-75718 A95-75718 A95-75718 A95-75716 A95-75715 A95-75725 A95-75725 A95-75725
BTN-95-EIX95152583254 BTN-95-EIX95152583255 BTN-95-EIX95152583256 BTN-95-EIX95152583256 BTN-95-EIX95152583256 BTN-95-EIX95152583260 BTN-95-EIX95152583260 BTN-95-EIX95152583260 BTN-95-EIX95152583267 BTN-95-EIX95152583270 BTN-95-EIX95152583276 BTN-95-EIX95152583286 BTN-95-EIX95152583286 BTN-95-EIX95152583286 BTN-95-EIX95152584677 BTN-95-EIX95152584678 BTN-95-EIX95152584678 BTN-95-EIX95152584678 BTN-95-EIX95152584678 BTN-95-EIX9515259292 BTN-95-EIX95172595294 BTN-95-EIX95172595294 BTN-95-EIX95172595296 BTN-95-EIX95172595296 BTN-95-EIX95172595296 BTN-95-EIX95172595296 BTN-95-EIX95172595296 BTN-95-EIX95172595298 BTN-95-EIX95172595298 BTN-95-EIX95172595298 BTN-95-EIX95172595298 BTN-95-EIX95182617454 BTN-95-EIX95182617454 BTN-95-EIX95182617456		P 306 P 306 P 266 P 267 P 267 P 267 P 267 P 268 P 298 P 298 P 298 P 298 P 298 P 282 P 282 P 282 P 282 P 282 P 287 P 288 P 288	A95-73554 * A95-73556 * A95-73556 * A95-73557 A95-73559 A95-73560 A95-73560 A95-73561 A95-73564 A95-7357 A95-7357 A95-7357 A95-73581 A95-73587 A95-73589 A95-73589 A95-73590 A95-75716 A95-75716 A95-75716 A95-75716 A95-75716 A95-75716 A95-75729 * A95-75729 * A95-75729 *
BTN-95-EIX95152583254 BTN-95-EIX95152583255 BTN-95-EIX95152583255 BTN-95-EIX95152583257 BTN-95-EIX95152583257 BTN-95-EIX95152583259 BTN-95-EIX95152583260 BTN-95-EIX95152583260 BTN-95-EIX95152583270 BTN-95-EIX95152583270 BTN-95-EIX95152583270 BTN-95-EIX95152583270 BTN-95-EIX95152583270 BTN-95-EIX95152583283 BTN-95-EIX95152583283 BTN-95-EIX95152583283 BTN-95-EIX95152584677 BTN-95-EIX95152584679 BTN-95-EIX95152584679 BTN-95-EIX95152584679 BTN-95-EIX95152584679 BTN-95-EIX95152584679 BTN-95-EIX95172595296 BTN-95-EIX95172595296 BTN-95-EIX95172595296 BTN-95-EIX95172595296 BTN-95-EIX95172595296 BTN-95-EIX95172595296 BTN-95-EIX95172595296 BTN-95-EIX95182617457 BTN-95-EIX95182617457 BTN-95-EIX95182617466		P 306 P 306 P 266 P 267 P 267 P 267 P 267 P 268 P 298 P 298 P 282 P 283 P 284 P 286 P 286 P 286 P 286 P 268 P 268 P 268 P 268	A95-73554 * A95-73556 * A95-73556 * A95-73556 * A95-73559 A95-73560 A95-73560 A95-73564 A95-73564 A95-73577 A95-73587 A95-73587 A95-73588 A95-73588 A95-73589 A95-73590 A95-75718 A95-75718 A95-75718 A95-75718 A95-75728 A95-75728 A95-75728 A95-75731 A95-75731 A95-75731 A95-75731
BTN-95-EIX95152583254 BTN-95-EIX95152583255 BTN-95-EIX95152583256 BTN-95-EIX95152583257 BTN-95-EIX95152583257 BTN-95-EIX95152583260 BTN-95-EIX95152583260 BTN-95-EIX95152583260 BTN-95-EIX95152583270 BTN-95-EIX95152583270 BTN-95-EIX95152583270 BTN-95-EIX95152583283 BTN-95-EIX95152583283 BTN-95-EIX95152583286 BTN-95-EIX95152583286 BTN-95-EIX95152584678 BTN-95-EIX95152584678 BTN-95-EIX95152584679 BTN-95-EIX95152647458 BTN-95-EIX95182617458		P 306 P 306 P 266 P 267 P 267 P 267 P 268 P 298 P 298 P 306 P 282 P 282 P 282 P 282 P 282 P 282 P 282 P 282 P 287 P 288 P 288	A95-73554 • A95-73556 • A95-73556 • A95-73556 • A95-73557 A95-73560 A95-73560 A95-73561 A95-73561 A95-73571 A95-73581 A95-73581 A95-73581 A95-73581 A95-73581 A95-73591 A95-75716 A95-75716 A95-75716 A95-75725 A95-75725 A95-75723 A95-75723 A95-75723 A95-75723 A95-75734
BTN-95-EIX95152583255 BTN-95-EIX95152583256 BTN-95-EIX95152583256 BTN-95-EIX95152583256 BTN-95-EIX95152583256 BTN-95-EIX95152583260 BTN-95-EIX95152583260 BTN-95-EIX95152583260 BTN-95-EIX95152583267 BTN-95-EIX95152583267 BTN-95-EIX95152583270 BTN-95-EIX95152583270 BTN-95-EIX95152583288 BTN-95-EIX95152583288 BTN-95-EIX95152583288 BTN-95-EIX95152584677 BTN-95-EIX95152584678 BTN-95-EIX95172595292 BTN-95-EIX95172595294 BTN-95-EIX95172595294 BTN-95-EIX95172595298 BTN-95-EIX95182617463 BTN-95-EIX95182617463		P 306 P 306 P 266 P 267 P 267 P 267 P 267 P 268 P 298 P 298 P 306 P 282 P 276 P 282 P 282 P 282 P 287 P 288 P 288	A95-73554 * A95-73556 * A95-73556 * A95-73557 A95-73559 A95-73560 A95-73560 A95-73561 A95-73564 A95-73564 A95-73568 A95-73577 A95-73581 A95-73587 A95-73589 A95-73589 A95-73590 A95-75716 A95-75716 A95-75716 A95-75716 A95-75729 * A95-75729 A95-75729 A95-75721 A95-75729 A95-75721 A95-75723 A95-75723 A95-75731 A95-75734 A95-75734 A95-75735
BTN-95-EIX95152583255 BTN-95-EIX95152583255 BTN-95-EIX95152583255 BTN-95-EIX95152583257 BTN-95-EIX95152583257 BTN-95-EIX95152583259 BTN-95-EIX95152583260 BTN-95-EIX95152583260 BTN-95-EIX95152583260 BTN-95-EIX95152583270 BTN-95-EIX95152583270 BTN-95-EIX95152583270 BTN-95-EIX95152583270 BTN-95-EIX95152583283 BTN-95-EIX95152583283 BTN-95-EIX95152584676 BTN-95-EIX95152584677 BTN-95-EIX95152584679 BTN-95-EIX95152584679 BTN-95-EIX95152584679 BTN-95-EIX95152584679 BTN-95-EIX95152584679 BTN-95-EIX95172595296 BTN-95-EIX95172595296 BTN-95-EIX95172595296 BTN-95-EIX95172595296 BTN-95-EIX95172595296 BTN-95-EIX95182617454 BTN-95-EIX95182617464 BTN-95-EIX95182617464 BTN-95-EIX95182617464 BTN-95-EIX95182617464		P 306 P 306 P 266 P 267 P 267 P 267 P 267 P 268 P 298 P 298 P 306 P 282 P 282 P 282 P 282 P 282 P 282 P 287 P 288 P 288	A95-73554 * A95-73556 * A95-73556 * A95-73556 * A95-73557 * A95-73559 * A95-73560 * A95-73564 * A95-73564 * A95-73564 * A95-7357 * A95-73581 * A95-73583 * A95-73584 * A95-73589 * A95-73589 * A95-73590 * A95-75716 * A95-75716 * A95-75718 * A95-75731 * A95-75731 * A95-75731 * A95-75733 * A95-75735 * A95-75735 * A95-75735 * A95-75736 *
BTN-95-EIX95152583254 BTN-95-EIX95152583255 BTN-95-EIX95152583256 BTN-95-EIX95152583257 BTN-95-EIX95152583257 BTN-95-EIX95152583260 BTN-95-EIX95152583260 BTN-95-EIX95152583260 BTN-95-EIX95152583270 BTN-95-EIX95152583270 BTN-95-EIX95152583270 BTN-95-EIX95152583283 BTN-95-EIX95152583283 BTN-95-EIX95152583283 BTN-95-EIX95152583283 BTN-95-EIX95152584678 BTN-95-EIX95152584678 BTN-95-EIX95152584679 BTN-95-EIX95152617463 BTN-95-EIX95182617463 BTN-95-EIX95182617463 BTN-95-EIX95182617463 BTN-95-EIX95182617463		P 306 P 306 P 266 P 267 P 267 P 267 P 267 P 268 P 298 P 298 P 306 P 282 P 276 P 282 P 282 P 282 P 287 P 288 P 288	A95-73554 • A95-73556 • A95-73556 • A95-73556 • A95-73557 A95-73560 A95-73560 A95-73561 A95-73561 A95-73561 A95-73561 A95-73561 A95-73561 A95-73581 A95-73581 A95-73581 A95-75716 A95-75716 A95-75716 A95-75716 A95-75725 A95-75733 A95-75734 A95-75734 A95-75734 A95-75734 A95-75736 A95-75736 A95-75736 A95-75736 A95-75736 A95-75736 A95-75736 A95-75736
BTN-95-EIX95152583255 BTN-95-EIX95152583255 BTN-95-EIX95152583255 BTN-95-EIX95152583257 BTN-95-EIX95152583257 BTN-95-EIX95152583259 BTN-95-EIX95152583260 BTN-95-EIX95152583260 BTN-95-EIX95152583260 BTN-95-EIX95152583270 BTN-95-EIX95152583270 BTN-95-EIX95152583270 BTN-95-EIX95152583270 BTN-95-EIX95152583283 BTN-95-EIX95152583283 BTN-95-EIX95152584676 BTN-95-EIX95152584677 BTN-95-EIX95152584679 BTN-95-EIX95152584679 BTN-95-EIX95152584679 BTN-95-EIX95152584679 BTN-95-EIX95152584679 BTN-95-EIX95172595296 BTN-95-EIX95172595296 BTN-95-EIX95172595296 BTN-95-EIX95172595296 BTN-95-EIX95172595296 BTN-95-EIX95182617454 BTN-95-EIX95182617464 BTN-95-EIX95182617464 BTN-95-EIX95182617464 BTN-95-EIX95182617464		P 306 P 306 P 266 P 267 P 267 P 267 P 267 P 268 P 298 P 298 P 306 P 282 P 283 P 284 P 286 P 286 P 268 P 268	A95-73554 * A95-73556 * A95-73556 * A95-73556 * A95-73557 * A95-73559 * A95-73560 * A95-73564 * A95-73564 * A95-73564 * A95-7357 * A95-73581 * A95-73583 * A95-73584 * A95-73589 * A95-73589 * A95-73590 * A95-75716 * A95-75716 * A95-75718 * A95-75731 * A95-75731 * A95-75731 * A95-75733 * A95-75735 * A95-75735 * A95-75735 * A95-75736 *
BTN-95-EIX95152583255 BTN-95-EIX95152583256 BTN-95-EIX95152583256 BTN-95-EIX95152583256 BTN-95-EIX95152583256 BTN-95-EIX95152583260 BTN-95-EIX95152583260 BTN-95-EIX95152583260 BTN-95-EIX95152583260 BTN-95-EIX95152583267 BTN-95-EIX95152583270 BTN-95-EIX95152583276 BTN-95-EIX95152583286 BTN-95-EIX95152583288 BTN-95-EIX95152583288 BTN-95-EIX95152584677 BTN-95-EIX95152584678 BTN-95-EIX95152584678 BTN-95-EIX95152584678 BTN-95-EIX95172595298 BTN-95-EIX95172595299 BTN-95-EIX95172595298 BTN-95-EIX95172595298 BTN-95-EIX95172595298 BTN-95-EIX95172595298 BTN-95-EIX95182617458 BTN-95-EIX95182617458 BTN-95-EIX95182617464 BTN-95-EIX95182617464 BTN-95-EIX95182617464 BTN-95-EIX95182617464 BTN-95-EIX95182617464 BTN-95-EIX95182617464 BTN-95-EIX95182617464 BTN-95-EIX95182617464 BTN-95-EIX95182617467		P 306 P 306 P 266 P 267 P 267 P 267 P 267 P 298 P 298 P 298 P 306 P 282 P 276 P 282 P 282 P 282 P 287 P 288 P 288	A95-73554 * A95-73556 * A95-73556 * A95-73557 A95-73559 A95-73560 A95-73560 A95-73561 A95-73564 A95-73564 A95-73568 A95-73577 A95-73581 A95-73587 A95-73589 A95-73589 A95-73589 A95-73590 A95-75716 A95-75716 A95-75716 A95-75716 A95-75729 A95-75729 A95-75729 A95-75734 A95-75734 A95-75734 A95-75735 A95-75735 A95-75735 A95-75735 A95-75735 A95-75735 A95-75735 A95-75735
BTN-95-EIX95152583255 BTN-95-EIX95152583255 BTN-95-EIX95152583255 BTN-95-EIX95152583257 BTN-95-EIX95152583257 BTN-95-EIX95152583259 BTN-95-EIX95152583260 BTN-95-EIX95152583260 BTN-95-EIX95152583270 BTN-95-EIX95152583270 BTN-95-EIX95152583270 BTN-95-EIX95152583270 BTN-95-EIX95152583270 BTN-95-EIX95152583283 BTN-95-EIX95152584676 BTN-95-EIX95152584676 BTN-95-EIX95152584679 BTN-95-EIX95152584679 BTN-95-EIX95152584679 BTN-95-EIX95152584679 BTN-95-EIX95152584679 BTN-95-EIX95152584679 BTN-95-EIX95172595294 BTN-95-EIX95172595295 BTN-95-EIX95172595296 BTN-95-EIX95172595296 BTN-95-EIX95172595296 BTN-95-EIX95182617457 BTN-95-EIX95182617464 BTN-95-EIX95182617464 BTN-95-EIX95182617466 BTN-95-EIX95182617466 BTN-95-EIX95182617466 BTN-95-EIX95182617808 BTN-95-EIX95182617808		P 306 P 306 P 266 P 267 P 297 P 297 P 298 P 298 P 306 P 298 P 306 P 282 P 283 P 284 P 284 P 285 P 286 P 286	A95-73554 * A95-73556 * A95-73556 * A95-73556 * A95-73557 * A95-73559 * A95-73560 * A95-73560 * A95-73564 * A95-73564 * A95-7357 * A95-73581 * A95-73583 * A95-73584 * A95-73589 * A95-73589 * A95-73589 * A95-73590 * A95-75716 * A95-75716 * A95-75718 * A95-75729 * A95-75731 * A95-75731 * A95-75731 * A95-75731 * A95-75731 * A95-75731 * A95-75735 * A95-75735 * A95-75736 * A95-75736 * A95-75736 * A95-75753 * A95-75753 * A95-75753 * A95-75754 * A95-75753 * A95-75754 * A95-75755 * A95-75754 * A95-757
BTN-95-EIX95152583254 BTN-95-EIX95152583255 BTN-95-EIX95152583255 BTN-95-EIX95152583257 BTN-95-EIX95152583257 BTN-95-EIX95152583260 BTN-95-EIX95152583260 BTN-95-EIX95152583260 BTN-95-EIX95152583270 BTN-95-EIX95152583270 BTN-95-EIX95152583270 BTN-95-EIX95152583270 BTN-95-EIX95152583283 BTN-95-EIX95152583283 BTN-95-EIX95152583283 BTN-95-EIX95152584676 BTN-95-EIX95152584677 BTN-95-EIX95152584677 BTN-95-EIX95152584678 BTN-95-EIX95152584678 BTN-95-EIX95152584678 BTN-95-EIX95172595294 BTN-95-EIX95172595296 BTN-95-EIX95182617463 BTN-95-EIX95182617463 BTN-95-EIX95182617463 BTN-95-EIX95182617463 BTN-95-EIX95182617807 BTN-95-EIX95182617807 BTN-95-EIX95182617808 BTN-95-EIX95182617808 BTN-95-EIX95182617808		P 306 P 306 P 266 P 267 P 267 P 267 P 268	A95-73554 • A95-73556 • A95-73556 • A95-73556 • A95-73557 A95-73560 A95-73560 A95-73561 A95-73561 A95-73561 A95-73561 A95-73581 A95-73581 A95-73581 A95-73581 A95-73581 A95-73571 A95-75716 A95-75716 A95-75718 A95-75731 A95-75731 A95-75731 A95-75731 A95-75731 A95-75731 A95-75733 A95-75734 A95-75734 A95-75735 A95-75735 A95-75735 A95-75735 A95-75736 A95-75735 A95-75755 A95-75755
BTN-95-EIX95152583254 BTN-95-EIX95152583255 BTN-95-EIX95152583255 BTN-95-EIX95152583257 BTN-95-EIX95152583256 BTN-95-EIX95152583260 BTN-95-EIX95152583260 BTN-95-EIX95152583260 BTN-95-EIX95152583267 BTN-95-EIX95152583270 BTN-95-EIX95152583270 BTN-95-EIX95152583270 BTN-95-EIX95152583280 BTN-95-EIX95152583280 BTN-95-EIX95152583280 BTN-95-EIX95152584678 BTN-95-EIX95152584677 BTN-95-EIX95152584678 BTN-95-EIX95152584679 BTN-95-EIX95172595294 BTN-95-EIX95172595292 BTN-95-EIX95172595298 BTN-95-EIX95172595298 BTN-95-EIX95172595298 BTN-95-EIX95172595298 BTN-95-EIX95172595298 BTN-95-EIX95182617464 BTN-95-EIX95182617464 BTN-95-EIX95182617463 BTN-95-EIX95182617463 BTN-95-EIX95182617463 BTN-95-EIX95182617463 BTN-95-EIX95182617463 BTN-95-EIX95182617460 BTN-95-EIX95182617460 BTN-95-EIX95182617800		P 306 P 306 P 266 P 267 P 297 P 298 P 298 P 298 P 298 P 298 P 306 P 282 P 282 P 282 P 282 P 282 P 282 P 283 P 284 P 284 P 287 P 287 P 287 P 287 P 287 P 287 P 288 P 268 P 268	A95-73554 * A95-73556 * A95-73556 * A95-73557 A95-73559 A95-73559 A95-73560 A95-73561 A95-73564 A95-73564 A95-73568 A95-73577 A95-73583 A95-73587 A95-73589 A95-73589 A95-73590 A95-75716 A95-75716 A95-75716 A95-75716 A95-75729 * A95-75729 A95-75734 A95-75734 A95-75734 A95-75734 A95-75735 A95-75735 A95-75735 A95-75755
BTN-95-EIX95152583255 BTN-95-EIX95152583255 BTN-95-EIX95152583255 BTN-95-EIX95152583257 BTN-95-EIX95152583257 BTN-95-EIX95152583257 BTN-95-EIX95152583259 BTN-95-EIX95152583260 BTN-95-EIX95152583260 BTN-95-EIX95152583270 BTN-95-EIX95152583270 BTN-95-EIX95152583270 BTN-95-EIX95152583270 BTN-95-EIX95152583283 BTN-95-EIX95152583283 BTN-95-EIX95152584676 BTN-95-EIX95152584677 BTN-95-EIX95152584679 BTN-95-EIX95152584679 BTN-95-EIX95152584679 BTN-95-EIX95152584679 BTN-95-EIX95152584679 BTN-95-EIX95172595294 BTN-95-EIX95172595295 BTN-95-EIX95172595296 BTN-95-EIX95172595296 BTN-95-EIX95172595296 BTN-95-EIX95182617457 BTN-95-EIX95182617464 BTN-95-EIX95182617464 BTN-95-EIX95182617466 BTN-95-EIX95182617468 BTN-95-EIX95182617808 BTN-95-EIX95182617808 BTN-95-EIX95182617808 BTN-95-EIX95182617808 BTN-95-EIX95182617818		P 306 P 306 P 266 P 267 P 267 P 267 P 267 P 267 P 268 P 298 P 306 P 282 P 282 P 282 P 287 P 287 P 267 P 268 P 288 P 268 P 298 P 268	A95-73554 • A95-73556 • A95-73556 • A95-73556 • A95-73550 A95-73560 A95-73560 A95-73561 A95-73561 A95-73561 A95-73581 A95-73581 A95-73581 A95-73581 A95-73581 A95-73581 A95-75718 A95-75718 A95-75718 A95-75735 A95-75735 A95-75735 A95-75735 A95-75735 A95-75735 A95-75735 A95-75754 A95-75755 A95-75755 A95-75756 A95-75756 A95-757575
BTN-95-EIX95152583254 BTN-95-EIX95152583255 BTN-95-EIX95152583255 BTN-95-EIX95152583257 BTN-95-EIX95152583256 BTN-95-EIX95152583260 BTN-95-EIX95152583260 BTN-95-EIX95152583260 BTN-95-EIX95152583267 BTN-95-EIX95152583270 BTN-95-EIX95152583270 BTN-95-EIX95152583270 BTN-95-EIX95152583280 BTN-95-EIX95152583280 BTN-95-EIX95152583280 BTN-95-EIX95152584678 BTN-95-EIX95152584677 BTN-95-EIX95152584678 BTN-95-EIX95152584679 BTN-95-EIX95172595294 BTN-95-EIX95172595292 BTN-95-EIX95172595298 BTN-95-EIX95172595298 BTN-95-EIX95172595298 BTN-95-EIX95172595298 BTN-95-EIX95172595298 BTN-95-EIX95182617464 BTN-95-EIX95182617464 BTN-95-EIX95182617463 BTN-95-EIX95182617463 BTN-95-EIX95182617463 BTN-95-EIX95182617463 BTN-95-EIX95182617463 BTN-95-EIX95182617460 BTN-95-EIX95182617460 BTN-95-EIX95182617800		P 306 P 306 P 306 P 266 P 267 P 267 P 267 P 267 P 278 P 298 P 306 P 282 P 282 P 282 P 282 P 287 P 267 P 268	A95-73554 * A95-73556 * A95-73556 * A95-73557 A95-73559 A95-73559 A95-73560 A95-73561 A95-73564 A95-73564 A95-73568 A95-73577 A95-73583 A95-73587 A95-73589 A95-73589 A95-73590 A95-75716 A95-75716 A95-75716 A95-75716 A95-75729 * A95-75729 A95-75734 A95-75734 A95-75734 A95-75734 A95-75735 A95-75735 A95-75735 A95-75755

BTN-95-EIX95182619075		р 307	A95-75760
BTN-95-EIX95182619076		p 269	A95-75761
BTN-95-EIX95182619077		p 307	A95-75762
BTN-95-EIX95182619078	•••••	p 269 p 269	A95-75763 A95-75765
BTN-95-EIX95182619080 BTN-95-EIX95182619087		p 291	A95-75772
BTN-95-EIX95182619088		p 283	A95-75773
BTN-95-EIX95182619093		p 269	A95-75778
BTN-95-EIX95182619097		p 283	A95-76582
BTN-95-EIX95182619099 BTN-95-EIX95182619100		p 295 p 307	A95-76584 A95-76585
BTN-95-EIX95182619101		p 308	A95-76586
BTN-95-EIX95182619103		p 321	A95-76588
BTN-95-EIX95182619104		p 269	A95-76589
BTN-95-EIX95182619105 BTN-95-EIX95182619115		p 269 p 321	A95-76590 A95-76592
BTN-95-EIX95182619121		p 321	A95-76598
BTN-95-EIX95182619125		p 322	A95-76602
BTN-95-EIX95182619126		p 291	A95-76603
BTN-95-EIX95182619127 BTN-95-EIX95182619128		p 276 p 269	A95-76604 A95-76605
BTN-95-EIX95182619129		p 291	A95-76606
BTN-95-EIX95182619130		p 291	A95-76607
BTN-95-EIX95182619131		p 291	A95-76608
BTN-95-EIX95182619132 BTN-95-EIX95182619138	••••	p 292 p 269	A95-76609 A95-76615
BTN-95-EIX95182619139		p 288	A95-76616
BTN-95-EIX95182619144		p 299	A95-76621
BTN-95-EIX95182619145		p 279	A95-76622
BTN-95-EIX95182619149		p 322	A95-76626
BTN-95-EIX95182619153 BTN-95-EIX95182619154		p 292 p 279	A95-76630 A95-76631
BTN-95-EIX95182619209		p 283	A95-76635
BTN-95-EIX95182619210		p 270	A95-76636
BTN-95-EIX95182619211	•	p 295	A95-76637
BTN-95-EIX95182619212 BTN-95-EIX95182619213		p 322 p 296	A95-76638 1 A95-76639 1
BTN-95-EIX95182619214		p 292	A95-76640
BTN-95-EIX95182619215		p 292	A95-76641
BTN-95-EIX95182619216		p 292	A95-76642
BTN-95-EIX95182619217 BTN-95-EIX95182619218		p 270 p 284	A95-76643 *
BTN-95-EIX95182619219		p 276	A95-76645
BTN-95-EIX95182619220		p 270	A95-76646
BTN-95-EIX95182619221		p 308	A95-76647
BTN-95-EIX95182619222 BTN-95-EIX95182619223		p 288 p 289	A95-76648 A95-76649
BTN-95-EIX95182619224		p 289	A95-76650
BTN-95-EIX95182619225		p 270	A95-76651
BTN-95-EIX95182619226 BTN-95-EIX95182619227		p 308 p 270	A95-76652 A95-76653
BTN-95-EIX95182619228		p 284	A95-76654
BTN-95-EIX95182619229		p 284	A95-76655
BTN-95-EIX95182619230	••••	p 271	A95-76656
BTN-95-EIX95182619231 BTN-95-EIX95182619232		p 319 p 308	A95-76657 A95-76658
BTN-95-EIX95182619233		p 271	A95-76659
BTN-95-EIX95182619234		p 308	A95-76660
BTN-95-EIX95182619235		p 271	A95-76661
BTN-95-EIX95202637592 BTN-95-EIX95202637603		p 279 p 308	A95-76697 A95-76686
BTN-95-EIX95202637606		p 279	A95-76683
BTN-95-EIX95202637608		p 292	A95-76681
BTN-95-EIX95202637613			A95-76676
BTN-95-EIX95202638962 BTN-95-EIX95202638963		p 2/9	A95-76674 A95-76673
BTN-95-EIX95212641069			A95-76734
BTN-95-EIX95212641070	•••••	p 287	A95-76735
BTN-95-EIX95212641071			A95-76736
BTN-95-EIX95212641072 BTN-95-EIX95212645688		פוניק 271 ם	A95-76737 A95-76740
BTN-95-EIX95212645690			A95-76742
BTN-95-EIX95212645692		p 271	A95-76744
BTN-95-EIX95212645694			A95-76746
BTN-95-EIX95212645695 BTN-95-EIX95212645706		p 2/2	A95-76747 A95-76758
BTN-95-EIX95212645707			A95-76759
BTN-95-EIX95212645712		p 272	A95-76764
BTN-95-EIX95212645713		p 261	A95-76765
CCMS-95-01		p 301	N95-23179

CONF-9404162-14 ...... p 297 N95-24019 #

# CONF-940440-5

CONF-940440-5						REPOR	INUN	MBEH INDEX
			•			NASA-TM-109177	- 330	N95-23009 * #
CONF-940440-5			NAS 1.15:106849			NASA-TM-109177	n 296	N95-23011 * #
CONF-940865-4			NAS 1.15:106870			NASA-TM-109102	D 272	
CONF-9411142-4			NAS 1.15:106872			NASA-TM-4602	D 309	N95-23015 * #
CONF-941129-9			NAS 1.15:106885			NASA-TM-4602	D 310	N95-23210 * #
CONF-941144-14	. р 324	N95-24076 #	NAS 1.15:106890			NASA-TM-4635	p 296	N95-23192 * #
			NAS 1.15:108860 NAS 1.15:109177			NASA-TM-4638	p 274	N95-23250 * #
CU-CAS-95-03	. p 289	N95-23088 * #	NAS 1.15:109177			NASA-TM-4661		N95-22804 * #
DE0. 0.7700	- 004	NOT 20004 #	NAS 1.15:4583			NASA-TM-4665		N95-24030 * #
DE94-017768			NAS 1.15;4602			NASA-TM-4676	p 284	N95-22829 * #
DE95-001360			NAS 1.15:4602					
DE95-002602 DE95-002988			NAS 1.15:4635			NASA-TP-3465	p 285	N95-22953 * #
DE95-003630			NAS 1.15:4638			NASA-TP-3537	p 284	N95-22806 * #
DE95-003703			NAS 1.15:4661					
DE33-003703	. p 524	1433-24070 #	NAS 1.15:4665			NAWCADPAX-95-10-RTR	p 288	N95-24030 * #
DOT/FAA/AM-95/1	n 278	N95-24071 #	NAS 1.15:4676					
DOT/FAA/AM-95/4			NAS 1.26:189099	. p 290	N95-24053 * #	NIAR-94-11	p 277	N95-24012 #
DOT/FAA/AM-95/6	. p 323	N95-23603 #	NAS 1.26:189141	p 316		NIAR-94-3	p 277	N95-24050 #
DOT/FAA/AM-95/8	p 277	N95-24024 #	NAS 1.26:189146				-05	N95-23161 #
,			NAS 1.26:194972			NLR-TP-93109-U	p 285	N93-23101 #
DSTO-TR-0049	. р 286	N95-23666	NAS 1.26:195026			NTSB/AAR-95/01	- 277	NOS 22500 #
			NAS 1.26:195032			N12B/AAH-95/01	p 2//	N93-23003 #
E-9016			NAS 1.26:195050			NTSB/RP-94/01-VOL-1	n 278	N95-24105 #
E-9207			NAS 1.26:195052			NTSB/RP-94/02-VOL-2		
E-9364			NAS 1.26:195421		N95-22675 * # N95-23222 * #	N138/HF/34/02-40L-2	p Z	7100 20000 77
E-9421			NAS 1.26:195445 NAS 1.26:195454			PB94-917005	n 278	N95-24105 #
E-9425			NAS 1.26:196313	🕶		PB94-917007		
E-9489			NAS 1.26:197383			PB95-136032		
E-9491			NAS 1.26:197419			PB95-139184		
E-9493 E-9521			NAS 1.26:197420		N95-23217 * #	PB95-910401		
E-9530			NAS 1.26:197421		N95-23183 * #			
E-9538			NAS 1.26:197438			SAND-94-2746C	p 299	N95-23532 #
E-9552			NAS 1.26:197439	p 301	N95-23179 * #			
E-9583			NAS 1.26:197440	. p 289	N95-23088 * #	TAE-698	p 316	N95-23662 #
E-9589			NAS 1.26:197661		N95-22908 * #			
			NAS 1.26:197699			TII-R9201-001-RD	p 316	N95-23/92 #
EOARD-TR-94-07	. p 276	N95-23201 #	NAS 1.26:197704			TR-112894-3570P	- 216	NOS 22670 * #
500 75 00 000			NAS 1.26:197867 NAS 1.26:197912			TR-94-A-019	p 288	N95-24030 * #
ESC-TR-93-293	. р зоо	N95-23/81 #	NAS 1.26:197931				<b>,</b>	- "
FAA-AC-91-70	n 277	N95-24065 #	NAS 1.26:197938			UCRL-JC-118476	p 297	N95-24019 #
			NAS 1.26:197944					
FAA-AFS-550	. p 277	N95-24065 #	NAS 1.26:4649			US-PATENT-APPL-SN-014581		
			NAS 1.26:4650			US-PATENT-APPL-SN-014584 US-PATENT-APPL-SN-056503		N95-23390 * N95-22578 *
GAO/NSIAD-95-52	. p 286	N95-24091 #	NAS 1.26:4651 NAS 1.60:3465			US-PATENT-APPL-SN-889347		N95-23389 *
H-1984	0.284	NG5-22806 * #	NAS 1.60:3537			US-PATENT-APPL-SN-926117		N95-23377 °
H-2040				F		US-PATENT-APPL-SN-935939	p 280	N95-23393 *
11-20-40	. р соч	1155 22525 11	NASA-CASE-ARC-11913-1	p 311	N95-23377 *			
HTN-95-A0861	p 317	A95-76265 *	NASA-CASE-ARC-11944-1		N95-23389 *	US-PATENT-CLASS-244-182	p 294	N95-23389 *
HTN-95-A0862			NASA-CASE-ARC-11979-1		N95-23390 °	US-PATENT-CLASS-244-199		N95-23390 *
HTN-95-A0863			NASA-CASE-ARC-11982-1		N95-23393 *	US-PATENT-CLASS-244-215 US-PATENT-CLASS-244-216		N95-23395 * N95-23395 *
		A95-77000	NASA-CASE-ARC-11990-1	. p 200	N95-23395 *	US-PATENT-CLASS-244-51		N95-23389 *
HTN-95-11295							n 294	N95-23389 *
HTN-95-11304	p 319	A95-77009	NASA.CASE.NPO.18733-1-CH	n 288	N95-22578 *			
HTN-95-11304 HTN-95-20976	р 319 р 261	A95-77009 A95-74042 *	NASA-CASE-NPO-18733-1-CU	. p 288	N95-22578 *	US-PATENT-CLASS-244-7R	p 294	N95-23389 *
HTN-95-11304 HTN-95-20976 HTN-95-41219	р 319 . р 261 . р 317	A95-77009 A95-74042 * A95-75031 *		•			p 294 p 294	
HTN-95-11304 HTN-95-20976 HTN-95-41219 HTN-95-41223	p 319 p 261 p 317 p 317	A95-77009 A95-74042 * A95-75031 * A95-75035	NASA-CR-189099	. p 290	N95-24053 * #	US-PATENT-CLASS-244-7R	p 294 p 294 p 286	N95-23389 *
HTN-95-11304 HTN-95-20976 HTN-95-41219 HTN-95-41223 HTN-95-41393	. p 319 . p 261 . p 317 . p 317 . p 288	A95-77009 A95-74042 * A95-75031 * A95-75035 A95-76389	NASA-CR-189099 NASA-CR-189141	. р 290 р 316	N95-24053 * # N95-23792 * #	US-PATENT-CLASS-244-7FR US-PATENT-CLASS-244-75R US-PATENT-CLASS-244-75R US-PATENT-CLASS-340-946 US-PATENT-CLASS-340-953	p 294 p 294 p 286 p 280 p 280	N95-23389 * N95-23390 * N95-23393 * N95-23393 *
HTN-95-11304 HTN-95-20976 HTN-95-41219 HTN-95-41223 HTN-95-41393 HTN-95-41394	p 319 p 261 p 317 p 317 p 288 p 283	A95-77009 A95-74042 * A95-75031 * A95-75035 A95-76389 A95-76390	NASA-CR-189099	. р 290 р 316 р 316	N95-24053 * # N95-23792 * # N95-24189 * #	US-PATENT-CLASS-244-77R US-PATENT-CLASS-244-75R US-PATENT-CLASS-340-946 US-PATENT-CLASS-340-953 US-PATENT-CLASS-340-961 US-PATENT-CLASS-340-961	p 294 p 294 p 286 p 280 p 280 p 280 p 280	N95-23389 * N95-23390 * N95-23393 * N95-2339 * N95-2350 * N95-2350 * N95-2350 * N95-2350 * N95-2350 * N95-2350
HTN-95-11304 HTN-95-20976 HTN-95-41219 HTN-95-41223 HTN-95-41393 HTN-95-401394 HTN-95-60779	p 319 p 261 p 317 p 317 p 288 p 283 p 317	A95-77009 A95-74042 • A95-75031 • A95-75035 A95-76389 A95-76390 A95-75976	NASA-CR-189099 NASA-CR-189141 NASA-CR-189146	p 290 p 316 p 316 p 325	N95-24053 * # N95-23792 * # N95-24189 * # N95-23276 * #	US-PATENT-CLASS-244-77R US-PATENT-CLASS-244-75R US-PATENT-CLASS-340-946 US-PATENT-CLASS-340-953 US-PATENT-CLASS-340-961 US-PATENT-CLASS-340-981	p 294 p 294 p 286 p 280 p 280 p 280 p 280 p 280	N95-23389 * N95-23390 * N95-23393 * N95-23393 * N95-23393 * N95-23393 * N95-23393 *
HTN-95-11304 HTN-95-20976 HTN-95-41219 HTN-95-41223 HTN-95-41393 HTN-95-41394 HTN-95-60779 HTN-95-80851 HTN-95-80852	p 319 p 261 p 317 p 317 p 288 p 283 p 317 p 290 p 290	A95-77009 A95-74042 * A95-75031 * A95-75035 A95-76389 A95-76389 A95-75976 A95-75093 A95-75093	NASA-CR-189099 NASA-CR-189141 NASA-CR-189146 NASA-CR-194972 NASA-CR-195026 NASA-CR-195032	p 290 p 316 p 316 p 325 p 292 p 314	N95-24053 * # N95-23792 * # N95-24189 * # N95-23276 * # N95-22674 * # N95-23466 * #	US-PATENT-CLASS-244-7R US-PATENT-CLASS-244-75R US-PATENT-CLASS-244-75R US-PATENT-CLASS-340-946 US-PATENT-CLASS-340-961 US-PATENT-CLASS-340-961 US-PATENT-CLASS-340-981 US-PATENT-CLASS-345-8	p 294 p 294 p 286 p 280 p 280 p 280 p 280 p 280 p 288	N95-23389 * N95-23390 * N95-23393 * N95-23393 * N95-23393 * N95-22578 *
HTN-95-11304 HTN-95-20976 HTN-95-41219 HTN-95-41223 HTN-95-41393 HTN-95-41394 HTN-95-60779 HTN-95-80851 HTN-95-80852	p 319 p 261 p 317 p 317 p 288 p 283 p 317 p 290 p 290	A95-77009 A95-74042 * A95-75031 * A95-75035 A95-76389 A95-76389 A95-75976 A95-75093 A95-75093	NASA-CR-189099 NASA-CR-189141 NASA-CR-189146 NASA-CR-194972 NASA-CR-195026 NASA-CR-195032 NASA-CR-195050	p 290 p 316 p 316 p 325 p 292 p 314 p 273	N95-24053 * # N95-23792 * # N95-24189 * # N95-23276 * # N95-22674 * # N95-23466 * # N95-23193 * #	US-PATENT-CLASS-244-7R US-PATENT-CLASS-244-75R US-PATENT-CLASS-244-75R US-PATENT-CLASS-340-946 US-PATENT-CLASS-340-961 US-PATENT-CLASS-340-981 US-PATENT-CLASS-345-8 US-PATENT-CLASS-362-62	p 294 p 294 p 286 p 280 p 280 p 280 p 280 p 280 p 288 p 288	N95-23389 ' N95-23390 ' N95-23393 ' N95-23393 ' N95-23393 ' N95-23393 ' N95-22578 ' N95-23393 '
HTN-95-11304 HTN-95-20976 HTN-95-41219 HTN-95-41223 HTN-95-41393 HTN-95-60779 HTN-95-80851 HTN-95-80852 HTN-95-80852 HTN-95-80853	. p 319 . p 261 . p 317 . p 317 . p 288 . p 283 . p 317 . p 290 . p 290 . p 290	A95-77009 A95-74042 * A95-75031 * A95-75035 A95-76389 A95-76390 A95-75976 A95-75093 A95-75095 * A95-75096 *	NASA-CR-189099 NASA-CR-189141 NASA-CR-189146 NASA-CR-194972 NASA-CR-195026 NASA-CR-195032 NASA-CR-195050 NASA-CR-195050	p 290 p 316 p 316 p 325 p 292 p 314 p 273 p 310	N95-24053 * # N95-23792 * # N95-24189 * # N95-23276 * # N95-22674 * # N95-23466 * # N95-23193 * # N95-23257 * #	US-PATENT-CLASS-244-77R US-PATENT-CLASS-244-75R US-PATENT-CLASS-340-946 US-PATENT-CLASS-340-953 US-PATENT-CLASS-340-961 US-PATENT-CLASS-340-961 US-PATENT-CLASS-345-8 US-PATENT-CLASS-362-62 US-PATENT-CLASS-362-62	p 294 p 294 p 286 p 280 p 280 p 280 p 280 p 288 p 280 p 288	N95-23389 * N95-23390 * N95-23393 * N95-23393 * N95-23393 * N95-22578 * N95-22578 * N95-22578 *
HTN-95-11304 HTN-95-20976 HTN-95-41219 HTN-95-41223 HTN-95-41393 HTN-95-60779 HTN-95-80851 HTN-95-80852 HTN-95-80853 HTN-95-80854 HTN-95-80855	. p 319 . p 261 . p 317 . p 317 . p 288 . p 283 . p 317 . p 290 . p 290 . p 290 . p 290 . p 267	A95-77009 A95-74042 * A95-75031 * A95-75035 A95-76389 A95-76380 A95-75996 A95-75094 A95-75094 A95-75096 * A95-75097 *	NASA-CR-189099 NASA-CR-189141 NASA-CR-189146 NASA-CR-194972 NASA-CR-195026 NASA-CR-195032 NASA-CR-195050 NASA-CR-195052 NASA-CR-195052 NASA-CR-195052	p 290 p 316 p 316 p 325 p 292 p 314 p 273 p 310 p 323	N95-24053 * # N95-23792 * # N95-24189 * # N95-22674 * # N95-22674 * # N95-23466 * # N95-23193 * # N95-23257 * # N95-22675 * #	US-PATENT-CLASS-244-77R US-PATENT-CLASS-244-75R US-PATENT-CLASS-340-946 US-PATENT-CLASS-340-953 US-PATENT-CLASS-340-961 US-PATENT-CLASS-340-961 US-PATENT-CLASS-345-8 US-PATENT-CLASS-362-62 US-PATENT-CLASS-364-578 US-PATENT-CLASS-395-152	p 294 p 294 p 286 p 280 p 280 p 280 p 280 p 288 p 280 p 288 p 288	N95-23389 ' N95-23393 ' N95-23393 ' N95-23393 ' N95-23393 ' N95-23393 ' N95-22578 ' N95-22578 ' N95-22578 '
HTN-95-11304 HTN-95-20976 HTN-95-41219 HTN-95-41223 HTN-95-41393 HTN-95-41394 HTN-95-80851 HTN-95-80852 HTN-95-80853 HTN-95-80854 HTN-95-80855 HTN-95-80855	. p 319 . p 261 . p 317 . p 317 . p 288 . p 283 . p 317 . p 290 . p 290 . p 290 . p 290 . p 267 . p 283	A95-77009 A95-74042 * A95-75031 * A95-75035 A95-76389 A95-76389 A95-75996 A95-75093 A95-75094 A95-75096 * A95-75097 * A95-75098	NASA-CR-189099 NASA-CR-189141 NASA-CR-189146 NASA-CR-194972 NASA-CR-195026 NASA-CR-195032 NASA-CR-195050 NASA-CR-195052 NASA-CR-195052 NASA-CR-19545	p 290 p 316 p 316 p 325 p 292 p 314 p 273 p 310 p 323 p 289	N95-24053 * # N95-23792 * # N95-24189 * # N95-23276 * # N95-22674 * # N95-23466 * # N95-23193 * # N95-23257 * # N95-23227 * # N95-23222 * #	US-PATENT-CLASS-244-77R US-PATENT-CLASS-244-75R US-PATENT-CLASS-340-946 US-PATENT-CLASS-340-961 US-PATENT-CLASS-340-961 US-PATENT-CLASS-340-981 US-PATENT-CLASS-345-8 US-PATENT-CLASS-36-578 US-PATENT-CLASS-364-578 US-PATENT-CLASS-364-578 US-PATENT-CLASS-364-578 US-PATENT-CLASS-364-578 US-PATENT-CLASS-364-578	P 294 P 294 P 286 P 280 P 280 P 280 P 280 P 288 P 288 P 288 P 288 P 288	N95-23389 ' N95-23390 ' N95-23393 ' N95-23393 ' N95-23393 ' N95-23393 ' N95-22578 ' N95-22578 ' N95-22578 ' N95-23377 '
HTN-95-11304 HTN-95-20976 HTN-95-41219 HTN-95-41223 HTN-95-41393 HTN-95-60779 HTN-95-80851 HTN-95-80852 HTN-95-80853 HTN-95-80855 HTN-95-80855 HTN-95-80855 HTN-95-80855 HTN-95-80855 HTN-95-80855	. p 319 . p 261 . p 317 . p 317 . p 288 . p 283 . p 317 . p 290 . p 290 . p 290 . p 290 . p 267 . p 283 . p 283	A95-77009 A95-74042 * A95-75031 * A95-75035 A95-76389 A95-76390 A95-75976 A95-75093 A95-75094 A95-75095 * A95-75097 * A95-75099 *	NASA-CR-189099 NASA-CR-189141 NASA-CR-189146 NASA-CR-194972 NASA-CR-195026 NASA-CR-195032 NASA-CR-195050 NASA-CR-195052 NASA-CR-195052 NASA-CR-195421 NASA-CR-195421 NASA-CR-195425 NASA-CR-195445 NASA-CR-195454	p 290 p 316 p 316 p 325 p 292 p 314 p 273 p 310 p 323 p 289 p 275	N95-24053 * # N95-23792 * # N95-24189 * # N95-23276 * # N95-22674 * # N95-23466 * # N95-23466 * # N95-23267 * # N95-22675 * # N95-23222 * # N95-23462 * #	US-PATENT-CLASS-244-77R US-PATENT-CLASS-244-75R US-PATENT-CLASS-340-946 US-PATENT-CLASS-340-953 US-PATENT-CLASS-340-961 US-PATENT-CLASS-340-961 US-PATENT-CLASS-340-981 US-PATENT-CLASS-362-62 US-PATENT-CLASS-363-578 US-PATENT-CLASS-364-578 US-PATENT-CLASS-364-578 US-PATENT-CLASS-364-578 US-PATENT-CLASS-364-578 US-PATENT-CLASS-364-578	P 294 P 294 P 286 P 280 P 280 P 280 P 280 P 288 P 288 P 288 P 288 P 288 P 311 P 311	N95-23389 N95-23393 N95-23393 N95-23393 N95-23393 N95-23393 N95-22578 N95-22578 N95-22578 N95-22578 N95-23377 N95-23377
HTN-95-11304 HTN-95-20976 HTN-95-41223 HTN-95-41223 HTN-95-41393 HTN-95-60779 HTN-95-80851 HTN-95-80852 HTN-95-80853 HTN-95-80855 HTN-95-80855 HTN-95-80856 HTN-95-80856 HTN-95-80856 HTN-95-80856	. p 319 . p 261 . p 317 . p 317 . p 288 . p 283 . p 317 . p 290 . p 290 . p 290 . p 290 . p 267 . p 283 . p 283	A95-77009 A95-74042 * A95-75031 * A95-75035 A95-76389 A95-76389 A95-75090 A95-75094 A95-75094 A95-75096 * A95-75097 * A95-75098 A95-75099 * A95-75100	NASA-CR-189099 NASA-CR-189141 NASA-CR-189146 NASA-CR-194972 NASA-CR-195026 NASA-CR-195032 NASA-CR-195050 NASA-CR-195052 NASA-CR-195421 NASA-CR-195445 NASA-CR-195454 NASA-CR-195454 NASA-CR-1956313	p 290 p 316 p 316 p 325 p 292 p 314 p 273 p 310 p 323 p 289 p 275 p 320	N95-24053 * # N95-23792 * # N95-24189 * # N95-23276 * # N95-22674 * # N95-23466 * # N95-23257 * # N95-23257 * # N95-23222 * # N95-23462 * # N95-23466 * #	US-PATENT-CLASS-244-77R US-PATENT-CLASS-244-75R US-PATENT-CLASS-340-946 US-PATENT-CLASS-340-961 US-PATENT-CLASS-340-961 US-PATENT-CLASS-340-961 US-PATENT-CLASS-345-8 US-PATENT-CLASS-362-62 US-PATENT-CLASS-364-578 US-PATENT-CLASS-395-152 US-PATENT-CLASS-364-578 US-PATENT-CLASS-364-578 US-PATENT-CLASS-364-578 US-PATENT-CLASS-416-34 US-PATENT-CLASS-416-61 US-PATENT-CLASS-43-307R	P 294 P 294 P 286 P 280 P 280 P 280 P 280 P 280 P 288 P 288 P 311 P 311 P 288	N95-23389 ' N95-23393 ' N95-23393 ' N95-23393 ' N95-23393 ' N95-22578 ' N95-22578 ' N95-22578 ' N95-22578 ' N95-23377 ' N95-2377 ' N95-22578 '
HTN-95-11304 HTN-95-20976 HTN-95-41219 HTN-95-41223 HTN-95-41393 HTN-95-41394 HTN-95-80851 HTN-95-80852 HTN-95-80853 HTN-95-80854 HTN-95-80856 HTN-95-80856 HTN-95-80857 HTN-95-80857 HTN-95-80858	. p 319 . p 261 . p 317 . p 318 . p 283 . p 317 . p 290 . p 290 . p 290 . p 290 . p 267 . p 263 . p 283 . p 283 . p 283 . p 267	A95-77009 A95-74042 * A95-75031 * A95-75031 * A95-76389 A95-76389 A95-75996 A95-75093 A95-75094 A95-75096 * A95-75097 * A95-75097 * A95-75098 A95-75099 * A95-75100 A95-75100	NASA-CR-189099 NASA-CR-189141 NASA-CR-189146 NASA-CR-194972 NASA-CR-195026 NASA-CR-195032 NASA-CR-195050 NASA-CR-195050 NASA-CR-195052 NASA-CR-195421 NASA-CR-195445 NASA-CR-195454 NASA-CR-195454 NASA-CR-196313 NASA-CR-197383	p 290 p 316 p 316 p 325 p 292 p 314 p 273 p 310 p 323 p 320 p 320 p 320	N95-24053 * # N95-23792 * # N95-2376 * # N95-23276 * # N95-23466 * # N95-23466 * # N95-23257 * # N95-232675 * # N95-23462 * # N95-23462 * # N95-23462 * # N95-23462 * # N95-23463 * #	US-PATENT-CLASS-244-77R US-PATENT-CLASS-244-75R US-PATENT-CLASS-340-946 US-PATENT-CLASS-340-953 US-PATENT-CLASS-340-961 US-PATENT-CLASS-340-961 US-PATENT-CLASS-340-981 US-PATENT-CLASS-362-62 US-PATENT-CLASS-363-578 US-PATENT-CLASS-364-578 US-PATENT-CLASS-364-578 US-PATENT-CLASS-364-578 US-PATENT-CLASS-364-578 US-PATENT-CLASS-364-578	P 294 P 294 P 286 P 280 P 280 P 280 P 280 P 288 P 288 P 288 P 311 P 311 P 288 P 288	N95-23389 N95-23393 N95-23393 N95-23393 N95-23393 N95-23393 N95-22578 N95-22578 N95-22578 N95-22578 N95-23377 N95-23377
HTN-95-11304 HTN-95-20976 HTN-95-41299 HTN-95-41293 HTN-95-41393 HTN-95-60779 HTN-95-80851 HTN-95-80852 HTN-95-80853 HTN-95-80854 HTN-95-80855 HTN-95-80856 HTN-95-80857 HTN-95-80856 HTN-95-80857 HTN-95-80858 HTN-95-80858	. p 319 . p 261 . p 317 . p 317 . p 288 . p 283 . p 317 . p 290 . p 290 . p 290 . p 290 . p 267 . p 283 . p 283 . p 283 . p 283 . p 283 . p 287 . p 287	A95-77009 A95-74042 * A95-75031 * A95-75035 A95-76390 A95-76390 A95-75976 A95-75093 A95-75094 A95-75095 * A95-75096 * A95-75097 * A95-75098 A95-75099 * A95-75100 A95-75100 A95-75101 A95-7534	NASA-CR-189099 NASA-CR-189141 NASA-CR-189146 NASA-CR-199172 NASA-CR-195026 NASA-CR-195032 NASA-CR-195050 NASA-CR-195052 NASA-CR-195052 NASA-CR-195421 NASA-CR-195445 NASA-CR-195454 NASA-CR-196313 NASA-CR-197383 NASA-CR-197419	p 290 p 316 p 316 p 325 p 292 p 314 p 273 p 310 p 323 p 323 p 320 p 320 p 309	N95-24053 * # N95-23792 * # N95-2376 * # N95-22676 * # N95-22674 * # N95-23193 * # N95-23265 * # N95-23265 * # N95-23222 * # N95-23222 * # N95-2322481 * # N95-2318 * #	US-PATENT-CLASS-244-77R US-PATENT-CLASS-244-75R US-PATENT-CLASS-340-946 US-PATENT-CLASS-340-961 US-PATENT-CLASS-340-961 US-PATENT-CLASS-340-961 US-PATENT-CLASS-345-8 US-PATENT-CLASS-36-578 US-PATENT-CLASS-364-578 US-PATENT-CLASS-364-578 US-PATENT-CLASS-364-578 US-PATENT-CLASS-364-578 US-PATENT-CLASS-364-578 US-PATENT-CLASS-364-578 US-PATENT-CLASS-364-578 US-PATENT-CLASS-416-34 US-PATENT-CLASS-416-378 US-PATENT-CLASS-434-307R US-PATENT-CLASS-434-307R	P 294 P 294 P 286 P 280 P 280 P 280 P 280 P 280 P 288 P 288 P 288 P 311 P 288 P 288 P 288 P 288	N95-23389 ' N95-23390 ' N95-23393 ' N95-23393 ' N95-23393 ' N95-23393 ' N95-22578 ' N95-22578 ' N95-22578 ' N95-23377 ' N95-23377 ' N95-23578 ' N95-23578 '
HTN-95-11304 HTN-95-20976 HTN-95-41219 HTN-95-41223 HTN-95-41393 HTN-95-41394 HTN-95-80851 HTN-95-80852 HTN-95-80853 HTN-95-80854 HTN-95-80856 HTN-95-80856 HTN-95-80857 HTN-95-80857 HTN-95-80858	. p 319 . p 261 . p 317 . p 317 . p 288 . p 283 . p 317 . p 290 . p 290 . p 290 . p 290 . p 267 . p 283 . p 283 . p 283 . p 283 . p 283 . p 287 . p 287	A95-77009 A95-74042 * A95-75031 * A95-75035 A95-76390 A95-76390 A95-75976 A95-75093 A95-75094 A95-75095 * A95-75096 * A95-75097 * A95-75098 A95-75099 * A95-75100 A95-75100 A95-75101 A95-7534	NASA-CR-189099 NASA-CR-189141 NASA-CR-189146 NASA-CR-194972 NASA-CR-195026 NASA-CR-195032 NASA-CR-195050 NASA-CR-195050 NASA-CR-19541 NASA-CR-195445 NASA-CR-195454 NASA-CR-195454 NASA-CR-197419 NASA-CR-197419 NASA-CR-197420 NASA-CR-197421	p 290 p 316 p 316 p 325 p 292 p 314 p 273 p 310 p 320 p 275 p 320 p 309 p 289 p 309	N95-24053 * # N95-23792 * # N95-23189 * # N95-23276 * # N95-22674 * # N95-23466 * # N95-23193 * # N95-23257 * # N95-23222 * # N95-23266 * # N95-23462 * # N95-23766 * # N95-23766 * # N95-23766 * # N95-23766 * # N95-23176 * #	US-PATENT-CLASS-244-77R US-PATENT-CLASS-244-75R US-PATENT-CLASS-244-75R US-PATENT-CLASS-340-946 US-PATENT-CLASS-340-961 US-PATENT-CLASS-340-961 US-PATENT-CLASS-340-961 US-PATENT-CLASS-362-62 US-PATENT-CLASS-362-62 US-PATENT-CLASS-362-578 US-PATENT-CLASS-362-578 US-PATENT-CLASS-362-62 US-PATENT-CLASS-363-6378 US-PATENT-CLASS-363-6378 US-PATENT-CLASS-416-61 US-PATENT-CLASS-434-372 US-PATENT-CLASS-434-372	P 294 P 294 P 286 P 280 P 280 P 280 P 280 P 288 P 288 P 288 P 311 P 311 P 288 P 288 P 288 P 288	N95-23389 ' N95-23393 ' N95-23393 ' N95-23393 ' N95-23393 ' N95-22578 ' N95-22578 ' N95-22578 ' N95-22578 ' N95-23377 ' N95-23377 ' N95-22578 '
HTN-95-11304 HTN-95-20976 HTN-95-41299 HTN-95-41293 HTN-95-41393 HTN-95-60779 HTN-95-80851 HTN-95-80852 HTN-95-80853 HTN-95-80854 HTN-95-80855 HTN-95-80856 HTN-95-80857 HTN-95-80856 HTN-95-80857 HTN-95-80858 HTN-95-80858	p 319 p 261 p 317 p 317 p 288 p 283 p 317 p 290 p 290 p 290 p 290 p 267 p 283 p 283 p 283 p 283 p 319	A95-77009 A95-74042 * A95-75031 * A95-75031 * A95-76389 A95-76389 A95-75093 A95-75094 A95-75095 * A95-75096 * A95-75097 * A95-75098 A95-75099 * A95-75090 A95-75100 A95-75101 A95-76394 A95-77334	NASA-CR-189099 NASA-CR-189141 NASA-CR-189146 NASA-CR-189172 NASA-CR-195026 NASA-CR-195032 NASA-CR-195050 NASA-CR-195052 NASA-CR-195451 NASA-CR-195454 NASA-CR-195454 NASA-CR-195454 NASA-CR-197383 NASA-CR-197419 NASA-CR-197419 NASA-CR-197420 NASA-CR-197421 NASA-CR-197421 NASA-CR-197438	p 290 p 316 p 316 p 325 p 292 p 314 p 273 p 310 p 320 p 320 p 320 p 320 p 274 p 274 p 275 p 309 p 274 p 309 p 309	N95-24053 * # N95-23792 * # N95-2376 * # N95-23276 * # N95-22674 * # N95-23466 * # N95-23193 * # N95-23257 * # N95-23227 * # N95-23222 * # N95-23462 * # N95-23766 * # N95-2318 * # N95-23183 * # N95-23183 * # N95-23183 * #	US-PATENT-CLASS-244-77R US-PATENT-CLASS-244-75R US-PATENT-CLASS-244-75R US-PATENT-CLASS-340-946 US-PATENT-CLASS-340-961 US-PATENT-CLASS-340-961 US-PATENT-CLASS-340-961 US-PATENT-CLASS-362-62 US-PATENT-CLASS-362-62 US-PATENT-CLASS-362-62 US-PATENT-CLASS-362-62 US-PATENT-CLASS-364-578 US-PATENT-CLASS-364-578 US-PATENT-CLASS-363-63 US-PATENT-CLASS-416-61 US-PATENT-CLASS-434-307R US-PATENT-CLASS-434-372 US-PATENT-CLASS-434-372 US-PATENT-CLASS-434-38 US-PATENT-CLASS-434-43 US-PATENT-CLASS-434-43	P 294 P 294 P 286 P 280 P 280 P 280 P 280 P 288 P 288 P 288 P 311 P 311 P 288 P 288 P 288 P 288 P 288	N95-23389 ' N95-23390 ' N95-23393 ' N95-23393 ' N95-23393 ' N95-23393 ' N95-22578 ' N95-22578 ' N95-23377 ' N95-23377 ' N95-22578 ' N95-23393 '
HTN-95-11304 HTN-95-20976 HTN-95-41223 HTN-95-41223 HTN-95-41393 HTN-95-60779 HTN-95-80851 HTN-95-80852 HTN-95-80853 HTN-95-80855 HTN-95-80856 HTN-95-80856 HTN-95-80856 HTN-95-80857 HTN-95-80859 HTN-95-80859 HTN-95-80859	p 319 p 261 p 317 p 317 p 288 p 283 p 317 p 290 p 290 p 290 p 290 p 283 p 283 p 283 p 283 p 283 p 283 p 283 p 319	A95-77009 A95-74042 * A95-75031 * A95-75031 * A95-76389 A95-76389 A95-75976 A95-75094 A95-75094 A95-75096 * A95-75097 * A95-75097 * A95-75099 * A95-75099 * A95-75100 A95-75101 A95-76394 A95-77334 N95-23466 * #	NASA-CR-189099 NASA-CR-189141 NASA-CR-189146 NASA-CR-199172 NASA-CR-195026 NASA-CR-195050 NASA-CR-195052 NASA-CR-195052 NASA-CR-195421 NASA-CR-195445 NASA-CR-195445 NASA-CR-195445 NASA-CR-197383 NASA-CR-197419 NASA-CR-197420 NASA-CR-197420 NASA-CR-197438 NASA-CR-197438 NASA-CR-197438 NASA-CR-197439	p 290 p 316 p 316 p 325 p 292 p 273 p 273 p 323 p 289 p 275 p 309 p 274 p 285 p 309 p 309	N95-24053 * # N95-23792 * # N95-2376 * # N95-23276 * # N95-22674 * # N95-23266 * # N95-23257 * # N95-23257 * # N95-23262 * # N95-23262 * # N95-23262 * # N95-23183 * # N95-23183 * # N95-23183 * # N95-23190 * # N95-23190 * #	US-PATENT-CLASS-244-77R US-PATENT-CLASS-244-75R US-PATENT-CLASS-340-946 US-PATENT-CLASS-340-961 US-PATENT-CLASS-340-961 US-PATENT-CLASS-340-961 US-PATENT-CLASS-340-961 US-PATENT-CLASS-362-62 US-PATENT-CLASS-362-62 US-PATENT-CLASS-363-578 US-PATENT-CLASS-363-578 US-PATENT-CLASS-363-578 US-PATENT-CLASS-416-34 US-PATENT-CLASS-416-61 US-PATENT-CLASS-418-61 US-PATENT-CLASS-418-61 US-PATENT-CLASS-434-372 US-PATENT-CLASS-434-38 US-PATENT-CLASS-434-38 US-PATENT-CLASS-434-38 US-PATENT-CLASS-434-43 US-PATENT-CLASS-373-178H US-PATENT-CLASS-373-178H	P 294 P 294 P 280 P 280 P 280 P 280 P 280 P 280 P 288 P 288 P 311 P 311 P 311 P 318 P 288 P 288 P 288 P 288 P 288 P 288	N95-23389 ' N95-23393 ' N95-23393 ' N95-23393 ' N95-23393 ' N95-22578 ' N95-22578 ' N95-22578 ' N95-22578 ' N95-23377 ' N95-23377 ' N95-22578 ' N95-22578 ' N95-22578 ' N95-22578 ' N95-22578 ' N95-22578 ' N95-23393 '
HTN-95-11304 HTN-95-20976 HTN-95-41219 HTN-95-41223 HTN-95-41393 HTN-95-41394 HTN-95-80851 HTN-95-80852 HTN-95-80853 HTN-95-80855 HTN-95-80856 HTN-95-80856 HTN-95-80857 HTN-95-80857 HTN-95-80858 HTN-95-80858 HTN-95-80859	P 319 P 261 P 317 P 317 P 288 P 283 P 290 P 290 P 290 P 290 P 267 P 283 P 283 P 283 P 283 P 319	A95-77009 A95-74042 * A95-75031 * A95-75031 * A95-75035 A95-76389 A95-76380 A95-75093 A95-75094 A95-75096 * A95-75097 * A95-75097 * A95-75099 * A95-75090 A95-75100 A95-75101 A95-76394 A95-77334  N95-23466 * #	NASA-CR-189099 NASA-CR-189141 NASA-CR-189146 NASA-CR-194972 NASA-CR-195032 NASA-CR-195050 NASA-CR-195050 NASA-CR-195052 NASA-CR-195445 NASA-CR-195445 NASA-CR-195454 NASA-CR-197454 NASA-CR-19749 NASA-CR-197419 NASA-CR-197420 NASA-CR-197421 NASA-CR-197421 NASA-CR-197439 NASA-CR-197439 NASA-CR-197440	p 290 p 316 p 325 p 325 p 292 p 313 p 313 p 313 p 323 p 289 p 275 p 320 p 320 p 320 p 320 p 320 p 320 p 320 p 320 p 320 p 320	N95-24053 * # N95-24189 * # N95-23276 * # N95-22674 * # N95-22676 * # N95-23466 * # N95-23257 * # N95-23222 * # N95-23222 * # N95-23462 * # N95-23468 * # N95-23183 * # N95-23183 * # N95-23183 * # N95-23199 * # N95-23199 * # N95-23199 * # N95-23198 * #	US-PATENT-CLASS-244-77R US-PATENT-CLASS-244-75R US-PATENT-CLASS-340-946 US-PATENT-CLASS-340-961 US-PATENT-CLASS-340-961 US-PATENT-CLASS-340-961 US-PATENT-CLASS-340-981 US-PATENT-CLASS-36981 US-PATENT-CLASS-368-78 US-PATENT-CLASS-368-778 US-PATENT-CLASS-368-778 US-PATENT-CLASS-368-778 US-PATENT-CLASS-395-152 US-PATENT-CLASS-416-34 US-PATENT-CLASS-434-307R US-PATENT-CLASS-434-307R US-PATENT-CLASS-434-372 US-PATENT-CLASS-434-378 US-PATENT-CLASS-434-38 US-PATENT-CLASS-33-178H US-PATENT-CLASS-33-178H US-PATENT-CLASS-33-178H US-PATENT-CLASS-33-178H US-PATENT-5-294-080 US-PATENT-5-5-15-296	P 294 P 294 P 286 P 280 P 280 P 280 P 280 P 288 P 288 P 288 P 311 P 311 P 288	N95-23389 ' N95-23393 ' N95-23393 ' N95-23393 ' N95-23393 ' N95-23393 ' N95-22578 ' N95-22578 ' N95-22578 ' N95-23377 ' N95-23377 ' N95-23377 ' N95-23377 ' N95-23378 ' N95-23393 '
HTN-95-11304 HTN-95-20976 HTN-95-41299 HTN-95-41293 HTN-95-41393 HTN-95-41394 HTN-95-80851 HTN-95-80852 HTN-95-80853 HTN-95-80855 HTN-95-80855 HTN-95-80856 HTN-95-80857 HTN-95-80858 HTN-95-80858 HTN-95-80859 HTN-95-91421	P 319 P 261 P 317 P 317 P 288 P 283 P 290 P 290 P 290 P 290 P 283 P 283 P 283 P 283 P 283 P 319 P 314	A95-77009 A95-74042 * A95-75031 * A95-75031 * A95-75035 A95-76389 A95-75396 A95-75094 A95-75096 * A95-75097 * A95-75098 A95-75098 A95-75099 * A95-75099 * A95-75100 A95-75100 A95-75101 A95-76394 A95-77334  N95-23466 * # N95-23377 * N95-23389 *	NASA-CR-189099 NASA-CR-189141 NASA-CR-189146 NASA-CR-189146 NASA-CR-195026 NASA-CR-195032 NASA-CR-195050 NASA-CR-195050 NASA-CR-195421 NASA-CR-19545 NASA-CR-195454 NASA-CR-195454 NASA-CR-197383 NASA-CR-197419 NASA-CR-197419 NASA-CR-197419 NASA-CR-197420 NASA-CR-197420 NASA-CR-197438 NASA-CR-197439 NASA-CR-197439 NASA-CR-197439 NASA-CR-197440 NASA-CR-197461	p 290 p 316 p 315 p 325 p 329 p 310 p 323 p 389 p 275 p 320 p 309 p 285 p 309 p 310 p 310 p 310 p 310 p 310 p 320	N95-24053 * # N95-23792 * # N95-2376 * # N95-23276 * # N95-22674 * # N95-23466 * # N95-23193 * # N95-23267 * # N95-23267 * # N95-23267 * # N95-23218 * # N95-23183 * #	US-PATENT-CLASS-244-77R US-PATENT-CLASS-244-75R US-PATENT-CLASS-340-946 US-PATENT-CLASS-340-953 US-PATENT-CLASS-340-961 US-PATENT-CLASS-340-961 US-PATENT-CLASS-340-961 US-PATENT-CLASS-362-62 US-PATENT-CLASS-362-62 US-PATENT-CLASS-362-62 US-PATENT-CLASS-362-62 US-PATENT-CLASS-364-578 US-PATENT-CLASS-364-578 US-PATENT-CLASS-361-61 US-PATENT-CLASS-416-61 US-PATENT-CLASS-434-307R US-PATENT-CLASS-434-372 US-PATENT-CLASS-434-38 US-PATENT-CLASS-434-39 US-PATENT-S-294-0800 US-PATENT-S-296-050	P 294 P 294 P 280 P 280 P 280 P 280 P 288 P 288 P 281 P 311 P 288 P 288 P 288 P 288 P 280 P 286 P 288 P 288	N95-23389 · N95-23393 · N95-23393 · N95-23393 · N95-23393 · N95-23393 · N95-22578 · N95-22578 · N95-23377 · N95-23377 · N95-22578 · N95-23393 · N95-23393 ·
HTN-95-11304 HTN-95-20976 HTN-95-41223 HTN-95-41223 HTN-95-41393 HTN-95-41394 HTN-95-60779 HTN-95-80851 HTN-95-80852 HTN-95-80853 HTN-95-80855 HTN-95-80856 HTN-95-80856 HTN-95-80857 HTN-95-80857 HTN-95-80859 HTN-95-80859 HTN-95-80859 HTN-95-91363 HTN-95-91363 HTN-95-91421 ICASE-95-5 INT-PATENT-CLASS-B64C-11/00 INT-PATENT-CLASS-B64C-19/00 INT-PATENT-CLASS-B64C-5/00	p 319 p 261 p 317 p 317 p 288 p 283 p 283 p 290 p 290 p 290 p 290 p 283 p 283 p 283 p 283 p 283 p 283 p 283 p 319 p 311 p 311 p 311 p 311 p 286 p 319	A95-77009 A95-74042 * A95-75031 * A95-75031 * A95-76389 A95-76389 A95-75094 A95-75094 A95-75095 * A95-75096 * A95-75097 * A95-75099 * A95-75099 * A95-75090 * A95-73040 * A95-73340 * N95-23466 * W95-23389 * N95-23380 *	NASA-CR-189099 NASA-CR-189141 NASA-CR-189146 NASA-CR-194972 NASA-CR-195032 NASA-CR-195050 NASA-CR-195050 NASA-CR-195052 NASA-CR-195445 NASA-CR-195445 NASA-CR-195454 NASA-CR-197454 NASA-CR-19749 NASA-CR-197419 NASA-CR-197420 NASA-CR-197421 NASA-CR-197421 NASA-CR-197439 NASA-CR-197439 NASA-CR-197440	p 290 p 316 p 316 p 325 p 329 p 310 p 323 p 323 p 320 p 329 p 320 p 320 p 320 p 309 p 309 p 301 p 301 p 301 p 303	N95-24053 * # N95-23792 * # N95-2376 * # N95-23276 * # N95-22674 * # N95-23266 * # N95-23257 * # N95-23257 * # N95-23262 * # N95-23262 * # N95-23262 * # N95-23218 * # N95-23218 * # N95-23180 * # N95-23190 * # N95-23088 * # N95-23088 * # N95-23067 * #	US-PATENT-CLASS-244-77R US-PATENT-CLASS-244-75R US-PATENT-CLASS-340-946 US-PATENT-CLASS-340-961 US-PATENT-CLASS-340-961 US-PATENT-CLASS-340-961 US-PATENT-CLASS-340-981 US-PATENT-CLASS-36981 US-PATENT-CLASS-368-78 US-PATENT-CLASS-368-778 US-PATENT-CLASS-368-778 US-PATENT-CLASS-368-778 US-PATENT-CLASS-395-152 US-PATENT-CLASS-416-34 US-PATENT-CLASS-434-307R US-PATENT-CLASS-434-307R US-PATENT-CLASS-434-372 US-PATENT-CLASS-434-378 US-PATENT-CLASS-434-38 US-PATENT-CLASS-33-178H US-PATENT-CLASS-33-178H US-PATENT-CLASS-33-178H US-PATENT-CLASS-33-178H US-PATENT-5-294-080 US-PATENT-5-5-15-296	P 294 P 294 P 280 P 280 P 280 P 280 P 280 P 288 P 280 P 288 P 311 P 311 P 288 P 289	N95-23389 ' N95-23393 ' N95-23393 ' N95-23393 ' N95-23393 ' N95-22578 ' N95-22578 ' N95-22578 ' N95-22578 ' N95-23377 ' N95-23377 ' N95-22578 ' N95-22578 ' N95-22578 ' N95-22578 ' N95-23393 '
HTN-95-11304 HTN-95-20976 HTN-95-41299 HTN-95-41293 HTN-95-41393 HTN-95-41394 HTN-95-80851 HTN-95-80852 HTN-95-80853 HTN-95-80855 HTN-95-80855 HTN-95-80856 HTN-95-80857 HTN-95-80858 HTN-95-80858 HTN-95-80859 HTN-95-91421	p 319 p 261 p 317 p 317 p 288 p 283 p 283 p 290 p 290 p 290 p 290 p 283 p 283 p 283 p 283 p 283 p 283 p 283 p 319 p 311 p 311 p 311 p 311 p 286 p 319	A95-77009 A95-74042 * A95-75031 * A95-75031 * A95-76389 A95-76389 A95-75094 A95-75094 A95-75095 * A95-75096 * A95-75097 * A95-75099 * A95-75099 * A95-75090 * A95-73040 * A95-73340 * N95-23466 * W95-23389 * N95-23380 *	NASA-CR-189099 NASA-CR-189141 NASA-CR-189146 NASA-CR-199172 NASA-CR-195026 NASA-CR-195050 NASA-CR-195052 NASA-CR-195052 NASA-CR-195421 NASA-CR-195445 NASA-CR-195445 NASA-CR-195445 NASA-CR-197383 NASA-CR-197419 NASA-CR-197419 NASA-CR-197420 NASA-CR-197420 NASA-CR-197420 NASA-CR-197420 NASA-CR-197440 NASA-CR-197440 NASA-CR-197440 NASA-CR-197661 NASA-CR-197661	p 290 p 316 p 316 p 325 p 292 p 310 p 323 p 330 p 330 p 309 p 309 p 285 p 309 p 301 p 301	N95-24053 * # N95-24189 * # N95-23276 * # N95-22674 * # N95-23266 * # N95-23193 * # N95-232675 * # N95-23222 * # N95-23266 * # N95-23266 * # N95-23462 * # N95-23468 * # N95-23218 * # N95-23218 * # N95-23183 * # N95-23190 * # N95-23199 * # N95-23199 * # N95-23080 * # N95-23600 * # N95-23670 * # N95-23670 * #	US-PATENT-CLASS-244-77R US-PATENT-CLASS-244-75R US-PATENT-CLASS-340-946 US-PATENT-CLASS-340-961 US-PATENT-CLASS-340-961 US-PATENT-CLASS-340-961 US-PATENT-CLASS-340-961 US-PATENT-CLASS-362-62 US-PATENT-CLASS-362-62 US-PATENT-CLASS-364-578 US-PATENT-CLASS-364-578 US-PATENT-CLASS-364-578 US-PATENT-CLASS-364-578 US-PATENT-CLASS-416-61 US-PATENT-CLASS-434-307R US-PATENT-CLASS-434-372 US-PATENT-CLASS-434-372 US-PATENT-CLASS-434-372 US-PATENT-CLASS-434-378 US-PATENT-CLASS-434-38 US-PATENT-CLASS-434-39 US-PATENT-S-324-080 US-PATENT-5-324-080 US-PATENT-5-326-050 US-PATENT-5-326,050 US-PATENT-5-326,050	P 294 P 294 P 280 P 280 P 280 P 280 P 288 P 288 P 288 P 281 P 288	N95-23389 ' N95-23393 ' N95-23393 ' N95-23393 ' N95-23393 ' N95-23393 ' N95-22578 ' N95-22578 ' N95-22578 ' N95-22578 ' N95-23377 ' N95-23377 ' N95-22578 ' N95-23373 ' N95-23393 ' N95-23393 ' N95-23393 ' N95-23393 ' N95-23393 ' N95-23397 ' N95-23397 '
HTN-95-11304 HTN-95-20976 HTN-95-41223 HTN-95-41223 HTN-95-41393 HTN-95-41394 HTN-95-60779 HTN-95-80851 HTN-95-80852 HTN-95-80853 HTN-95-80855 HTN-95-80856 HTN-95-80856 HTN-95-80857 HTN-95-80857 HTN-95-80859 HTN-95-80859 HTN-95-80859 HTN-95-91363 HTN-95-91363 HTN-95-91421 ICASE-95-5 INT-PATENT-CLASS-B64C-11/00 INT-PATENT-CLASS-B64C-19/00 INT-PATENT-CLASS-B64C-5/00	p 319 p 2617 p 317 p 317 p 288 p 283 p 283 p 290 p 290 p 290 p 290 p 290 p 290 p 290 p 290 p 291 p 293 p 283 p 283	A95-77009 A95-77009 A95-74042 A95-75031 A95-75031 A95-75036 A95-76389 A95-75093 A95-75096 A95-75096 A95-75097 A95-75097 A95-75097 A95-75097 A95-75098 A95-75098 A95-75100 A95-75100 A95-75101 A95-76394 A95-77334 N95-23466 #	NASA-CR-189099 NASA-CR-189141 NASA-CR-189146 NASA-CR-189146 NASA-CR-195026 NASA-CR-195026 NASA-CR-195052 NASA-CR-195052 NASA-CR-195421 NASA-CR-195445 NASA-CR-195445 NASA-CR-195445 NASA-CR-197431 NASA-CR-197419 NASA-CR-197419 NASA-CR-197419 NASA-CR-197419 NASA-CR-197419 NASA-CR-197419 NASA-CR-197420 NASA-CR-197440 NASA-CR-197440 NASA-CR-197440 NASA-CR-197440 NASA-CR-197661 NASA-CR-197699 NASA-CR-197704 NASA-CR-197704 NASA-CR-197704 NASA-CR-197704 NASA-CR-197707	p 290 p 316 p 316 p 316 p 325 p 329 p 314 p 273 p 320 p 300 p 300 p 300 p 301 p 303 p 303	N95-24053 * # N95-23792 * # N95-23796 * # N95-23276 * # N95-2366 * # N95-23267 * # N95-23261 * # N95-23183 * # N95-23183 * # N95-23183 * # N95-23183 * # N95-23190 * # N95-23190 * # N95-23190 * # N95-23088 * # N95-23080 * # N95-24032 * # N95-23049 * #	US-PATENT-CLASS-244-77R US-PATENT-CLASS-244-75R US-PATENT-CLASS-340-946 US-PATENT-CLASS-340-946 US-PATENT-CLASS-340-953 US-PATENT-CLASS-340-981 US-PATENT-CLASS-340-981 US-PATENT-CLASS-362-62 US-PATENT-CLASS-362-62 US-PATENT-CLASS-364-578 US-PATENT-CLASS-364-578 US-PATENT-CLASS-364-578 US-PATENT-CLASS-364-578 US-PATENT-CLASS-416-34 US-PATENT-CLASS-416-61 US-PATENT-CLASS-434-307R US-PATENT-CLASS-434-372 US-PATENT-CLASS-434-372 US-PATENT-CLASS-434-372 US-PATENT-CLASS-434-38 US-PATENT-CLASS-434-38 US-PATENT-S-326-050 US-PATENT-S-326-050 US-PATENT-S-326,090 US-PATENT-S-338,990	P 294 P 296 P 280 P 280 P 280 P 280 P 280 P 280 P 288	N95-23389 ' N95-23393 ' N95-23393 ' N95-23393 ' N95-23393 ' N95-22578 ' N95-22578 ' N95-22578 ' N95-22578 ' N95-23377 ' N95-23377 ' N95-22578 ' N95-22578 ' N95-22578 ' N95-23393 ' N95-23393 ' N95-23393 ' N95-23393 ' N95-23395 ' N95-23395 ' N95-23396 ' N95-23397 ' N95-23389 ' N95-23389 ' N95-23389 ' N95-23377 ' N95-22578 '
HTN-95-11304 HTN-95-20976 HTN-95-41219 HTN-95-41223 HTN-95-41393 HTN-95-41394 HTN-95-80851 HTN-95-80852 HTN-95-80853 HTN-95-80855 HTN-95-80856 HTN-95-80856 HTN-95-80857 HTN-95-80857 HTN-95-80858 HTN-95-80859 HTN-95-91363 HTN-95-91421 ICASE-95-5 INT-PATENT-CLASS-B64C-11/00 INT-PATENT-CLASS-B64C-5/00 INT-PATENT-CLASS-B64C-9/16 INT-PATENT-CLASS-B64C-9/16	P 319 P 261 P 317 P 317 P 317 P 283 P 317 P 290 P 290 P 290 P 290 P 283 P 283 P 283 P 283 P 283 P 319 P 311 P 314 P 314 P 386 P 286	A95-77009 A95-77009 A95-74042 A95-75031 A95-75035 A95-76389 A95-75093 A95-75094 A95-75096 A95-75096 A95-75097 A95-75099 A95-75099 A95-75099 A95-75090 A95-75100 A95-75101 A95-76394 A95-77334 N95-23466 # N95-23377 N95-23388 N95-23395 N95-23395 N95-23395	NASA-CR-189099 NASA-CR-189141 NASA-CR-189146 NASA-CR-194972 NASA-CR-195026 NASA-CR-195052 NASA-CR-195052 NASA-CR-195052 NASA-CR-195454 NASA-CR-195454 NASA-CR-195454 NASA-CR-197454 NASA-CR-197454 NASA-CR-197419 NASA-CR-197419 NASA-CR-197420 NASA-CR-197420 NASA-CR-197420 NASA-CR-197439 NASA-CR-197439 NASA-CR-197661 NASA-CR-197661 NASA-CR-197669 NASA-CR-197704 NASA-CR-197704 NASA-CR-197704 NASA-CR-197707 NASA-CR-197867 NASA-CR-197867 NASA-CR-197867 NASA-CR-197931	p 290 p 316 p 316 p 316 p 317 p 317 p 318 p 319	N95-24053 * # N95-23792 * # N95-23776 * # N95-23276 * # N95-22674 * # N95-23267 * # N95-23257 * # N95-23257 * # N95-23267 * # N95-23267 * # N95-23266 * # N95-23766 * # N95-23766 * # N95-2318 * # N95-23183 * # N95-23183 * # N95-23190 * # N95-23190 * # N95-23190 * # N95-23080 * # N95-23670 * # N95-23670 * # N95-23670 * # N95-23182 * # N95-23182 * # N95-23392 * #	US-PATENT-CLASS-244-77R US-PATENT-CLASS-244-75R US-PATENT-CLASS-340-946 US-PATENT-CLASS-340-961 US-PATENT-CLASS-340-961 US-PATENT-CLASS-340-961 US-PATENT-CLASS-340-981 US-PATENT-CLASS-345-8 US-PATENT-CLASS-362-62 US-PATENT-CLASS-363-778 US-PATENT-CLASS-364-778 US-PATENT-CLASS-364-778 US-PATENT-CLASS-395-152 US-PATENT-CLASS-416-34 US-PATENT-CLASS-434-307R US-PATENT-CLASS-434-307R US-PATENT-CLASS-434-378 US-PATENT-CLASS-434-39 US-PATENT-CLASS-434-39 US-PATENT-CLASS-334-318 US-PATENT-5-315-296 US-PATENT-5-315-296 US-PATENT-5-310-311 US-PATENT-5-330-131 US-PATENT-5-330-131	P 294 P 296 P 280 P 280 P 280 P 280 P 280 P 280 P 288	N95-23389 ' N95-23393 ' N95-23393 ' N95-23393 ' N95-23393 ' N95-22578 ' N95-22578 ' N95-22578 ' N95-22578 ' N95-23377 ' N95-23377 ' N95-22578 ' N95-22578 ' N95-22578 ' N95-23393 ' N95-23393 ' N95-23393 ' N95-23393 ' N95-23395 ' N95-23395 ' N95-23396 ' N95-23397 ' N95-23389 ' N95-23389 ' N95-23389 ' N95-23377 ' N95-22578 '
HTN-95-11304 HTN-95-20976 HTN-95-41299 HTN-95-41293 HTN-95-41393 HTN-95-41394 HTN-95-80851 HTN-95-80852 HTN-95-80853 HTN-95-80855 HTN-95-80855 HTN-95-80856 HTN-95-80857 HTN-95-80858 HTN-95-80858 HTN-95-80858 HTN-95-80858 HTN-95-80858 HTN-95-80859 HTN-95-91421 ICASE-95-5 INT-PATENT-CLASS-B64C-11/00 INT-PATENT-CLASS-B64C-9/16 INT-PATENT-CLASS-B64C-9/16 INT-PATENT-CLASS-G08B-21/00 ISBN-92-836-1010-5	P 319 P 261 P 317 P 317 P 288 P 283 P 317 P 290 P 290 P 290 P 290 P 290 P 291 P 283 P 283 P 283 P 283 P 283 P 283 P 284 P 311 P 311 P 294 P 286 P 286 P 280	A95-77009 A95-77009 A95-74042 A95-75031 A95-75031 A95-75036 A95-76389 A95-75096 A95-75096 A95-75097 A95-75097 A95-75097 A95-75097 A95-75097 A95-75098 A95-75098 A95-75100 A95-75100 A95-75101 A95-76394 A95-77334 N95-23466 # N95-23397 N95-23399 N95-23399 N95-23399 N95-23393 N95-23393	NASA-CR-189099 NASA-CR-189141 NASA-CR-189146 NASA-CR-194972 NASA-CR-195026 NASA-CR-195032 NASA-CR-195050 NASA-CR-195050 NASA-CR-195052 NASA-CR-195445 NASA-CR-195445 NASA-CR-195454 NASA-CR-196313 NASA-CR-197419 NASA-CR-197419 NASA-CR-197419 NASA-CR-197419 NASA-CR-197410 NASA-CR-197661 NASA-CR-197661 NASA-CR-197661 NASA-CR-197667 NASA-CR-197667 NASA-CR-197912 NASA-CR-197912 NASA-CR-197938	p 290 p 316 p 316 p 316 p 325 p 329 p 317 p 318 p 323 p 319 p 323 p 329 p 329 p 329 p 329 p 310 p 301	N95-24053 * # N95-23792 * # N95-2376 * # N95-23276 * # N95-23466 * # N95-23466 * # N95-23257 * # N95-23222 * # N95-23266 * # N95-23766 * # N95-23766 * # N95-23766 * # N95-23183 * # N95-23183 * # N95-23190 * # N95-23088 * # N95-23088 * # N95-23088 * # N95-23089 * # N95-23190 * #	US-PATENT-CLASS-244-77R US-PATENT-CLASS-244-75R US-PATENT-CLASS-340-946 US-PATENT-CLASS-340-953 US-PATENT-CLASS-340-961 US-PATENT-CLASS-340-961 US-PATENT-CLASS-340-981 US-PATENT-CLASS-362-62 US-PATENT-CLASS-362-62 US-PATENT-CLASS-362-62 US-PATENT-CLASS-364-578 US-PATENT-CLASS-364-578 US-PATENT-CLASS-364-578 US-PATENT-CLASS-364-578 US-PATENT-CLASS-416-61 US-PATENT-CLASS-416-61 US-PATENT-CLASS-434-372 US-PATENT-CLASS-434-372 US-PATENT-CLASS-373-178H US-PATENT-CLASS-373-178H US-PATENT-5-294-080 US-PATENT-5-5-315-296 US-PATENT-5-5-315-296 US-PATENT-5-5-330,131 US-PATENT-5-320,900 US-PATENT-5-388,990 VPI-E-94-09	P 294 P 294 P 296 P 280 P 280 P 280 P 280 P 280 P 280 P 288 P 280 P 288 P 288 P 286 P 286 P 294 P 311	N95-23389 ' N95-23393 ' N95-23393 ' N95-23393 ' N95-23393 ' N95-22578 ' N95-22578 ' N95-22578 ' N95-23377 ' N95-23377 ' N95-22578 ' N95-23393 ' N95-23393 ' N95-23393 ' N95-23397 ' N95-23397 ' N95-23399 ' N95-23399 ' N95-23399 ' N95-23399 ' N95-23399 ' N95-23377 ' N95-22578 '
HTN-95-11304 HTN-95-20976 HTN-95-41219 HTN-95-41223 HTN-95-41393 HTN-95-41394 HTN-95-80851 HTN-95-80852 HTN-95-80853 HTN-95-80855 HTN-95-80856 HTN-95-80856 HTN-95-80857 HTN-95-80857 HTN-95-80858 HTN-95-80859 HTN-95-91363 HTN-95-91421 ICASE-95-5 INT-PATENT-CLASS-B64C-11/00 INT-PATENT-CLASS-B64C-5/00 INT-PATENT-CLASS-B64C-9/16 INT-PATENT-CLASS-B64C-9/16	P 319 P 261 P 317 P 317 P 288 P 283 P 317 P 290 P 290 P 290 P 290 P 290 P 291 P 283 P 283 P 283 P 283 P 283 P 283 P 284 P 311 P 311 P 294 P 286 P 286 P 280	A95-77009 A95-77009 A95-74042 A95-75031 A95-75031 A95-75036 A95-76389 A95-75096 A95-75096 A95-75097 A95-75097 A95-75097 A95-75097 A95-75097 A95-75098 A95-75098 A95-75100 A95-75100 A95-75101 A95-76394 A95-77334 N95-23466 # N95-23397 N95-23399 N95-23399 N95-23399 N95-23393 N95-23393	NASA-CR-189099 NASA-CR-189141 NASA-CR-189146 NASA-CR-189146 NASA-CR-195026 NASA-CR-195026 NASA-CR-195052 NASA-CR-195052 NASA-CR-195052 NASA-CR-195445 NASA-CR-195445 NASA-CR-195445 NASA-CR-197441 NASA-CR-197419 NASA-CR-197419 NASA-CR-197420 NASA-CR-197420 NASA-CR-197420 NASA-CR-197420 NASA-CR-197440 NASA-CR-197661 NASA-CR-197661 NASA-CR-197661 NASA-CR-197667 NASA-CR-197704 NASA-CR-197704 NASA-CR-197704 NASA-CR-197912 NASA-CR-197912 NASA-CR-197931 NASA-CR-197938 NASA-CR-197944	p 290 p 316 p 316 p 316 p 325 p 329 p 327 p 329 p 329 p 329 p 329 p 329 p 320	N95-24053 * # N95-23792 * # N95-2376 * # N95-23267 * # N95-2366 * # N95-23267 * # N95-23261 * # N95-23183 * # N95-23183 * # N95-23183 * # N95-23190 * # N95-23088 * # N95-23088 * # N95-23088 * # N95-23089 * #	US-PATENT-CLASS-244-77R US-PATENT-CLASS-244-75R US-PATENT-CLASS-340-946 US-PATENT-CLASS-340-946 US-PATENT-CLASS-340-953 US-PATENT-CLASS-340-981 US-PATENT-CLASS-340-981 US-PATENT-CLASS-362-62 US-PATENT-CLASS-362-62 US-PATENT-CLASS-364-578 US-PATENT-CLASS-364-578 US-PATENT-CLASS-364-578 US-PATENT-CLASS-364-578 US-PATENT-CLASS-416-34 US-PATENT-CLASS-416-61 US-PATENT-CLASS-434-307R US-PATENT-CLASS-434-372 US-PATENT-CLASS-434-372 US-PATENT-CLASS-434-372 US-PATENT-CLASS-434-38 US-PATENT-CLASS-434-38 US-PATENT-S-326-050 US-PATENT-S-326-050 US-PATENT-S-326,090 US-PATENT-S-338,990	P 294 P 294 P 296 P 280 P 280 P 280 P 280 P 280 P 280 P 288 P 280 P 288 P 288 P 286 P 286 P 294 P 311	N95-23389 ' N95-23393 ' N95-23393 ' N95-23393 ' N95-23393 ' N95-22578 ' N95-22578 ' N95-22578 ' N95-23377 ' N95-23377 ' N95-22578 ' N95-23393 ' N95-23393 ' N95-23393 ' N95-23397 ' N95-23397 ' N95-23399 ' N95-23399 ' N95-23399 ' N95-23399 ' N95-23377 ' N95-22578 '
HTN-95-11304 HTN-95-11304 HTN-95-20976 HTN-95-41219 HTN-95-41293 HTN-95-41393 HTN-95-41394 HTN-95-80851 HTN-95-80852 HTN-95-80853 HTN-95-80855 HTN-95-80856 HTN-95-80856 HTN-95-80857 HTN-95-80857 HTN-95-80858 HTN-95-91363 HTN-95-91363 HTN-95-91421 ICASE-95-5 INT-PATENT-CLASS-B64C-11/00 INT-PATENT-CLASS-B64C-19/00 INT-PATENT-CLASS-B64C-5/00 INT-PATENT-CLASS-B64C-9/16 INT-PATENT-CLASS-B64C-9/16 INT-PATENT-CLASS-B64C-9/16 INT-PATENT-CLASS-B64C-9/16 INT-PATENT-CLASS-B64C-9/16 INT-PATENT-CLASS-B64C-9/16	. p 319 p 261 p 317 p 317 p 283 p 283 p 290 p 290 p 290 p 290 p 267 p 283 p 283 p 283 p 283 p 283 p 283 p 283 p 283 p 283 p 287 p 319 p 311 p 294 p 296 p 315 p 280 p 280 p 280 p 296 p 296 p 314 p 296 p 296 p 296 p 296 p 315 p 280 p 280 p 296 p 315 p 280 p 280 p 280 p 316 p 296 p 316 p 296 p 296 p 316 p 296 p 296 p 296 p 316 p 296 p 296 p 296 p 316 p 296 p 296 p 296 p 316 p 296 p 296 p 316 p 296 p 296 p 316 p 296 p 316 p 296 p 296 p 316 p 296 p 296 p 316 p 296 p 296 p 296 p 296 p 316 p 296 p 296 p 296 p 296 p 316 p 296 p 29	A95-77009 A95-77009 A95-74042 A95-75031 A95-75035 A95-76389 A95-75036 A95-75093 A95-75094 A95-75096 A95-75096 A95-75097 A95-75099 A95-75099 A95-75099 A95-75090 A95-75100 A95-75101 A95-76394 A95-77334 N95-23466 # N95-23377 N95-23389 N95-23390 N95-23390 N95-23393 N95-23393 N95-23393 N95-23393 N95-23393 N95-23393 N95-23496 #	NASA-CR-189099 NASA-CR-189141 NASA-CR-189146 NASA-CR-194972 NASA-CR-195026 NASA-CR-195052 NASA-CR-195052 NASA-CR-195052 NASA-CR-195454 NASA-CR-1954545 NASA-CR-195454 NASA-CR-195454 NASA-CR-197333 NASA-CR-197333 NASA-CR-197419 NASA-CR-197420 NASA-CR-197420 NASA-CR-197420 NASA-CR-197661 NASA-CR-197699 NASA-CR-197661 NASA-CR-197661 NASA-CR-197699 NASA-CR-197704 NASA-CR-197867 NASA-CR-197931 NASA-CR-197931 NASA-CR-197931 NASA-CR-197938 NASA-CR-197934 NASA-CR-197944 NASA-CR-197944 NASA-CR-197944 NASA-CR-197931 NASA-CR-197938 NASA-CR-197944	p 290 p 316 p 316 p 316 p 317 p 317 p 318 p 319 p 319 p 319 p 319 p 319 p 329 p 329 p 329 p 319 p 310 p	N95-24053 * # N95-23792 * # N95-2376 * # N95-23267 * # N95-22674 * # N95-23267 * # N95-23257 * # N95-23257 * # N95-23267 * # N95-23267 * # N95-23266 * # N95-23462 * # N95-23766 * # N95-23218 * # N95-23218 * # N95-23218 * # N95-23183 * # N95-23190 * # N95-23090 * # N95-23690 * # N95-23410 * # N95-23410 * # N95-23410 * #	US-PATENT-CLASS-244-77R US-PATENT-CLASS-244-75R US-PATENT-CLASS-340-946 US-PATENT-CLASS-340-953 US-PATENT-CLASS-340-961 US-PATENT-CLASS-340-961 US-PATENT-CLASS-340-981 US-PATENT-CLASS-362-62 US-PATENT-CLASS-362-62 US-PATENT-CLASS-362-62 US-PATENT-CLASS-364-578 US-PATENT-CLASS-364-578 US-PATENT-CLASS-364-578 US-PATENT-CLASS-364-578 US-PATENT-CLASS-416-61 US-PATENT-CLASS-416-61 US-PATENT-CLASS-434-372 US-PATENT-CLASS-434-372 US-PATENT-CLASS-373-178H US-PATENT-CLASS-373-178H US-PATENT-5-294-080 US-PATENT-5-5-315-296 US-PATENT-5-5-315-296 US-PATENT-5-5-330,131 US-PATENT-5-320,900 US-PATENT-5-388,990 VPI-E-94-09	P 294 P 294 P 296 P 280 P 280 P 280 P 280 P 280 P 280 P 288 P 280 P 288 P 288 P 286 P 286 P 294 P 311	N95-23389 ' N95-23393 ' N95-23393 ' N95-23393 ' N95-23393 ' N95-22578 ' N95-22578 ' N95-22578 ' N95-23377 ' N95-23377 ' N95-22578 ' N95-23393 ' N95-23393 ' N95-23393 ' N95-23397 ' N95-23397 ' N95-23399 ' N95-23399 ' N95-23399 ' N95-23399 ' N95-23377 ' N95-22578 '
HTN-95-11304 HTN-95-10976 HTN-95-41219 HTN-95-41223 HTN-95-41393 HTN-95-41394 HTN-95-80851 HTN-95-80852 HTN-95-80853 HTN-95-80855 HTN-95-80856 HTN-95-80856 HTN-95-80857 HTN-95-80858 HTN-95-80858 HTN-95-80858 HTN-95-80858 HTN-95-80859 HTN-95-80859 HTN-95-80859 HTN-95-91363 HTN-95-91421 ICASE-95-5 INT-PATENT-CLASS-B64C-11/00 INT-PATENT-CLASS-B64C-9/16	P 319 P 261 P 317 P 317 P 288 P 283 P 317 P 290 P 290 P 290 P 290 P 283 P 283 P 283 P 283 P 283 P 283 P 284 P 314 P 314 P 314 P 386 P 286 P 286 P 280	A95-77009 A95-77009 A95-74042 * A95-75031 * A95-75031 * A95-75035 A95-76389 A95-75396 A95-75096 * A95-75097 * A95-75097 * A95-75097 * A95-75098 A95-75099 * A95-75100 A95-75100 A95-75101 A95-7334  N95-23466 * # N95-23390 * N95-23393 * N95-23393 * N95-23496 # N95-23496 #	NASA-CR-189099 NASA-CR-189141 NASA-CR-189146 NASA-CR-189146 NASA-CR-195026 NASA-CR-195026 NASA-CR-195052 NASA-CR-195052 NASA-CR-195052 NASA-CR-195445 NASA-CR-195445 NASA-CR-195445 NASA-CR-197441 NASA-CR-197419 NASA-CR-197419 NASA-CR-197420 NASA-CR-197420 NASA-CR-197420 NASA-CR-197420 NASA-CR-197440 NASA-CR-197661 NASA-CR-197661 NASA-CR-197661 NASA-CR-197667 NASA-CR-197704 NASA-CR-197704 NASA-CR-197704 NASA-CR-197912 NASA-CR-197912 NASA-CR-197931 NASA-CR-197938 NASA-CR-197944	p 290 p 316 p 316 p 316 p 325 p 329 p 317 p 323 p 310 p 323 p 320 p	N95-24053 * # N95-23792 * # N95-2376 * # N95-23267 * # N95-23466 * # N95-23466 * # N95-23257 * # N95-23222 * # N95-23266 * # N95-23766 * # N95-23766 * # N95-23766 * # N95-23183 * # N95-23183 * # N95-23183 * # N95-23190 * # N95-23199 * # N95-23199 * # N95-23199 * # N95-23088 * # N95-23088 * # N95-23088 * # N95-23089 * # N95-23089 * # N95-23670 * # N95-23669 * # N95-23690 * #	US-PATENT-CLASS-244-77R US-PATENT-CLASS-244-75R US-PATENT-CLASS-340-946 US-PATENT-CLASS-340-953 US-PATENT-CLASS-340-961 US-PATENT-CLASS-340-961 US-PATENT-CLASS-340-981 US-PATENT-CLASS-362-62 US-PATENT-CLASS-362-62 US-PATENT-CLASS-362-62 US-PATENT-CLASS-364-578 US-PATENT-CLASS-364-578 US-PATENT-CLASS-364-578 US-PATENT-CLASS-364-578 US-PATENT-CLASS-416-61 US-PATENT-CLASS-416-61 US-PATENT-CLASS-434-372 US-PATENT-CLASS-434-372 US-PATENT-CLASS-373-178H US-PATENT-CLASS-373-178H US-PATENT-5-294-080 US-PATENT-5-5-315-296 US-PATENT-5-5-315-296 US-PATENT-5-5-330,131 US-PATENT-5-320,900 US-PATENT-5-388,990 VPI-E-94-09	P 294 P 294 P 296 P 280 P 280 P 280 P 280 P 280 P 280 P 288 P 280 P 288 P 288 P 286 P 286 P 294 P 311	N95-23389 ' N95-23393 ' N95-23393 ' N95-23393 ' N95-23393 ' N95-22578 ' N95-22578 ' N95-22578 ' N95-23377 ' N95-23377 ' N95-22578 ' N95-23393 ' N95-23393 ' N95-23393 ' N95-23397 ' N95-23397 ' N95-23399 ' N95-23399 ' N95-23399 ' N95-23399 ' N95-23377 ' N95-22578 '
HTN-95-11304 HTN-95-11304 HTN-95-20976 HTN-95-41223 HTN-95-41293 HTN-95-41393 HTN-95-41394 HTN-95-80851 HTN-95-80852 HTN-95-80853 HTN-95-80855 HTN-95-80856 HTN-95-80856 HTN-95-80857 HTN-95-80858 HTN-95-80859 HTN-95-80859 HTN-95-80859 HTN-95-91363 HTN-95-91363 HTN-95-91421 ICASE-95-5 INT-PATENT-CLASS-B64C-11/00 INT-PATENT-CLASS-B64C-9/16	. p 319 P 261 P 317 P 317 P 283 P 283 P 290 P 290 P 290 P 290 P 267 P 283 P 283 P 283 P 283 P 319 P 314 P 314 P 296 P 286 P 28	A95-77009 A95-74042 * A95-75031 * A95-75031 * A95-75035 A95-76389 A95-75396 A95-75094 A95-75094 A95-75096 * A95-75097 * A95-75097 * A95-75099 * A95-75099 * A95-75090 * A95-7334 * N95-23466 * M95-23380 * N95-23380 * N95-23390 * N95-23390 * N95-23390 * N95-23496 # N95-23496 # N95-23496 # N95-23496 #	NASA-CR-189099 NASA-CR-189141 NASA-CR-189146 NASA-CR-194972 NASA-CR-195026 NASA-CR-195052 NASA-CR-195052 NASA-CR-195052 NASA-CR-195052 NASA-CR-195454 NASA-CR-195454 NASA-CR-195454 NASA-CR-195454 NASA-CR-197833 NASA-CR-197833 NASA-CR-197419 NASA-CR-197420 NASA-CR-197420 NASA-CR-197420 NASA-CR-197420 NASA-CR-197661 NASA-CR-197699 NASA-CR-197661 NASA-CR-197699 NASA-CR-197931 NASA-CR-197931 NASA-CR-197931 NASA-CR-197931 NASA-CR-197934 NASA-CR-197934 NASA-CR-197934 NASA-CR-197934 NASA-CR-197934 NASA-CR-197934 NASA-CR-197934 NASA-CR-197934 NASA-CR-197944 NASA-CR-197944 NASA-CR-197944 NASA-CR-197944 NASA-CR-197944 NASA-CR-197944 NASA-CR-197944 NASA-CR-197944 NASA-CR-197940 NASA-CR-197944 NASA-CR-197940 NASA-CR-197944 NASA-CR-197940 NASA-CR-197940 NASA-CR-197940 NASA-CR-197940 NASA-CR-197940 NASA-CR-197940 NASA-CR-197940 NASA-CR-19650 NASA-CR-4650	p 290 p 316 p 316 p 316 p 317 p 317 p 318 p 319 p 319 p 319 p 319 p 329 p 329 p 329 p 329 p 329 p 310 p 329 p 310 p 310 p 389 p 310 p 389 p 273 p 273 p 273 p 273 p 273	N95-24053 * # N95-23792 * # N95-23766 * # N95-23266 * # N95-23267 * # N95-23268 * # N95-23183 * # N95-23190 * #	US-PATENT-CLASS-244-77R US-PATENT-CLASS-244-75R US-PATENT-CLASS-340-946 US-PATENT-CLASS-340-953 US-PATENT-CLASS-340-961 US-PATENT-CLASS-340-961 US-PATENT-CLASS-340-981 US-PATENT-CLASS-362-62 US-PATENT-CLASS-362-62 US-PATENT-CLASS-362-62 US-PATENT-CLASS-364-578 US-PATENT-CLASS-364-578 US-PATENT-CLASS-364-578 US-PATENT-CLASS-364-578 US-PATENT-CLASS-416-61 US-PATENT-CLASS-416-61 US-PATENT-CLASS-434-372 US-PATENT-CLASS-434-372 US-PATENT-CLASS-373-178H US-PATENT-CLASS-373-178H US-PATENT-5-294-080 US-PATENT-5-5-315-296 US-PATENT-5-5-315-296 US-PATENT-5-5-330,131 US-PATENT-5-320,900 US-PATENT-5-388,990 VPI-E-94-09	P 294 P 294 P 296 P 280 P 280 P 280 P 280 P 280 P 280 P 288 P 280 P 288 P 288 P 286 P 286 P 294 P 311	N95-23389 ' N95-23393 ' N95-23393 ' N95-23393 ' N95-23393 ' N95-22578 ' N95-22578 ' N95-22578 ' N95-23377 ' N95-23377 ' N95-22578 ' N95-23393 ' N95-23393 ' N95-23393 ' N95-23397 ' N95-23397 ' N95-23399 ' N95-23399 ' N95-23399 ' N95-23399 ' N95-23377 ' N95-22578 '
HTN-95-11304 HTN-95-10976 HTN-95-41219 HTN-95-41223 HTN-95-41393 HTN-95-41394 HTN-95-80851 HTN-95-80852 HTN-95-80853 HTN-95-80855 HTN-95-80856 HTN-95-80856 HTN-95-80857 HTN-95-80858 HTN-95-80859 HTN-95-80859 HTN-95-91363 HTN-95-91421 ICASE-95-5 INT-PATENT-CLASS-B64C-11/00 INT-PATENT-CLASS-B64C-9/16 INT-PATENT-CLASS-B64C-9/16 INT-PATENT-CLASS-B64C-9/16 INT-PATENT-CLASS-B64C-9/16 INT-PATENT-CLASS-B64C-9/16 INT-PATENT-CLASS-B64C-9/16 INT-PATENT-CLASS-B64C-9/16 INT-PATENT-CLASS-B64C-9/16 INT-PATENT-CLASS-B64C-19/00 INT-PATENT-CLASS-B64C-19/00 INT-PATENT-CLASS-B64C-19/10 INT-PATENT-CLASS-B64C-11/00 INT-PATENT-CLASS-	. p 319 . p 261 . p 317 . p 317 . p 283 . p 283 . p 290 . p 290 . p 290 . p 267 . p 283 . p 283 . p 283 . p 283 . p 283 . p 281 . p 319 . p 314 . p 314 . p 294 . p 296 . p 286 . p 319 . p 315 . p 319 . p 315 . p 319 . p 316 . p 316 . p 317 . p 316 . p 317 . p 316 . p 317 . p 316 . p 317 . p 317 . p 318 . p 319 . p 319 . p 319 . p 316 . p 316 . p 317 . p 316 . p 317 . p 317 . p 318 . p 319 . p 319 . p 319 . p 316 . p 316 . p 317 . p 316 . p 317 . p 317 . p 318 . p 319 . p 319	A95-77009 A95-74042 * A95-75031 * A95-75031 * A95-75035 A95-76389 A95-75396 A95-75096 * A95-75096 * A95-75096 * A95-75097 * A95-75097 * A95-75099 * A95-75099 * A95-75100 A95-75100 A95-75100 A95-75100 A95-7334 A95-77334  N95-23466 * # N95-23390 * N95-23390 * N95-23390 * N95-23496 # N95-23496 # N95-23496 # N95-23496 # N95-23496 # N95-23496 #	NASA-CR-189099 NASA-CR-189141 NASA-CR-189146 NASA-CR-194972 NASA-CR-195026 NASA-CR-195022 NASA-CR-195050 NASA-CR-195050 NASA-CR-195052 NASA-CR-195445 NASA-CR-195445 NASA-CR-195445 NASA-CR-197451 NASA-CR-197419 NASA-CR-197419 NASA-CR-197420 NASA-CR-197420 NASA-CR-197420 NASA-CR-197421 NASA-CR-197438 NASA-CR-197438 NASA-CR-197461 NASA-CR-197661 NASA-CR-197661 NASA-CR-197661 NASA-CR-197661 NASA-CR-197699 NASA-CR-197697 NASA-CR-197901 NASA-CR-197912 NASA-CR-197912 NASA-CR-197913 NASA-CR-197931 NASA-CR-197934 NASA-CR-197934 NASA-CR-1650 NASA-CR-4650 NASA-CR-4650 NASA-CR-4651	p 290 p 316 p 316 p 316 p 317 p 319	N95-24053 * # N95-23792 * # N95-23766 * # N95-22676 * # N95-23666 * # N95-23193 * # N95-23267 * # N95-23227 * # N95-23266 * # N95-23766 * # N95-23766 * # N95-23183 * # N95-23183 * # N95-23183 * # N95-23190 * #	US-PATENT-CLASS-244-77R US-PATENT-CLASS-244-75R US-PATENT-CLASS-340-946 US-PATENT-CLASS-340-953 US-PATENT-CLASS-340-961 US-PATENT-CLASS-340-961 US-PATENT-CLASS-340-981 US-PATENT-CLASS-362-62 US-PATENT-CLASS-362-62 US-PATENT-CLASS-362-62 US-PATENT-CLASS-364-578 US-PATENT-CLASS-364-578 US-PATENT-CLASS-364-578 US-PATENT-CLASS-364-578 US-PATENT-CLASS-416-61 US-PATENT-CLASS-416-61 US-PATENT-CLASS-434-372 US-PATENT-CLASS-434-372 US-PATENT-CLASS-373-178H US-PATENT-CLASS-373-178H US-PATENT-5-294-080 US-PATENT-5-5-315-296 US-PATENT-5-5-315-296 US-PATENT-5-5-330,131 US-PATENT-5-320,900 US-PATENT-5-388,990 VPI-E-94-09	P 294 P 294 P 296 P 280 P 280 P 280 P 280 P 280 P 280 P 288 P 280 P 288 P 288 P 286 P 286 P 294 P 311	N95-23389 ' N95-23393 ' N95-23393 ' N95-23393 ' N95-23393 ' N95-22578 ' N95-22578 ' N95-22578 ' N95-23377 ' N95-23377 ' N95-22578 ' N95-23393 ' N95-23393 ' N95-23393 ' N95-23397 ' N95-23397 ' N95-23399 ' N95-23399 ' N95-23399 ' N95-23399 ' N95-23377 ' N95-22578 '
HTN-95-11304 HTN-95-11304 HTN-95-20976 HTN-95-41219 HTN-95-41223 HTN-95-41393 HTN-95-41394 HTN-95-80851 HTN-95-80852 HTN-95-80853 HTN-95-80855 HTN-95-80855 HTN-95-80856 HTN-95-80856 HTN-95-80857 HTN-95-80859 HTN-95-80859 HTN-95-80859 HTN-95-91363 HTN-95-91363 HTN-95-91421 ICASE-95-5 INT-PATENT-CLASS-B64C-11/00 INT-PATENT-CLASS-B64C-9/16	. p 319 p 261 p 317 p 317 p 283 p 283 p 290 p 290 p 290 p 267 p 283 p 267 p 314 p 314 p 314 p 286 p 286	A95-77009 A95-77009 A95-74042 A95-75031 A95-75031 A95-75036 A95-75090 A95-75094 A95-75095 A95-75096 A95-75097 A95-75099 A95-75099 A95-75099 A95-75090 A95-7304 A95-7334 A95-7334 A95-7334 A95-23466 # N95-23389 N95-23390 N95-23390 N95-23390 N95-23496 # N95-23602 # N95-23602 # N95-23602 # N95-23602 # N95-2310	NASA-CR-189099 NASA-CR-189141 NASA-CR-189146 NASA-CR-194972 NASA-CR-195026 NASA-CR-195026 NASA-CR-195052 NASA-CR-195052 NASA-CR-195052 NASA-CR-195445 NASA-CR-195445 NASA-CR-195445 NASA-CR-195445 NASA-CR-197419 NASA-CR-197419 NASA-CR-197419 NASA-CR-197420 NASA-CR-197420 NASA-CR-197420 NASA-CR-197440 NASA-CR-197661 NASA-CR-197661 NASA-CR-197661 NASA-CR-197661 NASA-CR-197704 NASA-CR-197667 NASA-CR-197912 NASA-CR-197912 NASA-CR-197912 NASA-CR-197931 NASA-CR-197944 NASA-CR-197944 NASA-CR-197944 NASA-CR-197944 NASA-CR-197944 NASA-CR-197944 NASA-CR-197944 NASA-CR-4650 NASA-CR-4650 NASA-CR-4650 NASA-CR-4651	p 290 p 316 p 316 p 316 p 325 p 329 p 327 p 329 p 329 p 329 p 329 p 329 p 339 p 330 p 301 p 301 p 301 p 301 p 301 p 302 p 303 p 285 p 293 p 293 p 293 p 293 p 273 p 273 p 273	N95-24053 * # N95-23792 * # N95-23792 * # N95-23276 * # N95-23267 * # N95-23266 * # N95-23257 * # N95-23267 * # N95-23267 * # N95-23267 * # N95-23267 * # N95-23261 * # N95-23183 * # N95-23183 * # N95-23183 * # N95-23190 * # N95-23185 * # N95-23095 * # N95-24025 * #	US-PATENT-CLASS-244-77R US-PATENT-CLASS-244-75R US-PATENT-CLASS-340-946 US-PATENT-CLASS-340-953 US-PATENT-CLASS-340-961 US-PATENT-CLASS-340-961 US-PATENT-CLASS-340-981 US-PATENT-CLASS-362-62 US-PATENT-CLASS-362-62 US-PATENT-CLASS-362-62 US-PATENT-CLASS-364-578 US-PATENT-CLASS-364-578 US-PATENT-CLASS-364-578 US-PATENT-CLASS-364-578 US-PATENT-CLASS-416-61 US-PATENT-CLASS-416-61 US-PATENT-CLASS-434-372 US-PATENT-CLASS-434-372 US-PATENT-CLASS-373-178H US-PATENT-CLASS-373-178H US-PATENT-5-294-080 US-PATENT-5-5-315-296 US-PATENT-5-5-315-296 US-PATENT-5-5-330,131 US-PATENT-5-320,900 US-PATENT-5-388,990 VPI-E-94-09	P 294 P 294 P 296 P 280 P 280 P 280 P 280 P 280 P 280 P 288 P 280 P 288 P 288 P 286 P 286 P 294 P 311	N95-23389 ' N95-23393 ' N95-23393 ' N95-23393 ' N95-23393 ' N95-22578 ' N95-22578 ' N95-22578 ' N95-23377 ' N95-23377 ' N95-22578 ' N95-23393 ' N95-23393 ' N95-23393 ' N95-23397 ' N95-23397 ' N95-23399 ' N95-23399 ' N95-23399 ' N95-23399 ' N95-23377 ' N95-22578 '
HTN-95-11304 HTN-95-10976 HTN-95-41219 HTN-95-41223 HTN-95-41393 HTN-95-41394 HTN-95-80851 HTN-95-80852 HTN-95-80853 HTN-95-80855 HTN-95-80856 HTN-95-80856 HTN-95-80857 HTN-95-80858 HTN-95-80859 HTN-95-80859 HTN-95-91363 HTN-95-91421 ICASE-95-5 INT-PATENT-CLASS-B64C-11/00 INT-PATENT-CLASS-B64C-9/16 INT-PATENT-CLASS-B64C-9/16 INT-PATENT-CLASS-B64C-9/16 INT-PATENT-CLASS-B64C-9/16 INT-PATENT-CLASS-B64C-9/16 INT-PATENT-CLASS-B64C-9/16 INT-PATENT-CLASS-B64C-9/16 INT-PATENT-CLASS-B64C-9/16 INT-PATENT-CLASS-B64C-19/00 INT-PATENT-CLASS-B64C-19/00 INT-PATENT-CLASS-B64C-19/10 INT-PATENT-CLASS-B64C-11/00 INT-PATENT-CLASS-	. p 319 p 261 p 317 p 317 p 283 p 283 p 290 p 290 p 290 p 267 p 283 p 267 p 314 p 314 p 314 p 286 p 286	A95-77009 A95-77009 A95-74042 A95-75031 A95-75031 A95-75036 A95-75090 A95-75094 A95-75095 A95-75096 A95-75097 A95-75099 A95-75099 A95-75099 A95-75090 A95-7304 A95-7334 A95-7334 A95-7334 A95-23466 # N95-23389 N95-23390 N95-23390 N95-23390 N95-23496 # N95-23602 # N95-23602 # N95-23602 # N95-23602 # N95-2310	NASA-CR-189099 NASA-CR-189141 NASA-CR-189146 NASA-CR-189120 NASA-CR-195026 NASA-CR-195026 NASA-CR-195050 NASA-CR-195052 NASA-CR-195052 NASA-CR-195454 NASA-CR-195454 NASA-CR-195454 NASA-CR-195454 NASA-CR-197833 NASA-CR-197833 NASA-CR-197419 NASA-CR-197420 NASA-CR-197420 NASA-CR-197420 NASA-CR-197420 NASA-CR-197420 NASA-CR-197611 NASA-CR-197699 NASA-CR-197661 NASA-CR-197661 NASA-CR-197699 NASA-CR-197699 NASA-CR-197931 NASA-CR-197912 NASA-CR-197931 NASA-CR-197931 NASA-CR-197934 NASA-CR-197934 NASA-CR-197934 NASA-CR-197934 NASA-CR-197934 NASA-CR-197934 NASA-CR-197944 NASA-CR-4649 NASA-CR-4650 NASA-CR-4651 NASA-TM-106764 NASA-TM-106764 NASA-TM-106764 NASA-TM-106764 NASA-TM-106764 NASA-TM-106764	p 290 p 316 p 316 p 316 p 317 p 325 p 327 p 328 p 329	N95-24053 * # N95-23792 * # N95-2376 * # N95-23276 * # N95-23266 * # N95-23257 * # N95-23257 * # N95-23267 * # N95-23267 * # N95-23267 * # N95-23267 * # N95-23268 * # N95-23183 * # N95-23190 * #	US-PATENT-CLASS-244-77R US-PATENT-CLASS-244-75R US-PATENT-CLASS-340-946 US-PATENT-CLASS-340-953 US-PATENT-CLASS-340-961 US-PATENT-CLASS-340-961 US-PATENT-CLASS-340-981 US-PATENT-CLASS-362-62 US-PATENT-CLASS-362-62 US-PATENT-CLASS-362-62 US-PATENT-CLASS-364-578 US-PATENT-CLASS-364-578 US-PATENT-CLASS-364-578 US-PATENT-CLASS-364-578 US-PATENT-CLASS-416-61 US-PATENT-CLASS-416-61 US-PATENT-CLASS-434-372 US-PATENT-CLASS-434-372 US-PATENT-CLASS-373-178H US-PATENT-CLASS-373-178H US-PATENT-5-294-080 US-PATENT-5-5-315-296 US-PATENT-5-5-315-296 US-PATENT-5-5-330,131 US-PATENT-5-320,900 US-PATENT-5-388,990 VPI-E-94-09	P 294 P 294 P 296 P 280 P 280 P 280 P 280 P 280 P 280 P 288 P 280 P 288 P 288 P 286 P 286 P 294 P 311	N95-23389 ' N95-23393 ' N95-23393 ' N95-23393 ' N95-23393 ' N95-22578 ' N95-22578 ' N95-22578 ' N95-23377 ' N95-23377 ' N95-22578 ' N95-23393 ' N95-23393 ' N95-23393 ' N95-23397 ' N95-23397 ' N95-23399 ' N95-23399 ' N95-23399 ' N95-23399 ' N95-23377 ' N95-22578 '
HTN-95-11304 HTN-95-10976 HTN-95-41219 HTN-95-41223 HTN-95-41393 HTN-95-41394 HTN-95-80851 HTN-95-80852 HTN-95-80853 HTN-95-80856 HTN-95-80856 HTN-95-80857 HTN-95-80857 HTN-95-80858 HTN-95-80858 HTN-95-80859 HTN-95-80859 HTN-95-80859 HTN-95-80859 HTN-95-80859 HTN-95-80850 HTN-95-80850 HTN-95-80859 HTN-95-91421 ICASE-95-5 INT-PATENT-CLASS-B64C-11/00 INT-PATENT-CLASS-B64C-9/16 INT-PATENT-CLASS-B64C-9/16 INT-PATENT-CLASS-G08B-21/00 ISBN-92-836-1010-5 ISBN-92-836-1011-3 L-17233 L-17348 L-17348 L-17348	P 319 P 261 P 317 P 317 P 288 P 283 P 317 P 290 P 290 P 290 P 290 P 283 P 286 P 314 P 314 P 314 P 286 P 286 P 280 P 315 P 302 P 285 P 309 P 310 P 272 P 324	A95-77009 A95-77009 A95-77001 A95-75031 A95-75031 A95-75036 A95-75030 A95-75093 A95-75096 A95-75096 A95-75097 A95-75097 A95-75098 A95-75099 A95-75101 A95-75099 A95-75101 A95-76394 A95-77334 N95-23466 # N95-23397 N95-23393 N95-23393 N95-23393 N95-23393 N95-23496 # N95-23496 # N95-23496 # N95-23496 # N95-23496 # N95-23502 # N95-23210 # N95-23210 # N95-23210 # N95-23210 # N95-23202 # N95-23202 # N95-23202 # N95-23202 #	NASA-CR-189099 NASA-CR-189141 NASA-CR-189146 NASA-CR-194972 NASA-CR-195032 NASA-CR-195050 NASA-CR-195050 NASA-CR-195052 NASA-CR-195451 NASA-CR-1954545 NASA-CR-1954545 NASA-CR-197457 NASA-CR-197419 NASA-CR-197419 NASA-CR-197420 NASA-CR-197420 NASA-CR-197420 NASA-CR-197439 NASA-CR-197439 NASA-CR-197461 NASA-CR-197661 NASA-CR-197661 NASA-CR-197667 NASA-CR-197667 NASA-CR-197931 NASA-CR-197944 NASA-CR-1650 NASA-CR-4650 NASA-CR-4650 NASA-CR-4651 NASA-TM-106847 NASA-TM-106847 NASA-TM-106847 NASA-TM-106847 NASA-TM-106847	p 290 p 316 p 316 p 316 p 317 p 319 p 319 p 319 p 323 p 310 p 323 p 329 p 329 p 329 p 329 p 310 p 321 p 310 p 321 p 329 p 329 p 329 p 329 p 273	N95-24053 * # N95-23792 * # N95-23767 * # N95-23267 * # N95-2366 * # N95-23468 * # N95-23257 * # N95-23222 * # N95-23266 * # N95-23468 * # N95-23468 * # N95-23766 * # N95-23218 * # N95-23183 * # N95-23183 * # N95-23190 * # N95-23680 * # N95-23410 * # N95-23450 * # N95-23185 * # N95-23055 * # N95-22966 * # N95-22669 * # N95-22669 * # N95-22669 * # N95-23259 * #	US-PATENT-CLASS-244-77R US-PATENT-CLASS-244-75R US-PATENT-CLASS-340-946 US-PATENT-CLASS-340-953 US-PATENT-CLASS-340-961 US-PATENT-CLASS-340-961 US-PATENT-CLASS-340-981 US-PATENT-CLASS-362-62 US-PATENT-CLASS-362-62 US-PATENT-CLASS-362-62 US-PATENT-CLASS-364-578 US-PATENT-CLASS-364-578 US-PATENT-CLASS-364-578 US-PATENT-CLASS-364-578 US-PATENT-CLASS-416-61 US-PATENT-CLASS-416-61 US-PATENT-CLASS-434-372 US-PATENT-CLASS-434-372 US-PATENT-CLASS-373-178H US-PATENT-CLASS-373-178H US-PATENT-5-294-080 US-PATENT-5-5-315-296 US-PATENT-5-5-315-296 US-PATENT-5-5-330,131 US-PATENT-5-320,900 US-PATENT-5-388,990 VPI-E-94-09	P 294 P 294 P 296 P 280 P 280 P 280 P 280 P 280 P 280 P 288 P 280 P 288 P 288 P 286 P 286 P 294 P 311	N95-23389 ' N95-23393 ' N95-23393 ' N95-23393 ' N95-23393 ' N95-22578 ' N95-22578 ' N95-22578 ' N95-23377 ' N95-23377 ' N95-22578 ' N95-23393 ' N95-23393 ' N95-23393 ' N95-23397 ' N95-23397 ' N95-23399 ' N95-23399 ' N95-23399 ' N95-23399 ' N95-23377 ' N95-22578 '
HTN-95-11304 HTN-95-11304 HTN-95-20976 HTN-95-41219 HTN-95-41223 HTN-95-41393 HTN-95-41394 HTN-95-80851 HTN-95-80852 HTN-95-80853 HTN-95-80855 HTN-95-80855 HTN-95-80856 HTN-95-80856 HTN-95-80857 HTN-95-80859 HTN-95-80859 HTN-95-80859 HTN-95-91363 HTN-95-91363 HTN-95-91421 ICASE-95-5 INT-PATENT-CLASS-B64C-11/00 INT-PATENT-CLASS-B64C-9/16	P 319 P 261 P 317 P 317 P 288 P 283 P 317 P 290 P 290 P 290 P 290 P 283 P 286 P 314 P 314 P 314 P 286 P 286 P 280 P 315 P 302 P 285 P 309 P 310 P 272 P 324	A95-77009 A95-77009 A95-77001 A95-75031 A95-75031 A95-75036 A95-75030 A95-75093 A95-75096 A95-75096 A95-75097 A95-75097 A95-75098 A95-75099 A95-75101 A95-75099 A95-75101 A95-76394 A95-77334 N95-23466 # N95-23397 N95-23393 N95-23393 N95-23393 N95-23393 N95-23496 # N95-23496 # N95-23496 # N95-23496 # N95-23496 # N95-23502 # N95-23210 # N95-23210 # N95-23210 # N95-23210 # N95-23202 # N95-23202 # N95-23202 # N95-23202 #	NASA-CR-189099 NASA-CR-189141 NASA-CR-189146 NASA-CR-189146 NASA-CR-195026 NASA-CR-195026 NASA-CR-195052 NASA-CR-195052 NASA-CR-195052 NASA-CR-195445 NASA-CR-195445 NASA-CR-195445 NASA-CR-197441 NASA-CR-197419 NASA-CR-197419 NASA-CR-197420 NASA-CR-197420 NASA-CR-197420 NASA-CR-197440 NASA-CR-197440 NASA-CR-19740 NASA-CR-19740 NASA-CR-19740 NASA-CR-197699 NASA-CR-197699 NASA-CR-197704 NASA-CR-197691 NASA-CR-197912 NASA-CR-197912 NASA-CR-197931 NASA-CR-197931 NASA-CR-197934 NASA-CR-197934 NASA-CR-197934 NASA-CR-4650 NASA-CR-4650 NASA-CR-4650 NASA-TM-106847 NASA-TM-106847 NASA-TM-106847 NASA-TM-106847 NASA-TM-106870 NASA-TM-106870	p 290 p 316 p 316 p 316 p 317 p 325 p 327 p 327 p 328 p 329 p 329 p 329 p 330 p 330 p 330 p 331 p 331 p 331 p 331 p 283 p 330 p 330 p 330 p 323 p 330 p 323 p 330 p 323 p 273 p 262 p 309 p 309 p 309 p 309 p 309 p 320 p 323	N95-24053 * # N95-23792 * # N95-23792 * # N95-23764 * # N95-23767 * # N95-23267 * # N95-23261 * # N95-23180 * # N95-23180 * # N95-23180 * # N95-23190 * # N95-23190 * # N95-23190 * # N95-23190 * # N95-23182 * # N95-23182 * # N95-23182 * # N95-23182 * # N95-23185 * # N95-23185 * # N95-23185 * # N95-23095 * # N95-23185 * # N95-23185 * # N95-23095 * # N95-23185 * #	US-PATENT-CLASS-244-77R US-PATENT-CLASS-244-75R US-PATENT-CLASS-340-946 US-PATENT-CLASS-340-953 US-PATENT-CLASS-340-961 US-PATENT-CLASS-340-961 US-PATENT-CLASS-340-981 US-PATENT-CLASS-362-62 US-PATENT-CLASS-362-62 US-PATENT-CLASS-362-62 US-PATENT-CLASS-364-578 US-PATENT-CLASS-364-578 US-PATENT-CLASS-364-578 US-PATENT-CLASS-364-578 US-PATENT-CLASS-416-61 US-PATENT-CLASS-416-61 US-PATENT-CLASS-434-372 US-PATENT-CLASS-434-372 US-PATENT-CLASS-373-178H US-PATENT-CLASS-373-178H US-PATENT-5-294-080 US-PATENT-5-5-315-296 US-PATENT-5-5-315-296 US-PATENT-5-5-330,131 US-PATENT-5-320,900 US-PATENT-5-388,990 VPI-E-94-09	P 294 P 294 P 296 P 280 P 280 P 280 P 280 P 280 P 280 P 288 P 280 P 288 P 288 P 286 P 286 P 294 P 311	N95-23389 ' N95-23393 ' N95-23393 ' N95-23393 ' N95-23393 ' N95-22578 ' N95-22578 ' N95-22578 ' N95-23377 ' N95-23377 ' N95-22578 ' N95-23393 ' N95-23393 ' N95-23393 ' N95-23397 ' N95-23397 ' N95-23399 ' N95-23399 ' N95-23399 ' N95-23399 ' N95-23377 ' N95-22578 '
HTN-95-11304 HTN-95-10976 HTN-95-41219 HTN-95-41223 HTN-95-41393 HTN-95-41394 HTN-95-80851 HTN-95-80852 HTN-95-80853 HTN-95-80855 HTN-95-80856 HTN-95-80856 HTN-95-80857 HTN-95-80857 HTN-95-80858 HTN-95-80859 HTN-95-91363 HTN-95-91421 ICASE-95-5 INT-PATENT-CLASS-B64C-11/00 INT-PATENT-CLASS-B64C-19/00 INT-PATENT-CLASS-B64C-91/00 INT-PATENT-CLASS-B64C-91/00 INT-PATENT-CLASS-B64C-91/00 INT-PATENT-CLASS-B64C-91/00 INT-PATENT-CLASS-B64C-91/00 INT-PATENT-CLASS-B64C-91/00 INT-PATENT-CLASS-B64C-91/10 INT-PATEN	P 319 P 261 P 317 P 317 P 317 P 283 P 317 P 290 P 290 P 290 P 290 P 293 P 283 P 283 P 283 P 287 P 314 P 311 P 294 P 280 P 280 P 315 P 302 P 302 P 300	A95-77009 A95-77009 A95-74042 * A95-75031 * A95-75031 * A95-75035 A95-76389 A95-75390 A95-75094 A95-75096 * A95-75096 * A95-75097 * A95-75097 * A95-75099 * A95-75099 * A95-75100 A95-75100 A95-75100 A95-75100 A95-7534 A95-77334 A95-77334 A95-77334 S95-23390 * N95-23390 * N95-23390 * N95-23390 * N95-23496 # N95-23496 # N95-23496 # N95-23015 * N95-23015 * N95-23015 * N95-23015 * N95-23015 * N95-23016 # N95-23016 #	NASA-CR-189099 NASA-CR-189141 NASA-CR-189146 NASA-CR-189120 NASA-CR-195026 NASA-CR-195026 NASA-CR-195050 NASA-CR-195052 NASA-CR-195052 NASA-CR-195451 NASA-CR-195454 NASA-CR-195454 NASA-CR-195454 NASA-CR-197833 NASA-CR-197833 NASA-CR-197419 NASA-CR-197419 NASA-CR-197420 NASA-CR-197420 NASA-CR-197420 NASA-CR-197420 NASA-CR-197420 NASA-CR-197419 NASA-CR-197681 NASA-CR-197681 NASA-CR-197889 NASA-CR-197939 NASA-CR-197959 NASA-CR-197912 NASA-CR-197912 NASA-CR-197931 NASA-CR-197931 NASA-CR-197934 NASA-CR-197934 NASA-CR-197934 NASA-CR-197934 NASA-CR-197944 NASA-CR-4649 NASA-CR-4650 NASA-CR-4650 NASA-CR-4650 NASA-TM-106764 NASA-TM-106847 NASA-TM-106849 NASA-TM-106870	p 290 p 316 p 316 p 316 p 317 p 325 p 329 p 320 p 273	N95-24053 * # N95-23792 * # N95-23766 * # N95-23266 * # N95-23267 * # N95-23268 * # N95-23183 * # N95-23190 * # N95-23199 * # N95-23199 * # N95-23199 * # N95-23690 * # N95-23690 * # N95-23690 * # N95-23185 * # N95-23185 * # N95-23185 * # N95-23185 * # N95-23095 * # N95-23178 * # N95-23178 * # N95-23671 * # N95-23671 * #	US-PATENT-CLASS-244-77R US-PATENT-CLASS-244-75R US-PATENT-CLASS-340-946 US-PATENT-CLASS-340-953 US-PATENT-CLASS-340-961 US-PATENT-CLASS-340-961 US-PATENT-CLASS-340-981 US-PATENT-CLASS-362-62 US-PATENT-CLASS-362-62 US-PATENT-CLASS-362-62 US-PATENT-CLASS-364-578 US-PATENT-CLASS-364-578 US-PATENT-CLASS-364-578 US-PATENT-CLASS-364-578 US-PATENT-CLASS-416-61 US-PATENT-CLASS-416-61 US-PATENT-CLASS-434-372 US-PATENT-CLASS-434-372 US-PATENT-CLASS-373-178H US-PATENT-CLASS-373-178H US-PATENT-5-294-080 US-PATENT-5-5-315-296 US-PATENT-5-5-315-296 US-PATENT-5-5-330,131 US-PATENT-5-320,900 US-PATENT-5-388,990 VPI-E-94-09	P 294 P 294 P 296 P 280 P 280 P 280 P 280 P 280 P 280 P 288 P 280 P 288 P 288 P 286 P 286 P 294 P 311	N95-23389 ' N95-23393 ' N95-23393 ' N95-23393 ' N95-23393 ' N95-22578 ' N95-22578 ' N95-22578 ' N95-23377 ' N95-23377 ' N95-22578 ' N95-23393 ' N95-23393 ' N95-23393 ' N95-23397 ' N95-23397 ' N95-23399 ' N95-23399 ' N95-23399 ' N95-23399 ' N95-23377 ' N95-22578 '
HTN-95-11304 HTN-95-20976 HTN-95-41219 HTN-95-41223 HTN-95-41393 HTN-95-41394 HTN-95-80851 HTN-95-80852 HTN-95-80853 HTN-95-80856 HTN-95-80856 HTN-95-80857 HTN-95-80857 HTN-95-80858 HTN-95-80858 HTN-95-80859 HTN-95-80859 HTN-95-80859 HTN-95-80859 HTN-95-80859 HTN-95-80850 HTN-95-80850 HTN-95-80859 HTN-95-91421 ICASE-95-5 INT-PATENT-CLASS-B64C-11/00 INT-PATENT-CLASS-B64C-9/16 INT-PATENT-CLASS-B64C-9/16 INT-PATENT-CLASS-G08B-21/00 ISBN-92-836-1010-5 ISBN-92-836-1011-3 L-17233 L-17348 L-17348 L-17348	P 319 P 261 P 317 P 317 P 317 P 283 P 317 P 290 P 290 P 290 P 290 P 283 P 283 P 283 P 283 P 283 P 283 P 287 P 318 P 319 P 314 P 314 P 286 P 280 P 315 P 302 P 280 P 315 P 302 P 324 P 300	A95-77009 A95-77009 A95-77001 A95-75031 A95-75031 A95-75035 A95-76389 A95-75093 A95-75094 A95-75095 A95-75096 A95-75097 A95-75097 A95-75098 A95-75090 A95-75101 A95-75090 A95-75101 A95-76394 A95-77334 N95-23466 # N95-23397 N95-23395 N95-23395 N95-23395 N95-23395 N95-23496 # N95-23015 # N95-2302 # N95-2302 # N95-2302 # N95-2302 # N95-23015 # N95-23016 # N95-24076 # N95-24076 # N95-24076 # N95-24076 #	NASA-CR-189099 NASA-CR-189141 NASA-CR-189146 NASA-CR-189146 NASA-CR-195026 NASA-CR-195026 NASA-CR-195052 NASA-CR-195052 NASA-CR-195052 NASA-CR-195445 NASA-CR-195445 NASA-CR-195445 NASA-CR-197441 NASA-CR-197419 NASA-CR-197419 NASA-CR-197420 NASA-CR-197420 NASA-CR-197420 NASA-CR-197440 NASA-CR-197440 NASA-CR-19740 NASA-CR-19740 NASA-CR-19740 NASA-CR-197699 NASA-CR-197699 NASA-CR-197704 NASA-CR-197691 NASA-CR-197912 NASA-CR-197912 NASA-CR-197931 NASA-CR-197931 NASA-CR-197934 NASA-CR-197934 NASA-CR-197934 NASA-CR-4650 NASA-CR-4650 NASA-CR-4650 NASA-TM-106847 NASA-TM-106847 NASA-TM-106847 NASA-TM-106847 NASA-TM-106870 NASA-TM-106870	p 290 p 316 p 316 p 316 p 317 p 318 p 319 p 323 p 319 p 323 p 329 p 329 p 329 p 329 p 329 p 330 p 371 p 289 p 330 p 273 p 289 p 273	N95-24053 * # N95-24792 * # N95-23776 * # N95-23276 * # N95-23277 * # N95-23267 * # N95-23266 * # N95-23766 * # N95-23766 * # N95-23183 * # N95-23183 * # N95-23183 * # N95-23190 * # N95-23590 * #	US-PATENT-CLASS-244-77R US-PATENT-CLASS-244-75R US-PATENT-CLASS-340-946 US-PATENT-CLASS-340-953 US-PATENT-CLASS-340-961 US-PATENT-CLASS-340-961 US-PATENT-CLASS-340-981 US-PATENT-CLASS-362-62 US-PATENT-CLASS-362-62 US-PATENT-CLASS-362-62 US-PATENT-CLASS-364-578 US-PATENT-CLASS-364-578 US-PATENT-CLASS-364-578 US-PATENT-CLASS-364-578 US-PATENT-CLASS-416-61 US-PATENT-CLASS-416-61 US-PATENT-CLASS-434-372 US-PATENT-CLASS-434-372 US-PATENT-CLASS-373-178H US-PATENT-CLASS-373-178H US-PATENT-5-294-080 US-PATENT-5-5-315-296 US-PATENT-5-5-315-296 US-PATENT-5-5-330,131 US-PATENT-5-320,900 US-PATENT-5-388,990 VPI-E-94-09	P 294 P 294 P 296 P 280 P 280 P 280 P 280 P 280 P 280 P 288 P 280 P 288 P 288 P 286 P 286 P 294 P 311	N95-23389 ' N95-23393 ' N95-23393 ' N95-23393 ' N95-23393 ' N95-22578 ' N95-22578 ' N95-22578 ' N95-23377 ' N95-23377 ' N95-22578 ' N95-23393 ' N95-23393 ' N95-23393 ' N95-23397 ' N95-23397 ' N95-23399 ' N95-23399 ' N95-23399 ' N95-23399 ' N95-23399 ' N95-23377 ' N95-22578 '

N95-23325 \*#

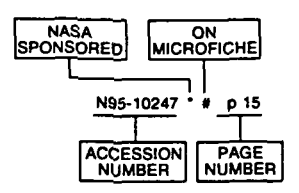
N95-23333 \*#

p 294

p 275

July 1995

# Typical Accession Number **Index Listing**



Listings in this index are arranged alphanumerically by accession number. The page number indicates the page on which the citation is located. The accession number denotes the number by which the citation is identified. An asterisk (\*) indicates that the item is a NASA report. A pound sign (#) indicates that the item is available on microfiche.

		<b>.</b>	
A95-73345	p 300	A95-73548 *	p 266
A95-73433	P 278	A95-73549	p 282
A95-73435	P 278	A95-73551	p 305
A95-73437	P 280	A95-73552 *	p 266
		A95-73553 *	p 305
A95-73438	P 286	A95-73554 *	p 306
A95-73439	P 304	A95-73555 *	р 306
A95-73441	p 262	A95-73556 *	p 306
A95-73444 A95-73451	p 262	A95-73557	p 266
A95-73451	p 286	A95-73558	p 267
A95-73454 *	p 304	A95-73559	p 297
A95-73454 A95-73457	р 304 р 304	A95-73560	p 267
A95-73458	p 304	A95-73561	p 267
A95-73460	p 305	A95-73564	p 298
A95-73461	p 263	A95-73568	p 298
A95-73462	p 263	A95-73571	p 278
A95-73465	p 263	A95-73577	p 298
A95-73471	p 321	A95-73583	p 298
A95-73477	p 305	A95-73584 A95-73587	p 306
A95-73479	P 305	A95-73588	p 282
A95-73486	p 305	A95-73589	p 276 p 282
A95-73493	p 263	A95-73590	p 282
A95-73494	p 263	A95-73591	p 282
A95-73495	p 263	A95-74042 *	p 261
A95-73496 *	p 264	A95-74496	p 306
A95-73497	p 264	A95-74554	p 295
A95-73498	p 305	A95-74612	p 306
A95-73516	p 264	A95-74629	p 295
A95-73517	p 316	A95-74702	p 306
A95-73518 *	p 264	A95-75031 *	p 317
A95-73519	p 264	A95-75035	p 317
A95-73520	P 264	A95-75093	p 290
A95-73521	p 316	A95-75094	p 290
A95-73522	p 276	A95-75095 *	p 290
A95-73523 A95-73524	p 264	A95-75096 *	p 290
A95-73525	P 265 P 265	A95-75097 *	p 267
A95-73526	p 281	A95-75098	p 283
A95-73527	p 265	A95-75099 *	p 283
A95-73529 *	p 265	A95-75100	p 283
A95-73530	P 265	A95-75101	p 267
A95-73531 *	p 281	A95-75494	p 323
A95-73532 *	p 265	A95-75516	p 307
A95-73533	P 281	A95-75532	p 317
A95-73535 *	p 281	A95-75714	p 279
A95-73536	p 276	A95-75716 A95-75717	p 287
A95-73537	p 281	A95-75717 A95-75718	p 287
A95-73538	p 323	A95-75718 A95-75720	p 287 p 287
A95-73539	p 266	A95-75725 *	p 298
A95-73540	p 281	A95-75728	-
A95-73541	p 266		p 267
A95-73542	p 282	A95-75729 °	p 268
A95-73544	p 282	A95-75731	p 268
A05-73546	0.266	A95.75733	n 268

A95-75733

A95-75734

p 268

p 298

A95-76681

A95-76683

p 279

p 292

p 279

A95-73546

A95-73547

p 266

A95-75735	p 298	
A95-75736	p 268	
A95-75752	p 261 p 261	
A95-75753 A95-75754	p 261	
A95-75755 A95-75756	p 300 p 261	
A95-75757	p 288	
A95-75758 A95-75760	p 268 p 307	
A95-75761 *	p 269	
A95-75762 A95-75763	p 307 p 269	
A95-75765 A95-75772	p 269 p 291	
A95-75773	p 283	
A95-75778 A95-75976	p 269 p 317	
A95-76265 *	p 317	
A95-76266 * A95-76267 *	p 318 p 318	
A95-76389 A95-76390	p 288 p 283	
A95-76394	p 318	
A95-76484 * A95-76489	p 307 p 307	
A95-76491	p 307	
A95-76582 A95-76584	p 283 p 295	
A95-76585 A95-76586	p 307 p 308	
A95-76588	p 321	
A95-76589 A95-76590	p 269 p 269	
A95-76592 A95-76598	p 321 p 321	
A95-76602	p 322	
A95-76603 A95-76604	p 291 p 276	
A95-76605	p 269	
A95-76606 * A95-76607 *	p 291 p 291	
A95-76608 A95-76609	p 291 p 292	
A95-76615	p 269	
A95-76616 A95-76621	p 288 p 299	
A95-76622 A95-76626	p 279 p 322	
A95-76630	p 292	
A95-76631 A95-76635 *	p 279 p 283	
A95-76636 *	p 270	
A95-76637 * A95-76638 *	p 295 p 322	
A95-76639 * A95-76640 *	p 296 p 292	
A95-76641 °	p 292	
A95-76642 * A95-76643 *	p 292 p 270	
A95-76644 A95-76645	p 284 p 276	
A95-76646	p 270	
A95-76647 A95-76648	p 308 p 288	
A95-76649	p 289	
A95-76650 A95-76651	p 289 p 270	
A95-76652 A95-76653	p 308 p 270	
A95-76654	p 284	
A95-76655 A95-76656	p 284 p 271	
A95-76657 A95-76658	p 319 p 308	
A95-76659	p 271	
A95-76660 * A95-76661	p 308 p 271	
A95-76673	p 289	
A95-76674 A95-76676	p 279 p 279	

A95-76686	р 308	N95-23377 *	p 311
A95-76697	p 279	N95-23389 *	p 294
A95-76734	p 287	N95-23390 *	p 286
	p 287	N95-23392 * #	p 294
A95-76736	p 287	N95-23393 *	p 280
A95-76737	p 319	N95-23395 *	p 286
A95-76740	p 271	N95-23410 * #	p 295
A95-76742	p 271	N95-23419.* #	p 322
A95-76742	p 271	N95-23423 * #	p 311
	p 272	N95-23425 *#	p 312
	p 272 p 272	N95-23429 *#	p 312
A95-76747		N95-23435 *#	p 312
A95-76758	p 299	N95-23435 #	p 312
A95-76759	p 299	N95-23438 * #	
A95-76764	p 272	N95-23440 ° #	p 312
A95-76765	p 261	N95-23440 # N95-23444 *#	p 313
A95-77000	p 319		p 313
A95-77009	p 319	N95-23446 *#	p 313
A95-77334	p 319	N95-23447 *#	p 314
		N95-23462 *#	p 275
N95-22481 °#	p 309	N95-23466 *#	p 314
N95-22510 #	p 284	N95-23496 # N95-23497 #	p 302
N95-22578 *	p 288	N95-23497 #	p 302
N95-22666 *#	p 272	N95-23500 #	p 302
N95-22669 °#	p 309	N95-23503 #	p 323
N95-22674 *#	p 292	N95-23505 #	p 314
N95-22675 * #	p 323	N95-23506 #	p 262
N95-22689 #	p 300	N95-23507 #	p 315
N95-22764 #	p 300	N95-23508 #	p 302
N95-22802 *#	p 272	N95-23509 #	p 302
N95-22804 *#	p 309	N95-23510 #	p 303
N95-22806 *#	p 284	N95-23512 #	p 315
N95-22829 *#	p 284	N95-23513 #	p 303
N95-22908 *#	p 293	N95-23515 #	p 303
N95-22917 *#	p 273	N95-23516 #	p 303
N95-22949 *#	p 285	N95-23517 #	p 303
N95-22953 *#	p 285	N95-23518 #	p 303
N95-22954 *#	p 293	N95-23519 #	p 262
N95-23009 * #	p 320	N95-23532 #	p 299
N95-23009 # N95-23011 #	p 296	N95-23550 *#	p 289
N95-23011 #	p 309	N95-23565 #	p 280
N95-23015 # N95-23031 *#	p 303	N95-23598 #	p 277
N95-23031 # N95-23038 *#	p 301	N95-23602 #	p 315
N95-23038 # N95-23088 *#	p 289	N95-23602 #	
		N95-23609 #	p 323
N95-23095 *#	p 273	N95-23630 *#	p 277
N95-23161 #	p 285		p 315
N95-23168 #	p 324		p 315
N95-23178 * #	p 323	N95-23662 #	p 316
N95-23179 * #	p 301	N95-23666	p 286
N95-23182 * #	p 273	N95-23669 *#	p 275
N95-23183 * #	p 309	N95-23670 *#	p 316
N95-23185 * #	p 273	N95-23671 *#	p 295
N95-23190 * #	p 310	N95-23761 *#	p 299
N95-23192 *#	p 296	N95-23766 *	p 320
N95-23193 * #	p 273	N95-23781 #	p 300
N95-23201 #	p 276	N95-23792 *#	p 316
N95-23210 *#	p 310	N95-23872 *#	p 325
N95-23217 * #	p 285	N95-23940 * #	
N95-23218 * #	p 274	N95-23947 *#	p 320
N95-23222 *#	p 289	N95-23948 *#	p 321
N95-23250 ° #	p 274	N95-23981 #	p 304
N95-23257 *#	p 310	N95-24012 #	p 277
N95-23259 * #	p 320	N95-24019 #	p 297
N95-23276 *#	p 325	N95-24024 #	p 277
N95-23277 °#	p 301	N95-24025 °#	p 262
N95-23283 * #	p 274	N95-24030 *#	p 288
N95-23284 * #	p 324	N95-24032 * #	p 300
N95-23287 * #	p 310	N95-24050 #	p 277
N95-23290 * #	p 310	N95-24053 * #	p 290
N95-23294 * #	p 274	N95-24065 #	p 277
N95-23297 * #	p 293	N95-24071 #	p 278
N95-23299 *#	p 296	N95-24076 #	p 324
N95-23300 °#	p 301	N95-24091 #	p 286
N95-23304 * #	p 297	N95-24105 #	p 278
N95-23308 *#	p 322	N95-24189 * #	p 316
N95-23309 *#	p 297		,
N95-23311 *#	p 311		
N95-23311 #	p 293		
N95-23317 *#	p 285		
N95-23317 #	p 280		
N95-23319 *#	p 294		
N95-23320 °#	p 324		
NID5.22225 * #	n 204		

# **AVAILABILITY OF CITED PUBLICATIONS**

# OPEN LITERATURE ENTRIES (A95-60000 Series)

Inquiries and requests should be addressed to NASA Center for AeroSpace Information, 800 Elkridge Landing Road, Linthicum Heights, MD 21090-2934. Orders are also taken by telephone, (301) 621-0390, e-mail, help@sti.nasa.gov, and fax, (301) 621-0134. Please refer to the accession number when requesting publications.

## STAR ENTRIES (N95-10000 Series)

One or more sources from which a document announced in *STAR* is available to the public is ordinarily given on the last line of the citation. The most commonly indicated sources and their acronyms or abbreviations are listed below, and their addresses are listed on page APP-3. If the publication is available from a source other than those listed, the publisher and his address will be displayed on the availability line or in combination with the corporate source line.

- Avail: CASI. Sold by the NASA Center for AeroSpace Information. Prices for hard copy (HC) and microfiche (MF) are indicated by a price code following the letters HC or MF in the STAR citation. Current values for the price codes are given in the tables on page APP-5.
  - NOTE ON ORDERING DOCUMENTS: When ordering publications from NASA CASI, use the N accession number or other report number. It is also advisable to cite the title and other bibliographic identification.
- Avail: SOD (or GPO). Sold by the Superintendent of Documents, U.S. Government Printing Office, in hard copy.
- Avail: BLL (formerly NLL): British Library Lending Division, Boston Spa, Wetherby, Yorkshire, England. Photocopies available from this organization at the price shown. (If none is given, inquiry should be addressed to the BLL.)
- Avail: DOE Depository Libraries. Organizations in U.S. cities and abroad that maintain collections of Department of Energy reports, usually in microfiche form, are listed in *Energy Research Abstracts*. Services available from the DOE and its depositories are described in a booklet, *DOE Technical Information Center Its Functions and Services* (TID-4660), which may be obtained without charge from the DOE Technical Information Center.
- Avail: ESDU. Pricing information on specific data, computer programs, and details on Engineering Sciences Data Unit (ESDU) topic categories can be obtained from ESDU International Ltd. Requesters in North America should use the Virginia address while all other requesters should use the London address, both of which are on page APP-3.
- Avail: Fachinformationszentrum Karlsruhe. Gesellschaft für wissenschaftlich-technische Information mbH 76344 Eggenstein-Leopoldshafen, Germany.
- Avail: HMSO. Publications of Her Majesty's Stationery Office are sold in the U.S. by Pendragon House, Inc. (PHI), Redwood City, CA. The U.S. price (including a service and mailing charge) is given, or a conversion table may be obtained from PHI.
- Avail: Issuing Activity, or Corporate Author, or no indication of availability. Inquiries as to the availability of these documents should be addressed to the organization shown in the citation as the corporate author of the document.
- Avail: NASA Public Document Rooms. Documents so indicated may be examined at or purchased from the National Aeronautics and Space Administration (JBD-4), Public Documents Room (Room 1H23), Washington, DC 20546-0001, or public document rooms located at NASA installations, and the NASA Pasadena Office at the Jet Propulsion Laboratory.

- Avail: NTIS. Sold by the National Technical Information Service. Initially distributed microfiche under the NTIS SRIM (Selected Research in Microfiche) are available. For information concerning this service, consult the NTIS Subscription Section, Springfield, VA 22161.
- Avail: Univ. Microfilms. Documents so indicated are dissertations selected from *Dissertation Abstracts* and are sold by University Microfilms as xerographic copy (HC) and microfilm. All requests should cite the author and the Order Number as they appear in the citation.
- Avail: US Patent and Trademark Office. Sold by Commissioner of Patents and Trademarks, U.S. Patent and Trademark Office, at the standard price of \$1.50 each, postage free.
- Avail: (US Sales Only). These foreign documents are available to users within the United States from the National Technical Information Service (NTIS). They are available to users outside the United States through the International Nuclear Information Service (INIS) representative in their country, or by applying directly to the issuing organization.
- Avail: USGS. Originals of many reports from the U.S. Geological Survey, which may contain color illustrations, or otherwise may not have the quality of illustrations preserved in the microfiche or facsimile reproduction, may be examined by the public at the libraries of the USGS field offices whose addresses are listed on page APP-3. The libraries may be queried concerning the availability of specific documents and the possible utilization of local copying services, such as color reproduction.

## FEDERAL DEPOSITORY LIBRARY PROGRAM

In order to provide the general public with greater access to U.S. Government publications, Congress established the Federal Depository Library Program under the Government Printing Office (GPO), with 53 regional depositories responsible for permanent retention of material, inter-library loan, and reference services. At least one copy of nearly every NASA and NASA-sponsored publication, either in printed or microfiche format, is received and retained by the 53 regional depositories. A list of the regional GPO libraries, arranged alphabetically by state, appears on the inside back cover of this issue. These libraries are *not* sales outlets. A local library can contact a regional depository to help locate specific reports, or direct contact may be made by an individual.

# **PUBLIC COLLECTION OF NASA DOCUMENTS**

An extensive collection of NASA and NASA-sponsored publications is maintained by the British Library Lending Division, Boston Spa, Wetherby, Yorkshire, England for public access. The British Library Lending Division also has available many of the non-NASA publications cited in *STAR*. European requesters may purchase facsimile copy or microfiche of NASA and NASA-sponsored documents, those identified by both the symbols # and \* from ESA — Information Retrieval Service European Space Agency, 8-10 rue Mario-Nikis, 75738 CEDEX 15, France.

## STANDING ORDER SUBSCRIPTIONS

NASA SP-7037 supplements and annual index are available from the NASA Center for AeroSpace Information (CASI) on standing order subscription. Standing order subscriptions do not terminate at the end of a year, as do regular subscriptions, but continue indefinitely unless specifically terminated by the subscriber.

# ADDRESSES OF ORGANIZATIONS

British Library Lending Division Boston Spa, Wetherby, Yorkshire England

Commissioner of Patents and Trademarks U.S. Patent and Trademark Office Washington, DC 20231

Department of Energy Technical Information Center P.O. Box 62 Oak Ridge, TN 37830

European Space Agency-Information Retrieval Service ESRIN Via Galileo Galilei 00044 Frascati (Rome) Italy

Engineering Sciences Data Unit International P.O. Box 1633 Manassas, VA 22110

Engineering Sciences Data Unit International, Ltd. 251-259 Regent Street London, W1R 7AD, England

Fachinformationszentrum Karlsruhe
Gesellschaft für wissenschaftlich-technische
Information mbH
76344 Eggenstein-Leopoldshafen, Germany

Her Majesty's Stationery Office P.O. Box 569, S.E. 1 London, England

NASA Center for AeroSpace Information 800 Elkridge Landing Road Linthicum Heights, MD 21090-2934

National Aeronautics and Space Administration Scientific and Technical Information Office (JT) Washington, DC 20546-0001 National Technical Information Service 5285 Port Royal Road Springfield, VA 22161

Pendragon House, Inc. 899 BroadwayAvenue Redwood City, CA 94063

Superintendent of Documents U.S. Government Printing Office Washington, DC 20402

University Microfilms A Xerox Company 300 North Zeeb Road Ann Arbor, MI 48106

University Microfilms, Ltd. Tylers Green London, England

U.S. Geological Survey Library National Center MS 950 12201 Sunrise Valley Drive Reston, VA 22092

U.S. Geological Survey Library 2255 North Gemini Drive Flagstaff, AZ 86001

U.S. Geological Survey 345 Middlefield Road Menlo Park, CA 94025

U.S. Geological Survey Library Box 25046 Denver Federal Center, MS914 Denver, CO 80225

# Page Intentionally Left Blank

# NASA CASI PRICE CODE TABLE

(Effective January 1, 1995)

CASI PRICE CODE	NORTH AMERICAN PRICE	FOREIGN PRICE
A01	\$ 6.00	\$ 12.00
A02	9.00	18.00
A03	17.50	35.00
A04-A05	19.50	39.00
A06-A09	27.00	54.00
A10-A13	36.50	73.00
A14-A17	44.50	89.00
A18-A21	52.00	104.00
A22-A25	61.00	122.00
A99	Call For Price	Call For Price

# IMPORTANT NOTICE

For users not registered at the NASA CASI, prepayment is required. Additionally, a shipping and handling fee of \$1.00 per document for delivery within the United States and \$9.00 per document for delivery outside the United States is charged.

For users registered at the NASA CASI, document orders may be invoiced at the end of the month, charged against a deposit account, or paid by check or credit card. NASA CASI accepts American Express, Diners' Club, MasterCard, and VISA credit cards. There are no shipping and handling charges. To register at the NASA CASI, please request a registration form through the NASA Access Help Desk at the numbers or addresses below.

# **RETURN POLICY**

Effective June 1, 1995, the NASA Center for AeroSpace Information will gladly replace or make full refund on items you have requested if we have made an error in your order, if the item is defective, or if it was received in damaged condition and you contact us within 30 days of your original request. Just contact our NASA Access Help Desk at the numbers or addresses listed below.

# NASA Center for AeroSpace Information

800 Elkridge Landing Road Linthicum Heights, MD 21090-2934

Telephone: (301) 621-0390 E-mail: help@sti.nasa.gov Fax: (301) 621-0134

# REPORT DOCUMENT PAGE

1.	Report No.	2. Government Acc	cession No.	3. Recipient's Catal	og No.	
	NASA SP-7037 (319)					
4.	Title and Subtitle	<del></del>		5. Report Date		
	Aeronautical Engineering		July 1995			
	A Continuing Bibliography	(Supplement 319	9)	6. Performing Organ	nization Code	
				JT	-11	
7.	Author(s)			8. Performing Organ	nization Report No.	
		•				
_		··	10. Work Unit No.			
9.	Performing Organization Name and Ad	O#:		_		
	NASA Scientific and Techn	lical information	Опісе	11. Contract or Grant	No.	
		•				
12.	Sponsoring Agency Name and Addres	is		1	nd Period Covered	
	National Aeronautics and S		ition	Special Publ	ication	
	Washington, DC 20546-000	01		14. Sponsoring Agency Code		
<u> </u>						
15.	Supplementary Notes					
ŀ						
16.	Abstract					
	This report lists 349 reports STI Database.	s, articles and ot	her documents re	ecently announced	d in the NASA	
	STI Dalabase.					
				•		
	•					
	· ·					
	·		•	,		
17.	Key Words (Suggested by Author(s))		18. Distribution State	ement		
	Aeronautical Engineering		1	d - Unlimited		
	Aeronautics Bibliographics		Subject Cat	egory - 01		
	Bibliographies					
				•		
19.	Security Classif. (of this report)	20. Security Classif	(of this page)	21. No. of Pages	22. Price	
- *	Unclassified	Unclassifie	-	136	A07/HC	
	· <del></del>					

# FEDERAL REGIONAL DEPOSITORY LIBRARIES

#### ALABAMA AUBURN UNIV. AT MONTGOMERY LIBRARY

Documents Dept. 7300 University Dr. Montgomery, AL 36117-3596 (205) 244-3650 Fax: (205) 244-0678

# UNIV. OF ALABAMA Amelia Gayle Gorgas Library Govt. Documents

P.O. Box 870266 Tuscaloosa, AL 35487-0266 (205) 348-6046 Fax: (205) 348-0760

# DEPT. OF LIBRARY, ARCHIVES, AND PUBLIC RECORDS Research Division

Third Floor, State Capitol 1700 West Washington Phoenix, AZ 85007 (602) 542-3701 Fax: (602) 542-4400

#### ARKANSAS ARKANSAS STATE LIBRARY

State Library Service Section Documents Service Section One Capitol Mall Little Rock, AR 72201-1014 (501) 682-2053 Fax: (501) 682-1529

#### **CALIFORNIA** CALIFORNIA STATE LIBRARY

Govt. Publications Section P.O. Box 942837 - 914 Capitol Mall Sacramento, CA 94337-0091 (916) 654-0069 Fax: (916) 654-0241

#### COLORADO UNIV. OF COLORADO - BOULDER

Libraries - Govt. Publications Campus Box 184 Boulder, CO 80309-0184 (303) 492-8834 Fax: (303) 492-1881

**DENVER PUBLIC LIBRARY**Govt. Publications Dept. BSG 1357 Broadway Denver, CO 80203-2165 (303) 640-8846 Fax: (303) 640-8817

## CONNECTICUT **CONNECTICUT STATE LIBRARY**

231 Capitol Avenue Hartford, CT 06106 (203) 566-4971 Fax: (203) 566-3322

#### **FLORIDA** UNIV. OF FLORIDA LIBRARIES

Documents Dept. 240 Library West Gainesville, FL 32611-2048 (904) 392-0366 Fax: (904) 392-7251

### **GEORGIA**

UNIV. OF GEORGIA LIBRARIES Govt. Documents Dept. Jackson Street Athens, GA 30602-1645 (706) 542-8949 Fax: (706) 542-4144

UNIV. OF HAWAII **Hamilton Library** Govt. Documents Collection 2550 The Mall Honolulu, HI 96822 (808) 948-8230 Fax: (808) 956-5968

#### IDAHO UNIV. OF IDAHO LIBRARY

Documents Section Raybum Street Moscow, ID 83844-2353 (208) 885-6344 Fax: (208) 885-6817

### ILLINOIS ILLINOIS STATE LIBRARY

Federal Documents Dept. 300 South Second Street Springfield, IL 62701-1796 (217) 782-7596 Fax: (217) 782-6437

#### INDIANA

INDIANA STATE LIBRARY Serials/Documents Section 140 North Senate Avenue

Indianapolis, IN 46204-2296 (317) 232-3679 Fax: (317) 232-3728

UNIV. OF IOWA LIBRARIES
Govt. Publications Washington & Madison Streets lowa City, IA 52242-1166 (319) 335-5926 Fax: (319) 335-5900

## KANSAS

UNIV. OF KANSAS

Govt. Documents & Maps Library 6001 Malott Hall Lawrence, KS 66045-2800 (913) 864-4660 Fax: (913) 864-3855

## KENTUCKY

UNIV. OF KENTUCKY King Library South Govt. Publications/Maps Dept. Patterson Drive Lexington, KY 40506-0039 (606) 257-3139 Fax: (606) 257-3139

# LOUISIANA

LOUISIANA STATE UNIV. Middleton Library

Govt. Documents Dept. Baton Rouge, LA 70803-3312 (504) 388-2570 Fax: (504) 388-6992

## LOUISIANA TECHNICAL UNIV.

Prescott Memorial Library Govt. Documents Dept. Ruston, LA 71272-0046 (318) 257-4962 Fax: (318) 257-2447

#### MAINE

UNIV. OF MAINE

Raymond H. Fogler Library Govt. Documents Dept. Orono, ME 04469-5729 (207) 581-1673 Fax: (207) 581-1653

MARYLAND
UNIV. OF MARYLAND - COLLEGE PARK

McKeldin Library
Govt. Documents/Maps Unit College Park, MD 20742 (301) 405-9165 Fax: (301) 314-9416

## **MASSACHUSETTS** BOSTON PUBLIC LIBRARY

Govt. Documents 666 Boylston Street Boston, MA 02117-0286 (617) 536-5400, ext. 226 Fax: (617) 536-7758

#### **MICHIGAN** DETROIT PUBLIC LIBRARY

5201 Woodward Avenue Detroit, MI 48202-4093 (313) 833-1025 Fax: (313) 833-0156

## LIBRARY OF MICHIGAN

Govt. Documents Unit P.O. Box 30007 717 West Allegan Street Lansing, MI 48909 (517) 373-1300 Fax: (517) 373-3381

#### **MINNESOTA UNIV. OF MINNESOTA**

Govt. Publications 409 Wilson Library 309 19th Avenue South Minneapolis, MN 55455 (612) 624-5073 Fax: (612) 626-9353

#### MISSISSIPPI UNIV. OF MISSISSIPPI

J.D. Williams Library 106 Old Gym Bldg. University, MS 38677 (601) 232-5857 Fax: (601) 232-7465

### MISSOURI

UNIV. OF MISSOURI - COLUMBIA 106B Ellis Library Govt. Documents Sect. Columbia, MO 65201-5149 (314) 882-6733 Fax: (314) 882-8044

# MONTANA

UNIV. OF MONTANA Mansfield Library Documents Division Missoula, MT 59812-1195 (406) 243-6700 Fax: (406) 243-2060

## NEBRASKA

UNIV. OF NEBRASKA - LINCOLN

D.L. Love Memorial Library Lincoln, NE 68588-0410 (402) 472-2562 Fax: (402) 472-5131

#### NEVADA THE UNIV. OF NEVADA **LIBRARIES**

Business and Govt. Information Center

Reno, NV 89557-0044 (702) 784-6579 Fax: (702) 784-1751

## **NEW JERSEY** NEWARK PUBLIC LIBRARY

Science Div. - Public Access P.O. Box 630 Five Washington Street Newark, NJ 07101-7812 (201) 733-7782 Fax: (201) 733-5648

#### **NEW MEXICO** UNIV. OF NEW MEXICO

General Library
Govt. Information Dept. Albuquerque, NM 87131-1466 (505) 277-5441 Fax: (505) 277-6019

# **NEW MEXICO STATE LIBRARY**

325 Don Gaspar Avenue Santa Fe, NM 87503 (505) 827-3824 Fax: (505) 827-3888

NEW YORK NEW YORK STATE LIBRARY

Cultural Education Center Documents/Gift & Exchange Section Empire State Plaza Albany, NY 12230-0001 (518) 474-5355 Fax: (518) 474-5786

#### NORTH CAROLINA UNIV. OF NORTH CAROLINA -**CHAPEL HILL**

Walter Royal Davis Library CB 3912, Reference Dept. Chapel Hill, NC 27514-8890 (919) 962-1151 Fax: (919) 962-4451

## NORTH DAKOTA NORTH DAKOTA STATE UNIV. LIB.

Documents P.O. Box 5599 Fargo, ND 58105-5599 (701) 237-8886 Fax: (701) 237-7138

# UNIV. OF NORTH DAKOTA

Chester Fritz Library University Station
P.O. Box 9000 - Centennial and University Avenue
Grand Forks, ND 58202-9000 (701) 777-4632 Fax: (701) 777-3319

STATE LIBRARY OF OHIO Documents Dept. 65 South Front Street Columbus, OH 43215-4163 (614) 644-7051 Fax: (614) 752-9178

## OKLAHOMA

OKLAHOMA DEPT. OF LIBRARIES U.S. Govt. Information Division 200 Northeast 18th Street

Oklahoma City, OK 73105-3298 (405) 521-2502, ext. 253 Fax: (405) 525-7804

#### OKLAHOMA STATE UNIV.

Edmon Low Library Stillwater, OK 74078-0375 (405) 744-6546 Fax: (405) 744-5183

## **OREGON**

PORTLAND STATE UNIV.

Branford P. Millar Library 934 Southwest Harrison Portland, OR 97207-1151 (503) 725-4123 Fax: (503) 725-4524

#### **PENNSYLVANIA** STATE LIBRARY OF PENN.

Govt. Publications Section 116 Walnut & Commonwealth Ave. Harrisburg, PA 17105-1601 (717) 787-3752 Fax: (717) 783-2070

#### SOUTH CAROLINA CLEMSON UNIV.

Robert Muldrow Cooper Library Public Documents Unit P.O. Box 343001 Clemson, SC 29634-3001 (803) 656-5174 Fax: (803) 656-3025

# UNIV. OF SOUTH CAROLINA

Thomas Cooper Library Green and Sumter Streets Columbia, SC 29208 (803) 777-4841 Fax: (803) 777-9503

#### **TENNESSEE** UNIV. OF MEMPHIS LIBRARIES

Govt. Publications Dept. Memphis, TN 38152-0001 (901) 678-2206 Fax: (901) 678-2511

#### **TEXAS**

TEXAS STATE LIBRARY United States Documents

P.O. Box 12927 - 1201 Brazos Austin, TX 78701-0001 (512) 463-5455 Fax: (512) 463-5436

## TEXAS TECH. UNIV. LIBRARIES

Documents Dept. Lubbock, TX 79409-0002 (806) 742-2282 Fax: (806) 742-1920

#### UTAH UTAH STATE UNIV.

Merrill Library Documents Dept. Logan, UT 84322-3000 (801) 797-2678 Fax: (801) 797-2677

#### **VIRGINIA**

UNIV. OF VIRGINIA

Alderman Library Govt. Documents University Ave. & McCormick Rd. Charlottesville, VA 22903-2498 (804) 824-3133 Fax: (804) 924-4337

#### WASHINGTON **WASHINGTON STATE LIBRARY**

Govt. Publications P.O. Box 42478 16th and Water Streets Olympia, WA 98504-2478 (206) 753-4027 Fax: (206) 586-7575

## **WEST VIRGINIA** WEST VIRGINIA UNIV. LIBRARY

Govt. Documents Section
P.O. Box 6069 - 1549 University Ave. Morgantown, WV 26506-6069 (304) 293-3051 Fax: (304) 293-6638

# WISCONSIN

ST. HIST, SOC, OF WISCONSIN LIBRARY Govt. Publication Section 816 State Street Madison, WI 53706 (608) 264-6525 Fax: (608) 264-6520

## MILWAUKEE PUBLIC LIBRARY

Documents Division 814 West Wisconsin Avenue Milwaukee, WI 53233 (414) 286-3073 Fax: (414) 286-8074 National Aeronautics and Space Administration Code JT Washington, DC 20546-0001

Official Business Penalty for Private Use \$300